Copyrighted Materials
Copyright © 2004 Editions Technip Retrieved from www.knovel.com

INSTITUT FRANÇAIS DU PÉTROLE PUBLICATIONS

Pierre TRAMBOUZE
Former Director of CEDI (IFP)

Jean-Paul EUZEN
Chief Engineer at CEDI (IFP)
Professor at the IFP School

CHEMICAL REACTORS

FROM DESIGN TO OPERATION

Translated by
Robert Bononno
Bowne Global Solutions

2004

Editions TECHNIP 27, rue Ginoux, 75737 PARIS Cedex 15, FRANCE

Translation of
Les réacteurs chimiques. De la conception à la mise en œuvre
P. Trambouze, J.-P. Euzen
© 2002, Éditions Technip, Paris

All rights reserved.

No part of this publication may be reproduced or transmitted in any form or by any means, electronic or mechanical, including photocopy, recording, or any information storage and retrieval system, without the prior written permission of the publisher.

© Editions Technip, Paris, 2004.

Printed in France

ISBN 2-7108-0845-5

Copyrighted Materials
Copyright © 2004 Editions Technip Retrieved from www.knovel.com

Table of Contents

FOREWORD V

CHAPTER 1 • **DEFINITIONS AND FUNDAMENTAL CONCEPTS** 1

1.1 Definitions of stoichiometric values 1
1.1.1 Stoichiometric relations 1
1.1.2 Extent of reaction, conversion, selectivity, and yield 2
1.1.3 Mass selectivity and yield 5
1.1.4 Concluding remarks 5

1.2 Chemical thermodynamics 5
1.2.1 Energy balance of the chemical transformation 5
1.2.2 Chemical equilibria 7

1.3 Chemical kinetics 9
1.3.1 Definition of rate of reaction 10
1.3.2 Ways of expressing the rate of reaction r_j 11
1.3.3 Influence of temperature 12
1.3.4 Formal kinetic expressions involving fractional or high orders 13
1.3.5 Other forms of kinetic expression associated with catalytic processes 13
1.3.6 Heterogeneous catalytic reactions 15
1.3.7 Groups of compounds 16
1.3.8 Kinetics based on elementary steps 23
1.3.9 Conclusion 23

1.4 Reactor types 23
1.4.1 Principal characteristics of a reactor 24
1.4.2 Classification of reactors 29
1.4.3 General expression of mass and enthalpy balances 30
1.4.4 Application of the general balance expressions to the various types of ideal reactor 32

1.5 Residence time distribution 35
1.5.1 Typical distribution functions of fluid flow 35
1.5.2 Experimental determination of distribution functions 38
1.5.3 Distribution functions for various types of flow 40
1.6 Macromixing and micromixing 42
1.6.1 Earliness of mixing 43
1.6.2 Segregation within a fluid 44
1.6.3 Micromixing 46
1.6.4 Use of computational fluid dynamics methods 49
References 49
Nomenclature 51

CHAPTER 2 • **SINGLE-PHASE REACTORS** 53
2.1 Batch reactors 53
2.1.1 Mass and energy balances 53
2.1.2 General case and practical implications 59
2.1.3 Thermal instability 61
2.1.4 Available technologies 69
2.1.5 Mixing systems 75
2.1.6 Reactors involving gradual injection of part of the reactants and gradual elimination of a product 84
2.1.7 Conclusion 89
2.2 Continuous tubular reactors 89
2.2.1 Mass and energy balances 90
2.2.2 Solutions for a few simple cases 92
2.2.3 Influence of backmixing 94
2.2.4 Available technologies 99
2.2.5 Concluding remarks 104
2.3 Continuous stirred tank reactors (CSTR) 104
2.3.1 Mass and energy balances 105
2.3.2 Solutions for some simple cases 107
2.3.3 Autothermal operation 110
2.3.4 The multistage reactor 115
2.3.5 Available technologies 116
2.3.6 Conclusion 123
2.4 Comparison of the different reactor types 123
2.4.1 Operating conditions and production capacity 123
2.4.2 Conversion 127
2.4.3 Selectivity 136
2.4.4 Concluding remarks 142
References 143
Nomenclature 144

CHAPTER 3 • **GENERAL CHARACTERISTICS OF REACTORS WITH TWO FLUID PHASES** 145

3.1 Review of two-film theory 145

3.2 Mass transfer accompanied by chemical reaction 148

3.2.1 Irreversible and isothermal reaction in a single phase and transfer toward the reaction phase 149

3.2.2 Calculating the local flux of a compound transferred from phase I to phase II 161

3.2.3 Efficiency in a reaction system with two fluid phases (first-order reaction) 161

3.2.4 Extending the study of transfer phenomena with chemical reaction to systems with more complex kinetics 164

3.2.5 Comparison of various theories of mass transfer accompanied by chemical reaction 166

3.3 Influence of mass transfer on chemical transformation 168

3.3.1 Apparent reaction order 168

3.3.2 Apparent activation energy 172

3.3.3 Influence of mass transfer on selectivity 173

3.4 Designing a reactor with two fluid phases 184

3.4.1 Batch reactor with two fluid phases 184

3.4.2 Semi-Continuous gas-liquid reactor 188

3.4.3 Tubular reactor with two fluid phases 192

3.4.4 Continuous stirred tank reactor with two fluid phases 196

3.4.5 Conclusion 197

References 199

Nomenclature 200

CHAPTER 4 • **EXPERIMENTAL DATA AND CORRELATIONS FOR GAS-LIQUID REACTORS** 201

4.1 Introduction and preliminary definitions 201

4.1.1 Specific interfacial area 203

4.1.2 Holdup 203

4.1.3 Current values of design parameters 203

4.2 Bubble columns 205

4.2.1 General characteristics 205

4.2.2 Hydrodynamics 207

4.2.3 Mass transfer 209

4.2.4 Heat transfer 226

4.2.5 General design considerations 226

4.2.6 Alternative designs 228

4.2.7 Concluding remarks 229

4.3 Gaslifts 229

4.3.1 General characteristics 229

4.3.2 Hydrodynamics 229

4.3.3 Mass transfer 232
4.3.4 Heat transfer at the wall 232
4.3.5 General design considerations 232
4.3.6 Concluding remarks 233
4.4 Plate columns 233
4.4.1 General features 233
4.4.2 Hydrodynamics 234
4.4.3 Mass transfer 236
4.4.4 Construction details 238
4.4.5 Submerged plate reactors 240
4.4.6 Concluding remarks 240
4.5 Packed columns 241
4.5.1 General characteristics 241
4.5.2 Hydrodynamics 245
4.5.3 Mass transfer 249
4.5.4 Unconventional packed columns 251
4.5.5 Selection criteria and construction details 253
4.5.6 Comparison of plate columns and packed columns 255
4.5.7 Concluding remarks 256
4.6 Falling film reactors 257
4.6.1 General characteristics 258
4.6.2 Hydrodynamics 259
4.6.3 Mass transfer 261
4.6.4 Heat transfer 262
4.6.5 Current uses 264
4.6.6 Practical applications 267
4.6.7 Technology 268
4.6.8 Concluding remarks 268
4.7 Mechanically agitated devices 269
4.7.1 General characteristics 269
4.7.2 Hydrodynamics 269
4.7.3 Mass transfer 277
4.7.4 Heat transfer 278
4.7.5 Construction details 278
4.7.6 Concluding remarks 279
4.8 Ejectors 279
4.8.1 Bubble generation 280
4.8.2 Droplet generation 283
4.9 Inline mixers 288
4.9.1 Empty pipes 288
4.9.2 Static mixers 289

4.10 Concluding remarks 290
References 292
Nomenclature 297

CHAPTER 5 • **EXPERIMENTAL DATA AND CORRELATIONS FOR LIQUID-LIQUID REACTORS** 299

5.1 Introduction 299
5.1.1 Hydrodynamic behavior 302
5.1.2 Mass transfer 305
5.1.3 Scale-up 307
5.2 Spray columns 308
5.2.1 Hydrodynamics 309
5.2.2 Mass transfer 311
5.2.3 Technology 312
5.2.4 Concluding remarks 313
5.3 Perforated plate columns 313
5.3.1 Hydrodynamics 313
5.3.2 Mass transfer 317
5.3.3 Technology 317
5.3.4 Concluding remarks 319
5.4 Packed columns 319
5.4.1 Hydrodynamics 320
5.4.2 Mass transfer 322
5.4.3 Technology 322
5.4.4 Pulsed packed columns 323
5.4.5 Concluding remarks 323
5.5 Static mixers 323
5.5.1 Hydrodynamics 323
5.5.2 Mass transfer 325
5.5.3 Technology 326
5.5.4 Concluding remarks 326
5.6 Columns with rotary agitators 326
5.6.1 Hydrodynamics 329
5.6.2 Mass transfer 334
5.6.3 Technology 335
5.6.4 Concluding remarks 336
5.7 Mixer-settlers 336
5.7.1 Hydrodynamics 337
5.7.2 Mass transfer 338
5.7.3 Consumed power 339

5.7.4 Technology 339
5.7.5 Concluding remarks 341
5.8 Other types of equipment 341
5.8.1 Centrifugal extractors 341
5.8.2 Microreactors 342
5.9 Concluding remarks 342
References 344
Nomenclature 346

CHAPTER 6 • **GENERAL CHARACTERISTICS OF HETEROGENEOUS CATALYTIC REACTORS** 347
6.1 Introduction 347
6.2 The catalyst 347
6.2.1 The solid 348
6.2.2 The grain 348
6.2.3 Granular mass 353
6.2.4 Monolithic catalysts 355
6.3 Internal diffusion 358
6.3.1 Plane surface 359
6.3.2 Homogeneous spherical particle 360
6.3.3 Spherical particle with an active zone on the periphery 363
6.3.4 Optimization of catalyst geometry 365
6.4 Extending the concepts of the Thiele modulus and effectiveness 367
6.4.1 Non-spherical geometric shapes 368
6.4.2 Other than first-order reactions 368
6.4.3 Reversible reactions 370
6.4.4 Non-isochorous reactions 371
6.4.5 Non-isothermal reactions 372
6.5 Influence of internal diffusion on the selectivity of catalytic chemical reactions 375
6.5.1 Independent parallel first-order reactions 375
6.5.2 First-order twin reactions 376
6.5.3 Consecutive reactions 377
6.6 Estimating the coefficient of diffusion $\mathcal{D}_e$ 382
6.7 Influence of external mass transfer: the concept of global effectiveness 384
6.7.1 Global transfer coefficient 384
6.7.2 Heat transfer on the outer surface of the grain 386
6.7.3 The concept of global grain effectiveness 386
6.7.4 Temperature and concentration gradients 387
6.8 Apparent activation energy of heterogeneous catalytic reactions 388

6.9 Catalyst deactivation 391
6.9.1 Causes of catalyst deactivation 391
6.9.2 Preventing catalyst deactivation 391
6.9.3 Equations for deactivation kinetics 391
6.9.4 Deactivation accompanied by internal diffusion limitation 392
6.9.5 Concluding remarks 393
6.10 Use of heterogeneous catalysts 394
6.10.1 Conditions for the optimal use of a catalyst 394
6.10.2 The fixed bed 394
6.10.3 The moving bed 396
6.10.4 Reactors with catalyst in suspension 398
6.10.5 Comparison of catalyst technologies 403
References 408
Nomenclature 408

CHAPTER 7 • **REACTORS EMPLOYING A FLUID PHASE AND A CATALYTIC SOLID PHASE: FIXED BED, MOVING BED, FLUIDIZED BED** 411

7.1 Introduction 411
7.2 Fixed-bed catalytic reactors 411
7.2.1 Writing the mass balance equations 411
7.2.2 Designing the catalytic bed 414
7.2.3 Discussion concerning the validity of the criteria used 417
7.2.4 Calculation of dynamic pressure drop in a catalytic reactor 418
7.2.5 Influence of external transfer in fixed-bed catalytic reactors 419
7.2.6 Criteria for determining the possible influence of external mass transfer 424
7.2.7 Heat transfer at the reactor wall 425
7.2.8 Thermal stability of fixed-bed catalytic reactors 428
7.2.9 Practical considerations 429
7.2.10 Concluding remarks 443
7.3 Moving-bed catalytic reactors 445
7.3.1 Introduction 445
7.3.2 Design of the moving-bed reactor 445
7.3.3 Applications of moving-bed technology 451
7.4 Fluidized-bed reactors with a single fluid phase 454
7.4.1 General remarks 454
7.4.2 The hydrodynamics of fluidized beds 455
7.4.3 Minimum superficial velocity of fluidization $(V_{SF})_m$ 457
7.4.4 The terminal velocity of a particle 460
7.4.5 Expansion in a fluidized bed 461

7.4.6 Fluidized-bed reactor models and correlations 463
7.4.7 Mass and heat transfer between a gas and a solid in the dense phase 471
7.4.8 Heat transfer between the wall and the fluidized bed 471
7.4.9 Introduction of reactants and withdrawal of products 472
7.4.10 Industrial applications 474
References 482
Nomenclature 483

CHAPTER 8 • **THREE-PHASE REACTORS: GAS, LIQUID, AND CATALYTIC SOLID** 485

8.1 Introduction 485
8.1.1 Reaction at the surface of an isolated catalyst particle 486
8.2 Characteristics of three-phase reactors 491
8.2.1 Bubble columns 492
8.2.2 Mechanically agitated reactors 501
8.2.3 Fixed beds with two-phase flow 502
8.2.4 Moving-bed reactors 528
8.2.5 Three-phase fluidized beds or ebullated beds 530
8.3 Current uses and comparison of three-phase reactors 542
References 545
Nomenclature 551

CHAPTER 9 • **CASE STUDIES** 553

9.1 Batch and semi-continuous homogeneous reactors 553
9.1.1 Fundamental data 553
9.1.2 Batch reactor 554
9.1.3 Semi-Continuous reactor 557
9.1.4 Concluding remarks 564
9.2 Packed column gas-liquid reactor 564
9.2.1 Fundamental data 565
9.2.2 Writing the molar and heat balances 568
9.2.3 Calculating the transfer parameters 571
9.2.4 Integration of the differential balances 572
9.2.5 Column geometrical characteristics 575
9.2.6 Concluding remarks 575
9.3 Fixed-bed catalytic reactor with a single fluid phase 577
9.3.1 Fundamental data 578
9.3.2 Calculating the volume of catalyst 579
9.3.3 Cost optimization 581

9.3.4 Presentation of the results 584
9.3.5 Calculating concentration and temperature profiles 586
9.3.6 Variants 589
9.3.7 Concluding remarks 590
9.4 Liquid-phase reactor with a catalyst in suspension 591
9.4.1 Fundamental data 591
9.4.2 Process flowsheet 592
9.4.3 Molar balances 593
9.4.4 Energy balances 595
9.4.5 Equipment design 597
9.4.6 Cost optimization 599
9.4.7 Final reactor design 602
9.4.8 Concluding remarks 603
9.5 Fixed-bed catalytic reactors with two fluid phases 603
9.5.1 Fundamental data 603
9.5.2 Process flow diagram 605
9.5.3 Material and heat balances 606
9.5.4 Examination of diffusion limitations 608
9.5.5 Calculating the transfer parameters 611
9.5.6 Volume of catalyst needed 616
9.5.7 Calculating the reactor dimensions 617
9.5.8 Calculations for other equipment 617
9.5.9 Concluding remarks 620
References 620

CHAPTER 10 • **MULTIFUNCTIONAL REACTORS AND FUTURE DEVELOPMENTS** 621

10.1 Classification of multifunctional reactors 621
10.2 Reaction with mass transfer 622
10.2.1 Reaction with adsorption 622
10.2.2 Reaction with distillation 622
10.2.3 Reaction with absorption 625
10.2.4 Reaction with extraction 625
10.2.5 Reaction with filtration 627
10.2.6 Reaction with fluid-reactive solid transfer 629
10.3 Reaction with energy transfer 630
10.3.1 Heat transfer through the wall 630
10.3.2 Heat transfer by direct contact between the phases 630
10.3.3 Radiative transfer 632
10.3.4 Transfer of electricity 634

10.4 Reaction with transfer of momentum 635
10.4.1 Transfer by friction or shear 635
10.4.2 Transfer by acceleration 637
10.4.3 Transfer by impulse or pressure 637
10.5 Future developments 638
References 640

GENERAL NOMENCLATURE 645
INDEX 651

Copyrighted Materials
Copyright © 2004 Editions Technip Retrieved from www.knovel.com

1 Definitions and Fundamental Concepts

1.1 DEFINITIONS OF STOICHIOMETRIC VALUES

1.1.1 Stoichiometric relations

For a chemical system participating in a reaction, the principle of mass conservation is implicit in the stoichiometric equations that define the chemical transformation. In general, we can write a stoichiometric relation of the form:

$$\sum \nu_i A_i = 0 \quad i = 1, S \tag{1.1}$$

where

A_i molecular compound of rank i
S total number of compounds participating effectively in the reaction
ν_i stoichiometric coefficient of compound A_i.

By convention, compounds that are consumed during a reaction described by a stoichiometric relation are assigned a negative stoichiometric coefficient and, similarly, compounds that are formed are assigned a positive stoichiometric coefficient:

$$\nu_i < 0 \text{ for } \textbf{reactants}, \quad \nu_i > 0 \text{ for } \textbf{products}$$

Equation (1.1) is in fact a balance that respects mass conservation, although it does not provide information about the feasibility of the reaction or the rate at which the reaction can occur. It should be immediately obvious that while the number of molecules can vary in an evolving system, the number of atoms is invariant.

If a system undergoing a chemical transformation can be described by a set of R simultaneous reactions, we have R equations:

$$\sum \nu_{i,j} A_i = 0 \quad \begin{matrix} i = 1, S \\ j = 1, R \end{matrix} \tag{1.2}$$

where $\nu_{i,j}$ is the stoichiometric coefficient of constituent A_i in reaction j.

With respect to the stoichiometric equations, note that inerts, catalysts, and solvents are generally not represented. Since stoichiometric relations are overall balances, compounds whose quantity remains unchanged during the course of the reaction can be excluded. This is true even when the transformation cannot proceed in their absence. Therefore, a stoichiometric description alone is inadequate for correctly defining a reaction system. As will be shown below, we also need to describe the system in terms of the "reaction scheme", which implies a thorough knowledge of the reaction paths.

The set of stoichiometric coefficients $\nu_{i,j}$ constitutes the stoichiometric coefficient matrix.

1.1.2 Extent of reaction, conversion, selectivity, and yield

1.1.2.1 Closed systems

When a single reaction:

$$\sum \nu_i A_i = 0 \tag{1.3}$$

takes place within a closed system we can characterize the **extent of reaction** by the variable ξ, defined as:

$$\xi = \frac{n_i - n_{i,0}}{\nu_i} \tag{1.4}$$

where

$n_{i,0}$ initial number of moles of compound A_i

n_i number of moles of compound A_i.

By definition, the value of ξ is independent of the compound A_i under consideration.

In a system in which R reactions occur simultaneously:

$$\sum \nu_{i,j} A_i = 0 \quad \begin{matrix} i = 1, S \\ j = 1, R \end{matrix} \tag{1.5}$$

we can define the extent of reaction ξ_j for each reaction and can write the molar balance for each compound A_i:

$$n_i = n_{i,0} + \sum \nu_{i,j} \xi_j \quad \begin{matrix} i = 1, S \\ j = 1, R \end{matrix} \tag{1.6}$$

If the values of ξ_j (one for each reaction) are known or can be calculated, it is easy to determine the different values of $(n_{i,0} - n_i)$ corresponding to the different compounds A_i.

Similarly, if we know the values of n_i and $n_{i,0}$, as well as the R stoichiometric equations involved, we can determine the corresponding values of ξ_j by resolving the system of R equations:

$$\sum \nu_{i,j} \xi_j = n_i - n_{i,0} \tag{1.7}$$

A solution exists only if the matrix of coefficients is not singular. In this case, the number of extents of reaction ξ_j we can determine is given by the rank of the non-singular matrix.

Introducing the concept of extent of reaction ξ_j into complex systems is of limited usefulness in interpreting experimental results. However, once we know the reaction scheme and have established the kinetic equations, reactor design can be greatly simplified through the use of the matrix of stoichiometric coefficients and the extent of the reactions.

We can define the **conversion of a reactant** A_i by the following equation:

$$X_i = \frac{n_{i,0} - n_i}{n_{i,0}} \tag{1.8}$$

This is a dimensionless number that is always positive. It is frequently expressed as a percent: $X_i(\%) = 100X_i$.

If we incorporate the definition of extent of reaction ξ_j, we have:

$$X_i = \frac{-\sum \nu_{i,j}\xi_j}{n_{i,0}} \tag{1.9}$$

Bear in mind that the concept of conversion applies only to reactants and that it includes all reactions in the system. For transformation products, we can define other values, known as **selectivity** and **yield**. In general, the molar selectivity of a compound A_i with respect to a compound $A_{i'}$ will be introduced as the following ratio:

$$S_{i,i'} = \frac{\left[\dfrac{\Delta n_i}{\Delta n_{i'}}\right]_{\text{real}}}{\left[\dfrac{\Delta n_i}{\Delta n_{i'}}\right]_{\text{ideal}}} \tag{1.10}$$

where

Δn_i number of moles of compound A_i at time t, less the number of moles of compound A_i after a period of time Δt

$\Delta n_{i'}$ number of moles of compound $A_{i'}$ at time t, less the number of moles of compound $A_{i'}$ after a period of time Δt

ideal according to an ideal reaction scheme.

The time t selected often refers to the initial state ($t = 0$); the value of Δt can vary within a broad range. If Δt is selected with a sufficiently low value, the selectivity defined is the instantaneous selectivity (s), whereas if Δt assumes non-negligible values, we obtain the integrated selectivity (S).

Unless otherwise indicated, the molar yield is generally defined as:

$$R_{i,i'} = X_{i'}S_{i,i'} \tag{1.11}$$

$A_{i'}$ being a reactant and A_i a product.

► ***Example:*** Consider a reaction between a C_3 olefin and a C_4 olefin that yields a C_7 olefin.

$$C_3^{=} + C_4^{=} \rightarrow C_7^{=}$$

The above ideal stoichiometric relation cannot completely describe the system because of the appearance of C_6, C_8, C_9, etc., olefins. Therefore, we need to recast the above as follows:

$$2C_3^= \rightarrow C_6^=$$
$$2C_4^= \rightarrow C_8^=$$
$$C_3^= + C_6^= \rightarrow C_9^= \quad \text{etc.}$$

In keeping with the notation introduced above, we have the following equivalencies:

$$C_3^= = A_1\ ; \quad C_4^= = A_2\ ; \quad C_6^= = A_3\ ; \quad C_7^= = A_4\ ; \quad C_8^= = A_5\ ; \quad C_9^= = A_6$$

We may also want to know the integrated selectivity of the transformation of $C_4^=(A_2)$ into $C_7^=(A_4)$: $S_{4,2}$:

$$\left[\frac{\Delta n_4}{\Delta n_2}\right]_{\text{real}} = \frac{n_{4,0} - n_4}{n_{2,0} - n_2}\ ; \quad \left[\frac{\Delta n_4}{\Delta n_2}\right]_{\text{ideal}} = -1$$

from which we determine that:

$$S_{4,2} = \frac{n_4 - n_{4,0}}{n_{2,0} - n_2}$$

The yield $C_7^=(A_4)$ with respect to $C_4^=(A_2)$ can be written: $R_{4,2} = X_2 S_{4,2}$. ◀

1.1.2.2 Open systems

What applies to closed systems can also be applied to open systems, providing we replace the number of moles n_i (mol) by the molar flow rate F_i (mol/s). For a reaction represented by $\sum \nu_i A_i = 0$, the extent of reaction ξ' is defined by:

$$\xi' = \frac{F_i - F_{i,0}}{\nu_i} \quad \text{and expressed in mol/s} \tag{1.12}$$

Similarly, for a set of reactions $\sum \nu_{i,j} A_i = 0$:

$$F_i = F_{i,0} + \sum \nu_{i,j} \xi'_j \tag{1.13}$$

The conversion X_i is written:

$$X_i = \frac{F_{i,0} - F_i}{F_{i,0}} = -\frac{\sum \nu_{i,j} \xi'_j}{F_{i,0}} \tag{1.14}$$

and the selectivity $S_{i,i'}$:

$$S_{i,i'} = \frac{\left[\dfrac{\Delta F_i}{\Delta F_{i'}}\right]_{\text{real}}}{\left[\dfrac{\Delta F_i}{\Delta F_{i'}}\right]_{\text{ideal}}} \tag{1.15}$$

The yield $R_{i,i'}$ is written as indicated above:

$$R_{i,i'} = X_{i'} S_{i,i'} \tag{1.16}$$

1.1.3 Mass selectivity and yield

It is often useful, and sometimes necessary, to express selectivity and yield in terms of mass ratio. This is especially true when one refers to groups of compounds in which it is difficult to identify molecules and when we are dealing with aggregates that are likely to be weighed. Hence the mass (or weight) selectivity of a group of products A_i with respect to a group of reactants $A_{i'}$ is defined by:

$$S^m_{i,i'} = -\frac{\Delta m_i}{\Delta m_{i'}} \tag{1.17}$$

where Δm is the change in mass.

Similarly, the mass yield can be written:

$$R^m_{i,i'} = X_{i'}\left[-\frac{\Delta m_i}{\Delta m_{i'}}\right] = X_{i'} S^m_{i,i'} \tag{1.18}$$

1.1.4 Concluding remarks

- Based on known or calculable values of ξ_j associated with reactions that actually follow the rules of stoichiometry, it is always possible to establish a correct material balance.
- Knowing the correct material balance, it is always possible to establish a list of independent stoichiometric equations with small, integer coefficients and determine the values of ξ_j. However, this procedure cannot be used to trace back the actual steps of the reaction path or calculate the actual molar extent ξ_j of those reactions.

1.2 CHEMICAL THERMODYNAMICS

When designing a chemical reactor, thermodynamics provides essential information for establishing the energy balance for the transformation as well as the limits imposed on the conversion.

1.2.1 Energy balance of the chemical transformation

The energy of a chemical system is the sum of different terms of varying importance:

- internal energy
- potential energy
- kinetic energy
- superficial energy, etc.

As the system evolves, it exchanges various forms of energy with the exterior:

- mechanical energy
- heat energy
- electrical energy
- radiant energy, etc.

Whenever the system changes from state 1 to state 2, the law of conservation of energy can be written:

energy content of state 2 = energy content of state 1
+ energy provided to the system from the exterior
− energy supplied by the system to the exterior

In practice it is more important to consider the change in energy in a system rather than its absolute value, which requires that we select a reference point.

The change in energy content can result from a modification of the intensive variables (pressure, temperature, partial molar enthalpy) or of the extensive variables (volume, entropy, number of moles).

In practice, when following the change in reaction systems, we have to distinguish two cases:

1. During the transformation, there is an exchange of heat at constant pressure or a change in enthalpy.
2. There is an exchange of heat at constant volume or a change in internal energy.

The first case is the most frequent and will be discussed here.

Change in enthalpy associated with a chemical reaction

In a reaction system described by a stoichiometric equation:

$$\sum \nu_i A_i = 0$$

we can express the change in enthalpy associated with this relation and corresponding to the complete transformation of reactants ($\nu_i < 0$) into products ($\nu_i > 0$) as being equal to:

$$(\Delta H_R)_T = \sum \nu_i \cdot \bar{h}_T(A_i) \tag{1.19}$$

In (1.19) $(\Delta H_R)_T$ is the change in enthalpy (expressed in joules) associated with the reaction $\sum \nu_i A_i = 0$ that takes place at temperature T.

In general the change in enthalpy is related to a mole of compound A_i. The heat of reaction then has a numerical value $\Delta H_R/|\nu_i|$ and is expressed in J/mol of A_i.

$\bar{h}_T(A_i)$ is the partial molar enthalpy of compound A_i at temperature T.

Partial molar enthalpy is calculated by classical procedures. For examples, readers may wish to consult standard works on thermodynamics such as the volume by J. Vidal [1997].

For complex systems defined by R stoichiometric equations, every equation j is characterized as above by an enthalpy of reaction:

$$\begin{aligned} &(\Delta H_j)_T = \sum \nu_{i,j} \cdot \bar{h}_T(A_i) && i = 1, S \\ &(\Delta H_j)_T \quad \text{is expressed in joules} && j = 1, R \end{aligned} \tag{1.20}$$

The R values of ΔH_j can be evaluated independently.

At times we may want to determine the change in enthalpy of a complex reaction system between state 1 and state 2. The change in enthalpy corresponding to reaction j, whose extent of reaction is ξ_j, is written:

$$\xi_j(\Delta H_j)_T = \xi_j \left[\sum \nu_{i,j} \cdot \bar{h}_T(\mathrm{A}_i) \right] \tag{1.21}$$

and the overall change in enthalpy in a system for respective values of ξ_j in the different reactions ($j = 1, R$) is:

$$(\Delta H)_T = \sum \left(\xi_j \Delta H_j\right)_T \tag{1.22}$$

It is important to recognize the difference between:

- the reaction enthalpy strictly speaking $(\Delta H_R)_T$ or $(\Delta H_j)_T$ at temperature T
- the enthalpy variation between two states of the chemical transformation, characterized by different extent of reaction values and frequently different temperatures.

In this last case in particular, we must take into account the presence of inert compounds. There is little ambiguity, however, if we are careful to correctly describe the thermodynamic path in going from state 1 to state 2 *via* a reference state carefully chosen so we can use the values from thermodynamic tables. These tables (see the references API, JANAF, TRC at the end of the chapter) should be used with caution and should be verified since it is not uncommon to find inconsistencies in them.

1.2.2 Chemical equilibria

1.2.2.1 Change in free enthalpy accompanying a chemical reaction

As indicated above, writing a stoichiometric equation tells us nothing about the feasibility of the reaction it is supposed to represent. To determine whether a reaction described by a stoichiometric equation is feasible, we must rely on thermodynamics and, in particular, on the standard free enthalpy data $G°$. The greater the decrease in free enthalpy accompanying a reaction, the more the reaction is favored. When only a single stoichiometric relation is involved, we can write:

$$\sum \nu_i \mathrm{A}_i = 0$$

We express the change in the standard free enthalpy of reaction at temperature T (standard free enthalpy of the products − standard free enthalpy of the reactants) by the expression:

$$\left(\Delta G_R^\circ\right)_T = \sum_{i=1}^{S} \left[\nu_i \Delta G_f^\circ(\mathrm{A}_i)\right]_T \quad \text{in joules for } \nu_i \text{ mol of } \mathrm{A}_i \tag{1.23}$$

$\left[\Delta G_f^\circ(\mathrm{A}_i)\right]_T$ being the change in the standard free enthalpy of formation of compound A_i at temperature T. To estimate these values, readers can refer to standard works on thermodynamics.

1.2.2.2 Equilibrium constant

It is relatively easy to determine the variation in standard free energy corresponding to a single reaction and determine the equilibrium constant K_a from:

$$\left(\Delta G_R^\circ\right)_T = -RT \ln(K_a) \tag{1.24}$$

K_a is expressed in terms of activities, every compound A_i being represented in the law of mass action by its activity at equilibrium $a_{i,\text{eq}}$:

$$K_a = \prod \left(a_{i,\text{eq}}\right)^{\nu_i} \tag{1.25}$$

In the kinetic expressions we introduce below, we will make use of the equilibrium constant expressed in terms of concentrations, partial pressures, or molar fractions. It is appropriate, therefore, to change K_a into K_c, K_p, K_x, depending on the circumstances.

Moreover, thermodynamics frequently provides knowledge of the equilibrium constant in the gas phase. However, when the reaction takes place in the condensed phase, it is often necessary to know the equilibrium constant in the condensed phase. In such cases we must make use of other thermodynamic data pertaining to the liquid-vapor equilibria of the different compounds A_i when making the transition from $K_{\text{vapor phase}}$ to $K_{\text{condensed phase}}$, unless we have direct access to thermodynamic values for the liquid phase.

1.2.2.3 Maximum extent of reaction of a chemical transformation

If we allow a chemical system to progress toward equilibrium and if this progression follows a path represented by the stoichiometric relation $\sum \nu_i A_i = 0$, the extent of reaction at equilibrium, ξ_{eq}, can be easily calculated from one of the equilibrium constants K defined above.

In the case of complex systems defined by R stoichiometric relations, $\sum \nu_{i,j} A_i = 0$, a change in free enthalpy can be associated with each reaction j:

$$\left(\Delta G_j^\circ\right)_T = \sum \nu_{i,j} \left[\Delta G_f^\circ(A_i)\right]_T \tag{1.26}$$

and therefore an equilibrium constant K_j.

If we want to determine the equilibrium state of the system as a whole, we must solve a system that simultaneously comprises:

- S linear balance equations of the following form:

$$n_{i,\text{eq}} = n_{i,0} + \sum \nu_{i,j} \xi_{j,\text{eq}} \quad i = 1, S \text{ and } j = 1, R \tag{1.27}$$

- R non-linear equations of the following form:

$$K_{x,j} = \prod \left(x_{i,\text{eq}}\right)^{\nu_{i,j}} \quad i = 1, S \text{ and } j = 1, R \tag{1.28}$$

where $x_{i,\text{eq}} = n_{i,\text{eq}}/n_{T,\text{eq}}$ and $n_{T,\text{eq}} = \sum n_{i,\text{eq}} + n_{\text{inerts}}$.

Because the solution of this system of equations is often complex, it is generally easier to use a method based on the minimization of free energy.

1.2.2.4 Effect of temperature on the equilibrium constant

We can use thermodynamics to calculate changes in K_a as a function of temperature:

$$\frac{\mathrm{d}\left(\ln K_a\right)}{\mathrm{d}\left(\frac{1}{T}\right)} = \frac{-\left(\Delta H_R^\circ\right)_T}{R} \tag{1.29}$$

$\left(\Delta H_R^\circ\right)_T$ being the change in standard enthalpy associated with the reaction at temperature T.

The graphic representation of $\ln(K_a)$ as a function of $1/T$ (abscissa) is a curve similar to a straight line, whose slope has the following value:

$$\frac{-\Delta \bar{H}_R^\circ}{R}$$

where $-\Delta \bar{H}_R^\circ$ is the average change in the enthalpy of reaction within the range of temperatures considered (in joules per ν_i moles of A_i, R being equal to 8.31 J/mol · K).

1.3 CHEMICAL KINETICS

Chemical kinetics can be used to define the extent of reactions as a function of the residence time of reactants in the reactor. The introduction of residence time is essential for determining the reaction volume needed for a chemical transformation to proceed to a given degree of advancement.

These rate laws constitute chemical kinetics, here considered to be a set of equations expressed as a function of observable and measurable parameters. These laws are used when designing a chemical reactor. In practice this means that we can make direct use of the rate laws, frequently qualified as formal kinetics, even if the actual mechanism has not been defined in all its details.

This does not imply any lack of interest in a detailed knowledge of phenomena but enables us to better identify the responsibilities of the researcher, who is focused on the laboratory, and those of the reactor designer, who is responsible for overall engineering and development.

However—and we will return to this subject when we discuss the various forms of the rate laws—it is important that we are at least familiar with the principal characteristics of the reaction, which are described below.

• Reaction phases and their location

In a reaction environment involving several phases, we frequently find that a chemical transformation takes place within a phase, at the interface between two phases, or within a phase but in the vicinity of the interface. Once the location of the reaction has been identified, we are in a position to increase the reaction space, whether this is a three-dimensional space (reactions developing within a single phase) or a two-dimensional space (surface reactions or reactions occurring within a phase but in the immediate proximity of an interface).

It should be obvious that prior knowledge of reaction location is crucial, especially when we have to scale-up a reactor on the basis of laboratory data. This is important because the distribution of phases and the ratio of surfaces to volumes can differ between a small-scale laboratory reactor and an industrial reactor. Ignorance of this difference has been the cause of a number of problems in reactor design.

• **Mode of activation**

There are several ways to initiate a chemical transformation, the most important of which are increasing the temperature, introducing catalysts and initiators, and using outside energy sources (UV radiation, electric arc, microwaves). These activation mechanisms make use of different processes, either separately or in combination:

- increasing the internal energy of the molecules until they reach the reaction threshold (supply of chemical, electrical, or radiation energy)
- decreasing the energy barrier of the reaction (the role of catalysts)
- seeding the process with foreign compounds that act by driving the reaction (the role of initiators).

• **Active intermediate forms**

The modes of activation mentioned above generate temporary compounds: ions, radicals, active molecules, complexes, etc. These are often highly reactive and rarely directly observable, but they play an essential role in consolidating the bonds formed during the transition from reactants to products.

1.3.1 Definition of rate of reaction

To simplify our description, we will first examine the case of a single reaction occurring within a closed vessel. Let us assume that we introduce $n_{i,0}$ mol of each of the S compounds A_i that react with one another. The reaction can be described stoichiometrically by $\sum \nu_i A_i = 0$. After a period of time t, we analyze the mixture, which enables us to calculate the extent of reaction by means of the following expression:

$$\xi = \frac{n_i - n_{i,0}}{\nu_i} \tag{1.30}$$

If we repeat the above, stopping the reaction at time $t + \Delta t$, we observe an extent of reaction $\xi + d\xi$, corresponding to a number of moles of A_i equal to $n_i + \Delta n_i$.

We can then write: $\Delta n_i = \nu_i \, d\xi$, or in its differential form:

$$\left(\frac{dn_i}{dt}\right)_t = \nu_i \left(\frac{d\xi}{dt}\right)_t \tag{1.31}$$

where

$\left(\frac{dn_i}{dt}\right)_t$ is the rate of appearance (or disappearance) of compound A_i as a function of time in the closed, batch system under consideration, and

$\left(\frac{d\xi}{dt}\right)_t$ is a measurement of the extensive rate of reaction for the entire volume of the reactor vessel.

More often, we relate the rate of change in the number of molecules to the unit volume of the reaction phase, obtaining:

$$\left(\frac{1}{V}\frac{\mathrm{d}n_i}{\mathrm{d}t}\right)_t = \nu_i\left(\frac{1}{V}\frac{\mathrm{d}\xi}{\mathrm{d}t}\right)_t = \nu_i r_t \tag{1.32}$$

where r_t is the rate of reaction per unit volume of reaction phase (r_t is sometimes referred to as the intensive rate, or intrinsic rate of reaction).

We can then write, omitting the subscript t for simplicity:

$$\frac{\mathrm{d}n_i}{\mathrm{d}t} = \nu_i r V \tag{1.33}$$

Note that the volume V occupied by all the molecules forming the homogeneous reaction medium (reactants, products, and inerts) can vary during the course of the reaction and in some cases must be taken into account.

If we then define the molar concentration $C_i = n_i/V$, we have:

$$\frac{1}{V}\frac{\mathrm{d}n_i}{\mathrm{d}t} = \frac{\mathrm{d}C_i}{\mathrm{d}t} + C_i\frac{\mathrm{d}(\ln V)}{\mathrm{d}t} \tag{1.34}$$

which can be simplified to:

$$\frac{1}{V}\frac{\mathrm{d}n_i}{\mathrm{d}t} = \frac{\mathrm{d}C_i}{\mathrm{d}t} \tag{1.35}$$

if the reaction volume remains constant.

In a more complex system, where R simultaneous reactions take place, each characterized by a rate of reaction r_j, we can write:

$$\frac{\mathrm{d}n_i}{\mathrm{d}t} = \sum \nu_{i,j}\left(r_j V\right) \tag{1.36}$$

and, if the reaction takes place at constant volume:

$$\frac{\mathrm{d}C_i}{\mathrm{d}t} = \sum \nu_{i,j}\left(r_j\right) \tag{1.37}$$

We can, therefore, describe the change in a reaction system if we have access to the various expressions of r_j, which, as we show below, incorporate the concentrations of the different species and the temperature of the system.

1.3.2 Ways of expressing the rate of reaction r_j

The rate r_j can assume different forms of expression. Yet in general, r_j is a more or less complex function of concentration C_i and temperature. The most common forms of expression r_j for homogeneous systems are given in Table 1.1.

The exponent (α_i, β_i) associated with concentration is called the partial order with respect to compound A_i. This coefficient should not be confused with the stoichiometric coefficient unless an elementary step of a reaction mechanism is involved.

Table 1.1 Different expressions of reaction kinetics.

Type of reaction	Forms of the rate of reaction	Comments
Irreversible or far from equilibrium	$r = k\prod_{i=1}^{S}(C_i)^{\alpha_i}$	Concentrations, C_i, can be expressed as partial pressures or molar fractions
With a reverse reaction	$r = k\prod_{i=1}^{S}(C_i)^{\alpha_i} - k'\prod_{i=1}^{S}(C_i)^{\beta_i}$	
Reversible	$r = k\left[\prod_{i=1}^{S}(C_i)^{\alpha_i} - \frac{1}{K_e}\prod_{i=1}^{S}(C_i)^{\beta_i}\right]$	$\beta_i = \alpha_i + \nu_i$

k and k' are rate constants.

K_e is an equilibrium constant.

The experimental values of the coefficients α_i, β_i are generally close to 1 or 2. If not, we can assume that either the precision of our results is not good or—and this is more common—that the written expression does not refer to a single reaction but a composite set of several interrelated reactions.

It should be pointed out that determining values for α_i, β_i that are equal to or close to 1 or 2, does not demonstrate the existence of an elementary step in the process.

In general writing the expression with both terms must respect the requirements for thermodynamic equilibrium. This can be expressed as follows: If equilibrium has been reached, the rate of reaction in the forward direction will balance the rate of reaction in the reverse direction, so that the net reaction rate will be zero ($r = 0$).

However, we frequently find kinetic expressions that do not respect the indicated thermodynamic constraints. This is of little importance as long as the system is far from equilibrium. In particular, it is common to write the expression without the term for the reverse reaction.

1.3.3 Influence of temperature

The rate constants k and k', whose units are dependent on the orders of reaction, vary with temperature as a first approximation according to the Arrhenius law:

$$k = k_0 \exp\left(\frac{-E}{RT}\right) \tag{1.38}$$

where

- E activation energy of the reaction (J/mol)
- R ideal gas constant (= 8.314 J/mol · K or 2 cal/mol · K)
- T temperature (K)
- k_0 frequency factor (same dimensions as k).

If the reaction is reversible, we can write:

$$\frac{k}{k'} = K_e \quad \text{according to which: } \Delta H_R = E - E' \tag{1.39}$$

where E' is the activation energy of the reverse reaction.

A few words about the above equality are in order: It is generally considered that, within a temperature interval corresponding to the range of operating conditions for a given reaction, the activation energies do not depend on temperature. This is only an approximation. The same holds true for ΔH_R. In reality this reflects the average change in the enthalpy of reaction within the range of temperatures under consideration.

It is often preferable to use the Arrhenius relation in a different form, choosing a reference temperature T_0:

$$k_T = k_{T_0} \exp\left[\frac{E}{R}\left(\frac{1}{T_0} - \frac{1}{T}\right)\right] \tag{1.40}$$

For example, T_0 can be the desired reaction temperature, or the temperature at the reactor inlet, or at the start of the reaction, or even the average temperature of the cooling fluid.

1.3.4 Formal kinetic expressions involving fractional or high orders

It often happens that a kinetic analysis results in apparent orders that are either fractional or high. In the vast majority of cases, this indicates that the kinetic relation established does not apply to an elementary reaction but rather to a group of elementary reactions involving transient forms that cannot be analyzed. This is true, in particular, of reactions involving free radicals such as those for the thermal cracking of hydrocarbons.

1.3.5 Other forms of kinetic expression associated with catalytic processes

Some chemical transformations can only take place in the presence of catalysts, substances introduced in small quantities with respect to the reactants and capable of forming complexes with them. These complexes lead to the formation of the reaction product with the liberation of the catalyst, which can then be used to continue the reaction cycle anew.

For example, assume a reaction A + B $\rightarrow$ 2C, which takes place in the presence of a catalyst K and is characterized by a rate of reaction r. Let us further assume that the reaction path can be described by the following j elementary steps, each characterized by its own rate of reaction r_j:

$$\mathrm{A} + \mathrm{K} \rightarrow \mathrm{AK} \qquad r_1 = k_1[\mathrm{A}][\mathrm{K}] - k_1'[\mathrm{AK}] \tag{1.41}$$

$$\mathrm{AK} + \mathrm{B} \rightarrow \mathrm{AKB} \qquad r_2 = k_2[\mathrm{AK}][\mathrm{B}] \tag{1.42}$$

$$\mathrm{AKB} \rightarrow 2\mathrm{C} + \mathrm{K} \qquad r_3 = k_3[\mathrm{AKB}] \tag{1.43}$$

If substance K acts as a catalyst, that is in small quantities with respect to the reactants, the concentrations of intermediate complexes will remain low compared to the concentrations of

reactants and products. This indicates that the rate of disappearance of A will be equal to the rate of disappearance of B and to half the rate of appearance of C.

We can then write:

$$r = r_1 = r_2 = \frac{2r_3}{2}$$

and, therefore:

$$r = k_1[\mathrm{A}][\mathrm{K}] - k_1'[\mathrm{AK}] = k_2[\mathrm{AK}][\mathrm{B}] = k_3[\mathrm{AKB}] \tag{1.44}$$

When determining the balance for the catalytic substance K, we find that the initial amount of catalyst (or rather, the concentration corresponding to it) $[\mathrm{K}]_0$ exists at any time either in a free form [K] or a combined form [AK] and [AKB] according to the following equation:

$$[\mathrm{K}]_0 = [\mathrm{K}] + [\mathrm{AK}] + [\mathrm{AKB}] \tag{1.45}$$

Based on the above expressions, we can deduce the following rate equation:

$$r = r_1 = r_2 = r_3 = \frac{k_1 k_2[\mathrm{K}]_0[\mathrm{A}][\mathrm{B}]}{k_1' + k_2[\mathrm{B}] + k_1[\mathrm{A}]\left(1 + \dfrac{k_2[\mathrm{B}]}{k_3}\right)} \tag{1.46}$$

This expression makes use of measurable analytical concentrations $[\mathrm{K}]_0$, [A], [B], and the rate constants for each step. Often, the expression can be simplified by using relative values for various terms as shown in the following example:

1. If $k_3 \ll k_2[\mathrm{B}]$, k_1' and $k_1[\mathrm{A}]$ we can write:

$$r = k_3[\mathrm{K}]_0 \tag{1.47}$$

   The rate of reaction becomes zero order with respect to [A] and [B] and first order with respect to the catalyst. The rate constant that appears is that of the third reaction; this is often expressed by referring to the third step as the limiting step in the process. In reality $r = r_1 = r_2 = r_3$ with [K] and [AK] near 0 and all the catalytic substance practically concentrated in [AKB].

2. $k_2[\mathrm{B}] \ll k_3$ and $k_1', k_1' \ll k_1[\mathrm{A}]$:

$$r = k_2[\mathrm{B}][\mathrm{K}]_0 \tag{1.48}$$

   Step 2 is said to be controlling. In fact $r = r_1 = r_2 = r_3$, but practically speaking all the catalyst exists in the form [AK].

In conclusion, we can say that whenever a chemical transformation involves the intervention of a catalytically active substance, introduced in small quantities with respect to the other compounds and capable of forming complexes with one of the compound A_i, it is very common to find kinetic expressions that include a denominator. This situation is often found, for example, in cases of homogeneous catalysis by coordination complexes, enzymatic catalysis, and heterogeneous catalysis.

1.3.6 Heterogeneous catalytic reactions

Chemical reactions catalyzed by a solid catalyst constitute a highly important family, justifying a separate analysis. Taylor introduced the concept of "active sites" on the catalyst surface. Langmuir and Hinshelwood developed a theory—the Langmuir-Hinshelwood model—that enables us to account for the great majority of experimental results obtained in heterogeneous catalysis. It is fitting that we provide an overview of this theory, which leads to the various forms of rate expression found in practice.

We assume that the population of active sites is distributed uniformly on the surface of the catalyst, this being understood as the exterior surface of the catalyst particles as well as the surface of the pores. Thus there is a proportional relationship between the number of active sites and the surface area of the catalyst. Moreover, we consider that a proportional relationship exists between the surface area and mass of the catalyst or volume of the bed, that is, the pores are uniformly distributed throughout the mass of the catalyst. The reaction rate can then be considered roughly proportional to the surface area, the mass, or the volume of the catalyst.

We can now examine the different steps in a catalytic reaction according to the Langmuir-Hinshelwood theory:

- approach of the reactants from the homogeneous fluid phase to the catalytic surface. This approach is governed by the laws of mass transfer and, with respect to penetration of the pores, by the laws of internal diffusion (see Chapter 6)
- chemisorption of the reactants on active sites
- surface reactions between adsorbed molecules
- desorption of the products
- movement of the products toward the homogeneous fluid phase.

The influence of external diffusion (diffusion from the homogeneous phase toward the outer surface of the particles) can be the dominant factor in the case of a very rapid surface reaction or when flow conditions are not favorable. For low-activity catalysts consisting of small particles with large and interconnected pores, internal diffusion is often negligible.

Each step proceeds at its own rate. Taken together, they determine the overall rate of reaction. Here, we consider only the steps that take place on the surface of the catalyst.

The development of quantitative rate expressions is based on combining various laws:

- activated adsorption
- surface reactions
- mass and heat transfer
- diffusion in porous media.

The following reaction:

$$A_1 + A_2 \rightleftarrows A_3 + A_4 \tag{1.49}$$

can be broken down into different steps.

- **Adsorption of A_1**

$$A_1 + \sigma \rightleftarrows A_1\sigma \qquad \text{(step 1)}$$

where

σ	free active site
$A_{1\sigma}$	active site occupied by A_1
k_1	adsorption rate constant of $A_1 = k_{1,0}\exp(-E_a/RT)$
k'_1	desorption rate constant of $A_1 = k'_{1,0}\exp(-E_d/RT)$
$k_1/k'_1 = b_1$	adsorption coefficient of A_1:

$$b_1 = b_{1,0}\exp\left[(-E_a + E_d)/RT\right] = b_{1,0}\exp\left[\lambda/RT\right]$$

λ	heat of adsorption of A_1.

- **Adsorption of A_2**

$$A_2 + \sigma \rightleftarrows A_2\sigma \qquad \text{(step 2)}$$

- **Reaction between adsorbed molecules**

$$A_1\sigma + A_2\sigma \rightleftarrows A_3\sigma + A_4\sigma \qquad \text{(step 3)}$$

where

k	reaction rate constant in the forward direction
k'	reaction rate constant in the reverse direction
$k/k' = K'$	equilibrium constant in the adsorbed phase.

- **Desorption of A_3**

$$A_3\sigma \rightleftarrows A_3 + \sigma \qquad \text{(step 4)}$$

- **Desorption of A_4**

$$A_4\sigma \rightleftarrows A_4 + \sigma \qquad \text{(step 5)}$$

Table 1.2 shows the different kinetic expressions for various cases, where one step can be considered rate controlling for the process.

Other classic reactions, such as parallel reactions, competing reactions, and consecutive reactions can be treated similarly, without any special complications.

1.3.7 Groups of compounds

The number of molecular compounds simultaneously involved in a chemical transformation can sometimes be very high. This is especially the case with petroleum cuts when they are subject to refining operations (catalytic reforming, catalytic cracking, hydrocracking, etc.).

To correctly describe kinetic phenomena, it is necessary to consolidate both reactants and products, a process known as **lumping**. Lumping changes the kinetic expressions substantially, even when we attempt to retain these expressions in a form similar to that shown above. Consequently, the reaction order changes considerably as well as the activation energy, although to a somewhat lesser extent.

Table 1.2 Expressions of reaction rate in heterogeneous catalysis according to the Langmuir-Hinshelwood theory. Case examined: $A_1 + A_2 \rightleftarrows A_3 + A_4$.

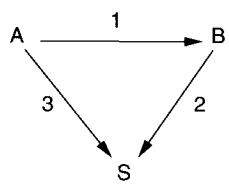
Rate-controlling step	Rate expression
Surface reaction	$r = kb_1b_2\dfrac{(C_1C_2 - C_3C_4/K)}{(1 + b_1C_1 + b_2C_2 + b_3C_3 + b_4C_4)^2}$
Adsorption of A_1	$r = k_1\dfrac{(C_1 - C_3C_4/C_2K)}{(1 + b_1C_3C_4/C_2K + b_2C_2 + b_3C_3 + b_4C_4)}$
Desorption of A_3	$r = k_3K\dfrac{(C_1C_2/C_4 - C_3/K)}{(1 + Kb_3C_1C_2/C_4 + b_1C_1 + b_2C_2 + b_4C_4)}$
Surface reaction (with adsorption and dissociation of A_1)	$r = kb_1b_2\dfrac{(C_1C_2 - C_3C_4/K)}{\left(1 + \sqrt{b_1C_1} + b_2C_2 + b_3C_3 + b_4C_4\right)^3}$
Reaction between adsorbed A_1 and non-adsorbed A_2 (A_3 and A_4 adsorbed)	$r = kb_1\dfrac{(C_1C_2 - C_3C_4/K)}{(1 + b_1C_1 + b_3C_3 + b_4C_4)^2}$

$$K = \text{equilibrium constant in the homogeneous phase} = \frac{C_{3,\text{eq}}C_{4,\text{eq}}}{C_{1,\text{eq}}C_{2,\text{eq}}} \tag{1.50}$$

1.3.7.1 Apparent overall order

The earliest example of lumping is probably that of gas oil cracking, which was investigated extensively by Weekman *et al.* [1976] and which we summarize below.

The simplified model used involves three groups:



A represents all the reactants in the gas oil, S all the byproducts (coke, light hydrocarbons), and B all the compounds forming the gasoline group.

For the reactions A → B and A → S, an apparent order of 2 has been observed for lump A. For the reaction B → S, the observed order is close to unity. The model was subsequently improved by taking into account 10 groups [Jacob, 1976].

These apparent orders are interpreted as follows: The gas oil consists of a number of molecular compounds with variable reactivities; the most reactive compounds crack first, with an order of 1. The preferential disappearance of the most reactive compounds slows the reaction down in a way that is more pronounced than would normally be expected of a first-order reaction. If viewed in terms of reaction order, the slowdown results in an apparent

order greater than 1. On the contrary, with respect to the gasoline group, we find that, vis-à-vis the cracking reaction, the spectrum of reactivities of the different compounds is much smaller. Consequently, the observed order remains close to unity.

A number of overall kinetic investigations have been made about the hydrodesulfurization of petroleum fractions, a phenomenon that lends itself well to the present topic. It has been known for quite some time in fact that sulfur compounds subjected to catalytic treatment with hydrogen react by liberating hydrogen sulfide with a reaction order of 1. Yet, when a petroleum fraction is subjected to the same catalytic treatment, the overall order observed with respect to the sulfur compounds falls between 1 and 2, and more specifically between 1.5 and 1.7, for gas oil fractions [Leprince 1998]. A number of theoretical studies have been conducted to mathematically describe the relation between a given distribution of the reactivities of molecular compounds undergoing transformation and the apparent kinetic expression that should be observed. Astarita and Sandler [1991] have edited a volume that includes developments on this subject.

As an example, we examine the case involving parallel reactions with chemical compounds that have a similar reactive chemical function (double or triple bond, sulfur or nitrogen atom, etc.) but different reactivities. We assume that the compounds react according to first-order kinetics and that their initial concentration in the feedstock being processed ($C_{i,0}$) is given as a function of the reactivity defined by the kinetic constant (k_i). The distribution of reactivities can be discrete or continuous.

If the distribution is discrete, it is given by a series of related values of $C_{i,0}$ and k_i ($i = 1, \ldots, n$). The overall chemical transformation can be represented by means of the following expressions:

$$C_0 = \sum_{i=1}^{n} C_{i,0} \tag{1.51}$$

$$C(t) = \sum_{i=1}^{n} C_i(t) = \sum_{i=1}^{n} C_{i,0} \exp(-k_i t) \tag{1.52}$$

The overall conversion, which is sometimes the only experimental measurement possible, is generally obtained from:

$$X = \frac{C_0 - C(t)}{C_0}$$

If the distribution of reactivities is a continuous distribution $k(x)$, we can then write:

$$C_0 = \int_0^{\infty} C_0(x)\, \mathrm{d}x \tag{1.53}$$

$$C(t) = \int_0^{\infty} C_0(x) \exp\left[-k(x)t\right] \mathrm{d}x \tag{1.54}$$

Since k is generally a monotonic function of x, we can use the value of k itself to determine reactivities. The above expression then becomes:

$$C(t) = \int_0^\infty C_0(k) \exp[-kt]\, dk \tag{1.55}$$

We can define the following normalized values:

$$U(t) = \frac{C(t)}{C_0}; \quad u(k,t) = \frac{C(t,k)}{C_0}$$

$$\bar{k} = \int_0^\infty k \cdot u(k,0)\, dk; \quad \tau = \bar{k}t \tag{1.56}$$

By using tables of integrals for Laplace transforms, it is easy to show that a distribution $u(k,0)$ of the following form:

$$g(k) = \frac{\alpha^\alpha k^{\alpha-1} \exp(-\alpha k)}{\Gamma(\alpha)} \tag{1.57}$$

leads to an expression of $U(t)$ whose form is identical to one corresponding to a reaction of order $n = (1+\alpha)/\alpha$, that is:

$$U(t) = \left(1 + \frac{\bar{k}t}{\alpha}\right)^\alpha \tag{1.58}$$

This provides us with a simple means for associating the apparent order n with the distribution of reactivities, $u(k,0) = g(k)$, characterized by the parameter α. As an example, Fig. 1.1 is a graphical representation of the distribution, $g(k)$, for several values of α.

A detailed kinetic analysis should be based on preliminary selection of compounds or groups of compounds as a function of their reactivities. If this is impossible, we are liable to observe fractional orders having no real physical significance.

We can, however, attempt to determine the influence a supposed distribution of reactivities will have on the overall kinetics of the system. For example, let us assume that the reactivities of the reacting compounds are uniformly distributed along an interval between k_1 and k_2. If the total concentration of reactive compounds is C_0, the distribution of reactivities can then be written:

$$g(k) = \frac{C_0}{k_2 - k_1} \quad \text{for } k_1 < k < k_2 \tag{1.59}$$

Therefore, we can easily calculate $U(t)$:

$$U(t) = \int_{k_1}^{k_2} g(k) \exp(-kt)\, dk = \frac{C_0}{(k_2 - k_1)t} \left[\exp(-k_1 t) - \exp(-k_2 t)\right] \tag{1.60}$$

We can perform the same calculation for any distribution of reactivities, either analytically if the form of the distribution is simple as it is above, or numerically in all other cases. In many cases a given distribution of reactivities corresponds to an apparent order between 1 and 2.

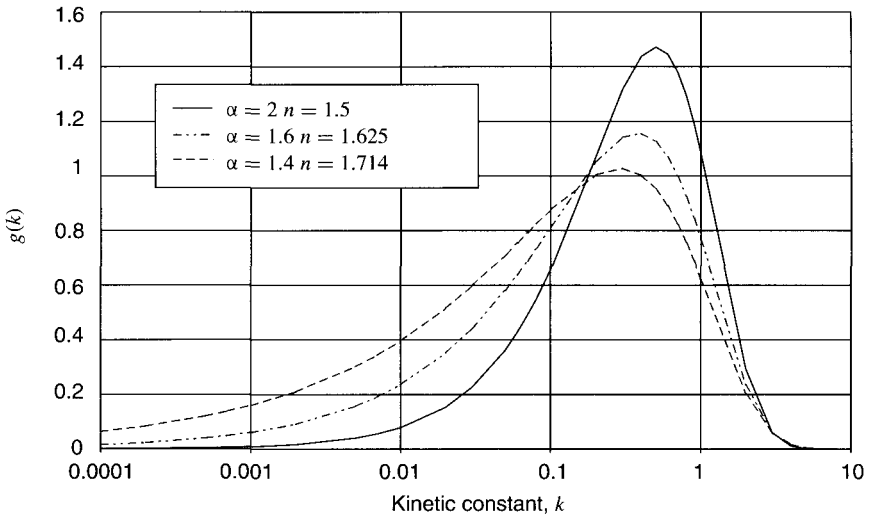


Figure 1.1 Examples of reactivity distribution curves corresponding to various values of α and apparent order n.

► ***Example:*** We use the following values for the variables shown above:

$$C_0 = 1$$

$$k_1 = 1 \quad \text{and} \quad k_2 = Rk_1 \quad \text{where } R \text{ varies between 1 and 10 000}$$

For an overall conversion of 99.5%, the curves in Fig. 1.2 show a correspondence between the apparent order N_{ap}, the associated rate constant K_{ap}, and the value of R. The conversion rates calculated according to the two formulations are also compared in Fig. 1.2 for the case where $R = 20$. ◄

1.3.7.2 Lumping procedure

Numerous theoretical studies have been made of the procedure of lumping into families, using groups with comparable reactivities. Ozawa [1973] has, for example, provided successful methods for lumping even when we do not have all the kinetic information for a given system.

Alongside these theoretical approaches, generally illustrated by numerical examples, we find experimental approaches that have been converted into reaction models, where the authors have lumped compounds in ways that seem to them both logical (on the reaction level) and feasible (on the analytic level) with respect to both reactants and products.

As an example, we cite the case of catalytic reforming, which has been the subject of numerous studies. Lumping is performed by hydrocarbon family (paraffins, naphthenes, aromatics) and by number of carbon atoms. Li and Rabitz [1993] have proposed a model comprising 26 reactions.

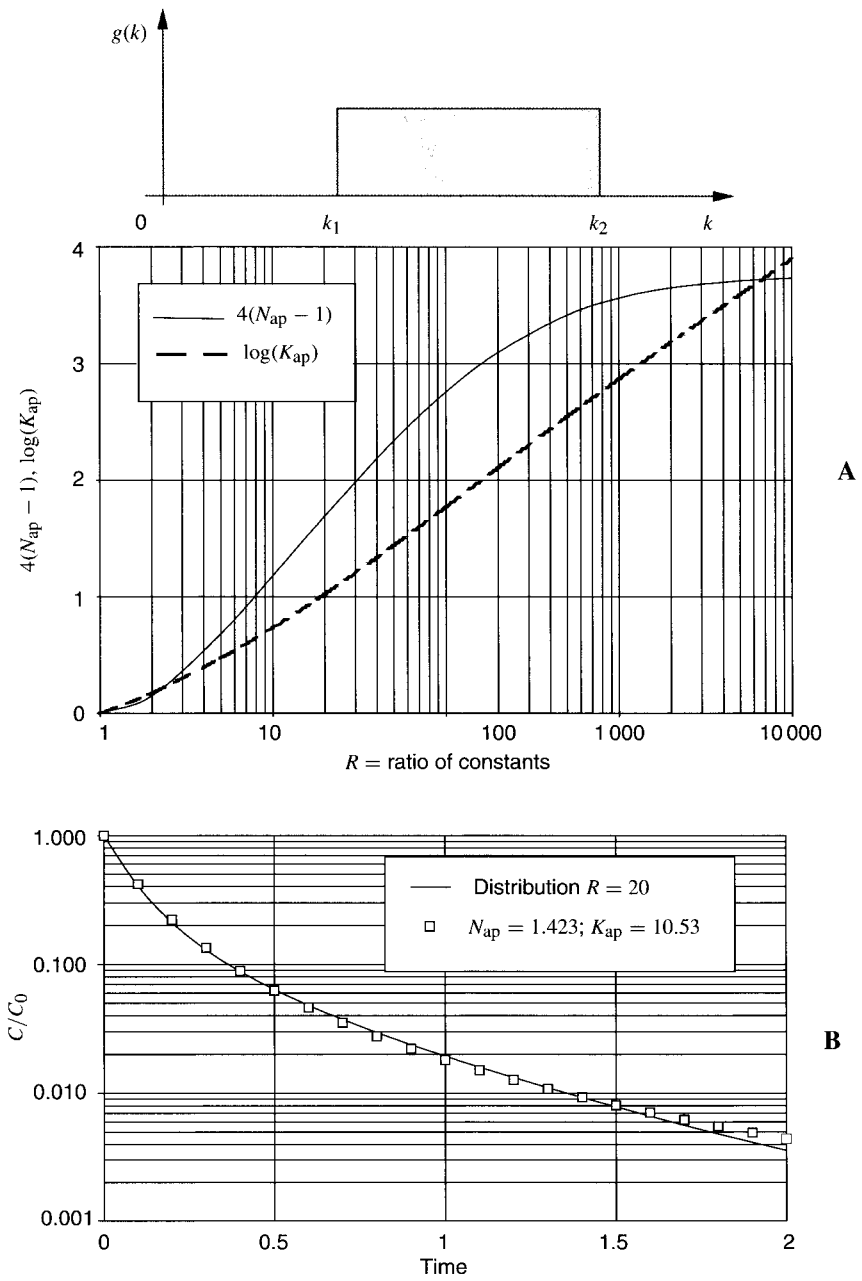


Figure 1.2 Case of uniform distribution of reactivities between two limit values: **A.** Relationship between apparent order (N_{ap}) and the apparent constant (K_{ap}) *vs.* the ratio R of limit kinetic constants. **B.** Curve showing the comparison of the two models: apparent order and distribution of constants.

These models probably do not provide sufficient mathematical reliability with respect to a strict separation of parameters. They provide no fundamental explanation but simply describe, as faithfully and as concisely as possible, the phenomena observed in the domain under consideration. None of the authors claims that his model can be used outside the limits of the observed domain.

1.3.7.3 "Overall" activation energy

It should be noted that when lumping compounds into families, even if considerable attention is paid to how they are grouped, the activation energy also assumes an apparent overall value that can vary with the extent and temperature of the reaction. This has been clearly demonstrated by Golikeri and Luss [1972], who have shown, based on a purely numerical example, that a conventional representation of $\ln t$ (where t is the time needed to obtain a given conversion) as a function of $1/T$, results in concave or convex curves, depending on the extent of reaction.

The ability to describe the effect of temperature on the transformation of a group of compounds, for example, by means of an Arrhenius expression involving overall activation energy, depends on the range of activation energies taken individually. If all the individual energies are equal, a form of the Arrhenius expression may be appropriate. In all other cases, however, the overall activation energy depends both on the degree of conversion and the temperature, according to a generally complex law, even for relatively simple cases.

1.3.7.4 Conclusions and suggestions

- Any lumping is legitimate providing it allows us to construct a reliable model within a sufficiently large domain.
- It is important to determine the most suitable form of lumping for the specific situation (by molecular mass, chemical family, change in a physico-chemical property, etc).
- The ideal breakdown is the one that, for a minimal number of groups, leads to a model containing the minimum number of parameters, after suitable adjustments have been made. We note in passing that a model containing more parameters does not necessarily lead to better results.
- Don't be overly surprised if the model that is used contains singularities (variable order as a function of the initial composition, activation energy that varies with conversion, etc.).
- Studying the kinetic behavior of model molecules chosen as representative of a complex feedstock can provide valuable additional information.
- An imperfect or improperly used model can lead to unsatisfactory reactor design. On the other hand, even a simple model is often sufficient for an initial approach to the problem of reactor design, at least during the pilot stage. The model can then be refined and adjusted to include observations made with the pilot plant.
- Research efforts should match actual problems. There is no point in completing an exhaustive kinetics study if it turns out that the transformation process is governed by mass transfer laws.

1.3.8 Kinetics based on elementary steps

We indicated above that the choice of families used to lump compounds depends largely on the ability to divide them analytically. With the development of analytical techniques, it has become possible in certain cases (catalytic reforming, for example) to identify all the chemical compounds involved. We might then assume that there are as many reactions as there are compounds taking part in the transformation. However, this is rarely possible in practice given the amount of experimental work that would be needed to identify all the kinetic equations.

Another approach, which takes into account all the possible reactions, has been proposed by Froment *et al.* [1991]. The kinetics of each reaction are here expressed in terms of elementary steps, which are limited in number.

This approach has been applied to vapor-phase reactions, like those that occur during steam cracking, which can be described on the basis of elementary reactions involving free radicals. The approach has been extended to catalytic reactions, even though the mechanisms on the surface of the catalyst are more complex and depend on the catalyst itself.

1.3.9 Conclusion

Knowledge of formal kinetic expressions for the transformation of reactants separately involved in a given process—for example, involving the same catalyst and under the same conditions of temperature and pressure—is generally not sufficient for constructing a complete reaction scheme in which all the reactants take part. This is possible only if all the limiting elementary steps of the process have been identified and if the numerical values of the constants for these key steps are known.

Although it is true that a formal kinetic expression can, in principle, enable us to design a chemical reactor, there are advantages in determining the implications of the basic mathematical expression. In this respect, it is worth noting that it is sometimes extremely difficult, even in the laboratory, to completely eliminate the influence of mass and heat transfer phenomena. Yet these phenomena may result in a substantial modification of the rate expression that completely masks the progress of the chemical reaction itself. A kinetics that is isolated from these contingencies is said to be true or intrinsic.

1.4 REACTOR TYPES

We refer to a **chemical reactor** as any device used to conduct a chemical reaction, that is, one where molecular compounds are transformed into other molecular compounds. However, we restrict the term to those cases where the chemical transformation is designed to produce one or more predetermined **chemical compounds** or to eliminate one or more compounds from a mixture. We exclude from our definition systems in which chemical reactions are used for other purposes, such as the production of energy.

The chemical reactor as we have defined it here constitutes the core of the chemical manufacturing units found in refineries and metallurgical plants as well as in bulk chemical and

allied plants. In these manufacturing plants, the reactor is generally surrounded by equipment, located upstream and downstream, used for the physical processing of raw materials and reaction products. We also find reactors in pollution control plants, where they are used to chemically purify various effluents.

In practice, the equipment where chemical transformations take place can assume a wide variety of shapes and sizes. They include furnaces, boilers, tanks, columns, drums, mixers, rotary kilns, blast furnaces, and even simple tubes. At first sight we might be tempted to consider any attempt at classifying chemical reactors to be futile and to feel that every piece of equipment found in practice is a special case.

However, all these devices perform a common function, namely to carry out a chemical transformation. Therefore, by referring to the principal characteristics of a chemical reaction, we should be able to determine a limited number of criteria that can be used to classify such devices. Any systematic analysis of the operation of these units depends upon first having classified them into a number of clearly defined types, with which existing industrial equipment can be identified.

1.4.1 Principal characteristics of a reactor

In Section 1.3 we introduced the different characteristics of a chemical transformation. From among them we will now select the characteristic that is most apparent on the macroscopic scale, namely the **number** and **nature of phases present**. This will serve as the basis for our classification.

1.4.1.1 Phases present

We distinguish among the following cases:

Single-phase systems

The reaction medium consists of a gas or liquid phase.

Multiphase or heterogeneous systems

- gas + liquid
- liquid + liquid
- gas + solid
- liquid + solid
- gas + liquid + solid, and, more generally speaking
- fluid + solid.

Here we should distinguish between cases where the solids involved serve as a **catalyst** and are not consumed during the reaction and those where the solids take part in the transformation, either as **reactants** or as **products**. In a number of cases, we can refer to both the gas phase and the liquid phase as the **fluid** phase, whether the system is single phase or multiphase.

1.4.1.2 Operating mode

A second criteria in our classification is determined by the practical requirements of the chemical process itself. Consequently, operating modes for reactors can be **batch** or **continuous**.

When working in batch mode (Fig. 1.3) reactants are loaded into a suitable reactor and the chemical transformation is allowed to take place as a function of time. We sometimes refer to these devices as **closed systems** because, while the reaction is taking place, there is no material flow entering or leaving the system. In contrast, continuous devices, known as **open systems**, are equipped with one or more inlets for introducing the reactants and one or more outlets through which the transformation products are evacuated.

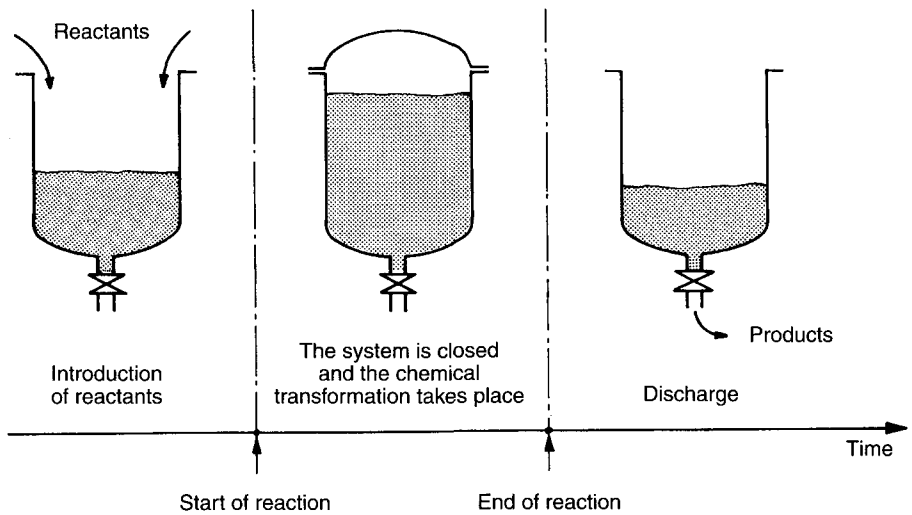


Figure 1.3 Batch operation. Illustration of the various steps.

In a variant of the batch system, some of the reactants are introduced throughout the operation and products are discharged at the end of the operation. This is known as **semi-continuous** operation (Fig. 1.4). There are also situations where reactants are introduced at the beginning of the operation, some reaction products being gradually eliminated during the course of the reaction.

In general we can characterize the two modes of operation defined above by the fact that the batch system operates under **non-steady state** conditions while the continuous system is generally designed to operate under **steady state conditions**.

In the case of multiphase systems, it may occur that one phase is confined within the reactor (operating in batch mode) while another phase feeds the reactor and is continuously eliminated. The process is then qualified as continuous or batch by referring to the phase containing the principal reactant. Thus, liquid-phase hydrogenation, in which the liquid containing the compounds to be hydrogenated remains in the reactor throughout the entire

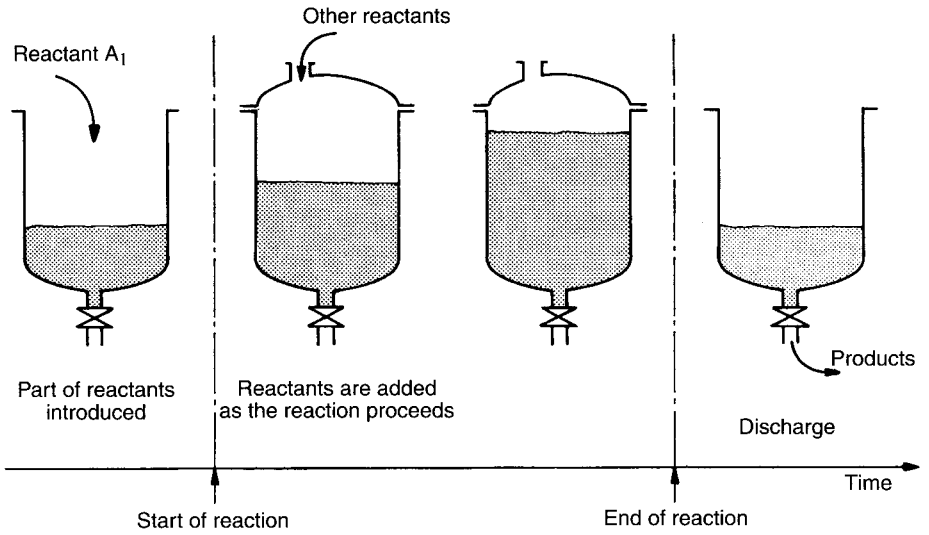


Figure 1.4 Semi-Continuous operation. Illustration of the various steps.

operation, while hydrogen is continuously introduced, is referred to as a batch operation (the hydrogenation of vegetable oils is an example). Similarly, a fixed-bed catalytic reactor will be classified as a continuous device although the catalyst remains confined in the reactor and can change over time.

Once we consider an operation to be continuous, the various phases within the reactor are assumed to flow from their point of introduction to their point of discharge. This internal flow can assume various forms, which obviously depend on the structure of the device. We can therefore define several well-characterized flow types with which the situations encountered in practice can be compared and sometimes identified. These typical flows, which can be considered as **ideal models**, are of two types (Fig. 1.5):

- **plug flow**, which occurs when a low-viscosity fluid is caused to flow at high speed within a tube
- flow through a **perfectly** mixed vessel.

The two flow models, which are very dissimilar at the structural level, have a significantly different impact on the process of chemical transformation within the device. This will become apparent if we consider the change in a chemical compound entering each of the two model reactors. In a **tubular** reactor the chemical compound progresses along with its environment throughout the length of the tube, undergoing gradual transformation. Between the reactor inlet and outlet, the concentration of the reactant appears to be continuously decreasing. For this reason these reactors are sometimes referred to as **concentration gradient reactors**.

In a perfectly mixed tank, however, the **concentrations** of the various chemical compounds are **uniform** throughout the reaction medium within the reactor. The reactant entering the reactor is immediately plunged into an environment (reaction medium) whose composition is

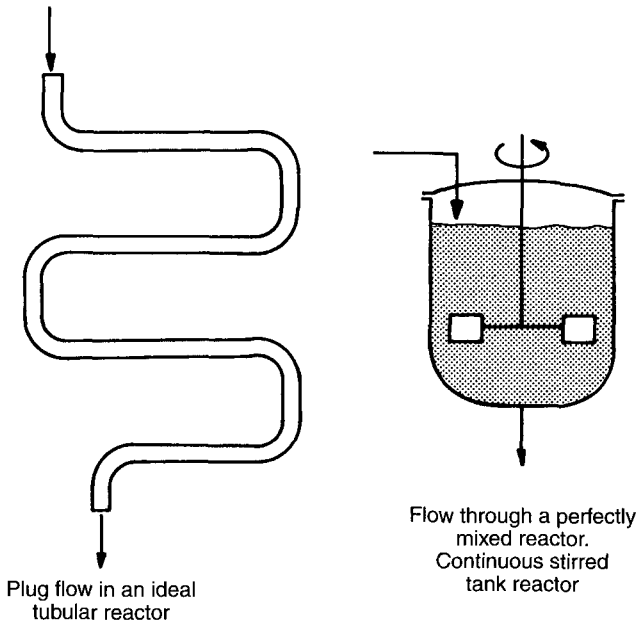


Figure 1.5 Continuous operation. The two ideal flow models.

identical to that of the reactor's outgoing stream. At the reactor inlet, there is a discontinuity of concentrations within the incoming stream.

An intermediate case between these two ideal models is that of the **multistage reactor**, consisting of a series of perfectly mixed zones. Instead of a sudden discontinuity of concentrations at the reactor inlet, we have a series of smaller discontinuities at the inlet of each of the perfectly mixed zones.

Using the model reactor types defined above, our classification now looks like this:

- batch (and semi-continuous)
- continuous
  - tubular
  - stirred tank
  - multistage.

A breakdown of the various reactor types in terms of change in concentration is illustrated in Fig. 1.6 for a single-phase system.

Of course, the devices found in practice will not have all the characteristics of the ideal models, but, to the extent that they are appreciably similar, their operation can be analyzed on the basis of the ideal model by introducing corrective terms if needed. As a first approximation, we can continue to speak of tubular reactors and continuous stirred tank reactors, following the ideal model retained.

As soon as one or more phases circulate within a reactor, we need to ensure adequate contact among them. In practice, contact between the phases allows for the transfer of

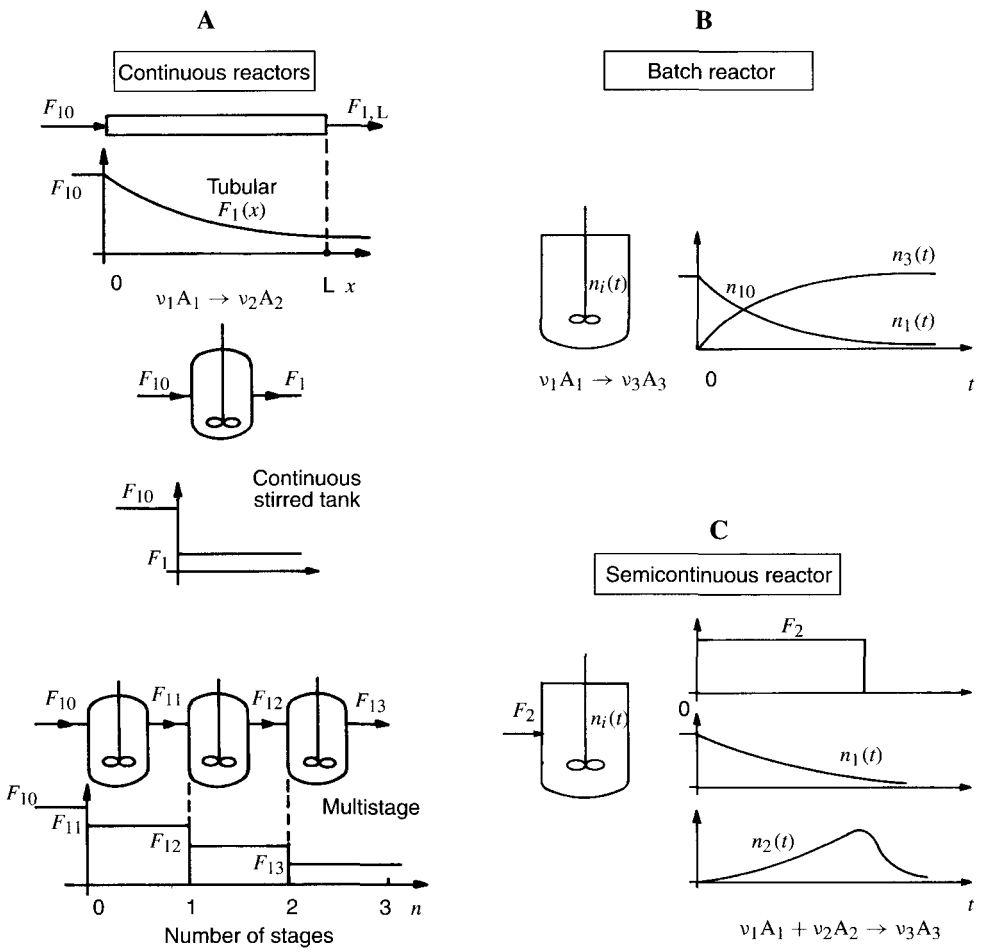


Figure 1.6 *Single-phase systems. The different reactor types are shown together with the changes in concentration.*

chemical compounds between phases, without which the reaction would not take place. The reactant or reactants need to reach the reaction phase and, similarly, some reaction products must often be eliminated from this same reaction phase. When we analyze the operation of such reactors, we encounter the same concepts that characterize the study of devices in which physical separations take place through mass transfer between phases, namely the conventional concepts of interfacial area between two phases and the coefficients of mass transfer associated with that interface.

1.4.1.3 Circulation of phases

As with separation devices, we can choose among the different flow patterns of phase circulation: **countercurrent**, **cocurrent**, and **crosscurrent**.

Because of the key role played by chemical transformation, countercurrent designs are not necessarily optimal, as is the case with many purely physical processes. It is for the same reason that phase **holdup**, especially that of the reaction phase, is such an important parameter when designing a multiphase reactor.

Lastly, it is important to recognize that in multiphase systems the phases may be characterized by different types of flow patterns. For example, we can conceive of a gas-liquid system in which the liquid phase is perfectly mixed while the gas phase would be characterized by plug flow (as in a fermenter).

1.4.1.4 Heat transfer

Another characteristic of the reaction, which often has a decisive influence on the structure of the reactor and its external appearance, is the thermal effect inevitably associated with any chemical transformation. Many industrial reactions have fairly high heats of reaction, whether the reactions are exothermic or endothermic. In these cases the reactor must be equipped with **heat exchange surfaces** capable of transferring the heat in the appropriate direction.

We frequently distinguish the following two cases:

- **isothermal** reactor
- **adiabatic** reactor.

The first case is realized if we use a continuous stirred tank reactor in the steady state regime, although this is an ideal limit case if the reactor is tubular. Here too, comparison of the real-world situation to an ideal tubular isothermal reactor sometimes provides an acceptable approximation.

The **adiabatic** reactor, often found in industry, is simply a particular case of the general situation where no heat transfer surface exists. The apparent differences indicated above are often dependent on the **location of the heat exchange surface**. In fact, heat exchange can take place:

- inside the reactor
- through the walls of the reactor
- outside the reactor.

If we also take into account the temperature at which the exchange occurs, the ensuing reactor designs can vary widely. For example, heat exchange can take place by radiation of a flame toward the reaction tube, by circulation of a heat transfer fluid inside an internal heat exchanger, or by circulation of the reaction medium in an external exchanger whose size may greatly exceed that of the reactor itself. Because of this, reactor designs can assume various forms, like furnaces, drums, or heat exchangers.

1.4.2 Classification of reactors

Using the criteria introduced above, it is now possible to classify the various reactor types found in practice (Table 1.3). The two principal characteristics we use for our classification are:

- the nature of the phases present
- the operating mode of the reactor.

Table 1.3 Classification of reactors together with typical examples found in refining and petrochemistry.

Phases present	**Tubular**	**Multistage**	**Continuous stirred tank**
Gas	Steam cracking		
Liquid	Visbreaking	Dimerization of olefins	
Gas + liquid	Clauspol process	Absorption in plate columns	
Liquid + liquid	HF alkylation	Sulfuric acid alkylation	
Fluid + catalyst	Steam reforming	Catalytic reforming	Catalytic cracking
Gas + liquid + catalyst	Hydrotreatment	Hydrotreatment	Hydrotreatment

In our detailed description of the various reactor types, we will point out additional differences. These differences are associated with the relative direction of phase flows or with mass and heat transfer phenomena. Nonetheless, for each of the classification criteria used, there are general concepts that are always applicable to a given row or column in the above table.

Table 1.3 also indicates some of the most common applications of the various reactor types, which provides an initial idea of the concrete nature of our classification.

Clearly, when faced with a specific piece of industrial equipment, we might hesitate before trying to position it somewhere in the above table. We have already pointed out situations where a reactor may be tubular for one phase and perfectly mixed for another. In spite of this, the dominant feature of the reactor will often be easy to determine by referring to the reaction phase or the phase containing the principal reactants and/or products.

There are, however, some reactors whose specific characteristics do not meet the criteria of our classification. Here, we would like specifically to mention those systems in which the reactions take place so rapidly that they are completed during the initial mixing phase of the reactants. This is the case for certain combustion processes in the gas phase. In the description of tubular systems, it was assumed that the reactants in a phase were mixed before entering the reactor. In contrast, in a continuous stirred tank reactor, the reactants are assumed to be mixed along with the entire reaction medium contained in the reactor. In the case of a very fast reaction, we would therefore tend to use a very compact unit, corresponding to an in-line mixer for the tubular version and a very small stirred tank for the perfectly mixed version. We see that in this specific instance, the two technologies tend to merge in a limiting case that should be considered separately.

1.4.3 General expression of mass and enthalpy balances

Here we will consider only single-phase systems. We assume an element of volume ΔV in the reaction phase, which is assumed to be uniform in composition and temperature. For each compound A_i contained in this volume ΔV, we can write a molar balance of the following

general form (see Fig. 1.7):

$$\frac{dn_i}{dt} = F_{i,e} - F_{i,s} + \mathcal{R}_i \Delta V \quad (i = 1, S) \tag{1.61}$$

where

$\frac{dn_i}{dt}$ is the rate of accumulation of A_i in the volume ΔV

$F_{i,e}$ and $F_{i,s}$ are respectively the molar flow rates entering and exiting the system by convection and/or diffusion

$\mathcal{R}_i$ is the rate of generation of compound A_i per chemical reaction, expressed per unit of volume ($\mathcal{R}_i = \sum \nu_{i,j} r_j$; for an inert, $\mathcal{R}_i = 0$).

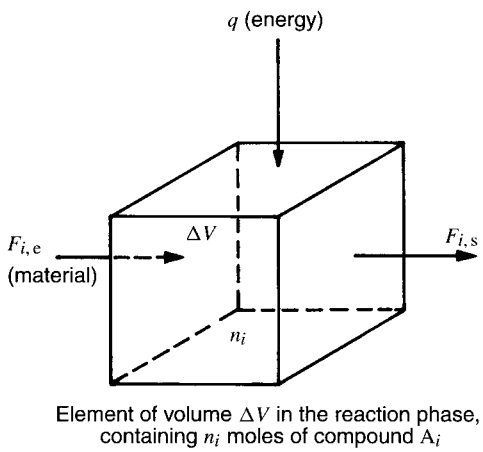


Figure 1.7 Diagram illustrating elementary mass and enthalpy balances considered.

For enthalpy, we can write an overall balance as follows:

$$\sum \frac{d(n_i \bar{h}_i)}{dt} = \sum F_{i,e} \bar{h}_{i,e} - \sum F_{i,s} \bar{h}_{i,s} + q \Delta V \tag{1.62}$$

In the above expression, the left term is the rate of accumulation of enthalpy in volume ΔV, $\sum F_{i,e} \bar{h}_{i,e}$ and $\sum F_{i,s} \bar{h}_{i,s}$ are respectively the incoming and outgoing enthalpy flows, q is the rate of transfer of enthalpy from outside of volume ΔV, which is considered positive if it is supplied to the system.

Comment: Note that there is no reason to introduce a term for the heat of reaction in Eq. (1.62) since it is implicitly accounted for by the partial molar enthalpies.

1.4.4 Application of the general balance expressions to the various types of ideal reactor

1.4.4.1 Single-phase batch reactor

For this type of reactor, we assume that temperature and composition are identical at any point of the reaction phase. Equations (1.61) and (1.62) written for an element ΔV, can then be applied to the entire volume V of the reaction phase. Moreover, the terms corresponding to the incoming and outgoing flows disappear since material is neither added nor subtracted (Fig. 1.8A).

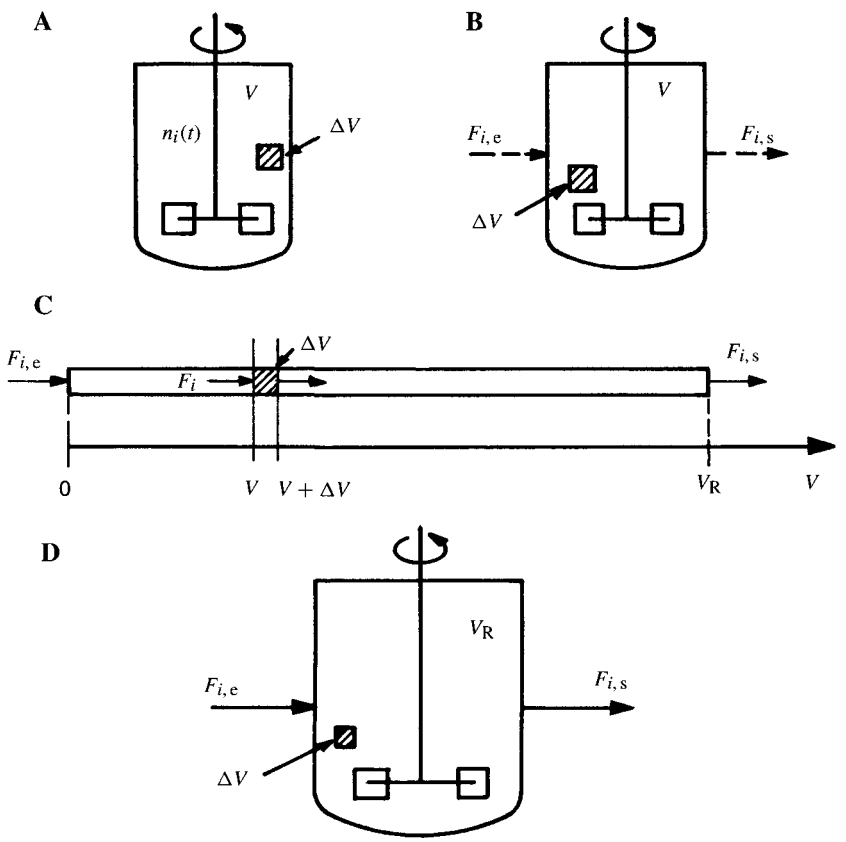


Figure 1.8 Representation of volume elements used as the basis for balances in the various idealized reactors.

As a result, the balance equations become:

- for the mass balances:

$$\frac{dn_i}{dt} = \mathcal{R}_i V = V\left(\sum \nu_{i,j} r_j\right) \quad i = 1, S \tag{1.63}$$

- for the enthalpy balance:

$$\frac{\mathrm{d}\left(\sum n_i \bar{h}_i\right)}{\mathrm{d}t} = qV \tag{1.64}$$

Equation (1.64) can also be written by introducing the extent of reaction ξ_j and the molar heat capacity $C_{\mathrm{P}i}$:

$$\sum\left(\Delta H_j \frac{\mathrm{d}\xi_j}{\mathrm{d}t}\right) + \left(\sum n_i C_{\mathrm{P}i}\right)\frac{\mathrm{d}T}{\mathrm{d}t} = qV \tag{1.65}$$

The first term of the enthalpy balance is associated with the heat produced or consumed by the reaction, while the second term reflects the accumulation of heat energy in the reaction phase.

We can integrate these equations by taking into account the boundary conditions that determine the initial values at $t = 0$, namely, the number of moles contained in the reactor ($n_{i,0}$) and the temperature T_0.

1.4.4.2 Semi-continuous single-phase reactor

In this case the assumption of the uniformity of the reaction phase is still valid. However, the terms corresponding to the incoming and outgoing flow are only partially conserved and are generally a function of time (Fig. 1.8B). As described above, some compounds are added as the reaction progresses and the balance equations are written as follows:

$$\frac{\mathrm{d}n_i}{\mathrm{d}t} = F_{i,\mathrm{e}} + \mathcal{R}_i V \quad i = 1, S \tag{1.66}$$

$$\frac{\mathrm{d}\left(\sum n_i \bar{h}_i\right)}{\mathrm{d}t} = \sum F_{i,\mathrm{e}} \bar{h}_{i,\mathrm{e}} + qV \tag{1.67}$$

The terms $F_{i,\mathrm{e}}$ are nonzero only for certain compounds A_i, precisely those that are added during the operation.

In those cases where compounds are removed during the operation, the equations are similarly written:

$$\frac{\mathrm{d}n_i}{\mathrm{d}t} = -F_{i,\mathrm{s}} + \mathcal{R}_i V \quad i = 1, S \tag{1.68}$$

$$\frac{\mathrm{d}\left(\sum n_i \bar{h}_i\right)}{\mathrm{d}t} = -\sum F_{i,\mathrm{s}} \bar{h}_{i,\mathrm{s}} + qV \tag{1.69}$$

The values $\bar{h}_{i,\mathrm{e}}$ and $\bar{h}_{i,\mathrm{s}}$ are taken respectively at the temperatures of injection and removal and for the physical state under consideration (solid, liquid, or gas). We refer the reader to Eq. (1.64) for an explanation of the left-hand side of Eqs. (1.67) and (1.69).

1.4.4.3 Plug-flow tubular reactor

By definition the flow in this type of reactor is such that a fluid element can pass through it without mixing with any of the fluid elements that precede it or follow it. Additionally, all the

fluid elements are assumed to have the same linear velocity, regardless of their radial position. This means that, throughout the reactor, the composition of the reaction phase varies from one point to the next, while concentrations are radially uniform. This is also true for temperature. In this case, the element ΔV that appears in the equations is infinitesimal and equal to dV (Fig. 1.8C), resulting in two equations with partial derivatives. Equation (1.61) can then be written:

$$\frac{\partial C_i}{\partial t} = -\frac{\partial F_i}{\partial V} + \mathcal{R}_i \quad i = 1, S \tag{1.70}$$

Similarly, Eq. (1.62) becomes:

$$\frac{\partial \left(\sum C_i \bar{h}_i\right)}{\partial t} = -\frac{\partial \left(\sum F_i \bar{h}_i\right)}{\partial V} + q \tag{1.71}$$

Note that the variable q is related to the volume unit of the tube and can be a function of the variable V.

These equations, combined with the initial conditions for $t = 0$ and $V = 0$, can be used to describe the behavior of an ideal tubular reactor under non-steady-state conditions. To determine the steady state conditions, consider the derivatives with respect to time as zero. In this case, Eqs. (1.70) and (1.71) become:

$$\frac{dF_i}{dV} = \mathcal{R}_i = \sum \nu_{i,j} \frac{d\xi'_j}{dV} \quad i = 1, S \tag{1.72}$$

$$\frac{d\left(\sum F_i \bar{h}_i\right)}{dV} = q \tag{1.73}$$

The reactor volume needed to process an incoming flow $F_{i,e}$ and an outgoing flow $F_{i,s}$, can be calculated by means of the following integral:

$$V_R = \int_{F_{i,e}}^{F_{i,s}} \frac{dF_i}{\mathcal{R}_i} \tag{1.74}$$

This expression can only be used unmodified in the case of an isothermal reactor. In all other situations, we need to simultaneously integrate the two differential Eqs. (1.72) and (1.73). As above, Eq. (1.73) can be developed to yield:

$$\sum \left[\Delta H_j \frac{d\xi'_j}{dV}\right] + \left(\sum F_i C_{Pi}\right) \frac{dT}{dV} = q \tag{1.75}$$

1.4.4.4 Perfectly stirred continuous reactor

In this case, the general expressions (1.70) and (1.71), written for an element of volume ΔV, can be extended to the entire volume V occupied by the reaction phase (Fig. 1.8D). When a steady-state condition has been established, the transient terms disappear and we obtain:

$$F_{i,e} - F_{i,s} + \mathcal{R}_i V = 0 \quad i = 1, S \tag{1.76}$$

$$\sum F_{i,e} \bar{h}_{i,e} - \sum F_{i,s} \bar{h}_{i,s} + qV = 0 \tag{1.77}$$

Once we know the reactor's operating temperature, we can calculate its volume from (1.76):

$$V_R = \frac{F_{i,e} - F_{i,s}}{-\mathcal{R}_i} \tag{1.78}$$

In this case the values $F_{i,e}$ and $\bar{h}_{i,e}$ represent the boundary conditions of the problem since they describe the reactor feed in terms of flow rate, composition and temperature

1.5 RESIDENCE TIME DISTRIBUTION

In the preceding paragraphs, we used ideal concepts corresponding to two types of simple flow to establish mass and enthalpy balances, namely:

- plug flow
- flow with perfect mixing.

However, it is important that we be able to better characterize these flows and have practical means at our disposal for recognizing them. Moreover, the behavior of a real reactor deviates more or less from the ideal model and it would be useful if we were able to quantify this deviation. Within this context, the concept of residence time distribution assumes increased interest.

When a fluid flows through a vessel of volume V, the various molecules of the fluid remain inside the volume V for times t_S that are directly dependent on the type of flow involved. These residence times, t_S, can deviate significantly from the mean residence time $\theta = V/Q$. This results in a distribution of residence times that depends on the flow type. In practice, the performance of the system as a reactor is often linked to the residence time distribution.

1.5.1 Typical distribution functions of fluid flow

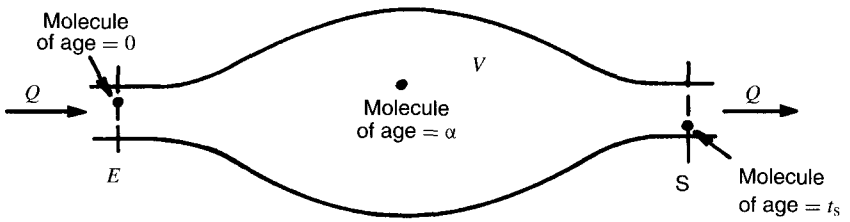
Consider a volume V of any form, within which circulates a fluid at flow rate Q, between an inlet cross-section I and an outlet cross-section O (Fig. 1.9). We can define various distribution functions that describe the characteristics of the circulating molecules, which are considered to be identifiable individuals.

If, by analogy, we were to refer to a population of identifiable living beings (humans, for example), we could choose age as a characteristic of the individual. We can also distinguish two age characteristics.

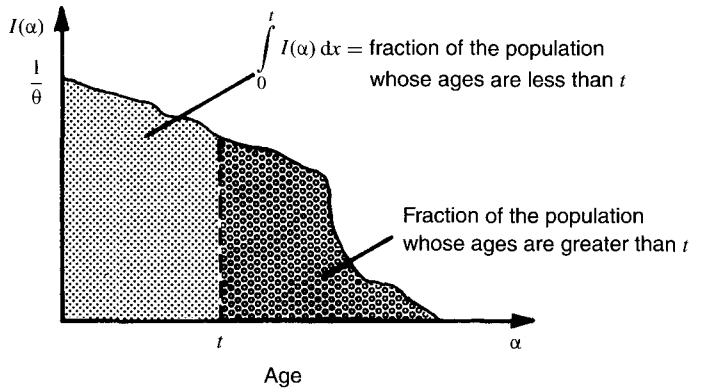
- The age α of an individual at the moment the population is observed (age pyramid).
- The age t_S at which this same individual will die and, therefore, leave the population of living beings.

For the population as a whole, we can then consider two age distribution functions that globally describe this population:

- the distribution function of the ages of the living $I(x)$
- the distribution function of the ages at which individuals die $E(t_S)$.



A



B

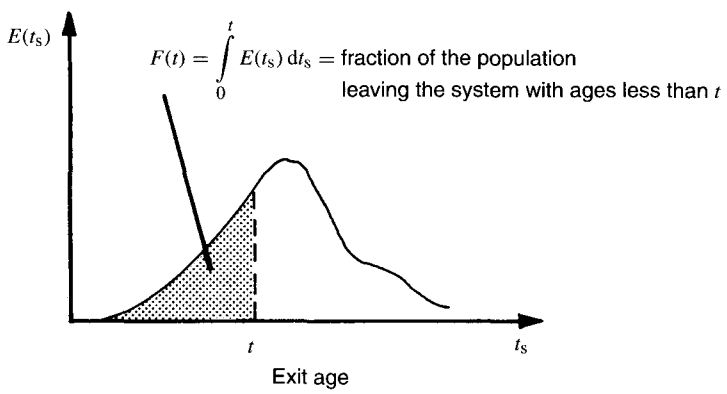


Figure 1.9 Diagram of an open system with continuous fluid flow and its age distribution functions: **A.** Example of the distribution function of ages within the system. **B.** Example of the distribution function for residence time, or the ages of molecules when they leave the system.

By analogy, we can define the following characteristics for a fluid that flows through a volume V:

- The **internal age** α of a molecule within volume V is the time that has passed since that molecule crossed the inlet section I.
- The **residence time**, t_S, of the molecule in volume V is the time that has elapsed during passage of the molecule between inlet I and outlet O. This time is simply the age of the molecule when it leaves outlet O.

Because of the large number of molecules and their different flow behaviors, there are distribution functions for these characteristics (Fig. 1.9A and 1.9B). Thus:

- $I(\alpha)$ is the distribution function for internal age
- $E(t_S)$ is the distribution function for residence time.

$I(\alpha)\,d\alpha$, therefore, represents the fraction of fluid within volume V whose internal age is comprised between α and $\alpha + d\alpha$. Similarly, $E(t_S)\,dt_S$ represents, for the outgoing stream at section O, the fraction of fluid whose residence time or age is comprised between t_S and $t_S + dt_S$.

Moreover, any distribution function can be represented in normalized form, so that:

$$\int_0^\infty I(\alpha)\,d\alpha = 1 \tag{1.79}$$

$$\int_0^\infty E(t_S)\,dt_S = 1 \tag{1.80}$$

We can also replace the variables t (real time), α (age in the reactor), and t_S (age at outlet) with a dimensionless time variable τ defined on the basis of the mean residence time $\theta = V/Q$:

$$\tau = \frac{t}{\theta} \quad \tau_i = \frac{\alpha}{\theta} \quad \tau_S = \frac{t_S}{\theta}$$

Which gives us:

$$\mathbf{I}(\tau_i) = \theta I(\alpha) \tag{1.81}$$

$$\mathbf{E}(\tau_S) = \theta E(t_S) \tag{1.82}$$

The function $I(\alpha)$ is always decreasing and tends toward 0 for high values of α. Moreover, when $\alpha = 0$, this function has a characteristic value of $1/\theta$, the inverse of the mean residence time θ. In the notation adopted: $\mathbf{I}(0) = 1$.

Note that these distribution functions for age and residence time, presented for the case of fluid flow through a volume V, can also be applied to any system in which there is a flow of particles or even objects through an enclosure equipped with an inlet and an outlet. These same concepts are, for example, used in hydrology and medicine. In chemical engineering, we also apply them to cases of solid granular flow, as with a catalyst.

We can define the overall distribution as follows:

$$F(t) = \int_0^t E(t_S)\,dt_S = \mathbf{F}(\tau) \tag{1.83}$$

This function represents, for the outgoing stream, the fraction of fluid whose residence time is less than t or whose dimensionless residence time is less than τ.

There are various relationships among these distribution functions, which are summarized below.

For $t = t_S = \alpha$:

$$\frac{1}{\theta}E(t_S) = -\frac{dI(\alpha)}{d\alpha} \tag{1.84}$$

$$\frac{1}{\theta}F(t) + I(\alpha) = I(0) = \frac{1}{\theta} \tag{1.85}$$

In the dimensionless notation we have adopted, for $\tau = \tau_S = \tau_i$:

$$\mathbf{F}(\tau) + \mathbf{I}(\tau_i) = \mathbf{I}(0) = 1 \tag{1.86}$$

$$\mathbf{E}(\tau_S) = -\frac{d\mathbf{I}(\tau_i)}{d\tau_i}$$

As with any distribution function, we can define **moments**. Frequently, we use:

- the first-order moment with respect to the origin or mean
- the second-order moment with respect to the mean or variance σ^2.

Based on the residence time distribution (RTD), we then have:

$$\bar{t}_S = \int_0^\infty t_S \cdot E(t_S)\, dt_S \tag{1.87}$$

$$\sigma^2 = \int_0^\infty (t_S - \bar{t}_S)^2 \cdot E(t_S)\, dt_S \tag{1.88}$$

Here the mean $\bar{t}_S$ should in principle be equal to the mean residence time $\theta = V/Q$. However, anomalies associated with specific flow characteristics sometimes lead to different values. The various moments of a distribution are often used to compare distributions with one another.

1.5.2 Experimental determination of distribution functions

When we defined the distribution functions, we assumed that the molecules were identifiable individuals. This can only be realized in part by using what is known as a **tracer**, which allows us to mark the molecules or at least some of the molecules. Miscible substances, those that do not modify the hydrodynamic characteristics of the fluid, can also be used. These substances can be detected by using a specific physical property such as radioactivity, electrical or thermal conductivity, absorption spectra, magnetic properties, and so on.

With a tracer, the experimental method consists in applying a **signal** at the inlet to the system without disturbing the flow, and observing the **response** at the outlet of the system. The signals injected into the system can, in theory, assume any form whatsoever. However,

most often we use specific signals whose form is such that the response can be easily exploited, typically **step** or **pulse** signals.

1.5.2.1 Response to a step

During a single step injection, the concentration of tracer at the inlet, E, changes suddenly from a value C_1 to a value C_2 at a time that is treated as the origin ($t = 0$). Most frequently, one of the two values, C_1 or C_2, is taken to be equal to 0.

From a mathematical standpoint, the step signal corresponds to the **unit step**, $H(t)$, which is characterized as follows:

$$H(t) = 0 \quad \text{for } t < 0$$
$$H(t) = 1 \quad \text{for } t > 0$$

At the outlet, S, of the system, we measure the concentration $C(t)$ of tracer from $t = 0$. If we assume $C_1 = 0$, we can define a dimensionless outlet function:

$$\mathrm{C}' = \frac{C(t)}{C_2} = 1 - \theta I(t) \tag{1.89}$$

or

$$\mathbf{C}' = \frac{C(\tau)}{C_2} = 1 - \mathbf{I}(\tau) \tag{1.90}$$

Using the relations described above, we obtain:

$$\mathbf{C}' = \mathbf{F}(\tau) \tag{1.91}$$

This signifies that the response to a step signal, or the indicial response, directly yields the cumulative distribution function $\mathbf{F}(\tau)$, from which we can deduce the other distribution functions **I** and **E**. Adoption of the dimensionless form $\mathbf{C}'$ for the response is equivalent to the use of a **unit-step** signal.

1.5.2.2 Response to a pulse

In this case we inject a known quantity of tracer (for example, n moles) into the inlet of the system for a very brief period of time. From the mathematical standpoint, the **pulse** signal corresponds to the Dirac function $\delta(t)$, which is the derivative of the unit step function.

Once again we measure the concentration $C(t)$ of the tracer in the outgoing stream. For a time t that begins at the moment of injection, the quantity of tracer leaving the reactor can be expressed in terms of the residence time distribution function:

$$QC(t)\,\mathrm{d}t = nE(t_\mathrm{S})\,\mathrm{d}t_\mathrm{S} \tag{1.92}$$

In this case t and t_S are identical.

If we take $C_0 = n/V$ as the reference concentration for the tracer, corresponding to the concentration of the tracer if it were uniformly distributed in volume V, we obtain the distribution function E from the experimental response:

$$E(t_\mathrm{S}) = \frac{1}{\theta}\frac{C(t)}{C_0} \tag{1.93}$$

If we denote $\mathbf{C} = C(\tau)/C_0$, the experimental response in dimensionless form, we obtain:

$$\mathbf{C} = \mathbf{E}(\tau) \tag{1.94}$$

The relation between the input signals is also found in the output signals:

$$\frac{\mathrm{d}\mathbf{F}(\tau)}{\mathrm{d}\tau} = \mathbf{E}(\tau)$$

1.5.3 Distribution functions for various types of flow

We can now relate the two types of ideal flow considered above to the distribution functions we have defined.

1.5.3.1 Plug-type flow

In this case, all the molecules move at the same velocity and the system acts as a simple delay line. All the incoming signals are transmitted unchanged and arrive at the outlet after time $t = \theta$ or $\tau = 1$. The distribution of residence times therefore reduces to the mean residence time $t_S = \theta$. The various distribution functions or signal responses can be represented as shown in Fig. 1.10.

1.5.3.2 Flow with perfect mixing

Consider the case of an incoming signal having the shape of a unit step. The molar balance of the tracer can be written if we take into account the fact that the volume V is perfectly mixed. In this case, we have:

$$QC_2 = Q \cdot C(t) + V\frac{\mathrm{d}C(t)}{\mathrm{d}t} \tag{1.95}$$

This equation is valid for $t \geqslant 0$, when the boundary condition is:

$$C(t) = 0 \quad \text{for } t = 0$$

By integrating, we obtain:

$$\mathrm{C}' = \frac{C(t)}{C_2} = 1 - \exp\left(-\frac{t}{\theta}\right) \tag{1.96}$$

From this we can directly derive the distribution function $\mathbf{F}(\tau)$:

$$\mathbf{F}(\tau) = 1 - \exp(-\tau) \tag{1.97}$$

The residence time distribution, $\mathbf{E}(\tau)$, is deduced from $\mathbf{F}(\tau)$ by simple derivation:

$$\mathbf{C}(\tau) = \mathbf{E}(\tau) = \frac{\mathrm{d}\mathbf{F}(\tau)}{\mathrm{d}\tau} = \exp(-\tau) \tag{1.98}$$

These functions are also represented in Fig. 1.10.

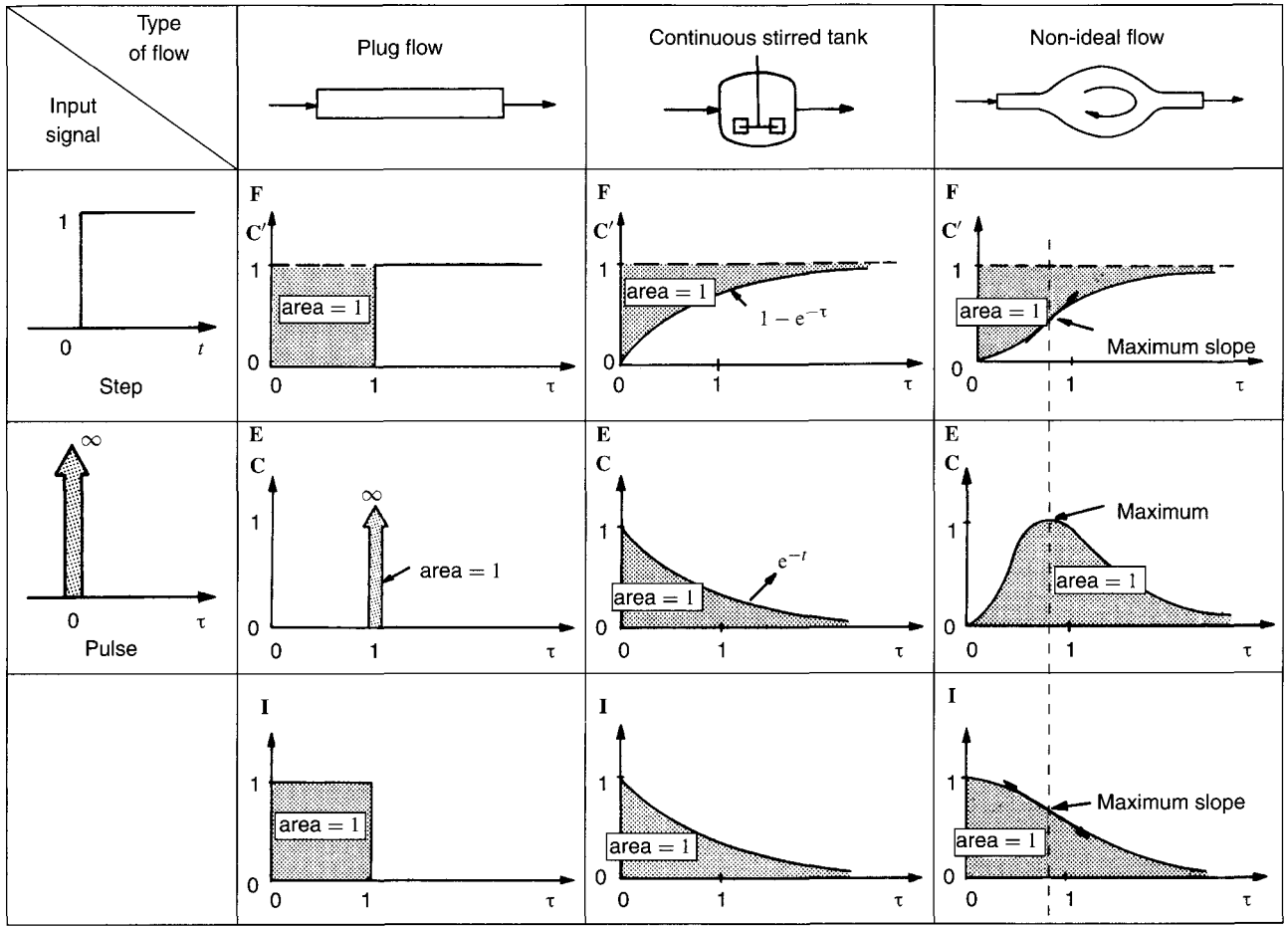


Figure 1.10 Representation of the various distribution functions and responses to input signals for three types of flow.

1.5.3.3 Non-ideal flow

For a non-ideal system, the distribution functions assume various forms while retaining the intrinsic properties of the functions we defined above. For example, Fig. 1.10 indicates the possible form of the curves for a non-ideal system.

Knowing these distribution functions for a given system is very important in practice for, by a comparison with the curves corresponding to ideal systems, we can determine which type of ideal flow the system under consideration most closely approaches. If the differences are minimal, we can assimilate the system to one of the ideal models. If the differences are significant, the ideal models can be made more complex or modified in such a way that they incorporate the real behavior of the system.

The technique of measuring residence time distribution (RTD) by means of a tracer provides a diagnostic method for determining the flow structure of continuous systems. For example, the simple fact that t_S might be different from θ can itself lead to certain conclusions: the existence of a short-circuit or a stagnant zone.

We will see in the following chapters how the performance of a continuous system used as a reactor can be influenced by residence time distribution. We would like to point out that the ideal systems that have been considered up to now have residence time distributions that are completely different and we can therefore expect significant differences in their behavior.

It is important to recognize that the correspondence between residence time distribution and system structure is not reciprocal. In other words, for a system of given structure, there will exist a single distribution function, whereas for a given distribution function, we can imagine various flow structures that can result in the same distribution function.

Additionally, the only information we can obtain from experimental investigation with a tracer involves the time intervals during which the various elements of the fluid remain in the system, independently of the interactions they undergo. We generally distinguish **macromixing**, or the group of phenomena associated with residence time distribution, from **micromixing**, which results from interactions among the elements of the flow fluid. Because of the scale at which they operate, these interactions are independent of macromixing. The residence time distribution functions are therefore incapable of supplying information about micromixing.

1.6 MACROMIXING AND MICROMIXING

In a reactor, the way we introduce and mix the reactants can have a significant impact on the conversion and selectivity. However, this is only one aspect of the mixing process, which takes place at various levels. We will see in the following chapter that the type of flow also has considerable importance for the overall process. This is especially true since chemical reactions take place at a molecular scale.

We therefore distinguish micromixing, which occurs at the molecular scale, from macromixing, which is directly associated with the type of flow and characterized by the residence time distribution.

Mixing within a turbulent flowing fluid is highly complex and we can distinguish several stages that occur at decreasing scales. These are generally referred to as macromixing, mesomixing, and micromixing.

Macromixing refers to mixing on the scale of the entire recipient.

Mesomixing refers to the turbulent exchange realized between the fresh feedstock and its environment, near the injection point. For a rapid reaction, a large part of the transformation takes place in this zone, which is much larger than the scales covered by micromixing. Mesomixing takes place through turbulent diffusion and the fragmentation of fresh feedstock elements entering the reactor.

Micromixing occurs through gradual reduction of the dimensions of fluid elements, by deformation and fragmentation, until uniformity is achieved by diffusion at the molecular level.

There are two approaches to the problems associated with mixing:

- The first was referred to in the preceding section, that is, the **earliness of mixing**.
- The second appears as soon as we attempt to specify the mixing process in detail. Within the mixed fluid there can coexist unmixed aggregates that create local heterogeneities, which lead to what is known as **segregation**.

When mixing in a vessel is examined from the point of view of "earliness of mixing," we focus on mixing between portions of fluid of different ages: This is its **temporal aspect**. On the other hand, when examined from the point of view of "fluid segregation," we focus on the fine details of mixing within the vessel: This is its **spatial aspect**.

1.6.1 Earliness of mixing

Earliness of mixing was the first concept to be considered and has helped clarify our approach to the problem of mixing. Zwietering [1959] has shown that knowledge of the residence time distribution can be used to construct two extreme models, which are illustrated in Fig. 1.11.

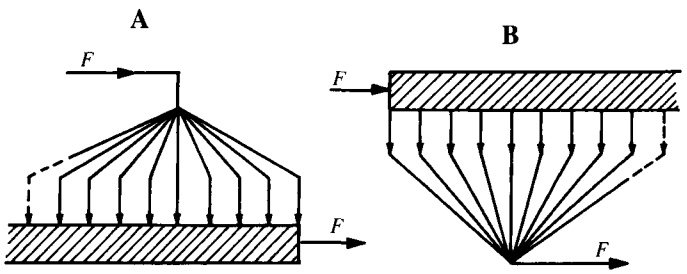


Figure 1.11 The two extreme states of fluid mixing from the temporal standpoint. **A.** Mixing at the earliest. **B.** Mixing at the latest.

The configuration for **maximum mixedness** is characteristic of a plug-flow type tubular vessel equipped with a number of lateral feed tubes. Fluid flow in these lateral feed tubes is such that the model reproduces the residence time distribution function in question. Since plug

flow implies that there is perfect mixing in every straight section of the tube, every incoming fluid element is mixed with fluid elements having different ages as soon as it enters the vessel.

The configuration for **minimum mixedness** is also characteristic of a plug-flow type tubular vessel, but one that is equipped with a number of lateral outlet tubes. Fluid flows in these lateral outlet tubes are such that the model reproduces the residence time distribution function in question. Because of the nature of plug flow, every fluid element, during its residence in the vessel, mixes only with fluid elements of the same age. It is only at the outlet of the vessel that fluid elements of different ages are mixed.

For every residence time distribution function for fluid flow in a vessel, there are two corresponding distinct extreme configurations.

In practice, since the residence time distribution function of a fluid flowing in a vessel can be used to construct several possible flow models, in certain cases we may want to identify the model that most closely mirrors reality. To do this, we can first eliminate the implausible models that do not conform to the type of equipment needed. For example, if we consider flow in a tubular vessel connected to an upstream premixing tank, the residence time distribution function obtained experimentally should reflect a model of maximum mixedness.

1.6.2 Segregation within a fluid

Although macroscopically homogeneous, a fluid can display a variable microscopic structure that is comprised between two limiting states (Fig. 1.12).

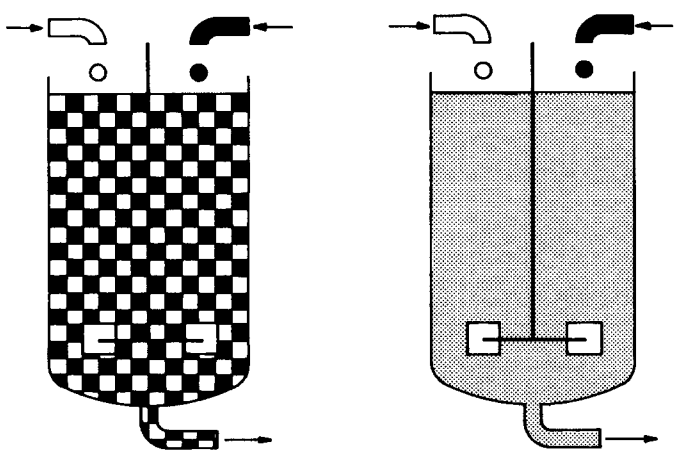


Figure 1.12 The two extreme states of the micromixing of a fluid considered from the spatial standpoint.

The first of these limiting states is that of a fluid that is thoroughly mixed on the molecular level, all the molecules being free to move about and come in contact with one another. In this case the fluid is said to be a **microfluid**.

The other limit state is that of a fluid whose molecules remain grouped into aggregates with hermetic boundaries. Although their dimensions are small on a macroscopic scale, they contain a very large number of molecules. These aggregates, or **segregation domains**, mix with one another, but molecules belonging to a given segregation domain remain bound to it and, in a continuous system, have the same internal age at any given moment. We refer to this as a **macrofluid**, or a fluid in a state of complete segregation. This limit state, which is obviously never achieved in a homogeneous fluid, can be compared to the dispersed phase of a liquid-liquid or gas-liquid system when there is no coalescence or interaction within the dispersed phase.

Between these two limit states, we say that the fluid is considered to be partially segregated, or in a state of partial segregation.

The degree of segregation, J, was defined by Zwietering as follows:

$$J = \frac{\text{variance of the ages of the aggregates}}{\text{variance of the ages of the molecules}} \tag{1.99}$$

Thus $J = 1$ for complete segregation and $J = 0$ for maximum mixing.

A second parameter needs to be considered if we want to completely characterize segregation. This is the segregation scale, which is associated with the size of the aggregates (Fig. 1.13).

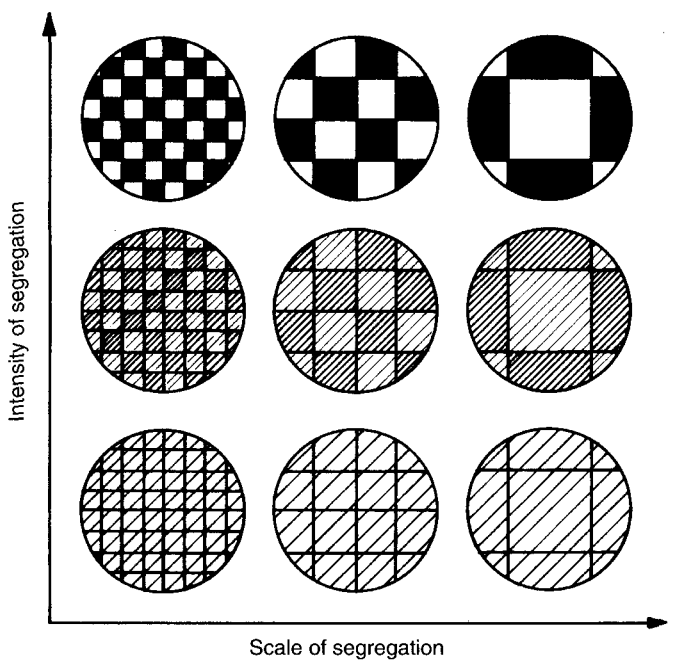


Figure 1.13 Characterization of segregation: scale and intensity of segregation.

If we now return to the ideal flow models defined above:

- plug type flow
- perfectly mixed system

what can we say about the state of segregation in such systems?

For plug type flow, the overall degree of segregation is 1 since infinitesimal slices of the flow fluid, treated as an aggregate, do not interact with other neighboring slices. However, radially within a slice, the degree of segregation should be 0. A nonzero segregation within a slice would have no significance to the extent that the reactants are premixed.

In the case of a perfectly mixed system, however, the degree of segregation is zero.

Every real fluid is partially segregated since it consists of aggregates of molecules formed by shear effects arising from mechanical agitation and friction, these aggregates exchanging matter with one another through diffusion. The intimate behavior of a real fluid thus results from the coupling of hydrodynamics (convection, turbulence) and the mass transfer by diffusion. It seems, therefore, that a real fluid, considered macroscopically homogeneous, can, under certain conditions (when diffusion is slow compared to other involved phenomena), turn out to be microscopically heterogeneous.

Note that the premixing of reactants will always have a beneficial effect on reducing segregation and, should this continue, will tend to minimize its harmful effects.

The concept of a macrofluid is especially important for multiphase systems, since at least one of the phases in these systems generally behaves like a partially or completely segregated fluid. Thus, the solid phase of fluid-solid systems can be compared to a macrofluid, since each particle of the solid is a distinct aggregate of molecules. Similarly, the dispersed phase of a fluid-fluid system is partially segregated. The degree of segregation varies with the nature of the interactions between liquid droplets or between gas bubbles dispersed in the continuous phase.

The concept of macrofluid (no interaction among segregation domains) also implies, once the residence time distribution function has been determined, identical behavior for every type of flow configuration, since the composition of the molecular aggregates depends only on the time they spend within the recipient. By treating the system as a macrofluid, we can directly calculate the behavior associated with a given residence time distribution function, without taking into account earliness of mixing.

1.6.3 Micromixing

Determination of the intensity and scale of segregation require great care but are useful for determining the various phenomena implied in micromixing. Understanding micromixing involves up-to-date knowledge of turbulence [Baldyga and Bourne, 1999]. In particular, we need to take into account the distribution of turbulent kinetic energy as a function of the size of the fluid elements (eddies) in a stream.

Engineers who study fluid mechanics make use of the spectral density function, $E(k)$, of kinetic energy, where k is the wavenumber and inversely proportional to the size of the fluid elements. Figure 1.14 illustrates the general form of this function along with that for the change in concentration, $G(k)$.

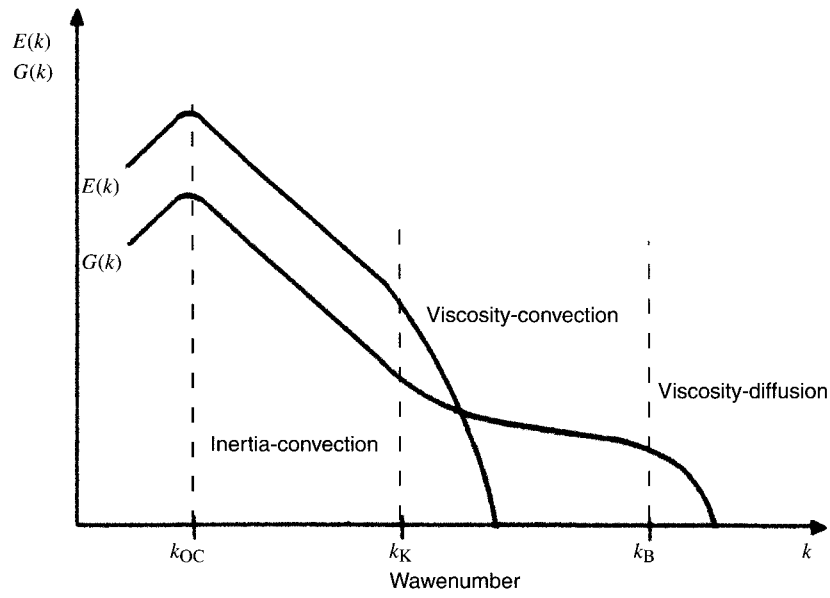


Figure 1.14 Spectra of fluctuations in kinetic energy densities, $E(k)$, and concentration, $G(k)$.

For liquids, three domains are generally distinguished on the scale of wavenumbers k:

1. The inertial-convective domain, in which the larger fluid elements are deformed and fragmented without any notable effect on micromixing. This domain extends from k_{OC} to k_K. The subscript OC corresponds to the largest fluid elements in the stream, while K corresponds to the Kolmogorov scale:

$$\lambda_K = \frac{1}{k_K} = \left(\frac{\nu^3}{\varepsilon}\right)^{1/4} \tag{1.100}$$

where

ν kinematic viscosity

ε intensity of energy dissipation from turbulence.

2. The viscous-convective domain, for $k_K < k < k_B$, corresponding to fluid element sizes comprised between the Kolmogorov and Batchelor scales. The fluid elements are then subjected to laminar stretching and diffusion can gradually play a role. The Batchelor scale is expressed by the following equation:

$$\lambda_B = \frac{1}{k_B} = \left(\frac{\nu \mathcal{D}^2}{\varepsilon}\right)^{1/4} = \lambda_K Sc^{-1/2} \tag{1.101}$$

where

$\mathcal{D}$ molecular diffusivity

Sc Schmidt number $= \nu/\mathcal{D}$.

3. The viscous-diffusive domain, for $k > k_B$. In this domain the kinetic energy of fluid eddies has practically disappeared and, consequently, molecular diffusion becomes the preponderant factor leading to the disappearance of concentration gradients.

It is the last two domains that need to be considered in micromixing. Moreover, the vorticity of the flow, which is responsible for the rollup of fluid lamellae, creates spiral structures in which diffusion can occur between various lamellae of different composition.

An estimation of the lifetime (τ_V) of vortices within which diffusion of the reactants takes place gives us:

$$\tau_V = 12\left(\frac{\nu}{\varepsilon}\right)^{1/2} \tag{1.102}$$

The characteristic diffusion time in the fluid element can be estimated by means of the following equation:

$$t_D = 2\left(\frac{\nu}{\varepsilon}\right)^{1/2} \operatorname{arcsinh}(0.05Sc) \tag{1.103}$$

This diffusion time should be compared to the characteristic reaction time. For a second-order reaction, we can use the half-reaction time, that is $t_R = (kC_0)^{-1}$. Comparison of these characteristic times can be used to determine the limiting phenomenon.

- $t_D \ll t_R$, the transformation is controlled by chemical kinetics
- $t_D \geqslant t_R$, the transformation will be more or less limited by diffusion and, therefore, micromixing will influence the process.

► ***Example:*** Using the following values for the parameters of a liquid-phase system:
$\varepsilon = 1$ W/kg; $\nu = 10^{-6}$ m^2/s; $\mathcal{D} = 10^{-9}$ m^2/s

$$Sc = 10^3$$

we obtain, for the characteristic values considered above:

$$\lambda_K = 30\ \mu\text{m}$$
$$\lambda_B = 1\ \mu\text{m}$$
$$\tau_V = 12\ \text{ms}$$
$$t_D \cong 10\ \text{ms}$$

This last value should be compared to the half-reaction time. ◄

It was on this basis that Baldyga and Bourne [1984] proposed their model of micromixing, known as the **engulfment model**, which is directly related to fundamental concepts of turbulence. Although this model, and many other more formal models that were proposed before it, can be used to interpret micromixing experiments in the presence of very fast reactions, they are inadequate for the a priori design of an apparatus in a novel situation.

To get a better overall view of the problem of micromixing in reactors, the reader should consult the available literature, especially Villermaux [1982], and more recently Bourne [1993] and Baldyga and Pohorecki [1995].

1.6.4 Use of computational fluid dynamics methods

Over the past ten years, a variety of new software tools (CFD) have been introduced commercially for the analysis of fluid dynamics, which can be used to describe fluid flow within a given geometry [Trambouze, 1993]. These programs can be very useful in describing micromixing and establishing the residence time distributions as a function of the various geometric and physical parameters.

As indicated above, in order to describe micromixing we need to consider turbulence phenomena in sufficient detail and couple chemical kinetics with purely physical phenomena. It is not easy to integrate both elements in a software program. Recently, however, new methods of addressing these problems have been proposed and look extremely promising. This is true in particular of methods involving the use of probability density functions (PDF) to describe turbulent reactive flows [Fox, 1995]. These methods were initially used to model combustion phenomena in a gas current.

We should point out, however, that the use of software to model macromixing, and especially micromixing, is the job of specialists working in close cooperation with process engineers.

REFERENCES

A.P.I. Selected Values of Physical and Thermodynamic Properties of Hydrocarbons and related Compounds. American Petroleum Institute, Project 44.

Astarita G, Sandler SI (1991) Kinetic and thermodynamic lumping of multicomponent mixtures. Proceedings of an A.C.S Symposium. Elsevier.

Baldyga J, Bourne JR (1984) A fluid mechanical approach to turbulent mixing and chemical reaction. Chem Eng Comm 28, pp 243–258.

Baldyga J, Bourne JR (1999) Turbulent Mixing and Chemical Reactions. John Wiley and Sons, New York.

Baldyga J, Pohorecki R (1995) Turbulent micromixing in chemical reactors — a review. Chem Eng J 58, 5, pp 183–195.

Bourne JR (1993) What does the modelling of reactive flows ask of CFD? Revue de l'Institut Français du Pétrole 48, 5, pp 615–630.

Fox RO (1995) Computational methods for turbulent reactive flows in the chemical process industry. Revue de l'Institut Français du Pétrole 51, 2, pp 215–243.

Froment GF (1991) Kinetic modeling of complex catalytic reactions. Revue de l'Institut Français du Pétrole 46, 4, pp 491–504.

Golikeri SV, Luss D (1972) Analysis of activation energy of grouped parallel reactions. AIChE J 18, 2, p 277.

Jacob SM *et al.* (1976) Ten-lump catalytic cracking kinetics. AIChE J 22, pp 701–713.

Leprince P (2000) Hydrotreating. *In:* Petroleum Refining. Vol. 3: Conversion Processes. Editions Technip, Paris.

Levenspiel O (1972) Chemical Reaction Engineering. 2nd Edition. John Wiley and Sons, New York.

Li G, Rabitz H (1993) The direct lumping approach: an application to a catalytic reforming model. Chem Eng Sci 48, 10, pp 1903–1909.

Osawa Y (1973) The structure of a lumpable monomolecular system for reversible chemical reactions. Ind Eng Chem Fund 12, p 191.

Pedley J, Naylor R, Kirkby S (1986) Thermochemical Data for Organic Compounds. Chapman & Hall.

Stull DR, Prophet H (1971) Janaf thermochemical tables. National Standard Reference, Data Series, NSRDS 37. US Department of Commerce National Bureau of Standards. US Government Printing Office, Washington.

Trambouze P (1993) CFD applied to chemical reaction engineering. Revue de l'Institut Français du Pétrole, 48, 5, pp 595–613.

TRC Data Project, Thermodynamic Research Center, Texas A. and M. University, Dept of Chemistry.

Vidal J (1997) Thermodynamique, Éditions Technip, Paris.

Villermaux J (1982) Mixing in chemical reactors. 7th International Symposium on Chem. Reaction Engineering, Boston.

Weekman VW *et al.* (1976) A lumping and reaction scheme for catalytic cracking. AIChE J 22, 4, p 701.

Zwietering TN (1959) Chem Eng Sci 11, 1.

NOMENCLATURE

(specific to Chapter 1)

Symbol	Definition	SI unit
a_i	Activity	–
b_i	Coefficient of adsorption	variable
C or **C**′	Dimensionless concentration	–
$E(t_S)$	Residence time distribution function	s^{-1}
$\mathbf{E}(\tau)$	Dimensionless residence time distribution function	–
$F(t)$	Cumulative residence time distribution function	–
$\mathbf{F}(\tau)$	Dimensionless cumulative residence time distribution function	–
$g(k)$	Distribution function for the rate constants k	–
$G(k)$, $E(k)$	Spectra of the fluctuations in concentration and kinetic energy densities	–
h_i	Molar enthalpy	J/mol
$\bar{h}_i$	Partial molar enthalpy	J/mol
$I(\alpha)$	Age distribution function	s^{-1}
$\mathbf{I}(\tau)$	Dimensionless age distribution function	–
J	Degree of segregation	–
k	Wavenumber	m^{-1}
R	Number of reactions in a system	–
S	Number of compounds in a system	–
t_S	Residence time of a molecule in a vessel	s
$\bar{t}_S$	Mean residence time	s
α	Age of a molecule since its entry into a vessel	s
β_i	Partial reaction order	–
θ	Mean residence time	s
λ_i	Heat of adsorption	J/mol
τ	Dimensionless time: t/θ	–
τ_i	Dimensionless age: α/θ	–
τ_S	Dimensionless residence time: t_S/θ	–
σ	Active catalytic site	–
σ^2	Variance	s^2
	Subscripts:	
a	relative to adsorption on a catalytic site	
d	relative to desorption from a catalytic site	
f	formation from elements	

Copyrighted Materials
Copyright © 2004 Editions Technip Retrieved from www.knovel.com

2 Single-Phase Reactors

In this chapter we consider several types of single-phase reactors defined in Chapter 1:

- batch reactors
- semi-continuous reactors
- continuous tubular reactors
- continuous stirred tank reactors (CSTR).

2.1 BATCH REACTORS

Of the various reactor types, the batch reactor is the simplest for carrying out a chemical transformation. It consists of a vessel in which the reactants are introduced at the start of the operation. As temperature and pressure are adjusted, the reaction progresses until the desired degree of conversion takes place. The operating conditions are then modified and the products removed.

A schematic drawing of the batch reactor appears in Fig. 2.1. The essential elements are:

- a vessel capable of containing a volume V of reaction fluid
- a surface that can be used for heat transfer
- a stirrer for mixing the reactants during the operation and facilitating heat transfer through the exchange surface.

As described, the device appears to be well suited for reactions in the liquid phase, but difficult to use for gas-phase reactions. Below, we implicitly assume that we are dealing with a homogeneous liquid phase; consequently, the pressure variable will not be taken into consideration.

2.1.1 Mass and energy balances

Consider a reaction system characterized by the general stoichiometric expressions:

$$\sum \nu_{i,j} \mathrm{A}_i = 0 \quad \begin{matrix} i = 1, S \\ j = 1, R \end{matrix} \tag{2.1}$$

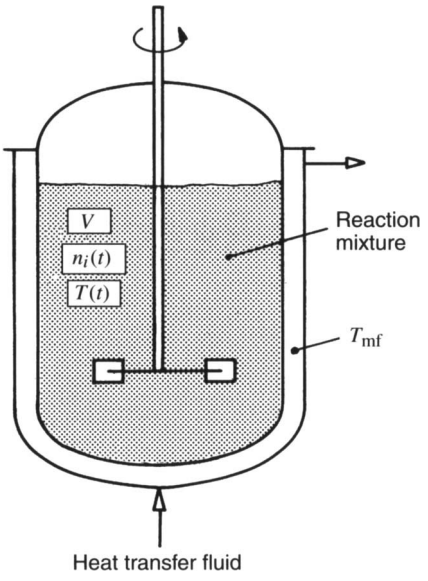


Figure 2.1 Batch reactor.

Let $n_{i,0}$ be the number of moles of A_i fed into the reactor at time $t = 0$ and at a temperature T_0. The initial volume of the reaction mixture is therefore:

$$V_0 = \sum V_{mi} \cdot n_{i,0} \tag{2.2}$$

V_{mi} being the molar volume of compound A_i. Bear in mind that the compounds A_i under consideration include not only those that take part in the reaction ($\nu_{i,j} \neq 0$) but also those that, although playing no role in the reaction ($\nu_{i,j} = 0$), are nevertheless present in the reactor feedstock. These include solvents, catalysts, and inerts.

We saw in the previous chapter (Eqs. 1.3 and 1.8) that for a single-phase batch reactor, the mass and energy balances can be written as follows:

$$\frac{dn_i}{dt} = \mathcal{R}_i V = V\left(\sum \nu_{i,j} r_j\right) \qquad (i = 1 \text{ to } S) \tag{2.3}$$

$$\sum\left(\Delta H_j \frac{d\xi_j}{dt}\right) + \left(\sum n_i C_{Pi}\right)\frac{dT}{dt} = qV \tag{2.4}$$

Equation (2.3) will in fact be replaced by the R equations reflecting the kinetics of the R reactions, namely:

$$\frac{d\xi_j}{dt} = r_j V \quad (j = 1 \text{ to } R) \tag{2.5}$$

Remember that the term qV is the energy exchanged with the exterior per unit of time, qV being positive if energy is supplied to the reaction medium. The term qV assumes different

forms depending on the type of energy exchange involved. Classically, qV contains two terms of generally unequal importance:

$$qV = \text{heat exchanged with the exterior } (q_1 V) + \text{mechanical energy dissipated by the stirrer } (q_2 V)$$

For heat exchange through an exchange surface (wall, coil, etc.), the term $q_1 V$ is often written:

$$q_1 V = U\Omega(T_{mf} - T)$$

and is therefore an indirect function of time.

T_{mf} is the mean temperature of the exchange fluid.

The term $q_2 V$ can, in the other hand, be considered constant and is often negligible compared to $q_1 V$. Moreover, in the general case, we have:

$$V = \sum V_{mi} n_i \tag{2.6}$$

Equations (2.3) and (2.4) constitute the system of differential equations, which, when integrated, enable us to describe the operation of a batch reactor. Integration is numerically simple when starting from the initial conditions defined above, where:

for $t = 0$:

$$n_i = n_{i,0} \quad T = T_0 \quad V = V_0$$

To further simplify the integration, possibly reducing it to an analytical solution, we can make certain assumptions, such as:

- constant volume (acceptable for a liquid phase, especially if it contains a solvent)
- isothermal system:

$$\frac{dT}{dt} = 0$$

or

- adiabatic system:

$$q = 0$$

Each of the last two assumptions corresponds to a limiting case that often provides an approximate representation of a real case.

• Isothermal system

The differential system reduces to Eqs. (2.5), which can be integrated once expressions for r_j are known. We are then faced with integration of the kinetic equations, examples of which are given in Table 2.1.

In the table are shown the differential mass balances and integrated solutions for some of the cases often found in practice. The differential equations are general in nature. If the reaction temperature and volume are not constant over time those changes must be taken into account when the equations are integrated.

The integrated forms are valid only within the following limits:

- isothermal in all cases
- isochorous when the reactions are not first order.

Table 2.1 Examples of molar differential and integrated balances for some simple kinetic equations.

Case	Reaction scheme	Kinetic equation	Order	Molar balances	
				Differential form	Integrated form
A	$A_1 \rightarrow A_2$	$r = k$	0	$\frac{d\xi}{dt} = kV$	$\xi = kVt$
B	$A_1 \rightarrow A_2$	$r = kC_1$	1	$\frac{d\xi}{dt} = k(n_{1,0} - \xi)$	$\xi = n_{1,0}\left[1 - \exp(-kt)\right]$
C	$A_1 \rightarrow A_2$	$r = kC_1^{\alpha}$	α ($\alpha \neq 1$)	$\frac{d\xi}{dt} = \frac{k(n_{1,0} - \xi)^{\alpha}}{V^{\alpha-1}}$	$\xi = n_{1,0}\left\{1 - \left[1 - (1-\alpha)kt\left(\frac{n_{1,0}}{V}\right)^{\alpha-1}\right]^{\frac{1}{1-\alpha}}\right\}$
D	$A_1 \rightleftarrows A_2$	$r = k_1C_1 - k_2C_2$	1	$\frac{d\xi}{dt} = k_1(n_{1,0} - \xi) - k_2(n_{2,0} + \xi)$	$\xi = \frac{(k_1 n_{1,0} - k_2 n_{2,0})}{k_1 + k_2}\{1 - \exp[-(k_1 + k_2)t]\}$
E	$A_1 + A_2 \rightarrow A_3$	$r = kC_1C_2$	2 $n_{1,0} \neq n_{2,0}$	$\frac{d\xi}{dt} = k\frac{(n_{1,0} - \xi)(n_{2,0} - \xi)}{V}$	$\xi = \frac{n_{1,0}\left\{1 - \exp\left[-\frac{k}{V}(n_{1,0} - n_{2,0})t\right]\right\}}{1 - \frac{n_{1,0}}{n_{2,0}}\exp\left[-\frac{k}{V}(n_{1,0} - n_{2,0})t\right]}$
Ebis	$\nu_1A_1 + \nu_2A_2 \rightarrow A_3$	$r = kC_1C_2$	2 $n_{1,0} \neq n_{2,0}$	$\frac{d\xi}{dt} = k\frac{(n_{1,0} + \nu_1\xi)(n_{2,0} + \nu_2\xi)}{V}$	$t = \frac{V}{k(\nu_2 n_{1,0} - \nu_1 n_{2,0})}\ln\left[\frac{(n_{2,0} + \nu_2\xi)n_{1,0}}{(n_{1,0} + \nu_1\xi)n_{2,0}}\right]$
F	$A_1 + A_2 \rightleftarrows A_3 + A_4$	$r = k_1C_1C_2 - k_2C_3C_4$	2	$\frac{d\xi}{dt} = \frac{k_1(n_{1,0} - \xi)(n_{2,0} - \xi)}{V} - \frac{k_2(n_{3,0} + \xi)(n_{4,0} + \xi)}{V}$	$\ln\left\{\frac{(2a\xi - b - f)(b - f)}{(2a\xi - b + f)(b + f)}\right\} = \frac{f}{V}t$ where $a = k_1 - k_2$ $b = k_1(n_{1,0} + n_{2,0}) + k_2(n_{3,0} + n_{4,0})$ $c = k_1 n_{1,0} n_{2,0} - k_2 n_{3,0} n_{4,0}$ $f = \sqrt{b^2 - 4ac}$
G	$A_1 \rightarrow A_2$ $A_1 \rightarrow A_3$	$r_1 = k_1C_1$ $r_2 = k_2C_1$	1 1	$\frac{d\xi_1}{dt} = k_1(n_{1,0} - \xi_1 - \xi_2)$ $\frac{d\xi_2}{dt} = k_2(n_{1,0} - \xi_1 - \xi_2)$	$\xi_1 = \frac{k_1 n_{1,0}\{1 - \exp[-(k_1 + k_2)t]\}}{k_1 + k_2}$ $\xi_2 = \frac{k_2}{k_1}\xi_1$
H	$A_1 \rightarrow A_2 \rightarrow A_3$	$r_1 = k_1C_1$ $r_2 = k_2C_2$	1 1	$\frac{d\xi_1}{dt} = k_1(n_{1,0} - \xi_1)$ $\frac{d\xi_2}{dt} = k_2(n_{2,0} + \xi_1 - \xi_2)$	$\xi_1 = n_{1,0}\left[1 - \exp(-k_1t)\right]$ $\xi_2 = n_{2,0}\left[1 - \exp(-k_2t)\right] + \frac{n_{1,0}\left\{k_2\left[1 - \exp(-k_1t)\right] - k_1\left[1 - \exp(-k_2t)\right]\right\}}{k_2 - k_1}$

For complex reaction systems, the concepts of selectivity and yield play an important role in describing phenomena. Below, we indicate how to calculate these values in two cases.

1. Twin parallel first order reactions (case G in Table 2.1)
   By definition, the instantaneous selectivity is written:

$$s_{2,1} = \frac{\dfrac{dn_2}{dn_1}}{\dfrac{\nu_{2,1}}{\nu_{1,1}}} = \frac{\nu_{1,1}k_1}{\nu_{1,1}k_1 + \nu_{1,2}k_2} \quad \text{(for a closed system)} \tag{2.7}$$

   $\nu_{2,1}/\nu_{1,1}$ represents the maximum number of moles of A_2 that can be obtained per mole of A_1 if reaction 2 does not take place. Similarly, the integrated selectivity is written:

$$S_{2,1} = \frac{\dfrac{\Delta n_2}{\Delta n_1}}{\dfrac{\nu_{2,1}}{\nu_{1,1}}} = \frac{\nu_{1,1}k_1}{\nu_{1,1}k_1 + \nu_{1,2}k_2} \tag{2.8}$$

   The yield can then be calculated:

$$R_{2,1} = X_1 S_{2,1} = -\frac{\nu_{1,1}k_1}{\nu_{1,1}k_1 + \nu_{1,2}k_2}\left(\frac{\nu_{1,1}\xi_1 + \nu_{1,2}\xi_2}{n_{1,0}}\right) \tag{2.9}$$

   Case G in Table 2.1 corresponds to:

$$\nu_{1,1} = \nu_{1,2} = -1 \quad \text{and} \quad \nu_{2,1} = \nu_{3,2} = +1$$

2. Consecutive first order reactions (case H in Table 2.1)
   In this case:

$$s_{2,1} = 1 + \frac{\nu_{2,2}k_2 n_2}{\nu_{2,1}k_1 n_1} = 1 + \frac{\nu_{2,2}}{\nu_{2,1}}\frac{k_2(n_{2,0} + \nu_{2,1}\xi_1 + \nu_{2,2}\xi_2)}{k_1(n_{1,0} + \nu_{1,1}\xi_1)} \tag{2.10}$$

   ξ_1 and ξ_2 have the values indicated in Table 2.1.
   $\nu_{2,1}/\nu_{1,1}$ represents the maximum number of moles of A_2 that can be obtained for each mole of A_1 if reaction 2 does not take place.
   The integrated selectivity is written:

$$S_{2,1} = \frac{\nu_{2,1}\xi_1 + \nu_{2,2}\xi_2}{\nu_{2,1}\xi_1} \tag{2.11}$$

   and the yield:

$$R_{2,1} = X_1 S_{2,1} = \frac{-\nu_{1,1}(\nu_{2,1}\xi_1 + \nu_{2,2}\xi_2)}{\nu_{2,1}n_{1,0}} \tag{2.12}$$

   Case H of Table 2.1 corresponds to:

$$\nu_{1,1} = \nu_{2,2} = -1 \quad \text{and} \quad \nu_{2,1} = \nu_{3,2} = +1$$

   Figure 2.2 represents, for different values of the ratio $m = \nu_{1,1}k_1/\nu_{2,2}k_2$, the value of $R_{2,1}$ as a function of the conversion X_1 for $n_{2,0} = 0$.
   We see from the above that the yield passes through a maximum, which is easily identified from the locus of the maxima indicated by the dashed line. The diagram can be used to determine the conversion corresponding to the maximum yield. This maximum yield depends only on m and is expressed by:

$$R_{2,1\,\max} = m^{\frac{1}{1-m}} \tag{2.13}$$

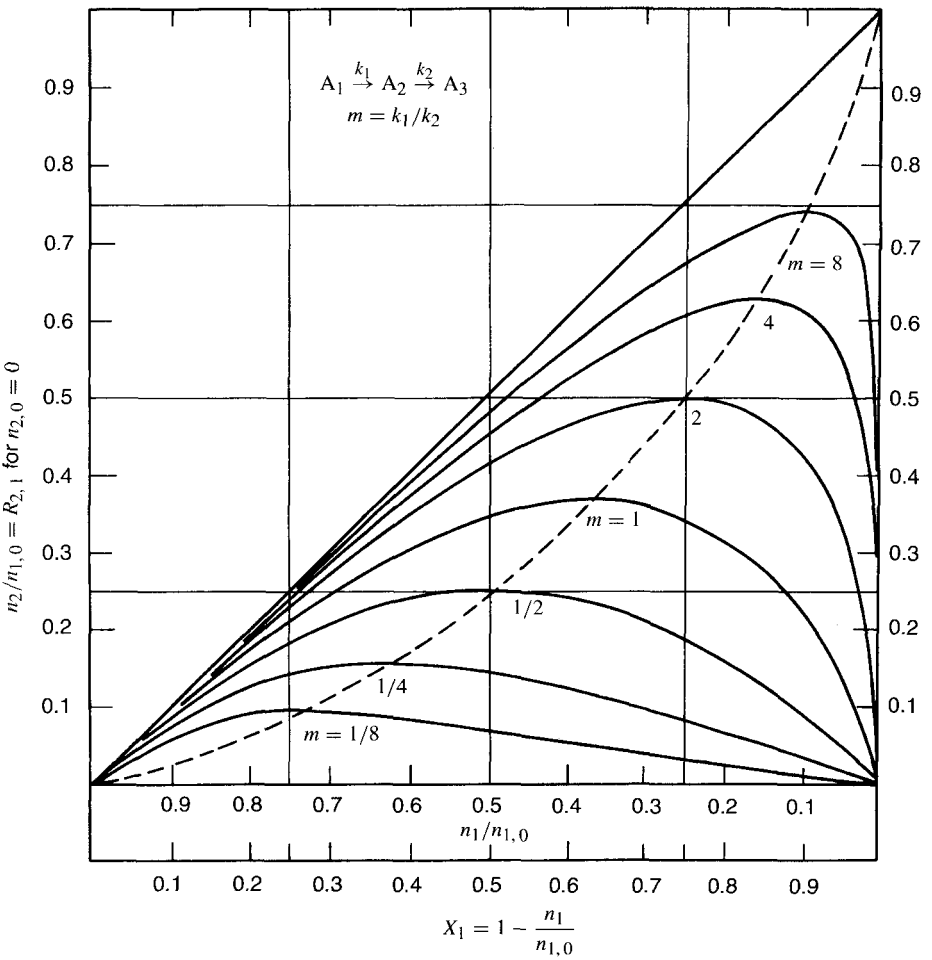


Figure 2.2 Consecutive reactions: change in yield of intermediate compound with conversion.

- **Adiabatic system**

In the case of a simple reaction system ($\sum \nu_i A_i = 0$), Eq. (2.4) reduces to:

$$\Delta H_R \frac{d\xi}{dt} + \left(\sum n_i C_{Pi}\right) \frac{dT}{dt} = 0 \tag{2.14}$$

and we can write:

$$\frac{dT}{d\xi} = \frac{-\Delta H_R}{\sum n_i C_{Pi}} \tag{2.15}$$

If we neglect changes on the right-hand side of the equation, the above can be integrated, resulting in the following equality:

$$T = T_0 - \frac{\Delta H_R}{\sum n_i C_{Pi}} \xi \tag{2.16}$$

We can then introduce Eq. (2.16) into Eq. (2.5), which can be numerically integrated without difficulty.

We can also calculate the change in temperature of the reaction medium if the transformation is complete and adiabatic. We refer to this value as ΔT_{ad}. We can express this using (2.16), replacing ξ by $n_{i,0}/\nu_i$:

$$\Delta T_{ad} = T - T_0 = -\frac{n_{i,0} \Delta H_R}{\nu_i \left(\sum n_{i,0} C_{Pi} \right)} \tag{2.17}$$

Compound A_i, taken as a reference, corresponds to the limiting reactant. Since ν_i is negative, ΔT_{ad} is positive if ΔH_R is negative, that is, if the reaction is exothermic.

2.1.2 General case and practical implications

In the most general situations found in practice, we simultaneously consider the mass balance and heat balance equations (2.3 and 2.4, for example). These equations can be solved numerically to the extent that the physico-chemical properties and chemical kinetics of the reaction system are perfectly known.

In general, an operation that takes place in a batch reactor can be divided into five successive steps that are more or less distinct:

1. loading the reactants into the reactor
2. adjusting temperature and pressure
3. reaction period proper
4. return to normal conditions of temperature and pressure
5. discharging the reactor.

The total duration of the operation will be the sum of the times needed to carry out each of the steps. Steps 1 and 5 are easily identifiable and distinct, and their duration is determined by taking into account the devices used to feed reactants to the reactor and discharge the reaction medium from the reactor. As a first approximation, we can state that the times needed to fill and empty the reactor are proportional to the volume V of the reaction phase in the reactor:

$$t_1 = \text{load time} = V/Q_c$$
$$t_2 = \text{discharge time} = V/Q_v$$

Q_c and Q_v being the average volume flow rates when the reactor is being filled and emptied.

Steps 2, 3, and 4, however, are generally not distinct but overlap considerably. To describe them we must make use of balance equations like those used for the system (2.3) + (2.4). In certain cases (polymerization, for example) we have to add to the five steps listed above a sixth step reserved for cleaning the reactor (duration t_6).

For example, let's look at a simple first-order reaction:

$$A_1 \rightarrow A_2$$

The molar balance of compound A_1 is written:

$$\frac{dn_1}{dt} = -kn_1 = -k_{T\mathrm{mf}} \exp\left[\frac{E}{R}\left(\frac{1}{T_{\mathrm{mf}}} - \frac{1}{T}\right)\right] n_1 \tag{2.18}$$

where

T_{mf} temperature of the heat transfer fluid circulating within the jacket, taken as a reference temperature

$k_{T\mathrm{mf}}$ kinetic constant at this temperature.

The heat balance will be identical to Eq. (2.4), that is, by using the expression for the extensive rate instead of $d\xi/dt$, we obtain:

$$\left(\sum n_i C_{\mathrm{P}i}\right) \frac{dT}{dt} + k_{T\mathrm{mf}} \exp\left[\frac{E}{R}\left(\frac{1}{T_{\mathrm{mf}}} - \frac{1}{T}\right)\right] n_1 \Delta H_R = qV \tag{2.19}$$

As indicated, qV is often identical to $q_1 V$:

$$qV \cong q_1 V = U\Omega(T_{\mathrm{mf}} - T) \tag{2.20}$$

At the beginning of the heating and reaction phases ($t = t_1$), that is, at the end of the loading step, the initial conditions can be written:

$$\text{for } t = t_1\,, \quad n_1 = n_{1,0}\,, \quad T = T_0$$

To simplify, we can assume that the terms $(\sum n_i C_{\mathrm{P}i})$ and $U\Omega$ are constant throughout the operation and that the temperature of the heat transfer fluid T_{mf} is also appreciably constant.

Equations (2.18), (2.19), and (2.20) describing the system, can then be rewritten by introducing the following dimensionless variables:

$$x = \frac{n_1}{n_{1,0}} \quad y = \frac{T}{T_{\mathrm{mf}}} \quad \theta = k_{T\mathrm{mf}}(t - t_1)$$

We then have:

$$\frac{dx}{d\theta} = -\exp\left[\frac{E}{RT_{\mathrm{mf}}}\left(1 - \frac{1}{y}\right)\right] x \tag{2.21}$$

$$\frac{dy}{d\theta} = \frac{n_{1,0}(-\Delta H_R)x}{T_{\mathrm{mf}}\left(\sum n_i C_{\mathrm{P}i}\right)} \exp\left[\frac{E}{RT_{\mathrm{mf}}}\left(1 - \frac{1}{y}\right)\right] + \frac{U\Omega(1-y)}{\left(\sum n_i C_{\mathrm{P}i}\right) k_{T\mathrm{mf}}} \tag{2.22}$$

The initial conditions then become:

$$\text{for } t = t_1, \quad x = 1, \quad y = T_0/T_{\mathrm{mf}}, \quad \theta = 0$$

The solution to the system of differential Eqs. (2.21) and (2.22) depends on four dimensionless numbers:

$$\alpha = \frac{n_{1,0}(-\Delta H_R)}{T_{\mathrm{mf}}\left(\sum n_i C_{\mathrm{P}i}\right)} = \left(\frac{C_{1,0}(-\Delta H_R)}{T_{\mathrm{mf}}\rho C_{\mathrm{PM}}}\right) \tag{2.23}$$

$$\beta = \frac{E}{RT_{\mathrm{mf}}} \tag{2.24}$$

$$\gamma = \frac{U\Omega}{k_{T\mathrm{mf}}\left(\sum n_i C_{\mathrm{P}i}\right)} = \left(\frac{U\mathcal{A}}{k_{T\mathrm{mf}}\rho C_{\mathrm{PM}}}\right) \tag{2.25}$$

$$y_0 = \frac{T_0}{T_{\mathrm{mf}}} \tag{2.26}$$

in which we have introduced the following variables:

$\mathcal{A}$ heat exchange surface area per unit of volume of the reactor $= \Omega/V$

C_{PM} specific heat capacity of the mixture

ρ density of the mixture.

This gives us:

$$\sum n_i C_{\mathrm{P}i} = V\rho C_{\mathrm{PM}} \tag{2.27}$$

The expressions between the large parentheses in (2.23) and (2.25) correspond to systems in which there is no change in volume.

The numerical solution of this system of equations is straightforward and can be used to draw sets of curves similar to those shown in Fig. 2.3, corresponding to an exothermic reaction. The different values for the parameters fall within the ranges shown in Table 2.2.

Examination of the entire set of curves $x = f(\theta)$ and $y = f(\theta)$ for different values of α, β, γ, and y_0, shows that we can roughly distinguish two situations:

1. An unstable situation in which it is impossible, with the exchange conditions given (γ is fixed), to prevent thermal runaway during the reaction.
2. A stable situation in which it is possible to control the reaction temperature and enable the reaction to take place in a reasonable amount of time.

The stability results from certain conditions that can be expressed, as shown below, in terms of the dimensionless numbers we have defined. Qualitatively, we can state that the stability of an exothermic reaction system will increase as γ increases. That is:

- the heat transfer area is larger
- the reaction is slower or less exothermic
- the heat capacity of the global system is higher.

2.1.3 Thermal instability

We first consider an intentionally simplified case in order to demonstrate how thermal instability can occur in a batch reaction.

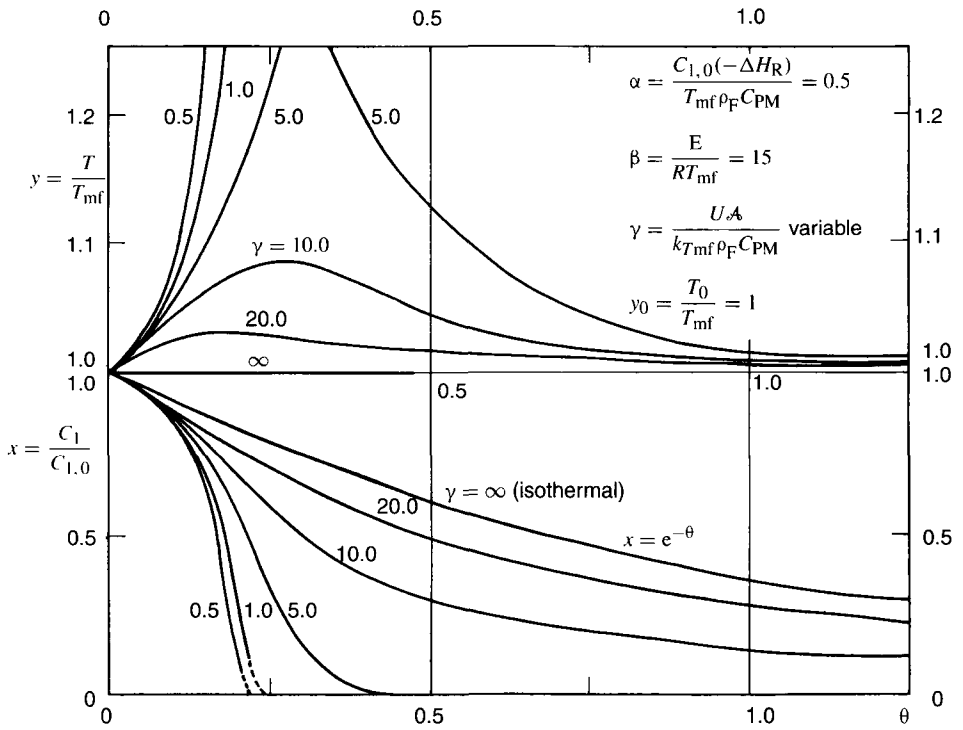


Figure 2.3 Change in temperature in a batch reactor as a function of time (first-order reaction at constant volume).

Table 2.2 Parameters used for Fig. 2.3.

Parameter values:				
10^{-4}	$<$	k_{Tmf}	$< 5 \cdot 10^{-3}$	(s^{-1})
1	$<$	$C_{1,0}$	< 10	($kmol/m^3$)
40	$<$	$-\Delta H_R$	< 150	(kJ/mol)
$5 \cdot 10^5$	$<$	ρC_{PM}	$< 4 \cdot 10^6$	($J/m^3 \cdot K$)
300	$<$	T_{mf}	< 500	(K)
100	$<$	U	< 500	($W/m^2 \cdot K$)
2	$<$	$\mathcal{A}$	< 10	(m^2/m^3)
40	$<$	E	< 150	($J/mol \cdot K$)
therefore:				
0.02	$<$	α	< 10	
10	$<$	β	< 60	
0.01	$<$	γ	< 100	

We assume a simple zero-order reaction, $A_1 \rightarrow A_2$, that takes place in a reactor similar to the one illustrated in Fig. 2.1. We can rewrite the heat balance by combining Eqs. (2.4) and (2.20):

$$\left(\sum n_i C_{Pi}\right) \frac{dT}{dt} + \frac{d\xi}{dt} \Delta H_R + U\Omega(T - T_{mf}) = 0 \tag{2.28}$$

We also know that:

$$\frac{d\xi}{dt} = kV = k_0 \exp\left(-\frac{E}{RT}\right) V \tag{2.29}$$

If the reaction is exothermic ($\Delta H_R < 0$), the entire transformation can take place at a fixed temperature T, to the extent the equality based on (2.28) holds:

$$U\Omega(T - T_{mf}) = k_0 \exp\left(-\frac{E}{RT}\right) V(-\Delta H_R) \tag{2.30}$$

This equation describes the equality between the heat exchanged and the heat produced. It can be graphically resolved by plotting each term *versus* T (Fig. 2.4). The reactor's operating temperature is then given on the abscissa by the point of intersection of the two curves. In Fig. 2.4 we see that it is possible to obtain two solutions, represented by points S and I.

Point I is an unstable operating point. If the temperature deviates slightly from the value of T found for (2.30), there is no reason to assume that the temperature will return to this value of T. For example, if the temperature exceeds T slightly, the heat produced then being greater than the heat exchanged, the temperature will increase until all of reactant A_1 is exhausted.

Point S, on the other hand, represents a stable operating point and is the only one used in practice.

If the heat transfer conditions change, following a modification of $U\Omega$ or T_{mf}, the stable operating point will shift. The limits of these changes can be evaluated by stating that the line representing $Q_E(T)$is tangent to the curve representative of $Q_P(T)$:

$$U\Omega = k_0 \frac{E}{RT^2} \exp\left(-\frac{E}{RT}\right) V(-\Delta H_R) \tag{2.31}$$

The equation describing the equality of the heat exchanged can then be written in the following form:

$$T_{mf} = T - \frac{RT^2}{E} \tag{2.32}$$

In both cases (modification of $U\Omega$ and T_{mf}) it is then possible to calculate the limiting temperature for stable operation at the point of tangency and then, depending on the situation, the minimum temperature T_{mf} or the corresponding product $U\Omega$.

- Case A: $U\Omega$ variable and T_{mf} fixed:

$$T_{lim} \leqslant \frac{E - \sqrt{E^2 - 4RET_{mf}}}{2R} \tag{2.33}$$

and:

$$U\Omega \geqslant k_0 \frac{E}{RT_{lim}^2} \exp\left(-\frac{E}{RT_{lim}}\right) V(-\Delta H_R) \tag{2.34}$$

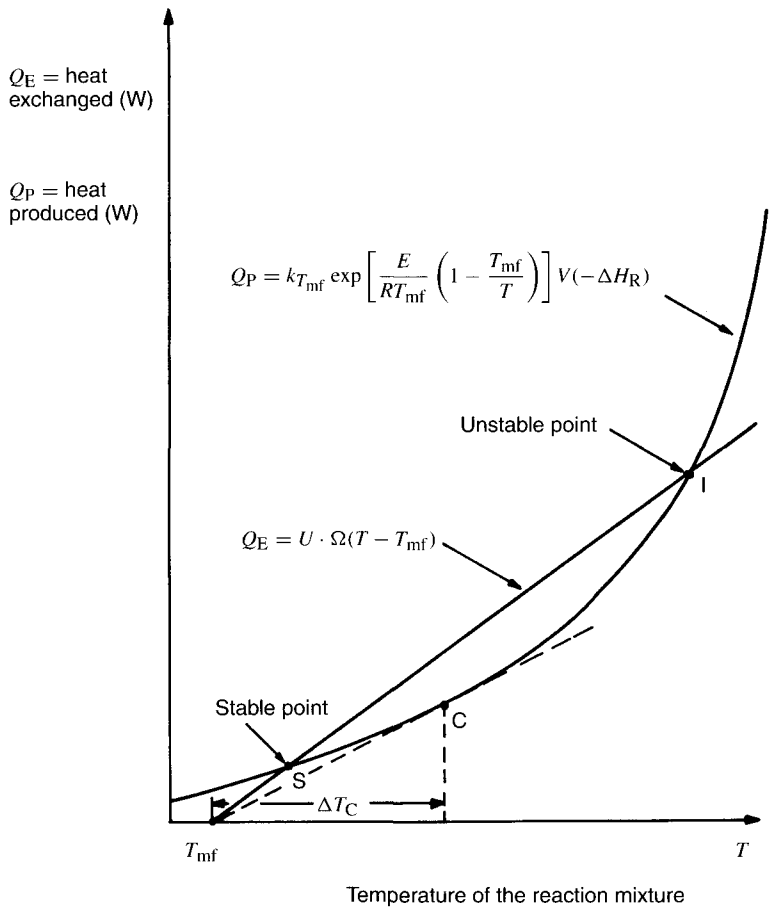


Figure 2.4 Graphic representation of the heat balance for a zero-order exothermic reaction.

- Case B: T_{mf} variable and $U\Omega$ fixed:
  T_{lim} is the solution for $U\Omega = k_0(E/RT_{lim}^2)\exp(-E/RT_{lim})V(-\Delta H_R)$ and we then have:

$$T_{mf} \leqslant T_{lim} - \frac{RT_{lim}^2}{E} \tag{2.35}$$

If a reaction must take place at a given temperature T, the heat generated is determined from:

$$Q_P = k_0 \exp\left(\frac{-E}{RT}\right) V(-\Delta H_R) \tag{2.36}$$

The maximum transfer conditions used to evacuate this heat correspond to the characteristics of the tangent to the curve Q_P at the abscissa T. We then immediately obtain

$(U\Omega)_{\text{lim}}$ and $(T_{\text{mf}})_{\text{lim}}$:

$$(U\Omega)_{\text{lim}} = k_0 \frac{E}{RT^2} \exp\left(-\frac{E}{RT}\right) V(-\Delta H_R) \tag{2.37}$$

and:

$$(T_{\text{mf}})_{\text{lim}} = T - \frac{RT^2}{E} \tag{2.38}$$

If we intend to control the reaction at the desired temperature T, we need to ensure that $U\Omega > (U\Omega)_{\text{lim}}$ and $T_{\text{mf}} < (T_{\text{mf}})_{\text{lim}}$, the first constraint often being the more difficult to realize in practice.

For example, we can calculate that for a reaction that occurs at 400 K and has an activation energy of 84 kJ/mol, the maximum temperature difference between the reaction mixture and the cooling fluid is 16 K.

This calculation, although based on a very simple case, clearly illustrates that the choice of T_{mf} must be made carefully and that, for a strongly exothermic reaction, it is preferable to increase the exchange surface Ω and, if possible, the heat transfer coefficient U, rather than counting on increased driving force $\Delta T = (T - T_{\text{mf}})$ to bring about the evacuation of the heat produced. In the event operating conditions are unstable, the temperature will change until it reaches a maximum value corresponding to the final temperature during adiabatic operation, as calculated from Eq. (2.17).

For example, reactions involving the polymerization of olefin monomers all have heats of reaction that are appreciably equal to 20 kcal/mol. This leads to high values for ΔT_{ad}, which can vary from approximately 400 K in the case of styrene to 1 000 K for vinyl chloride. Such uncontrolled increases in temperature are obviously capable of generating explosions.

A more general criterion for stability can be deduced by resolving the system of Eqs. (2.21) and (2.22) introduced above. For a first-order reaction, we describe the behavior of the batch reactor using the two differential Eqs. (2.21) and (2.22), whose coefficients are the dimensionless numbers α, β, γ, and y_0, which were previously defined (Eqs. 2.23 to 2.26).

We can then attempt to formulate a stability criterion using these four dimensionless parameters. To do this we numerically resolve the differential system (2.21) and (2.22) and then consider as stable those systems for which the temperature T does not exceed $1.25T_{\text{mf}}$ during the course of operation. This limit, although arbitrary, corresponds well to the reality of industrial practice. Moreover, modifying this limit (for example, by using 1.15 or $1.35T_{\text{mf}}$) would have little effect on the results for high values of α (that is for the most critical cases).

The curves shown in Fig. 2.5, drawn respectively for $y_0 = 0.8$–0.9 and 1.0, can be used to delimit the stability domain. It appears that below a limiting value of α, instability cannot occur. Above that value, the reactor is stable or unstable depending on the values of β and γ. The limiting value of α corresponds to the case where all the heat generated by the complete reaction is stored in the reaction fluid without any exchange with the exterior (adiabatic operation).

In this case, we can write:

$$n_{1,0}(-\Delta H_R) = V\rho C_{\text{PM}}(T_{\max} - T_0) \tag{2.39}$$

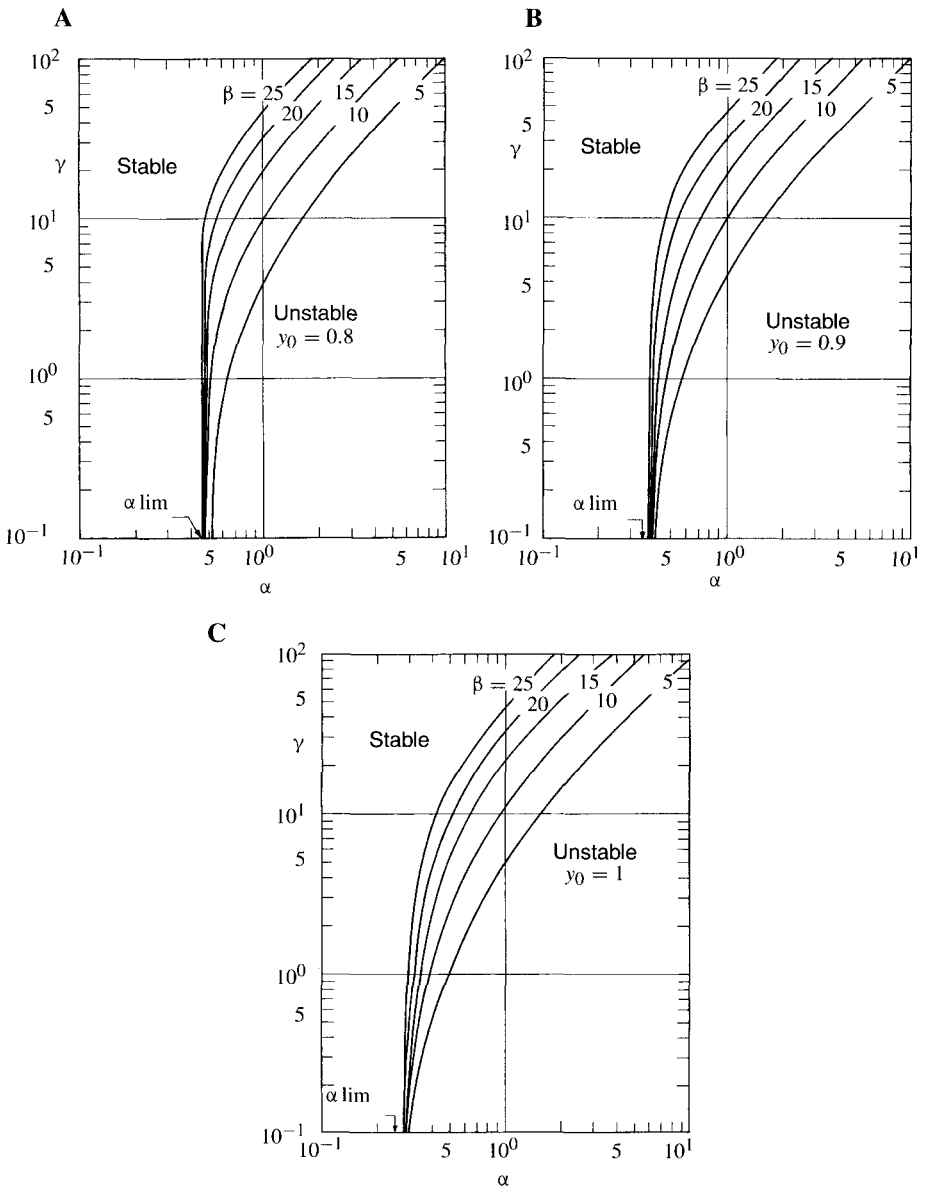


Figure 2.5 Stability of a batch reactor, $\gamma = f(\alpha)$ for: **A.** $y_0 = 0.8$. **B.** $y_0 = 0.9$. **C.** $y_0 = 1$.

If we let $T_{max} = 1.25T_{mf}$, we can obtain the value of α_{lim} by substituting (2.39) in the definition of α (2.23), that is:

$$\alpha_{lim} = \frac{T_{max} - T_0}{T_{mf}} = 1.25 - y_0 \tag{2.40}$$

Using the curves, it is easy to verify that this relation is satisfied. The inequality:

$$\alpha \leqslant \frac{T_{\max}}{T_{\mathrm{mf}}} - y_0 \quad (T_{\max} \text{ and } T_{\mathrm{mf}} \text{ in K}) \tag{2.41}$$

is therefore a first criterion indicating the upper limit of α for which adiabatic operation is feasible.

For larger values of α (highly exothermic reaction, low heat capacity), we need high values of γ (large exchange capacity) to achieve stability. Values of γ must be greater with increasing values of β (high activation energy).

In examining the curves in Fig. 2.5, we see that for values of α greater than 1, the curves have a tendency to become straight lines whose slope is close to unity. From this we can derive a semi-empirical stability criterion, namely:

$$\gamma \geqslant (\alpha\beta)^{1.18} \tag{2.42}$$

For $\alpha \geqslant 1$, this criterion is a reasonable approximation.

The significance of these dimensionless numbers is worth examining.

Based on (2.17) and (2.23), we can write:

$$\alpha = \frac{\Delta T_{\mathrm{ad}}}{T_{\mathrm{mf}}} \tag{2.43}$$

The significance of (2.42) becomes clear if, as a first approximation, we change the exponent 1.18 to 1. In this case we find that $\gamma = \alpha\beta$, and by replacing α, β, and γ with their definitions, Eqs. (2.23) to (2.25), we obtain:

$$UA\Delta T_C = k_{T_{\mathrm{mf}}} C_{1,0}(-\Delta H_R) \tag{2.44}$$

This equation reflects the following situation: At temperature T_{mf} and time $t = 0$, the rate of heat generation (right side of Eq. (2.44)) is equal to the rate of heat removal (left side of Eq. (2.44)), assuming a temperature difference equal to the corresponding critical ΔT.

In practice the temperature difference between the reaction mixture and the cooling fluid does not correspond to a single value but a domain ranging from $(T_{\mathrm{e,f}} - T)$ to $(T_{\mathrm{s,f}} - T)$. We can then use as a value for ΔT:

$$\Delta T = (T - T_{\mathrm{mf}}) = \mathrm{LMTD} = \frac{T_{\mathrm{e,f}} - T_{\mathrm{s,f}}}{\ln\left(\dfrac{T - T_{\mathrm{e,f}}}{T - T_{\mathrm{s,f}}}\right)}$$

where

LMTD logarithmic mean temperature difference, generally used when designing heat exchangers

$T_{\mathrm{e,f}}$ inlet temperature of the cooling fluid

$T_{\mathrm{s,f}}$ outlet temperature of the cooling fluid.

These considerations are particularly important during reactor scale-up. For if we multiply the volume of the reactor by a factor Z, the right-hand side of (2.30) will also be multiplied by Z. We must then ensure that ΩU as well is multiplied by Z. If the heat exchange occurs through the reactor wall (jacket), by maintaining $H = D$, the exchange area Ω will only be multiplied by $Z^{2/3}$ (in practice $\Omega/V = \mathcal{A} =$ approximately $5/D$, where D is the diameter of the reactor). During scale-up, we must anticipate some means of additional cooling while increasing the coefficient of heat transfer.

Careful attention must be given to this problem when using the same reactor for producing a large variety of products (such as occurs in the pharmaceutical industry). When a new product is synthesized in the laboratory, we may be tempted to duplicate the reaction in an existing production reactor. Such a procedure, if conducted too hastily, can result in serious accidents arising from the instability described above. For exothermic reactions, where the thermodynamics and kinetics are often poorly understood, it is essential to undertake a thermokinetic study before scale-up. This can be done with specially designed calorimeters that can be used to monitor the kinetics of the heat of reaction. With this information, it is then possible, using simulation procedures, to ensure that the existing reactor is indeed capable of sustaining the new reaction, which had previously been limited to small-scale laboratory production.

Problems associated with thermal instability have been the cause of various industrial accidents. For the past fifteen years, strict methodologies have been put in place by a number of fine chemical manufacturers to avoid any risk of accident during scale-up.

An article by Stoessel [1993] discusses Ciba-Geigy's approach to the problem. The synthesis reaction is studied in the laboratory on a very small scale using differential thermal analysis to detect the existence of possible secondary reactions that are strongly exothermic (decomposition, for example). The amount of heat liberated by the various reactions when the temperature is increased can be measured. An analysis of the results can then be used to calculate an overall activation energy and adiabatic temperature difference.

Another criterion taken into consideration is the critical runaway time, $t_{C,E}$, characterizing the rate at which temperature rises in the event of an accident:

This critical time is expressed as follows:

$$t_{C,E} = \frac{\sum n_{i,0} C_{Pi}}{-\Delta H_R} \Delta T_C = \frac{\sum n_{i,0} C_{Pi}}{-\Delta H_R} \frac{RT^2}{E} \tag{2.45}$$

and corresponds to the time it takes for the reaction to reach the critical temperature at which runaway occurs.

Based on the above criteria, a risk analysis is performed, which traditionally distinguishes the severity and probability of an accident (Table 2.3).

As indicated earlier, we see from the table that ΔT_{ad} is of prime importance. However, the probability criterion is a second parameter to consider and may seem exaggerated for a reaction that takes place in a device equipped with conventional instrumentation. Yet, if we consider equipment such as storage tanks, in which secondary reactions can occur, the importance of the probability criterion becomes easier to understand. The accident that occurred at Bhopal, India, in 1984, is appreciably similar to the situation we are describing here.

Table 2.3 Criteria used to assess the risk associated with a batch reaction.

Severity	Criterion	Probability	Criterion
High	$\Delta T_{ad} \geqslant 200\,K$	High	$t_{C,E} \leqslant 8\,h$
	or $T_0 + \Delta T_{ad} \geqslant T_{bp}$		
Medium	$50\,K \leqslant \Delta T_{ad} \leqslant 200\,K$	Medium	$8\,h \leqslant t_{C,E} \leqslant 24\,h$
Low	$\Delta T_{ad} \leqslant 50\,K$	Low	$t_{C,E} \geqslant 24\,h$

2.1.4 Available technologies

As indicated at the beginning of the chapter, the equipment needed to carry out a batch reaction is relatively simple. It should, however, include the following elements:

- A vessel capable of containing the volume V of fluid to be processed at the temperature and pressure conditions corresponding to the requirements of the reaction. This vessel is called the reactor.
- A heat exchange surface sufficient to supply or remove the calories absorbed or generated by the reaction. This heat exchange surface can be located inside the reactor (coil, plates), outside the reactor (conventional heat exchanger for the liquid phase or condenser for the vapor phase), or form the reactor wall (jacket). These various systems can sometimes be used simultaneously.

Some of the systems most frequently found in industry are illustrated in Fig. 2.6. With respect to the reactor itself, it often assumes the form of a vertical cylinder with an elliptical bottom. It is constructed in such a way that it can sustain a vacuum or internal pressure. The construction material is often selected to accommodate a variety of uses. Enameled steel, for example, is of considerable interest because of its resistance to corrosion and the ease with which it can be cleaned. Table 2.4 indicates the principal characteristics of some standard reactors sold commercially.

Table 2.4 Principal characteristics of commercially available reactors (Fig. 2.7).

Capacity (m^3)	0.16	0.63	1.6	2.5	4.0	6.3	8	20	40
Diameter D (m)	0.6	1	1.4	1.6	1.8	2	2.2	2.8	3.4
Total weight (kg)	640	1 500	3 200	4 150	5 900	8 070	8 600	19 200	34 500
Exchange area Ω (m^2)	1.25 J	3.1 J	7.3 WC	8.3 J	13.23 WC	15.6 J	18 WC	34 J	55.2 WC
Exchange area/Volume Ω/V (m^2/m^3)	7.8	5	4.5	3.3	3.3	2.5	2.2	1.7	1.4
$\Omega D/V$	4.7	5	6.3	5.3	5.9	5	4.8	4.8	4.8
Service pressure (bar)	6	6	6	6	6	6	6	6	6
Material	ES	ES	ES	ES	ES	ES	ES	ES	ES

J: jacket; WC: welded coil; ES: enameled steel.

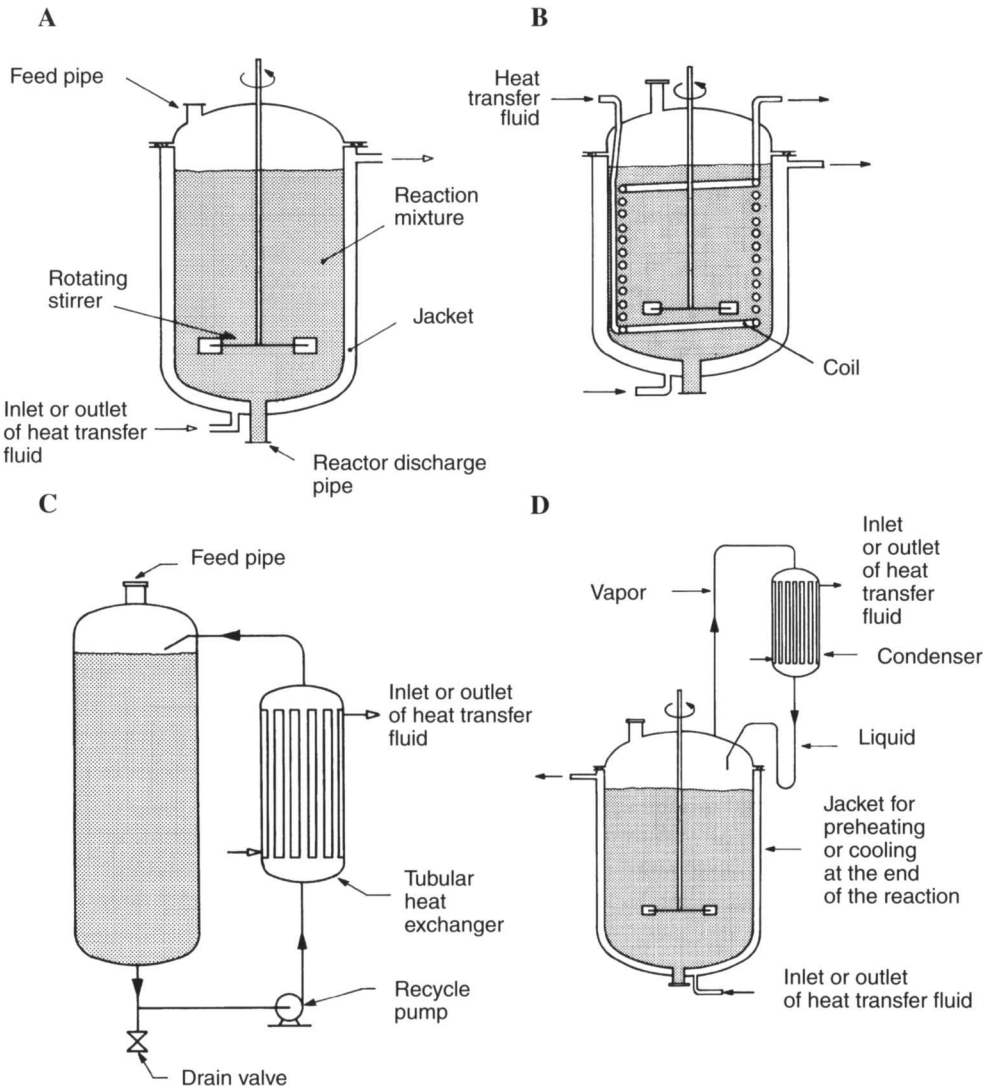


Figure 2.6 Various heat exchange technologies: **A.** Jacket. **B.** Jacket and internal coil. **C.** External heat exchanger on circulation loop. **D.** Cooling by vapor-phase condensation.

With respect to heat exchange, although the jacket is relatively simple to construct, it has a limited exchange surface area which decreases relative to the volume of the tank as the tank increases in size (2.5 m^2/m^3 for small reactors to 1.5 m^2/m^3 for 35 m^3 reactors). Moreover, the overall coefficient of heat transfer obtained with a jacket is relatively low (from 60 to 350 $W/m^2 \cdot K$). For this reason, the jacket is often replaced by a coil consisting of a half-tube wrapped around the exterior in spirals and welded to the wall of the reactor (Fig. 2.7) in order

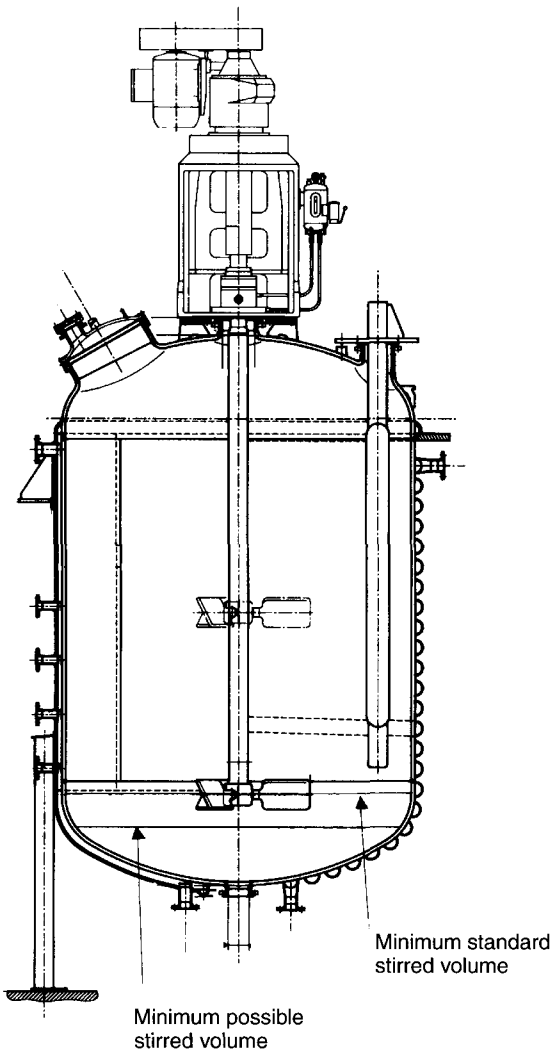


Figure 2.7 Typical industrial batch reactor (see photo 1).

to increase the linear velocity of the heat-transfer fluid and, therefore, the external transfer coefficient.

The use of a coil (Fig. 2.6B) or plates inside the reactor can provide relatively good heat transfer coefficients (700–800 $W/m^2 \cdot K$), but their exchange area is limited and their presence can hinder the action of the stirrer or cleaning operations.

The external heat exchanger, whether it is part of a liquid circulation loop (Fig. 2.6C) or operates as a condenser for the vapor phase (Fig. 2.6D), is the only system that provides the high exchange surface area required by highly exothermic reactions (such as polymerization).

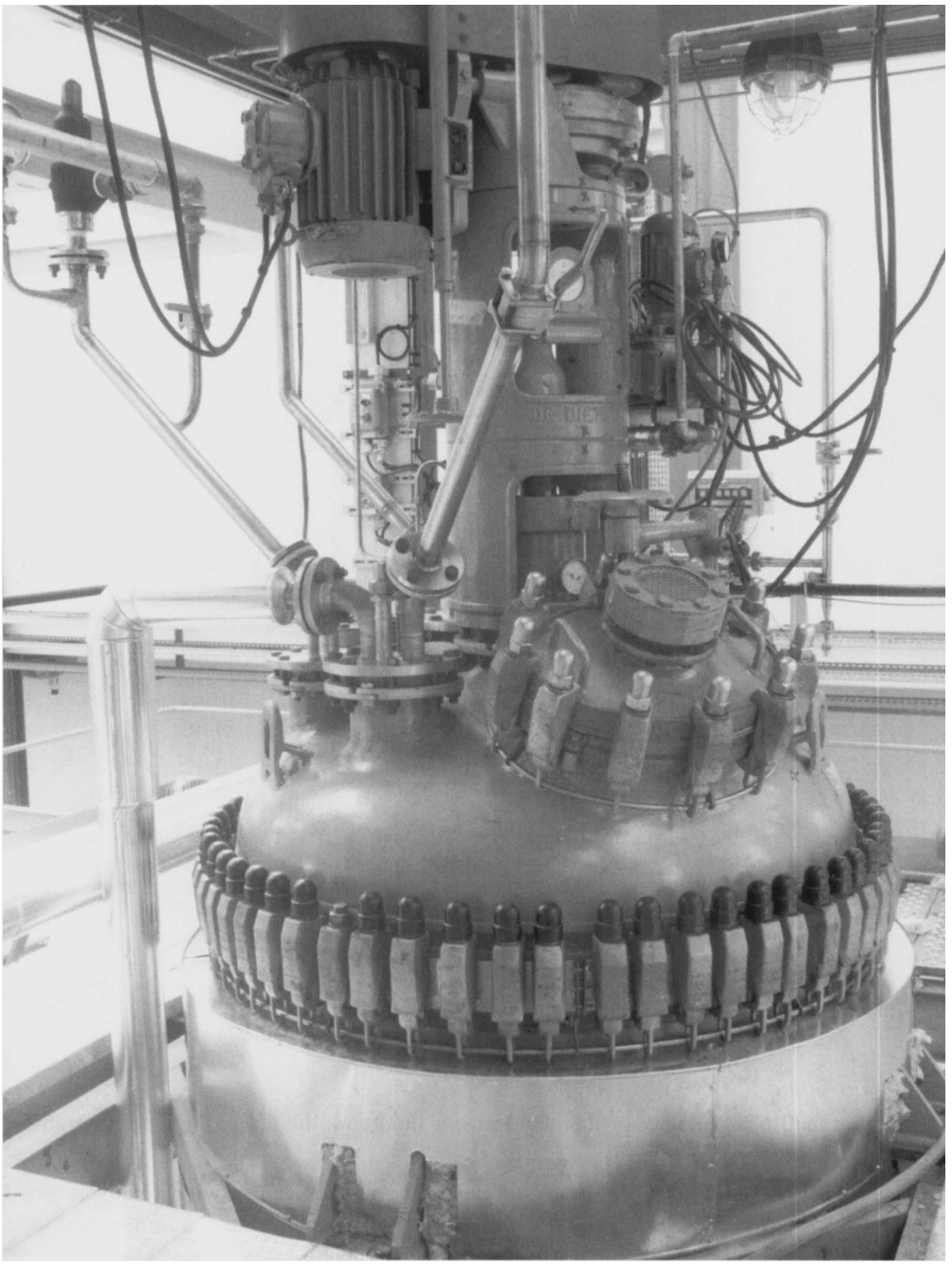


Photo 1 Stirred tank reactor. This type of reactor is most frequently used for batch or semi-continuous reactions (see case 1 in Chapter 9).

(*Photo France Wisten*).

The literature [Dream, 1999] provides correlations that can be used to calculate heat exchange coefficients associated with systems that are frequently found in practice.

It is important to remember that the overall coefficient of heat exchange U contains three components, which correspond to three sources of resistance located inside the reactor (h_{int}), through the wall (h_{p}), and on the heat-transfer fluid side (h_{ext}):

$$\frac{1}{U} = \frac{1}{h_{\text{int}}} + \frac{1}{h_{\text{p}}} + \frac{1}{h_{\text{ext}}} = \frac{1}{h_{\text{int}}} + \frac{e}{\lambda_{\text{p}}} + \frac{1}{h_{\text{ext}}} \tag{2.46}$$

where

λ_{p} thermal conductivity of the wall

e thickness of the wall

h_{int} depends on the nature of the reaction fluid (in particular, its viscosity) and the turbulence in the vicinity of the wall, which varies according to the type of agitation used. The presence of protective coatings against corrosion (enamel, plastic) tends to increase resistance due to the wall (e/λ_{p}).

h_{ext} depends on fluid flow in the vicinity of the wall. It is important to remember that if heat transfer is accompanied by a change of state (vapor condensation, for example), the film coefficient (h_{ext}) can be significantly larger than in the case of simple fluid circulation without a change of state. For this reason, we very often find that reactors are heated by condensation of a vapor within a jacket or in a coil.

To heat and cool the reactor, we can use water, steam, or a heat-transfer fluid suitable for the temperature range in question.

Note that during the total time needed to carry out a batch operation, times t_2 and t_4, which correspond to heating and cooling of the reaction mixture, are often considerable (sometimes several hours). These times can be calculated if we know the heat balances written for the reaction fluid and the fluid used for heating or cooling.

$$QC_{\text{F}}(T_{\text{e,f}} - T_{\text{s,f}}) = \left(\sum n_{i,0} C_{\text{P}i} + wC_w\right) \frac{\mathrm{d}T}{\mathrm{d}t} = \bar{U}\Omega(\text{LMTD})$$

where

Q fluid flow used for heat exchange (m^3/s)

C_{F} heat capacity of the heat exchange fluid ($\text{kcal}/\text{m}^3 \cdot \text{K}$)

w weight of those parts of the reactor subject to changes in temperature during heating or cooling (kg)

C_w average heat capacity for the weight w defined above ($\text{kcal}/\text{kg} \cdot \text{K}$)

LMTD logarithmic mean temperature difference, defined above (K)

$\bar{U}$ overall coefficient of heat exchange; mean values are used during heating or cooling ($\text{kcal}/\text{m}^2 \cdot \text{s} \cdot \text{K}$)

$T_{\text{e,f}}$ inlet temperature of heat exchange fluid (K)

$T_{\text{s,f}}$ outlet temperature of heat exchange fluid (K).

We thus obtain the following formulas:

$$t_2 = B \ln \left[\frac{T_{f,c} - T_R}{T_{f,c} - T_0} \right] \tag{2.47}$$

$$t_4 = B \ln \left[\frac{T_R - T_{f,r}}{T_F - T_{f,r}} \right] \tag{2.48}$$

where

$$B = \frac{\sum n_{i,0} C_{Pi} + w C_w}{Q_F C_F} \frac{\exp\left(\dfrac{\bar{U}\Omega}{Q_F C_F}\right)}{1 - \exp\left(\dfrac{\bar{U}\Omega}{Q_F C_F}\right)}$$

T_0 and T_F temperature of the reaction medium at the beginning and end of the operation
$T_{f,c}$ inlet temperature of the fluid used for heating
$T_{f,r}$ inlet temperature of the fluid used for cooling
T_R temperature at which the reaction should take place.

To shorten these unproductive waiting periods, we need to increase U and Ω at the same time. The only possibility available then is to use a system with a circulation loop and external exchanger (Fig. 2.6C). In this case, we can easily achieve the following values: $U = 1\,000$ W/m$^2 \cdot$ K and $\Omega/V = 10$ m^2/m^3, which enables us to reduce t_2 and t_4 by a factor of at least 10. However, we must also take into account the reaction volume contained in the exchanger.

Bear in mind that the use of a fluid heat carrier for heating is not the only possible solution, even if it is the one most frequently encountered in practice. Electric induction heating has recently been used with success on tanks as large as 4.5 m^3 (Fig. 2.8). About 270 kW of electrical power is then required to reach a temperature of 350°C [Salfati, 1997].

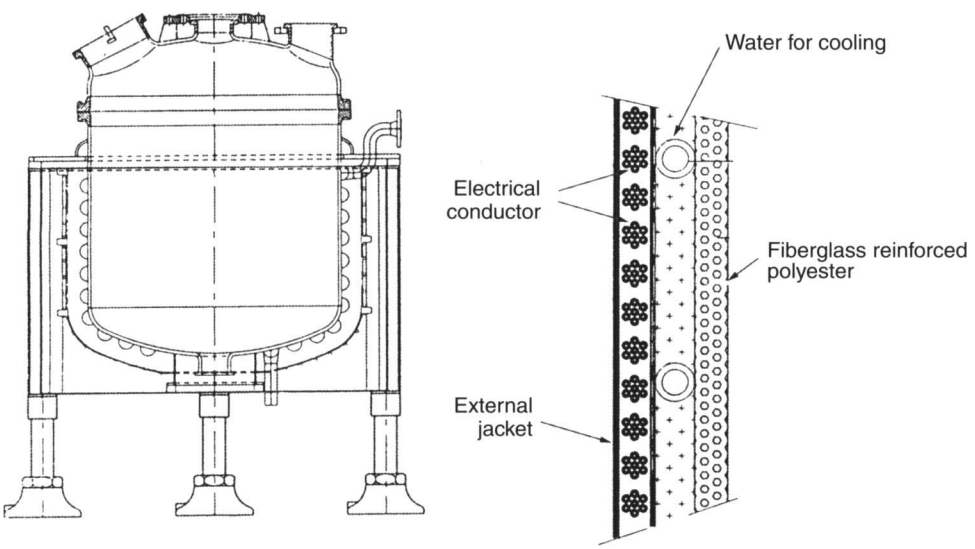


Figure 2.8 Electric induction heating.

2.1.5 Mixing systems

There are various types of rotary stirrers on the market. Here, we consider only those that are most commonly used in batch reactors. These stirrers are used to mix the reactants at the beginning of the operation and then to promote heat transfer to the vessel's specially designed walls.

A rotating stirrer consists of a motor that imparts, by means of a shaft, a rotational movement to a stirrer that mixes the fluid. The primary effect of these stirrers is to create fluid circulation within the tank. This circulation can be essentially axial, radial, or peripheral. Differently shaped stirrers have been designed to accommodate each of the different situations. In practice they are classified into four categories:

1. helix type or propeller stirrers
2. turbine stirrers
3. stirrers with a large radius of action (anchor, large paddle)
4. stirrers based on the Archimedes screw principle.

The various stirrer designs are shown in Figs. 2.9 to 2.12.

• **Propeller,** (Fig. 2.9) **stirrers**

The first propeller stirrers were based on marine propellers used for the propulsion of ships (Fig. 2.9). Since then, to improve energy efficiency, various models have come on the market containing thin, or flat, streamlined or multiplane blades. These generate an essentially axial movement with low shear and therefore are often used to homogenize fluid media. These stirrers are characterized by:

- the diameter, D_A, often equal to 1/3, sometimes 1/5 or 2/3, of the diameter of the reactor, D_T; the highest ratios of D_A/D_T tending to promote primarily axial flow and, therefore, homogenization and heat transfer, while the smallest ratios, associated with higher speeds, tend to promote turbulence and micromixing
- the number of blades (generally 2, 3, or 4)

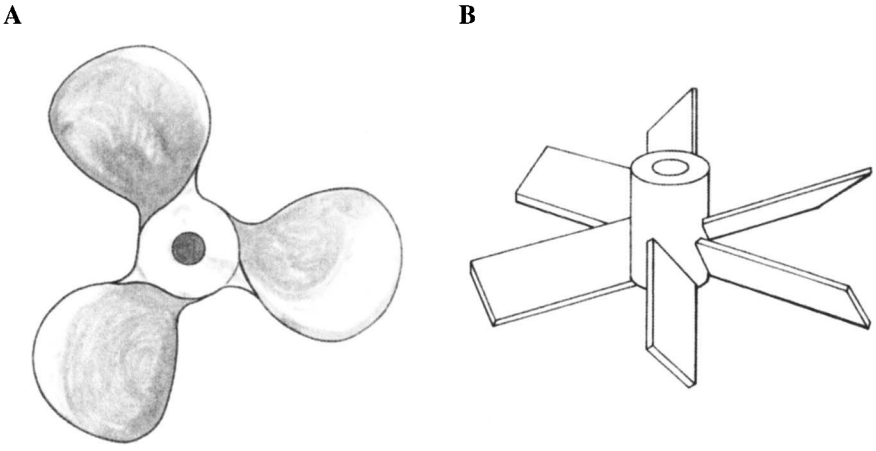


Figure 2.9 Propeller agitators: **A.** Marine propeller with three blades. **B.** Propeller with six inclined blades.

- the pitch, often equal to the diameter of the helix, but more generally comprised between 0.5 and 3 times the diameter
- the direction of rotation, which causes the fluid to ascend or descend.

• **Turbines** (Fig. 2.10)

Turbines typically consist of flat, vertical, radial blades, mounted on a horizontal disk. They produce primarily radial flow, with high shear at the blade tip (Fig. 2.10). They are very frequently used when it is necessary to fragment a fluid into bubbles or drops. The basic model with flat blades (called a Rushton turbine) is characterized by:

- the diameter, often equal to 1/3, sometimes between 1/5 and 2/3, of the diameter of the reactor
- the number of blades (most often 6)
- the dimensions of the blades compared to the diameter of the impeller, in particular, a width between 1/10 and 1/4 of the diameter of the impeller.

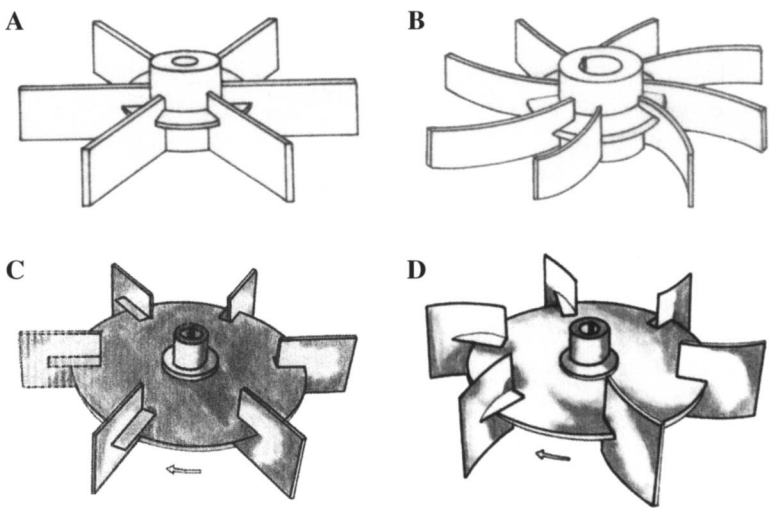


Figure 2.10 Turbine agitators: **A.** Turbine with six flat blades. **B.** Turbine with eight curved blades. **C.** Turbine with six flat blades mounted on a disk. **D.** Turbine with six curved blades mounted on a disk.

There are a large variety of turbine types, distinguished primarily by the number, shape, pitch, inclination and curvature of the blades, and by the presence or absence of a central disk.

• **Anchors** (Fig. 2.11)

Anchor stirrers consist of a U-shaped tube or flat ribbon of reduced width that rotates about its axis in the proximity of the vessel's walls. They produce a peripheral tangential flow and are suitable for mixing viscous products near the walls, in particular, to improve heat transfer.

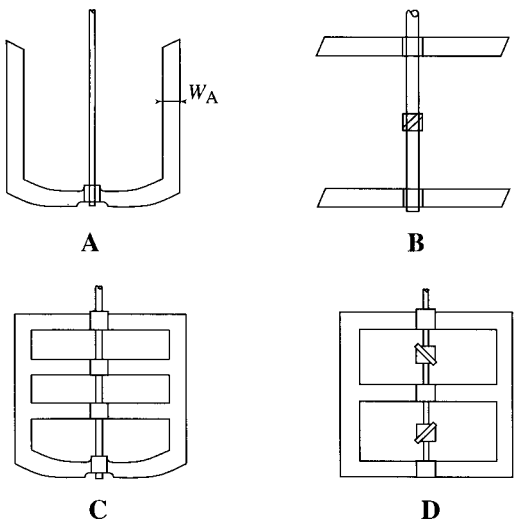


Figure 2.11 Wide radius stirrers: **A.** Simple anchor. **B.** Large inclined paddles (three blades at 90°). **C.** Reinforced anchor. **D.** Frame with large inclined paddles mounted perpendicular to the frame.

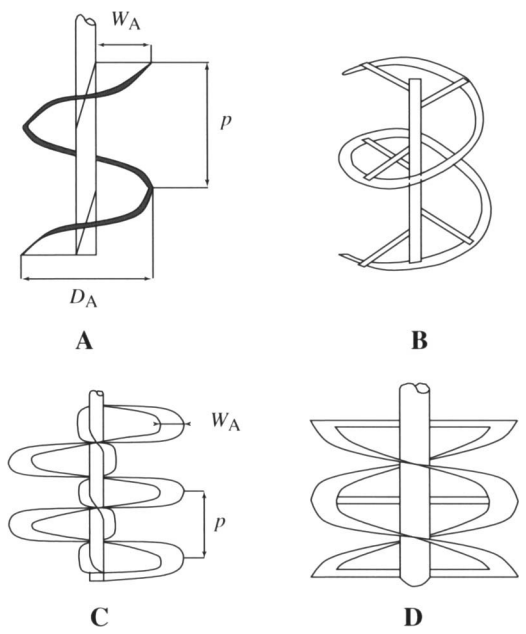


Figure 2.12 Archimedes screw type agitators: **A.** Simple Archimedes screw. **B.** Single helical ribbon. **C.**Single helical ribbon with screw (reversed pitch). **D.** Double helical ribbon (two ribbons with reverse pitch, 180°out of phase).

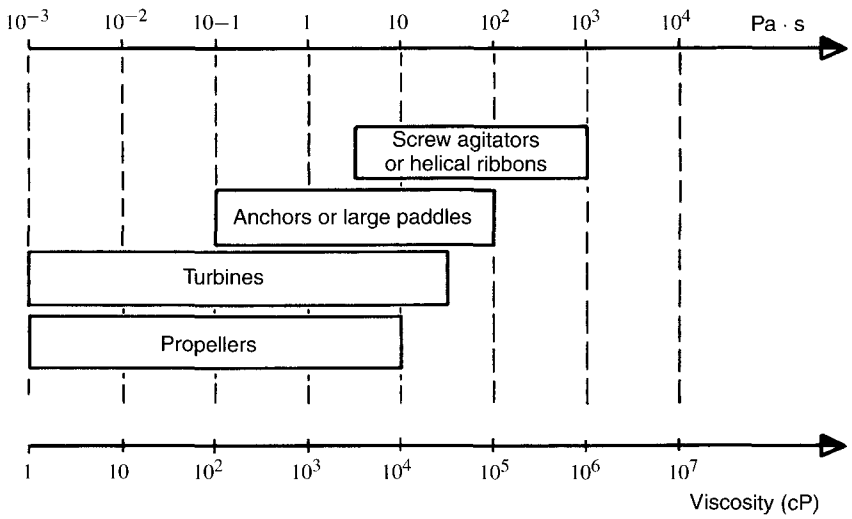


Figure 2.13 Viscosity range of use for various types of stirrers.

• Other types of impellers

There are a large variety of rotating stirrers. These include helical ribbons, Archimedes screws, discs, and turbines that can be hollow to some degree, etc. (Fig. 2.12), each of which is specific to a particular application.

The viscosity of the stirred fluid is often a key element in the choice of impeller. Figure 2.13 indicates the range of use for the various types of stirrer as a function of the viscosity of the fluid.

2.1.5.1 Power dissipated by an agitator

In the presence of a single liquid phase, the turbulence of the medium subjected to the action of a rotary stirrer is defined, as with other types of liquid flow, by means of the Reynolds number, which is the ratio of the inertial and viscous forces.

$$Re = \frac{\rho N_R D_A^2}{\mu} \tag{2.49}$$

where

N_R rotational speed of the impeller (s^{-1})
D_A characteristic diameter of the impeller (m)
ρ fluid density (kg/m^3)
μ fluid dynamic viscosity (Pa · s).

The hydrodynamic regimes found in practice are most often turbulent ($Re > 10\,000$), or laminar ($Re < 10$) when the fluid is especially viscous, and sometimes in the transition zone ($10 < Re < 10\,000$).

In general, the power dissipated by an impeller can be correlated with two dimensionless numbers characteristic of the system, namely the Reynolds number and the Froude number:

$$Fr = \frac{N_R^2 D_A}{g} \tag{2.50}$$

where g is the acceleration due to gravity (9.81 m/s^2).

The power P_A is then included in a third dimensionless number, the power number:

$$N_P = \frac{P_A}{\rho N_R^3 D_A^5} \quad \text{(or Newton number)} \tag{2.51}$$

These dimensionless numbers are related by an equation of the following type:

$$N_P = C(Re)^a (Fr)^b \tag{2.52}$$

or:

$$\Phi = \frac{N_P}{(Fr)^b} = C(Re)^a \tag{2.53}$$

Φ is generally referred to as the **power factor**.

In the case of a vessel provided with baffles or counterblades, in which a vortex cannot be formed, the influence of gravitational forces becomes negligible and the exponent b tends to 0. We then have: $\Phi = N_P$, a value that depends only on the Reynolds number. This case, which is the one most frequently encountered in practice, is discussed below. A graphical representation of Φ *versus* Re is shown in Fig. 2.14A. We distinguish three regions, depending on the value of the Reynolds number:

1. For low values of $Re(< 10)$, in the viscous or laminar domain, where Φ decreases as Re increases, $a = -1$ and, therefore, $N_P = C/Re$ (AB on the curve).
2. For Reynolds numbers comprised between 10 and 10^4, we observe a transition zone between the laminar and turbulent regimes. Note that, in the absence of baffles or counterblades, the vortex will occur when the Reynolds number is near 300 (point C).
3. For Reynolds numbers greater than 10^4 (DE on the curve), the turbulent regime is fully developed and the power number is practically invariant: $N_P \cong$ Cte.
   Note that sections C D′ E′ on the curve correspond to the transition and turbulent regimes observed when counterblades are not present.

Anchors and Archimedes screws, which are recommended for viscous or highly viscous liquids, operate within the range of Reynolds numbers below 10^3 (Fig. 2.14B). The power factors Φ vary significantly in this case, the exponent a of the Reynolds number in Eq. (2.52) often being in the range -0.5 to -1.0. The values of Φ, which vary between 1 and 100, are on the order of 1 for $Re = 10^3$.

In the literature, we often find curves similar to those shown in Fig. 2.14 for the various types of stirrer discussed above. With respect to these curves, we can make the following comments: the propellers and turbines used to mix liquids of relatively low viscosity generally operate in the turbulent domain ($Re > 10^4$). When there are baffles arranged near the vessel walls, the values for the power number generally show little variation:

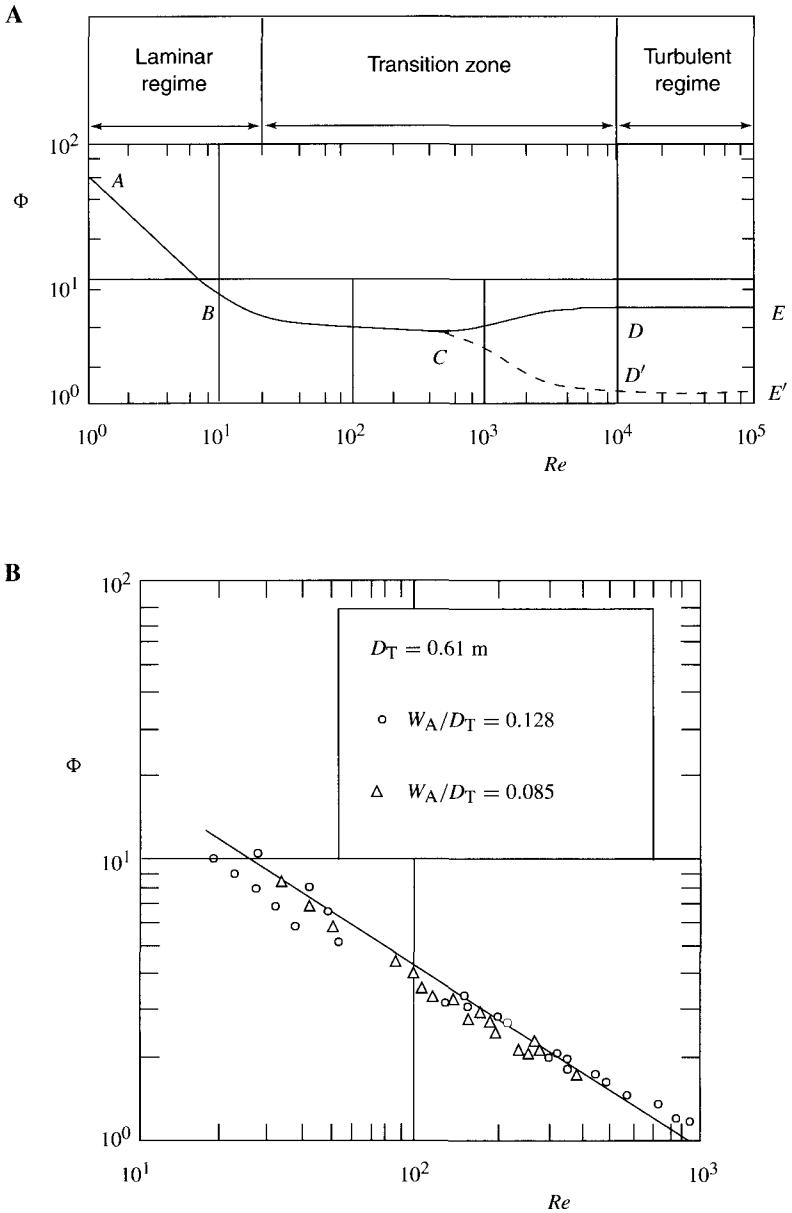


Figure 2.14 Variation of power factor as a function of the Reynolds number. **A.** Turbine with six-flat blades. **B.** Anchor.

- turbines: N_P is most often comprised between 1 and 6, and increases with the number of blades and their pitch.
- marine-type propellers and inclined blade turbines: N_P is comprised between 0.2 and 1.

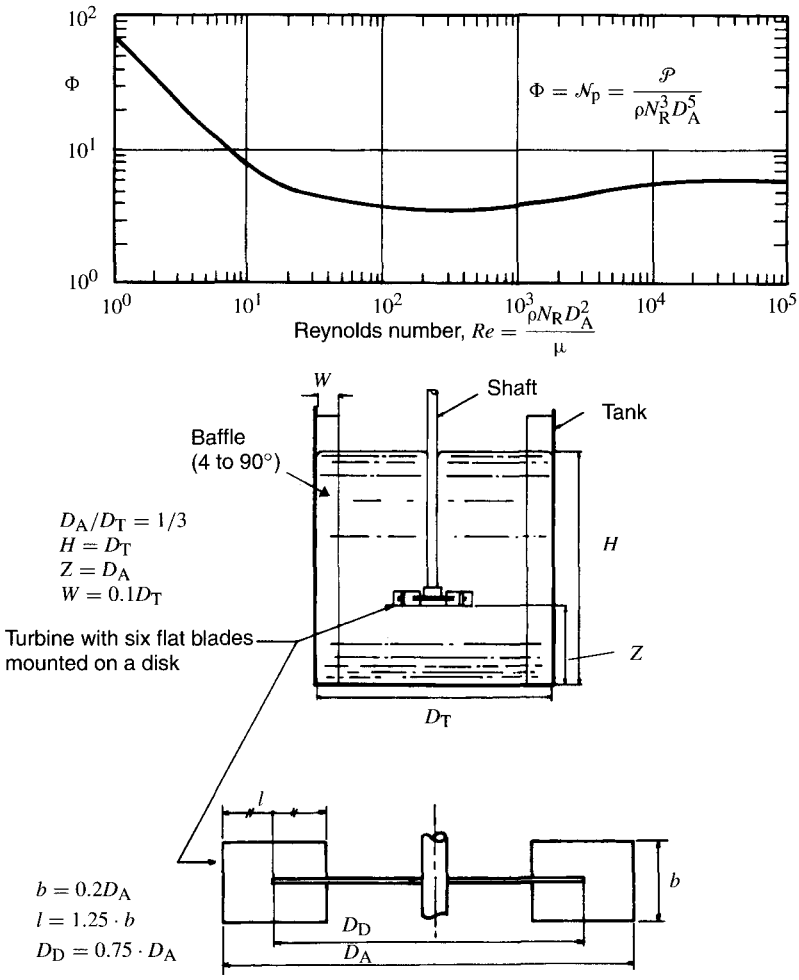


Figure 2.15 Variation of the power factor Φ for a turbine with six flat blades mounted on a disk, together with the definition of the corresponding system (standard configuration).

For example, Fig. 2.15 shows the variation in the power factor Φ for a turbine with six flat blades used under conditions that have been designated as the standard configuration. We see from the example the different geometric variables that have an influence on the behavior of the stirrer.

2.1.5.2 Heat transfer in stirred tanks

Heat transfer can occur either by using a wall of the tank as a heat exchange surface or by immersing a coil, or a bundle of tubes or plates into the vessel. To calculate enthalpy balances, we need to know the heat transfer coefficients, in particular, the transfer coefficient,

h_{int}, for the stirred fluid in the tank. The literature provides numerous correlations that can be used to calculate the transfer coefficient for a given system. In practice there are a large number of combinations between stirrer types and heat exchange surfaces. In general, the correlations are given in the dimensionless form, most frequently making use of the following dimensionless numbers:

$$\text{Nusselt number} \quad Nu_{\text{int}} = \frac{h_{\text{int}} D_{\text{T}}}{\lambda} \tag{2.54}$$

$$\text{Reynolds number} \quad Re = \frac{\rho N_{\text{R}} D_{\text{A}}^2}{\mu} \tag{2.55}$$

$$\text{Prandtl number} \quad \text{Pr} = \frac{C_{\text{PM}} \mu}{\lambda} \tag{2.56}$$

and the ratio of viscosities measured respectively at the wall temperature (T_w) and in the bulk of the fluid: vis $= \mu_w/\mu$.

Dimensional relations between certain elements characterizing the system can also play a role. In general, these correlations assume the following form:

$$Nu_{\text{int}} = K\,(Re)^a\,(Pr)^b\,(\text{vis})^c$$

In the majority of correlations the coefficients K, a, b, and c in the above equation are always close to the following values:

$$K = \text{between 0.1 and 1.0}$$
$$a = 0.5 \text{ to } 0.7$$
$$b = \text{close to } 0.3$$
$$c = -0.1 \text{ to } -0.2$$

Below we provide several examples of equations that describe the standard configuration described previously (Fig. 2.15):

• **Jacketed vessel** (Fig. 2.16A) [Dream, 1999]:

$$Nu_{\text{int}} = K\,(Re)^{0.67}\,(Pr)^{0.33}\,(\text{vis})^{-0.14} \tag{2.57}$$

where $K = 0.74$ for $Re > 400$ and $K = 0.54$ for $Re < 400$.

• **Immersed coil** (Fig. 2.16B):

$$Nu_{\text{int}} = 0.17\,(Re)^{0.67}\,(Pr)^{0.37}\,(\text{vis})^c \left(\frac{D_{\text{A}}}{D_{\text{T}}}\right)^{0.10} \left(\frac{D_c}{D_{\text{T}}}\right)^{0.50} \tag{2.58}$$

The exponent c varies as a function of the viscosity of the fluid at the operating temperature:

$$c = -0.97 \quad \text{for } \mu = 0.30 \text{ mPa} \cdot \text{s}$$
$$c = -0.18 \quad \text{for } \mu = 1\,000 \text{ mPa} \cdot \text{s}$$

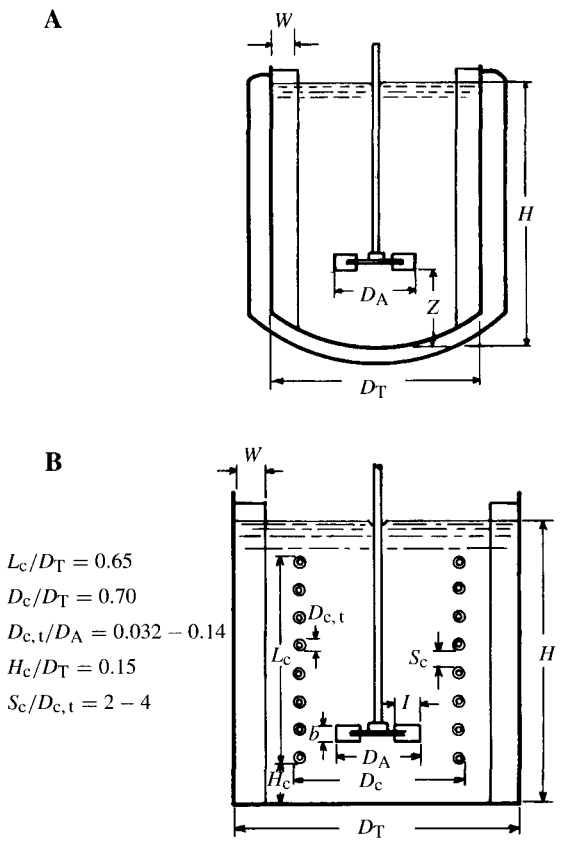


Figure 2.16 Tanks equipped for heat transfer: **A.** Jacket. **B.** Immersed coil.

• **Four-blade impeller with a 45° pitch and a jacketed vessel:**

The following equation is proposed [Dream, 1999]:

$$Nu_{int} = 0.42\,(Re)^{0.67}\,(Pr)^{0.25}\,(\text{vis})^{-0.14} \tag{2.59}$$

With respect to the **external heat transfer coefficient**, h_{ext}, some correlations exist [Dream, 1999] for calculating the corresponding Nusselt number:

$$Nu_{ext} = \frac{h_{ext} D_e}{\lambda} \tag{2.60}$$

D_e is the equivalent diameter defined for each case. It is also used to calculate the Reynolds number.

• **Simple jacketed vessel, operating in the turbulent regime:**

$$Nu_{ext} = 0.027(Re)^{0.8}(Pr)^{0.33}\left(1 + \frac{3.5D_e}{D_T + 0.5D_e}\right)\left(\frac{\mu_w}{\mu}\right)^{0.14} \tag{2.61}$$

where

D_e equivalent diameter $= [(D_{J,O})^2 - (D_{J,I})^2]/D_{J,I}$

$D_{J,O}$ diameter of the external wall of the jacket

$D_{J,I}$ diameter of the internal wall of the jacket.

The Reynolds number is calculated from the equivalent diameter D_e and the velocity in a cross-section equal to: $\pi\left[(D_{J,O}^2 - D_{J,I}^2)/4\right]$.

- **Spiral half-tube welded around the tank and operating in the turbulent regime:**

$$D_e\text{: equivalent diameter of the half-tube} = \frac{\pi d_{Co}}{2}$$

where d_{Co} is the internal diameter of the welded tube (m).

The cross-section used to calculate the Reynolds number is then equal to: $\pi d_{Co}^2/8$.

The Nusselt number is obtained from the following expression:

$$Nu = 0.027(Re)^{0.8}(Pr)^{0.33}\left(1 + \frac{3.5D_e}{D_T + 2e + 0.25d_{Co}}\right)\left(\frac{\mu}{\mu_w}\right)^{0.14} \tag{2.62}$$

where

e thickness of the tank wall (m)

D_T internal diameter of the tank (m).

When we consider the combined resistance to heat transfer (wall and films), the overall coefficient of heat transfer, U, in actual practice generally falls between 50 and 400 $W/m^2 \cdot K$. By convention thermal flux is calculated by taking the logarithmic mean of the temperature difference between the heat-transfer fluid and the fluid inside the tank. Additionally, when a stirred tank is being designed, we generally anticipate, as with any exchanger, a certain degradation of heat transfer due to fouling of the exchange surfaces.

When determining the most efficient impeller for heat transfer within a tank, we recommend the following:

- Large dimension impellers (anchors, helical ribbons) or those that result in intense circulation along the walls (propeller) provide the best performance for wall transfer.
- Impellers that create intense radial circulation (turbines or large blades) are preferable when using a coil.
- In those cases where tubes or heat exchangers are immersed, baffles are no longer essential with the impellers that generally require them (turbines, propellers, etc.), providing the exchange surfaces are properly designed.

2.1.6 Reactors involving gradual injection of part of the reactants and gradual elimination of a product

In certain cases it is sometimes advantageous not to introduce all the reactants at the start but rather to inject them gradually throughout the course of the operation. This results in what is sometimes referred to as semi-continuous operation, even though it retains all the principal characteristics of a batch operation.

2.1.6.1 Semi-Continuous reactor

The most typical and most frequently encountered case is that where one reactant is gradually injected throughout the course of the operation, the other reactants having been loaded at the beginning. Referring to the simple case of a reaction of type $A_1 + A_2 \rightarrow A_3$, we can diagram this type of operation as shown in Fig. 2.17.

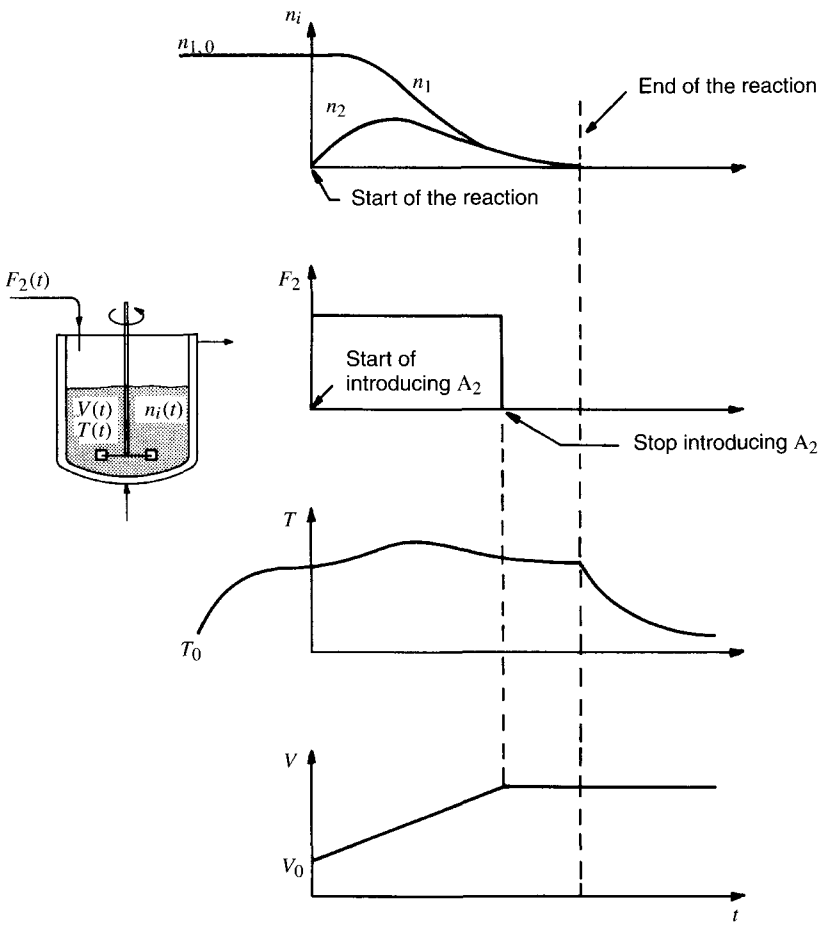


Figure 2.17 Operation of a semi-continuous reactor with gradual introduction of a reactant.

The mass balances with respect to A_1 and A_2 can be written as above, providing we replace $n_{2,0}$ with $n'_{2,0}$, which is a function of the injection rate, F_2, of reactant A_2. This gives:

$$n'_{2,0}(t) = n_{2,0} + \int_0^t F_2(t)\,\mathrm{d}t \tag{2.63}$$

F_2 being the rate of injection in kmol/s.

As a result the volume V of the reaction mixture also changes as follows:

$$V(t) = V_0 + \int_0^t V_{m,2} F_2(t)\, dt \tag{2.64}$$

$V_{m,2}$ being the molar volume of A_2 (m^3/kmol).

F_2 is not necessarily a continuous function of t but can, for example, represent a series of pulses of varying amplitude and duration.

The equation describing the change in the system:

$$\frac{d\xi}{dt} = \frac{k}{V}(n_{1,0} - \xi)(n'_{2,0} - \xi) \tag{2.65}$$

remains identical to the equation written previously, but (2.63) and (2.64) must be taken into account when it is integrated.

Semi-Continuous operation is especially useful in the following cases:

- A strongly exothermic reaction that is carried out in an apparatus with an insufficient heat exchange surface area. By regulating the injection of one of the reactants, the temperature can easily be controlled without any risk of a runaway reaction. This is the case, for example, with very fast exothermic reactions (neutralization of an acid with a base).
- A reaction whose selectivity decreases rapidly when the concentration of a reactant is too high. As an example, we examine the codimerization of propylene and butenes:

  $$C_3^= + C_4^= \rightarrow C_7^= \quad (j = 1)$$

  The reaction shown above, which is the one we want to perform, is accompanied by the two following competing reactions:

  $$C_3^= + C_3^= \rightarrow C_6^= \quad (j = 2)$$
  $$C_4^= + C_4^= \rightarrow C_8^= \quad (j = 3)$$

  Considering the rapidity with which the second reaction takes place ($k_2 = 50k_1 = 2\,500k_3$), to obtain maximum selectivity for heptenes ($C_7^=$), it is worthwhile keeping the concentration of propylene in the reaction mixture relatively low. We can then show that in this case, the maximum selectivity is obtained when there is a constant ratio between the concentrations of $C_3^=$ and $C_4^=$. We can accomplish this by gradually injecting propylene into the reactor, which has been fed with all the butenes at the start of the operation.

There are other situations, however, where it is advantageous to remove a constituent during the reaction. In this way we can reduce the limiting effect of thermodynamic equilibrium in the case of a reversible reaction or decrease the inhibitory effect of a product. One example is esterification, where the water formed can be removed by distillation (see Chapter 10 on multifunctional reactors).

2.1.6.2 Mixing time

An impeller is often used to homogenize a liquid phase. The homogenization is related to the circulation of the fluid caused by the impeller. The time needed to homogenize the tank, or mixing time t_M, can be measured experimentally. Its value depends on the characteristics of the medium (especially viscosity), the homogeneity criterion selected to characterize the end of the mixing and the size of the vessel. It varies from a few seconds in the case of small laboratory reactors to several minutes for industrial equipment.

For a batch reactor, the mixing time matters little since the mixing operation takes place at the beginning of the operation when the reactants are loaded and, therefore, under conditions when the reaction rate is still low. For a semi-continuous reactor, on the contrary, the mixing time is important throughout the duration of the operation, since the reaction is generally rapid.

In the case of consecutive or competing reactions, the selectivity of a specific product is often dependent on the rate of micromixing. For fast reactions, the mixing time will assume considerable importance and should be low compared to the reaction time.

There are few general correlations that enable us to estimate mixing time. For Rushton and inclined blade turbines, Rewatkar and Joshi [1991] suggest the following:

$$t_M = \frac{5.37}{N_R} A^{-0.87} \left(\frac{W}{D_A}\right)^{-0.314} n_P^{-0.842} \left(\frac{D_T}{D_A}\right)^{1.83} \left(\frac{C}{D_T}\right)^{-0.27} \left(\frac{H}{D_T}\right)^{0.413} \tag{2.66}$$

where

C distance between the blade and the bottom (m)

A angle of the plane of the blade (rad).

and where the following limitations hold:

$$0.57 \text{ m} < D_T < 1.5 \text{ m}, \qquad \frac{1}{6} < \left(\frac{D_A}{D_T}\right) < \frac{1}{2},$$

$$\frac{\pi}{6} < A < \frac{\pi}{3}, \qquad 4 < n_P < 8,$$

$$\frac{1}{8} < \left(\frac{C}{D_T}\right) < \frac{3}{4}, \qquad \frac{1}{4} \leqslant \left(\frac{W}{D}\right) \leqslant \frac{1}{3},$$

$$\frac{2}{3} \leqslant \left(\frac{H}{D_T}\right) \leqslant 1$$

Since the mixing time is always inversely proportional to the rotational speed of the impeller, there are specific correlations that link the group $N_R t_M$ to the characteristic variables of particular systems:

- In the turbulent regime, $N_R t_M$ is nearly constant for a given system. Depending on the geometry, this constant can be expressed simply by means of equations of the following type:

$$N_R t_M \cong a \left(\frac{D_T}{D_A}\right)^b \tag{2.67}$$

where:

$$N_R t_M \cong 6(D_T/D_A)^2 \quad \text{for propellers,}$$
$$N_R t_M \cong 4(D_T/D_A)^2 \quad \text{for turbines.}$$

- In the laminar regime, $N_R t_M$ remains appreciably constant for a given system, ranging from 40 to 150 for helical ribbon or screw type impellers, and anchors stirrers:

$$N_R t_M \cong 70 \quad \text{for helical screws,}$$
$$N_R t_M \cong 50 \quad \text{for helical ribbons.}$$

On the other hand, the mixing time is related to the pumping flow rate through the impeller:

$$t_M \approx \frac{V}{Q_P} \tag{2.68}$$

The pumping flow rate, Q_P, depends on the diameter, the speed of rotation, and the type of stirrer used. Every stirrer can be characterized by a "pumping number", N_Q:

$$N_Q = \frac{Q_P}{N_R D_A^3} \quad \text{or} \quad Q_P = N_Q N_R D_A^3 \tag{2.69}$$

In the turbulent regime range, the pumping number varies only slightly. For a vessel with baffles, the following values can be used as a first approximation:

- N_Q ranges from 0.5 to 1.0 for propellers
- N_Q ranges from 0.6 to 0.9 for straight or inclined blade turbines.

Table 2.5 provides values of power numbers and pumping numbers for several standard impellers.

Table 2.5 Power number and pumping number.

Agitator	N_P	N_Q
Rushton turbine	4.3 to 6	0.75 to 0.84
Turbine with four 25° inclined blades	0.51	0.47
Turbine with six 45° inclined blades	1.7	0.83
Propeller	0.30 to 0.35	0.52 to 0.56
Multiple flat inclined paddles	0.65	0.73

Since the pumping flow rate causes a complementary induced liquid flow rate in the vessel, there is an overall total recirculation rate, Q_C, the sum of the direct pumping rate and the induced flow rate. The induced flow rate is only slightly lower than the pumping flow rate, so that:

$$Q_C \cong 2Q_P \tag{2.70}$$

We can define a recirculation time based on the recirculation flow rate. It corresponds to the average time taken by a fluid element to make a complete circuit around the tank. The circulation time is four to five times lower than the mixing time.

In the case of very fast reactions, where the selectivity is essential, the performance of rotary impellers may be inadequate. The reason is that selectivity depends on micromixing, which takes place locally at the point where the reactants are introduced and which must be as rapid and complete as possible. In this case, inline mixing, within a circulation loop around a stirred tank, can be used to provide better performance.

2.1.7 Conclusion

Before concluding our examination of batch reactors, we would like to draw the reader's attention to two characteristics that are often critical in practice:

- These reactors are designed so that a single reactor can be used for a variety of purposes. This flexibility is especially useful whenever a large number of different products need to be produced in relatively small quantities (in the pharmaceutical industry, for example).
- The relatively low utilization factor for this type of device. By utilization factor, we refer to the ratio between the time during which the reaction effectively takes place (t_3) and the total time required to complete the operation ($t_1 + t_2 + t_3 + t_4 + t_5 + t_6$).

We should also point out that the recovery of calories through heat exchange between the effluent and the feedstock is difficult to carry out in practice due to the time lag between loading and discharge. This explains why batch reactors are used primarily for low tonnage operations, unless other factors strongly influencing the economy of the process dictate an alternate choice.

2.2 CONTINUOUS TUBULAR REACTORS

As indicated earlier, in its most basic form, the tubular reactor consists of a tube inside which the reaction medium flows. This is the simplest conceivable arrangement for a continuous system. The heat exchange, which is necessary either to provide calories to the system or to remove them, generally occurs through the walls of the tube. A typical device is shown in Fig. 2.18.

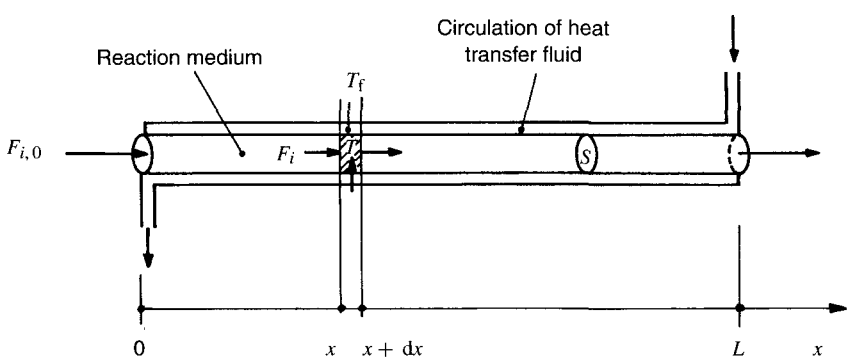


Figure 2.18 Continuous tubular reactor.

2.2.1 Mass and energy balances

We assume that a chemical transformation, symbolized by $\sum \nu_i A_i = 0$, takes place within the fluid flowing in the tubular reactor shown schematically in Fig. 2.18. The position of a volume element of the reaction fluid within the reactor can be identified by means of the distance x from the tube inlet.

We consider a fluid element of volume dV, delimited by two tube cross-sections, at distances x and $x + dx$ respectively from the tube inlet ($x = 0$). Molar and energy balances around this elementary volume can be calculated by assuming that a steady-state condition has been established.

Molar balance for a compound A_i:

$$(F_i)_x - (F_i)_{x+dx} + \mathcal{R}_i \, dV = 0 \quad (i = 1, S) \tag{2.71}$$

Overall energy balance:

$$\left(\sum F_i \bar{h}_i\right)_x - \left(\sum F_i \bar{h}_i\right)_{x+dx} + q \, dV = 0 \tag{2.72}$$

We also know that:

$$\Delta V = S \, dx$$

where S is the tube cross-section.

If all the terms of Eqs. (2.71) and (2.72) are divided by dx and let dx tend toward 0, the above equations become:

$$\frac{dF_i}{dx} - \mathcal{R}_i S = 0 \tag{2.73}$$

$$\sum \left(\frac{dF_i \bar{h}_i}{dx}\right) - qS = 0 \tag{2.74}$$

Here, qS is the heat transferred per unit of time and unit of tube length.

We saw in Chapter 1 that for a continuous system the extent of reaction of various reactions j could be defined by means of the variable ξ'_j. Thus:

$$F_i = F_{i,0} + \sum \nu_{i,j} \xi'_j \tag{2.75}$$

And since:

$$\mathcal{R}_i = \Sigma \nu_{i,j} r_j$$

Eq. (2.73) can be rewritten as follows:

$$\frac{d\xi'_j}{dx} = r_j S \quad (j = 1, R) \tag{2.76}$$

We rewrite Eq. (2.74) by developing the first term to obtain:

$$\sum_i \left(F_i C_{Pi} \frac{dT}{dx}\right) + \sum_j \left(\Delta H_j \frac{d\xi'_j}{dx}\right) - qS = 0 \tag{2.77}$$

The R Eqs. (2.76) and Eq. (2.77) can then be integrated simultaneously, taking into account the boundary conditions for $x = 0$:

$$F_i = F_{i,0} \quad \text{therefore} \quad \xi_j' = 0 \quad (j = 1, R) \quad \text{and} \quad T = T_0$$

Integrating (2.77) requires knowledge of the transfer term q. This variable corresponds to the energy supplied to the reaction fluid calculated per unit of volume. This energy transfer occurs upon contact with the wall in the form of exchanged heat. We can therefore write:

$$q = \pi d_T \frac{h_{int}}{S}(T_{int} - T) = \frac{4}{d_T} h_{int}(T_{int} - T) \tag{2.78}$$

where

d_T interior diameter of the tube
h_{int} heat transfer coefficient inside the tube
T_{int} temperature of the inside tube wall
T average temperature in the tube.

If the exchange of heat occurs through external circulation of a heat-transfer fluid whose temperature is locally T_f, Eq. (2.78) can then be written:

$$q = \frac{\pi d_T}{S} U(T_f - T) \tag{2.79}$$

where U is the overall coefficient of heat transfer, encompassing the various transfer resistances.

If the flow rate of the heat-transfer fluid is sufficiently high, we can, as a first approximation, assume that T_f is constant. If this is not the case, a new differential equation must be written reflecting the heat balance relative to the heat-transfer fluid:

$$Q_f \rho_f C_f \frac{dT_f}{dx} \pm qS = 0 \tag{2.80}$$

where

Q_f volume flow rate of the heat-transfer fluid (m^3/s)
ρ_f density of the heat-transfer fluid (kg/m^3)
C_f mass heat capacity (J/kg).

In Eq. (2.80), the sign refers to the direction of flow of the heat-transfer fluid and reaction fluid: minus for countercurrent flow, plus for cocurrent flow. The boundary condition for integrating (2.80) is obviously chosen on this basis:

$$T_s = T_{f0} \quad \text{for } x = 0 \text{ in cocurrent flow}$$
$$T_f = T_{fL} \quad \text{for } x = L \text{ in countercurrent flow}$$

Note that the way Eqs. (2.71) and (2.72) are written implies the following important assumption: the values $\mathcal{R}_i$ and $\bar{h}_i$ depend only on x and are invariant within a given cross-section of tube, regardless of the radial position. This assumption corresponds to the ideal model retained, namely the **plug-flow model**. By using this flow model, we assume that all the fluid elements have the same linear velocity when they pass through a given cross-section.

In writing Eqs. (2.71) and (2.72), we did not include terms for mass and energy exchange between successive fluid slices apart from those related to forced convection. This corresponds to **plug flow without backmixing**.

2.2.2 Solutions for a few simple cases

Referring to Eq. (2.77), the implications for certain specific situations become immediately obvious:

- isothermal reactor: $dT/dx = 0$.
  In this case only Eqs. (2.76) need to be integrated, the temperature variable being fixed.
- adiabatic reactor: $q = 0$.
  There is a one-to-one correspondence between the variables T and ξ'_j.

We now consider the case of a simple transformation, $\sum \nu_i A_i = 0$, that takes place in a tubular reactor under isothermal conditions. Equation (2.76) can now be written:

$$\frac{d\xi'}{dx} = rS \tag{2.81}$$

The rate term r can be replaced by its expression as a function of the concentrations of compounds A_i.

If we assume that the reaction is first order: $r = kC_1$,

$$C_1 = \frac{F_1}{Q} = \frac{F_{1,0} + \nu_1 \xi'}{Q}$$

Equation (2.81) then becomes:

$$\frac{d\xi'}{F_{1,0} + \nu_1 \xi'} = k\frac{S\,dx}{Q} \tag{2.82}$$

In the case of a system in which changes in volume can be ignored (an isochorous system), Eq. (2.82) can be easily integrated to give:

$$\xi' = \frac{F_{1,0}}{\nu_1}\left[\exp\left(\frac{\nu_1 kSx}{Q}\right) - 1\right] \tag{2.83}$$

Sx is the volume of the reactor needed to obtain an extent of reaction ξ'.
Sx/Q is the mean residence time (θ) of the reaction medium in the reactor for a distance x.

Equation (2.83) can then be used to express the molar flow rates of the various compounds A_i at the reactor outlet as a function of residence time (θ) alone. In this case, for the reaction $A_1 \rightarrow A_2$, Eq. (2.83) leads to:

$$\frac{F_1}{F_{1,0}} = \exp(-k\theta) \tag{2.84}$$

This equation is similar to the one obtained for a batch reactor:

$$\frac{n_1}{n_{1,0}} = \exp(-kt)$$

It follows that conversion of reactant A_1 can be expressed identically, that is:

$$X_1 = \frac{n_{1,0} - n_1}{n_{1,0}} = 1 - \exp(-kt) \quad \text{for the batch reactor}$$

$$X_1 = \frac{F_{1,0} - F_1}{F_{1,0}} = 1 - \exp(-k\theta) \quad \text{for the continuous tubular reactor.}$$

We see that only the reaction time t has been replaced by the residence time θ.

What we have found to apply to first-order reactions can in fact be generalized, and all the equations obtained for various reactions that take place in a batch reactor are directly applicable to a tubular reactor. We simply need to replace t by θ in these equations.

This correspondence between the performance of the two reactor types is readily understandable if we treat a volume element ΔV of the tubular reactor as a batch microreactor moving in space: It enters the tube at time $t = 0$ and leaves at time $t = \theta$. This identical performance, which manifested itself in the case of isothermal operation, can be generalized to the extent that changes in temperature are identical, that is, every time $T(\theta) = T(t)$ holds true. This is particularly the case for adiabatic operation.

Since tubular reactors are well suited for gas-phase reactions, the assumption of an isochorous system is not always valid. In this case an equation of state applicable to the gas mixture must be used in addition to the molar balances. As an example, we resume the simple case considered above: a first-order reaction characterized by the stoichiometric equation $\sum \nu_i A_i = 0$, where $\sum \nu_i = \bar{\nu} \neq 0$. We also assume that the ideal gas law can be used.

Equation (2.82) remains valid, but, since Q is now variable, it must be expressed as a function of ξ'.

The volumetric flow rate Q corresponds to the molar flow rates F_i, with inert species also accounted for. We can then write:

$$Q = \left(\sum F_i\right) \frac{RT}{P} \tag{2.85}$$

We also know that:

$$\sum F_i = \sum F_{i,0} + \sum \nu_i \xi' \tag{2.86}$$

Equation (2.82) then becomes:

$$\frac{(F_0 + \bar{\nu}\xi')}{(F_{i,0} + \nu_1 \xi')} = \frac{kSP}{RT}\,\mathrm{d}x \tag{2.87}$$

Assuming that the change in the system occurs isothermally, and that the pressure variations along the tube are negligible, we can integrate (2.87), obtaining:

$$\frac{1}{\nu_1}\left(F_0 - \frac{\bar{\nu}}{\nu_1} F_{1,0}\right) \ln\left[\frac{F_{1,0} + \nu_1 \xi'}{F_{1,0}}\right] + \frac{\bar{\nu}}{\nu_1}\xi' = \frac{kSP}{RT}x \tag{2.88}$$

For the general case, Eq. (2.87) must be integrated along with an equation derived from (2.77), which represents the energy balance:

$$\sum F_i C_{Pi} \frac{\mathrm{d}T}{\mathrm{d}x} + \Delta H_R \frac{\mathrm{d}\xi'}{\mathrm{d}x} - qS = 0 \tag{2.89}$$

and an equation representing the pressure drop due to fluid flow, which has the following form:

$$\frac{dP}{dx} = -f\frac{\bar{u}^2\rho}{d_T} \tag{2.90}$$

where f is the friction factor, which is dependent on the Reynolds number and the relative roughness of the tube, and $\bar{u} = Q/S$ is the mean velocity inside a tube of diameter d_T.

In designing a new reactor, the desired performance we want to obtain is fixed. Most often the degree of conversion of one of the main reactants will be selected as the objective. The above equations enable us to determine the mean residence time θ_L or the reactor volume $S \cdot L$ needed to bring about the desired conversion. Bear in mind, however, that these equations cannot be used to calculate S or L separately. The assumptions made in writing these equations are needed to proceed further, as shown in the following section.

2.2.3 Influence of backmixing

Until now we have considered the plug-flow tubular reactor, which is often referred to as an ideal tubular reactor. It is important, however, to compare this ideal model with real-world applications to determine its range of applicability in practice.

Whenever a fluid flows in a tube, two flow regimes can be distinguished:

- laminar flow, characterized by a Reynolds number:

$$\left(Re = \frac{\bar{u}d_T\rho}{\mu}\right) < 2\,000$$

- turbulent flow, observed for $Re \geqslant 4\,000$.

The two flow regimes differ, especially in the radial profile of the linear velocities of the fluid elements, which is established within the tube. Figure 2.19 illustrates the velocity profiles for the two types of flow regimes, together with the velocity profile for an ideal tubular reactor.

For laminar flow, the linear velocity profile is parabolic. In other words, the linear velocity of a fluid element situated a distance r from the axis of the tube can be expressed as follows:

$$u(r) = 2\bar{u}\left[1 - \left(\frac{2r}{d_T}\right)^2\right] \tag{2.91}$$

For turbulent flow, the linear velocity profile is relatively flat throughout the majority of the tube cross-section, with low amplitude fluctuations resulting from turbulence in the flow stream. Referring again to Fig. 2.19, we see that turbulent flow most closely resembles plug flow, which we retained as our model. The similarity increases with turbulence and the velocity profile tends to become increasingly flat as the Reynolds number increases.

Another way of characterizing the various types of flow is by the residence time distribution, which is obtained for each of the regimes. Figure 2.20 represents the response to a concentration pulse for each flow type, illustrating the similarity between the turbulent regime and plug flow.

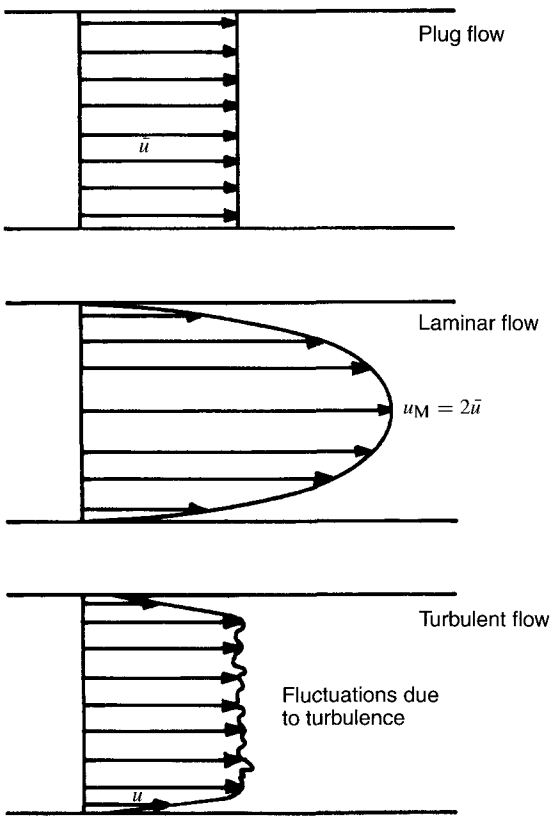


Figure 2.19 Velocity profiles for various flow regimes inside a tube.

We can develop a quantitative correlation between these two types of flow by treating turbulent flow as the combination of plug flow, with the same mean velocity, and diffusion in the axial direction, which we assume to be governed by Fick's law. The axial, or longitudinal, diffusion coefficient, $\mathcal{D}_A$, itself depends on flow conditions and, in particular, on the Reynolds number. Thus, for an element of volume $\Delta V = S\Delta x$ of a tube, in which such a flow occurs in the absence of any chemical reaction, the molar balance relative to a compound A_i, can be written:

$$(F_i)_x - (F_i)_{x+\Delta x} - \mathcal{D}_A S\left(\frac{\partial C_i}{\partial x}\right)_x + \mathcal{D}_A S\left(\frac{\partial C_i}{\partial x}\right)_{x+\Delta x} = \left(\frac{\partial C_i}{\partial t}\right)_x S\Delta x \tag{2.92}$$

Dividing by $S\Delta x$ and allowing Δx to tend toward 0, the above equation becomes:

$$-\frac{Q}{S}\frac{\partial C_i}{\partial x} + \mathcal{D}_A \frac{\partial^2 C_i}{\partial x^2} = \frac{\partial C_i}{\partial t} \tag{2.93}$$

If we integrate this equation, using boundary conditions corresponding to the injection of a pulse of compound A_i at time $t = 0$ and for $x = 0$, with $C_i = 0$ for all values of x, we

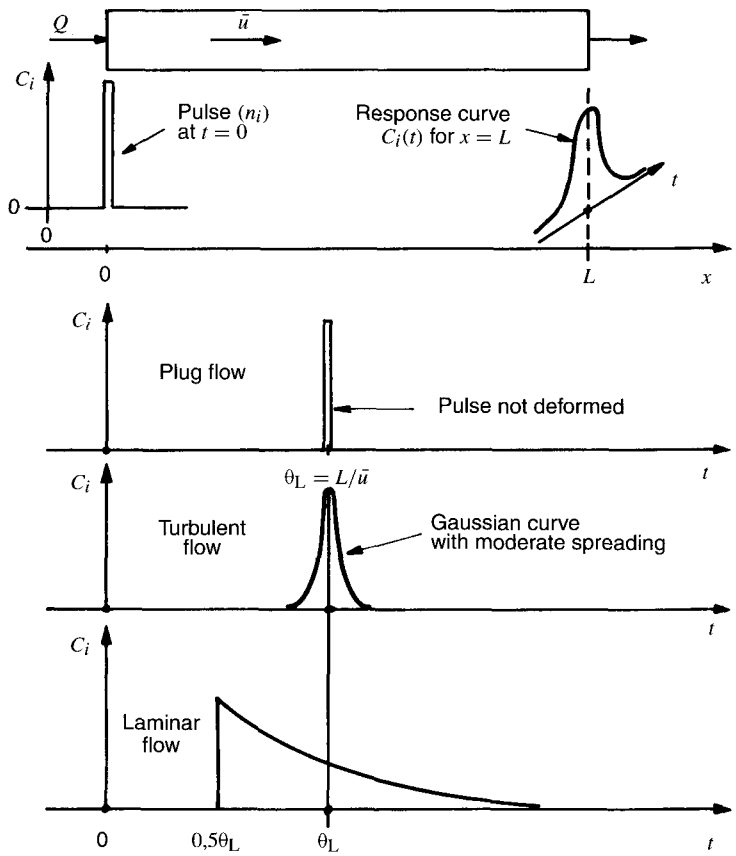


Figure 2.20 Comparison of residence time distribution curves for various flow regimes inside a tube.

obtain the residence time distribution function (Fig. 2.20). For relatively low values of $\mathcal{D}_A$, the solution of (2.93) can be written:

$$\left(\frac{C_i(t)}{C_0}\right)_{x=L} = \frac{1}{2\sqrt{\pi \dfrac{\mathcal{D}_A}{\bar{u}L}}} \exp\left[-\frac{\left(1-\dfrac{t}{\theta_L}\right)^2}{4\dfrac{\mathcal{D}_A}{\bar{u}L}}\right] \tag{2.94}$$

C_0 is defined as the reference concentration (see Chapter 1) corresponding to the injection of tracer A_i:

$$C_0 = \frac{n_i}{V}$$

where

n_i number of moles of A_i injected as a pulse

V reactor volume $= SL$.

A representation of this expression leads to a Gaussian curve with a maximum occurring at $t = \theta_L = SL/Q$. The variance is expressed as follows:

$$\sigma^2 = 2\frac{\mathcal{D}_A}{\bar{u}L} \tag{2.95}$$

The number $\mathcal{D}_A/\bar{u}L$, which is characteristic of the axial dispersion, is the product of two terms:

$$\frac{\mathcal{D}_A}{\bar{u}L} = \left(\frac{\mathcal{D}_A}{\bar{u}d_T}\right)\left(\frac{d_T}{L}\right) = \text{(dispersion intensity)(geometric factor)}$$

The dimensionless number $\bar{u}d_T/\mathcal{D}_A$ is commonly known as the axial Peclet number (Pe_A).

By comparing experimental measurements made with tracers against the solutions of Eq. (2.93), such as Eq. (2.94), it is possible to associate the dimensionless parameter $\mathcal{D}_A/(\bar{u}d_T)$ with flow conditions and, in particular, to determine its dependence on the Reynolds number, $Re = \bar{u}d_T\rho/\mu$. Results from the literature were used to draw the curves in Fig. 2.21. The curves show the considerable difference in dispersion that exists between laminar and turbulent flow regimes.

In the turbulent regime, the dependence of the parameter $\mathcal{D}_A/\bar{u}d_T$ on the Reynolds number can be expressed as follows:

$$\frac{\mathcal{D}_A}{\bar{u}d_T} = \frac{3 \cdot 10^7}{(Re)^{2.1}} + \frac{1.35}{(Re)^{0.125}} \tag{2.96}$$

The values of $\mathcal{D}_A/\bar{u}d_T$ based on the curves in Fig. 2.21 correspond to a straight tube. Corrections for these values can be provided to account for elbows or U-bends, which are commonly used in industry to join straight sections of tube. The corrective multiplication factor applied to $\mathcal{D}_A/\bar{u}d_T$ can be estimated as follows:

$$\text{Corrective factor: } 1 + \frac{2\mathcal{N}_C \cdot l_{eq}}{L}$$

where

$\mathcal{N}_C$ total number of bends for a length L of tube.

l_{eq} equivalent length of the bend used to calculate the pressure drop ($l_{eq} = 30d_T$ for a 90° elbow, $l_{eq} = 50d_T$ for a 180° U-bend).

Note that Eq. (2.94) is an accurate representation of the residence time distribution once $(\mathcal{D}_A/\bar{u}L) < 10^{-2}$. This condition is easily realized for $Re > 10^4$ and $L/d_T > 50$, as shown in Fig. 2.21.

We now consider the case of fluid flow accompanied by a chemical reaction. The molar balance relative to a compound A_i under steady state conditions is written by modifying Eq. (2.92). The left side of the equation remains unchanged while the right side will be replaced by a term expressing the chemical kinetics.

$$(F_i)_x - (F_i)_{x+\Delta x} - \mathcal{D}_A S\left(\frac{dC_i}{dx}\right)_x + \mathcal{D}_A S\left(\frac{dC_i}{dx}\right)_{x+\Delta x} = -\mathcal{R}_i S\Delta x \tag{2.97}$$

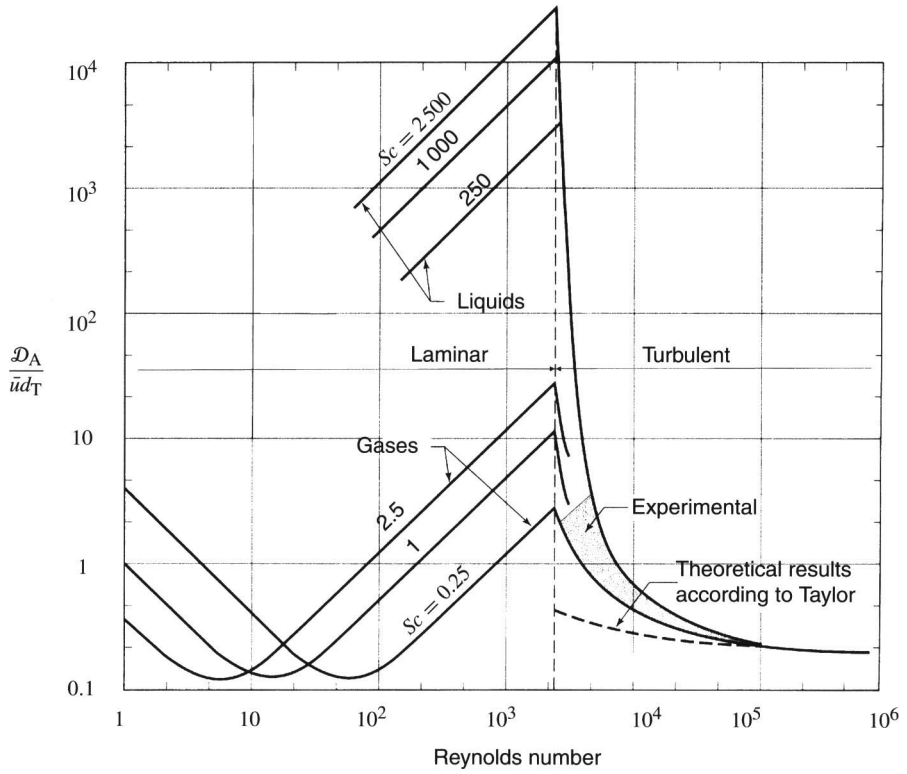


Figure 2.21 Dependence of $\mathcal{D}_A/\bar{u}d_T$, characterizing axial dispersion, on the Reynolds number [based on Levenspiel, 1999].

By allowing $\Delta x \to 0$ and neglecting changes in volume (Q is constant), the above equation becomes:

$$\frac{S\mathcal{D}_A}{Q}\frac{d^2C_i}{dx^2} - \frac{dC_i}{dx} + \frac{S}{Q}\mathcal{R}_i = 0 \tag{2.98}$$

This equation can be integrated once we have clarified the kinetic term $\mathcal{R}_i$ and introduced the appropriate boundary conditions, namely:

$$\text{for } x = 0 \qquad C_{i,0} = (C_i)_{x=0} - \frac{\mathcal{D}_A S}{Q}\left(\frac{dC_i}{dx}\right)_{x=0}$$

$$\text{for } x \to \infty \qquad C_i = 0$$

In the case of a simple first-order reaction ($A_1 \to A_2$), we have: $\mathcal{R}_i = -kC_1$ and Eq. (2.98) can be integrated analytically. The solution is written:

$$\frac{C_{1,L}}{C_{1,0}} = \frac{4\alpha \exp\left(\dfrac{\bar{u}L}{2\mathcal{D}_A}\right)}{(1+\alpha)^2 \exp\left(\alpha\dfrac{\bar{u}L}{2\mathcal{D}_A}\right) - (1-\alpha)^2 \exp\left(-\alpha\dfrac{\bar{u}L}{2\mathcal{D}_A}\right)} \tag{2.99}$$

Previous Page
Copyrighted Materials
Copyright © 2004 Editions Technip Retrieved from www.knovel.com

where:

$$\alpha = \sqrt{1 + 4k\theta_L \frac{\mathcal{D}_A}{\bar{u}L}} \tag{2.100}$$

Sets of curves can be plotted to represent $C_{1,L}/C_{1,0}$, or the conversion, as a function of the two dimensionless parameters $k\theta_L$ and $\mathcal{D}_A/\bar{u}L$. It should be obvious that for specific cases, we can always rewrite the molar balances in a form similar to Eq. (2.97) and perform the integrations numerically.

In the case of an ideal tubular reactor, the ratio of concentrations is expressed simply on the basis of (2.84):

$$\frac{C_{1,L}}{C_{1,0}} = \exp(-k\theta_L) \tag{2.101}$$

If we compare Eqs. (2.101) and (2.99) for low values of $\mathcal{D}_A/\bar{u}L$, identical conversions can be calculated from the two expressions by introducing a value θ_{id} in (2.101). A comparison of Eqs. (2.101) and (2.99) yields the following equation:

$$\theta_{id} = \frac{\theta_L}{1 + k\theta_L \frac{\mathcal{D}_A}{\bar{u}L}} \tag{2.102}$$

Similarly, if we take the residence times to be equal ($\theta_L = \theta_{id}$), using (2.99) and (2.101), we can calculate the corresponding values for C_1 as follows:

$$C_1 = (C_1)_{id}\left[1 + (k\theta_L)^2 \frac{\mathcal{D}_A}{\bar{u}L}\right] \tag{2.103}$$

Equations (2.102) and (2.103) indicate that the performance of a real tubular reactor may be similar in practice to that of an ideal reactor. For the difference between them to be less than 1%, it is sufficient that $\mathcal{D}_A/\bar{u}L$ be less than 10^{-2}, which is, as we saw above, easy to realize,

To generalize our conclusion, we propose to calculate the performance of a tubular reactor by using the ideal model. The tube dimensions simply need to be chosen so that the value of $\mathcal{D}_A/\bar{u}L$ is as low as possible. For example, we can use the following inequalities as constraints:

$$Re > 10^4 \quad \text{and} \quad L/d_T > 10^2 \tag{2.104}$$

2.2.4 Available technologies

As we saw earlier, the reactor consists of a tube in which the reaction medium flows. Heat exchange, either to add or remove calories from the system, takes place through the tube walls. Depending on the temperature of the reaction, several fairly distinct technologies are available:

- At moderate temperature (< 500°C) the system consists of concentric tubes with circulation of a heat-transfer fluid between the tubes as shown in Fig. 2.22. The fluid can be water, steam, an organic fluid, molten salt.

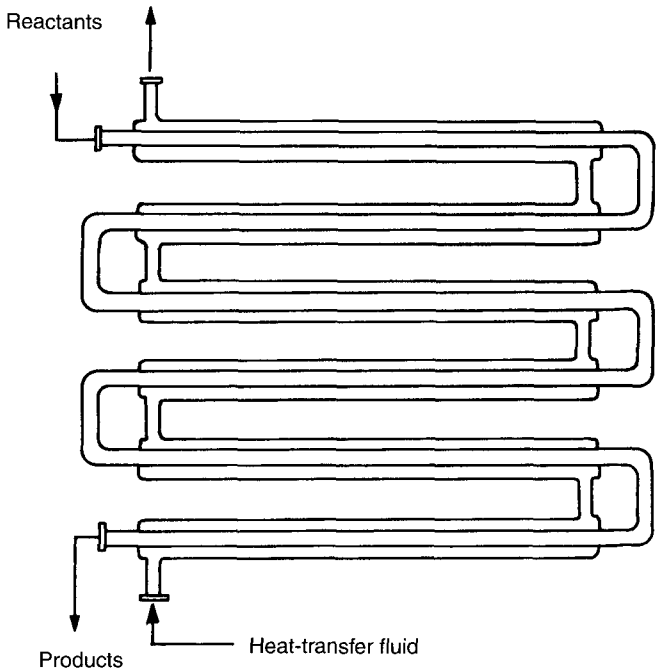


Figure 2.22 Tubular reactor with concentric tubes.

- At high temperature (> 500°C) the tube is placed in a furnace, heated by means of gas or fuel burners. In this case the tube is located in the radiation or convection zone (Fig. 2.23) and generally assumes the shape of a series of hairpin loops with straight lengths normally 6 to 10 m in length.

Typical examples of processes embodying these two technologies include the polymerization of ethylene and steam cracking of petroleum fractions to obtain olefins. Obviously such a reactor can be made to work adiabatically by insulating the outside of the tube.

As discussed earlier, the volume of the reactor is obtained from the molar and energy balances. To calculate the diameter and length, we must incorporate our assumption of plug flow by using the constraints given in (2.104). For example, in a steam cracking furnace, with an inside tube diameter close to 7 cm, the Reynolds number is greater than 10^6, while the residence time is less than one second. We see from this that the tubular reactor is well suited to fast reactions, especially in the gas phase.

In terms of practical implementation, if large reaction volumes are needed, the dimensions of the tube assume greater importance. For example, if a volume of 50 m^3 and significant residence time (one hour or more) are required, the tube will be on the order of 100 m with a diameter of approximately 80 cm. The costs of building such a reactor are relatively high, so it might be worthwhile using a tube with a larger diameter, providing it is filled with packing to ensure plug-type flow.

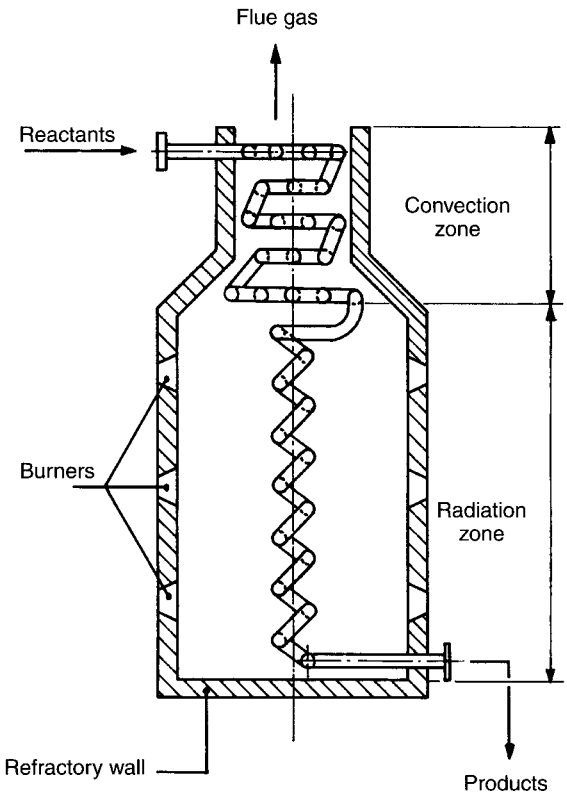


Figure 2.23 Tubular furnace for high-temperature reactions.

When a fluid flows through packing, the corresponding value of $\mathcal{D}_A/u_i d_p$ remains appreciably constant even with very large changes in the Reynolds number (u_i being the interstitial velocity $= \bar{u}/\varepsilon_F$, where ε_F is the volume fraction occupied by the fluid). For a liquid $\mathcal{D}_A/u_i d_p$ is close to 2, while for a gas, we obtain values less than 1. Since we can choose packing with a high void fraction ε_F (0.8 for example) and with nominal dimensions such that L/d_p is on the order of 10^3, finally we obtain:

$$\frac{\mathcal{D}_A}{\bar{u}L} = \frac{\mathcal{D}_A}{u_i d_p}\frac{1}{\varepsilon_F}\frac{d_p}{L} \simeq \frac{2}{0.8}10^{-3} = 2.5 \cdot 10^{-3}$$

This value is well below the limit considered previously, namely $\mathcal{D}_A/\bar{u}L = 10^{-2}$.

For example, in the case of a metal Pall ring, 10 mm in size, we have the following characteristics:

- nominal diameter, $d_p = 10^{-2}$ m
- void fraction, $\varepsilon_F = 0.92$.

By choosing a reactor length $L = 10$ m, we obtain $\mathcal{D}_A/\bar{u}L = 2.2 \cdot 10^{-3}$, and residence times of several hours are possible.

When designing a tubular reactor, along with the residence time, which is associated with the rate of reaction and the desired conversion, we need to consider heat transfer through the walls of the tube, which is responsible for the temperature profile along the length of the tube.

The heat transfer coefficients between the fluid flowing inside the tube and the wall are calculated using conventional methods. Outside the tube, we need to consider the way in which heat exchange takes place [Trambouze *et al.*, 2000]:

- transfer by forced convection in the case of concentric tubes
- radiative transfer in the case of a furnace, in which case heat fluxes can be considerable (3 to $8 \cdot 10^4$ W/m^2 on average in a steam cracker).

The problem of heat transfer presents difficulties when the reaction is fast and accompanied by a major thermal effect. If the reaction is exothermic, we may face problems of thermal instability identical to those encountered in batch reactors. Here too, the only way to stabilize the system is to increase γ (Eq. 2.25) while using a geometry that ensures that the specific contact area for heat transfer ($\mathcal{A}$) and the overall coefficient of transfer (U) are sufficiently high. The most favorable geometry is found when using a tube of small diameter together with high fluid velocities.

An example of an industrial implementation in which stability presents serious problems is that of the polymerization of ethylene at high pressure. Industrial tubular reactors have lengths ranging from 200 and 800 m, with inside diameters between 2.5 and 7 cm. They are constructed by joining straight sections 10 to 20 m long in series connected by U-bends. The reaction medium is cooled by circulating a fluid (such as pressurized water) in a jacket. The following operating conditions are used: pressure between 2 000 and 3 000 bars, temperature between 180 and 300°C. A first reactor zone (approximately 150 m) serves to preheat the ethylene to 180°C, and the terminal section cools the reaction mixture before expansion (Fig. 2.24).

Temperature control occurs through the combined effect of heat transfer across the wall and staggered injection of the polymerization initiator mixed with part of the cold monomer. Nevertheless, the temperature in the reaction zone rises from 180°C to approximately 280°C. These reactors operate at the limits of stability and polymer deposits on the reactor wall can lead to unstable conditions. The ethylene conversion in these reactors varies between 15 and 22%, while the residence time is on the order of 45 s.

It is also possible to use the tubes of a conventional tubular heat exchanger as a reactor. The reaction fluid velocity must however remain high, to ensure turbulent flow: 1 to 2 m/s for a liquid and 3 to 10 m/s for a gas. In a single-pass exchanger, the residence time will therefore be very short, on the order of 3 to 6 s for a liquid and 0.6 to 2 s for a gas flowing in 6 m tubes. We can then either place several exchangers in series or use a multipass exchanger (up to 8 passes). Regardless of the nature of the exchanger, the residence time in such systems will remain low. However, the values of $\mathcal{A}$ that can be obtained are very high (up to 400 m^2/m^3), while the transfer coefficient U will retain its conventional values (about 500 W/m$^2 \cdot$ K for a liquid and 50 W/m$^2 \cdot$ K for a gas).

Note that backmixing is more significant in a multipass exchanger than it is in a simple tube, even if the latter has U-bends. The only references to this found in the literature give a value of $\mathcal{D}_A/\bar{u}L$ on the order of 0.05. The tube side of an exchanger, therefore, will give

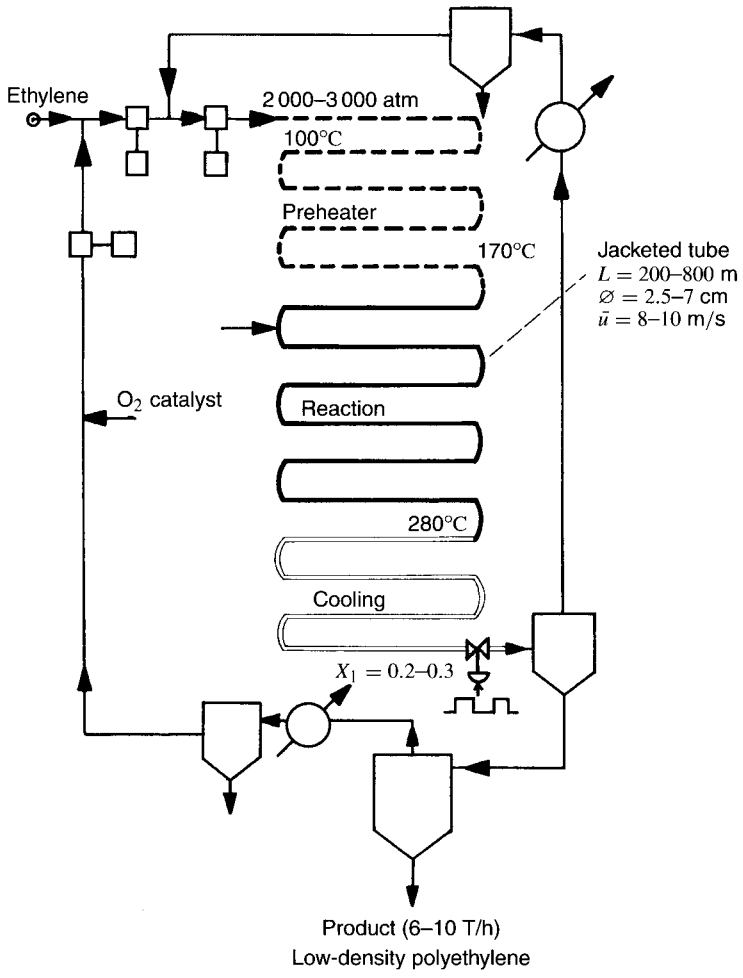


Figure 2.24 Schematic diagram of an ethylene polymerization unit.

results close to those for an ideal tubular reactor. A correction for residence time can always be made by using Eq. (2.102).

By contrast, the shell side of a heat exchanger is rarely considered as a reactor even though greater residence times can be obtained than on the tube side. The reason is that backmixing is relatively significant ($\mathcal{D}_A/\bar{u}L = 0.15$) and the model that has been considered up to now (plug flow + longitudinal diffusion) is inadequate for representing the behavior of such a system.

In certain cases a tubular exchanger can be combined with a portion of a reactor operating under adiabatic conditions (for example, a large diameter tube filled with packing). The exchanger can be used to carry out the initial rapid phase of the reaction, the final conversion being achieved under adiabatic conditions in the second device with a relatively long residence time.

For reaction systems that require lengthy residence times, and therefore low rates of reaction, adiabatic sections can be combined with intermediate heat exchangers keeping the temperature of the reaction medium within acceptable limits. In all cases, the heat transfer calculation can be performed conventionally, using basic reference works on heat exchangers.

Although stability is not a problem with fast and highly endothermic reactions, the problem of heat transfer must, in this case, be handled with extreme care. In practice the most typical example corresponds to the case of high-temperature thermal cracking, conducted in tubular furnaces. The specialized literature provides many references concerning heat transfer in such systems. It is important to be aware of the fact that the residence times obtained in these furnaces are always very short (about 1 second).

In the case of very fast reactions, if the reactants must be mixed at the reactor inlet and under the temperature conditions for the reaction, the influence of micromixing can affect selectivity. The use of an inline mixer to obtain rapid mixing of the reactants may be necessary [Trambouze *et al.*, 2000].

In practice, the operations carried out in such reactors consist essentially of:

- olefin production (ethylene, propylene) by steam cracking of petroleum fractions
- ketene manufacture by cracking of acetone or acetic acid
- vinyl chloride production from dichloroethane
- trichloroethylene manufacture through the thermal dehydrochlorination of tetrachloroethane.

For example, in a steam cracking furnace, the tubes generally have inside diameters between 5 and 10 cm, whereas their length in the radiation zone can vary between 30 and 50 m. The final temperature of the reaction medium is between 800 and 900°C.

2.2.5 Concluding remarks

In light of our earlier comments, the tubular reactor appears to be an ideal continuous system that is particularly well suited to carrying out reactions under a wide variety of operating conditions (in particular, high temperature and/or high pressure). However, the constraints associated with the need to guarantee a plug-type flow can lead to difficulties for practical implementation if we need to design systems capable of handling large quantities of feedstock and having lengthy residence times. In the next section, we will see why, in these cases, the continuous stirred tank reactor can provide a viable alternative.

2.3 CONTINUOUS STIRRED TANK REACTORS (CSTR)

In principle, as we saw in Chapter 1, the operation of a continuous stirred tank single-phase reactor is simple. It is assumed that at any point in the apparatus, the intensive variables, such as concentration or temperature, have the same value. Moreover, in this apparatus the reactants are continuously fed and the reaction mixture containing the reaction products is continuously withdrawn. Such a reactor can be represented schematically as shown in

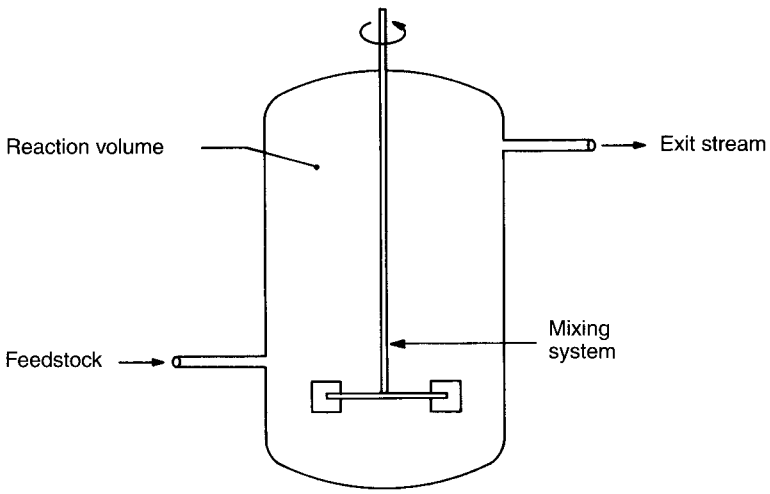


Figure 2.25 Single-phase continuous stirred tank reactor.

Fig. 2.25. Essentially, it contains a tank equipped with a stirring system, a feed pipe and a withdrawal pipe.

2.3.1 Mass and energy balances

Let us assume that a chemical transformation, symbolized by $\sum \nu_{i,j} A_i = 0$, takes place in the fluid contained in the reactor shown in Fig. 2.25. If V denotes the volume of reaction fluid contained in the reactor, the molar balance of each compound A_i accounted for between the reactor's inlet and outlet, can be written as follows for the steady-state:

$$(F_i)_e - (F_i)_s + \mathcal{R}_i V = 0 \quad (i = 1, S) \tag{2.105}$$

The subscripts e and s indicate that the variable corresponds respectively to inlet and outlet conditions.

The term for chemical kinetics, $\mathcal{R}_i$, is expressed on the basis of the conditions prevailing throughout volume V, which conditions also hold at the withdrawal point because of our assumption of perfect mixing.

The overall energy balance is similarly written:

$$\left(\sum F_i \bar{h}_i\right)_e - \left(\sum F_i \bar{h}_i\right)_s + qV = 0 \quad (i = 1, S) \tag{2.106}$$

If we use the two general equations we introduced earlier:

$$F_i = F_{i,0} + \sum \nu_{i,j} \xi'_j \quad i = 1, S \tag{2.107}$$

$$\mathcal{R}_i = \sum \nu_{i,j} r_j \quad j = 1, R \tag{2.108}$$

Eqs. (2.105) and (2.106) can be rewritten by substituting $F_{i,0}$ for $(F_i)_e$ and F_i for $(F_i)_s$:

$$\sum \nu_{i,j}\xi'_j = \sum \nu_{i,j} r_j V$$

or even:

$$\xi'_j = r_j V \tag{2.109}$$

and:

$$\sum F_{i,0}\left[(\bar{h}_i)_e - (\bar{h}_i)_s\right] - \sum_i \sum_j \nu_{i,j}\xi'_j(\bar{h}_i)_s + qV = 0 \tag{2.110}$$

In the above equations, the molar extents of reaction ξ'_j are those at the reactor outlet. The double sum of the above equation can be clarified as follows:

$$\sum_i \sum_j \nu_{i,j}\xi'_j \left(\bar{h}_j\right)_s = \sum_j \Delta H_j \xi'_j \tag{2.111}$$

The enthalpies of reaction ΔH_j are calculated for the conditions within the reactor, which are identical to those for the outgoing fluid. Equation (2.110) can then be written:

$$\sum F_{i,0}(\Delta \bar{h}_i) - \sum \Delta H_j \xi'_j + qV = 0 \tag{2.112}$$

The term $\Delta \bar{h}_i$ reflects the difference in partial molar enthalpies between the inlet and outlet of the reactor.

Equation (2.112) comprises three terms corresponding to the three components of the energy balance:

- 1st term: addition or removal of heat by the continuous flow of fluid
- 2nd term: thermal effect due to the chemical reaction
- 3rd term: energy exchange with the exterior.

To the extent that the change in partial molar enthalpy is essentially due to temperature variations, the first term can be written:

$$\sum F_{i,0}\bar{C}_{Pi}(T_e - T_s)$$

$\bar{C}_{Pi}$ being the mean value of C_{Pi} between T_e and T_s.

As for the third term, it is generally expressed, as is the case with batch reactors, in the form of a heat exchange term, namely:

$$qV = U\Omega(T_{mf} - T_s) \tag{2.113}$$

The simultaneous solution of (2.109) and (2.112) enables us to calculate the values of ξ'_j and T_s. To do this, we must obviously know all the characteristics of the reaction system (r_j, ΔH_j, C_{Pi}, $\nu_{i,j}$) as well as those for the reactor (V, U, Ω, T_{mf}). The operating conditions are defined by the values of $F_{i,0}$ and T_e. As with other types of reactors, we can simplify the above equations in the specific cases already mentioned by treating the system as either isothermal or adiabatic.

• **Isothermal system**

In this case: $T_e = T_s$.

It is important to recognize that in every case the same temperature, T_s prevails at every point of the reactor volume V. Letting $T_e = T_s$ results in only a minor modification when applying Eqs. (2.109) and (2.112). Generally, Eqs. (2.109) are resolved by assuming a value for T that is frequently chosen independently of T_e. In this case, an isothermal operation will appear more as a constraint than as an ideal case, for which the solution is simpler.

• **Adiabatic system**

As with the other reactor types, in an adiabatic system, we assume that the third term of Eq. (2.112) is zero, that is: $qV = 0$. Equation (2.112) can then be written:

$$\sum F_{i,0}\bar{C}_{Pi}(T_e - T_s) = \sum \Delta H_j \xi'_j \tag{2.114}$$

The adiabatic operating temperature, T_s is in this case derived from the simultaneous solution of Eqs. (2.109) and (2.114). We again find the general expression of the adiabatic temperature difference previously encountered:

$$T_e - T_s = \frac{\sum \Delta H_j \xi'_j}{\sum F_{i,0}\bar{C}_{Pi}} \tag{2.115}$$

When resolving Eqs. (2.109), the term r_j must be clarified and hence the concentrations, C_i, of the various chemical species within the reactor appear. If we call Q_s the volumetric withdrawal flow rate, we can write:

$$C_{i,s} = \frac{F_{i,s}}{Q_s} \tag{2.116}$$

In the reactor feed we can, if necessary, similarly specify the various concentrations $C_{i,0}$. In many cases, we can assign: $Q_s = Q_e = Q$.

2.3.2 Solutions for some simple cases

To compare the performance of the continuous stirred tank reactor with that of the tubular reactor for specific cases, we will solve Eq. (2.109) for some of the simple reaction systems already considered. In all cases we assume that we know the operating temperature T_s, which means that we can assign fixed values for the kinetic constants. We also assume that the reaction system volume is constant ($Q_s = Q_e = Q$).

2.3.2.1 Simple first-order reaction: $\nu_1 A_1 + \nu_2 A_2 = 0$

In this case, we have:

$$r = kC_{1,s} = k\frac{F_{1,s}}{Q}$$

Moreover, we know that:

$$\xi' = \frac{F_{1,s} - F_{1,0}}{\nu_1}$$

Equation (2.109) can then be written:

$$F_{1,s} - F_{1,0} = \nu_1 k \frac{F_{1,s}}{Q} V$$

or:

$$F_{1,s} = \frac{F_{1,0}}{1 - \nu_1 k \dfrac{V}{Q}} \tag{2.117}$$

Once again, the mean residence time, $\theta = V/Q$, is the principal parameter.

However, the expression for the molar flow rate, F_1, at the reactor outlet is completely different from the one found for the tubular reactor. We then have the following two expressions corresponding to a first-order reaction:

$$\frac{F_{1,s}}{F_{1,0}} = \exp(\nu_1 k\theta) \quad \text{for an ideal tubular reactor}$$

$$\frac{F_{1,s}}{F_{1,0}} = \frac{1}{1 - \nu_1 k\theta} \quad \text{for a continuous stirred tank reactor.}$$

2.3.2.2 Twin first-order reactions

$$\nu_{1,1}A_1 + \nu_{2,1}A_2 = 0 \quad r_1 = k_1 C_{1,s}$$
$$\nu_{1,2}A_1 + \nu_{3,2}A_3 = 0 \quad r_2 = k_2 C_{1,s}$$

Equation (2.109) is then written:

$$\xi_1' = k_1 C_{1,s} V$$
$$\xi_2' = k_2 C_{1,s} V \tag{2.118}$$

Additionally, we know that:

$$F_{1,s} = F_{1,0} + \nu_{1,1}\xi_1' + \nu_{1,2}\xi_2'$$

Through substitution, the above equations reduce to:

$$\frac{F_{1,s}}{F_{1,0}} = \frac{1}{1 - \nu_{1,1}k_1\theta - \nu_{1,2}k_2\theta} \tag{2.119}$$

This equation should be compared to the equation obtained for a tubular reactor:

$$\frac{F_{1,s}}{F_{1,0}} = \exp\left[(\nu_{1,1}k_1 + \nu_{1,2}k_2)\theta\right] \tag{2.120}$$

Using Eqs. (2.118) and (2.119), we can also specify the molar extents:

$$\xi_1' = k_1 F_{1,s}\theta = \frac{k_1\theta F_{1,0}}{1 - \nu_{1,1}k_1\theta - \nu_{1,2}k_2\theta}$$

$$\xi_2' = k_2 F_{1,s}\theta = \frac{k_2\theta F_{1,0}}{1 - \nu_{1,1}k_1\theta - \nu_{1,2}k_2\theta} \tag{2.121}$$

Similarly, we can write:

$$F_{2,s} = F_{2,0} + \nu_{2,1}\xi_1'$$
$$F_{3,s} = F_{3,0} + \nu_{3,2}\xi_2'$$

2.3.2.3 Consecutive first-order reactions

$$\nu_{1,1}A_1 + \nu_{2,1}A_2 = 0 \quad r_1 = k_1 C_{1,s}$$
$$\nu_{2,2}A_2 + \nu_{3,2}A_3 = 0 \quad r_2 = k_2 C_{2,s}$$

In this case, we write Eq. (2.109) for each reaction:

$$\xi_1' = k_1 C_{1,s} V$$
$$\xi_2' = k_2 C_{2,s} V \tag{2.122}$$

We then obtain:

$$F_{1,s} = F_{1,0} + \nu_{1,1}\xi_1' = F_{1,0} + \nu_{1,1}k_1 F_{1,s}\theta$$
$$F_{2,s} = F_{2,0} + \nu_{2,1}\xi_1' + \nu_{2,2}\xi_2' = F_{2,0} + \nu_{2,1}k_1 F_{1,s}\theta + \nu_{2,2}k_2 F_{2,s}\theta$$

By substitution, we obtain successively:

$$\frac{F_{1,s}}{F_{1,0}} = \frac{1}{1 - \nu_{1,1}k_1\theta}$$

and:

$$F_{2,s} = \frac{F_{2,0} + \dfrac{\nu_{2,1}k_1 F_{1,0}\theta}{1 - \nu_{1,1}k_1\theta}}{1 - \nu_{2,2}k_2\theta} \tag{2.123}$$

or, using the molar extents:

$$\xi_1' = k_1 F_{1,s}\theta = \frac{k_1\theta F_{1,0}}{1 - \nu_{1,1}k_1\theta}$$

$$\xi_2' = k_2 F_{2,s}\theta = \frac{k_2\theta F_{2,0} + k_1 k_2\theta^2(-\nu_{1,1}F_{2,0} + \nu_{2,1}F_{1,0})}{(1 - \nu_{1,1}k_1\theta)(1 - \nu_{2,2}k_2\theta)} \tag{2.124}$$

These equations differ considerably from those obtained in the case of a tubular reactor.

From the above examples, we can conclude that the two types of continuous reactor, tubular and CSTR, do not lead to identical extents of reaction for the same mean residence time θ. As indicated earlier (Chapter 1), the mean residence time θ corresponds to quite different residence time distributions, depending on the type of continuous reactor under consideration.

2.3.2.4 Calculating selectivity

As we saw earlier, the concept of selectivity often plays a key role in complex reaction systems. For the two reaction systems we have been considering, we will calculate the selectivities that would be obtained in a continuous stirred tank reactor, so we can compare them to the same values calculated for a batch or tubular reactor (see Section 2.11).

For a continuous stirred tank reactor, the instantaneous and overall selectivity are similar because at any point in the reactor, the chemical transformations occur at the same rate. We can calculate selectivities using the expressions obtained above.

• **Twin reactions**

$$S_{2,1} = \frac{\left(\frac{\Delta F_2}{\Delta F_1}\right)}{\left(\frac{\Delta F_2}{\Delta F_1}\right)_{\text{id}}}$$

$$\frac{\Delta F_2}{\Delta F_1} = \frac{\nu_{2,1}(r_1)_s}{\nu_{1,1}(r_1)_s + \nu_{1,2}(r_2)_s} \quad \text{and} \quad \left(\frac{\Delta F_2}{\Delta F_1}\right)_{\text{id}} = \frac{\nu_{2,1}}{\nu_{1,1}}$$

We obtain:

$$S_{2,1} = \frac{\nu_{1,1}}{\nu_{2,1}} \frac{\nu_{2,1}(r_1)_s}{\nu_{1,1}(r_1)_s + \nu_{1,2}(r_2)_s} = \frac{k_1}{k_1 + \frac{\nu_{1,2}}{\nu_{1,1}} k_2} \tag{2.125}$$

This is the same value we obtained for batch and tubular reactors.

• **Consecutive reactions**

$$\frac{\Delta F_2}{\Delta F_1} = \frac{\nu_{2,1}(r_1)_s + \nu_{2,2}(r_2)_s}{\nu_{1,1}(r_1)_s} \quad \text{and} \quad \left(\frac{\Delta F_2}{\Delta F_1}\right)_{\text{id}} = \frac{\nu_{2,1}}{\nu_{1,1}}$$

After substitution and development, we obtain:

$$S_{2,1} = \frac{\nu_{2,1} k_1 \theta F_{1,e} + \nu_{2,2} k_2 \theta F_{2,e} - \nu_{2,2} \nu_{1,1} k_1 k_2 \theta^2 F_{2,e}}{\nu_{2,1} k_1 \theta F_{1,e}(1 - \nu_{2,2} k_2 \theta)} \tag{2.126}$$

There is a marked difference between this and the expression found for the batch or tubular reactor.

We may want to determine the yield $R_{2,1}$ (for $F_{2,e} = 0$).

$$R_{2,1} = \frac{\frac{-F_{2,s}}{F_{1,e}}}{\frac{\nu_{2,1}}{\nu_{1,1}}}$$

expressing θ as a function of X_1, that is, $\nu_{1,1} k_1 \theta = -X_1/(1 - X_1)$ leads to:

$$R_{2,1} = \frac{m X_1 (1 - X_1)}{m(1 - X_1) + X_1}$$

with:

$$m = \frac{\nu_{1,1} k_1}{\nu_{2,2} k_2}$$

2.3.3 Autothermal operation

In general, the operation of a unit is said to be autothermal if that unit is capable of self sufficiency in terms of heat energy. In the case of a reactor, this means that the heat produced by the reaction is used to heat the reactants, fed at a lower temperature than the reaction

temperature. This corresponds to what we have described as adiabatic operation, the reaction being exothermic. To describe such a system, we will use Eq. (2.114) in conjunction with Eq. (2.109).

2.3.3.1 Simple reaction

Here, we consider a simple reaction system ($A_1 \rightarrow A_2$) with first-order kinetics. Equation (2.109) leads to the following expression:

$$F_{1,s} = \frac{F_{1,0}}{1 + k\theta}$$

and:

$$\xi' = \frac{F_{1,0} k\theta}{1 + k\theta} \tag{2.127}$$

Equation (2.114) can now be written:

$$\sum F_{1,0} \bar{C}_{Pi} (T_s - T_e) = \frac{-\Delta H_R F_{1,0} k\theta}{(1 + k\theta)} \tag{2.128}$$

The two sides of this equation respectively represent the heat (Q_E) removed from the reactor by the effluent and the heat (Q_P) generated by the chemical transformation. Equation (2.128) can therefore be written:

$$Q_E = Q_P$$

In the right-hand side of the equation, the constant k can be replaced by its expression as a function of temperature, that is:

$$k = k_0 \exp\left(-\frac{E}{RT_s}\right)$$

To obtain the solution of (2.128), we can plot each member of the equation on the same diagram as a function of the operating temperature T_s. We then obtain curves similar to those shown in Fig. 2.26.

The solution to Eq. (2.128) is represented by the point of intersection of the two curves plotted. The shape of curve $Q_P(T_s)$ is the result of both the exponential growth of the rate of reaction when the temperature increases and the limitation of the thermal effect to a maximum value ($-\Delta H_R F_{1,0}$) corresponding to a completed reaction.

In contrast, curve $Q_E(T_s)$ is appreciably a straight line passing through the abscissa $T = T_e$ when $Q_E = O$. The position of the point representing the solution will vary essentially as a function of the slope of Q_E and the value of T_e. Depending on the respective positions of the two curves Q_P and Q_E, various cases may be encountered, such as those shown in Fig. 2.26:

- Case (a): Since the slope of Q_E is relatively steep, the only possible solution occurs at low temperature and for an extent of reaction that is nearly zero, a situation of no practical interest. We could say that, in this case, the reactor is flooded by an excessively high flowrate of reactants.

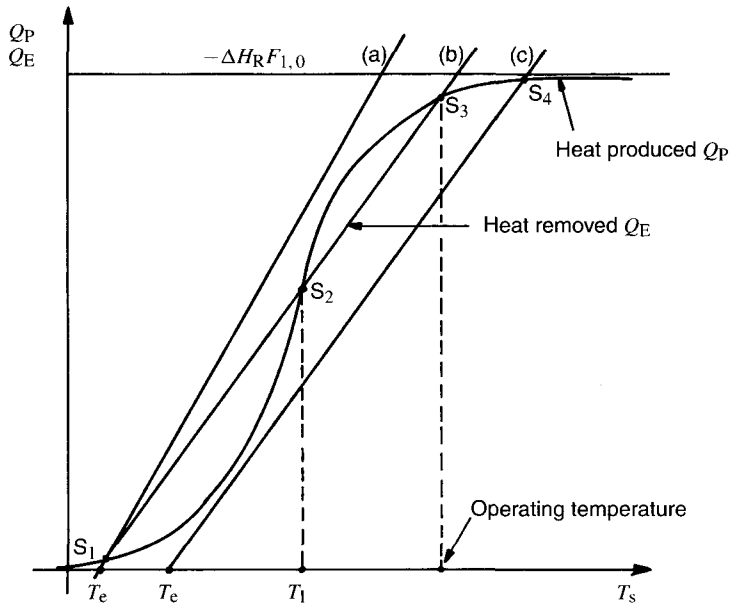


Figure 2.26 Autothermal operation of a continuous stirred tank reactor (CSTR) under different possible conditions.

- Case (b): There are three possible solutions, S_1, S_2, and S_3. For the same reasons as above, point S_1 is of no practical interest. S_2 and S_3, however, may be of interest, although S_2 is not a stable operating point. In practice, the least variation in T_s, starting from a value corresponding to S_2, results in a disequilibrium of the heat balance so that the operating point shifts either to S_1 (extinction) or S_3. Point S_3 is stable, however, and if the operating temperature is acceptable for the reaction system under consideration, it is certainly the operating point to be adopted. To reach this operating point, the system simply needs to exceed a temperature T_1 corresponding to S_2.
- Case (c): The inlet temperature T_e being relatively high, there is only a single point of intersection (S_4) between the two curves. This point corresponds to stable operation, for the same reasons as S_3. Starting from the corresponding operating temperature, even a small change in temperature destabilizes the heat balance so that the temperature tends to return to its initial value.

Point S_4, or any operating point corresponding to a nearly complete reaction, is often preferred providing the operating temperature does not rise too high. The same type of approach can obviously be applied to any exothermic reaction system. As an example, below we examine two cases: a reversible reaction and consecutive reactions.

2.3.3.2 Reversible reaction $A_1 \rightleftarrows A_2$

In this case the shape of curve Q_P will be modified by the fact that at high temperature the extent of reaction may be limited by thermodynamic equilibrium. We then have a graphic

representation of Eq. (2.128) as shown in Fig. 2.27. Here too, the points of intersection can correspond to stable (S_3, S_4) or unstable (S_2) operation. Assuming that the operating temperature (T_M) is not too high, point S_4, corresponding to the maximum extent of reaction, will obviously be the target.

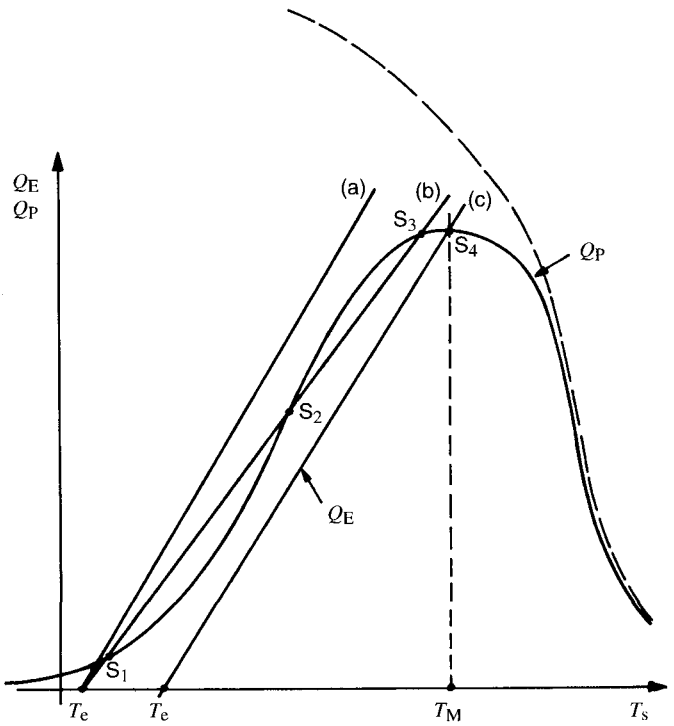


Figure 2.27 Autothermal operation of a CSTR for a reversible reaction.

2.3.3.3 Consecutive reactions $A_1 \rightarrow A_2 \rightarrow A_3$

If both consecutive reactions are exothermic, the heat generation curve can assume a more complex shape, with two inflection points (Fig. 2.28). This could result in five points of intersection for the curves corresponding to the production and elimination of heat: two being unstable (S_2 and S_4) and three being stable (S_1, S_3, and S_5). However, of the three last points, only one is generally of practical interest—S_3, for example, if we are looking for good selectivity in the intermediate product A_2. Although stable for small fluctuations, such systems can become unstable when there are larger fluctuations. Therefore, a reactor operating at point S_3, can become unstable following a relatively small drop in the feed rate or a slight increase in the feed temperature.

This type of situation is found, for example, in the case of partial oxidation reactions; since complete oxidation is highly exothermic, it can be triggered by slight variations in the operating conditions.

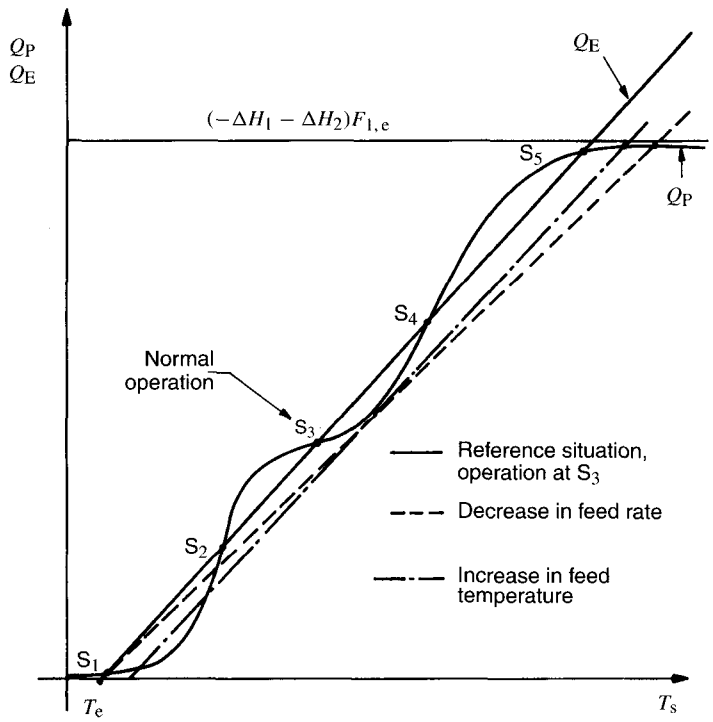


Figure 2.28 Autothermal operation of a continuous stirred tank reactor for consecutive reactions.

To make the operation of the continuous stirred tank reactor more stable, we can, as with batch reactors, add a heat exchange surface to the reactor (jacket or internal coil). In this case Eq. (2.128), reflecting the enthalpy balance, is modified as follows:

$$\sum F_{1,0}\bar{C}_{Pi}(T_s - T_e) - U \cdot \Omega(T_s - T_{mf}) = \frac{-\Delta H_R F_{1,0} k\theta}{(1 + k\theta)} \tag{2.129}$$

The effect of heat exchange within the reactor will increase the slope of line Q_E, making it easier to locate a stable operating point and avoid the possibility of the system shifting toward unstable conditions, as represented by point S_4 in Fig. 2.28.

On a practical level there are certain advantages associated with autothermal operation. For although—once the reaction is exothermic—we can in principle operate under autothermal conditions by exchanging heat between the reactor feed and the effluent, it is important to realize that this type of heat exchange occurs optimally inside the CSTR. If this least-cost internal exchange (no exchange surface) is insufficient, as we saw for case (a) of Fig. 2.26, we can add an external exchanger between the effluent and feed to increase T_e to a suitable value. Such operation is illustrated in Fig. 2.29.

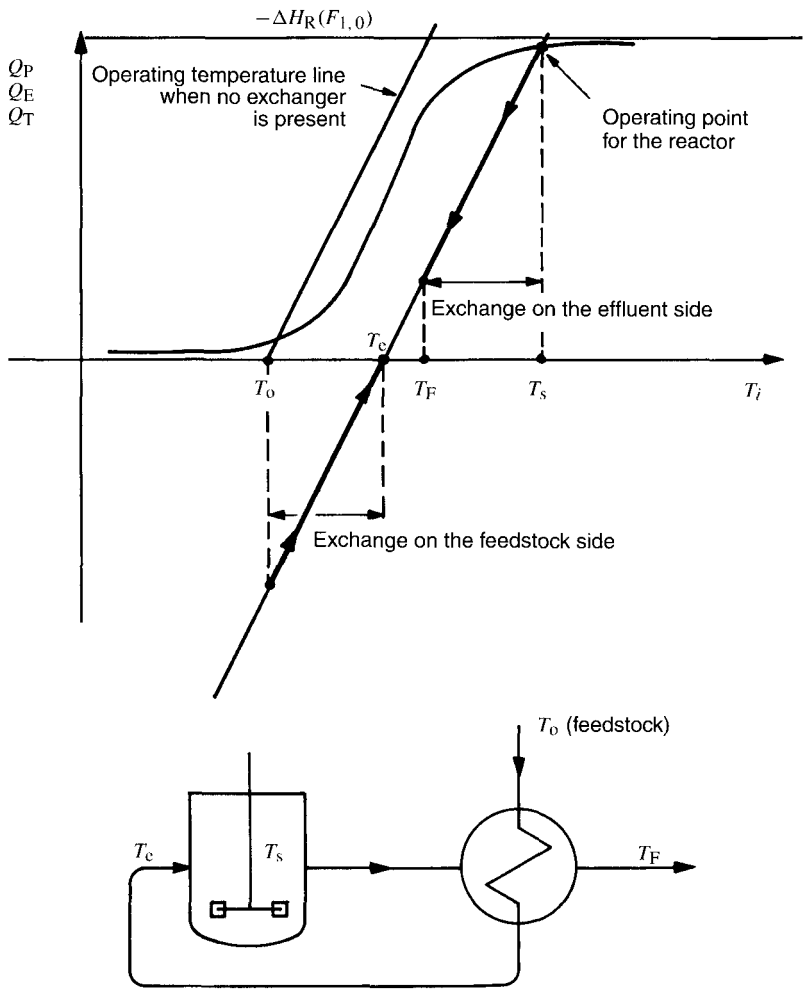


Figure 2.29 Autothermal operation of a CSTR with the addition of a heat exchanger.

2.3.4 The multistage reactor

We saw in Chapter 1 that we can sometimes combine several continuous stirred tank reactors in series, thereby creating what is known as a multistage reactor. Because the change in concentration of the various reactants and products takes place in successive steps, we can compare it to the change in concentration that occurs in a tubular reactor. Each stage in the cascade is treated as a continuous stirred tank reactor. All the calculations introduced in the previous sections are therefore applicable. Here, the outlet values for one stage $(m - 1)$ are used as the inlet values for the next stage m.

As an example, we examine the case of a simple first-order reaction (see Section 2.3.2.1). For a given stage m, we rewrite Eq. (2.117) as follows:

$$(F_1)_m = \frac{(F_1)_{m-1}}{1 - \nu_1 k_m \dfrac{V_m}{Q}} \tag{2.130}$$

If all the stages have equal volumes V_m and operate at the same temperature, the above equation can be written:

$$(F_1)_m = \frac{(F_1)_{m-1}}{1 - \nu_1 k \dfrac{V}{Q}} = \frac{(F_1)_{m-1}}{1 - \nu_1 k\theta}$$

Through recursion we then obtain the general solution:

$$(F_1)_m = \frac{F_{1,0}}{(1 - \nu_1 k\theta)^m} \tag{2.131}$$

For the general case we rewrite the molar and enthalpy balances introduced in (2.105) and (2.106) for each stage, that is:

$$(F_1)_{m-1} - (F_1)_m + (\mathcal{R}_1)_m V_m = 0 \tag{2.132}$$

$$\left(\sum F_i \bar{h}_i\right)_{m-1} - \left(\sum F_i \bar{h}_i\right)_m + q_m V_m = 0 \tag{2.133}$$

The subscript i varies from 1 to S (total number of compounds) and the subscript m from 1 to N (total number of stages). Very often, to minimize construction cost, the volumes of the various stages are chosen to be identical, that is, $V_m = V$.

If the operating temperatures of the various stages are chosen to be identical and fixed in advance, only Eqs. (2.132) will need to be solved simultaneously. However a temperature can be chosen for each stage without any additional difficulty; in fact varying the operating temperature throughout the series of stages can provide certain advantages.

Thus for a reversible exothermic reaction, it will be beneficial to reduce the operating temperature from stage to stage as the extent of reaction progresses. Each stage will then function adiabatically providing it is preceded by a heat exchanger that lowers the inlet temperature (Fig. 2.30). In the case of a reversible endothermic reaction, the opposite procedure is followed.

Temperature variations in the successive stages of a cascade can also be obtained by the staged injection of part of the feedstock. The injection temperature is then controlled so as to obtain the desired temperature staging. Staged injection of part of the reactants can also be beneficial when we want to improve the selectivity of complex reaction systems.

2.3.5 Available technologies

As illustrated in Fig. 2.25, the continuous stirred tank reactor strongly resembles the batch reactors we looked at earlier. To the extent that the pipework for the feedstock and effluent

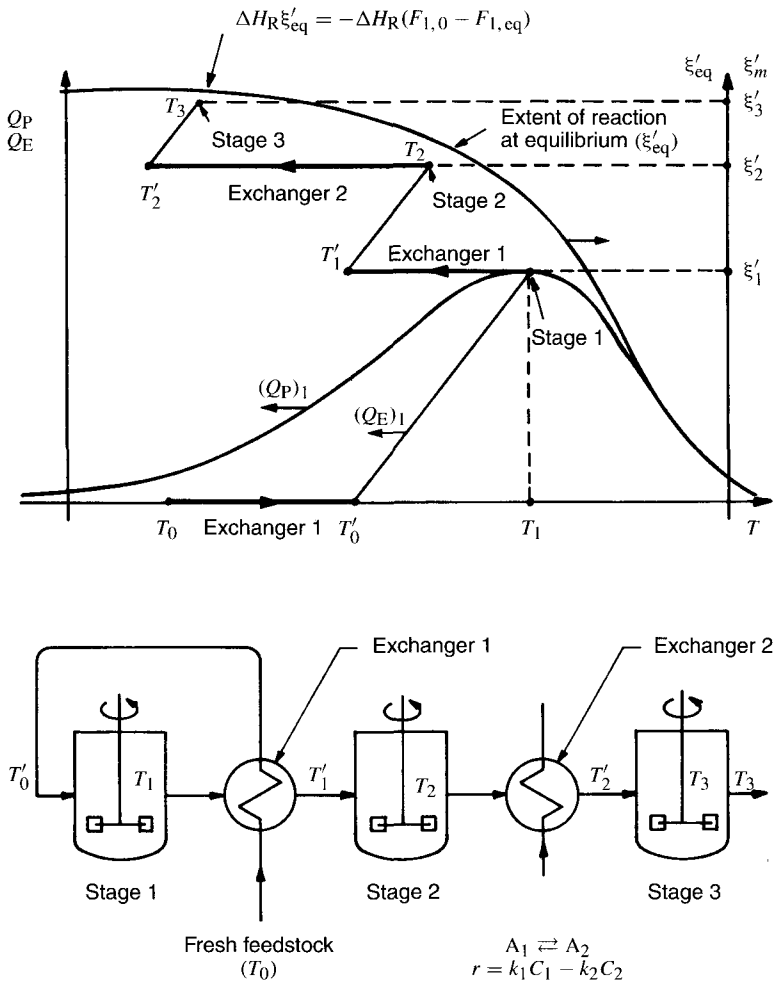


Figure 2.30 Battery of continuous stirred tank reactors with intermediate heat exchangers for a reversible exothermic reaction.

has been specified, the same technologies should be applicable. The situation then resembles that of the stirred tank, whether we use a rotating stirrer or external circulation.

2.3.5.1 Mechanically stirred tank

Figure 2.31 is a schematic diagram of a mechanically stirred tank. The cylindrical tank with a generally elliptical bottom is equipped with a rotating stirrer whose vertical motor shaft is generally introduced from the top, although they are sometimes introduced through the bottom of the tank. The tank can also be equipped with heat exchange surfaces: jacket, coil, submerged plates, etc. (see Fig. 2.6B).

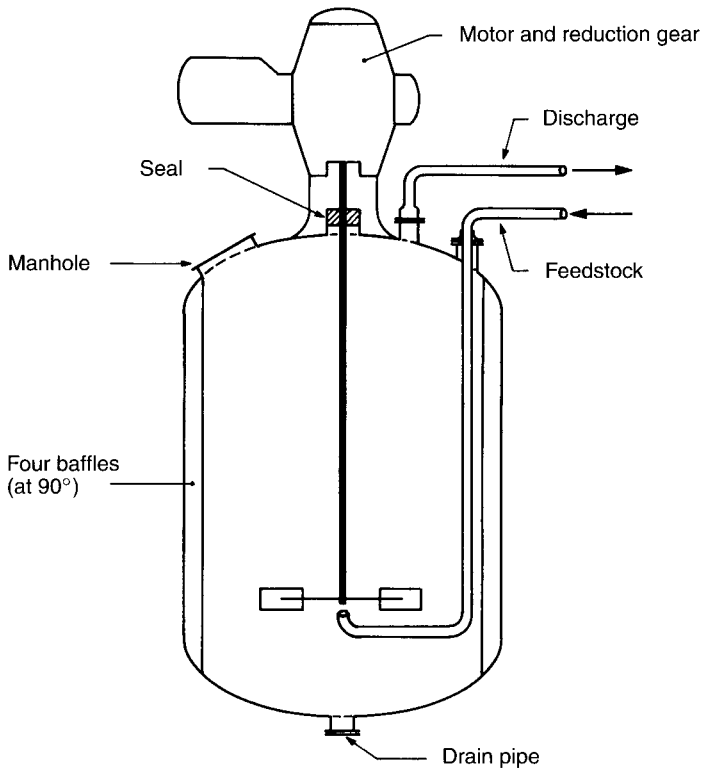


Figure 2.31 Continuous stirred tank reactor with mechanical agitation.

Although agitation plays a secondary role in the batch reactor, in the case of a continuous stirred tank reactor, it is critical. Note that rotating stirrers are essentially used for liquid phases. The type of stirrer used will depend primarily on the viscosity of the liquid phase present in the reactor.

Introduction of the feedstock should be done in such a way that mixing takes place as rapidly as possible. In most cases the feed pipe should discharge close to the stirrer, at a point where the circulation flowrate caused by the stirrer is at a maximum. The discharge pipe can in principle be located at any point in the reactor, but there is an advantage to placing it as far as possible from the feed pipe to avoid any possibility of a bypass between the inlet and the outlet. The discharge pipe is often located in the upper part of the reactor.

This type of reactor can operate either filled with liquid or with a gas-phase blanket. The choice between these two solutions is often related to problems of tightness around the stirrer shaft, which is often achieved through the use of a stuffing box, a mechanical seal, or a magnetic drive.

The presence of internal elements for heat exchange, such as coils, is not recommended because they can reduce the efficiency of the stirrer and create problems if there is a risk of fouling.

Stirrer systems are designed to obtain a quality of mixing that is appropriate for the desired objective. This mixing quality can be expressed by means of two criteria:

1. Mixing time t_M, which should be no more than a tenth of the mean residence time
2. The range of action for the agitation system which should cover the entire volume of the reactor [Trambouze, *et al.*, 2000].

Earlier, we provided information about estimating mixing time. Generally, mixing times are less than a minute. Therefore setting up a continuous stirred tank reactor for reactions with mean residence times greater than 10 minutes should present no problem.

The choice of agitation system is made in such a way that the entire tank volume is uniformly mixed. For low viscosity and Newtonian fluids, this condition is easy to obtain, whereas highly viscous and non-Newtonian systems must be given careful consideration to avoid stagnant zones.

Multistage systems can be designed by arranging several stirrers on the same shaft mounted in the center of a compartmentalized column (Fig. 2.32). In this way up to ten stages in series can easily be obtained.

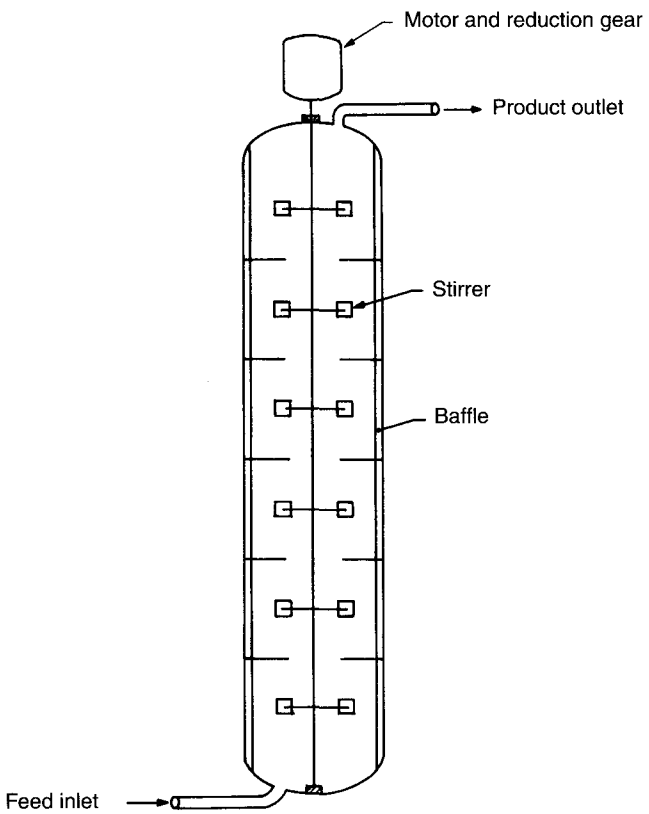


Figure 2.32 A mechanically stirred multistage reactor (six stages in series).

2.3.5.2 Tank with external circulation

As with the batch reactor, the reactants and the reaction mixture can be mixed through the use of an external circulation system incorporating a pump (Fig. 2.33). If necessary, heat exchange can be achieved by inserting a conventional heat exchanger—tubular or plate, depending on the circumstances—into the circulation loop.

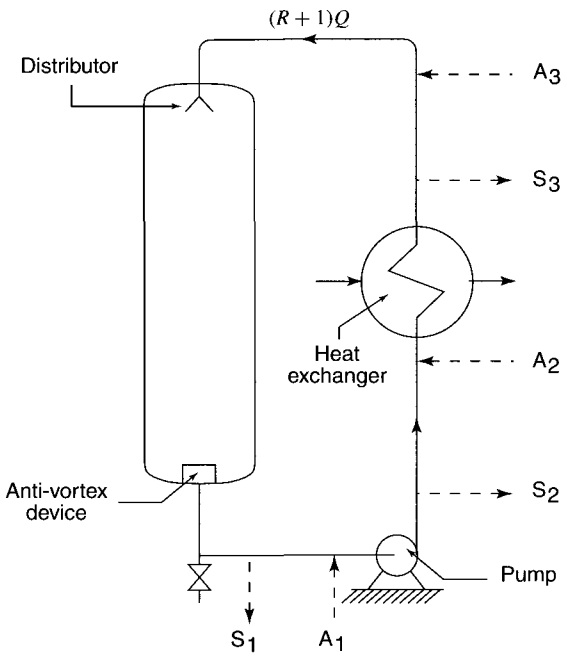


Figure 2.33 A continuous stirred tank reactor with a circulation loop. A_1, A_2, and A_3 three reactant feed possibilities. S_1, S_2, and S_3 three discharge possibilities. Q = feed stock flow rate.

Reactants are introduced just before or after the exchanger to ensure optimal use of the heat exchange area. To decide which method to use, we must consider both the feed temperature compared to the mean temperature in the exchanger and the sign of the heat effect of the reaction (endothermic or exothermic). In certain cases we can introduce fresh reactants upstream of the pump to take advantage of the lower pressure at that point and to bring about rapid mixing of fresh reactants with the reaction medium (to avoid problem with micromixing).

In all cases effluent is removed from the circulation loop at a point slightly upstream of the feed inlet to avoid bypass between the feed and the discharge (points A and S having the same subscript in Fig. 2.33).

The design of such reactors is based on the mean residence time θ required. Once the total volume of reaction medium has been determined, the tank volume can be obtained by taking

into account the volumes corresponding to the circulation loop and the exchanger. The tank is designed as a vertical drum with a height-to-diameter ratio between 3 and 10.

The recirculation flow rate is adjusted to be between 15 and 20 times the feed rate Q. We can show that for a recirculation ratio equal to or greater than 20, the conversions that can be calculated, assuming plug flow in a vertical drum, are appreciably identical to those evaluated on the basis of perfect mixing.

Strictly speaking, the recirculation ratio R between the recirculation flow rate and the feed rate Q should increase with the conversion. Another element needed for determining the rate of recirculation is related to heat exchange. The temperature difference between the exchanger inlet and outlet decreases as the rate of recirculation increases. For a simple reaction system with a given ΔT_{ad}, the temperature difference between the exchanger inlet and outlet can be expressed as follows:

$$(\Delta T)_{ech} = \frac{X_I \Delta T_{ad}}{R+1}$$

X_1 being the conversion achieved in the reactor and expressed with respect to the principal reactant A_1.

In general we want to limit the value of $(\Delta T)_{ech}$ to less than 10 degrees, which, for reactions having values of ΔT_{ad} above 200°C, will lead to recirculation ratios on the order of 15 to 20.

Note that flow in a vertical drum is not precisely characterized. This is not a problem in itself, providing no part of the volume forms a stagnant zone. To prevent this, it is useful to add a distributor at the recirculation inlet at the top of the reactor. The distributor serves primarily to break up the jet issuing from the pipe introducing the fluid (Fig. 2.34A).

In certain cases, when perfect mixing is needed for reasons of selectivity, the recirculation stream can be injected through an ejector nozzle, producing an internal recirculation current throughout the entire tank. In this case the height-to-diameter ratio of the drum is chosen to be smaller than previously indicated (on the order of 2 to 3) (Fig. 2.34B). This arrangement can be adapted for use with a gas-phase reaction, for which the other systems we have been describing are difficult to implement. An example of this arrangement is the industrial chlorination of methane.

2.3.5.3 Some applications

A number of reactions are carried out industrially using CSTR or multistage systems. These include mass and solution polymerization reactions. Given the high viscosities of the reaction medium, most units are mechanically agitated tanks, with the mixing device being an anchor or Archimedes screw. To avoid a too wide distribution of molecular weight of the polymers, which is dependent on residence time distribution, a multistage system is often used. CSTR systems may still be of interest when producing copolymers, however. In this case all the copolymers will have the same composition, corresponding to the concentrations of monomers, which are uniform throughout the entire reactor volume. A recirculating loop system can also be used.

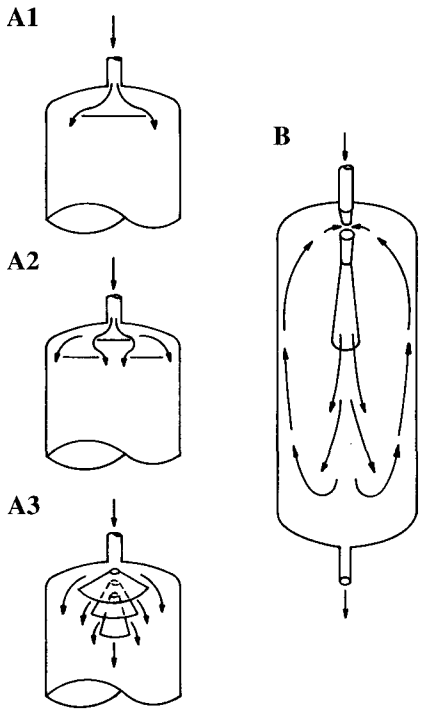


Figure 2.34 Internal devices to avoid stagnant zones in recirculation loop reactors: **A.** Distributors: **A.1** Single impact plate. **A.2** Double plate. **A.3** Concentric cones. **B.** Ejector.

As indicated earlier, CSTR or multistage systems are suitable for liquid-phase reactions. There are now a number of applications for liquid phase homogeneous catalysis, which can easily be carried out in the systems described above. Examples include the manufacture of hexenes, heptenes, and octenes through the dimerization of propylene and butenes. In practice one or more reactors are used with external recirculation. When producing hexenes from propylene, a single reactor is sufficient to achieve 90% conversion (mean residence time on the order of 2 hours). If we want to increase the conversion, we can use two reactors in series. In the case of the dimerization of butenes, the reaction is slower and four reactors in series may be needed. When manufacturing heptenes from a mixture of propylene and butenes, three or four stages will be necessary. In this case propylene is added at every stage in such a way that the ratio of concentrations of propylene and butenes is maintained at an optimal value leading to the maximum selectivity of heptenes.

In terms of practicality and reliability, the circulating loop system presents a certain number of advantages over other technologies, especially for high-capacity units. Pumps are certainly easier to implement than mechanical stirrers and two pumps can be mounted in parallel on a single reactor to avoid any shutdown of the plant as a result of mechanical failure. It is only for highly viscous reaction fluids that the mechanically stirred tank has an advantage.

2.3.6 Conclusion

We have described continuous stirred tank reactors on the basis of their principal features, which are summarized below:

- These systems are well suited to liquid-phase reactions, where the reaction rate is moderate or low.
- Mean residence times greater than one hour can easily be realized.
- Autothermal operation presents an enormous advantage since it enables us to eliminate a heat exchanger and make direct use of the heat produced by the reaction.
- The very broad distribution of residence times can, in certain cases, be a disadvantage.
- The uniformity of temperature and concentration for the entire reaction volume can, however, provide certain advantages over other systems.

These will be discussed at greater length in the following sections, in which we compare the three reactor types considered.

2.4 COMPARISON OF THE DIFFERENT REACTOR TYPES

In the previous sections we presented three types of reactor and analyzed their behavior by limiting our discussion to single-phase systems. But before extending the discussion to heterogeneous systems, it would be useful to compare the three reactor types to highlight their respective advantages and disadvantages. The comparison will look at the various aspects of reactor operation, each of which plays a specific role in achieving the final objective: to carry out a chemical transformation under suitable operating conditions for the purpose of producing a given quantity of product within a given period of time, while ensuring a conversion and/or selectivity that are predetermined or maximal.

2.4.1 Operating conditions and production capacity

By operating conditions we refer to the operating mode (batch or continuous), the intensive operating variables (temperature, pressure, and initial or inlet concentrations), and mean residence time.

2.4.1.1 Operating mode and production capacity

When we first classified reactors (Chapter 1), we made a preliminary distinction based on the mode of operation. The choice between continuous and batch operation is often related to the production capacity. As a first approximation we can say that for high capacities (greater than 10 000 tons per year), continuous systems are generally preferred. On the contrary, when manufacturing relatively small quantities of product, involving several steps in succession, a batch reactor that can be adapted for the various steps is preferable (for example, the manufacture of dyes, pharmaceuticals, cosmetics, etc.). Although the continuous tubular reactor is well suited for processes in the gas phase, all reactor types, as noted earlier, are appropriate for liquid-phase reactions.

The principal advantage of continuous systems is their high capacity, while the principal advantage of the batch reactor is its flexibility and adaptability to various reaction types. When working with intermediate capacities, the choice is based on economic comparisons, bearing in mind that a continuous system requires constant attention by plant personnel (5 or 6 shifts). Batch operation, by contrast, can often be carried out in a single day with one or two shifts or, at most, with personnel working only five days a week in shifts.

2.4.1.2 Intensive variables (T and P)

As noted earlier, it is the tubular reactor that is most suitable for severe operating conditions (high temperature and pressure). There are examples of reactors operating at pressures of 3 000 bar or temperatures reaching 900°C.

Of course, batch and continuous stirred tank reactors can operate at high temperature or pressure. But because of the technology used and the geometry of these reactors, it is harder to achieve high operating pressure and high reaction temperature simultaneously. This would, however, be relatively easy to carry out in a tube, which can support temperatures as high as 800°C and pressures of 100 bar.

The batch reactor is certainly the least suitable to severe operating conditions. For if high temperature conditions are required, the time needed to heat and then cool the reactor system becomes prohibitive. The use of high pressure can also present problems. For example, if pressure is generated by a compressor operating in batch mode and with a variable compression ratio, the cost of equipment can quickly become significant.

The higher the temperature, the more economically important it becomes to recover sensible heat from the reactor effluent. This can easily be accomplished with continuous systems, but it is much more difficult in a batch reactor. From this standpoint, we saw earlier that the continuous stirred tank reactor is particularly well suited for heat exchange operations in the case of an exothermic reaction.

2.4.1.3 Mean residence time θ and residence time distribution

In the sections concerning reactor types, we indicated that their respective possibilities with respect to mean residence time θ, were significantly different. Thus the batch reactor is unsuitable for short residence times ($<$ 15 min) but can easily accommodate very long reaction times (10 to 20 h, for example). By contrast, the tubular reactor is very well suited for short reaction times (0.5 s to 1 h). The continuous stirred tank reactor falls somewhere between them, and can easily accommodate a range of residence times between 10 min and 4 h. Obviously, we can achieve higher residence times by using a multistage reactor.

In Fig. 2.35 we have tried to summarize our remarks comparing the various reactor types, specifically with respect to capacity, residence time, and operating conditions. There are no strict limits to the fields of application indicated, however; they are intended only to serve as a guide in choosing the most suitable type of reactor.

We see from the above figure that the fields of application overlap considerably, which clearly shows that the final choice must also take into account other criteria, economic considerations in particular (capital investment, operating costs, and yield).

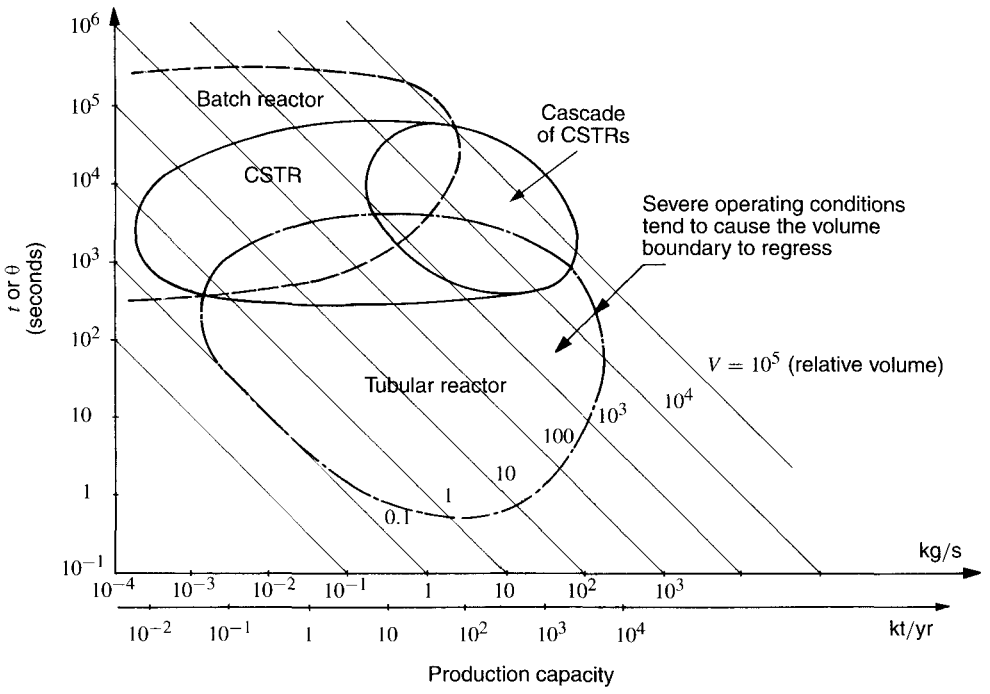


Figure 2.35 Comparison of the various reactor types.

Moreover, a strict comparison on the basis of mean residence time is of limited interest. As we saw in Chapter 1 for continuous systems, the mean residence time can correspond either to a true residence time (ideal tubular reactor) or it may only be the mean of a distribution of residence times, which range from 0 to infinity. From this point of view, the ideal tubular reactor and the batch reactor are equivalent, since in both cases all the elements of the reaction phase spend the same amount of time in the reactor.

Real tubular reactors have residence times that cluster around the mean value θ. We have seen that this distribution can be represented by a simple model, assuming plug-type flow with the superposition of axial diffusion. The continuous stirred tank reactor behaves completely differently, while the multistage reactor falls somewhere between the two types of ideal reactor.

The residence time distribution for a system consisting of m stirred tanks in series is expressed as follows:

$$\mathbf{E}(\tau) = \frac{m^m \tau^{(m-1)}}{(m-1)!} \exp(-m\tau) \tag{2.134}$$

where $\tau = t/\theta$.

We can verify that for $m = 1$, $\mathbf{E}(\tau) = \exp(-\tau)$, the residence time distribution function found earlier for the continuous stirred tank reactor. Figure 2.36 represents the function $\mathbf{E}(\tau)$

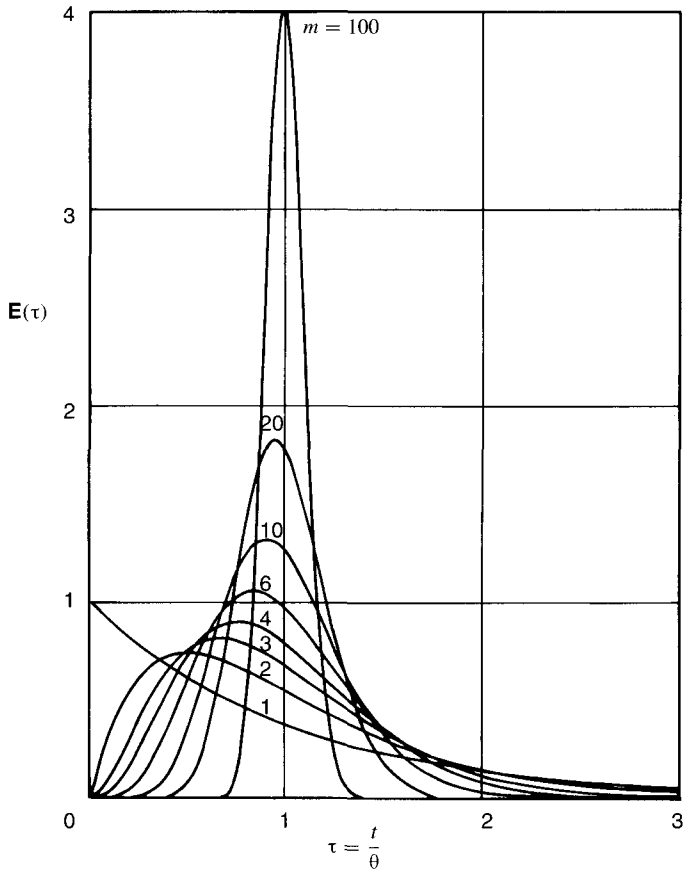


Figure 2.36 Residence time distribution curves for a series of m continuous stirred tank reactors.

of Eq. (2.134) for various values of m. We see that as m increases, the distribution curves tend to narrow and mimic those for a tubular reactor with axial diffusion.

The two models (plug flow + axial diffusion and the multistage reactor) tend to merge for low values of axial diffusivity $\mathcal{D}_A$ and for a high number m of stages in series. If the variances for the residence time distribution curves are equal (Fig. 2.36, for example), the following equation holds:

$$\frac{2\mathcal{D}_A}{\bar{u}L} = \frac{1}{m} \tag{2.135}$$

which expresses the equivalence between the two models.

If we want to extend the range of comparison between the two models, we are led to the following equivalence:

$$\frac{2\mathcal{D}_A}{\bar{u}L}\left[1 - \frac{\mathcal{D}_A}{\bar{u}L}\left(1 - \exp\left(-\frac{\bar{u}L}{\mathcal{D}_A}\right)\right)\right] = \frac{1}{m} \tag{2.136}$$

Equations (2.135) and (2.136) are graphically represented in Fig. 2.37.

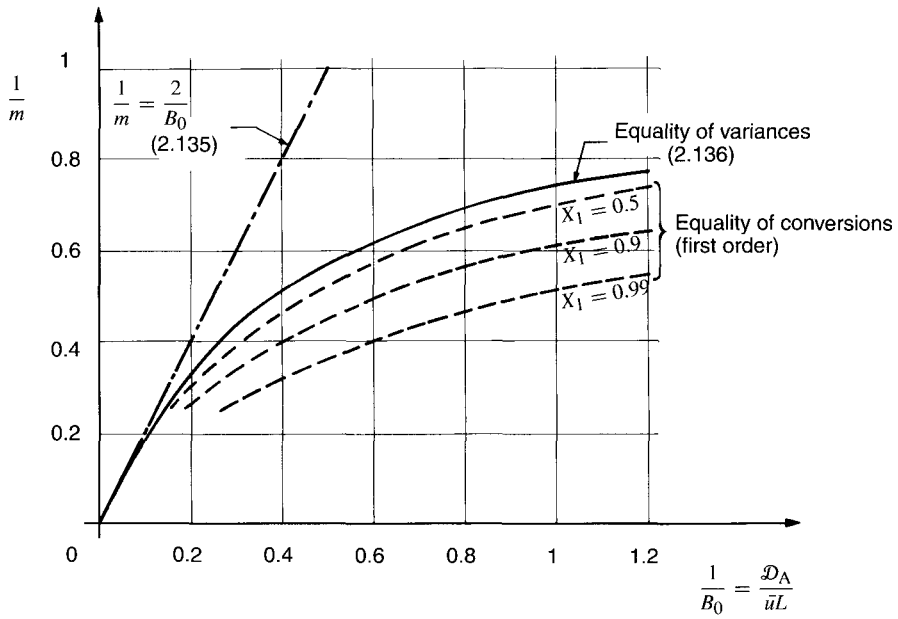


Figure 2.37 Equivalence between a tubular reactor with axial diffusion and a cascade of m CSTRs (constant total volume): **A.** With respect to flow (Bo compared to m according to Eqs. (2.135) and (2.136)) (continuous line). **B.** With respect to conversion for a first-order reaction (Eqs. (2.99) and (2.131)) (dashed line).

2.4.2 Conversion

With respect to performance, the various reactor types can be compared on the basis of the conversion. Below, we compare the volumes of various systems needed to achieve a given conversion and a fixed production level in the case of a simple reaction.

We consider the case of a simple first-order reaction $A_1 \rightarrow A_2$ and calculate the volume of each of the reactors needed to achieve the conversion X_1 of reactant A_1. We assume that, in all cases, the reaction takes place isothermally and at the same temperature. We can use the expressions derived in the previous sections:

- For a batch reactor:

$$X_1 = 1 - \exp(-kt) \tag{2.137}$$

- For an ideal tubular reactor:

$$X_1 = 1 - \exp(-k\theta_T) \tag{2.138}$$

- For a continuous stirred tank reactor:

$$X_1 = \frac{k\theta_{CSTR}}{1 + k\theta_{CSTR}} \tag{2.139}$$

We have already seen that conversions in the batch and tubular reactor are the same as soon as the reaction time t in batch mode is equal to the residence time θ in continuous mode. A comparison of volumes between a batch system and a continuous system holds little interest given the fact that the volume required for the batch reactor depends essentially on the scheduling of successive operations. We simply note that the batch reactor can lead to the same conversion as the tubular reactor and we limit our comparison to the two continuous systems.

We can equate expressions (2.138) and (2.139) to derive a relation between the Damköhler numbers corresponding respectively to a tubular reactor and a continuous stirred tank reactor, namely:

- tubular reactor: $(Da)_T = (k\theta)_T$
- continuous stirred tank reactor: $(Da)_{CSTR} = (k\theta)_{CSTR}$.

The result of such a calculation is shown in Fig. 2.38, where the ratio $(Da)_{CSTR}/(Da)_T$ is plotted on the ordinate *versus* $1 - X_1$ on the abscissa. The diagram also shows the results of the same calculation for a second-order reaction: the Damköhler number is then expressed as $Da = C_{1,0}k\theta$. In the case of a zero-order reaction, $Da = k\theta/C_{1,0}$, the two types of continuous reactor being strictly equivalent.

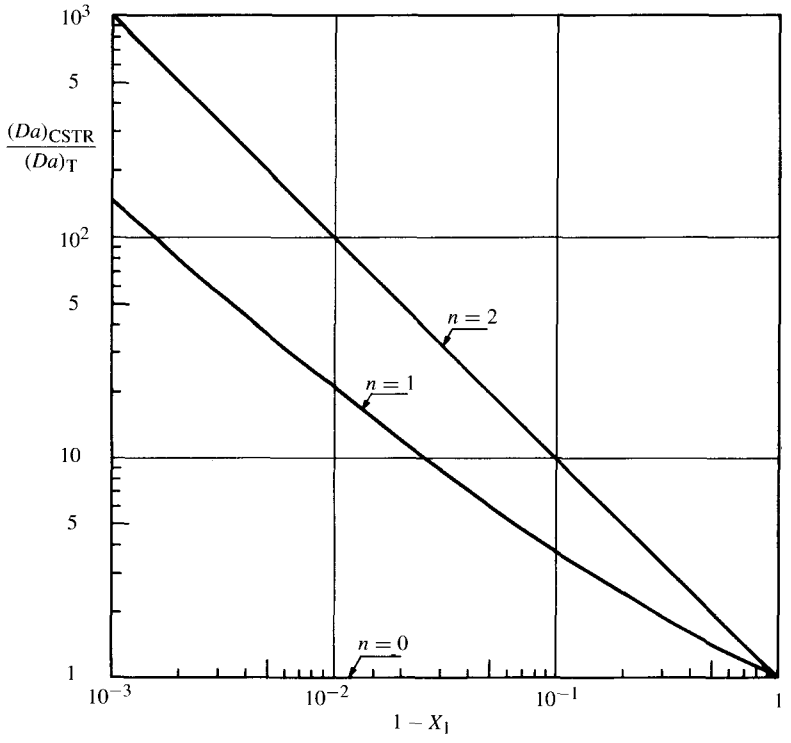


Figure 2.38 Comparison of tubular (T) and continuous stirred tank (CSTR) reactors for an n-order reaction $A_1 \rightarrow A_2$. The ratio of Damköhler numbers (Da) is used to calculate the ratio of residence times needed to obtain the same conversion X_1 (isochorous system).

Based on these simple cases, we see that the tubular reactor is more efficient per unit volume than the continuous stirred tank reactor once the reaction order becomes positive. This result is not surprising if we refer to the earlier general equations that were established for the individual reactor types.

With respect to the tubular reactor, we use the general expression for volume V_T as a function of the conversion $X_{1,s}$ we wish to achieve:

$$V_T = \int_0^{X_{1,s}} \frac{F_{1,0}\, dX_1}{-\mathcal{R}_1} \tag{2.140}$$

where:

$$\mathcal{R}_1 = \sum \nu_{1,j} r_j$$

For the continuous stirred tank reactor, we use a different expression to calculate the volume V_{CSTR}:

$$V_{CSTR} = \frac{F_{1,0} X_{1,s}}{-(\mathcal{R}_1)_s} \tag{2.141}$$

The subscript s indicates that the quantity is taken at the reactor outlet for an extent $X_{1,s}$. In the case of a simple reaction $A_1 \rightarrow A_2$, we have $\mathcal{R}_1 = -r$.

The two expressions (2.140) and (2.141) can be graphically represented as shown in Fig. 2.39.

The quantities $V_T/F_{1,0}$ and $V_{CSTR}/F_{1,0}$ correspond to the two crosshatched areas. It should be immediately apparent that the volume of the tubular reactor is smaller than that of the continuous stirred tank reactor for the same conversion and production output, to the extent that the reaction rate decreases as a function of extent (case a in Fig. 2.39). This behavior is the most frequent and corresponds to what might be referred to as normal kinetics with a positive order. In the case of a zero-order reaction, the expressions (2.140) and (2.141), shown graphically in Fig. 2.39B, clearly illustrate that both reactor types are equivalent (this is already apparent from Fig. 2.38). However, if the kinetic behavior of the reaction is abnormal, where the rate of reaction increases with extent (negative order or autocatalytic reaction), the continuous stirred tank reactor becomes more efficient than the tubular reactor (case c in Fig. 2.39).

All the above comparisons have been made on the assumption of isothermal operation of a tubular reactor at a temperature equal to that of the CSTR. In practice the comparison may not be presented in such terms and problems associated with heat exchange can, under certain conditions, alter these conclusions.

For example, in the case of an exothermic reaction, an adiabatic CSTR (autothermal) can operate at a temperature higher than the mean temperature obtained in an adiabatic tubular reactor. Thus the effect of temperature on the rate constant may sometimes offset the lower efficiency of the CSTR. However, if the desired conversion is high, the above conditions may be difficult to achieve; and in this case the combination of a CSTR and a tubular reactor may be optimal.

As with our comparison of residence time distribution, it is often useful to compare a tubular reactor with axial diffusion (PAD) with a multistage reactor, using conversion this

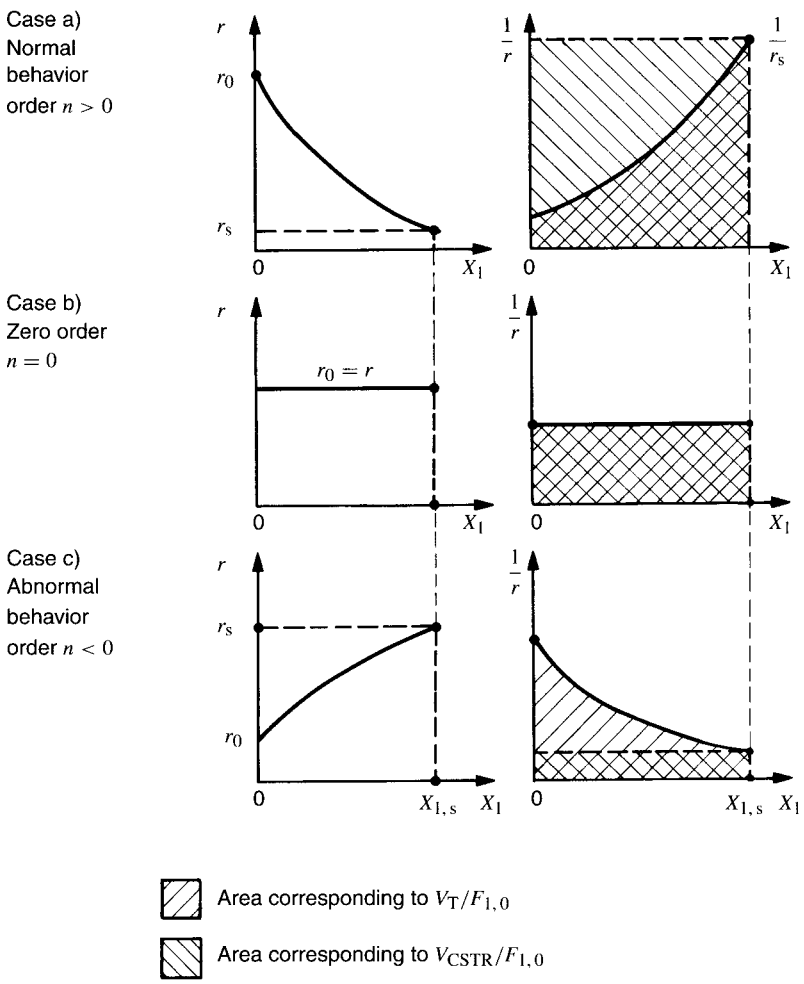


Figure 2.39 Comparison of volumes V_T and V_{CSTR} needed to achieve the same conversion $X_{1,s}$.

time as the point of comparison. The comparison is straightforward for a first-order reaction. We simply use Eqs. (2.99) and (2.131) to calculate the conversions obtained respectively in a tubular reactor characterized by a Bodenstein number, $Bo = \bar{u}L/\mathcal{D}_A$, and in a multistage reactor with m identical stages.

By direct identification of the two equations (identical conversions), we obtain a relation between the Bodenstein number and the number m of stages. This equation is shown in Fig. 2.37 by the three curves (dashed lines) that correspond to three different conversions. The curves in Fig. 2.37 clearly illustrate that the two models cannot be used indiscriminately outside a limited range, where $m > 5$ and $Bo > 10$. Consequently, the choice of model must be based on the physical structure of the reactor used.

In practice, the comparison of volumes is of limited interest. The only valid comparison is economic, and it is based on capital investment and operating costs. Also, the general guidelines given above can help orient our choice but must be supplemented by additional calculations, taking into account the various reactor types that can be used.

2.4.2.1 Multistage reactors

In addition to the two types of continuous reactor compared above, it would be useful to consider the intermediate case of the multistage reactor consisting of m stages of equal volumes, where the sum of the volumes is designated by $V_{m,E} = mV_{Et}$. A comparison with the tubular reactor can be done as before, on the basis of identical conversion X_1 and identical production output. Figure 2.40 represents the ratio of Damköhler numbers *versus* the conversion for different values of m.

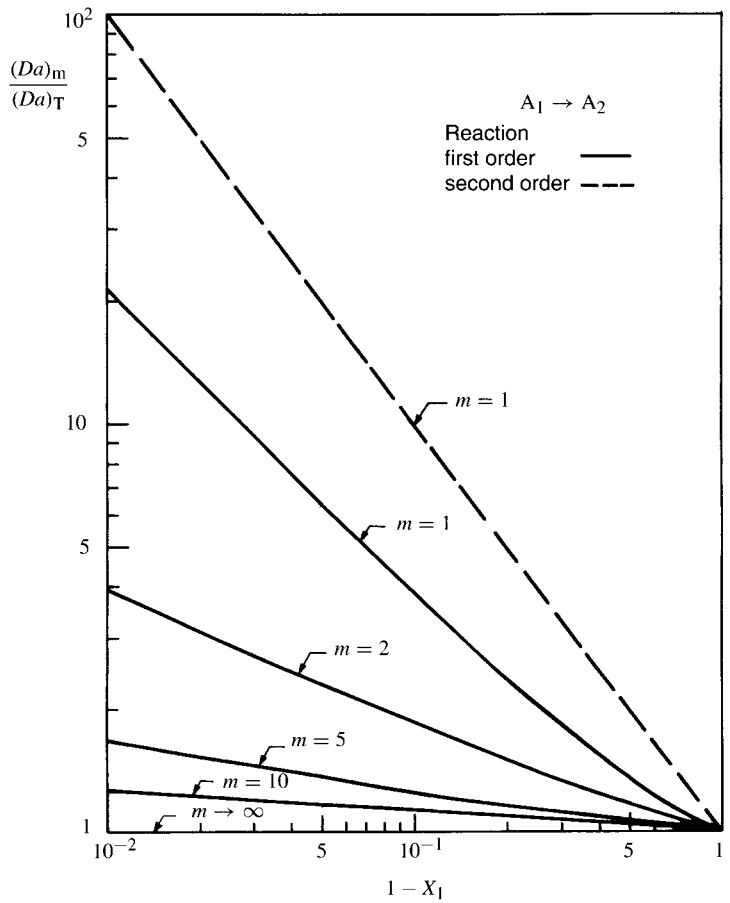


Figure 2.40 Comparison of multistage and tubular reactors. $(Da)_m$ is related to the overall residence time.

It might also be useful to determine the influence of the number of stages in series on conversion. For example Fig. 2.41 illustrates the variation in conversion X_1 for a first-order reaction $A_1 \rightarrow A_2$ as a function of the residence time θ in a stage and for various stages m in series. The case shown in the graph corresponds to a reaction where no change of volume occurs and assumes that all the reaction stages have the same volume and operate at the same temperature.

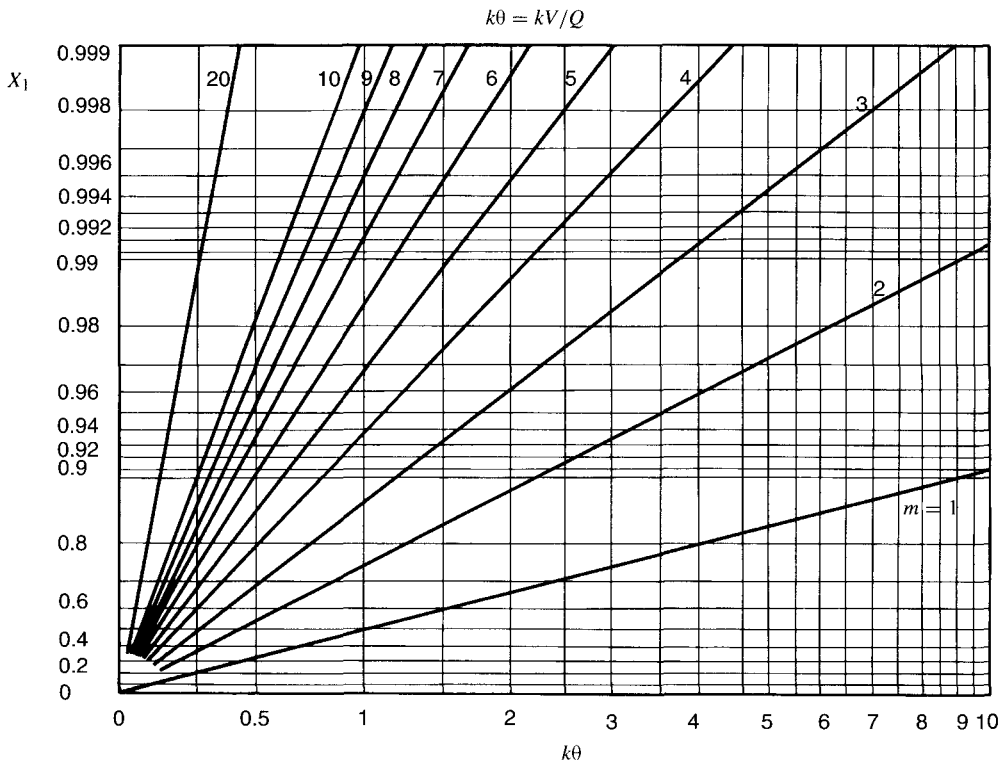


Figure 2.41 Comparison *versus* $k\theta$ of a battery of m stirred tank reactors of the same volume (first order). θ is the residence time per stage.

2.4.2.2 Tubular reactor with recycling

We can also alter the performance of a tubular reactor by recycling outgoing product to the reactor inlet. We saw earlier that a system with a high rate of recycling operates like a continuous stirred tank reactor. Below we provide further details about the effect of the recycle ratio on conversion.

Assume a system like that shown in Fig. 2.42: It consists of an ideal tubular reactor of volume V, with a flow rate of fresh feed Q in which reactant A_1 is present at a concentration $C_{1,0}$. Output from the reactor is recycled to the inlet at a flow rate RQ. At the reactor inlet,

we have a concentration of A_1, $C_{1,e}$, which can be calculated from the following expression:

$$C_{1,e} = \frac{QC_{1,0} + RQC_{1,s}}{(R+1)Q} = \frac{C_{1,0} + RC_{1,s}}{1+R} \tag{2.142}$$

$C_{1,s}$ being the concentration of A_1 at the reactor outlet.

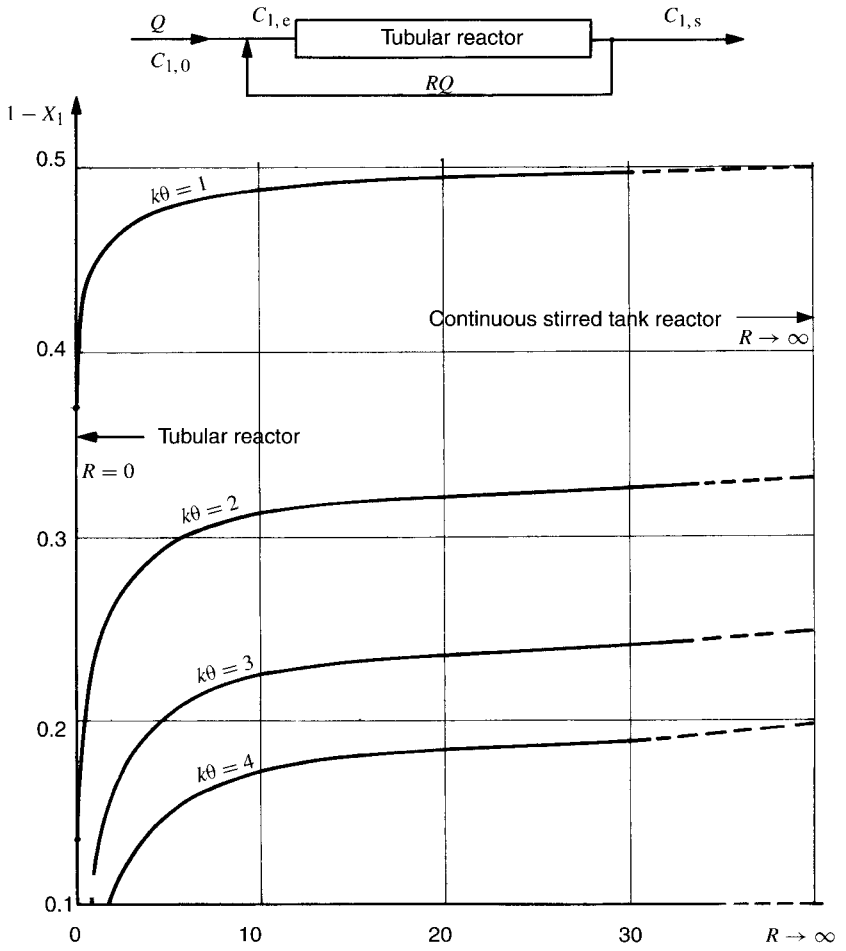


Figure 2.42 Tubular reactor with recycling.

If we also assume that the reaction is first order, we can write:

$$C_{1,s} = C_{1,e} \exp(-k\theta') \tag{2.143}$$

where:

$$\theta' = \frac{V}{(1+R)Q} = \frac{\theta}{1+R}$$

By combining the above equations, we obtain:

$$\frac{C_{1,s}}{C_{1,0}} = \frac{1}{(1+R)\exp\left(\dfrac{k\theta}{1+R}\right) - R} \tag{2.144}$$

If the recycle ratio R is high, we can reduce the above expression to:

$$\frac{C_{1,s}}{C_{1,0}} = \frac{1}{1+k\theta} \tag{2.145}$$

which corresponds to the case of a CSTR.

The transition from (2.144) to (2.145) is justified, however, only to the extent that the exponential function can be replaced by the first term of its series expansion. This assumes that $k\theta/(1+R)$ is sufficiently small, for example, less than 0.1.

In the previous section we indicated that a recycling ratio of 15 to 20 was necessary to realize a continuous stirred tank reactor. Given the limits set earlier, a recycling ratio of 20 would be valid for values of $k\theta$ less than 2, that is, for conversion of up to 70%, whereas a recycling ratio of 15 would be sufficient for conversion below 60%.

In Fig. 2.42 we have represented changes in conversion *versus* the recycle ratio R for a first-order reaction (Eq. 2.144). Bear in mind that the previous calculation applies to an ideal tubular reactor with recycling. In practice (see Fig. 2.33) recycling is carried out around vessels in which there is significant backmixing. Hence the value $R = 20$ leads to performance similar to that for a CSTR system. As indicated earlier, this value should only be exceeded for the purposes of heat exchange.

2.4.2.3 Autocatalytic reactions

Autocatalytic reactions have specific kinetic characteristics and it is worthwhile treating them separately. Consider a reaction:

$$A_1 \rightarrow A_2$$

whose kinetics is expressed by the equation: $r = kC_1C_2$.

If we assume that the change in volume due to the reaction is negligible, the change in the reaction mixture during batch operation can be described by the following equation:

$$-\frac{dC_1}{dt} = kC_1C_2$$

where:

$$C_1 + C_2 = C_{1,0} + C_{2,0}$$

The reaction rate will pass through a maximum, corresponding to a value C_1, which can easily be obtained from the above equation, namely:

$$C_1 = \left(\frac{C_{1,0} + C_{2,0}}{2}\right)$$

or: $C_1 = C_2$.

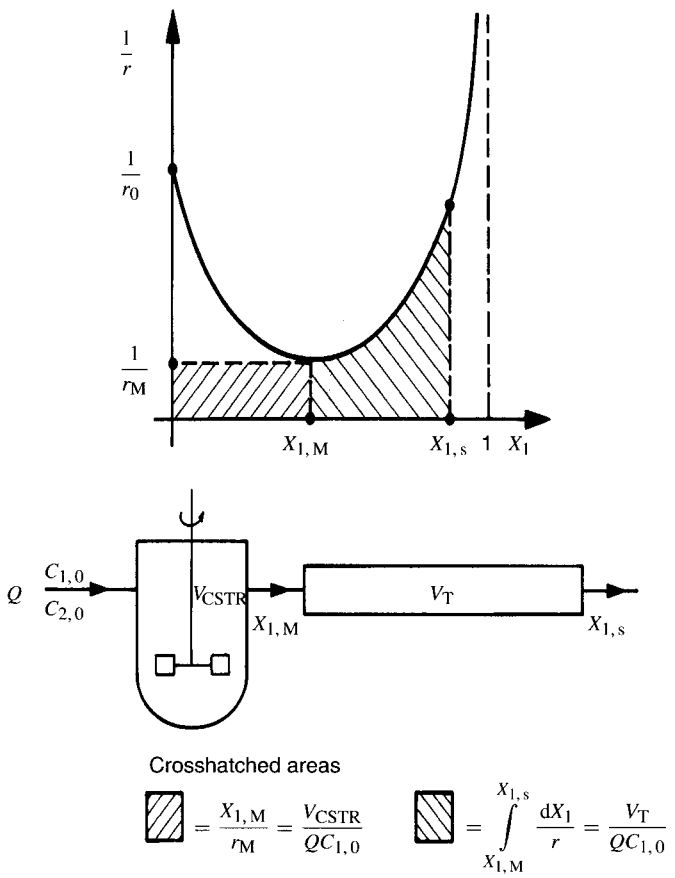


Figure 2.43 Autocatalytic reaction: $A_1 \rightarrow A_2$; $r = kC_1C_2$.

Referring to Fig. 2.43, to carry out this reaction in continuous mode, two reactors must be combined in series:

- a continuous stirred tank reactor, for $C_1 > C_2$ (zone of increasing reaction rate)
- a tubular reactor, for $C_1 < C_2$ (zone of decreasing reaction rate).

We wish to emphasize that the above reaction cannot be carried out in batch mode (or in a tubular reactor) unless the initial concentration of product A_2 is not zero ($C_{2,0} \neq 0$). In a continuous stirred tank reactor, however, we need only initiate the reaction by injecting a small amount of A_2 at the start for it to continue on its own. In an oxidation reaction, for example, this practice is known as "initiation", while in the case of fermentation, the initial supply of product is referred to as "seeding".

Using the notation adopted in Fig. 2.43, we can write:

$$r_M = \frac{k(C_{1,0} + C_{2,0})^2}{4} \quad \text{and} \quad X_{1,M} = \frac{C_{1,0} - C_{2,0}}{2C_{1,0}}$$

these two equations being valid only if $C_{1,0} > C_{2,0}$.

The volumes required for each reactor are calculated as indicated previously:

$$V_{\mathrm{CSTR}} = \frac{QC_{1,0}X_{1,\mathrm{M}}}{r_{\mathrm{M}}}$$

$$V_{\mathrm{T}} = QC_{1,0}\int_{X_{1,\mathrm{M}}}^{X_{1,\mathrm{s}}} \frac{\mathrm{d}X_1}{r}$$

Note that these expressions remain valid for $C_{2,0} = 0$.

2.4.3 Selectivity

In complex reaction systems it is often selectivity that serves as a basis for determining the type of reactor to use. In this case the profitability of the operation is directly related to the selectivity of the transformation of a principal reactant A_1 into one or more desired products.

Let us assume a complex reaction system of the type: $\sum \nu_{i,j}\mathrm{A}_i = 0$. We are interested in transforming as much as possible of reactant A_1 into compound A_2. The ideal reaction could be expressed, for example, as $\nu_{1,1}\mathrm{A}_1 \rightarrow \nu_{2,1}\mathrm{A}_2$. We can then write the overall selectivity resulting from an operation in a batch reactor:

$$S_{2,1} = \frac{\Delta n_2}{\Delta n_1}\frac{\nu_{1,1}}{\nu_{2,1}} \tag{2.146}$$

Similarly, we define the instantaneous selectivity to be:

$$s_{2,1} = \frac{\mathrm{d}n_2}{\mathrm{d}n_1}\frac{\nu_{1,1}}{\nu_{2,1}} \tag{2.147}$$

We see that the instantaneous selectivity is determined by considering the reaction mixture under well-defined conditions and by allowing it to evolve over an infinitesimal period of time dt, leading to changes in the number of moles of A_1 and A_2 equal to $\mathrm{d}n_1$ and $\mathrm{d}n_2$. The instantaneous selectivity can then be calculated directly from the kinetic equations.

We saw earlier that the continuous tubular reactor provided the same performance as the batch reactor operating under the same conditions. This implies, in particular, that the selectivities obtained will be identical. In what follows we limit our discussion to a comparison of the two types of continuous reactors (tubular and CSTR).

If the extent of a reaction in a continuous reactor is such that the molar flow rate of A_1 changes from $F_{1,0}$ at the inlet to $F_{1,\mathrm{s}}$ at the outlet, we can write:

$$X_1 = \frac{F_{1,0} - F_{1,\mathrm{s}}}{F_{1,0}} \quad \text{(conversion of A}_1\text{)}$$

The overall selectivity can then be written:

$$S_{2,1} = \frac{\Delta F_2}{\Delta F_1}\frac{\nu_{1,1}}{\nu_{2,1}}$$

In a tubular reactor the instantaneous selectivity changes throughout the reactor as the conversion increases. The instantaneous selectivity is written:

$$s_{2,1} = \frac{\mathrm{d}F_2}{\mathrm{d}F_1} \frac{\nu_{1,1}}{\nu_{2,1}}$$

Through integration, we can calculate the overall selectivity:

$$(S_{2,1})_T = \frac{1}{F_{1,s} - F_{1,0}} \int_{F_{1,0}}^{F_{1,s}} s_{2,1}\, \mathrm{d}F_1 \tag{2.148}$$

For a continuous stirred tank reactor, this same value can be expressed as follows:

$$(S_{2,1})_{CSTR} = (s_{2,1})_s \tag{2.149}$$

where $(s_{2,1})_s$ is the instantaneous selectivity at the reactor outlet as well as throughout the volume of the reactor.

If, as a first approximation, we consider that variations in instantaneous selectivity are associated solely with the conversion X_1, it is easy to compare Eqs. (2.148) and (2.149).

If $s_{2,1}$ increases as F_1 decreases, that is, as the extent of reaction increases, we obtain, for a continuous stirred tank reactor, a selectivity greater than that obtainable in a tubular reactor for the same conversion of A_1. Conversely, if $s_{2,1}$ decreases as the extent of reaction increases, the reverse occurs and the tubular reactor will provide a better selectivity. These two situations are illustrated in Fig. 2.44 (case **A** and **B**).

Other situations can arise where the change in $s_{2,1}$ as a function of X_1 is not monotone. We can, for example, have a maximum (Fig. 2.44C) or minimum (Fig. 2.44D). In these cases, for a fixed conversion $X_{1,s}$, the maximum selectivity will be obtained by combining the two types of reactors in series:

- In case C the first reactor will be a continuous stirred tank reactor operating at the maximum instantaneous selectivity, followed by a tubular reactor (see photo 2).
- In case D we reverse the order of the reactors so that the conditions under which the continuous stirred tank reactor operates are such that the final conversion is $X_{1,s}$, for which the selectivity is $(s_{2,1})_s$.

Note that our assumption regarding the exclusive dependence of $s_{2,1}$ on X_1 is not always confirmed in practice.

In fact, we can achieve the same conversion $X_{1,s}$ using either reactor type (tubular or CSTR). The selectivities obtained will not be the same, which implies that the composition of the effluents at the reactor outlets is not the same. Under these conditions, it is highly probable that the instantaneous selectivities corresponding to the outlet conditions of the reactors are not the same.

In practice, therefore, the guidelines for selection described above can only be used with caution if we do not know the exact behavior of the reaction system. There are situations, however, where the exclusive dependence of instantaneous selectivity on extent of reaction turns out to be correct because of kinetics or can be taken as a valid first approximation (this is the case for low conversion).

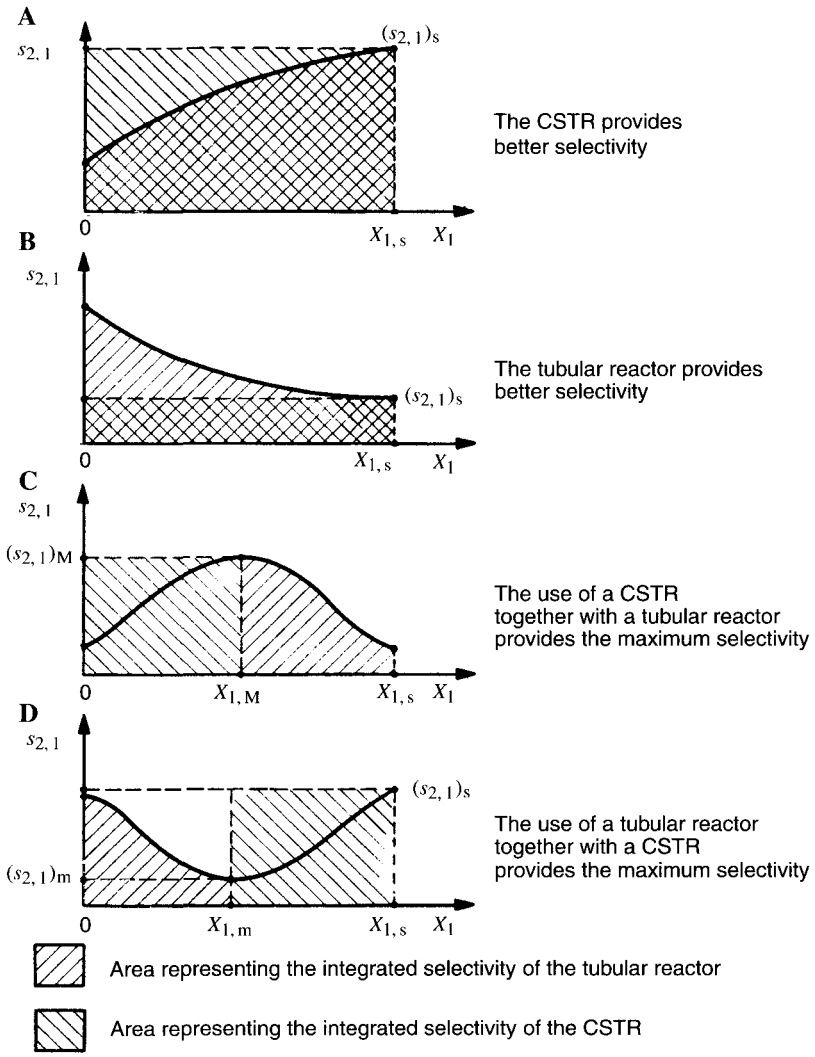


Figure 2.44 Change in selectivity with conversion.

The invariance of $s_{2,1}$ with increasing conversion is valid for a simple reaction; in this case the two reactor types will have the same selectivity, independent of the extent of reaction (case E).

The various cases, shown graphically in Fig. 2.44, can be expressed analytically:

- Case (A): $\dfrac{ds_{2,1}}{dX_1} > 0 \qquad \text{for} \quad 0 \leqslant X_1 \leqslant X_{1,s}$
- Case (B): $\dfrac{ds_{2,1}}{dX_1} < 0 \qquad \text{for} \quad 0 \leqslant X_1 \leqslant X_{1,s}$



Photo 2 Reaction unit for an olefin dimerization process (Dimersol) with two CSTR stages (vertical tanks with recirculation) in which a conversion rate greater than 90% is obtained. The remainder of the conversion takes place in the tubular reactor (shown in the foreground on the right).

(*IFP Photo Library: Dimersol G unit*).

- Case (C): $\dfrac{ds_{2,1}}{dX_1} > 0$ for $0 \leqslant X_1 \leqslant X_{1,M}$

  $\dfrac{ds_{2,1}}{dX_1} < 0$ for $X_{1,M} \leqslant X_1 \leqslant X_{1,s}$

- Case (D): $\dfrac{ds_{2,1}}{dX_1} < 0$ for $0 \leqslant X_1 \leqslant X_{1,M}$

  $\dfrac{ds_{2,1}}{dX_1} > 0$ for $X_{1,M} \leqslant X_1 \leqslant X_{1,s}$

- Case (E): $\dfrac{ds_{2,1}}{dX_1} = 0$ for $0 \leqslant X_1 \leqslant X_{1,s}$

2.4.3.1 Example

Consider the following reaction system:

$$\nu_{1,1}A_1 \rightarrow \nu_{2,1}A_2 \quad \text{(constant } k_1\text{, order } p\text{)}$$
$$\nu_{1,2}A_1 \rightarrow \nu_{3,2}A_3 \quad \text{(constant } k_2\text{, order } q\text{)}$$

The balance equations for a batch reactor can be written:

$$\frac{1}{V}\frac{dn_1}{dt} = \nu_{1,1}k_1\left(\frac{n_1}{V}\right)^p + \nu_{1,2}k_2\left(\frac{n_1}{V}\right)^q \tag{2.150}$$

$$\frac{1}{V}\frac{dn_2}{dt} = \nu_{2,1}k_1\left(\frac{n_1}{V}\right)^p \tag{2.151}$$

The instantaneous selectivity $s_{2,1}$ is then expressed as:

$$s_{2,1} = \frac{\nu_{1,1}}{\nu_{2,1}}\frac{dn_2}{dn_1} = \frac{k_1 n_1^p}{k_1 n_1^p + \dfrac{\nu_{1,2}}{\nu_{1,1}}k_2 n_1^q V^{p-q}} \tag{2.152}$$

We assign:

$$k_2' = \frac{\nu_{1,2}}{\nu_{1,1}}k_2 V^{p-q}$$

from which:

$$s_{2,1} = \frac{k_1 n_1^p}{k_1 n_1^p + k_2' n_1^q} \tag{2.153}$$

Moreover, the conversion X_1 can be written:

$$X_1 = \frac{n_{1,0} - n_1}{n_{1,0}} = 1 - \frac{n_1}{n_{1,0}} \tag{2.154}$$

$$\frac{ds_{2,1}}{dX_1} = \frac{ds_{2,1}}{dn_1}\frac{dn_1}{dX_1} = -n_{1,0}\frac{ds_{2,1}}{dn_1} \tag{2.155}$$

From (2.153) and (2.155) we derive:

$$\frac{ds_{2,1}}{dX_1} = n_{1,0}\frac{(q-p)k_1k_2'n_1^{p+q-1}}{(k_1n_1^p + k_2'n_1^q)^2} \tag{2.156}$$

The sign of the equation depends only on the difference $(q-p)$. In light of the remarks made earlier, we can conclude that:

- if $q > p$:

$$\frac{ds_{2,1}}{dX_1} > 0$$

and the continuous stirred tank reactor will have greater selectivity;

- if $q < p$:

$$\frac{ds_{2,1}}{dX_1} < 0$$

and the tubular reactor will have better selectivity;

- if $p = q$:

$$\frac{ds_{2,1}}{dX_1} = 0$$

we have the case of a simple reaction of the type: $\nu_1A_1 \rightarrow \nu_2A_2 + \nu_3A_3$, and the choice of reactor will be irrelevant.

2.4.3.2 Determination of instantaneous selectivity

The above calculations assume that the reaction scheme and the kinetics of the various reactions are well known. In practice however we often have only an approximate and partial understanding of these mechanisms.

Experimentally we can obtain the value of instantaneous selectivity from a continuous stirred tank reactor. However, as indicated, the relation between instantaneous selectivity and conversion, which can thus be obtained, is not necessarily equivalent to the relation that exists in a tubular reactor. Nonetheless, we are often forced by circumstances to assume this to be the case, at least as a first approximation.

Assume we have a reaction system that can be used to produce compound A_2 from reactant A_1. On the basis of the molecular structure of A_1 and A_2, we can always write an ideal reaction: $\nu_{1,1}A_1 \rightarrow \nu_{2,1}A_2$.

The conversion of A_1 is written as above for a continuous tubular system:

$$X_1 = \frac{F_{1,0} - F_{1,s}}{F_{1,0}} \tag{2.157}$$

and the instantaneous selectivity is:

$$s_{2,1} = \frac{dF_2}{dF_1}\frac{\nu_{1,1}}{\nu_{2,1}} \tag{2.158}$$

The overall selectivity for a conversion X_1 is written:

$$S_{2,1} = \frac{F_{2,0} - F_2}{F_{1,0} - F_1}\frac{\nu_{1,1}}{\nu_{2,1}} \tag{2.159}$$

From the above equations, we determine that:

$$F_{2,0} - F_2 = F_{1,0} X_1 \frac{\nu_{2,1}}{\nu_{1,1}} S_{2,1} \tag{2.160}$$

Through derivation with respect to F_1, we obtain:

$$\frac{dF_2}{dF_1} = -\frac{\nu_{2,1}}{\nu_{1,1}} \left[(F_{1,0} - F_1) \frac{dS_{2,1}}{dF_1} - S_{2,1} \right]$$

or:

$$s_{2,1} = S_{2,1} + X_1 \frac{dS_{2,1}}{dX_1} \tag{2.161}$$

This equation, which was determined for a tubular reactor, is also valid for a batch reactor. Equation (2.161) can be rewritten as follows:

$$s_{2,1} = \frac{d}{dX_1} (X_1 S_{2,1}) \tag{2.162}$$

We see that, if we measure the overall selectivity by using a batch or tubular reactor, we can calculate the instantaneous selectivity by means of Eq. (2.162). This value of $s_{2,1}$ can then be used for a continuous stirred tank reactor.

2.4.4 Concluding remarks

As we have seen, the final choice of the type of reactor needed to realize a given chemical transformation will be made on the basis of economic considerations. If the reaction system is simple (a single stoichiometric equation), the problem of selectivity doesn't arise so that capacity and conversion become the only fixed objectives. The cost of production, including capital outlays and variable operating costs, will have to be minimized by choosing the most suitable reactor type.

At this stage the following general guidelines should be borne in mind:

- If the reaction order is positive and if high conversion is required ($> 95\%$), the tubular reactor is preferred.
- If the reaction is autocatalytic, the continuous stirred tank reactor is generally preferred.

However, these choices, based solely on reaction kinetics, often need to be modified to take into account other factors, such as the operating conditions and thermal behavior of the reaction. In particular, for high-thermicity reactions, the CSTR or multistage reactor is often preferable.

If the reaction system is complex, selectivity is often the most important factor when choosing a reactor type and no general guidelines can be offered out of context. Nonetheless, for consecutive systems and whenever the desired products are intermediates, the tubular reactor should generally provide the best results.

The selection criteria we have developed in this chapter, based on the kinetic characteristics of the reactions involved, can also be applied to the heterogeneous systems that we examine in the following chapters. However, they must be modified to take into account the multiphase nature of these systems.

Our comparisons of various reactor types have most often been based on the assumption that the conversion of a reactant has been determined in advance. In practice, the optimal conversion must often be found through a consideration of the reactor environment, in particular the part of the unit where the reactor effluent is fractionated. Reactor optimization must therefore be carried out globally, and not simply limited to the vessel in which the reaction takes place.

REFERENCES

Dream RF (1999) Heat transfer in agitated jacketed vessels. Chem Eng 106, 1, pp 90–96.

Documentation De Dietrich « Cat F04/96 »

Levenspiel O (1999) Chemical Reaction Engineering (3e édition). John Wiley and Sons, New York.

Rewatkar V, Joshi JB (1991) Effect of impeller design on liquid phase mixing in mechanically agitated reactors. Chem Eng Comm 102, pp 1–33.

Salfati S (1997) Électricité : le vecteur énergétique de la chimie nouvelle. Informations Chimie 384, pp 117–128.

Stoessel F (1993) What is your thermal risk? Chem Eng Prog October 1993, pp 68–75.

Trambouze P *et al.* (2000) Petroleum Refining. Vol. 4: Materials and Equipment. Editions Technip, Paris.

NOMENCLATURE

(specific to Chapter 2)

Symbol	Definition	SI unit
Bo	Bodenstein number $= \bar{u}L/\mathcal{D}_A$	–
Da	Damköhler number (for a first-order reaction, $Da = k_0$)	–
$\bar{C}_{Pi}$	Mean value of C_{Pi} in the temperature range under consideration	J/mol · K
d_T	Interior diameter of a tube	m
e	Wall thickness	m
f	Friction factor	
l_{eq}	Equivalent length of an bend	m
m	$m = \nu_{1,1}k_1/\nu_{2,2}k_2$	–
m	Number of a stage in series in a battery	–
N	Number of stages	–
$\mathcal{N}_C$	Number of bends for a tube length L	–
PDA	plugflow + axial dispersion	
Q_C	Volumetric flow rate of feedstock	m^3/s
Q_V	Volumetric flow rate of discharge stream	m^3/s
Q_E	Heat exchanged	W
Q_P	Heat generated	W
r	Radial distance from the center of the tube	m
R	Ratio between recirculation and feed rate	–
t_M	Mixing time	s
$\bar{u}$	Mean velocity in the tube $= Q/S$	m/s
u_i	Interstitial velocity $= \bar{u}/\varepsilon_F$	m/s
$u(r)$	Velocity at radius r	m/s
$\bar{\nu}$	$= \sum \nu_i$	–
	Subscripts:	
ad	adiabatic	
L	corresponding to the total length of the tube	
id	corresponding to an ideal plug-flow reactor	
m	relative to stage m	
ech	relative to the exchanger	
M	indicates an optimal partition point for autocatalytic reactions	
CSTR	continuous stirred tank reactor	
T	tubular with plug flow	

Copyrighted Materials
Copyright © 2004 Editions Technip Retrieved from www.knovel.com

3 General Characteristics of Reactors with Two Fluid Phases

3.1 REVIEW OF TWO-FILM THEORY

Consider two fluid phases separated by an interface. If the two phases are not in concentration equilibrium for at least one of the compounds A_i, the compound will migrate from one phase to the other across the interface. The transfer of A_i will cease when both phases reach the concentration equilibrium for compound A_i.

Let us examine a situation in which A_i is transferred from phase I, where its concentration is $C_{i,I}$, to phase II, where its concentration is $C_{i,II}$. For the sake of convenience, we assume that the concentrations $C_{i,I}$ and $C_{i,II}$ are constant over time (equivalent to the situation existing at a given point in a gradient reactor operating in the steady state or the one existing at any point in a continuous stirred tank reactor in the steady state).

The simplest transfer law to express the flow of A_i is:

$$N_i = K_{i,I}\left(C_{i,I} - C_{i,I}^{E}\right) \tag{3.1}$$

where N_i is the flux of A_i from phase I to phase II, expressed in SI units as moles of $A_i/s \cdot m^2$ of interfacial area ($mol/s \cdot m^2$).

$C_{i,I}^{E}$ is the **equilibrium concentration**, that is, the concentration that would be found in phase I if it were in equilibrium with phase II, where the concentration is $C_{i,II}$. If the concentrations C_i are expressed in mol/m^3, $K_{i,I}$ is in m/s.

The overall transfer coefficient $K_{i,I}$ has the dimensions of **velocity**. It is also possible to express transfer flux with respect to the receptor phase (here phase II) since, in the steady state, the flow leaving phase I is equal to the flow reaching phase II. We can then write:

$$N_i = K_{i,II}\left(C_{i,II}^{E} - C_{i,II}\right) \tag{3.2}$$

$C_{i,II}^{E}$ is the concentration of compound A_i found in phase II when its concentration is in equilibrium with phase I, where the concentration is $C_{i,I}$.

The equilibrium equation between the concentrations in the two phases is generally expressed as a curve where $C_{i,\mathrm{I}}$ is a function of $C_{i,\mathrm{II}}$, as shown in Fig. 3.1. This curve can often be considered a straight line, at least in the range of concentrations that is of interest. The equilibrium line can therefore be described by the equation:

$$C_{i,\mathrm{I,e}} = mC_{i,\mathrm{II,e}} + p \tag{3.3}$$

Using the definitions of $C^{\mathrm{E}}_{i,\mathrm{I}}$ and $C^{\mathrm{E}}_{i,\mathrm{II}}$, we then have:

$$C^{\mathrm{E}}_{i,\mathrm{I}} = mC_{i,\mathrm{II}} + p$$

$$C_{i,\mathrm{I}} = mC^{\mathrm{E}}_{i,\mathrm{II}} + p \quad \text{that is,} \quad C^{\mathrm{E}}_{i,\mathrm{II}} = \frac{C_{i,\mathrm{I}} - p}{m}$$

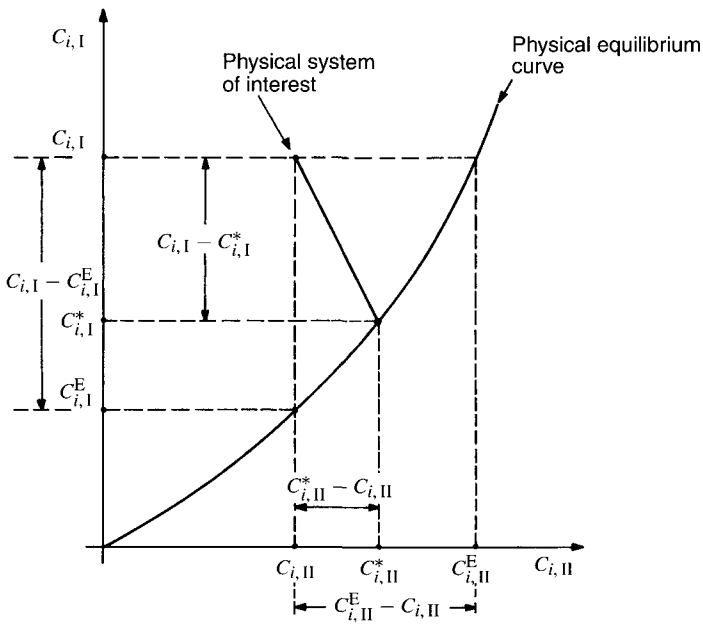


Figure 3.1 Deviations from equilibrium during transfer between two fluid phases.

It is easy to show that $K_{i,\mathrm{II}} = mK_{i,\mathrm{I}}$. In general it is assumed that equilibrium is established exactly at the interface. If we refer to $C^{*}_{i,\mathrm{I}}$ and $C^{*}_{i,\mathrm{II}}$ as the concentrations occurring at the phase I side and the phase II side of the interface, we can define the flux by:

$$N_i = k_{i,\mathrm{I}}(C_{i,\mathrm{I}} - C^{*}_{i,\mathrm{I}}) \tag{3.4}$$

or by:

$$N_i = k_{i,\mathrm{II}}(C^{*}_{i,\mathrm{II}} - C_{i,\mathrm{II}}) \tag{3.5}$$

Here, we introduce other transfer coefficients $k_{i,\mathrm{I}}$ and $k_{i,\mathrm{II}}$, referred to as the film transfer coefficients for phases I and II respectively. These also have the dimensions of velocity. It can be shown that:

$$\frac{1}{K_{i,\mathrm{I}}} = \frac{1}{k_{i,\mathrm{I}}} + \frac{m}{k_{i,\mathrm{II}}} \tag{3.6}$$

and:

$$\frac{1}{K_{i,\mathrm{II}}} = \frac{1}{k_{i,\mathrm{II}}} + \frac{1}{mk_{i,\mathrm{I}}} \tag{3.7}$$

We thus have four means of expressing flux that can be used according to the available data or the specific phenomenon we wish to express. For reasons of convenience in presentation, we will mainly use (3.5) as the basic expression, since we are primarily interested in the phenomena that occur in phase II, which will be assumed to be the reaction phase. We see that the flux expression reveals the existence of a transfer potential based on a difference in concentration. These potentials are shown as straight line segments in Fig. 3.1. The higher the transfer potential, the greater the transfer, in other words the system is further from equilibrium.

Several theories have been proposed to explain a phenomenological transfer law and, in particular, to link the transfer coefficient to the physicochemical properties of the phases present and the hydrodynamic conditions governing their flow [Sherwood *et al.*, 1975]. Here we consider only those aspects associated with two-film theory, which assumes that the resistance to mass transfer is found in two films in each of the phases, these films being located on either side of the interface and in immediate proximity to it. This situation is shown schematically in Fig. 3.2, which refers, as above, to a local situation in which $C_{i,\mathrm{I}}$ and $C_{i,\mathrm{II}}$ are invariant over time. The films are assumed to be immobile and of thickness δ_{I} and δ_{II}. Applying Fick's law relative to transfer by molecular diffusion, we can write:

$$N_i = \mathcal{D}_{i,\mathrm{I}} \left(\frac{C_{i,\mathrm{I}} - C^*_{i,\mathrm{I}}}{\delta_{\mathrm{I}}} \right) = \mathcal{D}_{i,\mathrm{II}} \left(\frac{C^*_{i,\mathrm{II}} - C_{i,\mathrm{II}}}{\delta_{\mathrm{II}}} \right) \tag{3.8}^{(1)}$$

$\mathcal{D}_{i,\mathrm{I}}$ and $\mathcal{D}_{i,\mathrm{II}}$ are the coefficients of molecular diffusion for A_i in phase I and phase II respectively (in $L^2 \cdot \theta^{-1}$, or m^2/s). We then derive:

$$k_{i,\mathrm{I}} = \frac{\mathcal{D}_{i,\mathrm{I}}}{\delta_{\mathrm{I}}} \tag{3.9}$$

$$k_{i,\mathrm{II}} = \frac{\mathcal{D}_{i,\mathrm{II}}}{\delta_{\mathrm{II}}} \tag{3.10}$$

Note that Eqs. (3.6) and (3.7) reflect the addition of two localized resistances in each of the fluid phases.

1. Note that two-film theory implies that the thicknesses δ_{I} and δ_{II} are the same, regardless of the species A_i that is transferred and even if several species are transferred simultaneously (which is why the subscript i has been dropped from the symbol δ.)

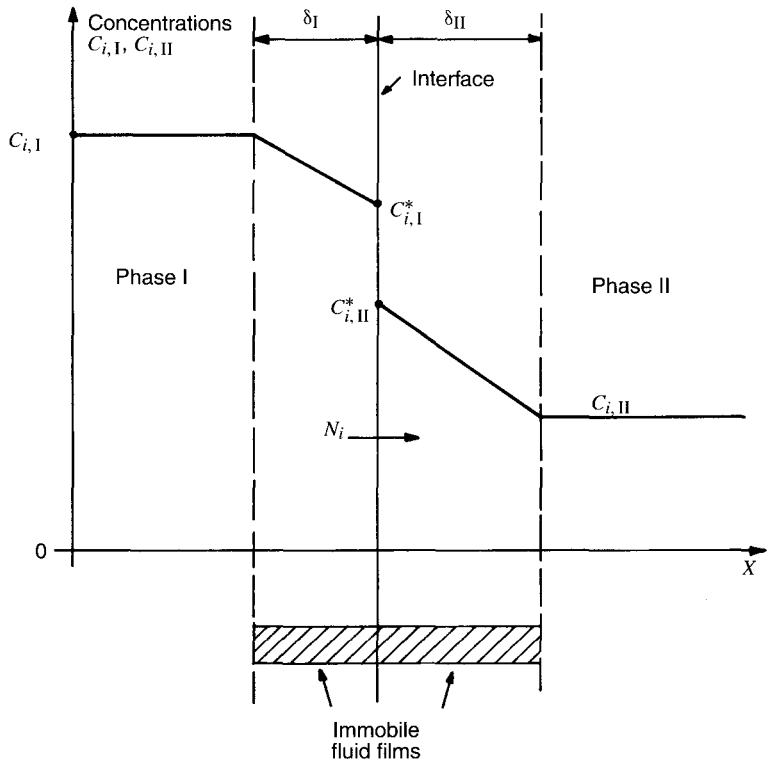


Figure 3.2 Two-film theory: concentration profiles on either side of the interface.

Comment: If phase I is a gas phase, partial pressures p_i are often used in place of concentrations, C_i. The flux expressions then become:

$$N_i = K_{i,\mathrm{I}}\left(C_{i,\mathrm{I}} - C^{\mathrm{E}}_{i,\mathrm{I}}\right) = K_{i,\mathrm{G}}\left(p_{i,\mathrm{G}} - p^{\mathrm{E}}_{i,\mathrm{G}}\right)$$
$$N_i = k_{i,\mathrm{I}}\left(C_{i,\mathrm{I}} - C^{*}_{i,\mathrm{I}}\right) = k_{i,\mathrm{G}}\left(p_{i,\mathrm{G}} - p^{*}_{i,\mathrm{G}}\right) \tag{3.11}$$

Since for ideal gases $C_i = p_i/(RT)$, we see that:

$$\frac{K_{i,\mathrm{I}}}{K_{i,\mathrm{G}}} = \frac{k_{i,\mathrm{I}}}{k_{i,\mathrm{G}}} = RT$$

The dimensions of $K_{i,\mathrm{G}}$ and $k_{i,\mathrm{G}}$ are in mol/s · m^2 · Pa.

3.2 MASS TRANSFER ACCOMPANIED BY CHEMICAL REACTION

We now turn our attention to the disturbances in mass transfer caused by a chemical reaction [Astarita, 1967; Danckwerts, 1970]. It is fairly obvious that a chemical reaction, since it modifies the concentration profile at the interface, will also affect the transfer flux toward the phase where the reaction is taking place.

3.2.1 Irreversible and isothermal reaction in a single phase and transfer toward the reaction phase

Assume we have a phase I containing compound A_1 and a phase II containing compound A_2. We further assume that compound A_1 is transferred from phase I to phase II and that an irreversible reaction occurs in this second phase:

$$\nu_1 A_1 + \nu_2 A_2 \rightarrow \nu_3 A_3 \tag{3.12}$$

The rate of reaction in phase II, wherever the concentrations are $C_{1,\mathrm{II}}$ and $C_{2,\mathrm{II}}$, can be expressed conventionally in moles per second per cubic meter of the reaction phase:

$$r = f(C_{1,\mathrm{II}}, C_{2,\mathrm{II}}) \quad (\mathrm{mol/m^3 \cdot s}) \tag{3.13}$$

It must be stressed that this rate expression is considered valid at every point of phase II, that is both in the film near the interface and in the bulk of reaction phase II. Below we make use of three distinct notations for the concentration $C_{i,\mathrm{II}}$:

- $C_{i,\mathrm{II}}$ designates the concentration of A_i at any point in phase II, as shown in the previous rate expression.
- $C_{i,\mathrm{IIb}}$ designates the concentration of A_i in the bulk of phase II, beyond the film.
- $C_{i,\mathrm{II}}(x)$ designates the concentration of A_i at a point of the film located a distance x from the interface. We then have:

$$C_{i,\mathrm{II}}(\delta_{\mathrm{II}}) = C_{i,\mathrm{IIb}}$$

The subscript II will be omitted in the following discussion since it refers only to reaction phase II.

We now examine the situation illustrated in Fig. 3.3, where compound A_1 is transferred from phase I to phase II. Once it crosses the interface, A_1 participates in the reaction with A_2. It is assumed that compounds A_2 and A_3 do not cross the interface and, therefore, do not diffuse into phase I. Figure 3.3 indicates the shape of the concentration profiles for a local situation where the concentrations are $C_{1,\mathrm{Ib}}$, $C_{1,\mathrm{IIb}}$, $C_{2,\mathrm{IIb}}$, $C_{3,\mathrm{IIb}}$, these being invariant over time.

3.2.1.1 General case

We can write a material balance for compound A_i for a slice of film of thickness dx and for a unit cross-section of the interface by applying Fick's law relative to molecular diffusion in quasi-immobile media:

(flux of A_i entering at x on the abscissa)

+ (quantity of A_i that appears or disappears per unit of time)

= (flux of A_i leaving at $x + dx$ on the abscissa)

$$-\mathcal{D}_i \left[\frac{dC_i(x)}{dx}\right]_x + \nu_i r\, dx = -\mathcal{D}_i \left[\frac{dC_i(x)}{dx}\right]_{x+dx} \tag{3.14}$$

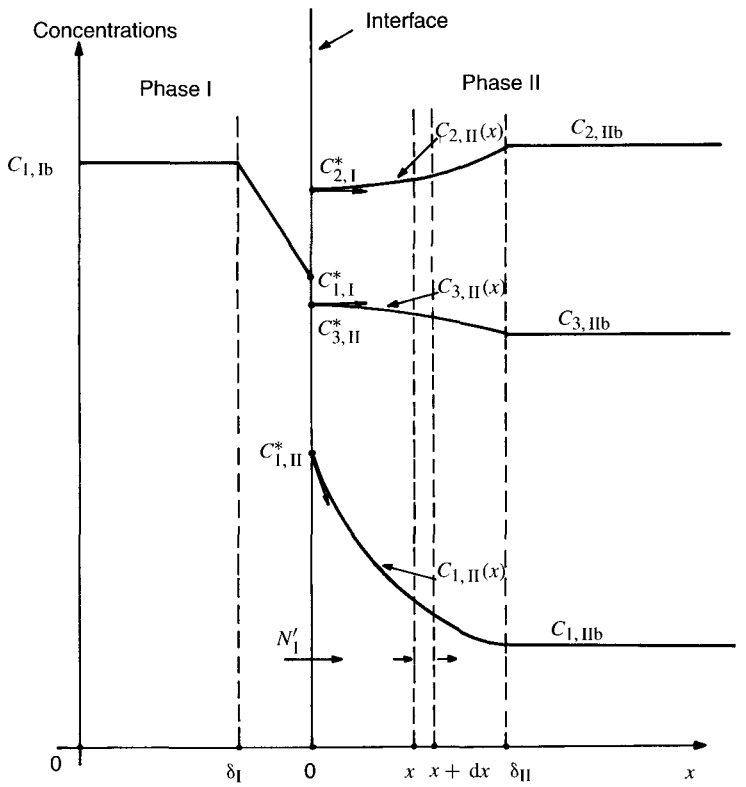


Figure 3.3 Concentration profiles for constituents A_1, A_2, A_3 in the phase II film when constituent A_1 is transferred. A_1 participates in the chemical reaction in phase II that follows the stoichiometric relation $\nu_1 A_1 + \nu_2 A_2 \rightarrow \nu_3 A_3$.

If $\mathrm{d}x$ tends toward 0, we can write, for each compound A_i:

$$\mathcal{D}_i \left[\frac{\mathrm{d}^2 C_i(x)}{\mathrm{d}x^2} \right] + \nu_i r = 0 \tag{3.15}$$

The boundary conditions will be:

$$C_i(0) = C_i^* \quad \text{for } x = 0 \tag{3.16}$$

$$C_i(\delta) = C_{i,b} \quad \text{for } x = \delta \tag{3.17}$$

Remember that, according to two-film theory, δ is the thickness of the phase II film defined by $\delta = \mathcal{D}_1/k_1 = \mathcal{D}_2/k_2 = \mathcal{D}_i/k_i$, ($k_1$, k_2, k_i being the film transfer coefficients on the phase II side, defined in the case of transfer *without chemical reaction*).

3.2.1.2 Pseudo-first-order reaction

We now consider the case of an irreversible first-order reaction with respect to each of the two reactants [$r = kC_1(x)C_2(x)$], where we can assume that $C_2(x)$ is constant throughout the film and equal to $C_{2,b}$ (below we examine the implications of this assumption).

The solution of (3.15) with the boundary conditions (3.16) and (3.17) is written:

$$C_1(x) = \frac{C_{1,b}\sinh[\rho x] + C_1^*\sinh[-\rho(\delta - x)]}{\sinh[\rho\delta]} \tag{3.18}$$

where:

$$\rho = \sqrt{\frac{-\nu_1 k C_{2,b}}{\mathcal{D}_1}}$$

We can determine the flux crossing the interface by writing:

$$[N_1']_{x=0} = -\mathcal{D}_1\left[\frac{dC_1(x)}{dx}\right]_{x=0} = k_1\frac{\rho\delta}{\tanh[\rho\delta]}\left[C_1^* - \frac{C_{1,b}}{\cosh[\rho\delta]}\right] \tag{3.19}$$

The variable N' represents the flux with chemical reaction, N being reserved for the flux *without* chemical reaction.

Similarly, we can calculate the flux at the other end of the film, when $x = \delta$:

$$[N_1']_{x=\delta} = -\mathcal{D}_1\left[\frac{dC_1(x)}{dx}\right]_{x=\delta} = k_1\frac{\rho\delta}{\tanh[\rho\delta]}\left[\frac{C_1^*}{\cosh[\rho\delta]} - C_{1,b}\right]$$

The term $\rho\delta$ is a dimensionless number, which is generally referred to as the Hatta number, $Ha = \sqrt{-\nu_1 k C_{2,b}\mathcal{D}_1}/k_{1,II}$. The rate of absorption of A_1 per unit of time and unit interfacial area, in the presence of a chemical reaction, is written:

$$[N_1']_{x=0} = k_1\frac{Ha}{\tanh[Ha]}\left[C_1^* - \frac{C_{1,b}}{\cosh[Ha]}\right]$$

Recalling that the flux in the absence of a chemical reaction can be expressed as:

$$[N_1]_{x=0} = k_1(C_1^* - C_{1,b})$$

the ratio of fluxes with and without a chemical reaction is then written:

$$E = \frac{Ha}{\tanh[Ha]}\,\frac{1 - \dfrac{\mathcal{N}_3}{\cosh[Ha]}}{1 - \mathcal{N}_3} \tag{3.20}$$

where $\mathcal{N}_3$ is the dimensionless number $C_{1,b}/C_1^*$.

We can also express the enhancement factor E by means of the following equation:

$$E = \frac{[N_1']_{x=0}}{[N_1]_{x=0}} = -\left(\frac{dC_1(x)}{dx}\right)_{x=0}\cdot\frac{\delta}{C_1^* - C_{1,b}} \tag{3.21}$$

The change in mass transfer brought about by the chemical reaction becomes appreciable only when $Ha \geqslant 0.3$.

It is also worthwhile examining the value of the flux of A_1 when it reaches the end of the film ($x = \delta$) and comparing its value to the flux entering the film ($x = 0$).

By assigning:

$$\mathcal{F} = \frac{\left[N_1'\right]_{x=\delta}}{\left[N_1'\right]_{x=0}}$$

we obtain:

$$\mathcal{F} = \frac{1 - \mathcal{N}_3 \cosh[Ha]}{\cosh[Ha] - \mathcal{N}_3} \tag{3.22}$$

- If Ha is less than 0.3 (that is, if the reaction is slow), $\cosh[Ha]$ and $\mathcal{F}$ both tend toward 1. The reaction takes place essentially in the bulk of phase II and is practically insignificant in the film. The absorption flux per unit of interfacial area is close to:

$$\left[N_1'\right]_{x=0} \cong [N_1]_{x=0} = k_1(C_1^* - C_{1,b}) \quad \text{(see Eq. 3.5)}$$

that is, $E \cong 1$.

- If Ha is > 5 (that is, if the reaction is fast), we can assume that $\mathcal{N}_3$ is small; the reaction will take place almost entirely within the film. Under these conditions:

$$\mathcal{F} = \frac{1}{\cosh[Ha]}$$

We see that the fraction of compound transferred that reaches the film boundary becomes insignificant as soon as Ha approaches 5. Under these conditions $E \cong Ha$. The absorption flux per unit interfacial area is then written:

$$\left[N_1'\right]_{x=0} \cong k_1 Ha C_1^* = C_1^* \sqrt{-\nu_1 k C_{2,b} \mathcal{D}_1} \tag{3.23}$$

- If $0.3 < Ha < 5$, the intermediate situation is governed by (3.20).

3.2.1.3 Second-order reactions

The previous equations were easy to derive because $C_2(x)$ was assumed to be constant throughout the film:

$$C_2(x) \cong C_{2,b} \quad \text{and therefore} \quad \frac{dC_2(x)}{dx} \cong 0$$

This enabled us to integrate Eq. (3.15).

However, we also need to examine the situation when this assumption is not true. In this case it is not possible to obtain an analytic expression for $\left[N_1'\right]_{x=0}$. However, a numeric solution can be obtained. First, we rewrite the balance equations for the compounds A_1, A_2, A_3:

$$\mathcal{D}_i \left[\frac{d^2 C_i(x)}{dx^2}\right] + \nu_i k C_1(x) C_2(x) = 0 \quad (i = 1, 2, 3) \tag{3.24}$$

The following boundary conditions are used:

$$x = 0 \quad C_1(0) = C_1^* \qquad \frac{dC_2(0)}{dx} = 0 \qquad \frac{dC_3(0)}{dx} = 0 \tag{3.25}$$

$$x = \delta \quad C_1(\delta) = C_{1,b} \qquad C_2(\delta) = C_{2,b} \qquad C_3(\delta) = C_{3,b} \tag{3.26}$$

By combining (3.15; $i = 1$) and (3.15; $i = 2$) and integrating twice using the above boundary conditions, we obtain:

$$C_2(x) = C_{2,b}\left\{1 + \frac{\nu_2}{\nu_1}\frac{\mathcal{D}_1}{\mathcal{D}_2}\frac{C_1(x) - C_{1,b}}{C_{2,b}}\left[1 + \frac{(\delta - x)\left(\dfrac{dC_1}{dx}\right)_{x=0}}{C_1(x) - C_{1,b}}\right]\right\} \tag{3.27}$$

Writing the above equation for the interface conditions and taking into account Eq. (3.21), we then obtain:

$$C_2^* = C_{2,b}\left\{1 + \frac{(1 - \mathcal{N}_3)(1 - E)}{\mathcal{N}_2}\right\} \tag{3.28}$$

where:

$$\mathcal{N}_2 = \frac{\nu_1}{\nu_2}\frac{\mathcal{D}_2}{\mathcal{D}_1}\frac{C_{2,b}}{C_1^*} \tag{3.29}$$

It can also be assumed that $C_2(x)$ is appreciably constant in a region near the interface (a situation close to reality), that is:

$$\left(\frac{dC_2(x)}{dx}\right)_{x=0} = 0$$

Using (3.28), we can then derive the following equation, which is implicit for E:

$$E = \frac{Ha\sqrt{1 - \dfrac{(E-1)(1-\mathcal{N}_3)}{\mathcal{N}_2}}}{\tanh\left[Ha\sqrt{1 - \dfrac{(E-1)(1-\mathcal{N}_3)}{\mathcal{N}_2}}\right]} \frac{1 - \dfrac{\mathcal{N}_3}{\cosh\left[Ha\sqrt{1 - \dfrac{(E-1)(1-\mathcal{N}_3)}{\mathcal{N}_2}}\right]}}{1 - \mathcal{N}_3} \tag{3.30}$$

Figure 3.4 represents (for $\mathcal{N}_3 = 0$) the enhancement factor E as a function of Ha with $\mathcal{N}_2$ as a parameter (Eq. 3.30).

An examination of Fig. 3.4 calls for the following comments:

1. It is rare to be able to consult a graph such as the one shown above for values of $\mathcal{N}_3$ other than $\mathcal{N}_3 = 0$. We explain below why this is the case. Recall that ε_{II} is the fraction of the reactor volume occupied by phase II and $\mathcal{A}$ is the interfacial area per unit volume of the reactor. Then, for the unit volume of the reactor, a balance for the compound A_1 crossing the film boundary can be written, using the steady-state conditions but without including the terms for incoming and outgoing convective flows:

$$\mathcal{A}\left[N_1'\right]_{x=\delta} = -\nu_1\left[\varepsilon_{II} - \mathcal{A}\delta\right]kC_{1,b}C_{2,b} \tag{3.31}$$

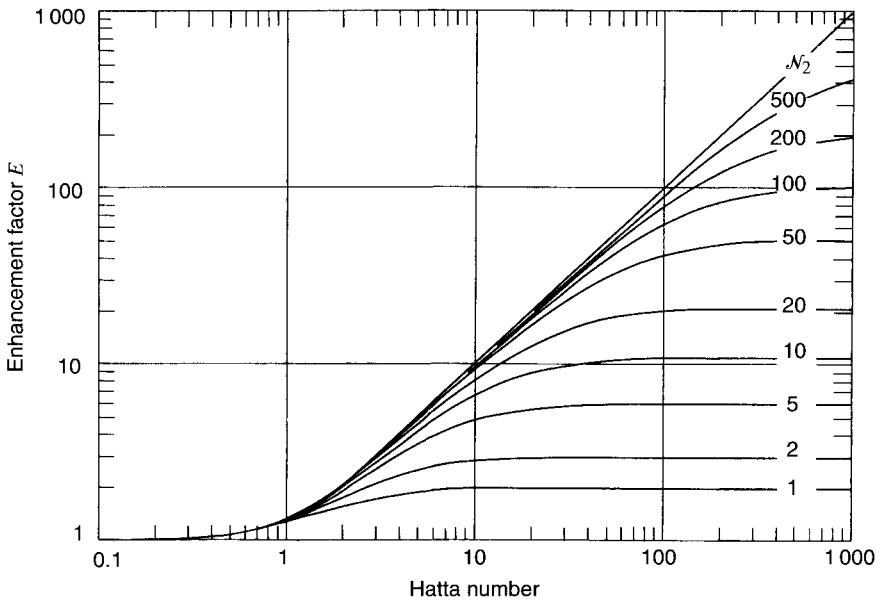


Figure 3.4 Enhancement factor as a function of the Hatta number and $\mathcal{N}_2$ ($\mathcal{N}_3 = 0$).

This expression indicates that the quantity of A_1 crossing the film boundary is equal to the quantity consumed within phase II. For a pseudo-first-order reaction, we derive, after expansion:

$$\mathcal{N}_3 = \frac{\dfrac{1}{\cosh[Ha]}}{1 + Ha\left[\dfrac{k_{1,\mathrm{II}}\varepsilon_{\mathrm{II}}}{\mathcal{A}\mathcal{D}_{1,\mathrm{II}}} - 1\right]\tanh[Ha]} \tag{3.32}$$

After inserting realistic values for $k_{1,\mathrm{II}}$, $\varepsilon_{\mathrm{II}}$, $\mathcal{A}$, and $\mathcal{D}_{1,\mathrm{II}}$ (Table 3.1), we find that β, which is equal to $(k_{1,\mathrm{II}}\varepsilon_{\mathrm{II}})/(\mathcal{A}\mathcal{D}_{1,\mathrm{II}})$, remains between 10 and 5 000. Note that β is the ratio of the volume of phase II to the volume of the film in phase II. Figure 3.5 represents the value of $\mathcal{N}_3$ as a function of Ha and β.

Table 3.1 Practical values of the parameters $\varepsilon_{\mathrm{II}}$, $k_{1,\mathrm{II}}$, and $\mathcal{D}_{1,\mathrm{II}}$, $\mathcal{A}$ and β.

0.2	$<$	$\varepsilon_{\mathrm{II}}$	$<$	0.99
$5 \cdot 10^{-5}$	$<$	$k_{1,\mathrm{II}}$	$<$	$5 \cdot 10^{-4}$ m/s (for a phase II liquid)
10^{-9}	$<$	$\mathcal{D}_{1,\mathrm{II}}$	$<$	$5 \cdot 10^{-9}$ m^2/s
100	$<$	$\mathcal{A}$	$<$	1 000 m^2/m^3 of reactor
10	$<$	β	$<$	5 000

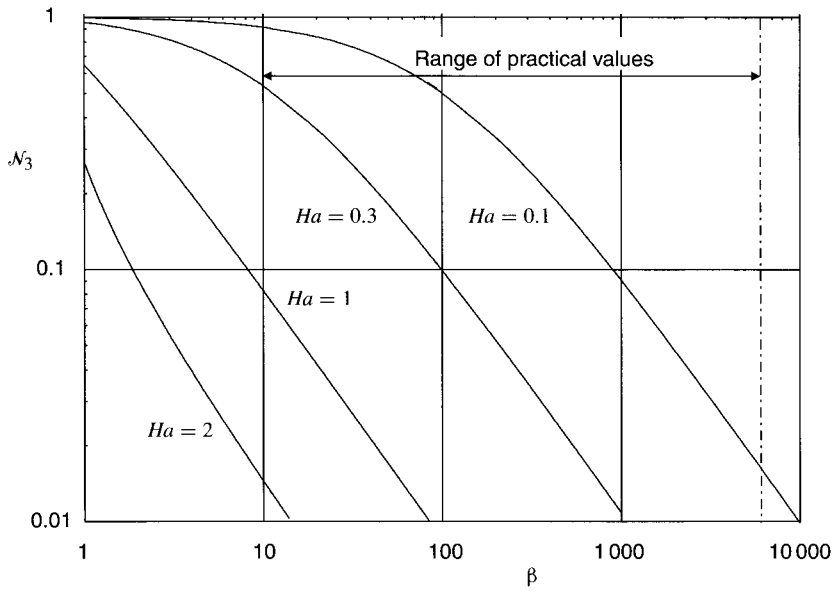


Figure 3.5 $\mathcal{N}_3$ as a function of β and the Hatta number.

Examination of the above curves leads to the following conclusions:

- Whenever Ha is relatively high ($Ha > 0.3$), so that E may be greater than 1, the value of $\mathcal{N}_3$ rarely exceeds 0.1 for values of Ha between 0.3 and 1 and never exceeds 0.01 when Ha is greater than 2.
- Whenever Ha is low ($Ha < 0.3$), $\mathcal{N}_3$ can assume non-negligible values, which sometimes approach unity. However, this has little effect, for under these conditions, E is practically equal to 1.

As a result, in both cases there is little deviation from a value of E calculated for $\mathcal{N}_3 = 0$. Table 3.2 shows the very weak influence of the parameter β on the numerical value of E for a pseudo-first-order reaction. It can also be shown that this is true for a second-order reaction. This justifies the use of the following expression for the enhancement factor E represented in Fig. 3.4:

$$E = \frac{Ha\sqrt{1 - \dfrac{(E-1)}{\mathcal{N}_2}}}{\tanh\left[Ha\sqrt{1 - \dfrac{(E-1)}{\mathcal{N}_2}}\right]} \tag{3.33}$$

2. When, for a given value of $\mathcal{N}_2$, Ha increases, the enhancement factor levels off at a value that can be calculated from (3.30):

$$E_{\text{lim}} = \frac{\mathcal{N}_2}{1 - \mathcal{N}_3} + 1 \tag{3.34}$$

which, as we have seen, is appreciably equal to:

$$E_{\text{lim}} = 1 + \mathcal{N}_2 \tag{3.35}$$

Table 3.2 Influence of β on the enhancement factor for a pseudo-first-order reaction.

Ha	*Ha*/ tanh(*Ha*)	β	$\mathcal{N}_3$	*E*
0.5	1.082	10	0.288	1.169
0.5	1.082	1 000	0.040	1.082
0.7	1.159	10	0.166	1.206
0.7	1.159	1 000	0	1.159
1	1.312	10	0.082	1.354
1	1.312	1 000	0	1.312
2	2.075	10	0.015	2.098
2	2.075	1 000	0	2.075
5	5.0	10	0	5.0
5	5.0	1 000	0	5.0

Physically, this arises from the fact that C_2^* tends to decrease rapidly as *Ha* increases. Below, we refer to this as the instantaneous reaction regime.

3. The case when $C_2^* = C_{2,b}$, which implies that $C_2(x)$ is constant within the film, corresponds to: $[(E-1)(1-\mathcal{N}_3)]/\mathcal{N}_2 = 0$ [based on (3.28)]. This can only be satisfied when $\mathcal{N}_2$ becomes very large. If we examine the expression for $\mathcal{N}_2$, we see that for a given reaction system, the only way to increase $\mathcal{N}_2$ is to increase $C_{2,b}/C_1^*$ in such a way that:

$$\frac{C_{2,b}}{C_1^*} \gg \frac{\nu_2}{\nu_1}\frac{\mathcal{D}_1}{\mathcal{D}_2}$$

Under these conditions, the enhancement factor assumes the simplified form indicated previously:

$$E = \frac{Ha}{\tanh[Ha]}\frac{1-\dfrac{\mathcal{N}_3}{\cosh[Ha]}}{1-\mathcal{N}_3} \tag{3.36}$$

This becomes $E = Ha$ for $Ha > 5$. The same equality is also found in the expression for the flux with a chemical reaction in (3.23).

4. Equation (3.33) is implicit. Kishinevskii [1971] has supplied an approximate explicit expression:

$$E = 1 + \frac{Ha}{A}\left[1 - \exp(-0.65 \cdot Ha\sqrt{A})\right] \tag{3.37}$$

where:

$$A = \frac{Ha}{\mathcal{N}_2} + \exp\left[\frac{0.68}{Ha} - \frac{0.45 \cdot Ha}{\mathcal{N}_2}\right] \tag{3.38}$$

The numerical values obtained from this equation are very close (on average the difference is less than 5%) to those given by the implicit Eq. (3.33). This equation provides the limits of the fast reaction regime ($Ha > 5$). It also makes it easier to identify the limits for both the fast pseudo-first-order and instantaneous reaction regimes:

- Fast pseudo-first-order reaction:

$$E = Ha \quad \text{when } Ha > 5 \text{ and } Ha/\mathcal{N}_2 < 10^{-1}$$

- Instantaneous reaction:

$$E_{\text{lim}} = 1 + \mathcal{N}_2 \quad \text{when } Ha > 5 \text{ and } Ha/\mathcal{N}_2 > 10$$

Other empirical equations have been proposed, but the one provided by Kishinevskii appears to be the best. Nonetheless, resolution of Eq. (3.33), which is relatively easy using current computational methods, is recommended.

5. The combination of Eqs. (3.22) and (3.32) allows us to calculate $\mathcal{F}$, the fraction of reactant A_1 entering the bulk of phase II without having reacted in the film. We find:

$$\mathcal{F} = \frac{Ha(\beta - 1)}{\sinh[Ha] + Ha(\beta - 1)\cosh[Ha]} \tag{3.39}$$

This equation, which is graphed in Fig. 3.6, shows that β has little effect on this fraction. Moreover, the transition from a situation where more than 85% of the reactants are transformed in the bulk of phase II to one where only 25% enter the phase occurs when the Hatta number changes from 0.5 to 2.

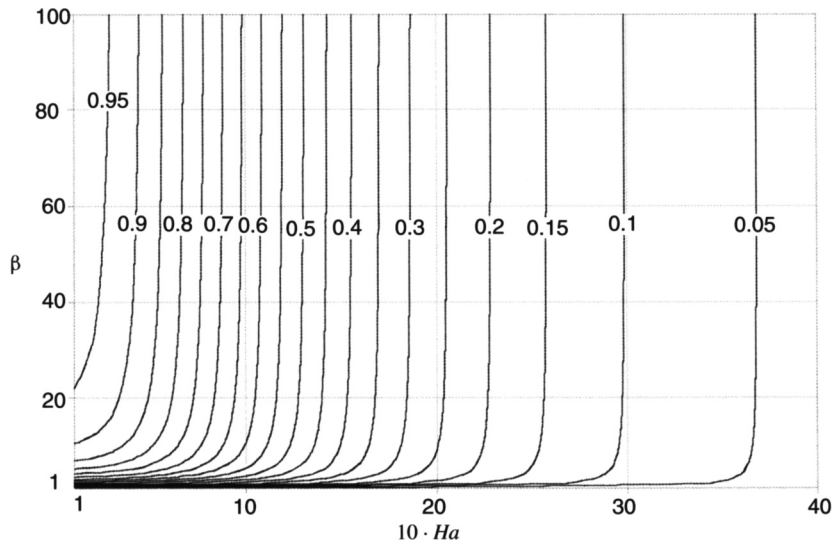


Figure 3.6 Iso-value contours for the fraction $\mathcal{F}$ as a function of β and the Hatta number.

3.2.1.4 Instantaneous reactions

If the reaction $\nu_1 A_1 + \nu_2 A_2 \rightarrow \nu_3 A_3$ is considered instantaneous, and assuming again that A_1, and A_1 alone, is transferred from phase I to phase II, the phase containing reactant A_2, this means that A_1 and A_2 cannot coexist.

The situation illustrated in Fig. 3.7 occurs in the film. Within a distance z, A_1 (and A_3) can be present but not A_2. Beyond that distance, A_2 (and A_3) can be present but not A_1. The distance z indicates the existence of a reaction location. At that point the respective fluxes in opposite directions of the constituents A_1 and A_2 are in the ratio of their stoichiometric coefficients. If this were not the case, there would be an excess of one of the reactants at point z, resulting in the displacement of point z until the indicated condition be fulfilled:

$$\text{Flux of } A_1 \text{ measured in the direction of increasing } x = -\mathcal{D}_1 \left(\frac{C_1^* - 0}{0 - z} \right) = +\mathcal{D}_1 \frac{C_1^*}{z} \cdot$$

$$\text{Flux of } A_2 \text{ measured in the direction of increasing } x = -\mathcal{D}_2 \left(\frac{C_{2,b} - 0}{\delta - z} \right) = -\mathcal{D}_2 \frac{C_{2,b}}{(\delta - z)} \cdot$$

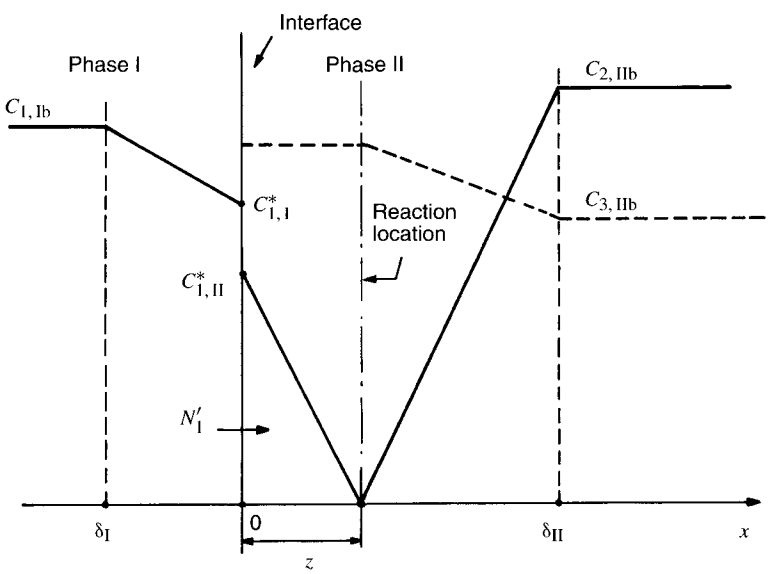


Figure 3.7 Concentration profiles near the interface for an irreversible instantaneous reaction: $\nu_1 A_1 + \nu_2 A_2 \rightarrow \nu_3 A_3$.

The flux ratio must equal the ratio of stoichiometric coefficients (the sign for the flux of A_2 is changed to account for the fact that this flux moves in the direction opposite that of A_1). We thus obtain:

$$z = \frac{\nu_2 \mathcal{D}_1 C_1^* \delta}{\nu_1 \mathcal{D}_2 C_{2,b} + \nu_2 \mathcal{D}_1 C_1^*} \tag{3.40}$$

In the absence of a chemical reaction (and with $C_{1,b} = 0$ to make the comparison valid), we would have:

$$[N_1]_{x=0} = \frac{\mathcal{D}_1}{\delta} C_1^*$$

In the presence of a chemical reaction, we have:

$$[N_1']_{x=0} = \frac{\mathcal{D}_1}{z} C_1^*$$

in such a way that the factor E becomes equal to δ/z.

$$E = \frac{\delta}{z} = 1 + \frac{\nu_1 \mathcal{D}_2 C_{2,b}}{\nu_2 \mathcal{D}_1 C_1^*} = 1 + \mathcal{N}_2 \tag{3.41}$$

which is identical to (3.35).

3.2.1.5 Surface reactions

The above case involving instantaneous reactions results in high enhancement factors. In reality, for very fast reactions, the transformation is sometimes controlled by diffusion in phase I. The concentrations of $C_{1,I}^*$ and therefore $C_{1,II}^*$ decrease, z decreases, and $C_{1,I}^*$, $C_{1,II}^*$, and z tend to 0 at the limit. The reaction front shifts toward the interface and we then have the situation shown in Fig. 3.8. We saw earlier, however, that for an instantaneous reaction $E = 1 + \mathcal{N}_2$. Therefore, we can write:

$$[N_1']_{x=0} = k_{1,I}(C_{1,Ib} - C_{1,I}^*) = k_{1,II}(1 + \mathcal{N}_2) C_{1,II}^* = k_{1,II}\left(C_{1,II}^* + \frac{\nu_1}{\nu_2}\frac{\mathcal{D}_{2,II}}{\mathcal{D}_{1,II}} C_{2,IIb}\right)$$

where, since concentrations are very low, $C_{1,I}^* = m_0 C_{1,II}^*$ and we obtain:

$$C_{1,II}^* = \frac{k_{1,I} C_{1,Ib} - k_{1,II}\dfrac{\nu_1}{\nu_2}\dfrac{\mathcal{D}_{2,II}}{\mathcal{D}_{1,II}} C_{2,IIb}}{m_0 k_{1,I} + k_{1,II}} \tag{3.42}$$

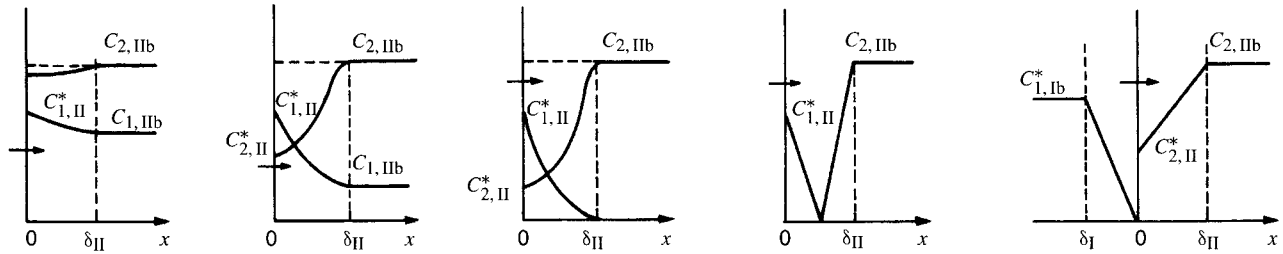
The conditions for a so-called **surface reaction** occur when $C_{1,II} = 0$, that is when:

$$\frac{C_{2,IIb}}{C_{1,Ib}} = \frac{k_{1,I}}{k_{1,II}}\frac{\nu_2}{\nu_1}\frac{\mathcal{D}_{1,II}}{\mathcal{D}_{2,II}} \tag{3.43}$$

3.2.1.6 Summary of transfer regimes

The various regimes examined are shown in Fig. 3.8. We have added values for the characteristic dimensionless numbers. Distinguishing among these regimes will obviously be very important when choosing equipment for a desired transformation.

For example, in the case of regime 1 in Fig. 3.8, where the reaction takes place essentially within the bulk of phase II, there is no advantage in developing the interfacial area. However, the proportion of phase II in the reactor, referred to as phase II **holdup**, ε_{II}, should be increased as much as possible.



①	②	③	④	⑤
Slow reaction	Moderate reaction	Fast reaction	Instantaneous reaction	Surface reaction
$Ha < 0.3$	$0.3 < Ha < 5$	$Ha > 5$	$Ha > 5$ and $Ha/\mathcal{N}_2 > 10$	$Ha > 5$ and $Ha/\mathcal{N}_2 > 10$ and $\dfrac{C_{2,\mathrm{IIb}}}{C_{1,\mathrm{Ib}}} > \dfrac{k_{1,\mathrm{I}}\nu_2\mathcal{D}_{1,\mathrm{II}}}{k_{1,\mathrm{II}}\nu_1\mathcal{D}_{2,\mathrm{II}}}$
$E = 1$	$E = f(Ha \cdot \mathcal{N}_2)$	$E = f(Ha \cdot \mathcal{N}_2)$	$E = 1 + \mathcal{N}_2$	
$[N'_1] = k_{1,\mathrm{II}}\left(C^*_{1,\mathrm{II}} - C_{1,\mathrm{IIb}}\right)$	$[N'_1] = k_{1,\mathrm{II}}E\left(C^*_{1,\mathrm{II}} - C_{1,\mathrm{IIb}}\right)$	$[N'_1] = k_{1,\mathrm{II}}E\left(C^*_{1,\mathrm{II}} - C_{1,\mathrm{IIb}}\right)$	$[N'_1] = k_{1,\mathrm{II}}C^*_{1,\mathrm{II}}(1 + \mathcal{N}_2)$	$[N'_1] = k_{1,\mathrm{I}}C_{1,\mathrm{Ib}}$
		if $Ha/\mathcal{N}_2 < 0.1$		
		$E = Ha$		
		$[N'_1] = k_{1,\mathrm{II}}Ha\left(C^*_{1,\mathrm{II}} - C_{1,\mathrm{IIb}}\right)$		

Figure 3.8 Possible regimes for transfer between two fluid phases accompanied by a phase II chemical reaction having the stoichiometry: $\nu_1 A_1 + \nu_2 A_2 \rightarrow \nu_3 A_3$. The interface between the two phases is located at $x = 0$.

By contrast in cases corresponding to conditions of regimes 3, 4, and 5, we need to minimize phase II holdup and increase the specific interfacial area $\mathcal{A}$ to as great an extent as possible. We will return to these selection criteria when we discuss the different types of technology available in practice.

3.2.2 Calculating the local flux of a compound transferred from phase I to phase II

We assume that values for $\mathcal{A}$, ε_{II}, $k_{1,I}$, $k_{1,II}$, $C_{1,Ib}$, $C_{2,IIb}$, ν_1, ν_2, $\mathcal{D}_{1,II}$, $\mathcal{D}_{2,II}$ have been determined, as well as the equilibrium equation $C_{1,I,e} = mC_{1,II,e} + p$ in the range of concentrations considered. We begin by calculating Ha:

$$Ha = \frac{\sqrt{-\nu_1 k C_{2,IIb} \mathcal{D}_{1,II}}}{k_{1,II}}$$

We estimate an initial value for E, for example, by assigning $E_{(1)} = Ha$. We can then write:

$$\left[N'_1\right]_{x=0} = k_{1,I}(C_{1,Ib} - C^*_{1,I}) = E_{(1)}k_{1,II}(C^*_{1,II} - C_{1,IIb})$$

where:

$$C^*_{1,I} = mC^*_{1,II} + p$$

which gives us:

$$C^*_{1,II} = \frac{E_{(1)}k_{1,II}C_{1,IIb} + k_{1,I}(C_{1,Ib} - p)}{E_{(1)}k_{1,II} + mk_{1,I}} \tag{3.44}$$

We can then calculate:

$$\mathcal{N}_2 = \frac{\nu_1}{\nu_2}\frac{\mathcal{D}_{2,II}}{\mathcal{D}_{1,II}}\frac{C_{2,IIb}}{C^*_{1,II}}$$

By referring to Fig. 3.4 or using Eq. (3.33), we obtain a value for $E_{(2)}$ that differs from $E_{(1)}$. We can continue our calculation iteratively until $E_{(n+1)} \cong E_{(n)}$. $E_{(n)}$ is then used as the value of E and we can write:

$$\left[N'_1\right]_{x=0} = E_{(\text{final})}k_{1,II}(C^*_{1,II,\text{final}} - C_{1,IIb}) \tag{3.45}$$

3.2.3 Efficiency in a reaction system with two fluid phases (first-order reaction)

In a reaction system with two fluid phases, the **efficiency** is defined as the ratio of the observed rate of transformation for the transferred reactant (in mol/s · m^3 of reactor) to the theoretical rate we could obtain when there is no limitation due to physical transfer.

$$\text{Efficiency} = \eta = \frac{r_{1,\text{app}}}{r_{1,\text{ max}}} \tag{3.46}$$

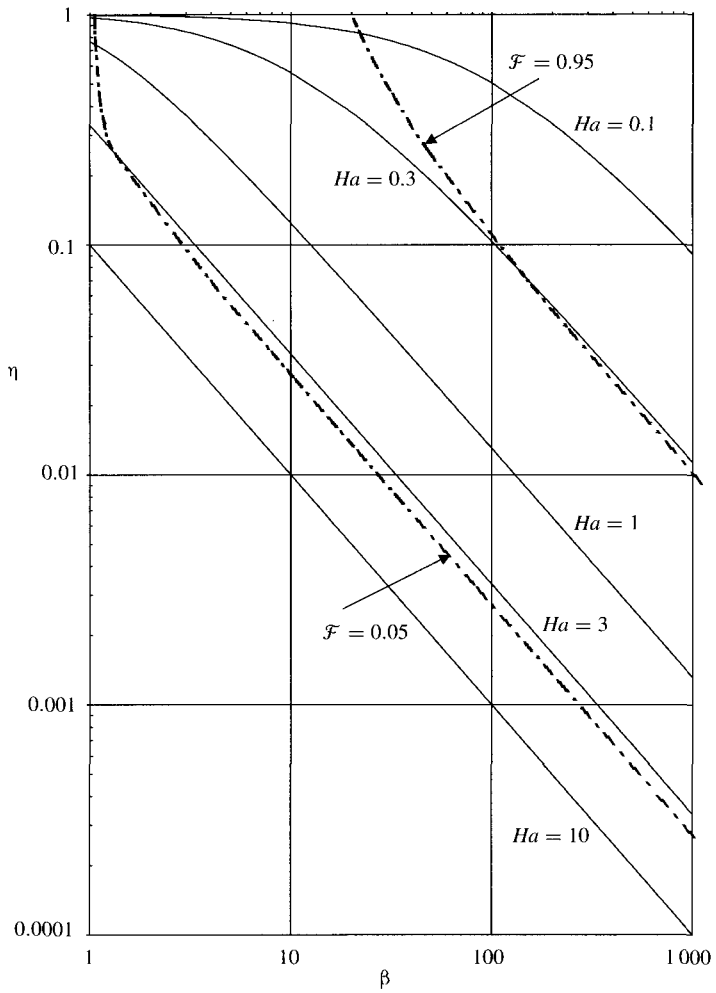


Figure 3.9 Efficiency η as a function of β and *Ha*.

Here, the subscript 1 refers to compound A_1; r_1 is therefore the rate of consumption of reactant A_1 and is positive. For a first-order reaction with respect to A_1:

$$r_{1\,\max} = -\nu_1 k \varepsilon_{II} C^*_{1,\,II}$$
$$r_{1,\,app} = \mathcal{A}\left[N'_1\right]_{x=0}$$

Using the equations previously established, we can then write:

$$\eta = \frac{1}{\beta Ha}\left[\frac{\tanh\left[Ha\right] + (\beta - 1)Ha}{1 + (\beta - 1)Ha\tanh\left[Ha\right]}\right] \tag{3.47}$$

We can also show that $\eta = [E(1 - \mathcal{N}_3)]/(\beta Ha^2)$.

As noted earlier, β is the ratio of the volume of phase II to the volume of film in phase II and, therefore, $\beta - 1$ is the ratio of the volume of the bulk of phase II to the volume of film in phase II.

Figure 3.9 represents, for an irreversible first-order reaction, the relation between η and β for different values of *Ha*. Two dotted line curves have also been drawn, corresponding to the two extremes cases: a reaction that takes place almost entirely within the film and a reaction that takes place almost entirely in the bulk of the liquid phase.

Although use of the graph is limited to first-order reactions, other values of η can be obtained for more complex kinetics. The practical limits of the various parameters are given in Table 3.1. Values of β less than 10 correspond to foaming gas-liquid systems, in which the majority of the liquid is found in the foam. The minimum value of β is equal to 1, in which case all of phase II exists in the form of a film.

The curve $\eta = f[Ha]$ can be transformed by defining the parameter $Ha^2\eta$.

$$Ha^2\eta = \frac{\mathcal{D}_{1,\mathrm{II}} r_{1,\mathrm{app}}}{\varepsilon_{\mathrm{II}} k_{1,\mathrm{II}}^2 C_{1,\mathrm{II}}^*} \tag{3.48}$$

This definition makes use of measurable values and does not require any prior knowledge of the kinetics. By measuring $r_{1,\mathrm{app}}$ and estimating $\varepsilon_{\mathrm{II}}$, $k_{1,\mathrm{II}}$, $\mathcal{D}_{1,\mathrm{II}}$, and $C_{1,\mathrm{II}}^*$, we have access to $Ha^2\eta$.

Figure 3.10 is a graphic representation of Eq. (3.47) for a first-order reaction, with $Ha^2\eta$ on the abscissa, η on the ordinate, and β as a parameter.

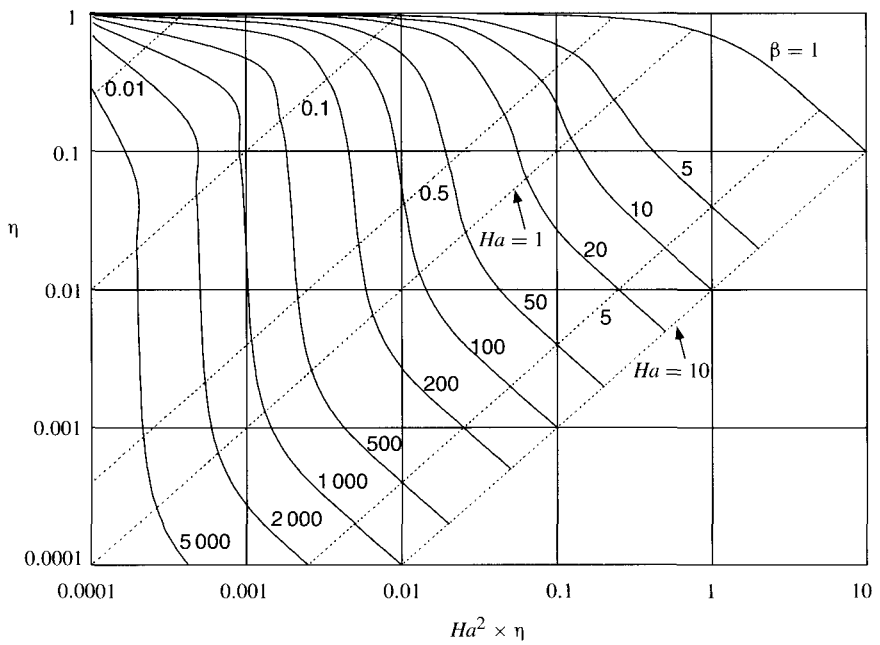


Figure 3.10 Efficiency η as a function of $Ha^2\eta$ and β.

The concept of efficiency assumes its fullest meaning when we are faced with the problem of selecting a reactor. For a gas-liquid system, where the reaction has been shown to take place in the bulk of the liquid phase, we must ensure a reasonable rate of transfer so that the liquid remains appreciably saturated with gas. To do this we need to supply energy to the system. Once the desired level of saturation has been obtained, any additional supply of energy is unnecessary. For such systems reactors with high liquid holdup are most suitable (for example, bubble column reactors). However, if the reaction takes place essentially in the film, it is best to increase the interfacial area as much as possible. In this case we should use a plate column, packed column, or other reactor type, which will be described in subsequent chapters.

3.2.4 Extending the study of transfer phenomena with chemical reaction to systems with more complex kinetics

The transfer models considered until now essentially involve simple kinetics: a single first- or second-order irreversible chemical reaction that takes place in phase II, with the transfer of reactant A_1 from phase I to phase II, which may ultimately contain a coreactant A_2. We also assumed that no coreactant A_2 could transfer to phase I, that a steady-state existed in the volume element of the reactor, and that the transformation was isothermal. Although these conditions may seem restrictive, they can be found, at least approximately, in practice, which justifies an exhaustive treatment of these simplified cases.

Below we discuss more complex situations:

1. The chemical reaction is irreversible but the kinetics are complex.
2. The chemical reaction is reversible.
3. Several reactants are transferred simultaneously from phase I to phase II and react with one another in phase II or with one or more reactants already in phase II.
4. One or more reaction products are transferred back to phase I.

Before examining the above cases, we wish to point out that the equations describing them have generally assumed that phase I is gas and phase II is liquid. We will also make frequent use of Fig. 3.4, which is a graphic representation of implicit Eq. (3.30) and its simplified form (3.33).

3.2.4.1 Irreversible reactions with other than first-order kinetics

Here the reaction is of the type $\nu_1 A_1 + \nu_2 A_2 \rightarrow$ products, where A_1 is transferred from phase I to phase II, and A_2 is contained in phase II. The reaction takes place in phase II, with a rate of reaction that can be expressed by $r = k_{m,n} C_{1,\mathrm{II}}^m C_{2,\mathrm{II}}^n$. For such a situation it has been shown that we can make use of the curves in Fig. 3.4 or the Kishinevskii equation, providing that Ha and $E_{\lim}$ are defined as follows:

$$Ha = \frac{\sqrt{\dfrac{-2\nu_1 \mathcal{D}_{1,\mathrm{II}}}{1+m} k_{m,n} (C_{1,\mathrm{II}}^*)^{m-1} (C_{2,\mathrm{IIb}})^n}}{k_{1,\mathrm{II}}}$$

$$E_{\lim} = \left(\frac{\mathcal{D}_{1,\mathrm{II}}}{\mathcal{D}_{2,\mathrm{II}}}\right)^p (1 + \mathcal{N}_2)$$

The exponent p is generally between 0.3 and 0.5, reflecting the dependence of $k_{l,II}$ on $\mathcal{D}_{l,II}$. If Ha is greater than 3, we can write [Sharma and Shah, 1976]:

$$E = Ha\left[\frac{E_{lim} - E}{E_{lim} - 1}\right]^{\frac{m}{2}}$$

In these equations the number $\mathcal{N}_3 = C_{1,IIb}/C^*_{1,II}$ is considered to be zero, which, as indicated above, is perfectly valid in the vast majority of cases.

3.2.4.2 Transfer accompanied by a reversible reaction

Consider the reaction $\nu_1 A_1 + \nu_2 A_2 \rightleftarrows \nu_3 A_3 + \nu_4 A_4$, characterized by a rate of reaction:

$$r = k\left[C^{\alpha}_{1,II} C^{\beta}_{2,II} - \frac{1}{K} C^{\gamma}_{3,II} C^{\delta}_{4,II}\right]$$

Danckwerts [1970] has suggested that Fig. 3.4 be used with the following values for E_{lim}:

$$E_{lim} = \frac{\mathcal{C}^*_{1,II} - \mathcal{C}_{1,IIb}}{\mathcal{C}^*_{1,II} - \mathcal{C}^E_{1,IIb}}$$

and a value of Ha:

$$Ha = \frac{\sqrt{\dfrac{-2\nu_1 \mathcal{D}_{1,II}}{1+\alpha} k (C^*_{1,II})^{\alpha-1} (C_{2,IIb})^{\beta}}}{k_{1,II}}$$

where

$\mathcal{C}^*_{1,II}$ and $\mathcal{C}_{1,IIb}$ total concentrations (free and combined) of A_1 at the interface and in the bulk of phase II respectively

$\mathcal{C}^E_{1,IIb}$ concentration of free A_1 in the bulk of phase II if this phase were in chemical equilibrium.

3.2.4.3 Simultaneous transfer of two compounds reacting together

When two reactants are transferred simultaneously, we need to define two enhancement factors [Hikita *et al.*, 1977]. For a reaction $\nu_1 A_1 + \nu_2 A_2 \rightarrow$ products, characterized by $r = k_{m,n} C^m_{1,II} C^n_{2,II}$, with the simultaneous transfer of A_1 and A_2 from phase I to phase II, the enhancement factors are calculated as follows:

$$E_1 = \frac{\lambda Ha_1}{\tanh[\lambda Ha_1]} \qquad Ha_1 = \frac{\sqrt{\dfrac{-2\nu_1 \mathcal{D}_{1,II}}{1+m} k_{m,n} (C^*_{1,II})^{m-1} (C^*_{2,II})^{n}}}{k_{1,II}}$$

where, for:

$$n = 0 \quad \lambda = 1$$

$$n = 1 \quad \lambda = \sqrt{(1-a) + a\left(\frac{m+1}{m+2}\right)}$$

$$n = 2 \quad \lambda = \sqrt{(1-a)^2 + 2a(1-a)\left(\frac{m+1}{m+2}\right) + a^2\left(\frac{m+1}{m+3}\right)}$$

and:

$$a = \left(1 - \frac{C_{2,\mathrm{IIb}}}{C^*_{2,\mathrm{II}}} - \frac{\nu_2}{\nu_1}\frac{\mathcal{D}_{1,\mathrm{II}}}{\mathcal{D}_{2,\mathrm{II}}}\frac{C^*_{1,\mathrm{II}}}{C^*_{2,\mathrm{II}}}\right)\frac{1}{E_1} + \frac{\nu_2}{\nu_1}\frac{\mathcal{D}_{1,\mathrm{II}}}{\mathcal{D}_{2,\mathrm{II}}}\frac{C^*_{1,\mathrm{II}}}{C^*_{2,\mathrm{II}}}$$

$$E_2 = 1 + \frac{(E_1 - 1)\nu_2 C^*_{1,\mathrm{II}}\mathcal{D}_{1,\mathrm{II}}}{\left(1 - \dfrac{C_{2,\mathrm{IIb}}}{C^*_{2,\mathrm{II}}}\right)\nu_1 C^*_{2,\mathrm{II}}\mathcal{D}_{2,\mathrm{II}}}$$

E_1 and E_2 are then obtained by iteration.

3.2.4.4 Simultaneous transfer of two compounds reacting with a third compound present in phase II

A number of detailed studies have been made for the important case where two compounds are transferred and react with the same solute (for example, the simultaneous absorption of CO_2 and SH_2 in alkanolamine solutions). Consider the following reactions:

$$\nu_{1,1}\mathrm{A}_1 + \nu_{3,1}\mathrm{A}_3 \rightarrow P \quad \text{where } r_1 = k_1 C_{1,\mathrm{II}} C_{3,\mathrm{II}}$$
$$\nu_{2,2}\mathrm{A}_2 + \nu_{3,2}\mathrm{A}_3 \rightarrow Q \quad \text{where } r_2 = k_2 C_{2,\mathrm{II}} C_{3,\mathrm{II}}$$

where A_1 and A_2 are transferred from phase I to phase II and A_3 is present in phase II. If the limiting enhancement factors are appreciably greater than 1, we can obtain the values for E_{lim} shown below:

$$E_{i\,\mathrm{lim}} = \sqrt{\frac{\mathcal{D}_{i,\mathrm{II}}}{\mathcal{D}_{3,\mathrm{II}}}}\left[1 + \frac{\mathcal{D}_{3,\mathrm{II}}C_{3,\mathrm{IIb}}}{\dfrac{\nu_{3,1}}{\nu_{1,1}}C^*_{1,\mathrm{II}}\mathcal{D}_{1,\mathrm{II}} + \dfrac{\nu_{3,2}}{\nu_{2,2}}C^*_{2,\mathrm{II}}\mathcal{D}_{2,\mathrm{II}}}\right] \quad (i = 1, 2)$$

These values are appreciably smaller than those obtained for each reactant taken individually. The enhancement factors E_1 and E_2 can be obtained from Fig. 3.4, using the appropriate Hatta number for each compound.

3.2.5 Comparison of various theories of mass transfer accompanied by chemical reaction

The two-film model is not the only theory that describes transfer phenomena; Higbie's penetration theory and Danckwerts [1970] surface renewal theory are also used. We will not discuss

the various approaches here, but refer the reader to the specialized literature on the subject [Astarita, 1967]. It is worthwhile however to examine the form of the enhancement factor in the three theories for an irreversible first-order reaction and an instantaneous irreversible second-order reaction. The different expressions for E are shown in Table 3.3. They have been established for $\mathcal{N}_3 = 0$, although, as we have seen, this does not have a significant impact. For slow reactions, corresponding to $Ha < 0.3$, the enhancement factor is equal to 1 in the three theories.

For fast reactions, corresponding to $Ha > 5$, the enhancement factor is equal to Ha in all three theories. In the intermediate domain ($Ha < 5$), the equations are different but the numerical values are similar.

Thus, for $Ha = 1$, we obtain the following values for E:

Two-film theory	$E = 1.31$
Penetration theory	$E = 1.38$
Surface renewal theory	$E = 1.41$

Similarly, for an instantaneous second-order reaction, the difference between the numerical values given by the different expressions will decrease as the values for $\mathcal{D}_{1,\mathrm{II}}$ and $\mathcal{D}_{2,\mathrm{II}}$ approach one another.

We can make use of this agreement when referring to Fig. 3.4. The graph is valid, regardless of the theory retained, providing E is read from the curve whose asymptotic ordinate corresponds to the extreme value of E, as calculated from the respective equations in Table 3.3. In short, all the theories lead to equivalent expressions and we can, therefore, use the values provided by the simplest expressions. It is for this reason that our discussion has focused on two-film theory.

Table 3.3 Expressions of the enhancement factor E as given by the three principal mass transfer theories. $\mathcal{N}_3 = 0$.

Type of reaction	Reaction regime and *Ha* value	Theory		
		Whitman two-film theory	Higbie penetration theory	Danckwerts surface renewal theory
$\nu_1 A_1 \rightarrow \nu_2 A_2$ first order	Slow reaction $Ha < 0.3$	$E = 1$		
	Moderate reaction rate $0.3 < Ha < 5$	$E = \dfrac{Ha}{\tanh[Ha]}$	$E = Ha\left(1 + \dfrac{\pi}{8Ha^2}\,\mathrm{Erf}\left(\dfrac{2Ha}{\sqrt{\pi}}\right) + \dfrac{1}{2}\exp\left(\dfrac{-4Ha^2}{\pi}\right)\right)$	$E = \sqrt{1 + Ha^2}$
	Fast reaction $Ha > 5$	$E = Ha$		
$\nu_1 A_1 + \nu_2 A_2 \rightarrow \nu_3 A_3$ second order	Instantaneous reaction	$E_{\mathrm{lim}} = 1 + \mathcal{N}_2$	$E_{\mathrm{lim}} = (1 + \mathcal{N}_2)\sqrt{\dfrac{\mathcal{D}_{1,\mathrm{II}}}{\mathcal{D}_{2,\mathrm{II}}}}$	

3.3 INFLUENCE OF MASS TRANSFER ON CHEMICAL TRANSFORMATION

3.3.1 Apparent reaction order

Until now we have addressed the question of mass transfer in the presence of a chemical reaction by assuming that transfer could be modified by the reaction, whose specific character has been preserved. The problem can, however, be looked at somewhat differently and treated as if the chemical reaction is modified by mass transfer. In this case we speak of an **apparent** kinetics of the chemical reaction.

The basic equations governing the phenomenon are written:

$$r_{1,\text{app}} = \mathcal{A}\left[N_1'\right]_{x=0} = k_{1,\text{II}} E\left(C_{1,\text{II}}^* - C_{1,\text{IIb}}\right) \tag{3.49}$$

$$\mathcal{A}\left[N_1'\right]_{x=\delta} = \left(\varepsilon_{\text{II}} - \mathcal{A}\delta_{\text{II}}\right) r_1 \tag{3.50}$$

As before, in these equations we assume the existence of a steady-state condition. The three cases described above can easily be distinguished:

1. The Hatta number is high and $C_{1,\text{IIb}}$ is zero: the entire reaction occurs within the film and $\left[N_1'\right]_{x=\delta} = 0$. The apparent kinetics is governed by the equations given in the previous sections.
2. The Hatta number is low and β is sufficiently high so that we can neglect what occurs in the film: $\left[N_1'\right]_{x=\delta} = \left[N_1'\right]_{x=0}$. We will use this case to discuss transfer phenomena in greater detail.
3. The intermediate case where the reaction takes place both within the film and in the bulk of phase II.

The solution of the system of Eqs. (3.49) and (3.50) is still possible, at least numerically. For a first-order reaction, the set of equations discussed will yield an analytic solution to the problem. In cases (2) and (3) it must nevertheless be recalled that the solution depends on the concentration $C_{1,\text{IIb}}$ at the inlet of the unit.

An examination of (3.49) and (3.50) shows that the apparent rates depend on the equation used to calculate E. The apparent order with respect to the reactants has no relation to their true order. Thus, there is no point in examining the kinetics of a reaction system with two fluid phases by treating it as a homogeneous system.

As an example, we look at a reaction that is first-order with respect to a reactant A_1 arriving from phase I, and first order with respect to a coreactant A_2, present only in phase II. We also assume that coreactant A_2 is present in excess compared to reactant A_1 in phase II (this occurs frequently if the solubility of A_1 in phase II is low). We can then write that in the steady state the apparent rate is equal to the absorption flux of A_1 in phase II, that is:

$$r_{1,\text{app}} = N_1 = k_{1,\text{II}} \mathcal{A} Ha C_{1,\text{II}}^* \left[\frac{Ha\,(\beta - 1) + \tanh\,(Ha)}{1 + Ha\,(\beta - 1)\tanh(Ha)}\right] \tag{3.51}$$

Earlier we saw that:

$$Ha = \frac{\sqrt{kC_{2,\text{IIb}}\mathcal{D}_{1,\text{II}}}}{k_{1,\text{II}}} \quad \text{and} \quad \beta = \frac{\varepsilon_{\text{II}} k_{1,\text{II}}}{\mathcal{A}\mathcal{D}_{1,\text{II}}}$$

Below we examine two cases that clearly demonstrate how the true kinetics can be affected by mass transfer phenomena. This holds true for the apparent order with respect to reactants A_1 and A_2 as well as the apparent activation energy.

3.3.1.1 Order with respect to reactants A_1 and A_2

A. Order with respect to reactant A_2

Beginning with Eq. (3.51), it can easily be shown that the apparent order with respect to A_2 is not 1. Take the case where $Ha = 5 \cdot 10^{-2}$, a very small value. Starting from this point, we increase Ha by a factor of 10^2 (up to 5) by changing $C_{2,\mathrm{IIb}}$ alone, which will be increased by a factor of 10^4. Figure 3.11 shows the results of the calculations for different values of β. We see that, for the range of Ha values considered, β is highly significant: If β is too large (that is, if the interfacial area is too small, less than 100 m^2/m^3), it is impossible to observe first order with respect to coreactant A_2. The apparent order is much closer to 0.

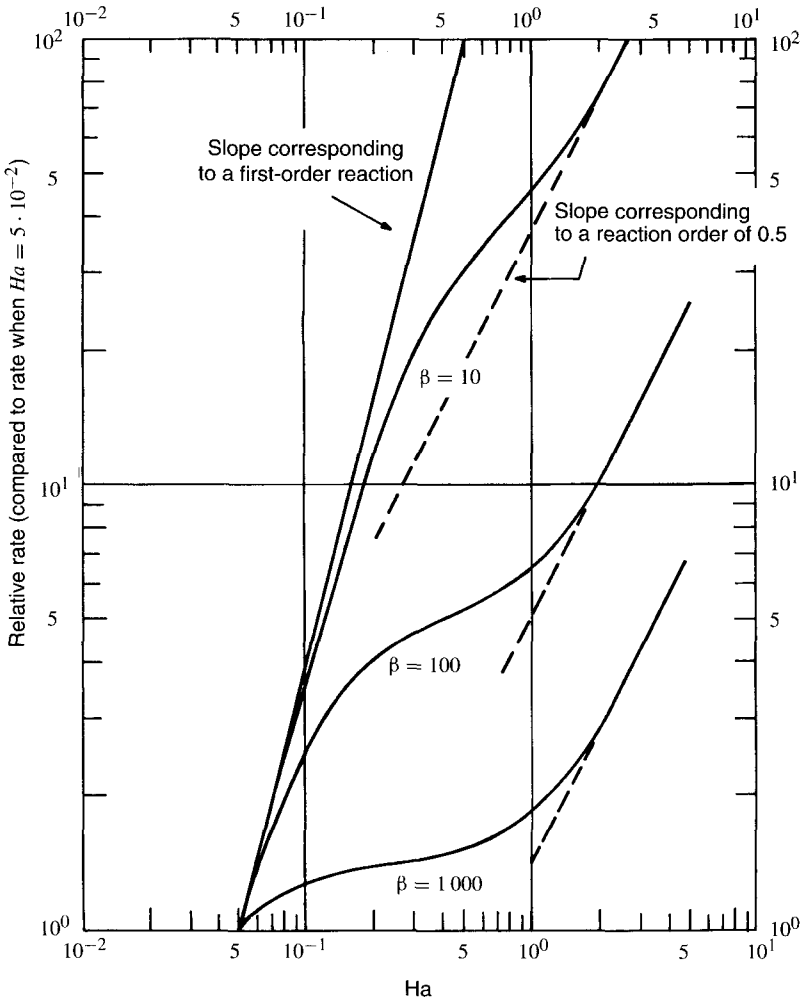


Figure 3.11 Apparent order with respect to the coreactant.

Although the situation is improved when $\beta = 100$ ($\mathcal{A}$ approximately 1 000 m^2/m^3), there still exists a range of Hatta numbers between 0.1 and 1 where the apparent order is particularly low. Reactors with a high foam ratio ($\beta = 10$, $\mathcal{A}$ approximately 10 000 m^2/m^3) are needed in order to observe an apparent order close to 1.

In all cases, however, regardless of the value of β, for Hatta numbers greater than 5 the apparent order is 0.5. This is easy to explain based on the simplifications made in Eq. (3.51) for $Ha > 5$:

$$N_1 = k_{1,\mathrm{II}}\mathcal{A}HaC^*_{1,\mathrm{II}} = \mathcal{A}C^*_{1,\mathrm{II}}\sqrt{kC_{2,\mathrm{IIb}}\mathcal{D}_{1,\mathrm{II}}} \tag{3.52}$$

The origin of this behavior is easy to understand. The observed near-zero order at low values of $\mathcal{A}$ results from the fact that each time $C_{2,\mathrm{IIb}}$ increases there is a corresponding decrease in $C_{1,\mathrm{IIb}}$, since the transfer rate and interfacial area are insufficient to maintain $C_{1,\mathrm{IIb}}$ at its previous level. This is compensated for by a very slight increase in the observed rate. The order 0.5 observed for higher values of Ha simply reflects the fact that the reaction takes place entirely in the film of phase II, since the concentration of $C_{1,\mathrm{IIb}}$ has fallen to 0. In real cases $C_{2,\mathrm{IIb}}$ almost never varies in the proportions shown above (1 to 10^4). The range covered will correspond to only a portion of Fig. 3.11, in such a way that, in the majority of cases, we observe an apparent order that is constant but differs from the true order throughout the reaction or throughout the length of the reactor.

B. Order with respect to reactant A_1

Consider a true first order in phase II for the transferred reactant A_1. This first-order is often very difficult to observe in practice. Once the reaction becomes somewhat rapid, the concentration of $C_{1,\mathrm{IIb}}$ tends to 0, regardless of the concentration of $C_{1,\mathrm{Ib}}$. Under these conditions, the concept of order with respect to $C_{1,\mathrm{IIb}}$ becomes meaningless. There are times, however, when we may want to define an apparent order with respect to $C_{1,\mathrm{Ib}}$, that is with respect to the concentration of A_1 in phase I. We have the following basic equations:

$$r_{1,\mathrm{app}} = N_1 = k_{1,\mathrm{I}}\mathcal{A}\left(C_{1,\mathrm{Ib}} - C^*_{1,\mathrm{I}}\right) = k_{1,\mathrm{II}}E\mathcal{A}\left(C^*_{1,\mathrm{II}} - C_{1,\mathrm{IIb}}\right) = -\nu_1 C^*_{1,\mathrm{II}}C_{2,\mathrm{IIb}}\varepsilon_{\mathrm{II}}\eta$$

We can examine the different cases discussed in the previous sections:

1. If the reaction is fast enough to be considered a surface reaction, we have $C^*_{1,\mathrm{I}} = C^*_{1,\mathrm{II}} = 0$ and, therefore, $r_{1,\mathrm{app}} = k_{1,\mathrm{I}}\mathcal{A}C_{1,\mathrm{Ib}}$. We observe first order with respect to $C_{1,\mathrm{Ib}}$ regardless of the true order with respect to $C_{1,\mathrm{IIb}}$.
2. Whenever the reaction is not instantaneous and as long as the concentration of A_2 is sufficiently high so that the concentration profile of A_2 in the film can be considered flat, we find, regardless of the extent of the gas side resistance:

$$\begin{aligned} r_{1,\mathrm{app}} &= k_{1,\mathrm{I}}\mathcal{A}\left(C_{1,\mathrm{Ib}} - C^*_{1,\mathrm{I}}\right) = k_{1,\mathrm{II}}E\mathcal{A}\left(C^*_{1,\mathrm{II}} - C_{1,\mathrm{IIb}}\right) \\ &= k_{1,\mathrm{II}}\mathcal{A}C^*_{1,\mathrm{II}}\left(\frac{Ha^2(\beta-1) + Ha\tanh[Ha]}{1 + Ha(\beta-1)\tanh[Ha]}\right) \end{aligned}$$

Since $C^*_{1,\mathrm{I}} = m_0 C^*_{1,\mathrm{II}}$, we obtain:

$$C^*_{1,\mathrm{II}} = \frac{k_{1,\mathrm{I}}C_{1,\mathrm{Ib}}}{m_0 k_{1,\mathrm{I}} + k_{1,\mathrm{II}}\left(\dfrac{Ha^2(\beta-1) + Ha\tanh[Ha]}{1 + Ha(\beta-1)\tanh[Ha]}\right)}$$

$$N_1 = r_{1,\mathrm{app}} = K'_{1,\mathrm{I}}\mathcal{A}C_{1,\mathrm{Ib}}$$

where:

$$\frac{1}{K'_{1,\mathrm{I}}} = \frac{1}{k_{1,\mathrm{I}}} + \frac{m_0}{k_{1,\mathrm{II}}\left(\dfrac{Ha^2(\beta-1)+Ha\tanh[Ha]}{1+Ha(\beta-1)\tanh[Ha]}\right)}$$

Neither Ha nor β depend on the concentrations relative to A_1, so that we again have first order with respect to $C_{1,\mathrm{Ib}}$. There are also a number of interesting limiting cases:

- gas side resistance is negligible:

$$r_{1,\mathrm{app}} = k_{1,\mathrm{II}}\mathcal{A}\frac{C_{1,\mathrm{Ib}}}{m_0}\left(\frac{Ha^2(\beta-1)+Ha\tanh[Ha]}{1+Ha(\beta-1)\tanh[Ha]}\right)$$

- gas side resistance is negligible and $Ha > 5$ (fast reaction), $\tanh[Ha] = 1$ and then:

$$r_{1,\mathrm{app}} = k_{1,\mathrm{II}}\mathcal{A}\frac{C_{1,\mathrm{Ib}}}{m_0}Ha$$

- gas side resistance is negligible and the reaction is slow: $\tanh[Ha] = Ha$:

$$r_{1,\mathrm{app}} = k_{1,\mathrm{II}}\mathcal{A}\frac{C_{1,\mathrm{Ib}}}{m_0}\left(\frac{1}{1+(\beta-1)Ha^2}\right)\beta Ha^2$$
$$= -\nu_1 k\varepsilon_{\mathrm{II}}\frac{C_{1,\mathrm{Ib}}}{m_0}C_{2,\mathrm{IIb}}\left(\frac{1}{1+(\beta-1)Ha^2}\right)$$

Moreover, if $\beta Ha^2 < 0.01$ (very slow reaction) and $\beta > 10$ (more than 90% of the liquid is outside the film):

$$r_{1,\mathrm{app}} = -\nu_1\varepsilon_{\mathrm{II}}k\frac{C_{1,\mathrm{Ib}}}{m_0}C_{2,\mathrm{IIb}}$$

This is the only case where the true kinetic constant can be obtained.

3. If our assumption of an excess of A_2 with respect to A_1 in the film is not satisfied, the enhancement factor E will depend on the parameter:

$$\mathcal{N}_2 = \frac{\nu_1}{\nu_2}\frac{\mathcal{D}_{2,\mathrm{II}}}{\mathcal{D}_{1,\mathrm{II}}}\frac{C_{2,\mathrm{IIb}}}{C^*_{1,\mathrm{II}}}$$

which contains the concentration $C^*_{1,\mathrm{II}}$: The apparent order will be different from 1. For example, for an instantaneous reaction without resistance in phase I, we find:

$$N_{\mathrm{I}} = r_{1,\mathrm{app}} = k_{1,\mathrm{II}}\mathcal{A}\left(\frac{C_{1,\mathrm{Ib}}}{m_0} + \frac{\nu_1}{\nu_2}\frac{\mathcal{D}_{2,\mathrm{II}}}{\mathcal{D}_{1,\mathrm{II}}}C_{2,\mathrm{IIb}}\right)$$

It is obvious that the apparent order with respect to $C_{1,\mathrm{Ib}}$ will fall between 0 and 1.

This analysis, which applies to the very simple case where the true order is 1, shows that observation of the apparent order with respect to $C_{1,\mathrm{Ib}}$ or $C_{1,\mathrm{IIb}}$ is generally not of much help in determining the limiting step in the process or the true order. It is also obvious that we must exercise caution in interpreting experimental kinetics results obtained in a heterogeneous fluid-fluid system. For this reason it is likely that many published results are of little significance.

3.3.2 Apparent activation energy

We now examine the case of a true first-order irreversible reaction carried out at various temperatures. The apparent rate of reaction in the steady state is equal to the rate of absorption. The absorption flux per unit volume of reactor can be expressed as we saw earlier by:

$$N_1 = k_{1,II}\mathcal{A}C^*_{1,II}Ha\left(\frac{Ha(\beta-1)+\tanh[Ha]}{1+Ha(\beta-1)\tanh[Ha]}\right) \tag{3.53}$$

Comparing the absorption flux at two different temperatures is appreciably the same as comparing two apparent rates. By applying the classic Arrhenius equation, we can determine an apparent activation energy:

$$\ln\left(\frac{N_1(T)}{N_1(T')}\right) = \frac{E_{app}}{R}\left[\frac{1}{T'}-\frac{1}{T}\right] \tag{3.54}$$

There are several possible cases:

1. If $Ha > 5$ in the temperature range T to T' under consideration, then $\tanh[Ha] = 1$, and we have:

$$\frac{N_1(T)}{N_1(T')} = \frac{k_{1,II}(T)}{k_{1,II}(T')}\frac{\mathcal{A}(T)}{\mathcal{A}(T')}\frac{C^*_{1,II}(T)}{C^*_{1,II}(T')}\frac{Ha(T)}{Ha(T')}$$

   If we assume that:

$$\frac{k_{1,II}(T)}{k_{1,II}(T')}\frac{\mathcal{A}(T)}{\mathcal{A}(T')}\frac{C^*_{1,II}(T)}{C^*_{1,II}(T')} = 1 \quad \text{and} \quad \frac{\mathcal{D}_{1,II}(T)}{\mathcal{D}_{1,II}(T')} = 1$$

   and that the change in temperature has an appreciable effect only on the rate constant, we have:

$$\frac{N_1(T)}{N_1(T')} = \sqrt{\frac{k(T)}{k(T')}} \tag{3.55}$$

   This equation enables to determine an apparent activation energy that is equal to half the true activation energy.

2. If $Ha < 0.3$ in the temperature range T to T' under consideration, $\tanh[Ha] \cong Ha$.

$$\frac{N_1(T)}{N_1(T')} = \frac{k_{1,II}(T)}{k_{1,II}(T')}\frac{\mathcal{A}(T)}{\mathcal{A}(T')}\frac{C^*_{1,II}(T)}{C^*_{1,II}(T')}\frac{\dfrac{Ha^2(T)\beta(T)}{1+Ha^2(T)\beta(T)}}{\dfrac{Ha^2(T')\beta(T')}{1+Ha^2(T')\beta(T')}}$$

   The above equation introduces the parameter $Ha^2\beta$. It is worthwhile examining the physical significance of this parameter:

$$Ha^2\beta = \frac{kC^*_{1,II}C_{2,IIb}\varepsilon_{II}}{k_{1,II}\mathcal{A}C^*_{1,II}}$$

   Here $Ha^2\beta$ appears as the ratio of the maximum rate of chemical reaction to the maximum rate of physical transfer. If we assume that $k_{1,II}$, $\mathcal{A}$, $C^*_{1,II}$, β, and $\mathcal{D}_{1,II}$ do not change with temperature and that β remains appreciably greater than 1, we have:

$$\frac{N_1(T)}{N_1(T')} = \frac{k(T)}{k(T')}\frac{1+Ha^2(T')\beta(T')}{1+Ha^2(T)\beta(T)}$$

There are two extreme cases:

- $Ha^2(T)\beta(T)$ and $Ha^2(T')\beta(T')$ are small compared to 1.

$$\frac{N_1(T)}{N_1(T')} = \frac{k(T)}{k(T')} \tag{3.56}$$

  and the apparent activation energy is equal to the true activation energy.

- $Ha^2(T)\beta(T)$ and $Ha^2(T')\beta(T')$ are large compared to 1.

$$\frac{N_1(T)}{N_1(T')} = \frac{k(T)}{k(T')}\frac{k(T')}{k(T)} = 1 \tag{3.57}$$

  The apparent activation energy is zero.

3. For the general case, depending on changes in the various parameters as a function of temperature, we find a range of situations, even including, for certain temperature domains, a negative apparent activation energy. This is observed principally when the solubility of A_1 in phase II is a decreasing function of temperature.

Figure 3.12 is based on the following values:

$$E_v = 83.6 \text{ kJ/mol}$$
$$R = 8.31 \text{ J/mol} \cdot \text{K}$$
$$\beta = 1\,000\text{-}100\text{-}10$$
$$Ha(300 \text{ K}) = 10^{-2.5}$$

Above 500 K we gradually approach the domain where $E_{app} = E_v/2$.

3.3.3 Influence of mass transfer on selectivity

When several chemical reactions take place simultaneously in a system with two fluid phases, selectivity problems can arise. As in the case of a single reaction, we can analyze the phenomenon from two points of view:

- the influence of the chemical reactions on transfer between the phases (case of simultaneous absorption of two gaseous compounds by a liquid reactant)
- the influence of mass transfer on the chemical reactions (this is the case, for example, with chlorination, hydrogenation, and oxidation reactions).

Below we limit our discussion to a qualitative analysis of gas-liquid systems.

3.3.3.1 Influence of chemical reactions on transfer selectivity

In general a chemical reactant is used to accelerate absorption only if the reactant is sufficiently effective, that is, if the rate of reaction is high. This means that, in the majority of cases, we will be working with fast ($Ha > 5$) or even instantaneous or surface reactions.

It frequently happens that the chemical reaction is reversible—for obvious economic reasons. This is the case, for example, with the absorption of acidic gases in aqueous amine solutions. These systems often follow the stoichiometric relations:

$$A_{1,G} + A_{3,L} \rightleftarrows A_{4,L}$$
$$A_{2,G} + A_{3,L} \rightleftarrows A_{5,L}$$

(For convenience we consider all the $|\nu_{i,j}|$ to be equal to 1.)

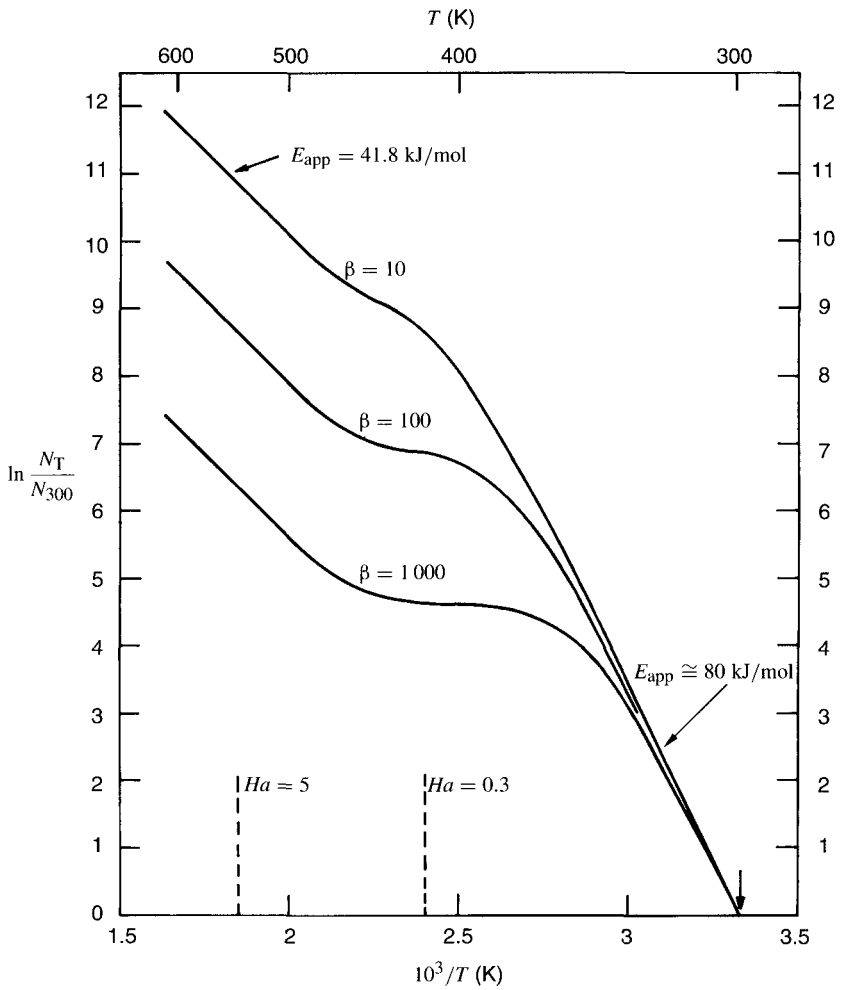


Figure 3.12 Apparent activation energy as a function of temperature for $Ha = 10^{-2.5}$ at 300 K, $E_v = 83.6$ kJ/mol.

We also assume, for the purpose of our example and for compatibility with the cases presented earlier in the chapter, that the rate equations are written:

$$r_1 = k_1 C_{1,\text{II}} C_{3,\text{II}} \quad \text{mol/s} \cdot \text{m}^3 \text{ of phase II}$$
$$r_2 = k_2 C_{2,\text{II}} C_{3,\text{II}} \quad \text{mol/s} \cdot \text{m}^3 \text{ of phase II}$$

Since the reactions are reversible, some selectivity may result from the different values of the equilibrium constants. This thermodynamic selectivity is rarely very high.

On the other hand, the transfer coefficients, both on the gas and on the liquid side, are generally very close. Thus no selectivity can be attributed directly to mass transfer. However,

the increase in the transfer coefficients on the liquid side can be attributed to the chemical reactions (enhancement factor).

In this regard, a recent study by Vas Bhat *et al.* [1999] presents the results of calculations for various kinetic schemes, using penetration theory to model mass transfer with chemical reaction. The various reactions (reversible and irreversible) were examined and the results supplied as a network of curves with E as a function of the Hatta number for the first reaction (see Fig. 3.13).

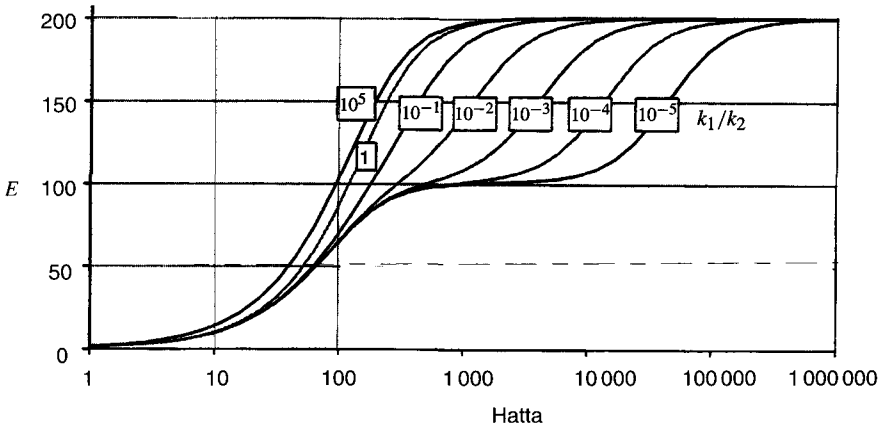


Figure 3.13 Enhancement factor for the transfer of a compound A_1 followed by an irreversible consecutive reaction: $A_{1,G} + A_{2,L} \rightarrow A_{3,L}$; $A_{1,G} + A_{3,L} \rightarrow A_{4,L}$ as a function of the Hatta number on the abscissa and with the ratio of the two kinetic constants k_1/k_2 as a parameter [after Vas Bhat *et al.* 1999].

Several possible cases are to be considered when examining selectivity:

1. The two reactions can be fast reactions, similar to pseudo-first-order reactions ($Ha > 2$ and $\mathcal{N}_2 > 10Ha$). In this case the concentration profiles in the film are those shown in Fig. 3.14A. The concentration profile of the coreactant present in phase II (liquid) is flat and the ratio of absorption rates is close to:

$$\frac{N_1}{N_2} \approx \sqrt{\frac{k_1 \mathcal{D}_{1,\mathrm{II}}}{k_2 \mathcal{D}_{2,\mathrm{II}}}} \frac{C^*_{1,\mathrm{II}}}{C^*_{2,\mathrm{II}}} \quad \text{[Following (3.23)]} \tag{3.58}$$

   We see that a given kinetic selectivity can be realized since the ratio of absorption fluxes is proportional to the square root of the ratio of kinetic constants.

2. The two reactions are instantaneous ($Ha > 2$, $\mathcal{N}_2 < 0.1Ha$). The concentration profiles are shown in Fig. 3.14B. It is obvious that there is a unique reaction location and, consequently, the ratio of absorption fluxes can be written:

$$\frac{N_1}{N_2} \approx \frac{\mathcal{D}_{1,\mathrm{II}}}{\mathcal{D}_{2,\mathrm{II}}} \frac{C^*_{1,\mathrm{II}}}{C^*_{2,\mathrm{II}}} \tag{3.59}$$

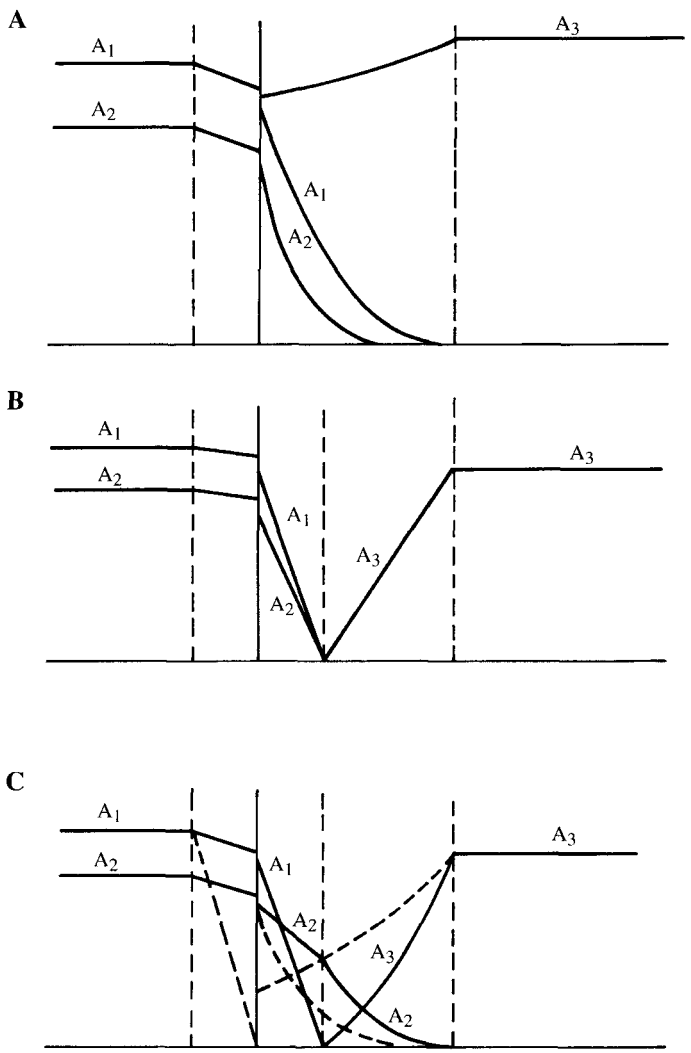


Figure 3.14 Concentration profiles on either side of the interface. System examined: $A_{1,G} + A_{3,L} \rightarrow A_{4,L}$; $A_{2,G} + A_{3,L} \rightarrow A_{5,L}$.
A. Both reactions are fast. **B.** Both reactions are instantaneous. **C.** One reaction is fast and the other instantaneous.

We see that there is little chance, in terms of current applications, of being able to observe any effect of absorption selectivity due to the chemical reaction.

3. One reaction can be considered instantaneous (r_1) and the other fast (r_2). The concentration profiles are shown in 3.14C. Here, depending on the position of the reaction location (that is, depending on the values of diffusivity and concentration), the absorption fluxes can be very different. Enhancement of the transfer of the compound reacting in the

instantaneous regime can even inhibit absorption of the second compound, even if this second compound is more concentrated or more soluble. As an extreme case, the absorption of compound A_1 can take place as a surface reaction limited only by the resistance in the gas phase (dotted lines).

As noted, the two following criteria can be used to identify the reaction regime:

- Instantaneous: $\dfrac{\sqrt{-\nu_i k_i \mathcal{D}_{i,\mathrm{II}} C_{3,\mathrm{IIb}}}}{k_{i,\mathrm{II}}} > 10 \dfrac{\nu_i}{\nu_3} \dfrac{\mathcal{D}_{3,\mathrm{II}}}{\mathcal{D}_{i,\mathrm{II}}} \dfrac{C_{3,\mathrm{IIb}}}{C^*_{i,\mathrm{II}}}$
- Surface: $\dfrac{C_{3,\mathrm{IIb}}}{C_{i,\mathrm{Ib}}} > \dfrac{\nu_3}{\nu_i} \dfrac{\mathcal{D}_{i,\mathrm{II}}}{\mathcal{D}_{3,\mathrm{II}}} \dfrac{k_{i,\mathrm{I}}}{k_{i,\mathrm{II}}}$

(A_3 is a coreactant, A_i a reactant transferred from the gas phase).

We can draw the following qualitative conclusions from this discussion based on the third case examined:

- Given the concentration gradients at the interface, a kinetic selectivity for absorption can be obtained.
- The equipment must be chosen in such a way that both fluids circulate with plug flow and with limited contact time. Lengthy contact times and backmixing lead to thermodynamic equilibrium, which is often less favorable for selectivity.

In conclusion we can say that only when both reactions take place at different regimes (one instantaneous, the other fast) does the kinetic selectivity favor the compound absorbed in the instantaneous regime. Nonetheless, systematic experimentation is needed to determine the optimal operating conditions and particular attention must be paid to the design of equipment to avoid excessive residence times and overly broad residence time distributions.

3.3.3.2 Influence of mass transfer on the selectivity of the chemical transformation

Above we examined the role played by the chemical reactions in the absorption selectivity between two reactants, generally in the gas phase. Conversely, we will also consider the influence of transfer phenomena between phases on the selectivity of complex chemical reactions. Such reactions occur, for example, when we have a phase I coreactant that is common to several chemical reactions that take place in phase II. Here we examine two important practical cases, the consecutive reactions represented by:

$$\mathrm{A}_{1,\mathrm{G}} + \mathrm{A}_{2,\mathrm{L}} \rightleftarrows \mathrm{A}_{3,\mathrm{L}} \quad (\text{rate } r_1)$$
$$\mathrm{A}_{1,\mathrm{G}} + \mathrm{A}_{3,\mathrm{L}} \rightleftarrows \mathrm{A}_{4,\mathrm{L}} \quad (\text{rate } r_2)$$

where:

$$r_1 = k_1 C_{1,\mathrm{II}} C_{2,\mathrm{II}}$$
$$r_2 = k_2 C_{1,\mathrm{II}} C_{3,\mathrm{II}}$$

and the parallel reactions represented by:

$$\mathrm{A}_{1,\mathrm{G}} + \mathrm{A}_{2,\mathrm{L}} \rightleftarrows \mathrm{A}_{3,\mathrm{L}} \quad (\text{rate } r_1)$$
$$\mathrm{A}_{1,\mathrm{G}} + \mathrm{A}_{4,\mathrm{L}} \rightleftarrows \mathrm{A}_{5,\mathrm{L}} \quad (\text{rate } r_2)$$

where:

$$r_1 = k_1 C_{1,\mathrm{II}} C_{2,\mathrm{II}}$$
$$r_2 = k_2 C_{1,\mathrm{II}} C_{4,\mathrm{II}}$$

The twin reactions:

$$\mathrm{A}_{1,\mathrm{G}} + \mathrm{A}_{2,\mathrm{L}} \rightleftarrows \mathrm{A}_{3,\mathrm{L}} \quad (\text{rate } r_1)$$
$$\mathrm{A}_{1,\mathrm{G}} + \mathrm{A}_{2,\mathrm{L}} \rightleftarrows \mathrm{A}_{4,\mathrm{L}} \quad (\text{rate } r_2)$$

are of no interest since there is no chance of changing the selectivity resulting from the transfer of A_1 from phase I to phase II.

If the reactions are slow enough for phase II (bulk + film) to be considered always as saturated with compound A_1, we have the classic case of single-phase reactions. This can be used as a reference case to test any possible variations in selectivity. It should be obvious that a change in selectivity can only be observed in the case of fast reactions.

A. Consecutive reactions

If both reactions are fast (rates r_1 and r_2), a majority, if not all, of the reaction will take place within the film at the interface (Fig. 3.15). The diffusion fluxes of compound A_2 toward this reaction zone (from the bulk to the film) and of compound A_3 out of this reaction zone (from the film to the bulk) will determine local selectivity.

If we examine, even qualitatively, the concentration gradients of A_2 and A_3 in the film (Fig. 3.15 for example), we find that the mean value $\bar{C}_{2,\mathrm{II}}$ in the film is less than the measurable concentration $C_{2,\mathrm{IIb}}$, and the mean value $\bar{C}_{3,\mathrm{II}}$ in the film is greater than $C_{3,\mathrm{IIb}}$.

The ratio of concentrations $\bar{C}_{2,\mathrm{II}}/\bar{C}_{3,\mathrm{II}}$ which governs the selectivity—because the entire transformation occurs in the film—is less favorable than the ratio $C_{2,\mathrm{IIb}}/C_{3,\mathrm{IIb}}$. As a result the selectivity of the intermediate compound will be lower than the reference selectivity based on a single-phase reaction. Van de Vusse [1966] was the first to examine the influence of the mass transfer of a coreactant on the selectivity of consecutive chemical reactions.

The basic equations describing the local steady-state situation within the film have already been introduced.

$$\mathcal{D}_i \left[\frac{\mathrm{d}^2 C_i(x)}{\mathrm{d}x^2} \right] + \sum \nu_{i,j} r_j = 0$$

In the present situation, these become:

$$\mathcal{D}_1 \left[\frac{\mathrm{d}^2 C_1(x)}{\mathrm{d}x^2} \right] = r_1 + r_2 = k_1 C_1(x) C_2(x) + k_2 C_1(x) C_3(x) \tag{3.60}$$

$$\mathcal{D}_2 \left[\frac{\mathrm{d}^2 C_2(x)}{\mathrm{d}x^2} \right] = k_1 C_1(x) C_2(x) \tag{3.61}$$

$$\mathcal{D}_3 \left[\frac{\mathrm{d}^2 C_3(x)}{\mathrm{d}x^2} \right] = k_2 C_1(x) C_3(x) - k_1 C_1(x) C_2(x) \tag{3.62}$$

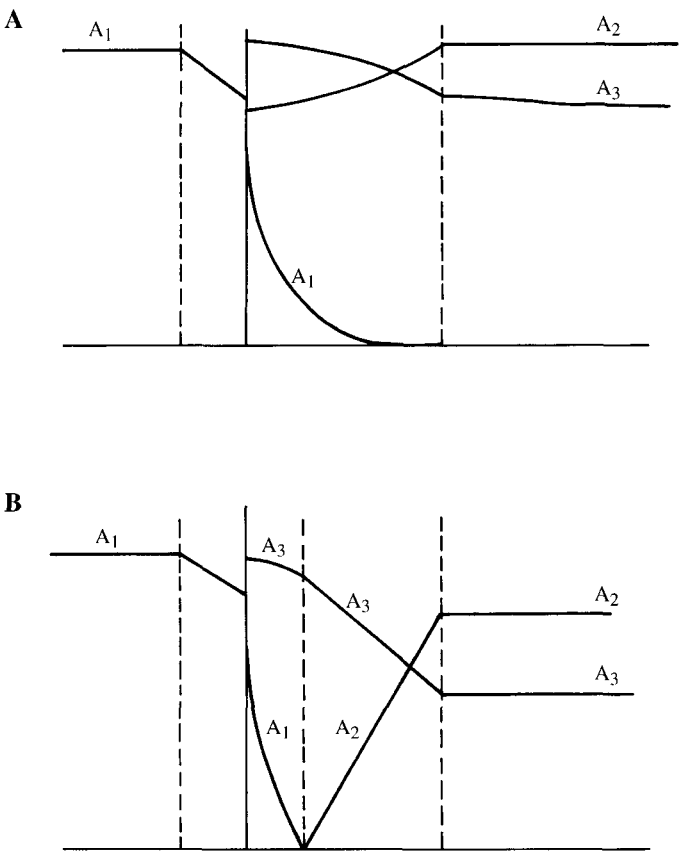


Figure 3.15 Concentration profiles on either side of the interface. System examined: $A_{1,G} + A_{2,L} \rightarrow A_{3,L}$; $A_{1,G} + A_{3,L} \rightarrow A_{4,L}$. **A.** Both reactions are fast. **B.** One reaction is instantaneous, the other fast.

Where the boundary conditions are:

- For $x = 0$, that is, at the interface:

$$C_1(0) = C_1^*$$

$$\frac{dC_2}{dx} = 0 \quad \text{and} \quad \frac{dC_3}{dx} = 0$$

because compounds 2 and 3 do not cross the interface.

- For $x = \delta$, that is, at the edge of the film:

$$C_2(\delta) = C_{2,b}$$

$$C_3(\delta) = C_{3,b}$$

- The last boundary condition, involving $C_1(\delta)$, is expressed differently by different authors. We have, for example:

$$C_1(\delta) = C_{1,b}$$

$$C_1(\delta) = 0$$

$$\left[\frac{dC_1}{dx}\right]_{x=\delta} = 0 \quad \text{the boundary condition used by Van de Vusse}$$

$$\mathcal{D}_1 \mathcal{A} \left[\frac{dC_1}{dx}\right]_{x=\delta} = -(r_1 + r_2)_b \, (\varepsilon_{II} - \mathcal{A}\delta) \tag{3.63}$$

This was boundary condition N° 1 for Teramoto *et al.* [1973] and expresses the fact that the flux of A_1 that crosses the film feeds the reaction in the bulk of the liquid phase.

$$\mathcal{D}_1 \mathcal{A} \left[\frac{dC_1}{dx}\right]_{x=\delta} dV = -(r_1 + r_2)_b \, (\varepsilon_{II} - \mathcal{A}\delta) \, dV - Q \, dC_{1,b} \tag{3.64}$$

(the second boundary condition N° 2 used by Teramoto *et al.* [1973])
where

Q volume flow rate of phase II flowing through the volume dV

dV volume element for which the temperature and composition can be considered uniform.

This last condition expresses the fact that the flux of A_1, which crosses the boundary of the film in the direction of the bulk of the liquid phase, is combined with a phase II flow Q that contributes to the overall balance.

This same type of boundary condition was adopted by Darde *et al.* [1983], who examined the problem both theoretically and experimentally. The authors have shown that the selectivity of an intermediate compound A_3 was promoted by an increase in the following key parameters: concentration of reactant A_2, mass transfer coefficient of A_1, and the ratio of the kinetic constants k_1/k_2.

Because all the studies mentioned above used film theory to model transfer, they had to address the difficult problem of the boundary condition for $x = \delta$. Penetration theory, which has been used by Vas Bhat *et al.* [1999], eliminates this problem. Applying their model to the chlorination of p-cresol, they were able to show that the selectivity of the formation of the monochlorinated compound, compared to the bichlorinated compound, decreased as the Hatta number for the first reaction increased, while the overall conversion increased.

Van de Vusse summarized his findings (Table 3.4), which can be used to evaluate the effect of the following parameters:

$$Ha = \frac{\sqrt{k_1 \mathcal{D}_{1,II} C_{2,IIb}}}{k_{1,II}} \qquad \mathcal{N}_2 = \frac{\mathcal{D}_{2,II}}{\mathcal{D}_{1,II}} \frac{C_{2,IIb}}{C^*_{1,II}} \quad \text{and} \quad \beta = \frac{k_{1,II}\varepsilon_{II}}{\mathcal{A}\mathcal{D}_{1,II}}$$

on the rate and selectivity of the transformation.

Note that in the Table 3.4, the definition of the Hatta number only takes reaction one into account and that the number $\mathcal{N}_2$, which is related to compound A_3, is ignored. In the event the kinetic constants are not too different, this approximation is sufficient to derive valid criteria.

Table 3.4 Effect of Ha, $\mathcal{N}_2$ and β on selectivity.

<table>
<tr><th colspan="2">$Ha > 2$</th><th colspan="2">$Ha < 0.5$</th></tr>
<tr><td>$\mathcal{N}_2 > 10Ha$</td><td>No effect on selectivity</td><td colspan="2">No effect on selectivity</td></tr>
<tr><td>$\mathcal{N}_2 \cong Ha$</td><td>Harmful effect on selectivity</td><td rowspan="2">$Ha^2\beta \ll 1$

Observed rate = rate of the chemical reaction</td><td rowspan="2">$Ha^2\beta \gg 1$

Observed rate = rate of physical transfer</td></tr>
<tr><td>$\mathcal{N}_2 < 0.1Ha$</td><td>Very harmful effect on selectivity</td></tr>
</table>

It is also important to remember that it is generally not worth considering the selectivity of slow reactions. These reactions take place in phase II and the selectivity is purely chemical.

When dealing with fast reactions, several cases are possible. Figure 3.15 indicates the corresponding concentration profiles.

1. Both reactions are fast ($Ha > 2$, $\mathcal{N}_2 > 10Ha$). The profiles shown in 3.15A show that there is an influence on selectivity but it remains moderate.
2. Reaction 1 is instantaneous, reaction 2 is fast. The profiles shown in Fig. 3.15B show that the effect on selectivity is considerable. The mean concentration of compound A_2 in the film is low and clearly less than $C_{2,\mathrm{IIb}}$, while the mean concentration of the intermediate compound A_3 in the film is appreciably higher than the concentration in the bulk of the fluid phase $C_{3,\mathrm{IIb}}$.
3. There is little point in examining the case when both reactions are instantaneous since we can no longer speak of selectivity: the intermediate compound cannot be observed in phase II.

To conclude, it is important to determine whether or not, within the diffusion film in phase II, the respective profiles of $C_{2,\mathrm{II}}(x)$ and $C_{3,\mathrm{II}}(x)$ can be considered nearly flat.

Recall that in our examination of a simple chemical reaction, we considered two separate cases. First, we examined the case where the concentration profile of the coreactant in the film was flat, which corresponded to the case we referred to as a pseudo-first-order reaction, governed by a single equation $E = f(Ha)$ and, more specifically, $E = Ha$ for $Ha > 2$. Second, we examined the situation where the profile of the coreactant was not flat. This led us to consider the reaction as second order and to introduce the dimensionless number $\mathcal{N}_2$, as shown in Fig. 3.4, for example.

For every value of Ha, we can read two values for the enhancement factor, one corresponding to pseudo-first order (straight profile), the other corresponding to second order (more or less pronounced profile). The difference between the values read off the graph is, in a way, a measurement of the flatness of the concentration profile of the coreactant.

We see from Fig. 3.4 that:

- For $Ha < 0.5$, and regardless of the value of $\mathcal{N}_2$, the enhancement factor is close to unity. This corresponds to the flat profiles for A_2 and A_3 and, as a consequence, does not lead to a loss of selectivity.

- For $Ha > 2$ and $\mathcal{N}_2 > 10Ha$, the two values read for the enhancement factor tend to merge: E(pseudo-first order) $\cong E$(second order), and consequently, the profiles for A_2 and A_3 are flat and there is no influence on selectivity.

On the other hand, when $\mathcal{N}_2 < 10Ha$, the difference in the two values for E increases with the difference between $\mathcal{N}_2$ and Ha. Whenever the combination of values of Ha and $\mathcal{N}_2$ leads to a value of E (second order) along a curve that is appreciably horizontal, the selectivity becomes not just poor but unacceptable.

B. Parallel reactions

The findings summarized in Table 3.4 can be considered perfectly valid, as shown by the profiles in Fig. 3.16. Here the definition of the Hatta number becomes:

$$Ha = \frac{\sqrt{\mathcal{D}_{1,\mathrm{II}}(k_1 C_{2,\mathrm{IIb}} + k_2 C_{3,\mathrm{IIb}})}}{k_{1,\mathrm{II}}} \tag{3.65}$$

and there are two different $\mathcal{N}_2$:

$$\mathcal{N}_{2,2} = \frac{\nu_1}{\nu_2}\frac{\mathcal{D}_{2,\mathrm{II}}}{\mathcal{D}_{1,\mathrm{II}}}\frac{C_{2,\mathrm{IIb}}}{C^*_{1,\mathrm{II}}} \quad \text{and} \quad \mathcal{N}_{2,3} = \frac{\nu_1}{\nu_3}\frac{\mathcal{D}_{3,\mathrm{II}}}{\mathcal{D}_{1,\mathrm{II}}}\frac{C_{3,\mathrm{IIb}}}{C^*_{1,\mathrm{II}}} \tag{3.66}$$

- **Two fast reactions** (Fig. 3.16A)

This situation is realized for high concentrations of reactants A_2 and A_3, while the concentration of A_1 remains low (low partial pressure or a relatively insoluble compound). This implies that:

$$\frac{\mathcal{N}_{2,2}}{Ha} > 10 \quad \text{and} \quad \frac{\mathcal{N}_{2,3}}{Ha} > 10$$

In this case the concentration profiles remain flat and the influence on selectivity is not only limited but unobservable.

- **An instantaneous reaction (r_1) and a fast reaction (r_2)** (Fig. 3.16B)

In this case, for reaction 1 the criterion $\mathcal{N}_{2,2}/Ha > 10$ is no longer satisfied and depletion of the corresponding reactant A_2 in the film has an effect. This will have a favorable or unfavorable effect on the desired selectivity, for it is the fastest reaction that will be most affected by mass transfer phenomena. We can rephrase this by saying that the ratio of mean concentrations of the two reactants A_2 and A_3 in the film is less than the ratio of concentrations in the bulk of the fluid phase. Since it is this ratio that governs selectivity, it is reaction 1, the faster reaction, that will be disadvantaged.

- **Two instantaneous reactions** (Fig. 3.16C)

In this case, for both reactions, $\mathcal{N}_{2,2}/Ha < 0.1$ and $\mathcal{N}_{2,3}/Ha < 0.1$. As a result, the selectivity, that is the flux ratio of compounds A_2 and A_3 towards the reaction location, can be written as follows:

$$\frac{N_2}{N_3} = \frac{\mathcal{D}_{2,\mathrm{II}}}{\mathcal{D}_{3,\mathrm{II}}}\frac{C_{2,\mathrm{IIb}}}{C_{3,\mathrm{IIb}}} \tag{3.67}$$

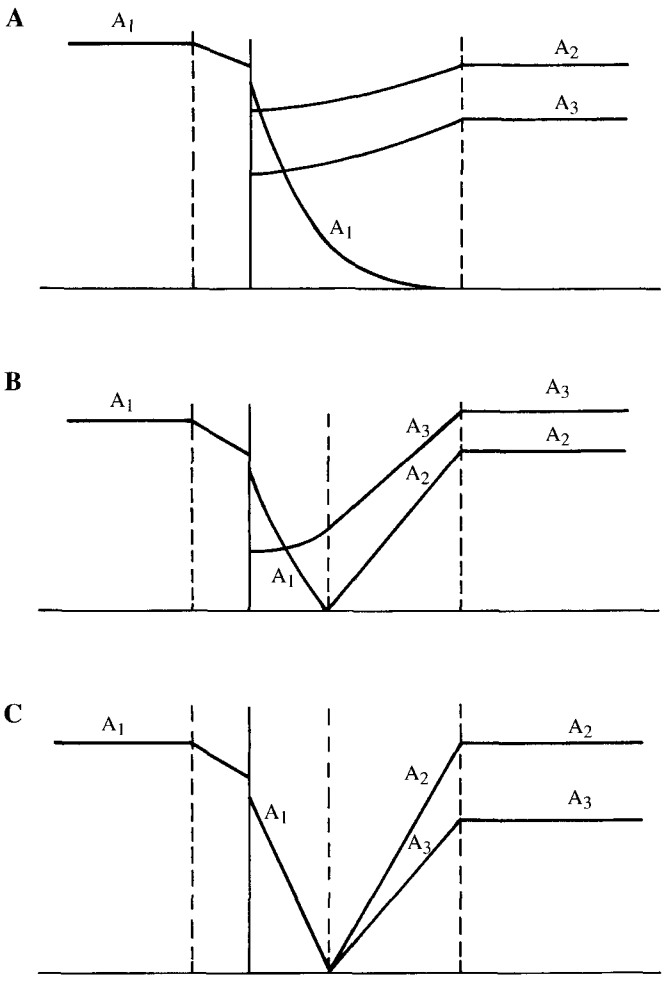


Figure 3.16 Concentration profiles on either side of the interface. System examined: $A_{1,G} + A_{2,L} \rightarrow A_{4,L}$; $A_{1,G} + A_{3,L} \rightarrow A_{5,L}$.
A. Both reactions are fast. **B.** One reaction is instantaneous, the other fast.
C. Both reactions are instantaneous.

We see that it is no longer the ratio of kinetic constants that governs the selectivity of the transformation but the ratio of diffusion coefficients. The resulting physical selectivity is very different from the chemical selectivity, which can be expressed as:

$$\frac{r_1}{r_3} = \frac{k_1 C_{2,\mathrm{IIb}}}{k_2 C_{3,\mathrm{IIb}}} \tag{3.68}$$

To conclude our discussion of the effects of mass transfer on chemical selectivity, we can say that mass transfer does not have a significant effect on selectivity unless $Ha > 2$ and

$\mathcal{N}_2/Ha$ for one or both of the reactions falls below 10. In this case specific experimentation is needed to determine the selectivities that can be obtained effectively with an industrial reactor.

The selectivity of an existing reactor can only be improved by increasing $\mathcal{N}_2$, that is by increasing the concentration of A_2 or A_3 (or both) and possibly by lowering the concentration of A_1.

3.4 DESIGNING A REACTOR WITH TWO FLUID PHASES

We will now examine how the theoretical concepts developed in the previous pages can be used to design a reactor in which two fluid phases are present. We distinguish three types of reactor:

- the batch reactor together with its variant, the semi-continuous reactor
- the tubular reactor, or concentration gradient reactor
- the continuous stirred tank reactor, or one with uniform concentration.

There are three ways in which interactions between mass transfer and chemical reactions occur in practice:

- slow reaction: Mass transfer is not influenced by the chemical reaction. The fraction of the reaction that takes place in the film is negligible.

$$Ha < 0.3 \quad \text{for } \beta > 50 \quad \text{(see Fig. 3.6)}$$

- fast reaction: Mass transfer is strongly influenced by the chemical reaction and the entire reaction takes place in the film.

$$Ha > 5 \quad \text{regardless of the value of } \beta$$

- intermediate rate reaction: Mass transfer is moderately influenced by the chemical reaction, which takes place both in the film and in the bulk of phase II. This last fact significantly complicates the balance equations. However, in light of Fig. 3.9, we can conclude that this case is not found unless $0.5 < Ha < 2$.

When $0.3 < Ha < 0.5$, we assume that the chemical reaction accelerates transfer but that the reaction nevertheless takes place essentially in the bulk of phase II, with classic kinetics and a calculable concentration $C_{1,\text{IIb}}$.

Above $Ha = 1$ (and even, in some cases, for $Ha > 0.5$) the concentration of $C_{1,\text{IIb}}$ becomes very low. Consequently, we can consider it zero, reducing this case to that of a fast reaction, with good approximation. In the sections below we treat two situations:

- slow reactions
- fast reactions (including surface and instantaneous reactions).

3.4.1 Batch reactor with two fluid phases

When the two fluid phases are a gas and a liquid, the batch reactor is not used in actual practice. Here we examine the use of a batch reactor to process two liquid phases (Fig. 3.17), which is the situation encountered most often in practice. Specifically, we are going to examine a

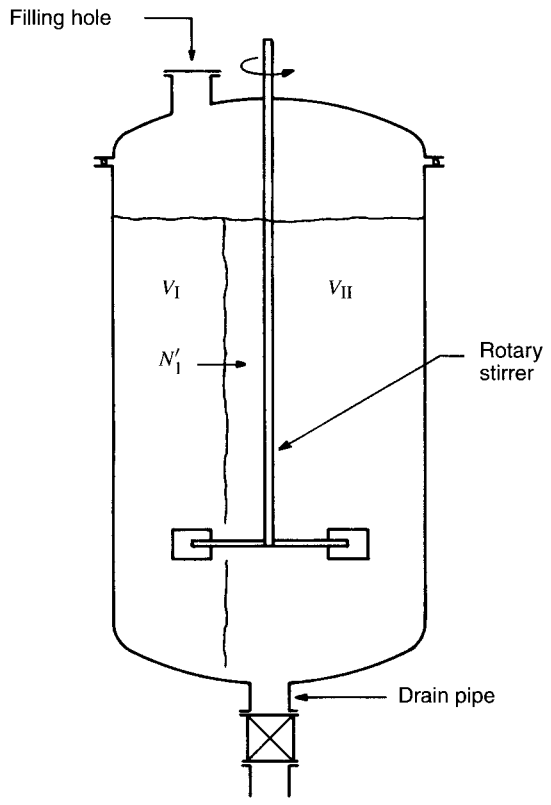


Figure 3.17 Batch reactor with two liquid phases.

second-order irreversible reaction $\nu_1 A_1 + \nu_2 A_2 \rightarrow \nu_3 A_3$ that takes place in phase II with a rate r. The reactant A_2 and the product A_3 cannot be transferred to phase I. We assume the presence of a perfectly dispersed mixture of the two phases in the reactor, phase I occupying volume V_I, phase II occupying volume V_{II}.

3.4.1.1 Writing the mass balance equations

Below we derive the mass balance equations for a slow reaction and a fast reaction.

A. Slow reaction

When the reaction is slow, we can assume that the concentrations in the film are not very different from those in the bulk of phase II. We treat the bulk and film similarly, assuming the conditions are the same everywhere throughout volume V_{II}.

Bear in mind that with a slow reaction and a low value of β, phase II will be constantly saturated with reactant A_1—ideal conditions for realizing the chemical transformation. With other values of β, phase II will be more or less saturated with reactant A_1 and the concentration will change as a function of time, as shown below.

The mass balance equations are written:

$$\frac{dn_{1,I}}{dt} = -N_1 V \tag{3.69}$$

$$\frac{dn_{1,II}}{dt} = N_1 V + \nu_1 r V_{II} \tag{3.70}$$

$$\frac{dn_{2,II}}{dt} = \nu_2 r V_{II} \tag{3.71}$$

$$\frac{dn_{3,II}}{dt} = \nu_3 r V_{II} \tag{3.72}$$

with:

$$\begin{aligned} N_1 &= \mathcal{A}\left[N_1'\right]_{x=0} \\ V &= V_I + V_{II} \\ V_I &= \sum n_{i,I} \bar{v}_{m,i,I} \\ V_{II} &= \sum n_{i,II} \bar{v}_{m,i,II} \\ r &= k C_{1,II} C_{2,II} \\ \left[N_1'\right]_{x=0} &= k_{1,I}(C_{1,Ib} - C_{1,I}^*) = k_{1,II}(C_{1,II}^* - C_{1,IIb}) \\ C_{1,I}^* &= p + m C_{1,II}^* \end{aligned}$$

$\bar{v}_{m,i,I}$ molar volume of constituent i in phase I
$n_{i,I}$ number of moles of constituent i in phase I.

We assume that ν_1, ν_2, ν_3, $(n_{i,I})_0$, $(n_{i,II})_0$, V_I, V_{II}, k, $k_{1,I}$, $k_{1,II}$, $\mathcal{A}$, m, and p are known. Equations (3.69) and (3.71) can then be written:

$$\frac{dn_{1,I}}{dt} = -K_{1,II}\mathcal{A}V\left[\frac{\left(\frac{n_{1,I}}{V_I}\right) - p}{m} - \frac{n_{1,II}}{V_{II}}\right] \tag{3.73}$$

$$\frac{dn_{2,II}}{dt} = \nu_2 k V_{II}\left(\frac{n_{1,II}}{V_{II}}\right)\left(\frac{n_{2,II}}{V_{II}}\right) \tag{3.74}$$

with:

$$\frac{1}{K_{1,II}} = \frac{1}{k_{1,II}} + \frac{1}{m k_{1,I}}$$

The initial conditions are:

$$\left(\frac{n_{1,I}}{V_I}\right)_0 = (C_{1,Ib})_0 \quad \left(\frac{n_{1,II}}{V_{II}}\right)_0 = (C_{1,IIb})_0 \quad \left(\frac{n_{2,II}}{V_{II}}\right)_0 = (C_{2,IIb})_0$$

After integration up to time t, we obtain:

$$n_{1,I}(t),\ n_{1,II}(t),\ n_{2,II}(t),\ n_{3,II}(t),\ V_I(t),\ V_{II}(t)$$

B. Fast reaction

The mass balance equations are modified as follows:

$$\frac{dn_{1,I}}{dt} = -N_1 V \tag{3.75}$$

$$\frac{dn_{1,II}}{dt} = 0 \quad \text{where } n_{1,II} = 0 \quad \text{and } C_{1,IIb} = 0 \tag{3.76}$$

$$\frac{dn_{2,II}}{dt} = -\frac{\nu_2}{\nu_1} N_1 V \tag{3.77}$$

$$\frac{dn_{3,II}}{dt} = -\frac{\nu_3}{\nu_1} N_1 V \tag{3.78}$$

with:

$$[N_1']_{x=0} = k_{1,I}(C_{1,Ib} - C_{1,I}^*) = Ek_{1,II}C_{1,II}^*$$

and:

$$C_{1,I}^* = mC_{1,II}^* + p$$

The value of E must be estimated. For example, if:

$$E = Ha = \frac{\sqrt{-\nu_1 k C_{2,IIb} \mathcal{D}_{1,II}}}{k_{1,II}}$$

we can determine that:

$$C_{1,II}^* = \frac{k_{1,I}(C_{1,Ib} - p)}{Ek_{1,II} + mk_{1,I}}$$

We can then calculate $\mathcal{N}_2$. Referring to Fig. 3.4 or Eq. (3.37), we can obtain a corrected value for E, which enables us to continue the iteration until we obtain correct values for E and $C_{1,II}^*$. We can then express N_1 and, as a result, integrate (3.76) and (3.77) as before, calculating Ha, E, and $C_{1,II}^*$ at each integration step. Finally, we obtain:

$$n_{1,I}(t),\ n_{1,II}(t),\ n_{2,II}(t),\ n_{3,II}(t),\ V_I(t),\ V_{II}(t)$$

3.4.1.2 Writing the enthalpy balances

The heat balance is written:

$$\sum \left[\frac{d(n_i \bar{h}_i)_I + d(n_i \bar{h}_i)_{II}}{dt} \right] = Q_E \tag{3.79}$$

Q_E being the heat supplied to the system per unit of time. For the current case, we have:

$$-\frac{dn_{1,I}}{dt} = N_1 V \quad \text{and} \quad \frac{dn_{i,II}}{dt} = 0 \quad \text{for } i \neq 1$$

$$\frac{dn_{1,II}}{dt} = N_1 V + \nu_1 r V_{II} \quad \text{(slow reaction) or } n_{1,II} = 0 \quad \text{(fast reaction)}$$

$$\frac{dn_{2,II}}{dt} = \nu_2 r V_{II}$$

$$\frac{dn_{3,II}}{dt} = \nu_3 r V_{II}$$

$$\frac{dn_{i,II}}{dt} = 0 \quad \text{for } i \neq 1,2,3 \text{ (inert species)}$$

$$\frac{d\bar{h}_{i,I}}{dt} = C_{Pi,I}\frac{dT_I}{dt}$$

$$\frac{d\bar{h}_{i,II}}{dt} = C_{Pi,II}\frac{dT_{II}}{dt}$$

$$\sum \nu_i \bar{h}_{i,II} = \Delta H_R$$

Equation (3.79) then assumes the following form:

$$\left(\sum n_{i,I} C_{Pi,I}\right)\frac{dT_I}{dt} + \left(\sum n_{i,II} C_{Pi,II}\right)\frac{dT_{II}}{dt} + \sum \bar{h}_{i,I}\frac{dn_{i,I}}{dt} + \sum \bar{h}_{i,II}\frac{dn_{i,II}}{dt} = Q_E$$

which can here be written:

$$\left(\sum n_{i,I} C_{Pi,I}\right)\frac{dT_I}{dt} + \left(\sum n_{i,II} C_{Pi,II}\right)\frac{dT_{II}}{dt} + \left[\bar{h}_{1,II}(N_1 V + \nu_1 r V_{II}) + \bar{h}_{2,II}\nu_2 r V_{II} + \bar{h}_{3,II}\nu_3 r V_{II}\right] + \bar{h}_{1,I}(-NV)_1 = Q_E$$

or, if $T_I = T_{II}$ and $\bar{h}_{i,I} \cong \bar{h}_{i,II}$:

$$\left(\sum n_i C_{Pi}\right)\frac{dT}{dt} + r V_{II}\Delta H_R = Q_E \tag{3.80}$$

If we cannot assume $\bar{h}_{i,I} \cong \bar{h}_{i,II}$ (as for evaporation or condensation, for example), then we must introduce one or more terms for latent heat into the enthalpy balance. If T_I differs from T_{II}, then we must introduce a term for heat transfer between phases. This situation is not examined here, however. Equation (3.80) is identical to the equation obtained for a single-phase batch reactor.

3.4.2 Semi-Continuous gas-liquid reactor

Although the batch reactor examined above works well when both fluids are liquid phases, it is highly unsuitable when one of the fluid phases is a gas. In this case the semi-continuous reactor is recommended. This type of reactor is illustrated in Fig. 3.18. A stirred vessel

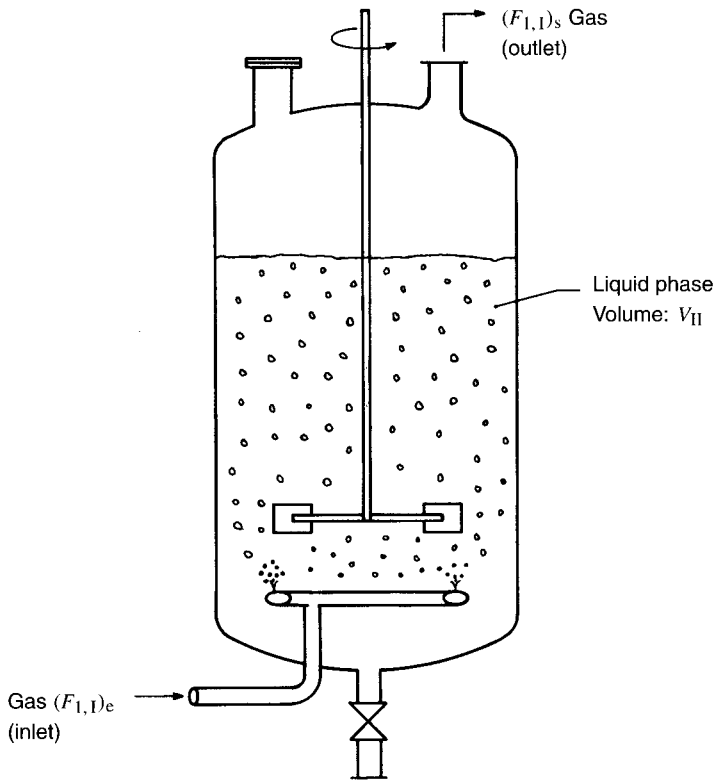


Figure 3.18 Semi-Continuous gas-liquid reactor.

contains a volume V_{II} into which gas is injected continuously with a molar flow rate F_e, which results in expansion and increases the total volume (gas + liquid) to V. Again consider the second-order irreversible reaction:

$$\nu_1 A_1 + \nu_2 A_2 \rightarrow \nu_3 A_3 \quad (\text{rate } r)$$

We also assume that the liquid phase can be perfectly mixed. Flow is considerably more complex in the gas phase, however. For small laboratory apparatus, the assumption of perfect mixing is not totally unrealistic; for industrial reactors the assumption of plug flow can be used as a first approximation. For greater accuracy a backmixing term for the gas phase should be introduced. In the following equations we assume gas phase plug flow.

• Slow reaction

The mass balance equations are written:

$$\frac{\partial C_{1,I}}{\partial t} = \frac{\partial F_{1,I}}{S \partial \ell} + N_1 \tag{3.81}$$

$$\frac{\mathrm{d}n_{2,\mathrm{II}}}{\mathrm{d}t} = \int_0^H \nu_2 \varepsilon_{\mathrm{II}} r S \,\mathrm{d}\ell \tag{3.82}$$

$$\frac{\mathrm{d}n_{1,\mathrm{II}}}{\mathrm{d}t} = \int_0^H \nu_1 \varepsilon_{\mathrm{II}} r S \,\mathrm{d}\ell + N_1 S \,\mathrm{d}\ell \tag{3.83}$$

with:

$$r = kC_{1,\mathrm{IIb}} C_{2,\mathrm{IIb}} = f(t)$$
$$N_1 = \mathcal{A}\left[N_1'\right]_{x=0} = g(t,\ell)$$

This system of equations is quite complex. It can be simplified in the majority of practical cases by decoupling the time and space integrations. In doing so we assume that changes in the concentration $C_{1,\mathrm{I}}$ over time are slow. Equation (3.81) can then be written:

$$N_1 + \frac{\mathrm{d}F_{1,\mathrm{I}}}{S\,\mathrm{d}\ell} = 0 \tag{3.84}$$

The above equation can be integrated independently. For a slow reaction, we can write:

$$N_1 = k_{1,\mathrm{II}} \mathcal{A} (C^*_{1,\mathrm{II}} - C_{1,\mathrm{IIb}})$$

The value of $C^*_{1,\mathrm{II}}$ is calculated from (3.44):

$$C^*_{1,\mathrm{II}} = \frac{k_{1,\mathrm{II}} C_{1,\mathrm{IIb}} + k_{1,\mathrm{I}} (C_{1,\mathrm{Ib}} - p)}{k_{1,\mathrm{II}} + m k_{1,\mathrm{I}}}$$

Using the following equations (see Chapter 2):

$$F_{1,\mathrm{I}} = F_{1,\mathrm{I,e}} + \nu_1 \xi'$$
$$F_{\mathrm{T,I}} = F_{\mathrm{T,I,e}} + \nu_1 \xi'$$
$$C_{1,\mathrm{Ib}} = \frac{F_{1,\mathrm{I,e}} + \nu_1 \xi'}{F_{\mathrm{T,I,e}} + \nu_1 \xi'} \frac{P}{RT}$$

we find that:

$$-\nu_1 \frac{\mathrm{d}\xi'}{\mathrm{d}V} = A\left[B\left(\frac{F_{1,\mathrm{I,e}} + \nu_1 \xi'}{F_{\mathrm{T,I,e}} + \nu_1 \xi'}\right) - C\right] = \frac{A\left[\left(BF_{1,\mathrm{I,e}} - CF_{\mathrm{T,I,e}}\right) + \nu_1 \xi'(B - C)\right]}{F_{\mathrm{T,I,e}} + \nu_1 \xi'} \tag{3.85}$$

with:

$$A = K_{1,\mathrm{I}} \mathcal{A} \quad B = \frac{P}{RT} \quad C = C^{\mathrm{E}}_{1,\mathrm{Ib}} = p + m C_{1,\mathrm{IIb}}$$

After integration, we obtain:

$$AV = \frac{-\nu_1 \xi'_s}{B - C} + \frac{B(F_{1,\mathrm{I,e}} - F_{\mathrm{T,I,e}})}{(B - C)^2} \ln\left[\frac{(BF_{1,\mathrm{I,e}} - CF_{\mathrm{T,I,e}}) + \nu_1 \xi'_s (B - C)}{BF_{1,\mathrm{I,e}} - CF_{\mathrm{T,I,e}}}\right] \tag{3.86}$$

This equation can be used to calculate ξ'_s from the constants, $C_{1,\mathrm{IIb}}$, and the total volume V.

However:

$$-\nu_1 \xi_s' = \int_0^H N_1 S \, d\ell \quad \text{following (3.84)}$$

We can therefore calculate:

$$\frac{dn_{1,II}}{dt} = \nu_1 \left(-\xi_s' + r\varepsilon_{II} V\right) \tag{3.87}$$

$$\frac{dn_{2,II}}{dt} = \nu_2 \left(r\varepsilon_{II} V\right) \tag{3.88}$$

Equations (3.87) and (3.88) are integrated stepwise from the initial values of $C_{2,IIb}$ and $C_{1,IIb}$. If we consider that the volume flow rate of gas remains constant during its passage through the reactor, that is $F_{T,I} \cong F_{T,I,e}$, Eq. (3.85) can be simplified:

$$\frac{d\xi'}{dV} = \frac{-A}{\nu_1} \frac{\left[\left(BF_{1,I,e} - CF_{T,I,e}\right) + \nu_1 \xi' B\right]}{F_{T,I,e}} \tag{3.89}$$

which can be integrated to:

$$AV = \frac{F_{T,I,e}}{B} \ln \left[\frac{\left(BF_{1,I,e} - CF_{T,I,e}\right)}{\left(BF_{1,I,e} - CF_{T,I,e}\right) + \nu_1 \xi_s' B} \right]$$

but:

$$\frac{F_{T,I,e}}{B} = Q_I \quad \text{and} \quad -\nu_1 \xi_s' = Q_I \left(C_{1,Ib,e} - C_{1,Ib,s}\right)$$

and:

$$K_{1,I} \mathcal{A} V = Q_I \ln \frac{C_{1,Ib,e} - C}{C_{1,Ib,s} - C} \tag{3.90}$$

However, the total quantity of A_1 transferred throughout the entire reactor is:

$$\bar{N}_1 V = Q_I \left(C_{1,Ib,e} - C_{1,Ib,s}\right) \tag{3.91}$$

We can then write:

$$\bar{N}_1 = K_{1,I} A \frac{\left(C_{1,Ib,e} - C\right) - \left(C_{1,Ib,s} - C\right)}{\ln \left(\dfrac{C_{1,Ib,e} - C}{C_{1,Ib,s} - C} \right)}$$

$$-\nu_1 \xi_s' = \bar{N}_1 V = K_{1,I} \mathcal{A} V (\text{LMCD}) \tag{3.92}$$

where LMCD is a logarithmic mean concentration difference, with C being equal to $C^E_{1,Ib}$, that is, to the concentration that would exist in phase I if it were in equilibrium with phase II, where we find the concentration, $C_{1,IIb}$.

• **Fast reaction**

The entire reaction takes place in the film. We have $C_{1,\mathrm{IIb}} = 0$ and $\mathrm{d}n_{1,\mathrm{II}}/\mathrm{d}t = 0$. Equation (3.84) still applies:

$$\frac{\mathrm{d}F_{1,\mathrm{I}}}{\mathrm{d}V} = -N_1 \quad \text{or} \quad \frac{\mathrm{d}\xi'}{\mathrm{d}V} = -\frac{N_1}{\nu_1}$$

$$\frac{\mathrm{d}n_{2,\mathrm{II}}}{\mathrm{d}t} = -\frac{\nu_2}{\nu_1}N_1$$

N_1 can be expressed as:

$$N_1 = k_{1,\mathrm{II}}E\mathcal{A}C^*_{1,\mathrm{II}} \tag{3.93}$$

where:

$$C^*_{1,\mathrm{II}} = \frac{k_{1,\mathrm{I}}(C_{1,\mathrm{Ib}} - p)}{Ek_{1,\mathrm{II}} + mk_{1,\mathrm{I}}}$$

and:

$$C_{1,\mathrm{Ib}} = \frac{F_{1,\mathrm{I,e}} + \nu_1\xi'}{F_{\mathrm{T,I,e}} + \nu_1\xi'}\frac{P}{RT}$$

from which we derive:

$$-\nu_1\frac{\mathrm{d}\xi'}{\mathrm{d}V} = \frac{k_{1,\mathrm{I}}k_{1,\mathrm{II}}E\mathcal{A}}{Ek_{1,\mathrm{II}} + mk_{1,\mathrm{I}}}\left[\left(\frac{F_{1,\mathrm{I,e}} + \nu_1\xi'}{F_{\mathrm{T,I,e}} + \nu_1\xi'}\right)\frac{P}{RT} - p\right] \tag{3.94}$$

which is solved as before to determine a value for ξ'_s.

The only difficulty lies in the choice of E, which is determined iteratively, as indicated in Section 3.2.2. At the limit the reaction can be considered a surface reaction, entirely controlled by gas-phase diffusion. We then have:

$$N_1 = k_{1,\mathrm{I}}\mathcal{A}C_{1,\mathrm{Ib}} \tag{3.95}$$

The enthalpy balance is established taking into account gas phase flow, which can entrain a number of liquid-phase compounds in the vaporized phase. In this case we have:

$$\frac{\mathrm{d}\left(n_i\bar{h}_i\right)}{\mathrm{d}t} - \sum\left(F_{i,\mathrm{I}}\bar{h}_{i,\mathrm{I}}\right)_{\mathrm{e}} + \sum\left(F_{i,\mathrm{I}}\bar{h}_{i,\mathrm{I}}\right)_{\mathrm{s}} = Q_{\mathrm{E}} \tag{3.96}$$

The subscript i is applied to all the compounds present, whether or not they participate in the reaction, as well as inerts and the solvent. To evaluate the term $\sum\left(F_{i,\mathrm{I}}\bar{h}_{i,\mathrm{I}}\right)_{\mathrm{s}}$ we must calculate the liquid-vapor equilibrium for the gas phase exiting the reactor and the liquid phase present in the reactor. The calculation must be performed at all times to account for variations in $n_{i,\mathrm{II}}$ and possibly temperature.

3.4.3 Tubular reactor with two fluid phases

In tubular reactors with two fluid phases, we generally assume that both phases are characterized by plug flow behavior. Contact between the two phases can occur in two ways: countercurrent or cocurrent. In the following sections we consider only the case of a slow reaction, as an illustration.

3.4.3.1 Countercurrent operation

Countercurrent operation is the one most frequently found in practice, being typical of packed columns. As in the previous cases, we write the molar balances for compound A_1, which is transferred from phase I to phase II, and for compound A_2, a coreactant present in phase II. These balances will be established for a differential element in the column, located between z and $z + dz$ (Fig. 3.19). In the steady state we can write:

$$(F_{1,I})_z - N_1 S\,dz = (F_{1,I})_{z+dz}$$
$$(F_{1,II})_{z+dz} + N_1 S\,dz + \nu_1 r \varepsilon_{II} S\,dz = (F_{1,II})_z$$
$$(F_{2,II})_{z+dz} + \nu_2 r \varepsilon_{II} S\,dz = (F_{2,II})_z$$

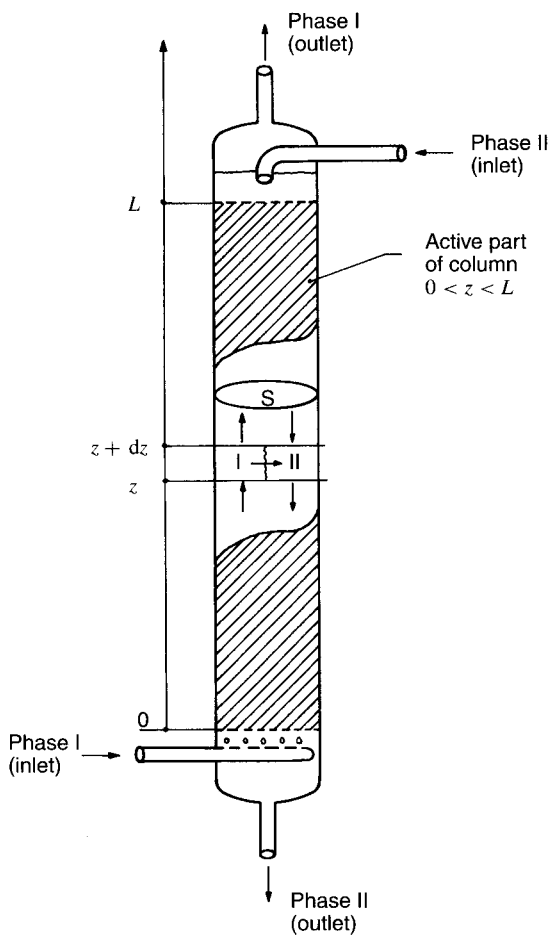


Figure 3.19 Tubular reactor with two fluid phases (countercurrent operation).

where: $r = kC_{1,\mathrm{IIb}}C_{2,\mathrm{IIb}}$, which is applicable to all of phase II (bulk + film). In their differential form these equations become:

$$\frac{\mathrm{d}F_{1,\mathrm{I}}}{\mathrm{d}z} + N_1 S = 0 \tag{3.97}$$

$$\frac{\mathrm{d}F_{1,\mathrm{II}}}{\mathrm{d}z} + N_1 S + \nu_1 r \varepsilon_{\mathrm{II}} S = 0 \tag{3.98}$$

$$\frac{\mathrm{d}F_{2,\mathrm{II}}}{\mathrm{d}z} + \nu_2 r \varepsilon_{\mathrm{II}} S = 0 \tag{3.99}$$

These equations are identical in form to (3.69), (3.70), and (3.71) and are therefore solved in the same way.

If we know all the necessary variables at level 0, that is:

$$(F_{1,\mathrm{I}})_0,\ (F_{1,\mathrm{II}})_0,\ (F_{2,\mathrm{II}})_0,\ (C_{1,\mathrm{Ib}})_0,\ (C_{1,\mathrm{IIb}})_0,\ (C_{2,\mathrm{IIb}})_0,$$
$$k,\ k_{1,\mathrm{I}},\ k_{1,\mathrm{II}},\ m,\ p,\ \varepsilon_{\mathrm{II}},\ \mathcal{A},\ \nu_1,\ \nu_2$$

we can integrate step by step throughout the length of the column and obtain:

$$(F_{1,\mathrm{I}})_L,\ (F_{1,\mathrm{II}})_L,\ (F_{2,\mathrm{II}})_L,\ (C_{1,\mathrm{Ib}})_L,\ (C_{1,\mathrm{IIb}})_L,\ (C_{2,\mathrm{IIb}})_L$$

In other cases we may only have access to the values at the inlets:

$$(F_{1,\mathrm{I}})_0,\ (F_{1,\mathrm{II}})_L,\ (F_{2,\mathrm{II}})_L,\ (C_{1,\mathrm{Ib}})_0,\ (C_{1,\mathrm{IIb}})_L,\ (C_{2,\mathrm{IIb}})_L$$

and we will have to determine the values at the outlets:

$$(F_{1,\mathrm{I}})_L,\ (F_{1,\mathrm{II}})_0,\ (F_{2,\mathrm{II}})_0,\ (C_{1,\mathrm{Ib}})_L,\ (C_{1,\mathrm{IIb}})_0,\ (C_{2,\mathrm{IIb}})_0$$

In this case we make assumptions about the outlet values and perform the calculation using these hypothetical values. We then compare the calculated values to the initial values. After a series of iterative calculations, the values will converge.

Using the enthalpy balance per slice of column, we can calculate the change in temperature throughout the length of the column. The balance is written:

$$\sum \left[\frac{\mathrm{d}\left(F_{i,\mathrm{I}}\bar{h}_{i,\mathrm{I}} - F_{i,\mathrm{II}}\bar{h}_{i,\mathrm{II}}\right)}{\mathrm{d}z} \right] = q_{\mathrm{e}} \tag{3.100}$$

q_{e} being the enthalpy supplied to the system per unit length of column.

If one of the phases is a gas phase, we may need to know the pressure profile in the column. This is easy enough to calculate once we have access to the correlations for pressure drop in the unit concerned.

3.4.3.2 Cocurrent operation

This type of operation is illustrated in Fig. 3.20. For convenience dimensions on the reactor are measured from the inlet for phase II, that is, from the top of the reactor. The balance equations are written:

$$\frac{dF_{1,I}}{dz} + N_1 S = 0 \tag{3.101}$$

$$\frac{dF_{1,II}}{dz} - N_1 S - \nu_1 r \varepsilon_{II} S = 0 \tag{3.102}$$

$$\frac{dF_{2,II}}{dz} - \nu_2 r \varepsilon_{II} S = 0 \tag{3.103}$$

The only difference between Eqs. (3.102), (3.103) and (3.98), (3.99) is the sign of $dF_{1,I}/dz$ and $dF_{2,II}/dz$.

In practice cocurrent devices are used far less frequently than countercurrent devices. Nonetheless, we can consider them in the same way as countercurrent reactors whenever the chemical reaction is not limited by chemical equilibrium.

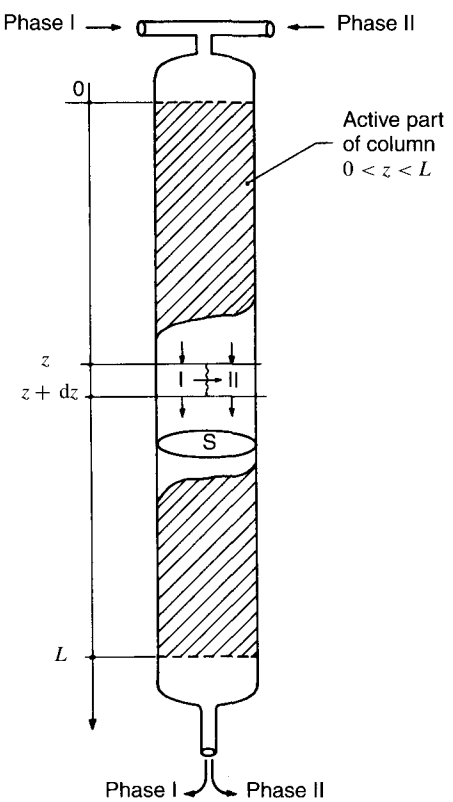


Figure 3.20 Tubular reactor with two fluid phases (cocurrent operation).

3.4.4 Continuous stirred tank reactor with two fluid phases

This type of device is shown in Fig. 3.21; there are two separate versions, depending on whether the phases are gas + liquid or liquid + liquid. The difference is based on the separation of the phases. This generally takes place in the reactor itself for a gas-liquid system, while liquid-liquid systems require the addition of a separator (by settling, for example).

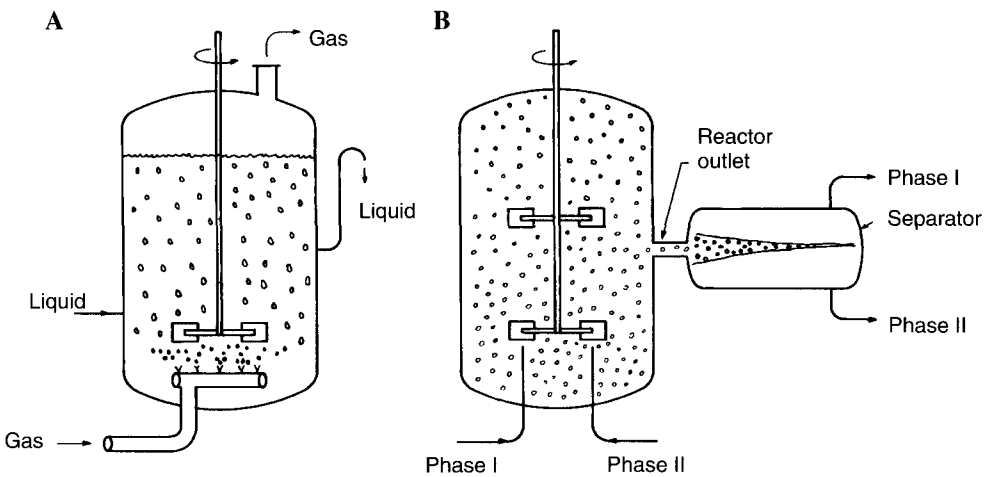


Figure 3.21 Continuous stirred tank reactor with two fluid phases.
A. Gas-liquid. **B.** Liquid-liquid.

We will ignore the separation issue and write the balance equations for the reactor alone. Looking again at a reaction of the type $\nu_1 A_1 + \nu_2 A_2 \rightarrow \nu_3 A_3$, governed by second-order kinetics, we see that compound A_1 is transferred from phase I to phase II, compound A_2 being in phase II, which is the reaction phase.

- If the reaction is slow enough, we can assume that the rate expression $r = kC_{1,\mathrm{IIb}}C_{2,\mathrm{IIb}}$ applies to all of phase II contained in the reactor:

$$(F_{1,\mathrm{I}})_e - N_1 V = (F_{1,\mathrm{I}})_s \tag{3.104}$$

$$(F_{1,\mathrm{II}})_e + N_1 V + \nu_1 r \varepsilon_{\mathrm{II}} V = (F_{1,\mathrm{II}})_s \tag{3.105}$$

$$(F_{2,\mathrm{II}})_e + \nu_2 r \varepsilon_{\mathrm{II}} V = (F_{2,\mathrm{II}})_s \tag{3.106}$$

where:

$$N_1 = \mathcal{A}\,[N_1']_{x=0} = k_{1,\mathrm{II}}(C^*_{1,\mathrm{II}} - C_{1,\mathrm{IIb}})\mathcal{A}$$

- If the reaction is fast enough, we can assume that phase II contains no reactant A_1:

$$(F_{1,\mathrm{I}})_e - N_1 V = (F_{1,\mathrm{I}})_s \tag{3.107}$$

$$[(F_{2,\mathrm{II}})_e - (F_{2,\mathrm{II}})_s] = \frac{\nu_2}{\nu_1}[(F_{1,\mathrm{I}})_e - (F_{1,\mathrm{I}})_s] \tag{3.108}$$

where:

$$N_1 = \mathcal{A}\left[N_1'\right]_{x=0} = k_{1,\mathrm{II}} E(C_{1,\mathrm{II}}^*)\mathcal{A}$$

Based on these equations, we can design the reactor using iterative procedures similar to those introduced earlier. In all cases, the enthalpy balance is written:

$$\sum \left[F_{i,\mathrm{I}}\bar{h}_{i,\mathrm{I}} + F_{i,\mathrm{II}}\bar{h}_{i,\mathrm{II}}\right]_e - \sum \left[F_{i,\mathrm{I}}\bar{h}_{i,\mathrm{I}} + F_{i,\mathrm{II}}\bar{h}_{i,\mathrm{II}}\right]_s + Q_{\mathrm{E}} = 0 \qquad (3.109)$$

Where Q_{E} is the enthalpy supplied to the reactor per unit of time.

Very often in practice this type of reactor is used as part of a series of identical stirred reactors. Consequently, there are three possible ways of arranging the vessels (Fig. 3.22):

- cocurrent arrangement
- countercurrent arrangement
- cross-current arrangement.

The cocurrent arrangement offers the advantage of not requiring intermediate separators. However, except in special situations (for example, when large volumes of reaction phase are needed), this arrangement has no specific advantage over the tubular cocurrent reactor.

The countercurrent arrangement is most frequently encountered in column reactors. The stages often consist of plates or stirred compartments. For a liquid-liquid system, we must ensure that the phases are in contact and settling takes place (see Chapter 5). For this reason countercurrent columns are sometimes unusable and mixer-settlers designed for countercurrent operation are then recommended. Crosscurrent operation is sometimes used, but almost exclusively with gas-liquid systems.

3.4.5 Conclusion

The above discussion was chiefly intended to illustrate how to approach the design of different types of reactor. For simplicity we made a number of assumptions, which in practice are not always verified. Also, before applying these equations to practical situations, it is essential to make sure that the actual unit is identical to the one on which the initial calculations are based.

In particular, the following need to be examined:

- For a continuous tubular reactor, the assumption of "plug" flow is sometimes no more than a first approximation with respect to the continuous phase. If the data are available, it would be useful to consider the effect of backmixing by introducing a term for axial diffusivity into the mass balance equations.
- For a continuous stirred tank reactor, the gas phase cannot always be assumed to be perfectly mixed. In this case we make use of the treatment presented for the semi-continuous reactor.

We see that designing a two-phase industrial reactor can be relatively complex if we want to take into account the effect of all the variables. However, the equations shown on the previous pages can often lead to a first approximation, which can serve as a guide in finding a more rigorous solution of the problem.

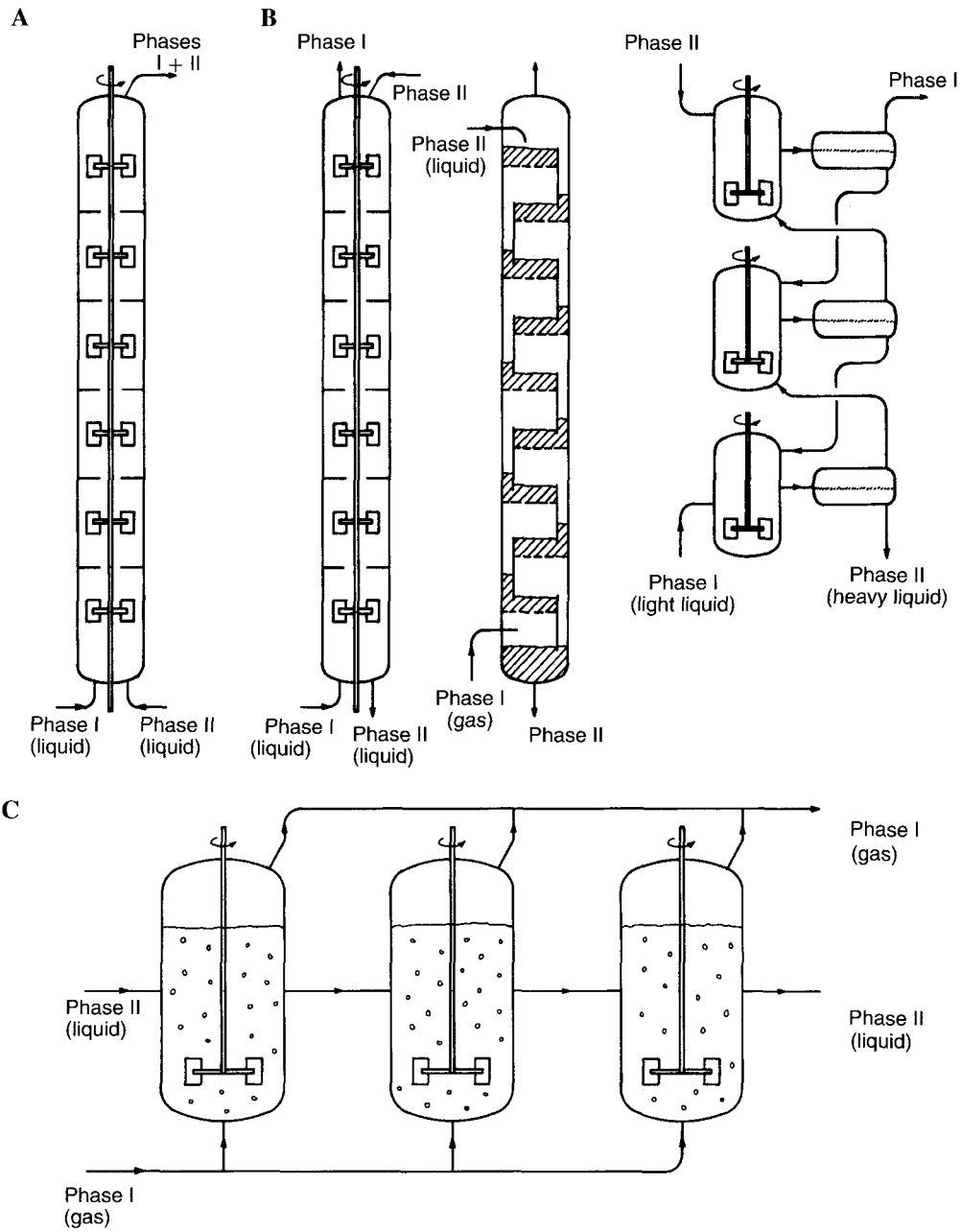


Figure 3.22 Cascade of continuous stirred tank reactors with two fluid phases: **A.** Cocurrent arrangement. **B.** Countercurrent arrangement (column with agitated compartments, plate column, cascade of mixer-settlers). **C.** Cross-flow arrangement (gas + liquid).

It is worth noting that we are often limited, when applying these equations, by the lack of data. These include:

- reaction characteristics (kinetics)
- physical constants (solubilities, diffusivities)
- device characteristics (transfer coefficients, interfacial area, holdup).

With respect to the latter point, the literature does contain data for the various types of equipment found in practice, such as those examined in the following two chapters.

REFERENCES

Astarita G (1967) Mass Transfer with Chemical Reaction. Elsevier.

Danckwerts PV (1970) Gas-Liquid Reactions. McGraw-Hill, New York.

Darde T, Midoux N, Charpentier JC (1983) Chem Eng Comm, 22, pp 221–241 and 26 (1984), pp 33–54.

Hikita H, Asai S, Ishikawa H (1977) Ind Eng Chem Fund, 16, 2, p 215.

Kishinevskii MK (1971) Theor Fund Chem Eng, 4, p 641.

Sharma MM, Shah YT (1976) Trans Inst Chem Eng, 54, p 1.

Sherwood TK, Pigford RL, Wilke CR (1975) Mass Transfer. McGraw-Hill, New York.

Teramoto M, Nagayasu T, Matsui T, Hashimoto K, Nagata S (1973) Chem Eng Japan, 6, no.6, pp 522–527.

Van de Vusse JG (1966) Chem Eng Sci, 21, pp 631–645 and p 1239.

Vas Bhat RD, Van Zwaaij WPM, Kuipers JAM, Versteeg GF (1999) Chem Eng Sci, 54, pp 121–147.

NOMENCLATURE

(specific to Chapter 3)

Symbol	Definition	SI Unit
$\mathcal{C}$	Total concentration (free + combined) for reversible reactions	mol/m^3
E_{lim}	Limit of the enhancement factor E for a very high Ha	–
$\mathcal{F}$	Fraction of reactant that disappears in the film	–
K_I	Overall coefficient of transfer with respect to the initial phase I	m/s
m	Slope of the equilibrium line	–
p	Ordinate at the origin of the equilibrium line	mol/m^3
m_0	Slope of the equilibrium line when it passes through the origin (partition coefficient)	–
m	Partial reaction order relative to the transferred compound	–
N	Transfer flux per unit volume	$mol/m^3 \cdot s$
n	Partial reaction order relative to the coreactant	
N_i'	Transfer flux with chemical reaction	$mol/m^2 \cdot s$
$\mathcal{N}_2$	Dimensionless number $= \nu_1 \mathcal{D}_{2,II} C_{2,IIb} / \nu_2 \mathcal{D}_{1,II} C_{1,II}^*$	–
$\mathcal{N}_3$	Dimensionless number $= C_{1,IIb} / C_{1,II}^*$	–
LMCD	Logarithmic mean concentration difference	mol/m^3
q_e	Heat supplied to the system per unit of length and unit of time	W/m
Q_E	Heat supplied to the system per unit of time	W
x	Distance in the film measured from the interface	m
z	Distance of the reaction location to the interface for instantaneous reactions	m
β	Dimensionless number $= k_{1,II} \varepsilon_{II} / \mathcal{A} \mathcal{D}_{1,II}$	–
δ	Thickness of film	m
	Subscripts:	
v	true	
app	apparent	
	Exponents:	
E	$C_{i,I}^E$: concentration in phase I when this phase is in equilibrium with phase II, where the concentration is $C_{i,II}$	
*	at the interface	

Copyrighted Materials
Copyright © 2004 Editions Technip Retrieved from www.knovel.com

4 Experimental Data and Correlations for Gas-Liquid Reactors

4.1 INTRODUCTION AND PRELIMINARY DEFINITIONS

For years equipment in which a gas and liquid phase are reacted with one another has been used in a wide variety of fields: chemistry, biochemistry, refining, petrochemistry, metallurgy, food processing, pharmacy, and so on [Danckwerts, 1970]. Highly varied in shape and size, this equipment also differs in the arrangement of the internal components used to promote contact between the phases: physical supports for the gas-liquid interface of varying complexity, stationary or moving elements, etc. (Fig. 4.1).

Through the application of fluid mechanics, some hydrodynamic behaviors of gas-liquid reactors have begun to be understood [Kumar *et al.*, 1995; Trambouze, 1996; Lübbert and Lapin, 1996; Lance *et al.*, 1996; Cockx *et al.*, 1997, among others], but interface phenomena are still imperfectly interpreted and poorly represented. Global methods remain essential in the design of these reactors.

The current chapter includes information on hydrodynamics and fluid distribution as well as data and correlations that can be used to estimate the parameters needed to design chemical reactors. Among the large variety of contactors that have been studied, we specifically examine those that are most commonly used, classifying them according to the predominant method of introducing energy:

- potential energy in bubble columns, with and without baffles, plate columns, and packed columns
- mechanical energy in mechanically stirred tanks
- kinetic energy in ejectors and inline mixers.

These devices are designed to promote mass transfer and chemical reaction between two fluid phases. Their efficiency is, therefore, associated with certain typical hydrodynamic values such as interfacial area and phase holdup. To avoid any ambiguity we define these terms below.

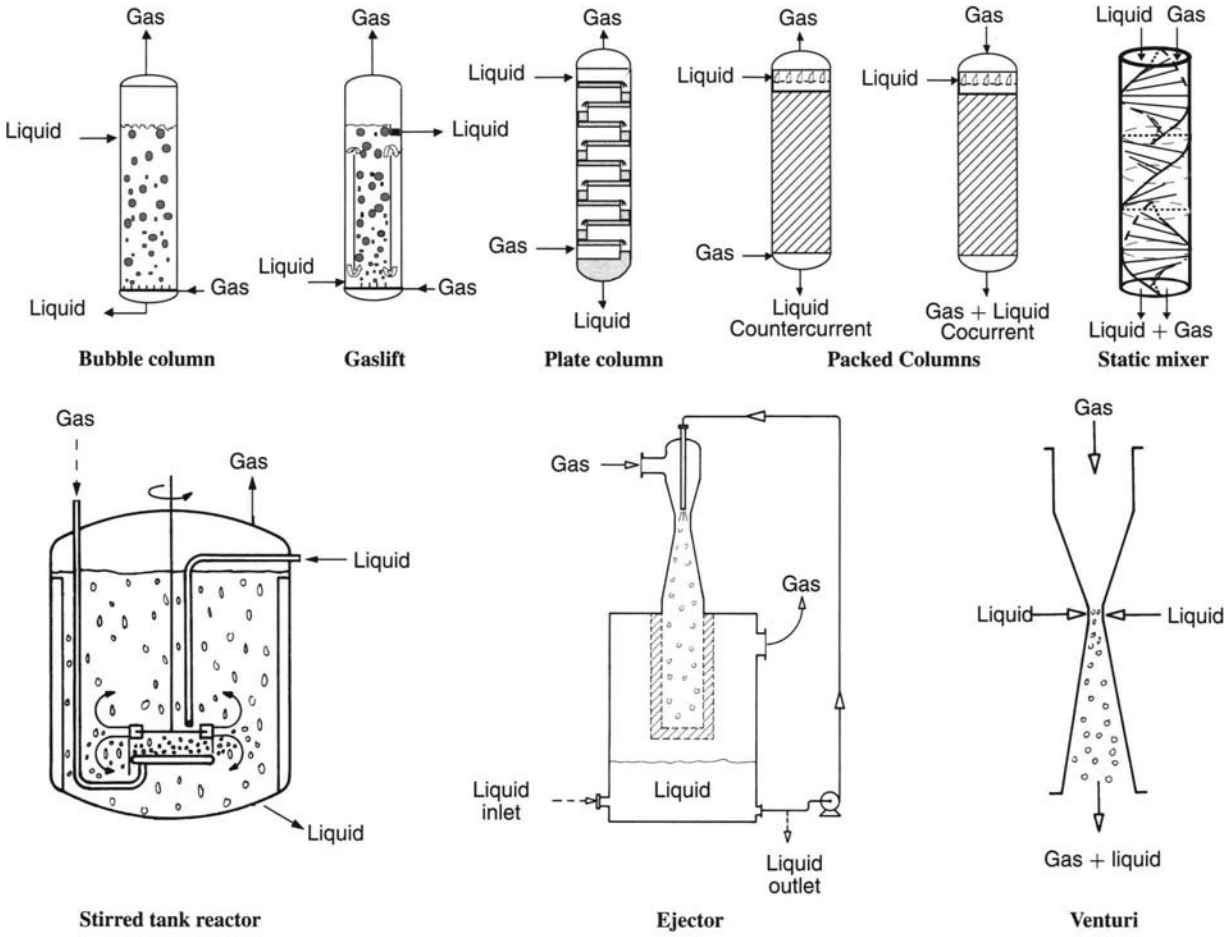


Figure 4.1 Examples of gas-liquid contactors discussed in this chapter.

4.1.1 Specific interfacial area

The specific interfacial area $\mathcal{A}$ is the gas/liquid interfacial area (surface of droplets or bubbles) developed in the active unit volume of the reactor. The volume considered is the expanded volume of the liquid phase for bubble columns and stirred tanks, the volume occupied by the gas-liquid suspension in scrubbers, or the volume of the packed bed in packed columns. The upper part of a bubble column or packed column is practically all gas. Assumed to be inactive, it is not taken into account when considering the active volume of the corresponding reactor. Occasionally certain interfacial areas are expressed with respect to the unexpanded liquid phase ($\mathcal{A}_L$) or the active area of a plate in a plate column ($\mathcal{A}'$). In this latter case, $\mathcal{A}'$ is dimensionless.

4.1.2 Holdup

Holdup in gas (ε_G) or liquid (ε_L) is the ratio of the volume occupied by the gas or liquid to the total active volume of the reactor. If the reactor contains only two fluid phases, we have the equation $\varepsilon_G + \varepsilon_L = 1$. In a packed column where a solid is present $\varepsilon_G + \varepsilon_L + \varepsilon_P = 1$. As with interfacial area, in a plate column the gas volume comprised between the zones of expanded liquid is considered to be inactive, or dead, when calculating holdup or interfacial area. To summarize, we have:

$\mathcal{A}$ interfacial area with respect to the active volume of the reactor (m^2/m^3)

$\mathcal{A}_L$ interfacial area with respect to the volume of liquid, where

$$\mathcal{A}_L = \frac{\mathcal{A}}{\varepsilon_L} \quad (m^2/m^3)$$

ε_G gas phase holdup (-)

ε_L liquid phase holdup (-), with $\varepsilon_L = 1 - \varepsilon_G$ except for packed columns, where $\varepsilon_L = 1 - \varepsilon_G - \varepsilon_P$

ε_P fraction of volume occupied by packing (-).

4.1.3 Current values of design parameters

The current ranges for the essential mass-transfer parameters are indicated in Table 4.1 for the principal industrial gas-liquid reactors. Contactors are classified by decreasing liquid holdup, that is, proceeding from the bubble column to the scrubber, they are designed to accommodate increasingly fast reactions, which occur increasingly closer to the gas-liquid interface. The table also shows that the values for k_G and k_L are, overall, very similar among the devices examined.

In general, by using a classification based on decreasing liquid holdup, we imply that the chemical reaction takes place in the liquid phase alone. This corresponds to the majority of cases found in practice. However, there are cases in which the reaction takes place both in the liquid phase and in the gas phase (for example, the absorption of nitrous vapors during the manufacture of nitric acid). The device must then be designed with this in mind.

Table 4.1 Orders of magnitude for mass-transfer parameters in various industrial reactors.

	Liquid holdup [1] ε_L (%)	**Gas holdup** [1] ε_G (%)	**Gas side film transfer** k_G (m/s)	**Liquid side film transfer** k_L (m/s)	**Interfacial area** [1] $\mathcal{A}$ (m^{-1})	[1] $k_L\mathcal{A}$ (s^{-1})	**Specific energy input** [1] $\mathcal{P}/V$ (kW/m^3)	**Volume** [2] V (m^3)
Bubble columns	> 60	< 40	$(1–5)\cdot10^{-2}$	$(1–5)\cdot10^{-4}$	50–500	0.01–0.2	0.01–1	0.01–3 000
Mechanically stirred tanks	> 70	< 30	$(1–5)\cdot10^{-2}$	$(1–5)\cdot10^{-4}$	100–4 000	0.005–0.8	0.5–10	0.002–300
Plate columns	4–25	75–95	$(1–5)\cdot10^{-2}$	$(1–5)\cdot10^{-4}$	200–500	0.01–0.1	0.01–0.2	0.01–1 000
	5–30 [2]	70–95 [2]			40–100 [2]	0.002–0.02	0.002–0.04	
Countercurrent packed columns	2–20	> 80	$(1–5)\cdot10^{-2}$	$(0.5–2)\cdot10^{-4}$	50–300	0.002–0.1	0.01–0.2	0.01–1 000
Cocurrent packed columns	2–95	5–98	$(0.3–5)\cdot10^{-2}$	$(0.4–6)\cdot10^{-4}$	10–2 000	0.01–1	0.05–10	0.01–400
Falling film	1–15	> 85	$(0.3–5)\cdot10^{-2}$	$(0.4–6)\cdot10^{-4}$	300–600 [1] 3 – 100 [2]	0.01–1	0.05–10 [3]	0.1–200
Venturi ejector	2–10	> 90	$(1–5)\cdot10^{-2}$	$(1–10)\cdot10^{-4}$	50–5 000	0.1–0.8	< 100	0.01–100
Spray column	2–20	> 80	$(0.5–2)\cdot10^{-2}$	$(1–15)\cdot10^{-4}$	10–500	0.001–0.02		0.01–400
Static mixer	> 50	< 50	$(1–5)\cdot10^{-2}$	$(5–20)\cdot10^{-4}$	200–1 000	0.1–2	< 100	< 10
Horizontal pipes	0–100	0–100	$(0.5–4)\cdot10^{-2}$	$(1–10)\cdot10^{-4}$	50–700	0.005–0.7		

(1) Relative to the sum of active volumes for the two phases (phase I + phase II).
(2) Relative to the total volume of the column (phase I + phase II + volume occupied by internal components + inactive volumes).
(3) Relative to the area in m^2 of the film surface.

4.2 BUBBLE COLUMNS

4.2.1 General characteristics

A conventional bubble column is a vertical cylindrical vessel filled with liquid; a distributor at the base is used to inject gas in the form of bubbles into the column (Fig. 4.2A). In general the height-to-diameter ratio is greater than 1 (3 to 10), even though large fermenters of this type are often quite squat. The top of the column is sometimes enlarged to facilitate disengagement of the gas. Gas is introduced through perforated pipes, perforated plates, and more rarely through sintered metal elements. Biological treatment tanks for wastewater are frequently equipped with porous tubes. The superficial velocities[1] of the gases vary, but normally range from 1 to 30 cm/s. Operation above these velocities is possible, but problems with mechanical entrainment of the liquid (priming) can occur, especially with fluids that have a tendency to foam. The liquid is introduced continuously or in batches, and flows generally cocurrent with respect to the gas. Heating or cooling is performed through the wall or by means of internal exchangers, otherwise through an external circuit. The temperature is quite uniform because of the considerable mass of liquid and the homogenization brought about by the gas. The frequent absence of internal components and the simplicity of construction are important advantages in these devices, which can assume considerable size: 100 to 200 m^3 for chemical applications, all the way up to 3 000 m^3 for fermentation and 20 000 m^3 for the treatment of certain effluents.

Occasionally the units are modified to improve the behavior of fluids, sometimes through the addition of vertical compartments or horizontal partitions. Different arrangements, shown in Figs. 4.2, are discussed below (see Section 4.2.6 and 4.3).

We previously indicated that reactor design becomes increasingly difficult when the interfacial area appears spontaneously, without a physical support such as packing in packed columns, for example. When the interface is associated only with the surface of the bubbles or drops, without expanding and stabilizing itself on a solid support, it becomes particularly sensitive to interfacial properties that govern bubble formation and coalescence. Coalescence theories are still incapable of predicting with a sufficient degree of precision the behavior of a large number of systems in which, for example, polar molecules (as in certain petroleum cuts) or surface active substances are present (during fermentation), or systems in which significant mass transfer modifies local interfacial tension (Marangoni effect). In some cases the effects of temperature and pressure on coalescence also need to be considered.

There is good reason, therefore, to be cautious when using the following correlations (Table 4.2). The value of the estimates should be verified by means of tests conducted in the laboratory or in pilot units. Measurements should be made under actual operating conditions using fluids that are as similar as possible to industrial fluids. When all else fails, comparison with known systems remains a possible solution for approaching scale-up.

It is also preferable to avoid large scaling factors. In the tests used for the scale-up, a diameter above 0.15 m is recommended [Wilkinson, 1991] to limit wall effects on gas holdup,

1. By superficial velocity we refer to the ratio of the volumetric flow rate at local conditions of temperature and pressure to the cross-section of the vessel that is assumed to be empty.

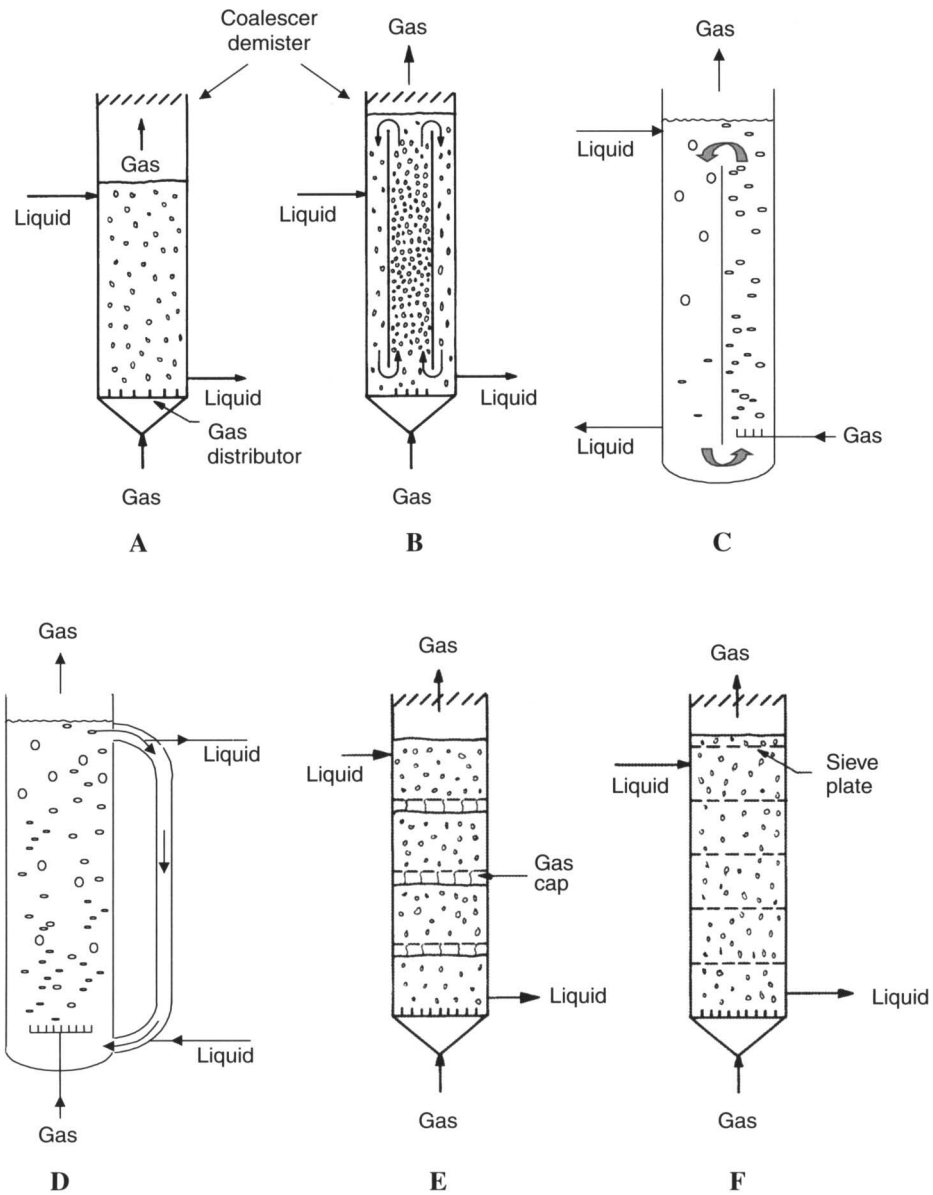


Figure 4.2 Bubble column designs.

at low and high pressure alike, whether or not viscous liquids are present. A sufficiently tall (greater than 2 to 3 m) and slender (H/D greater than 4 to 5) column helps limit end effects (distributor, upper portion of the fluid medium) and liquid recirculation. Finally, sufficient safety margins must be included to compensate for any accidental modification or any gradual evolution of the properties of the medium.

4.2.2 Hydrodynamics

4.2.2.1 Hydrodynamic regimes

Depending on operating conditions (superficial velocity of the gas and efficiency of the distributor), the physical properties of the medium, and the column diameter, the gas will traverse the column in the form of bubbles (bubble flow) or slugs (slug flow). Bubble flow is itself subdivided into two, sometimes three, clearly distinct hydrodynamic regimes: homogeneous (homogeneous flow, or dispersed bubble flow) and heterogeneous (heterogeneous, or churn turbulent flow). These two regimes are separated by a transition regime (Fig. 4.3).

Homogeneous flow occurs whenever the gas makes its way through the column in the form of fine bubbles, with a minimum of coalescence. The bubbles, similar to spheres from one to several millimeters in diameter, rise nearly uniformly at a fairly consistent velocity on the order of 0.2 m/s. The bubbles rise one behind the other, in vertical chains, throughout the entire bulk of expanded liquid, without forming clusters or packets.

In the case of heterogeneous flow, larger, irregularly shaped bubbles form a short distance from the distributor mouth. They rise turbulently and chaotically, frequently coalescing and fragmenting, giving rise to two bubble populations of very distinct diameters: approximately 5 mm for small bubbles and 50 mm for large bubbles [Krishna *et al.*, 1991]. Their velocity can easily exceed 0.5 m/s, when superficial gas velocities exceed 0.06 m/s. The bubbles create increased global turbulence in the medium and impart an effective homogenization to the liquid phase.

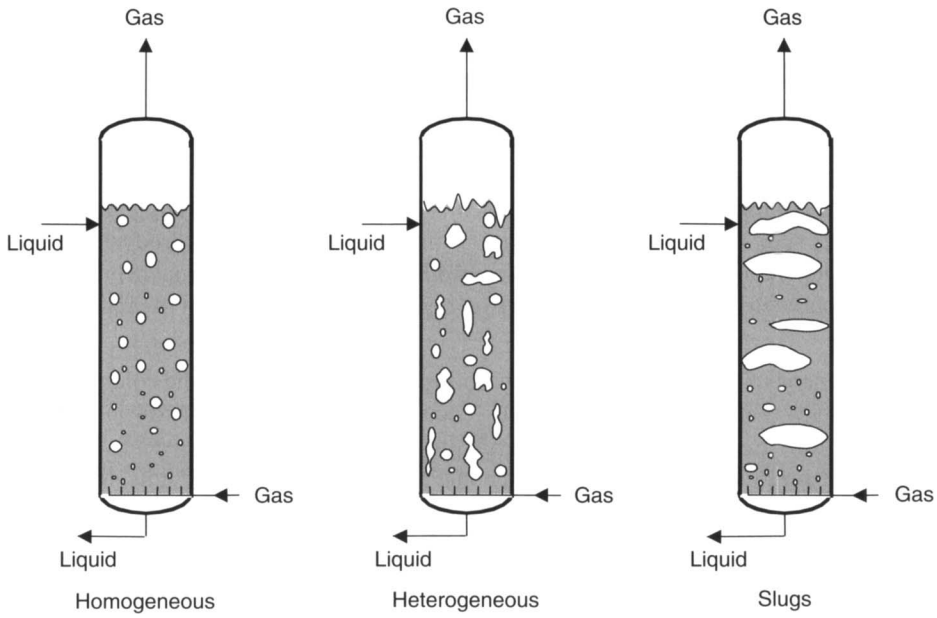
Slug flow corresponds to the uniform rise of relatively tall gas slugs whose diameter is close to that of the column. The liquid rises, partially entrained in the wake of the gas pockets, then flows down along the walls.

These regimes depend essentially on the nature of the medium, the flow rate, the density (and therefore the pressure) of the gas, and the diameter of the column. The homogeneous regime is observed with low superficial gas velocities ($V_{SG} < 0.02$ to 0.04 m/s) and when using sintered or porous distributors. The heterogeneous regime is found in the majority of low-viscosity liquids when the superficial gas velocity V_{SG} is greater than 0.03 to 0.05 m/s (for a perforated pipe or sintered distributor, respectively). In viscous solutions the regime becomes rapidly heterogeneous. This is also true when suspensions are present, for the solid particles promote coalescence and sharply reduce the extent of the homogeneous regime [Koïde, 1996].

The slug regime is only observed in narrow columns (diameters less than 0.10–0.20 m) with gas velocities ranging from 0.07 to 0.15 m/s in low-viscosity solutions and around 0.03 m/s in viscous solutions. Column height promotes this behavior.

4.2.2.2 Axial dispersion of the liquid

Although the liquid is often initially considered to be perfectly mixed and homogeneous, more detailed examination leads to a representation of the behavior of the liquid phase by



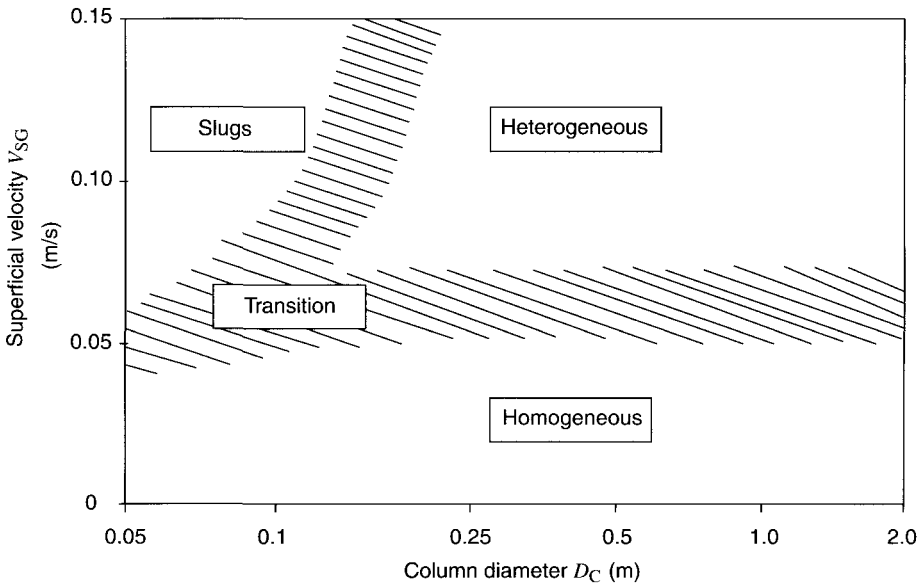


Figure 4.3 Hydrodynamic regimes for bubble columns (low-viscosity medium).

means of an axial dispersion flow model. The coefficient of axial dispersion then depends essentially on the superficial velocity of the gas and the diameter of the column [Deckwer and Schumpe, 1993], which can be represented by a relation between two dimensionless numbers:

$$\text{Peclet number}\left(Pe_{\mathrm{L}} = \frac{V_{\mathrm{SL}} D_{\mathrm{C}}}{\mathcal{D}_{\mathrm{A,L}}}\right) \tag{4.1}$$

$$\text{Froude number}\left(Fr_{\mathrm{G}} = \frac{V_{\mathrm{SG}}}{(gD_{\mathrm{C}})^{0.5}}\right) \tag{4.2}$$

$$Pe_{\mathrm{L}} = 2.85 Fr_{\mathrm{G}}^{0.67} \tag{4.3}$$

Under pressure, the coefficient of axial dispersion of the liquid increases slightly, as does liquid holdup [Wilkinson *et al.*, 1993].

4.2.2.3 Radial dispersion of the liquid

The composition and temperature radial uniformities of the medium are quite good. At most we find a conversion for the gas reactants that is slightly greater near the wall as a result of the longer residence time of small gas bubbles caused by the descending liquid or even by solid particles along the walls.

4.2.2.4 Axial dispersion of the gas

Gas is often considered to follow a plug flow model in the narrowest columns but, in large-diameter reactors, the large variety of bubble sizes and the turbulence they cause, often justify the inclusion of a significant backmixing effect using an axial dispersion model. Wachi and Nojima [1990] have proposed the following equation, which fairly well represents a number of experimental results in an air-water medium:

$$\mathcal{D}_{\mathrm{A,G}} = 20 D_{\mathrm{C}}^{1.5} V_{\mathrm{SG}} \tag{4.4}$$

Wilkinson *et al.* [1993] introduced the effect of pressure by looking at holdup values.

4.2.3 Mass transfer

Table 4.2 summarizes the most reliable correlations and experimental values; Table 4.3 indicates the valid ranges for several of the correlations in Table 4.2. We should point out, however, that these are applicable only when gas flow turbulence is neither too large nor too small. They are based on some rather wide-ranging summaries, primarily those by Deckwer *et al.* [1992, 1993], the result of extensive experience in the field, Koïde [1996], especially concerning the work of Japanese researchers, and several articles by Wilkinson *et al.* [beginning in 1990], which take pressure effects into account.

Table 4.2 Correlations for bubble columns *(pages 210 to 215)*.

			Author	Equation no.
Coefficient of liquid axial dispersion $\mathcal{D}_{A,L}$ (m^2/s)	$Pe_L = 2.85 Fr_G^{0.67}$		Deckwer and Schumpe [1993]	(4.3)
Coefficient of gas axial dispersion $\mathcal{D}_{A,G}$ (m^2/s)	$(\mathcal{D}_{A,G})_P = (\mathcal{D}_{A,G})_{P_0}\left[\frac{(\varepsilon_L)_{P_0}}{(\varepsilon_L)_P}\right]$ where $(\mathcal{D}_{A,G})_{P_0} = 20 D_C^{1.5} V_{SG}$		Wilkinson *et al.* [1993]	(4.4)
Mean bubble diameter, $\overline{d_B}$ (m)	Sieve plates: $\overline{d_B} = 9.5\left(\frac{d_0\sigma}{g\rho_L}\right)^{0.33} Mo^{0.053}$ where the Morton number, $Mo = \frac{g^{3n-2}m^4}{\rho_L^{2-n}\sigma^{n+2}}$ m and n the coefficient and exponent of the power law of the non-Newtonian fluid		Miyahara and Hayashino [1995]	(4.5)
	$\frac{\overline{d_B}}{D_C} = 26\left(\frac{gD_C^2\rho_L}{\sigma}\right)^{-0.50}\left(\frac{gD_C^3\rho_L^2}{\mu_L^2}\right)^{-0.12}\left(\frac{V_{SG}}{\sqrt{gD_C}}\right)^{-0.12}$ If $D_C > 0.6$ m, use $D_C = 0.6$ m	Homogeneous flow	Akita and Yoshida [1974]	(4.6)
	$\frac{g\rho_L\overline{d_B}^2}{\sigma} = 8.8\left(\frac{V_{SG}\mu_L}{\sigma}\right)^{-0.04}\left(\frac{\rho_L\sigma^3}{g\mu_L^4}\right)^{-0.12}\left(\frac{\rho_L}{\rho_G}\right)^{0.22}$	Under pressure	Wilkinson *et al.* [1994]	(4.7)

Note: Equations not shown in the table appear in the text.

Table 4.2 *(continued).*

			Author	Equation no.
Bubble velocity (m/s)	$u_B = 2.25\frac{\sigma}{\mu_L}\left(\frac{\sigma^3\rho_L}{g\mu_L^4}\right)^{-0.273}\left(\frac{\rho_L}{\rho_G}\right)^{0.03}$	Homogeneous regime	Wilkinson *et al.* [1992]	(4.8)
	$u_B = 2.5V_{SG}^{0.69}$		Hyndmann and Guy [1995]	(4.9)
	$u_B = \left(\frac{\sigma(\rho_L - \rho_G)g}{\rho_L^2}\right)^{0.25}\left(0.014 + 0.116V_{SG} + 0.5V_{SG}^2 + 0.8V_{SG}^3\right)$		Trambouze *et al.* [1988]	(4.10)
	$u_B = u_{SB} + 2.4\frac{\sigma}{\mu_L}\left[\frac{\mu_L\,(V_{SG} - V_{SGtrans})}{\sigma}\right]^{0.757}\left(\frac{\sigma^3\rho_L}{g\mu_L^4}\right)^{-0.077}\left(\frac{\rho_L}{\rho_G}\right)^{0.077}$	Heterogeneous regime	Wilkinson *et al.* [1992]	(4.11)
Gas holdup (ε_G)	$\varepsilon_G = kV_{SG}^n$ where n is between 0.7 and 1.2 and k is between 0.05 and 1, depending on the liquids	Homogeneous regime	Reilly *et al.* [1994]	(4.12)
	$\varepsilon_G = kV_{SG}^n$ where n is between 0.4 and 0.7 and k is between 0.05 and 1, depending on the liquids	Heterogeneous regime		
	$\varepsilon_G = 4V_{SG}$ where V_{SG} is in m/s	Homogeneous regime	Krishna *et al.* [1991]	(4.13)
	$\frac{\varepsilon_G}{(1-\varepsilon_G)^4} = K\left(\frac{V_{SG}\mu_L}{\sigma}\right)\left(\frac{\rho_L\sigma^3}{g\mu_L^4}\right)^{0.29}$ $K = 0.20$ for pure liquids, $K = 0.25$ for electrolytes.	Homogeneous regime	Akita and Yoshida [1973]	(4.14)
	$\varepsilon_G = 0.73B^{0.25} - 0.485B^{0.5} + 0.0975B^{0.75}$, where $B = \left[\frac{V_{SG}^4\rho_L^2}{\sigma\,(\rho_L - \rho_G)\,g}\right]$	Homogeneous regime	Kumar *et al.* [1976]	(4.15)

Table 4.2 *(continued).*

			Author	Equation no.
	Homogeneous regime: $\varepsilon_G(1-\varepsilon_G) = 2.8\rho_G^{0.04}\sigma^{0.12}V_{SG}$ Transition: $(V_{SG})_{trans} = V_s\dfrac{\varepsilon_{trans}}{(1-\varepsilon_{trans})}$ Where $V_s = 0.35\rho_G^{-0.04}\sigma^{0.12}$ $\varepsilon_{trans} = 0.6B^{1.5}\sqrt{\dfrac{\rho_G^{0.96}\sigma^{0.1}}{\rho_L}}$ and B is between 4 and 6, depending on the liquids.	Homogeneous and transition regimes	Reilly *et al.* [1994]	(4.17)
	$\varepsilon_G = \varepsilon_B + \varepsilon_e(1-\varepsilon_B)$ where $\varepsilon_e = \varepsilon_{trans} = 4.5\sqrt{\dfrac{\rho_G^{0.96}\sigma^{0.1}}{\rho_L}}$ and $\varepsilon_B = 0.27D_C^{-0.18}\left[V_{SG} - (V_{SG})_{trans}\right]^{0.58}$ D_C: column diameter (if $D_C > 0.6$ m, use $D_C = 0.6$ m)	Heterogeneous regime	Krishna and Ellenberger [1996]	(4.18)
	$\varepsilon_G = 0.67\left(\dfrac{V_{SG}\mu_L}{\sigma}\right)^{0.58}\left(\dfrac{\rho_L\sigma^3}{\mu_L^4 g}\right)^{0.13}\left(\dfrac{\rho_G}{\rho_L}\right)^{0.06}\left(\dfrac{\mu_G}{\mu_L}\right)^{0.11}$	Heterogeneous regime	based on Hikita *et al.* [1980]	(4.19)
	Homogeneous regime: $V_{SG} < (V_{SG})_{trans}$ $\varepsilon_G = \dfrac{V_{SG}}{u_{SB}}$ Heterogeneous regime: $V_{SG} > (V_{SG})_{trans}$ $\varepsilon_G = \dfrac{(V_{SG})_{trans}}{u_{SB}} + \dfrac{V_{SG} - (V_{SG})_{trans}}{u_{lB}}$	Homogeneous and heterogeneous regimes	Wilkinson *et al.* [1992]	(4.20)

Table 4.2 *(continued).*

			Author	Equation no.
Regime transition	$\varepsilon_{G,\text{trans}} = 0.5\exp\left(-193\rho_G^{-0.61}\mu_L^{0.5}\sigma^{0.11}\right)$ $(V_{SG})_{\text{trans}} = \varepsilon_{G,\text{trans}} u_{SB}$	Homogeneous/ heterogeneous	Wilkinson [1991]	(4.21)
Interfacial area ($\mathcal{A}$) (m^2/m^3)	$\mathcal{A} = \dfrac{6\varepsilon_G}{\overline{d_B}}$			(4.22)
Transfer coefficient (k_L) (m/s)	$\dfrac{k_L\overline{d_B}}{\mathcal{D}_L} = 0.5\left(\dfrac{\mu_L}{\rho_L\mathcal{D}_L}\right)^{0.5}\left(\dfrac{gd_B^2\rho_L}{\sigma}\right)^{0.375}\left(\dfrac{gd_B^3\rho_L^2}{\mu_L^2}\right)^{0.25}$	Homogeneous flow	Akita and Yoshida [1974]	(4.28)
	$k_L\mathcal{A} = 0.6\dfrac{\mathcal{D}_L}{D_C^2}\left(\dfrac{\mu_L}{\rho_L\mathcal{D}_L}\right)^{0.50}\left(\dfrac{gD_C^2\rho_L}{\sigma}\right)^{0.62}\left(\dfrac{gD_C^3\rho_L^2}{\mu_L^2}\right)^{0.31}\varepsilon_G^{1.1}$ D_C: diameter of the column; for $D_C > 0.6$ m, use $D_C = 0.6$ m		Akita and Yoshida [1973]	(4.29)
	$k_L = 0.31\left(\dfrac{g\mu_L}{\rho_L}\right)^{0.33}\left(\dfrac{\mathcal{D}_L\rho_L}{\mu_L}\right)^{0.66}$ $\overline{d_B} \leqslant 2.5$ mm $k_L = 0.42\left(\dfrac{g\mu_L}{\rho_L}\right)^{0.33}\left(\dfrac{\mathcal{D}_L\rho_L}{\mu_L}\right)^{0.5}$ $\overline{d_B} > 2.5$ mm		Calderbank and Moo-Young [1961]	(4.30)

Table 4.2 *(continued).*

		Author	Equation no.
$k_L a = 3.31 \frac{\mathcal{D}_L}{\overline{d_B^2}} \left(\frac{\mu_L}{\rho_L \mathcal{D}_L}\right)^{0.33} \left[\overline{d_B} \rho_L \left(\frac{0.8 V_{SG}}{\varepsilon_G}\right)\right]^{0.5} \varepsilon_G$		Fair [1962]	(4.31)
$Sh = (1 - \varepsilon_G)\, Sh' = 0.018\,(1 - \varepsilon_G)\, Sc^{0.50} Bo^{0.20} Ga^{0.62} Fr^{0.51}\,[1 + 0.12 Wi]^{-1}$	Viscoelastic media	Suh *et al.* [1991]	(4.32)
$\frac{k_l a V_{SG}}{g} = 14.9 f \left(\frac{V_{SG}\mu_L}{\sigma}\right)^{1.76} \left(\frac{\rho_L \sigma^3}{g \mu_L^4}\right)^{0.25} \left(\frac{\mu_G}{\mu_L}\right)^{0.24} \left(\frac{\mu_L}{\rho_L \mathcal{D}_L}\right)^{-0.6}$ where $f = 1$ the medium is non-electrolytic $f = 10^{0.07 I}$ if $I < 1.0$ g-ion/l $f = 1.1 \cdot 10^{0.02 I}$ if $I > 1.0$ g-ion/l		Hikita *et al.* [1981]	(4.33)
$\frac{k_l a \overline{d_B}^2}{\mathcal{D}_L} = 0.62 \left(\frac{\mu_L}{\rho_L \mathcal{D}_L}\right)^{0.5} \left(\frac{g \rho_L \overline{d_B}^2}{\sigma}\right)^{0.33} \left(\frac{g \rho_L^2 \overline{d_B}^3}{\mu_L^2}\right)^{0.29} \left(\frac{V_{SG}}{\sqrt{g \overline{d_B}}}\right)^{0.68} \left(\frac{\rho_G}{\rho_L}\right)^{0.04}$		Öztürk *et al.* [1987]	(4.34)
$k_l a = 9.3 \cdot 10^{-5} \frac{V_{SG}}{D_C} \left(\frac{D_C V_{SG} \rho_L}{\mu_L}\right)^{0.56} \left(\frac{V_{SG}\mu_L}{\sigma}\right)^{0.09} \left(\frac{V_{SG}}{\sqrt{g D_C}}\right)$	Viscous media	Zhao *et al.* [1994]	(4.35)

Table 4.2 *(continued).*

		Author	Equation no.
Mass transfer coefficient (k_G) (m/s)	$k_G = 0.08\dfrac{\overline{d_B}}{t_G}\exp\left(\dfrac{-40\mathcal{D}_G t_G}{\overline{d_B}^2}\right)$	Sharma and Mashelkar [1968]	(4.37)
	$k_G = 6.6\dfrac{\mathcal{D}_G}{\overline{d_B}}$ for $u_B = 0.3$ m/s and height > 0.5 m		(4.38)
Heat transfer coefficient α_W (W/m^2 · K)	$\dfrac{\alpha}{\rho_L C_{PL} V_{SG}} = 0.121(1-\varepsilon)\left(\dfrac{V_{SG}^3\rho_L}{\mu_L g}\right)^{-0.25}\left(\dfrac{C_{PL}\mu_L}{\lambda_L}\right)^{-0.5}$ $\varepsilon = \dfrac{1}{2+(0.35/V_{SG})}$	Verma [1989]	(4.39)
	$St = 0.1\left(Re_G Fr_G \mathrm{Pr}_L^2\right)^{-025}$ where $St = \dfrac{\alpha_W}{\rho_L C_{PML} V_{SG}}$ $Re_G = \dfrac{V_{SG} D_C \rho_L}{\mu_L}$ $Fr_G = \dfrac{V_{SG}^2}{gD_C}$ $\mathrm{Pr}_L = \dfrac{\mu_L C_{PML}}{\lambda_L}$	Deckwer [1992]	(4.40)
	$\rho_{SL} = \Phi_S\rho_S + \Phi_L\rho_L$ $\mu_{SL} = \mu_L(1 + k_S\Phi_S)$ $C_{PSL} = w_S C_{PS} + w_L C_{PL}$ Φ_S, Φ_L: volume fraction of solid, volume fraction of liquid w_S, w_L: weight fraction of solid, weight fraction of liquid	Lee and Tsui [1999]	(4.41)

Table 4.3 Range of validity for the correlations shown in Table 4.2.

	ρ_L kg/m^3	μ_L mPa · s	σ N/m	V_{SG} m/s	ρ_G kg/m^3	D_C m	H_c m	P MPa	Comments
Wilkinson [1991]	683–2 960	0.4–55	0.02–0.07	0–0.5	0.09–38	0.15–2.6	1.2–5		
Hikita *et al.* [1980]	800–1 240	0.7–18	0.02–0.07	0.04–0.38	0.08–1.84	0.1	1.5		
Reilly *et al.* [1994]	740–1 460	0.5–1	0.02–0.07	0.006–0.23	0.16–1.8	0.15	2.7	0.1–1.1	
Krishna and Ellenberger [1996]	760–1 000	1–2.9	0.03–0.07	0.001–0.9	0.2–6.7	0.1–0.6	0.3–2.2	0.1	
Wilkinson *et al.* [1994]	684–1 113	0.4–21	0.02–0.07	< 0.15	0.16–6.16	0.16	1.5	0.1–0.4	Water, aqueous solutions, glycol, heptane.
Hikita *et al.* [1981]	800–1 230	0.8–11.1	0.02–0.74	0.04–0.38	0.08–1.86	0.10 0.19	1.3 2.2	0.1	Water, aqueous solutions, alcohols, air, H_2, CH_4, CO_2.
Zhao *et al.* [1994]	884–1 120	1–1 260	0.03–0.07	0.008–0.06	1–1.86	0.14	0.02–1.5		Water, oils, CMC, CO_2, N_2.
Öztürk *et al.* [1987]	714–1 600	0.33–20	0.02–0.07	0.08–0.1	0.1–2.4	0.09	0.8	0.1	Organic liquids, pure liquids, mixtures, air, N_2, CO_2, He, H_2.
Wachi and Nojima [1990]	1 000	1	0.07	0.007–0.5	1.2	0.2–0.5	4.5	0.1	Water, air.

4.2.3.1 Bubble diameter

The diameter $\overline{d_B}$ considered is in general the Sauter diameter defined by the following equation:

$$\overline{d_B} = \frac{\sum n_i d_i^3}{\sum n_i d_i^2}$$

The mean bubble diameter, which often varies between several millimeters and several centimeters, depends on the distributor and is a decreasing function of pressure and the gas and liquid densities, but an increasing function of the interfacial tension σ. It is relatively unaffected by the gas flowrate.

A. Influence of the distributor

The influence of the distributor is complex. Bubble diameter, like pressure drop near the opening, depends on the velocity through the opening, its diameter, as well as the shape of the edges of the opening, wall thickness, etc. Fortunately this influence is limited, especially if the column diameter is greater than 0.15 m and its height greater than 1 m, or if the column is sufficiently elongated ($H/D_C > 5$) and the distributor openings large enough ($d_0 > 2$ mm) [Wilkinson *et al.*, 1992; Zhao *et al.*, 1994]. For small openings, Deckwer [1992] found that there was a noticeable difference depending on the size of the openings. Thus, for an aqueous system and a superficial gas velocity V_{SG} of 0.03 m/s, we obtain:

Hole diameter (mm)	Bubble diameter (mm)
1	6.5
0.5	5.1
Sintered metal	3

Trambouze *et al.* [1988] have proposed equations that depend on the hydrodynamic regime:

Re_{hole}	Correlation
$Re_{hole} < 10$	$\overline{d_B} \approx d_0^{0.56}$
$10 < Re_{hole} < 2\,100$	$\overline{d_B} \approx d_0^{0.92}$
$4\,000 < Re_{hole}$	$\overline{d_B} \approx d_0^{0.1}$

In various media, especially those that are non-Newtonian (carboxymethyl-cellulose solutions), Miyahara and Hayashino [1995] have proposed a correlation for bubbles generated by a plate perforated with holes 0.7 to 1.5 mm in size:

$$\overline{d_B} = 9.5 \left(\frac{d_O \sigma}{g \rho_L} \right)^{0.33} Mo^{0.053} \tag{4.5}$$

where:

$$\overline{d_B} = \left(\frac{\Sigma (6V_b/\pi)}{n} \right)^{0.33} \quad \text{and} \quad Mo = \frac{g^{3n-2} m^4}{\rho_L^{2-n} \sigma^{n+2}}$$

Mo is the Morton number, a dimensionless number in which m and n are respectively the coefficient and exponent of the rheological power law for the liquid.

B. Influence of the medium

Aside from the distributor, bubble size depends a great deal on the coalescence properties of the medium. Specifically, the variation in surface tension as a function of the concentration at the interface has a significant effect on coalescence and, therefore, on bubble size. The estimate of $\overline{d_B}$ established by Akita and Yoshida [1973] for columns up to 0.3 m in diameter and gas superficial velocity up to 0.07 m/s, must be used with considerable caution. The size of the bubbles depends somewhat on the distributor but greatly on coalescence phenomena. Akita and Yoshida limit the range of use of their correlation to values of ε_G below 15%. The influence of column diameter is discussed by some authors ($\overline{d_B} \approx D_C^{-0.3}$); it remains limited to $20\overline{d_B}$, that is, approximately 0.15 m.

C. Homogeneous flow

Several correlations collected by Koïde [1996] can be used, in particular the correlation of Akita and Yoshida [1974] (Eq. 4.6), which has been verified for column diameters larger than 5 m.

D. Heterogeneous flow

The bubbles have complex shapes. Under pressure, rupture is accelerated following the increase in gas density. The number of large bubbles decreases and there is a narrower distribution of sizes. Wilkinson *et al.* [1994] have proposed a correlation that takes pressure into account by means of gas density:

$$\frac{g\rho_L\overline{d_B}^2}{\sigma} = 8.8\left(\frac{V_{SG}\mu_L}{\sigma}\right)^{-0.04}\left(\frac{\rho_L\sigma^3}{g\mu_L^4}\right)^{-0.12}\left(\frac{\rho_L}{\rho_G}\right)^{0.22} \tag{4.7}$$

According to Jiang *et al.* [1995], this is valid up to 1.5 MPa.

4.2.3.2 Bubble rise velocity

Bubble rise velocity, u_B, although not very useful by itself, is a characteristic of the system that is needed to calculate the contact time of the gas and establish certain correlations. Typical are those related to transfer and backmixing. Less than 0.2 or 0.3 m/s in the homogeneous regime, bubble velocity can exceed 0.5 m/s in the heterogeneous regime with perforated distributors and superficial gas velocities of at least 0.2 m/s. It is related to gas holdup through the formula: $u_B = V_{SG}/\varepsilon_G$.

In the homogeneous regime, bubble rise velocity depends essentially on the medium. For small bubbles, Wilkinson *et al.* [1992] propose a correlation that also accounts for pressure by means of gas density:

$$u_B = 2.25\left(\frac{\sigma}{\mu_L}\right)\left(\frac{\sigma^3\rho_L}{g\mu_L^4}\right)^{-0.273}\left(\frac{\rho_L}{\rho_G}\right)^{0.03} \tag{4.8}$$

In the heterogeneous regime, gas velocity has a marked influence on bubble rise velocity, as Hyndmann and Guy [1995] demonstrated for water/air systems:

$$u_B = 2.5V_{SG}^{0.69} \tag{4.9}$$

The effect associated with the medium is accounted for in a correlation [Trambouze *et al.*, 1988] that consolidates nearly 400 measurements made in very different media, with values of V_{SG} as high as 0.15 m/s, distributor holes of 1 to 3 mm, and columns from 5 to 10 cm in diameter:

$$u_B = \left(\frac{\sigma(\rho_L - \rho_G)g}{\rho_L^2}\right)^{0.25} \left(0.014 + 0.116V_{SG} + 0.5V_{SG}^2 + 0.8V_{SG}^3\right) \qquad (4.10)$$

Wilkinson *et al.* [1992] also consider the role of the medium, but add to this the influence of pressure by means of gas density (Eq. 4.11, Table 4.2).

4.2.3.3 Holdup

In this section we discuss gas holdup ε_G alone; in bubble columns liquid holdup ε_L can be directly determined from the relation $\varepsilon_G + \varepsilon_L = 1$. A number of correlations have been identified and consolidated by Fan [1989], Deckwer [1992], and Koïde [1996]. Although there are a large number of correlations, many of them quite sophisticated, their precision is often poor since relative uncertainties of 10 to 20% are common.

In fact, gas holdup can vary considerably, ranging from values less than 10% to more than 40%, depending on the hydrodynamic regime and the gas flow rate (Fig. 4.4). A large number of results are covered by a simplified general law of the type $\varepsilon_G = kV_{SG}^n$ (Eq. 4.12, Table 4.2), where k depends on the system (k, an increasing function of gas density, can vary from 1 to 5) and n on the regime (n varies from 0.7 to 1.2 in the homogeneous regime and from 0.4 to 0.7 in the heterogeneous regime) [Reilly *et al.*, 1994].

Other factors that can have an appreciable effect on gas holdup include the physicochemical properties of the medium and the distributor, variables that are often specific to the problem at hand. The velocity of the liquid crossing the column, generally low with respect to the bubble rise velocity, has no significant influence. For superficial liquid velocities greater than 0.05 m/s, it may be more precise to substitute in the correlations a bubble slip velocity for the superficial gas velocity. Bubble slip velocity is defined by the following equation:

$$u_{Gl} = \frac{V_{SG}}{\varepsilon_G} \pm \frac{V_{SL}}{1 - \varepsilon_G}$$

where the sign is:

- $-$ for the liquid flowing upward
- $+$ for the liquid flowing downward.

In the absence of a liquid flow rate, this velocity is equal to the bubble rise velocity, $u_B = u_{Gl}$.

A. Homogeneous flow

In the homogeneous regime Krishna *et al.* [1991] have proposed a very simple formula, which is valid for water if $V_{SG} < 0.05$ m/s:

$$\varepsilon_G = 4V_{SG} \quad \text{where } V_{SG} \text{ in m/s} \qquad (4.13)$$

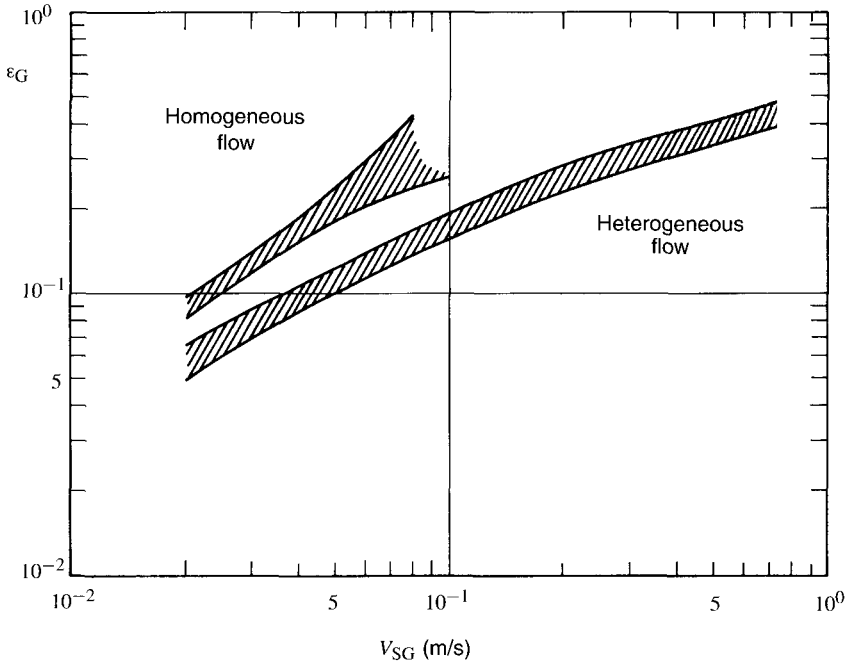


Figure 4.4 Bubble columns. Gas holdup ε_G as a function of the superficial gas velocity V_{SG}.

However, apart from the gas flow rate, the properties of the medium play a significant role. One generally accepted correlation is that of Akita and Yoshida [1973]:

$$\frac{\varepsilon_G}{(1-\varepsilon_G)^4} = K\left(\frac{V_{SG}\mu_L}{\sigma}\right)\left(\frac{\rho_L\sigma^3}{g\mu_L^4}\right)^{0.29} \tag{4.14}$$

(where $K = 0.20$ for pure liquids and $K = 0.25$ for electrolytes), which is well suited to a variety of media, including aqueous or non aqueous solutions, and superficial gas velocities up to 0.4 m/s. The effect of gas density is introduced later, but only in terms of the difference with the density of the liquid (Eq. 4.15, Table 4.2).

The distributor can also play an important role, at least for gas velocities up to 0.2 m/s. Thus, perforated pipes or sieve plates will result in lower holdup values than the sintered or porous plates often used in the laboratory to obtain experimental data. Certain ejectors will even give ε_G values that are nearly double those for perforated pipe.

B. Heterogeneous flow

In the heterogeneous regime the gas flow rate and the nature of the medium have considerable influence on holdup. In this respect Eq. (4.16) does a good job of summarizing several of the correlations provided by Deckwer [1992] for water-air systems at atmospheric pressure, with gas velocities from 0.01 to 1 m/s and columns 5 m or more in diameter.

$$\varepsilon_G = 0.6V_{SG}^{0.6} \tag{4.16}$$

To fully account for the bimodal distribution of bubble diameters, Krishna *et al.* [1991, 1996] suggest that when $V_{SG} > 0.1$ m/s holdup be divided into two fractions, one for large and one for small bubbles. The large bubbles, or clusters, pass quickly through the column without actually participating in gas-liquid reactions. The small, individual, bubbles a few millimeters in diameter, provide interfacial areas and residence times favorable to the chemical reaction. In the heterogeneous regime the holdup for small bubbles no longer depends on the superficial velocity of the gas. Krishna recommends the correlation of Reilly *et al.* [1994], which was validated for more than 3 000 data points, including various gas densities and columns 0.6 m in diameter:

$$\varepsilon_G = \varepsilon_{G,\text{trans}} = 0.6B^{1.5}\sqrt{\frac{\rho_G^{0.96}\sigma^{0.1}}{\rho_L}} \tag{4.17}$$

In (4.17) $B = 3.85$ for air-water and air-tetradecane systems. The large-bubble fraction does not depend on the properties of the liquid, or the density of the gas phase, or the distributor, but on the diameter of the column (at least up to 0.6 m). For large bubbles, Krishna and Ellenberger [1996] propose a formula that takes into account the effect of column diameter (confirmed up to 0.6 m) and holdup at the regime transition ($\varepsilon_{G,\text{trans}}$):

$$\varepsilon_B = 0.27D_C^{-0.18}\left[V_{SG} - (V_{SG})_{\text{trans}}\right]^{0.58} \tag{4.18}$$

where:

$$(V_{SG})_{\text{trans}} = 0.35\frac{\varepsilon_{\text{trans}}}{1-\varepsilon_{\text{trans}}}\rho_G^{-0.04}\sigma^{0.12}$$

Influence of fluid properties

Hikita *et al.* [1980] have proposed a rather general correlation based on some twenty different media, in particular gases of different densities, which has been confirmed by numerous results in the literature (Eq. 4.19, Table 4.2). Foamy systems have much higher holdup values. Until now quantitative forecasting of these phenomena has not been very reliable; however there are known chemical, mechanical, and thermal methods that can limit or even eliminate the foam.

The presence of electrolytes also modifies bubble coalescence and leads to an increase in gas holdup of approximately 10 to 20% [Hikita *et al.*, 1980]. The results obtained with a suspension comprising a second immiscible liquid phase or a solid phase [Trambouze *et al.*, 1988] differ only slightly from those obtained with a single liquid phase. The presence of solid particles has a tendency to decrease gas holdup.

Influence of pressure

Until around 1975 most correlations had been based on measurements carried out at atmospheric pressure with air. However, they can still supply us with trends and orders of magnitude. Gas holdup increases slightly with pressure or gas density [Wilkinson *et al.*, 1992] (Eqs. 4.20 and 4.21, Table 4.2).

Influence of internal components

The influence on holdup of horizontal baffles of perforated plate depends on the number of perforations. With few perforations (open area < 10% of the plate area) a more or less stable

gas cap forms beneath each plate, which reduces the volume occupied by the liquid. When there are a large number of perforations (perforation ratio > 25%), the baffles increase gas holdup (by approximately 4% when holdup is 20 to 30%). Pressure drop through the plates depend on the superficial velocity of the gas and the number and diameter of perforations but remains moderate (for example, ΔP per plate $\cong$ 1 kPa for air that moves through the reactor with a superficial velocity $V_{SG} = 0.5$ m/s, plates with 3 mm holes, and a perforation ratio of 50%).

Vertical obstacles or a cylindrical baffle produce consistent circulation of the liquid, which generally results in a notable decrease (5 to 7%) of the mean gas holdup. This arrangement will be examined in detail in section 4.3 in our discussion of the gaslift reactor.

Holdup can be used to calculate the height of the expanded liquid. To determine the total column height, we also need to incorporate a free board, whose height (at least 1 m) is approximately equal to the diameter of the column.

4.2.3.4 Interfacial area, $\mathcal{A}$

The interfacial areas of bubble columns range from 100 to 400 m^2/m^3. There are a number of direct (photographic, physical methods) and indirect (chemical) methods for determining interfacial area, but these lead to values that easily vary by a factor of 2 to 3, and sometimes 5 [Deckwer, 1992].

When a bubble column operates in the homogeneous regime, good estimates of interfacial area can be obtained using the mean dimension of the bubbles and gas holdup. For spherical bubbles, we have:

$$\mathcal{A} = \frac{6\varepsilon_G}{\overline{d_B}} \tag{4.22}$$

This equation is a good first approximation if the gas velocities are low, but $\overline{d_B}$ as well as ε_G must be estimated. The combination of correlations is difficult and imprecise; scale-up must be performed with care, using data obtained from the physicochemical system itself whenever possible. An increase in pressure leads to an increase in gas holdup and a reduction in bubble size, and therefore to an increase in interfacial area.

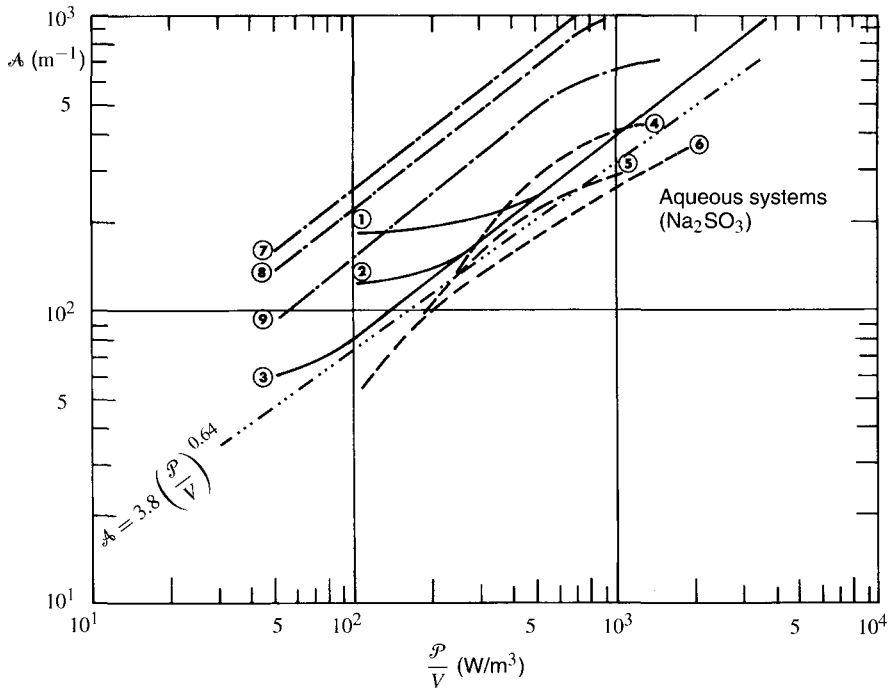
For direct evaluation of the interfacial area, it is worthwhile knowing that, for a given system, $\mathcal{A}$ is a function of the amount of energy introduced (Fig. 4.5), according to a power law of the following form:

$$\mathcal{A} = K\left(\frac{\mathcal{P}}{V}\right)^n \quad \text{in } m^2/m^3 \tag{4.23}$$

where n is appreciably comprised between 0.60 and 0.70 and K is about 3.8.

The equation has been established primarily on the basis of research on fermentation tanks. In this case energy consumption can represent a non-negligible fraction of the cost of the products obtained [Trambouze *et al.*, 1988]. To calculate the optimal superficial velocity for the gas, we use the energy of isothermal expansion of the gas at the temperature of the column, together with a small contribution from the kinetic energy of the gas jet. Neglecting this last term, we obtain:

$$\mathcal{P} = \frac{Q_M R T_L}{M} \ln \frac{P_e}{P_s} \tag{4.24}$$



Reith's data [1968]	– Mechanically agitated columns (Rushton turbines): (1) $D = 0.19$ m (2) $D = 0.45$ m (3) $D = 1.20$ m Equation for the straight line common to curves (1) (2) (3): $\mathcal{A} = 3.32\left(\frac{\mathcal{P}}{V}\right)^{0.69}$ $\quad 100 < \mathcal{A} < 1\,000$ m^2/m^3 – Bubbles columns: (4) $D_C = 0.29$ m $\quad H = 1.6$ m (5) $D_C = 0.29$ m $\quad H = 3.7$ m (6) $D_C = 0.14$ m $\quad H = 2$ and 3.4 m
Data from Nagel *et al.* [1970]	– $D_C = 0.3$ m $\quad H = 2.6$ m (7) $Q_{VG} = 9.12$ m^3/h (8) $Q_{VG} = 4.65$ m^3/h (9) $Q_{VG} = 2.28$ m^3/h

Figure 4.5 Change in interfacial area versus the power introduced per unit volume.

where

$\mathcal{P}$ power input (W)
Q_M total mass flow rate (kg/s)
R ideal gas constant ($R = 8.31$ J/mol · K)
T_L temperature of the liquid in the column (K)
M molecular weight of the gases (kg/mol)
P_e, P_s gas inlet (base of column) and outlet pressure (Pa).

If the difference $(P_e - P_s) = \Delta P$ is small compared to P_s, we can write:

$$\mathcal{P} = \frac{Q_M R T_L}{M} \ln\left(1 + \frac{\Delta P}{P_s}\right) \approx \frac{Q_M R T_L}{M P_s} \Delta P = Q_{VG} \Delta P \tag{4.25}$$

where: $Q_{VG} = V_{SG} S$ and $\Delta P = H \rho_L g$

Here

Q_{VG} volume flow rate at the outlet (m^3/s)
S column cross-section (m^2)
H height of the (non-expanded) liquid (m)
V_L volume of the (non-expanded) liquid (m^3).

Since:

$$V_L = HS = V\varepsilon_L$$

we find that:

$$\frac{\mathcal{P}}{V_L} = V_{SG} \rho_L g \tag{4.26}$$

In a liquid such as water ($\rho_L = 10^3$ kg/m^3), we find:

$$\frac{\mathcal{P}}{V_L} = 9\,810 V_{SG} \text{ W/m}^3 \quad \text{if } V_{SG} \text{ in m/s} \tag{4.27}$$

A superficial gas velocity of 0.1 m/s, therefore, corresponds to the introduction of approximately 1 kW/m^3 of non-expanded liquid, which produces an interfacial area of about 320 m^2/m^3.

Finally, a column with a low gas flow rate, operating in the homogeneous regime, can provide greater gas holdup and interfacial area than a column operating at the same superficial gas velocity in the heterogeneous regime (Fig. 4.4). Since there is also less backmixing of the gas phase, use of this operating mode is worth investigating, even though most industrial plants running at atmospheric pressure operate in the heterogeneous regime [Deckwer, 1992].

4.2.3.5 Coefficient of mass transfer k_L and the product $k_L a$

The coefficient of mass transfer, k_L, is approximately $2 \cdot 10^{-4}$ m/s for slightly viscous liquids. It is essentially a function of the gas velocity and the properties of the medium. There are few correlations that can be used to estimate k_L alone. The correlation supplied by Akita and Yoshida [1974] (Eq. 4.28) provides values that are proportional to $\left(\overline{d_B}\right)^{0.5}$ and comprised between $6 \cdot 10^{-5}$ and $7 \cdot 10^{-4}$ m/s, and would be especially valid under conditions

of homogeneous flow. In fact, values of k_L depend primarily on the physical properties of fluids and the size of the bubbles. For a sodium sulfite solution the values are around $k_L = 4 \cdot 10^{-4}$ m/s.

The group $k_L\mathcal{A}$, which is approximately 0.05 to 0.2 s^{-1}, depends neither on the diameter of the column (if $D_C > 0.60$ m) nor on the type of distributor (if $H_C > 1$ m, $V_{SG} > 0.05$ m/s and if the gas velocity, u_O, at the outlet of the distributor orifice is not too high: $u_O < 50$ m/s) but on the properties of the fluids (essentially, the density of the liquid and interfacial tension), and increases sharply with the superficial velocity of the gas (Eqs. 4.29 to 4.32). Hikita *et al.* [1981] discuss the results obtained with pure or aqueous liquids, with good precision over a large range of superficial gas velocities. For electrolyte media, in which the coalescence is slowed and there are more bubbles with small diameters, they provide a correction associated with the ionic force (I) of the solution.

$$\frac{k_l\mathcal{A}V_{SG}}{g} = 14.9f\left(\frac{V_{SG}\mu_L}{\sigma}\right)^{1.76}\left(\frac{\rho_L\sigma^3}{g\mu_L^4}\right)^{0.25}\left(\frac{\mu_G}{\mu_L}\right)^{0.24}\left(\frac{\mu_L}{\rho_L\mathcal{D}_L}\right)^{-0.6} \tag{4.33}$$

where

$f = 1$ for non-electrolyte solutions
$f = 10^{(0.07 \cdot I)}$ if $I < 1.0$ g-ion/l
$f = 10^{(0.02 \cdot I)}$ if $I > 1.0$ g-ion/l.

Muller and Davidson [1992, 1995] have shown that, in the heterogeneous regime, the contribution of small bubbles to $k_L\mathcal{A}$ is greater than 60% if $V_{SG} = 0.15$ m/s in water-air and ranges from 20 to 50% in highly viscous media. The addition of small quantities of surfactants increases the holdup of small bubbles, which results in an appreciable increase in mass transfer (50% increase in $k_L\mathcal{A}$ after the addition of 0.025% octanol in a 1% CMC solution, according to Muller).

The correlation supplied by Öztürk *et al.* [1987] (Eq. 4.34), which has been confirmed in about fifty different media, principally organic liquids, takes into account the influence of the properties of the gas and liquid with a precision of roughly 13%.

Whenever the viscosity increases, the decrease in $k_L\mathcal{A}$, which can decline by as much as a factor of 5, is most likely associated with an increase in coalescence [Suh *et al.*, 1991; Muller and Davidson, 1992 and 1995]. Zhao *et al.* [1994] used this to explain the decrease in local values of $k_L\mathcal{A}$ within a distance of one meter above the distributor (Eq. 4.35).

Under pressure, the increase of ε_G and decrease of $\overline{d_B}$ lead to an increase of $k_L\mathcal{A}$. Wilkinson *et al.* [1992, 1994] have suggested modifying the values obtained at atmospheric pressure using a correction coefficient based on the change in holdup:

$$k_L\mathcal{A} \approx (\varepsilon_G)^{1.1} \tag{4.36}$$

4.2.3.6 Coefficient of mass transfer k_G and the product $k_G\mathcal{A}$

In most situations bubble columns are used for slow reactions or absorptions, when the resistance to transfer on the gas side is generally negligible. Consequently, a bubble column is normally not the best choice if resistance on the gas side controls mass transfer.

For conventional values of $k_G a$ ranging from 1 to 3 s^{-1} [0.5 to 1.5 · 10^{-3} mol/(m^3Pa · s)], the equation of Sharma, cited in Trambouze *et al.* [1988] can be used for confirmation. The equation takes into account the medium and operating conditions, and can be written:

$$k_G = 0.08 \frac{\overline{d_B}}{t_G} \exp\left(\frac{-40 \mathcal{D}_G t_G}{\overline{d_B}^2}\right) \tag{4.37}$$

where

$\mathcal{D}_G$ diffusivity in the gas (m^2/s)

t_G contact time of the bubble, with $t_G = H/u_B$, where H is the height of the column of expanded liquid and u_B the mean rise velocity of the bubbles.

If $u_B \cong 0.3$ m/s, for column heights greater than 0.5 m, the above equation can be simplified:

$$k_G \cong 6.6 \frac{\mathcal{D}_G}{\overline{d_B}}, \quad \text{which can be written: } \mathrm{Sh} = \frac{k_G \overline{d_B}}{\mathcal{D}_G} = 6.6 \tag{4.38}$$

4.2.4 Heat transfer

When direct exchanges, such as the addition of fluids or evaporation, fail to provide or eliminate the desired quantity of heat, indirect heat transfer across exchange surfaces (walls or tubes immersed in the gas-liquid medium) becomes necessary. Large surfaces can in fact be developed in bubble columns through the use of coils or bundles of tubes parallel or perpendicular to the column axis, even if such obstacles to free flow sometimes modify the hydrodynamics of the system.

The coefficient of heat transfer α_W, on the order of 2 000 to 8 000 W/(m^2 · K), appreciably increases with the superficial gas velocity but decreases with the viscosity of the medium. Verma's [1989] correlation (Eq. 4.39), which has been confirmed for gas-liquid media with various properties and under severe operating conditions, provides a good starting point. But Deckwer [1992] (Eq. 4.40) and Schlüter *et al.* [1995] have collected and compared correlations and models that, in addition to operating conditions, take into account the number, arrangement, and geometry of the exchange tubes, as well as the local turbulence they generate. The equations these authors provide introduce a number of parameters, notably bubble diameter and gas holdup, which clearly limits the precision of the predictions but can be useful when scaling up.

In the case of suspensions of solid particles, the coefficient of heat transfer increases with the concentration of solids and the size of the particles (Eq. 4.41).

4.2.5 General design considerations

4.2.5.1 General dimensions

The volume V of a bubble column designed for a given conversion and selectivity is based on the materials balance and the selected operating conditions. By calculating iteratively, we can determine the geometry. Actually, by starting with an initial presumed value for

the superficial gas velocity V_{SG}, we can calculate the corresponding cross-section A of the column, the diameter D_C, and the head of liquid H using the standard equations:

$$A = \frac{Q_G}{V_{SG}} \rightarrow D_C = \sqrt{\frac{4A}{\pi}} \rightarrow H = \frac{V}{A} \tag{4.42}$$

We must then verify that the selected superficial velocity leads to acceptable values for the holdup, the contact time for the gas, and the overall pressure drop. The final determination of total column size must take into account the gas holdup and the height needed to remove the gas from the drops of liquid. Once the general dimensions of the column are known, the arrangement of the internal components must be determined, especially the gas distributor.

4.2.5.2 Gas distributor

A bubble column needs a gas distributor that provides uniform gas distribution to avoid over- or undersaturated zones in the column. In laboratory or pilot plant columns the distributor is generally made of porous glass or metal (pores of 10 to 100 μm); in industrial facilities, plates, rings, or perforated pipes are preferable. The diameter of the openings is generally between 1.5 and 15, sometimes 20 mm, and the number of openings is determined so as to ensure that flow is appreciably equal through each orifice. It is therefore recommended that the pressure drop through each opening (roughly a few thousand pascals) be at least 10 to 20 times greater than the pressure drop in the tube. This leads to gas velocities through the orifice on the order of 20 to 80 m/s or corresponding Reynolds numbers greater than 5 000. In industrial columns performance depends somewhat on the method of introducing the gas, but the influence of the distributor is not critical in determining the hydrodynamics of the column. This is because, above a height approximately equal to 5 times the column diameter [Joshi *et al.*, 1990], or at most 1 meter, we find that coalescence phenomena and bubble fragmentation have a greater effect on the distribution of bubble sizes.

We can precisely calculate the diameter of the holes by using an initial diameter d_o, taking into account technological requirements (risk of plugging, mechanical strength, etc.), and calculating a critical diameter $d_{o,c}$:

$$d_{o,c} = 2.3\left[\frac{\sigma}{\rho_G g}\right]^{0.5}\left[\frac{\rho_G}{\rho_L - \rho_G}\right]^{0.62} \tag{4.43}$$

The number of holes is based on calculation of the gas velocity $u_{G,o}$ through the openings based on either of the following expressions:

$$\begin{aligned} d_o < d_{o,c} \qquad & \frac{\rho_G d_o u_{Go}^2}{\sigma} > 2 \\ d_o > d_{o,c} \qquad & \frac{u_{Go}^2}{d_o g}\left[\frac{\rho_G}{\rho_L - \rho_G}\right]^{1.25} > 0.37 \end{aligned} \tag{4.44}$$

When making our calculations, we are therefore free to choose, for a given gas flow rate, the diameter of the perforations or their number. In rings and perforated pipes, the openings are often oriented toward the bottom to prevent plugging from debris or solid particles.

4.2.5.3 Separator

At the top of the column, drops of liquid, sometimes entrained by the gas stream, are stopped and collected by a demister often consisting of a woven metallic mat a few tens of centimeters in height.

4.2.5.4 Thermal exchange surfaces

If exchange through the wall is inadequate, tubes, coils, or plates can be arranged inside the column. Their surface area and arrangement depend on the heat balance and their influence on the hydrodynamics of the system.

4.2.6 Alternative designs

4.2.6.1 Horizontal bubble columns

Although most bubble columns are simple vertical cylinders, several different alternative designs exist that can be useful. Trambouze *et al.* [1988] describe a horizontal bubble column (Fig. 4.6) with and without mechanical agitation. The orders of magnitude of k_L, k_G, and $\mathcal{A}$, are similar to those found in conventional columns, but $\mathcal{A}$ is inversely proportional to the diameter of the column D_C and proportional to u_{Go}, while k_G and k_L depend on $u_{Go}^{0.2}$ (u_{Go} being the gas velocity at the orifice).

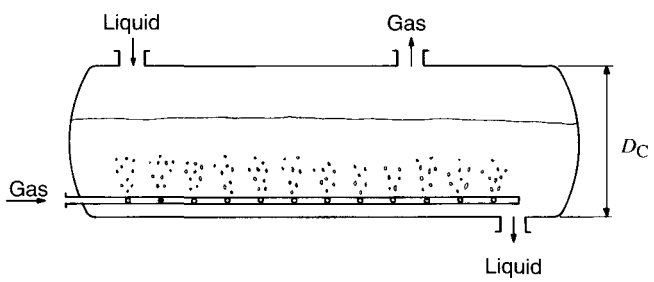


Figure 4.6 Horizontal bubble column.

The advantages of the horizontal configuration are:

- low static head (most of the pressure drop comes from the injector)
- $k_L\mathcal{A}$ is larger for a given pressure drop.

The major drawback is the short travel time of the bubble in the liquid phase, thereby preventing any significant exhaustion. In practice horizontal bubble columns are used primarily when the chemical reaction is slow and does not involve high conversion of the gas phase.

4.2.6.2 Large basins

This approach is also used in the large, shallow basins found in water treatment facilities. In this case, the gas is often distributed through porous tubes or rubber linings pierced with very fine openings.

4.2.7 Concluding remarks

Bubble columns have the following principal characteristics:

Advantages

- high liquid holdup and residence time
- good mass and heat transfer and good thermal inertia
- moderate interfacial area
- simple construction
- no moving parts
- low construction, operating, and maintenance costs
- ability to process liquids containing solid particles.

Disadvantages

- non-negligible gas pressure drop if the column is high
- high liquid homogenization throughout the column.

4.3 GASLIFTS

4.3.1 General characteristics

A cylindrical baffle (Fig. 4.2B), a vertical compartment (Fig. 4.2C), or external bypass (Fig. 4.2D) can transform a simple bubble column into a gaslift with an internal or external loop. These changes result in the creation of two zones that communicate through the top and bottom of the device, creating a loop. The gas, introduced at the bottom of the first zone, rises to the upper part as in a simple bubble column. In the second zone, the liquid, freed of the gas, returns to the bottom of the device.

The difference in the gas holdup between the two zones results in a difference in their average densities ($\rho_{\text{descending}} - \rho_{\text{ascending}} > 0$) and results in systematic circulation of the liquid in the loop.

If the gas flow is moderate, all the bubbles will rise to the gas-liquid interface and the liquid will fall, freed of any trapped gas. When gas flow increases, the liquid flows more rapidly in the loop and entrains more and more gas bubbles in the downcomer, which reduces the density difference between the two zones. Under these conditions, the rate of circulation decreases and the system moves toward equilibrium. However, if the falling liquid is too rich in gas and the turbulence in the lower part of the reactor too strong, systematic recirculation may be suppressed, at least temporarily. The range of stabilized operation is still quite extensive, however, even when gas bubbles flow downward to significant depths along with the liquid.

4.3.2 Hydrodynamics

Gaslifts have many hydrodynamic similarities with bubble columns. What makes them different is the one-to-one correspondence that is established between the rate of circulation of the liquid in the loop and the gas holdup. Fairly complete summaries of results and models have been assembled by Christi [1989] and Joshi *et al.* [1990] among others.

4.3.2.1 Holdup

Compared to simple bubble columns, the rate of liquid circulation results in a significant decrease in average gas holdup throughout the column (approximately 0.05 to 0.07 in the holdup range 0.20 to 0.30).

Mean gas holdup increases with the superficial gas velocity and the ratio A_d/A_m between downcomer and riser cross-sections. It also depends on the properties of the medium and the relative change in pressure from the bottom to the top of the gaslift. Joshi *et al.* [1990] have presented a number of results obtained for gas velocities ranging from 0.08 to 0.35 m/s and columns of more than 0.1 m in diameter using the following formulas:

$$\varepsilon_G = 0.25 V_{SG}^{0.56} \mu_L^{-0.11} \sigma^{-0.10} \quad \text{no surface-active agents present} \tag{4.45}$$

$$\varepsilon_G = 0.07 V_{SG}^{0.5} \mu_L^{-0.04} \sigma^{-0.75} \quad \text{aliphatic alcohols present} \tag{4.46}$$

Dhaouadi [1997] proposed a more precise formula for gas holdup in the riser:

$$\varepsilon_{G,m} = a V_{SG}^{b} \left(\frac{A_d}{A_m}\right)^{c} \left(\frac{\rho_L g H_0}{P_0}\right)^{d} \left(\frac{\mu_L}{\mu_{water}}\right)^{e} \tag{4.47}$$

where, for example, $a = 0.27$, $b = 0.64$, $c = -0.30$, $d = -0.31$, $e = -0.06$ for more or less viscous aqueous media ($0.004 \leqslant \mu \leqslant 0.033$ Pa · s) in an external-loop gaslift up to 6 m in height with downcomers of moderate cross-section ($0.04 < (A_d/A_m) < 0.33$), and moderate gas velocities ($V_{SG} \leqslant 0.16$ m/s). The holdup in the downcomer is too dependent on gas removal conditions at the top of the gaslift to be represented by a correlation that is both precise and general, but it obviously increases with the velocity of the liquid in the downcomer and therefore with the flow rate of the gas.

Gaslifts with external loops have lower holdup than gaslifts with internal recirculation, which does not favor mass transfer. When the transfer is limiting, static mixers can be introduced into the riser to fragment large gas bubbles into smaller and more uniform bubbles, which, according to Gaspillo and Goto [1991], increases gas holdup and mass transfer (up to 30%).

4.3.2.2 Circulation velocity

Liquid circulation velocities of 0.5 to 1 and sometimes 2 m/s are easily obtainable in columns a few meters high. In fact, the velocity of circulation is based on the balance of pressures in the complete loop: the difference in holdup between the two vertical zones, riser and downcomer, and the pressure drops in the loop. We can write the following balance:

$$gH(\rho_{descending} - \rho_{ascending}) \cong \frac{1}{2}\rho_L \sum (K V_{SL}^2) \tag{4.48}$$

where H is the height of the gas-liquid mixture and K a coefficient of friction that is calculated for each zone [Joshi, 1990; Cockx, 1997; Cockx *et al.*, 1997; Abashar *et al.*, 1998].

By neglecting pressure drop in the vertical regions compared to pressure drop in the bends of the connecting zones, and by assuming holdup to be negligible in the downflow region, the superficial liquid velocity V_{Lm} in the riser has the following values:

- for internal-loop gaslifts:

$$V_{Lm} = \left[\frac{2gH\varepsilon_{G,\,ascending}}{K_B \left(\frac{A_m}{A_d} \right)^2} \right]^{0.5} \tag{4.49}$$

- for external-loop gaslifts

$$V_{Lm} = \left[\frac{2gH\varepsilon_{G,\,ascending}}{K_B \left(\frac{1}{\left(1 - \varepsilon_{G,\,ascending}\right)^2} + \left(\frac{A_m}{A_d} \right)^2 \right)} \right]^{0.5} \tag{4.50}$$

where:

$$K_B = 11.4 \left(\frac{A_d}{A_b} \right)^{0.79}$$

Here

A_b flow area at the base of the gaslift

$\varepsilon_{G,\,downcomer} \cong 0$ if gas removal at the top is effective.

Overall, the velocity of circulation increases with the gas flow rate, the liquid head, the ratio of the cross-sections, and the effectiveness of gas removal [Christi, 1989; Dhaouadi, 1997]:

$$V_{Lm} = \alpha V_{SGm}^{\beta} \left(\frac{A_d}{A_m} \right)^{\gamma} \tag{4.51}$$

where, depending on the geometry and properties of the system,

$$0.2 < \alpha < 1.8$$
$$0.26 < \beta < 0.4$$
$$0.6 < \gamma < 1.0$$

Moreover, the velocity of circulation decreases with the viscosity of the medium and increases with surface tension [Wachi and Nojima, 1990]. This velocity varies little in the presence of solid concentrations of a few percent, however [Choi *et al.*, 1996].

4.3.2.3 Fluid flow

The liquid descends with nearly perfect plug flow but is accompanied by slight dispersion as it rises. This is reflected in the fact that Peclet numbers from 40 to 100 are common for gas velocities below 0.10 m/s.

4.3.3 Mass transfer

In terms of mass transfer, the advantage of the gaslift reactor over the bubble column is not clear because, as a result of the velocity of circulation, the global interfacial area $\mathcal{A}$ may decrease while the coefficient k_L increases only slightly. In an external-loop gaslift, in the presence of an aqueous medium and air, Christi [1989] proposed the use of the following expression:

$$k_L\mathcal{A} = 0.35V_{SG}^{0.84}\left(1 + \frac{A_d}{A_m}\right)^{-1} \tag{4.52}$$

4.3.4 Heat transfer at the wall

The coefficients of heat transfer at the wall, α_W, on the order of 2 000 to 8 000 $W/(m^2 \cdot K)$, also depend on the superficial gas velocity according to power laws that change slightly from regime to regime [Dhaouadi, 1997]:

$$\alpha_W = aV_{SG}^b \quad \text{in aqueous media and air} \tag{4.53}$$

if	$V_{SG} < 0.04$ m/s	$a = 26\,000$	$b = 0.48$
and if	$0.04 < V_{SG} < 0.10$	$a = 16\,000$	$b = 0.33$

4.3.5 General design considerations

The cross-section area of each zone as well as the height of the column must be chosen as a function of the overall volume of liquid contained in the reactor and the desired gas flow rate. A first estimate of the superficial velocity of the liquid can be used to calculate the corresponding holdup and the pressure drop throughout the loop, and thus determine the liquid circulation velocity. An iterative calculation is performed until it converges on the anticipated liquid velocity and gas holdup for the reactor. It is useful to take into account the influences summarized in the following table.

Parameter ↗	Liquid velocity (riser)	Liquid velocity (downcomer)	Gas holdup (riser)	Gas holdup (downcomer)
Viscosity	↘	↘	↘	↘
Solid concentration	↘	↘	↘	↘
Height of central tube	↗	↗	↘	↗
$\frac{A_{ascending}}{A_{ascending} + A_{descending}}$	↘	↗	↘	↗

The gas distributor is similar to that used in bubble columns but it plays a more critical role since it has a direct influence on holdup and therefore on the velocity of circulation in the loop. The distributor is frequently a perforated or sintered pipe. It is located just above

the bottom of the riser so that the liquid that passes around it and the ejected gas bubbles are distributed uniformly throughout the section.

4.3.6 Concluding remarks

Gaslifts have a number of advantages over bubble columns or mechanically stirred tanks. They are simple in design and contain no moving parts, and are therefore easy to maintain. Because of systematic circulation, gaslifts provide good homogeneity and temperature uniformity in the liquid, while preserving good mass transfer characteristics—an important factor in fermentation for example. Their operating range is also appreciably greater than that of bubble columns. Gaslifts are relatively economical and well suited for systems that require long liquid residence times, occasionally high gas flow rates, efficient heat transfer, and moderate, but especially uniform, turbulence.

4.4 PLATE COLUMNS

Commonly used for purely physical operations, such as distillation, absorption, or stripping, plate columns are less commonly used than packed columns for chemical reactions. Below we briefly describe how these reactors operate, then provide several correlations that can be used to calculate their principal characteristics.

4.4.1 General features

The general design of a plate column is shown in Fig. 4.7. The liquid, injected at the top of the column, falls by gravity into the downcomers and flows horizontally in a narrow (3 to 8 cm) liquid layer over each plate. For the column as a whole, liquid flow is countercurrent to the gas, which is introduced at the base of the column. The gas moves from plate to plate through orifices whose size and shape can vary considerably. Generally, the liquid descends from one plate to the next through downcomers located along the wall of the column or along the axis of very large-diameter columns. This arrangement is useful for limiting the thickness gradient of the liquid film between the liquid inlet and outlet, which can be appreciable in bubble-cap trays. The variation in thickness, caused by pressure drops across the plate, results in non-uniform flows of gas, which tends to pass through the thinnest layer of liquid.

A typical bubble-cap tray together with its downcomers is shown in Fig. 4.8. Obviously other designs are possible, but the tray in the illustration will be useful for specifying some typical dimensions used in the correlations. In the case of sieve trays, with or without valves, the overall geometry is generally the same. Sieve trays without a downcomer have operating ranges that are too narrow to make them useful as reactors [Trambouze *et al.*, 1988].

The transverse flow of liquid across the plate causes a change in composition between the plate inlet and outlet. This cross-flow circulation of liquid and gas is not uniform, which makes a detailed mathematical description especially complex. It is also often assumed that each plate behaves like a bubble column for both the gas and the liquid. Plate columns are then treated as a succession of N reactors in a cascade, N being equal to the number of plates.

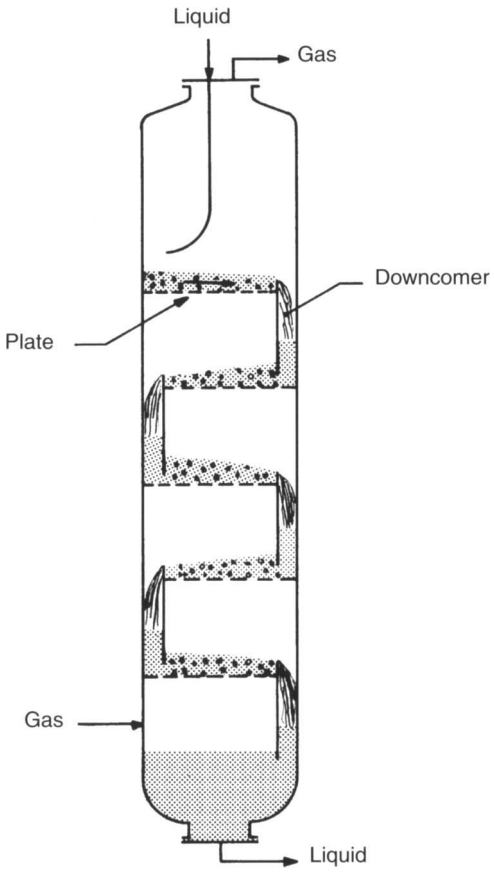


Figure 4.7 Sieve-plate column.

As a first approximation, the volume of gas between the plates is treated as an inactive, or dead, volume. In fact, in certain cases, such as those when gas velocities are high, this volume plays an important role because of the excellent gas-liquid contact provided by the droplet mist entrained by the gas as it crosses each liquid layer. In the case of a purely physical operation (absorption or distillation without chemical reaction), we often assume that the plate behaves as a fraction of a theoretical plate (concept of plate efficiency). This approach is not considered here.

4.4.2 Hydrodynamics

A detailed discussion of the design of this type of equipment is beyond the scope of this text, but there are a number of excellent presentations, including those by Gourlia and Trambouze [2000], Ptak *et al.* [1998], Cicile [1994], and Perry [1997]. A number of important characteristics are simple to calculate and are discussed below.

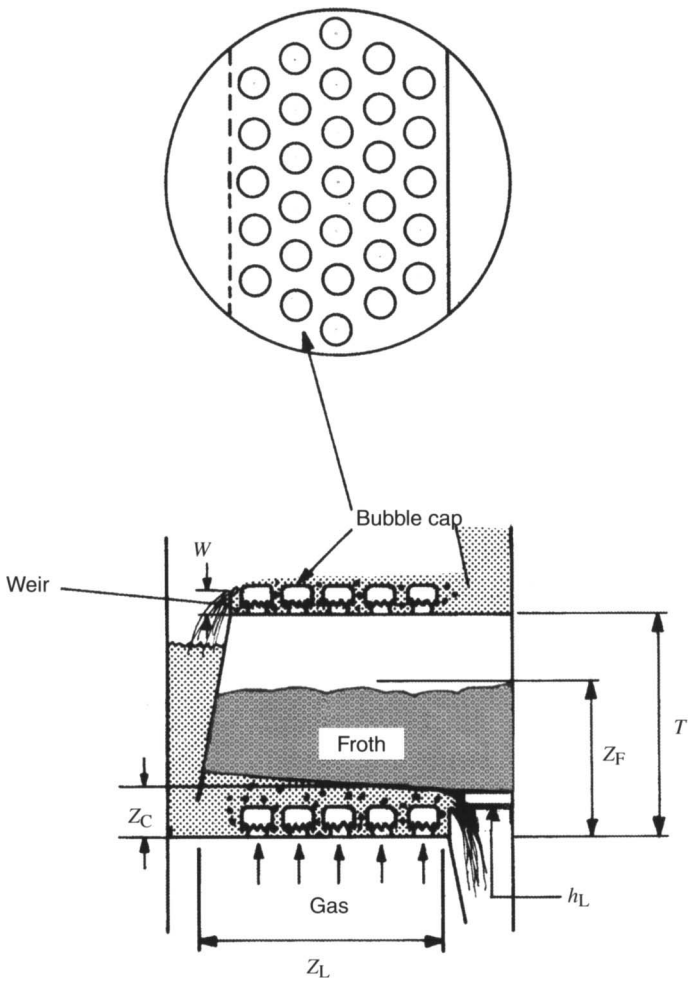


Figure 4.8 Bubble-cap tray column. Tray details.

4.4.2.1 Maximum gas velocity

Beyond a certain gas velocity $V_{SG\,max}$, mechanical entrainment becomes unacceptable. A careful correlation based on data cited by Trambouze *et al.* [1988] is written:

$$V_{SG\,max} = K\sqrt{\frac{\rho_L - \rho_G}{\rho_G}} \quad \text{m/s} \tag{4.54}$$

$$K = -0.052 + 0.33T - 0.28T^2$$

T being the distance between plates in m (between 0.3 and 0.9 m).

The equation provides increasingly satisfactory values the higher the surface tension and the greater the holdup on the tray.

4.4.2.2 Flooding

The choice of reactor cross-section and the design of downflow regions must be such that the hydrostatic head of the liquid in the downcomers balances the pressure losses in the gas phase. These depend on the hydrostatic column of liquid on the trays and pressure drops in the perforations. Construction details for the trays are of considerable importance. In the majority of configurations, there is a risk that foaming will cause premature flooding of the trays and downcomers. Column design does not take into account the effect of backmixing of the liquid on the plate except for large size trays.

Gourlia and Trambouze [2000] proposed a fairly detailed method for calculating tray characteristics.

One final remark concerns the use of plate columns as chemical reactors. In this case the calculation does not associate each tray with a fraction of a theoretical tray where the phases are in equilibrium. On the contrary, each tray is in this case considered to be a continuous stirred tank.

Under these conditions, liquid holdup must be high or low when the rate of the reaction is slow or fast, a factor that is not a part of classical models of plate-by-plate calculation. However, holdup can be an essential characteristic in the case of simultaneous absorption of two gases. It happens that the two gases (CO_2 and SH_2, for example) present similar solubility in the solvent (for example, alkanolamines in an aqueous solution) at equilibrium. Therefore, at equilibrium there is no selectivity. In terms of the kinetics, however, one of the gases (SH_2, in this example) can be absorbed under conditions of instantaneous absorption, while the other reacts much less quickly. To take advantage of this kinetic selectivity, it is critical that the liquid-gas system not reach equilibrium, a factor that will have a direct influence on column design. We return to this point in the following section.

4.4.3 Mass transfer

The interfacial area per volume of liquid present on the plate is approximately 100 to 500 m^2/m^3. Given the complexity of flow, there are a number of criteria that must be respected during the design phase. The majority of studies have examined purely physical contact and been interpreted in terms of efficiency [Cicile, 1994]. Nonetheless, some mass transfer correlations are possible, but they must be used with caution. They are useful for estimating orders of magnitude, but given the wide variety of designs for trays, downcomers, and orifices, general correlations are inaccurate. Those we have retained are shown in Table 4.4. The correlations by Nakoua *et al.* [1999] distinguish two regimes, a drop regime and a jet regime, and take into account the properties of the two fluids.

Tableau 4.4 Correlations for plate columns.

1. Bubble-cap trays

Coefficient of transfer

$$k_G = 3.64 V_{SG}^{0.25} Z_C^{0.5} \mathcal{D}_G^{0.5} \quad (\text{m/s})$$ Sharma *et al.* [1969] (4.55)

$$k_L = 4.11 V_{SG}^{0.25} Z_C^{-0.5} \mathcal{D}_L^{0.5} \quad (\text{m/s})$$ Sharma *et al.* [1969] (4.56)

Z_C being the height of the liquid on the plate, estimated by: Sherwood *et al.* [1975] (4.57)

$$Z_C = 4.04 \cdot 10^{-2} + 0.29W - 1.35 \cdot 10^{-2} F + 2.46 L' \quad (\text{m})$$

where

W height of the weir (m),

F factor $= V_{SG} \rho_G^{0.5} \left(\text{kg}^{0.5}\text{m}^{-0.5}\text{s}^{-1}\right)$,

L' specific discharge of the liquid $\left(\dfrac{\text{volume flow rate m}^3/\text{s}}{\text{width of weir (m)}}\right)$.

Interfacial area

$$\mathcal{A} = 240 V_{SG}^{0.5} Z_C^{-0.17} \quad (\text{m}^{-1})$$ Sharma *et al.* [1969] (4.58)

$\mathcal{A}$ being the interfacial area compared to the expanded volume of liquid retained on the trays (m^2/m^3)

$$\mathcal{A} = 2.45 (f/f_{max})^{0.28} \left[(\rho_L - \rho_G)\, g/\sigma\right]^{0.5} \quad \text{if } f/f_{max} \leqslant 0.1 \text{ (bubbling regime)}$$ (4.59)

$$\mathcal{A} = 1.6 (f/f_{max})^{0.28} \left[(\rho_L - \rho_G)\, g/\sigma\right]^{0.5} \quad \text{if } 0.1 < f/f_{max} < 0.65 \text{ (transition)}$$ Nakoua *et al.* [1999] (4.60)

$$\mathcal{A} = 2\left[1 - (f/f_{max})^{0.28}\right] f^2 \Phi^2 \sigma \quad \text{if } f/f_{max} \geqslant 0.65 \text{ (mist regime)}$$ (4.61)

where $f = U_G \sqrt{\rho_G}$ $\quad f_{max} = 2.5 \Phi^2 \sigma \left[(\rho_L - \rho_G)\, g\right]^{1.4}$

U_G gas velocity calculated for the active area of the tray (m/s)

Φ open fraction of the tray (−).

2. Sieve trays

$$1.5 \cdot 10^{-4} < k_L < 4.5 \cdot 10^{-4} \quad (\text{m/s})$$

$$2 \cdot 10^{-2} < k_G < 10^{-1} \quad (\text{m/s})$$

Calderbank [1959]

$$\mathcal{A} d_o = 0.38 \left(\frac{V_{SG}}{u_t}\right)^{0.775} \left(\frac{V_{SG} \rho_L}{n_t d_o \mu_L}\right)^{0.125} \left(\frac{g \rho_L d_o^2}{\sigma}\right)^{0.33}$$ Calderbank and Moo-Young [1961] (4.62)

$$\mathcal{A} = 250 V_{SG}^{0.5} \rho_G^{0.25} \quad (\text{m}^{-1})$$ Charpentier [1981] (4.63)

where

$\mathcal{A}$ interfacial area compared to the expanded volume of liquid retained on the trays (m^2/m^3)

u_t terminal velocity of bubbles (≈ 0.3 m/s)

n_t number of holes per unit surface

d_o diameter of orifices.

Comments

• Bubble-cap trays

The Sharma correlations cited by Trambouze *et al.* [1988] for k_G, k_L, and $\mathcal{A}$ require knowledge of the height Z_c, which is appreciably equal to the mean height of the liquid traversed by the gas along the tray. To estimate this value, the difference between the height of the weirs and the mid-height of the slits in the bubble caps is sometimes used.

• Sieve trays

Depending on the type of tray, the values of k_G are comprised between $2 \cdot 10^{-2}$ and 10^{-1} m/s and those of k_L between $1 \cdot 10^{-4}$ and $5 \cdot 10^{-4}$ m/s. For the coefficient of transfer k_L, correlations for bubble columns can be employed. For the interfacial area $\mathcal{A}$, with respect to the volume of the gas-liquid mixture alone, the customary values are comprised between 200 and 500 m^2/m^3, which is slightly greater than what we would expect in a bubble column. Since, in this case, the gas can only cross a limited thickness of liquid before being redistributed, this seems logical: during the gas's brief passage through the liquid, the chances of bubble coalescence are in fact reduced. A rather simple correlation suggested by Charpentier [1981] can be written as follows:

$$\mathcal{A} = 250 V_{SG}^{0.5} \rho_G^{0.25} \tag{4.63}$$

The maximum values of 800 m^2/m^3 for the gas-liquid mixture observed by Calderbank seem abnormally high and should be considered as upper limits for the correlation he provides. In the particular case of the absorption of CO_2 in amines, Kohl and Riesenfeld [1985] have proposed several specific correlations.

The values of $k_L\mathcal{A}$ and $k_G\mathcal{A}$ with respect to the volume of the dispersed gas-liquid medium are almost independent on the flow rates of the gas or liquid. In a review of the state of the art, Zuiderweg [1982] proposed, for two hydrodynamic regimes, a series of correlations that can be used to calculate pressure drops, holdup, axial mixing of the liquid, entrainment, and the mass transfer efficiency of the sieve trays. Table 4.4 summarizes the correlations for interfacial area and transfer coefficients.

4.4.4 Construction details

Figure 4.9 illustrates the most used types of trays. There are three fundamental designs:

- trays that incorporate a system of chimneys or a moving mechanical element to retain a layer of liquid on the tray, even when gas and liquid flow rates are very low
- sieve trays of varying design but with no liquid holdup at low flow rates
- extremely simple inclined baffle plates.

• The first group contains the oldest device of this type: the bubble-cap tray (Fig. 4.9A). Even though the contact performance and hydrodynamics of this type of tray are well known, its high price and relatively strong pressure drop limit its use to situations where liquid flow rates are low. The market is primarily dominated by valve trays (Fig. 4.9B), both ballasted and unballasted. These trays have the advantage of considerable flexibility with respect to gas and liquid flow rates. They are not as widely used when gas flow rates are high and there is relatively little liquid or if solid particles are present in the gas or liquid (there is a risk of accumulation on the tray and plugging of the valves).

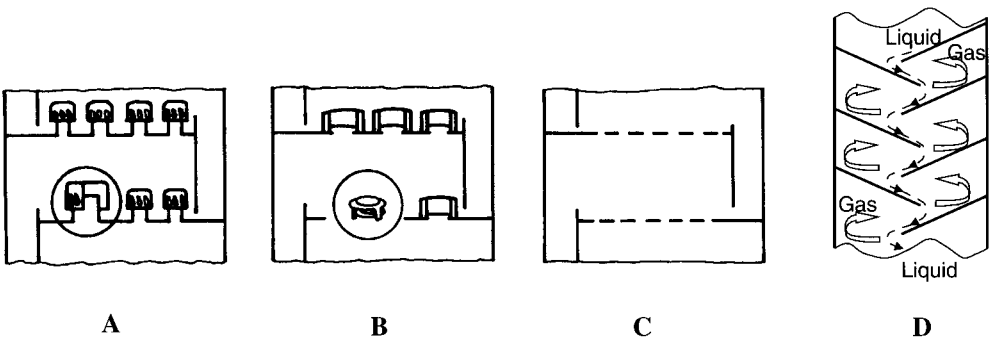


Figure 4.9 Various tray configurations. **A.** Bubble-cap tray. **B.** Valve tray. **C.** Sieve tray. **D.** Inclined baffle plate.

- Sieve trays (Fig. 4.9C) are very simple in design. The impact tray, a slightly more elaborate variant, is considered effective for fines removal accompanied by absorption for particle sizes up to 1 to 2 μm (flue gas scrubbers). These trays are particularly sensitive to level defects; the slope must be less than 0.5%, otherwise there is a risk the liquid will flow into the lower sections filled with liquid, while the gas traverses the thinnest layers of liquid in the upper part of the tray. To avoid enlargement of the holes and unequal gas-liquid contact, construction materials must be resistant to corrosion and erosion.
- Simple inclined baffle plates (Fig. 4.9D) are covered with a thin film of liquid that overflows the tray and flows downward in a liquid curtain. The gas passes through this curtain and atomizes the liquid as it rises from stage to stage. These trays have several advantages: they are very simple and inexpensive, they create almost no pressure drop and easily accommodate slurries. Precise levelling of the edge of the trays is essential. These trays, which are efficient for reactions, very fast heat exchange operations, or simple fines removal, sometimes have diameters greater than 6 m [Fair, 1993].

New and highly efficient trays for distillation equipment are periodically introduced by the major manufacturers (Koch and Norton, for example).

To avoid the entrainment of liquid droplets by the gas to the column outlet, demisters (grids, inclined plates) are arranged above the last tray (Fig. 4.10). At the bottom of the reactor, a vortex breaker is sometimes incorporated in the liquid drain tubing. These devices, made of two perpendicular flat plates are very efficient and inexpensive; unfortunately they also create an obstacle in the column and are used only for clean fluids. A number of construction details and design guidelines are provided in Gourlia and Trambouze [2000] and Kister [2003].

It is important to note that, in the case of gas scrubbing involving a fast chemical reaction (such as an acid-base reaction), the scrubbing solution is frequently recycled around one or more trays to achieve the liquid flow rates needed for good efficiency.

Sieve-plate contactors generally have the advantage of low pressure drop and allow better control of liquid residence time. This last point is especially important for reactions where kinetic selectivity during absorption is important. This is the case, for example, in the selective absorption of SH_2 in the presence of CO_2 in amines, as indicated above.

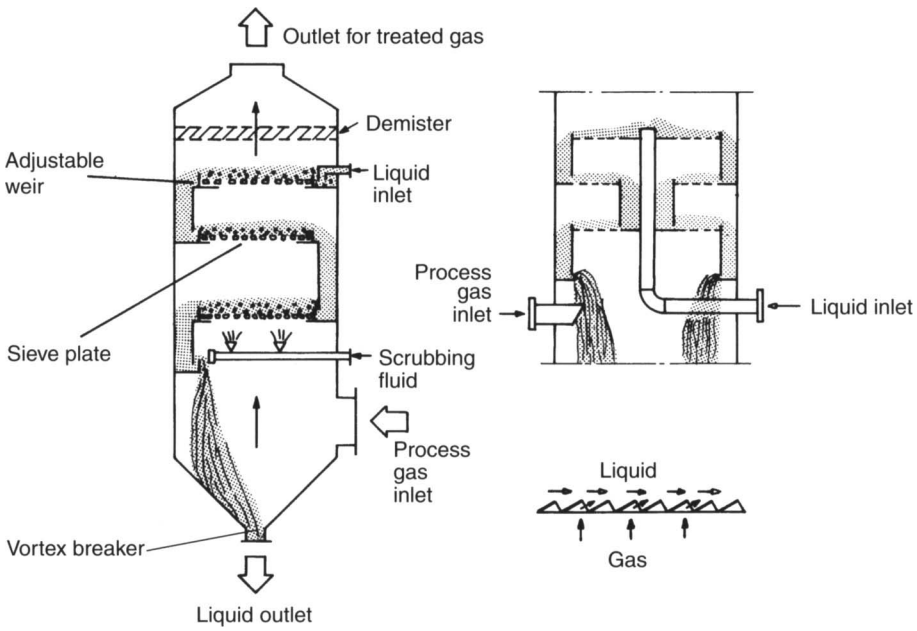


Figure 4.10 Plate absorbers.

4.4.5 Submerged plate reactors

A variant design involves flooding the plate reactor by filling it with liquid. This arrangement is practically identical to the bubble column equipped with horizontal perforated plates. The liquid flows downward in the column as the gas rises.

The space between two successive plates is treated as a small bubble column. The plates promote the systematic flow of fluids from one compartment to another without backmixing. This is especially true in the case of a gas that is regularly redistributed in the form of small bubbles. Sometimes, however, there is a risk the liquid will be subject to large convection currents, with backmixing if the flow rate is low or the perforations poorly adapted to the respective flow rates of the fluids. Again, a non perfectly horizontal plate can lead to preferential flows.

4.4.6 Concluding remarks

Gas-liquid reactors equipped with plates have the following characteristics:

- average gas holdup falls between bubble columns and packed columns
- no backmixing
- solids can be present
- fairly good mass and heat transfer
- considerable flexibility in flow rates

- relatively high capital investment
- not recommended where frothing occurs.

These plate reactors are especially well suited when reactions are realized under pressure or large-diameter tanks used. Liquid holdup is still considerable, although lower than it is in bubble columns. Consequently, plate columns can be used when the reaction does not occur only in the film. On the other hand, plate columns create efficient compartments, thereby avoiding the bypasses that are often present and harmful in bubble columns, poorly filled packed columns, or those that operate too far from the load point (see below). However, because of their fairly complex design, plate columns are more generally used for large-scale installations.

4.5 PACKED COLUMNS

4.5.1 General characteristics

The packed column is without doubt the simplest and most traditional gas-liquid contactor in use (see photo 3 on the next page). It consists of a column equipped with a support tray and fluid distributors, and is filled with packing [Copigneaux, 1993]. The packing, of which there are a great variety of types and sizes (see Fig. 4.11 for examples), is generally loaded in bulk in random fashion but can be arranged uniformly when large Raschig or Pall rings are employed. In recent years structured packing, prepared in cylinders or pre-sized blocks, has been used, arranged in systematic fashion within the column. The liquid trickles by gravity along the packing, after being distributed by means of a device located at the top of the column. The gas generally circulates countercurrent to the liquid, although cocurrent and cross-flow designs are also used. At the top of the column, any droplets of liquid are removed by a demister, often consisting of a woven metal blanket a few tens of centimeters in height.

Table 4.5 lists characteristic values needed for the correlations discussed below. The following definitions apply:

d_p nominal dimension of packing element as provided by the manufacturer
N number of elements dumped in bulk per unit volume
$\mathcal{A}_p$ specific area or external surface of the packing exposed to fluids per unit volume
ε void fraction between packing elements in the bed (where $\varepsilon = 1 - \varepsilon_p$)
F_p packing factor, which characterizes the difficulty of fluid to flow through the bed.

Comments:

F_p is in principle determined experimentally; otherwise it is assumed that $F_p = \mathcal{A}_p/\varepsilon^3$.
F_p is inversely proportional to the hydraulic capacity of the packed volume.

Some of these values vary somewhat depending on how the packing is arranged. This uncertainty is inherent in the relative arrangement of packing elements; it is a factor not only when determining experimental data but also applies to industrial units in their initial state, and even after months or years of service. Any correlations must take this uncertainty into account and, consequently, be used with caution.



Photo 3 Packed column used for gas treatment connected to the outlet of a Claus furnace (elimination of H_2S and SO_2 in the Clauspol process). Columns such as this are sometimes 10 m in diameter and 40 m in height.

(*IFP Photo Library: Clauspol 150*).

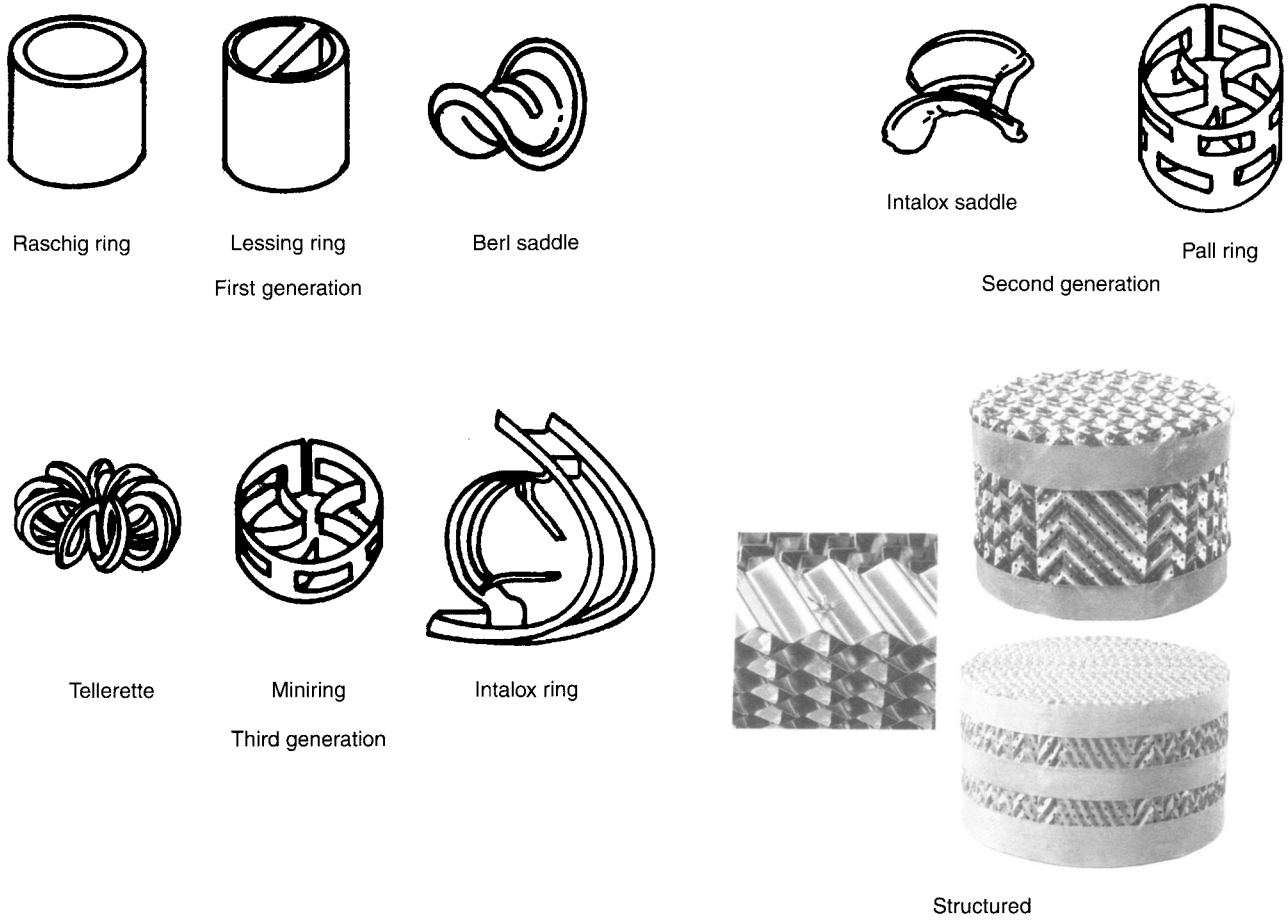


Figure 4.11 Different types of packing.

Table 4.5 Characteristics of packing elements.

	d_p (")	d_p (mm)	N	$\mathcal{A}_p$ (m^2/m^3)	ε (–)	F_p (m^2/m^3)	α	β
Ceramic Raschig ring	1/4"	6.3	3 000	800	0.70	3 300		
	1/2"	13.0	370	370	0.70	1 700	1 328	0.1
	3/4"	19.0	100	240	0.72	840		
	1"	25.0	48	200	0.73	525	292	0.045
	1 1/2"	38.0	15	130	0.75	310		
	2"	51.0	6	95	0.75	210	133	0.03
	3"	76.0	1.90	70	0.83	120	98	0.03
Metal Raschig ring	1/4"	6.3	3 000	800	0.82			
	1/2"	13.0	370	400	0.91	1 000	226	0.043
	3/4"	19.0	100	290	0.93	500		
	1"	25.0	48	210	0.93	380	159	0.04
	1 1/2"	38.0	15	140	0.94	280		
	2"	51.0	6	100	0.94	190	126	0.03
	3"	76.0	1.90	70	0.94	105		
Ceramic Pall ring	1"	25.0	46	220	0.73		193	0.033
	1 1/2"	38.0	18.50	165	0.76			
	2"	51.0	6	120	0.77		73	0.025
	3"	76.0	2.20	105	0.78			
Metal Pall ring	1/2"	13.0	200	370	0.93			
	1"	25.0	50	240	0.94	150	80	0.03
	1 1/2"	38.0	19	145	0.95	80	53	0.03
	2"	51.0	6	105	0.95	55	33	0.025
	3"	76.0	1.6	78	0.95			
Plastic Pall ring	1"	25.0	52	225	0.89	200	80	0.03
	1 1/2"	38.0	17	151	0.91	140		
	2"	51.0	6.8	111	0.92	90	33	0.025
Ceramic Berl saddle	1/4"	6.3	4 600	1 000	0.62	3 000		
	1/2"	13.0	620	480	0.65	1 250	664	0.04
	3/4"	19.0	195	300	0.67	560		
	1"	25.0	80	250	0.70	360	200	0.035
	1 1/2"	38.0	22	150	0.75	210	80	0.03
	2"	51.0	8.80	110	0.77	150		

Table 4.5 *(continued).*

	d_p (")	d_p (mm)	N	$\mathcal{A}_p$ (m^2/m^3)	ε (–)	F_p (m^2/m^3)	α	β
Ceramic Intalox saddle	1/4"	6.3	5000	985	0.62	2000		
	1/2"	13.0	630	480	0.73	870	571	0.04
	3/4"	19.0	210	300	0.73	430	266	0.035
	1"	25.0	85	250	0.74	320	226	0.033
	1 1/2"	38.0	23	160	0.74	170	73	0.03
	2"	51.0	8.80	110	0.75	120		
	3"	76.0	1.87	92	0.77	70		
Plastic Intalox saddle	1"	25.0	85	260	0.88	110	226	0.033
	2"	51.0	8.80	122	0.91	80		
Ceramic miniring	2"	51.0				190		
	3"	76.0				80		
Metal miniring	1"	25.0				113		
	2"	51.0				73		
	3"	76.0				46		
Plastic miniring	1"	25.0				90		
	2"	51.0				57		
	3"	76.0				40		
Plastic Tellerette	1"	25.0	36	190	0.92			

N: Number of elements per liter; $\mathcal{A}_p$: specific area;
ε: void fraction of bed; F_p: packing factor.

4.5.2 Hydrodynamics

4.5.2.1 Pressure drop and flooding

Pressure drop ($\Delta P/H$) in conventional randomly packed columns is about 300 Pa/m of packing. A general approach used to calculate pressure drop is the empirical formula proposed by Leva [1953, 1992]:

$$\frac{\Delta P}{H} = \alpha 10^{\beta L} \frac{G^2}{\rho_G} \quad \text{in Pa/m of packed height} \tag{4.64}$$

This formula, established for water and air, takes into account the type and size of packing by means of the two coefficients α and β, with the values indicated in Table 4.5.

To account for the properties of fluids, other equations are used, which are directly related to flooding characteristics. The conventional curves (Fig. 4.12) can be represented by correlations between π_1 and π_2, two dimensionless groups of variables (Table 4.6).

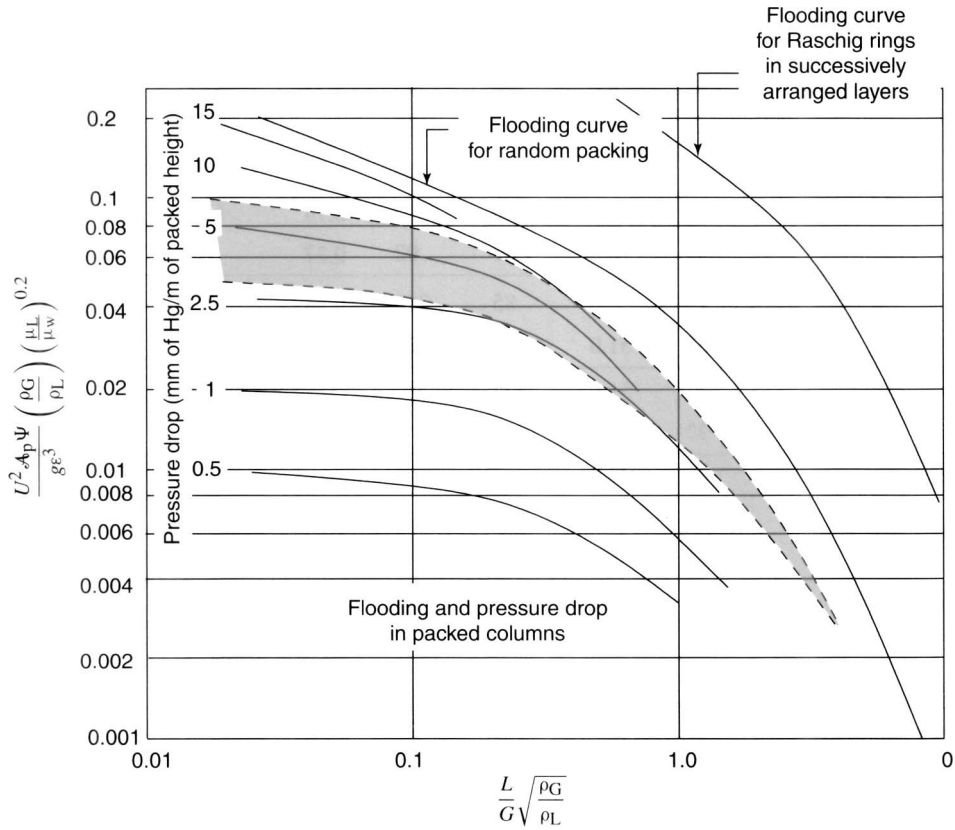


Figure 4.12 Countercurrent packed column: flooding curves.

These curves are also used to determine the operational superficial gas velocity V_{SG} in industrial columns. This superficial velocity is a fraction, on the order of 50 to 80%, of the velocity that causes flooding. In the correlation considered, this corresponds, for a given number π_2, to an actual number π_1 comprised between 0.3 and 0.7 times the number π_{1e}, which characterizes flooding. The calculated velocity can be used to determine the diameter of the column and estimate the pressure drop from correlation (4.68).

The correlations and curves accurately reflect the pressure drop measured with simple first-generation packings. For the highly varied second- or third-generation shapes that many manufacturers offer, it is advisable to adjust the coefficients with a few experimental data points.

Next Page

Table 4.6 Hydrodynamics of packed columns.

Flooding correlation

$$\pi_1 = \frac{F_P}{g}\frac{\rho_G}{\rho_L}\frac{\rho_w}{\rho_L}\left(\frac{\mu_L}{\mu_w}\right)^{0.2} V_{SG}^2 \tag{4.65}$$

and:

$$\pi_2 = \frac{V_{SL}}{V_{SG}}\sqrt{\frac{\rho_L}{\rho_G}} \tag{4.66}$$

where

F_P	packing factor (see Table 4.5)
ρ_w, μ_w	density, dynamic viscosity of water at 20°C
V_{SG}	superficial gas velocity
V_{SGe}	superficial gas velocity at flooding.

Flooding equation (that is, when $V_{SG} = V_{SGe}$)

$$\ln \pi_{1e} = 0.1117 - 4.012\pi_2^{0.25} \tag{4.67}$$

Pressure drop

$$\frac{\Delta P}{L} = \frac{98\pi_1}{\pi_{1e}}\left(A_1 + A_2\frac{\pi_1}{\pi_{1e}}\right) \quad \text{(Pa/m)} \tag{4.68}$$

$$A_1 = 21.79 - 36.19\pi_2^{0.25} + 16.60\pi_2^{0.5}$$

$$A_2 = 7.06 + 10.30\pi_2^{0.25} - 10.36\pi_2^{0.5}$$

The pressure drop at the flood point, on the order of 900 to 1 200 Pa/m, can also be estimated using the following simple formula proposed by Kister [1992]:

$$\left(\frac{\Delta P}{H}\right)_{\text{flooding}} = 41F_p^{0.7} \text{ (Pa/m)} \tag{4.69}$$

A first estimate of the maximum recommended flow rate for simple random packing is given in the following table.

d_p characteristic packing size (mm)	Maximum recommended liquid flow rate $(m^3/(m^2 \cdot s))$
25	0.03
51	0.05
87	0.085

Rocha *et al.* [1993] have proposed correlations that were confirmed for structured packings of the corrugated plate type.

Previous Page
Copyrighted Materials
Copyright © 2004 Editions Technip Retrieved from www.knovel.com

4.5.2.2 Minimum wetting rate

Although the superficial liquid velocity used is approximately 0.01 m/s, it must provide a minimum wetting of the packing without leading to flooding. To wet the entire packing surface, the superficial liquid velocity must exceed a threshold, the minimum wetting rate $(V_{SL})_m$. Below this value, the fraction of packing that is actually wetted is too low. This minimum liquid flow rate depends on the packing but falls within the following ranges:

- structured packing $0.07-0.2 \cdot 10^{-3}$ m^3/(m^2 · s)
- random packing $0.4-1.4 \cdot 10^{-3}$ m^3/(m^2 · s).

This rate decreases as the surface of the material is wetted by the liquid (contact angle, roughness, and aging of the material have an appreciable effect). Morris and Jackson established a relation that leads to a reasonable basis for avoiding excessive under-wetting conditions:

$$V_{SL} \geqslant 2.2 \cdot 10^{-5} \mathcal{A}_p \quad \text{(m/s) for packing elements smaller than 51 mm;}$$
$$V_{SL} \geqslant 3.3 \cdot 10^{-5} \mathcal{A}_p \quad \text{(m/s) for packing elements larger than 51 mm.}$$

Manufacturer data appears to indicate that lower values, obtained from an equation that involves a critical surface tension for each material, could be used (Table 4.8):

$$V_{SL} \geqslant 1 \cdot 10^{-6} \mathcal{A}_P \left(\frac{\sigma}{\sigma_c}\right)^2 \quad \text{(m/s)} \tag{4.70}$$

A margin of error is useful, however, to ensure consistent wetting in spite of fouling and the alteration of the surfaces of the packing elements over time.

4.5.2.3 Holdup

Liquid holdup is a useful characteristic when we intend to use the column as a chemical reactor in which a slow reaction takes place ($Ha < 0.3$). Generally less than 0.1, holdup has almost no dependence on the gas flow rate. Trambouze *et al.* [1988] provide a correlation for calculating holdup:

$$\varepsilon_L = 2.57 \left(\frac{d_p V_{SL} \rho_L}{\mu_L}\right)^{0.43} \left(\frac{d_p^3 g \rho_L}{\mu_L^2}\right)^{-0.37} (\mathcal{A} d_P)^{0.85} \tag{4.71}$$

where d_p is the characteristic size of the packing.

More recently, Mackowiak [1991] proposed a formula that is valid when operating at less than 65% of flooding conditions:

$$\varepsilon_L = \left[\mu_L^{0.33} \frac{V_{SL}}{d_p} \frac{1-\varepsilon}{\varepsilon^2}\right]^{0.5} \tag{4.72}$$

with the following limits:

$$d_p > 25 \text{ mm} \qquad 660 < \rho_L < 1\,260 \text{ kg/m}^3$$
$$1 < \mu_L < 14 \text{ cP} \qquad 2 < Re_L < 200$$

These correlations have been established globally for the oldest packing elements of simple design, made of ceramic for example. To obtain additional detail about the behavior of the liquid, we need to distinguish static holdup ε_{Ls}—which persists when the gas and liquid flow rates are cut—from dynamic holdup ε_{Ld}. For complex packing elements, which are becoming increasingly frequent in materials such as metal and plastic, the correlations are often imprecise. Raw data, similar to the data proposed by Billet [1995] in his excellent work on packed columns, are to be preferred. At the load point, he proposes the following equation:

$$\varepsilon_L = 2.3 Re^{-0.33} Fr^{0.33} \tag{4.73}$$

in which the dimensionless Reynolds (Re) and Froude (Fr) numbers are calculated with a length estimated from the specific area of the packing ($1/\mathcal{A}_p$).

4.5.2.4 Backmixing

It was generally felt that backmixing was relatively limited in packed columns and that its potential effect was accounted for by the correlations for gas-liquid transfer coefficients. A critical examination leads to the following conclusions:

The liquid Peclet numbers ($Pe_L = V_{SL} d_p / \mathcal{D}_{AL}$) fall between 0.1 and 0.5.

The gas Peclet numbers ($Pe_G = V_{SG} d_p / \mathcal{D}_{AG}$) fall between 1 and 5; axial mixing of the gas is therefore approximately 10 times less than that of the liquid.

For systems where a low packing height is sufficient for high conversion rates, the use of a plug-flow model for the calculations can result in a column height that is off by a factor of two (columns for which the calculations predict a height of only 0.2–0.3 m). The effects of poor liquid distribution can also be the source of a considerable increase in bypass, resulting in performance losses similar to those caused by backmixing. Distributor design is therefore very important.

4.5.3 Mass transfer

Compared to what we have examined until now, the best estimates we have are those for mass transfer in packed columns. In fact, we can assume the correlations in Table 4.7 to be valid to approximately 20–30%. The numerical values needed for the equations in Table 4.7 are given in Tables 4.5 on page 244 and 4.8 on the next page.

Correlations for $k_L\mathcal{A}$ take into account the effects of backmixing under the experimental conditions for which they have been established. Their precision can decrease appreciably under different conditions, however, especially for superficial liquid velocities, V_{SL}, that are outside the conventional range (0.5–2 cm/s).

A few words of comment are needed, especially with respect to interfacial area. It has been found experimentally that not all the gas-liquid interface is active for mass transfers: the stagnant zones, where the reactant is exhausted and the solvent saturated by the gaseous compound, are inactive. It is obvious that a solution rich in a coreactant will be less affected by this exhaustion, which means the active interfacial area can differ considerably from one

Table 4.7 Packed columns: mass transfer correlations.

$$\frac{k_G}{\mathcal{A}_P \mathcal{D}_G} = 5.23\,(\mathcal{A}_P d_P)^{-2}\left(\frac{V_{SG}\rho_G}{\mu_G \mathcal{A}_P}\right)^{0.7}\left(\frac{\mu_G}{\rho_G \mathcal{D}_G}\right)^{0.5} \tag{4.74}$$

$$\frac{k_L}{\mathcal{A}_P \mathcal{D}_L} = 0.0051\,(\mathcal{A}_P d_P)^{0.4}\left(\frac{V_{SL}\rho_L}{\mu_L \mathcal{A}_P}\right)^{1.33}\left(\frac{\mu_L}{\rho_L \mathcal{D}_L}\right)^{0.5}\left(\frac{V_{SL}^2 \mathcal{A}_P}{g}\right)^{-0.33} \tag{4.75}$$

$$\mathcal{A} = \mathcal{A}_P\left\{1 - \exp\left[-1.45\left(\frac{\sigma_c}{\sigma}\right)^{0.75}\left(\frac{V_{SL}\rho_L}{\mu_L \mathcal{A}_P}\right)^{0.1}\left(\frac{V_{SL}^2 \rho_L}{\sigma \mathcal{A}_P}\right)^{0.2}\left(\frac{V_{SL}^2 \mathcal{A}_P}{g}\right)^{-0.05}\right]\right\} \tag{4.76}$$

where

$\mathcal{A}$ interfacial area (m^2/m^3 of bed)

$\mathcal{A}_P$ geometric area of packing (theoretical m^2/m^3 of bed)

d_P characteristic dimension of packing

σ_c critical surface tension (see Table 4.8).

Minimum wetting rate

$$V_{SL} \geqslant 1 \cdot 10^{-6} \mathcal{A}_P \left(\frac{\sigma}{\sigma_c}\right)^2 \quad \text{(m/s)} \tag{4.77}$$

Table 4.8 Critical surface tension, σ_c for different packing materials.

Material	σ_c (mN/m)
Steel	71
Carbon	56
Unglazed ceramic	61
Oxidized or treated metal	75
Polished metal	35
Paraffin	20
Polyethylene or polypropylene	33
PVC	40
Glass	73

reaction to another since physical absorption is generally highly sensitive to the existence of stagnant zones. Joosten and Danckwerts, cited in Trambouze *et al.* [1988], have introduced the parameter γ to characterize this phenomenon, γ being the ratio between the increase in the absorption capacity of the liquid and the acceleration of the rate of absorption, both effects being due to the chemical reaction.

Interfacial areas determined using reactions where $\gamma \gg 1$ will give values that are too high and unusable, especially in the case of physical absorption.

4.5.4 Unconventional packed columns

An excellent review [Charpentier, 1976] of the behavior of bubble columns referred to two unconventional uses of packed columns: flooded packed columns and high-throughput columns with downward cocurrent flow. Later, in the nineties, new industrial uses were found for packed columns in reactive distillation operations (the topic is discussed in Chapter 10). Here, we briefly examine these three types of packed columns.

4.5.4.1 Flooded packed columns

Bubble columns are cheap and efficient gas-liquid contactors (see above). Their principal drawback is the considerable backmixing found in them. To overcome this, packing was introduced, transforming the bubble column into a flooded packed column with upward cocurrent flow. Packing with a very high void fraction (Pall rings) is the most efficient. Its presence normally does not increase $k_L\mathcal{A}$ or $k_G\mathcal{A}$. Their values depend primarily on the hydrodynamic regime:

- in the bubble regime ($V_{SG} \leqslant 0.05$ m/s) $k_L\mathcal{A}$ remains appreciably constant and equal to 0.15 s^{-1}
- in the intermediate regime ($0.1 < V_{SL} < 0.2$ cm/s) $k_L\mathcal{A}$ is proportional to $V_{SG}^{0.5}$
- under high-throughput conditions, the influence of the specific energy input is taken into account by the following formula:

$$k_L\mathcal{A} = 0.017\frac{\mathcal{P}}{V_L}\left(\frac{\mathcal{D}_L}{2.4 \cdot 10^{-9}}\right)^{0.5} \tag{4.78}$$

The interfacial area increases with the surface of the packing, the gas velocity, and the pressure. The correlations developed for irrigated packed columns, for example by Midoux *et al.* [1984], can be used to estimate interfacial area with a precision of approximately 60%. Scale-up from results obtained with a small column appear to be correct [Molga and Westerterp, 1997].

4.5.4.2 High-throughput downward cocurrent operation

The operation of a packed column with downward cocurrent flow provides values for the coefficient of transfer and interfacial area that are very similar to those obtained for countercurrent flow, as long as the liquid trickles through the packing (trickle-flow operation). However, during downward cocurrent flow, flooding is not a problem, which means the reactor can operate at specific flow rates that are much greater than those possible during countercurrent operation. At these flow rates, other flow regimes (pulsed and mist) appear. Under these conditions, the values of the transfer parameters are considerably higher, but at the cost of increased pressure drop, with the attendant consumption of energy.

This type of flow occurs most frequently in heterogeneous catalytic reactors, those with particles between 1 and 6 mm in diameter. (This topic is covered in Chapter 8.) However, some authors have examined these operating conditions using conventional packing elements [Trambouze *et al.*, 1988]. Although definitive correlations may not be available, Charpentier

[1976] suggests using Reiss's [1967] equations (for regimes other than trickle-flow):

$$k_L\mathcal{A} = 0.017E_L^{0.5} \qquad \text{where} \quad E_L = \left(\frac{\Delta P}{L}\right)_{LG} V_{SL} \tag{4.79a}$$

$$k_G\mathcal{A} = 2.0 + 0.1E_G^{0.66} \quad \text{where} \quad E_G = \left(\frac{\Delta P}{L}\right)_{LG} V_{SG} \tag{4.79b}$$

E_L and E_G are terms for the dissipation of energy, expressed in W/m^3 of column, if $(\Delta P/L)_{LG}$ is expressed in Pa/m and V_S in m/s. The values of $k_L\mathcal{A}$ and $k_G\mathcal{A}$ obtained are very high (for example, values of $k_L\mathcal{A} > 1$ s^{-1}), which is difficult to realize in other gas-liquid contactors. However, even if the value of $k_L\mathcal{A}$ depends only on $(\Delta P/L)_{LG}$ and V_{SL}, the corresponding power input is equal to:

$$E_T = \left(\frac{\Delta P}{L}\right)_{LG} (V_{SL} + V_{SG}) \tag{4.80}$$

Figure 4.13 shows Reiss's [1967] equation, together with some experimental results. The input of specific energy, plotted on the abscissa, corresponds only to the energy introduced by the liquid.

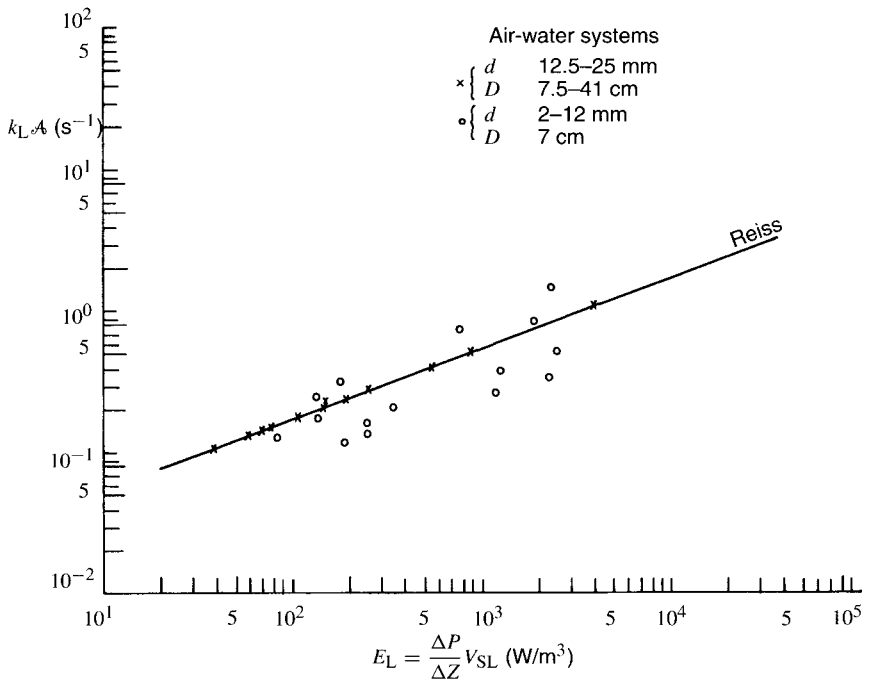


Figure 4.13 Packed columns: Transfer coefficient (downward cocurrent flow).

Because the energy introduced by the gas is systematically on the order of 5 to 10 times greater, the total energy input is itself on the order of 5 to 10 times greater. We can also obtain values of $k_L\mathcal{A}$ of 0.5 s^{-1} for $E_L = 800$ W/m^3. If we accept a value of $k_L = 4 \cdot 10^{-4}$ m/s, this

corresponds to an interfacial area of 1 250 m^2/m^3. Taking E_T to be eight times greater than E_L, we find that $E_T = 6\,400$ W/m^3. This result is comparable to the result obtained using Reith's correlation for agitated reactors (Fig. 4.5):

$$\mathcal{A} = 3.2\left(\frac{\mathcal{P}}{V}\right)^{0.69} \cong 1\,400 \text{ m}^2/\text{m}^3 \text{ of reactor} \tag{4.81}$$

It appears that this operation can be used to design a compact reactor with high transfer efficiency, but in terms of energy, one whose performance is comparable to that of other equipment.

4.5.4.3 Reactive distillation columns

If a liquid and gas flow countercurrently through a packed column, the packing surface improves mass transfer for chemical reactions and distillation alike, but is especially favorable for the immediate offtake of reaction products. If temperature and pressure conditions are carefully chosen, this local coupling of reaction and distillation can be used to shift chemical equilibria and appreciably increase the conversion obtained.

Moreover, certain types of packing can be impregnated with active substances and play a catalytic role in the chemical reaction (catalytic reactive distillation). This is particularly the case with alkylation, esterification, and etherification reactions that take place on an industrial scale. Random or structured packings in various shapes are used. The conventional characteristics and guidelines for sizing packings (pressure drop, flooding, load point, holdup, transfer coefficients, etc.) are generally applicable. Under certain conditions, specific correlations must be used, based most often on experimental results for the case under consideration. These columns, filled with packing and operating under conditions of countercurrent fluid flow, provide an attractive alternative to three-phase cocurrent-flow reactors.

4.5.5 Selection criteria and construction details

Packed columns are devices with low liquid holdup. They are therefore used primarily for absorption accompanied by fast chemical reactions. Consequently, values for the interfacial area are critical. Design parameters and operating conditions have little effect on the transfer coefficients (k_L and k_G). In itself holdup is not an important parameter when designing these devices. The selection of the packing is, therefore, influenced by its compatibility with operating conditions (temperature, corrosion, etc.) and especially by the cost per square meter of exchange surface actually available and the cost of the shell and the various structural elements.

The nominal size of packing elements should result from a compromise between smaller elements, which promote the efficiency of mass transfer, and the largest elements, which increase the capacity of the column and reduce the pressure drop. In practice recommended packing diameters are less than 1/10 and usually 1/20 of the diameter of the column, to avoid bypass at the wall. Generally, the most economical sizes range from 19 to 38 mm (3/4" to 1 1/2"). Under 19 mm (3/4"), capacity is reduced because of pressure drop and the risk of flooding, while the effective surface has a tendency to decline; over 51 mm (2"), the interfacial area is too small, which increases the cost of the column.

Given the wide variety of existing models, the most efficient packing elements will be those with a high void fraction to limit pressure drop and a large extended surface to promote the formation of droplets.

Structured packing is most often employed when an existing column is revamped because of its superior performance, higher efficiency, and lower pressure drop [Kister *et al.*, 1994; Bravo, 1997], even though it is more expensive than random packing. In general, we can conclude that:

- Plastic packing elements have effective interfacial areas that are approximately half that of the corresponding ceramic models when polar liquids are involved (frequent in the case of absorption with chemical reaction). For hydrocarbons, this is not an impediment. Aside from this particular drawback, plastic packing has a number of advantages:
  - because elements can have thin walls and are therefore highly aerated (Pall rings, minirings, Tellerettes), the resulting pressure drop is very low
  - very lightweight, which reduces the cost of the column structure
  - resistant to shock
  - inexpensive
  - easy to load

  and a number of disadvantages:
  - limited chemical and heat resistance
  - low resistance to crushing.
- Metal elements (essentially stainless steel) are less subject to wetting than ceramic elements but better than plastic; they have good mechanical characteristics and high resistance to corrosion. Because of their thin-wall design, they are lightweight and highly aerated (Multiknit wire mesh, for example), but more expensive than ceramic elements, even when the savings in shell construction are taken into account. Preferred designs include Pall rings, minirings, and more complex—and also more expensive—packing elements from Sulzer and Multiknit, intended primarily for reduced-pressure operations.
- Ceramic packing (especially unglazed) is less expensive and has the best ratio of effective area to geometric area. The least expensive shapes are those obtained by extrusion (Raschig rings, Intalox saddles) and, of these, Intalox saddles are by far those with the best characteristics (flooding, operational flexibility[1], etc.).
- The behavior of Tellerette and Spiralpac packing seems to be quite different from the other types. The interfacial area is developed at the points of contact between the different threads that constitute the packing element, these threads being highly entangled. Therefore, it is no longer the geometric support strictly speaking that forms the interfacial area. The good performance obtained depends more on fluid properties than it does for other packing types.

Liquid distribution must be very carefully implemented [see Klemas and Bonilla, 1995], at least 50 to 100 identical wetting points per square meter being needed. The distribution plate must be perfectly horizontal (for a diameter, a maximum allowable deviation from the horizontal of 5 to 10 mm). Moreover, the distribution plate must be placed in the immediate

1. Flexibility: ratio between maximum and minimum possible flow rates with acceptable performance.

proximity of the upper surface of the packing (within approximately 0.2 m). If preferential paths are created by non-horizontal distribution plates and poor design of the network of downcomers or perforated tubes, these will persist in the column. Figure 4.14 provides examples of distribution plates for packed columns.

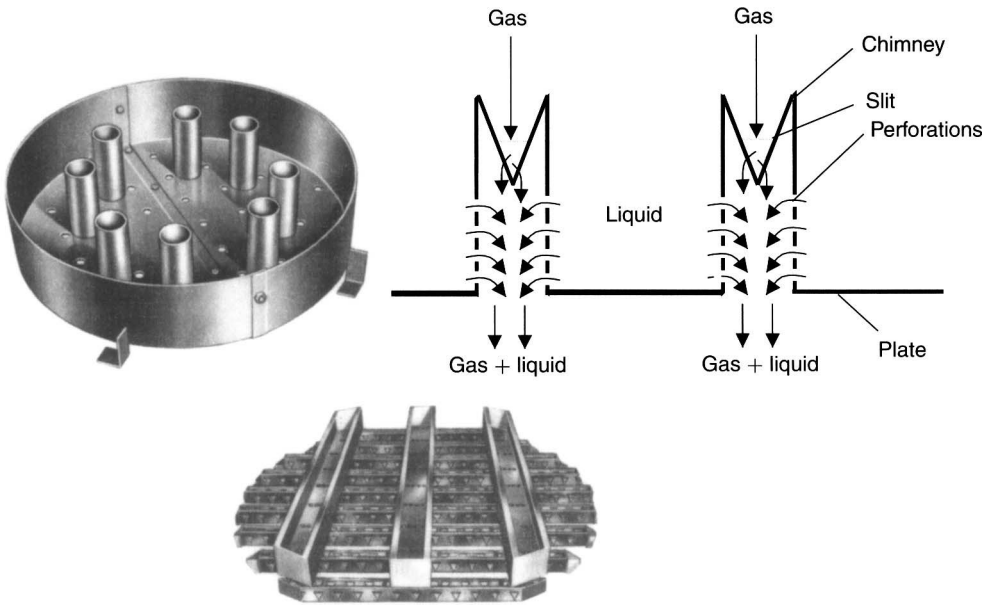


Figure 4.14 Packed columns: distribution trays.

On the other hand, there seems to be little necessity in devoting additional effort to gas distribution. The packing will handle gas distribution except when the bed height is low or gas flow rates are very low.

The accumulation of liquid at the wall, a phenomenon that is well known and results from the failure to reflect liquid streams at that point, is harmful only for narrow columns (< 2 m). In these cases, the liquid should be redistributed from time to time through the use of redistributors (Fig. 4.15). Generally, a height between redistributors of 5 to 6 times the column diameter—but sometimes as little as 2.5 to 3 meters—is used. Intermeshed packing (Tellerette) and, to a lesser extent, Intalox saddles, are less subject to this phenomenon.

4.5.6 Comparison of plate columns and packed columns

The following points are relevant when choosing between a plate column and a packed column:

- Pressure drop: Pressure drop in a packed column is lower, which gives it a clear advantage when columns are at atmospheric pressure or under vacuum.

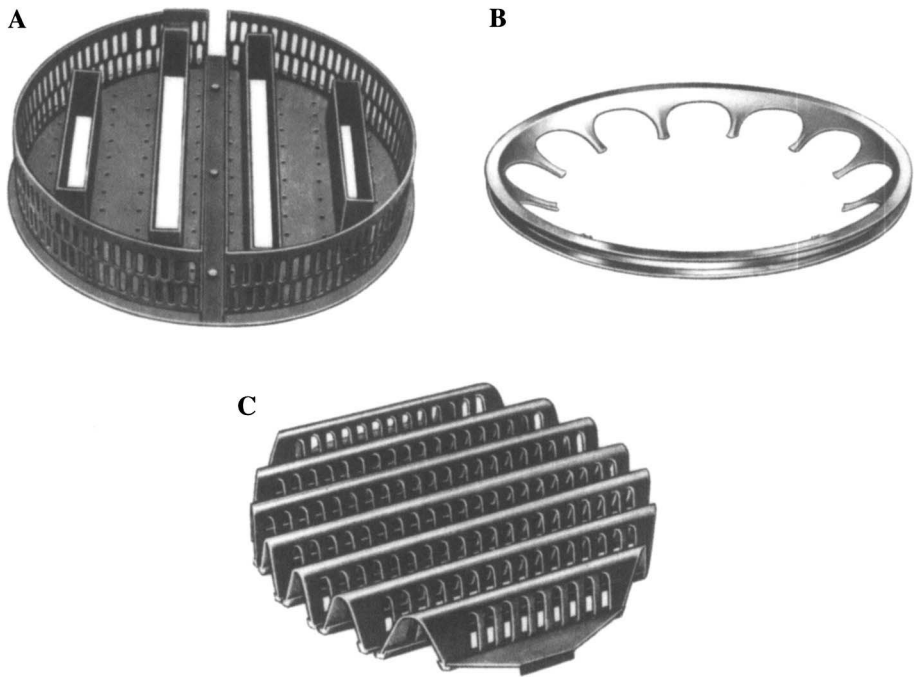


Figure 4.15 Packed column internals: **A.** and **B.** Redistribution trays. **C.** Support tray at the base of the column.

- Cost: For columns whose diameter is less than 1 m, random, and or even structured, packings are generally less expensive. Above this diameter the plate column is generally less expensive, but if the flow factor π_2 is low ($\pi_2 = (V_{SL}/V_{SG})\sqrt{\rho_L/\rho_G} < 0.1$), a packed column may still be viable, whereas if $\pi_2 > 0.2$, a plate column will be less costly.
- Performance: Better control of bypass and backmixing is possible in a plate column. Because holdup is different the plate column can still be used for reactions that take place partially in the liquid phase, which is not the case for a packed column.
  A plate column with downcomers is extremely flexible. On the other hand, a packed column that operates too far from its flood point must be very uniformly wetted to avoid gas phase bypass.

4.5.7 Concluding remarks

Countercurrent or cocurrent packed columns are characterized by the following:

- well suited to narrow-diameter columns (< 0.40 m)
- low liquid holdup
- lack of flexibility, especially when liquid flow is countercurrent
- flow nearly resembles plug flow

Table 4.9 Comparison between plate columns, packed columns, and their variants.

Criterion	Plate columns		Packed columns	
	Perforated or valve	Bubble-cap	Random	Structured
Efficiency	2	2	2	3
$P < 10$ kPa	2	1	2	3
P medium	3	2	2	1
$P > 1$ MPa	3	2	2	0
Low liquid flow rate	1	3	1	3
High liquid flow rate	2	1	3	0
Low liquid holdup	1	1	2	3
Low pressure drop	1	0	2	3
Heat control	2	2	1	1
Flexibility (1)	1	2	1	3
Foaming system	2	1	3	0
Solids present	1	1	1	0
Viscous liquid	2	1	3	0
Corrosive fluids	2	2	3	2
Multiple inlets or outlets	3	3	1	0
Low cost	2	1	3	1
Column diameter < 0.5 m	2	1	3	2
Column diameter > 1 m	3	2	2	2

0: not recommended, 1: problematic, 2: typical, 3: recommended.

(1) Flexibility: ratio between the maximum and minimum flow rates possible with acceptable performance.

- good mass transfer
- poor heat transfer
- not recommended when solids are present
- well suited to corrosive media
- performance affected by distribution quality
- simple and inexpensive construction in terms of investment, operation, and maintenance.

These characteristics help explain the large number of implementations of gas-liquid reactors and the amount of research that has been devoted to them. The basic studies include works by Danckwerts [1970], Charpentier [1981], Copigneaux [1993], Cicile [1994], Dudukovic *et al.* [1995], Gourlia and Trambouze [2000].

4.6 FALLING FILM REACTORS

Thin-layer devices, although generally designed for physical operations such as distillation, absorption, and stripping, have specific characteristics that can be put to good use in chemical reaction engineering.

4.6.1 General characteristics

Whether a simple falling film or one stirred by a rotor, these devices can be described as follows (see Fig. 4.16):

- flow from top to bottom of a liquid phase in the form of a thin film along a vertical wall, generally the internal wall of a cylindrical tube
- flow from a gas phase in the center of the tubes (downward or upward)
- possible heat transfer between the liquid film and the wall
- possible mass transfer at the gas-liquid interface.

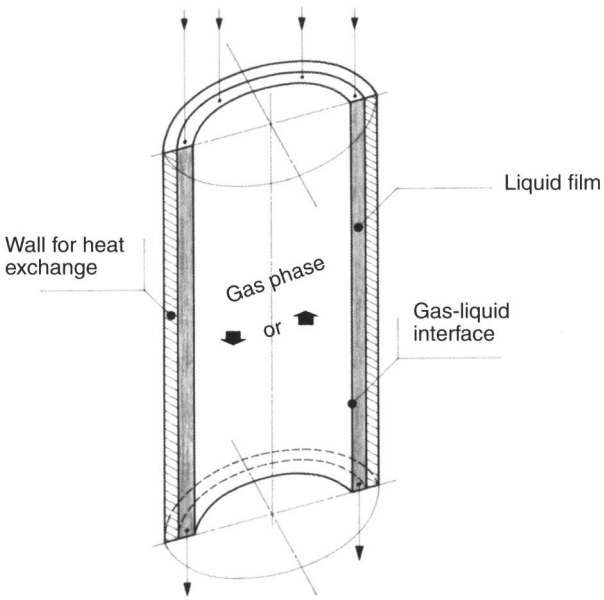


Figure 4.16 Principal features of a thin-film reactor.

A falling film unit can be used as a continuous reactor for:

- homogeneous liquid-phase reactions (the gas phase plays no role)
- heterogeneous gas-liquid reactions
- heterogeneous gas-liquid-solid reactions in the presence of a suspended catalyst (slurry).

To provide a better idea of how these devices are used, we describe below some of their characteristics and typical applications when used as reactors.

Liquid-phase flow occurs in a thin film along an interior or exterior wall of a tube. It is important, therefore, to know the thickness of the film, the mean flow velocity, and its structure (velocity profile). With this information we can calculate the capacity of falling film devices, liquid holdup, mean residence time, and residence-time distribution. Specifically, at this point, we need to distinguish between the following types of equipment:

- simple falling film device
- agitated falling film device.

In the first case, liquid flow is the result of gravity alone, while in the second case, shear forces, due to the rotation of a rotor whose blades spin very near the wall, are superimposed on gravitational forces.

4.6.2 Hydrodynamics

4.6.2.1 Falling film

Flow is characterized by a Reynolds number, defined as:

$$Re_L = \frac{\bar{u} e \rho_L}{\mu_L} \tag{4.82}$$

where

$\bar{u}$ mean velocity of the liquid

e thickness of the liquid film

ρ_L and μ_L respectively, the density and viscosity of the liquid.

Different flow regimes are observed depending on the value of Re_L:

$$\begin{aligned} Re_L &\leqslant 25 && \text{laminar regime} \\ 25 < Re_L &< 400 && \text{transition regime} \\ Re_L &\geqslant 400 && \text{turbulent regime} \end{aligned}$$

The thickness of the liquid film often fluctuates because of the presence of ripples or waves that form surface undulations. However, to reflect the influence of the properties of the system and the liquid flowrate, a mean value for the thickness can be calculated using the following formula:

$$e = A \left(\frac{3\mu_L^2}{g\rho_L^2} \right)^{0.33} (Re)_L^B \tag{4.83}$$

where the values of the coefficients A and B are a function of the Reynolds number Re_L, as indicated below:

Re_L	A	B
< 100	1	1/3
100 to 420	0.93	1/3
> 420	0.37	1/2

The film thickness varies due to surface ripples between a minimum e_m and a maximum e_M. The difference between e_m and e_M increases with the Reynolds number in such a way that the ratio e_M/e_m can vary between 3 and 10. The mean velocity $\bar{u}$ of liquid flow is then calculated from the volume flow rate Q_L and the length L of the downcomer or wetted perimeter:

$$\bar{u} = \frac{Q_L}{eL} \tag{4.84}$$

In the case of n parallel tubes of diameter d, we have: $L = n\pi d$.

Because of the velocity profile between the wall (where the velocity is very low or even zero) and the gas-liquid interface, where the velocity is a maximum (u_M), there is a relatively large residence time distribution. In the laminar regime $u_M/\bar{u} = 1.5$, while in the turbulent regime this ratio decreases and tends to 1.15. In practice liquid flow is most often treated as plug flow.

Table 4.10 lists the orders of magnitude obtainable in practice for the various parameters. Note that the use of simple falling films is generally recommended only for liquids whose viscosity is less than 1.5 Pa · s.

Table 4.10 Flow characteristics in thin-film devices.

	Falling film	**Agitated film**
Film surface (m^2)	0.1 to 100	0.1 to 25
Diameter of tubes (m)	5 to $6 \cdot 10^{-2}$	$2 \cdot 10^{-2}$ to 1.25
Number of tubes	1 to 60	1
Height of apparatus (m)	1 to 10	1 to 10
Mean residence time (s)	5 to 100	5 to 600
Film thickness (mm)	0.2 to 6	1 to 8
Specific flow rate (Q_L/L) ($m^3/h \cdot m$)	0.2 to 4	0.2 to 4.5
Liquid holdup (m^3)	$0.2 \cdot 10^{-3}$ to 0.5	$0.2 \cdot 10^{-3}$ to 0.2
Acceptable viscosity (Pa · s)	< 1.5	< 2000

4.6.2.2 Agitated film

Here the flow is much more complex and less well known than for falling films. The rotor blades create a circular movement and the resulting flow assumes a helical trajectory. At the same time, the resulting turbulence completely destroys the velocity profiles observed for falling films, which reduces the spread of the residence time distributions and increases their mean value. Consequently, film thicknesses are slightly greater. Table 4.10 provides orders of magnitude for these parameters.

With respect to residence time distribution, we can characterize flow by means of a Peclet number ($Pe = \bar{u}H/\mathcal{D}_A$), corresponding to axial turbulent diffusion ($\mathcal{D}_A$) superimposed on plug flow. The experimental results lead to values of the Peclet number between 3 and 100. This Peclet number decreases as residence time increases, especially when the increase occurs through the use of a retaining ring.

Whenever flow occurs in a tube under turbulent conditions, the Peclet[1] numbers observed are greater than 20. This means that, in general, in an agitated thin-film device, flow is similar to plug flow or a series of at least five continuous stirred tanks.

1. In this case we also make use of the term Bodenstein number, *Bo*.

4.6.3 Mass transfer

4.6.3.1 Interfacial area

In either case (falling film or agitated film) we can consider the interfacial area equal to the surface of the tube in which the thin film is formed. We can then write, for an interfacial area per unit volume of reactor $\mathcal{A}$:

$$\mathcal{A} = \frac{4\pi d}{\pi d^2} = \frac{4}{d} \quad (\mathrm{m}^2/\mathrm{m}^3) \tag{4.85}$$

Although this characteristic value can be used to make a straightforward comparison with other types of gas-liquid reactors, it is also useful to know, for thin-film devices, the interfacial area per unit volume of liquid, that is $\mathcal{A}_\mathrm{L}$:

$$\mathcal{A}_\mathrm{L} = \frac{\pi d}{\pi d e} = \frac{1}{e} \quad (\mathrm{m}^2/\mathrm{m}^3) \tag{4.86}$$

Given the irregularities of the film surface, the actual interfacial area is always somewhat greater than the geometric surface calculated above; nonetheless, this increase in surface area is in general low. Because we can obtain relatively precise knowledge of the interfacial area, falling film devices are used for studying gas-liquid reactions [Trambouze *et al.*, 1988].

4.6.3.2 Gas-phase transfer coefficient

The gas-phase transfer coefficient is somewhat dependent on the rates of circulation of the liquid and the gas. To calculate $k_{i,\mathrm{G}}$ we can, for example, make use of the dimensionless formulas given in Trambouze *et al.* [1988]:

- For countercurrent operation (gas flows upward):

$$Sh_{\mathrm{CC}} = 0.013(Re)_\mathrm{G}^{0.75}(Re)_\mathrm{L}^{0.16}(Sc)_\mathrm{G}^{0.44}\left[1 + 5.2\left(\frac{H}{d}\right)^{-0.75}\right] \tag{4.87}$$

- For cocurrent operation (gas flows downward):

$$Sh_{\mathrm{CoC}} = 0.015(Re)_\mathrm{G}^{0.4}(Re)_\mathrm{L}^{0.16}(Sc)_\mathrm{G}^{0.44}\left[1 + 6.4\left(\frac{H}{d}\right)^{-0.75}\right] \tag{4.88}$$

where:

$$(Sh)_\mathrm{G} = \frac{k_{i,\mathrm{G}} d}{\mathcal{D}_{i,\mathrm{G}}} \quad \text{(gas Sherwood number)}$$

$$(Re)_\mathrm{G} = \frac{4Q_\mathrm{G}\rho_\mathrm{G}}{\pi d \mu_\mathrm{G}} \quad \text{(gas Reynolds number)}$$

$$(Re)_\mathrm{L} = \frac{Q_\mathrm{L}\rho_\mathrm{L}}{\pi d \mu_\mathrm{L}} \quad \text{(liquid Reynolds number)}$$

$$(Sc)_\mathrm{G} = \frac{\mu_\mathrm{G}}{\rho_\mathrm{G}\mathcal{D}_{i,\mathrm{G}}} \quad \text{(gas Schmidt number)}$$

In the case of agitated films, we have no access to experimental values. Therefore, the formulas given below must be used with caution, given the fact that they were obtained with a tube 0.04 m in diameter. The resulting Sh value should be corrected by multiplying by a factor equal to $d/0.04$.

4.6.3.3 Liquid-phase transfer coefficient

In falling films the liquid transfer coefficient depends only on the flow rate of the liquid; we can use the correlation given in Trambouze *et al.* [1988]:

$$\left(\frac{k_{i,\mathrm{L}}}{\mathcal{D}_{i,\mathrm{L}}}\right)\left(\frac{\mu_{\mathrm{L}}^2}{\rho_{\mathrm{L}}^2 g}\right)^{0.33} = a(Re)_{\mathrm{L}}^{b}\,(Sc)_{\mathrm{L}}^{0.5} \tag{4.89}$$

where the following values are used for the coefficient a and exponent b:

	a	b
$(Re)_{\mathrm{L}} \leqslant 300$	$1.1 \cdot 10^{-2}$	0.4
$300 < (Re)_{\mathrm{L}} \leqslant 1\,600$	$3.0 \cdot 10^{-2}$	0.2
$1600 < (Re)_{\mathrm{L}} \leqslant 10\,500$	$9.8 \cdot 10^{-2}$	0.7

In the absence of specific data for agitated films, we are forced to make use of those for falling films. In this case it is likely that transfer coefficients will be underestimated, especially in the liquid phase, given the very high turbulence found in agitated films.

4.6.4 Heat transfer

In addition to the heat transfer between the film and the tube wall, we also need to examine heat transfer between the gas and liquid phases. In both cases, the exchange surface is known and can, like the interfacial area, be taken as the surface of the tube.

4.6.4.1 Transfer at the wall

It is at the wall that thin-film devices develop interesting characteristics. The exchange surface, measured per unit volume of liquid phase, assumes large values that are far greater than those obtainable with conventional equipment. In terms of the unit volume of the corresponding liquid film, the transfer surface at the wall is equal to:

$$\Omega_{\mathrm{L}} = \frac{\pi d}{\pi d e} = \frac{1}{e} \quad (\mathrm{m}^2/\mathrm{m}^3) \tag{4.90}$$

Given the practical values for film thickness, e, we see that Ω_{L} can reach values greater than 10^3 (between 125 and 5 000).

A number of correlations have been proposed for calculating the coefficient of heat transfer, h_{L}. For falling films we can, for example, make use of a simple formula that has been in use for a long time, namely:

$$\frac{h_{\mathrm{L}}}{\lambda_{\mathrm{L}}}\left(\frac{\mu_{\mathrm{L}}^2}{\rho_{\mathrm{L}}^2 g}\right)^{0.33} \cong 7 \cdot 10^{-3}(Re)_{\mathrm{L}}^{0.35}\,(Pr)_{\mathrm{L}}^{0.4} \tag{4.91}$$

where:

$$(Pr)_L = \frac{\mu_L C_{PM}}{\lambda_L} \quad \text{(liquid Prandtl number)}$$

This equation is valid over a large range of Reynolds (3 to 10 000) and Prandtl numbers (3.6 to 950).

With respect to agitated films, in addition to the dimensionless number already discussed and the number of rotor blades (n_P), a new Reynolds number for the rotor is introduced, $(Re)_R$:

$$(Re)_R = \frac{N_R d_R^2 \rho_L}{\mu_L} \tag{4.92}$$

Here, N_R is the speed of rotation of the rotor (revolutions per second) and d_R is the rotor diameter (m). We then have the following two correlations:

- Heat exchange without vaporization:

$$(Nu)_L = 0.018(Re)_L^{0.46}(Re)_R^{0.6}(Pr)_L^{0.87}\left(\frac{d}{H}\right)^{0.48}(n_P)^{0.24} \tag{4.93}$$

- Heat exchange with vaporization:

$$(Nu)_L = 0.65(Re)_L^{0.25}(Re)_R^{0.4}(Pr)_L^{0.3}(n_P)^{0.33} \tag{4.94}$$

where $(Nu)_L$ is the corresponding Nusselt number, that is: $(Nu)_L = h_L d/\lambda_L$.

4.6.4.2 Heat transfer at the gas-liquid interface

Although heat transfer at the gas-liquid interface is not as important as that at the wall, under certain conditions it needs to be evaluated. Here too, most of the information available is for falling films and we have to assume they are equally valid for agitated films.

In this case resistance to transfer is largely dependent on the gas phase. We can therefore use the gas-phase transfer coefficient, h_G, as the basis for our calculations. This can be calculated by means of the following equation:

$$(Nu_G) = 0.175(Re)_{GL}^{0.82} \tag{4.95}$$

where:

$$(Nu)_G = \frac{h_G d}{\lambda_L} \quad \text{and} \quad (Re)_{GL} = \frac{u_r \rho_G d}{\mu_G}$$

The Reynolds number shown above is calculated on the basis of the relative velocity, u_r, of the gas with respect to the liquid at the surface of the film. In this case, as with the gas-phase mass transfer coefficient, use of this equation with agitated films must be approached with caution, after correcting the value of $(Nu)_G$ obtained by multiplying by a factor equal to $d/0.04$.

For the sake of completeness, when comparing thin-film devices with other reactor types, we must also take into account the consumption of mechanical energy. Although the falling film device is, from this point of view, similar to a packed column, agitated film systems require the use of an electric motor, whose power can be on the order of one kW/m^2 of film surface.

4.6.5 Current uses

In light of the above characteristics, it should be clear that reactions carried out in these devices must be rapid, in other words residence times must be no greater than a few minutes.

Compared to other types of continuous reactor, thin-film devices appear to have a specific advantage in terms of heat transfer. Therefore, a second criterion for choosing these devices would be a high heat of reaction, whether the reactions are endothermic or exothermic. We can treat the two cases introduced earlier separately:

- a reaction that requires a liquid phase alone
- a reaction that requires a liquid phase and a gas phase.

4.6.5.1 Continuous single-phase reactor

It is certainly possible to carry out a fast liquid-phase reaction in a thin-film device. Given the characteristics discussed in Section 4.6.1, such a device would be a kind of tubular reactor. We can see how this is so by referring to Fig. 4.17, which illustrates the range of use for various types of reactors based on mean residence time, θ, and processing capacity. The illustration shows that the range of use for thin-layer devices falls well within that of conventional tubular reactors (see Chapter 2).

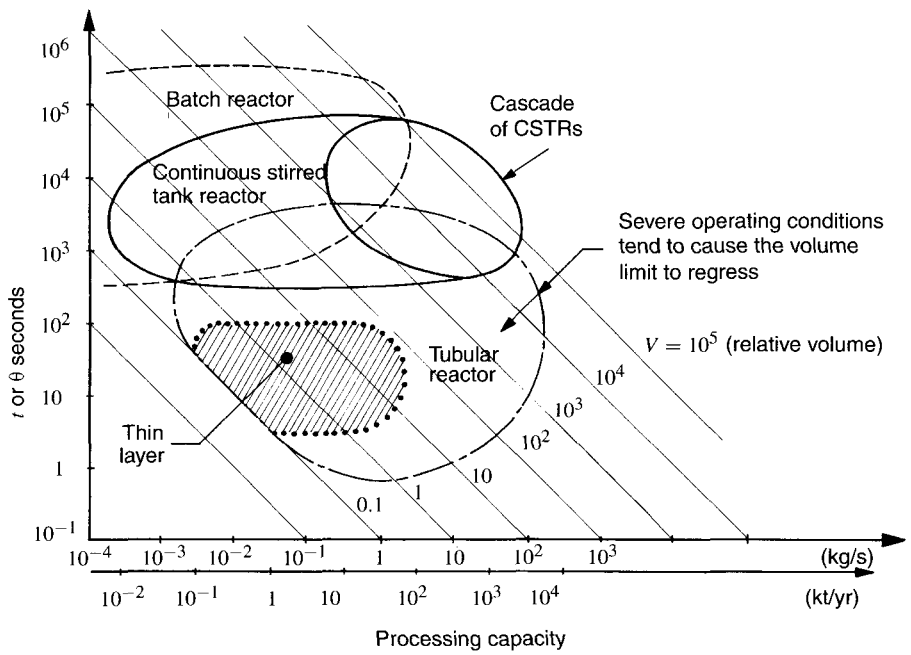


Figure 4.17 Range of use for thin-film reactors.

Since thin-film devices are structurally more complex, in practice they are used only when they provide a definite advantage, usually with respect to heat transfer.

In the field of reactor design, most of the thermal problems that are difficult to resolve occur when highly exothermic reactions with high activation energy are involved. To ensure stable reactor operation in such cases, a suitable value for the term γ (see Chapter 2, Eq. 2.25) is needed. γ is defined as follows:

$$\gamma = \frac{h_L \Omega}{K_{T_P} \rho_L C_{PM} V} \tag{4.96}$$

where T_P is the wall temperature (K).

Even if we ignore the fact that the transfer coefficients, h_L, are higher in thin-layer devices than in a tube, we can make the comparison on the basis of Ω/V alone, which is the exchange surface per unit volume of the reaction phase.

For the thin layer, we have: $\Omega/V = \Omega_L = 1/e$.

For a tube of diameter d_T, which can accommodate the same reaction volume, V, the value of Ω/V is given by the following equation:

$$\left(\frac{\Omega}{V}\right)_T = \frac{4}{d_T}$$

The two values of Ω/V are identical for a diameter d_T such that $d_T = 4e$, which results in a tube having a diameter of about 1 cm. For example, if we want to obtain the same reaction volume V as an agitated thin-film device with the following characteristics:

$$d = 1.25 \text{ m} \quad H = 6.10 \text{ m} \quad \Omega = 24 \text{ m}^2 \quad V = 0.072 \text{ m}^3$$

the equivalent tubular reactor must have a length of 160 m and a diameter of 1.2 cm, which is conceivable. However, if the liquid phase is viscous, the transfer coefficient will be much lower in the tube than in the agitated thin-film device, and problems of thermal stability are liable to occur in the tube. Moreover, the pressure drop in the tube could present an obstacle to its use. In conclusion we can state that in very specific situations (polymerization, for example), an agitated thin-film device can be useful as a type of single-phase tubular continuous reactor.

4.6.5.2 Gas-liquid reactors

When comparing a thin-layer device to the more conventional reactors used for gas-liquid reaction systems, the following parameters need to be taken into consideration:

- interfacial area $\mathcal{A}$ (m^2/m^3)
- liquid-phase holdup, ε_L
- interfacial area per liquid-phase unit volume, $\mathcal{A}_L$
- the dimensionless number $\beta_L = (k_{i,L}\varepsilon_L)/\mathcal{A}\mathcal{D}_{i,L}$, which determines the reaction efficiency of the liquid phase.

Table 4.11 lists ranges for each of these parameters and various types of equipment. From the table we can see that thin-film devices can be compared to packed columns, which makes sense since the liquid phase flows over the packing as a film.

Table 4.11 Comparison of falling-film and other gas-liquid reactors.

	Mechanically agitated tank	Bubble column	Packed column	Thin-film reactor
$\mathcal{A}$ (m^{-1})	200 to 2 000	100 to 500	50 to 250	3 to 100
ε_L	> 0.7	> 0.7	0.05 to 0.15	0.01 to 0.15
$\mathcal{A}_L$ (m^{-1})	220 to 2 500	120 to 700	1 000 to 1 600	300 to 600
β_L	> 100	> 100	10 to 100	10 to 200
$(\Delta P)_{gas}$	Moderate	High	Low	Negligible

It is worth noting that the very low pressure drop of the gas during its passage through a thin-layer device can be highly advantageous in certain situations. Like packed columns, thin-film devices are well suited to fast gas-liquid reactions, characterized by a Hatta number greater than 3 (see Chapter 3). Nonetheless, thin-film devices can be distinguished from packed columns by their ability to handle viscous, even highly viscous, liquid phases, and to accommodate reactions with significant thermal effects. The superiority of thin-film devices is obvious in situations that have the following characteristics:

- absorption reaction with a fast and highly exothermic chemical reaction
- highly endothermic reaction producing a volatile compound whose desorption is desirable to shift the equilibrium or avoid secondary reactions.

In the case of highly exothermic reactions, we can again turn to the problem of the stability of such systems or at least evaluate the local rise in temperature that can occur. Indeed, for such reactions there is a risk of overheating at the gas-liquid interface, resulting in a loss of selectivity.

Figure 4.18 illustrates the temperature and concentration profiles that can result during the absorption of a compound A_1 present in the gas phase and reacting very rapidly in the liquid phase. The reaction, assumed to be exothermic, occurs within a very thin reaction film near the interface. A heat balance can be written for a film element perpendicular to the wall and of unit cross-section.

If we examine the system from within the reactor, at the point where the temperature of the liquid, flowing vertically from top to bottom, reaches its maximum, we can neglect the terms associated with liquid flow in the heat balance.

The heat generated in the thin-film element is written:

$$\text{Heat generated} = k_{1,G}\left(C_{1,G} - C^*_{1,G}\right)(-\Delta H_R) \tag{4.97}$$

The heat eliminated through transfer at the wall and transfer to the gas phase is written:

$$\text{Heat eliminated} = h_G\,(T_R - T_G) + \varphi\lambda_L\,(T_R - T_L) \tag{4.98}$$

where $\varphi = \alpha/e$, α being a coefficient related to the turbulence of the thin film.

By neglecting the resistance to transfer on the gas side of the film, we have:

$$\text{Heat eliminated} = \frac{h_L\varphi\lambda_L}{h_L + \varphi\lambda_L}\,(T_R - T_P) \tag{4.99}$$

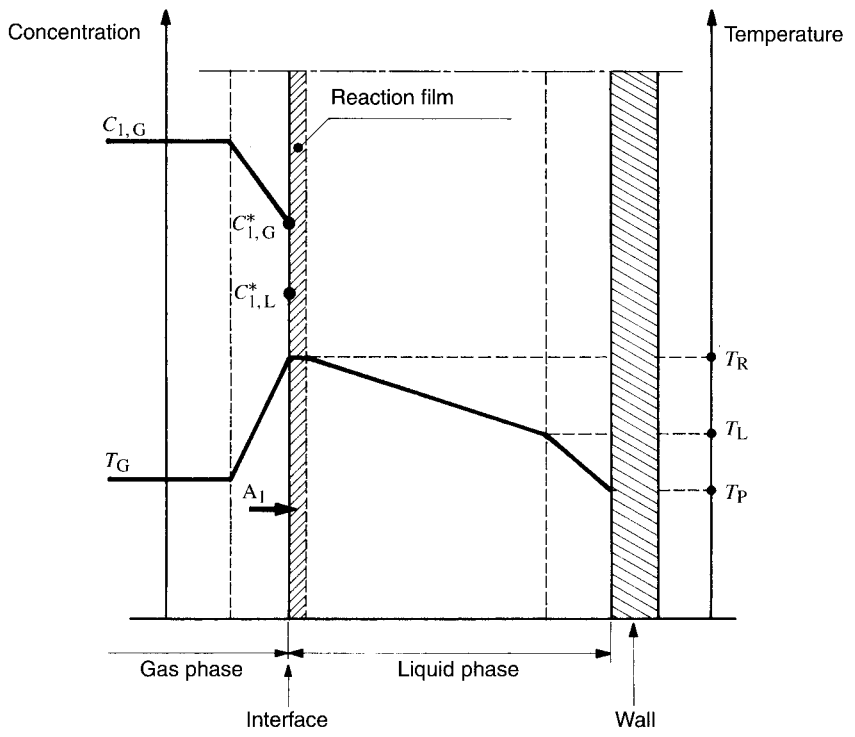


Figure 4.18 Temperature and concentration profiles in a thin-film device in which a fast exothermic reaction takes place.

If the reaction is very fast, given the high enhancement factor E ($E = Ha$), we can assume that the resistance to transfer is restricted to the gas phase alone, which implies:

$$C^*_{I,G} \ll C_{I,G}$$

The simplified heat balance can then be written:

$$T_R - T_P = C_{I,G}\,(-\Delta H_R)\left(\frac{Sh_G}{Nu_L}\right)\frac{Nu_L + \varphi d}{\varphi \lambda_L}\,\frac{\mathcal{D}_{I,G}}{d} \tag{4.100}$$

This equation can be used to calculate the rise in temperature of the reaction interface, which in many cases must be limited if secondary reactions are to be avoided.

4.6.6 Practical applications

In light of the above, we see that there are three reaction systems for which thin-film devices are suitable:

1. Highly exothermic reactions that occur in a highly viscous liquid phase
2. Highly exothermic reactions in a liquid phase, one of the reactants being transferred from a gas phase

3. Endothermic reactions in a viscous liquid phase accompanied by the production of a compound whose vaporization or desorption is of interest from the point of view of thermodynamics (reversible reaction) or selectivity (undesirable consecutive reactions).

Table 4.12 lists a number of such applications, classified according to the three categories listed above.

Table 4.12 Some practical applications of thin-film devices.

Single-phase reactor	Absorption with reaction	Reaction with desorption
Polymerization of vinyl acetate	SO_3 sulfonation: – of dodecylbenzene – of fatty alcohols – of petroleum cuts	Polycondensation
Condensation of phenol with formaldehyde	Production of dichlorohydrins	Esterification reactions
	Chlorination of ethylene	
	Nitration of aromatics	
	Wastewater treatment	

4.6.7 Technology

Technologically, the efficiency of falling film reactors is particularly sensitive to the design of tubes and distributors in particular. In the case of reactor tubes, their diameter, height, even number, are determined using the customary guidelines governing pressure drop, mass and heat transfer. The nature of the material and surface quality must also be selected with care to promote the development, adhesion, and permanence of the film throughout the height of the tube.

Distributors are also key components. Gas and even more so liquid distributors are designed to distribute fluids uniformly along the periphery of the tube(s). The film thickness is adjusted simply by overflow or by allowing the liquid to pass through a circular diaphragm.

4.6.8 Concluding remarks

As we saw above, thin-film devices can be used as reactors. When they are compared to more conventional reactors, they appear to have potential advantages in very specific situations, namely:

- when the reaction is fast and highly exothermic
- when the liquid phase in which the reaction occurs is relatively viscous.

However, aside from these specific situations, thin-film devices do not appear to present any advantages as chemical reactors because of the increased investment cost, especially when agitated film devices are used. Yet, in certain circumstances, they may be the only viable technological solution for implementing a chemical reaction on an industrial scale.

4.7 MECHANICALLY AGITATED DEVICES

4.7.1 General characteristics

Mechanically agitated reactors can be used to rapidly obtain uniform composition and temperature throughout the vessel. Such devices are, therefore, to be recommended especially when there is a marked thermal effect associated with the reaction, mixing, or dissolution.

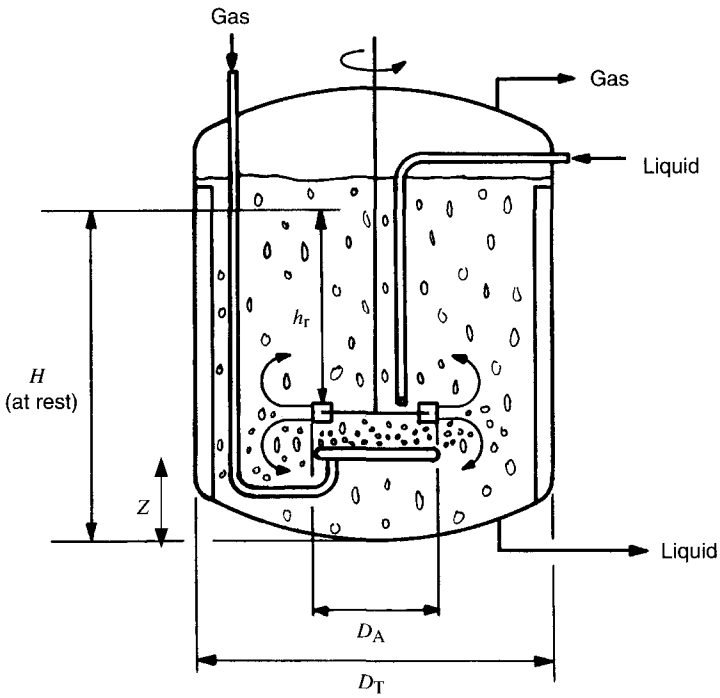


Figure 4.19 Continuous stirred tank reactor with liquid and gas.

Figure 4.19 is a schematic illustration of such a device. Aside from the gas injector, it differs little from devices used for single-phase reactions. However, while single-phase reactors require good mixing, gas-liquid reactors also require good transfer between the phases. To obtain this, high-shear impellers (Rushton turbines, for example) are generally preferred to propellers that generate greater pumping rates with less energy expenditure but are less effective at creating an interface. The standardization introduced in the 1950s by Rushton is now commonplace in the industry.

4.7.2 Hydrodynamics

A mechanically agitated reactor can have three principal hydrodynamic regimes, depending on the values of two key parameters that operate inversely to one another: the speed of rotation of the agitator and the gas flow rate.

At very low rotational speeds, the impeller plays almost no role, has no interaction with the gas, so that in practice the reactor behaves like a simple bubble column. This situation corresponds to rotational speeds less than the minimum value N_{Rm}.

At very high rotational speeds and high gas flow rates, the impeller becomes flooded and the moving elements can, at some point, slip in a gas cap without promoting gas-liquid contact.

Between these two extremes, bubble fragmentation, mixing, and recirculation change gradually (the following reference works are particularly useful: Uhl and Gray [1967], Oldshue [1983], Tatterson [1999], Harnby [1992]). The most efficient operating conditions occur when the energy supplied by the mechanical agitator is 3 to 5 times greater than that corresponding to the expansion of the gas.

Table 4.13 lists the generally accepted correlations for estimating the numerical value of the most important parameters. They must be used with caution, however. For, as with bubble columns, interface properties, responsible for the formation of bubbles and their coalescence, are not fully described by interfacial tension. Therefore, scale-up must be based on a set of experiments made with actual fluids and retain modest scaling factors.

All the suggested correlations assume that the impeller's rotational speed exceeds the minimal speed, N_{Rm}, below which the impeller has no effect on the behavior of the system. This speed appreciably corresponds to a minimum peripheral speed ($= \pi N_{Rm} D_A$) of 2 m/s. It depends on the geometry of the system and the physical properties of the liquid, as shown in the correlations in Table 4.13. A summary of these effects has been published by Joshi *et al.* [1982].

4.7.2.1 Power input

The power input is frequently correlated by first calculating, using the conventional equations, the power absorbed by the unaerated liquid medium ($\mathcal{P}_L$). This power is the result of a correlation between a power number $N_P = \mathcal{P}/(\rho_L N_R^3 D_A^5)$ and a Reynolds number $Re = N_R D_A^2 \rho_L / \mu_L$. This correlation is often presented in the form shown in Fig. 4.20.

The actual power in the presence of a gas ($\mathcal{P}_{LG}$) is then obtained by calculating the ratio $\mathcal{P}_{LG}/\mathcal{P}_L$ in different ways. The aeration number $N_{QG} = Q_{VG}/(N_R D_A^3)$ often appears in these correlations. Calderbank proposed Fig. 4.21, which has been used as a reference in this field for a number of years. Some of the more recent equations are given in Table 4.13. Note that the equation by Michel and Miller [1962] is valid solely for aqueous systems.

No correlation is truly satisfactory, but by examining all the experimental results, we find that $\mathcal{P}_{LG}/\mathcal{P}_L$ always falls between 0.3 and 0.6 for current industrial applications, with a value of 0.4 being the most frequent. This is a good basis to use when designing a reactor, in the absence of more precise data. Nonetheless, it is essential that the installed power be sufficient to mix the liquid, even in the absence of a gas, whether accidental or not.

Note that in the presence of several superimposed impellers, the total absorbed power is appreciably equal to the sum of the absorbed powers of each impeller considered individually.

Table 4.13 Stirred tank reactors *(continued on the following pages).*

1. Minimum rpm needed to disperse the gas

Pure liquids:

$$\text{for } D_T < 1.0\text{ m} \quad \left(\frac{N_{Rm}D_A^2}{D_T}\right)(gD_T)^{-0.5} = 0.07 \qquad \text{Van Dierendonck } \textit{et al.} \text{ [1968]} \qquad (4.101)$$

$$\text{for } D_T \geqslant 1.0\text{ m} \quad \text{if } V_{SG} < 0.03\text{ m/s} \quad \text{and if } 0.1 < (h_r/D_T) < 0.6$$

$$\left(\frac{N_{Rm}D_A^2\mu_L}{\sigma D_T}\right)\left(\frac{\rho_L\sigma^3}{g\mu_L^4}\right)^{0.25} = 2\left(\frac{h_r}{D_T}\right)^{0.5} \qquad (4.102)$$

where h_r: height of liquid above the stirrer when at rest

For coalescent systems with $D_T < 1.8$ m and conventional turbines in reactors with standard geometry ($H = D_T$ and $Z = D_T/4$)

$$\frac{Q_{VG}}{N_{Rm}D_A^3} = 30\left(\frac{D_A}{D_T}\right)^{3.5}\left(\frac{N_{Rm}^2 D_A}{g}\right) \qquad (4.103)$$

For electrolyte solutions:

$$\left(\frac{N_{Rm}D_A^2\mu_L}{\sigma D_T}\right)\left(\frac{\rho_L\sigma^3}{g\mu_L^4}\right)^{0.25} \cong 1 \quad \text{if } V_{SG} < 0.05\text{ m/s} \qquad (4.104)$$

2. Absorbed power

$$\mathcal{P}_{LG} = K\left(\mathcal{P}_L^2 N_R D_A^3/Q_{VG}^{0.56}\right)^{0.45} \qquad \text{Michel and Miller [1962]} \qquad (4.105)$$

$K = 1$ in SI units (aqueous systems)

$$\frac{\mathcal{P}_{LG}}{\mathcal{P}_L} = \exp\left[-442\left(\frac{D_A}{D_T}\right)^{4.38}\left(\frac{N_R D_A^2\mu_L}{\rho_L}\right)^{0.115}\left(\frac{N_R^2 D_A}{g}\right)^{1.9D_A/D_T}\left(\frac{Q_{VG}}{N_R D_A^3}\right)\right] \qquad \text{Nagata [1975]} \qquad (4.106)$$

Table 4.13 *(continued).*

3. Gas holdup

$$\varepsilon_G = K\left(\frac{Q_{VG}N_R^2}{\sigma}\right)^Z$$ Hassan and Robinson [1977] (4.107)

Non-electrolytes: $Z = 0.6 \quad K = 0.1$

Aqueous electrolytes: $0.4 < Z < 0.5 \quad 0.2 < K < 0.3$

Pure liquids:

$$\varepsilon_G = 0.31\left(\frac{\mu_L V_{SG}}{\sigma}\right)^{0.67}\left(\frac{\rho_L\sigma^3}{g\mu_L^4}\right)^{0.17} + 0.45\frac{(N_R - N_{Rm})\,D_A^2}{D_T\sqrt{gD_T}}$$ (4.108)

if $\varepsilon_G < 0.2 \quad V_{SG} < 0.05$ m/s $\quad H/D_T = 1$

Electrolytes:

$$\varepsilon_G = 0.075\left(\frac{\mu_L\,(N_R - N_{Rm})\,D_A^2}{\sigma D_T}\right)\left(\frac{\rho_L\sigma^3}{g\mu_L^4}\right)^{0.25}$$ Van Dierendonck [1968] (4.109)

if $\varepsilon_G < 0.3 \quad V_{SG} < 0.03$ m/s $\quad H/D_T = 1$

For water-air systems:

$$\varepsilon_G = 0.23\left(\frac{\mathcal{P}}{V}\right)^{0.31} V_{SG}^{0.67}$$ (4.110)

For non-electrolytes:

$$\varepsilon_G = \left(\frac{V_{SG}\varepsilon_G}{0.26}\right)^{0.50} + 1.5\cdot 10^{-4}\mathcal{A}$$ (4.111)

Table 4.13 *(continued).*

4. Transfer coefficient k_L

Small bubbles:

$$\overline{d_B} < 2.5 \text{ mm} \quad k_L = 0.31 \left(\frac{g\mu_L}{\rho_L}\right)^{0.33} \left(\frac{\mathcal{D}_L \rho_L}{\mu_L}\right)^{0.67}$$ Calderbank and Moo-Young [1961] (4.112)

Large bubbles:

$$\overline{d_B} > 2.5 \text{ mm} \quad k_L = 0.42 \left(\frac{g\mu_L}{\rho_L}\right)^{0.33} \left(\frac{\mathcal{D}_L \rho_L}{\mu_L}\right)^{0.5}$$ (4.113)

In practice $2 \cdot 10^{-4} < k_L < 6 \cdot 10^{-4}$ m/s, frequently $k_L \cong 5 \cdot 10^{-4}$ m/s

For hydrogen, this coefficient k_L is approximately twice as large as it is for other gases. This is because of hydrogen's greater diffusivity.

5. Interfacial area $\mathcal{A}$

$$\mathcal{A} = K \left(\frac{\mathcal{P}}{V}\right)^n \quad 0.65 < n < 0.70$$ Reith [1968] (4.114)

For aqueous systems, $K = 4$ if $\mathcal{A}$ is in m^2/m^3 and $\mathcal{P}/V$ in W/m^3.

$$\mathcal{A}_0 = 1.44 \left(\frac{\mathcal{P}}{V_L}\right)^{0.4} \frac{\rho_L^{0.2}}{\sigma^{0.6}} \left(\frac{V_{SG}}{u_t}\right)^{0.5}$$ Calderbank [1958] (4.115)

$$\mathcal{A} = \frac{\mathcal{A}_0}{2.3} 10^B \quad \text{where } B = 2 \cdot 10^{-5} \left(\frac{N_R D_A \rho_L}{\mu_L}\right)^{0.7} \left(\frac{N_R D_A}{V_{SG}}\right)^{0.3}$$ (4.116)

u_t: rise velocity of a bubble (approximately 0.3 m/s).

Table 4.13 *(continued).*

6. Transfer coefficient $k_L\mathcal{A}$

$$\frac{k_L\mathcal{A}D_A^2}{\mathcal{D}_L} = 0.06\left(\frac{N_R D_A^2 \rho_L}{\mu_L}\right)^{1.5}\left(\frac{N_R^2 D_A}{g}\right)^{0.19}\left(\frac{\mu_L}{\rho_L \mathcal{D}_L}\right)^{0.5}\left(\frac{\mu_L V_{SG}}{\sigma}\right)^{0.6}\left(\frac{N_R D_A}{V_{SG}}\right)^{0.32}$$ Yagi and Yoshida [1975] (4.117)

$$k_L\mathcal{A} = 2.6\cdot 10^{-2}\left(\frac{\mathcal{P}}{V}\right)^{0.4} V_{SG}^{0.5}$$ for non-electrolyte air and water media — Lee and Tsui [1999] (4.118)

$$k_L\mathcal{A} = 2.0\cdot 10^{-3}\left(\frac{\mathcal{P}}{V}\right)^{0.7} V_{SG}^{0.2}$$ in the presence of electrolytes — Lee and Tsui [1999] (4.119)

7. Coefficient of heat transfer

Exchange with the side wall:

$$h = a\frac{\lambda_L}{D_T}\left(\frac{N_R D_A^2 \rho_L}{\mu_L}\right)^{b}\left(\frac{C_{PL}\mu_L}{\lambda_L}\right)^{0.33}\left(\frac{\mu_L}{\mu_W}\right)^{m}$$ (4.120)

where:

$a = 0.36$ $b = 0.67$ $m = 0.21$ for a propeller

$a = 0.53$ $b = 0.67$ $m = 0.14$ for a turbine

Exchange with a immersed coil of diameter d_t:

$$h = 0.17\frac{\lambda_L}{d_t}\left(\frac{N_R D_A^2 \rho_L}{\mu_L}\right)^{0.67}\left(\frac{C_{PL}\mu_L}{\lambda_L}\right)^{0.37}\left(\frac{D_A}{D_T}\right)^{0.1}\left(\frac{d_t}{D_T}\right)^{0.5}$$ Trambouze *et al.* [2000] (4.121)

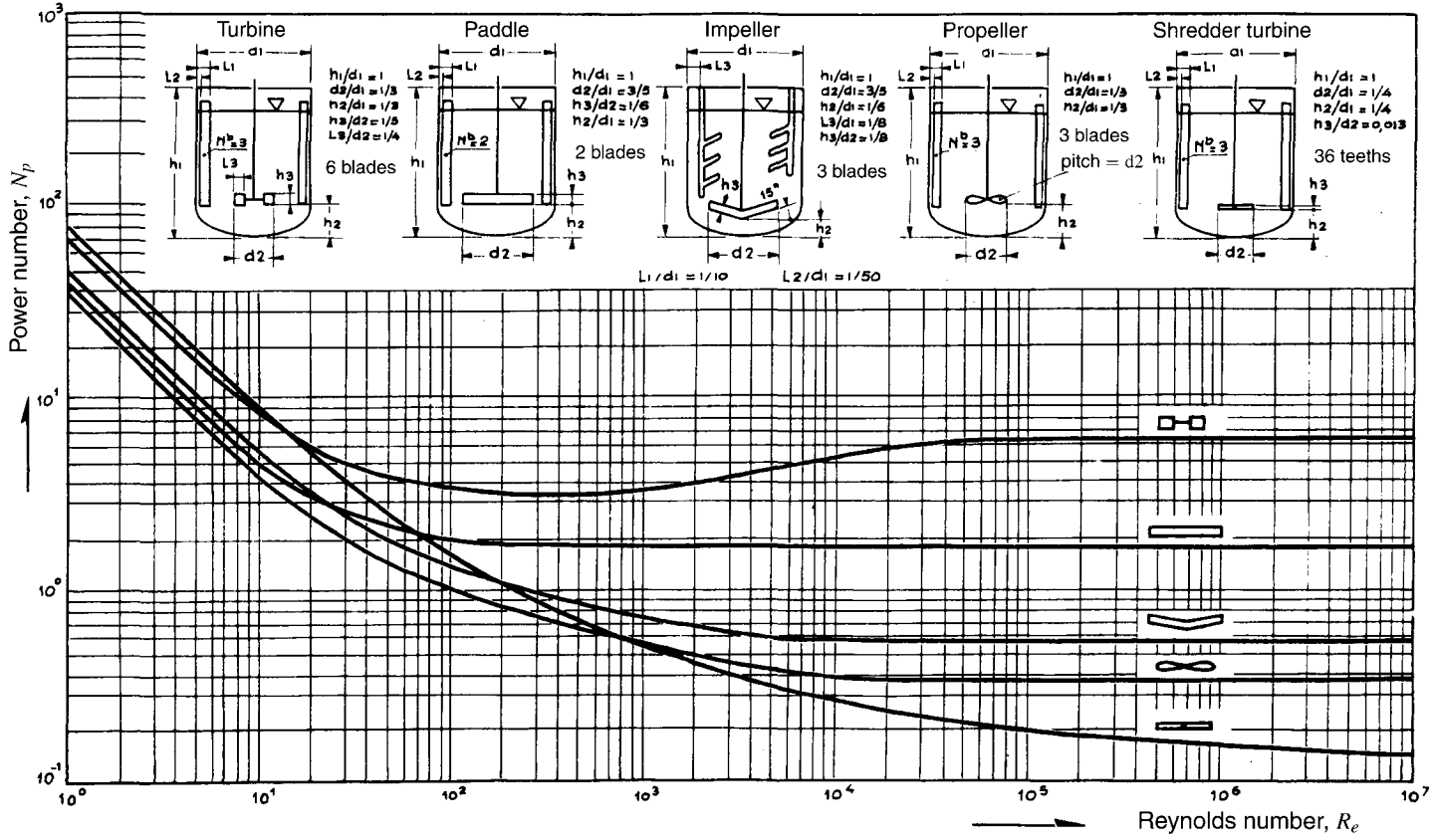


Figure 4.20 Examples of variations in the power number N_P as a function of the Reynolds number for different mixing devices (Missenart-Quint Industries, Mixel) in the presence of a liquid alone.

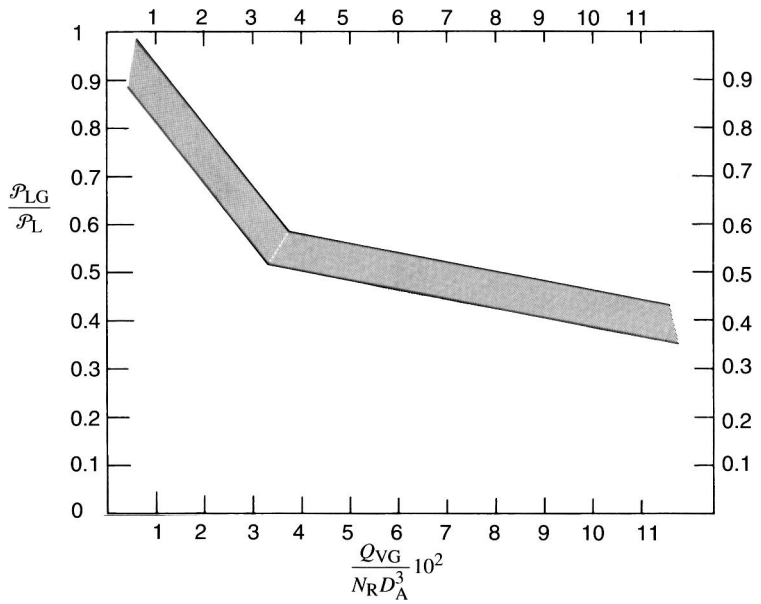


Figure 4.21 Stirred tank reactors: power variation associated with the presence of a gas.

4.7.2.2 Gas holdup

Gas holdup is directly dependent on the gas flow rate and the mechanical power introduced into the medium:

$$\varepsilon_G \approx \mathcal{P}_{LG}^{0.4} V_{SG}^{0.5} \sigma^{-0.6} \tag{4.122}$$

As has been frequently observed, however, since even in an aerated medium, $\mathcal{P}_{LG}$ is proportional to N_R^3, the previous expression can be written in the following form:

$$\varepsilon_G \approx N_R^{1.2} V_{SG}^{0.5} \sigma^{-0.6} \tag{4.123}$$

Robinson has generalized this equation, which is valid for relatively small units (see Table 4.13). The equation is dimensional, however, and can only provide semiquantitative information.

The geometry of the gas injector has little influence on holdup, assuming there is nearly uniform distribution underneath the turbine and the gas inlet is placed in the field of radial circulation, in other words, no more than a few centimeters beneath the blades. Holdup increases with the pressure of the medium.

Thijert *et al.* [1992] have proposed a useful correlation for scaling-up stirred tank reactors in the presence of a gas and a liquid:

$$\varepsilon_G = \frac{1}{H}\left(5.1 \cdot 10^{-3} + 0.88 V_{SG} + 3.1 \cdot 10^{-2} (N_R - N_{Rm}) \left(\frac{D_A}{D_T}\right)^2\right) \tag{4.124}$$

This equation has been established for $5 \cdot 10^{-3} \leqslant V_{SG} \leqslant 3 \cdot 10^{-2}$ m/s, $D_T = H = 0.3$ m.

4.7.3 Mass transfer

4.7.3.1 Interfacial area $\mathcal{A}$

The interfacial area $\mathcal{A}$ is highly dependent on the mixing conditions and in particular on the power input per unit volume of reactor (so-called specific power). The interfacial area is little affected by system pressure except for extremely high gas flow rates.

A relation between interfacial area and the specific power introduced into the reactor for a given physicochemical system has been proposed by Trambouze *et al.* [1988] (Fig. 4.5). This equation can be expressed as shown in Table 4.13. It was also referred to in the section on bubble columns. Calderbank's equations are valid for pure liquids. u_t is the mean rise velocity of a bubble (approximately 0.3 m/s). In this case we find that bubble size does not fall below 2.5 mm.

4.7.3.2 Mass transfer coefficient k_L and the product $k_L\mathcal{A}$

Most authors, aside from certain reservations they may have, acknowledge that k_L depends primarily on the intrinsic characteristics of the liquid and very little on the specific power introduced into the tank: with respect to the liquid, the bubbles appear to have a relative velocity that is nearly independent of the intensity of mixing. Estimates of k_L can be obtained using the equations proposed by Calderbank (Table 4.13).

$k_L\mathcal{A}$ depends on the power introduced by the turbine. For a given geometry and constant V_{SG}, a power-type law holds. Simpler, but sufficiently precise, correlations for a number of media associate $k_L\mathcal{A}$ with various parameters that affect the energy introduced into the medium by the gas and the turbine (Table 4.13). The presence of electrolytes improves transfer, a fact reflected in a law of the same form but with slightly different coefficients. On the other hand, the increase in the viscosity of the liquid leads to a noticeable decrease of $\mathcal{A}$ and $k_L\mathcal{A}$.

Note that the exponent of V_{SG} (proportional to the power introduced with the gas) is small, while $k_L\mathcal{A}$ tends to 0 at zero rpm, which is obviously false. It appears therefore that the validity of the equation must be limited to low superficial gas velocities (< 0.01 m/s based on the experimental range) for turbines operating beyond the minimum rotational speed.

To maintain the same values for the interfacial area $\mathcal{A}$ and the transfer coefficient k_L when scaling-up, we must also use the same specific power and the same gas superficial velocity.

Comments:

1. The amounts of energy introduced by the gas are far from negligible in an industrial reactor. Earlier, we showed how an approximation of this quantity could be written:

$$\mathcal{P} = Q_{VG}\Delta P$$

where ΔP corresponds to the hydrostatic head.
This gives the following equation for the specific energy injected:

$$\frac{\mathcal{P}}{V} = V_{SG}\rho_L g\varepsilon_L \quad \text{W/m} \tag{4.125}$$

It appears then that for superficial velocities above 1 cm/s, we need to take into consideration the energy of expansion of the gas. Above 5 to 10 cm/s this can become

the dominant factor, making the choice of a mechanical stirrer critical. In fact there is an optimum value for the superficial velocity for which a value of $k_L\mathcal{A}$ can be realized with the minimum expenditure of energy. For fermentation—and therefore for an aqueous system—this minimum corresponds to a gas velocity between 0.03 and 0.05 m/s.

2. The aeration number can be expressed as a function of V_{SG}. For a conventional geometry, where $D_T/D_A = 3$, we find that:

$$N_{QG} = \frac{Q_{VG}}{N_R D_A^3} = \frac{9\pi Q_{VG}}{4N_R D_A S} \cong 7\frac{V_{SG}}{N_R D_A} \tag{4.126}$$

Since $N_R D_A$ is often between 1 and 3 m/s, we find that:

$$2V_{SG} < N_{QG} = \frac{Q_{VG}}{N_R D_A^3} < 7V_{SG} \tag{4.127}$$

We see in Fig. 4.21 that the decrease in dissipated power due to the presence of the gas is sensitive to values of the aeration number up to 0.1. However, this value of 0.1 roughly corresponds to a superficial velocity of 1 cm/s. This again confirms the fact that the introduction of a gas with superficial velocities of several centimeters per second quickly leads to a loss of efficiency for the stirrer. The energy provided by the gas becomes much larger than the mechanical energy of agitation.

4.7.3.3 Bubble diameter

Bubble diameter varies considerably with the medium and the rotational speed and location relative to the impeller blades. Near the ends of the blades bubbles are smaller (often on the order of a millimeter) and their size distribution is more limited. Near the walls and top of the reactor, coalescence effects lead to the production of bubbles as large as one or more centimeters in size. There is also a much greater distribution of diameters. An increase in pressure tends to decrease the mean size of the bubbles.

4.7.4 Heat transfer

The high turbulence found in stirred tank reactors strongly favors transfer. The exchange surface is often distributed between the reactor wall and coils or plates immersed in the medium. The coefficients shown in Table 4.13 provide mean values; the influence of the gas is sharply reduced, so that the correlations for a liquid alone are often used. Further details can be found in Uhl and Gray [1967]. Safety margins are always useful, especially since there is a possibility the medium will alter the characteristics of the wall and, consequently, the exchange characteristics.

4.7.5 Construction details

The stirred tanks used as gas-liquid contactors differ only slightly from equipment used for single-phase reactions (see Chapter 2). The differences involve the choice of impeller and the means for introducing fluids.

In the case of gas-liquid contactors, impellers are chosen to provide significant shear in order to reduce bubble size efficiently. The most commonly used impellers are radial turbines. These devices are fairly small (a third of the tank diameter) and rotate relatively quickly. Their use would appear to be unsuitable with viscous fluids and, in fact, this type of device is rarely used for gas-liquid reactions when the viscosity exceeds 500, or even 100 mPa · s.

The presence of 3, 4, and sometimes 6 counterblades can be used to increase the introduction of specific energy. They prevent the formation of a vortex and are generally justified if the gas cap does not need to be recycled. In certain cases adjustable blades can be used to match the reactor's geometry and energy consumption to the specific needs of the reaction system.

The following recommendations can be followed when determining the placement of the fluid inlets:

- If possible, gas should be introduced in the region swept by the radial circulation of the turbine. For example, the gas can be introduced by means of a central tube beneath the turbine or, preferably, through a perforated ring located a few centimeters below the blades.
- In a continuous reactor liquid should be introduced in the region subject to the greatest mixing, just above the turbine disk.

In light of the energy considerations discussed above, mechanically agitated gas-liquid contactors of this type should be limited to a maximum of 10 to 20 m^3 in size.

A number of variant designs for mechanically agitated tanks have been used [Schügerl, 1980]. For example, if we want to take advantage of exchange between the gas cap and the liquid in a small reactor (< 1 m^3), a device for recycling the gas cap, similar to that found in bubble columns, or a specially designed impeller, can be used. The gas is then introduced through the hollow shaft and hollow blades. The values for $\mathcal{A}$ and $k_L\mathcal{A}$ are the same as those obtained with conventional equipment for an equivalent specific power. Energy consumption can be calculated using the customary equations.

4.7.6 Concluding remarks

Stirred tank reactors have the following characteristics:

- high liquid holdup
- excellent gas and liquid mixing
- high mass transfer and heat transfer
- good temperature control
- ability to process viscous liquids and solutions containing solid particles
- presence of moving parts (as well as reducers, fittings, and bearings) that increase capital investment, operating, and maintenance costs.

4.8 EJECTORS

Ejectors make use of the kinetic energy of a fast moving fluid to disperse another fluid in the form of fine bubbles or droplets and generate an interfacial area of considerable size. We examine these two situations below, considering their operating characteristics and technological design features before discussing specific applications.

4.8.1 Bubble generation

4.8.1.1 Ejector connected to a bubble column

In these ejectors the liquid, injected at high speed through a narrow opening sometimes shaped like a venturi, entrains the gas current. The high shear between the two fluids disperses the gas in the form of fine bubbles (Fig. 4.22). This creates significant interfacial area near the nozzle, associated with a considerable expenditure of energy. The suspension of fine bubbles can give rise to a fairly large mean interfacial area, providing it remains stable within the expanded phase of the column. The effect on the values of k_L is less clear. Mass transfer in these devices is also much better than in conventional bubble columns, so that the complete treatment of a gas is possible providing we are willing to accept the large energy requirements. If very short contact times and high pressure drop (liquid side) are acceptable, significant gas flow rates can be accommodated. Scale-up of these ejectors to industrial sizes is not very common. In such cases ejectors are generally used in a parallel arrangement and are always accompanied by relatively high energy consumption.

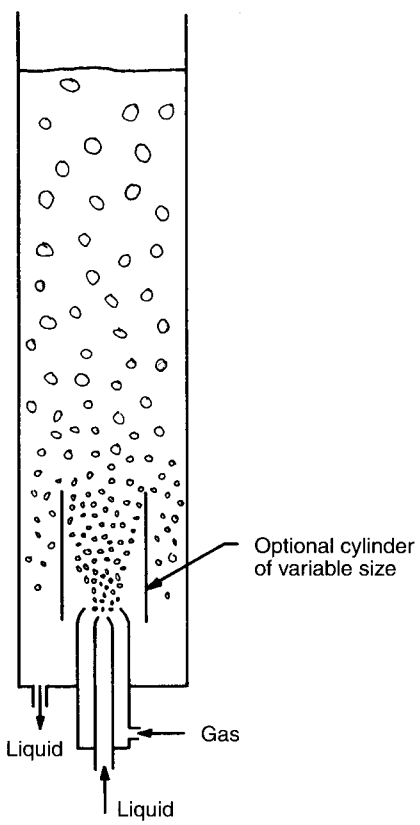


Figure 4.22 Bubble column incorporating a gas ejector.

The exchange surface is created by the venturi effect as a result of the considerable liquid circulation around the reactor. No gas overpressure is needed, but energy is supplied as the liquid is recirculated; more than 120 times the volume of the reactor can be recycled in an hour. For example, assuming that the discharge pressure, expressed as the height H_R of clear liquid, is 5 m, we can calculate, in the case of water, a specific power equal to:

$$\frac{\mathcal{P}}{V_L} = \frac{Q_{VL}}{V_L} H_R \rho_L g = \frac{120}{3\,600} 5 \cdot 10^3 \cdot 9.81 = 1\,635 \text{ W/m}^3 \qquad (4.128)$$

This value is comparable to the power introduced into other systems, as are the interfacial areas obtained. Possible benefits would include the lower capital investment needed and the homogeneity of the medium.

4.8.1.2 Practical applications

The ejector can be placed either at the base of the column (Fig. 4.22) or in the upper section (Figs. 4.23 and 4.24).

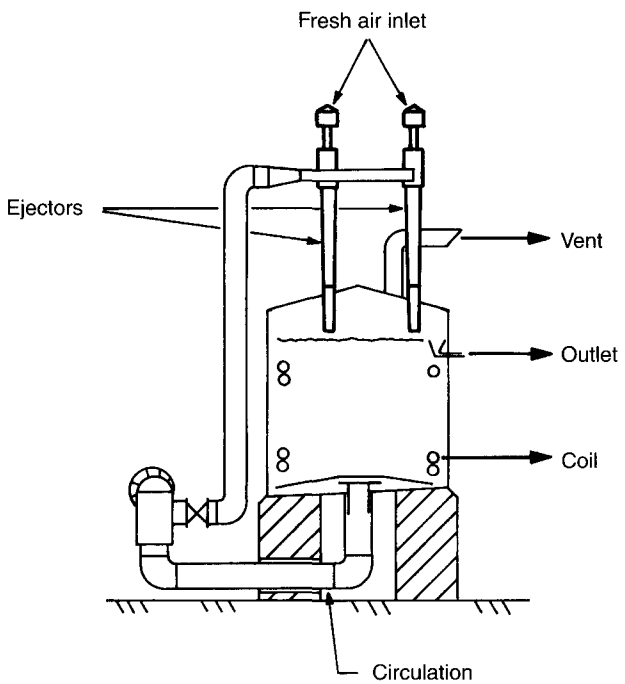


Figure 4.23 Bubble column with liquid recirculation device.

• In the first arrangement, the ejector issues directly into the aerated liquid medium. The entrance zone, which is especially rich in bubbles, is extended a variable distance into the reactor depending on the energy of the jet and the height of the equipment. Tests conducted

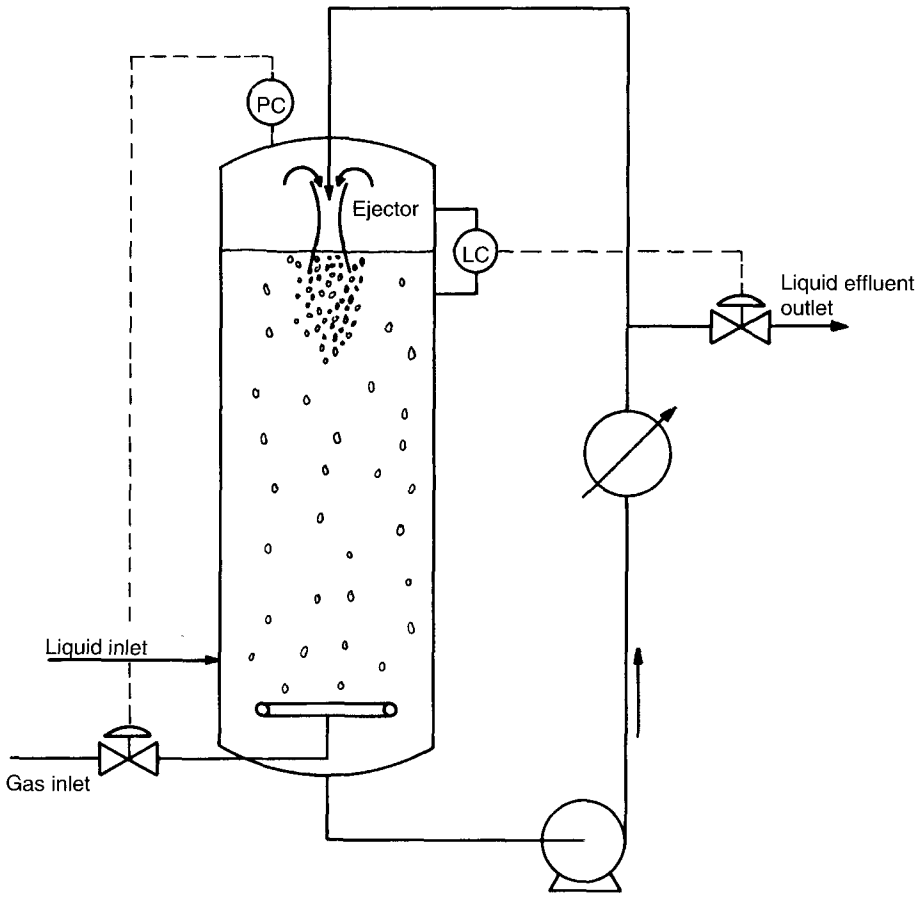


Figure 4.24 Bubble column with ejector for recycling the gas cap.

with a liquid ejector placed at the base of a column 0.15 m in diameter and filled with an aqueous medium led Ogawa *et al.* [1983] to propose the following correlations:

$$\overline{d_B} = 0.012 V_{SG}^{0.2} Fr^{-0.37} \tag{4.129}$$

$$\varepsilon_G = 0.35 V_{SG}^{0.55} Fr^{0.3} \tag{4.130}$$

$$k_L a = 0.084 V_{SG}^{0.6} Fr \tag{4.131}$$

where:

V_{SG} superficial gas velocity calculated in the reaction zone:

$$Fr = V_{LO}^2/(gD_O)$$

Here V_{LO} is the velocity at the orifice and D_O the diameter of the orifice.

• In the second arrangement, the ejector is located above the interface and projects gas bubbles into the bulk of the gas-liquid mixture. Depending on the device, the entrained gas can then be supplied either in the form of fresh makeup gas from outside the reactor (Fig. 4.23), or as recycled gas from a gas cap inside the reactor (Fig. 4.24).

The mass transfer characteristics depend on the gas and liquid flow rates, the diameter D_C of the column, and the distance H_{O-M} between the ejector orifice and the medium, as shown in Table 4.14.

Table 4.14 Bubble column with liquid recirculation and fresh gas inlet: influence of an increase in the variables V_{SG}, V_{SL}, D_C, H_{O-M} on mass transfer characteristics.

	V_{SG} ↗	V_{SL} ↗	D_C ↗	H_{O-M} ↗
$\mathcal{A}$	↗	↗	↘	↘
$k_G\mathcal{A}$	↗	–	↘	↘
k_G	↗	–	–	
k_L	↗	↗	–	

The fresh gas aspirator and disperser is often used in fermenters as well as in the aerobic treatment of waste water.

Gas cap recycling (Fig. 4.24) can be used to overcome one of the drawbacks of the bubble column. In vertical and especially horizontal columns, the reduced residence time of the gas phase sometimes limits its exhaustion. Not only is the emission of unconverted gases often unacceptable, it occasionally leads to problems in controlling the equipment. When a chemical reaction takes place by means of a pure gas reactant, it is not unusual to regulate the introduction of the gas by controlling the pressure of the gas cap. It is obvious that the accumulation of unconverted gas in the cap leads to a system where the gas-liquid exchange is practically limited to the gas-liquid interface at the top of the reactor, the fresh gas feed being too weak to ensure a sufficient exchange surface within the liquid phase. The problem can be resolved by using a liquid recycling circuit (frequently needed to control temperature in the reactor), where the return circuit passes through an ejector arranged in the reactor gas cap in such a way as to recirculate the gas phase. Exact design and calculation of the effectiveness of this ejector is highly dependent on the reaction system, but its usefulness should be obvious. These types of ejectors are frequently used both as laboratory and industrial equipment.

4.8.2 Droplet generation

4.8.2.1 Venturi scrubbers

Venturi scrubbers consist of a convergent-divergent system traversed by a stream of process gas. The liquid is introduced through one or more nozzles, either immediately before the venturi neck (Fig. 4.25A) or at the venturi wall and level with the neck (Fig. 4.25B). In both cases the liquid is broken up into fine droplets as a result of the high gas velocity at the venturi neck.

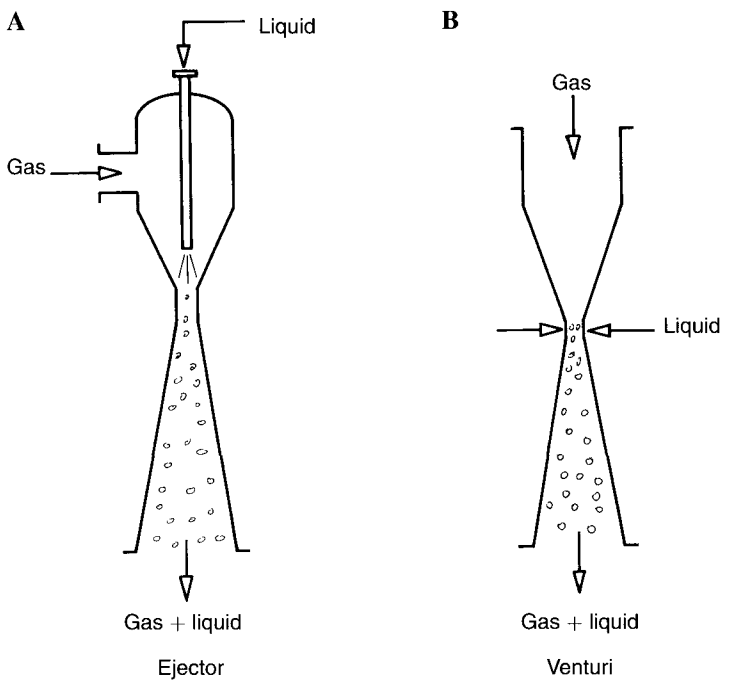


Figure 4.25 Two types of venturi scrubber.

Although there are a number of variant designs in use, our knowledge of the optimal design guidelines is still limited. The pressure drop in the gas is on the order of $5 \cdot 10^3$ Pa. It can be evaluated by means of the following equation:

$$\Delta P_G = 10^3 V_{GC}^2 \frac{Q_L}{Q_G} \tag{4.132}$$

V_{GC} is the gas velocity at the neck of the venturi (m/s).

Given the flow rates involved, these pressure drops represent significant consumption of energy. Some experimental data can be found in the literature but they apply only to small size units. Some typical orders of magnitude are shown below.

$k_L \cong 7 \cdot 10^{-4}$ m/s, nearly independent of the gas and liquid flow rates;

$10^{-2} < k_G < 3 \cdot 10^{-2}$ m/s;

$150 < \mathcal{A} < 300$ m^{-1};

$\overline{d_B} \cong 100 \cdot 10^{-6}$ m;

for the following operating conditions and physical properties:

$30 < V_{GC} < 100$ m/s;

$5 \cdot 10^{-2} < Q_{LC} < 15 \cdot 10^{-2}$ m^2/s (m^3/s · m of circumference at the neck);

$40 < \sigma < 70$ mN/m;

$\mu_L \cong 1$ mPa · s

In the majority of the cases found in practice, the following equation can be used to estimate k_G:

$$Sh = 2 + 0.347 Re^{0.62} Sc^{0.31} \tag{4.133}$$

where:

$$Sh = \frac{k_G \overline{d_B}}{\mathcal{D}_G} \quad Re = \frac{V_{SG} \overline{d_B} \rho_G}{\mu_G} \quad Sc = \frac{\mu_G}{\rho_G \mathcal{D}_G}$$

With respect to the interfacial area, the uncertainty of experimental measurement arises from the fact that the reference volume is not precisely defined. Any liquid spray system must include a gas/liquid separator downstream (such as a cyclone), whose volume is often at least as large as that of the throat of the venturi in which gas-liquid contact first takes place. Yet contact continues in the separator as long as the phases coexist.

The most logical way to approach venturi scrubbers is to treat the flow of the gas and the liquid droplets as cocurrent and evaluate the transfer using conventional methods. The interfacial area is calculated with the following equation:

$$\mathcal{A} = \frac{6\varepsilon_L}{\overline{d_B}} \tag{4.134}$$

As a first approximation ε_L can be taken to be equal to $Q_L/(Q_L + Q_G)$.

$\overline{d_B}$ is calculated using the following equation [Trambouze *et al.*, 1988]:

$$\overline{d_B} = 0.6 \frac{\sqrt{\rho_L}}{V_{r,C}\sqrt{\sigma}} + 0.017 \left[\frac{\mu_L}{\sqrt{\sigma \rho_L}}\right]^{0.45} \left[\frac{Q_L}{Q_G} 10^3\right]^{1.5} \tag{4.135}$$

where

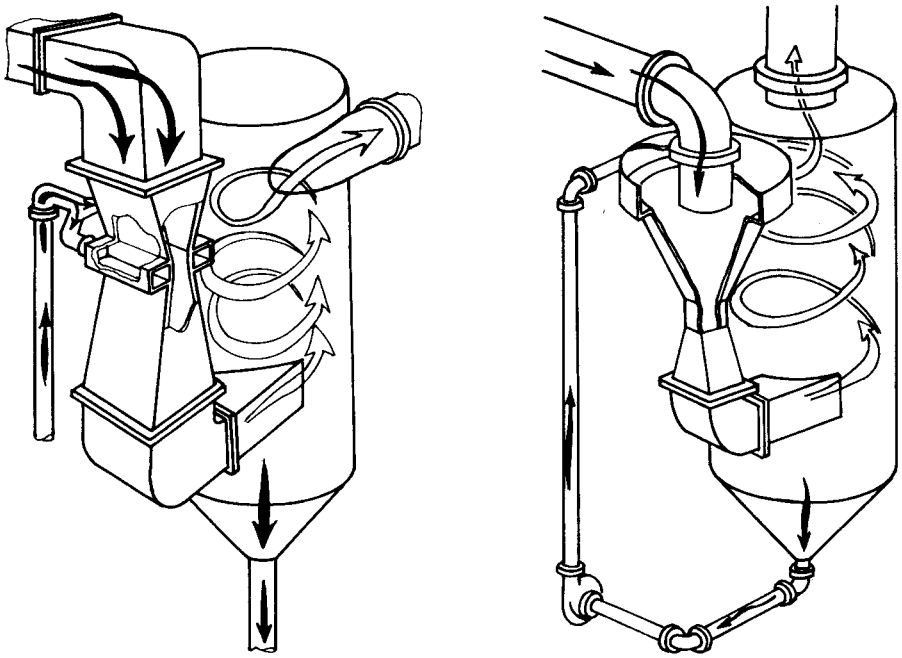
$V_{r,C}$ relative gas/liquid velocity at the neck (m/s)
V_{GC} gas velocity at the neck, on the order of 100 m/s
Q_G, Q_L gas and liquid volume flow rates (m^3/s).

A. Practical applications

Venturi scrubbers are extensively used to scrub gases, remove micron- or submicron-size solids from various effluents (catalytic cracking, flue gas, mist, vapor, etc.) (Fig. 4.26). The size and velocity of the liquid droplets has a direct effect on the efficiency of collection. The efficiency decreases rapidly with the size of the particles (typically, for power plant flue gas: 94% for 1.7 μm particles, 81% for 0.65 μm particles, and 29% for 0.3 μm particles). The liquid is frequently recycled around the device.

B. Gas scrubbers

Gas scrubbers are designed to process high flow rates of gas and eliminate dust at the same time (wet fines removal). Most reactions that occur in scrubbers are "neutralization" reactions between an acid and a base, one of the two reactants being found in the gas phase. These reactions are very fast, even instantaneous, and therefore characterized by a high enhancement factor with frequently non negligible resistance on the gas side. Very brief residence times are characteristic of these devices.



Venturi-scrubber, type P-A

Venturi-scrubber, type W-A

Figure 4.26 Two venturi scrubber designs: Type P-A: liquid injected through nozzles. Type W-A: liquid film stripping at the neck.

Two types of equipment are suitable for use: venturi scrubbers and atomizers. Venturi scrubbers offer the advantage of being able to process large volumes of gas efficiently but do so with significant pressure drop and consequently rather high energy consumption. So-called "atomizers" are certainly more appropriate from this perspective, but the risks of bypass for a portion of the gas are greater, while their ability to remove dust is not as good.

In both devices the formation of a mist of fine droplets entrained at the outlet represents a potential risk. To counteract this effect, in practice scrubbers are often connected to demisters.

The most efficient separators are equipped with metal or plastic mesh but they are less flexible (they are inefficient at low flow rates and flood at high flow rates). Moreover, they present risks of fouling when fines removal is poor or incomplete. Static centrifugal separators do not have this drawback but the separation is not as good.

In some scrubbers the energy needed for gas-liquid contact is provided by the liquid alone. Known as liquid ejectors (Fig. 4.27), these devices are also used to remove process gas. They have relatively low capacity and are generally used to purify exhaust gases or absorb components produced by certain types of reaction (acidic gases or ammonia, for example).

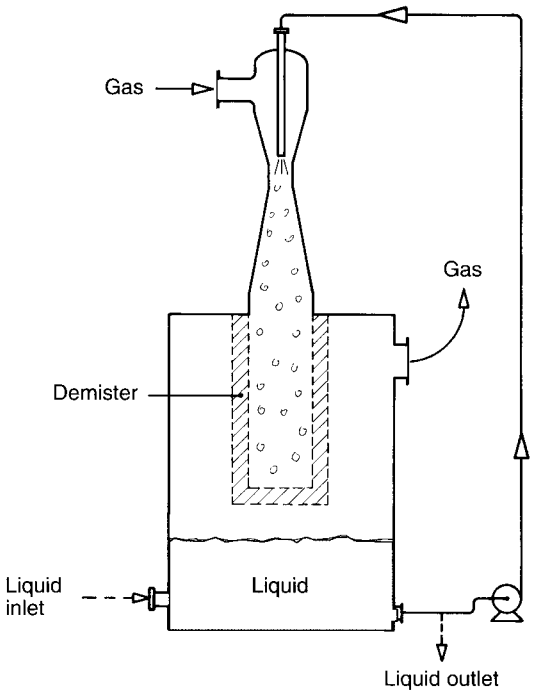


Figure 4.27 Gas scrubber equipped with an ejector with liquid phase recirculation.

4.8.2.2 Atomizers and spray towers

In atomizers and spray columns, liquid is sprayed through nozzles at the top of a large chamber (Fig. 4.28). The spray operation entails significant pressure drop on the liquid side. The fine droplets that are formed describe trajectories that are dependent on their size, the circulation of the gas, the geometry of the chamber and nozzle, and so on. These droplets must be distributed uniformly throughout the entire column section, even though some of them are projected against the wall, forming a film. Few systematic studies are available [Taniguchi *et al.*, 1999]. Trambouze *et al.* [1988] provide the following orders of magnitude:

$$\begin{aligned} 1.5 \cdot 10^{-4} < \quad & \rho_L \quad < 3.0 \cdot 10^{-4} \text{ (m/s)} \\ 0.4 < \quad & k_G \quad < 1 \text{ (mol/m}^2 \cdot \text{atm} \cdot \text{s)} \\ 10^{-2} < \quad & k_G RT \quad < 2.5 \cdot 10^{-2} \text{ (m/s)} \\ 30 < \quad & \mathcal{A} \quad < 70 \text{ (m}^{-1}\text{)} \end{aligned}$$

These atomizers are especially appropriate when:

- the available pressure drop on the gas side is very low
- one or two theoretical contact stages are sufficient
- the gas is very soluble
- the reactions are exothermic.

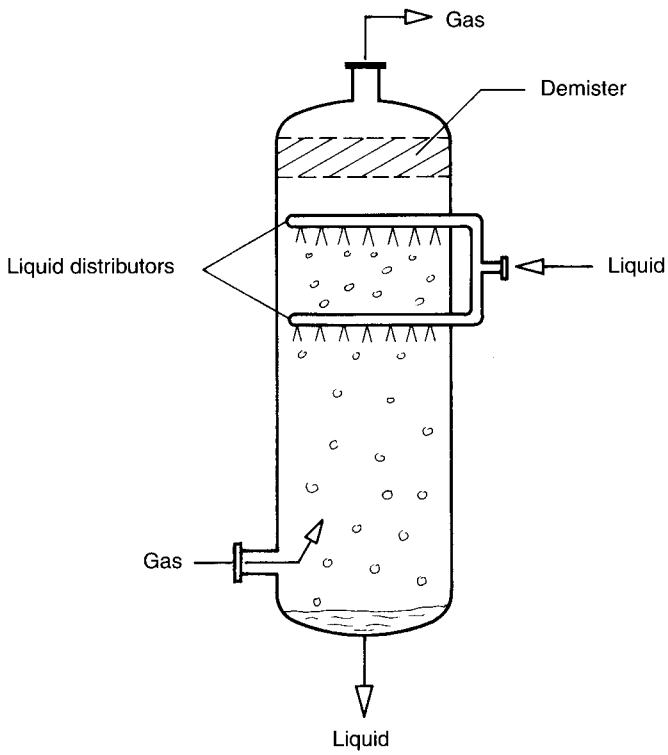


Figure 4.28 Operation of an atomizer.

To conclude, these ejectors and atomizers are characterized by significant mass transfer and short contact times. The pump, which entrains the liquid, accounts for the bulk of the initial—and non-negligible—investment and maintenance costs. These ejectors are well suited for the very rapid absorption of highly soluble gases and can accept gas under low pressure. However, they do have high operating costs because of the amount of energy required to atomize the liquid.

4.9 INLINE MIXERS

The gas-liquid contact that takes place in simple empty pipes or those equipped with stationary obstacles for turbulent flow generation is sometimes adequate for promoting a reaction.

4.9.1 Empty pipes

When a gas-liquid mixture passes through a straight horizontal pipe, a number of hydrodynamic regimes are possible. Depending on the flow rates and properties of the two fluids, the flow can assume various forms: bubble, slug, annular, stratified, wave, plug,... A number

of correlations or regime charts can be used to specify the limits of these regimes and calculate the corresponding pressure drops.

For bubble or slug regimes, the mass transfer and especially the heat transfer are favorable. The following correlation, established for horizontal pipes, takes into account the properties of the fluids [Scott and Hayduk, 1966].

$$k_L a = 9.03 \cdot 10^{-3} V_{SL} \left(\frac{V_{SG}}{V_{SL} + V_{SG}} \right)^{0.78} \sigma_L^{0.5} \mu_L^{0.09} \left(10^5 \mathcal{D}_A\right)^{0.4} D_C^{-1.9} \qquad (4.136)$$

This type of gas-liquid contactor is very simple, compact, inexpensive, and tolerates large variations in flow rates. If the pipe is not horizontal and straight, the hydrodynamic behavior becomes complex.

A number of devices can be used to inject the minority fluid (Fig. 4.29). Moreover, obstacles of more or less complex shape placed in the pipe can noticeably improve contact between the phases, although with appreciable pressure drop.

4.9.2 Static mixers

Static mixers are inline mixers that contain a flat helical ribbon that is systematically twisted 90 to 180° into right- and left-hand elements (Fig. 4.29). They separate fluids into independent

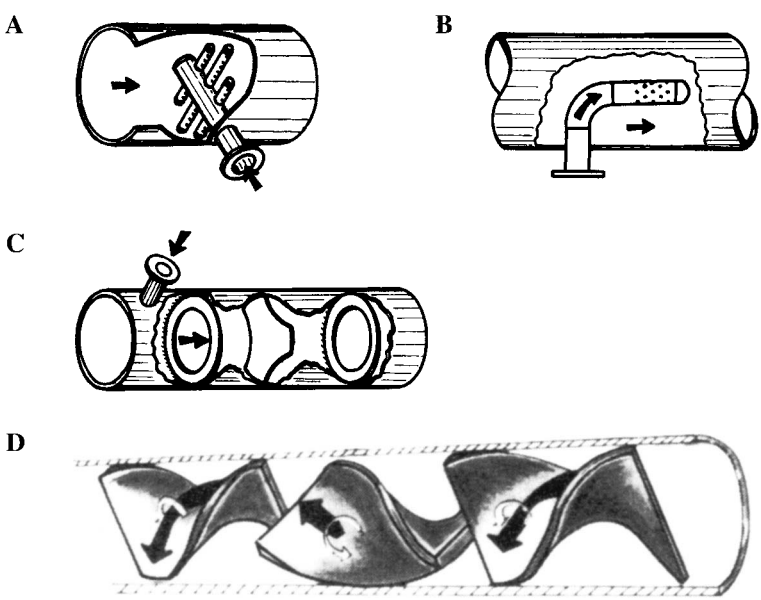


Figure 4.29 Examples of inline and static mixers. **A.** Perforated pipe distributors. **B.** Injection of a fluid through a strainer into the axis of the pipe. **C.** Injection through a T-shaped pipe and mixing by passage through alternating baffles. **D.** Static mixer for viscous or pasty fluids (Kenics).

streams, then rotate these streams, and finally recombine them in a relative position different from their starting position.

Placed in pipes through which a gas-liquid mixture passes, they uniformly fragment the gas bubbles and produce a narrow distribution of bubble sizes, where mean diameter decreases when the liquid velocity increases. Mass and heat transfer are improved through the rotation and fragmentation process without an appreciable increase in pressure drop compared to the empty pipe.

Generally, several static mixers are placed in series in pipes less than 1 m in diameter rather than in bubble columns strictly speaking. However, there exist open structured packings that can be placed in columns several meters in diameter, resulting in an appreciable increase in interfacial area and therefore in $k_L a$. Wang and Fan [1978] have provided a series of correlations, but since the publication of their findings useful correlations have become rare.

These static mixers have the following advantages:

- good gas-liquid contact
- short, well-controlled residence times, but dependent on flow rates
- very good heat transfer
- good flexibility
- moderate pressure drop
- the presence of moderate quantities of fine solids is acceptable
- no moving parts
- made of a variety of corrosion-resistant materials.

4.10 CONCLUDING REMARKS

We currently have access to a large number of correlations for gas-liquid contactors. These can be used to efficiently guide the selection of equipment for a chemical reaction whose characteristics are relatively well known. However, the quantitative values needed to design and engineer devices other than packed columns are not yet completely reliable. This arises from the fact that interfacial areas depend to a large extent on the coalescence properties of the physicochemical system and, at present, these have not yet been fully described. It is also recommended that the scaling factor be limited and that scale-up be based only on tests conducted on the same reaction system. Simulation of the behavior of an industrial reactor by means of a small test apparatus in which the same chemical reaction takes place is a useful approach, providing the laboratory device is truly representative of the industrial reactor (Laurent, cited in Trambouze *et al.* [1988]).

Several reliable publications are available and can be consulted when selecting equipment, in particular Gourlia and Trambouze [2000] and Perry [1997]. Table 4.15 summarizes the criteria introduced throughout Chapters 3 and 4 and can be used as a basis for making an informed decision.

Of all the gas-liquid contactors seen so far, bubble columns stand out for their reasonable capital investment and operating costs. Unfortunately they do not provide very high interfacial area. They are recommended for slow reactions that do not require significant interfacial areas or gas holdup.

Table 4.15 Selection of gas-liquid contactors.

	Bubble column	Partitioned bubble column	Horizontal bubble column	Bubble column with gas recycling	Mechanically stirred tank	Bubble-cap plate column	Valve plate column	Countercurrent packed column	Crosscurrent or cocurrent packed column	Venturi scrubber	Spray tower	Static mixer
Fast reaction	−	−	0	−	0	0	0	+	+	+	+	+
Slow reaction	+	+	+	+	0	0	0	−	−	−	−	−
High conversion of the reactant in gas phase	−	0	−	+	−	+	+	+	0	0	0	0
High conversion of the reactant in liquid phase	0	0	0	−	0	+	+	+	0	−	−	0
Low pressure drop for gas	−	−	0	−	0	−	0	+	0	+	+	0
Thermal control	+	+	+	+	+	0	0	0	0	+	+	+
Foaming	+	+	0	0	−	−	−	+	0	0	+	0
Presence of solids	+	+	+	+	0	−	−	−	−	0	0	−
Fines removal	0	0	0	−	−	−	−	−	−	+	+	−
Maintenance cost	+	+	+	+	−	+	+	0	0	0	0	+
Capital investment	+	+	0	0	0	−	0	+	+	0	0	+

+: recommended; 0: acceptable; −: unsuitable.

REFERENCES

Abashar M, Narsingh U, Rouillard A, Judd R (1998) Hydrodynamic flow regimes, gas holdup and liquid circulation in airlift reactors. Ind Eng Chem Res 37, pp 1251–1259.

Akita K, Yoshida F (1973) Gas holdup and volumetric mass transfer coefficient in bubble columns. Ind Eng Chem Proc Des Dev 12, 1, p 76–80.

Akita K, Yoshida F (1974) Bubble size, interfacial area and liquid phase mass transfer coefficient in bubble columns. Ind Eng Chem Proc Des Dev 13, 1, p 84–91.

Billet R (1995) Packed towers in processing and environmental technology. VCH, Weinheim.

Bravo JL (1997) Select structured packings or trays? Chem Eng Prog, July 1997, pp 3641.

Calderbank PH (1958) Physical Rate Processes in Industrial Fermentation: Part I: The Interfacial Area in Gas-Liquid Contacting with Mechanical Agitation. Trans Inst Chem Eng 36, p 443–463.

Calderbank PH (1959) Physical rates processes in industrial fermentation. Part II: Mass transfer coefficients in gas-liquid contacting with and without mechanical agitation. Trans Inst Chem Eng 37, p 173–85.

Calderbank PH, Moo young MB (1961) Chem Eng Sci 16, p 39.

Charpentier JC (1976) Recent Progress in Two Phase Gas-Liquid Mass Transfer in Packed Beds. Chem Eng J 11, p 161–181.

Charpentier JC (1981) Mass-Transfer Rates in Gas-Liquid Absorbers and Reactors. Adv Chem Eng XI, pp 1–133. Ed. Academic.

Chisti MY (1989) Airlift bioreactors. Elsevier.

Choi KH, Chisti Y, Moo-young M (1996) Comparative evaluation of hydrodynamic and gas-liquid mass transfer characteristics in bubble column and air-lift slurry reactors. Chem Eng J 62, pp 223–229.

Cicile JC (1994) Distillation Absorption. Généralités sur les colonnes de fractionnement – Colonnes plateaux : dimensionnement. Techniques de l'ingénieur J2610 to J2627.

Cockx A (1997) Modélisation de contacteurs gaz-liquide : application de la mécanique des fluides numérique aux airlifts. INSA dissertation, Toulouse.

Cockx A, Liné A, Roustan M, Do-quang Z, Lazarova V (1997) Numerical simulation and physical modeling of the hydrodynamics in an air-lift internal loop reactor. Chem Eng Sc 52, 21/22, pp 3787–3793.

Copigneaux P (1993) Distillation, Absorption, 4. Colonnes garnies. Techniques de l'ingénieur J2626, p 1–24

Danckwerts PV (1970) Gas Liquid Reactions. McGraw-Hill, London.

Deckwer W, Schumpe A (1993) Improved tools for bubble column reactor design and scale-up. Chem Eng Sci 48, 5, pp 889–911.

Deckwer WD (1992) Bubble column reactors. John Wiley and Sons, New York.

Dhaouadi H (1997) Étude d'un réacteur à gazosiphon à recirculation externe. INPL dissertation, Nancy.

Dudukovic MP, Devanathan N, Holub R (1995) Packed Towers in processing and environmental Technology. VCH, Weinheim.

Fair JR, Lambright AJ, Andersen JW (1962) Heat transfer and gas holdup in a sparged contactor. Ind Eng Chem Proc Des Dev 1, p 33–6.

Fair JR (1993) How to design baffle tray columns. Hydrocarbon Processing, May 1993, pp 75–80.

Fan L (1989) Gas-Liquid-Solid Fluidization Engineering. Butterworths, Boston.

Gaspillo PAD, Goto S (1991) Mass transfer in bubble slurry column with static mixer in draft tube. J Chem Eng Japan 24, 5, pp 680–682.

Gourlia JP, Trambouze P (2000) Petroleum Refining. Vol. 4: Materials and Equipment. Editions Technip, Paris.

Harnby N (1992) Mixing in the process industries (2nd edition). Butterworth-Heinemann, Boston.

Hassan ITM, Robinson CW (1977) Stirred-tank mechanical power requirement and gas holdup in aerated aqueous phases. AIChE J 23, 1, p 48–56.

Hikita H, Asai S, Tanigawa K, Segawa K, Kitao M (1981) The volumetric liquid-phase mass transfer coefficient in bubble columns. Chem Eng J, 22, pp 61–69.

Hikita H, Asai S, Tanigawa K, Segawa K, Kitao M (1980) Gas holdup in bubble columns. Chem Eng J 20, pp 59–67.

Hyndmann CL, Guy C (1995) Gas phase hydrodynamics in bubble columns. Trans Inst Che. Eng 73, April 1995, p 302–307.

Hyndmann CL, Guy C (1996) Gas holdup in bubble column reactors operating in the churn-turbulent flow regime. AIChE J, 42(9), 2627–2634.

Jiang P, Lin T, Luo *et al.* (1995) Flow vizualisation of high pressure bubble columns: bubble characteristics. Trans Inst Chem Eng 73, pp 269–274.

Joshi J, Ranade V, Gharat S, Lele S (1990) Sparged loop reactors. Can J Chem Eng 68, pp 705–741.

Joshi JB, Pandit AB, Sharma MM (1982) Mechanically agitated gas-liquid reactors. Chem Eng Sci 37, 6, pp 813–844.

Kister H, Larson K, Yanagi T (1994) How do trays and packing stack up? Chem Eng Progress, Feb. 1994, pp 23–32.

Kister HZ (2003) What caused tower malfunctions in the last 50 years?, Trans IchemE, Vol 81, Part A, January 2003, 5–26.

Kister HZ (1992) Distillation design. McGraw-Hill, New York.

Klemas L, Bonilla JA (1995) Accurately assess packed column efficiency. Chem Eng Progress, July 1995, 27–44.

Kohl A, Riesenfeld F (1985) Gas purification (4th Ed.). Gulf Publishing Company.

Koïde K (1996) Design parameters of bubble column reactors with and without solid suspensions. J Chem Eng Japan 29, 5, pp 745–759.

Koïde K (1996) Effect of packed bed on mass transfer in external-loop airlift bubble column. J Chem Eng Japan 29, 4, pp 582–587.

Krishna R, Wilkinson P, Van Dierendonck L (1991) A model for gas holdup in bubble columns incorporating the influence of gas density on flow regime transitions. Chem Eng Sci 46, 10, pp 2491–2496.

Krishna R, Ellenberger J (1996) Gas holdup in bubble column reactors operating in the churn turbulent flow regime. AIChE J. 42, 9, pp 2627–2634.

Kumar S, Vanderheyden W, Devanathan N, Padial N, Dudukovic M, Kashiwa N (1995) Numerical simulation and experimental verification of the gas-liquid flow in bubble columns. AIChE Symposium series 305, 91, pp 11–19.

Kumar A, DegaleesanTE, Laddha GS, Hoelscher HE (1976) Bubble swarm characteristics in bubble columns. Can J Chem Eng 54, p 503–508.

Lance M, Tran M, Petersen K (1996) Simulation numérique des écoulements à bulles dans les réacteurs gaz-liquide. Revue de l'Institut Français du Pétrole 51, 2, pp 279–290.

Lee SY, Tsui YP (1999) Succeed at gas/liquid contacting. Chem Eng Prog July 1999, pp 23–49.

Leva M (1953) Tower Packings and Packed Tower Design. US Stoneware Co., Akron.

Leva M (1992) Reconsider packed tower pressure-drop correlations. Chem Eng Prog Jan. 1992, pp 65–72.

Lübbert A, Lapin A (1996) Dynamical numerical experiments with 3-D bubble columns. Analysis of some key mixing mechanisms. Revue de l'Institut Français du Pétrole 51, 2, pp 269–277.

Mackowiak J (1991) Pressure drop in irrigated packed columns. Chem Eng Proc 29, pp 93–105.

Michel BJ, Miller SA (1962) Power requirements of gas-liquid agitated systems. AIChE J, 8, p 262–6.

Midoux N, Morsi BI, Purwasasmita M, Laurent A, Charpentier JC (1984) Interfacial area and liquid-side mass transfer coefficient in trickle bed reactors operating with organic liquids. Chem Eng Sci 39, pp 781–794.

Miyahara T, Hayashino T (1995) Size of bubbles generated from perforated plates in non-newtonian liquids. J Chem Eng of Japan, 28, 5, pp 596–600.

Molga EJ, Westerterp K (1997) Experimental study of a cocurrent upflow packed bed bubble column reactor: pressure drop, holdup and interfacial area. Chem Eng Proc 36, pp 489–495.

Muller F, Davidson J (1992) On the contribution of small bubbles to mass transfer in bubble columns containing highly viscous liquids. Chem Eng Sci 47, 13/14, pp 3525–3532.

Muller F, Davidson J (1995) On the effects of surfactants on mass transfer to viscous liquids in bubble columns. Trans Inst Chem Eng, 73, April 1995, pp 291–296.

Nagata S (1975) Mixing, Principles and Applications. John Wiley and Sons, New York.

Nagel O, Kurten H, Sinn R (1970) Power-jet reactors: I. Application of the ejector principle to the improvement of gas absorption in bubble columns. Chem Ing Tech 42, p 474–480.

Nakoua M, Dribika M, Besher E (1999) Interfacial area in valve and bubble cap tray columns. J Chem Eng of Japan 32, 1, pp 126–129.

Ogawa S, Yamaguchi H, Tone S, Otake T (1983) Gas-liquid mass transfer in the jet reactor with liquid jet ejector. J Chem Eng of Japan 16, 5, pp 419–425.

Oldshue JY (1983) Fluid mixing technology. McGraw-Hill, New York.

Öztürk S, Schumpe A, Deckwer W (1987) Organic liquids in a bubble column: holdups and mass transfer coefficients. AIChE J 33, 9, pp 1473–1480.

Perry RH (1997) Gas in liquid dispersion. Chemical Engineers Handbook, p 14.74, 7th edition and p 5.48, 5th edition, McGraw-Hill, New York.

Ptak C, Bonfils P, Marty C (2000) Distillation, absorption and stripping in the petroleum industry. *In:* Petroleum Refining. Vol. 2: Separation Processes. Editions Technip, Paris.

Reilly I, Scott D, De Bruijn T, Mc Intyre D (1994) The role of gas phase momentum in determining gas holdup and hydrodynamic flow regimes in bubble column operations. Can J Chem Eng 72, Feb 1994, pp 3–12.

Reiss LP (1967) Cocurrent Gas-Liquid Contacting in Packed Columns. Ind Chem Proc Des Dev 6, 4, pp 486–498.

Reith Th (1968) Physical Aspects of Bubble Dispersions in Liquids. Dissertation, Delft.

Rocha JA, Bravo JL, Fair JR (1993) Distillation columns containing structured packings. Ind Eng Chem Res 1993, 32, pp 641–651.

Schlüter S, Steiff A, Weinspach PM (1995) Heat transfer in two and three phase bubble column reactors with internals. Chem Eng Proc 34, pp 157–172.

Schügerl K (1980) Neue Bioreaktoren für aerobe Prozesse. Chem Ing Tech 52, pp 951–965.

Scott DS, Hayduk W (1966) Can J Chem Eng 44, pp 130–136.

Sharma MM, Jhaveri AS (1969) Chem Eng Sci 24, p 189.

Sharma MM, Mashelkar RA, Metha VD (1969) Mass transfer in plate columns. Br Chem Eng 14, 1, p 70–6.

Sharma MM, Mashelkar RA (1968) Chem Eng Symp Ser, 28, p 10.

Sherwood TK, Pigford RL, Wilke CR (1975) Mass Transfer. McGraw-Hill, New York.

Suh I, Schumpe A, Deckwer W, Kulicke W (1991) Gas-liquid mass transfer in the bubble column with viscoelastic liquid. Can J Chem Eng 69, pp 506–512.

Taniguchi I, Yokoyama H, Asano K (1999) Mass transfer in absorption of lean gas using a small spray column. J Chem Eng Japan 32, pp 145–150.

Tatterson GB (1991) Fluid mixing and gas dispersion in agitated tanks. McGraw-Hill, New York.

Thijert M, Oyevaar M, Kuper W, Westerterp K (1992) Residence time distribution of the gas phase in a mechanically agitated gas-liquid reactor. Chem Eng Sci 47, p 3339–3346.

Trambouze P, Van Landeghem H, Wauquier JP (1988) Chemical Reactors. Editions Technip, Paris.

Trambouze P (1996) CFD applied to process engineering; an introduction. Revue de l'Institut Français du Pétrole 51, 2, pp 199–203.

Trambouze P *et al.* (2000) Petroleum Refining. Vol. 4: Materials and Equipment. Editions Technip, Paris.

Uhl VW, Gray JB (1967) Mixing Theory and Practice. Academic Press, New York.

Van Dierendonck L, Fortuin JMH, Venderbos D (1968) Proc IV Eur Symp Chem React Eng.

Verma AK (1989) Heat transfer mechanism in bubble columns. Chem Eng J 42, pp 205–208.

Wachi S, Nojima Y (1990) Gas-phase dispersion in bubble columns. Chem Eng Sci 45, 4, pp 901–905.

Wang KB, Fan LT (1978) Mass transfer in bubble columns packed with motionless mixers. Chem Eng Sci 33, p 945–52.

Wilkinson P (1991) Physical aspects and scale-up of high pressure bubble columns. Dissertation, Université de Groningen (Hollande).

Wilkinson P, Haringa H, Van Dierendonck L (1994) Mass transfer and bubble size in a bubble column under pressure. Chem Eng Sci 49, 9, pp 1417–1427.

Wilkinson P, Haringa H, Stokman F (1993) Liquid mixing in a bubble column under pressure. Chem Eng Sci 48, 10, pp 1785–1791.

Wilkinson P, Spek A, Van Dierendonck L (1992) Design parameters estimation for scale-up of high pressure bubble columns. AIChE J 38, 4, pp 544–554.

Wilkinson P, Van Dierendonck L (1994) A theoretical model for the influence of gas properties and pressure on single-bubble formation at an orifice. Chem Eng Sci 49, 9, pp 1429–1438.

Wilkinson PM, Van Dierendonck L (1990) Pressure and gas density effects on bubble break-up and gas hold-up in bubble columns. Chem Eng Sci 45, 8, pp 2309–2315.

Yagi H, Yoshida E (1975) Gas absorption by Newtonian and non-Newtonian fluids in sparged agitated vessels. Ind Eng Chem Proc Des Dev 14, 4, p. 488–493.

Zhao M, Niranjan K, Davidson J (1994) Mass transfer to viscous liquids in bubble columns and airlift reactors: influence of baffles. Chem Eng Sci 49, 14, pp 2359–2369.

Zuiderweg FJ (1982) Sieve trays: A view on the state of the art. Chem Eng Sci 37, 10, pp 1441–1464.

NOMENCLATURE

(specific to Chapter 4)

Symbol	Definition	Dimension	SI unit
$\mathcal{A} = \mathcal{A}_h$	Interfacial area per unit surface of tray	–	–
$\mathcal{A}_L = \mathcal{A}/\varepsilon_L$	Interfacial area per volume of liquid	L^{-1}	m^2/m^3
d	Pipe diameter	L	m
d_p	Nominal dimension of packing	L	m
e	Thickness of liquid film	L	m
E_G, E_L, E_T	Energy per unit volume of packed column dissipated by the gas, by the liquid, total	$ML^{-1}\theta^{-3}$	W/m^3
F_P	Packing factor (see Table 4.5)	L^{-1}	m^2/m^3
h_L	Height of clear liquid above the bubble caps of a plate (Fig. 4.8)	L	m
h_r	Height of liquid above the stirrer at rest	L	m
L	Wetted perimeter	L	m
L'	Specific flow of liquid per unit length of weir	$L^3\theta^{-1}L^{-1}$	m^2/s
n	Number of pipes	–	–
n_P	Number of rotor blades	–	–
n_t	Number of holes per unit surface in a perforated plate	–	–
$\mathcal{P}_L$	Total power input in the degassed liquid	$ML^2\theta^{-3}$	W
$\mathcal{P}_{LG}$	Total power input in the expanded liquid	$ML^2\theta^{-3}$	W
T	Distance between plates (Fig. 4.8)	L	m
t_G	Bubble contact time $= H/u_B$	θ	S
u_B	Mean rise velocity of bubbles	$L\theta^{-1}$	m/s
u_r	Relative velocity of the two phases	$L\theta^{-1}$	m/s
u_t	Rise velocity of a bubble	$L\theta^{-1}$	m/s
$V_{r,C}$	Relative gas-liquid velocity at the neck of the venturi	$L\theta^{-1}$	m/s
W	Height of weir (Fig. 4.8)	L	m
Z_C	Height of liquid on a plate (Fig. 4.8)	L	m
Z_F	Height of foam on a plate (Fig. 4.8)	L	m
π_1, π_2	Dimensionless numbers (Eqs. (4.65) to (4.68))	–	–
Ω_L	Surface compared to the unit volume of liquid	L^{-1}	m^2/m^3
Bo	Bond number $= gD_C^2\rho_L/\sigma$	–	–
Fr	Froude number $= V_{SG}/(gD_C)^{0.5}$	–	–
Ga	Galileo number $= gD_C^3\rho_L^2/\mu_{eff}^2$	–	–
Pe	Peclet number $= \dfrac{V_{SL}D_C}{\mathcal{D}_{AL}}$	–	–
Re_R	Reynolds number relative to the rotor $(Re)_R = \dfrac{N_R d_R^2 \rho_L}{\mu_L}$	–	–
Sc	Schmidt number $= \mu_{eff}/\rho_L\mathcal{D}_L$	–	–
Sh	Sherwood number $= k_L\mathcal{A}D_C^2/\mathcal{D}_L$	–	–
Wi	Weissenberg number $= N_1/\tau$	–	–
	Subscripts:		
B	relative to the bubbles		
C	at the Venturi neck, in the column		
e	at flooding		

Copyrighted Materials
Copyright © 2004 Editions Technip Retrieved from www.knovel.com

5 Experimental Data and Correlations for Liquid-Liquid Reactors

5.1 INTRODUCTION

Liquid-liquid contactors are used extensively for physical extraction with a solvent, but these same devices can also be used when the two liquid phases react chemically with one another. From this point of view the design of liquid-liquid reactors is similar to that of gas-liquid reactors. The same physical parameters are involved (interfacial area, transfer coefficients, etc.), the location of the reaction is important, and similar reactors are used. However, the ratio of phases remains generally closer to the ratios of inlet flow rates than in gas-liquid reactors.

In the current chapter our presentation of liquid-liquid reactors is based on the type of energy introduced and the dispersed phase fragmentation process employed (Fig. 5.1):

- spray towers
- plate columns (pulsed and non-pulsed)
- packed columns
- static mixers
- mechanically agitated columns
- mixer-settlers
- other equipment.

For each of these reactor types we provide the following information:

- hydrodynamic
  - phase holdup
  - interfacial area
  - flooding
  - backmixing
- mass transfer
- technology.

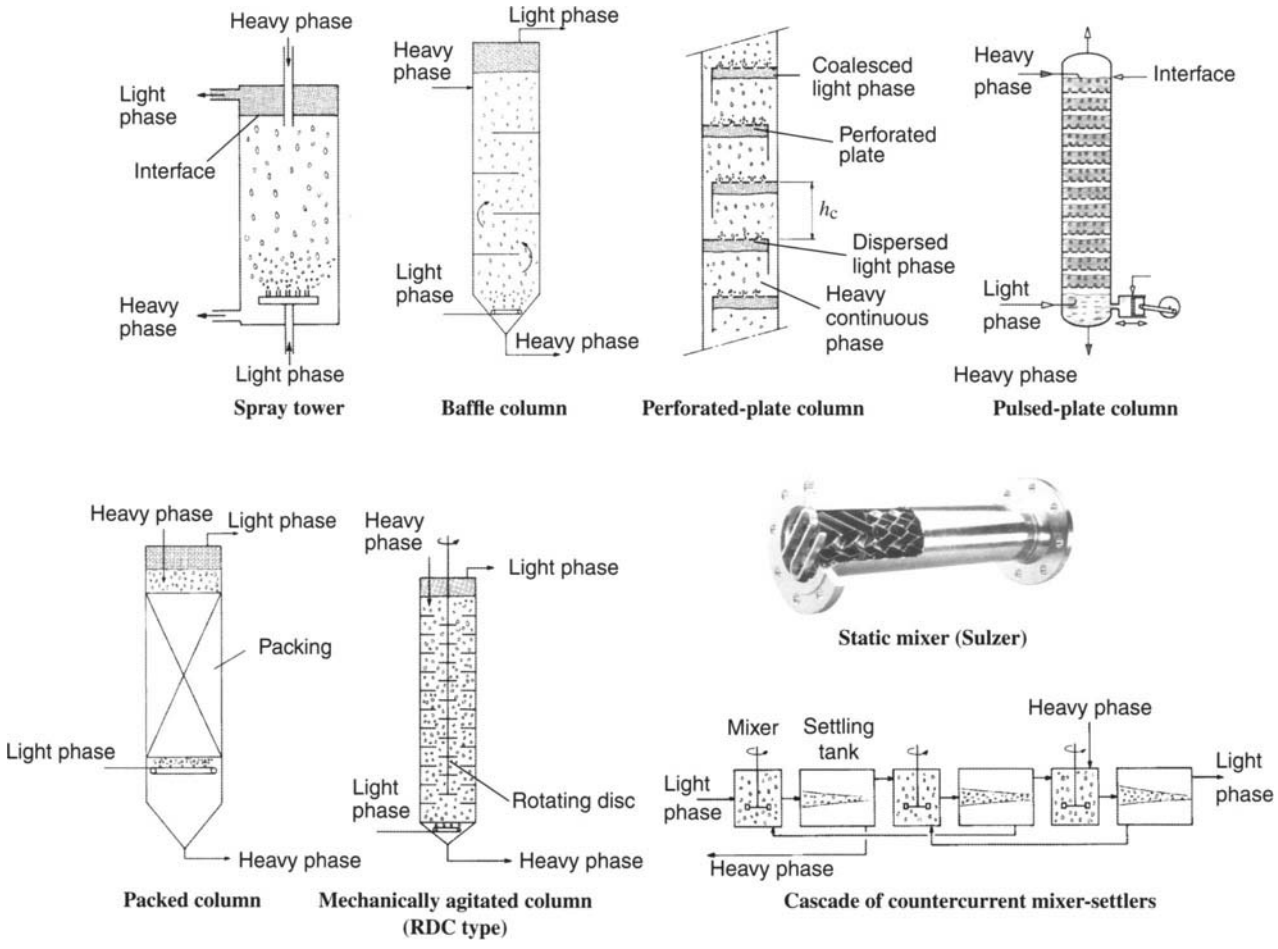


Figure 5.1 Different types of liquid-liquid contactors.

It is sometimes difficult to formulate reliable general correlations for liquid-liquid contactors because the associated physicochemical properties have a very considerable influence on transfer parameters that is difficult to quantify. The situation is even more critical than it is with gas-liquid reactors because various phenomena complicate the interpretation of experimental results. These primarily involve turbulence at the interfaces due to interfacial tension gradients, which are themselves the result of concentration gradients (Marangoni effect). Sawitowski [1975] classifies the phenomena into two types:

1. Appearance of interfacial convection currents. These currents increase the transfer coefficients by modifying turbulence at the interface. Although the interface is subject to deformation from these currents, the influence of the deformation on the interfacial area is frequently negligible.
2. Under certain conditions, especially if fluid circulation is already turbulent or if the transfer flux is large, these interface deformations can look like dispersed phase packets erupting into the continuous phase. In this case there is, quite obviously, an increase in the interfacial area.

The importance of these phenomena depends on several factors. Some of them are responsible for the appearance of turbulence (primary factors), others influence only their intensity (secondary factors).

The primary factors are:
- the direction of mass transfer
- the sign of the gradient $\mathrm{d}\sigma/\mathrm{d}C$ (normally negative—the interfacial tension decreases when a solute is added)
- the ratio of diffusivities: $\mathcal{D}_a/\mathcal{D}_d$ [1]
- the ratio of kinematic viscosities: ν_a/ν_d [1].

The secondary factors are:
- the numerical value of $\mathrm{d}\sigma/\mathrm{d}C$
- the concentrations in the two phases C_a and C_d of transferred solute
- the value of the partition coefficient
- the values of $\mathcal{D}_a$ and $\mathcal{D}_d$
- the values of ν_a and ν_d.

We can conclude that these phenomena greatly complicate the interpretation of experimental results. But their importance is felt most when the concentration gradients at the interfaces are large: when the phases come into contact and transfer first begins, in other words, when droplets are being formed. In nearly all cases they accelerate transfer rates in such a way that the majority of the correlations discussed below are valid essentially during stabilized periods. They are always conservative and provide relatively low numerical values.

When designing the reactor vessels, transfer is primarily associated with:
- the intensity and type of shear of the dispersed phase
- the efficiency of settling and drop coalescence
- the temperature.

1. The subscripts a and d refer to the incoming and outgoing phase respectively.

We first identify a number of characteristics typical of all liquid-liquid contactors. In spite of the impressive number of studies on the behavior of isolated drops, we limit our discussion to research involving correlations for drop clouds and dispersions.

Ray [1994] provides a detailed bibliography, and important summaries of liquid-liquid contactors have been provided by Godfrey and Slater [1994], Kumar and Hartland [1995], Lo [1997], Schweitzer [1997], Wauquier [2000], and Trambouze [2000].

5.1.1 Hydrodynamic behavior

5.1.1.1 Observation of the dispersed phase

To design liquid-liquid contactors we must first determine which of the phases is continuous. In general this is the phase with the greatest surface tension; it is often the polar phase. However, beyond a certain phase ratio, a phase inversion occurs. This critical ratio depends on the system in question, the operating mode, and the intensity of agitation. For the water-heptane system, for example, it has been found that inversion occurs only when the heptane/water ratio is greater than three. Nonetheless, there remains a zone of uncertainty, which increases when the interfacial tension decreases. For example, if we start out with a suspension of water in oil and add water, we can maintain the oil as the continuous phase for higher concentrations of water than if we began with a suspension of oil in water.

5.1.1.2 Holdup and interfacial area

Holdup and interfacial area are important hydrodynamic parameters and need to be estimated. This is possible if we can determine the average droplet size and a characteristic relative velocity. When vertical velocities are essentially the result of gravitational forces (column contactors), we can write the following continuity equation:

$$u_r = \frac{V_{SD}}{\varepsilon_D} \pm \frac{V_{SC}}{\varepsilon_C} \quad \begin{matrix} + \text{ countercurrent system} \\ - \text{ cocurrent system} \end{matrix} \tag{5.1}$$

where

u_r	relative overall velocity of the two phases (considered as positive in the direction of circulation of the dispersed phase)
V_{SC}, V_{SD}	superficial velocity of the continuous and dispersed phases respectively
ε_C, ε_D	volume fraction of the reactor occupied by the continuous and dispersed phases respectively.

This equation assumes that there is no backmixing or change in the velocity of the phases. For a packed column, it is valid providing we remember that, in this case:

$$\varepsilon_C + \varepsilon_D + \varepsilon_B = 1 \tag{5.2}$$

where ε_B is the volume fraction of reactor occupied by the packing.

The relative velocity u_r is associated with the rise (or fall) velocity of a cloud of drops in a continuous medium that is infinite and immobile. This velocity depends primarily on

the physicochemical properties of the system and, to a certain extent, on the conditions under which the dispersed phase is introduced. This intrinsic cloud velocity is known as the characteristic velocity of the system, u_g, and can be assumed to describe the relative velocity of the two phases. For example, in a device such as a drop column, the rise of a drop creates circulation of the continuous phase in the opposite direction. The characteristic velocity u_g is therefore not equal to the overall relative velocity u_r because we must take into account the circulation of the continuous phase during the passage of drops:

$$u_g = \frac{u_r(1 - \varepsilon_B)}{\varepsilon_C} \tag{5.3}$$

Substituting in (5.1) yields:

$$u_r = u_g \frac{\varepsilon_C}{1 - \varepsilon_B} = \frac{V_{SD}}{\varepsilon_D} \pm \frac{V_{SC}}{\varepsilon_C} \tag{5.4}$$

where u_g is the characteristic relative velocity or slip velocity.

For the relationship between interfacial area, holdup ε_D, and mean drop diameter $\overline{d_B}$, the following equation is approximately valid:

$$\mathcal{A} = \frac{6\varepsilon_D}{\overline{d_B}} \tag{5.5}$$

where

$\overline{d_B}$ mean drop diameter: $\overline{d_B} = 6\Sigma V_i / \Sigma S_i = d_{32} = d_{Sauter}$

ΣV_i volume of drops

ΣS_i surface area of drops.

If we have access to correlations that enable us to estimate u_g and $\overline{d_B}$, we can calculate $\mathcal{A}$ since ε_D is obtained by combining (5.2) and (5.4).

With respect to holdup, the extensive efforts of compilation and synthesis undertaken by Kumar and Hartland [1995] have resulted in a correlation that is valid for a large number of liquid-liquid contactors (eight types of column and more than 7 000 data points from a wide variety of sources were included). Based on a lumping of characteristic parameters with varying effects (specific power, flow rates and physical properties of phases, geometry), the following correlation, which is general and empiric, can be used to predict holdup in the dispersed phase with relatively good precision:

$$\varepsilon_C = A \cdot B \cdot C \cdot D \tag{5.6}$$

$$A = \left[0.27 + \left\{\frac{P_m}{9.81}\left(\frac{\rho_C}{9.81\sigma}\right)^{0.25}\right\}^{0.78}\right]\left[V_{SD}\left(\frac{\rho_C}{9.81\sigma}\right)^{0.25}\right]^{0.87}$$

$$B = \exp\left[3.34 V_{SC}\left(\frac{\rho_C}{9.81\sigma}\right)^{0.25}\right]\left(\frac{\Delta\rho}{\rho_C}\right)^{-0.58}$$

$$C = \left(\frac{\mu_D}{\mu_W}\right)^{0.18} e^{F}\left[l\left(\frac{9.81\rho_C}{\sigma}\right)^{0.5}\right]^{-0.39}$$

D : coefficient that depends on the column (see Table 5.1)

where

P_m specific power (W/kg)

ρ_C, $\Delta\rho$ density of the continuous phase, difference relative to the dispersed phase (kg/m^3)

σ interfacial tension (N/m)

μ_D, μ_W viscosity of the dispersed phase and of water at 20°C ($\mu_W = 10^{-3}$ Pa · s) (Pa · s)

e free fraction of column cross-section; $e = (D_R/D_c)^2$ for rotating disc columns, where D_c is the column diameter and D_R the diameter of the rotor

F exponent that depends on the column:
- $F = -1$ for packed columns and Kühni columns
- $F = 0$ for other agitated columns

l characteristic length; depending on the device, this is equal to:
- h_c height of the compartment for a plate column
- $1/\mathcal{A}_P$ inverse specific area for a packed column
- d_{32} diameter of the drops for a spray column.

Table 5.1 Coefficient D in Eq. (5.6) from Kumar and Hartland [1995].

Column type	D
Normal (RDC) and asymmetric (ARDC) rotating disc	8.28
Kühni	4.35
Wirz II	21.9
Pulsed sieve tray	9.70
Karr	4.93
Packed	3.33
Spray	1.86

In describing the average drop size, the same authors, Kumar and Hartland [1995], provide several correlations specific to the various contactors. For mechanically agitated systems in which gravity is not a factor, Eq. (5.4) cannot be used; in this case the holdup $\varepsilon_D/(\varepsilon_C + \varepsilon_D)$ is close to the ratio $Q_D/(Q_C + Q_D)$, providing there is sufficient agitation. Consequently, it is appropriate to characterize the minimum agitation beyond which $\varepsilon_D/(\varepsilon_C + \varepsilon_D) = Q_D/(Q_C + Q_D)$. As with gas-liquid contactors, droplet size depends on the power dissipated and the physicochemical properties, but Eq. (5.5) remains valid in principle. The value of $\overline{d_B}$, which is about 0.1 to several millimeters, more infrequently 1 to 2 cm, depends to a large extent on the properties of the fluids and the direction of transfer of the solutes, as well as the method of dispersion.

In the preceding chapter we indicated how poorly understood are coalescence phenomena in gas-liquid contactors. The situation is similar for liquid-liquid contactors. However, the tendency to coalesce is one of the fundamental characteristics on which the numerical values of interfacial area depends. Therefore, the following methods for estimating these values are no more than approximate. The calculated values are almost always too low because

the presence of small quantities of surfactants generally inhibits coalescence, which in turn reduces the average drop size and increases the interfacial area, sometimes considerably.

5.1.1.3 Backmixing

Mixer-settlers obviously behave like cascades of continuous stirred tanks. For the other types of equipment, we will limit our discussion to models that exhibit plug flow accompanied by turbulent axial diffusion. Flow can then be characterized by a Peclet number (see Chapter 2). In spite of the somewhat summary nature of this description, it is sufficient for our purposes. On the other hand, the fact that backmixing can have an unfavorable influence on column performance is well known. Ingham's review [1975] provides useful information on this subject.

5.1.2 Mass transfer

Mass transfer between two liquid phases and between a gas and a liquid phase are identically described. The concept of local resistance in two zones or films on either side of the interface is also used. The overall resistance to transfer is then the sum of these two resistances: the resistance in the dispersed phase and the resistance in the continuous phase. Laddha and Degaleesan [1976] and Skelland and Conger [1973] have supplied lists of equations for estimating these transfer coefficients. We reproduce the most useful sections in Tables 5.2 and 5.3 [Trambouze *et al.* 1988].

Use of the correlations shown in 5.2 and 5.3 calls for the following comments:

1. The correlations are shown in a form that employs current dimensionless numbers. This does not always correspond to the original presentation of the authors. We have also retained the characteristic velocity u_g as the "velocity" variable in all the correlations. In certain cases the author of a given correlation has not specified the velocity used or has introduced a different concept, such as drop formation time or the settling time of a cloud of drops. In general these ambiguities cannot be resolved by referring to the original publication.

   To conclude, we recommend that the correlations be used as shown in the tables. Possible errors will be small given the lack of precision associated with the other terms.

2. Another source of ambiguity—and therefore of possible error—results from the definition of dispersed phase holdup. Many authors relate the dispersed phase fraction, referred to as *holdup*, to the sum of the volumes occupied by the two liquids. The holdup thus defined corresponds to $\varepsilon_D / (\varepsilon_C + \varepsilon_D)$. The sum $(\varepsilon_C + \varepsilon_D)$ is not necessarily equal to 1, especially if the column is packed, so that holdup may differ appreciably from ε_D.

3. The use of a given correlation is not always immediately obvious. It is recommended that numerical values be calculated for the various correlations and a value chosen that is a mean value, a conservative value, or one that is the result of a correlation that seems most appropriate for the unit or the part of the unit considered.

Table 5.2 Mass transfer coefficients, dispersed phase.

During drop formation	
$Sh_D = 0.057\left(d_O/\overline{d_B}\right)^{1.333}\left(u_O/u_g\right)^{0.84} Re_D^{1.27} Sc_D^{0.67} We_D^{-0.3} Fr^{0.089}$	(5.7)
In the cloud	
Rigid, motionless drops	
$Sh_D = -0.17\left(\overline{d_B}/L\right) Re_D Sc_D \ln\left[1 - 2\pi\left(\overline{d_B}/L\right)^{-0.5} Re_D^{-0.5} Sc_D^{-0.5}\right]$	(5.8)
$Sh_D = 6.6$ (conservative estimate)	(5.9)
Drops with circulation (internal convection)	
$Sh_D = 19.6\left(\overline{d_B}/L\right)^{0.34} Re_D^{0.34} Sc_D^{0.215} We_C^{0.37}$	(5.10)
$Sh_D = 0.023 Re_D Sc_D^{0.5}$	(5.11)
Oscillating drops	
$Sh_D = 0.26\left(\overline{d_B}/L\right)^{0.14} Re_D^{0.14} Sc_D^{0.14} We_C^{-0.2} Re_C^{1.08} Bo^{-0.1}$	(5.12)
During coalescence	
$Sh_D = 0.24\left(d_O/\overline{d_B}\right)^{1.71}\left(u_O/u_g\right)^{0.85} Re_D^{1.15} Sc_D^{0.031} Bo^{1.30}$	(5.13)

Table 5.3 Mass transfer coefficients, continuous phase.

During drop formation	
$Sh_C = 0.50\left(d_O/\overline{d_B}\right)^{1.22}\left(u_O/u_g\right)^{0.61} Re_C^{0.91} Bo^{-0.41} Fr^{-0.15}$	(5.14)
In the cloud	
Rigid drops	
$Sh_C = 0.74 Re_C^{0.5} Sc_C^{0.33}$	(5.15)
$Sh_C = 2 + 0.95 Re_C^{0.5} Sc_C^{0.25}$	(5.16)
$Sh_C = 0.98 Re_C^{0.33} Sc_C^{0.33}$	(5.17)
$Sh_C = 0.31 Re_C^{0.67} Sc_C^{0.33} We_C^{-0.33} Bo^{0.33}$	(5.18)
Drops with circulation	
$Sh_C = 50 + 0.0085 Re_C Sc_C^{0.7}$	(5.19)
$Sh_C = 1.3 Re_C^{0.5} Sc_C^{0.42}$	(5.20)
$Sh_C = 0.725\left(1 - \varepsilon_D\right) Re_C^{0.57} Sc_C^{0.42}$	(5.21)
$Sh_C = 0.92 Re_C^{0.67} Sc_C^{0.5} We_C^{-0.33} Bo^{0.33}$	(5.22)
Oscillating drops	
$Sh_C = 3.5 Re_C^{0.5} Sc_C^{0.5}$	(5.23)
$Sh_C = 2 + 0.084 Re_C^{0.53} Sc_C^{0.39} Fr^{-0.024}$	(5.24)
During coalescence	
$Sh_C = 7.3 \cdot 10^{-4}\left(d_O/\overline{d_B}\right)\left(u_O/u_g\right)^{0.5} Re_C^{0.83} Sc_C^{0.5} We_C^{0.52} Re_D^{0.52} Fr^{0.33}$	(5.25)

4. The values obtained for motionless and rigid drops are always low and approximately 3 to 5 times lower than the values obtained for moving or oscillating drops.
5. The values measured during coalescence and especially during drop formation are considerably higher, but the zones of coalescence and formation remain limited in most vessels. Only compartmentalized columns (plates, RDC) and possibly packed columns operating near the flood point present operating characteristics that are favorable throughout their entire height. Moreover, the drop coalescence does not always have a positive effect on the transfer coefficients, in fact, coalescence can impede circulation at the interfaces due to interfacial tension gradients. Obviously, coalescence leads to other types of motion, but these are not necessarily more effective than those indicated above for promoting mass transfer. Coalescence is especially beneficial in systems where the presence of surfactive substances tends to immobilize the interface.
6. The numerical values of the coefficients of transfer have the same order of magnitude for the continuous and dispersed phases. We would expect, therefore, to find correlations that combine the two coefficients in a global coefficient, while taking into account the partition coefficients. In no case, however, we can neglect either of the two sources of resistance.
7. Correlations (5.18) and (5.22), established by Calderbank [1967], show that the transfer coefficients are a function of the difference of the density of the phases, $\Delta\rho$. Calderbank makes specific reference to this, noting that it may be the source of the low transfer values observed in some extraction columns where $\Delta\rho$ is low. Other authors do not introduce this parameter. It should be noted, however, that Calderbank's correlation was obtained from gas-liquid absorption data.

5.1.3 Scale-up

During scale-up, several parameters must remain constant or otherwise be taken into account. The most important are:

- in the medium:
  - the physicochemical properties of the medium (especially interfacial tension, density differences, viscosity) under the reaction conditions
  - the nature of the dispersed phase and the direction of transfer
  - the size distribution of dispersed phase droplets
  - the possible presence of solids
- in the reactor:
  - the method and degree of agitation or shear
  - the nature of the materials and their wetting properties for the continuous phase
  - the effects of axial dispersion
  - the wall and end effects
  - the kinetics of coalescence and dispersion.

Scale-up is the result of a judicious compromise among these various—and sometimes incompatible—requirements, as well as the requirements of capacity, conversion, and selectivity associated with the process.

Minotti *et al.* [1998] have proposed a general method for designing liquid-liquid extractors considered as a cascade of mixers operating in countercurrent or cocurrent mode. The method can be applied to any number of components and reactions. It can be used to study the influence of various parameters, such as the number of stages, the flow rate of solvent, the phase holdup, or the reactant conversion rates.

5.2 SPRAY COLUMNS

The spray column is the simplest form of liquid-liquid contactor. In a column in which the continuous phase circulates, a countercurrent dispersed phase is introduced by a suitable means—a perforated plate or series of nozzles (Fig. 5.2). The dispersed drops flow through the continuous phase and are collected at the other end of the column, forming a homogeneous layer that is continuously removed from the column. Depending on whether the dispersed phase is lighter or heavier than the continuous phase, it is introduced either from the bottom or the top of the column.

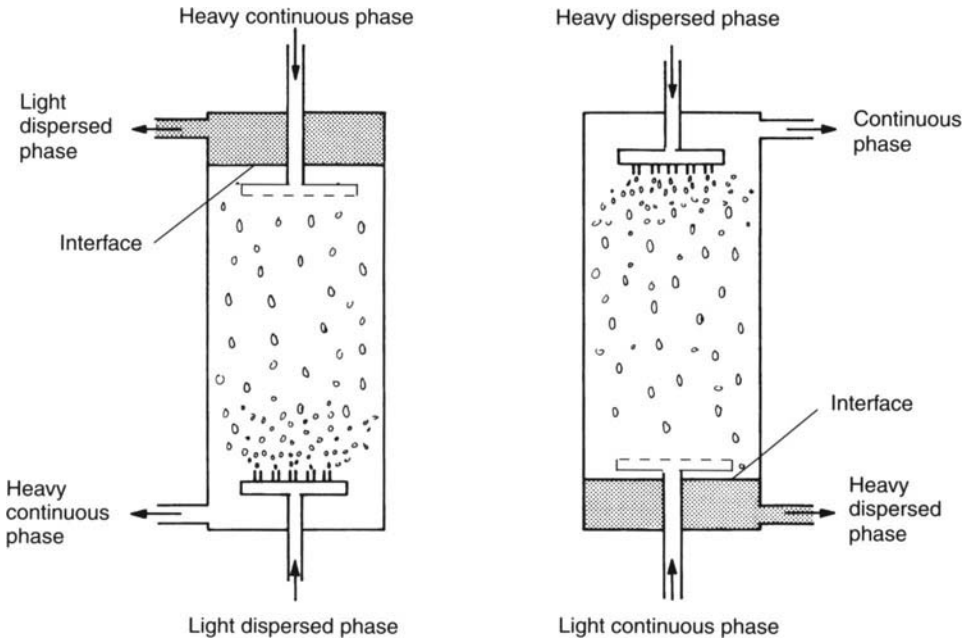


Figure 5.2 Spray column without internal components.

The geometry of the distributor, the diameter of the openings d_O, and the velocity of the dispersed phase at the distributor u_O have an influence on the size of the droplets and, thus, on the interfacial area. However, given the coalescence and rupture of drops that takes place further away in the column, it might be expected that the influence of these factors would

remain negligible in an industrial column. The same holds true for the transfer coefficients: the high values observed during the periods of droplet formation are of limited importance in these units.

Backmixing of the continuous phase, however, is quite important if no device has been installed to prevent the formation of convection currents. Moreover, the individual movement of drops, when no intermediary remixing occurs, limits material transfer.

5.2.1 Hydrodynamics

Depending on the flow rates and properties of the phases, two hydrodynamic regimes can occur. They are sharply differentiated by their respective holdup values:

- loose bed ($\varepsilon_D < 0.2$) with clearly separate and independent drops
- dense bed ($\varepsilon_D > 0.4$), where the drops are often close or packed and move as a group.

5.2.1.1 Holdup and interfacial area

We saw earlier that the interfacial area $\mathcal{A}$ can be calculated from the slip velocity u_g and the mean drop diameter $\overline{d_B}$. In reactors without internal components:

$$\varepsilon_B = 0 \quad \text{and therefore} \quad u_g = \left(\frac{V_{SD}}{\varepsilon_D} + \frac{V_{SC}}{\varepsilon_C}\right)\frac{1}{\varepsilon_C} \tag{5.26}$$

The holdup ε_D of the dispersed phase is about 0.10 to 0.20 in the loose-bed regime, which is the most frequently used.

Drops in the dispersed phase are quite large, with a narrow distribution of sizes when measured at a sufficient distance from the jet formed at the outlet of the orifice. Their mean diameter $\overline{d_B}$, on the order of a few millimeters, can, along with the slip velocity u_g, be obtained from Laddha's [1976] equations:

$$\overline{d_B} = 1.6\left(\frac{\sigma}{\Delta\rho \cdot g}\right)^{0.5}\left(\frac{u_O^2}{2gd_O}\right)^{-0.067} \tag{5.27}$$

$$u_g = \alpha_2\left(\frac{\sigma \cdot \Delta\rho \cdot g}{\rho_C^2}\right)^{0.25}\left(\frac{u_O^2}{2gd_O}\right)^{\beta_2} \tag{5.28}$$

where the coefficients depend on the direction of transfer:

- with no transfer or with transfer from the continuous to the dispersed phase:

$$\alpha_2 = 1.09 \quad \beta_2 = -0.082$$

- with transfer of the dispersed phase to the continuous phase:

$$\alpha_2 = 1.42 \quad \beta_2 = +0.125$$

The influence of the geometry of the openings and the operating conditions is very small. It may seem surprising that no term for viscosity appears in these equations. In fact, few

columns operate with viscous liquids. Consequently, we should reserve the use of these correlations for relatively fluid systems.

A correlation proposed by Kumar and Hartland [in Godfrey and Slater, 1994] is based on results obtained with distributors having several openings. It eliminates the effects associated with the direction of transfer:

$$\frac{d_{32}}{d_O} = E\ddot{o}_O^{-0.35}\left[0.80 + \exp\left(-2.73 \cdot 10^{-2}\frac{We_O}{E\ddot{o}_O}\right)\right]$$

Here, the Weber and Eötvos numbers are calculated with respect to the conditions at the outlet of the orifice:

$$E\ddot{o}_O = \frac{d_O^2 g \Delta\rho}{\sigma} \quad \text{and} \quad We_O = \frac{\rho_D d_O u_O^2}{\sigma}$$

By making use of these various equations, we can calculate the interfacial area, since:

$$\mathcal{A} = \frac{6\varepsilon_D}{d_B} \tag{5.5}$$

In fairly complete studies, Mersmann, then Horvath, cited in Trambouze *et al.* [1988], suggest the use of equations similar to (5.27) and (5.28)—with certain recommendations and reservations regarding their use.

To calculate the dispersed phase holdup directly, the general Eq. (5.6) of Kumar and Hartland [1995] can also be used with the appropriate coefficients; these have been optimized from a database of more than 900 experimental data points for spray columns.

5.2.1.2 Backmixing

In a spray column, backmixing of the continuous phase is essentially the result of the axial and transverse movement of dispersed phase droplets, which entrain the continuous phase as they move about. This flow is often represented by an axial diffusivity model whose coefficient of axial diffusion in the continuous phase can be calculated by means of an approximate, but simple, equation proposed by Trambouze *et al.* [1988]:

$$\mathcal{D}_{A,C} = 0.12\,(V_{SD} D_T)^{0.5} \tag{5.29}$$

D_T is the column diameter.

More recently, Kumar and Hartland [in Godfrey and Slater, 1994] proposed an equation that, although not very precise, is more complete since it takes into account the effects associated with the size of the droplets and the properties of the medium:

$$\mathcal{D}_{A,C} = 9.9 \cdot 10^{-3}\frac{\mu_C}{\Delta\rho}\left[\frac{\mu_C}{(\sigma\Delta\rho d_{32})^{0.5}}\right]^{-1.47}\left(\frac{\mu_C}{\mu_D}\right)^{-0.75}\left(\frac{\Delta\rho}{\rho_C}\right)^{1.39}\left(\frac{D_T}{d_{32}}\right)^{1.47}\varepsilon_D^{-0.34} \tag{5.30}$$

For the dispersed phase, we can state that backmixing is significantly less pronounced ($\mathcal{D}_{A,D} \leqslant 0.3$ m^2/s) than it is in the continuous phase, primarily as a result of the range of sizes of the droplets. Laddha and Degaleesan [1976] have pointed out the close relationship between droplet dispersion and holdup:

- For holdup values that vary between 10 and 40%, the Peclet number of the dispersed phase is quite stable, being about 20, which corresponds to the irregular movement of a large number of droplets of different sizes.

- For holdup values that are less than 10%, the Peclet number reaches values as high as 140, reflecting the ordered movement of a smaller number of drops of fairly uniform size, nearly all of which have the same velocity.

5.2.1.3 Flooding

Spray columns are subject to flooding problems. In the absence of transfer, the hydrodynamic behavior of liquid-liquid extraction equipment has been studied extensively [Laddha and Degaleesan, 1976, Godfrey and Slater, 1994]. The equation that is easiest to use shows that flooding occurs for values of V_{SD} and V_{SC} such that:

$$|V_{SD}|^{0.5} + |V_{SC}|^{0.5} = A \tag{5.31}$$

The value of A, which is constant for a given system, can be determined with a small laboratory device. Generalized correlations do not appear to be available. According to Thornton (see Trambouze *et al.* [1988]), at the flood point the dispersed-phase fraction ε_{DE} reaches a maximum that results in:

$$\begin{aligned} V_{SD} &= 2u_g\varepsilon_{DE}^2(1-\varepsilon_{DE}) \\ V_{SC} &= u_g(1-\varepsilon_{DE})^2(1-2\varepsilon_{DE}) \\ \varepsilon_{DE} &= \frac{\left[\left(\frac{V_{SD}}{V_{SC}}\right)^2 + 8\left(\frac{V_{SD}}{V_{SC}}\right)\right]^{\frac{1}{2}} - 3\left(\frac{V_{SD}}{V_{SC}}\right)}{4\left(1-\frac{V_{SD}}{V_{SC}}\right)} \end{aligned} \tag{5.32}$$

Equation (5.32) can be used to calculate ε_{DE} for an imposed flow rate ratio. By then using Eq. (5.4), and assuming we know the value of u_g, we can calculate the flow rate of the continuous (or dispersed) phase that gives rise to flooding, and choose a column diameter that enables the column to operate at approximately 50% of this superficial velocity.

5.2.2 Mass transfer

It is reasonable to assume that the equations shown in Tables 5.2 and 5.3, referring to drops with circulation, can be used when designing spray columns. However, the lowest numerical value for the correlations shown should probably be used. For each of the reactants (subscript i) the global coefficient is written:

- for a reaction in the continuous phase:

$$\frac{1}{K_{i,DC}} = \frac{1}{k_{i,D}} + \frac{m_i}{k_{i,C}E_C} \tag{5.33}$$

where:

$$m_i = \frac{C_{i,Deq}}{C_{i,Ceq}}$$

- similarly, for a reaction in the dispersed phase:

$$\frac{1}{K_{i,\mathrm{CD}}} = \frac{1}{k_{i,\mathrm{C}}} + \frac{1}{m_i k_{i,\mathrm{D}} E_{\mathrm{D}}} \tag{5.34}$$

E_{D} and E_{C} are the enhancement factors due to the chemical reaction.

Some studies provide estimates of transfer coefficients during drop formation from liquid jets both in the dispersed phase and the continuous phase. Since the drop formation stage is relatively unimportant for the overall operation of the column, we will not pursue the subject further.

5.2.3 Technology

Spray columns have superficial flow rates of around 10 to 20 $\mathrm{m^3/(m^2 \cdot h)}$. Their construction requires no further commentary. In our opinion, dense bed columns are of little interest because of their mediocre hydrodynamic stability and transfer characteristics. No further mention will be made of them here.

The region of the column where the dispersed phase is introduced must be sufficiently large so that the velocity of the continuous phase is reduced (30 to 80% of the superficial velocity of the continuous phase calculated for the remainder of the column). Drops of the dispersed phase are formed during their passage through a perforated plate or nozzles and are distributed with as much uniformity as possible throughout the column cross-section. The holes are designed to promote the formation of jets that break apart into uniform drops.

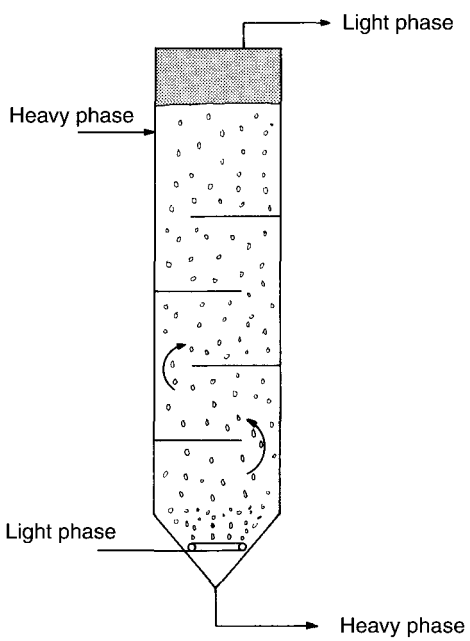


Figure 5.3 Baffle column.

Baffle columns (Fig. 5.3) can be treated as deriving from spray columns. Few studies have been made of their operation. The baffles promote intermediary remixing of the dispersed phase, but drop dispersion is poorly controlled. Backmixing of the continuous phase is very limited.

The final settling of dispersed phase droplets occurs at the top or bottom of the column, or in special settling tanks that are sometimes equipped with devices that promote coalescence (inclined plates, fiber beds, packing, etc.).

5.2.4 Concluding remarks

Spray columns are not the most efficient of the various types of liquid-liquid reactors: contact efficiency is no more than average and backmixing is sometimes significant. Their major advantage is simplicity, which makes them highly economical and relatively unaffected by the presence of media containing high concentrations of solids.

5.3 PERFORATED PLATE COLUMNS

There are two distinct types of perforated plate columns:

- The static column, which greatly resembles the column described in the section on gas-liquid contactors (Fig. 5.4); it contains no moving parts. The dispersed phase moves from stage to stage through a series of perforated plates; it is systematically dispersed as it crosses each plate and then coalesces again. The continuous phase crosses each compartment horizontally and moves vertically from one stage to the next through a downcomer. Some static columns are more than 2 m in diameter and 20 m in height.
- The pulsed column, in which the fluids move across the plates with a reciprocating motion. In small columns plates are sometimes mounted on a shaft that moves up and down. In industrial reactors internal components are stationary but the liquid phases are pulsed by means of a reciprocating piston, mounted in the continuous phase circuit (Fig. 5.5).

The calculations used to determine holdup and interfacial area are comparable to those used for spray columns. However, backmixing effects are much weaker while the series of steps leading to drop coalescence and formation has a favorable influence on the transfer coefficients.

5.3.1 Hydrodynamics

5.3.1.1 Holdup and interfacial area

Dispersed phase holdup can be determined from the following equation, which was introduced earlier:

$$u_g\,(1-\varepsilon_D) = \frac{V_{SD}}{\varepsilon_D} + \frac{V_{SC}}{1-\varepsilon_D} \tag{5.26}$$

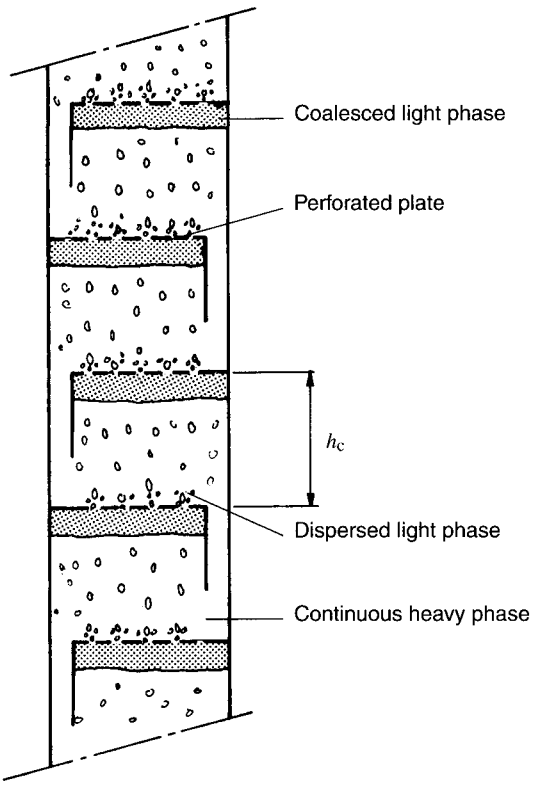


Figure 5.4 Perforated plate column.

A few comments concerning its use are called for, however:

- In static columns that incorporate a downcomer (Fig. 5.4), the continuous phase circulates in cross-flow mode with respect to the dispersed phase. Treybal [1963] suggests that V_{SC}, the superficial velocity of the continuous phase, be assigned a value of zero, which yields:

$$\varepsilon_D (1 - \varepsilon_D) = \frac{V_{SD}}{u_g} \tag{5.35}$$

u_g can be calculated from Eq. (5.28), which was proposed for spray columns.

To calculate the mean drop diameter, Treybal [1963] proposes a method that has been used by many other authors. In this case $B = d_O\sqrt{\Delta\rho \cdot g/\sigma}$ is estimated first, then:

$$\frac{d_O}{d_J} = 1 + 0.485B^2 \quad \text{if } B \leqslant 0.78 \tag{5.36}$$

$$\frac{d_O}{d_J} = 0.12 + 1.51B \quad \text{if } B > 0.78 \tag{5.37}$$

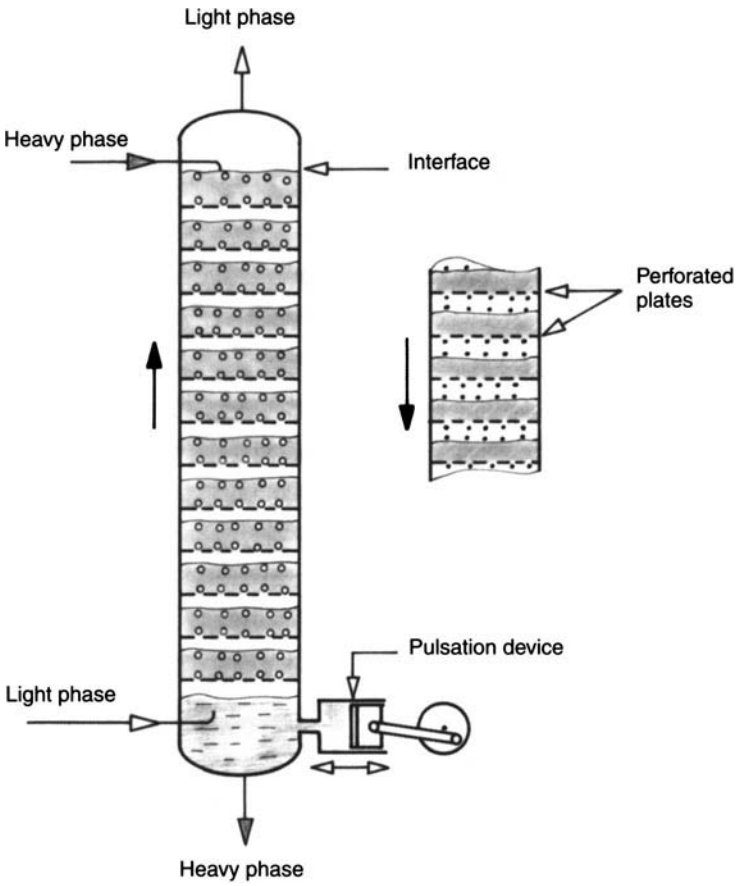


Figure 5.5 Pulsed plate column.

where

d_O diameter of the orifice

d_J diameter of the jet.

The velocity at the orifice u_{OM} resulting in the maximum exchange surface, is given by the following equation:

$$u_{OM} = 2.69 \left(\frac{d_J}{d_O} \right)^2 \left[\frac{\sigma}{d_J (0.51\rho_D + 0.47\rho_C)} \right]^{0.5} \tag{5.38}$$

Knowing d_J, Treybal suggests that we assign:

$$\overline{d_B} = 2d_J$$

$\overline{d_B}$ can also be calculated from the equation suggested by Laddha, which was introduced earlier (5.27) for spray columns. The interfacial area is then $\mathcal{A} = 6\varepsilon_D/\overline{d_B}$, which is the standard equation.

• In pulsed columns Eq. (5.4) is valid. To calculate u_g, the following equations were proposed by Treybal [1963]:

$$\frac{u_g \mu_C}{\sigma} = 0.6 \left(\frac{\Sigma \mu_C^5}{\rho_C \sigma^4}\right)^{-0.24} \left(\frac{d_O \rho_C \sigma}{\mu_C^2}\right)^{0.9} \left(\frac{\mu_C^4 g}{\Delta\rho \sigma^3}\right) \left(\frac{\Delta\rho}{\rho_C}\right)^{1.8} \left(\frac{\mu_D}{\mu_C}\right)^{0.3} \tag{5.39}$$

$$\Sigma = \frac{\pi^2 \left[\left(\frac{S_t}{S_O}\right)^2 - 1\right] (Af)^3}{0.72 h_c} \tag{5.40}$$

where

Σ power input per unit mass

$\frac{S_t}{S_O}$ total area of the plate/area of the orifices

h_c compartment height

A pulse amplitude

f pulse frequency.

It has been suggested that the drop diameter $\overline{d_B}$ can be estimated, as is the case with static columns, by assuming for u_O the maximum velocity for the fluid as it crosses the holes in the plates. Laddha and Degaleesan [1976] provide methods for calculating the power consumption required to create the pulse.

The general equation of Kumar and Hartland [1995] (5.6), used with suitable coefficients (established from nearly 1 300 data points for perforated plate columns), provides fairly precise results for holdup values. In a chapter in Godfrey and Slater [1994], Kumar and Hartland also proposed various correlations for calculating drop diameter.

5.3.1.2 Backmixing

A. Static columns

Backmixing of the dispersed phase can be considered nearly nonexistent, while the compartments between the plates can be considered perfectly mixed for the continuous phase.

B. Pulsed columns

The results and correlations that have been published for diffusion in pulsed columns vary widely and have been contested. The correlation proposed by Tung and Luecke [1986] reflects the majority of observations with a precision of 35%, which is still acceptable:

$$\frac{\mathcal{D}_{A,C}}{h_c V_{SC}} = 0.25 (S_t - S_O)^{-1.30} \left(\frac{d_O}{h_c}\right)^{0.565} \left(\frac{Af}{V_{SC}}\right)^{0.606} \tag{5.41}$$

where

d_O diameter of the holes in the plates

h_c compartment height.

5.3.1.3 Flooding

The flooding velocity is an important characteristic of the system and is used when designing the column. The column diameter is generally established on the basis of a superficial velocity of the continuous phase equal to 50 to 70% of the flooding velocity, to allow a margin of safety. Unfortunately the available data are not very useful in practice. The orders of magnitude of the flux limits are 70 $m^3/(m^2 \cdot h)$ for static columns and only 60 $m^3/(m^2 \cdot h)$ for pulsed columns.

A. Static columns

As with gas-liquid columns, flooding is determined by a set of pressure balances together with the characteristics of the downcomer cross-sections. Overall, plate columns lack flexibility and their performance diminishes rapidly when operating conditions deviate from the initial design conditions. Relevant details can be found in Treybal [1963], Laddha and Degaleesan [1976], Trambouze *et al.* [1988], and Godfrey and Slater [1994].

B. Pulsed columns

Pulsed columns are quite sensitive to flooding, which can occur either from too little or too much pulsing. According to Godfrey and Slater [1994], reliable data are largely unavailable. Thornton [1957, 1966] describes a method for spray columns that could serve as a first approximation, but it must be used with considerable caution.

5.3.2 Mass transfer

In perforated plate columns we would expect to find high transfer coefficients, influenced by periods of drop formation and coalescence. Skelland and Conger [1973] present a method for calculating transfer coefficients that takes into account these various periods (see Tables 5.2 and 5.3). Their approach, which is fairly complex, is beyond the scope of our presentation. Moreover, current reactor design techniques can make do with more approximate values. Laddha and Degaleesan [1976] suggest that the following equations be used:

$$\frac{k_C \overline{d_B}}{\mathcal{D}_C} = 2\left(\frac{\overline{d_B} u_g}{\pi \mathcal{D}_C}\right)^{0.5} \tag{5.42}$$

$$\frac{k_D}{u_g} = 0.023\left(\frac{\mu_D}{\rho_D \mathcal{D}_D}\right)^{-0.5} \tag{5.43}$$

The values of the transfer coefficients for an oscillating drop are frequently overestimated. We again wish to point out that the direction of transfer ($C \rightarrow D$ or $D \rightarrow C$) has a moderate influence on the values of k_C, k_D, and $\mathcal{A}$, and that even this influence is controversial.

5.3.3 Technology

The plates, generally spaced 0.1 to 0.60 m apart, must be designed with the greatest care and manufactured from a material that is preferentially wetted by the continuous phase. The perforations have diameters that are most often between 3 and 8 mm. The greater the

interfacial tension, the greater the tendency to reduce this dimension. Laddha and Degaleesan [1976] suggest using the following equation to determine the diameter d_O of the perforations:

$$0.5 < B = d_O\sqrt{\frac{\Delta\rho g}{\sigma}} < \pi \tag{5.44}$$

The distance between the perforations on the plates must be at least 3 to 4 times d_O to avoid coalescence of adjacent drops. The number of holes is such that the velocity through the orifices u_O is close to u_{OM} (Eq. 5.38). In general perforations make up 3 to 8% of the surface. Drops are smaller when the dispersed phase does not wet the perforated plate. To obtain drops of uniform size, it is recommended that the plates be checked during manufacture to ensure that the edges of the holes are smooth and free of burrs. Note that smaller holes are not always preferable. It is easier for the very small drops they create to flood the column or be entrained by the continuous phase, which limits the capacity of the unit. Moreover, mass transfer is not promoted either by internal mixing of reactants within a droplet or by the interface regeneration observed in larger drops. Studies have shown that a decrease in the diameter of the perforations from 13 to 6 mm has a favorable influence on transfer but reduces the capacity of the column and has no influence on backmixing.

Lastly, critical system variables should be verified to make sure they do not vary too much between the bottom and top of the column and that the same characteristic design values can be used for all the plates. These perforated plate columns are also quite sensitive to corrosion and the presence of solids.

In pulsed columns two different methods can be used to improve transfer:

1. The perforated plates are mobile, actuated up and down by a shaft with a reciprocating motion or vibrating (Karr columns). In this case the vibrations have an amplitude of about 1 or 2 cm and a frequency of 100 to 150 cycles per minute. The plates are fairly close together, 2 to 15 cm apart, and heavily perforated (holes of approximately 1 cm in diameter and a ratio of perforation of 50 to 60%). These characteristics result in much greater efficiency than in packed columns, with quite moderate energy consumption. Moreover, the columns support the presence of solid particles and are easy to scale up.
2. The plates are stationary but the total mass of liquid moves periodically. This method is the one most commonly used in midsize or large columns. A piston (for columns with a diameter greater than 0.5 m) or a reciprocating pump (for columns with a diameter less than 0.3 m) is used to move the continuous phase up and down. The pulsed vertical motion of the continuous phase more or less entrains the dispersed phase through the plates, which occupy the entire column cross-section. In industrial columns (up to 3 m in diameter and 30 m in height) the diameter of the holes is generally from 2 to 6 mm, with spacing of approximately 5 cm, for a perforated surface of roughly 20 to 25%. Holes with finished edges seem to improve transfer. Pulse frequencies of 100 to 300 cycles/minute and amplitudes of from 5 to 30 mm are customary. Depending on frequency and amplitude, the resulting regime can be gentle or agitated. In the first case (slow pulses of low amplitude), transfer is improved and the interfaces are quite stable. In the second case (rapid pulses and high amplitude) drops no longer have time to coalesce and the column fills with a relatively uniform emulsion. The most favorable regimes are those that operate near the flood point.

Capacities are relatively high (60 to 80 $m^3/m^2 \cdot h$) in industrial units, which can have diameters up to 2 to 3 m and are sometimes more than 25 m in height.

5.3.4 Concluding remarks

Perforated plate columns play an important role because of their high capacity and simplicity—and consequently low cost. Unfortunately, however, they have certain drawbacks, including a lack of flexibility, a limited number of theoretical stages, and susceptibility to plugging in the presence of solids, as well as corrosion.

5.4 PACKED COLUMNS

The general structure of packed columns is shown in Fig. 5.6. Because of the packing (random or structured) backmixing effects are much smaller than in spray columns and, with respect to the continuous phase, even lower than they are in plate columns. Like plate columns they can operate in the static or pulsed regime. There is little published data on pulsed columns, so we will limit our discussion to static columns.

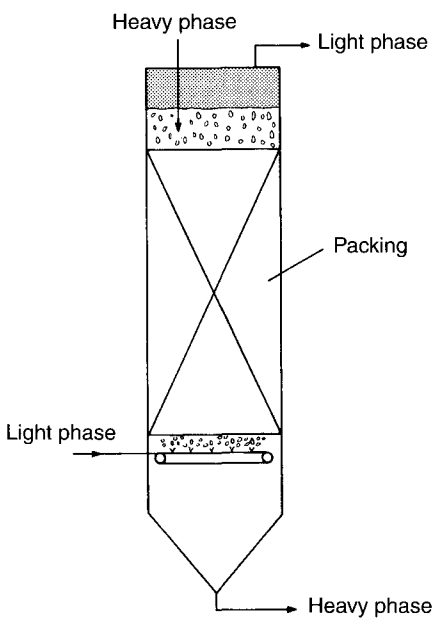


Figure 5.6 Packed column.

Depending on the type of packing, its size, the material used (more specifically, its wetability with respect to the phases), and the fluid flow rates, we can obtain highly variable values for transfer coefficients, holdup, and interfacial area. These values are contingent

upon the solid-liquid interactions that take place in the reactor, which are responsible for coalescence and redispersion effects. The capacity of packed columns is also smaller than that of spray towers or plate columns, especially if the density difference between the two phases is small.

Preferential wetting of the packing by either of the phases must also be taken into account. If the dispersed phase wets the packing, it will flow as a film through the packing. If the continuous phase wets the packing, the dispersed phase will flow as more or less deformed drops, which has a favorable influence on the coefficients of transfer and the interfacial area. Below we limit our discussion to this last case (wetting by the continuous phase), which provides better performance and is more commonly found in practice.

5.4.1 Hydrodynamics

5.4.1.1 Holdup and interfacial area

For a packed column, Eq. (5.4) is written:

$$u_g \left(\frac{\varepsilon_C}{1 - \varepsilon_B} \right) = \frac{V_{SD}}{\varepsilon_D} + \frac{V_{SC}}{\varepsilon_C} \tag{5.45}$$

where $\varepsilon_B = 1 - \varepsilon$.

According to Laddha and Degaleesan [1976], for Raschig or Lessing rings and different types of saddles, the characteristic velocity can be correlated as follows:

$$u_g = 0.68 \left(\frac{\mathcal{A}_P \rho_C}{(1 - \varepsilon_B)\, g \Delta\rho} \right)^{-0.5} \tag{5.46}$$

The coefficient 0.68 becomes 0.97 if spherical particles are used for the packing material.

Although estimating u_g plays a large role in calculating the fraction of the dispersed phase in the column, drop deformation and the frequent coalescence and rupturing of drops make estimates of interfacial area from holdup and mean drop size less reliable. Under these conditions we prefer to use only correlations that yield values for $(k_L\mathcal{A})_D$ and $(k_L\mathcal{A})_C$ directly. However, if an independent estimate of interfacial area is needed, the equation found in Trambouze *et al.* [1988] can be used:

$$\overline{d_B} = 0.92 \left(\frac{\sigma}{\Delta\rho g} \right)^{\frac{1}{2}} \left(\frac{u_g \varepsilon_D}{V_{SD}} \right) \tag{5.47}$$

and:

$$\mathcal{A} = \frac{6\varepsilon_D}{\overline{d_B}} \tag{5.48}$$

Correlation (5.6) and the coefficients established by Kumar and Hartland [1995], based on more than 2 000 data points for packed columns, provide results that are quite close to the experimental values.

5.4.1.2 Backmixing

Backmixing has been studied by Vermeulen *et al.* [1966] for both the dispersed phase and the continuous phase.

For the dispersed phase:

$$\frac{d_p V_{SD}}{\mathcal{D}_{A,D}} \cong 0.4 \tag{5.49}$$

where d_p is the nominal diameter of the packing.

For the continuous phase the correlation is more complex. However, as a first approximation, the following two correlations can be used, depending on the value of the dimensionless number Ψ_T, which represents the hydrodynamic regime:

$$\Psi_T = \left(\frac{d_p V_{SC} \rho_C}{\lambda \mu_C}\right)^{0.5} \frac{V_{SC}}{V_{SD}}$$

where $\lambda = 1$ for spheres and $\lambda = 0.63$ for Raschig rings, saddles, and other shapes:

$$\text{if } \Psi_T > 22 \qquad \frac{d_p V_{SC}}{\mathcal{D}_{A,C}} = 0.2 \tag{5.50}$$

$$\text{if } \Psi_T < 22 \qquad \frac{d_p V_{SC}}{\mathcal{D}_{A,C}} = 0.0135 \left(\Psi_T\right)^{0.87} \tag{5.51}$$

Structured packing, because of the regularity and optimization entailed in its design, results in very good radial homogeneity and strongly inhibits axial backmixing.

5.4.1.3 Flooding

A correlation as general as that presented for gas-liquid packed columns does not yet seem to exist for liquid-liquid columns. Laddha and Degaleesan [1976] suggest the use of the following correlation, which, among those published, is the most general and is also dimensionless.

$$\left[1 + 0.835 \left(\frac{V_{SD}}{V_{SC}}\right)_E^{0.5} \left(\frac{\rho_D}{\rho_C}\right)^{0.25}\right] \left(\frac{\left(V_{SC}^2\right)_E \mathcal{A}_P \rho_C}{g \left(1 - \varepsilon_B\right)^3 \Delta\rho}\right)^{0.25} = C \left(\frac{\mathcal{A}_P \left(1 - \varepsilon_B\right) \sigma}{\rho_C \left(V_{SC}^2\right)_E}\right)^n \tag{5.52}$$

where C and n have the following values:

Type of packing	C	n
Raschig rings	0.894	−0.078
Berl saddles	0.882	−0.052
Lessing rings	0.853	−0.046

Trambouze *et al.* [1988] have proposed a correlation, established by Watson, which, unfortunately, is not dimensionless (CGS):

$$\left(V_{SC}^{0.5}\right)_E + \left(0.84 \Delta\rho^{0.15} d_p^{0.3} \mu_C^{-0.08} \varepsilon_D^{-0.08}\right) \left(V_{SD}^{0.5}\right)_E = 23.8 \Delta\rho^{0.27} d_p^{0.44} \mu_C^{-0.08} \varepsilon_D^{0.5} \tag{5.53}$$

There is a tendency to choose operating conditions that are relatively far from flooding conditions (V_{SC} approximately 30–50% of V_{SC} at flooding conditions). Laddha and Degaleesan [1976] suggest a procedure for calculating pressure drop. Pressure drop is first estimated when the continuous phase circulates alone with the same superficial velocity throughout the bed: $\Delta P_0/Z$ (in Pa/m of packing). Pressure drop is then calculated from the following equation:

$$\frac{\Delta P}{Z} = \frac{\Delta P_0}{Z} + 2.82 \frac{\Delta \rho g \varepsilon_D}{(1-\varepsilon_B)} \left(\frac{V_{SC}^2 \mathcal{A}_P \rho_C}{g (1-\varepsilon_B)^3 \Delta \rho} \right)^{0.25} \tag{5.54}$$

5.4.2 Mass transfer

Numerical values for $(k_C \mathcal{A})$ and $(k_D \mathcal{A})$ are fairly abundant in the literature but the suggested correlations are generally too specific. The correlation proposed by Laddha and Degaleesan [1976] is somewhat more general:

$$k_j \mathcal{A} = 0.06 \varepsilon_D \varepsilon_C \left(\frac{\mathcal{A}_P \rho_C (1-\varepsilon_B)}{g \Delta \rho} \right)^{-0.5} \left(\frac{\mu}{\rho \mathcal{D}} \right)_j^{-0.5} \left(\frac{\sigma}{g \Delta \rho} \right)^{-0.5} \tag{5.55}$$

The subscript j is relative either to the dispersed phase, $j = D$, or the continuous phase, $j = C$.

The above equation is valid for systems where transfer is one-way, that is, where the transfer of a solute is measured from the dispersed phase to the continuous phase, the dispersed phase first being saturated by the continuous phase and *vice versa*. The results are somewhat different when counter-diffusion occurs.

5.4.3 Technology

Distribution of the dispersed phase requires the same care as in packed gas-liquid columns. The remarks made in that section are valid here. Specifically, in tall reactors, redistributors are needed (approximately every 4 to 5 m) to adequately distribute the dispersed phase throughout the entire height of packing and compensate for any irregularities in the distribution of phases. If the dispersed phase is introduced with too great a velocity at the distributor, early flooding may occur. For this reason, the velocity of the dispersed phase at the orifices is limited to approximately 0.40 m/s.

The type of packing used depends on the capacity of the column. At the lowest flow rates (up to approximately 2 m^3/h), random packing is generally preferred over structured packing, which causes lower pressure drops but is more costly. At the highest flow rates structured packing is preferable because of its capacity and better performance (up to 100 $m^3/m^2 \cdot h$ for both phases combined compared to approximately 20 to 30 $m^3/m^2 \cdot h$ for conventional random packing). We have already pointed out the advantage of using a material that is wetted by the continuous phase so that the dispersed phase flows in the form of droplets. Metal and plastic materials are frequently used.

With random packing it appears that the best price/performance compromise is found with Intalox saddles or Pall rings (see Chapter 4), which are obtained by extrusion or injection in the case of plastic. In terms of size, there is a critical size below which the influence of the

packing on the droplet size is greater, which results in an increase in the values of $k_j a$. In most applications this critical size, which is calculated by means of the following equation: $d_{p,c} = 2.4\sqrt{\sigma/(g\Delta\rho)}$, rarely exceeds 0.5 to 1 cm. Therefore, fairly small packing elements 5 to 15 mm should be used to take advantage of this phenomenon, which promotes transfer. In any case, packing must be less than 1/10 the diameter of the column to limit harmful phenomena associated with wall effects.

Structured packing can be used to improve conversion, selectivity, and the capacity of the reactor while maintaining very small pressure drops. It is well suited to systems with low interfacial tension or small density differences. In spite of these important advantages over random packed columns, its use remains limited by problems of corrosion, the risk of fouling, and the high capital outlay and installation costs.

5.4.4 Pulsed packed columns

Pulsation plays the same role as in pulsed columns with perforated plates. The packing is selected to promote wetting by the continuous phase. Superficial velocities are quite close to flooding conditions (65%). Efficiency and size are often greater than in unpulsed packed columns. Some columns, for example those used to process effluents, are as much as 3 m in diameter and 10 m in height.

5.4.5 Concluding remarks

Simple, resistant to corrosion, and inexpensive, packed columns provide certain advantages over spray columns in terms of interfacial area and backmixing. They are used extensively in industry in spite of their relatively low efficiency and the serious risk of plugging in the presence of solids.

5.5 STATIC MIXERS

Static mixers contain obstacles consisting of smooth or corrugated baffles, often helical in shape, individual or stacked, placed along the pipe. A number of baffles have been proposed in a wide variety of shapes, both open and complex (Fig. 5.7), but always with the goal of separating fluid streams and recombining them, in a more or less turbulent way, with other streams coming from another section of the pipe cross-section. The turbulence fragments the dispersed phase into droplets. Several baffles are often placed in series in the pipe.

5.5.1 Hydrodynamics

In static mixers the phases circulate in cocurrent mode. As indicated in Chapter 4, during our discussion of gas-liquid contactors, static mixers promote very good radial homogeneity of fluids while axial flow of the phases is nearly plug-like. The Peclet number based on a single element is always greater than 20. The residence time distribution of the two phases, therefore, clusters around the theoretical mean residence time, which can cover a broad range (a few seconds to a few minutes).

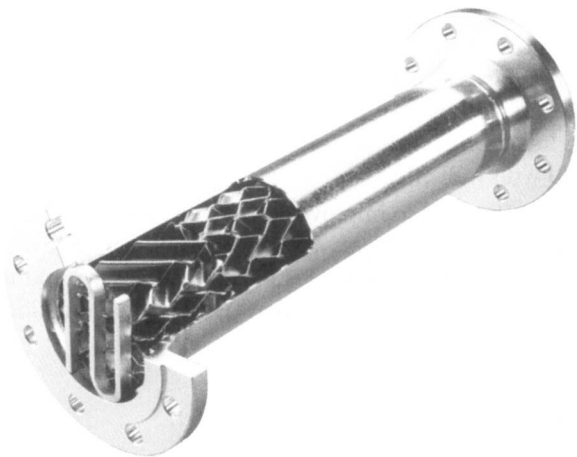


Figure 5.7 Static mixer (Sulzer).

Pressure drop, which is fairly low, can be calculated by multiplying the conventional pressure drop in an empty pipe by a coefficient K that varies from 5 to 100, depending on the Reynolds number of the flow and the geometry of the static mixer. On average, the following relation holds:

$$\Delta P_{\text{mixer}} = K_1 \Delta P_{\text{pipe}}$$

where:

$$K_1 \cong 0.4 Re^{0.7} \quad \text{and} \quad \Delta P_{\text{pipe}} = C \left(\frac{L}{d_t} \right) \left(\frac{\rho V_{SL}^2}{2} \right) \tag{5.56}$$

L length of a mixer element

d_t diameter of the piping in which the mixer element is placed.

Here, C is the coefficient of friction, which depends on the Reynolds number and the roughness of the pipe.

Other authors have used the hydraulic diameter d_h (d_h = 4/surface area of the mixer element per unit volume) in similar formulas:

$$\Delta P_{\text{mixer}} = K_2 \left(\frac{L}{d_h} \right) \left(\frac{\rho V_{SL}^2}{2} \right)$$

where $K_2 = aB$, in which a and B vary with the type of mixer and the regime, as indicated below. Note that the function B depends on the Reynolds number calculated either from the hydraulic diameter of the element Re_h or from the pipe diameter Re_{pipe}:

Mixer	Regime	a	B
Kenics	$100 < Re_h < 2\,000$	12.6	$Re_h^{0.5}$
Kenics	$600 < Re_{\text{pipe}} < 30\,000$	1.1	$Re_{\text{pipe}}^{-0.11}$
Sulzer	$Re_h < 100$	145	Re_h^{-1}

5.5.2 Mass transfer

The interfacial area is directly related to the energy dissipated in the form of a pressure drop:

$$\mathcal{A}_{LL} \approx (\Delta P)^{0.75} \tag{5.57}$$

It is typically between 200 and 500 m^2/m^3 for an energy expenditure of 1 kW/m^3. Beyond this overall influence, precise correlations relative to liquid-liquid media are rare and highly specific. To situate the orders of magnitude, it is possible to examine the values obtained in the presence of gas and liquid. The interfacial area can be estimated if we know the gas holdup ε_G and the drop size, since we can use the customary equation: $\mathcal{A}_{GL} = 6\varepsilon_G/\overline{d_B}$.

Droplets have a distribution of diameters d_B that clusters tightly around a mean value that varies between 0.1 and 1 mm, and depends only on the velocities and properties of the phases. It is often related to the Weber and Reynolds numbers, according to an equation of the following form:

$$\frac{\overline{d_B}}{d_t} = C We_{pipe}^{\alpha} Re_{pipe}^{\beta} \tag{5.58}$$

where:

$$We_{pipe} = \frac{\rho_m d_t u^2}{\sigma} \quad \text{and} \quad Re_{pipe} = \frac{\rho_m d_t u}{\mu_m} \quad \text{relative to the diameter of the pipe}$$

where

u actual linear velocity of the mixture in the mixing element.

For example, for a Kenics mixer: $C = 0.39$, $\alpha = -0.43$, and $\beta = 0$.

With Sulzer mixers, for velocities u below 1 m/s, a formula similar to (5.58) [Sulzer, 1994] is used, but with Reynolds and Weber number that are this time based on the hydraulic diameter d_h of the mixer element and the mean physical properties of the mixture:

$$\frac{\overline{d_B}}{d_h} = 0.21\,(We_h)^{-0.5}\,(Re_h)^{0.15} \tag{5.59}$$

where:

$$We_h = \frac{\rho_m d_h u^2}{\sigma} \quad \text{and} \quad Re_h = \frac{\rho_m d_h u}{\mu_m}$$

For velocities above 1 m/s, this equation underestimates diameters. A more complete equation, which takes into account pressure drop through the static mixer, has also been proposed; it is based on work by Streiff *et al.* [1997]:

$$\overline{d_B} = 0.62 d_{max} = 0.58 \left(\frac{\sigma}{\rho_C}\right)^{0.6} \left(\frac{\rho_C}{\rho_D}\right)^{0.1} \Sigma^{-0.4} \tag{5.60}$$

where:

$$\Sigma = \frac{Q_{VL} L \Delta P}{\rho V}$$

5.5.3 Technology

The various manufacturers (Kenics, Koch, Lightnin, Mixel, Sulzer, etc.) have proposed modules that are placed in series inside the piping. Easy to install, some of them can have diameters of 1 m or more. The shape of the internals varies with the manufacturer and the application, some inline mixers, for example, being specifically designed to accommodate viscous products.

There is little published data concerning scale-up and design for these mixers, but the key variables are, for the media, flow rate, residence time, and fluid viscosity, and, for the mixer, length, pitch, number of streams that ultimately correspond to the number of divisions or rotations, the degree of turbulence, and the overall pressure drop (which is moderate, about 0.2 to $0.5 \cdot 10^5$ Pa in general).

5.5.4 Concluding remarks

Static mixers are well suited to situations that are otherwise difficult to resolve in the process industries (see, for example, Baker [1991], Harnby *et al.* [1992], Sulzer [1994], Myers [1996]). They include:

- fast reactions
- complex reactions in which backmixing will have a harmful effect
- reactions in the presence of fragile solids.

The practical limitations on these devices are primarily associated with the lengthy residence times needed (greater than several minutes), the extreme viscosity, the difficulty, if not the impossibility, of mechanically cleaning the unit, and a certain lack of flexibility.

5.6 COLUMNS WITH ROTARY AGITATORS

Columns with rotary agitators consist of a series of compartments each of which comprises an agitation zone and a calm zone (Fig. 5.8). The agitator shaft passes through all the compartments and imparts rotational and shear, along with vertical movement. In general the two phases circulate countercurrent to one another, the light phase entering from the bottom of the column while the heavy phase is introduced from the top. The different devices are differentiated by their internal components (separator baffles and geometry of the compartments, agitator). In any case, the presence of an agitator, whose rotational speed can be adjusted, provides the operator with an additional controllable parameter in operating the unit. The introduction of energy can be used to increase the interfacial area and therefore promotes mass transfer. However, these systems are complex, have all the problems inherent in rotating machinery, consume more energy—which increases operating costs—and may present difficulties in the subsequent separation of phases.

One of the best known and most studied devices of this kind is the rotating disc contactor (RDC), originally developed in the 1950s by Reman for Shell. It consists of a column divided into compartments partially enclosed by annular discs. A solid disc rotates in the center of

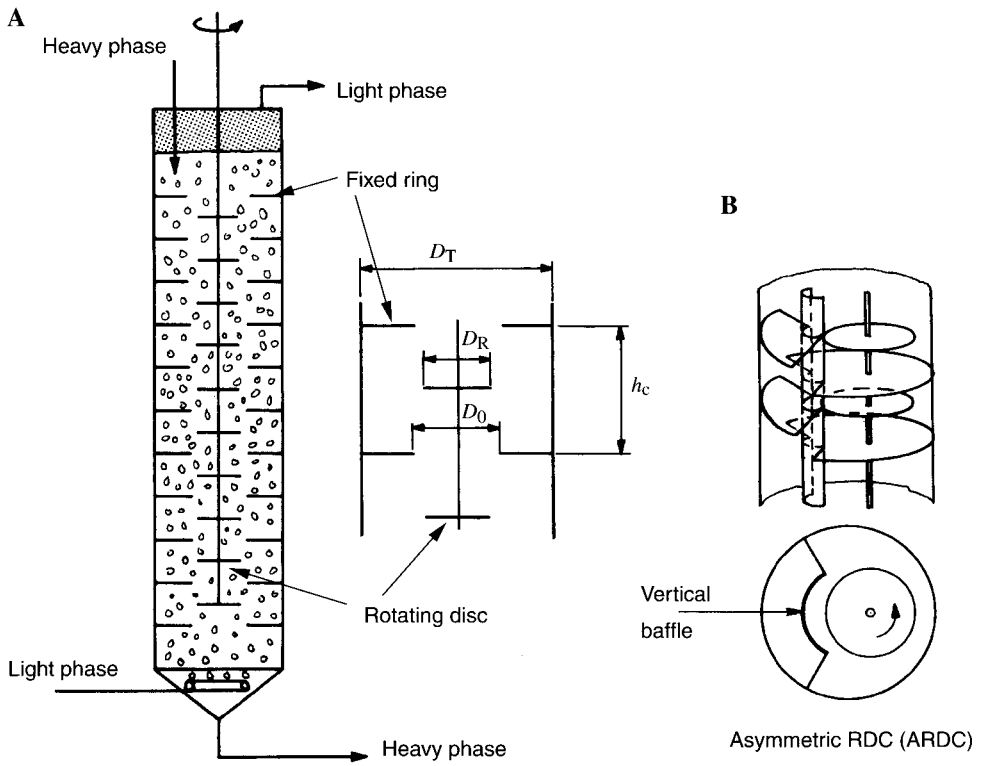


Figure 5.8 Mechanically agitated column. **A.** RDC. **B.** ARDC.

each compartment. All the solid discs are mounted on a single axial shaft; their diameter is slightly less than the diameter of the opening in the annular discs, greatly facilitating assembly. The characteristic dimensions are given in Fig. 5.8.

A number of variants, somewhat different from the RDC, have been developed. They include:

- The asymmetric rotating disc contactor (ARDC) (Fig. 5.8B), in which the shaft supporting the discs is not in the center of the column. The compartments are nearly tight and flow between compartments occurs through settling zones located on the side of the apparatus. Some industrial units are more than 3 m in diameter.
- The Oldshue-Rushton contactor (Fig. 5.9), in which the discs are replaced by Rushton-type turbines with 4 to 6 blades. The openings between stages are smaller. This column, which can accommodate the presence of suspended solids, would be easy to scale up to diameters of 2.7 m.
- The Kühni contactor (Fig. 5.9), in which the agitators are turbines that rotate between stators, the compartments being separated by sieve plates. Kumar and Hartland [in Godfrey and Slater, 1994] provide the hydrodynamic characteristics of these units, which are sometimes more than 3 m in diameter.

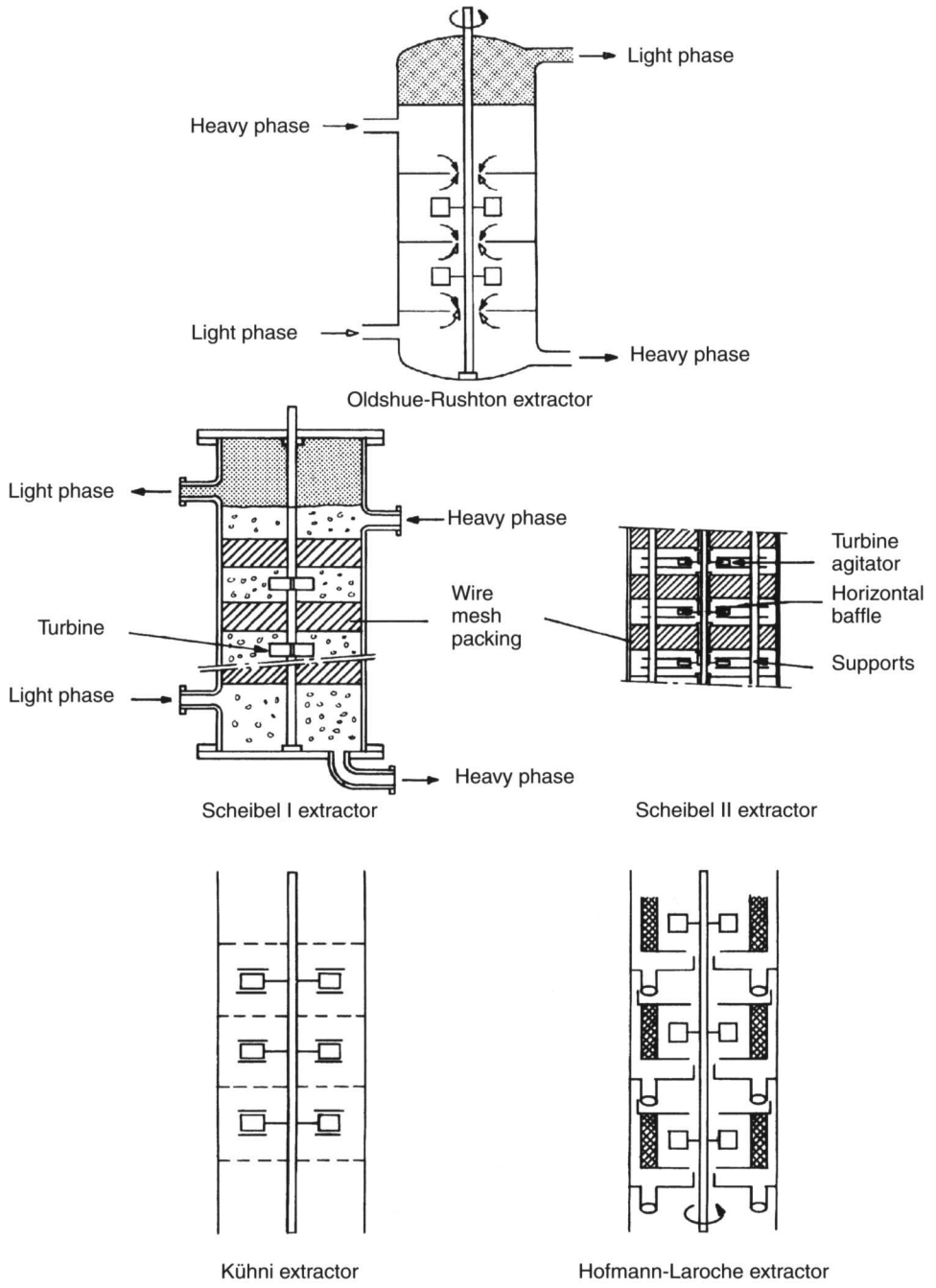


Figure 5.9 Examples of mechanically agitated columns.

- The Scheibel contactor (Fig. 5.9), in which the agitators are flat paddles and the compartments are separated by settling-coalescence zones equipped with a wire mesh packing. The packing increases the overall efficiency but decreases the capacity of the column. Moreover, in the presence of solids, the packing can become plugged.
- The Hofmann-Laroche contactor (Fig. 5.9), in which the agitators are turbines, with packing along the periphery and within the field of radial circulation; the compartments are separated by plates with downcomers.

5.6.1 Hydrodynamics

5.6.1.1 Power input

As indicated elsewhere (Section 2.1.5.1), the power input for a rotating rotor in a liquid phase can be correlated by means of a dimensionless number known as the power number. A first approximation consists of assuming this power number to be constant for an RDC:

$$\frac{\mathcal{P}_c}{\rho_m N_R^3 D_R^5} = N_P \cong 0.03 \quad \text{if} \quad \frac{D_R^2 N_R \rho_m}{\mu_m} > 10^5 \tag{5.61}$$

where

N_R speed of rotation of the rotor in rpm

D_R rotor diameter

$\rho_m = \varepsilon_D \rho_D + (1 - \varepsilon_D)\, \rho_C$ density of the mixture (5.62)

$\mathcal{P}_c$ power dissipated in a compartment

$$\mu_m = \exp\left[\frac{2.5\varepsilon_D}{\varepsilon_C}\left(\frac{0.4 + \dfrac{\mu_D^*}{\mu_C}}{1 + \dfrac{\mu_D^*}{\mu_C}}\right)\right] \quad \text{apparent viscosity of the mixture} \tag{5.63}$$

$\mu_D^* = \mu_D + \mu_S$ interfacial viscosity.

Interfacial viscosity is determined experimentally (with no surfactant present $\mu_S = 0$). If it cannot be determined from experimental values, an older equation may be useful, since it depends only on the viscosities of the two phases and the holdup:

$$\mu_m = \frac{\mu_C}{\varepsilon_D}\left(1 + \frac{1.5\mu_D\varepsilon_D}{\mu_C + \mu_D}\right)$$

This equation is valid for the following geometries (see the symbols in Fig. 5.8):

$$0.05 < D_T < 2 \quad \text{(in m)}$$

$$0.7 < \frac{D_O}{D_T} < 0.8 \qquad 0.45 < \frac{D_R}{D_T} < 0.625 \qquad 0.12 < \frac{h_c}{D_T} < 0.25$$

If the rotating disc is replaced by a Rushton turbine, as in Scheibel and Oldshue extractors, the power number N_P increases from 0.03 to 1.85. In fact, the power number N_P is not constant for all hydrodynamic regimes but depends on the Reynolds number, the type of contactor, the geometry of the system, and, under certain conditions, the Froude number:

- For RDCs and ARDCs Kumar and Hartland [1995] have proposed the following law:

$$N_P = \frac{C_1}{Re_R} + C_2 \left[\frac{1\,000 + 1.2 Re_R^{C_3}}{1\,000 + 3.2 Re_R^{C_3}} \right]^{C_4} \tag{5.64}$$

where:

$$Re_R = \frac{N D_R^2}{\rho_C \mu_C}$$

where

D_R rotor diameter

C_1, C_2, C_3, C_4 constants with the following values:

	C_1	C_2	C_3	C_4
RDC	109.36	0.74	0.72	3.30
ARDC	90.0	0.62	0.73	3.17

- For Kühni columns, the value of N_P is:

$$N_P = 1.08 + \frac{10.94}{Re_R^{0.5}} + \frac{257}{Re_R^{1.5}} \tag{5.65}$$

In a column with N_c compartments, the total absorbed power is obviously equal to $\mathcal{P}_{total} = N_c \mathcal{P}_c$.

5.6.1.2 Holdup and interfacial area

A. Holdup

The general empirical correlation (5.6) and the specific coefficients established by Kumar and Hartland [1995], using more than 1100 data points for rotating disc columns, provide results that are quite close to the values for holdup found experimentally. From a more theoretical point of view, the general equation, which relates dispersed phase holdup to the superficial velocities and a characteristic velocity, is valid in this case:

$$u_g (1 - \varepsilon_D) = \frac{V_{SD}}{\varepsilon_D} + \frac{V_{SC}}{1 - \varepsilon_D} \tag{5.66}$$

The correlations used to calculate u_g are obviously specific to this type of device and depend on the system and geometry of the extractor. However, if the discs rotate slowly, the hydrodynamic behavior is close to that of drop columns—taking into account the limitations imposed by the column internals on phase circulation—and u_g is appreciably constant. At high rotational velocities, however, turbulence has an influence on the droplet size and recirculation in the compartments, and u_g decreases sharply as N_R increases.

This characteristic is reflected in the discontinuity in correlations for u_g as a function of the speed of rotation.

Laddha *et al.* [1978] have published a general correlation that relates u_g to various system parameters. The correlation is based on the experimental results of a number of authors. It is different for systems with and without mass transfer. Note that the limit between the region of "low speed of rotation" (zone I) and the region of "high speed of rotation" (zone II) is not found for the same conditions, but depends on whether mass transfer occurs from the dispersed phase to the continuous phase or in the opposite direction. To account for these factors, Laddha introduced two dimensionless groups:

$$\text{"properties group"} \quad \Psi_P = \left(\frac{\sigma^3 \rho_C}{\mu_C^4 g}\right)^{\frac{1}{4}} \left(\frac{\Delta\rho}{\rho_C}\right)^{\frac{3}{5}}$$

$$\text{"geometry group"} \quad \Psi_G = \left(\frac{h_c}{D_R}\right)^{0.9} \left(\frac{D_O}{D_R}\right)^{2.1} \left(\frac{D_R}{D_T}\right)^{2.4}$$

The limit between the two operating zones satisfies the following criteria:

$$\text{transfer } C \rightarrow D \quad \frac{g}{D_R N_R^2} \Psi_P^{\frac{1}{2}} = 25$$

$$\text{transfer } D \rightarrow C \quad \frac{g}{D_R N_R^2} \Psi_P^{\frac{1}{2}} = 16$$

The estimated value of u_g, therefore, depends on the operating zone according to the following equations:

Zone I: transfer from $D \rightarrow C$ or $C \rightarrow D$:

$$u_g = 1.5 \left[\left(\frac{\sigma \Delta\rho g}{\rho_C^2}\right)^{0.25} \Psi_G\right] \left[\Psi_P^{\frac{1}{2}} \left(\frac{g}{D_R N_R^2}\right)\right]^{0.08} \tag{5.67}$$

Zone II:

$$u_g = \beta \left[\left(\frac{\sigma \Delta\rho g}{\rho_C^2}\right)^{0.25} \Psi_G\right] \left[\Psi_P^{\frac{1}{2}} \left(\frac{g}{D_R N_R^2}\right)\right] \tag{5.68}$$

where

$\beta = 0.110$ for transfer from $D \rightarrow C$

$\beta = 0.077$ for transfer from $C \rightarrow D$.

Figure 5.10 is a graphic representation of Laddha's equations for transfer from $C \rightarrow D$.

B. Interfacial area

The general equation $\mathcal{A} = 6\varepsilon_D / \overline{d_B}$ remains valid and leads to an estimate of drop size and holdup. It seems logical therefore to distinguish the same zones used in predicting u_g. Correlations have been proposed by various authors, but we again want to point out the risk in using them without verification: the interfacial phenomena associated with mass transfer and the presence of surfactive, or even polar, substances at the interface can have a significant impact on these general correlations.

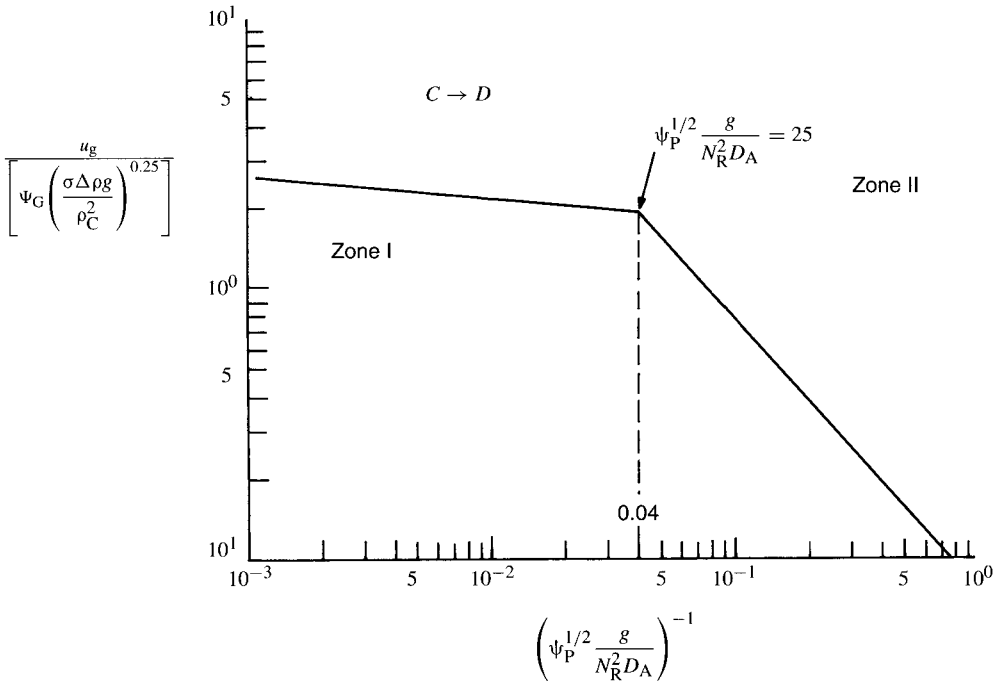


Figure 5.10 Mechanically agitated extractors: determination of the characteristic velocity u_g.

To estimate drop size it is preferable to make a distinction between the two hydrodynamic regimes. For zone I, at low rotational velocities, $\overline{d_B}$ can be estimated from:

$$\overline{d_B} \cong 1.4\left(\frac{\sigma}{\Delta\rho g}\right)^{0.5} \tag{5.69}$$

In region II, at high rotational velocities, the dissipated power directly influences drop size, just as it does in gas-liquid contactors. Trambouze *et al.* [1988] suggest first calculating the maximum stable drop size in a turbulent shear field:

$$\overline{d_{B\max}} = C\left(\frac{\sigma}{\rho_C}\right)^{0.6}\Sigma^{-0.4} \tag{5.70}$$

where

C constant $\cong 0.5$ if the dispersed phase is organic

C constant $\cong 1$ if the dispersed phase is aqueous

Σ is the power input per unit mass calculated as shown above (5.61).

The average size is then taken to be equal to approximately $0.7\overline{d_{B\max}}$, bearing in mind that the distribution of sizes will widen appreciably under these conditions.

Another approach is provided by Kumar and Hartland [1986], who consolidate results from 23 independent systems in two correlations with a mean precision of 12%, using the formulas shown below.

- For $Re \leqslant 50\,000$:

$$\overline{d_B} = k_1 D_R \left(\frac{N_R D_R^2 \rho_C}{\mu_C}\right)^{-1.12} \left(\frac{\mu_C}{\sqrt{\sigma \rho_C D_R}}\right)^{-1.38} \left(\frac{\Delta\rho}{\rho_C}\right)^{-0.24} \left(\frac{D_R^2 \rho_C g}{\sigma}\right)^{-0.05} \left(\frac{H}{D_R}\right)^{0.42}$$

- For $Re \geqslant 50\,000$:

$$\overline{d_B} = k_2 D_R \left(\frac{N_R D_R^2 \rho_C}{\mu_C}\right)^{-0.55} \times \exp\left[-0.23 \frac{N_R^2 D_R}{g}\right] \left(\frac{\mu_C}{\sqrt{\sigma \rho_C D_R}}\right)^{-1.30} \left(\frac{\rho_D}{\rho_C}\right)^{0.75} \left(\frac{D_R^2 \rho_C g}{\sigma}\right)^{-0.30} \left(\frac{h_c}{D_R}\right)^{0.28}$$

where

h_c compartment height (m)

the values of k_1 and k_2 depend on the direction of transfer:

Transfer	k_1	k_2
None	0.18	$7.0 \cdot 10^{-3}$
$C \rightarrow D$	0.17	$7.0 \cdot 10^{-3}$
$D \rightarrow C$	0.20	$7.9 \cdot 10^{-3}$

5.6.1.3 Backmixing

Strand *et al.* [1962] have suggested the following equation for both the continuous phase and the dispersed phase:

$$\frac{\varepsilon_j \mathcal{D}_{A,j}}{V_{Sj} h_c} = 0.5 + 0.09 \varepsilon_j \left(\frac{D_R N_R}{V_{Sj}}\right) \left(\frac{D_R}{D_T}\right)^2 \left[\left(\frac{D_O}{D_T}\right)^2 - \left(\frac{D_R}{D_T}\right)^2\right] \tag{5.71}$$

The equation is valid when $\left(D_R N_R / V_{Sj}\right) > 30$, the subscript j being relative either to the dispersed phase, $j = D$, or the continuous phase, $j = C$.

Stemerding *et al.* [1963] provide a simpler expression for the continuous phase, but it is numerically little different from the equation that results from using (5.71). Although published in 1963, it remains more precise than many later correlations.

$$\frac{\mathcal{D}_{A,C}}{V_{SC} h_c} = 0.5 + 0.012 \left(\frac{D_R N_R}{V_{SC}}\right) \left(\frac{D_O}{D_T}\right)^2 \tag{5.72}$$

The coefficient $\mathcal{D}_{A,D}$ is estimated to be approximately $3\mathcal{D}_{A,C}$.

5.6.1.4 Flooding

There are few published data and correlations for flooding in these columns and most of them lack generality. Figure 5.11, which appeared in Reman [1966], gives a fairly good idea of the operating limits.

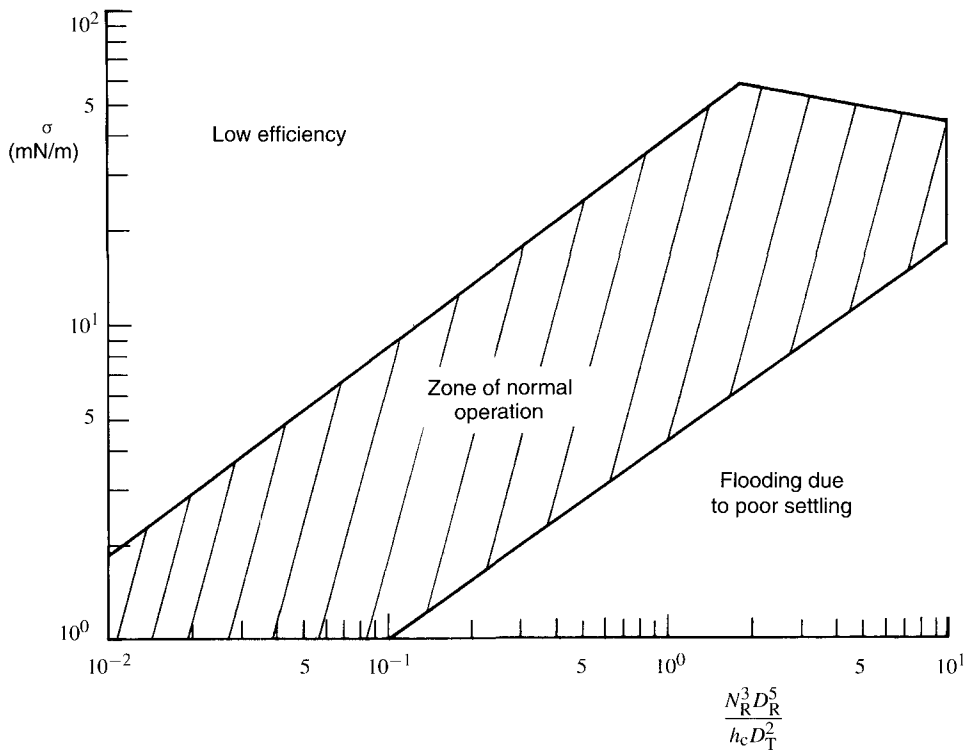


Figure 5.11 Flooding in mechanically agitated extractors.

Another, and fairly efficient, method consists in identifying the conditions that correspond to a holdup value of 10 to 20%. Lacking any simple and precise correlations, Kumar and Hartland [1988] proposed a correlation, although somewhat complex and relative to Karr columns, that could provide an estimate of the flooding velocity for columns with a rotating agitator.

5.6.2 Mass transfer

Korchinsky's detailed summary in Godfrey and Slater [1994] suggests that no precise general correlation currently exists. The individual coefficients, k_C and k_D, can be calculated from correlations valid for rigid drops, it being understood that the drop size is small enough for

this assumption to be reasonable. This gives, for example:

$$\frac{k_D\overline{d_B}}{\mathcal{D}_D} = 6.6 \tag{5.73}$$

$$\frac{k_C\overline{d_B}}{\mathcal{D}_C} = 2 + 0.95\left(\frac{\overline{d_B}u_g\rho_C}{\mu_C}\right)^{\frac{1}{2}}\left(\frac{\mu_C}{\rho_C\mathcal{D}_C}\right)^{\frac{1}{4}} \tag{5.74}$$

These equations could provide estimates that are two times too small for drops of ordinary size.

Laddha *et al.* [1978] supply the following correlations for the global coefficient:

- Zone I:

$$K_{DC} = 0.068\varepsilon_D(1-\varepsilon_D)\left(\frac{g^3\Delta\rho^3}{\sigma\rho_C^2}\right)^{0.25}\left[\sqrt{\frac{\mu_D}{\rho_D\mathcal{D}_D}} + m\sqrt{\frac{\mu_C}{\rho_C\mathcal{D}_C}}\right]^{-1} \tag{5.75}$$

- Zone II:

$$K_{DC} = 0.95\varepsilon_D(1-\varepsilon_D)\left(\frac{g^3\Delta\rho^3}{\sigma\rho_C^2}\right)^{0.25}\left(\frac{D_R N_R^2}{g}\right)^{-0.5} \times \Psi_P^{-0.5}\left[\sqrt{\frac{\mu_D}{\rho_D\mathcal{D}_D}} + m\sqrt{\frac{\mu_C}{\rho_C\mathcal{D}_C}}\right]^{-1} \tag{5.76}$$

where m is the partition coefficient C_D/C_C.

5.6.3 Technology

The construction and installation of rotating disc contactors is relatively simple because the diameter of the discs is smaller than the openings in the stator. The dimensional ranges given above (Section 5.6.1.1) provide an indication of the customary geometries. The sum of the superficial velocities of the two phases (capacity) is between 1 and 2.5 cm/s. The speed of rotation, of course, depends on the dimensions of the column (normally in the turbulent regime) $\left(N_R D_R^2 \rho_C/\mu_C\right) > 10^4$, but this velocity is a parameter that is optimized when the device is put into operation: if agitation is too low, transfer is restricted, if agitation is too high, stable emulsions that no longer coalesce are liable to form. The influence of operating parameters on performance is summarized in the following table:

Parameter ↗	Capacity	Efficiency
Rotational speed	↘	↗↘
Diameter of rotor discs	↘	↗
Diameter of passages between stages	↗	↘
Vertical spacing between stages	↗	↘

The rotational characteristics of the unit present the greatest handicap during scale-up, for turbulence in a compartment is not uniformly distributed (as it always is in rotating agitators). This lack of homogeneity does not present too many problems in a small unit. But for larger sizes, we encounter the same difficulty found when scaling up mechanically agitated vessels. In such cases nearly calm zones can form, near the shaft, for example, creating a bypass of the compartments for part of the dispersed phase, resulting in a sharp drop in the efficiency of the unit. Following Reman [1966], scale-up generally involves keeping the ratio of the diameter of the stator to the diameter of the rotor constant. In spite of these precautions, units greater than 2.5 m in diameter are rarely found.

The major drawback of the RDC is its significant backmixing. The simplicity of construction requires fairly large compartment heights (at least 0.2 m for a reactor 2 m in diameter) and the openings between compartments are such that circulation between them is inevitable. For this reason some manufacturers have introduced devices that are more complicated to build but in which backmixing is strongly reduced.

5.6.4 Concluding remarks

Columns with rotary agitators have given rise to a number of variant designs intended to increase efficiency and capacity and reduce mixing between compartments. Simple to build, relatively unaffected by the presence of suspended solids, and highly flexible, they are in common use, in spite of the difficulty of scale-up.

5.7 MIXER-SETTLERS

Mixer-settlers are often arranged in series (cascade) and constitute the second category of devices containing rotary agitators. In principle, a mixer-settler is a very simple device (Fig. 5.12), containing two zones: a mixing zone and a settling zone.

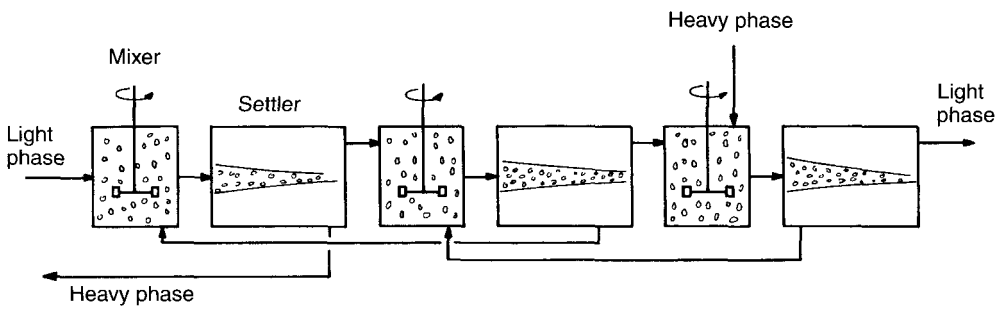


Figure 5.12 Cascade of countercurrent mixer-settlers.

In the mixing zone, a mechanical agitator (generally a turbine) disperses the two phases and sometimes ensures their transport from one compartment to the next (shear and pumping

effects). The mixers are ordinarily equipped with fairly small agitators that turn rapidly and produce high shear (for example, impellers with a tip speed about 3 m/s). By carefully choosing the geometry of the stirrer, a pumping effect can be created. Highly specific agitation conditions can be used to control the phase ratios and selective agitation in each stage when the agitators are mounted on separate shafts. Backmixing is limited.

The volume of the settling zones is always greater than the volume of the mixers. Very effective agitation sometimes leads to settling problems, but residence times can be established over fairly broad ranges (a few seconds to a few minutes, and sometimes as much as an hour). If the settling operation is carefully carried out, the contactor will function without backmixing between stages, and each compartment will operate as if it were a theoretical stage at thermodynamic equilibrium.

5.7.1 Hydrodynamics

5.7.1.1 Dispersion homogeneity

Dispersed phase holdup in a mechanically agitated tank is equal to the ratio $V_{SD}/(V_{SD} + V_{SC})$ providing the agitation exceeds a minimum value, thus providing nearly homogeneous dispersion. Skelland and Seksaria [1978] have determined this minimum velocity N_{min} for systems characterized by the type and position of the agitator in various liquid-liquid media. They proposed a dimensionless correlation having the following form:

$$\frac{D_A^{0.5} N_{min}}{g^{0.5}} = C_1 \left(\frac{D_C}{D_A}\right)^{C_2} \left(\frac{\mu_C}{\mu_D}\right)^{0.11} \left(\frac{\Delta\rho}{\rho_C}\right)^{0.25} \left(\frac{\sigma}{D_A^2 \rho_C g}\right)^{0.3} \tag{5.77}$$

where C_1 and C_2 vary respectively from 3 to 15 and from 0.2 to 1.6 depending on the system examined. A mixing index can also be defined to characterize the homogeneity:

$$I_m = \frac{\varepsilon_D (V_{SD} + V_{SC})}{V_{SD}} \tag{5.78}$$

It is obvious that I_m must be close to 1 everywhere in the vessel, which corresponds to a specific power input in the tank between 0.2 kW/m^3 and 0.4 kW/m^3. Treybal [1963] stated that a specific power of 0.32 kW/m^3 will provide a mixing index greater than 0.95 at every point in the tank.

Skelland and Moon Lee [1978] found that the mixing index exceeds 0.98 if the number of revolutions is approximately 8% higher than the number of revolutions needed to eliminate distinct layers of the continuous and dispersed phases. They correlated the latter speed of rotation with dimensionless numbers, but the constants used in the equation depend on the geometry of the system. However, the speed of rotation should not be so great that the shear caused by the agitator leads to the formation of secondary emulsions that are difficult to separate. These two limits are summarized by Lorrain [1999] in the following inequalities:

$$N^3 D_A^2 < 1.9 \quad \text{and} \quad \pi N D_A < 1.6$$

5.7.1.2 Holdup and interfacial area

By providing sufficient agitation, the phase ratio is very close to the ratio of incoming flow rates for each compartment. We can then write:

$$\varepsilon_D = \frac{V_{SD}}{V_{SD} + V_{SC}} \tag{5.79}$$

To determine the interfacial area, we simply need to determine the mean drop size $\overline{d_B}$ and use the well-known formula $\mathcal{A} = 6\varepsilon_D/\overline{d_B}$.

Various correlations relate the mean drop diameter in the dispersed phase to the speed of rotation N_R and the diameter D_A of the agitator. These often have the following general form: $\overline{d_B} \approx N_R^{\alpha} D_A^{\beta}$, where the value of the exponents α and β varies considerably with the system:

$$-0.7 < \alpha < 1.5 \quad \text{and} \quad -0.7 < \beta < 2.5$$

A correlation established by Vermeulen [Trambouze *et al.*, 1988] takes into account the influence of the properties of the medium:

$$\overline{d_B} = 2.24 \left(\frac{\sigma^{0.6}}{\left(\frac{\mathcal{P}}{V}\right)^{0.4} \rho_C^{0.2}} \right) \varepsilon_D^{0.5} \left(\frac{\mu_D}{\mu_C}\right)^{0.25} \tag{5.80}$$

This correlation illustrates the advantage of scaling up the results obtained in small mixers and keeping the volumetric power $\mathcal{P}/V$ constant. Nonetheless, it must be used with great caution since high speeds of rotation will result in the formation of many very fine drops that will have a significant effect on interfacial area and coalescence that is difficult to quantify.

5.7.2 Mass transfer

Given the fact that non-negligible amounts of energy are introduced into these mixers, the droplet size is often quite small, resulting in transfer coefficients that are similar to the equations for rigid spheres:

$$\frac{k_D \overline{d_B}}{\mathcal{D}_D} = 6.6 \tag{5.81}$$

$$\frac{k_C \overline{d_B}}{\mathcal{D}_C} = 2 + 0.95 \left(\frac{\overline{d_B} u_g \rho_C}{\mu_C} \right)^{\frac{1}{2}} \left(\frac{\mu_C}{\rho_C \mathcal{D}_C} \right)^{\frac{1}{4}} \tag{5.82}$$

Coalescence-redispersion phenomena in these systems partially compensate for the rigid behavior of droplets. For this reason these correlations may be too conservative. Treybal [1963] suggests using the above equation for k_D, but with a modified diffusivity, which is 2.5 times greater than the molecular diffusivity. This gives:

$$\frac{k_D \overline{d_B}}{\mathcal{D}_D} = 16.5 \tag{5.83}$$

For the continuous phase, he was able to correlate the results obtained for dispersed phase viscosities less than 10 mPa · s:

$$\frac{k_C D_T}{\mathcal{D}_C} = 0.052 \left(\frac{N_R D_A^2 \rho_C}{\mu_C} \right)^{0.83} \left(\frac{\mu_C}{\rho_C \mathcal{D}_C} \right)^{0.5} \tag{5.84}$$

Correlations (5.18) and (5.22) are also useful.

5.7.3 Consumed power

The power input can be estimated in a manner similar to that for a stirred tank reactor with a single liquid phase (see Section 2.1.5.1). The Reynolds and power numbers correspond to the definitions used in Eqs. (2.49) and (2.51):

$$Re = \frac{\rho N_R D_A^2}{\mu} \tag{2.49}$$

$$N_P = \frac{\mathcal{P}_A}{\rho N_R^3 D_A^5} \tag{2.51}$$

where $N_P = f(Re)$ according to the curve in Fig. 2.14, given that:

- the density of the medium is a weighted average based on the density of each of the liquid phases: $\rho_m = \rho_C \varepsilon_C + \rho_D \varepsilon_D$
- the viscosity can be calculated using the following formula:

$$\mu_m = \frac{\mu_C}{\varepsilon_C} \left(1 + \frac{1.5 \mu_D \varepsilon_D}{\mu_D + \mu_C} \right)$$

5.7.4 Technology

The mixer is generally scaled-up from tests with a pilot unit while maintaining the same geometry and absorbed power per unit volume. Following this procedure, it is important to ensure that the maximum shear velocities do not become too high. This is the most cautious, if not always the most economical, approach.

The many variant designs are distinguished by the arrangement of the mixing and settling zones, or their connections. The first mixer-settlers were horizontal: the mixing compartments (sometimes parallelepipeds) were arranged next to the settling zones, which were equipped with devices to promote coalescence (wire mesh or packing). Transfer between compartments took place primarily through overflow of the light phase and underflow of the heavy phase. Each compartment could have an optimized speed of rotation. A typical mixer-settler is the Denver extractor (Fig. 5.13A). These units have the following principal advantages:

- high efficiency per stage
- operational flexibility
- ease of scale-up.

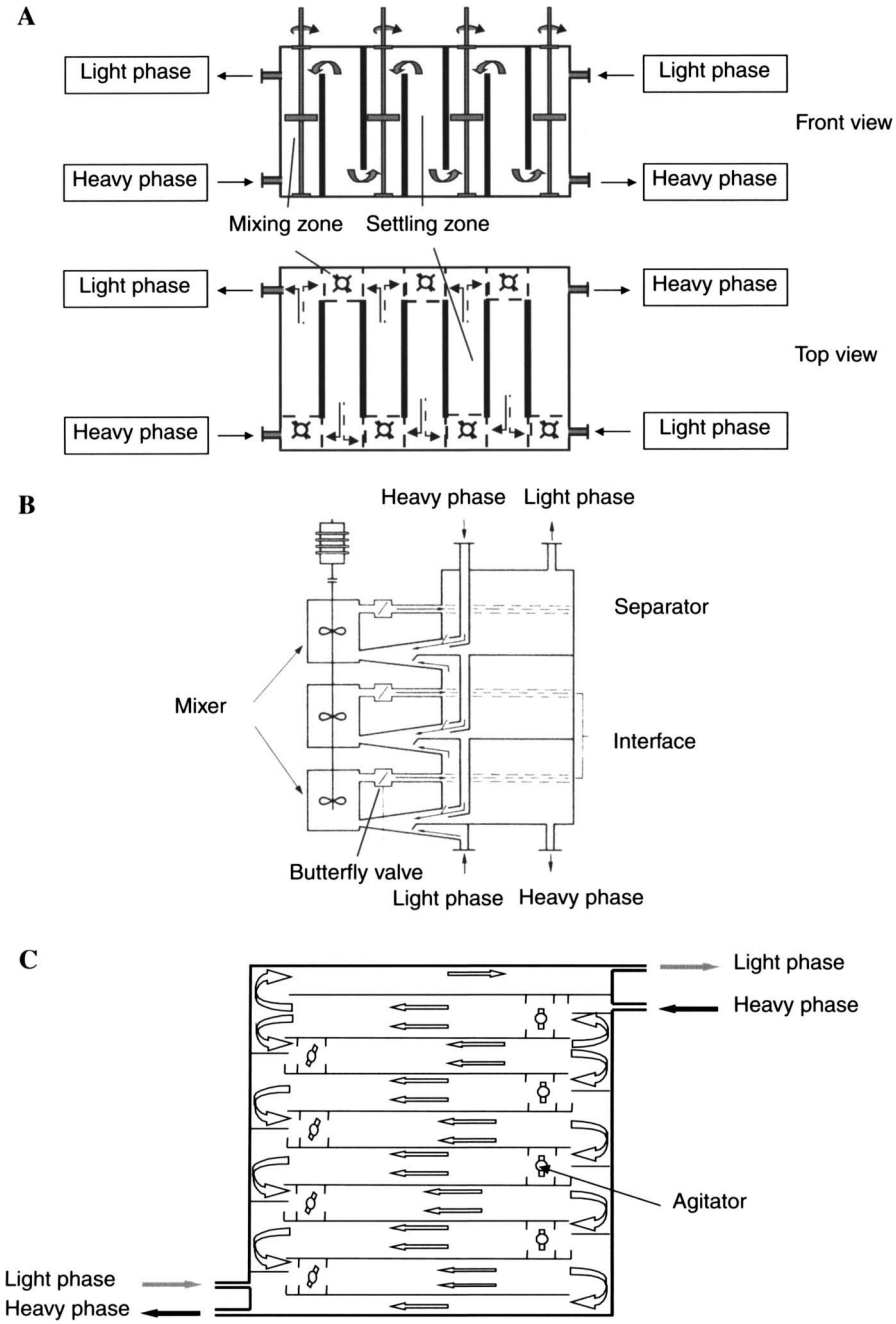


Figure 5.13 Mixer-settlers.
A. Denver mixer-settler. **B.** Stacked Lurgi mixer-settlers.
C. Stacked De Smet mixer-settlers.

However, they have the following drawbacks:
- large number of agitation shafts
- high cost
- large ground space required.

To overcome these drawbacks an extraction tower (Fig. 5.13) was developed in which the compartments are stacked. Unfortunately, the two most significant advantages of the mixer-settler, that is, excellent control of circulation of the two phases and the absence of bypass and backmixing, are not necessarily assured in the extraction tower. To overcome these problems, Lurgi proposed a device (Fig. 5.13B) in which the mixer also serves as a pump, pushing the heavy phase from a higher to a lower stage while simultaneously recirculating a large portion of the light phase. The extent of the recirculation depends on operating conditions, especially the flow rates of the two phases. These units can sometimes reach 30 m in height and 8 m in diameter and comprise as many as 24 stages.

Settling zone

After phase dispersion and contact, a settling zone is always necessary but the settler is sometimes completely separate. Since residence time in this zone is often several minutes, the capacity of the mixer-settler as a whole is primarily determined by the performance of the coalescer-settler. Models are available that can be used to describe the separation of dispersion based on a variety of parameters and scale-up laboratory data obtained during batch operation with greater precision [Jeelani *et al.* 1999]. Settlers are more efficient if the velocity and degree of turbulence at the inlet are low and the drops large. Devices to promote coalescence are sometimes installed. These consist of special internal components such as plates slightly inclined to the flow axis, cartridges or tubes, coalescer blankets, or even centrifugal or electric coalescers (from manufacturers such as Pall, for example).

5.7.5 Concluding remarks

Notwithstanding their high investment and maintenance costs, and their size, mixer-settlers are in common use because of their simplicity, flexibility, ability to process viscous products, and high flow rates. Since they accommodate lengthy residence times and efficient mass and heat transfer, they are well suited to slow or highly exothermic or endothermic reactions. They can also be easily scaled up from data obtained from pilot units. Volume scaling factors of 200-to-1 are standard.

5.8 OTHER TYPES OF EQUIPMENT

5.8.1 Centrifugal extractors

Centrifugal extractors consist essentially of a cylinder with plates attached to a horizontal (Podbielnak, Westfalia) or vertical (Robatel) shaft rotating at high speed (several thousand rpm). A number of different plate types have been proposed. The phases circulate in countercurrent mode while the centrifuge is used to promote settling. Well suited to fragile

products, they are infrequently used as reactors because of their relatively high investment, operating, and maintenance costs. Moreover, solids should be avoided in these units, even though the Podbielnak extractor can accommodate up to 30% by volume of solids if they are regularly eliminated. In spite of these drawbacks, these extractors are preferable when the phases have similar densities (differences of 10 to 50 kg/m^3). Used with continuous countercurrent flow of phases, capacities can reach 100 m^3/h; although residence times are generally very short, they can also be as long as one or more minutes. More detailed information is provided by E. Blass in Godfrey and Slater [1994].

5.8.2 Microreactors

On the opposite end of the spectrum from conventional efforts to scale-up to large industrial units, tests conducted in microreactors by Burns and Ramshaw [1999] have yielded promising results by using microtubes (interior diameters of 127 and 254 μm). In these microchannels it is possible to flow two immiscible liquids in cocurrent mode in the form of stable, stacked streams in the laminar regime. Mass and heat transfer are especially favorable and therefore these reactors are very well suited to fast reactions in a heterogeneous liquid-liquid medium. Moreover, heat exchange through the walls can be used to easily control the temperature, even for exothermic reactions, which strongly limits the appearance of byproducts. Scale-up can involve the use of a large number (several thousand) of microchannels in parallel. Problems of distribution, plugging, and pressure drop are the key issues. Compact and efficient, microreactors can be useful in obtaining the high added-value products that result from very fast reactions.

5.9 CONCLUDING REMARKS

Today we have access to a rather rich set of semiquantitative data that can be used as a reasonable guide in designing liquid-liquid reactors. Unfortunately, it is not always possible to design units of this type accurately, using a simple calculation based on kinetic data. As with gas-liquid reactors, it is the lack of a correct model that can be used to predict the physicochemical behavior of the liquid-liquid suspension that is the heart of the problem. A better knowledge of interface phenomena, a quantitative description of coalescence, and realization of the importance of impurities at the interface is needed to make progress in this field.

The choice of equipment is based largely on technological considerations [for example, see Lo *et al.*, 1983; Cusak *et al.*, 1991; Godfrey and Slater, 1994; Lo, 1997; Wauquier, 2000; Lorrain, 1999; and Trambouze, 2000]. Nevertheless, there are some simple criteria that can be used to orient our choices (Table 5.4). As with gas-liquid contactors, if the reaction is slow ($Ha < 1$), holdup in the reactive phase must be large. Therefore, devices are chosen in which this phase ratio is easy to control (mixer-settlers, Lurgi columns).

The ease of phase separation is another extremely important criteria. If the phase properties are such that settling problems could occur, devices that require a large energy input should be avoided. These include mixer-settlers and, especially, columns with rotary agitators in which

Table 5.4 Characteristics of different liquid-liquid reactors.

	Static mixer	**Spray columns**	**Columns with random packing**	**Columns with structured packing**	**Perforated-plate columns**	**Mixer-settlers**	**RDC**	**ARDC**	**Scheibel**	**Oldshue**	**Kühni**	**Pulsed columns**	**Centrifuges**
Maximum flow $m^3/(h \cdot m^2)$	150	20	30	100	70	1 000	35	35	25	25	50	60	100
H maximum (m)			15		12		15	12		40			
Maximum diameter (m)	2	2	2	1	5	8	8	3	1–3	3	5	2–3	0.8
Cost	average	low	low	high	average	high	average	average	average	average	average	average	high
Viscous products	yes	no	no	no	no	yes	no	no	no	no	no	no	limited
Corrosion	suitable	suitable	suitable	suitable	average	suitable	suitable	suitable	suitable	suitable	suitable	average	average
Comments	similar bubble sizes		fouling	fouling	fouling	large						can handle solids	$\Delta\rho$ low / small

the settling volume is quite small. If, however, effective extraction is most important—for example, in the case of a reaction from which a relatively transient intermediary product is to be extracted—a mechanical dispersion device must be used. Also, since a liquid-liquid device is generally quite large, the choice between a column or a horizontal arrangement depends to a large extent on the available space.

Finally, extraction devices such as centrifuges (Podbielniak) can be used for very short contact times, good exchange, and efficient separation, but the initial investment is high. These devices are preferable if the phases have similar densities and the flow rates are modest since scale-up is difficult and limited. They are described in books on extraction technology, in particular Godfrey and Slater [1994].

REFERENCES

Baker JR (1991) Motionless mixers stir up new uses. Chem En. Prog, June 1991, pp 32–38.

Burns JR, Ramshaw C (1999) Trans Inst Chem Eng 77, may 1999, pp 206–211.

Calderbank PH, (1967) Mass Transfer in: Mixing, Theory and Practice. V.W. Uhl, J.B. Gray, Eds, Academic Press, New York.

Cusak RW, Karr A, Fremeaux P (1991) A fresh look at liquid-liquid extraction. Chem Eng March 1991, pp 132–138 and April 1991, pp 112–119.

Danckwerts PV (1965) Chemical Engineering Practice 8, chap. 6. Butterworths. London.

Godfrey JC, Slater MJ (1994) Liquid-liquid extraction equipment. John Wiley and Sons, New-York.

Harnby N, Edwards M, Nienow A (1992) Mixing in the process industries, Second edition. Butterworth-Heinemann, Boston.

Ingham J (1975) Longitudinal Mixing in liquid-liquid Extraction. *In*: Recent advances in liquid-liquid Extraction. C. Hanson. Pergamon Press, Oxford.

Jeelani SAK, Panoussopoulos K, Hartland S (1999) Effect of turbulence on the separation of liquid-liquid dispersions in batch settlers of different geometries. Ind Eng Chem Res 38, pp 493–501.

Kumar A, Hartland S (1984) Correlation for drop size in liquid-liquid spray columns. Chem Eng Comm 31, 193–207.

Kumar A, Hartland S (1988) Prediction of Dispersed-Phase Holdup and Flooding Velocities in Karr Reciprocating-Plate Extraction Columns. Ind Eng Chem Res 27, pp 131–138.

Kumar A, Hartland S (1995) A unified correlation for the prediction of dispersed phase hold-up in liquid-liquid extraction columns. Ind Eng Chem Res 34, 11, pp 3925–3940.

Kumar A, Hartland S (1986) Prediction of drop size in Rotating Disc Extractors. Can J Chem Eng 4, dec. 1986, pp 915–923.

Laddha GS, Degaleesan TE (1976) Transport Phenomena in liquid-liquid Extraction. McGraw-Hill, New Dehli.

Laddha GS, Degaleesan TE, Kannappan R (1978) Can J Eng 56, p 137.

Lo TC (1997) *In:* Commercial liquid-liquid extraction equipment. Handbook of Separation Techniques for Chemical Engineers, Third Edition, McGraw-Hill, New York, pp 1449–1518.

Lo TC, Baird MH, Hanson C (1983) Handbook of solvent extraction. Wiley Interscience, New York.

Lorrain C (1999) Extraction liquide-liquide, aspects pratiques, Techniques de l'ingénieur, 1999, J 2755–2757.

Minotti M, Doherty MF, Malone MF (1998) Design for simultaneous reaction and liquid-liquid extraction. Ind Eng Chem Res 37, 12, pp 4748–4755.

Myers K, Reeder M, Rigden M (1996) Agitating for success. Chem Eng, Oct. 10, 1996, pp 39–42.

Ray MS (1994) Liquid-liquid Extraction: a bibliography update (1992–1993). Separation Science and Technology, 29, 18, pp 2541–2554.

Reman GH (1966) Chem Eng Prog 62, 9, p 57.

Sawistowski H (1975) Interfacial Phenomena. *In*: Recent Advances in liquid-liquid Extraction. (C. Hanson, Ed.) Pergamon Press, Oxford.

Schweitzer PA (1997) Handbook of separation techniques for chemical engineers. McGraw-Hill, New York.

Skelland AHP, Conger WL (1973) A rate approach to design of perforated-plate extraction columns. Ind Eng Chem Proc Des Dev 12, 4, pp 448–454.

Skelland AHP, Seksaria R (1978) Ind Eng Chem Proc Des Dev 17, 1, pp 56–61.

Skelland APH, Moon Lee JA (1978) Ind Eng Chem Proc Des Dev 17, 4, p 473.

Stemerding S, Lumb EC, Lips J (1963) Chem Ing Techn 35, p 844.

Strand CP, Olney RB, Ackerman GH (1962) AIChE J 8, p 253.

Streiff FA, Mathys P, Fischer T (1997) New fundamentals for liquid-liquid dispersion using static mixers. Récents progrès en Génie des procédés, 11, 51, 307–314, Lavoisier, Paris.

Sulzer (1994) Static mixers for refineries. Doc. Sulzer.

Thornton JD (1957) Trans Inst Chem Eng 35, p 316.

Thornton JD (1966) Chem Eng Sci, 5, p 201.

Trambouze P (2000) Petroleum Refining. Vol. 4: Materials and Equipment. Editions Technip, Paris.

Trambouze P *et al.* (1988) Chemical Reactors. Editions Technip, Paris.

Treybal RE (1963) Liquid Extraction. 2. McGraw-Hill, New York.

Tung L, Luecke R (1986) Mass transfer and drop size in pulsed-plate extraction columns. Ind Eng Chem Proc Des Dev 25, pp 664–673.

Vermeulen T, Moon JS, Hennico A, Miyauchi T (1966) Axial Dipersion in Extraction Columns. Chem Eng Prog 62, 9, pp 95–102.

Wauquier JP (2000) Petroleum Refining. Vol. 2: Separation Processes. Editions Technip, Paris.

NOMENCLATURE

(specific to Chapter 5)

Symbol	Definition	Dimension	SI unit
A	Pulse amplitude	L	m
D_O	Ring diameter (RDC)	L	m
D_R	Rotor diameter (RDC)	L	m
$d_{p,c}$	Critical packing diameter	L	m
$\mathcal{D}_a$, $\mathcal{D}_d$	Coefficient of diffusion in the incoming phase, outgoing phase	$L^2\theta^{-1}$	m^2/s
$\mathcal{D}_{A,C}$, $\mathcal{D}_{A,D}$	Coefficient of axial diffusion in the continuous phase, dispersed phase	$L^2\theta^{-1}$	m^2/s
E_C, E_D	Chemical enhancement factor in the continuous phase, dispersed phase	–	–
f	Pulse frequency	θ^{-1}	s^{-1}
h_c	Compartment height	L	m
k_C, k_D	Coefficient of transfer in the continuous phase, dispersed phase	$L\theta^{-1}$	m/s
L	Drop cloud trajectory (in Table 5.2 on page 306)	L	m
m	Partition coefficient $\frac{C_D}{C_C}$	–	–
n_O	Number of openings	–	–
N_c	Number of compartments	–	–
ΔP, ΔP_0	Overall pressure drop, single phase	$ML^{-1}\theta^{-2}$	Pa
Q_C, Q_D	Volumetric flow rate of the continuous phase, dispersed phase	$L^3\theta^{-1}$	m^3/s
S_O, S_t	Free cross-sectional area in the openings, total plate cross-section	L^2	m^2
S_i	Drop surface	L^2	m^2
u_g	Slip velocity or characteristic relative velocity	$L\theta^{-1}$	m/s
u_O	Velocity through the opening	$L\theta^{-1}$	m/s
u_r	Overall relative velocity	$L\theta^{-1}$	m/s
V_i	Drop volume	L^3	m^3
α_i, β_i	Constants (Eq. 5.27 and 5.28)	–	–
ε	Void fraction of packing	–	–
ε_D	Fraction of reactor occupied by the dispersed phase	–	–
λ	Packing factor	–	–
μ_C, μ_D, μ_m	Continuous phase viscosity, dispersed phase viscosity, mean	$ML^{-1}\theta^{-1}$	$Pa \cdot s$
ν_a, ν_d	Kinematic viscosity of incoming phase, outgoing phase	$L^2\theta^{-1}$	m^2/s
ρ_C, ρ_D, ρ_m	Density of continuous phase, dispersed phase, mean	ML^{-3}	kg/m^3
$\Delta\rho$	Density difference	ML^{-3}	kg/m^3
σ	Interfacial tension	$M\theta^{-2}$	N/m
Σ	Power input per unit mass	$L^2\theta^{-3}$	W/kg
Ψ_G, Ψ_P, Ψ_T	Dimensionless numbers	–	–
Z	Column height	L	m
Bo	(Bond number) $= \frac{g\overline{d_B^2}\Delta\rho}{\sigma}$	–	–
	Subscripts:		
j	C or D (continuous or dispersed phase)		
E	at flooding		

Copyrighted Materials
Copyright © 2004 Editions Technip Retrieved from www.knovel.com

6 General Characteristics of Heterogeneous Catalytic Reactors

6.1 INTRODUCTION

In Chapter 1 we indicated that reactions involving a solid catalyst formed a large class that justified a separate kinetic analysis, and we provided the most usual equations for reaction rates (Table 1.2). In those equations the reaction rate for heterogeneous catalysis is expressed as the number of moles per unit of time and unit of catalytic surface. The associated rate constant will be referred to as k_S. For convenience the reaction rate is generally defined per catalytic mass unit and not by surface unit. The rate constant then becomes k_M.

We can easily convert k_S to k_M by means of the following equation:

$$k_M = k_S S_P \tag{6.1}$$

in which S_P represents the surface area per unit mass of catalyst.

For a given mass of catalyst, there is an advantage in increasing the active surface as much as possible, which is accomplished by using porous or finely divided catalytic masses. The pores must remain accessible to the reactants, however. Consequently the diameter of the pores and their mean length must be suitable for the reactions involved. Obviously, for reasons of penetration efficiency, it is best to try to minimize the difficulty of access in a porous medium and therefore to divide the catalytic mass into fragments or grains. We will first examine the problem of a catalytic reaction with respect to the porous grain and then extend it to all the grains contained in the reactor.

6.2 THE CATALYST

For the reasons discussed above, it is common to employ a solid catalyst consisting of a large number of individual grains. Taken as a whole, the grains can be used in the following forms:

- a fixed bed, if the packed catalyst grains form a stationary packed bed in whose interstices the reaction fluids flow

- a moving bed, if the packing is subject to generally vertical translation, with the entire bed moving under the influence of gravity
- a fluidized bed, in which the catalyst grains are present in the form of fine particles that are maintained in suspension and agitated by an ascending current of reaction fluid
- an entrained bed, where fluids and particles are entrained in the same direction while crossing a reaction zone
- a slurry of catalytic solids immersed in the liquid reaction fluid.

More rarely the catalytic mass can form a monolithic body consisting of a compact porous mass crossed by generally straight-line channels through which the fluid reaction medium passes. This applies, for example, if small rigid beds are needed to withstand impact and vibrations. In the most common cases, it will always be possible to characterize the solid forming the catalytic structure, the catalyst grain, and the system of grains by means of simple physicochemical values.

6.2.1 The solid

Aside from its chemical composition, the solid is characterized by its density ρ_S (kg/m^3). In the case of supported catalysts, the density of the material forming the support can often be used for the density of the solid.

6.2.2 The grain

The catalyst grain is characterized by its shape and size (Fig. 6.1, photo 4). Depending on how it is used, the grain size can vary considerably, from a few micrometers for a suspended catalyst to a hundred micrometers for a fluidized bed, up to a centimeter or more in a fixed bed.

6.2.2.1 Mean diameter

In the case of catalysts that appear in the form of identical spherical beads, the diameter of the beads will be the characteristic dimension. Whenever the particles are not all the same size, whether spherical or not, a mean diameter $\overline{d_1}$ can be defined:

$$\overline{d_1} = \frac{6\,(\text{Total volume of particles in an average sample})}{(\text{Total exterior surface of particles in an average sample})}$$

The diameter $\overline{d_1}$ can be obtained from the cumulative numerical distribution curve: $a_i = f(t_i)$, where a_i is the ratio of the number of particles whose size is less than or equal to t_i to the total number of particles counted. It can be shown that:

$$\overline{d_1} = \frac{\Sigma \bar{t}_i^3 \Delta a_i}{\Sigma \bar{t}_i^2 \Delta a_i}$$

where

Δa_i difference on the ordinate of the curve $a_i = f(t_i)$ between t_{i-1} and t_i

$\bar{t}_i$ mean size in the interval t_{i-1} to t_i, that is: $\bar{t}_i = (t_{i-1} + t_i)/2$.

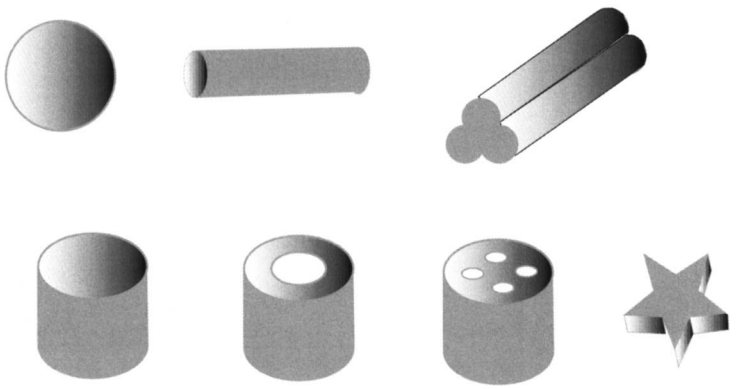


Figure 6.1 Catalyst shapes: sphere, extruded cylinder, cloverleaf, cylindrical pellet, ring, pellet with holes, star-shaped pellet.

Generally we have access to the mass distribution $x_i = f(t_i)$, x_i being the ratio of the mass of particles whose size is less than or equal to t_i to the total mass of particles. The following equation can then be used:

$$\frac{1}{\overline{d_1}} = \Sigma \frac{\Delta x_i}{\bar{t}_i}$$

Δx_i is the difference on the ordinate of the curve $x_i = f(t_i)$ between t_{i-1} and t_i.

The definition of mean diameter: To each physical or chemical phenomenon considered, there corresponds a distinct mean diameter. With respect to internal diffusion, that is the penetration in a porous medium, it has been observed that the best definition corresponds to:

$$\overline{d_1} = \frac{6\Sigma V}{\Sigma S} \tag{6.2}$$

where

ΣV sum of particle volumes contained in a unit volume of reactor

ΣS sum of the external surfaces of the particles contained in a unit volume of reactor.

Later, when we turn to the problem of pressure drop in a fixed bed and the phenomenon of fluidization, we will consider a mean diameter $\overline{d_2}$ such that:

$$\overline{d_2}^3 = \frac{6\Sigma V}{\pi n}$$

where

n number of grains per unit volume of reactor

$\overline{d_2}$ diameter of a sphere whose volume would be the average of the volumes of n particles contained in the unit volume of the reactor.

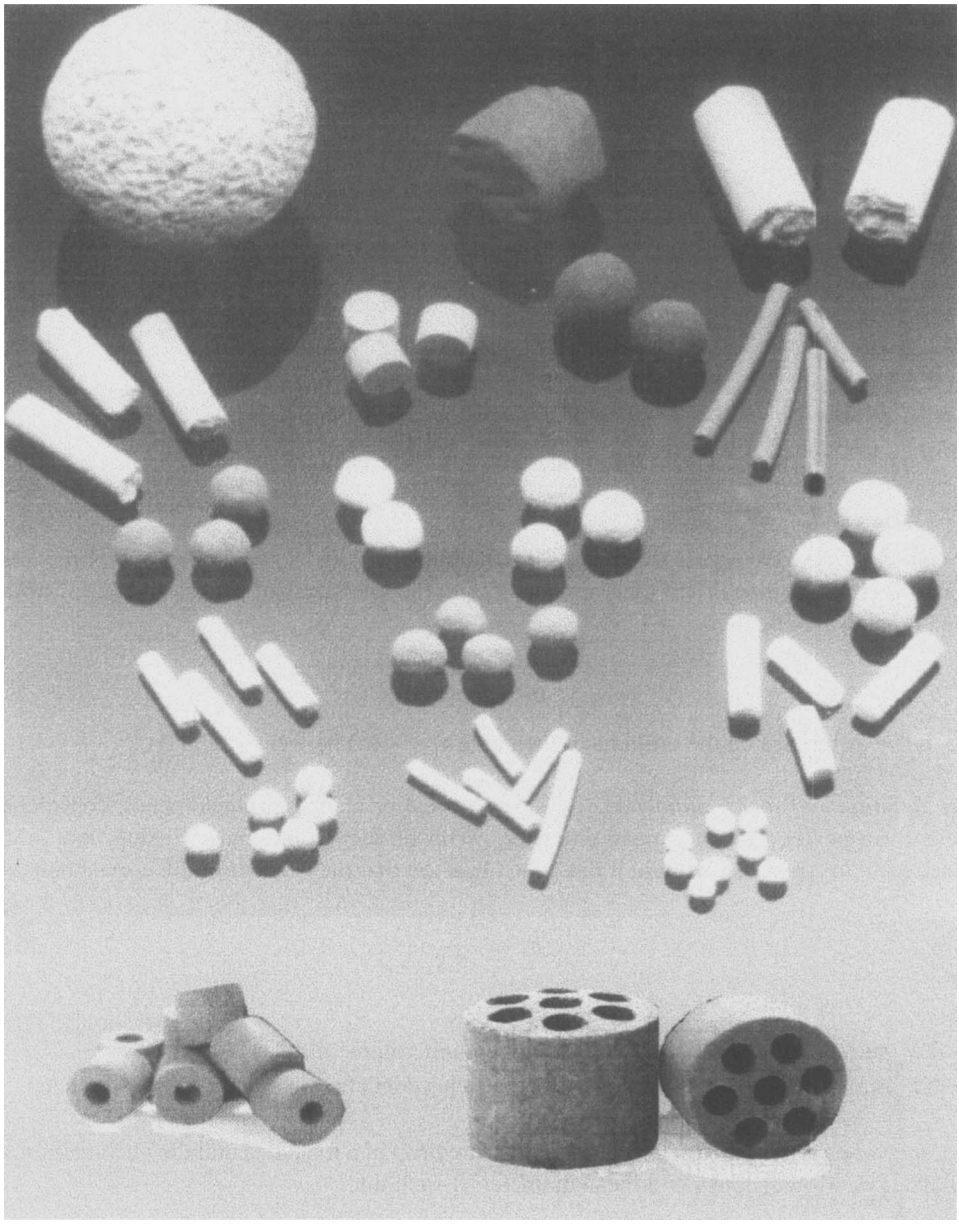


Photo 4 Different kinds and shapes of catalysts: spheres, extruded cylinders, rings, and six-hole pellets.

(*IFP Photo Library*).

When estimating the coefficients of mass and heat transfer between the particles and a fluid, we will have to introduce a mean diameter $\overline{d_3}$ such that:

$$\overline{d_3}^2 = \frac{\Sigma S}{\pi n}$$

$\overline{d_3}$ being the diameter of a sphere whose external surface would be the arithmetic mean of the external surfaces of the n particles contained in the unit volume of the reactor.

By combining the equations for $\overline{d_1}$, $\overline{d_2}$, and $\overline{d_3}$, we obtain:

$$\overline{d_1} = \frac{\overline{d_2}^3}{\overline{d_3}^2}$$

- For identical spheres of diameter d, we have:

$$\overline{d_1} = \overline{d_2} = \overline{d_3} = d$$

- For pellets (cylinders whose height is appreciably equal to the diameter D), we have:

$$\overline{d_1} = D$$

$$\overline{d_2} = \left(\sqrt[3]{\frac{3}{2}}\right) D = 1.14D$$

$$\overline{d_3} = \left(\sqrt{\frac{3}{2}}\right) D = 1.22D$$

The shapes of the grains vary and depend on the manufacturing procedure used: granulation, extrusion, pelletization, etc. [Lepage, 1978]. Catalyst particles frequently have one of the following geometries (Fig. 6.1):

- sphere
- cylinder whose height is equal to or less than its diameter (pellet)
- cylinder whose length is 1 to 20 times its diameter (extrudate)
- cylindrical ring characterized by an external diameter D_e, a cylinder height H, and an internal diameter D_e/κ
- cylindrical pellet containing several cylindrical holes
- extruded catalysts of various shapes (cloverleaf, for example).

Based on the previous definition, for solid cylindrical particles:

$$\overline{d_1} = \frac{3DH}{2H + D} \quad \text{if } D = H, \text{ then } \overline{d_1} = D$$

The same calculation can be performed for other geometries; the results are summarized in Table 6.1.

Table 6.1 Characteristics of various grain geometries.

Geometry	Parameter	Equivalent diameter	Example
Extruded cylinder	Diameter D Length L	$\overline{d_l} = \dfrac{3DL}{2L+D}$	$L = 10D$ $\overline{d_l} = 1.43D$
Pellet	Diameter D Height H	$\overline{d_l} = \dfrac{3DH}{2H+D}$	$H = D$ $\overline{d_l} = D$
Ring	External diameter D_e Internal diameter D_e/κ Height H	$\overline{d_l} = 3\dfrac{D_eH\left(1-\frac{1}{\kappa}\right)}{D_e\left(1-\frac{1}{\kappa}\right)+2H}$	$H = D_e$ $\kappa = 2$ $\overline{d_l} = 0.6D_e$
Pellet with holes	Diameter D Height H Diameter (holes) D/κ Number of holes n	$\overline{d_l} = \dfrac{3DH\left(1-\frac{n}{\kappa^2}\right)}{D\left(1-\frac{n}{\kappa^2}\right)+2H\left(1+\frac{n}{\kappa}\right)}$	$H = D$ $n = 4$ $\kappa = 4$ $\overline{d_l} = 0.47D$
Clover leaf	Lobe diameter D Length L	$\overline{d_l} = \dfrac{26.6D \cdot L}{8.88D+12.56L}$	$D = 2$ $L = 12$ $\overline{d_l} = 1.9D$

6.2.2.2 Surface area per unit mass

The second characteristic of the grain is the surface area per unit mass S_P (m^2/kg). The higher this specific area (and assuming active sites can form everywhere) the more active the catalyst, that is, the greater the ability of the unit mass to transform material per unit of time. The presence of pores in the grains naturally leads to an increase in the specific area. The porosity of the catalyst, or volume fraction of pores in the grain, is designated by θ.

The density ρ_p (kg/m^3) of the grain will always be less than the density of the constituent solid. The equation that associates these two densities is expressed as:

$$\rho_p = \rho_S(1-\theta) \quad \text{or} \quad \theta = 1 - \frac{\rho_p}{\rho_S} \tag{6.3}$$

If we treat the catalyst grain as a bundle of pores whose mean length is $\bar{l}$ and whose mean radius is $\bar{r}$, we can define the porous volume per unit mass of grain V_p in m^3/kg in several ways:

$$V_p = p\pi\bar{r}^2\bar{l} = 2p\pi\bar{r}\bar{l}\frac{\bar{r}}{2} = S_p\frac{\bar{r}}{2}$$

p being the number of pores per unit mass. Several obvious equations follows from the above

equalities:

$$\bar{r} = \frac{2V_p}{S_p} \tag{6.4}$$

$$V_p = \frac{1}{\rho_p} - \frac{1}{\rho_S} = \frac{\theta}{\rho_p} \tag{6.5}$$

If the catalyst has a bimodal pore size distribution, the above definitions are not applicable, unless a microporosity θ_1 and a macroporosity θ_2 are defined, such that $\theta = \theta_1 + \theta_2$. Table 6.2 provides some of the principal characteristics for commonly used industrial catalysts.

6.2.2.3 Mechanical strength of the grains

Catalyst grains should be able to resist crushing when stacked inside a reactor. The static mechanical strength of the grain is determined by subjecting it to a grain-by-grain crushing test [Lepage, 1978], which can vary considerably from one catalyst to another. Depending on the situation, grain-by-grain mechanical strength is evaluated in:

- Newton (N) (for more or less spherical particles), where the value can vary from 30 to 400 N
- N/m^2 (for flat pellets)
- N/m (for pellets or extrudates elongated along a generatrix).

6.2.3 Granular mass

6.2.3.1 Density, void fraction of stacked grains, exterior surface area

Assume we have a granular material, consisting of particles some of which may be in contact, contained in a reaction space known as a reactor. This material is characterized by:

- a catalyst mass per unit volume of reactor ρ_c (kg/m^3)
- a void fraction of the reactor $(1 - \varepsilon_p)$, where $\varepsilon_p = \rho_c/\rho_p$
- an external grain surface area per unit volume of reactor $\mathcal{A}_S$ (m^2/m^3).

There exists an obvious relation between $\mathcal{A}_S$, $\overline{d_1}$, and ρ_p. If the particle sample in question is contained in a unit volume of the reactor, then, by definition:

$$\Sigma V = \varepsilon_p$$
$$\Sigma S = \mathcal{A}_S$$

and consequently:

$$\mathcal{A}_S = \frac{6\varepsilon_p}{\overline{d_1}} = \frac{6\rho_c}{\overline{d_1}\rho_p} \tag{6.6}$$

For a mass of spherical particles or cylinders of uniform size in a compact stack, the void fraction $(1 - \varepsilon_p)$ can vary between 0.3 and 0.45. This contrasts with cylindrical rings, where the void fraction can achieve much higher values, up to approximately 0.7, which can constitute a significant advantage as discussed below. The void fraction of a mass of cylindrical rings can be calculated from the void fraction of a mass of cylindrical particles

Table 6.2 Characteristics of some industrial catalysts*.

Name	Use	Support	Active element	Shape	Dimensions (mm)	Surface area (m^2/g)	Porous volume (cm^3/g)	Manufacturer
RG482	Naphtha reforming	Al_2O_3	Pt-Re	Extrudate	1.2	210	0.60	Axens
CR201	Naphtha reforming	Al_2O_3	Pt-Sn	Sphere	1.8	160	0.45	Axens
HR306C	HDS	Al_2O_3	Co-Mo	Extrudate	1.2	210	0.60	Axens
HR945	HDS	Al_2O_3	Ni-Mo	Sphere	2–4			Axens
LT271	Selective hydrogenation	Al_2O_3	Pd + promoter	Sphere	1.5–3	70	0.60	Axens
HT308	Residue HDT	Al_2O_3	Co-Mo	Extrudate	1.2	200	0.50	Axens
CRS21	Claus process	Al_2O_3	Promoter	Sphere	4–8	250	0.12	Axens
DN190	Hydroprocessing	Al_2O_3	Ni-Mo	Cloverleaf	1.3	185	0.44	Criterion
HTZ4	Absorption of sulfur	–	ZnO	Extrudate	3–4			Topsoe
R67–7H	Natural gas steam reforming	Magnesium aluminate	Ni	Seven-hole cylinder	16 × 8 7 × 3.5			Topsoe
LK821	CO shift conversion	Al_2O_3	Cu-Zn	Pellet	4.5 × 3.2			Topsoe
PK5	Methanation	Al_2O_3	Ni	Ring	(6–1.7) × 4	250		Topsoe
FK2	Formaldehyde		Fe-Cr-Mo	Ring	(4.5–1.7) × 4			Topsoe
VK48	Sulfuric acid	Diatoms	$V_2O_5 + K_2O$	Ring	6 to 12			Topsoe
E221P	Hydrogenation	Al_2O_3	Pd	Sphere	2–4	230	0.54	Degussa
F154KP	Hydrogenation	Carbon	Pt	Extrudate	2–3	1 500	1.03	Degussa
Metalyst	Fine chemicals	–	Ni	Cylinder	3 × 3			Degussa
B2112Z	Fine chemicals	–	Co	Powder	35 μm	–	–	Degussa
XZ25	Catalytic cracking	Silica-Alumina	Zeolite	Sphere	65 μm ± 30	130	0.45	Davidson

* The numerical data shown in the above table has been taken from sales brochures supplied by the manufacturers.

and the ratio κ of the external and internal diameters of the particle:

$$\varepsilon_{\text{rings}} = \varepsilon_{\text{cyl}} \left(1 - \frac{1}{\kappa^2}\right) \tag{6.7}$$

6.2.3.2 Mechanical strength of a granular mass

Bulk crushing tests exist that can be used to classify catalysts according to their mechanical strength. The tests are performed in a special press equipped with a hollow cylinder and a piston. The particles (about thirty or forty) are placed in the cylinder and gradually compressed by the piston. After sieving, the fines are isolated. The result is expressed as the pressure needed to produce 0.5% of fines, the support area being that of the moving piston in the press.

Grain wear, caused by friction among the grains or with the wall, is determined by means of an attrition test: the percentage of fines produced is measured as a function of time, while specifying the apparatus used. Additional details can be found in Lepage [1978].

6.2.4 Monolithic catalysts

Over the past twenty years monolithic structures have appeared on the market. These are most often obtained by the extrusion of various materials (alumina, cordierite, mullite, zirconia, silicon carbide, etc.) or from rolled sheets, obtained by coating fibers or corrugated metal sheets (aluminum, steel, etc.) [Cybulski and Moulijn, 1994]. Their use as catalyst supports has developed gradually over the years, especially for pollution control in automobile exhaust systems. Catalysts are generally obtained from these monolithic supports through the deposition of a thin layer of alumina (washcoat) over the entire surface of channels, most often square or triangular in shape, followed by impregnation of the thin layer with an active element, as with a conventional catalyst (Fig. 6.2).

Monoliths can also be extruded from mixtures containing active elements; their surface area and porosity are such that they can be used directly without the deposition of an active layer.

In considering the use of monolithic structures as catalysts, where they can replace beds of particles (beads, extrudates, or pellets), it is important to have some method of comparison for deciding between these two options. We will limit our comparison to spheres and monoliths, spheres being suitably representative of solid particles in general. The following assumptions have been used for this comparison:

- the diameter of the spheres (d) is equal to the size of the cell (M) of the monolith, which is assumed to be square ($d = M$)
- the wall thickness of the monolith support is uniform and equal to e
- the porous layer deposited on the surface of the channels is assumed to be of uniform thickness δ and to vary between 25 and 100 μm
- the spheres and the active layer consist of the same catalytic porous solid, and therefore have the same characteristics with respect to the reaction.

For the comparison, several criteria that are important during a catalytic reaction can be used. We first consider the external surface of the catalytic solid, which is in contact with the

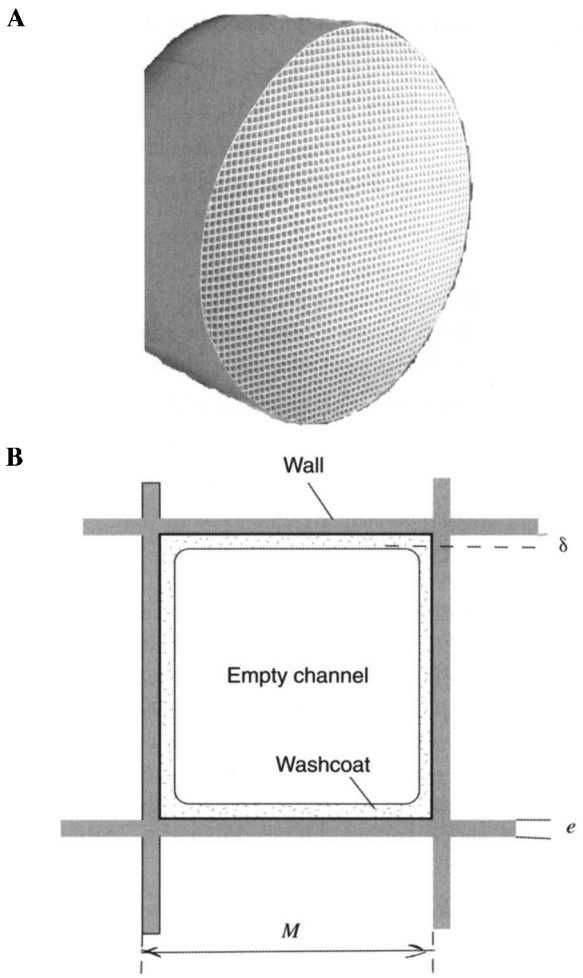


Figure 6.2 Monolith catalyst. **A.** Photograph of a cross-section of a square-mesh monolith. **B.** Cutaway view of a monolith channel showing the wall of the support structure and the active layer (washcoat).

flowing reactive fluid, needed to ensure mass transfer between the fluid and the catalyst. We will also compare the catalyst volumes needed for a given conversion to take place during a catalytic transformation. For this, knowledge of the volume fraction occupied by the active mass is required.

In the following chapter it will be shown that the pressure drop experienced by the flowing fluid is an important criteria for the comparison, pressure drop being primarily dependent on the void fraction $(1 - \varepsilon_M)$.

Assume a monolith with a square mesh equal to M and a wall thickness equal to e. The thickness of the active layer is δ. The following magnitudes can be successively calculated:

- Geometric area for fluid-monolith contact:
  - Surface area of the monolithic support (m^2/m^3)

$$S_M = \frac{4(M-e)}{M^2} \tag{6.8}$$

  - Surface area of the active phase (m^2/m^3)

$$S_{act} = \frac{4(M-e-2\delta)}{M^2} \tag{6.9}$$

- Void fraction of the monolith without a washcoat ($1-\varepsilon_M$)

$$(1-\varepsilon_M) = \frac{(M-e)^2}{M^2} \tag{6.10}$$

Fraction of active volume:

$$\mathcal{F}_{AV} = \frac{(M-e)^2-(M-e-2\delta)^2}{M^2} \tag{6.11}$$

The void fraction of the bed of beads ($1-\varepsilon_p$) depends on the reference catalyst, for example $(1-\varepsilon_p) = 0.4$ for spherical particles.

For example, Table 6.3 is a comparison of the characteristics of monoliths with beads for the same base dimension ($M = d$), a wall thickness of $0.15M$, and $\delta = 100\ \mu m$.

Table 6.3 Comparison of the geometric characteristics of beds of beads and monoliths.

Dimension ($d = M$)	Area of beads (m^{-1})	e (mm)	Monolith area (m^{-1})	Active volume fraction
1.3	2769	0.195	2615	0.238
1.5	2400	0.225	2267	0.209
1.75	2057	0.263	1943	0.181
2	1800	0.300	1700	0.160
2.5	1440	0.375	1360	0.130
3	1200	0.450	1133	0.109
3.5	1029	0.525	971	0.094
5	720	0.750	680	0.066
6	600	0.900	567	0.056

Figure 6.3 is a graphical representation of the comparison of geometric areas of beads and monoliths (support or active phase) *versus* diameter d or mesh M. We see that with both beads and monoliths appreciably the same geometric area of the external surface can be achieved. The void fraction, however, is much greater for the monolith ($1-\varepsilon_M = 0.723$) than it is for the spherical particles, and the active catalytic material volume is much lower. Below we discuss the influence of these characteristics in practice.

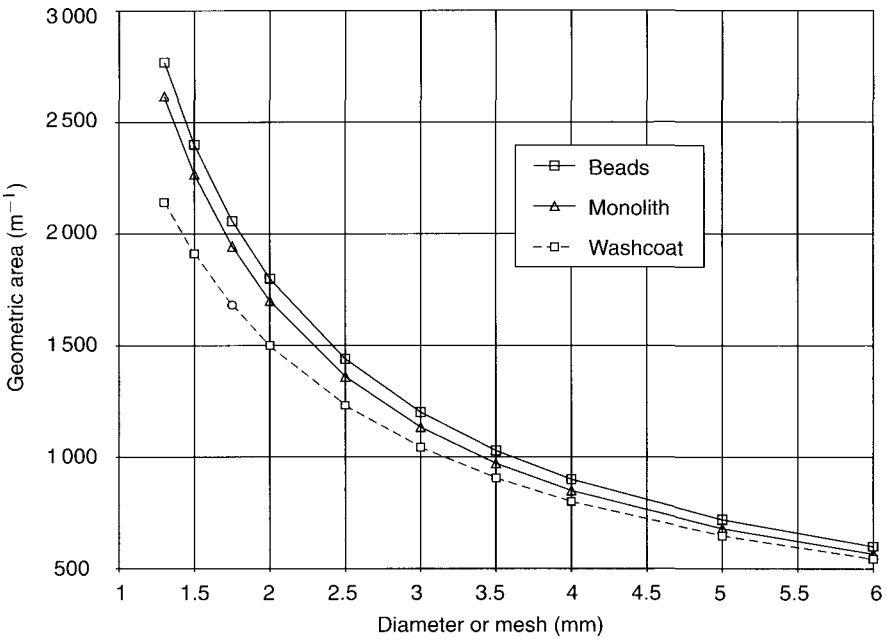


Figure 6.3 Comparison of geometric areas that can be achieved with a stack of spherical particles and a monolith (see Table 6.3).

6.3 INTERNAL DIFFUSION

A consequence of the porous structure of catalysts is their limited access. Designing a structure to increase the surface area per unit volume of reactor will do little if, at the same time, problems in reaching this surface compromise the reduction of catalyst volume. For this reason great care must be taken when examining the path taken by reactants and products in the porous medium that forms the catalytic mass. We will examine the problem for the ideal case of an isothermal catalytic reaction that takes place within a porous catalytic material by considering various geometries:

- plane surface
- spherical particle with a homogeneous structure containing active sites that are uniformly distributed throughout the volume of the grain
- spherical particle with a heterogeneous structure containing active sites in the external layer of the grain alone.

For each case we will consider a reactant A_1, present in the fluid phase in contact with the catalyst, which gives rise to a reaction whose stoichiometric equation is:

$$\nu_1 A_1 + \nu_2 A_2 = 0$$

Here we examine a rate expression of the form $r' = k_M C_1$, a first-order reaction, r' being expressed in mol/s · kg of catalyst. Under these conditions the rate constant k_M will be

expressed in $m^3/s \cdot kg$. We will then show how the results obtained for this simple case can be generalized to situations found in practice. Through the introduction of an effective diffusion coefficient $\mathcal{D}_{1e}$, an expression similar to Fick's law can be used to determine the molar balance around a catalytic volume element of thickness dz.

6.3.1 Plane surface

Assume we have a plate of porous catalytic material in contact with a fluid containing the reactant A_1. The fluid phase is in contact with only one of the surfaces of the plate of thickness L (Fig. 6.4). We consider one unit of interfacial area on the surface of the plate and write a molar balance for A_1 around a slice of thickness dz:

$$-\mathcal{D}_{1e}\left(\frac{dC_1}{dz}\right)_z + \nu_1 k_M \rho_p C_1 \, dz = -\mathcal{D}_{1e}\left(\frac{dC_1}{dz}\right)_{z+dz} \tag{6.12}$$

from which:

$$\frac{d^2C_{1,z}}{dz^2} = \frac{-\nu_1 k_M \rho_p C_{1,z}}{\mathcal{D}_{1e}}$$

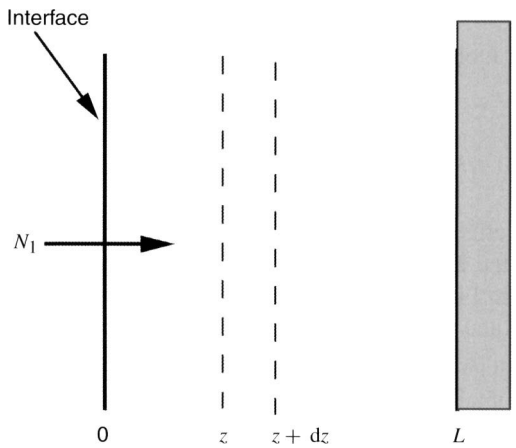


Figure 6.4 Diffusion flux in a flat plate of catalytic material.

If the following dimensionless term, known as the Thiele modulus, is introduced into the above equation:

$$\Phi' = L\sqrt{\frac{-\nu_1 k_M \rho_p}{\mathcal{D}_{1e}}} \tag{6.13}$$

we obtain:

$$\frac{d^2C_{1,z}}{dz^2} = \frac{\Phi'^2}{L^2}C_{1,z}$$

The boundary conditions are written:

$$C_{1,z} = C_{1,S} \quad \text{for } z = 0$$
$$\frac{dC_{1,z}}{dz} = 0 \quad \text{for } z = L$$

We can then easily calculate:

$$\frac{dC_{1,z}}{dz} = \frac{\Phi'}{L} C_{1,S} \frac{\sinh\left[\Phi'\left(1 - \frac{z}{L}\right)\right]}{\cosh[\Phi']}$$

$$C_{1,z} = C_{1,S} \frac{\cosh\left[\Phi'\left(1 - \frac{z}{L}\right)\right]}{\cosh[\Phi']}$$

The flux entering per unit surface of interfacial area is equal to:

$$[N'_1]_{z=0} = -\mathcal{D}_{1e}\left[\frac{dC_{1,z}}{dz}\right]_{z=0}$$

However, the flux that would enter if there were no diffusion limitation within the porous plate would be equal to:

$$[N'_1]_{z=0} = -\nu_1 k_M \rho_p C_{1,S} L$$

The effectiveness factor η of the catalytic solid can be defined as the ratio of these two fluxes, that is:

$$\eta = \frac{-\mathcal{D}_{1e}\frac{\Phi'}{L}\tanh[\Phi']}{-\nu_1 k_M \rho_p L} = \frac{\tanh[\Phi']}{\Phi'} \tag{6.14}$$

This shows that the effectiveness factor depends only on the Thiele modulus Φ', which plays the same role as the Hatta number for gas-liquid reactions. A graphic representation of Eq. (6.14) is shown in Fig. 6.7. The graph shows that for values of Φ' less than 0.2, the effectiveness factor is equal to 1.

The above equations can be directly applied in the case of a monolith, calculation of the Thiele modulus being obtained by substitution of L by δ, the thickness of the active layer for a monolith with a washcoat, or by $e/2$ if the monolithic structure is itself porous and active. Since L is always very small, the Thiele modulus will have values greater than 0.2 only for very high rates of reaction. This explains why monoliths are employed for high-temperature gas-phase reactions, such as those that take place in catalytic converters, where high conversions in as small a volume as possible are sought.

6.3.2 Homogeneous spherical particle

Figure 6.5A represents a spherical grain of catalyst with uniform activity. We can imagine a spherical layer around which we determine the molar balance.

The catalyst grain, with radius R, is immersed in a fluid containing the reactant A_1. Under steady-state conditions, the number of moles of reactant A_1 entering at radius z per unit

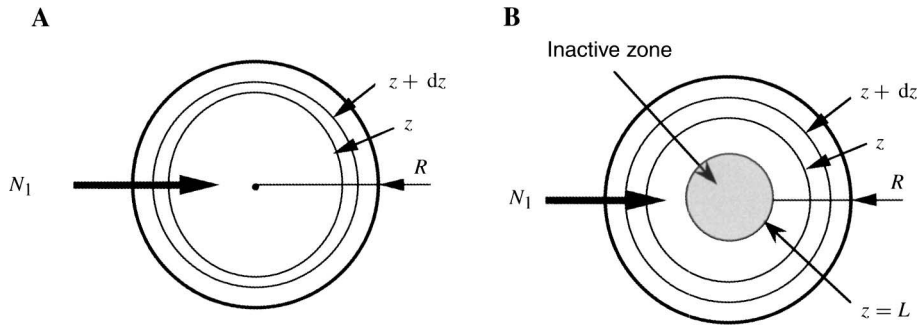


Figure 6.5 Diffusion flux in a spherical layer of a grain of catalyst. **A.** Completely active particle. **B.** Partially active particle for $R > L$.

of time $-4\pi z^2 \mathcal{D}_{1e} \left(\mathrm{d}C_{1,z}/\mathrm{d}z\right)_z$, plus the number of moles reacting in the spherical layer $+\nu_1 4\pi z^2\,\mathrm{d}z \cdot \rho_p \cdot r'$ (since ν_1 is negative, there is actually a loss of reactant), is equal to the number of moles leaving at radius $z + \mathrm{d}z$, that is: $-4\pi\,(z + \mathrm{d}z)^2\,\mathcal{D}_{1e} \left(\mathrm{d}C_{1,z}/\mathrm{d}z\right)_{z+\mathrm{d}z}$.

After development and simplification, the balance is written:

$$\frac{\mathrm{d}^2 C_{1,z}}{\mathrm{d}z^2} + \frac{2}{z}\frac{\mathrm{d}C_{1,z}}{\mathrm{d}z} + \frac{\nu_1 \rho_p k_M C_{1,z}}{\mathcal{D}_{1e}} = 0 \tag{6.15}$$

By changing the variable $y = zC_{1,z}$, we can write:

$$\frac{\mathrm{d}^2 y}{\mathrm{d}z^2} = \frac{-\nu_1 \rho_p k_M}{\mathcal{D}_{1e}} y = \frac{\Phi^2}{R^2} y \tag{6.16}$$

where:

$$\Phi = R\sqrt{\frac{-\nu_1 \rho_p k_M}{\mathcal{D}_{1e}}} \tag{6.17}$$

This is the Thiele modulus, but in this case relative to a spherical geometry, and can also be expressed as:

$$\Phi = R\sqrt{\frac{-\nu_1 \rho_p S_p k_S}{\mathcal{D}_{1e}}} \tag{6.18}$$

The differential Eq. (6.15) is solved with the following boundary conditions:

$$\text{for } z = R \quad C_{1,z} = C_{1,R}$$

$C_{1,R}$ is the concentration of A_1 at the outer surface of the grain.

$$\text{for } z = 0 \quad \frac{\mathrm{d}C_{1,z}}{\mathrm{d}z} = 0 \quad \text{(because of symmetry)}$$

The general solution of (6.16) is written:

$$y = B_1 \exp\left(\Phi\frac{z}{R}\right) + B_2 \exp\left(-\Phi\frac{z}{R}\right)$$

and finally:

$$C_{1,z} = \frac{C_{1,\mathrm{R}} \sinh\left(\Phi\dfrac{z}{R}\right)}{\dfrac{z}{R}\sinh\Phi} \tag{6.19}$$

in the neighborhood of $z = 0$, we obtain:

$$C_{1,0} \cong C_{1,\mathrm{R}}\frac{\Phi}{\sinh\Phi}$$

The concentration profiles are shown in Fig. 6.6 for different values of Φ. It can be seen that the concentration of reactant A_1 decreases more or less rapidly inside the particle depending on the value of the Thiele modulus Φ; the higher the modulus the faster the decrease in concentration. For example, when $\Phi = 10$, the concentration tends to zero for $z/R = 0.4$, and consequently the center of the sphere ($z/R < 0.4$) does not participate in the chemical transformation. We will return to this later on.

The molar flux of A_1 that diffuses to the interior of the particle where it reacts, is expressed by:

$$\mathbf{N}_{1,\mathrm{R}} = -4\pi R^2 \mathcal{D}_{1\mathrm{e}} \left(\frac{\mathrm{d}C_{1,z}}{\mathrm{d}z}\right)_{z=R} \tag{6.20}$$

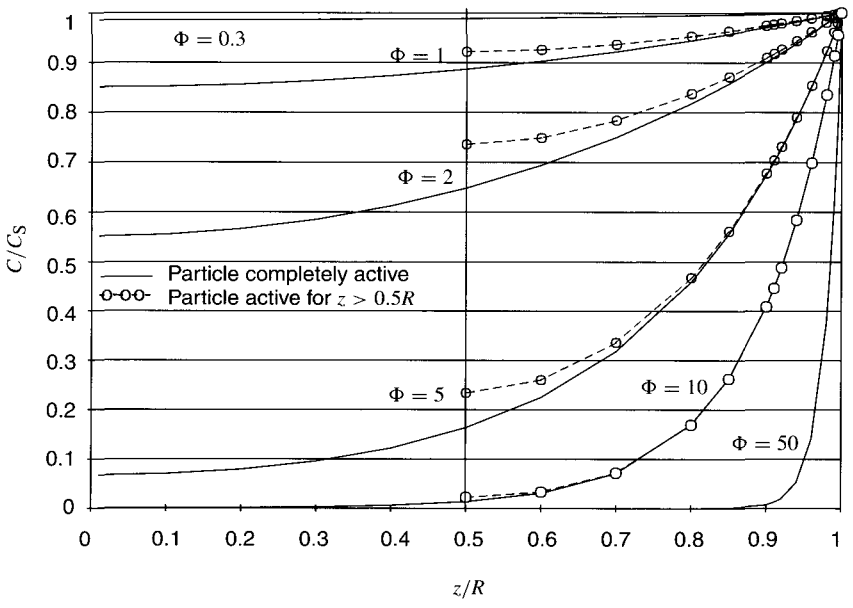


Figure 6.6 Concentration profiles inside a spherical grain. **a.** Completely active particle (solid line). **b.** Partially active particle for $R > L$ (the curves corresponding to $L/R = 0.5$ are represented by dashed lines).

Taking the derivative of Eq. (6.19), we obtain:

$$\frac{dC_{1,z}}{dz} = \frac{RC_{1,R}}{\sinh \Phi} \frac{\frac{z\Phi}{R}\cosh\left(\frac{z\Phi}{R}\right) - \sinh\left(\frac{z\Phi}{R}\right)}{z^2}$$

and therefore:

$$\mathbf{N}_{1,R} \text{ (with diffusion limitation)} = -4\pi R \mathcal{D}_{1e} C_{1,R} \Phi \left[\frac{1}{\tanh \Phi} - \frac{1}{\Phi}\right] \tag{6.21}$$

If the diffusion of reactant A_1 is sufficiently fast so that the concentration is $C_{1,R}$ everywhere in the particle, the incoming flux $\mathbf{N}_{1,R}$ will be equal to the rate of reaction with respect to the entire catalyst grain:

$$\mathbf{N}_{1,R} \text{ (without diffusion limitation)} = \nu_1 \frac{4}{3}\pi R^3 \rho_p k_M C_{1,R} \tag{6.22}$$

As in the case of a flat plate, we can then define an effectiveness factor η:

$$\eta = \frac{\mathbf{N}_{1,R} \text{ (with diffusion limitation)}}{\mathbf{N}_{1,R} \text{ (without diffusion limitation)}} = \frac{3}{\Phi}\left[\frac{1}{\tanh \Phi} - \frac{1}{\Phi}\right] \tag{6.23}$$

which is dependent on the Thiele modulus alone.

Figure 6.7 represents the variation of η as a function of Φ for spherical particles and an irreversible first-order reaction that occurs isothermally in the grain:

- for $\Phi < 1$, $\eta \cong 1$
- for $\Phi > 10$, $\eta = 3/\Phi$.

With the introduction of the effectiveness factor η, the flux of A_1 and therefore the rate of reaction of A_1 per grain is written:

$$\mathbf{N}_{1,R} = \nu_1 \frac{4}{3}\pi R^3 \rho_p k_M C_{1,R} \eta \tag{6.24}$$

It appears that the smaller the value of Φ, the closer η will be to unity, that is, the particles will be small, the reaction slow, and diffusion unproblematic. The obvious practical conclusion is that the active catalysts (high k_M) used will always be as small in size as possible, given the other constraints that need to be respected (primarily pressure drop through the bed). Another practical conclusion of interest is that it may be worthwhile to deposit active catalytic substances only on the outer layer of porous grains, abandoning the use of the entire available pore volume. We consider this situation in the following section.

6.3.3 Spherical particle with an active zone on the periphery

Assume we have a porous catalyst particle for which the active substance is located on the periphery in a spherical layer comprised between the radii $z = L$ and $z = R$ (Fig. 6.5B). This type of configuration is obtained during the fabrication of the catalyst by controlling the conditions governing the impregnation of the porous support. This is particularly useful when the active element deposited on the catalyst is expensive (noble metals, for example). The previous Eqs., (6.15) and (6.16), remain valid, only the boundary conditions are different:

- for $z = R$, $C_{1,z} = C_{1,R}$
  $C_{1,R}$ is the concentration of A_1 on the outer surface of the grain

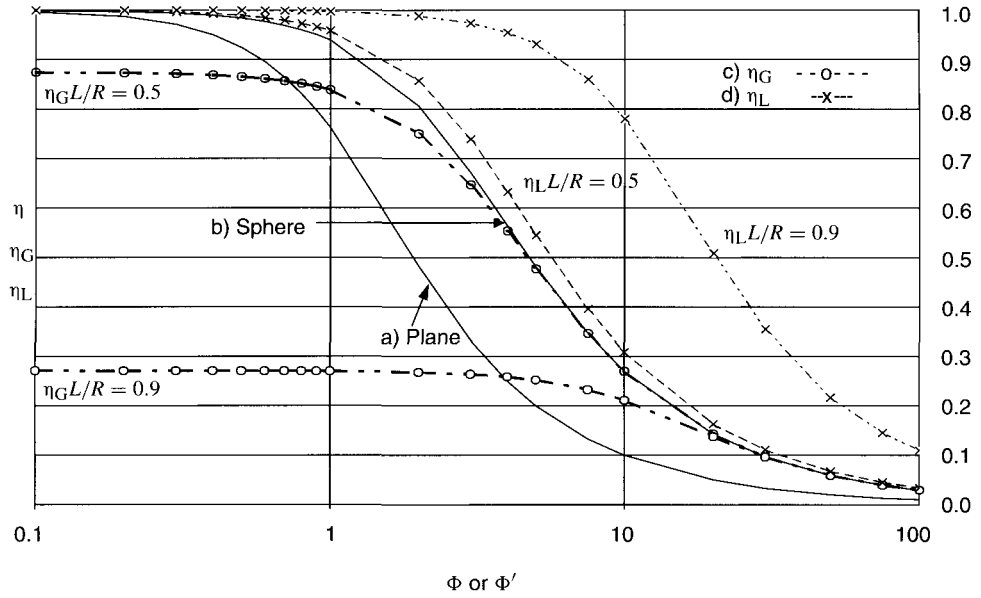


Figure 6.7 Relation between the effectiveness factor and the Thiele modulus. First-order isothermal, isochoric reaction. **a.** for a flat plate (Eq. 6.14). **b.** for spherical grains that are active throughout the entire catalyst (Eq. 6.23). **c.** for partially active spherical grains, η_G (Eq. 6.26); **d.** for partially active spherical grains, η_L (Eq. 6.27).

- for $z = L$, $dC_{1,z}/dz = 0$.

In addition to the Thiele modulus considered above, a second modulus, modified by the ratio L/R, needs to be considered:

$$\Phi'' = (R - L)\sqrt{\frac{-\nu_1 k_M \rho_p}{\mathcal{D}_{1e}}} = \left(1 - \frac{L}{R}\right)\Phi \tag{6.25}$$

Finally, the solution to (6.15) can be written:

$$C_{1,z} = C_{1,R}\frac{\frac{L}{R}\Phi\cosh\left[\frac{\Phi}{R}(L-z)\right] - \sinh\left[\frac{\Phi}{R}(L-z)\right]}{\frac{z}{R}\left(\sinh\left[\Phi''\right] + \Phi''\cosh\left[\Phi''\right]\right)}$$

As with homogeneous spherical particles, we have plotted on Fig. 6.6 the concentration profiles of A_1 inside the particle for various values of Φ and for $L/R = 0.5$. Note that for the same value of Φ, the concentrations in a partially active particle ($L/R = 0.5$, dashed line) are greater than those obtained in a fully active particle (solid line). The two profiles overlap only for values of Φ equal to or greater than 10, since for these values of Φ, as we have seen, the center of the particle remains inactive.

As before, we can calculate the effectiveness factor of the catalytic particle:

$$\eta_G = \frac{3}{\Phi^2} \frac{\Phi'' \cosh\left[\Phi''\right] + \left(\frac{L}{R}\Phi^2 - 1\right) \sinh\left[\Phi''\right]}{\sinh\left[\Phi''\right] + \frac{L}{R}\Phi \cosh\left[\Phi''\right]} \tag{6.26}$$

It can be shown that for $L = 0$, that is for a uniformly impregnated particle, $\Phi'' = \Phi$, and the above equations, now simplified, yield the results obtained in the previous section. The preceding calculation uses the entire particle as a reference, although it is only partially active. We can therefore calculate another effectiveness factor relative to the active part of the particle alone, that is η_L:

$$\eta_L = \frac{1}{1 - \left(\frac{L}{R}\right)^3} \eta_G \tag{6.27}$$

The effectiveness factors η_G and η_L are shown in Fig. 6.7 for two values of L/R (0.5 and 0.9). It is clear from the graph that the effectiveness factor η_G with respect to the total volume of the particle is less than that of the uniformly active particle, at least in the defined range of values of Φ that vary as a function of L/R. This corresponds to the fact mentioned above, namely, that beyond a certain value of Φ the uniformly active particle is only partially used. In contrast, the effectiveness factor η_L associated with the active part of the particle alone remains greater than that of the uniformly active particle, and this is true for all values of Φ.

6.3.4 Optimization of catalyst geometry

As we have seen, we can choose between various geometries for a solid catalyst. Using the information introduced so far, we can compare various catalyst shapes in the search for an optimized catalyst geometry.

6.3.4.1 Bead-monolith comparison

Continuing our comparison of beads and monolithic catalysts, we can calculate the rates of transformation for reactant A_1 per unit volume, respectively for a stack of beads and a monolithic structure with a washcoat. Consider a unit volume of catalytic mass, either in the form of beads or a monolith. As above, we take the diameter of the beads to be d and the mesh of the monolith to be M, and will assume that the active phase of the monolith has the same properties as that of the beads (activity, density, porosity, etc.).

For the simple reaction $\nu_1 A_1 + \nu_2 A_2 = 0$ we have been considering, a global rate of transformation of A_1 can be written (N_{V1}: moles per unit of time and unit volume) for each of the geometries:

- For a mass of beads:

$$N_{V1} = \varepsilon_p \eta k_M \rho_p C_{1,S}$$

- For a monolith:

$$N_{\mathrm{VI}} = \eta_{\mathrm{L}} k_{\mathrm{M}} \rho_{\mathrm{p}} \frac{(M-e)^2 - (M-e-2\delta)^2}{M^2} C_{\mathrm{I,S}}$$

The following ratio can then be calculated:

$$\frac{N_{\mathrm{VI}}\ (\text{monolith})}{N_{\mathrm{VI}}\ (\text{beads})} = \frac{\eta_{\mathrm{L}}}{\eta} \frac{(M-e)^2 - (M-e-2\delta)^2}{M^2} \varepsilon_{\mathrm{p}} \tag{6.28}$$

where η_{L} is calculated from Eq. (6.14) with $L = \delta$; η is obtained from (6.23).

Based on the numbers shown in Table 6.3, the same assumptions as for comparing the equivalent geometric surfaces for the two structures will be made: $d = M + e$, $e = 0.15M$, $\varepsilon_{\mathrm{p}} = 0.6$ and $\delta = 0.1$ mm.

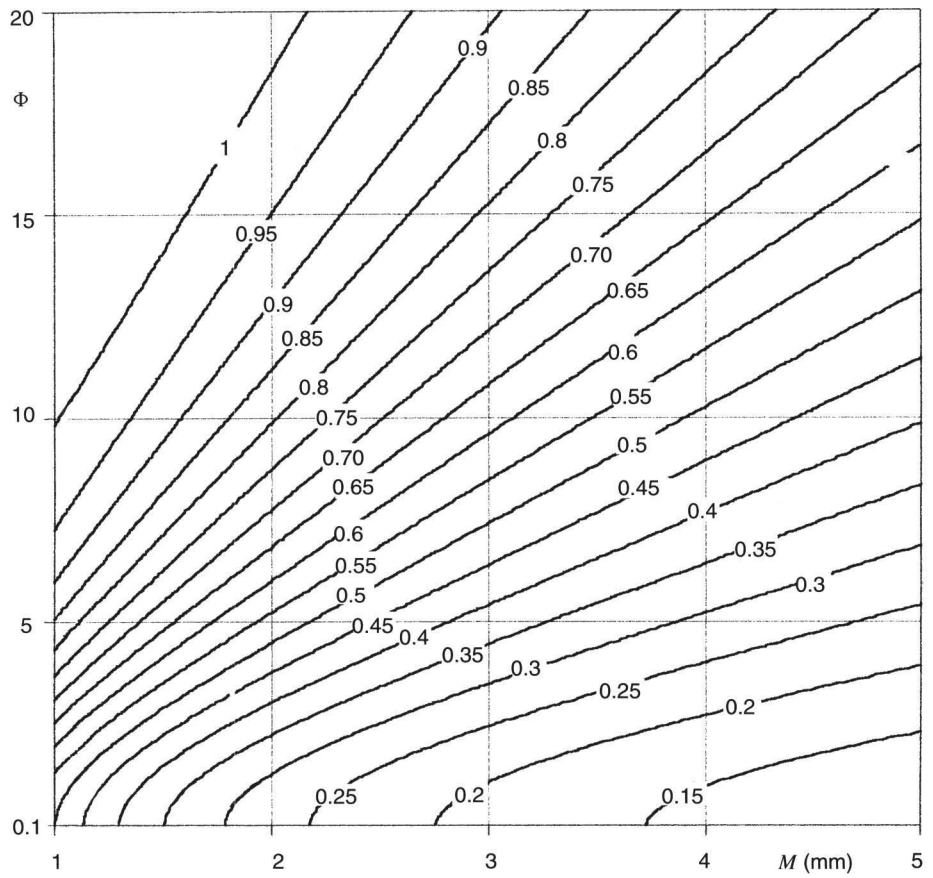


Figure 6.8 Isoline curves for the ratio of transformation rates per unit volume of a monolith compared to spherical particles as a function of the mesh M and the Thiele modulus Φ.

Figure 6.8 shows isoline contours of the ratio of the transformation rates (Eq. 6.28) for pair values of Φ and M. The graph shows that for values of Φ greater than 10 and cell dimensions less than 2 mm, a monolith can be more active per unit volume. However, this comparison is very sensitive to the thickness δ of the active layer.

6.3.4.2 Comparison of uniformly and partially active beads

This comparison was introduced previously during the calculation of the effectiveness factors η_G and η_L shown in Fig. 6.7. The choice of a uniformly active or partially active (near the outer surface) particle will depend on whether the total volume of the catalytic mass, the volume of the active phase, or the amount of active element (a noble metal, for example) is the deciding economic factor.

6.3.4.3 Comparison of solid and hollow cylindrical pellets

Here too the comparison is based on the equations developed above, (6.3) and (6.7). For cylindrical particles whose height is equal to their external diameter D_e, the rate of transformation of A_1 can be calculated by considering the particle as solid or hollow ($\kappa = D_e/D_{int}$). For each of the particles the Thiele modulus is calculated by using the corresponding equivalent diameter and from this the effectiveness factor is evaluated.

The ratio of the rates of transformation is then written:

$$\text{Ratio of transformation rates} = \frac{\eta_{PE}}{\eta_{PP}}\left[1 - \left(\frac{1}{\kappa}\right)^2\right] \tag{6.29}$$

The subscript PP refers to a solid particle, while PE refers to the hollow particle whose ratio of external and internal diameters is κ.

Figure 6.9 presents the contours of the calculated ratios as a function of κ and the Thiele modulus calculated using the exterior diameter D_e. Here the rate in a hollow particle can be appreciably higher than that in a solid particle for a range of values of κ and Φ, so that approximately $\Phi > 10/\kappa$.

6.4 EXTENDING THE CONCEPTS OF THE THIELE MODULUS AND EFFECTIVENESS

We can extend the concepts of the Thiele modulus and effectiveness to the following cases:

- non-spherical particles
- reaction orders other than first-order
- non-isochorous reactions
- non-isothermal reactions.

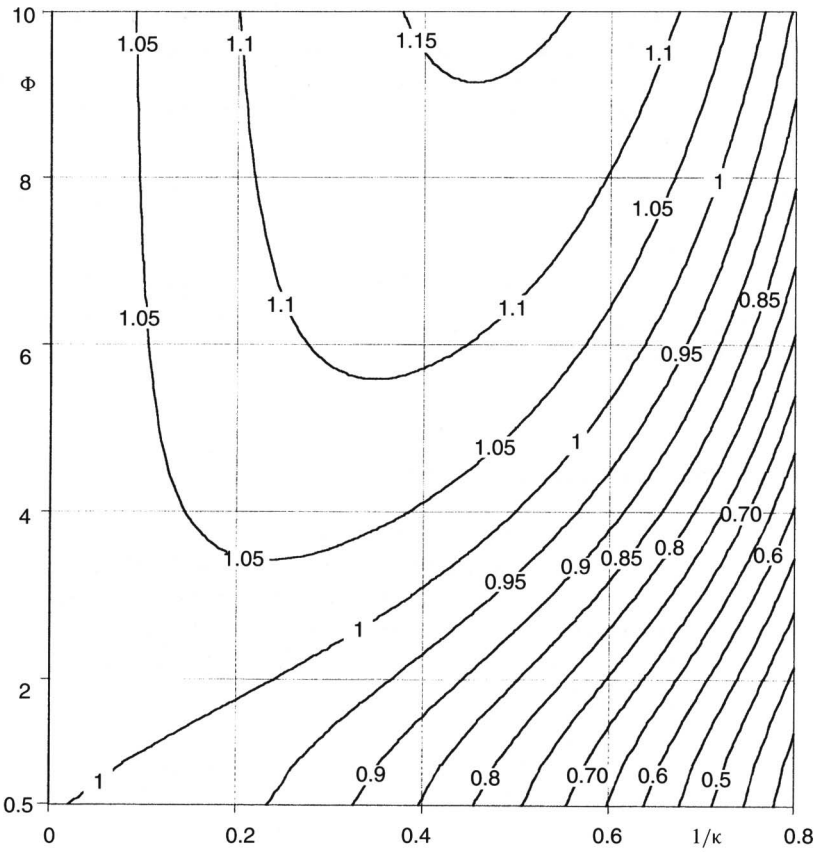


Figure 6.9 Isoline curves of the ratio of transformation rates per unit volume of hollow and solid cylindrical particles.

6.4.1 Non-spherical geometric shapes

For particles consisting of long cylinders or other geometric shapes, calculations similar to those shown for spheres can be performed. This is especially true of hollow cylindrical particles in the shape of rings [Wijngaarden *et al.*, 1998]. In reality it is probably preferable to make use of the equivalent diameter and a Thiele modulus defined as:

$$\Phi = \frac{\overline{d_l}}{2}\sqrt{\frac{-\nu_l k_M \rho_p}{\mathcal{D}_{le}}} = 3\frac{\varepsilon_p}{\mathcal{A}_S}\sqrt{\frac{-\nu_l k_M \rho_p}{\mathcal{D}_{le}}} \tag{6.30}$$

6.4.2 Other than first-order reactions

Similar to the procedure for determining a modified Hatta number for fluid-fluid reactions that were not first-order for the transferred reactant, modified expressions of the Thiele modulus

for non-first-order reactions with respect to reactant A_1 have been proposed [Wijngaarden *et al.*, 1998].

For an order n, the following equation is used:

$$\Phi = \sqrt{\frac{n+1}{2}}\,\frac{\overline{d_1}}{2}\sqrt{\frac{-\nu_1 k_M \rho_p C_{1,R}^{n-1}}{\mathcal{D}_{1e}}} \tag{6.31}$$

In the case of Langmuir-Hinshelwood kinetics, and depending on the form of the rate equation, it has been proposed that a Thiele modulus having one of the following definitions be used:

- For a law of the form $r_1 = KC_1/(1 + KC_1)$

$$\Phi = \frac{\overline{d_1}}{2}\sqrt{\frac{-\nu_1 k_M \rho_p}{\mathcal{D}_{1e}}}\,\frac{KC_{1,R}}{1+KC_{1,R}}\sqrt{\frac{1}{2\left[KC_{1,R} - \ln(1+KC_{1,R})\right]}} \tag{6.32}$$

- For a law of the form $r_1 = KC_1/(1 + KC_1)^2$

$$\Phi = \frac{\overline{d_1}}{2}\sqrt{\frac{-\nu_1 k_M \rho_p}{\mathcal{D}_{1e}}}\sqrt{\frac{KC_{1,R}}{1+KC_{1,R}}}\left\{2\left[\frac{1+KC_{1,R}}{KC_{1,R}}\ln(1+KC_{1,R}) - 1\right]\right\}^{-0.5} \tag{6.33}$$

- If the reaction is of the type $A_1 + A_2 \rightarrow$ products, with a kinetics of the following form:

$$r = kC_1C_2$$

we can convert to second-order kinetics by writing an equation reflecting the proportionality of the diffusion fluxes of A_1 and A_2, that is:

$$\mathcal{D}_{1e}(C_{1,S} - C_1) = \mathcal{D}_{2e}(C_{2,S} - C_2) \tag{6.34}$$

In those (rather frequent) cases when reactant A_2 is greatly in excess and diffuses more rapidly than A_1 (as in hydrogenation), we have a pseudo-first-order reaction, with a Thiele modulus that is written:

$$\Phi = \frac{\overline{d_1}}{2}\sqrt{\frac{k_M \rho_p C_{2,S}}{\mathcal{D}_{1e}}}$$

In the case of more complex kinetic expressions, although similar calculations are often impossible analytically, we should, depending on the nature of the kinetic expression:

- either assimilate the kinetics in question to a reaction of order n or a Langmuir-Hinshelwood reaction and use Eqs. (6.31), (6.32), or (6.33)
- or numerically integrate the differential equation similar to Eq. (6.15), in which the specific kinetic expression for the case under consideration appears.

6.4.3 Reversible reactions

Assume a reaction of the type $\nu_1 A_1 \rightleftarrows \nu_2 A_2$ with a kinetics that can be expressed as follows:

$$r = k_{1M} C_1 - k_{2M} C_2$$

Here we consider the case of a flat plate of solid catalyst as in 6.3.1. In this case the molar balance Eq. (6.12) can be rewritten in the following form:

$$\frac{d^2 C_{1,z}}{dz^2} = \frac{\Phi_1^2}{L^2} C_1 - \frac{\Phi_2^2}{L^2} C_2 \tag{6.35}$$

with the following Thiele moduli:

$$\Phi_1 = L\sqrt{\frac{-\nu_1 k_{1M} \rho_p}{\mathcal{D}_{1e}}} \quad \text{and} \quad \Phi_2 = L\sqrt{\frac{-\nu_1 k_{2M} \rho_p}{\mathcal{D}_{1e}}}$$

We can then write:

$$\frac{\Phi_2^2}{\Phi_1^2} \cdot \frac{\mathcal{D}_{1e}}{\mathcal{D}_{2e}} = m$$

and:

$$K = \sqrt{\Phi_1^2 + \frac{\mathcal{D}_{1e}}{\mathcal{D}_{2e}} \Phi_2^2} = \Phi_1 \sqrt{1 + m} \tag{6.36}$$

As above, we can write the equality of the diffusion fluxes of A_1 and A_2 associated with the reaction: $\mathcal{D}_{1e}(C_{1,S} - C_1) = -\mathcal{D}_{2e}(C_{2,S} - C_2)$. The solution to (6.35) is easily obtained using the following boundary conditions:

$$z = 0 \qquad C_1 = C_{1,S} \quad \text{and} \quad C_2 = C_{2,S}$$
$$z = L \qquad \frac{dC_1}{dz} = \frac{dC_2}{dz} = 0$$

We then have:

$$C_1(z) = H \frac{\cosh\left[\dfrac{K}{L}(L - z)\right]}{\cosh[K]} + \text{Cte} \tag{6.37}$$

The flux of A_1 that penetrates the catalytic solid is then expressed using the standard equation:

$$N_1' = -\mathcal{D}_{1e} \left(\frac{dC_1}{dz}\right)_{z=0} = \mathcal{D}_{1e} \frac{K}{L} H \tanh[K]$$

The effectiveness factor of the catalyst is calculated as before:

$$\eta = \frac{N_1'}{N_1} = \frac{\tanh[K]}{K} \tag{6.38}$$

This equation has the same form as the one obtained for an irreversible first-order reaction (6.14) but with a modified Thiele modulus to account for the reverse reaction. When $\nu_1 = -\nu_2$ and $\mathcal{D}_{1e}/\mathcal{D}_{2e} = 1$ (isomerization, for example), we obtain: $\Phi_2^2/\Phi_1^2 = k_{2M}/k_{1M} = m$.

6.4.4 Non-isochorous reactions

So far we have examined isochorous reactions of the following kind:

$$\nu_1 A_1 + \nu_2 A_2 = 0 \quad \text{where} \quad \nu_1 = -\nu_2$$

Under these conditions, for each molecule of A_1 transformed in the grain, a mole of product will be formed that will travel in the direction opposite A_1 and leave the grain. Since in this case there is equimolar diffusion, the simplified form of Fick's law can be applied:

$$N_{1,z} = -\mathcal{D}_{1e}\left(\frac{dC_1}{dz}\right)$$

When ν_2 differs from $-\nu_1$, a convection flux is superimposed on the diffusion flux and Fick's law is written:

$$N_{1,z} = -\mathcal{D}_{1e}\left(\frac{dC_1}{dz}\right) + \frac{C_1}{\Sigma C_i}\left(N_{1,z} + N_{2,z}\right) \tag{6.39}$$

where $N_{1,z} \neq -N_{2,z}$ and ΣC_i is the total concentration in mol/m^3.

At this point writing the mass balance equations becomes complex and it is impossible to find an analytic solution for $C_{1,z} = f(z)$.

In general:

- if $\nu_2 > (-\nu_1)$, effectiveness decreases
- if $\nu_2 < (-\nu_1)$, effectiveness increases.

Weekman and Gorring [1965] introduced a volume change modulus:

$$w = \left(\frac{\nu_2}{-\nu_1} - 1\right)\left(\frac{C_{1,S}}{\Sigma C_{i,S}}\right)$$

where

$C_{1,S}$ concentration of reactant A_1 on the outer surface of the grain

$\Sigma C_{i,S}$ sum of the concentrations of all the compounds (inerts included) on the outer surface of the grain.

They calculated the ratio of the effectiveness factor η_V (with a change of volume) to the effectiveness factor η without a change in volume for different values of the reaction order, the Thiele modulus Φ, and the modulus w. In analyzing their conclusions, we find that η_V/η remains between 0.7 and 1.3 for the customary values of $(-\nu_2/\nu_1)$, $C_{1,S}/\Sigma C_{i,S}$, and Φ.

We can conclude that the effect of the variation in the number of moles during the reaction will rarely be determining, especially given the lack of precision of the numerical value of the effective coefficient of diffusivity.

6.4.5 Non-isothermal reactions

It is easy to see that an exothermic reaction in a porous medium would give off calories that would then escape the grain. This will result in a rise in temperature, an increase in reaction rate, and so on. Given the ability of the grain to transfer this heat, a thermal gradient will be established in the grain with, in the case of exothermic reactions, a mean temperature greater than the surface temperature and, in the case of endothermic reactions, a mean temperature less than the surface temperature.

The parameters that need to be taken into consideration when studying this thermal phenomenon are:

- enthalpy of reaction ΔH_R (J/mol)
- energy of activation of the reaction, E (J/mol)
- main reactant concentration at the surface of the grain, $C_{1,S}$ (mol/m^3), which we have called $C_{1,R}$ for spherical grains
- effective thermal conductivity of the porous grain, λ_e (W/m · K)
- surface temperature, T_S (K)
- diffusivity of the reactant in the porous medium, $\mathcal{D}_{1e}$ (m^2/s).

It makes sense to lump the different parameters as dimensionless numbers. For example:

$$\beta_1 = \frac{C_{1,S}\,(-\Delta H_R)\,\mathcal{D}_{1e}}{\lambda_e T_S} \qquad \text{Prater number} \tag{6.40}$$

$$\beta_2 = \frac{E}{RT_S} \qquad \text{Arrhenius number} \tag{6.41}$$

R is the ideal gas constant (8.31 J/mol · K).

Recall that the effectiveness factor is the ratio of the apparent reaction rate, relative to the grain, to the theoretical reaction rate at a temperature T_S and a concentration $C_{1,S}$ at every point in the grain. Therefore, it is entirely possible, according to this definition, to obtain effectiveness factors that are appreciably greater than 1.

When $\beta_1 < 0$, the effectiveness factor will always be less than 1. This corresponds to endothermic reactions where the mean temperature in the grain is less than T_S and the mean concentration in the grain is less than $C_{1,S}$.

When $\beta_1 > 0$ (exothermic reactions), two effects act in opposite directions. The mean temperature of the grain can be appreciably greater than T_S, but the mean concentration can be significantly lower than $C_{1,S}$. Consequently, depending on the values of Φ, β_1, and β_2, η can be less than or greater than 1.

With respect to β_2, it can be shown that, for the same surface temperature T_S and the same value of β_1, the increase in the effectiveness factor will be greater as the activation energy E increases.

In practice β_1, which is positive for exothermic reactions and negative for endothermic reactions, generally remains within the following limits: $-0.8 < \beta_1 < 0.8$ and frequently $10 < \beta_2 < 40$.

***The significance of* β_1**

If we calculate the heat balance for a layer of thickness dz, in the steady state regime, we can write:

$$-\mathcal{D}_{1e}\frac{dC_{1,z}}{dz}(-\Delta H_R) = \lambda_e\frac{dT}{dz} \tag{6.42}$$

If λ_e, $\mathcal{D}_{1e}$, and ΔH_R are considered constant, the above equation can be integrated to obtain:

$$(T_z - T_S) = \frac{(-\Delta H_R)\,\mathcal{D}_{1e}}{\lambda_e}\left(C_{1,S} - C_{1,z}\right) \tag{6.43}$$

Since the smallest possible value of $C_{1,z}$ is $C_{1,z} = 0$, it follows that:

$$\Delta T \text{ maximum in the grain} = \frac{(-\Delta H_R)\,\mathcal{D}_{1e}}{\lambda_e}C_{1,S}$$

and:

$$\beta_1 = \frac{\Delta T_{max}}{T_S} = \frac{(-\Delta H_R)\,\mathcal{D}_{1e}}{\lambda_e T_S}C_{1,S} \tag{6.44}$$

Therefore, β_1 represents the maximum relative temperature increase (or decrease) in the grain. If $\left[(-\Delta H_R \cdot \mathcal{D}_{1e})/\lambda_e\right]C_{1,S}$ does not exceed 5 K, the effect of temperature on effectiveness can be ignored. When $T_S = 500$ K, then $\beta_1 = 0.01$.

The principal difficulty in estimating β_1 lies in estimating values for $\mathcal{D}_{1e}$ and especially λ_e, which is generally comprised between 0.2 and 0.5 W/m · K.

Figure 6.10A illustrates the variation in effectiveness factor with the Thiele modulus and the Prater number β_1 for an Arrhenius number β_2 of 20, which corresponds to the mean. In the illustration:

- The curve $\beta_1 = 0$ corresponds to a previously seen case and simply reproduces the curve for a sphere shown in Fig. 6.7.
- For $\beta_1 < 0$ (endothermic reaction), the effectiveness factor is always less than that when $\beta_1 = 0$.
- For $\beta_1 > 0$ (exothermic reaction), the effectiveness factor can be less than, equal to, or greater than 1.

Within a relatively limited region, when Φ is low and β high (thus, small particles accompanied by a slow exothermic reaction or unrestricted diffusion), the curve $\eta = f(\Phi)$ can have three solutions for the same value of Φ.

Physically this signifies that at the same exterior temperature T_S and the same surface concentration $C_{1,S}$ (and therefore the same values of β_1 and β_2), the particle can theoretically have two different stable operating states:

- A **hot state**, characterized by a high temperature gradient and a mean operating temperature that is appreciably higher than T_S, as well as by a pronounced concentration gradient, with an overall high reaction rate and, therefore, a very high effectiveness factor, in the sense defined here.
- A **cold state**, characterized by less pronounced temperature and concentration gradients and an effectiveness factor that is in general barely greater than 1.

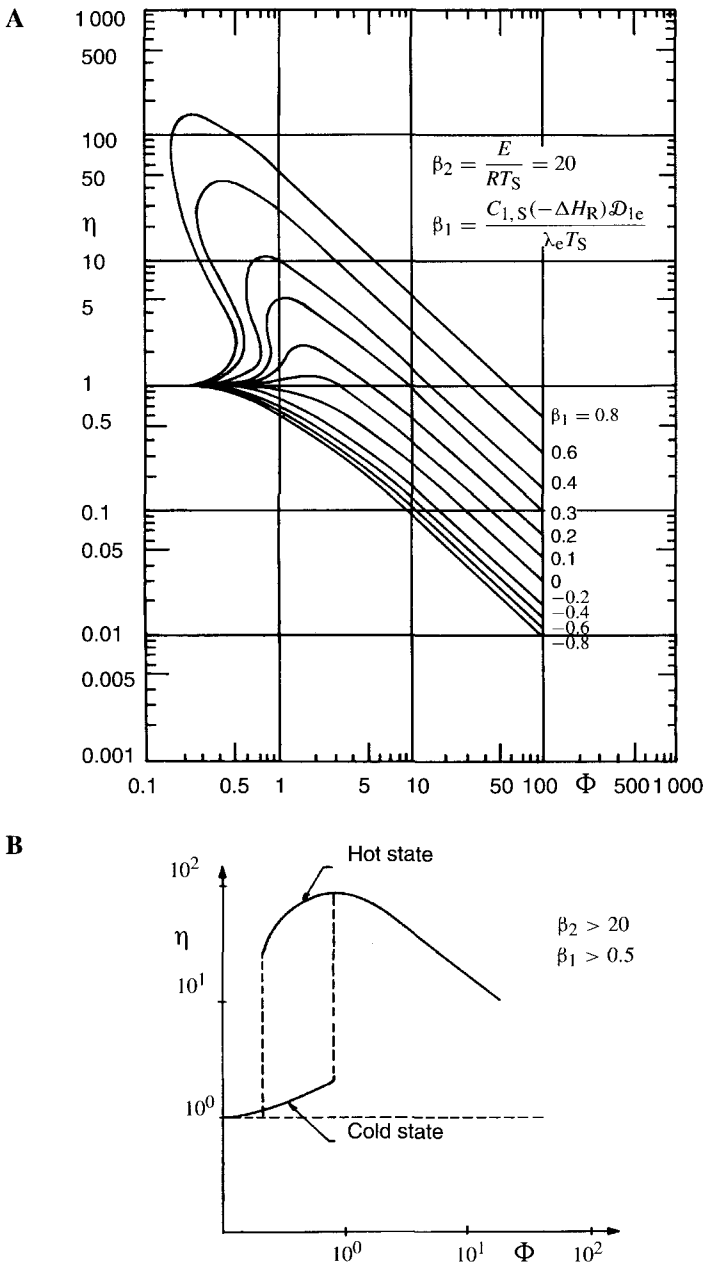


Figure 6.10 Relationship between the effectiveness factor and the Thiele modulus: influence of thermal effects. **A.** Variation of the effectiveness factor η with Φ, β_1, and β_2. **B.** Variation of the effectiveness factor η with Φ, for $\beta_2 > 20$ and $\beta_1 > 0.5$; possible stable states of a porous catalyst particle.

The third numerical solution, corresponding to an intermediate effectiveness factor, has no physical reality. Consequently, it seems preferable to represent this portion of the domain as shown in Fig. 6.10B, where only two possible stable states for the particle are shown.

The state assumed by the particle in this region between hot and cold will depend essentially on its prior thermal history. If the particle has been in use and has approached the operating temperature (corresponding to an exterior temperature T_S) slowly and from below, the stable state will be the cold state. If, on the contrary, the particle has been previously raised to a high temperature and is slow to reach its equilibrium state in operation, it will move toward the hot state.

Unforeseen circumstances, operating irregularities, runaway reactions or extinction can cause a grain or a mass of grains to shift from the hot to the cold state, or vice versa, if these grains are within the region of multiple stable states. This phenomenon interferes with proper operation of the reactor and should, if possible, be avoided by modifying the Thiele modulus. This can also be accomplished through judicious selection of the operating temperature, by controlling heat exchange, or by any other means appropriate to the circumstances. Note that it is the difference in the magnitude of the internal gradients that characterizes the two possible stable states. Later on we will see how the existence of external gradients can also lead to a multiplicity of stable operating states.

6.5 INFLUENCE OF INTERNAL DIFFUSION ON THE SELECTIVITY OF CATALYTIC CHEMICAL REACTIONS

Because internal diffusion predominately limits fast rather than slow reactions, a decrease in selectivity might be expected when the faster reaction is the desired reaction.

6.5.1 Independent parallel first-order reactions

Assume we have two first-order parallel reactions:

$$\nu_{1,1}A_1 \rightarrow \text{product} \quad r_1 = k_{1M}C_1$$
$$\nu_{2,2}A_2 \rightarrow \text{product} \quad r_2 = k_{2M}C_2$$

As shown in Chapter 1, the instantaneous selectivity is defined as:

$$s_{1,2} = \frac{\left(\dfrac{dF_1}{dF_2}\right)_{\text{real}}}{\left(\dfrac{dF_1}{dF_2}\right)_{\text{ideal}}}$$

however:

$$F_1 = F_{1,0} + \Sigma\nu_{1,j}\xi'_j$$
$$dF_1 = \Sigma\nu_{1,j}r_j \cdot dV\rho_c = \nu_{1,1}r_1 \cdot dV\rho_c$$
$$dF_2 = \Sigma\nu_{2,j}r_j \cdot dV\rho_c = \nu_{2,2}r_2 \cdot dV\rho_c$$

and therefore:

$$\frac{dF_1}{dF_2} = \frac{\nu_{1,1} k_{1M} C_1 \, (dV \rho_c)}{\nu_{2,2} k_{2M} C_2 \, (dV \rho_c)} = \frac{\nu_{1,1} k_{1M} C_1}{\nu_{2,2} k_{2M} C_2}$$

The selectivity $s_{1,2}$ without diffusion limitation, can then be written:

$$s_{1,2} \text{ (without diffusion limitation)} = \frac{\dfrac{\nu_{1,1} k_{1M} C_1}{\nu_{2,2} k_{2M} C_2}}{\left(\dfrac{dF_1}{dF_2}\right)_{\text{ideal}}}$$

The denominator does not need to be explicated. Its value depends on what is considered to be an ideal case. For example:

$$\left(\frac{dF_1}{dF_2}\right)_{\text{ideal}} = \frac{\nu_{1,1}}{\nu_{2,2}}$$

Since we know that each of the reactions can take place independently of the other whenever internal diffusion is non-negligible, we have to take into account two independent effectiveness factors η_1 and η_2 such that:

$$s_{1,2} \text{ (with diffusion limitation)} = \frac{\dfrac{\nu_{1,1} k_{1M} C_1 \eta_1}{\nu_{2,2} k_{2M} C_2 \eta_2}}{\left(\dfrac{dF_1}{dF_2}\right)_{\text{ideal}}}$$

and:

$$\frac{s_{1,2}(\text{AD})}{s_{1,2}(\text{SD})} = \frac{\eta_1}{\eta_2}$$

If the diffusion limitations are severe for both r_1 and r_2, the values of η_j will be inversely proportional to Φ_j and we can write:

$$\frac{s_{1,2}(\text{AD})}{s_{1,2}(\text{SD})} = \frac{\eta_1}{\eta_2} = \frac{\Phi_2}{\Phi_1} = \sqrt{\frac{\nu_{2,2} k_{2M} \mathcal{D}_{1e}}{\nu_{1,1} k_{1M} \mathcal{D}_{2e}}} \tag{6.45}$$

$s_{1,2}(\text{AD})$ may be greater than $s_{1,2}(\text{SD})$, depending on the respective values of $\nu_{2,2}/\nu_{1,1}$, k_{2M}/k_{1M}, and $\mathcal{D}_{1e}/\mathcal{D}_{2e}$.

6.5.2 First-order twin reactions

Assume we have the system of twin reactions represented by:

$$\nu_{1,1} A_1 \rightarrow \nu_{2,1} A_2 \quad r_1 = k_{1M} C_1$$
$$\nu_{1,2} A_1 \rightarrow \nu_{3,2} A_3 \quad r_2 = k_{2M} C_1$$

For a continuous reactor, the instantaneous selectivity $s_{2,1}$ is, by definition:

$$s_{2,1} = \frac{\dfrac{dF_2}{dF_1}}{\dfrac{\nu_{2,1}}{\nu_{1,1}}}$$

since $\nu_{2,1}/\nu_{1,1}$ represents the maximum number of moles of A_2 that can be obtained per mole of A_1 if reaction 2 does not take place:

$$dF_2 = \nu_{2,1} r_1 \cdot dV\rho_c = \nu_{2,1} k_{1M} C_1 \cdot dV\rho_c$$
$$dF_1 = \left(\nu_{1,1} r_1 + \nu_{12} r_2\right) dV\rho_c = \left(\nu_{1,1} k_{1M} + \nu_{1,2} k_{2M}\right) C_1 \cdot dV\rho_c$$

$$s_{2,1}(\mathrm{SD}) = \frac{\dfrac{\nu_{2,1} k_{1M}}{\nu_{1,1} k_{1M} + \nu_{1,2} k_{2M}}}{\dfrac{\nu_{2,1}}{\nu_{1,1}}} = \frac{1}{1 + \dfrac{\nu_{1,2}}{\nu_{1,1}} \dfrac{k_{2M}}{k_{1M}}}$$

Whenever internal diffusion occurs in such a way as to appreciably limit the rate of penetration of A_1, a Thiele modulus can be defined:

$$\Phi = R \sqrt{\frac{-\left(\nu_{1,1} k_{1M} + \nu_{1,2} k_{2M}\right) \rho_p}{\mathcal{D}_{1e}}}$$

and an effectiveness factor $\eta \cong 3/\Phi$ such that:

$$s_{2,1}(\mathrm{AD}) = \frac{\dfrac{\nu_{2,1} k_{1M} \eta}{\nu_{1,1} k_{1M} \eta + \nu_{1,2} k_{2M} \eta}}{\dfrac{\nu_{2,1}}{\nu_{1,1}}} = \frac{1}{1 + \dfrac{\nu_{1,2}}{\nu_{1,1}} \dfrac{k_{2M}}{k_{1M}}} = s_{2,1}(\mathrm{SD}) \qquad (6.46)$$

It should come as no surprise that diffusion limitation has no effect on the selectivity of twin reactions.

6.5.3 Consecutive reactions

For the following reactions:

$$\nu_{1,1} A_1 \rightarrow \nu_{2,1} A_2 \quad r_1 = k_{1M} C_1$$
$$\nu_{2,2} A_2 \rightarrow \nu_{3,2} A_3 \quad r_2 = k_{2M} C_2$$

the instantaneous selectivity for a continuous reactor is, by definition:

$$s_{2,1} = \frac{\dfrac{dF_2}{dF_1}}{\dfrac{\nu_{2,1}}{\nu_{1,1}}}$$

since $-\nu_{2,1}/\nu_{1,1}$ represents the maximum number of moles of A_2 that can be obtained per mole of reacted A_1 if reaction 2 does not take place.

The selectivity without diffusion limitation is written:

$$s_{2,1}(\mathrm{SD}) = \frac{\nu_{2,1}k_{1\mathrm{M}}C_1 + \nu_{2,2}k_{2\mathrm{M}}C_2}{\nu_{1,1}k_{1\mathrm{M}}C_1}\frac{\nu_{1,1}}{\nu_{2,1}}$$

or:

$$s_{2,1}(\mathrm{SD}) = 1 + \frac{\nu_{2,2}}{\nu_{2,1}}\frac{k_{2\mathrm{M}}C_2}{k_{1\mathrm{M}}C_1} \tag{6.47}$$

The effectiveness factor of a catalytic particle can be calculated as shown before. Plane geometry is used for the sake of simplicity.

The molar balance equations in Paragraph 6.3.1 are identical for compound A_1:

$$\frac{\mathrm{d}^2C_{1,z}}{\mathrm{d}z^2} = \frac{\Phi_1^2}{L^2}C_{1,z}$$

where:

$$\Phi_1 = L\sqrt{\frac{-\nu_{1,1}k_{1\mathrm{M}}\rho_\mathrm{p}}{\mathcal{D}_{1\mathrm{e}}}}$$

The solution is written:

$$C_{1,z} = C_{1,\mathrm{S}}\frac{\cosh\left[\Phi_1\left(1-\frac{z}{L}\right)\right]}{\cosh\left[\Phi_1\right]}$$

In the case of compound A_2, the molar balance is written:

$$\frac{\mathrm{d}^2C_2}{\mathrm{d}z^2} = \frac{\Phi_2^2}{L^2}C_2 - \frac{\Phi_3^2}{L^2}C_1 \tag{6.48}$$

where:

$$\Phi_2 = L\sqrt{\frac{-\nu_{2,2}k_{2\mathrm{M}}\rho_\mathrm{p}}{\mathcal{D}_{2\mathrm{e}}}} \quad \text{and} \quad \Phi_3 = L\sqrt{\frac{\nu_{2,1}k_{1\mathrm{M}}\rho_\mathrm{p}}{\mathcal{D}_{2\mathrm{e}}}}$$

Therefore:

$$\Phi_3^2 = \frac{\mathcal{D}_{2\mathrm{e}}}{\mathcal{D}_{1\mathrm{e}}}\frac{\nu_{2,1}}{-\nu_{1,1}}\Phi_1^2$$

The solution of (6.48) can be easily obtained using the following boundary conditions:

$$z = 0 \qquad C_1 = C_{1,\mathrm{S}} \quad \text{and} \quad C_2 = C_{2,\mathrm{S}}$$
$$z = L \qquad \frac{\mathrm{d}C_1}{\mathrm{d}z} = \frac{\mathrm{d}C_2}{\mathrm{d}z} = 0$$

By defining the following variables:

$$\Psi = \frac{\Phi_3^2}{\Phi_2^2 - \Phi_1^2} \quad \text{and} \quad \Gamma = C_{2,\mathrm{S}} - \Psi C_{1,\mathrm{S}}$$

we obtain:

$$C_2(z) = \Gamma \frac{\cosh\left[\Phi_2\left(1-\frac{z}{L}\right)\right]}{\cosh\left[\Phi_2\right]} + \Psi C_{1,S} \frac{\cosh\left[\Phi_1\left(1-\frac{z}{L}\right)\right]}{\cosh\left[\Phi_1\right]} \tag{6.49}$$

The flux of A_2 from the catalyst surface is generally expressed as:

$$N_2 = -\mathcal{D}_{2e}\left(\frac{dC_2}{dz}\right)_{z=0}$$

and the flux of A_1 penetrating the catalyst is similarly written:

$$N_1 = -\mathcal{D}_{1e}\left(\frac{dC_1}{dz}\right)_{z=0}$$

The instantaneous selectivity can then be calculated:

$$s_{2,1}(\mathrm{AD}) = \frac{N_2}{N_1}\frac{\nu_{1,1}}{\nu_{2,1}} = \frac{\nu_{1,1}}{\nu_{2,1}}\frac{\mathcal{D}_{2e}}{\mathcal{D}_{1e}}\frac{\left(\frac{dC_2}{dz}\right)_{z=0}}{\left(\frac{dC_1}{dz}\right)_{z=0}}$$

And finally:

$$s_{2,1}(\mathrm{AD}) = \frac{\Phi_1^2}{\Phi_1^2-\Phi_2^2}\left[1-\frac{\Phi_2}{\Phi_1}\frac{\tanh\left[\Phi_2\right]}{\tanh\left[\Phi_1\right]}\right] + \frac{\nu_{1,1}}{\nu_{2,1}}\frac{C_{2,S}}{C_{1,S}}\frac{\mathcal{D}_{2e}}{\mathcal{D}_{1e}}\frac{\Phi_2}{\Phi_1}\frac{\tanh\left[\Phi_2\right]}{\tanh\left[\Phi_1\right]} \tag{6.50}$$

The contour lines shown in Fig. 6.11A are a graphic representation of Eq. (6.50) as a function of Φ_1 and Φ_2, for the initial reaction conditions ($C_{2,S} = 0$). The curves show that the selectivity only approaches unity for low values of Φ_2, even when Φ_1 is large. Figure 6.11B represents selectivity *versus* Φ_1 for three values of the ratio Φ_2/Φ_1, assuming that $C_{2,S} = 0$. It can be shown that if the diffusion is highly limiting ($\Phi_1 > 10$), the selectivity tends toward a value equal to $1/\left[1+(\Phi_2/\Phi_1)\right]$.

This same figure shows two curves for $\left(\nu_{1,1}/\nu_{2,1}\right)\left(C_{2,S}/C_{1,S}\right)\left(\mathcal{D}_{2e}/\mathcal{D}_{1e}\right) = 0.5$, and $\Phi_2/\Phi_1 = 0.1$ and 1, demonstrating that selectivity decreases when the reaction takes place in the presence of compound A_2 ($C_{2,S} > 0$), that is as reaction 1 advances. The selectivity can even become negative if the concentration of the intermediate compound A_2 becomes too great. To maintain selectivity, the conversion of reaction 1 should be limited.

Other ways of increasing selectivity operate by decreasing both Φ_1 and the ratio Φ_2/Φ_1. We can also reduce L, the characteristic dimension of the catalyst particles, make use of catalyst particles that are active only near the surface, or even make use of a monolithic catalyst.

If the reactions are bimolecular, with a coreactant in excess, such that the kinetics are pseudo-first order, the concentration of coreactant can be reduced and the two reactions slowed down (this is the case with hydrogenation, for example, where the partial pressure of hydrogen can be reduced).

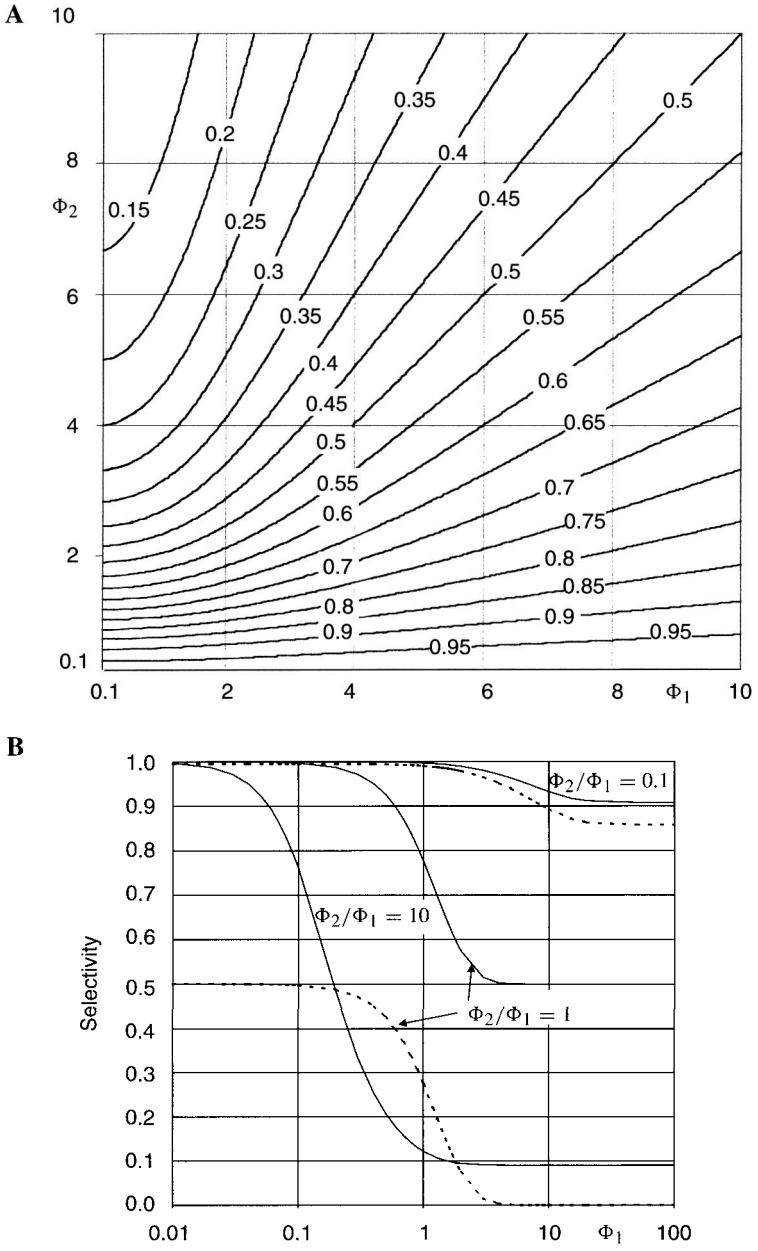


Figure 6.11 Selectivity of consecutive reactions. **A.** Selectivity contour lines as a function of Φ_1 and Φ_2. **B.** Selectivity *versus* Φ_1 for three values of the ratio Φ_2/Φ_1 for $C_{2,S} = 0$ (solid line). The two dashed lines correspond to values of the parameter $(\nu_{1,1}/\nu_{2,1})\,(C_{2,S}/C_{1,S})\,(\mathcal{D}_{2e}/\mathcal{D}_{1e}) = 0.5$.

Next Page

If both reactions do not have the same activation energy, the temperature effect can be used to influence their behavior; for example, the temperature can be reduced when $E_1 < E_2$.

If $m = (\nu_{1,1} k_{1M}) / (\nu_{2,2} k_{2M})$, Eq. (6.47) is written:

$$s_{2,1}(\mathrm{SD}) = 1 + \frac{\nu_{1,1}}{\nu_{2,1}} \frac{1}{m} \frac{C_2}{C_1} \tag{6.51}$$

When both reactions are clearly affected by internal diffusion, the instantaneous selectivity can be obtained from (6.50):

$$s_{2,1}(AD) = \frac{\sqrt{m}}{1+\sqrt{m}} + \frac{\nu_{1,1}}{\nu_{2,1}} \frac{\mathcal{D}_{2e}}{\mathcal{D}_{1e}} \frac{1}{\sqrt{m}} \frac{C_{2,S}}{C_{1,S}} \tag{6.52}$$

The integrated selectivity:

$$S_{2,1} = \frac{\dfrac{F_{2,0} - F_2}{F_{1,0} - F_1}}{\dfrac{\nu_{2,1}}{\nu_{1,1}}}$$

is obtained by integrating (6.51), assuming that $n_{2,0} = 0$, in other words, there is no intermediate compound in the reactor feed. Since $F_1 = F_{1,0}(1 - X)$, we can finally write:

$$S_{2,1} = \frac{m}{1-m} \frac{1}{X_1} \left[(1 - X_1) - (1 - X_1)^{\frac{1}{m}} \right] \tag{6.53}$$

and:

$$R_{2,1} = S_{2,1} X_1 = \frac{m}{1-m} \left[(1 - X_1) - (1 - X_1)^{\frac{1}{m}} \right]$$

The integrated selectivity in the presence of diffusion can be calculated from:

$$\frac{\mathrm{d}F_2}{\mathrm{d}F_1} = \frac{\nu_{2,1}}{\nu_{1,1}} \frac{\sqrt{m}}{1+\sqrt{m}} + \frac{\mathcal{D}_{2e}}{\mathcal{D}_{1e}} \frac{1}{\sqrt{m}} \frac{F_2}{F_1}$$

Assuming $\mathcal{D}_{1e} = \mathcal{D}_{2e}$ and $n_{2,0} = 0$, after integration the above equation yields:

$$\frac{F_2}{F_{1,0}} = \left(\frac{\nu_{2,1}}{\nu_{1,1}} \right) \left(\frac{\sqrt{m}}{1+\sqrt{m}} \right) \left(\frac{1}{1 - \dfrac{1}{\sqrt{m}}} \right) \left[\left(\frac{F_1}{F_{1,0}} \right) - \left(\frac{F_1}{F_{1,0}} \right)^{1/\sqrt{m}} \right]$$

that is:

$$\frac{F_2}{F_{1,0}} = \left(\frac{\nu_{2,1}}{\nu_{1,1}} \right) \left(\frac{m}{m-1} \right) \left[(1 - X_1) - (1 - X_1)^{1/\sqrt{m}} \right]$$

and, consequently:

$$S_{2,1} = \left(\frac{m}{1-m} \right) \frac{1}{X_1} \left[(1 - X_1) - (1 - X_1)^{1/\sqrt{m}} \right] \tag{6.54}$$

Previous Page
Copyrighted Materials
Copyright © 2004 Editions Technip Retrieved from www.knovel.com

and:

$$R_{2,1} = \left(\frac{m}{1-m}\right)\left[(1-X_1) - (1-X_1)^{1/\sqrt{m}}\right]$$

There is one aspect of Eq. (6.52) that should be considered. At the very start of the reaction, we would normally expect to see the only appearance of A_2 without the intervention of the subsequent reaction and consequently an initial selectivity of 1.

If the diffusion limitation is severe, we find that the initial selectivity is equal to $\left[\sqrt{m}/\left(1+\sqrt{m}\right)\right]$, which implies that, as soon as the reaction begins, product A_3 will appear and A_2 will disappear. This clearly shows that A_2, caught in the pores of the catalyst, cannot escape without being involved in the subsequent reaction in such a way that even an initial observation of the bulk of the fluid phase will reveal the presence of product resulting from the disappearance of A_2. This phenomenon can be used advantageously to reveal any potential diffusion limitation.

6.6 ESTIMATING THE COEFFICIENT OF DIFFUSION $\mathcal{D}_e$

The use of Fick's law to model diffusion within a solid catalyst results in a rough approximation. Various phenomena, whose relative importance varies considerably depending on the system considered, contribute to the displacement of molecules within the pores of the catalyst. The following mechanisms can occur simultaneously:

- molecular diffusion
- so-called Knudsen diffusion
- viscous flux resulting from pressure gradients
- surface diffusion of adsorbed molecules.

• Molecular diffusion

When the pores are relatively large and the pressure sufficiently high (atmospheric pressure and above), an approximate equation can be used to estimate $\mathcal{D}_e$. This involves modification of the coefficient of diffusion in the homogeneous phase, corrected for the void fraction of the particles as well as for the tortuosity and changes in pore cross-section:

$$\mathcal{D}_{1e} \cong \mathcal{D}_{1me} = \frac{\theta \mathcal{D}_{1m}}{\tau} \tag{6.55}$$

$\mathcal{D}_{1m}$ can be estimated from correlations for molecular diffusion either in a gas or in a liquid [Reid *et al.*, 1987]. The porosity θ and the tortuosity τ are related to the grain. θ is about 0.3 to 0.7, while τ varies from 2 to 10. In the absence of precise information, τ is assumed to fall between 2 and 4.

Note that the diffusivity in the gas phase is about 10^{-5} m^2/s, while in the liquid phase the values are much lower, roughly 10^{-9} m^2/s. In a mixed (gas + liquid) phase, where the catalyst pores are filled with liquid, it is the value of the diffusivity in the liquid phase that must be used to calculate the Thiele modulus.

• Knudsen diffusion

When the pores are very small and pressure low, the diffusion regime may no longer be comparable to the homogeneous phase regime. Since the value of the mean free path of molecules is high and the distances between the walls low, the molecule moves by successive hops along the pore. The diffusion regime is then referred to as the Knudsen regime and calculation of the corresponding diffusion coefficient makes use of the kinetic theory of gases. By assuming the mean free path is equivalent to the mean diameter of the pore, it can be shown that:

$$\mathcal{D}_{1ke} = 6.14 \frac{\theta^2}{\tau S_p \rho_p} \sqrt{\frac{T}{M_1}} \tag{6.56}$$

where

$\mathcal{D}_{1ke}$ effective diffusion in the Knudsen regime (m^2/s)
θ void fraction of the particle (dimensionless)
τ tortuosity factor (dimensionless)
S_p specific surface area (m^2/kg)
ρ_p density of the particle (kg/m^3)
T temperature (K)
M_1 molecular weight (kg/mol).

Orders of magnitude

θ 0.5
τ 2
S_p $2 \cdot 10^5$ m^2/kg
ρ_p 1 500 kg/m^3
T 600 K
M_1 0.2 kg/mol
$\mathcal{D}_{1ke}$ $1.4 \cdot 10^{-7}$ m^2/s.

When $\mathcal{D}_{1m} \gg \mathcal{D}_{1k}$, $\mathcal{D}_{1k}$ should be used.

When $\mathcal{D}_{1m} \ll \mathcal{D}_{1k}$, $\mathcal{D}_{1m}$ should be used.

For intermediate cases, a mean coefficient $\bar{\mathcal{D}}_{1e}$, defined by the following equation, is used:

$$\frac{1}{\bar{\mathcal{D}}_{1e}} = \frac{1}{\mathcal{D}_{1ke}} + \frac{1}{\mathcal{D}_{1me}} \tag{6.57}$$

• Viscous flow

Due to the effect of volume changes in the reaction medium, pressure gradients can appear in the interior of porous solids; the gradients will result in fluid flow governed by Darcy's law. This flow is superimposed on the diffusion flux associated with the concentration gradients.

• Surface diffusion

Molecules adsorbed at the surface of the pores may have considerable mobility. Migration of these molecules in the adsorbed phase can also contribute to molecular transfer inside the pores. This type of diffusion can be modeled similarly to other types of diffusion by

making use of a concentration gradient for the adsorbed compound and a coefficient of surface diffusion.

In the case of micropores, surface forces are considerable and the migration of adsorbed molecules may be significant, even leading in certain cases to unexpected selective steric effects [Krishna and Wesselingh, 1997].

To account for the interactions resulting from the various mechanisms, different models are used to better represent the actual situation. In general, the Stefan-Maxwell formulation must be used in place of Fick's law. A number of models have been proposed, especially to represent the transition between the Knudsen regime and molecular diffusion. One such model is known as the Dusty Gas Model (DGM), and we refer the reader to the literature for additional details [Wijngaarden *et al.*, 1998; Krishna and Wesselingh, 1997].

6.7 INFLUENCE OF EXTERNAL MASS TRANSFER: THE CONCEPT OF GLOBAL EFFECTIVENESS

6.7.1 Global transfer coefficient

Sometimes, in the case of fast catalytic reactions, diffusion of the reactants to the catalyst grains can limit the reaction. This is referred to as external diffusion limitation at the grain (Fig. 6.12). Referring to $C_{1,b}$ as the concentration within the fluid phase and $C_{1,S}$ as the concentration of the reactant on the exterior surface of the grain, a molar balance relative to reactant A_1 per unit volume of reactor can be written. In the steady state regime, this balance is written:

$$N_1 = k_{1,S}\mathcal{A}_S\left(C_{1,b} - C_{1,S}\right) = -\nu_1 r'_M \eta \rho_c \tag{6.58}$$

where the rate of reaction r'_M is expressed as the surface condition $\left(C_1 = C_{1,S}\right)$ in mol/s · kg of catalyst.

For a first-order reaction:

$$r'_M = k_M C_{1,S} \tag{6.59}$$

From (6.58) and (6.59) an expression for $C_{1,S}$ can be derived:

$$C_{1,S} = \frac{C_{1,b}}{1 - \dfrac{\nu_1 k_M \eta \rho_c}{k_{1,S}\mathcal{A}_S}} \tag{6.60}$$

If a global transfer coefficient K_1 is defined by the following equation:

$$N_1 = K_1 \mathcal{A}_S C_{1,b} \tag{6.61}$$

we then have:

$$\frac{1}{K_1} = \frac{1}{k_{1,S}} + \frac{\mathcal{A}_S}{-\nu_1 k_M \eta \rho_c} \tag{6.62}$$

K_1 is a global transfer coefficient that takes into account external mass transfer (through $k_{1,S}$) outside the grain, diffusion through the pores (through η), and the chemical reaction inside

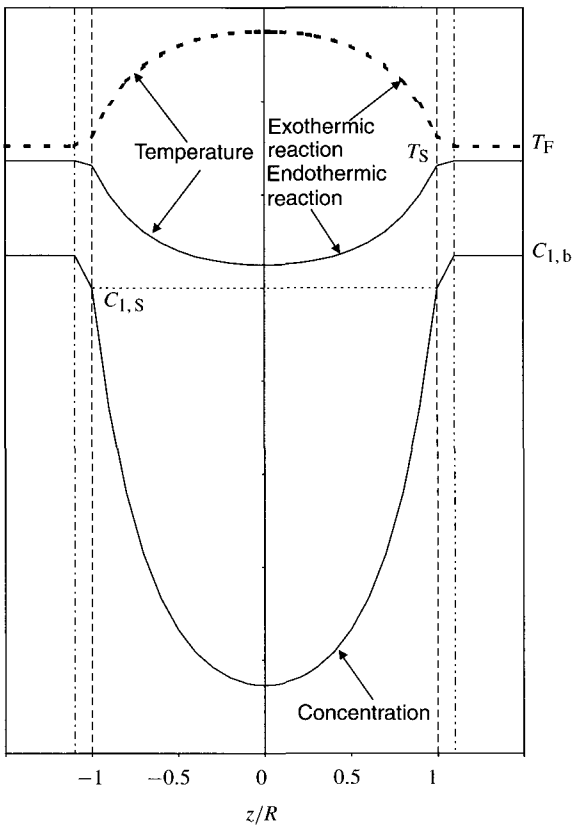


Figure 6.12 Concentration and temperature profiles around and within an active catalytic particle.

the grain (through k_M). Figure 6.12 represents a concentration profile around and within an active catalytic particle.

Particular case

1. The catalyst consists of spherical grains of diameter d_p:

$$\overline{d_1} = d_p = \frac{6\varepsilon_p}{\mathcal{A}_S} = \frac{6\rho_c}{\mathcal{A}_S \rho_p}$$

In this case:

$$\frac{1}{K_1} = \frac{1}{k_{1,S}} + \frac{6}{-\nu_1 k_M \eta \rho_p d_p} \tag{6.63}$$

2. The catalyst consists of particles of varied shapes that are characterized by their effective mean diameter $\overline{d_1}$:

$$\frac{1}{K_1} = \frac{1}{k_{1,S}} + \frac{6}{-\nu_1 k_M \eta \rho_p \overline{d_1}}$$

Bear in mind that the external and internal resistances are of the same type since they are associated with the diffusion of reactant molecules. The difference is based on two factors: 1) the free surface available for the passage of molecules, which is limited by the porosity in the interior of the particle, and 2) movement of the fluid phase, which is flowing at the exterior and stagnant in the interior. The result of these two factors is that the external mass transfer can play a role in the global resistance only if the effectiveness factor is significantly less than one.

In contrast, in Eq. (6.62) the two terms respectively associated with external transfer and the chemical reaction inside the particle present very different behavior towards the molecular compound involved. There is little influence of external transfer here, whereas the chemical reaction is highly specific for a molecular compound. As a result, in order to maintain the selectivity of a reaction, it is imperative that the resistance associated with external mass transfer be negligible.

6.7.2 Heat transfer on the outer surface of the grain

As with mass transfer, in certain cases heat transfer at the surface of the catalytic solid can play a role. The exchange of heat between solid and fluid is represented by an equation similar to the one used for mass transfer (6.58), namely:

$$Q_{\text{exch}} = h\mathcal{A}_S\,(T_S - T_F) = \nu_I r'_M \eta \rho_c \Delta H_R \tag{6.64}$$

where

Q_{exch} quantity of heat exchanged between the solid and the fluid in contact with the catalyst
h coefficient of fluid-solid heat transfer, $J/s \cdot K \cdot m^2$ of external surface of solid
T_S temperature at the surface of the solid
T_F temperature of the fluid
ΔH_R enthalpy of the reaction (J/mol of A_I).

In Fig. 6.12 are shown, together with the concentration profiles of reactant A_I, typical temperature profiles in the interior of the catalyst grain and in the vicinity of the surface in the fluid phase. There is a narrow region where the transfer resistance is found, the temperature difference being $T_S - T_F$. The profiles inside the grain show maximum and minimum values, depending on whether the reaction is exothermic or endothermic.

The coefficient of heat transfer h, as well as the coefficient of mass transfer $k_{I,S}$, depend on the nature of fluid flow around the solid. In the following chapter, as part of a more detailed examination of various technologies, we will see how these coefficients can be estimated depending on the specific implementation used.

6.7.3 The concept of global grain effectiveness

Just as we defined an internal grain effectiveness, we can define a global effectiveness **E** by relating the flux of the reactant transferred per unit volume of reactor to the theoretical rate of reaction expressed for the conditions prevailing within the fluid phase $(C_{I,b}, T_F)$. For a first-order reaction, the global effectiveness is defined by:

$$N_I = \mathcal{A}_S K_I C_{I,b} = -\nu_I k_M \mathbf{E} C_{I,b} \rho_c$$

from which we derive:

$$\mathbf{E} = \frac{\mathcal{A}_S K_1}{-\nu_1 k_M \rho_c} \tag{6.65}$$

It can be shown that:

$$\frac{1}{\mathbf{E}} = \frac{1}{\eta} - \frac{\nu_1 k_M \rho_c}{\mathcal{A}_S k_{1,S}}$$

The final equation for global grain effectiveness includes, in addition to the Thiele, Prater, and Arrhenius numbers (Φ, β_1, β_2), two new dimensionless numbers, the mass Biot number and the thermal Biot number, which are defined by:

$$Bi_m = \frac{k_{1,S} L}{\mathcal{D}_{1e}} \quad \text{and} \quad Bi_c = \frac{hL}{\lambda_e}$$

where

L characteristic dimension
$\mathcal{D}_{1e}$ coefficient of internal diffusion
h coefficient of heat transfer relative to the fluid phase
λ_e effective internal thermal conductivity of the particle.

In examining the changes in **E** based on the values of the various dimensionless numbers, we again encounter the existence of multiple stable states. These can arise from the presence of internal gradients, as previously examined, or external gradients, or the simultaneous coexistence of internal and external gradients (although this situation is rarely found in practice).

6.7.4 Temperature and concentration gradients

For heterogeneous catalytic reactions involving **gases**, it has been found that:

- the internal temperature gradient is generally low (rarely more than a few degrees difference between surface temperature and the maximum or minimum interior temperature of the grain)
- the external temperature gradient can be high (several tens of degrees difference between the surface temperature and the temperature within the gas phase)
- the internal concentration gradient can be high (internal concentrations of zero can occur)
- the external concentration gradient is generally low, except for very fast reactions.

For heterogeneous catalytic reactions involving **liquids**, it has been found that:

- the internal temperature gradient is low
- the external temperature gradient is also low
- the internal concentration gradient depends on the intrinsic activity of the catalyst
- the external concentration gradient can be non-negligible (external mass transfer limitation).

For heterogeneous catalytic reactions involving both **a gas and a liquid**, our findings for a liquid alone hold. Various criteria have been proposed to ensure that these gradients are negligible [Mears, 1971]:

- No temperature gradient inside the particle:

$$\frac{|\Delta H|\,\mathcal{R}_V R_p}{\lambda_e T_S} < 0.75\frac{RT_S}{E} \tag{6.66}$$

- No temperature difference between the fluid and the particle:

$$\frac{|\Delta H|\,\mathcal{R}_V R_p}{hT_F} < 0.15\frac{RT_F}{E} \tag{6.67}$$

where

ΔH enthalpy of reaction (J/mol)
$\mathcal{R}_V$ rate of reaction per unit volume of particle (mol/m^3 · s)
T_S surface temperature of the particle (K)
λ_e thermal conductivity of the particle (W/m · K)
R_p radius of the particle (m)
T_F temperature of the fluid phase (K)
h coefficient of fluid-solid heat transfer (W/m^2 · K)
E activation energy of the reaction (J/mol)
R ideal gas constant (= 8.31 J/mol · K).

6.8 APPARENT ACTIVATION ENERGY OF HETEROGENEOUS CATALYTIC REACTIONS

The cases involving endothermic and exothermic reactions have already been discussed. Earlier we saw how the temperature inside the catalyst grains could be appreciably different from the surface temperature. We also saw that when external heat transfer becomes limiting, the surface temperature can differ from the temperature in the bulk of the reaction fluid. This case is less common, however, and we will only consider the case when $T_F = T_S$.

If we examine an element of the bed where the temperature is T_F and the concentration $C_{1,L}$, the transformation rate per unit volume of porous bed can be expressed as:

$$N_1 = K_1 \mathcal{A}_S C_{1,L} \tag{6.68}$$

where:

$$\frac{1}{K_1} = \frac{1}{k_{1,S}} + \frac{\mathcal{A}_S}{-\nu_1 k_M \eta \rho_c}$$

At a temperature T'_F, and for the same concentration $C_{1,L}$, we have:

$$N'_1 = K'_1 \mathcal{A}_S C_{1,L}$$

where:

$$\frac{1}{K'_1} = \frac{1}{k'_{1,S}} + \frac{\mathcal{A}_S}{-\nu_1 k'_M \eta' \rho_c}$$

The ratio of the two apparent rates is:

$$\frac{N_1}{N_1'} = \frac{K_1}{K_1'} = \frac{\dfrac{1}{k_{1,S}'} + \dfrac{\mathcal{A}_S}{-\nu_1 k_M' \eta' \rho_c}}{\dfrac{1}{k_{1,S}} + \dfrac{\mathcal{A}_S}{-\nu_1 k_M \eta \rho_c}}$$

and if we define an *apparent* Arrhenius activation energy, we have:

$$\ln \frac{K_1}{K_1'} = \frac{E_{app}}{R}\left[\frac{1}{T_F'} - \frac{1}{T_F}\right] \tag{6.69}$$

We can then compare this apparent activation energy with the *true* activation energy E_v, defined by:

$$\ln \frac{k_M}{k_M'} = \frac{E_v}{R}\left[\frac{1}{T_F'} - \frac{1}{T_F}\right] \tag{6.70}$$

We then have:

$$\frac{E_{app}}{E_v} = \frac{\ln \dfrac{K_1}{K_1'}}{\ln \dfrac{k_M}{k_M'}}$$

Several extreme cases are possible:

1. The reaction is slow at temperatures T_F and T_F', and athermic, for example, if the temperature is low. Under these conditions:
   $1/k_{1,S}$ can be ignored compared to $\mathcal{A}_S/(-\nu_1 k_M \eta \rho_c)$
   $1/k_{1,S}'$ can be ignored compared to $\mathcal{A}_S/(-\nu_1 k_M' \eta' \rho_c)$
   η and η' remain close to 1.
   We have:
   $$\frac{K_1}{K_1'} \cong \frac{k_M}{k_M'}$$
   from which: $E_{app} = E_v$.
2. The reaction, although rapid, is not limited by external diffusion. Moreover, it is athermic in such a way that the temperature can be considered uniform in both the particles and the fluid. Here too:
   $1/k_{1,S}$ can be ignored compared to $\mathcal{A}_S/(-\nu_1 k_M \eta \rho_c)$, as can $1/k_{1,S}'$. We then have:
   $$\frac{K_1}{K_1'} = \frac{k_M \eta}{k_M' \eta'}$$
   Since the Thiele modulus is high, the effectiveness factor η is inversely proportional to it: $\eta \cong 3/\Phi$. Since $\Phi \approx \sqrt{k_M}$, we have:
   $$\frac{K_1}{K_1'} = \frac{k_M \eta}{k_M' \eta'} = \frac{k_M \sqrt{k_M'}}{k_M' \sqrt{k_M}} = \sqrt{\frac{k_M}{k_M'}}$$
   and thus:
   $$E_{app} = \frac{E_v}{2}$$

3. The reaction is very fast and entirely controlled by external diffusion:
   $\mathcal{A}_S/(-\nu_I k_M \eta \rho_c)$ can be ignored compared to $1/k_{I,S}$
   $\mathcal{A}_S/(-\nu_I k'_M \eta' \rho_c)$ can be ignored compared to $1/k'_{I,S}$
   We obtain:

$$\frac{K_I}{K'_I} = \frac{k_{I,S}}{k'_{I,S}}$$

Given the slow variation in the mass transfer coefficient with temperature, the apparent activation energy will be approximately several kJ/mol; in other words, the apparent reaction rate is relatively insensitive to temperature.

In the general case of non-athermic reactions that are moderately fast, it is easy to see that there are a number of possible situations, depending on the respective values of the Thiele modulus, the transfer coefficient $k_{I,S}$, the coefficients β_I and β_2, and the temperature interval under consideration. These different situations can occur whenever the temperature range is very broad, as shown in Fig. 6.13.

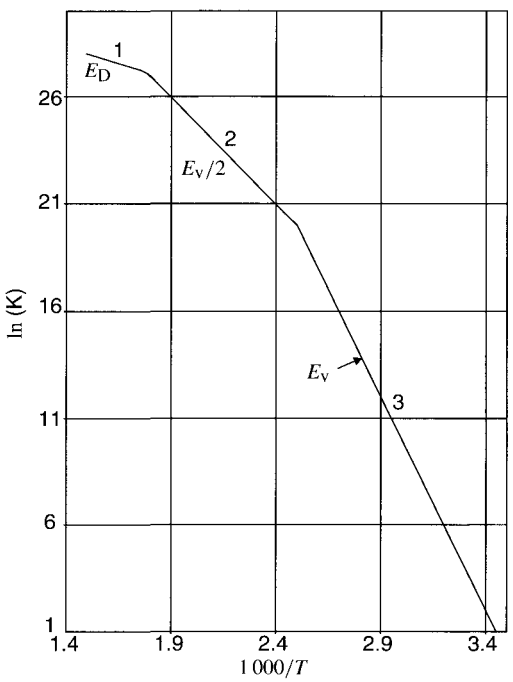


Figure 6.13 Change in the apparent rate with temperature ($\log K$ apparent *vs.* $1/T$). 1. External diffusion limitation, fast reaction, very low slope, $E_{app} = E_D$ of 10–20 kJ/mol. 2. Internal diffusion limitation, fast reaction, slope $= -E/2R$, $E_{app} = E_{true}/2$, 20 to 60 kJ/mol 3. True kinetic regime, slow reaction, no limitation due to transfer, slope $= -E/R$, $E_{app} = E_{true}$ of 60 to 180 kJ/mol.

6.9 CATALYST DEACTIVATION

During use, even during periods of inactivity, catalysts sometimes lose their physical and chemical integrity. They undergo alterations that lead to their deactivation—the speed, severity, and seriousness of the deactivation varying with circumstances.

6.9.1 Causes of catalyst deactivation

There are three principal causes of deactivation:

1. The gradual buildup of reaction byproducts, such as coking tar, that obstruct the active pores and eventually lead to the extinction of the catalyst.
2. Catalyst poisoning. Poisoning is provoked by substances contained in the feed being processed, even when they exist in small, and sometimes undetectable, concentrations. During their passage through the reactor, these substances are adsorbed on active sites and the cumulative effect of this preferential adsorption eventually leads to a significant reduction of the activity of the catalytic mass.
3. The slow structural transformation of the catalytic species or the agglomeration and growth of microcrystallites leading to a gradual decrease in the number of active sites per unit surface or—which amounts to the same thing—to a decrease of the active surface area. This is possibly the most harmful of the three causes of deactivation.

6.9.2 Preventing catalyst deactivation

Deposits of tar or coke can be eliminated by combustion, using a stream of oxygen-containing gas. Fortunately, this regeneration procedure can restore the activity of the partially coked catalyst. For example, a catalyst used for cracking petroleum fractions can sustain thousands of reaction-combustive regeneration cycles.

To overcome catalyst poisoning, the substance responsible for poisoning must be identified and the feed treated to eliminate the unwanted compounds, or a catalyst better resistant to poisoning can be used, or a portion of the catalytic bed located ahead of the actual bed can be sacrificed.

Structural transformation must be attacked at the root, for it is during the development of catalysts that the means to prevent transformation of the crystalline phases or recrystallization are tested. When designing reactors, engineers must obtain the maximum benefit from commercially available catalysts, whatever their advantages and disadvantages. Together with the equations describing the chemical kinetics of the process, at least one deactivation equation must be taken into consideration, regardless of the ultimate causes of deactivation.

6.9.3 Equations for deactivation kinetics

A number of authors have attempted to describe the intrinsic deactivation of the catalyst through the use of kinetic equations. We feel that the approach taken by Levenspiel [1999] is the simplest and most general. It is the one used here. It makes use of a phenomenological

equation, that is to say, one based on empirical laws without concern for any of the underlying —and infinitely complex— mechanisms. It turns out that deactivation processes, which most frequently cannot be analyzed because of their complexity, can generally be represented by relatively simple kinetic equations.

If the initial rate of a process can be expressed by:

$$r_0 = kC_1^n$$

the rate at time t, all other conditions being equal, can, by definition, be written:

$$r = kC_1^n a$$

where a is defined as a relative activity.

The variation of a with time ($\mathrm{d}a/\mathrm{d}t$) is a function of concentration, temperature, and the activity a at time t, according to a general expression:

$$-\frac{\mathrm{d}a}{\mathrm{d}t} = k_\mathrm{d} \Sigma C_i^m a^d$$

where

k_d deactivation rate constant

ΣC_i cumulative concentration of one or more compounds A_i.

A general expression such as this can be used to explain the intrinsic kinetics observed, for example:

$$r = \frac{kC_1^n}{1 + k_\mathrm{d} t} \quad \text{(hyperbolic form)}$$

where

t cumulative time (s)

k_d deactivation rate constant (s^{-1})

or:

$$r = kC_1^n \exp(-k_\mathrm{d} t) \quad \text{(exponential form)}$$

or:

$$r = kC_1^n [1 + k_\mathrm{d} t]^p \quad \text{(power law form, } p < 0)$$

The most frequently found values for d, m, and the number of compounds included in ΣC_i are:

d comprised between 1 and 3, and generally 1

m comprised between 0 and 2, and generally 1

The number of compounds included in ΣC_i is between 0 and 2, and is generally 1.

The different expressions suggest different possible mechanisms, although these will not be discussed here.

6.9.4 Deactivation accompanied by internal diffusion limitation

Research has led to the determination of two types of deactivation accompanied by diffusion limitation in the pores: uniform poisoning throughout the porous mass and poisoning that affects only the pore inlets, or, macroscopically, the external layer of the catalyst particles.

By defining a poisoned fraction α, it can be shown that, in the case of uniform poisoning, the ratio F of rates with and without deactivation is equal to $1 - \alpha$ if the effectiveness factor η is close to 1. When the effectiveness factor is low ($\eta \ll 1$), $F = \sqrt{1 - \alpha}$.

In the case of poisoning in the pore inlets, it can be shown that, for a first-order reaction:

$$\frac{1}{F} = \frac{1}{1-\alpha} + \frac{\eta\Phi^2\left[1 - (1-\alpha)^{\frac{1}{3}}\right]}{3\,(1-\alpha)^{\frac{1}{3}}}$$

where Φ is the Thiele modulus.

For example, if $\alpha = 0.10$ and $\Phi = 10$, $\eta = 3/\Phi = 0.3$, and $F \cong 0.68$. Poisoning that affects 10% of the catalyst surface causes a rate reduction of 32%. The crux of the problem, however, is the determination of the value of α after a specific period of time while the catalyst is in service.

It is here that the approach used by Levenspiel [1999], and discussed in Section 6.9.3, comes into play. Levenspiel does not try to define a poisoned fraction α but tries to establish a phenomenological equation for the rate of reaction strictly speaking as well as for the rate of deactivation. Either, or both, of these rates can be affected by internal diffusion. The exponent d in particular, often close to 1 in intrinsic kinetics, can assume higher observed values depending on the respective values of the Thiele moduli (corresponding to the reaction and to the deactivation) and the type of deactivation.

6.9.5 Concluding remarks

Although there are a number of theoretical studies concerning the problem of deactivation and in spite of the efforts of engineers, who have attempted to produce catalysts that are resistant to all forms of aging, more often than not, we must make use of empirical deactivation equations, often remarkably simple, such as those observed by Voorhies [1945].

Voorhies's equations can be summarized as follows:

- In a reaction process characterized by several reactions and, therefore, several distinct kinetic equations, each rate constant (or each rate for a given set of concentrations) follows a deactivation law characterized by a linear relation between the logarithm of the rate constant at cumulative time t and the square root of the cumulative time t.
- The coefficient of proportionality characterizes the reaction under consideration.
- This remarkable correlation has even been observed when there is diffusion limitation and when an apparent rate constant is plotted on the ordinate instead of the true rate constant.

When rapid catalyst deactivation cannot be avoided, technology must be used to compensate, primarily through the use of convenient regeneration procedures, by planning for the continuous or periodic renewal of the catalyst in the reactor, and by drawing off spent catalyst and supplying new catalyst material (moving bed, fluidized bed, transported bed). The use of such practices implies that the catalyst regeneration process is convenient and effective. These cases will be examined in the following chapters.

6.10 USE OF HETEROGENEOUS CATALYSTS

6.10.1 Conditions for the optimal use of a catalyst

It should be obvious that the catalyst's intrinsic characteristics must be maintained during use. These include:

- its activity, that is, the ability to transform the greatest amount of material in the shortest amount of time with the minimum amount of catalyst
- its selectivity, that is, the ability to obtain the maximum desired product from a given quantity of reactant
- its stability, that is, the ability to process the maximum amount of reactant
- its regeneratability.

These characteristics must be maintained, or even enhanced, during operation.

We saw earlier that diffusion phenomena could have a negative or harmful influence and, therefore, should be avoided to as great an extent as possible. With respect to internal diffusion, it is clear that the grains should be as small as possible and the porosity as great as possible. With respect to external diffusion, transfer conditions should be optimized. This can be done through increased turbulence of the fluid phase around the grain and the use of large heat and mass exchange surfaces (which is yet another argument in favor of the use of small grains).

In general the overall order of chemical reactions is greater than 0 (and often close to 1). Under these conditions there is an advantage, from the point of view of activity as well as selectivity, in considering a concentration gradient reactor or a plug flow reactor. However, other considerations, especially with respect to reaction thermicity, can influence this choice and lead us to consider CSTRs, in which thermal control is simpler. It is easy to see that the choice of reactor for a given application is in no way obvious from inception. This explains the great diversity of methods found for implementing catalysts in reactors.

In the following sections, we present a range of possible catalyst technologies, with their advantages and disadvantages; methods of calculation will be discussed later on in the book.

6.10.2 The fixed bed

As indicated previously, the fixed bed consists of a compact, immobile stack of catalyst grains within a generally vertical vessel. The catalyst grains have an equivalent diameter of $\overline{d_1}$, which is generally between 1 and 5 mm. Figure 6.14 corresponds to the case where a single fluid phase flows through the catalyst bed; Figure 6.15 represents a reactor with two-phase flow (gas + liquid).

If heat exchange must occur while the reaction takes place, exchange surfaces will have to be introduced within the catalytic bed. The most commonly employed technology is known as *multitubular* (Fig. 6.16). In this case the catalyst is contained in a number of tubes arranged in parallel and bathed in a heat exchange fluid.

If the operating temperature is high, the tubes are placed in a furnace and heated directly by means of burners. Here too, flow within the tubes can be single-phase or two-phase.

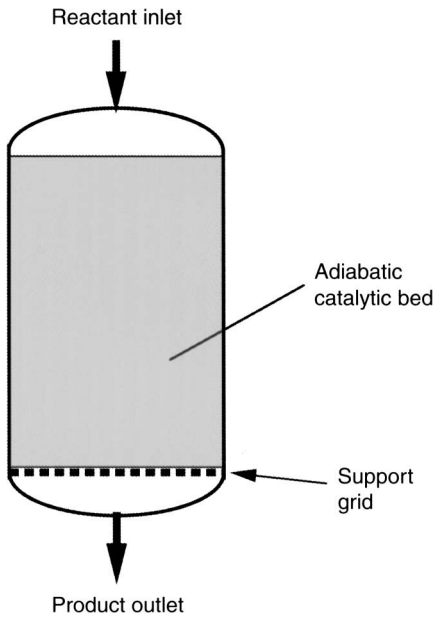


Figure 6.14 Adiabatic fixed-bed reactor with single-phase flow.

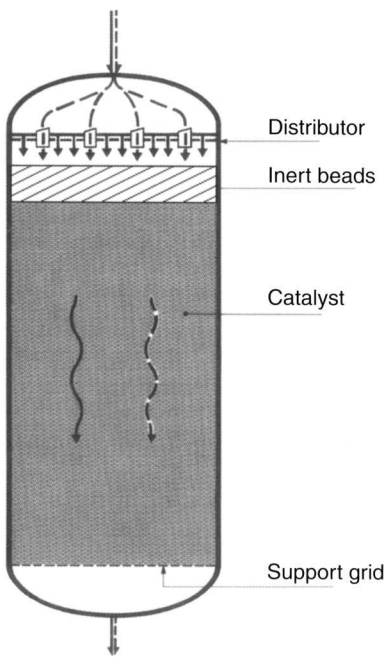


Figure 6.15 Adiabatic fixed-bed reactor with two-phase flow.

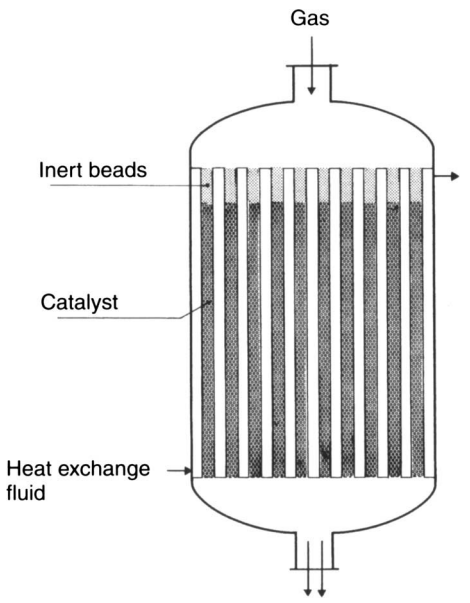


Figure 6.16 Multitubular fixed-bed reactor.

As we have described them, fixed beds are most frequently used as continuous tubular reactors. However, it is not impossible to conceive of a fixed bed being used as a batch reactor, or a CSTR, or a multistage reactor. In these cases the fixed bed is inserted in a recirculation loop for the reaction fluid (or fluids). However, the technology most commonly found in industrial use is the adiabatic fixed bed (Fig. 6.14 and Fig. 6.15), because of its great simplicity.

Adiabatic technology is even used for reactions with non-negligible thermicity. The catalyst bed is then divided into several sections between which the temperature of the reaction fluid(s) is readjusted by heat exchange (for example, in the case of catalytic reforming) or by introducing cold reactants (quenching) (Fig. 6.17). This technology is often used in refining, where practically all hydrogen treatments of petroleum cuts are performed in this way.

Monolithic catalysts can also be used in tubular reactors for specific applications involving fast reactions. This particular case is discussed in the following chapter during our detailed examination of the available technologies.

6.10.3 The moving bed

The moving bed also consists of a stack of catalyst grains inside a tube. In this case, however, the force of gravity is used to shift the catalyst from top to bottom (Fig. 6.18). Although other arrangements are possible, this design is frequently used in continuous tubular reactors through which a single fluid (gas) phase circulates.

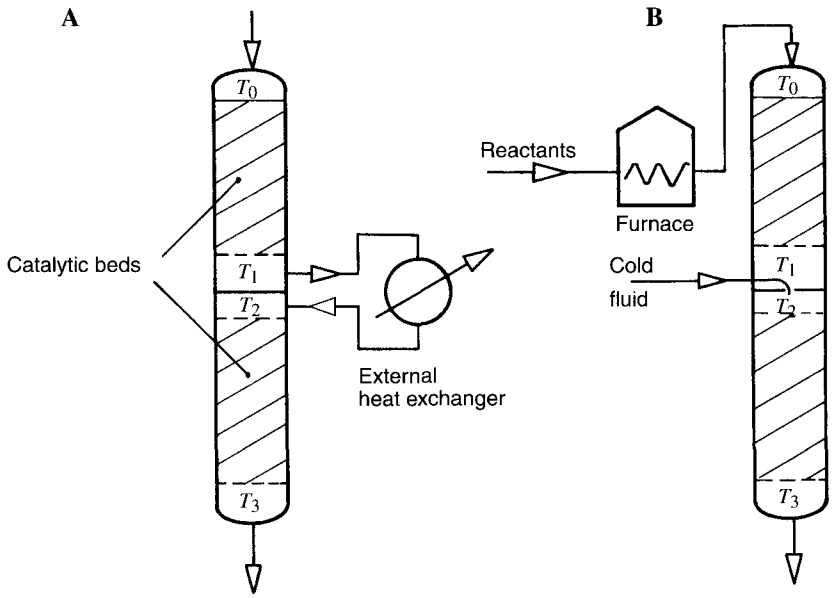


Figure 6.17 Adiabatic fixed-bed reactors with intermediate cooling. **A.** External heat exchanger. **B.** Introduction of cold fluid (one of the reactants, for example).

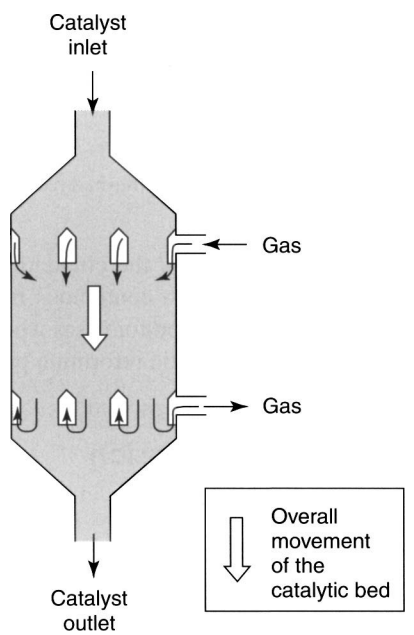


Figure 6.18 Cocurrent moving-bed reactor.

There are three possible arrangements for the direction of flow of the fluid-phase:

- top to bottom (Fig. 6.18)
- bottom to top (countercurrent, rarely used)
- horizontal (cross-flow, Fig. 6.19).

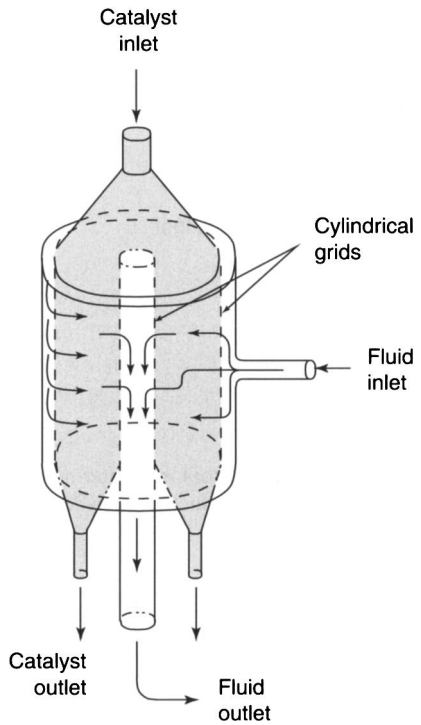


Figure 6.19 Cross-flow moving-bed reactor.

The complications introduced to the system by the circulation of the catalyst are counteracted by the ability to regenerate catalyst on a continuous basis. As a result, practical applications of moving bed technology are reserved for cases where the rapid deactivation of catalyst is encountered, for example, in the catalytic reforming process.

6.10.4 Reactors with catalyst in suspension

In this case the catalyst consists of relatively small particles ($d_p = 50\,\mu m$ to 1 mm) maintained in suspension within the reaction fluid(s). The suspension can be produced in various ways, namely through:

- mechanical agitation
- fluidization
- pneumatic transport.

6.10.4.1 Mechanical agitation

Mechanical agitation is conceptually simple. For example, a tank equipped with a rotary agitator can be filled with a liquid containing the reactants. Powdered catalyst can be added to the tank and maintained in suspension in the liquid by agitation. This simple case can be illustrated as shown in Fig. 6.20. If a gas phase is also needed to introduce some of the reactants, the gas can be bubbled through the liquid. The technology can be used either for a batch reactor or a conventional or multistage CSTR. In the case of continuous operation, the difficulty lies in separating the catalyst from the reactor effluent and recycling it to the reactor (dashed line in Fig. 6.20).

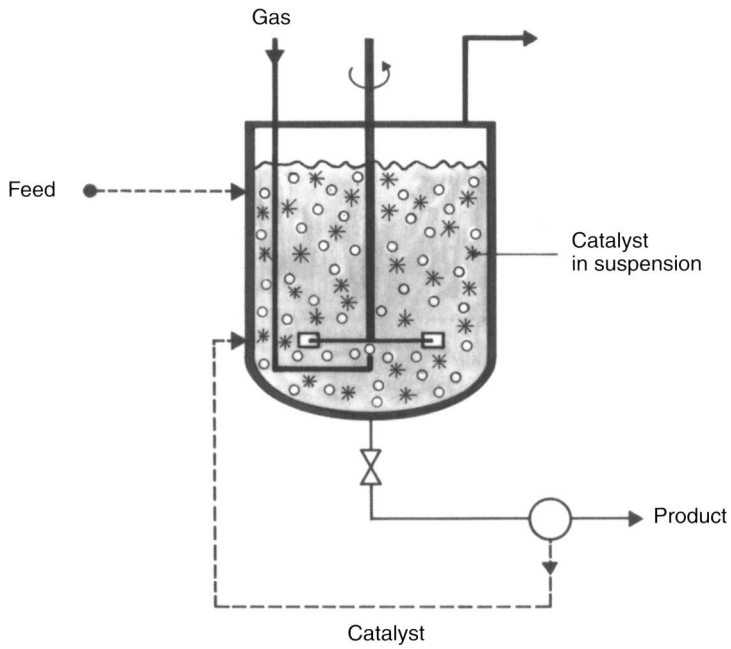


Figure 6.20 Batch reactor with catalyst in suspension and mechanical agitation.

The rotary agitator is not the only means available for generating sufficient agitation to maintain the catalyst in suspension. Another technology found in industrial use incorporates a pump that circulates the liquid phase in a closed loop and maintains the catalyst in suspension (Fig. 6.21). The major advantage of this technology is the ability to insert a heat exchanger in the recirculation loop. For example, it is used for the liquid-phase hydrogenation of benzene. In this specific case the difficulty of catalyst separation within the effluent is avoided by extracting the reaction product in the form of a vapor.

Clearly, mechanical agitation will only be used on an industrial scale if the fluid phase or one of the fluid phases is a liquid, mechanical agitation of a gas phase being less than optimal. However, continuous stirred-tank catalytic reactors that operate with a gas phase are found in the laboratory.

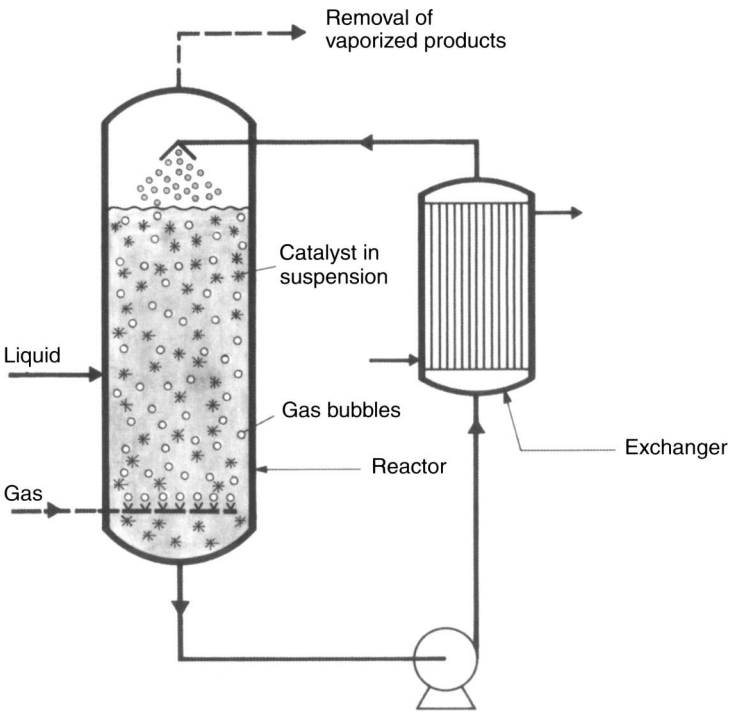


Figure 6.21 Continuous reactor with suspended catalyst and a recirculation loop.

6.10.4.2 The fluidized bed

Catalyst particles are placed in a reactor consisting of a vertically arranged cylindrical envelope. A grid placed in the lower section prevents particles from flowing to the bottom, while the reaction fluid is introduced through the same grid. As a result of upward fluid flow, catalyst particles are fluidized, a state characterized by random movement of all the particles. The fluid + particle mass then behaves, at least in certain respects, as a liquid.

Whenever fluidization is promoted by the presence of a gas, the fluid bed is far from being homogeneous; in fact, it consists of particle rich (dense phase) and particle poor (dilute phase) zones. This situation is illustrated in Fig. 6.22. In the case of liquid fluidization, the fluid bed is much more homogeneous and results in what is referred to as particulate fluidization. Similarly, fairly homogeneous fluidization can be achieved by introducing two fluid phases (gas + liquid) into the bottom of the reactor. This results in what is known as an ebullated bed (Fig. 6.23).

Fluidized beds, although more difficult to implement than fixed or even moving beds, have real advantages in the following situations:

- whenever the operation requires that large amounts of heat be removed or supplied (depending on whether the reaction is exothermic or endothermic)

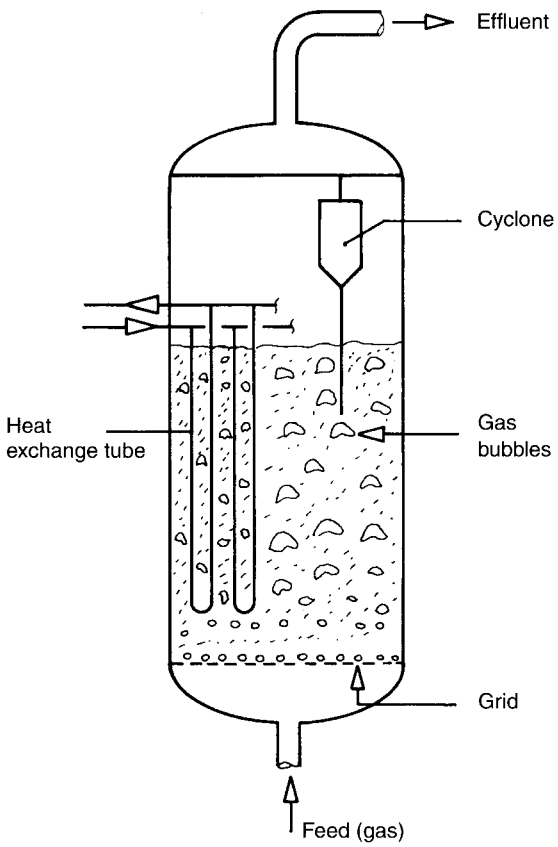


Figure 6.22 Gas fluidized bed.

- whenever it is necessary to frequently regenerate the catalyst by withdrawing used catalyst and introducing fresh or regenerated catalyst, fluidized-bed, as well as moving-bed, technology is recommended
- whenever the reaction temperature must be uniform and carefully controlled.

One of the most spectacular applications of the fluidized bed is its use in catalytic cracking. It is also used in a number of oxidation processes in which temperature control is critical but difficult to resolve.

6.10.4.3 The entrained-catalyst reactor

The reactor consists of one or more long tubes in which particles are entrained by the reaction fluid. This type of reactor is appropriate when, for various reasons (frequent regeneration, diffusion limitation, need for heat exchange), very small particles or very high rates of circulation must be employed. The density ρ_c (mass of catalyst per unit volume of reactor) in these reactors is much lower than it is in the fixed or fluidized bed.

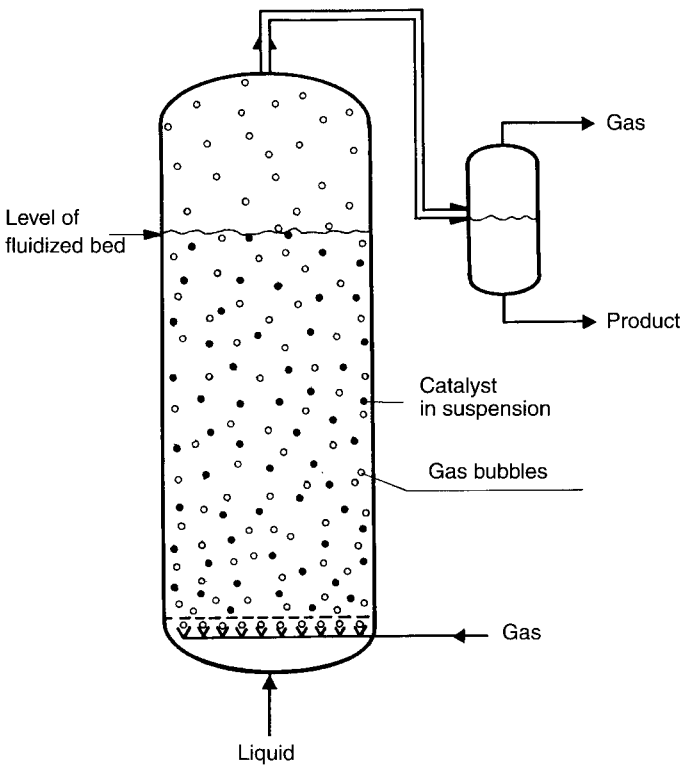


Figure 6.23 Fluidized bed with two fluid phases (ebullated bed).

A reactor of this type comprises three zones:

- a zone for introducing catalyst into the fluid stream
- a tube in which the fluid + catalyst mixture circulates and where the reaction takes place
- a separation zone for the catalyst, which is generally recycled.

The three zones are illustrated in Fig. 6.24.

Referring to our comments at the beginning of this section, we see that entrained-catalyst technology in principle possesses most of the desired characteristics for an ideal implementation of a catalyst, namely:

- fine catalyst particles
- high fluid turbulence around the particle
- gradient reactor
- ability to easily exchange heat with the exterior
- ability to continuously regenerate the catalyst.

In spite of these potential advantages, there have been few industrial applications of entrained-catalyst technology. However, the technology is used for catalytic cracking —and is alone responsible for the highest tonnage of catalyst used worldwide. The feedstock is introduced in the ascending flux of regenerated catalyst, at the base of the riser. After

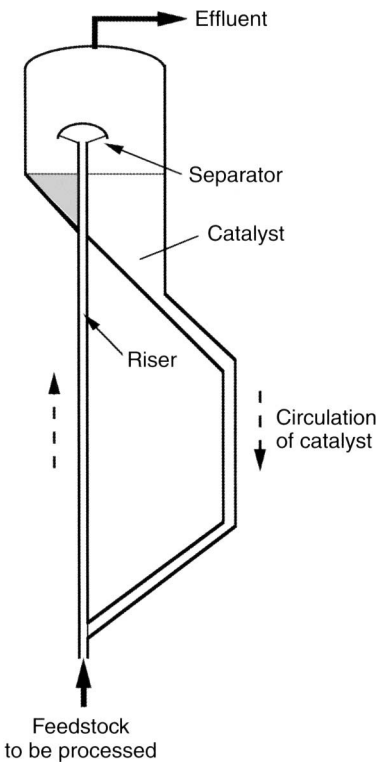


Figure 6.24 Entrained-catalyst reactor.

crossing the reaction zone, inside the riser, the feedstock and catalyst are quickly separated. An entrained bed is used inside the riser.

6.10.5 Comparison of catalyst technologies

Having briefly reviewed the various catalyst technologies available, we can now compare them. For the purposes of our comparison, we will use several criteria, shown in Table 6.4. When choosing a technology for industrial use, the information in the table, which is based on objective criteria, can be compared with any observations made while surveying the various industrial processes involving one of these technologies. Thus, in Tables 6.5, 6.6, and 6.7 we provide examples of processes that employ fixed-bed, moving-bed, and suspended-catalyst technologies. Finally, in Table 6.8, we present an overall comparison of the available technologies based on their frequency of use in industry.

The tables show that the adiabatic fixed bed, with one or two fluid phases, is by far the most extensively used system in industry. This is primarily the result of its simplicity and ability to accommodate very large feedstock capacities (greater than two million tons annually). In the following chapters we will examine each of the technologies introduced here in detail and discuss their design criteria.

Table 6.4 Comparison of available solid catalyst technologies.

Characteristics of the technology / Criteria for comparison	Implementation of the catalyst	Fixed bed				Moving bed	Catalyst in suspension				
							Mechanical agitation		Fluidized bed		Entrained bed
							Batch	Continuous			
	Heat exchange	Adiabatic		Multitubular		Adiabatic					
	Fluid phases	G or L	G + L	G or L	G + L	G or L	G + L	G + L	G or L	G + L	G or L
Preservation of characteristics associated with the catalyst grain:											
a. Activity.		+	0	+	0	+	++	++	++	+	++
b. Selectivity.		+	0	+	0	+	++	++	++	+	++
c. Stability.		+	0	+	0	0	+	+	+	+	+
d. Regeneratability.		+	+	0	0	++	0	−	++	++	++
e. Cost of catalyst.		++	++	++	++	−	−	0	−	−	−
Characteristics associated with the technology:											
a. Concentration gradient.		++	+	++	+	++	++	−	−	−	++
b. Temperature control.		−	−	0	+	−	++	++	+	++	+
c. Capacity.		++	++	+	+	+	−	0	+	+	+
d. Flexibility.		+	0	0	−	0	++	+	−	−	−
e. Simplicity.		++	++	−	−	−	++	+	0	0	0
f. Separation of catalyst/product.		++	++	++	++	+	0	−	0	0	−
g. Replacement of catalyst.		−	−	−	−	+	++	0	+	+	+
h. Pressure drop.		+	0	+	0	+	0	0	+	0	+
i. Design reliability.		++	++	+	0	0	++	++	+	0	0

++: very good; +: good; 0: average; −: poor.

Table 6.5 Examples of fixed-bed processes.

Implementation		Process
Adiabatic	Single fluid phase	Oxidation of SO_2 to SO_3
		Methanol synthesis
		Production of styrene
		Dehydrogenation of butene
		Catalytic reforming
		CO conversion ($CO + H_2O \rightarrow CO_2 + H_2$)
		C_5-C_6 isomerization
		Hydrodesulfurization of naphtha
		Selective hydrogenation of acetylene to ethylene
	Two fluid phases	Hydrodesulfurization of gasoils and residues
		Hydrocracking
		Hydroprocessing
		Selective hydrogenation of acetylenic and dienic compounds in C_3-C_4 gasoline cuts
With heat exchange	Single fluid phase	Steam reforming of methane or naphtha
		Ammonia synthesis
		Methanol synthesis
		Oxidation syntheses:
		— phthalic anhydride
		— maleic anhydride
		— acrolein
		— acrylonitrile
		— ethylene oxide
		— formol
		Fischer-Tropsch synthesis
	Two fluid phases	Selective hydrogenation

Table 6.6 Examples of moving-bed processes.

Single fluid phase	Catalytic cracking
	Regenerative reforming
Two fluid phases	Hydrodesulfurization of residues

Table 6.7 Processes involving a catalyst in suspension.

Implementation		**Process**
Mechanical agitation	Batch	Liquid-phase hydrogenation:
		— vegetable oils
		— fatty nitriles
		— adiponitrile
		— nitrated derivatives
	Continuous	Fischer-Tropsch synthesis
		Hydrogenation of benzene
		Hydrogenation of vegetable oils
Fluidized bed	Single gas phase	Catalytic cracking
		Oxychlorination of ethylene
		Maleic anhydride
		Aniline synthesis
		Acrylonitrile synthesis
		Fischer-Tropsch synthesis
	Two fluid phases	Hydrodesulfurization of residues
		Hydrocracking
Entrained catalyst	Gas phase	Catalytic cracking
		Fischer-Tropsch synthesis

Table 6.8 Frequency of use of various solid catalyst technologies.

Frequency of use	Method of operation				Heat exchange		Fluid phases	
	Batch	Continuous			Without (adiabatic)	With	One G or L	Two G + L
		Tubular	CSTR	Multistage				
Fixed bed	+	+ + +	+	+	+ + +	++	G + + + L +	+ + +
Moving bed	−	++	−	−	++	+	G ++ L +	+
Catalyst in suspension Mechanically agitated bed	++	−	++	+	+	++	G + L ++	++
Fluidized bed	−	−	++	+	++	++	G ++ L +	++
Entrained catalyst	−	++	−	−	++	+	G ++ L +	+

+ + +: Preferred implementation.
++ : Frequently encountered implementation.
+ : Possible but uncommon implementation.
− : Not applicable.

REFERENCES

Cybulski A, Moulijn JA (1994) Monoliths in Heterogeneous Catalysis. Catal Rev Sci Eng 36(2), pp 179–270.

Krishna R, Wesselingh JA (1997) The Maxwell-Stephan approach to mass transfer. Chem Eng Sci 52, 6, pp 861–911.

Le Page JF (1987) Applied Heterogeneous Catalysis. Design. Manufacture. Use of Solid Catalysts. Editions Technip, Paris.

Levenspiel O (1999) Chemical Reaction Engineering (third edition). John Wiley and Sons, New York.

Mears DE (1971) Diagnostic Criteria for Heat Transport Limitations in Fixed Bed Reactors. J Catalysis 20, pp 127–131.

Reid RC, Prausnitz JM, Poling BE (1987) The Properties of Gases and Liquids (fourth Edition). McGraw-Hill, New York.

Satterfield CN (1981) Mass Transfer in Heterogeneous Catalysis. R E. Krieger Pub. Company. New York.

Voorhies A (1945) Ind Eng Chem 38, p 318.

Weekman VW, Gorring RI (1965) J. Catalysis 4, p 260.

Wijngaarden RJ, Kronberg A, Westerterp KR (1998) Industrial Catalysis: Optimizing Catalysts and Processes. Wiley-VCH.

NOMENCLATURE

(specific to Chapter 6)

Symbol	Definition	SI unit
a_i	Ratio of number of particles of size $\leqslant t_i$ to the total number of particles	–
a	Relative activity: current rate/initial rate	–
Bi_m	Mass Biot number: $k_{i,S}L/\mathcal{D}_{ie}$	–
Bi_c	Thermal Biot number: hL/λ_e	–
$\overline{d_i}$	Mean particle diameter: $6\Sigma V/\Sigma S$	m
$\overline{d_2}$	Mean particle diameter: $\sqrt[3]{6\Sigma V/\pi n}$	m
$\overline{d_3}$	Mean particle diameter: $\sqrt[2]{\Sigma S/\pi n}$	m
D	Diameter of a cylindrical pellet	m
$\mathcal{D}_{ik}$	Knudsen coefficient of diffusion of compound A_i	m^2/s
$\mathcal{D}_{im}$	Molecular coefficient of diffusion of compound A_i	m^2/s
$\mathcal{D}_{ic}$	Effective coefficient of diffusion	m^2/s
d_p	Particle diameter	m
$\mathbf{E}$	Global effectiveness of a particle	–
F	Ratio of reaction rates, with and without deactivation	–

Symbol	Definition	SI unit
h	Coefficient of heat transfer	$W/K \cdot m^2$
H	Height of a cylindrical pellet	m
k_S	Rate constant with respect to the catalyst surface	variable
k_M	Rate constant with respect to the catalyst mass	variable
K_i	Overall transfer coefficient	m/s
$k_{i,S}$	Fluid film-solid transfer coefficient	m/s
k_d	Deactivation rate constant	s^{-1}
$\bar{l}$	Mean pore length	m
p	Number of pores per unit mass	–
L	Thickness of a plate	m
n	Number of grains per unit volume of reactor	–
m	$m = \dfrac{\nu_{1,1} k_{1M}}{\nu_{2,2} k_{2M}}$	–
R	Radius of a spherical particle	m
$\bar{r}$	Mean pore radius	m
r'_M	Rate of reaction with solid catalyst (with respect to the mass)	$mol/(kg \cdot s)$
r'_S	Rate of reaction with solid catalyst (with respect to the surface area)	$mol/(m^2 \cdot s)$
t_i	Particle size	m
$\bar{t}_i$	Mean size of a class of particles	m
w	Volume change modulus	–
x_i	Ratio of the mass of particles of size $\leqslant \bar{t}_i$ to the total mass of particles	–
z	Distance in a particle measured from the center	m
β_1	Prater number $\beta_1 = \dfrac{C_{1,S}(-\Delta H_R)\mathcal{D}_{1e}}{\lambda_e T_S}$	–
β_2	Arrhenius number $\beta_2 = \dfrac{E}{RT_S}$	–
η_V	Effectiveness factor for a non-isochorous reaction	–
θ	Porosity of a particle	–
λ_e	Effective heat conductivity of a particle	$W/(m \cdot K)$
ρ_c	Density of a mass of particles	kg/m^3
ρ_p	Density of a particle	kg/m^3
ρ_S	Density of the solid constituting the particle	kg/m^3
τ	Tortuosity	–
Φ	Thiele modulus: $\Phi = R\sqrt{\dfrac{-\nu_1 \rho_p k_M}{\mathcal{D}_{1e}}}$	–
Φ'	Thiele modulus: $\Phi' = L\sqrt{\dfrac{-\nu_1 \rho_p k_M}{\mathcal{D}_{1e}}}$	–
ΣS	Total external surface of n particles contained in a unit volume	m^2
ΣV	Total volume of n particles contained in a unit volume	m^3

Copyrighted Materials
Copyright © 2004 Editions Technip Retrieved from www.knovel.com

7 Reactors Employing a Fluid Phase and a Catalytic Solid Phase: Fixed Bed, Moving Bed, Fluidized Bed

7.1 INTRODUCTION

In this chapter we examine reactors employing both a fluid phase and a solid with catalytic properties. These include:

- 7.2: Fixed-bed catalytic reactors
- 7.3: Moving-bed catalytic reactors
- 7.4: Fluidized-bed catalytic reactors.

In fixed-bed reactors the catalyst particles are arranged in a vessel, generally a vertical cylinder, with the flux of reactants and products passing through the stationary bed.

In moving-bed reactors the bed can be removed either continuously or periodically in portions. Fluid circulation is similar to that in a fixed bed.

In fluidized-bed reactors the catalytic solid is present in the form of fine particles that are maintained in suspension by the upward flow of fluid.

There are a number of implementations of the three principal reactor types, as discussed in Chapter 6. As we will see later on, fixed-bed and moving-bed reactors present many of the characteristics of plug-flow reactors, while fluidized-bed reactors most resemble the CSTR model.

7.2 FIXED-BED CATALYTIC REACTORS

7.2.1 Writing the mass balance equations

Designing a fixed-bed catalytic reactor is similar to that of a single-phase reactor: mass and enthalpy balances are established for an elementary volume of bed. We saw, however, that in

heterogeneous catalysis the intrinsic reaction rates are ordinarily expressed either by unit of catalyst surface or by mass unit of catalyst. Therefore, these must be related to a unit volume of bed. Additionally, internal and external diffusion limitations can play a role. We will examine the simple case of a first-order reaction that is isothermal, isobaric, and isochoric, the fluid carrying the reactants and removing the products. A steady-state situation like the one shown in Fig. 7.1 is assumed.

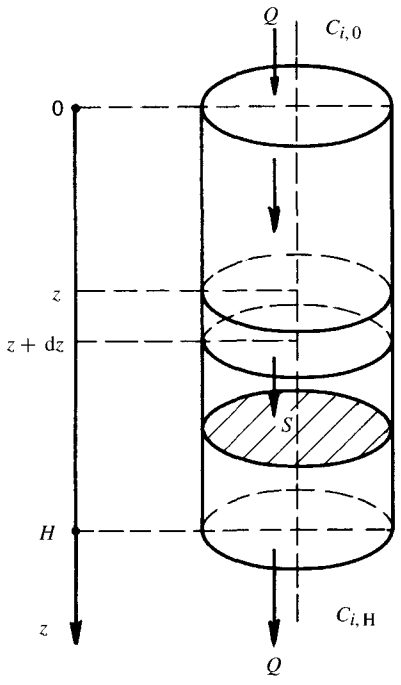


Figure 7.1 Fixed-bed catalytic reactor. Mass balance for a slice of thickness dz.

We will initially assume that flow is plug-type, which enables us to write, for an element of volume of reactor dV ($= S\,dz$), a mass balance for a compound A_i:

$$(F_i)_z - (F_i)_{z+dz} - K_i \mathcal{A}_S C_{i,z} S\,dz = 0$$

or:

$$(QC_i)_z - (QC_i)_{z+dz} - K_i \mathcal{A}_S C_{i,z} S\,dz = 0 \tag{7.1a}$$

where

Q volumetric flow rate of the fluid (here assumed constant throughout the bed)
$C_{i,z}$ concentration of compound A_i in the fluid at point z
$\mathcal{A}_S$ external surface area of grains per unit volume of bed
S cross-sectional area of bed

z length of the bed measured from the reactor inlet

K_i apparent rate constant for the disappearance or appearance of compound A_i, which takes into account the chemical kinetics as well as internal and external diffusion, as defined in Chapter 6 (Eq. 6.62).

Note: The molar balance relative to a reactant A_i can be expressed in two ways:

1. According to Eq. (7.1a), by using the apparent rate constant K_1:

$$QC_{i,z} - Q\left(C_{i,z} + \frac{dC_{i,z}}{dz}\,dz\right) - K_i \mathcal{A}_S C_{i,z} S\,dz = 0 \tag{7.1b}$$

2. By using the global effectiveness **E**:

$$QC_{i,z} - Q\left(C_{i,z} + \frac{dC_{i,z}}{dz}\,dz\right) + \nu_1 k_M \rho_c \mathbf{E} C_{i,z} S\,dz = 0 \tag{7.1c}$$

Naturally, the two modes of expression are equivalent, since $\mathbf{E} = \mathcal{A}_S K_1/(-\nu_1 k_M \rho_c)$ (see Eq. 6.65).

For the simple case of a first-order reaction, which is examined here, integration along the length of the bed is immediate, and we obtain:

$$C_{i,H} = C_{i,0} \exp\left\{\frac{-K_i \mathcal{A}_S S H}{Q}\right\} = C_{i,0} \exp\left\{\frac{-K_i \mathcal{A}_S V}{Q}\right\} \tag{7.2}$$

where

$C_{i,0}$ concentration of constituent A_i at the reactor inlet

$C_{i,H}$ outlet concentration.

In other cases, if the equation for the rate of reaction is more complex, step-by-step numerical integration is required.

Equation (7.2) introduces the parameter V/Q, which has the dimension of time, sometimes incorrectly referred to as "contact time". V/Q is more commonly referred to as the space velocity or VVH. To avoid ambiguity in the definitions, they should, strictly speaking, be applied to the actual mean conditions of pressure and temperature prevalent in the reactor slice under consideration. For the sake of convenience, the inlet conditions are often used to express Q. Obviously the balance Eq. (7.1a) refers to the actual conditions at every point in the reactor.

Sometimes VVH is replaced with PPH: the weight flow rate of feed with respect to the weight of the bed. The equation relating VVH to PPH is written:

$$\text{PPH} = \frac{\text{VVH}\rho_F}{\rho_c}$$

where

ρ_F density of the fluid when conditions are identical to those prevailing for the definition of VVH

ρ_c density of the bed.

Since:

$$\mathcal{A}_S = \frac{6\varepsilon_p}{\overline{d_p}} = \frac{6\rho_c}{\overline{d_p}\rho_p}$$

we have:

$$\frac{C_{i,H}}{C_{i,0}} = \exp\left\{\frac{-K_i\mathcal{A}_S}{VVH}\right\} = \exp\left\{\frac{-6K_i\rho_F}{PPH\overline{d_p}\rho_p}\right\} \tag{7.3}$$

where the space velocity VVH and ρ_F are expressed for actual mean conditions.

Obviously, for reactions that are not first order or are not isochorous, isobaric, or isothermal, each local situation corresponding to successive steps of the integration must be taken into account throughout the length of the reactor. We must then determine, through numerical integration, either the volume of the bed needed to realize a desired conversion or the conversion obtained for a reactor of a given volume.

The differential equations applicable in this case are written, for the mass balance:

$$Q_V C_{i,V} - Q_{V+dV}\left(C_{i,V} + \frac{dC_{i,V}}{dV}\,dV\right) + \nu_i \mathbf{E} r'_M \rho_c\,dV = 0$$

If the volumetric flow rate Q_V can be considered constant and equal to Q:

$$-Q\frac{dC_i}{dV} = -\nu_i \mathbf{E} \cdot r'_M \rho_c \tag{7.4}$$

r'_M is expressed as a function of the concentrations within the fluid.

For the heat balance:

$$Q_V \rho_F C_{PM}(T - T_{ref}) - Q_{V+dV}\rho_F C_{PM}\left(T + \frac{dT}{dV}\,dV - T_{ref}\right) + (-\Delta H_R)\, r'_M \rho_c\,dV + q\,dV = 0$$

and, if $Q_V = Q$:

$$Q\rho_F C_{PM}\frac{dT}{dV} = (-\Delta H_R)\, r'_M \rho_c + q \tag{7.5}$$

(Recall that q is the heat supplied to the system per unit volume of bed and unit of time.)

Note that these procedures can be used to determine the volume of the bed or the mass of catalyst to use, but not the shape of the bed. This question will be discussed below.

7.2.2 Designing the catalytic bed

Once the volume or mass of the bed has been determined, the reactor dimensions (height and diameter) must be specified. For this, as with homogeneous reactors, flow phenomena must be taken into consideration. Plug flow is generally recommended to eliminate backmixing, bypass, and stagnant zones in the reactor. In the case of fixed-bed reactors, where only a single fluid-phase circulates (the case under consideration here), this is fairly easy to bring about.

In Chapter 2 we showed that backmixing in a chemical reactor can be accounted for by making use of the concept of turbulent diffusion. We also indicated that plug flow was the ideal model, in which axial diffusivity is considered zero and radial diffusivity infinite. The real case could therefore be described by means of equations that introduce these diffusion phenomena, such as Eq. (7.6), which establishes the molar balance for a compound A_i in a cylindrical reactor:

$$\frac{\partial C_i}{\partial t} - \mathcal{D}_A \frac{\partial^2 C_i}{\partial z^2} - \mathcal{D}_R \left(\frac{\partial^2 C_i}{\partial r^2} + \frac{1}{r} \frac{\partial C_i}{\partial r} \right) + \frac{Q}{S} \frac{\partial C_i}{\partial z} - \mathcal{R}'_{Mi} \rho_c = 0 \tag{7.6}$$

where

$\mathcal{R}'_{Mi}$ observed rate of appearance or disappearance of compound A_i, in mol/kg of catalyst · s

$\frac{Q}{S} \frac{\partial C_i}{\partial z}$ term for forced convection, where $Q/S = V_{SF}$ (superficial velocity of the fluid)

$\mathcal{D}_A \frac{\partial^2 C_i}{\partial z^2}$ term for axial turbulent diffusion

$\mathcal{D}_R \left(\frac{\partial^2 C_i}{\partial r^2} + \frac{1}{r} \frac{\partial C_i}{\partial r} \right)$ term for radial turbulent diffusion

$\frac{\partial C_i}{\partial t}$ accumulation term, which vanishes under steady-state conditions.

The generally accepted boundary conditions are:

- at the reactor inlet ($z = 0$):

$$(C_i)_{z=0} = C_{i,0} + \frac{\mathcal{D}_A}{V_{SF}} \left[\frac{\partial C_i}{\partial z} \right]_{z=0}$$

  This condition indicates a concentration discontinuity at the reactor inlet, which is more pronounced with higher values of $\mathcal{D}_A$:
  - $C_{i,0}$ corresponds to the concentration immediately before the inlet
  - $(C_i)_{z=0}$ corresponds to the concentration immediately after the inlet
- at the reactor outlet ($z = L$): $\partial C_i / \partial z = 0$
- along the reactor axis ($r = 0$): $\partial C_i / \partial r = 0$ because of symmetry
- along the periphery of the reactor ($r = R$): $\partial C_i / \partial r = 0$ because of the inability to cross the boundary formed by the wall of the reactor
- after the steady-state regime has been established: $\partial C_i / \partial t = 0$.

By using a dimensionless form for the previous mass balance equation and introducing a characteristic length, such as the mean diameter $\overline{d_p}$ of catalyst grains, we can define:

- a dimensionless number known as the axial mass Peclet number:

$$Pe_{ma} = \frac{\overline{d_p} V_{SF}}{\mathcal{D}_A} \tag{7.7}$$

- a dimensionless number known as the radial mass Peclet number:

$$Pe_{mr} = \frac{\overline{d_p} V_{SF}}{\mathcal{D}_R} \tag{7.8}$$

- two geometric ratios:
  - n: ratio of the reactor height to the mean grain diameter
  - m: ratio of the reactor diameter to the mean grain diameter.

With respect to the numerical values of the Peclet numbers, the specialized literature contains correlations, $Pe = f(Re)$, for each type of reactor, where:

$$Re = \frac{\overline{d_p} V_{SF} \rho_F}{\mu_F}$$

This enables us to account for turbulent diffusion phenomena. For gases, once Re reaches 10, Pe_{ma} tends to a limit value close to 2; for liquids, the Reynolds number must approach 10^3 before Pe_{ma} tends toward 2 (Fig. 7.2). From this we can estimate $\mathcal{D}_A$. Under the same conditions Pe_{mr} tends toward a value near 10, which can be used to determine $\mathcal{D}_R$. The values of Re indicated are often achieved. Note that Pe_{mr} is appreciably higher than Pe_{ma}, which corresponds to a situation where $\mathcal{D}_A$ is greater than $\mathcal{D}_R$. This means that if there is poor distribution of reactants at the reactor inlet, there is no guarantee of uniform composition in a cross-section of the reactor. An estimate of the coefficients $\mathcal{D}_A$ and $\mathcal{D}_R$ can be used to determine, to a reasonable approximation, the deviation from plug flow.

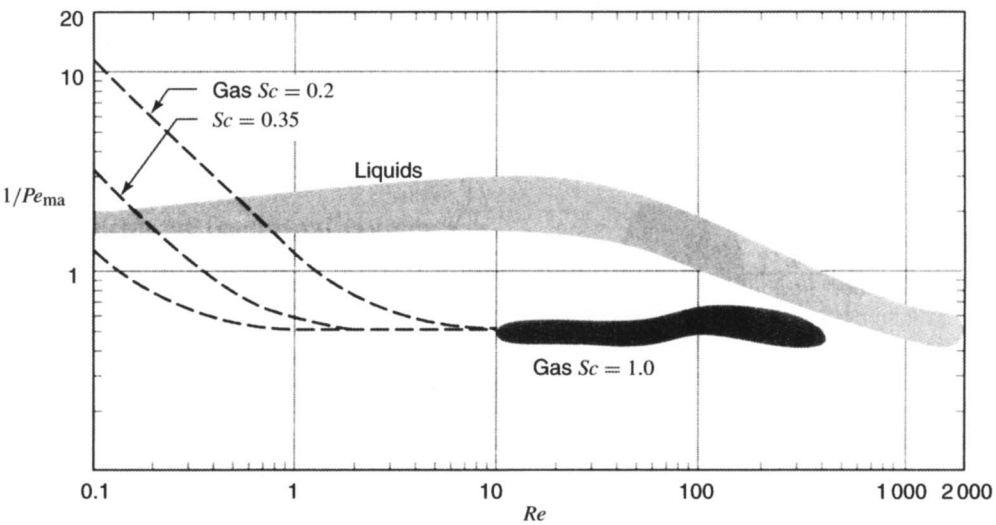


Figure 7.2 Variation of the reciprocal of Pe_{ma} with the Reynolds number in a fixed bed [after Levenspiel, 1999].

The assumption of plug-flow behavior can be more immediately verified by referring to the previously examined homogeneous reactor. We saw earlier that the dimensionless group $\mathcal{D}_A/V_{SF}L$ must be less than 10^{-2}. By making use of the limit value of the axial mass Peclet number $V_{SF}\overline{d_p}/\mathcal{D}_A = 2$, we see that the ratio of reactor length to the diameter of the grains must be greater than 50:

$$\frac{L}{\overline{d_p}} > 50$$

This condition, which is easily realized in the majority of industrial reactors (with the exception of catalytic gauze pad reactors such as those used for the oxidation of ammonia), must be taken into account when designing small pilot or laboratory reactors.

As for the radial distribution, particular care must be taken when introducing reactants into the catalytic bed.

The reactants must first be mixed correctly before entering the bed, for the values of radial diffusivity are such that satisfactory mixing of the reactants generally does not take place throughout the entire diameter of the bed. The use of ring-shaped particles can significantly increase radial mixing, however.

Once the reactants are mixed (for a single-phase system this presents no particular problems when static mixers, for example, are used) fluid flow occurs without difficulty.

It is generally considered that the risk of bypass is reduced with the increase in pressure drop per unit length of bed caused by the passage of fluid. In practice the threshold is often established at around 2 500 Pa/m, which is frequently achieved without any special care in conventional situations.

Generally, an n/m ratio (height of bed/diameter of bed) greater than 0.5 is recommended. In small reactors, such as pilot units, a ratio m (diameter of bed/diameter of particles) greater than 20 is desirable to reduce wall effects.

7.2.3 Discussion concerning the validity of the criteria used

The criteria used in the above paragraph should not be considered definitive. Consider the following:

- If care is taken when mixing the reactants at the inlet, the catalytic bed itself behaves as an excellent fluid distributor, providing the catalyst particles and the voids between the grains are regularly distributed (dense loading).
- The current trend in the design of some reactors (catalytic reforming, postcombustion) is to maintain low pressure drop. Consequently, there is increasing use of catalytic beds with radial circulation or beds that employ monolith catalysts.

Some radial reactors consist of beds whose thickness is only 20 to 30 cm and have low pressure drop of about 1 000 to 2 000 Pa. The catalyst particles are typically 1 to 3 mm. In these cases, the condition $L/\overline{d_p} > 50$ is by and large achieved. These beds are capable of high conversion rates (greater than 99%), which demonstrates that flow is completely satisfactory. In this case care must be taken to arrange the flow, distribution, and collection of fluids in the inlet and outlet zones: local pressure drop at these points must not interfere with uniform feedstock flow to the bed.

- Beds that make use of ion-exchange resins can be designed satisfactorily with height /diameter ratios below 0.5, providing that liquid is introduced through a large number of distributors uniformly arranged throughout the entire cross-section (strainers, for example).

It would seem, therefore, that flow problems are not critical in the design of fixed catalytic bed industrial reactors operating with a *single fluid phase*. By ensuring that the reactants

are fully mixed at the reactor inlet, a properly designed distributor will provide flow that is generally close to plug flow. An important special case is one in which heat transfer at the wall of the reactor becomes necessary. This leads to the establishment of a radial temperature gradient. This gradient will cause reaction rates that differ depending on the radial position in the reactor. This in turn will lead to radial concentration gradients. This phenomenon, associated with reaction thermicity, will be discussed in a subsequent section. It is the one factor that most frequently influences the design of catalytic beds.

7.2.4 Calculation of dynamic pressure drop in a catalytic reactor

7.2.4.1 Granular catalytic bed

Dynamic pressure drop across a granular bed can be estimated by means of the Ergun equation. The equation is dimensionally consistent:

$$\frac{\Delta P}{\Delta L} = A\frac{\varepsilon_p^2}{(1-\varepsilon_p)^3}\frac{\mu_F V_{SF}}{\overline{d_p}^2} + B\frac{\varepsilon_p}{(1-\varepsilon_p)^3}\frac{\rho_F V_{SF}^2}{\overline{d_p}} \tag{7.9}$$

where

ε_p volume fraction occupied by the solid
$(1-\varepsilon_p)$ void fraction of the bed.

For homogeneous beds, consisting of spherical particles of similar dimension, the coefficients A and B are:

$$A = 150,$$
$$B = 1.75$$

To adapt Ergun's equation to beds consisting of spheres of different diameter or non-spherical particles, laboratory measurement of the pressure drop can be used to determine the parameters A and B, and even the grouped parameters:

$$A\frac{\varepsilon_p^2}{(1-\varepsilon_p)^3}\frac{1}{\overline{d_p}^2} \quad \text{and} \quad B\frac{\varepsilon_p}{(1-\varepsilon_p)^3}\frac{1}{\overline{d_p}}$$

The measurement is taken in a tube whose diameter is such that $m = D/\overline{d_p}$ is greater than 10, using a gas of some kind (generally air). Ergun's equation remains valid for gases having different properties.

In the presence of a liquid, the coefficients A and B generally vary from one liquid to another. In this case it is recommended that A and B be determined from laboratory experiments in the presence of the catalyst being studied and the actual fluid; otherwise a fluid having at least the same density and viscosity should be used. In any event it is important to correctly evaluate ε_p since pressure drop is highly sensitive to this parameter.

If laboratory measurement is impossible, an estimate can always be made on the following basis:

- A bed of normally packed particles has a void fraction $(1-\varepsilon_p)$ that is generally between 0.38 and 0.42.
- When the catalyst is loaded, $(1-\varepsilon_p)$ is closer to 0.42.

After a certain period of operation, the void fraction tends toward 0.38, which often represents the maximum packing of the bed. The method of loading can influence the value of ε_p. This will be discussed below.

Finally, any possible fouling must be accounted for since this could further reduce $(1-\varepsilon_p)$, at least locally, and thus increase pressure drop.

With respect to the dimension $\overline{d_p}$ used in the Ergun equation, for particles of any kind:

$$\overline{d_p} = \frac{6\varepsilon_p}{\mathcal{A}_S} = 6\frac{\Sigma V}{\Sigma S}$$

For cylindrical particles pierced by one (ring) or more holes, the value of ε_p will certainly be decreased, which will lead to reduced pressure drop. For rings in which the ratio of external/internal radius is equal to κ, the value of ε_{CC} relative to a hollow cylinder is expressed by: $\varepsilon_{CC} = \varepsilon_{CP}\left((\kappa^2-1)/\kappa^2\right)$, where ε_{CP} is the volume fraction occupied by the solid cylinder. A similar calculation can be performed for cylinders with several holes.

7.2.4.2 Monolith catalysts

Flow in the channels of a monolith catalyst is most often laminar. Since the channels are generally short, an inlet effect corresponding to the development of the radial profile of the velocities complicates the problem somewhat. When evaluating pressure drop, a simple equation of the Hagen-Poiseuille type provides satisfactory results:

$$\Delta P = 32\frac{\mu_F V_{SF} L}{d_H^2} \tag{7.10}$$

where

d_H hydraulic diameter of the elementary channel

L length of the channels or thickness of the monolith.

Employing the notation introduced in Chapter 6, we can write:

$$d_H = M - e - 2\delta \tag{7.11}$$

7.2.5 Influence of external transfer in fixed-bed catalytic reactors

In the mass and enthalpy balance equations that describe the operation of a catalytic reactor, for the sake of accuracy, the terms for external mass and heat transfer should be introduced. This was discussed in Chapter 6. The constant K_i in Eq. (7.1a) takes these influences into account. The same is true for **E** in Eq. (7.4).

7.2.5.1 Balance equations

In the case of a fixed-bed catalytic reactor, the balance equations are written as follows for a first-order steady-state reaction at any point in the bed. See Fig. 7.3.

- For mass transfer:

$$k_{IS}\mathcal{A}_S(C_{i,F} - C_{i,S}) = -\nu_i r'_M \rho_c \eta \tag{7.12}$$

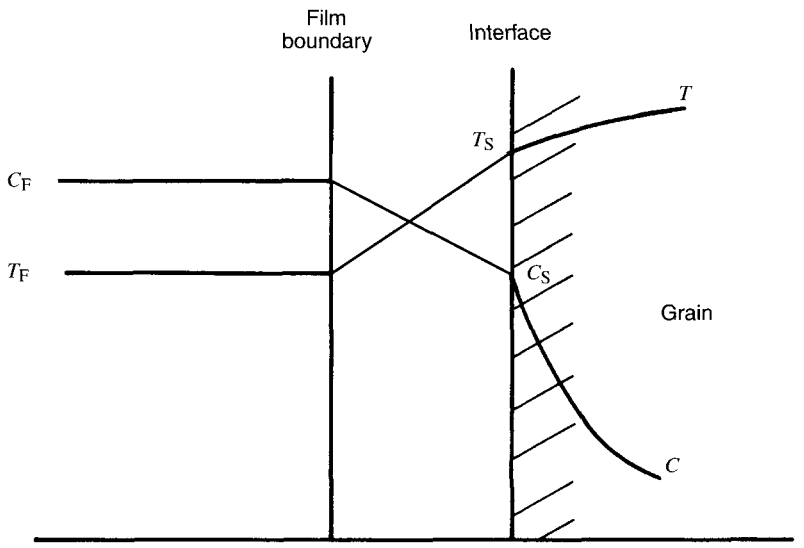


Figure 7.3 Temperature and concentration profiles in the fluid phase, in the film, and in the grain for an exothermic reaction (planar interfaces are shown).

where

r'_M	reaction rate (mol/kg s) at the external surface of the grain
ρ_c	density of the bed (kg/m^3 of bed)
$\nu_i r'_M \rho_c \eta$	actual rate of disappearance of reactant A_i (moles of A_i/m^3 of bed · s)
k_{lS}	coefficient of fluid-solid mass transfer (m/s)
$\mathcal{A}_S$	external surface area of grains per unit volume of bed (m^2/m^3).

If the constituent A_i is a reactant, $C_{i,F} - C_{i,S}$ is positive and $C_{i,F} > C_{i,S}$.

If the constituent A_i is a product, $C_{i,F} - C_{i,S}$ is negative and $C_{i,F} < C_{i,S}$.

- For heat transfer:

$$h_{FS}\mathcal{A}_S(T_F - T_S) = r'_M \eta \rho_c (\Delta H_R) \tag{7.13}$$

where

T_F	fluid temperature
T_S	surface temperature of the particles
ΔH_R	enthalpy change associated with the reaction $\sum \nu_i A_i = 0$.

If ΔH_R is negative, the reaction is exothermic, $T_F - T_S$ is negative and $T_S > T_F$.

If ΔH_R is positive, the reaction is endothermic, $T_F - T_S$ is positive and $T_S < T_F$.

These local balances give rise to a system of implicit equations that must be solved for every integration step throughout the length of the reactor. In the case of a sufficiently exothermic reaction, in order that $T_F - T_S$ not be negligible, the balance equations for a slice of thickness

dV are written:

$$\frac{dF_i}{dV} = \nu_i r'_M \eta \rho_c \qquad r'_M \text{ and } \eta \text{ vary with } V$$

$$\frac{dT_F}{dV} = \frac{r'_M \eta \rho_c \Delta H_R}{\sum F_i C_{Pi}}$$

where

$\sum F_i C_{Pi} = Q \rho_F C_{PM}$

Q volumetric flow rate of the fluid

C_{PM} specific heat of the fluid.

$$T_F = T_S + \frac{r'_M \eta \rho_c \Delta H_R}{h_{FS} \mathcal{A}_S}$$

$$C_{i,F} = C_{i,S} - \frac{\nu_i r'_M \eta \rho_c}{k_{iS} \mathcal{A}_S} \tag{7.14}$$

In order to use these expressions, estimates of the coefficients of mass and heat transfer are needed.

A. Bed of granular solid

To estimate the transfer coefficients between the circulating fluid and the catalyst grains, we have made use of the equations given by Satterfield [1981], which are shown in Table 7.1.

Based on the correlations shown in Table 7.1, k_{iS} and h_{FS} can be expressed. For example, for gases, when Re is between 3 and 2 000:

$$k_{iS} = \frac{0.36}{(1-\varepsilon_p)} \left(\frac{\mu_F}{\rho_F \mathcal{D}_{iF}} \right)^{-0.67} V_{SF} \left(\frac{\overline{d_p} V_{SF} \rho_F}{\mu_F} \right)^{-0.36}$$

that is:

$$k_{iS} = \frac{0.36}{(1-\varepsilon_p)} \mu_F^{-0.31} \rho_F^{0.31} \mathcal{D}_{i,F}^{0.67} \overline{d_p}^{-0.36} V_{SF}^{0.64}$$

and:

$$h_{FS} = \frac{0.43}{(1-\varepsilon_p)} \left(\frac{\overline{d_p} V_{SF} \rho_F}{\mu_F} \right)^{-0.36} \left(\frac{C_{PM} \mu_F}{\lambda_F} \right)^{-0.67} (C_{PM} \rho_F V_{SF})$$

that is:

$$h_{FS} = \frac{0.43}{(1-\varepsilon_p)} \mu_F^{-0.31} \rho_F^{0.64} \overline{d_p}^{-0.36} C_{PM}^{0.33} V_{SF}^{0.64} \lambda_F^{0.67}$$

The developments shown above can be used to determine the individual influence of each parameter.

Table 7.1 Correlations for mass and heat transfer between catalyst grains and the flowing fluid (fixed bed).

Correlation	Range of validity
$j_D = \frac{0.36}{(1-\varepsilon_p)Re^{0.36}}$	Gases: $3 < Re < 2\,000$
$j_D = \frac{0.25}{(1-\varepsilon_p)Re^{0.31}}$	Liquids: $55 < Re < 1\,500$
$j_D = \frac{1.1}{(1-\varepsilon_p)Re^{0.67}}$	Liquids: $0.0016 < Re < 55$
$j_H = 1.2 j_D$	Gases and liquids: $15 < Re < 1\,500$

where:

$$j_D = \frac{k_{iS}}{V_{SF}} Sc^{\frac{2}{3}}$$

$$j_H = \frac{h_{FS}}{C_{PM}\rho_F V_{SF}} Pr^{\frac{2}{3}}$$

$$Re = \frac{\overline{d_p} V_{SF}\rho_F}{\mu_F} \quad \text{Reynolds number}$$

$$Sc = \frac{\mu_F}{\rho_F \mathcal{D}_{iF}} \quad \text{Schmidt number}$$

$$Pr = \frac{C_{PM}\mu_F}{\lambda_F} \quad \text{Prandtl number}$$

B. Monolithic catalyst

Above we indicated that flow in the channels of a monolith is laminar and accompanied by an inlet effect. The correlations established for mass and heat transfer between the fluid and the wall take into account this inlet effect and have the following form:

$$Sh = C\left(1 + B\,Re\,Sc\frac{d_H}{L}\right)^{\alpha} \tag{7.15}$$

$$Nu = C\left(1 + B\,Re\,Pr\frac{d_H}{L}\right)^{\beta} \tag{7.16}$$

where:

$$Sh = \frac{k_{iS}}{\mathcal{D}_{im}} d_H \quad \text{Sherwood number}$$

$$Nu = \frac{h_{FS}}{\lambda_F} d_H \quad \text{Nusselt number}$$

B is a roughness factor, while C is the limit value used respectively for the Sherwood or Nusselt numbers when the flow regime has been completely established. Several numerical values have been proposed; here we make use of those established by Hawthorn, which are given by Cybulski and Moulijn [1994]:

$$\alpha = \beta = 0.45$$
$$B = 0.095$$
$$\text{and } C = 2.98 \text{ for a square channel.}$$

As indicated in Chapter 6, in fixed-bed catalytic reactors the influence of external transfer phenomena should be minimized. The importance of heat transfer and mass transfer in fixed beds is discussed below.

7.2.5.2 Grain-fluid heat transfer

A simple, steady-state, balance for a single reaction shows that the heat developed by the exothermic reaction within the grain and corresponding to the reactant flux must be equal to the heat flux from the grain to the fluid phase:

$$k_{iS}\left(C_{i,F} - C_{i,S}\right)\left(\frac{\Delta H_R}{-\nu_i}\right) = h_{FS}\left(T_F - T_S\right) \tag{7.17}$$

After development, this leads to:

$$T_S - T_F = \left(\frac{j_D}{j_H}\right)\left(\frac{Pr}{Sc}\right)^{\frac{2}{3}}\left(\frac{\Delta H_R C_{i,F,0}}{\nu_i \rho_F C_{PM}}\right)\left(\frac{C_{i,F} - C_{i,S}}{C_{i,F,0}}\right) \tag{7.18}$$

$\Delta H_R / -\nu_i$ heat of reaction corresponding to 1 mole of constituent A_i.

We recognize in the group $\left(\Delta H_R C_{i,F,0}\right) / \left(\nu_i \rho_F C_{PM}\right)$ the "adiabatic ΔT", an important characteristic in determining reactor stability (Chapter 2). The magnitude $\left(C_{i,F} - C_{i,S}\right)/C_{i,F,0}$ represents a relative concentration decrease between the fluid phase and the catalytic surface. In the complete absence of diffusion limitation for the mass flux, we have $C_{i,F} = C_{i,S}$ and $T_F = T_S$. If, on the contrary, the reaction is extremely fast, and therefore entirely controlled by mass transfer, $C_{i,S} = 0$ and $(T_F - T_S)$ can become very large.

j_D is of the same order of magnitude as j_H and, in the gas phase, $Pr \cong Sc$. We then have:

$$T_S - T_F \cong \left(\frac{\Delta H_R C_{i,F,0}}{\nu_i \rho_F C_{PM}}\right) = \Delta T_{\text{adiabatic}} \tag{7.19}$$

For example, this situation is often encountered in the regeneration of catalysts by combustion of carbon deposits.

In the case of liquids for which $Sc \gg Pr$ (factor of 100–1 000), the chances of seeing significant temperature differences are very small. The real risk in the liquid phase is the appearance of a boiling zone, heat transfer then occurring between solid and vapor, which is similar to the previous case. This can lead to the appearance of hot pockets, which are stable and difficult to eliminate. This problematic case will be discussed in greater detail in the following chapter.

7.2.6 Criteria for determining the possible influence of external mass transfer

Satterfield [1981] proposed a simple practical rule for detecting the possible influence of mass transfer: If, for a gaseous fluid phase, a bed height greater than $100\overline{d_p}$ is needed to achieve a conversion of 90% of the principal reactant, there is a strong chance that the reaction will not be limited by mass transfer. We will follow the reasoning that led Satterfield to the formulation of his rule but will modify it to obtain more realistic values. We saw that the molar balance of a reactant A_i led to Eq. (7.2), which is given again below:

$$C_{1,H} = C_{1,0} \exp\left\{\frac{-K_1 \mathcal{A}_S S H}{Q}\right\} \tag{7.20}$$

We can clarify the value of the global constant K_1, as shown in the previous chapter (Eq. 6.62):

$$\frac{1}{K_1} = \frac{1}{k_{1S}} + \frac{\mathcal{A}_S}{-\nu_1 k_M \eta \rho_c}$$

The above equation reflects the addition of two specific resistances, due respectively to mass transfer and to the chemical reaction in the catalyst particle.

In order for the influence of external mass transfer to be negligible, the value of k_{1S} must be much greater than that of the group $(-\nu_1 k_M \eta \rho_c)/\mathcal{A}_S$. If we assume a sufficiently large value for this ratio—50, for example, which implies that mass transfer will represent less than 2% of the overall resistance—we can write:

$$k_{1S} = 50\left(\frac{-\nu_1 k_M \eta \rho_c}{\mathcal{A}_S}\right) \quad \text{and therefore:} \quad K_1 = \frac{k_{1S}}{51}$$

Equation (7.20) can then be written:

$$\ln \frac{C_{1,0}}{C_{1,H}} = \frac{k_{iS}}{51} \mathcal{A}_S \frac{HS}{Q} = \frac{k_{1S}}{51} \mathcal{A}_S \frac{H}{V_{SF}} \tag{7.21}$$

Since we know that $\mathcal{A}_S$ can be estimated from $\mathcal{A}_S = 6\varepsilon_p/\overline{d_p}$, where ε_p is about 0.6, and:

$$\frac{k_{iS}}{V_{SF}} = j_D Sc^{-\frac{2}{3}} = \frac{0.36}{0.4} Re^{-0.36} Sc^{-0.67}$$

we obtain:

$$\ln \frac{C_{1,0}}{C_{1,H}} \cong \frac{0.064}{Re^{0.36} Sc^{0.67}} \frac{H}{\overline{d_p}} \tag{7.22}$$

Knowing that, for a gas, the Schmidt number is close to 1 under non-extreme conditions and that the order of magnitude of the Reynolds number is 100, we can write, for a conversion of 90%, that is: $C_{1,0}/C_{1,H} = 10$:

$$\frac{H}{\overline{d_p}} = 15.7\left(\ln \frac{C_{1,0}}{C_{1,H}}\right)(100^{0.36}) = 192$$

To obtain a conversion of 99%, the calculation leads to a value of $H/\overline{d_p}$ equal to 384.

This confirms Satterfield's rule ($H/\overline{d_p} > 100$) while making it more precise. For catalyst particles that have a mean diameter of 2 mm, a catalytic bed of 40 to 80 cm would be needed, depending on the target conversion. This constraint is not difficult to work with in an industrial setting. However, the constraint can become more difficult to maintain in small experimental laboratory reactors or pilot units.

If the fluid phase is a liquid, the situation is different. Here, under these same conditions, the Schmidt number is in the neighborhood of 10^4. In this case we obtain, for $C_{1,0}/C_{1,H} = 10$, a limit value of $H/\overline{d_p}$ that is very high, approximately 10^4: $H/\overline{d_p} > 10^4$. As a result of this high value, it is much more difficult to escape the influence of external diffusion phenomena when the fluid phase is a liquid.

7.2.7 Heat transfer at the reactor wall

As long as the adiabatic increase (or decrease) in temperature remains reasonable, it is generally preferable to operate industrial reactors adiabatically. To restrict temperature differences between the reactor inlet and outlet to values generally below 50°C, the catalyst zone is often divided into several beds. Between these beds heat exchange zones are arranged, where it is possible to introduce fresh reactant or recycled effluent for temperature control. Whenever this approach is feasible, it generally results in simple units that are easy to operate.

For some highly exo-(or endo-)thermic reactions, an adiabatic design is nearly impossible. In these cases heat must be removed from (or supplied to) the catalyst zone itself. In the case of a fixed bed, the elimination or supply of heat will be accompanied by a radial temperature gradient in the bed. This gradient, together with the axial temperature gradient, can be described by introducing terms for thermal diffusivity, as with concentration gradients. The enthalpy balance equation would then include:

- an axial heat Peclet number that contains an axial effective thermal conductivity
- a radial heat Peclet number that contains a radial effective thermal conductivity
- a coefficient of heat transfer at the wall.

Aside from the fact that there is little experimental data on effective thermal conductivity, the introduction of heat exchange at the wall complicates writing the balance and integrating the corresponding equation. For this reason we have chosen to address the problem on a global level by making use of film theory applied to granular beds.

A radial thermal conductivity that is not infinite (the values are approximately 1 to 2 $W/m \cdot K$), creates a continuous temperature gradient along a radius of the bed. In applying film theory to the case that interests us, the continuous temperature gradient of the fluid between the bed core and the wall is replaced by a gradient concentrated in a film near the wall. We assume that the temperature along the radius is appreciably uniform and represents the mean temperature of the bed, except for the immediate vicinity of the wall, where a linear temperature gradient between T_r and T_{pi} is considered, where

T_r mean temperature of the fluid

T_{pi} fluid temperature at the wall, on the bed side.

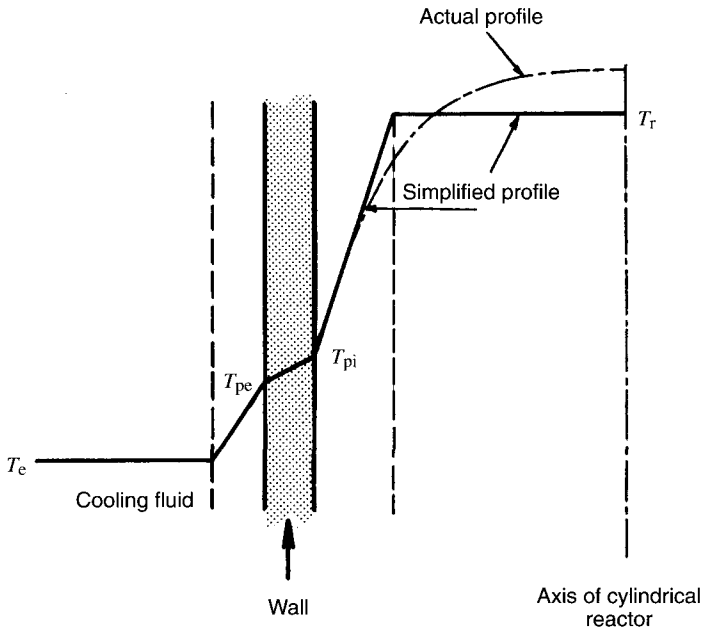


Figure 7.4 Film theory applied to the case of heat transfer at the wall for granular beds.

Figure 7.4 illustrates the realized transposition. In this representation, the enthalpy balance for a cylindrical slice of thickness dz can be written in simplified form:

$$p\frac{\pi d_t^2}{4}\,dz = \rho_F V_{SF}\frac{\pi d_t^2}{4}C_{PM}\frac{dT_r}{dz}\,dz + \pi d_t U\,(T_r - T_e)\,dz \tag{7.23}$$

where

- p rate of heat generation under mean temperature T_r and concentration conditions at a distance z from the reactor inlet (W/m^3)
- d_t reactor diameter (m)
- ρ_F fluid density for $T = T_r$ (kg/m^3)
- V_{SF} superficial velocity of the fluid for $T = T_r$ ($m^3/m^2 \cdot s$)
- C_{PM} specific heat of the fluid for $T = T_r$ ($J/kg \cdot K$)
- T_e temperature of the cooling fluid (K)
- U global coefficient of heat transfer at the wall ($W/m^2 \cdot K$)
- G $\rho_F V_{SF}$, mass flow rate of the fluid per unit cross-section ($kg/m^2 \cdot s$) (independent of the conditions of temperature and pressure).

Equation (7.23) can be written:

$$p = GC_{PM}\frac{dT_r}{dz} + \frac{4}{d_t}U\,(T_r - T_e) \tag{7.24}$$

Note that the enthalpy balances are written for the fluid phase without reference to the local temperature of the catalyst grains, which, as we saw earlier, can be appreciably different from that of the surrounding fluid. This has no effect in a system that has reached a steady state.

As noted, the temperature differences between the grain and the fluid are governed by the correlation for j_H, which was introduced earlier (Table 7.1).

The global coefficient of heat transfer is defined by the equation:

$$\frac{1}{U} = \frac{1}{h_L} + \frac{e}{\lambda}\frac{A_L}{A_m} + \frac{1}{h_e}\frac{A_L}{A_e} \tag{7.25}$$

where

h_L film coefficient of transfer, on the bed side ($W/m^2 \cdot K$)

h_e film coefficient of transfer, on the exchange fluid side ($W/m^2 \cdot K$)

e thickness of the wall of the pipe (m)

λ thermal conductivity of the pipe material ($W/m \cdot K$)

A_L exchange surface area measured on the bed side (m^2)

A_e exchange surface area measured on the cooling fluid side (m^2)

A_m logarithmic mean between A_L and A_e (m^2).

If the wall is sufficiently thin and the material sufficiently conductive, the term containing e/λ can be eliminated and $A_L \cong A_e \cong A_m$. Therefore:

$$\frac{1}{U} = \frac{1}{h_L} + \frac{1}{h_e}$$

The overall resistance to heat transfer consists of the two film resistances.

The transfer coefficient h_e is a conventional coefficient whose numerical value depends on the flow conditions of the cooling fluid (the values are approximately 150 $W/m^2 \cdot K$). h_L can be estimated, for example, by means of a correlation given in Perry and Green [1984]:

$$\frac{h_L d_t}{\lambda_F} = 1.22\left(\frac{\overline{d_p}G}{\mu_F}\right)^{0.83}\left(\frac{C_{PF}\mu_F}{\lambda_F}\right)d_t^{0.17} \tag{7.26}$$

where

λ_F thermal conductivity of the fluid for the film conditions

d_t diameter of the reactor tube

$\overline{d_p}$ mean equivalent diameter of the particle.

The thermal balance (7.24) can be used to evaluate the difference $(T_r - T_e)$ for a given T_e and d_t. In practice it is not realistic to use tubes whose diameter is greater than 60 mm in order to avoid the formation of unacceptable radial gradients. This leads, as a consequence, to the design of multitubular reactors. This type of reactor is easy to scale up: the pilot unit comprises a single tube that is operated under representative conditions, and the

scaled-up reactor consists of the juxtaposition of several hundred, if not thousands, of tubes in parallel.

7.2.8 Thermal stability of fixed-bed catalytic reactors

Fixed-bed catalytic reactors are not exempt from the laws governing thermal stability. In particular, our comments in Chapter 2 regarding homogeneous batch reactors—which in fact apply to all plug-flow tubular reactors—can also be applied to fixed-bed catalytic reactors since the two can be directly compared.

Under these conditions it is possible to determine the thermal profile along a longitudinal axis of a fixed-bed reactor, whether adiabatic or non-adiabatic, and examine its behavior quantitatively as a function of the operating parameters (reactant concentration in the incoming flux, inlet temperature, temperature of the heat exchange fluid) and the thermal, thermodynamic, and kinetic characteristics of the chemical reaction that occurs. We will not, therefore, discuss this aspect of the problem. However, aside from what may be described as normal behavior, fixed-bed catalytic reactors are subject to several specific problems:

1. In the case of multitubular reactors, that is, when there is heat transfer to the wall, we often observe, even with small diameter tubes, hot zones at the center of the tubes or temperature variations among the tubes. The existence of such hot zones interferes with proper operation of the reactor. In fact they can even lead to deviations in the activity and/or selectivity, and occasionally to the complete and rapid destruction of the catalytic sites involved. This phenomenon arises from the formation of radial temperature gradients that are much larger than is the case with homogeneous reactors as a result of the low thermal conductivity of the bed and poor heat exchange at the wall.
2. Fixed-bed catalytic reactors, whether multitubular or adiabatic, present more significant risks of runaway reactions than single-phase tubular reactors, especially for gaseous reactant fluids. This results from the frequently high initiation temperature and the narrow spread between the minimum initiation temperature and the maximum allowable temperature. This phenomenon is related to the often high value of the activation energy. The significant thermicity (endo- or exo-) added to the high activation energy frequently makes operation of the reactor difficult.
3. In Chapter 6 we saw that the existence of internal and external temperature gradients at the grain could result in instability and cause any part of the bed to shift from a hot state to a cold state and vice versa, depending on the direction of thermal approach.

The existence of transient hot zones is a manifestation of this instability. The persistence of stationary hot zones is generally associated with defective fluid flow. When designing catalytic reactors in which there is a risk of thermal instability, it is advisable to:

- anticipate the possibility of rapidly introducing cold fluid into the reactor
- use oversize exchange surfaces
- limit the bed length between quench operations
- install a device for rapidly cutting off the reactant feed flow while protecting the catalyst
- incorporate a control system with a sufficient number of sensors arranged at critical points, without interfering with fluid flow.

7.2.9 Practical considerations

7.2.9.1 Adiabatic reactors

A. Axial flow

The simplest fixed-bed technology is the "axial-flow reactor" design, as shown in Fig. 6.14. The catalyst is arranged in a more or less thick layer in the cylindrical part of the reactor (Fig. 7.5). The reactants are mixed before their introduction into the reactor, which takes place by means of a tube with an external flange. The tubing penetrates the interior of the reactor and a distributor prevents a stream of fluid from striking the top of the particle bed.

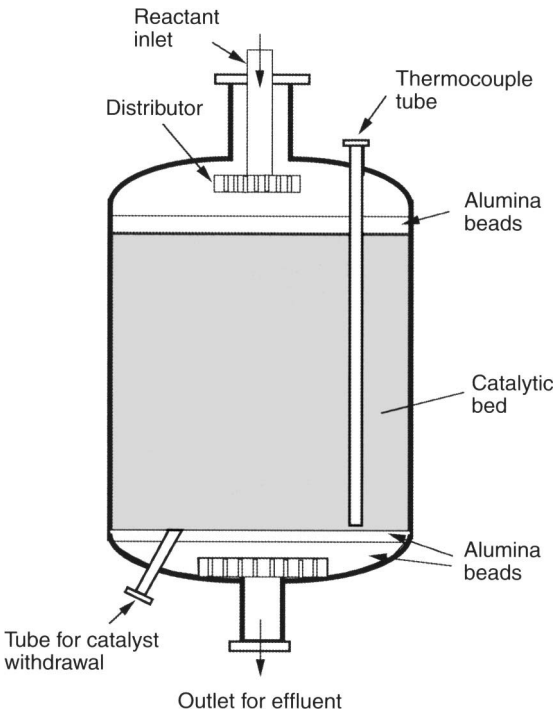


Figure 7.5 Adiabatic fixed-bed reactor with axial flow.

Any distribution problems can be overcome through the use of a layer of inert beads at the top of the bed. The use of metal filter baskets can help retain any solid particles (such as rust) entrained by the fluid entering the reactor. These reactors generally make use of downward flow, which avoids any expansion of the bed under conditions of high superficial velocity.

At the base of the reactor is an outlet collector for the reaction products as well as a tube for withdrawing the catalyst. The lower section of the reactor is filled with inert beads of alumina to avoid the need for a support grid for the catalyst layer. Generally, two sizes of alumina beads are superposed to reduce pressure drop.

The behavior of an adiabatic bed is well described by the set of differential Eqs. (7.4) and (7.5). Because of the exponential nature of the reaction rates as a function of temperature, the axial temperature profile is generally also exponential. Therefore, in a simplified calculation of the reactor design, we cannot use the axial mean temperature of the bed.

Additionally, for a temperature difference ΔT throughout the entire bed, we must make sure that the inlet temperature is sufficient for the reaction to begin. This is referred to as initiating a reaction. Consequently, the furnace or exchanger used to heat the reactants before they enter the reactor must be designed to ensure initiation regardless of conditions (deactivated catalyst, nonreactive feedstock, initial startup, etc.).

Adiabatic technology is even used for reactions whose thermicity is not negligible. The catalytic bed is then divided into several sections between which the temperature of the reaction fluid is readjusted. Within an **adiabatic** catalytic bed, the temperature T_F of the fluid changes along with the extent of the reaction ξ:

$$T_F - T_0 = \frac{\Delta H_R}{Q\rho_F C_{PM}}\xi$$

This change can be represented graphically as $\xi = f(T_F)$ (adiabatic conversion), which yields a straight line segment (AB, CD) (Fig. 7.6). In some cases the chemical reaction may be limited by thermodynamic equilibrium; thermal control is then used to shift the temperatures in the various sections of the catalytic bed into a region where the reaction rate is not too limited by the thermodynamics.

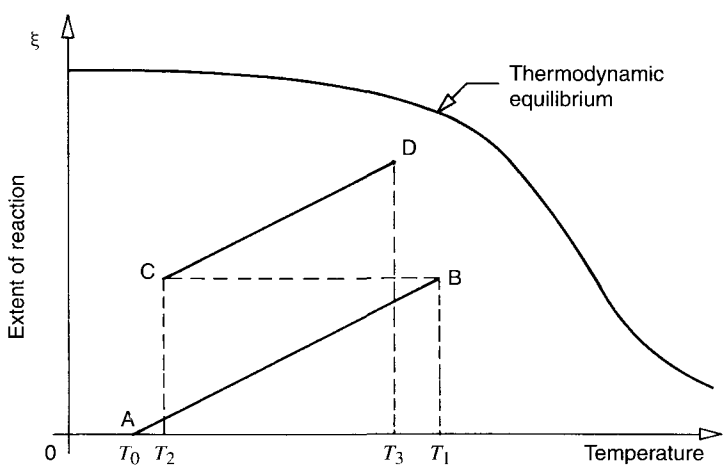


Figure 7.6 Concomitant changes in temperature and extent of reaction in an adiabatic fixed bed for a reversible reaction.

For an exothermic reaction the readjustment of the fluid temperature between catalyst sections can be accomplished either by heat exchange or by introducing a colder fluid. Both possibilities are shown in Fig. 6.17. The introduction of cold fluid can make use of a gas

or a liquid; preferably one of the reactants participating in the reaction is chosen. Thus, in the hydroprocessing of petroleum cuts (hydrocracking, hydrodesulfuration), the temperature inside the reactor is maintained within acceptable limits by introducing recycled hydrogen between the catalytic beds. On the other hand, when converting CO during the production of hydrogen, liquid water is introduced between the catalytic beds (Fig. 7.7B and 7.7C).

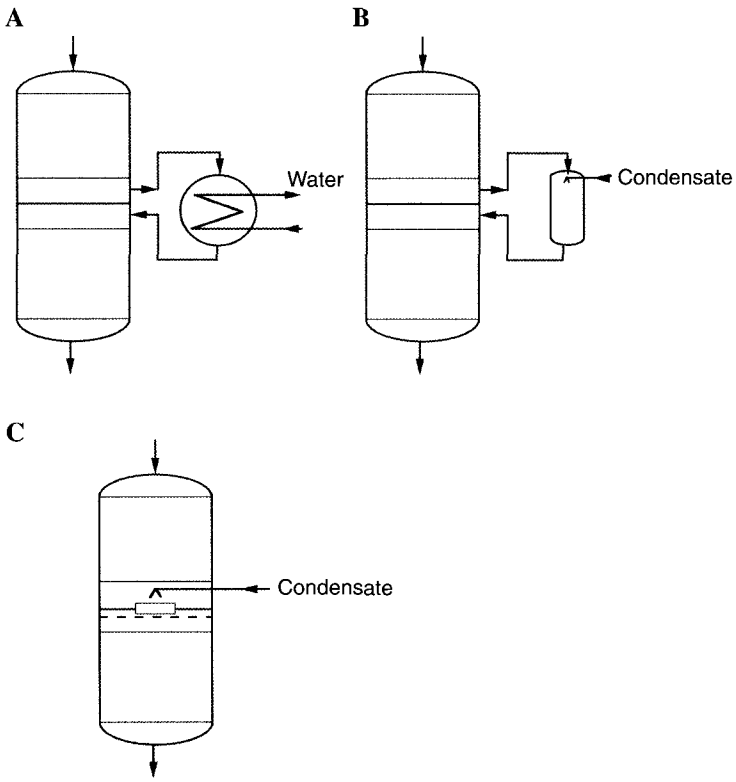


Figure 7.7 Different methods of controlling temperature in fixed-bed catalytic reactors: **A.** External heat exchanger. **B.** Introduction of condensate into an external inline mixer. **C.** Introduction of condensate into a reactor equipped with a mixing plate. Cases **B** and **C** can be applied to the conversion of CO in which water is one of the reactants.

The intermediate fluid quenching must be carried out with care: the quenching fluid coming from the exterior of the reactor and the fluid leaving a section of the catalytic bed must be correctly mixed in mixing chambers equipped with baffles, where the turbulence needed to mix them can be developed (Fig. 7.7).

With endothermic reactions, the fluid phase must be reheated between the catalytic beds. Depending on the operating temperature, heat exchangers or furnaces can be used. For example, in the catalytic reforming process three or four reactors are arranged in series, with a heating or reheating furnace before each reactor (photo 5).

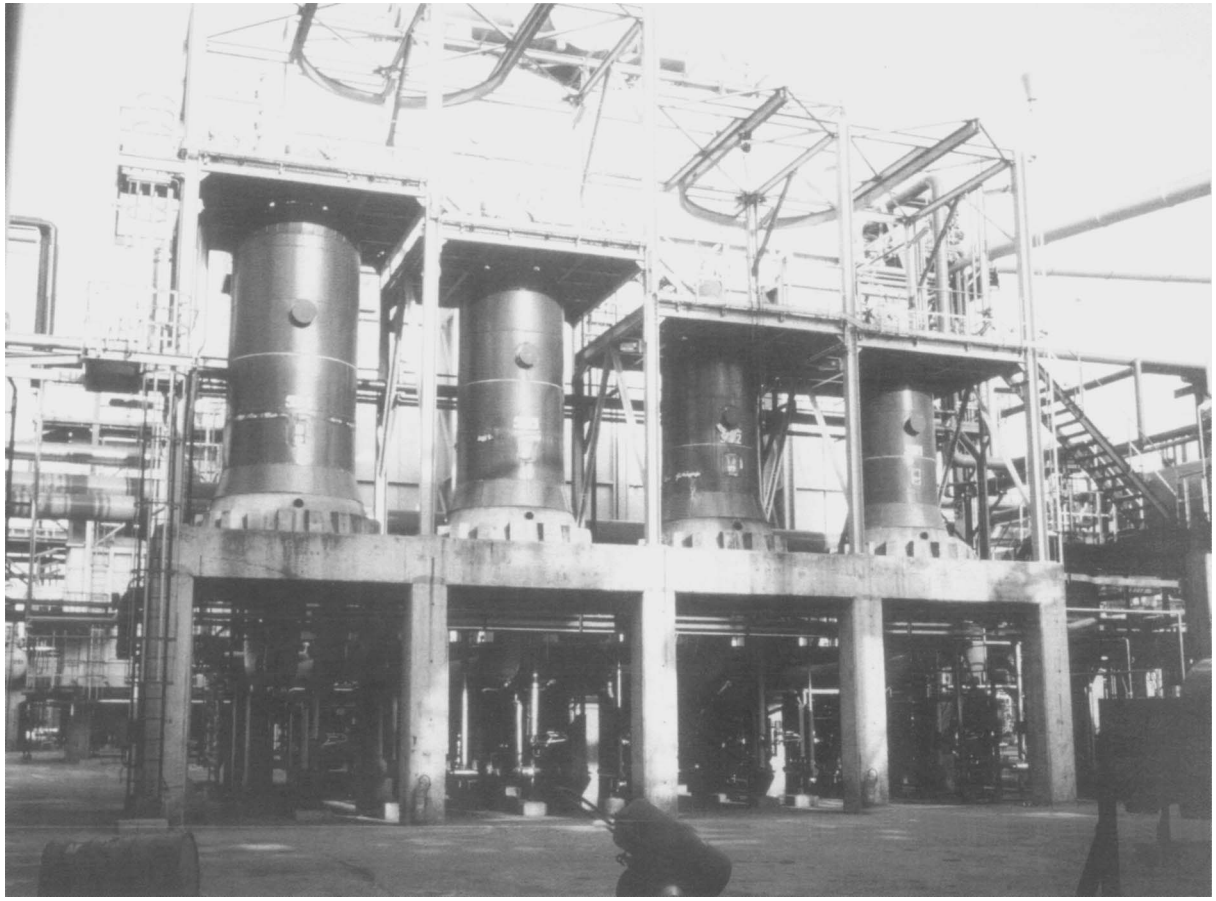


Photo 5 Fixed-bed catalytic reactors used for gasoline reforming. The photograph shows four reactors in series, whose size increases with the degree of conversion.

(*IFP Photo Library: Catalytic Reforming*).

The pressure drop in the fluid throughout the reactor can easily be calculated by multiplying the linear pressure drop (Eq. 7.9) by the height of the catalyst layer. When performing the calculation it is preferable to use average conditions in the bed for temperature and pressure as well as the molecular composition of the reaction fluid.

Earlier, we indicated that when the catalytic beds are being loaded, the void fraction $(1 - \varepsilon_p)$ is often in the neighborhood of 0.42. This fraction will decrease over time, finally reaching a value close to 0.38. Over the past 15 years loading systems have appeared that can be used to obtain an initial dense catalytic bed as soon as the reactor is started.

In these systems the catalyst particles are sprayed downward so that:

- Each particle is in a position of equilibrium before it is obstructed by other particles.
- The appearance of sloping catalyst piles that result in the segregation of the particles (the largest particles roll to the bottom of the pile) and preferential paths, which are always detrimental to optimum operation of the bed, are avoided.

Different systems (Arco, CFR, Catapac IFP) use rotating distributors to create a uniform particle spray. A similar result can be obtained by introducing the particles through a perforated plate, the perforations having diameters of 10 to 15 mm, depending on the size of the particles, and each hole covering approximately 150 cm^2 of bed.

The increase of ε_p can be significant (10 to 15%), especially for particles whose length is much greater than their diameter (extrudates, for example), and is accompanied by an increase in pressure drop (Eq. 7.9).

Dense loadings have significant advantages:

- the external void fraction is smaller and more homogeneous
- the reactor volume is used more efficiently and there is increased capacity for the chemical reaction
- bed structure does not change after the initial loading
- the distribution of fluid is more homogeneous and flow is closer to plug flow, which improves the conversion and selectivity for identical operating conditions.

Dimensioning

Above we indicated the different constraints involved in selecting a diameter-height combination for a catalytic bed, the volume being determined from the kinetics, depending on the desired conversion and the flow rate of the reaction fluid being transformed. Although the nature of the catalyst is determined, the size and shape of the grains may also be additional variables that need to be considered. Assume that the shape and size of the grains is imposed for various reasons, if only because of the manufacturing requirements for the catalyst. The problem can then be resolved by optimizing the economics of the catalytic reactor, taking into account the investment and operating expenses associated with:

- the reactor (I_R)
- the pump or compressor (I_{PC}) needed to overcome the pressure drop in the catalytic bed
- the catalyst (C_{cat}), with a life cycle of t_V (h)
- the additional energy consumed by the pump or compressor.

The economic function we want to minimize is then written as:

$$F_{eco} = (I_R + I_{PC}) \frac{t_V}{t_R} + C_{cat} + Q \cdot 3\,600 \frac{\Delta P}{\Delta L} H \cdot t_V \frac{C_{energy}}{R_{PC}} \tag{7.27}$$

where

t_R amortization period for the investment, expressed in hours
Q total flow rate of reaction fluid (m^3/s)
R_{PC} overall yield of the pump or compressor
C_{energy} cost of the energy used to operate the pump or compressor (US$/day)
H total height of the catalyst bed(s) (m).

The following simple relations hold among the variables in question:

$$H = \frac{4V}{\pi D^2} \qquad V_{SF} = \frac{4Q}{\pi D^2}$$

$$C_{cat} = V \cdot \text{price of catalyst (US\$/m}^3\text{)}$$

D is the internal diameter of the reactor (m) and V the volume of catalyst.

To calculate the height H_R of the reactor shell, a factor between 1.1 and 1.2 is applied to H to compensate for internal components (distributor, inert beads, support grid, etc.).

The investments I_R and I_{PC} are calculated conventionally as a function of the variables: D, H_R, P, and T for the reactor, and Q, suction and discharge pressures for a compressor or pump [Chauvel *et al.*, 1981]. Bear in mind that the cost of the reactor is appreciably proportional to its weight, which depends on D and H_R as well as the thickness. For pressure vessels the required thickness is proportional to the operating pressure and the diameter D. For high-pressure reactions, the term I_R will increase greatly if a low superficial velocity V_{SF} is used, implying a large diameter vessel.

The pressure drop depends on the properties of the fluid (ρ_F and μ_F) and the catalyst ($\overline{d_p}$ and ε_p), which are imposed, and increases with the superficial velocity V_{SF}.

The variable to be optimized will therefore be the superficial velocity V_{SF}, with which D and H_R can easily be calculated, An example of this type of calculation is given in Chapter 9 (Section 9.3.3) for a methanation reactor in a production line used to make synthesis gas for the production of ammonia.

It is useful to consider the various terms of the economic balance (Eq. 7.27) separately:

- The cost of the catalyst is often significant (between 4 and 30 US$/kg), but the volume V required varies little with V_{SF}; therefore it plays only a minor role in the optimization process once a choice has been made concerning the catalyst and grain size.
- The investment for the reactor I_R is often large, especially for high-pressure processes. Minimization of the cost of the reactor alone will lead to diameters that decrease as pressure increases and, consequently, to heights H_R that are often excessive.
- The additional investment I_{PC} required for the pump or compressor used to overcome pressure drop in the catalytic bed is generally low compared to I_R.
- The energy cost from pressure drop is often large and will increase rapidly as V_{SF} increases.

Thus, optimization is based primarily on the relationship between the investment relative to the reactor (I_R) and energy expenditure. There is an advantage then in decreasing the catalyst volume by making use of a dense loading. However, this will increase ε_p and especially the pressure drop and the energy expenditure.

If choices exist regarding the size and shape of the catalyst particles, the calculations can be redone using the different available options. It is important to realize that ring-shaped or pierced cylindrical particles can provide a significant advantage in terms of pressure drop and the related expenditure of energy.

In the previous chapter, we compared the productivity of solid cylindrical particles with rings having the same exterior diameter (Fig. 6.9). The illustration shows that for a ring with an interior diameter/exterior diameter ratio of approximately 0.5, productivity could be increased by 15%. The fraction of free volume would then increase from 0.38 to 0.53 and the pressure drop would be divided by 4; clearly these two terms of the economic balance (Eq. 7.27) have an appreciable impact on cost optimization.

B. Radial flow

To reduce energy consumption related to pressure drop in the catalytic bed without overly increasing the diameter of the reactor, which will increase costs, a catalytic bed with radial flow is often used. This geometry is particularly advantageous when using small size catalysts, which generate higher pressure drop. In this case the catalyst is maintained between two concentric cylindrical grids and the reaction mixture crosses the catalytic mass radially.

Flow can occur from the periphery to the center (which is the model used in Fig. 7.8) as well as from the center to the periphery. The molar balance of reactants and products can easily be written, as it was for axial flow (Eq. 7.1a), by referring to Fig. 7.8:

$$(QC_i)_{r+\mathrm{d}r} - (QC_i)_r \pm K_i \mathcal{A}_S C_i(r)\,[2\pi r H]\,\mathrm{d}r = 0 \tag{7.28}$$

The sign (plus or minus) is determined by the direction of flow; it is positive if flow is from the periphery to the center and negative if it moves in the opposite direction. Assuming that external mass transfer is sufficiently rapid to have no influence on the rate of transformation—that is the constant K_1 is independent of the superficial velocity V_{SF} and can be considered constant (first-order isothermal reaction)—after integration of (7.28) we obtain:

$$C_{i,s} = C_{i,e} \exp\left\{\frac{-\pi\left(R_1^2 - R_2^2\right) K_i \mathcal{A}_S H}{Q}\right\} = C_{i,0} \exp\left\{\frac{-K_i \mathcal{A}_S V}{Q}\right\} \tag{7.29}$$

where

$C_{i,e}$	concentration of A_i at the reactor inlet
$C_{i,s}$	concentration of A_i at the reactor outlet
R_1 and R_2	external and internal radius of the catalytic bed
H	bed height.

Equation (7.29), like Eq. (7.2), can be used to calculate the volume of catalyst required to obtain a given conversion, but gives no indication concerning the selection of the dimensions R_1, R_2, and H. To determine these values we will use the same procedure as above, assuming a value of k_{1S} such that mass transfer represents less than 2% of the overall resistance: $K_1 = k_{1S}/51$. Equation (7.28) can then be written:

$$\mathrm{d}C_1 = \frac{k_{1S}}{51} \mathcal{A}_S \frac{2\pi r H}{Q} C_1(r)\,\mathrm{d}r = \frac{1}{51} \frac{k_{1S}}{V_{SF}} \frac{6\varepsilon_p}{d_p} C_1(r)\,\mathrm{d}r \tag{7.30}$$

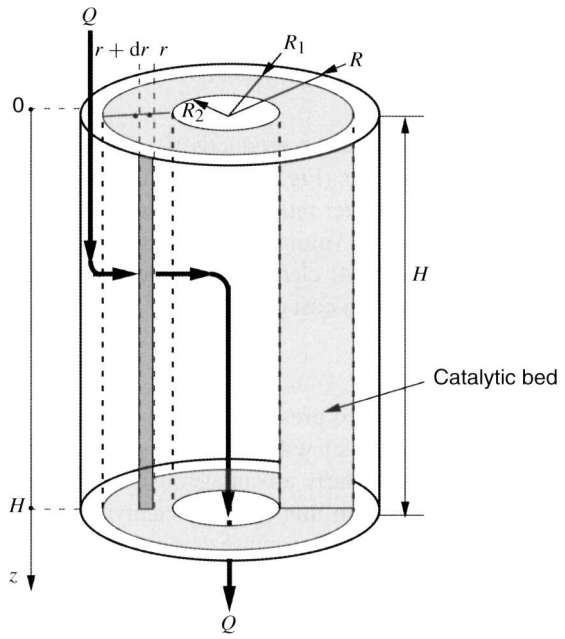


Figure 7.8 Cutaway of a fixed-bed catalytic reactor with radial flow.

V_{SF} varies between the inlet and outlet of the bed and, as a result, the same holds true for k_{1S}. However, the ratio k_{1S}/V_{SF} does not vary much and can be expressed as in Section 7.1.6:

$$\frac{k_{iS}}{V_{SF}} = j_D Sc^{-0.67} = \frac{0.36}{0.4} Re^{-0.36} Sc^{-0.67}$$

Using a mean value for the ratio k_{1S}/V_{SF}, corresponding to a Reynolds number of 80, for example, which corresponds to the maximum for radial flow, Eq. (7.30) can then be integrated:

$$\ln \frac{C_{1,e}}{C_{1,s}} \cong \frac{1}{51} \frac{3.2}{Re^{0.36} Sc^{0.67}} \frac{(R_1 - R_2)}{\overline{d_p}}$$

For a conversion of 90%, that is $C_{1,e}/C_{1,s} = 10$, the minimum value of the ratio $(R_1 - R_2)/\overline{d_p}$ required to ensure negligible external mass transfer is then:

$$\frac{R_1 - R_2}{\overline{d_p}} = \frac{51 \left(\ln \dfrac{C_{1,e}}{C_{1,s}} \right) (80^{0.36})}{3.2} = 177 \tag{7.31}$$

To obtain a conversion rate of 99%, the calculation results in a value of $(R_1 - R_2)/\overline{d_p}$ equal to 354.

If we choose the radii R_1 and R_2 of the catalytic bed such that the cross-sections through which feedstock is supplied and product eliminated are approximately 10% of the cross-

section of the reactor, whose shell has an internal radius R, we obtain:

$$\frac{R_2}{R} = 0.32 \quad \frac{R_1}{R} = 0.94$$

In order to satisfy the above conditions, a reactor diameter $R > (354/0.62)\overline{d_p} \cong 570 d_p$ must be used, which is feasible in an industrial context.

Pressure drop is calculated by integrating the elementary pressure balance:

$$\frac{dP}{dr} = \pm\frac{\Delta P}{\Delta L} = \pm\left(A_1 V_{SF}(r) + B_1 \left(V_{SF}(r)\right)^2\right) \tag{7.32}$$

$\Delta P/\Delta L$ is given by Eq. (7.9) and expressed as a function of radial position in the bed. As with the molar balance, the plus or minus sign depends on the direction of flow: it is positive if flow is from the periphery to the center, negative if flow is from the center to the periphery. The coefficients A_1 and B_1 can be determined from Eq. (7.9):

$$A_1 = 150\frac{\varepsilon_p^2}{(1-\varepsilon_p)^3}\frac{\mu_F}{\overline{d_p}^2} \quad B_1 = 1.75\frac{\varepsilon_p}{(1-\varepsilon_p)^3}\frac{\rho_F}{\overline{d_p}}$$

The superficial velocity V_{SF} can be easily calculated from the radius r:

$$V_{SF} = \frac{Q}{2\pi r H}$$

where Q is the flow rate of the fluid crossing a catalytic bed of height H.

Integration of Eq. (7.32) between the boundaries R_1 and R_2 yields:

$$\Delta P = \frac{Q}{2\pi H}\left[A_1 \ln\left(\frac{R_1}{R_2}\right) + B_1 \left(V_{SF}(R_2) - V_{SF}(R_1)\right)\right]$$

If we use the ratios of the radii given previously, the above equation becomes:

$$\Delta P = \frac{Q}{2\pi H}\left[1.1 \cdot A_1 + 1.94 \cdot B_1 \cdot V_{SF}(R_1)\right] \tag{7.33}$$

$V_{SF}(R_1)$ being the superficial velocity at the periphery of the bed.

Because of the geometry of radial flow reactors, occupancy of the reactor volume by the catalyst is not as good as in axial flow reactors, since at least 20% of the cross-section must be left empty to allow for flow of the reactants and products. Unlike axial beds, the optimal dimensions cannot be calculated only by considering the cost of the reactor and the expenditure of energy. For, minimizing these two cost factors works in favor of a reduction of the radius R of the reactor shell and an increase in height H. It is important, however, to ensure that external mass transfer remain negligible (Eq. 7.31), which functions as a constraint in the search for an optimum value.

Pressure drop in the distributors and collectors is an additional constraint and must remain negligible compared to the values for catalytic beds to ensure uniform distribution of the reaction fluid.

In the distribution zones along the periphery and the collection zones at the center, fluid flow—and therefore velocity—varies with the vertical position z, which is measured from the inlet in the distribution zone. The maximum fluid velocity in these zones is found at the inlet of the distribution zone or the outlet of the collection zone. We can then write:

$$\text{Velocity in the distribution zone:} \quad V_D = \frac{10Q}{\pi R^2}\left[1 - \frac{z}{H}\right]$$

$$\text{Velocity in the collection zone:} \quad V_C = \frac{10Q}{\pi R^2}\left[\frac{z}{H}\right]$$

Pressure drop from friction at the walls of the peripheral layer and in the center are negligible compared to the kinetic energy terms resulting from variations in the global velocity. Moreover, some compensation occurs as a result of the path followed by a fluid stream in the distribution and collection zones before and after crossing the catalytic bed (Fig. 7.8). On the other hand, as fluid streams enter and leave the catalytic bed, they undergo a pressure drop equal to the kinetic energy term $1/2\rho_F V^2$. The pressure drop experienced by each stream crossing the catalytic bed at height z can then be evaluated:

$$\Delta P_T = \Delta P_D + \Delta P_L + \Delta P_G + \Delta P_C = \frac{\rho_F V_D^2}{2} + \Delta P_L + \Delta P_G + \frac{\rho_F V_C^2}{2}$$

$$= \frac{\rho_F}{2}\left(\frac{10Q}{\pi R^2}\right)^2\left[1 - \frac{2z}{H} + \frac{2z^2}{H^2}\right] + \Delta P_L + \Delta P_G$$

ΔP_L is given by (7.33) and ΔP_G, the pressure drop across the concentric grids can, as a first approximation, be taken to be $0.1 \cdot \Delta P_L$.

To ensure the most uniform distribution possible, the following term must be minimized:

$$\frac{\rho_F}{2}\left(\frac{10Q}{\pi R^2}\right)^2\left[1 - \frac{2z}{H} + \frac{2z^2}{H^2}\right] = (\Delta P_D + \Delta P_C)$$

with respect to $\Delta P_L + \Delta P_G$, which is independent of z.

The term $(\Delta P_D + \Delta P_C)$ passes through a minimum when $z = H/2$ and a maximum at $z = 0$ and $z = H$. It is this maximum value that needs to be taken into consideration for the comparison with $\Delta P_L + \Delta P_G$.

In Eq. (7.33) the terms between square brackets generally have similar values, so we can use the following simplified equation:

$$\Delta P_L + \Delta P_G = 2.2\left[\frac{Q}{2\pi H}1.94 \cdot B_1 \cdot V_{SF}(R_1)\right] = 75\frac{\rho_F \cdot R_1}{\overline{d_p}}\left(V_{SF}(R_1)\right)^2$$

We can then write the ratio of the terms for the total pressure drop, which is:

$$\frac{\Delta P_D + \Delta P_C}{\Delta P_L + \Delta P_G} = \frac{\frac{\rho_F}{2}\left(\frac{10Q}{\pi R^2}\right)^2}{75\frac{\rho_F R_1}{\overline{d_p}}\left(V_{SF}(R_1)\right)^2} = \frac{200\left(\frac{R_1}{R}\right)^2\left(\frac{H}{R}\right)^2\left(V_{SF}(R_1)\right)^2}{75\frac{R_1}{\overline{d_p}}\left(V_{SF}(R_1)\right)^2} = 2.3\left(\frac{H}{R}\right)^2\frac{\overline{d_p}}{R_1}$$

If we assume the upper limit of this ratio to be 0.2, we limit the ratio H/R:

$$\frac{H}{R} \leqslant \sqrt{0.09 \frac{R_1}{\bar{d}_p}}$$

Given the constraints associated with external mass transfer, we will use a ratio $R_1/\overline{d_p}$ of approximately 600, which results in $H/R \leqslant 7.2$, which appears to be a reasonable constraint.

Figure 7.9 shows a cutaway drawing of a radial-flow reactor. The catalyst is located between two grids, the reactants enter through the outside grid and the effluent is withdrawn through the inside grid; as noted earlier the reverse arrangement is also possible. The collector or central distributor is made from a tube perforated with relatively large holes, covered on the outside by a fine metallic mesh. The external collector or distributor most often consists

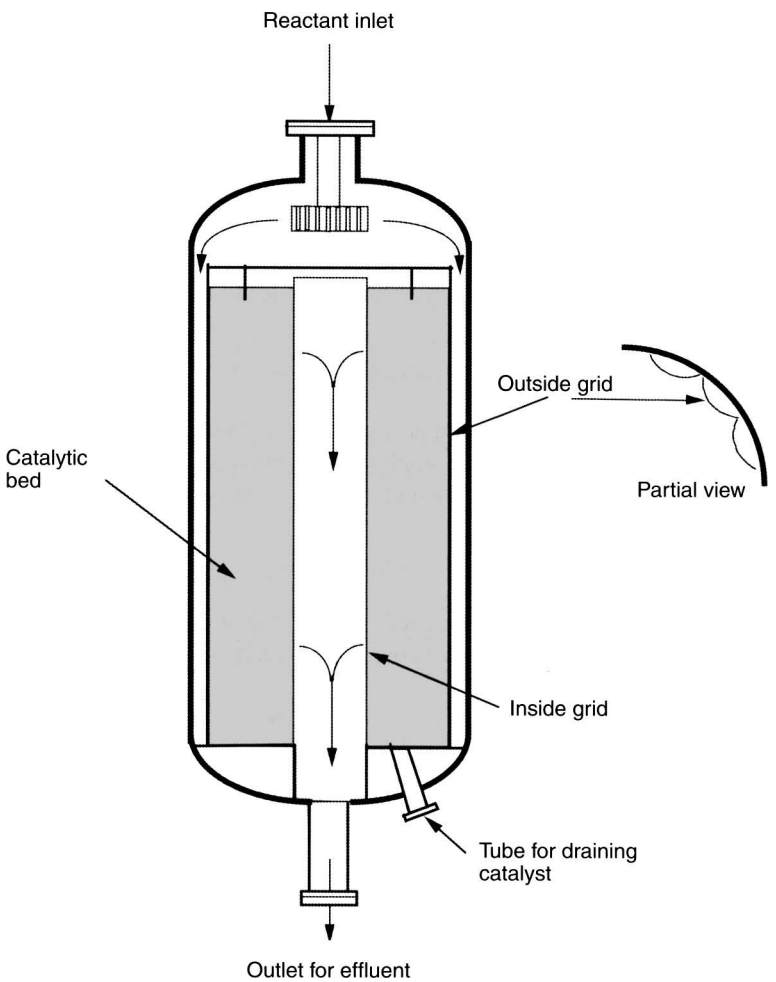


Figure 7.9 Cutaway of a fixed-bed catalytic reactor with radial flow.

of a succession of scalloped, perforated sheet metal panels, joined together and resting on the outside shell of the reactor. The upper region of the bed incorporates a zone without perforations and equipped with a cylindrical baffle that penetrates the interior of the catalytic bed; this is done to prevent any possible bypass of the gases. As a result of the gradual compaction of the catalytic bed, this zone is sometimes partially without catalyst. In this case it is easy to understand why the catalytic bed must be densely packed.

We indicated that the direction of circulation can, in principle, be chosen from the exterior to the interior and vice versa. For an endothermic reaction either reversible or one whose apparent kinetics is greater than first order, circulation from the center to the periphery is preferable to take advantage of the higher coefficient of mass transfer k_{1S} in the center of the bed. The opposite will be true for an exothermic reaction or one whose apparent order is less than 1.

C. Monolith reactor

Where very fast reactions are concerned, involving large gas flow rates, there may be an advantage in using a monolith catalyst to minimize pressure drop, and this to a far greater extent than is possible with a radial-flow bed. In the previous chapter we briefly discussed monolith catalysts and showed how they could be used to obtain geometric contact area equivalent to those provided by catalyst particles. In the previous sections we provided equations for evaluating pressure drop as well as mass transfer between the solid and the fluid flowing in the channels of the catalyst. In general it is difficult to avoid the effects of mass transfer (Eq. 7.15). The calculation of conversion is similar to that for a fixed bed with axial flow (Eq. 7.20):

$$C_{1,L} = C_{1,0} \exp\left\{\frac{-K_1 \mathcal{A}_S S L}{Q}\right\}$$

As we did for catalyst beads, we can calculate the length of the channel when fluid-solid mass transfer alone is the controlling factor. By applying the above equation and assuming that the overall constant K_1 is equal to k_{1S}, the coefficient of mass transfer, derived from (7.15), we have:

$$\ln \frac{C_{1,0}}{C_{1,L}} = k_{1S} \mathcal{A}_S \frac{L}{V_{SF}}$$

L is the length of square channels in the catalyst with unit dimension M. Their hydraulic diameter, $d_H = M - e = 0.85M$ (the washcoat is neglected, $\delta = 0$) can be calculated. We also have:

$$\mathcal{A}_S = \frac{4(M-e)}{M^2} = \frac{3.4}{M} = \frac{2.9}{d_H}$$

$$Sh = 2.98\left(1 + 0.095 Re \cdot Sc \frac{d_H}{L}\right)^{0.45}$$

We then obtain:

$$\frac{L}{d_H} = \left[\frac{1}{8.6\left(1 + 0.095 Re \cdot Sc \frac{d_H}{L}\right)^{0.45}}\right] Re \cdot Sc \cdot \ln\left[\frac{C_{1,0}}{C_{1,L}}\right] \tag{7.34}$$

This equation can be solved to determine L/d_H for various values of Re and the conversion, by using $Sc = 1$. To achieve a conversion of 90%, with mass transfer alone as the controlling mechanism, the length L must be such that:

$$\frac{L}{d_H} \geqslant 0.229Re \tag{7.35}$$

Similarly, for a conversion of 99% we find that:

$$\frac{L}{d_H} \geqslant 0.495Re \tag{7.36}$$

Since d_H is most often between 1 and 3 mm, the required lengths are small, even for high Reynolds numbers (above 1 000, for example). Also, note that to achieve 99% conversion it would be advantageous to split the monolith into two sections, each achieving a conversion of 90%. This results from the fact that flow in the channels is laminar ($Re < 2\,000$), but is established only after a given length Z_e, corresponding to the transitional zone at the inlet, has been traversed. This length can be estimated: $Z_e/d_H \cong 0.05 \cdot Re$.

In conclusion, depending on the situation, the transitional zone will occupy between 10 and 20% of the total length of the monolith, thereby influencing mass transfer.

The effect on mass transfer is not, however, the most important factor. The fact that the laminar regime, once established, occupies between 80 and 90% of the monolith, can have a noticeable influence by increasing the residence time distribution of reactants and products, which will have a pronounced effect on conversion or selectivity. Therefore, it is important to split the monolith reactor into several sections, thereby limiting the zone in which the laminar regime is established.

If the reactions have a significant thermal effect, generally exothermic as is the case with catalytic combustion, for example, heat exchange between the fluid and the solid wall must be taken into account since the heat transfer coefficient is also affected by the length of the channels (Eq. 7.16).

These devices are most commonly used for cleaning gaseous effluents. Some examples include the catalytic converters on gasoline and diesel engines, and the treatment of flue gas to eliminate NO_x. In the case of catalytic converters, the size of the reactor is minimized (a monolith of approximately 20 to 25 cm in length and 10 to 15 cm in diameter; the hydraulic diameter of the channels is roughly a millimeter), resulting in very low pressure drop. These reactors work for the most part in the non-stationary regime and, consequently, thermal inertia is an important factor. When the engine is started, the cold catalyst is inactive and the temperature must be quickly raised to the normal operating temperature (400 to 500°C) to meet existing regulatory requirements for the conversion of CO, hydrocarbons, and NO_x. In this context metallic monoliths may have an advantage over those made of ceramic materials.

Reactors for treating industrial gas effluents generally consist of several layers of monolithic parallelepiped elements, joined side by side in units including as much as 1 000 m^3 of catalyst (Fig. 7.10). The monolith element may have a cross-section of 15 cm × 15 cm, a specific area between 400 and 900 m^2/m^3, and a length that can vary from 30 cm to more than 1 m.

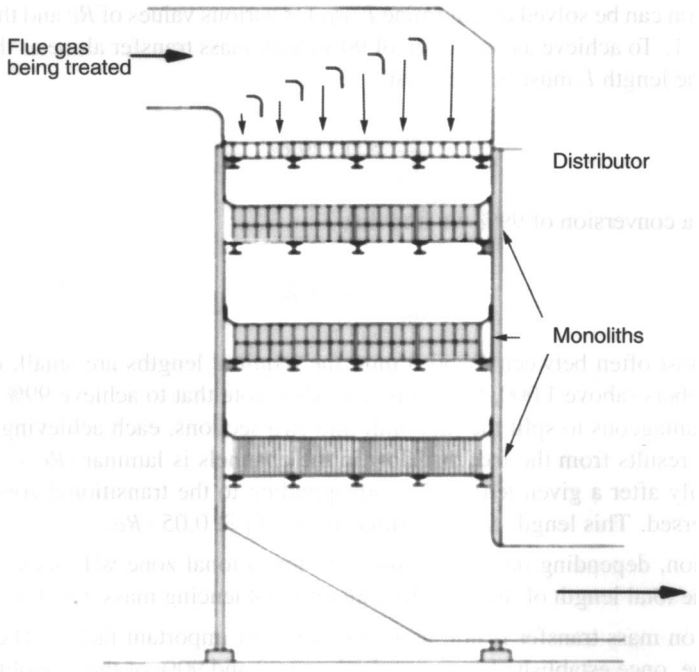


Figure 7.10 Monolith catalytic reactor for cleaning industrial flue gas.

7.2.9.2 Reactors with heat exchange at the wall

It is almost impossible to build an adiabatic implementation for a reaction that is highly exothermic (or endothermic). In this case heat must be removed (or supplied) from (or to) the catalytic zone itself, and the catalyst bed must be provided with exchange surfaces. The technology that is often used is referred to as *multitubular*. The catalyst is contained in a number of parallel tubes that are bathed in a heat exchange fluid (Fig. 7.11). Fluid circulation around the tubes is guided by lateral baffles, as in a conventional heat exchanger. Various fluids are used for heat exchange and are selected on the basis of the operating temperature [Eigenberger, 1992]:

- pressurized water up to 220°C
- organic fluids up to 300°C
- mixtures of molten salts (nitrates or carbonates) from 300°C up to 600°C.

The temperature difference between the fluid circulating around the tubes and the wall of the tube can be kept very low, whereas the temperature difference between the fluid inlet and outlet is about 5°C. For some applications under very high pressure (ammonia or methanol synthesis), the opposite arrangement is used: tubes in which the heat exchange fluid flows are immersed within the catalytic bed.

When the operating temperature is very high (above 500°C), the tubes are placed in a furnace and directly heated by the radiation produced by burners (Fig. 7.12). A typical example of the use of such a technology is the steam reforming of hydrocarbons.

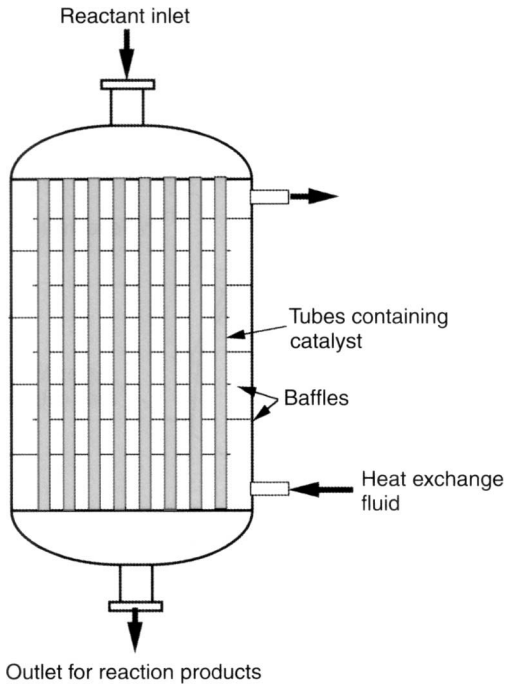


Figure 7.11 Multitubular catalytic reactor.

The calculation of heat exchange is similar to that for heat exchangers or furnaces [Trambouze *et al.*, 2000]. Problems arise in correctly estimating the heat transfer coefficient inside the catalyst tube. In practice it is not recommended to make use of tubes whose diameters are greater than 60 mm because of the risk of creating significant radial gradients.

Multitubular reactors are also subject to specific problems involving hydrodynamics. To bring about the same fluid flow rate in each tube, the texture of the bed must be absolutely identical from tube to tube. To do this, each tube must contain the exact same weight of catalyst, occupying exactly the same volume. During loading, the homogeneity of catalyst batches must be carefully monitored and any fines and clumps that have accumulated in the bottom of containers must be removed. After filling, the pressure drop is measured on each tube (if possible), using a predetermined fluid flow rate. Any tubes showing abnormal pressure drop are reloaded.

7.2.10 Concluding remarks

To summarize, in the case of fixed-bed catalytic reactors, the choice of which technology to use is based on the characteristics of the reaction being carried out. The adiabatic fixed bed remains the simplest and is generally preferred—except for highly exothermic reactions that could result in thermal instability. The following points should be considered:

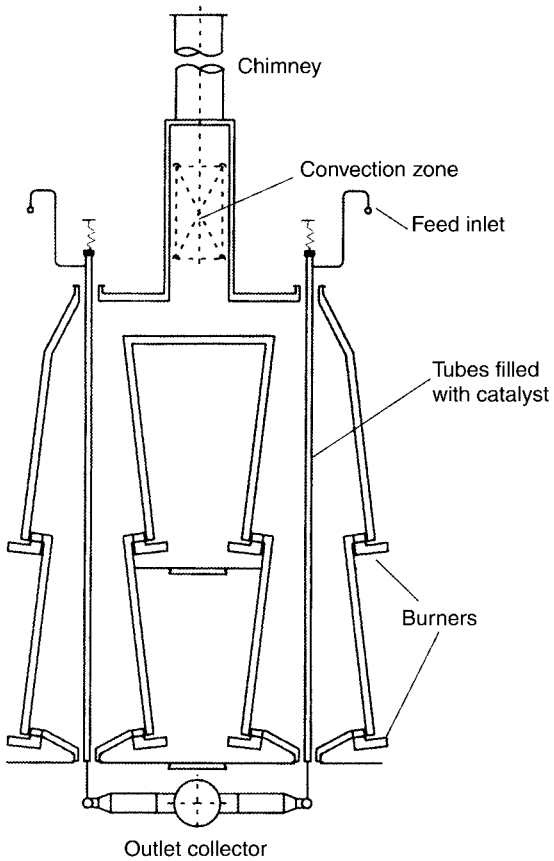


Figure 7.12 Steam reforming furnace for the production of synthesis gas.

- Plug flow will occur as long as the constraints indicated for the Reynolds number, pressure drop, and the geometric ratios n and m are followed.
- Axial diffusivity (mass and heat) will have a negligible influence in most cases.
- For mass transfer, the radial diffusivity ($\mathcal{D}_R$), although appreciably less than axial diffusivity, will have no appreciable effect, as long as there is satisfactory distribution of reactants at the reactor inlet.
- For heat transfer, the radial diffusivity will have no influence on purely adiabatic reactors but will, on the contrary, have considerable influence on reactors where there is heat exchange at the wall, and is particularly dependent on flow conditions, fluid characteristics, and the relative dimensions of the reactor and particle.
- The influence of mass transfer can easily be minimized or even eliminated providing that the above mentioned criteria are met.

For fast, high-temperature reactions a monolith catalyst can be an effective and attractive solution.

7.3 MOVING-BED CATALYTIC REACTORS

7.3.1 Introduction

In a moving-bed catalytic reactor, gravity causes the catalyst grains to flow while maintaining their relative positions to one another: the bed moves with respect to the wall of the vessel in which it is contained. The reactants move through this bed with cocurrent, countercurrent, or cross flow. Plug flow is the preferred mode for both the reactants and the catalysts. The moving bed also offers the ability to withdraw catalyst continuously or intermittently, so it can be regenerated outside the reactor and reintroduced into the circuit later on.

There is an advantage to using a moving bed when the catalyst has a short active life and can be continuously regenerated. It is important to avoid stagnant zones in the bed, which implies, as discussed below, that internal components be designed with great care. However, if these requirements are met, the moving bed retains all the characteristics of a fixed bed together with the advantages of the concentration gradient reactor. It can be used to obtain high conversion rates under good conditions for selectivity. Nonetheless, moving-bed technology suffers from the drawbacks associated with the manipulation of large quantities of granular solids. Attrition resistance is an important quality of a catalyst.

Moving beds are routinely operated adiabatically, especially when endothermic reactions are involved. Here, a large part of the heat energy needed for the reaction is provided by the catalyst grains themselves, which have stored sensible heat during the regeneration process. In other cases, however, it is the feed that provides the majority of this energy. When the catalyst also functions as a thermal vector, it is important to ensure that the temperature cycle imposed on the grain does not have a deleterious effect on mechanical strength and, ultimately, the activity of the catalyst.

The catalyst can be reheated by combustion of the coke deposited in the pores (reheating and regeneration then occur simultaneously), by direct heat exchange with flue gas, or by the indirect exchange of heat with a heat-exchange fluid.

7.3.2 Design of the moving-bed reactor

When a reactor has been designed as a fixed bed (assuming activity is constant over time and variable in space, in other words, that it is a function of the height in the bed and, therefore, the progress of reactants), it is important that all the related functions associated with the mobility of the solid be addressed. With respect to the reactor itself—for that is what we are here most concerned with—it is essential to determine how feedstock will be introduced and how effluent will be withdrawn. All the problems concerning catalyst circulation should also be dealt with at this time.

7.3.2.1 Behavior of a flowing granular solid

Figure 7.13 represents a cylindrical enclosure equipped with an inlet on top and an outlet on the bottom. Figure 7.13A shows a reactor being filled: in the upper part, the unfilled region is characterized by the angle α, known as the angle of repose. Figure 7.13B represents a reactor that has been emptied: there remains a zone containing the catalyst, characterized

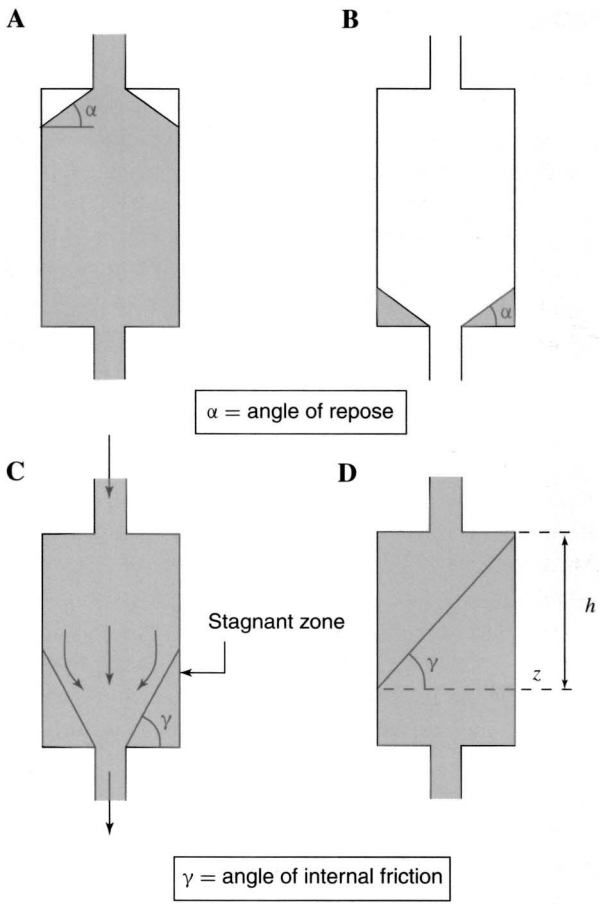


Figure 7.13 Characteristic angles of a mass of flowing grains (cylindrical vessels).

by the same angle α. The value of α can vary from 25 to 70°, flow being easier when α is smaller. For catalysts it is often between 30 and 45°, and lower for spheres than for extrudates. Figure 7.13C represents a reactor being emptied. There is a mobile zone and a stagnant zone; the border between the two zones is characterized by an angle γ, known as the angle of internal friction.

The static load supported by a layer of grains located at point z in the reactor is equal to the height of a column of bed defined by the angle of internal friction, as shown in Fig. 7.13D.

The value of the angle of internal friction is directly associated with the mechanical behavior of the catalytic bed and, especially, its resistance to shear; it is generally between 60 and 80°. It should be noted that the characteristic angles α and γ can be appreciably modified by the passage of a fluid current through the bed. In this case real or simulated conditions must be used to determine these angles.

Previous Page
Copyrighted Materials
Copyright © 2004 Editions Technip Retrieved from www.knovel.com

7.3.2.2 Pressure drop caused by flow through the granular medium

The correct evaluation of pressure drop is extremely important, both in the design of the reactor itself and to ensure a dynamic seal between parts of the reactor with different functions. Obviously valves cannot be used to prevent the passage of gas between two recipients connected by a conduit containing flowing catalyst, except for cutting off the flow of catalyst.

Communication between the two enclosures, generally with a different atmosphere and pressure, can be prevented by injecting an inert gas into the connecting pipes, at a pressure greater than that prevailing in the two enclosures. From the point of introduction in the connecting pipe, part of the gas rises into the upper vessel, the other part flows with the catalyst into the lower vessel. Although catalyst flow is assisted by the cocurrent downward flow of the gas and the catalyst, the countercurrent flow of gas interferes with the flow of catalyst and reduces the capacity of the pipe.

The calculation of the connecting legs and scavenger flows is based on an evaluation of the pressure drop in the piping and the nominal flow rate in the pipes.

Pressure drop can be calculated from Ergun's equation (Eq. 7.9). For this, a correct estimate of $(1 - \varepsilon_p)$ is needed: the void fraction of a moving bed under dense flow conditions is practically equal to that of a fixed bed consisting of the same particles, but loose, that is about 42 to 45%.

The second important term in Ergun's equation is the superficial velocity of the fluid V_{SF}. If the linear velocity of the displacement of the solid is low compared to that of the fluid, V_{SF} can be used without modification. Otherwise, the term $\Delta u\,(1 - \varepsilon_p)$ is used as the velocity term in Ergun's equation, where Δu is the solid-fluid linear slip velocity. Note that if Δu is equivalent to u_F (actual velocity of the fluid), the value of $\Delta u\,(1 - \varepsilon_p)$ will be equal to V_{SF}.

7.3.2.3 Introducing feedstock

The method of introducing feedstock presents no particular problems when the feed is in the form of a gas. For example, feed can be introduced into the bulk of the bed through nozzles whose openings are directed downward or through perforated grids along the walls. When mixed (liquid and gas) feedstocks are used, the method of introduction requires more care; this topic will be discussed later in the chapter on three-phase reactors (Chapter 8).

7.3.2.4 Effluent withdrawal

The removal of effluent has been the subject of considerable attention. At present effluent withdrawal can be controlled and various solutions are well understood. Figure 7.14 represents a now conventional embodiment for cocurrent or countercurrent flow conditions. In the case of cross flow, the introduction of feedstock and the withdrawal of products occur through vertical grids, as illustrated in Fig. 7.15.

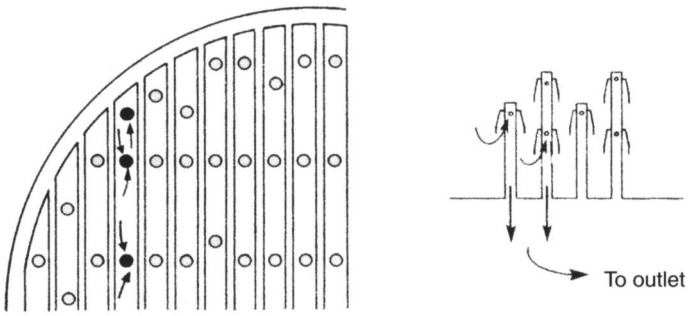


Figure 7.14 Device for removing products from a cocurrent moving bed. Left: top view of the removal channels. Right: Front view of those same channels.

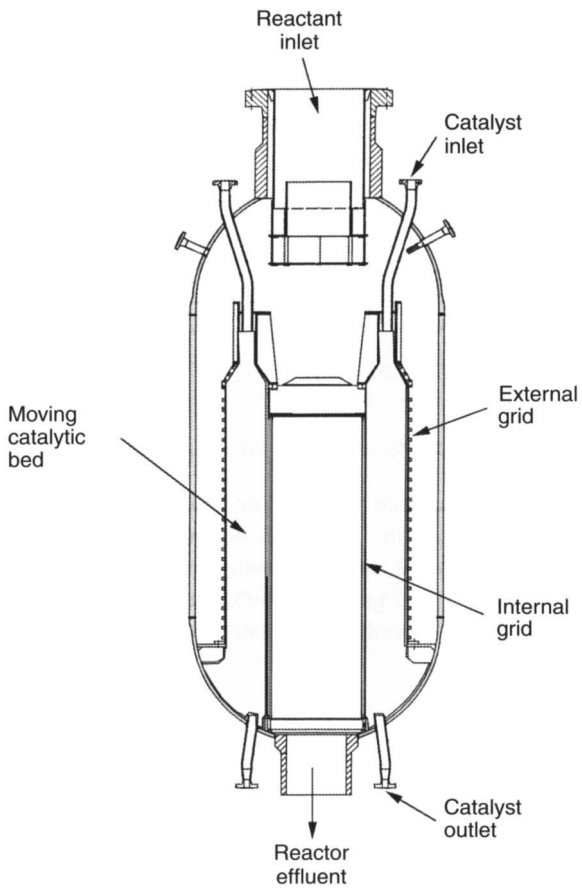


Figure 7.15 Cutaway of a cross-current moving-bed reactor.

7.3.2.5 Catalyst circulation

Gas lift is generally used for catalyst circulation. At the base of the assembly consisting of the reactor and regenerator, which are always filled with catalyst, the granular solid is introduced into a lift pot (Fig. 7.16).

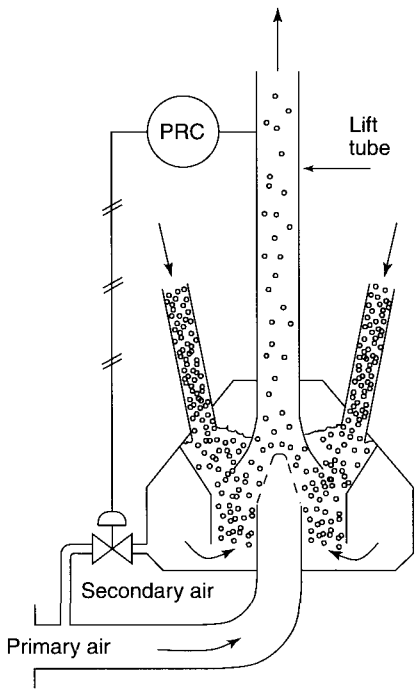


Figure 7.16 Schematic of lift pot operation.

A current of so-called secondary gas pushes the catalyst toward an ascending stream, where it is drawn upward by a current bearing the primary gas. The catalyst is then drawn upward in a dilute phase to the upper catalyst reservoir, from which the catalyst moves downward again by gravity toward the reactor under dense flow conditions. The catalyst flow rate in the unit is controlled by the flow rate of the vertical gas lift.

For a given catalyst flow rate—which is easy to achieve by pneumatic methods—it is critical that catalyst flow in the dense phase not become a bottleneck. The large capacities offered by the reactor and regenerator do not limit the flow process. In contrast, the connecting pipes between the devices and the withdrawal openings are only capable of limited flow rates. Therefore, it is important that the number and diameter of these connectors be designed so that they can accommodate the imposed flow rate.

The flow rate of solid through openings and pipes is given by the following equations:

$$Q_{(\text{nozzle})} = 2.16\,(d_0 - n)^{2.5}$$

$$Q_{(\text{piping})} = 1.73\,(d_t - n)^{2.33}$$

where

Q in m^3 of loose catalyst per second

d_0, d_t diameter of the nozzle or tube in m

n experimentally determined constant, approximately 10^{-2} m.

The correlations are valid for $d = 0.05$ m and above and as long as the reserve height above the nozzle or tube inlet is greater than $5d$.

The flow rate in a tube decreases when a fluid flows countercurrent to the solid. In particular, flow can stop entirely if, at any point in the tube, an equilibrium of opposite forces is achieved. This equilibrium is expressed by the following equation:

$$\frac{dP}{dz} = \rho_c g \, (\sin\theta - \tan\alpha \cos\theta) \sin\theta$$

where

$\frac{dP}{dz}$ local pressure drop per unit length of interconnecting leg

ρ_c density of the bed

g acceleration due to gravity

θ angle of inclination of the tube with respect to the horizontal

α characteristic angle of repose of the catalyst.

This equation determines the unit pressure drop $\Delta P/L$ above which there will be a blockage. Thus, in a vertical pipe the blockage will be obtained for $(\Delta P/L)_{max} = \rho_c g$.

It is very important to carefully manage this phenomenon: long before any blockage occurs, the flow capacity of the tube will be reduced. So, for a pressure drop that is half the maximum allowable pressure drop, the flow rate of catalyst will already have decreased by 20% with respect to the flow rate without back pressure.

To calculate the connecting leg's diameter and the scavenger flow of the fluid through the pipe, the following value:

$$\left(\frac{\Delta P}{L}\right)_{\text{nominal}} = 0.5 \left(\frac{\Delta P}{L}\right)_{\text{max}}$$

must be such that there is a reasonable margin of safety. Additionally, angles of inclination θ that are less than the angle of internal friction should be avoided.

7.3.2.6 Catalyst removal from a large-diameter vessel

Because of the necessity of maintaining uniform catalyst flow throughout the reactor cross-section, large-diameter vessels must be equipped with a significant number of catalyst drains. These drains feed into one or more collectors and the catalyst is routed by gravity toward the vessel below. The collection system can also provide an opportunity to install a gas seal and, if necessary, a catalyst stripper.

The problem is very directly related to the residence time distribution of solid particles. The distribution must be as close as possible to that corresponding to plug flow. The shape of reactor bottoms of the various vessels must be designed to avoid the presence of stagnant zones; from this point of view, conical bottoms are generally preferred. Cross flows of fluids

and solids create an additional problem: the crosscurrent fluid stream has a tendency to push the catalyst against the vertical fluid removal grid. The design of the grids and the catalyst drain system in the lower part of the reactor, as well as the choice of good crosscurrent flow conditions depend a great deal on experience and are often covered by patents.

7.3.3 Applications of moving-bed technology

The solid catalyst moving bed has found relatively few applications in industry but they are extremely important. They include catalytic cracking of gas oils and regenerative catalytic reforming of naphthas. Here we describe catalytic reforming, which is currently the most important industrial application of single-phase flow moving-bed technology. Catalytic cracking in a moving bed has no more been seen in refineries for the past twenty years and has been replaced by fluidized bed technology (discussed below).

Regenerative catalytic reforming of naphthas. The catalytic reforming process is primarily designed to modify the composition of light petroleum fractions to increase their octane number.

A large number of different chemical reactions between gaseous reactants are involved, but they all take place at around 500°C and in the presence of extruded or spherical platinum on alumina based catalysts. The principal reactions are dehydrogenation, dehydrocyclization, and isomerization, which are reversible and, in the case of the first two, highly endothermic reactions. However, along with these reactions, which increase the octane number of the feed, parasitic cracking and coking reactions occur. The rates of the various reactions depend especially on the pressure and temperature, the type of catalyst, and the type of feed.

Thus, a decrease in pressure increases the production of hydrogen and improves the quality and quantity of the reformate. On the other hand, it results in increased coking. The coke that is deposited on the catalyst particles is responsible for a loss of activity and selectivity, which eventually requires regeneration of the catalyst by combustion.

The influence of temperature is more complex. Although favorable from the point of view of the thermodynamic equilibria and kinetics of the principal reactions (dehydrogenation of naphthenes and dehydrocyclization of paraffins), an increase in temperature has the disadvantage of also accelerating parasitic reactions (hydrocracking, hydrogenolysis, and especially catalyst deactivation).

Catalytic reforming was initially used in fixed-bed adiabatic reactors, preferably with radial flow. The high flow rates of recycled gas prompt to minimize pressure drop in the reactor. The clearly endothermic nature of the reactions resulted in the use of three, four, sometimes five beds in succession, separated by reheating furnaces.

Economic constraints have made it necessary to improve the yield and quality of the reformate, as well as an increase in hydrogen production. These objectives can be achieved through a moderate increase in temperature but especially by a drop in pressure, as a quick glance at the chemical reactions involved will show. One of the inevitable consequences of the more severe operating conditions is increased coking and the resulting catalyst deactivation. To limit these drawbacks, methods for semi-continuous and continuous regeneration have been proposed. The systematic circulation of catalyst through the reactor and toward a

regeneration zone, without stopping production, is without doubt a significant technological improvement in the process of catalytic reforming. During the process, the downward flow of catalyst by gravity within the reactors must be carefully controlled, along with its transfer by gas lift between the reactors in the processing unit and the regeneration section.

Figure 7.15 illustrates the structure of a moving-bed reactor used for catalytic reforming. It displays the same radial flow of gaseous reactants between two grids as the fixed-bed reactor. But here the catalyst flows by gravity between the two concentric grids. This required a modification in the structure of the grids to minimize catalyst friction along the grids and avoid any risk of blocking the moving bed. The catalyst is introduced at the top of the reactor through a series of tubes distributed uniformly around a circumference whose diameter is equal to the mean diameter of the catalytic bed. Similarly, at the base of the reactor, a series of tubes is used to remove catalyst.

Depending on the licensor, the reactors can be arranged side by side (IFP) or stacked (UOP), each arrangement having its advantages and disadvantages. When the bases of the reactors are at the same level, overly tall structures are avoided; however, provision must be made for moving the catalyst from the bottom of one reactor to the top of the following reactor. This is accomplished by gas lift, using the recycle hydrogen gas (Fig. 7.17, photo 6). In the case of stacked reactors, there is no need to move catalyst from one reactor to the next, but the superstructure required to support the stacked reactors and the regenerator can reach considerable height, sometimes exceeding 75 m.

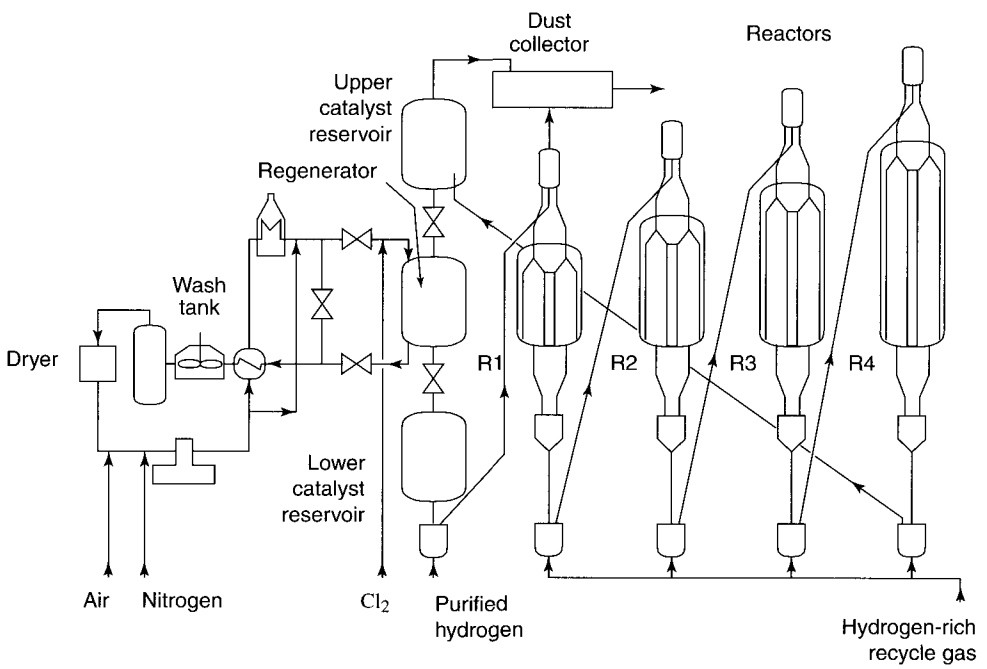


Figure 7.17 Catalytic reforming of naphthas in a moving bed. General arrangement showing the circulation of the catalyst.

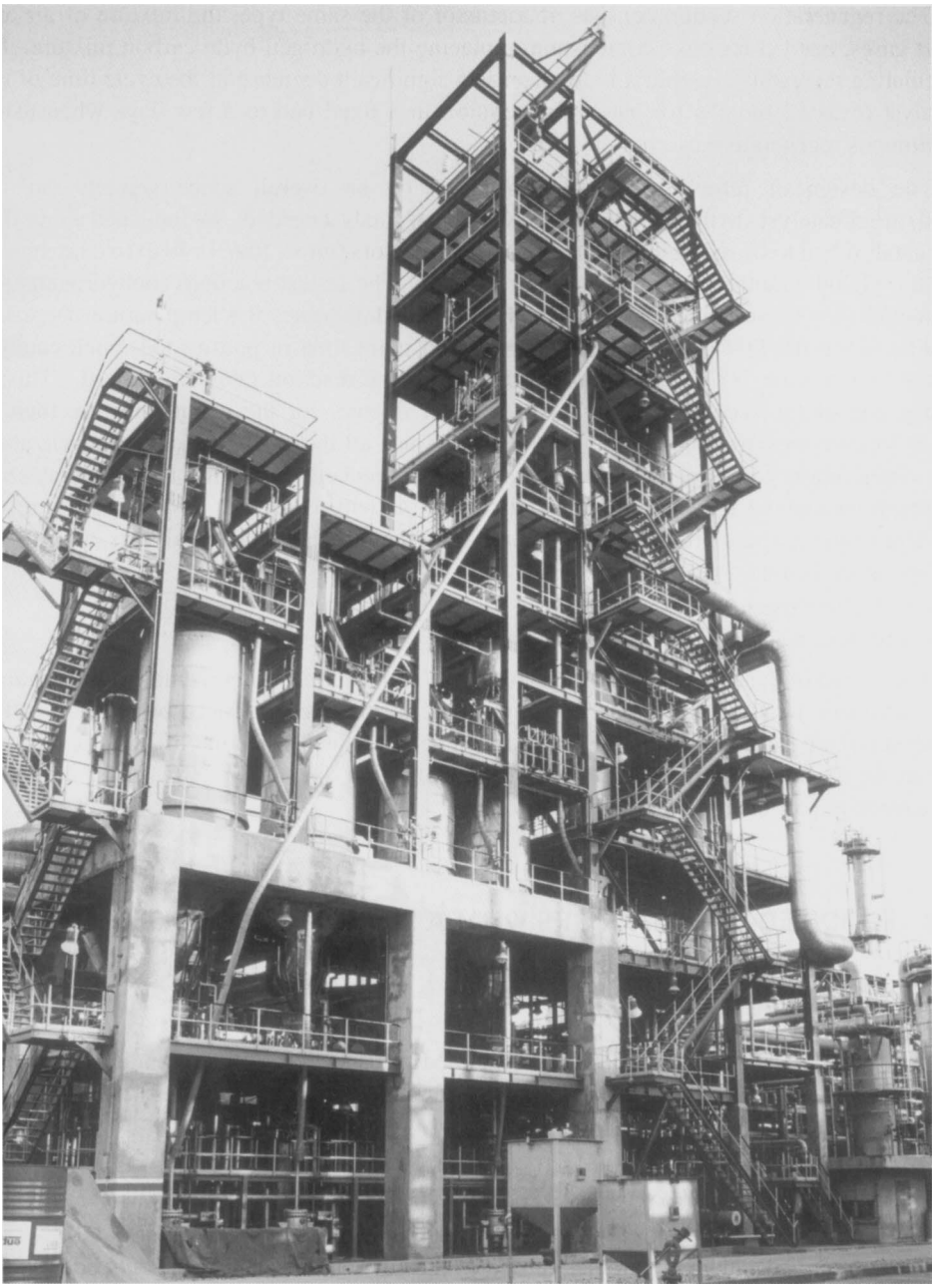


Photo 6 Moving-bed reactors for gasoline reforming. The photo shows four reactors in series, whose size, as in photo 5 on page 432, increases with the progress of the conversion. In the foreground can be seen the pipe carrying outgoing catalyst from the last reactor (on the left) to the regeneration section located on the upper right.
(*IFP Photo Library*).

The regeneration section consists of a reactor of the same type, the mixture of air and inert gases, needed for coke combustion, replacing the hydrogen-hydrocarbon mixture. By circulating the catalyst within a loop, there is a significant decrease in the cycle time of the catalyst (6 to 12 months for batch regeneration in a fixed bed to a few days when using continuous regeneration in a moving bed).

The design of reforming reactors is based on an overall space velocity (m^3 of feed/m^3 of catalyst · h) that yields the total volume of catalyst needed. We indicated above that the catalyst had to be redistributed among several reactors (three, four, or five) to compensate for the highly endothermic nature of the reactions. The fastest reactions (dehydrogenation of naphthenes to aromatics) also being the most endothermic, the temperature decreases rapidly along the first catalytic bed. There is no point then in putting too much catalyst in the first reactor, for once the temperature drops the reaction rates are slowed. This is partly true of the second reactor, but to a lesser degree, for the naphthenes are then in much lower concentrations. In the third reactor, since all the reactions (dehydrocyclization + isomerization + hydrocracking) have become appreciably athermic, the temperature is identical throughout the catalytic bed and catalyst activity is used at its peak. As a result the size of the reactors progressively increases and the distribution of catalyst is close to the figures given below:

- with three reactors: 15–25–60%
- with four reactors: 10–15–30–45%.

The design of the catalytic bed makes use of the conventional criteria employed for radial-flow adiabatic fixed-bed reactors. Although some of the fines produced by attrition of the catalyst (which must at all costs be limited) can be eliminated when the lift gas is cycloned, it may be useful—even necessary—to add an elutriation unit to correctly adjust the mean dimension of particles and their size distribution.

7.4 FLUIDIZED-BED REACTORS WITH A SINGLE FLUID PHASE

7.4.1 General remarks

A fluidized bed is a bed of solid particles maintained in suspension by the ascending circulation of one or more fluids. Depending on the type of fluid involved, we distinguish:

- gas-solid fluidized beds
- liquid-solid fluidized beds
- gas-liquid-solid fluidized beds (referred to as ebullated beds), which will be examined in Chapter 8.

The random movement of particles caused by the circulation of fluids can only occur if the upward velocity of the fluid exceeds a certain limit. This limit is generally referred to as the minimum fluidization velocity $(V_{SF})_m$. Above this minimum velocity, the bed begins to move and expand. Below it, the relative position of particles is unchanged; the bed is said to be fixed. The choice of a fluidized-bed reactor for use with a catalyst will depend on a number of qualitative factors whose advantages and disadvantages are given below.

Advantages

- Ability to withdraw and reintroduce solids continuously. This is particularly useful whenever the catalyst is rapidly deactivated.
- Elimination of any internal diffusion phenomena because of the small particle size.
- Elimination of internal and external concentration and temperature gradients.
- Elimination of radial gradients.
- Elimination of axial gradients.
- Minimization of the risk of hotspots and thermal instability. The fluidized bed is well suited to exothermic reactions.
- Experience shows that the heat transfer coefficients on the surfaces immersed in the bed are high.

Disadvantages

- For the same weight of catalyst, expansion of the bed requires an increase in the reactor volume.
- The random movement and backmixing result in overall reactor behavior that is much closer to a CSTR than to a plug-flow reactor. In the majority of reaction systems, this leads to an increase in the reaction volume and a loss of selectivity.
- Reactor hydrodynamics and modeling are complex. Consequently, scale-up presents serious problems, which limits use of these reactors to applications that can justify the significant research and development efforts involved, such as high-tonnage production units or widely used processes.
- The inevitable entrainment of solid particles necessitates the use of a large freeboard and a device for separating and recycling fines (cyclone).
- Erosion of internal components.

The problems presented by the hydrodynamics of catalytic fluidized beds and the development of models will be discussed in the following sections.

7.4.2 The hydrodynamics of fluidized beds

In general two fluidization regimes are distinguished:

- *Particulate fluidization*: In this case the bed has a nearly constant mean particle density from one point to another. On the macroscopic scale the bed can be considered homogeneous: there are no zones without solids and no bubbles. This type of fluidization is found especially when the fluid is a liquid or when fluidization by a gas takes place with very fine particles.
- *Aggregative fluidization*: In this case bubbles that are practically free of solids are found. This is the situation most frequently encountered in gas-solid fluidization and in ebullating beds.

Before beginning a study of a fluidized bed reactions, it is worthwhile examining the feasibility of their operation. Geldart [1973] succeeded in classifying powdered solids into four categories according to their aptitude for fluidization (Fig. 7.18). The parameters used for this classification are: the apparent density of the grains $(\rho_p - \rho_F)$ and the equivalent mean diameter $\overline{d_p}$.

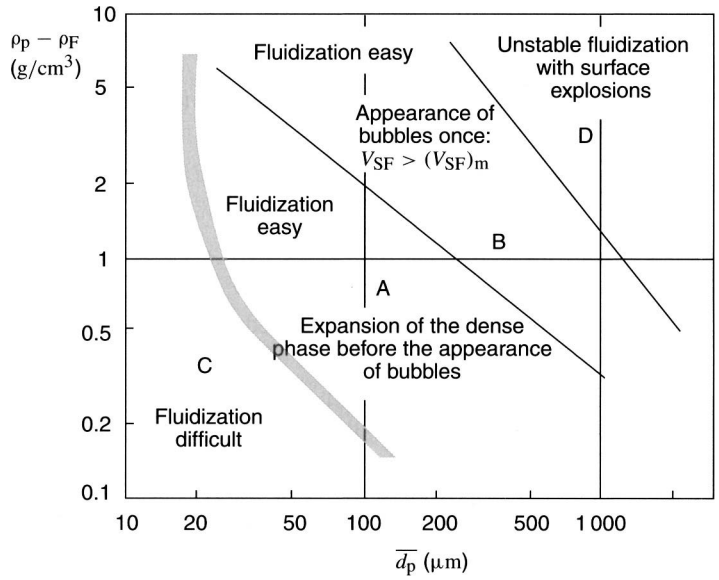


Figure 7.18 Classification of particles on the basis of their ability to be fluidized (based on Geldart, 1973).

According to Geldart, the particle size distribution does not present an obstacle to good fluidization, providing that the distribution is approximately normal, in other words, gaussian.

The following four classes were identified by Geldart:

- Class A: Fluidization is easy and particulate in nature.
- Class B: Fluidization is easy and aggregative in nature.
- Class C: Fluidization is nearly impossible because of the very high surface forces between grains.
- Class D: Fluidization is possible but of poor quality.

Geldart's classification does not take into account other factors that can have an influence in certain specific circumstances: the tendency to cake in humid atmospheres, the tendency to stick, the agglomeration of ash when near the melting point.

Once the feasibility of fluidization has been established, three hydrodynamic values must be determined:

- the minimum superficial velocity of fluidization $(V_{SF})_m$
- the superficial velocity leading to the entrainment of at least a part of the solid
- the expansion of the bed as a function of (V_{SF}).

The following comments are called for:

1. Whenever a fluidization unit is being designed, optimal use of the reaction volume requires that minimum expansion occur to ensure good mobility of the solid as well as good mixing. This is normally obtained for modest expansions of about 10 to 25%. The use of superficial velocities leading to greater expansion is not justified in most circumstances. However, it can happen that the operational flexibility of the facility requires operating at values of V_{SF} that differ significantly from those determined during the design phase. In this case it is important to understand the response of the bed to these variations.
2. According to the conventional design of the fluidized bed, the solid is confined in the bed and any entrainment is prevented by the use of cyclones or devices for capturing entrained particles. In fact, after several years and, more especially, after the development of the fluidized catalytic cracking process (FCC), the reaction zone has been shifted from the fluidized bed itself to the transfer lines for solids. As a result the cracking reactor has become, in this case, a pipe in which reactants and catalyst circulate with cocurrent flow.

7.4.3 Minimum superficial velocity of fluidization $(V_{SF})_m$

There are several ways to understand the physical meaning of the minimum superficial velocity of fluidization. We discuss the simplest of them.

When a fluid is made to circulate from bottom to top through a bed of solid particles, the pressure drop can be measured as a function of the superficial velocity of the fluid. We obtain a curve that qualitatively has the shape shown in Fig. 7.19. As long as the superficial velocity of the fluid is less than $(V_{SF})_m$, there is an increase in pressure drop with V_{SF}. The recorded pressure drop is the same as that resulting from conventional fluid flow through a granular material in a fixed bed. As noted earlier, this pressure drop can be estimated by means of Ergun's equation (Eq. 7.9):

$$\frac{\Delta P}{L} = A\frac{\varepsilon_p^2}{(1-\varepsilon_p)^3}\frac{\mu_F V_{SF}}{\overline{d_p}^2} + B\frac{\varepsilon_p}{(1-\varepsilon_p)^3}\frac{\rho_F V_{SF}^2}{\overline{d_p}}$$

where ε_p is the fraction of the bed occupied by the particles.

It is obvious that the force exercised on the bed by fluid friction—the pressure drop being the direct manifestation of this—increases with the flow rate of the fluid. At a given point this force is as great as the apparent weight of the bed. The bed, which has until this point retained a degree of consistency, begins to rise, resulting in the loss of consistency and a rearrangement of the particles. The situation in the bed begins to resemble that found at the end of a period of solid particle sedimentation in a fluid.

From the moment the position of the particles begins to shift, the bed becomes fluidized and the pressure drop becomes appreciably independent of the superficial velocity of the fluid: with each increase in the flow rate of the fluid there is a corresponding increase in bed expansion and, therefore, in the volume fraction occupied by the fluid in the bed, which leads to a stabilization of the pressure drop. It seems reasonable, then, to estimate the minimum

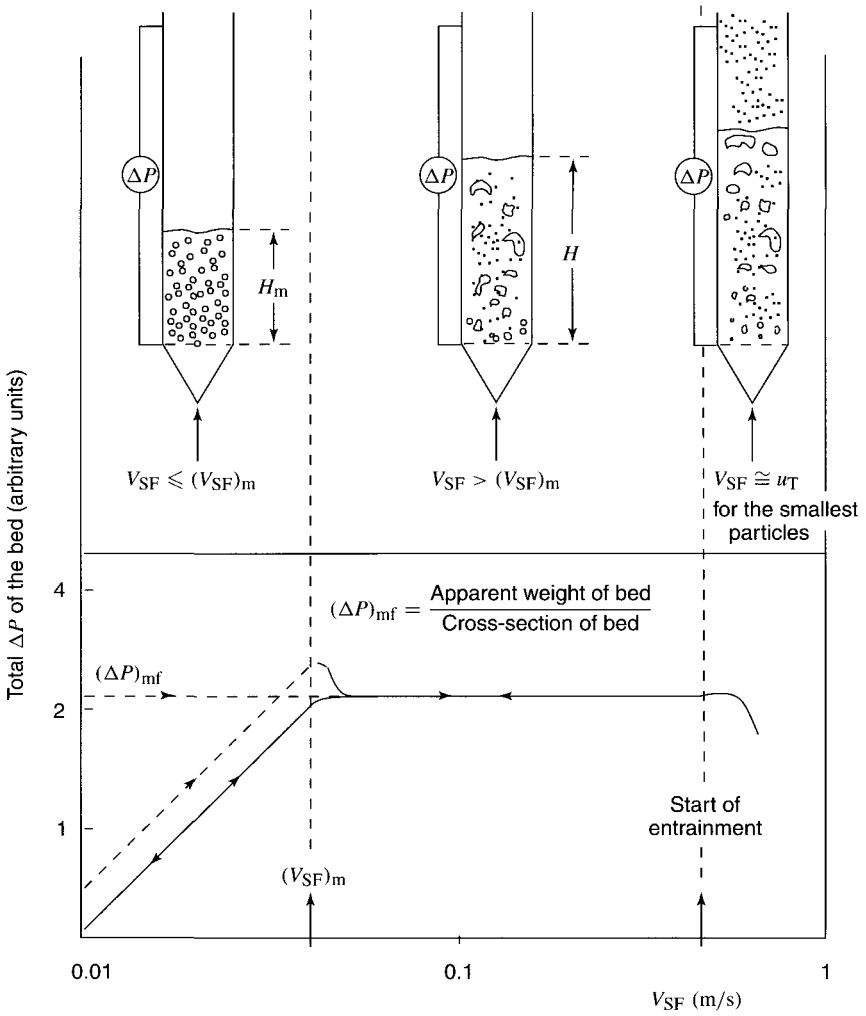


Figure 7.19 Total pressure drop of the bed as a function of the superficial velocity of the fluid. The dashed line corresponds to the first expansion of the bed: the void fraction is less than the void fraction of a bed first expanded by fluidization.

superficial velocity of fluidization from the equilibrium between the frictional force and the gravitational force:

$$\frac{\Delta P}{L_m} = A\frac{\varepsilon_{pm}^2}{(1-\varepsilon_{pm})^3}\frac{\mu_F (V_{SF})_m}{\overline{d_p}^2} + B\frac{\varepsilon_{pm}}{(1-\varepsilon_{pm})^3}\frac{\rho_F (V_{SF})_m^2}{\overline{d_p}} = (\rho_p - \rho_F)\varepsilon_{pm} g$$

where

ε_{pm} volume fraction of bed occupied by the particles at the threshold of fluidization

ρ_p density of a particle.

In order to obtain a dimensionless form of the equation, it is customary to multiply the terms in the equation by $\left(\rho_F \overline{d_p^3}\right) / \left(\mu_F^2 \varepsilon_{pm}\right)$ and to introduce two dimensionless numbers, a Reynolds number:

$$Re_m = \frac{\overline{d_p}\,(V_{SF})_m\,\rho_F}{\mu_F}$$

and an Archimedes number:

$$Ar = \frac{\rho_F\left(\rho_p - \rho_F\right)\overline{d_p^3} g}{\mu_F^2}$$

We then obtain:

$$Ar = A\frac{\varepsilon_{pm}}{\left(1-\varepsilon_{pm}\right)^3} Re_m + B\frac{1}{\left(1-\varepsilon_{pm}\right)^3} Re_m^2$$

It has been observed that:

- the value of $A\left[\varepsilon_{pm}/\left(1-\varepsilon_{pm}\right)^3\right]$ is frequently about 1 650
- the value of $B\left[1/\left(1-\varepsilon_{pm}\right)^3\right]$ is frequently about 24.5.

We can then write:

$$24.5\,(Re_m)^2 + 1\,650\,(Re_m) - Ar = 0$$

solving for Re_m:

$$Re_m = 33.7\left[\left(1 + 3.6\cdot 10^{-5} Ar\right)^{0.5} - 1\right] \tag{7.37}$$

or:

$$(V_{SF})_m = \frac{33.7\mu_F}{\overline{d_p}\rho_F}\left[\left(1 + \frac{3.6\cdot 10^{-5}\rho_F\left(\rho_p-\rho_F\right)\overline{d_p^3} g}{\mu_F^2}\right)^{0.5} - 1\right] \tag{7.38}$$

The value $\overline{d_p}$, the mean diameter of the particles, appears in the equation for $(V_{SF})_m$.

In contrast to the situation with fixed-bed reactors, where the granulometric distribution is relatively narrow and the particle geometry well defined, here we are in the presence of particles with a variety of shapes, with a distribution that varies with the circumstances. For $\overline{d_p}$ we use the value taken from the cumulative weight distribution curve by applying:

$$\frac{1}{\overline{d_p}} = \Sigma\frac{\Delta x_i}{\left(\frac{t_{i-1}+t_i}{2}\right)}$$

Δx_i is the weight fraction of catalyst for particles whose size falls between t_{i-1} and t_i. This definition corresponds to the $\bar{d}_1$ given in Chapter 6 $\left(\bar{d}_1 = 6\Sigma V/\Sigma S\right)$.

There can be two extreme cases for Eq. (7.37), depending on the value of Re_m:

$$Re_m < 20 \qquad Re_m = \frac{Ar}{1\,650} \quad \text{and} \quad (V_{SF})_m = \frac{\overline{d_p}^2\left(\rho_p-\rho_F\right)g}{1\,650\mu_F} \tag{7.39a}$$

$$Re_m > 1\,000 \qquad (Re_m)^2 = \frac{Ar}{24.50} \quad \text{and} \quad (V_{SF})_m^2 = \frac{\overline{d_p}\left(\rho_p-\rho_F\right)g}{24.50\rho_F} \tag{7.39b}$$

To improve the estimated value of $(V_{SF})_m$, we can, of course, conduct a direct measurement in the laboratory using simulation fluids such as water, air, or others which will enable us to empirically determine the values of the coefficients:

$$A\frac{\varepsilon_{pm}^2}{(1-\varepsilon_{pm})^3} \quad \text{and} \quad B\frac{\varepsilon_{pm}}{(1-\varepsilon_{pm})^3}$$

The method for estimating the minimum superficial velocity of fluidization can be used for gas-solid systems as well as for liquid-solid systems. It cannot be used for three-phase systems.

A word of caution is in order concerning systems involving a liquid and particles whose dimensions are less than 200 to 300 μm. In this case, capillary forces must be taken into account when determining the equilibrium of forces. These capillary forces can become dominant, to the point of completely altering the value of $(V_{SF})_m$ and even making all fluidization impossible in the presence of a liquid phase.

7.4.4 The terminal velocity of a particle

Entrainment velocity

As the rate of fluid flow through the fluidized bed is increased, eventually the smallest particles are carried away by the fluid current. This phenomenon of elutriation is often made use of to eliminate fines from a catalyst. However, entrainment of the catalyst is rarely acceptable and, therefore, the significance of the phenomenon must be evaluated, if only to correctly design the cyclones intended to return the entrained catalyst to the bed.

By comparing a particle of dimension t_i to a sphere of diameter $\overline{d_p}$, it can be shown that the terminal velocity results from a balance of forces:

Apparent weight of the particle = drag force

$$\frac{\pi\overline{d_p^3}}{6}(\rho_p - \rho_F)\,g = F_T \tag{7.40}$$

As would be expected, the equation for drag force introduces the parameters μ_F, $\overline{d_p}$, and u_t, the terminal velocity.

Dimensional analysis of the phenomenon shows the existence of a relationship between two dimensionless numbers $C_D = f(Re)$, where:

$$Re = \frac{\overline{d_p} u_t \rho_F}{\mu_F} \qquad \text{Reynolds number}$$

and:

$$C_D = \frac{F_T}{\left(\rho_F \frac{u_t^2}{2} \frac{\pi\overline{d_p^2}}{4}\right)} \qquad \text{drag coefficient}$$

At low values of the Reynolds number ($Re < 1$): $C_D = 24/Re$, and:

$$u_t = \frac{(\rho_p - \rho_F)\,\overline{d_p^2}\,g}{18\mu_F} \tag{7.41}$$

which is Stokes's law.

At high values of the Reynolds number ($Re > 10^3$):

$$C_D \cong 0.43$$

and:

$$u_t^2 = 3.1\frac{(\rho_p - \rho_F)\,\overline{d_p}\,g}{\rho_F} \tag{7.42}$$

which is Newton's law.

In the intermediate case, $1 < Re < 10^3$, the following analytic equation can be used:

$$\ln C_D = -5.50 + \frac{69.43}{\ln [Re] + 7.99} \tag{7.43}$$

Recall that these equations can only be used if the particles under consideration can be reasonably treated as spheres.

To avoid excessive particle entrainment, the fluidization operation must be conducted so that:

$$(V_{SF})_m < V_{SF} < u_t$$

However, the minimum superficial velocity of fluidization is calculated on the basis of a mean diameter $\overline{d_p}$ for the entire bed, whereas, when using u_t, only the mean diameter of the fraction corresponding to the smallest particles is taken into consideration. In practice it has been observed that the ratio $u_t/(V_{SF})_m$ (where u_t is calculated for $\overline{d_p}$) remains between 10 (large particles, $Re > 10^3$) and 90 (fines, $Re > 0.4$). Since, most often, V_{SF} is 5 to 10 times greater than $(V_{SF})_m$, the risks of entrainment are limited and can, in fact, be eliminated simply by the installation of cyclones.

Obviously, whenever we intend to design entrained fluidized beds, it is advisable to use a value of V_{SF} that is at least equal to a value of u_t corresponding to the largest particles that will be entrained.

7.4.5 Expansion in a fluidized bed

In a bed of particles at rest, the volume fraction of the bed occupied by the solid is ε_p. Whenever a fluid is made to circulate from bottom to top through the bed of particles, causing the superficial velocity to increase, no change in the height of the bed is observed until a threshold value is reached, at which point the bed suddenly expands. The total pressure drop of the bed is then stabilized at a value corresponding to the apparent weight of the column of catalyst. If the superficial velocity is increased again, we can expect the bed expansion to be reflected in an increase in the height of the bed and a reduction of ε_p. It is important to make a distinction, however, depending on whether the fluid is a liquid or a gas.

7.4.5.1 Fluidization by a liquid

Whenever V_{SL} is increased, fluidization remains homogeneous and ε_p decreases regularly with V_{SL} according to an empirical law established by Richardson and Zaki [1954]:

$$\left(1-\varepsilon_p\right)^n = \frac{V_{SL}}{u_t}$$

u_t corresponds to the terminal velocity of a particle with mean diameter $\overline{d_p}$; the exponent n, which is always positive, depends on the Reynolds number $Re = \left(u_t \rho_L \overline{d_p}\right)/\mu_L$, the shape of the particles, and the ratio $\overline{d_p}/D$, where D is the diameter of the reactor. Various aspects of liquid fluidization hydrodynamics and heat transfer have been analyzed by Jamialahmadi [2000].

7.4.5.2 Fluidization by a gas

Whenever V_{SG} is increased beyond $(V_{SG})_m$, either of two situations can occur:

1. Fluidization remains homogeneous, in which case the equation of Richardson and Zaki is applicable. Fluidization is said to be particulate. This case is uncommon, however, and corresponds to highly specific conditions, which are rarely encountered in industrial practice.
2. Fluidization becomes heterogeneous, with the appearance of gas bubbles almost as soon as $(V_{SG})_m$ is exceeded. This is the normal gas-solid fluidization regime, sometimes called aggregative fluidization. The phenomenon has been studied extensively, and we will return to the subject in the section on modeling fluidized-bed reactors.

There are no reliable correlations for estimating the volume fraction of bubbles in the bed or its expansion H/H_m as a function of the superficial velocity of the gas.

Whenever aggregative fluidization occurs, it should be made uniform, that is *slugging* and *channeling* must be eliminated. When slugging occurs, gas bubbles pressing against the walls of the reactor create plugs with solid projections. Generally, this is corrected by increasing the bed diameter to bed height ratio or by arranging internal components (heat exchangers) in the bed. Channeling corresponds to the creation of preferential paths through the bed. It is corrected by designing a suitable distributor.

It is important to note that in the aggregative fluidization regime, the volume fraction occupied by the gas in the phase consisting of the homogeneous particles-gas emulsion (also known as the dense phase), is identical to $\left(1-\varepsilon_{pm}\right)$, that is, the value corresponding to the fluidization threshold. It is as if, once the fluidization threshold is reached, any gas in excess of $(V_{SG})_m$ passes completely into the bed in the form of bubbles. This information can be used when modeling the process.

The different types of fluidization observed for increasing velocities are sometimes referred to as follows [Levenspiel, 1999]:

- bubbling fluidization
- turbulent fluidization
- fast fluidization
- pneumatic transport.

Figure 7.20 indicates the domains where the various fluidization regimes occur, as a function of particle size and the linear gas velocity.

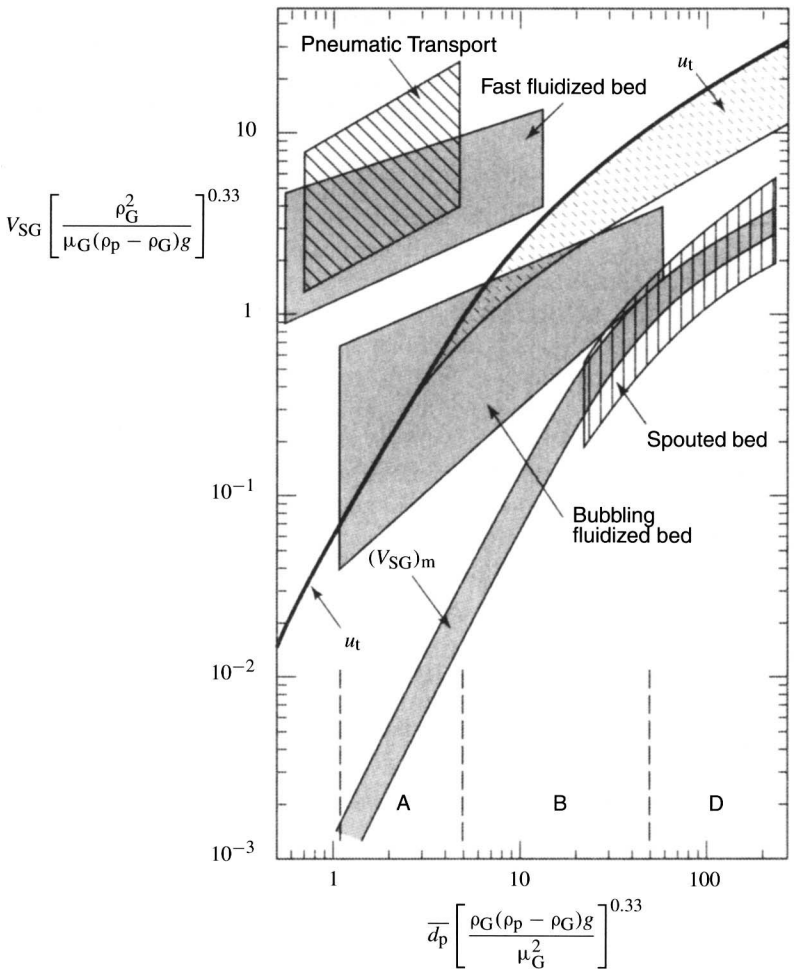


Figure 7.20 The various fluidization regimes.

7.4.6 Fluidized-bed reactor models and correlations

The description of fluidized-bed reactors varies significantly depending on whether the reactor is gas-solid, liquid-solid, or three-phase. This is primarily because of the distinct hydrodynamic behaviors associated with them, which require the use of very different flow models.

7.4.6.1 Liquid-solid fluidized reactors

We previously indicated that liquid-solid fluidization is normally particulate. The bed of suspended solids is pseudo-homogeneous and recirculation of both the liquid and the solid is sufficiently intense for reactor behavior to globally approximate that of CSTRs.

When the bed height is greater than twice the diameter, a more realistic picture might consider the bed as consisting of a cascade of CSTRs, each having a height equal to the diameter of the bed. This situation is consistent with observations made using small-scale reactors, and is somewhat analogous to a bubble column (Chapter 4) operating in the pseudo-homogeneous regime.

It has been observed that a density gradient from the bottom to the top of the reactor promotes (or inhibits, depending on the direction of the gradient) the convection currents responsible for backmixing. In this way the development of an exothermic reaction results in a temperature gradient and, therefore, a decrease in the density of the liquid with height, which impedes convection. This is especially significant when designing a reactor whose thermal stability must be determined by a careful choice of the inlet temperature. If the reactor is considered to be an ideal continuous stirred tank, the temperature at any point in the reactor will be identical to the outlet temperature, which often results in a satisfactory reaction rate as well as satisfactory thermal stability. If, however, the behavior of the reactor diverges too far from this model, the inlet temperature will be too low and the reaction will not start. It is recommended, therefore, in a liquid fluidized bed where an exothermic reaction is taking place, to incorporate an exterior recirculation system to provide a minimal recycling stream so that the temperature in the vicinity of the reactant inlet can be effectively controlled.

7.4.6.2 Gas-solid fluidized-bed reactors

The majority of gas-solid fluidized beds operate in the aggregative regime, that is to say, under conditions where large bubbles, relatively free of solids, pass through the bed. For years this type of fluidized bed has been considered to consist of two phases:

- an *emulsion*, or *dense*, *phase*, in which nearly all the solid is found and a relatively reduced fraction of the gaseous phase, where:

$$\frac{\text{volume of gas phase in the emulsion}}{\text{volume of emulsion phase}} = 1 - \varepsilon_{pm}$$

- a *bubble phase*, comprising the major part of the gas that passes through the bed, entraining in its wake a relatively large cloud of solid particles.

The behaviors of these two phases are, obviously, quite different, and their description as well as the modeling of mass transfer between them have given rise to a large number of models of varying complexity.

A. Werther's model

An interesting approach to the problem is provided in the work and associated correlations presented by Werther [1980]. In this simple model, reactant is transferred from the bubble phase to the emulsion phase, across an interfacial area $\mathcal{A}_{Be}$, $\mathcal{A}_{Be}$ = the external surface area of the bubbles per unit volume of fluidized bed. The size of the bubbles is considered to increase from the bottom at the diffuser to a height h^*, which is approximately 1 m. Beyond this, and up to the total height of the fluidized bed H, the combined and contrasting effects of bubble rupture and coalescence keep the bubble diameter nearly constant.

The bubble diameter is calculated by means of the following equation:

$$d_b = 0.54 \left(\frac{V_{SG} - (V_{SG})_m}{\sqrt{g}} \right)^{2/5} \left(h^* + 4\sqrt{A_O} \right)^{4/5} \tag{7.44}$$

A_O is the area fed by an opening in the distributor. For a porous plate A_O is taken to be equal 56 mm^2. The maximum size of the bubbles is generally between 30 and 45 cm, which makes it difficult to carry out experiments in a laboratory reactor or a pilot unit.

The assumptions that underlie Werther's model are given below (Fig. 7.21):

- $V_{SG} \gg (V_{SG})_m$: all the gas exists in the form of bubbles
- the bubble phase is characterized by plug flow
- the emulsion phase is stagnant: no significant gas flow
- the transfer of the bubble phase to the emulsion phase is controlled by a transfer coefficient $k_{l,e}$ and a bubble-emulsion interfacial area $\mathcal{A}_{Be}$ (m^2/m^3 of fluid bed)
- the reaction in the emulsion phase is first order and isothermal.

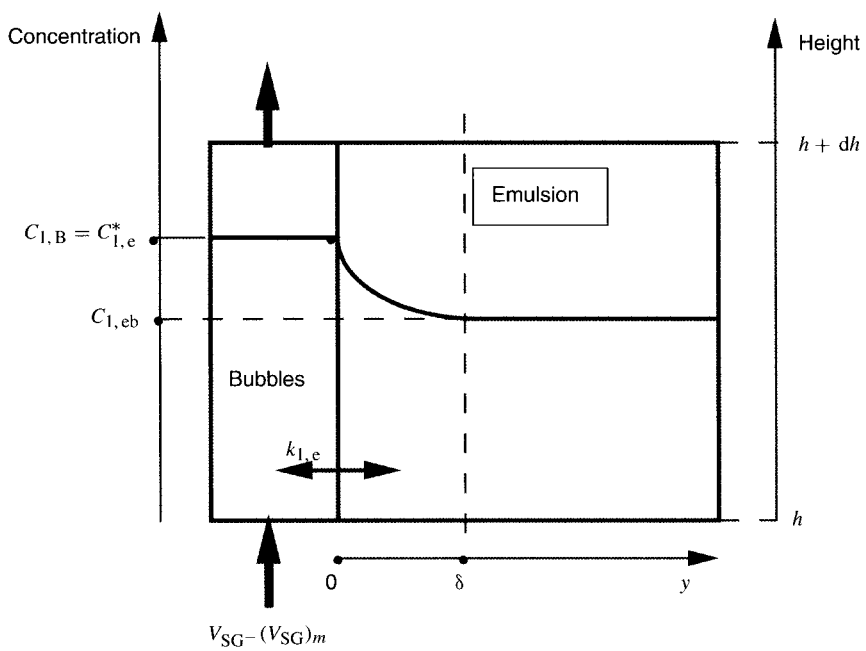


Figure 7.21 Werther's model.

Under the conditions indicated, the phenomenon of (bubble phase → dense phase) transfer serves as a perfect analogy for (fluid phase I → fluid phase II) transfer, in which the departure phase I is the bubble phase (B) and the arrival and reaction phase is the emulsion phase (e).

The pseudo-first order reaction takes place in this emulsion phase. The balance equations based on the model are shown below.

Balances for the film:

$$\mathcal{D}_{1,e}\frac{d^2C_{1,e}(y)}{dy^2} + \nu_1 k C_{1,e}(y) = 0$$

$$\mathcal{D}_{1,e}\mathcal{A}_{Be}\left[\frac{dC_{1,e}(y)}{dy}\right]_{y=\delta} + \nu_1 k\left[(1-\varepsilon_B) - \mathcal{A}_{Be}\delta\right]C_{1,eb} = 0$$

Boundary conditions:

$$y = 0 \qquad C^*_{1,e} = C_{1,B} \quad \text{(no discontinuity at the interface)}$$
$$y = \delta \quad C_{1,e}(\delta) = C_{1,eb}$$

Balances for a reactor slice:

$$-V_{SG}S\frac{dC_{1,B}}{dh} = -\mathcal{D}_{1,e}\left[\frac{dC_{1,e}(y)}{dy}\right]_{y=0}\mathcal{A}_{Be}S$$

where the boundary condition for $h = 0$ is:

$$C_{1,B} = C_{1,0} = \text{concentration in the gas at the reactor inlet}$$

$$\left[N'_1\right]_{x=0} = k_{1,e}E\left(C^*_{1,e} - C_{1,eb}\right)$$

$$E = \frac{Ha}{\tanh[Ha]}\,\frac{1 - \dfrac{\mathcal{N}_3}{\cosh[Ha]}}{1-\mathcal{N}_3} \tag{7.45}$$

$$\mathcal{N}_3 = \frac{\dfrac{1}{\cosh[Ha]}}{1 + Ha\tanh[Ha](\beta - 1)} \tag{7.46}$$

$$Ha = \frac{\sqrt{-\nu_1 k\mathcal{D}_{1,e}}}{k_{1,e}}$$

where

k	first-order rate constant for the emulsion phase (s^{-1})
$\mathcal{D}_{1,e}$	coefficient of diffusivity for constituent A_1 in the emulsion phase (m^2/s)
$k_{1,e}$	transfer coefficient of component A_1, in the emulsion phase (m/s)
$\beta = \dfrac{k_{1,e}\varepsilon_e}{\mathcal{A}_{Be}\mathcal{D}_{1,e}}$	
ε_e	volume fraction of the fluidized bed occupied by the emulsion phase
$\mathcal{A}_{Be}$	bubble-emulsion interfacial area (m^2/m^3 of fluidized bed).

The maximum rate of disappearance of reactant A_1 per unit volume of bed is equal to: $r_{1\,max} = -\nu_1 k C^*_{1,e}\varepsilon_e$. The actual rate, equal to the rate of transfer, is expressed by:

$$r_1 = \left[N'_1\right]_{x=0}\mathcal{A}_{Be}$$

and therefore, the efficiency η is:

$$\eta = \frac{r_l}{r_{l\,max}} = \frac{1}{Ha\,\beta}\left[\frac{\tanh[Ha] + [Ha](\beta - 1)}{1 + Ha\tanh[Ha](\beta - 1)}\right] \tag{7.47}$$

Therefore, all the equations developed in Chapter 3 can be easily transposed.

If we treat the bubble phase as moving with plug flow, a mass balance can be written for a slice of bed of thickness dh:

$$Q_B dC_{l,B} + \nu_l \eta k \varepsilon_e C_{l,B} S\,dh = 0 \tag{7.48}$$

where

h	bed height measured from the gas diffuser
$C_{l,B}$	concentration of reactant A_l in the bubble phase
$Q_B = (V_{SG} - (V_{SG})_m)S$	volumetric flow rate of the bubble phase
S	cross-section of the bed.

By integrating along the length of the bed, we obtain:

$$C_{l,B}(H) = C_{l,B}(0)\exp(\nu_l \eta k \theta) \tag{7.49}$$

where

$\theta = \dfrac{\varepsilon_e V}{Q_B}$ residence time

$V = SH$ volume of the bed.

Obviously, the primary difficulty in Eq. (7.49) lies in estimating η and k. For k, a rate constant per unit volume of the emulsion phase, it is generally possible to use the equation:

$$k = \varepsilon_{pm}\rho_p k_M$$

where k_M is the rate constant per unit mass of catalyst, which is sometimes easier to obtain than k.

As for η, based on (7.47), we need to be able to estimate $\mathcal{A}_{Be}$, $\mathcal{D}_{l,e}$, ε_e, $k_{l,e}$.

Table 7.2 provides usable correlations for reactors whose height and diameter are greater than 1 m. The orders of magnitude are shown in Table 7.3. We have decided not to provide correlations for bubble diameter, even though the question has been addressed in numerous publications. Werther's model implicitly contains a correlation expressed in terms of the interfacial area $\mathcal{A}_{Be}$.

B. Botton's model

Botton [Botton, 2000] revised one of the earliest models for fluidized beds, first described by May and based on the following assumptions:

- two phases: bubble and dense
- the dense phase contains all the catalyst
- the majority of the gas passes through the bubble phase with plug flow behavior

Table 7.2 Correlations for industrial gas-solid fluidized beds (height and diameter greater than 1 m).

Sand: $k_{l,e} = 2.3 \cdot 10^{-3}\sqrt{1 + 27.2(V_{SG} - (V_{SG})_m)}$ (m/s)
Porous catalyst: $k_{l,e} = 6.25 \cdot 10^{-3}\sqrt{1 + 27.2(V_{SG} - (V_{SG})_m)}$ (m/s)
$\mathcal{A}_{Be} = 18.2\dfrac{(V_{SG} - (V_{SG})_m)}{\sqrt{1 + 27.2(V_{SG} - (V_{SG})_m)}}\dfrac{1}{F}$ (m^2/m^3 of fluidized bed)
where: $F = \dfrac{H}{0.12 + 0.025H}$
Sand: $k_{l,e}\mathcal{A}_{Be} = \dfrac{(V_{SG} - (V_{SG})_m)}{24F}$ (s^{-1})
Porous catalyst: $k_{l,e}\mathcal{A}_{Be} = \dfrac{(V_{SG} - (V_{SG})_m)}{8.8F}$ (s^{-1})
$(1 - \varepsilon_e) = \varepsilon_B = \dfrac{1.54(V_{SG} - (V_{SG})_m)J}{[1 + 27.2(V_{SG} - (V_{SG})_m)]^{0.17}}$
where: $J = 0.291 + \dfrac{0.182}{H}$ and $\varepsilon_B = 1 - \dfrac{H_m}{H}$
$\mathcal{D}_{l,e} \cong \mathcal{D}_{lG}$ (m^2/s)

Table 7.3 Gas-solid fluidized-bed reactors. Orders of magnitude.

$\mathcal{D}_{l,e}$	=	10^{-5} to 10^{-4} (m^2/s) (as gas phase diffusivity)
$k_{l,e}$	=	10^{-2} (m/s)
$\mathcal{A}_{Be}$	=	10 (m^2/m^3 of fluidized bed)
ε_B	=	0.04
for porous catalyst and:		
D	=	1 m
H	=	2 m
V_{SG}	=	0.1 m/s
$(V_{SG})_m$	=	0.01 m/s

- the volume of the dense phase and the flow rate through it are independent of the total gas flow rate and equal to their values during the appearance of the first bubbles at the start of fluidization
- contact between the gas and the catalyst in the dense phase is assumed to be identical to what it would be in a fixed bed.

The model makes use of two coefficients: a transfer coefficient (K) between the bubbles and the dense phase gas, and a gas axial mixing coefficient (E) in the dense phase. The value of

Botton's model is that the author has been able to show, based on numerous experiments, that these two parameters could be obtained from the minimum velocity of fluidization $(V_{S,G})_m$. The model is formulated using the conventional concepts of transfer unit, dispersion, and reaction.

The equations for the model are then:

$$H_{0K} = 0.9 \left(\frac{(V_{SG})_m}{0.2} \right)^{1.25} \tag{7.50}$$

$$H_{0E} = 1.25 \cdot H_{0K} \left(\frac{(V_{SG})_m}{0.2} \right) \left(\frac{V_{SG} - V_{SGd}}{0.1} \right) \tag{7.51}$$

Range of validity:

$$0.08 \leqslant (V_{SG})_m \leqslant 0.5 \text{ cm/s}$$
$$V_{SG} - V_{SGd} \geqslant 0.10 \text{ m/s}$$
$$D \geqslant 0.25 \text{ m} \quad \text{and} \quad h > 2 \text{ m}$$

where

H_{0K} height of transfer unit between bubbles and dense phase gas
H_{0E} height of dense phase gas dispersion unit
V_{SGd} gas velocity within the dense phase
D reactor diameter
h height of the catalytic bed in the dense phase.

The author also provides a methodology for small-scale experimentation (laboratory, pilot unit) and transposition of the results to industrial scale requirements. Equations identical to (7.50) and (7.51) are provided for small reactors operating in slugging regime. The method has proven applicable for industrial chemical processes requiring high conversion rates (> 99%).

C. Kunii-Levenspiel (K-L) model

This model, more elaborate than those of Werther or Botton, attempts to take into account numerous observations concerning the behavior of bubbles in fluidized beds. The model considers three distinct phases in the bed [Levenspiel, 1999] (Fig. 7.22):

- an emulsion phase, as in Werther's model
- a bubble phase free of all solids, consisting of bubbles having the same diameter d_B
- a phase consisting of the cloud of solid particles around the bubble and entrained by it.

The model describes the successive transfer operations between these phases:

$$\text{(bubbles} \rightarrow \text{cloud)} \quad \text{and} \quad \text{(cloud} \rightarrow \text{emulsion)}$$

and the reactions in the two phases containing the catalyst.

The rise velocity of the bubbles $(V_{r,B})$ within the bed, which is at the minimum fluidization velocity, is an important magnitude and is used in all estimates:

$$V_{r,B} = 0.711 \, (g d_B)^{0.5} \tag{7.52}$$

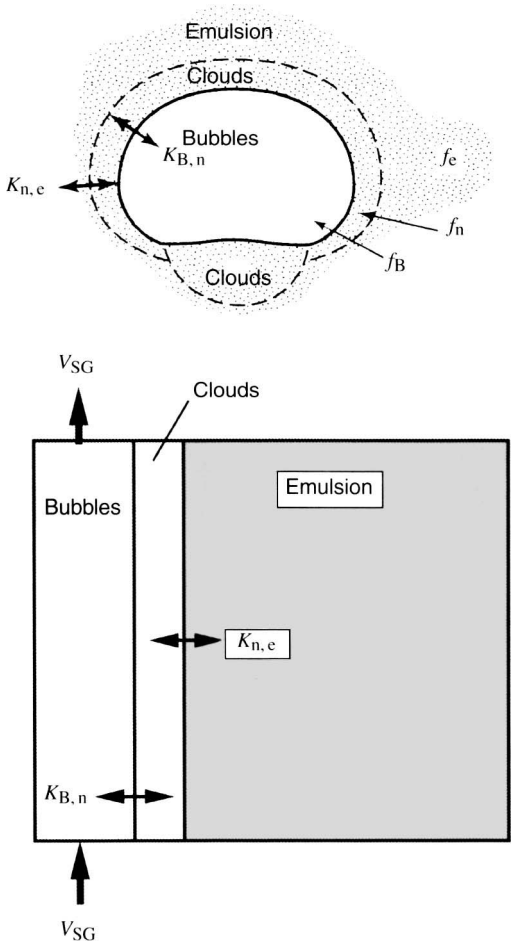


Figure 7.22 Kunii-Levenspiel model.

The fraction of the bed occupied by the bubbles can be calculated as follows:

$$f_B = \frac{V_{SG} - (V_{SG})_m}{V_{r,B}} \tag{7.53}$$

The ratio of the cloud volume to the bubble volume ($f_{n,B}$) varies from 0.2 to 2 for fines, but is very small for larger particles.

The ratio of the volume of solid in the clouds to the total volume of the bed is expressed as:

$$f_{S,n} = f_B(1 - \varepsilon_{mf}) \left[\frac{3\dfrac{(V_{SG})_m}{\varepsilon_{mf}}}{V_{r,B} - \dfrac{(V_{SG})_m}{\varepsilon_{mf}}} + f_{n,B} \right] \tag{7.54}$$

where ε_{mf} is the void fraction of the bed at the fluidization minimum.

The ratio of the volume of solid in the emulsion to the total volume of the bed is then:

$$f_{S,e} = (1 - \varepsilon_{mf})(1 - f_B) - f_{S,n}$$

The coefficients of transfer between the phases are calculated from the following correlations:

- between bubbles and clouds:

$$K_{B,n} = 4.5 \left(\frac{(V_{SG})_m}{d_B} \right) + 5.85 \left(\frac{\mathcal{D}_l^{0.5} g^{0.25}}{d_B^{1.25}} \right) \tag{7.55}$$

- between clouds and emulsion:

$$K_{n,e} = 6.77 \left(\frac{\varepsilon_{mf} \mathcal{D}_l V_{r,B}}{d_B^3} \right)^{0.5} \tag{7.56}$$

The calculation is then fairly conventional and takes into account the resistance in series and the reaction in the cloud and emulsion phases.

7.4.7 Mass and heat transfer between a gas and a solid in the dense phase

Transfer between the gas and the solid in the emulsion phase is governed by two factors:

- the transfer coefficients
- the interfacial area.

Although correlations of the type j_H or $j_D = f(Re)$ can be established for mass and heat transfer, there seems little point in developing them here, for, given the high values of the two factors given above, transfer within the dense phase is extremely rapid, so that:

- the temperatures of the solid and the gas are identical
- the concentrations in the gas phase of the emulsion and at the surface of the particles are identical.

Therefore, there are no measurable external concentration and temperature gradients at any point of the dense phase. Moreover, because of the intense backmixing of the solid, it can be safely assumed that the temperature is appreciably identical throughout the dense phase volume. Additionally, the size of the particles is sufficiently small so that neither an internal temperature gradient nor an internal concentration gradient can be observed. The emulsion phase reaction is partially controlled by the diffusion of the bubble phase reactants to the emulsion phase.

7.4.8 Heat transfer between the wall and the fluidized bed

Experts have long debated the beneficial or harmful effects of internal components. Such components are, however, often necessary, whether in the form of tubes or plates designed to supply or remove heat. Some authors claim that internals, through their arrangement, can be used to obtain better fluidization, limit the growth of bubbles, and improve reactor performance.

Given our current knowledge of the behavior of fluidized beds, we prefer to treat internal components as providing no specific advantages or disadvantages. The assertion that the presence of a bundle of vertical tubes will interfere with bubble growth beyond a diameter corresponding to the free space between the tubes should be approached with caution: bubbles have been observed whose diameter is such that they envelop several tubes in the same bundle. Nonetheless, the literature, especially patent literature, is highly prolix concerning methods for arranging internal components.

The value of the heat transfer coefficient between the wall and the fluidized bed depends on several factors. It is known that the value is high (20 to 40 times higher than with a single fluid at the same superficial velocity). It seems to depend a great deal on local flow conditions for the dense phase near the exchange surfaces. It is difficult to supply a correlation for general use.

The correlations that are used depend on the nature of the object through which heat passes: the wall (vertical cylinder) of the reactor, vertical tubes, horizontal tubes, immersed objects, etc. Davidson and Harrison [1971] provide recommendations for the use of such correlations.

The order of magnitude for the wall-fluidized bed heat transfer coefficient is $h_w = 150$ to $300\ W/m^2 \cdot K$. The Nusselt number $Nu = \left(h_w \overline{d_p}\right) / \lambda_F$ is approximately 0.5 to 2, with 1 being the mean value.

H.F. Rase [1982] has indicated the qualitative effect of the different parameters of a fluidized bed on the transfer coefficient h_w: mean particle diameter, shape and condition of the particle surface, heat capacity of the particle, thermal conductivity of the fluid and the particle, bed height and diameter, tube diameter, angle of inclination of the tubes with respect to the horizontal, baffles, distribution grids.

7.4.9 Introduction of reactants and withdrawal of products

7.4.9.1 Fluid distribution

The distribution of fluid to the lower section of the fluidized bed requires considerable care: good initial distribution determines the performance of the fluidized bed. In particular, it is important to avoid channeling, which is the cause of severe heterogeneity. Moreover, the fluid jets near the distributors are a region of intense activity, both in terms of the reaction and in terms of transfer. Some authors feel the region is characterized by an inlet effect that has a decisive influence on the bed and can be modeled (note that a phenomenon of the same type, known as an outlet effect, appears near the top of the fluidized bed, where gas bubbles burst).

A correctly designed distributor:

- can be used to evenly distribute fluid flow throughout the entire fluidized bed
- allows the use of fluid containing solid fines
- keeps the solid at rest
- allows rapid shutdowns and restarts without excessive fluctuation and without loss of solids.

The most generally accepted design criterion for distributors requires a value for the pressure drop caused by the passage of fluid through it that is at least equal to the highest of the following three values [Kunii and Levenspiel, 1991]:

- 10% of the pressure drop through the bed (equal to the apparent weight of the bed)
- 35 cm of height of a column of water (approximately 350 Pa)
- 100 times the calculated pressure drop of the fluid through the empty reactor.

Nonetheless, this pressure drop should be limited to a reasonable value because of the cost of compression energy.

Distributor manufacturers have displayed great imagination in the design of their products, and there have been a number of patented designs. However, it must be acknowledged that the simplest distributors are often the most efficient. Figure 7.23 illustrates some typical designs that provide satisfactory performance. Figure 7.23A illustrates a simple perforated plate. This type of distributor cannot be used to completely contain the solid at rest. Figure 7.23B illustrates two perforated plates on top of one another, which can be used to overcome this drawback. Figure 7.23C illustrates a section of packing that is sandwiched between two perforated grids. This arrangement can be used to inject a second miscible fluid into the packing. Large diameter distributors are preferably formed into concave plates (Fig. 7.23D), which increases their mechanical strength and corrects the tendency to collect streams of bubbles near the center. Figure 7.23E illustrates a grid element with a bubble cap, which prevents any reflux of solids into the fluid inlet region. Figure 7.23F shows a distribution system consisting of a number of perforated tubes arranged uniformly at the bottom of the bed.

7.4.9.2 Product withdrawal

During normal operation of the fluidized bed, part of the solid—whether it is the fraction with the smallest particle size from the original bed or fines resulting from wear of the larger particles—is entrained by the gas. To limit this entrainment, the freeboard above the fluidized bed can be used to allow the largest particles to fall back to the bed by gravity.

The concentration of solids in this zone changes from a value that is close to, but distinct from, the concentration in the bed, to a stationary value corresponding to the entrainment by pneumatic transport. The minimum height needed to achieve this stationary concentration, referred to as the *transport disengagement height* (TDH), determines the position of cyclones above the bed. The leg of the particle collector from the cyclone descends below the surface of the bed and a catalyst level is established in this leg.

If necessary, a second cyclone stage, inside or outside the reactor enclosure, can be used for dust removal and to eliminate the fines collected in the leg of the second cyclone.

The use of one- or two-stage cyclones somewhat complicates the design of the upper section of the reactor and increases investment costs. However, the cyclones themselves are inexpensive, robust, reliable, and have no rotating parts; the only operating cost involved is for the energy consumed by friction in the form of a pressure drop. Once again we find that the pressure balance for a unit with a fluidized bed must be examined with great care [Gauthier, 2000].

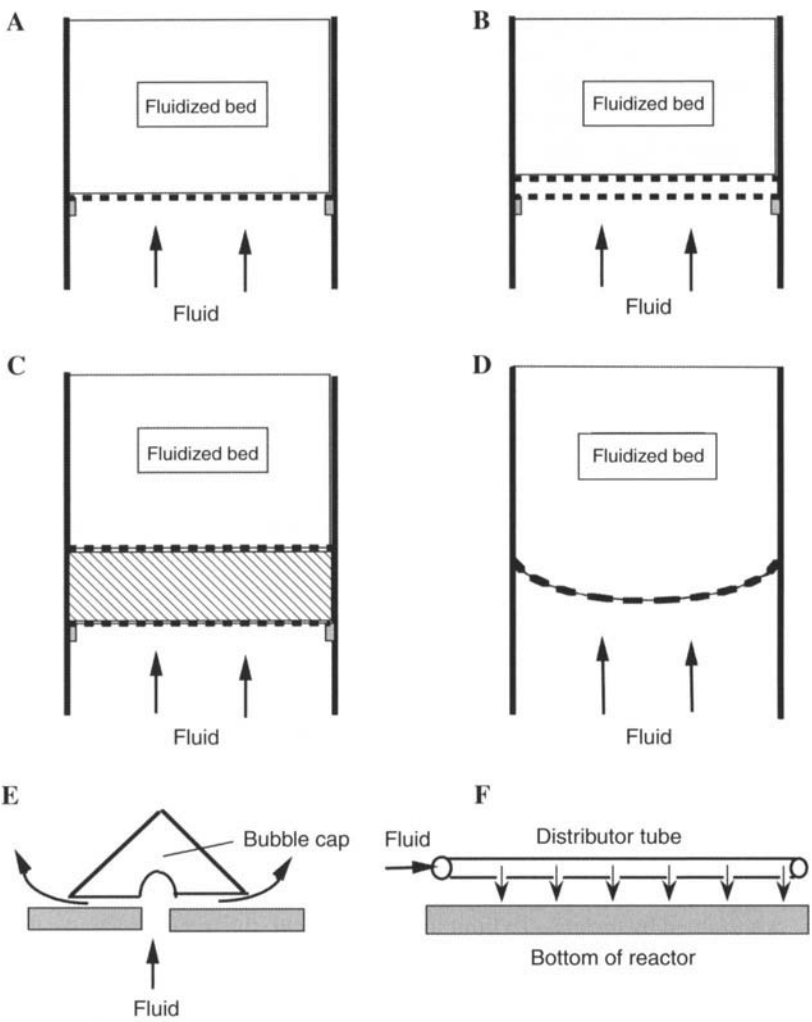


Figure 7.23 Fluid distributors in a fluidized bed.

7.4.10 Industrial applications

7.4.10.1 Catalytic cracking

No industrial application of fluidized bed technology has generated as much development interest and led to as much technological success as the catalytic cracking of gas-oils and middle distillates, later extended to residues. The process consists in using a solid catalyst, such as silica-alumina, to crack heavy hydrocarbons into lighter fractions (LPG, gasoline, and gas-oil). In the past, all three possible methods—fixed bed, moving bed, and fluidized bed—have been successively used for catalytic cracking. The technology has

seen considerable improvement, together with the development of new catalysts, especially the appearance of zeolites. At this time only fluidized bed technology is used in catalytic cracking units.

Shell introduced an important innovation to the process, namely, the *riser* with a short residence time, initially followed by a conventional fluidized bed. Gradually, the technology evolved, each operator or licenser following their own logic to improve both the reaction side and the regeneration side of the process. Over time the characteristics that are found in modern catalytic cracking units, commonly known as FCC (Fig. 7.24), were introduced. In terms of the reaction, it is characterized by short residence times in the riser, atomization of the feed at various points with steam assistance, fast separation of the effluents, improved stripping of the catalyst followed by regeneration. Regeneration itself has also been considerably improved through control of catalyst circulation within the regenerator, through improvement of air distribution, and through the inclusion of two regeneration stages in series (Fig. 7.25, photo 7).

Referring to Fig. 7.25, we find the essential elements common to all modern FCC units.

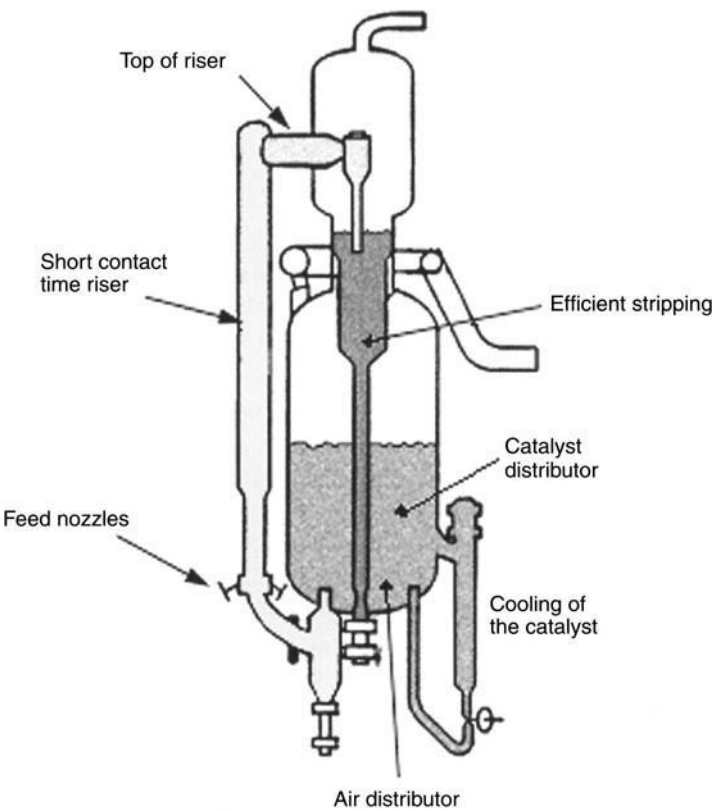


Figure 7.24 Catalytic cracking unit, illustrating important aspects of the technology.

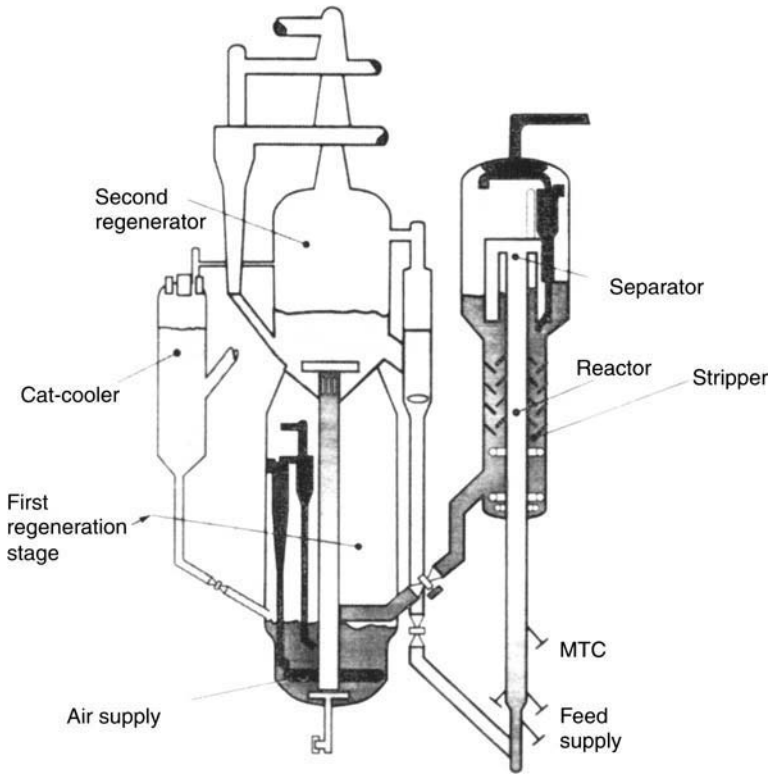


Figure 7.25 Fluid catalytic cracker for residues; the unit has two regeneration stages and a cat-cooler (based on Heinrich *et al.*, 1997).

• **Reactor-riser**: This consists of a vertical tube at the base of which the feed, preheated to approximately 500°C, and high-temperature (650 to 700°C) catalyst from the regenerator are introduced. At the bottom of the riser, the feed is introduced in fine droplets through several nozzles distributed around the periphery of the riser. The quality of feed dispersion and the extent of mixing with the catalyst are key elements for obtaining good selectivity. In some units a second introduction of feed is sometimes carried out in the middle of the riser, to adjust the temperature at the top of the riser and avoid secondary cracking of the reaction products. The outlet temperature of the riser is between 500 and 550°C.

Within the riser, whose diameter can exceed 1 m, catalyst flow is far from uniform. Radial density measurements of the catalyst have shown the existence of a parabolic distribution, with a relatively dilute axial zone, and much greater density along the periphery, with downward flow along the walls. The residence time, calculated for the reaction products, is between 1 and 2.5 seconds. The risers are generally 30 m in length or more, with a L/D ratio greater than 20.

It is important that the diameter of the riser where the feed is introduced be designed to supply a velocity of at least 4.5 to 6 m/s (based on complete vaporization of the feed). The



Photo 7 Fluidized-bed reactors: R2R catalytic cracking. The right side of the unit consists of the two regeneration stages on top of which can be seen the external cyclones. (*IFP Photo Library*).

diameter of the riser can be increased near the top to accommodate molar expansion. The narrow part of the riser, near the bottom, is often called the acceleration zone. The velocity at the riser outlet is generally about 18 m/s.

- **Separation of the catalyst from the reaction products:** An initial mechanical separation is carried out directly at the top of the riser using a ballistic or impact device. The reactor effluent is run through cyclones to remove catalyst fines before passing through the various fractionation columns in the unit. The catalyst then descends by gravity through a steam stripping section, where it is stripped of hydrocarbons adsorbed on the surface. Contact between the catalyst and the steam is generally carried out by means of concentric inclined baffles.

To provide good circulation of the catalyst, the standpipes, which are of relatively small diameter, must be carefully designed. They are ordinarily designed to accept from 500 to 1 500 kg of catalyst/$m^2 \cdot s$. They are preferably vertical, although angles as great as 35° from the vertical are acceptable.

Many standpipes require additional aeration to prevent the catalyst stream from becoming too dense. Typically, 0.55 to 0.85 m^3STP of gas per ton of circulating catalyst is added for a 30 m vertical standpipe. As a first approximation, complete aeration is uniformly distributed throughout the line. For optimum aeration, the density of the catalyst should be between 480 and 560 kg/m^3.

Of all the elements in an FCC unit, the standpipes are without doubt the most critical, and many catalyst circulation problems in FCCs result from problems in aerating the standpipes. Granulometric distribution of the catalyst and, especially, the proportion of fines can have a significant effect on circulation.

- **Regeneration section:** Here, the catalyst comes into contact with an oxidizing atmosphere so that the coke deposited during cracking in the riser is burned. Increasingly frequently, this combustion is made to take place in two stages. During the first stage, carbon deposits containing some proportion of hydrogen, and which are therefore more reactive, are burned. This first step in the regeneration process gives off CO_2 as well as steam, which at high temperature can result in a loss of catalyst activity. The temperature is deliberately limited by controlling the concentration of oxygen in the regeneration gas to prevent the loss of activity.

During the second stage, the oxygen concentration is greater to completely burn off the coke, and the temperature is higher. Good carbon combustion depends both on the circulation of catalyst through the regenerator and good distribution of oxygen in the various parts of the fluidized bed.

The kinetics of carbon combustion is influenced by the concentration of coke (roughly first order), by the partial pressure of oxygen (first order), and temperature. The CO/CO_2 combustion gas ratio depends on the temperature at the surface of the catalyst. The final combustion of CO in the gas phase in the bed is, however, inhibited by the presence of the solid. Also, some catalysts contain CO combustion promoters to reduce the presence of too much CO at the outlet of the fluidized bed and subsequent postcombustion in the upper part of the regenerator. The excess oxygen, which is beneficial for burning coke, must therefore be controlled with care to limit this postcombustion.

Ideally, catalyst flow should be plug-like to obtain the most uniform possible residence time distribution; the presence of two regenerators in series can improve this distribution. The residence time of the catalyst varies depending on the units from 1 to 10 min. Consequently, the fluidized bed must be large, with a height-diameter ratio between 0.3 and 0.7. Additionally, significant disengagement height (5 to 6 m) is needed to avoid excessive catalyst entrainment in the cyclones, which are generally two-stage.

The distribution of oxygen is difficult to adjust, since most frequently a simple perforated tube distributor (Fig. 7.23F) or grid are used even though they do not allow significant variations in the local flow rates introduced per unit volume of fluidized bed. To ensure approximately equal flow rate for each opening, the pressure drop is adjusted to approximately 30% of the pressure drop in the bed.

The combustion gas leaving the regenerator is cooled in an exchanger and any particles are removed in an electrostatic precipitator; any carbon monoxide in the gas is burned to carbon dioxide in a special boiler (CO boiler). When the regenerators operate at higher pressure, it is often economical to include an expansion turbine ahead of the precipitator. Whenever more restrictive SO_x and NO_x emission control limits require it, treatment of the combustion gas must be improved, and a washer incorporated for the SO_x and a selective catalytic reducer for controlling NO_x.

Several fluidization regimes are found throughout such a unit, as illustrated in Fig. 7.26.

An FCC catalyst becomes completely fluidized for values of V_{SG} approaching 0.25 cm/s. Between 0.3 and 1 cm/s, the catalyst is fluidized without any observable gas bubbles (particulate regime). An increase in superficial velocity brings about the appearance of the bubble regime. In narrow tubes (such as transfer lines) the bubbles can become so large that they approach the size of the tube itself (slugging).

Above 1 m/s the bubbles become unstable and break apart; this is known as the turbulent regime. If velocities reach 1.8 m/s, solid agglomerates are projected outside the bed as other agglomerates fall down the walls (rapid fluidization). Beyond approximately 1.8 m/s, the largest agglomerates are broken into smaller chunks, clusters which are entrained outside the tube, with relatively little fallback along the walls. An essential characteristic of an FCC unit is the rapid circulation of catalyst, which also happens to be a solid heat carrier, thus allowing the overall thermal balance to be maintained. The rates of circulation must therefore be adjusted at every point in the unit to values that are often critical, as indicated in Table 7.4.

Control of the unit is, for the most part, focused on the global heat balance, as indicated in Fig. 7.27. The heat produced by combustion of the coke in the regenerators must be removed and used as efficiently as possible for cracking the feedstock and producing steam, which is introduced at various points in the unit. Control of the FCC is carried out by means of two slide valves:

- The valve on the conduit that brings regenerated catalyst to the bottom of the riser controls the temperature of the riser by adjusting the flow of hot regenerated catalyst to the riser.
- The valve on the standpipe running from the stripper to the regenerator controls the level of the stripper by adjusting the flow of catalyst leaving the stripper (Fig. 7.25).

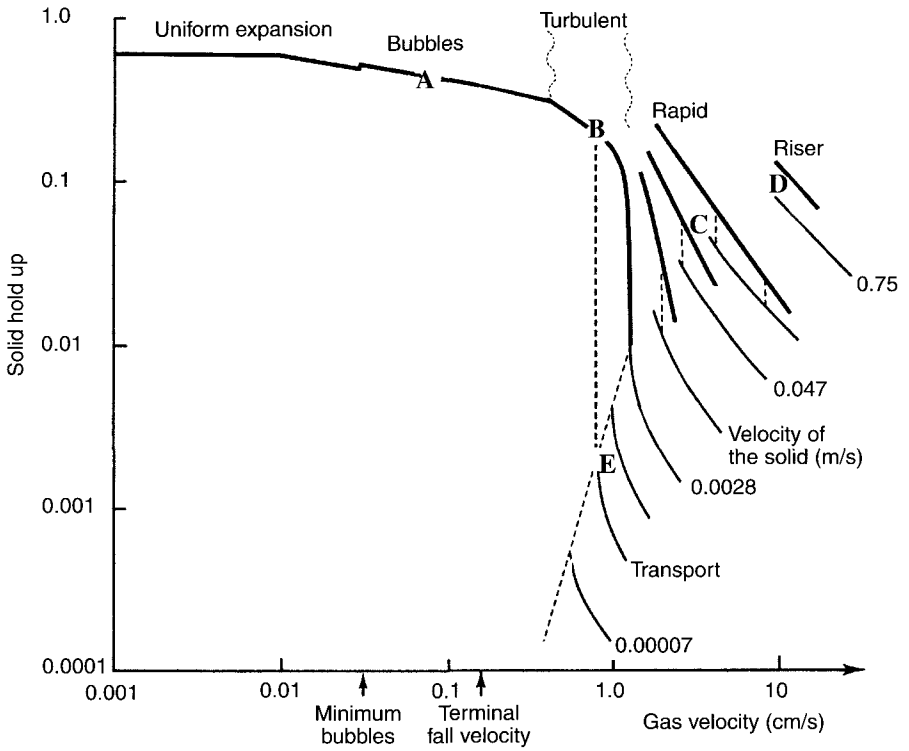


Figure 7.26 The various fluidization regimes found in a catalytic cracking unit: **A.** Dense regime with bubbles (standpipes). **B.** Dense turbulent regime (regenerator). **C.** Fast transport regime between the regenerator stages. **D.** Transport in the riser. **E.** Entrainment in the regenerator freeboard.

Table 7.4 Orders of magnitude of velocities and flow rates in the various parts of a catalytic cracking unit.

Riser	Bottom velocity	4–6 m/s
	Outlet velocity	15–20 m/s
	Maximum velocity	27.5 m/s
Stripper	Steam velocity	0.15–0.3 m/s
	Catalyst flow	30–75 kg/s · m^2
	Maximum flow	90 kg/s · m^2
Standpipe	Catalyst flow	500–1 500 kg/s · m^2
Regenerator	Gas velocity	0.6–1 m/s
	Residence time of catalyst:	
	One stage	5–10 min.
	Two stages	3–5 min/stage

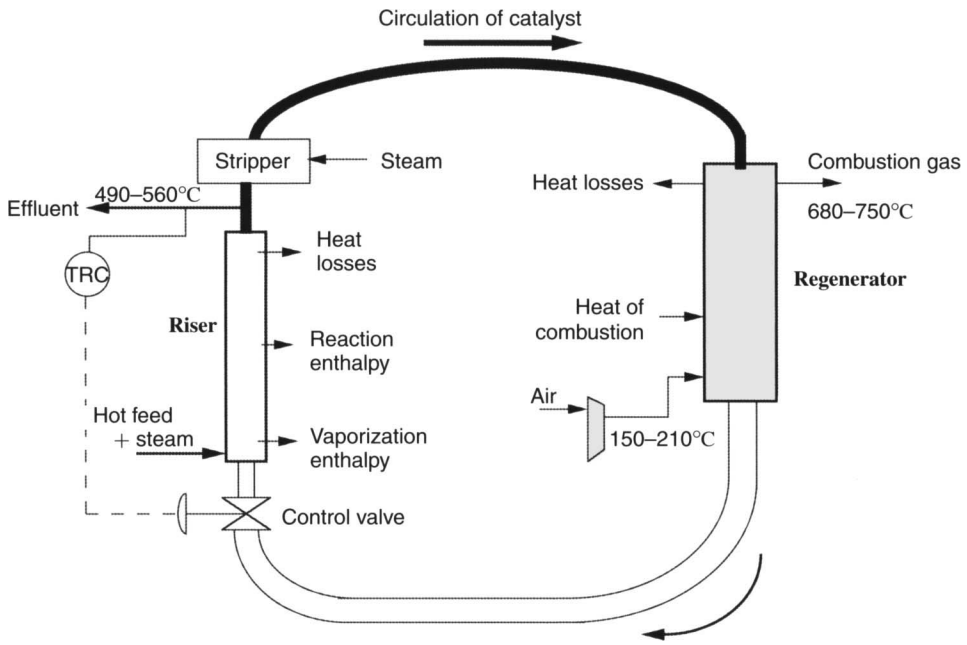


Figure 7.27 Heat balance of a catalytic cracking unit.

Much research has also been carried out on the use of increasingly heavier feedstocks (residues) and significant improvements have been introduced. In particular, for processing residues it is necessary to extract the excess heat produced in the regenerator, since more coke is produced than in the cracking of conventional feeds. The use of two regenerators and catalyst coolers (cat coolers) is essential in such cases (Fig. 7.25).

Because of the high temperatures in the various parts of the unit, all the metal walls are covered with refractory cement, to provide heat insulation and reduce the temperature of the metal, which provides the unit as a whole with mechanical strength.

7.4.10.2 Other applications of fluidized beds

Given the potential advantages of the fluidized bed, considerable effort has been made in applying the technology to a range of chemical processes. Here we list a few of the applications now in industrial use:

- polymerization of ethylene or propylene
- oxidation reactions, including:
  - naphthalene → phthalic anhydride
  - xylenes → phthalic acids
  - butane → maleic anhydride
  - ammoxidation of propylene to acrylonitrile
  - oxychlorination of ethylene for the production of vinyl chloride.

The advantage of the fluidized bed for these processes lies in its ability to evacuate the heat produced by the reaction throughout the reactor and provide good selectivity during the transformation.

More recently, Dupont has developed a process whose technology is similar to that of FCC (entrained bed) to produce tetrahydrofuran by oxidation of butane.

Other applications of the fluidized bed or entrained bed are found in industry for the transformation of solid products: reduction of ores, pyrite oxidation, manufacture of lime through the decomposition of calcium carbonate, coal combustion, the incineration of solid wastes, and so on. These are reactors in which the solid takes part in the reaction and, therefore, are not included in the present chapter, even though the general characteristics of fluidized beds are equally applicable.

REFERENCES

Botton R (2000) Lits fluidisés pour l'industrie chimique. Oil and Gas Science and Technology - Revue de l'IFP, 55, 1, pp 87–121.

Chauvel A *et al.*(1981) Manual of economic analysis of chemical processes. McGraw-Hill, New York.

Cybulski A, Moulijn JA (1994) Monoliths in Heterogeneous Catalysis. Catal Rev Sci Eng 36(2), 179–270.

Davidson JF, Harrison D (1971) Fluidization. Academic Press, London.

Eigenberger G (1992) Ullman's Encyclopedia of Industrial Chemistry. Vol. B4, Fixed Bed Reactors, pp 199–238.

Gauthier Th (2000) Petroleum Refining. Vol. 4: Materials and Equipment. Editions Technip, Paris, pp 128–131.

Geldart D (1973) Powder Technology. Vol. 7, p 285.

Heinrich G, Gauthier Th, Del Pozo M (1997) R2R: A Suite of Technologies for Residue Catalytic Cracking: Upgrading Heavy Ends with IFP, IFP.

Jamialahmadi M, Müller-Steinhagen (2000) Hydrodynamics and heat transfer of liquid fluidized bed systems. Chem. Eng. Comm. 2000, Vol. 179, pp 35–79.

Kunii D, Levenspiel O (1991) Fluidization Engineering, Second edition Butterworth-Heinemann, Boston.

Levenspiel O (1999) Chemical Reaction Engineering, third edition. Ed. John Wiley & Sons.

Perry RH, Green CH (1984) Chemical Engineer's Handbook, 6e édition. McGraw-Hill, New York.

Rase HF (1977) Chemical Reactor Design for Process Plants. Vol. I. Wiley Interscience, New York.

Satterfield CN (1981) Mass Transfer in Heterogeneous Catalysis. Krieger, New York.

Trambouze P (2000) Petroleum Refining. Vol. 4: Materials and Equipment. Editions Technip, Paris.

Werther J (1978) Chem Ing Tech 50, 11, pp 850–860, et Werther J, Hegner B (1980) Chem Ing Tech 52, 2, pp 106–113.

Werther J (1980) Chem Eng Sci 35, pp 372–379.

NOMENCLATURE

(specific to Chapter 7)

Symbol	Definition	SI Unit
A	$= -\nu_1 k_M \rho_c$	s^{-1}
Ar	Archimedes number $Ar = \dfrac{\rho_F (\rho_p - \rho_F) \overline{d_p^3} g}{\mu_F^2}$	–
$\mathcal{A}_{Be}$	Bubble phase – emulsion phase interfacial area	m^2/m^3
C_D	Drag coefficient	–
$\mathcal{D}_R$	Coefficient of radial dispersion	m^2/s
D	Reactor diameter	m
$\overline{d_p}$	Mean particle diameter	m
d_t	Tube diameter	m
$\mathcal{D}_{l,e}$	Emulsion phase diffusion coefficient	m^2/s
e	Tube thickness	m
F_T	Drag force	N
G, L	$= \rho_F V_{SF}$ fluid flow per unit cross-section	$kg/m^2 \cdot s$
H	Height of expanded fluidized bed	m
H_m	Height of fluidized bed at the fluidization threshold	m
h^*	Characteristic height in Werther's model	m
$k_{l,e}$	Bubble phase – emulsion phase transfer coefficient	m/s
m	Ratio of the diameter of a cylindrical reactor to the mean particle diameter	–
n	Ratio of the height of a cylindrical reactor to the mean particle diameter	–
PPH	Ratio of the hourly weight flow rate of feed to the weight of the catalyst	h^{-1}
Pe_{ma}	Axial mass Peclet number $Pe_{ma} = \dfrac{\overline{d_p} V_{SF}}{\mathcal{D}_A}$	–
Pe_{mr}	Radial mass Peclet number $Pe_{mr} = \dfrac{\overline{d_p} V_{SF}}{\mathcal{D}_R}$	–
p	Rate of heat generation	W/m^3
r	Distance to the axis of a cylindrical reactor	m
$\mathcal{R}_i'$	Rate of generation or disappearance of a compound $= \sum \nu_{i,j} r_j'$	$mol/kg \cdot s$
R	Radius of a cylindrical reactor	m
T_r	Mean temperature of the reactor	K
T_{pi}	Temperature at the internal wall of the reactor	K

Symbol	Definition	SI Unit
T_e	Temperature at the exterior of the reactor: coolant temperature	K
u_t	Terminal velocity of a particle	m/s
VVH	Ratio of the hourly volume flow rate of feed to the volume of the catalytic bed	h^{-1}
y	Distance from the interface, in the film, emulsion phase side	m
α	Angle of repose	–
γ	Angle of internal friction	–
θ	Angle of inclination to the horizontal	–
	Subscripts:	
B	relative to the bubble phase	
e	relative to the emulsion phase	
m	at the fluidization threshold	
ref	in the reference state	

Copyrighted Materials
Copyright © 2004 Editions Technip Retrieved from www.knovel.com

8 Three-Phase Reactors: Gas, Liquid, and Catalytic Solid

8.1 INTRODUCTION

Chemical reactions requiring the presence of three phases are commonplace in industrial settings. They include the many examples of catalytic hydrogenation found in practice, as well as facilities for oxidation and the treatment of effluents.

In practice there are several possibilities for bringing the three phases into contact with one another in such systems. The catalytic solid can be placed in a fixed or moving bed, maintained in suspension within the liquid phase, or even entrained by fluids. Two methods are frequently used for bringing the fluid phases (gas and liquid) into contact:

- gas flow through a captive liquid within the reactor
- flow of two fluid phases through the catalytic bed.

Different devices (Fig. 8.1) are used for bringing together the various phases; those most frequently found in industrial practice include:

- Systems with a catalyst dispersed in the liquid phase; the following devices are the most commonly used:
  - bubble columns
  - mechanically stirred reactors
  - three-phase fluidized beds.
- Systems with a catalyst arranged in a fixed or moving bed, through which the fluid phases flow, in either cocurrent (downflow or upflow) or countercurrent mode.

In terms of the reactor classification provided earlier (Chapter 1), three-phase reactors generally operate in batch mode with respect to the catalyst. In contrast, the gas phase generally passes continuously through the reactor. Depending on the circumstances, the liquid phase may or may not be fed continuously, as shown in Table 8.1.

Before describing the various units in greater detail, we will, as in Chapter 6, consider an isolated catalyst particle, but this time in the presence of two fluid phases—liquid and gas.

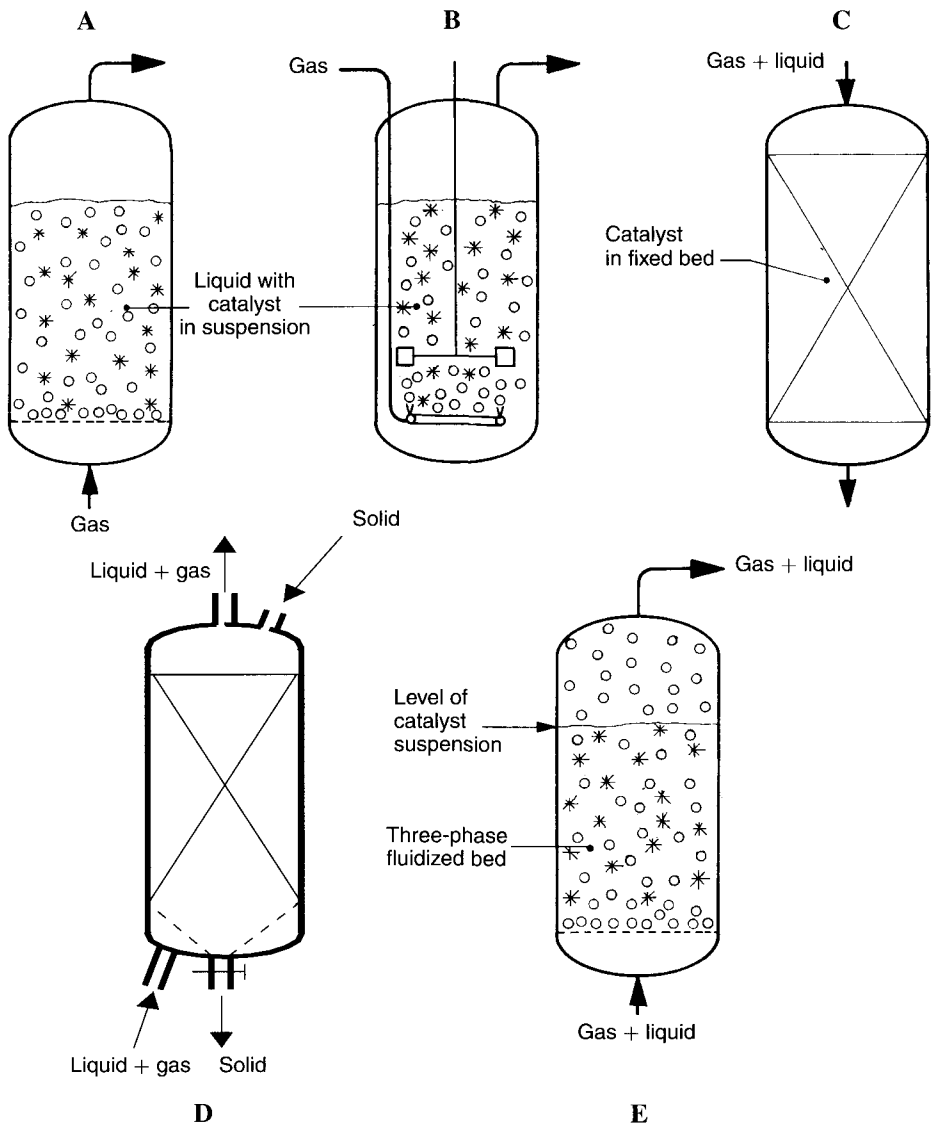


Figure 8.1 Three-phase catalytic reactors: **A.** Bubble column. **B.** Mechanically stirred tank. **C.** Fixed-bed reactor with two-phase cocurrent downflow. **D.** Moving-bed reactor. **E.** Three-phase fluidized bed, or ebullated bed.

8.1.1 Reaction at the surface of an isolated catalyst particle

Assume we have a catalytic reaction between a compound A_1 in the gas phase and a compound A_2 in the liquid phase:

$$\nu_1 A_1(\text{gas}) + \nu_2 A_2(\text{liquid}) \rightarrow \nu_3 A_3(\text{liquid})$$

Table 8.1

Liquid is fed in batches	Liquid is fed continuously	
	Tubular	**CSTR**
Bubble column	Fixed bed with two-phase flow	Three-phase fluidized bed
Mechanically stirred reactor	Moving bed	

To write the respective mass flows of A_1, A_2, and A_3, refer to Fig. 8.2.

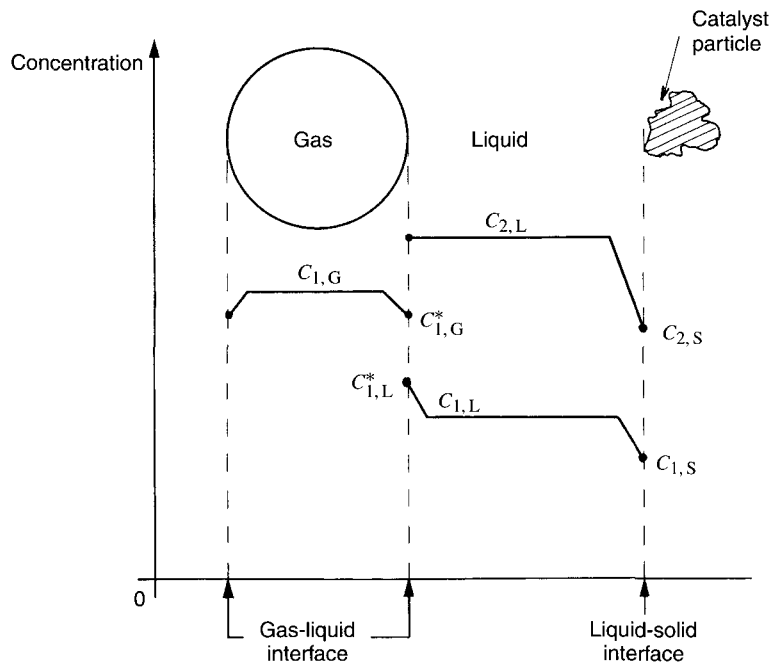


Figure 8.2 Concentration profiles of the reactants A_1 and A_2 in the vicinity of the catalyst grain suspended in a liquid phase.
Reaction: $\nu_1 A_1(\text{gas}) + \nu_2 A_2(\text{liquid}) \rightarrow \nu_3 A_3(\text{liquid})$.

In the steady-state regime, the number of moles of A_1 transferred per unit volume of reactor per unit time, N_1, can be evaluated by successively examining the gas-liquid interface and the liquid-solid interface or by using the reaction kinetics at the surface of the catalyst:

$$\text{Gas-liquid interface:} \quad N_1 = K_{1,L} a_{LG} \left(\frac{C_{1,G}}{m_1} - C_{1,L} \right) \tag{8.1}$$

$$\text{Liquid-solid interface:} \quad N_1 = k_{1,S} a_S \left(C_{1,L} - C_{1,S} \right) \tag{8.2}$$

$$\text{Chemical reaction:} \quad N_1 = -\nu_1 r'_S S_p \rho_c \eta \tag{8.3}$$

where:

$$C^*_{1,G} = mC^*_{1,L} \qquad \text{[specific case of (3.3)]}$$

$$\frac{1}{K_{1,L}} = \frac{1}{k_{1,L}} + \frac{1}{m_1 k_{1,G}} \qquad \text{[specific case of (3.7)]}$$

where

$\mathcal{A}_{LG}$	gas-liquid interfacial area per unit volume of reactor (m^2/m^3)
$\mathcal{A}_S$	grain superficial area per unit volume of reactor or liquid-solid interfacial area (m^2/m^3)
$C_{1,G}$	concentration of A_1 in the gas phase, far from the gas-liquid interface (mol/m^3 of gas)
$C_{1,L}$	concentration of A_1 in the liquid phase, far from the gas-liquid interface (mol/m^3 of liquid)
$C_{1,S}$	concentration of A_1 in the liquid phase, at the external surface of the particle (mol/m^3 of liquid)
$K_{1,L}$	global mass transfer coefficient with respect to the liquid phase (m/s)
$k_{1,G}$, $k_{1,L}$	gas side and liquid side film transfer coefficient (m/s)
$k_{1,S}$	liquid-solid film transfer coefficient (m/s)
m_1	partition coefficient of compound A_1 between the liquid phase and gas phase
N_i	transfer flow of compound A_i per unit volume of reactor (mol/$m^3 \cdot$ s)
r'_S	reaction rate for surface conditions on the outside of the grain (mol/s $\cdot$ m^2 of outside grain surface)
S_p	specific surface of the grain (m^2 of catalytic surface of grain/kg)
ρ_c	catalyst mass per unit volume of reactor (kg/m^3)
η	effectiveness factor of the reaction or use of the catalytic surface.

The rate of reaction is expressed for the external surface conditions of the particle.

For compound A_2, we can write:

$$N_2 = k_{2,S}\mathcal{A}_S\left(C_{2,L} - C_{2,S}\right) \tag{8.4}$$

and:

$$N_2 = N_1\frac{\nu_2}{\nu_1} \tag{8.5}$$

and therefore:

$$N_2 = -\nu_2 r'_S S_p \rho_c \eta \tag{8.6}$$

And for compound A_3:

$$N_3 = k_{3,S}\mathcal{A}_S\left(C_{3,L} - C_{3,S}\right) \tag{8.7}$$

$$N_3 = N_1\frac{\nu_3}{\nu_1} \quad (N_3 \text{ and } N_1 \text{ have opposite signs}) \tag{8.8}$$

$$N_3 = -\nu_3 r'_S S_p \rho_c \eta \tag{8.9}$$

For an overall reaction order of 2 (first order with respect to A_1 and first order with respect to A_2), we have:

$$r'_S = k_S C_{1,S} C_{2,S} \tag{8.10}$$

Moreover, it is still possible to define an apparent rate constant. Thus, for a second-order reaction, that is first order with respect to A_1 and first order with respect to A_2, an apparent rate constant can be defined by the equation:

$$N_1 = \mathcal{K}'_1 \mathcal{A}_S C_{1,G} C_{2,L} \tag{8.11}$$

The numerical value of $\mathcal{K}'_1$ depends on k_S, $k_{1,G}$, $k_{1,S}$, and η in a manner that is generally complex. However, if the reaction is first order with respect to A_1, a simple analytic relation can be established. For example, if it is assumed that reactant A_2 is greatly in excess in the liquid phase and, consequently, $C_{2,S} \cong C_{2,L} = \text{constant}$, a decay in the reaction order is observed, and the above equation becomes:

$$N_1 = \mathcal{K}_1 \mathcal{A}_S C_{1,G} \tag{8.12}$$

which is similar to (6.68) with $\mathcal{K}_1 = \mathcal{K}'_1 C_{2,L} = \text{Cte}$.

Comparing (8.1), (8.2), (8.3), (8.10), and (8.12), the following equation can be established, which illustrates the dependence of $\mathcal{K}_1$ on $K_{1,L}$ (which comprises $k_{1,G}$ and $k_{1,L}$), $k_{1,S}$, k'_S, and η:

$$\frac{1}{\mathcal{K}_1} = m_1 \left[\frac{\mathcal{A}_S}{\mathcal{A}_{LG}} \frac{1}{K_{1,L}} + \frac{1}{k_{1,S}} + \frac{\mathcal{A}_S}{-\nu_1 k'_S S_P \rho_c \eta} \right] \tag{8.13}$$

where:

$$k'_S = k_S C_{2,S} \tag{8.14}$$

Particular cases

- If it is assumed that the resistance to transfer in the gas phase is negligible ($k_{1,G}$ is very large), then:

$$\frac{1}{\mathcal{K}_1} = m_1 \left[\frac{\mathcal{A}_S}{\mathcal{A}_{LG}} \frac{1}{k_{1,L}} + \frac{1}{k_{1,S}} + \frac{\mathcal{A}_S}{-\nu_1 k'_S S_P \rho_c \eta} \right] \tag{8.15}$$

- If, however, there is little resistance to transfer in the liquid phase ($k_{1,L}$ is very large), then:

$$\frac{1}{\mathcal{K}_1} = m_1 \left[\frac{1}{k_{1,S}} + \frac{\mathcal{A}_S}{-\nu_1 k'_S S_P \rho_c \eta} \right] \tag{8.16}$$

- If there is little resistance to liquid-solid transfer ($k_{1,S}$ is very large), in such a way that the controlling process is the chemical reaction itself, then:

$$\frac{1}{\mathcal{K}_1} = \frac{m_1 \mathcal{A}_S}{-\nu_1 k'_S \eta S_P \rho_c} \tag{8.17}$$

and we have the equation for the intrinsic kinetics:

$$N_1 = \mathcal{K}_1 \mathcal{A}_S C_{1,G} = -\nu_1 k'_S S_P \rho_c \eta \frac{C_{1,G}}{m_1}$$

$$N_1 = -\nu_1 k'_S S_P \rho_c \eta C_{1,L} = -\nu_1 k'_S S_P \rho_c \eta C_{1,S} \tag{8.18}$$

- There can be a specific solution to the general Eq. (8.13) if the catalyst grains are non-porous or very small. For in this case the surface area available for the reaction and the external surface area are the same:

$$S_p \rho_c = \mathcal{A}_S \quad \text{and} \quad \eta = 1$$

Eq. (8.13) becomes:

$$\frac{1}{\mathcal{K}_l} = m_l \left[\frac{\mathcal{A}_S}{\mathcal{A}_{LG}} \frac{1}{K_{l,L}} + \frac{1}{k_{l,S}} + \frac{1}{-\nu_l k'_S} \right] \tag{8.19}$$

In general, the above considerations would lead us to question any changes in the chemical kinetics because of the physical phenomena that occur along with the chemical reactions. Equation (8.13)—valid only for first-order reactions—can be used to estimate the values of different resistance terms. $\mathcal{A}_{LG}$ and $\mathcal{A}_S$ can be estimated from the bubble size $(\overline{d_B})$, the gas holdup (ε_G), the size of the catalyst particles $(\overline{d_p})$, and the volume fraction occupied by the catalyst (ε_p). By convention:

$$\mathcal{A}_{LG} = \frac{6\varepsilon_G}{\overline{d_B}}$$

$$\mathcal{A}_S = \frac{6\varepsilon_p}{\overline{d_p}} = \frac{6\rho_c}{\overline{d_p}\rho_p}$$

which leads to:

$$\frac{C_{l,G}}{m_l N_l} = \frac{\overline{d_B}}{6K_{l,L}\varepsilon_G} + \frac{1}{\rho_c} \left[\frac{\overline{d_p}\rho_p}{6k_{l,S}} + \frac{1}{-\nu_l k'_S \eta S_p} \right] \tag{8.20}$$

or:

$$\frac{C_{l,G}}{m_l N_l} = A + \frac{B}{\rho_c}$$

The first term of this equation can be measured experimentally. By repeating the measurement with different amounts of catalyst (variable ρ_c), the results can be plotted in the form of a curve:

$$\frac{C_{l,G}}{N_l} = f\left(\frac{1}{\rho_c}\right) \tag{8.21}$$

If Eq. (8.20) is applicable (first-order or pseudo-first-order reaction), we should obtain a straight line whose slope and y value when $x = 0$ can be used to estimate the terms A and B. This procedure, which can be used in simple cases [Satterfield, 1970], is not generalizable. Depending on the reaction kinetics, the interaction of physical phenomena results in apparent kinetic equations that are more or less complex. There are a number of publications in the literature that discuss this issue [Shah, 1979, Levenspiel, 1999].

One general method for approaching these problems consists in introducing a global effectiveness factor that takes into account the various phenomena involved. Equations of this global effectiveness factor for various chemical kinetics can be found in the literature [Wijngaarden *et al.*, 1998]. They include different effectiveness factors (gas-liquid, liquid-solid, and the

catalyst particle), which compete to reduce global effectiveness. The effectiveness factor of the particle (η) has already been introduced in Chapter 6; it is evaluated using the Thiele modulus, with the understanding that the effective diffusivity $\mathcal{D}_{le}$ must be estimated for pores filled with the liquid phase. This has the effect of considerably reducing the value of the diffusivity compared to its value in the gas phase (smaller by about a factor of 10^4). This diffusivity is heavily influenced by temperature, directly, but also by the viscosity of the liquid, as shown by the Stokes-Einstein equation:

$$\mathcal{D}_{l,L} \approx \frac{T}{\mu_L} \tag{8.22}$$

Moreover, when the dimensions of the diffusing molecule approach the mean diameter of the pores, a sharp decrease in effective diffusivity $\mathcal{D}_{le}$ has been observed. This phenomenon can assume importance when heavy petroleum residues are processed, for example, during desulfurization. In general, the values of the tortuosity factors used to calculate $\mathcal{D}_{le}$ are, as in the gas phase, comprised between 2 and 3.

There is little question that it is through internal diffusion that the size of catalyst particles has its greatest effect, and, from this point of view, the different reactor types considered in the present chapter may present significant differences. Most often, the initial result of the interaction of the various physical phenomena with chemical phenomena is to reduce the rate of chemical transformation, but, in the case of reaction systems involving several simultaneous or consecutive reactions, the selectivity of the transformation can also be strongly altered.

8.2 CHARACTERISTICS OF THREE-PHASE REACTORS

Below, we discuss the different types of reactors mentioned at the beginning of this chapter, namely:

- bubble columns
- mechanically stirred reactors
- fixed beds with two-phase flow
- moving beds
- three-phase fluidized beds.

For each reactor we indicate what is known about the various physical phenomena that characterize the behavior of each type of device:

- hydrodynamics
- gas-liquid mass transfer
- liquid-solid mass transfer
- heat transfer.

In addition to general reference works on three-phase reactors, such as those by Shah [1979], Gianetto and Silveston [1986], Froment and Bishoff [1990], Wijngaarden *et al.* [1998], and Levenspiel [1999], we would like to point out the excellent review by Dudukovic *et al.* [1999], concerning the qualitative aspects of multiphase systems, and the various articles by Larachi and his team, who discuss the quantitative aspects.

8.2.1 Bubble columns

The bubble columns examined here consist of a cylindrical shell in which are contained the fluids and solid particles. The gas is introduced at the base of the column by means of a distributor. The flow rate of the liquid, which constitutes the continuous phase in the column, is zero or very low (generally $V_{SL} < 0.1$ m/s),upward or downward. The bubble columns contain suspended small catalyst particles (terminal velocity u_t less than 5 to 7 cm/s). These columns, known as slurry reactors when the size of catalyst particles is less than approximately 0.2 mm, have been studied extensively because they are used in important processes such as Fischer-Tropsch synthesis. Solid concentrations can reach 40% by volume; superficial gas velocities of about 0.3 m/s are also attained. These reactors differ from those described in Chapter 4 because of the finely divided solid that must be maintained in suspension in the liquid. The fines follow the turbulence of the liquid, at least as long as the solid concentration remains moderate (< 20%). A typical device is shown in Fig. 8.3.

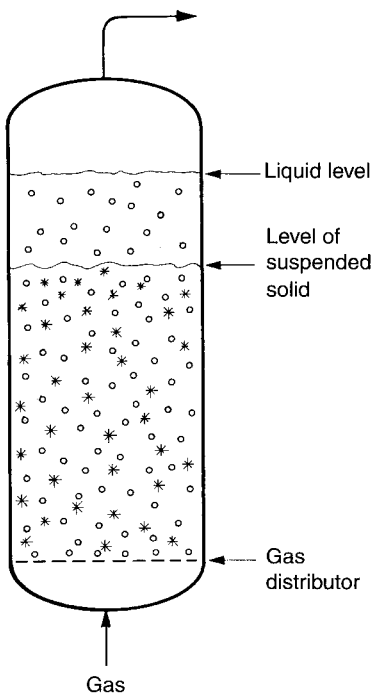


Figure 8.3 Bubble column with catalyst in suspension, with the liquid phase operating in batch mode.

Many of the conclusions regarding gas-liquid bubble columns are perfectly justified as long as the concentration of the solid is low. Here, we want to stress the specific circumstances that occur when a solid is present; in our presentation we have drawn upon the work of Fan [1989] and the excellent summary provided by Koïde [1996].

8.2.1.1 Hydrodynamics

A. Hydrodynamic regimes

The hydrodynamic regimes found in slurry columns more closely approximate two-phase gas-liquid bubble columns when fines and their concentration are low. Gas flow has a decisive influence: when it increases, the regime, initially homogeneous, becomes progressively turbulent:

- The homogeneous regime, which corresponds to the lowest gas superficial velocities (V_{SG} < approximately 3 cm/s), is characterized by a high proportion of small ($\overline{d_B} \leqslant 5$ mm), regularly shaped, dispersed bubbles. The regime is sometimes referred to as the *dispersed bubble regime*. These bubbles have trajectories that oscillate slightly, with mean rise velocities of about 0.15 to 0.25 m/s.
- The heterogeneous, or turbulent, regime corresponds to higher gas superficial velocities, typically $V_{SG} \geqslant 0.2$ to 0.5 m/s; large, shapeless bubbles appear ($10 < \overline{d_B} \leqslant 80$ mm), resulting from the coalescence of smaller bubbles, which gives the regime its name: *coalesced bubble regime*. Moving at a velocity of 1 to 2 m/s, the bubbles provide significant mixing, independent of the solid concentration. Solid particles and finer bubbles are entrained in their turbulent wake. Krishna [2000] represents the medium, in this turbulent regime, with a model that has two distinct phases: a "dense phase" and a "dilute phase", as in gas-solid fluidized beds. The dense phase contains the small bubbles and the solid particles dispersed in the liquid; the dilute phase contains the larger bubbles.

The presence of the solid has the effect of promoting the coalescence of small bubbles in the form of large bubbles, characteristic of the heterogeneous regime, which reduces the range of operation in the homogeneous regime. For solid concentrations of 30 to 40% by volume, the small bubbles disappear almost completely and large bubbles appear. In industrial settings, the homogeneous regime is found much more infrequently than the heterogeneous or transition regime.

The transition between the two regimes depends on the fineness of the initial gas distribution, the properties of the fluids and their flow rates. According to Wilkinson [1991], it corresponds to a gas holdup given by the following formula:

$$\varepsilon_{trans} = 2.16 \exp\left(-5.86 C_S - 13.1 \rho_G^{-0.10} \mu_L^{0.16} \sigma^{0.11}\right) \tag{8.23}$$

Since the transition velocity depends on several physicochemical parameters of the system, it should be determined experimentally for each situation. Whenever this is not possible, the following formula, proposed by Reilly *et al.*, [1994], can be used:

$$V_{SG\,trans} \cong 0.35 \frac{\sigma^{0.12}}{\rho_G^{0.04}} \varepsilon_{trans} (1 - \varepsilon_{trans}) \tag{8.24}$$

At this transition point, the velocity of small bubbles may be obtained from the following formula:

$$V_B = 2.25 \frac{\sigma}{\eta_L} \left(\frac{\sigma^3 \rho_L}{g \mu_L^4}\right)^{-0.27} \left(\frac{\rho_L}{\rho_G}\right)^{0.03} \tag{8.25}$$

The diameter of the bubbles, which is relatively independent of the gas velocity, can then be estimated from the following equation:

$$\overline{d_B} = 3g^{-0.44}\sigma^{0.34}\mu_L^{0.22}\rho_L^{-0.45}\rho_G^{-0.11} \tag{8.26}$$

During the nineties, several numerical models (Euler-Euler or Euler-Lagrange) were used to represent the behavior of bubble columns in the presence of small quantities of solids [Koïde, 1996]. These have confirmed the observations and qualitative conclusions given above, revealing the existence of typical zones of hydrodynamic behavior, sometimes combined axially or radially, in large reactors.

B. Suspension of the solid

It is important to emphasize the fact that, in bubble columns, the gas flow rate alone provides the agitation for the liquid phase and, therefore, the suspension of the solid. Consequently, the gas distributor must be designed in such a way that the solid does not remain stagnant anywhere in the column. A simple example of such a distributor (perforated plate) is shown in Fig. 8.3.

The minimum gas superficial velocity $(V_{SG})_m$ used to ensure the suspension of the solid can be calculated from the correlation of Abraham *et al.* [1992], established from experiments conducted in a number of columns:

$$(V_{SG})_m = 0.54u_t^{0.46}\varepsilon_G^{0.66}\varepsilon_S'^{0.39}D_C^{0.27} \tag{8.27}$$

where

u_t terminal velocity of an isolated particle in the liquid (m/s)
ε_G gas holdup (–)
ε_S' volume of solid present in the column, divided by the cross-sectional area of the column (ε_S' varies from 6 to 80 mm)
D_C column diameter (here, up to 0.38 m) (m).

Moreover, there exists a concentration profile of the solid particles as a function of height, which can be described by a turbulent diffusion model using axial Peclet numbers ($Pe_A = u_t H_S/\mathcal{D}_{A,S}$) of approximately 2 to 5 for gas superficial velocities ranging from 2 to 7 cm/s.

Systematic circulation of the liquid is often used to obtain a more uniform suspension; this is created either by the gas stream (gaslift, see Chisti, 1989, Fig. 8.4A) or generated by an external pump (Fig. 8.4B). In the latter case, the energy used to circulate the liquid can also be used to disperse the gas within the liquid phase by means of an ejector, as shown in Chapter 4 (Fig. 8.4C).

C. Gas phase holdup

Gas phase holdup, ε_G, is one of the essential parameters of three-phase bubble columns. In the absence of solid particles, we saw that the gas-phase holdup can be correctly evaluated from the gas superficial velocity V_{SG} and the characteristics of the liquid (see Eq. 4.12 to 4.15 of Table 4.2). In the presence of a solid, a slight reduction in ε_G is observed, at least for superficial velocities below 30 cm/s. Above this velocity, the solid does not appear to have a noticeable influence on the value of ε_G. This reduction is reflected in a corrective factor, B,

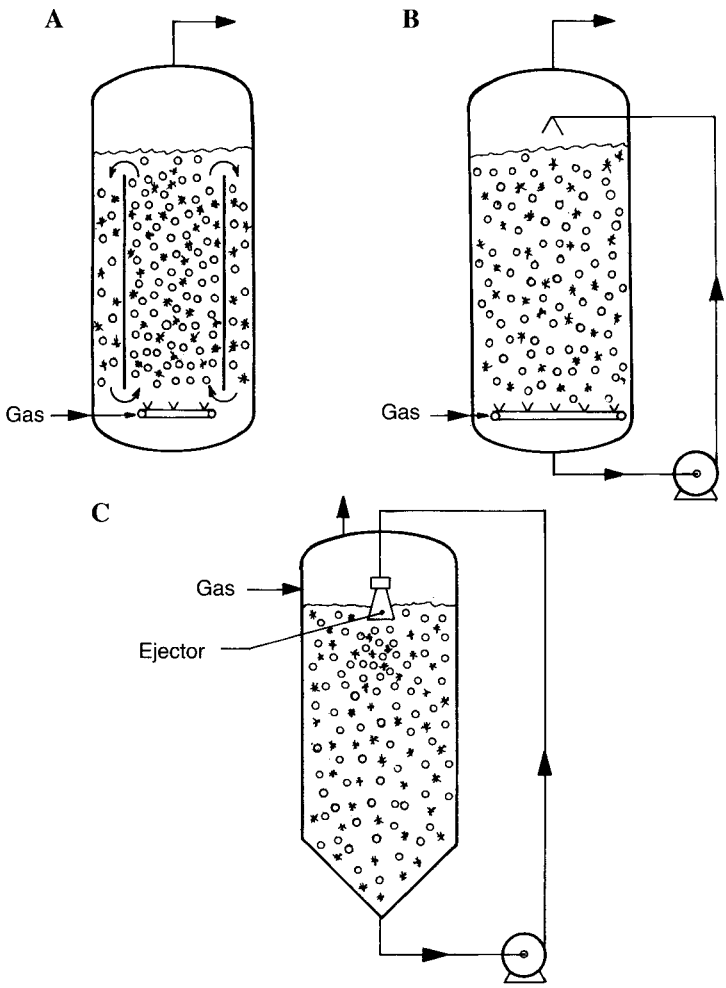


Figure 8.4 Different methods of circulating a liquid-solid mixture in a bubble column. **A.** Gaslift. **B.** External circulation with a pump. **C.** External circulation and gas recycling with an ejector.

which Koïde *et al.* [1984] introduced as follows:

$$\frac{\varepsilon_G}{(1-\varepsilon_G)^4} = \left[\frac{A}{B}\left(\frac{V_{SG}\mu_L}{\sigma}\right)^{0.92}\left(\frac{\rho_L\sigma^3}{g\mu_L^4}\right)^{0.25}\right] \tag{8.28}$$

where:

$$B = 1 + 4.35\left(\frac{C_S}{\rho_S}\right)^{0.75}\left(\frac{\rho_S-\rho_L}{\rho_L}\right)^{0.88}\left(\frac{D_C V_{SG}\rho_L}{\mu_L}\right)^{-0.17} \tag{8.29}$$

$A = 0.28$ for water and aqueous glycerol solutions, and 0.36 for solutions of inorganic electrolytes.

In fact, depending on the regime, ε_G depends more or less on the different parameters of the system, according to the following breakdown [Krishna, 2000]:

- In the dilute phase, $\varepsilon_{G,\text{dilute}}$, which corresponds primarily to large bubbles, it increases linearly with the gas superficial velocity but depends neither on the concentration of the solid nor on the properties of the liquid. In contrast, it decreases slightly as the diameter of the column increases, at least, up to approximately 1 m.
- In the dense phase, $\varepsilon_{G,\text{dense}}$, which is essentially associated with the presence of small bubbles, it is independent of the gas superficial velocity, V_{SG}, but decreases if the solid concentration increases. The gas-phase holdup depends on the distributor but not on the diameter of the column. Pressure promotes the presence of small bubbles, which decreases the rise velocity of the largest bubbles and results in an appreciable increase in the overall holdup. This effect is closely related to the gas density ρ_G:

$$\varepsilon_{G,\text{dense}} = 2.16 \exp\left(-5.86 C_S - 13.1 \rho_G^{-0.10} \mu_L^{0.16} \sigma^{0.11}\right) \tag{8.30}$$

The overall holdup is ultimately a decreasing function of the concentration in the slurry.

Measurements for systems used specifically for Fischer-Tropsch synthesis have led to the development of simplified correlations [Trambouze *et al.*, 1988]:

$$\varepsilon_G = 8.4 \cdot V_{SG}^{1.1} \pm 0.02 \quad (\text{where } V_{SG} \leqslant 0.04 \text{ m/s}) \tag{8.31}$$

$$V_B = 0.7\sqrt{g d_B} \tag{8.32}$$

D. Backmixing

The solid does not appear to exert any significant influence on backmixing, either in the gas or liquid phase. We refer the reader to our comments on backmixing in Chapter 4 (Eq. 4.3 and 4.4). Among the simple equations that can be used to estimate turbulent axial diffusivity of the liquid ($\mathcal{D}_{A,L}$ is approximately 0.1 m^2/s to 5 m^2/s), the following correlation has been verified by Deckwer [1992] for reactor diameters up to 0.6 m.

$$\mathcal{D}_{A,L} = 0.68 V_{SG}^{0.3} D_{\text{turb}}^{1.4} \tag{8.33}$$

where D_{turb} is the diameter of large vortices, which are most often limited by the diameter of the reactor, D_C, but generally less than 2 m. The viscosity of the medium has a slight influence, which is reflected in the following correlation based on Krishna [2000]:

$$\mathcal{D}_{A,L} = 0.2 V_{SG}^{0.37} D_C^{1.5} (g\nu)^{-0.12} \tag{8.34}$$

In the turbulent regime large bubbles create strong radial and axial mixing of the liquid, where circulation is somewhat systematic, rising along the axis and descending along the periphery. Krishna [2000] has analyzed in detail the velocity profiles of the liquid and relates the coefficient of axial diffusion of the liquid to the axial velocity, which can reach values of 4 to 5 m/s.

For the gas phase ($\mathcal{D}_{A,G}$ is approximately 0.1 m^2/s), a simple equation is also recommended by Deckwer [1992]:

$$\mathcal{D}_{A,G} = 50 \left(\frac{V_{SG}}{\varepsilon_G}\right)^3 D_C^{1.5} \tag{8.35}$$

In large diameter columns (5 m and above), the behavior of the medium resembles that of several, more or less independent parallel columns of reduced dimension (approximately 2 m in diameter) with several rising and falling zones.

8.2.1.2 Mass transfer

A. Gas-liquid mass transfer

Compared to simple gas-liquid bubble columns, the existing experimental results do not clearly demonstrate the influence of the solid on gas-liquid transfer parameters. No doubt, the most significant effect is on interfacial area, since the solid promotes bubble coalescence. If the correlations provided in Chapter 4 (Table 4.2) are used, it is best to assign the interfacial area calculated from the equation in Table 4.2 a coefficient of approximately $(1 - \varepsilon_S)$. The size of the bubbles is then corrected in such a way that Eq. (4.22) remains valid. More specifically, the influence of the presence of catalytic particles depends on the hydrodynamics of the system and is particularly sensitive in the turbulent regime.

In the turbulent regime mass transfer is primarily effected by small bubbles because of their greater interfacial area and longer residence time in the medium. In contrast, larger bubbles play an important role in absorbing and frequently creating smaller bubbles, whose concentration in the reactant corresponds to that of the large bubbles, which prevents their exhaustion. In terms of modeling the system, the gas phase is described by taking into account both the dense zone with its small bubbles and the dilute zone with its large bubbles. Each of the zones undergoes exchange with the liquid zone, which is in contact with the catalyst. Krishna [2000] proposed a simple correlation that has been confirmed for the heterogeneous regime under pressure and in the presence of concentrated solid mixtures:

$$\frac{k_L \mathcal{A}}{\varepsilon_B} = 0.5\sqrt{\frac{\mathcal{D}_L}{\mathcal{D}_{ref}}} \tag{8.36}$$

where

ε_B holdup for large bubbles

$\mathcal{D}_{ref} = 2 \cdot 10^{-9}$ m^2/s, reference coefficient of diffusion

$\mathcal{D}_L$ coefficient of diffusion of the gas in the liquid.

The transfer coefficient $k_L\mathcal{A}$ is related to that for gas-liquid bubble columns without a solid by a corrective factor, B, which Koïde *et al.* [1984] express as follows:

$$\frac{k_L \mathcal{A} \sigma_L}{\rho_L \mathcal{D}_L g} = \frac{1}{B}\left[2.11\varepsilon_G^{1.2}\left(\frac{\mu_L}{D_C \rho_L}\right)^{0.5}\left(\frac{\rho_L \sigma^3}{g\mu_L^4}\right)^{0.16}\right] \tag{8.37}$$

where:

$$B = 1 + 1.47 \cdot 10^{-4}\left(\frac{C_S}{\rho_S}\right)^{0.61}\left(\frac{u_t}{\sqrt{D_C g}}\right)^{0.49}\left(\frac{D_C^2 g \rho_L}{\sigma_L}\right)^{-0.49}\left(\frac{D_C V_{SG} \rho_L}{\mu_L}\right)^{-0.34} \tag{8.38}$$

B. Liquid-solid mass transfer

A number of studies have been conducted to determine the transfer coefficient $k_{l,S}$ for a solid particle submerged in a flowing fluid. Most of these theoretical studies lead to an equation of the following form:

$$(Sh)_S = 2 + K\,(Re)^{\frac{1}{2}}\,(Sc)_L^{\frac{1}{3}} \tag{8.39}$$

where:

$$(Sh)_S = \frac{k_{l,S}\overline{d_p}}{\mathcal{D}_{l,L}} \tag{8.40}$$

$$(Sc)_L = \frac{\mu_L}{\rho_L \mathcal{D}_{l,L}} \tag{8.41}$$

The Reynolds number (Re) is expressed in different ways, depending on the theoretical approach taken: the correlation of Sano *et al.* [1974] can be used, for it integrates a large number of earlier experimental results. The Reynolds number is then defined as follows:

$$Re = \frac{\Sigma_L \tilde{d}_p^4 \rho_L^3}{\mu_L^3} \tag{8.42}$$

Σ_L is the power dissipated per unit mass of liquid (W/kg), with:

$$\Sigma_L = g V_{SG} \tag{8.43}$$

The general correlation is then expressed as follows:

$$(Sh)_S = \left[2 + 0.4\,(Re)^{\frac{1}{4}}\,(Sc)_L^{\frac{1}{3}}\right] \varphi_C \tag{8.44}$$

φ_C is the Carman shape factor, determined from the diameter d'_p obtained by sieving:

$$\varphi_C = \frac{6\varepsilon_s}{\mathcal{A}_S d'_p} \tag{8.45}$$

8.2.1.3 Heat transfer at the wall

Heat transfer increases with the superficial velocity of the gas but decreases if pressure increases [Fan *et al.*, 1999], as in simple two-phase media (gas-liquid). However, it is known that the presence of a divided solid within a liquid phase can significantly increase heat transfer at the wall, to such an extent that, in practice, it is easy to achieve rather high transfer coefficients: twice as great as in bubble columns without a solid and sometimes five times as great as in fixed-bed columns. In three-phase bubble columns, the heat transfer coefficients can exceed 10^3 W/m^2 · K, values that make these bubble columns particularly attractive for highly exothermic reactions.

The correlation by Deckwer and Schumpe [1980], regularly cited by many authors, appears to be suitable for a number of media, providing the properties of the medium (ρ_{SL}, C_{PSL}, μ_{SL}, λ_{SL}) are included in the dimensionless numbers:

$$St_{SL} = 0.1 \left(Re_{SL} Fr_G Pr_{SL}^2\right)^{-0.25} \tag{8.46}$$

where:

$$St_{SL} = \frac{h_w}{\rho_{SL} C_{PSL} V_{SG}} \qquad Re_{SL} = \frac{V_{SG} \overline{d_p} \rho_{SL}}{\mu_{SL}}$$

$$Fr_G = \frac{V_{SG}^2}{g \overline{d_p}} \qquad Pr_{SL} = \frac{C_{PSL} \mu_{SL}}{\lambda_{SL}}$$

and:

$$\rho_{SL} = \rho_S \varepsilon_S + \rho_L \varepsilon_L$$
$$C_{PSL} = C_{PS} w_S + C_{PL} w_L$$

where w_S and w_L are weight fractions of solid and liquid.

$$\lambda_{SL} = \lambda_L \frac{2\lambda_L + \lambda_S - 2\varepsilon_S (\lambda_L - \lambda_S)}{2\lambda_L + \lambda_S + \varepsilon_S (\lambda_L - \lambda_S)}$$
$$\mu_{SL} = \mu_L (1 + K \varepsilon_S)$$

K, which is approximately 5, depends on the medium.

For additional details on specific configurations, readers are referred to the detailed bibliography provided by Saxena [1995].

8.2.1.4 Computational models

Given the current lack of precision in estimating hydrodynamic and gas-liquid transfer parameters, the computational model used for a bubble column reactor with a suspended catalyst must be as simple as possible. In this way the liquid and solid phases can be considered to be perfectly mixed in the reactor and the gas phase as moving with plug flow. The calculation shown in Chapter 4, in the absence of a catalyst, can be used as a starting point.

The assumption of perfect mixing in the liquid and solid phases is totally justified in the case of systems with external recirculation (Fig. 8.4). Note that, in practice, this external circulation has the advantage of simplifying heat exchange with the exterior. Thus reactions that are highly thermic in nature, such as the hydrogenation of benzene, can be easily carried out. It should be obvious that the hydrodynamic regime in the bubble column is modified by the forced circulation of the liquid cocurrent or countercurrent to that of the gas. In the absence of specific data for these cases, the information given above for a stagnant liquid is used.

Following Krishna [2000], a more precise model considers two distinct phases: a dilute phase (large bubbles) with plug flow and a dense phase (small bubbles and catalyst) that is perfectly mixed. Exchange between these two phases must frequently be taken into account.

Note also that we have examined the case where the liquid is captive in the reactor. In practice it can be renewed through the continuous introduction of a liquid phase containing one of the reactants, with the elimination, in a liquid or vapor phase, of one or more of the reaction products (which is the case for the hydrogenation of benzene).

8.2.1.5 Technology

Bubble columns are very simple to design and operate. Like two-phase bubble columns, a gas distributor is placed in the lower part of the column. In the case of three-phase media, there must be consistent turbulence throughout the column so that the catalyst particles do not settle in a calm zone. In particular, the zones located near the edges or between the holes of the distributor must not remain stagnant. The holes or small tubes for gas distribution should be as small and numerous as possible (a few centimeters from one another) to create sufficient movement of the liquid throughout the column. Over time the catalyst can erode these holes, and the introduction and distribution of the gas can become uneven, leading to particle accumulations in certain low-turbulence regions. The injector tubes do not present these problems but the materials must be chosen with care to avoid erosion or corrosion.

To remove the high amounts of heat generated by strongly exothermic reactions, such as Fischer-Tropsch synthesis [see De Swart *et al.*, 1997], cooling tubes are generally submerged in the medium. Purge nozzles are also often needed to completely remove catalyst and liquid when the unit is stopped. In this case the inevitable return of liquid and solid particles in the gas line will also require the use of a purge system.

These reactors are quite large, up to 8 m in diameter and 30 m in height. For example, in the Fischer-Tropsch syntheses, typical characteristic dimensions are:

- diameter: 6 to 10 m
- height: 20 to 40 m
- submerged exchangers: tube diameter is 0.05 m and total surface area is 500 to 8 000 m^2
- V_{SG}: 0.2 to 0.4 m/s
- ε_S: 0.3 to 0.4.

8.2.1.6 Concluding remarks

Overall, three-phase bubble column reactors have the following advantages and disadvantages.

Advantages

- Considerable operational flexibility
- Simple transition from continuous to batch operation
- Very good heat exchange capacity, simplified temperature control and heat recovery
- Ability to use very active catalysts and high rates of reaction
- Very good liquid-solid contact, leading to high values for effectiveness, selectivity, and catalyst life (important for fast or exothermic reactions)
- Effectiveness factor of the catalyst is close to unity when small particles are used
- Regular introduction of new catalyst and removal of spent catalyst is simplified.

Disadvantages

- Strong backmixing, which limits conversion
- Need to separate the total volume in several reactors to achieve high conversion rates
- High ratio of liquid/solid volume, promoting secondary reactions in the liquid phase
- Liquid/solid separation is sometimes difficult (filtration, cycloning)
- Catalyst is sometimes irregularly distributed.

One of the significant advantages of three-phase bubble columns is associated with the efficiency of heat transfer, with the attendant ability to conduct highly exothermic reactions in them. In practice, industrial three-phase bubble columns are used for highly varied reactions: hydrogenation, oxidation, chlorination, alkylation, conversion of synthesis gas, as well as for wastewater treatment and biotreatment.

8.2.2 Mechanically agitated reactors

The solid particles used in these reactors are in general rather fine (diameter < 1 mm) for reasons of mechanical strength. Consequently, they follow the behavior and turbulence of the liquid. Mechanically agitated reactors are, therefore, analogous to those discussed in Chapter 4 concerning two-phase gas-liquid media. The correlations introduced in Table 4.13 are used, with the assumption that the presence of the solid has negligible influence as long as the solid concentration remains low.

8.2.2.1 Hydrodynamics

In Chapter 4 three regimes were introduced to characterize the interactions between bubbles and agitation in gas-liquid media. Preference was given to the intermediate regime, which provides good bubble fragmentation and dispersion throughout the entire reactor (in this case the energy supplied by the impeller is two to five times greater than that supplied by the gas). In three-phase media, an additional factor is added—the solid particles. The rotational speeds must be chosen so that the particles are maintained in a uniform suspension throughout the entire reactor, even in the absence of a gas.

The power calculations are similar to those for reactors with a liquid alone. To account for the three phases, it is generally sufficient to use the properties of solid-liquid mixture to gain an accurate idea of the consumed power; however, the suspension process can present serious problems if the concentration of solids is high.

8.2.2.2 Mass transfer

The liquid-solid transfer coefficient, $k_{l,s}$, is calculated by using Sano's correlation, shown for three-phase bubble columns (Eq. 8.44). Calculation of the Reynolds number (Eq. 8.42) takes into account the mechanical power dissipated by the impeller (see Chapter 4). Midoux and Charpentier [1981] have studied the influence of various factors that affect the interfacial areas.

8.2.2.3 Heat transfer

In these stirred reactors, heat transfer between the three-phase reaction mixture and a solid wall (wall or submerged coil) is often an important factor. Readers are referred to the articles by Steiff and Weinspach [1980].

8.2.2.4 Computational models

For modeling purposes the assumptions made for bubble columns are used, namely:

- perfectly stirred liquid and solid phases
- gas phase characterized by plug flow.

8.2.2.5 Technology

In terms of design, we again wish to point out that these stirred reactors are very similar to those used with two-phase gas-liquid media. In terms of the choice of impeller, a compromise must be found between a purely radial movement, favorable to fragmentation of the gas into fine bubbles, and a more axial movement, which promotes effective circulation between the various zones of the reactor. Reaching a balance between these two solutions depends totally on the medium and the desired objective. Pitched blade turbines or stacked radial and axial devices are often used.

Also, the presence of solid particles requires that careful attention be paid to the bottom of the reactor, since the catalyst can settle there and form, beneath the impeller, a small, concentrated cone of catalyst that is relatively stationary (risk of parasite reactions). A special valve must also be used for catalyst removal. Additional information is provided by Oldshue [1983] and Harnby *et al.* [1992].

8.2.2.6 Concluding remarks

Stirred reactors have the following advantages compared to three-phase bubble columns:

- turbulence can be higher in stirred reactors but, most importantly, it is easier to adjust since it is independent of the gas flow rate
- mass and heat transfer are greater than in bubble columns.

However, there are certain drawbacks as a result of the mechanical components involved:

- high energy consumption
- significant investment and maintenance costs.

In practice, stirred reactors are often used for three-phase reactions in batch or continuous mode when the flow rates are not too high. This is especially true in the field of pharmaceuticals or fine chemicals. For example, liquid-phase hydrogenation is one well-known application (the production of edible oils, for example).

8.2.3 Fixed beds with two-phase flow

As indicated above, there are three possible configurations, depending on the respective direction of flow of the gas and liquid phases:

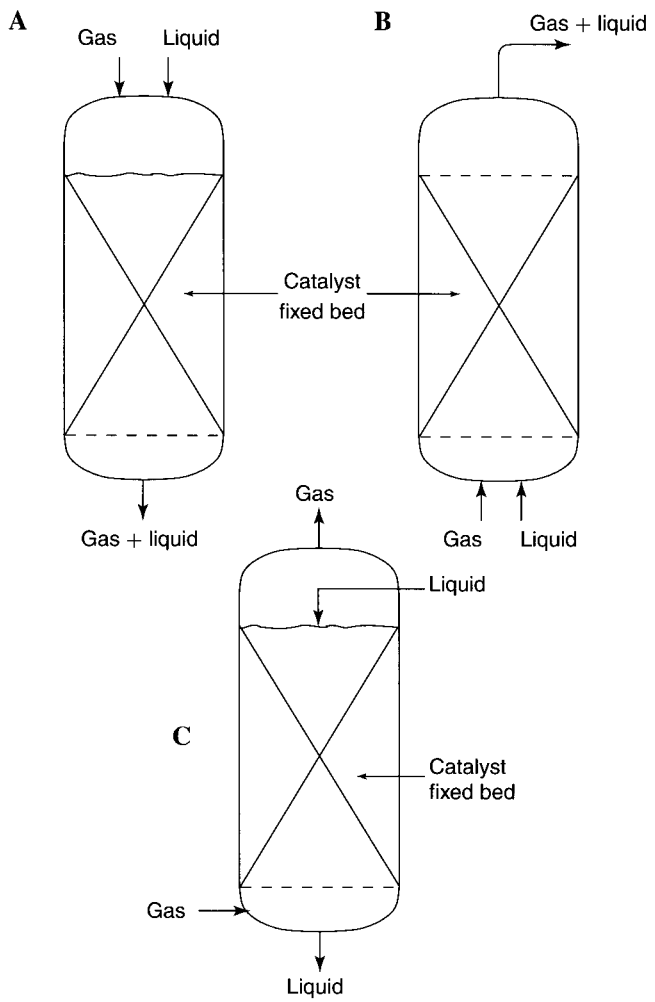


Figure 8.5 Fixed-bed catalytic reactors with two-phase flow. **A.** Cocurrent downflow. **B.** Cocurrent upflow. **C.** Countercurrent.

- cocurrent downflow systems (Fig. 8.5A)
- cocurrent upflow systems (Fig. 8.5B)
- countercurrent systems (Fig. 8.5C).

In practice the first of these configurations (cocurrent downflow) is the most commonly used.

8.2.3.1 Cocurrent downflow reactors

Fixed-bed catalytic reactors with two-phase flow have been studied extensively because of their commercial importance, especially during the years 1980 to 2000 [Gianetto and

Spechia, 1992; Larachi *et al.*, 1996; Saroha and Nigam, 1996; Al-Dahhan *et al.*, 1997; Attou and Boyer, 1999, Dudukovic, 1999, 2000]. Many publications, although not always consistent with one another, discuss flow regimes, the determination of pressure drop and liquid holdup, and gas-liquid and liquid-solid mass transfer. Here we examine these various factors, with special attention paid to those elements that are important for practical reactor design (phase distribution, for example) and modeling. The knowledge and understanding of how these reactors operate have progressed rapidly as a result of numerical modeling in two or three dimensions (2D and 3D CFD), which has been verified through local measurements, in particular, those using X- or γ-ray tomography or particle tracing [Dudukovic, 2000].

A. Hydrodynamics

a. Flow regimes

Four basic types of flow regimes have been observed, depending on the relative flow rates of the liquid and gas phases [Ng, 1986]:

1. For low liquid flow rates and low to moderate gas flow rates, a *trickle flow regime* or *regime of low interaction* between the fluid phases appears. The liquid phase trickles, dispersed in the form of streams or films that flow between and on the particles, while the gas phase is continuous and slips through the external openings unoccupied by the liquid. We note in passing that there has been some confusion between the term "trickle flow" and "trickle bed", the latter term sometimes being used—incorrectly—to apply to fixed-bed reactors with cocurrent downflow, sometimes even when they operate in a completely different regime.
2. With low liquid flow rates and high gas flow rates, a *mist regime* with a continuous gas phase and a liquid phase dispersed in fine droplets entrained by the gas current is observed.
3. For average liquid and gas flow rates, a high-interaction flow regime, or *pulsed regime*, occurs, with the more or less periodic passage of slugs composed almost exclusively of liquid then of gas.
4. When liquid flow rates are high, an *entrained bubble regime* is found, with a continuously flowing liquid phase that entrains the gas, dispersed in the form of bubbles. This regime is rather uncommon in industrial reactors.

The last three regimes involve strong fluid interaction.

Two principal types of diagrams have been proposed to represent these various regimes:

- the *G versus L* diagram by Sato *et al.* [1973] (Fig. 8.6A)
- the *L/G versus G* diagram by Charpentier and Favier [1975] and Morsi *et al.* [1978] (Fig. 8.6B).

L and G are the superficial mass flow rates ($L = \rho_L V_{SL}$ and $G = \rho_G V_{SG}$).

This last diagram has the drawback of using the same magnitude, G, on both the X and Y axes, which somewhat masks the influence of the liquid flowrate, L. However, the authors have used the corrective terms λ and ψ, which take into account the physical properties of

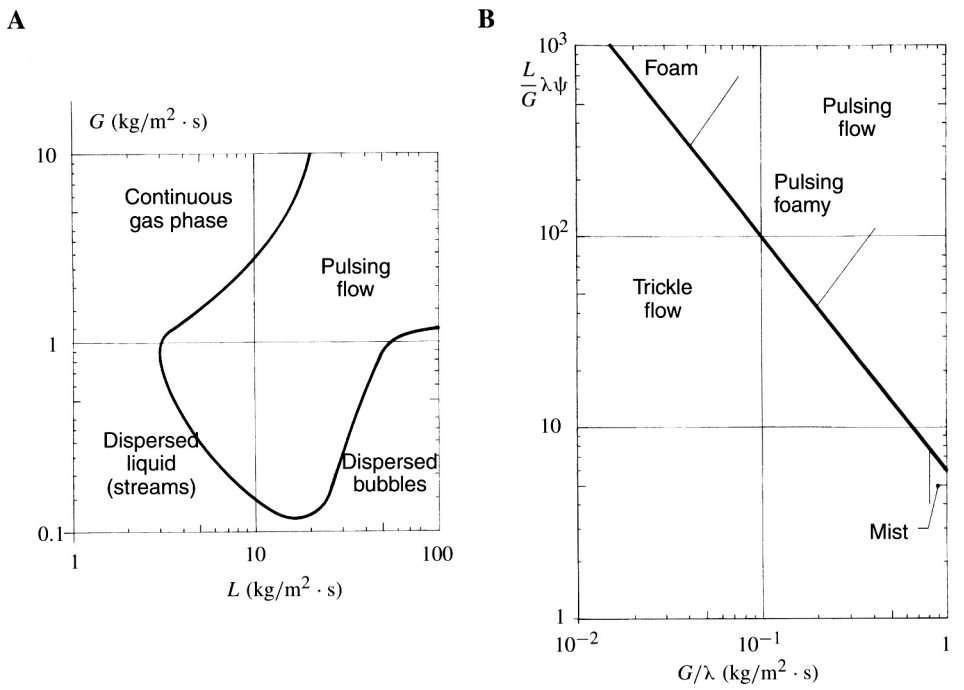


Figure 8.6 Two-phase flow regimes with cocurrent downflow of the gas and the liquid through the catalytic bed. **A.** Sato's diagram (air-water). **B.** Charpentier's diagram.

the fluids:

$$\lambda = \left(\frac{\rho_L}{\rho_{water}} \frac{\rho_G}{\rho_{air}} \right)^{\frac{1}{2}} \tag{8.47}$$

$$\psi = \frac{\sigma_{water}}{\sigma_L} \left[\frac{\mu_L}{\mu_{water}} \left(\frac{\rho_{water}}{\rho_L} \right)^2 \right]^{\frac{1}{3}} \tag{8.48}$$

Charpentier *et al.* have shown the influence of the foaming nature of the liquid. They have also taken into account the gas density, which can be used to compensate for pressure effects.

Larachi *et al.* [1993] have proposed a more complete correlation for the trickle-pulsed transition; Iliuta *et al.* [1999] have used more than 700 measurements in a neural network to devise a correlation, somewhat complex but much more precise, that introduces many more variables.

It is important to recognize that industrial reactors operate in the pulsed or trickle-flow regime, with superficial velocities frequently limited to 3 cm/s for V_{SL} and 30 cm/s for V_{SG}, whereas pilot reactors always operate in the trickle-flow regime, and at much lower velocities.

b. Pressure drop and liquid holdup

Ever since the work of Larkins *et al.* [1961], a number of findings concerning pressure drop and liquid holdup have been published, including those by Trambouze *et al.* [1988], Ellman *et al.* [1988, 1990], Wild *et al.* [1991], Al Dahhan *et al.* [1998], and Attou and Boyer [1999]. Illiuta *et al.* [1999] have proposed somewhat complex (21 coefficients) but precise (with an error of approximately 20%) correlations that have been established using neural networks applied to an extensive and varied range of data. Here, we reproduce the empirical correlations initially proposed by Ellman *et al.* [1988, 1990] and readjusted by Larachi *et al.* [1991, 1996] using several thousand experimental data points from various sources, including measurements taken under high pressure (10 MPa).

When the liquid or gas passes unaccompanied through the catalytic bed, the pressure drop due to the presence and passage of the fluid is given by an experimental correlation, otherwise by Ergun's correlation:

$$\delta'_{\mathrm{L}} = A\frac{\varepsilon_{\mathrm{s}}^2}{(1-\varepsilon_{\mathrm{s}})^3}\frac{\mu_{\mathrm{L}} V_{\mathrm{SL}}}{\overline{d_{\mathrm{p}}}^2} + B\frac{\varepsilon_{\mathrm{s}}}{(1-\varepsilon_{\mathrm{s}})^3}\frac{\rho_{\mathrm{L}} V_{\mathrm{SL}}^2}{\overline{d_{\mathrm{p}}}} \tag{8.49a}$$

or for the gas alone:

$$\delta'_{\mathrm{G}} = A\frac{\varepsilon_{\mathrm{s}}^2}{(1-\varepsilon_{\mathrm{s}})^3}\frac{\mu_{\mathrm{G}} V_{\mathrm{SG}}}{\overline{d_{\mathrm{p}}}^2} + B\frac{\varepsilon_{\mathrm{s}}}{(1-\varepsilon_{\mathrm{s}})^3}\frac{\rho_{\mathrm{G}} V_{\mathrm{SG}}^2}{\overline{d_{\mathrm{p}}}} \tag{8.49b}$$

The coefficients A and B are preferably determined experimentally, especially for liquids; the default values of $A = 150$ and $B = 1.75$ are not very precise for liquids. The void fraction $(1 - \varepsilon_{\mathrm{s}})$ is approximately 0.4 but difficult to predict or even measure experimentally. Moreover, it is likely to change over time (settling, fouling, clogging of the bed with fines, etc.). Since ε_{s} has a rather significant influence on pressure drop, generous safety margins are recommended.

The pressure drop from friction, caused by the passage of the gas-liquid mixture through the bed is much greater than the sum of the pressure drops of each fluid alone. This corrective effect, associated with the interaction between the fluids, is expressed, for example, with respect to the gas, by means of the empirical correlations provided in Table 8.2.

To overcome the uncertainty of predicting the pressure drops of the individual fluids, the parameter of Lockhart and Martinelli, χ_{G}, is often replaced by an approximate value, X_{G}, the simple ratio between the forces of inertia of each of the fluids (Eq. 8.56bis). The liquid saturation ratio can be obtained from Eqs. (8.57) and (8.58).

The pressure difference between two points of the reactor (pressure drop from friction and the difference in the static head due to the presence of the mixture) will finally be given by:

$$\left(\frac{\Delta P}{H}\right)_{\mathrm{GL\,total}} = \delta'_{\mathrm{GL}} - g\left[\beta_{\mathrm{L}}\rho_{\mathrm{L}} + (1-\beta_{\mathrm{L}})\rho_{\mathrm{G}}\right] \tag{8.59}$$

Note that these correlations, like nearly all those found in the literature, have been obtained in small-diameter columns (often less than 20 cm). Therefore, the results are most often

Table 8.2 Pressure drop and liquid holdup during downward gas and liquid flow.

$$\delta'_{GL} = FLGG\frac{2\rho_G V_{SG}^2}{d_h} \tag{8.50}$$

where:

$$d_h = d_p\left(\frac{16(1-\varepsilon_s)^3}{9\pi\cdot\varepsilon_s^2}\right)^{0.33} \tag{8.51}$$

$$FLGG = \kappa^{-1.5}(31.3 + 17.3\cdot\kappa^{-0.5}) \tag{8.52}$$

with:

$$\kappa = \chi_G(Re_L We_L)^{0.25} \tag{8.53}$$

$$Re_L = \frac{\rho_L V_{SL} d_p}{\mu_L} \tag{8.54}$$

$$We_L = \frac{(\rho_L V_{SL})^2 d_p}{\rho_L \sigma_L} \tag{8.55}$$

and

$$\chi_G = \sqrt{\frac{\delta'_G}{\delta'_L}} \tag{8.56}$$

$$\chi_G \cong X_G = \frac{G}{L}\sqrt{\frac{\rho_L}{\rho_G}} \tag{8.56bis}$$

$$\beta_L = 1 - 10^{-\Gamma} \tag{8.57}$$

where

$$\Gamma = 1.22\cdot\chi_G^{-0.15} Re_L^{-0.20} We_L^{0.15} \tag{8.58}$$

biased by wall phenomena (as long as D_C/d_p is less than 15 or 20, the local porosity will be different from the mean). For industrial dimensions (diameters of 1 to 4 m), these correlations are not very precise; consequently, the values obtained must be used with care. This restriction is not too limiting in practice though, since it is customary to assume a comfortable safety margin to take into account the inevitable fouling of the catalytic bed and the consequent increase in pressure drop over time.

Attou and Boyer [1999] assume a more fundamental point of view by modeling fluid flow in the interstitial space of the bed as a form of annular flow in which the gas and the liquid behave as two continuous phases separated by a stable interface. The macroscopic mass and momentum balances are integrated for each phase, as are the forces of interaction between the phases. The value of this physical model is that it can predict pressure drop and liquid holdup with good precision, without requiring the adjustment of empirical parameters other than those of the Kozeny-Carman correlation (the values A and B used here are 180 and 1.8), which is used to evaluate the pressure drop of a single fluid through the bed. Although it is somewhat more complicated to use than the simple empirical correlations, Attou's model can be recommended to precisely model flow in a fixed bed using the methods of fluid dynamics.

B. Mass transfer

a. Gas-liquid mass transfer

Gas-liquid mass transfer is especially sensitive to the presence of very small amounts of products that promote coalescence or foaming, which can easily cause the transfer coefficients to shift by a factor of 3 to 5. Moreover, pressure has a very noticeable influence that is almost never taken into account in the correlations that appeared before 1990 [Al-Dahhan *et al.*, 1997]. Fortunately, the pressure effect is generally well represented by the effect of gas density. Nonetheless, there is reason to remain cautious when using these correlations.

Here, we make use of the correlations of Wild *et al.* [1992], which, aside from a general formulation based on the Lockart-Martinelli parameter, associated with energy dissipation during flow through the catalytic bed, take into account regimes of weak or strong interaction. For the transfer coefficients, as for the interfacial area, Wild proposed rather general correlations, but they contain parameters adjusted for the appropriate hydrodynamic regime:

- For the film coefficient of transfer on the liquid side:

$$Sh_L = a\chi_G^b Re_L^c We_L^d Sc_L^e \varphi^f \tag{8.60}$$

with the following values for the parameters:

Regime	a	b	c	d	e	f
Strong interaction	0.45	0.65	1	0.26	0.65	0.32
Weak interaction	$2.8 \cdot 10^{-4}$	0.85	0.68	0.68	1.7	0.85
Transition	0.09	0.95	0.76	0.76	1.14	0.95

- For the film transfer coefficient on the gas side:

$$Sh_G = a\chi_G^b Re_L^c We_G^d Sc_G^e \varphi^f \tag{8.61}$$

with the following values for the parameters:

Regime	a	b	c	d	e	f
Strong interaction	0.123	0.45	0.72	0.27	0.45	0.22
Weak interaction	0.067	0.55	0.88	0.22	0.55	0.27
Transition	0.123	0.45	0.72	0.27	0.45	0.22

- For the interfacial area, the following correlation has the same form, but is somewhat simpler:

$$\frac{\mathcal{A}_{GL}}{\mathcal{A}_S} = a\chi_G^b Re_L^c We_G^d Sc_G^e \varphi^f \tag{8.62}$$

with the following values for the parameters:

Regime	a	b	c	d	e	f
Strong interaction	1 550	0.7	−0.35	0.7	0	−3.5
Weak interaction	10	0.7	−0.35	0.7	0	1
Transition	21.3	0.5	−0.25	0.5	0	−1

All the correlations make use of conventional dimensionless numbers, which we reproduce below for convenience:

$$Re_L = \frac{Ld_p}{\mu_L} \qquad We_G = \frac{G^2 d_p}{\rho_G \sigma_L} \qquad We_L = \frac{L^2 d_p}{\rho_L \sigma_L} \qquad \chi_G = \frac{G}{L}\sqrt{\frac{\rho_L}{\rho_G}}$$

$$Sc_G = \frac{\mu_G}{\rho_G \mathcal{D}_G} \qquad Sc_L = \frac{\mu_L}{\rho_L \mathcal{D}_L} \qquad Sh_G = \frac{k_G \mathcal{A}_{GL} d_h^2}{\mathcal{D}_G} \qquad Sh_L = \frac{k_L \mathcal{A}_{GL} d_h^2}{\mathcal{D}_L}$$

$$\varphi = \frac{\mathcal{A}_S d_h}{\varepsilon_s} \qquad d_h = d_P \left[\frac{16(1-\varepsilon_s)^3}{9\pi\varepsilon_s^2}\right]^{0.33}$$

The coefficients of mass transfer and interfacial area have also been subject to a comprehensive approach using neural networks involving thousands of data points, some of which have been obtained in systems under pressure. Correlations by Iliuta *et al.* [1999] have resulted in much better precision because of the relatively high number of coefficients (relative errors of approximately 20% on several thousand data points from a wide variety of sources).

b. Liquid-solid mass transfer

Liquid-solid transfer is rarely limiting when the particles are overlaid with liquid (wetting is much more limiting than transfer itself), so that there is a limited amount of data available [Bartelmus, 1989, 1993]. $k_{LS}\mathcal{A}_p$ is roughly 0.01 to 0.05 s^{-1}. Although it does not take into account the effects of particle shape, a correlation by Lakota and Levec [1990], incorporating a number of experimental results, remains an acceptable approximation for any flow regime. Their correlation makes use of a modified Reynolds number:

$$Sh_S = 0.49 Sc_L^{-0.33} \left(Re_L^*\right)^{0.5} \tag{8.63}$$

which is valid for:

$$0.2 < \left(Re_L^* = Re_L' \frac{1-\varepsilon_s}{\varepsilon_{L\,\text{dynamic}}}\right) < 600 \quad \text{where} \quad Re_L' = \frac{L\overline{d_p}}{\varepsilon_s \mu_L}$$

$$Sh_S = \frac{k_S \overline{d_P}}{\mathcal{D}_L} \frac{1-\varepsilon_s}{\varepsilon_s} \tag{8.64}$$

C. Heat transfer

Although three-phase reactions are often exothermic and temperature control can present a problem, heat transfer in trickle-bed reactors has been studied less extensively than mass transfer. Some authors have investigated the following two characteristic coefficients:

- the coefficient of thermal conductivity (Λ_r is roughly 50 to 100 W/m·K), which depends on the dry bed as well as the fluids and, globally, the hydrodynamic regimes
- the coefficient of transfer with the walls (h_W is about 1 000 to 10 000 W/m·K), although there is little research available.

Among the published correlations, the majority of them are the result of tests with water and air. So there is good reason to remain cautious. Since hydrodynamics has a strong influence, different correlations have been proposed for regimes with weak or strong interaction. Those by Lamine *et al.* [1996] show good precision:

$$\text{Regime of strong interaction:} \quad \frac{\Lambda_r}{\lambda_L} = \frac{\lambda_{L=0}}{\lambda_L} + 1.76\,(\beta_L Pe_L)^{0.66} \tag{8.65}$$

$$\text{Regime of weak interaction} \quad \frac{\Lambda_r}{\lambda_L} = \frac{\lambda_{L=0}}{\lambda_L} + 0.17 Pe_L \tag{8.66}$$

In the above correlations, the term $\lambda_{L=0}$, relative to transfer in the absence of flow, can be neglected in most cases. Remember that the thermal conductivity of porous catalysts in air, at 90°C, and under atmospheric pressure, is about 0.3–0.4 W/m · K [Satterfield, 1980]. The heat transfer in the presence of a gas alone, without a liquid, is much less favorable (100 to 1 000 times) than in the presence of a mixture of gas and liquid, which again shows that the nature of the distribution is critical.

For exchange with the wall, Lamine proposed a single correlation:

$$h_W = 318\beta_L L \tag{8.67}$$

Bear in mind that transfer with the wall is negligible in industrial reactors as well as in beds composed of large diameter particles (approximately > 6 mm).

When heat transfer is impossible to control in a large-diameter reactor, a fixed bed solution can be found: the multitubular reactor discussed in Chapter 7. In this case, the difficulty lies in successfully supplying each of the many tubes while maintaining a perfect distribution of gas and liquid flow rates.

D. Modeling

Here too, given the uncertainties concerning the parameters describing two-phase flow in a catalytic bed, it is best to use the simplest possible model to describe reactor operation. As a first approximation, we can assume that the linear velocity of the gas is the same at any point in a cross-section (plug flow) of the reactor. The same holds true for the liquid phase. In certain critical cases, it is best to err on the side of caution and examine the possible effect of turbulent diffusion superimposed on plug flow [Chaudhari and Ramachandran, 1992, Stegemen *et al.*, 1996].

Equations exist for evaluating the axial Peclet numbers in the gas and liquid phases [Shah, 1979]:

$$(Pe)_G = \frac{V_{SG}\overline{d_p}}{\mathcal{D}_{A,G}} = 1.8\left[\frac{(Re)_G}{\varepsilon_s}\right]^{-0.7} 10^{\frac{-0.005(Re)_L}{\varepsilon_s}} \tag{8.68}$$

$$(Pe)_L = \frac{V_{SL}\overline{d_p}}{\mathcal{D}_{A,L}} = 0.042\left[\frac{(Re)_L}{\varepsilon_s}\right]^{0.5} \tag{8.69}$$

Generally, we are interested in the conversion of the reactant present in the liquid phase. Therefore, it is the liquid-phase Peclet number that will be of greatest importance. Based

on (8.69), it can be seen that $(Pe)_L$ will generally fall between 0.3 and 1. If we apply the criteria defined by Mears [1971] in order to consider the axial diffusivity to be negligible, namely:

$$\frac{H}{d_p} > \frac{20}{(Pe)_L} \ln \frac{C_{2,L}(H=0)}{C_{2,L}(H)} \tag{8.70}$$

where H is the total height of the catalytic bed, then, for a conversion of 90%:

$$\frac{H}{d_p} > \frac{20}{0.3} 2.3 = 150 \tag{8.71}$$

It can be seen that this condition is easily realized in practice, given that the dimension of the catalyst grains is generally between 1 and 5 mm.

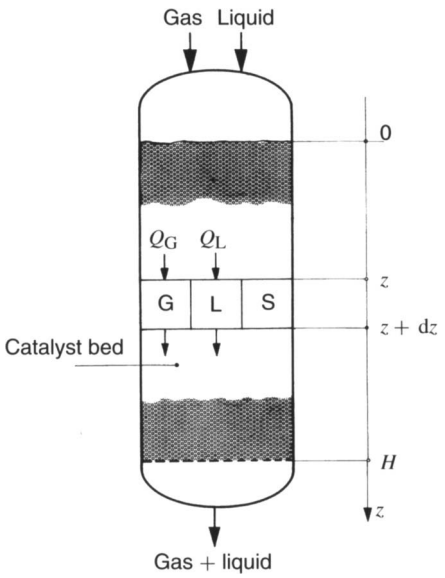


Figure 8.7 Basis for modeling a fixed-bed reactor with cocurrent downflow.

Therefore, if we adopt the assumption of plug flow for the two phases, equations for the molar balances of each of the constituents taking part in the reaction can be written. As with packed columns (see Chapter 4), these balances are based on an elementary slice of a reactor with cross-section S and thickness dz (Fig. 8.7). For example, taking the reaction introduced at the beginning of this chapter:

$$\nu_1 A_1(g) + \nu_2 A_2(l) \rightarrow \nu_3 A_3(l)$$

The molar balances for A_1 and A_2 are written as follows:

- In the gas phase:

$$\frac{d\left(Q_G C_{1,G}\right)}{dz} + \mathcal{A}_{GL} K_{1,L} \left(\frac{C_{1,G}}{m_1} - C_{1,L} \right) S = 0 \tag{8.72}$$

- In the liquid phase:

$$\frac{\mathrm{d}\left(Q_{\mathrm{L}}C_{1,\mathrm{L}}\right)}{\mathrm{d}z}+\left[\mathcal{A}_{\mathrm{S}}k_{1,\mathrm{S}}\left(C_{1,\mathrm{L}}-C_{1,\mathrm{S}}\right)-\mathcal{A}_{\mathrm{GL}}K_{1,\mathrm{L}}\left(\frac{C_{1,\mathrm{G}}}{m_1}-C_{1,\mathrm{L}}\right)\right]S=0 \tag{8.73}$$

$$\frac{\mathrm{d}\left(Q_{\mathrm{L}}C_{2,\mathrm{L}}\right)}{\mathrm{d}z}+\mathcal{A}_{\mathrm{S}}k_{2,\mathrm{S}}\left(C_{2,\mathrm{L}}-C_{2,\mathrm{S}}\right)S=0 \tag{8.74}$$

At the catalyst surface, and for a first-order reaction with respect to A_1 and A_2:

$$N_1=\mathcal{A}_{\mathrm{S}}k_{1,\mathrm{S}}\left(C_{1,\mathrm{L}}-C_{1,\mathrm{S}}\right)=-\nu_1 k_{\mathrm{S}}\eta S_{\mathrm{p}}\rho_{\mathrm{c}}C_{1,\mathrm{S}}C_{2,\mathrm{S}} \tag{8.75}$$

$$N_2=\mathcal{A}_{\mathrm{S}}k_{2,\mathrm{S}}\left(C_{2,\mathrm{L}}-C_{2,\mathrm{S}}\right)=\frac{\nu_2}{\nu_1}N_1 \tag{8.76}$$

If the reactor is adiabatic, the temperature $T(z)$ is related to the molar extent of reaction, ξ', by the equation:

$$T=T_0-\frac{\Delta H_{\mathrm{R}}\xi'}{\Sigma\left(F_i C_{\mathrm{P}i}\right)} \tag{8.77}$$

These reactors often operate under high pressure (greater than 10 MPa, or 100 bars), so that variations in pressure throughout the catalytic bed are negligible. If this is not the case, the equations given in Section 8.2.3.1.A must be used to calculate the change in pressure as a function of z.

Equations (8.72), (8.73), and (8.74) are then simultaneously integrated, taking into account Eqs. (8.75), (8.76), and (8.77), beginning the integration from the initial conditions, for $z = 0$:

$$\begin{aligned}C_{1,\mathrm{G}}&=C_{1,\mathrm{G}}(0)\\ C_{1,\mathrm{L}}&=C_{1,\mathrm{L}}(0)\\ C_{2,\mathrm{L}}&=C_{2,\mathrm{L}}(0)\\ T&=T_0\end{aligned}$$

In practice the solution to these equations can be simplified considerably to the extent that some phenomena play a negligible role. For example, in the case of slow reactions, all the phases are considered to be in equilibrium:

$$\begin{aligned}C_{1,\mathrm{S}}&=C_{1,\mathrm{L}}=\frac{C_{1,\mathrm{G}}}{m_1}\\ C_{2,\mathrm{S}}&=C_{2,\mathrm{L}}\end{aligned}$$

Moreover, if reactant A_1, in the gas phase, is greatly in excess (hydrogen, for example, in certain hydrogenation reactions), $C_{1,\mathrm{G}}(z)=C_{1,\mathrm{G}}(0)$, and we are left only with a differential equation to solve:

$$\frac{\mathrm{d}\left(Q_{\mathrm{L}}C_{2,\mathrm{L}}\right)}{\mathrm{d}z}-\nu_2 k_{\mathrm{S}}C_{2,\mathrm{L}}S_{\mathrm{p}}\rho_{\mathrm{c}}\frac{C_{1,\mathrm{G}}(0)}{m_1}S=0 \tag{8.78}$$

The analytic solution is immediate if we also assume that the liquid flow rate (Q_{L}) and temperature are invariable with respect to z:

$$\frac{C_{2,\mathrm{L}}(z)}{C_{2,\mathrm{L}}(0)}=\exp\left(-\frac{\nu_2 k_{\mathrm{S}}S_{\mathrm{p}}\rho_{\mathrm{c}}\eta C_{1,\mathrm{G}}(0)}{m_1 Q_{\mathrm{L}}}Sz\right) \tag{8.79}$$

This equation makes use of the concept of space velocity for the liquid phase alone, which is often used in practice, and designated by VVH, namely:

$VVH = Q_L/(SH)$: volume flow rate of the liquid phase per unit volume of catalytic bed. In the literature, this magnitude is often referred to as the *liquid hourly space velocity*, or LHSV.

Recall that, when considering the difficulties associated with changes in volume, it is sometimes more practical to use a similar notation but one that is expressed in terms of weight: PPH, the *weight flow rate of feed* related to the weight of the catalyst bed (see Section 7.2.1).

During scale-up of the results obtained on a pilot unit to industrial size reactors, the space velocity, VVH, is often kept constant to simplify matters. This is not without risk, however. For, in the pilot unit, the fluid velocities are much lower (frequently 10 to 100 times lower) than those of the industrial reactor. The transfer conditions and limitations can be considerably different, therefore, and result in very different performance, in terms of conversion and yield as well as selectivity. This approach has the virtue of simplicity but lacks rigor as long as the influence of the fluid velocities has not been carefully studied.

E. Technology

Trickle-bed reactors are commonly used in industry. For metallurgical reasons, or because of their size, they are often limited to diameters of approximately 4 m and heights of approximately 30 m. When the capacity and degree of conversion require it, several reactors can be arranged in series or in parallel. After examining several key technological problems that deserve particular attention—phase distribution, catalyst loading, and pressure drop through the bed—we will briefly discuss a non-steady state operating mode of trickle-bed reactors and the question of just how representative small reactors really are.

a. Distribution of fluid phases

Many authors [Moller *et al.*, 1996, Marcandelli *et al.*, 2000] have recognized that in practice the distribution of fluids at the top of the reactor could have a significant influence on the overall efficiency of the catalytic bed. This is easily explained since the most stable flow regime from the point of view of energy, is one in which there is complete segregation of the gas and liquid, which occupy distinct regions of the catalytic bed, with a minimum interface between the phases. In spite of the importance of the problem, contact efficiency in industrial reactors is poorly understood and there is little published literature on the subject. However, we will attempt to provide some indication of current trends, which can be used to avoid some of the most serious errors.

• The distributor plate

The role played by the quality of the initial distribution of the liquid at the top of the catalytic bed is critical. Different steps can be taken to promote and maintain this distribution. They are based on the distribution of liquid in the form of a fine, uniform rain at the top of the bed. For example, when recommending distribution plates that operate on the same basis as those described in Chapter 4 for packed columns, the density of the liquid distribution points

must be at least 40 to 100 per square meter of cross-section of catalytic bed. To fully wet all the grains, the spacing between the holes must be adjusted in proportion to the size of the particles [Jacobs, 2000]. Additionally, the liquid distribution openings (holes or chimneys) must be distributed uniformly throughout the cross-section, up to the walls. The diameter of these openings (rarely less than 1 cm) is calculated to provide a liquid level of about 10 cm throughout the distributor; the quality of the bore must also be checked. Periodic examination of distributor holes is recommended to quickly correct any plugging or enlargement (tolerance less than 1%). Improved devices can be used to obtain much more precise distribution [Harter *et al.*, 2001]. For reactors of very large diameter, two-stage distributors can promote good distribution.

• The catalytic bed

The free surface of the catalytic bed must be as flat and horizontal as possible to prevent poor liquid redistribution. To ensure that the upper surface of the catalytic bed remains flat throughout the operation of the reactor, several layers of spheres of decreasing size, but slightly larger and denser than the catalyst (for example, tabular alumina, $d_p = 0.6$ to 1 cm) are carefully arranged at the top of the catalyst layer (Fig. 8.8).

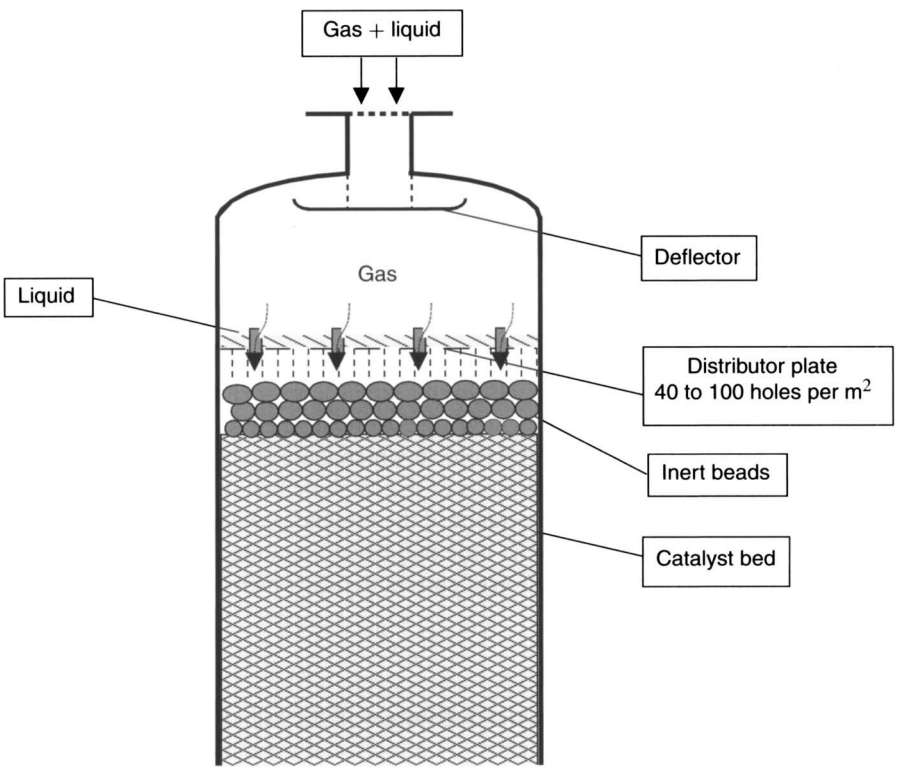


Figure 8.8 Internal components at the top of a fixed catalytic bed with downward cocurrent gas and liquid flow.

• Operating conditions

Maintaining good initial distribution of the phases throughout the catalytic bed depends on the linear velocities of the fluids. It appears that good contact efficiency is obtained once the interaction between the phases is strong. This contact efficiency tends toward 1 for a liquid superficial velocity of about 1 cm/s. If the liquid is foaming, a superficial velocity two to three times less may be sufficient.

A very high gas flow rate will destroy the good initial distribution of the liquid. So, when $V_{SG} > 10$ cm/s, it is essential that $V_{SL} > 1$ cm/s, especially if the liquid is not foaming.

In practice these recommendations, which are based on observations with models, are not always put into practice for reasons associated with reactor construction and cost. It is important to realize, however, that the consequence is, at a minimum, irregular irrigation of the catalyst particles and incomplete use of the catalytic bed, as well as either a decrease in the performance of the reactor or an increase in the volume of the catalytic bed needed to compensate for the loss of efficiency.

In addition to the poor use of catalyst, improper distribution of the liquid phase can create even greater problems during operation, such as the rapid deactivation of a part of the catalyst or unacceptable thermal instability. The latter phenomenon, observed in some industrial reactors (for hydrocracking or hydrogenation) appears to be the result of the fact that, in poorly irrigated regions of the catalytic bed, the liquid film can be completely evaporated locally, resulting in dry grains with greatly increased activity and much lower heat transfer values, along with significantly higher temperatures [Marcandelli *et al.*, 2000]. Because of the highly exothermic nature of the reactions, dry grains can reach temperatures that are much higher than those normally expected for a properly wetted bed. There can be several consequences from the presence of such hot spots, and they are generally serious and follow in succession: change of hydrodynamic or chemical regime, loss of selectivity, deactivation of the catalyst, even a rise in temperature of the entire reactor.

Abnormal fluid flow or bypass broadens the residence time distribution, which can seriously jeopardize the complete elimination of traces of some products and will, in any case, limit the conversion of reactants, or even the selectivity of intermediate products when several reactions are in competition. Vergel *et al.* [1995] have examined selective hydrogenation reactions, whose kinetics involve parallel and consecutive reactions. They have shown that the consequences of imperfect phase distribution on selectivity can be strongly attenuated by the use of two or three redistributors.

In the case of exothermic reactions, as with single-phase fixed beds (see Chapter 7), the catalytic bed is divided into several sections, separated by intermediate cooling devices (Fig. 7.7). For two-phase flow systems, cold fluid (hydrogen, for example, in hydrogenation reactions) is generally introduced into the zone separating the various sections of the catalytic bed. Here, the cold fluid must be mixed with the hot two-phase mixture from the previous catalytic bed and the new two-phase mixture must be redistributed at the top of the next catalytic bed. Mixing takes place by means of a perforated plate or inline mixer, redistribution by means of a plate distributor that is identical to the one previously described (Fig. 8.8).

b. Catalyst loading

Loading the catalyst into the reactor also plays a role in the distribution of fluids and must be achieved with great care for optimum performance. In particular, the separation of particles according to diameter and the formation of cavities must be avoided. Any unevenness in the porosity will result in a corresponding unevenness in gas-liquid distribution, liquid holdup, pressure drop, and the overall hydrodynamics of the system—effects that are both spatial and temporal, because of settling in the bed. Dudukovic [2000] has shown that even a normal global void fraction can hide the presence of uneven distributions of internal spaces and local void fractions, which result in enormous differences in fluid flow and, consequently, in performance. The problem is more difficult to correct in reactors of very small diameter than in large reactors, where several loading methods can be used to provide uniformity. Instead of sock loading, different methods of *dense loading* promote more uniform distribution and better particle packing. These operate according to the same basic principles: the use of a rotating element to project a rain of particles throughout the entire cross-section of the reactor at a controlled rate of flow. This flow rate must be chosen so that each particle, regardless of its size, has sufficient time to settle on the existing bed while maintaining the maximum number of contact points with grains already in place. It is important to prevent the grains from becoming wedged or stuck, thereby forming a vault that serves as an abnormally high local void fraction. These conclusions are applicable to spherical catalysts (commercial catalysts are relatively uniform in shape and size) as well as to simple or multilobe extrudates [Li *et al.*, 2000].

c. Operational problems associated with pressure drop

In some cases the feed introduced into the reactor contains debris, rust scales, catalyst fines, colloids, and compounds in varying stages of decay, which are deposited on and between the catalyst grains, creating a very rapid increase in pressure drop through the bed, especially when stopping and starting the unit. These disturbances can be so severe that it becomes necessary to frequently interrupt operation of the unit. Several solutions are used in practice to overcome this problem (see, in particular, Shaban and Kahn, 1995).

One solution, used in the hydroprocessing of petroleum cuts, involves placing baskets near the top of the fixed bed. Although helpful in protecting the bed, their use is controversial because they interfere with fluid distribution (in some cases they can occupy as much as a third of the available bed cross-section). Their use should be restricted to the introduction of dirty fluids. In other configurations the baskets are eliminated and replaced with a horizontal layer (0.5 to 1 m in height) of inert beads of alpha alumina (1" and 1/2" in diameter). These highly macroporous beads form a protective layer that absorbs impurities and helps improve the radial distribution of fluids. In the most serious cases, two independent beds, operating in rotation, can be used; these can be successively unloaded and reloaded without interrupting the continuous operation of the unit.

d. Trickle beds: effect of forced nonsteady operation

Rather than attempting to distribute fluids in a uniform and stable manner, several authors have used models and pilot-scale trials to test the consequences of the more or less cyclic fluid

feeds [Nieken *et al.*, 1995]. Khadilkar *et al.* [1999] have obtained significant performance improvements (up to 60%) by modulating the liquid feed flow rate in systems in which the gas is the limiting reactant. Adjustment of the duration and amplitude of the cycles must be examined for each reaction system. In 1996, Matros reviewed more than thirty systems that displayed improved performance through the effect of forced nonsteady operation. In fact, he concluded that operating in the forced nonsteady regime would never be less efficient than in the optimal continuous regime.

In practice, the variations in flow rates sometimes result in a change in the hydrodynamic regime that can have an overall positive effect on performance. Moreover, variable conditions for wetting the catalyst can also be used to avoid the continuous formation of distribution irregularities and dry zones over extended periods.

e. Small reactors

Several types and sizes of reactors are used to test industrial catalysts in their final form without grinding. For the tests to be meaningful, various constraints must be respected.

- The superficial velocities of the liquid must be chosen so that the dynamic pressure drop is significantly greater than the simple pressure drop due to gravity, which is reflected in the following inequality [Sie, 1991]:

$$W = \frac{\mu_L V_{SL}}{g \rho_L \bar{d}_p^2} \geqslant 5\ 10^{-6} \quad \text{where } W \text{ is the wetting number}$$

- The reactor diameter must be large enough so that wall effects can be neglected:

$$\frac{\Phi_{reactor}}{\Phi_{particle}} \geqslant 25$$

- To ensure that flow is as close to plug flow as possible, the following inequality must be maintained:

$$Pe > 8n \operatorname{Log} \frac{1}{1 - X}$$

where n is the reaction order, X the desired conversion, and Pe the Peclet number, $Pe = HV_{SL}/\mathcal{D}_A$.

To meet the previous criteria using industrial catalysts, pilot reactors a few centimeters in diameter and at least 1 m tall are used. To avoid the need to use large volumes while respecting these criteria, the catalyst can be diluted with much finer particles (roughly 10 times smaller), which determines the hydrodynamics of the reactor and promotes catalyst wetting and thermal uniformity. This technique also allows the catalyst grains to correctly reproduce the local operating conditions of industrial reactors. For correct dilution of the catalyst bed, great precision is required during loading operation [Sie, 1991; Al Dahhan *et al.*, 1995, 1996].

Other solutions are sometimes preferred, including the use of upflow reactors, which ensures good wetting of the particles without the need for dilution.

Next Page

F. Concluding remarks

The advantages and disadvantages of fixed-bed reactors with cocurrent downflow are listed below.

Advantages

- Flow is similar to plug flow, resulting in higher conversion rates
- Ability to operate at high temperature and pressure
- Ability to use variable liquid and gas flow rates
- No catalyst loss
- Low ratio of liquid/solid volumes and, consequently, little possibility of secondary reactions in the liquid phase
- Limited investment and operating cost
- Large size reactors can be used when needed
- No moving parts.

Disadvantages

- Strong influence of hydrodynamic regime on reactor performance: risk of poor liquid distribution and partial wetting of the catalyst
- Low catalyst effectiveness because of large particle size (internal diffusion limitation)
- Fairly low liquid-solid mass transfer
- Poor radial heat transfer
- Pressure drop through the bed
- Risk of impurity deposits and fouling of catalyst particles
- Unsuitable for use with viscous liquids
- Limited capacity in the event of rapid catalyst deactivation.

Finally, these reactors are in wide use because of their simplicity, compact size, and ability to process important flow rates of fluid with high conversion rates. If the reaction is highly exothermic, the variant multitubular fixed bed can be used. In the Table 8.3, multitubular fixed beds are compared to slurry columns.

Remarks

In pilot or laboratory reactors operating with downward flow, the liquid distribution is often a problem. To overcome this problem and promote catalyst wetting, the catalyst particles are often ground (which modifies the transfer conditions, especially internal mass transfer) or diluted with inert fines, which ensures better liquid contact as well as better thermal uniformity.

New catalysts that have innovative, multilobe shapes (three or four lobes) or are hollow have been proposed. Compared to the conventional spherical or cylindrical shapes, they offer a much larger external surface area than conventional grains and provide the reactants with easier access to the core of the grain, which has a favorable effect on the reaction rate and selectivity —at least theoretically. The greater external void fraction of the bed results in a decrease in pressure drop, although it also weakens the particles and leads to an increase in bed size to ensure that the real volume of catalyst is the same. The global balance is not always clearly favorable and depends on the specific conditions, including economic conditions, process conditions, and so on (see Chapters 6, 7, and 9).

Previous Page
Copyrighted Materials
Copyright © 2004 Editions Technip Retrieved from www.knovel.com

Table 8.3

	Multitubular fixed bed	Slurry column
Catalyst diameter (mm)	1–3	0.01–0.2
Capacity	+	++
Internal diffusion limitation	−	+
Use of reaction volume	++	−
Axial gradient of catalyst activity	++	−
Gas staging	+	−
Gas/liquid transfer limitation	+	+
Isothermal operation	−	+
Heat transfer to external fluid	−	++
Catalyst replacement	−	+
Solid/liquid separation	++	−−
Catalyst attrition	+	+ or −
Demonstration unit needed	no	yes
Development delay	++	−−

−− unfavorable, − somewhat favorable, + favorable, ++ highly favorable.

Trickle-bed reactors have obvious industrial advantages, and large size reactors are used for hydrodesulfurization, hydrogenation, hydrocracking of petroleum cuts (photo 8), as well as a variety of hydrogenation and oxidation reactions in chemistry.

8.2.3.2 Reactors with cocurrent upflow

Fixed-bed reactors with cocurrent upflow are very similar to the fixed-bed reactors with cocurrent downflow examined above. However, the change in the direction of circulation appreciably alters a number of hydrodynamic characteristics. This family of reactors is less frequently used and, consequently, our understanding of them is still quite limited. Below we provide only the most important information for designing such systems.

A. Hydrodynamics

a. Flow regimes

As with cocurrent downflow, various hydrodynamic regimes exist, and they depend on the flow rates and properties of the fluids as well as particle size.

- The dispersed bubble phase with a continuous liquid phase is observed when gas flow rates are very low. It seems that this regime is frequently found in industrial reactors and more generally in the presence of particles greater than 4 mm in diameter. According to data provided in the literature, this regime is established for low gas flow rates, namely:

$$G \leqslant 0.01 \text{ to } 1 \text{ kg/(m}^2 \cdot \text{s)}$$

- The pulsed regime appears when gas flow rates are high.
- The mist regime occurs when flow rates for both fluids are high (as with cocurrent downflow).

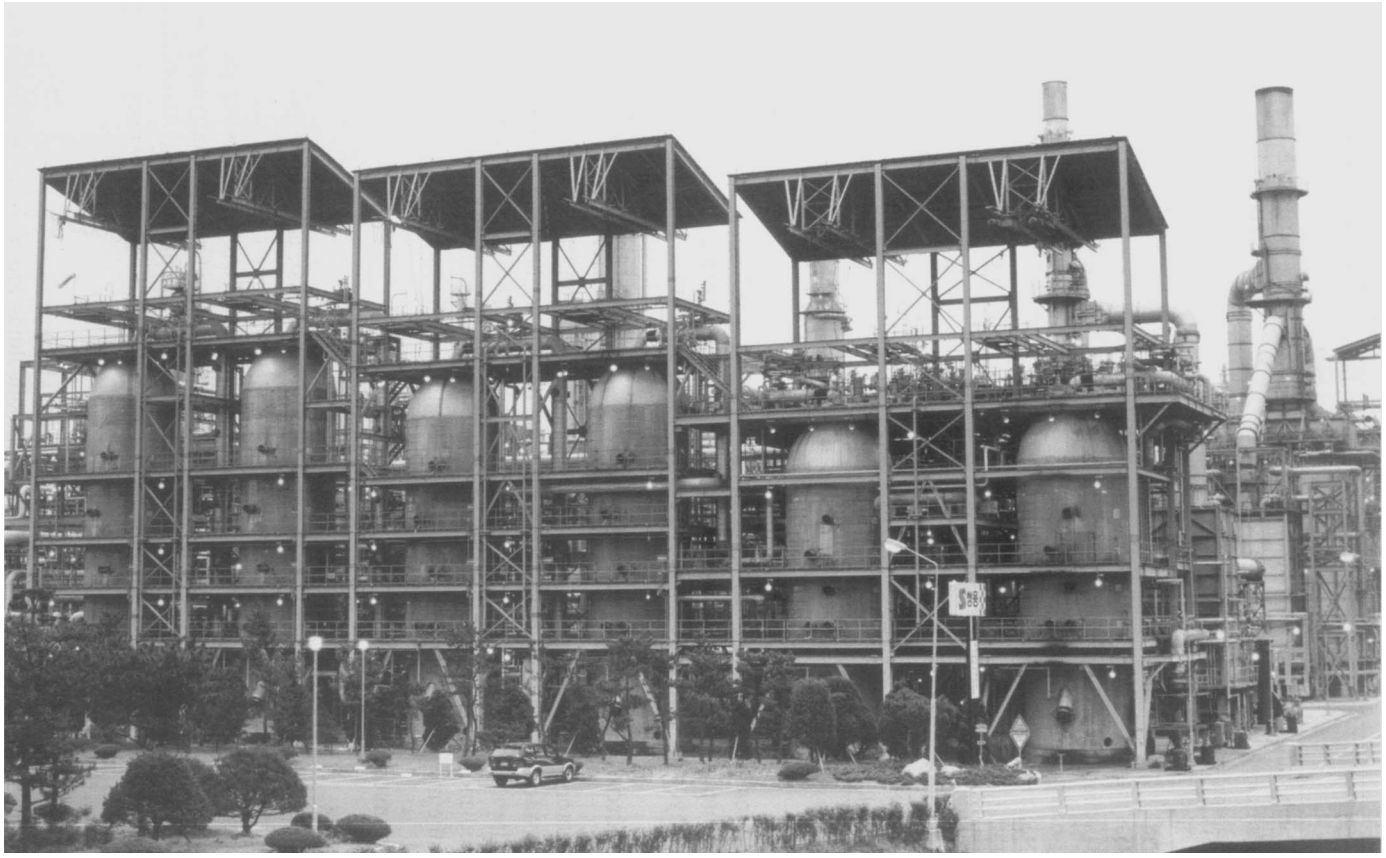


Photo 8 Catalytic reactors with two-phase flow (trickle bed): treatment of heavy petroleum fractions. Several reaction stages are arranged in series with different catalysts to carry out the various demetalation, desulfurization, and denitrogenation reactions. Because of the volumes that are processed, two reactors are placed in parallel at each stage.

(*IFP Photo Library*).

b. Pressure drop

For identical flow rates, the pressure drop and liquid holdup are generally higher with upward flow than with downflow. Some correlations have been proposed to calculate the pressure drop. However, these equations must be used with caution since they are frequently based on data for water-air systems. As a first approximation, the semi-empirical Ellman equation, established for trickle-bed reactors in the strong interaction regime, can be used. According to Yang *et al.* [1992], this equation is acceptable for upflow reactors.

$$\left(\frac{\Delta P}{\Delta H}\right)_{LG} = f_{LG}\frac{2G^2}{d_h \rho_G} \tag{8.80}$$

where:

$$f_{LG} = 6.96\,(X_G\xi)^{-2} + 53.3\,(X_G\xi)^{-1.5} \tag{8.81}$$

$$d_h = d_p\left[\frac{16\varepsilon_s^3}{9\pi\,(1-\varepsilon_s)^2}\right]^{0.33} \tag{8.82}$$

$$\xi = \frac{Re_L^{0.25} We_L^{0.2}}{\left(1 + 3.17 Re_L^{1.65} We_L^{1.2}\right)^{0.1}} \tag{8.83}$$

$$X_G = \left(\frac{We_G}{We_L}\right)^{0.5} \tag{8.84}$$

$$Re_L = \frac{\overline{d_p} L}{\mu_L} \tag{8.85}$$

$$We_L = \frac{V_{SL}^2 \rho_L d_p}{\sigma} \quad \text{and} \quad We_G = \frac{V_{SG}^2 \rho_G d_p}{\sigma} \tag{8.86}$$

c. Liquid holdup

Liquid holdup increases with the superficial velocity and the viscosity of the liquid, and decreases sharply with the gas flow rate, density, or pressure. The other parameters do not have as marked an influence. Yang *et al.* [1992, 1993] have proposed a simple equation that has been validated for a large number of media:

$$\varepsilon_L = (1-\varepsilon_s) - C_0\frac{V_{SG}}{V_{SG} + V_{SL}} \tag{8.87}$$

where

$C_0 = 0.16$ for non-foaming liquids

$C_0 = 0.28$ for foaming liquids

and:

$$\varepsilon_L + \varepsilon_G = 1 - \varepsilon_s$$

Molga and Westertep [1997] later returned to the concept of slip velocity and, on the basis of their tests, some of which were conducted under pressure, developed a correlation that can be written in the following form:

$$\varepsilon_L = (1 - \varepsilon_s) \frac{V_{SL} + 0.39 V_{SG}^{0.85}}{V_{SG} + V_{SL}} \tag{8.88}$$

There is also a dimensionless correlation that was proposed by Larachi [1999], which is expressed for the liquid saturation ratio $\beta = \varepsilon_L / (\varepsilon_L + \varepsilon_G)$:

$$\log\left(\frac{1}{1-\beta}\right) = 0.93 \frac{We_L^{0.08}}{Re_L^{0.2} X_G^{0.15}} \tag{8.89}$$

Much more complete models have been proposed, in particular, by Bensetiti *et al.* [1997] and Belfares *et al.* [2000]. Based on extremely large databases, their polynomial regressions also take into account the (moderate) effect of pressure and various properties, and incorporate a large number of parameters. The precision is quite good.

The liquid holdup in these reactors is appreciably higher than in downflow reactors under identical conditions. This has several important consequences, such as uniform wetting of catalyst particles and better thermal homogeneity (at least radial), which sharply decrease the risk of hot spots and considerably limit parasite reactions likely to produce unwanted products or poor conversion and selectivity.

d. Backmixing

Tests conducted over a broad range of temperatures and pressures, using hydrocarbons and hydrogen in small-size pilot reactors (diameter 2.5 cm, height 1 m) have provided—for the liquid phase—Peclet numbers, *Pe*, of 0.1 to 50 [Thanos *et al.*, 2001]. The Peclet number increases with the liquid flow rate but decreases very rapidly with the gas flow rate. However, *Pe* is said to be independent of the properties of the gas and the pressure. Papayanakos *et al.* [1992] proposed a correlation based on experimental data points obtained in the presence of hydrocarbons, near 400°C, with cylindrical pellets diluted with carborundum:

$$Pe = 45 \exp(-0.15) \frac{V_{SG}}{V_{SL}} \tag{8.90}$$

In spite of these findings, the effect of the properties of the medium is still not very clear, even though Belfares *et al.* [2000] have proposed a complete and precise correlation, using a neural network with 1 000 experimental data points.

B. Mass transfer

a. Gas-liquid mass transfer

For an equivalent expenditure of energy, the values of the interfacial area and the mass transfer coefficient observed with upward flows are slightly greater than those obtained under downward flow conditions.

As with downward flow, the best correlations refer to energy dissipation of flow. Unfortunately, as we have just seen, only rough estimations of this energy can be obtained. The

influence of pressure does not appear to be too important [Molga and Westertep, 1997], but data obtained under pressure are quite scarce. Among the published correlations, the following are noteworthy:

$$\frac{\mathcal{A}_{GL}}{\mathcal{A}_S} = 0.02\left[\left(\frac{\Delta P}{H}\right)_{LG}\frac{1-\varepsilon_s}{\mathcal{A}_S}\right]^{1.17} + 0.61 \tag{8.91}$$

$$10^3\frac{k_{l,L}(1-\varepsilon_s)}{V_{SL}} = 7.96\left[\left(\frac{\Delta P}{H}\right)_{LG}\frac{1-\varepsilon_s}{\mathcal{A}_S\rho_L V_{SL}^2}\right]^{0.275} - 9.41 \tag{8.92}$$

b. Liquid-solid mass transfer

The values of $k_{l,S}$ observed for upward flow are appreciably equivalent to those measured for downward flow. Some authors have even proposed a single correlation for calculating $k_{l,S}$ regardless of the direction of flow [Bartelmus, 1993]. In the absence of more recent data, the somewhat dated correlation provided by Mochizuki [1978] can be used:

$$Sh = \frac{k_{l,S}d_h}{\mathcal{D}_{l,L}} = 0.75\,(Sc)_L^{0.33}\left[(Re)_L^{0.5} + 4\,(Re)_G^{0.55}\,(Re)_L^{-0.2}\right] \tag{8.93}$$

The Reynolds numbers are calculated on the basis of the hydraulic diameter of the particles, d_h, that is:

$$d_h = \frac{(1-\varepsilon_s)\,\overline{d_p}}{1.5\varepsilon_s} \tag{8.94}$$

$$(Re)_L = \frac{\rho_L V_{SL} d_h}{\mu_L} \tag{8.95}$$

$$(Re)_G = \frac{\rho_G V_{SG} d_h}{\mu_G} \tag{8.96}$$

C. Heat transfer

The thermal stability of reactors with cocurrent upflow is better overall than in reactors with cocurrent downflow because liquid holdup is generally greater. This advantage is especially noticeable in regimes characterized by low interaction. During cocurrent upflow, the thermal conductivity of the bed is 20 to 30% greater than that of the downward cocurrent configuration; in regimes characterized by strong interaction, conductivity is appreciably equivalent.

As with the other fixed beds, homogeneous models with two parameters are pertinent:

- For the coefficient of thermal conductivity, Λ_{rad}, which is about 10 to 200 times λ_L, Colli-Serrano and Midoux [2000] have proposed a somewhat general correlation derived from the one they proposed for liquid flow alone.

For the liquid alone:
$$\frac{\Lambda_{rad}}{\lambda_L} = \frac{\lambda_{L=0}}{\lambda_L} + 0.06Re^{1.23}Pr^{0.7} \tag{8.97}$$

For the gas-liquid mixture:
$$\frac{\Lambda_{rad}}{\lambda_L} = \frac{\lambda_{L=0}}{\lambda_L} + 0.06Re^{1.23}Pr^{0.7}\frac{34.8Re_G}{1+2.16Re_G} \tag{8.98}$$

- The coefficient of transfer with the walls (h_W is approximately 800 to 10 000 W/m^2 · K), increases with the liquid velocity and particle diameter, but depends on the hydrodynamic regimes in a complex manner. Lamine *et al.* [1992] distinguish different cases depending on the size of the particles.

When $G > 0.05$ kg/m^2 · s and $L > 1$ kg/m^2 · s, the Biot number ($Bi = h_W\overline{d_p}/\Lambda_{rad}$) varies as follows:

$\overline{d_p}$ (mm)	1	2	4	6
Biot number	0.2	0.4	0.6	0.6

When there is low interaction regime, h_W is nearly independent of the gas flow rate when the bed consists of small particles ($\overline{d_P} \leqslant 2$ mm).

D. Modeling

Modeling a cocurrent upflow reactor resembles that for cocurrent downflow configurations (see Section 8.2.3.1.D). Here too, we must determine if the assumption of plug flow with axial dispersion can be used for each of the fluids or if the presence of stagnant liquid in the catalyst pores requires the addition of an exchange term [Yang *et al.*, 1990]. When catalytic beds with a height greater than $150 \cdot \overline{d_p}$, or approximately 50 cm, are used, backmixing in the liquid phase can be neglected. To accurately represent small reactors using "plug + diffusion" models, the coefficients of liquid axial diffusion proposed by Belfares *et al.* [2000], which are well suited to a variety of media, can be used. Molar balance equations can be written that are identical to Eqs. (8.72) to (8.76).

Here too we assume that the catalytic bed operates adiabatically. To carry out intermediate cooling operations when necessary, depending on the structure of the reactors (Fig. 8.9), it is certainly preferable to arrange several reactors in series rather than trying to introduce into the individual reactor vessel a large number of internal devices for introducing cold fluids and mixing them with the hot reaction fluids.

E. Technology

Fluid distribution

Although the distribution of the liquid phase does not present the same problems as with downward flow, suitable distribution of the gas phase must be achieved and the catalytic bed must remain stationary. Several possible implementations are possible, some of which are shown in Fig. 8.9.

- In Fig. 8.9A, the following two features are worth noting:
  - There is a conventional gas distributor at the base of the reactor, placed beneath the horizontal grid that supports the catalytic bed.
  - At the top of the catalytic bed is a conical grid. It allows the two fluid phases to pass through but, because of the sharp reduction in the diameter of the conical grid, keeps the catalyst in place by preventing it from traveling upward. The cylindrical volume of smallest diameter above the grid is filled with granular solid (catalyst or inert), which constitutes a reserve that will flow downward if the catalytic bed settles.

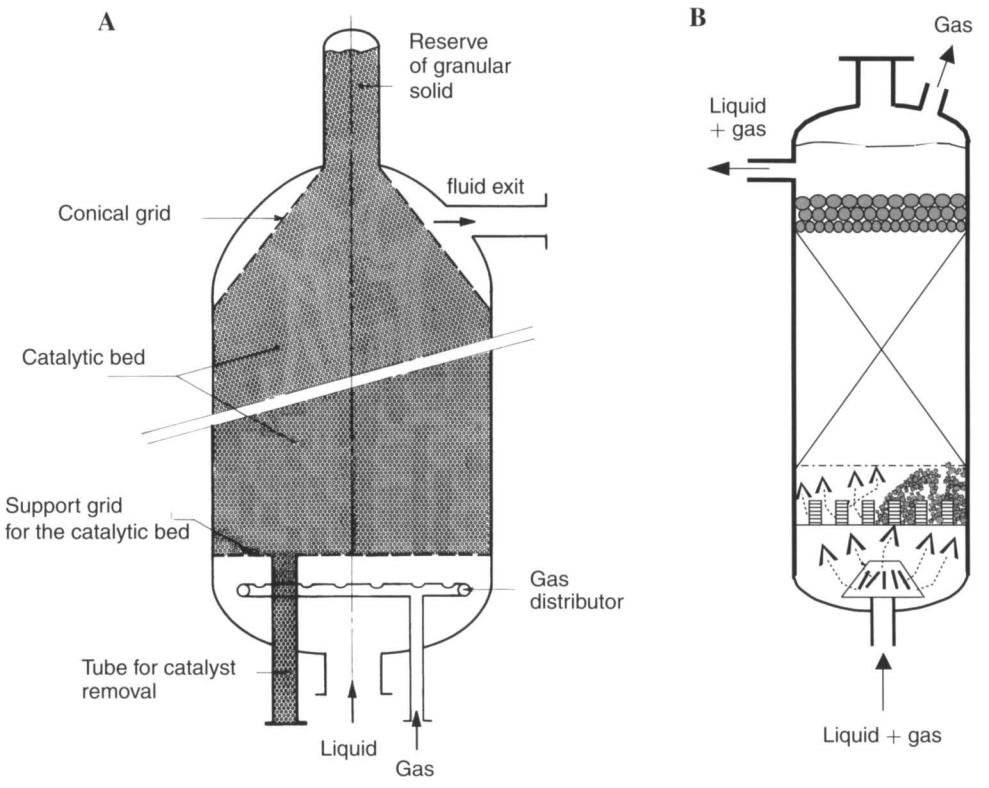


Figure 8.9 Possible designs for a fixed-bed catalytic reactor with two-phase cocurrent upflow.

- In the solution shown in Fig. 8.9B, the upper part of the bed is horizontal. Accidental expansion of the bed resulting from abnormal fluid movement, is prevented by the presence of several layers of inert support beads, whose diameters and densities are much greater than those of the catalyst.

F. Concluding remarks on cocurrent upflow reactors and comparison with downflow reactors

This type of fixed-bed reactor, in which the liquid and gas phases pass through the catalytic bed from bottom to top is not often used on an industrial scale, but it is frequently used for small pilot units. This results from the fact that it can be difficult to keep the catalytic bed stationary when the two-phase mixture passes through it, and because any movement of the catalyst particles caused by fluid flow leads to unacceptable attrition in an industrial facility. In contrast, the technology has the advantage of providing a simple and effective solution to the problem of radial distribution of the liquid, which handicaps downflow reactors.

The influence of the direction of fluid circulation, upward or downward, has been examined by a number of authors: Wild *et al.* [1991], Lara Marquez *et al.* [1992], Yang *et al.* [1992],

Vergel *et al.* [1995], Burghardt and Bartelmus [1996], Khadilkar *et al.* [1996]. Several phenomena occur more or less at the same time:

- The hydrodynamics, associated with the fluid flow rates and the size and shape of particles, plays a role on the degree of wetting of the particles and, therefore, on the interactions between the gas, the liquid, and the catalyst pores. These competing factors interfere with the kinetic regimes and, therefore, the conversion and selectivity. For, when a liquid film completely covers the catalyst, the gas cannot reach the catalytic sites directly but must pass through the liquid phase. However, when the surface area of the grains is not completely wet, the reactants present in the gas phase can easily access the catalyst pores. The situation can therefore change considerably depending on the direction of circulation.
- The interfacial area, gas-liquid transfer coefficients, reactant concentrations, as well as the pressure and temperature, can play a critical role in determining the apparent rates of reaction.
- The fluid flow rates, pressure, temperature, reactant concentrations, and physicochemical properties of the medium will have considerable effect on the different stages of transfer, on the kinetics, and globally on performance, conversion, and selectivity.
- The final result of the comparison depends on several parameters, but overall on the fluid phase, which controls the reaction and, in particular, according to Khadilkar *et al.* [1996], on the relative values of the concentrations and diffusivities of the reactants present in each of the phases. Globally, downflow is more favorable when the gas phase is the limiting phase; conversely, the upflow reactor is preferable when the liquid limits transfer. Nevertheless, their performance becomes similar as the flow rates of the fluids increase.

Finally, upflow reactors are often used on a small scale, in pilot units, for example, when developing hydrotreatment processes for petroleum refining. The hydrodynamic regime chosen is the bubble regime, in which the catalytic bed, submerged in the liquid, is traversed by the gas, which rises in the form of fine distinct bubbles. The transposition to a trickle-bed design is quite straightforward, at least when gas-liquid transfer and liquid-solid transfer are not limiting.

Comments: Monolith catalysts are currently undergoing a stage of intense development. They can be used as fixed-bed reactors with downward or, more rarely, upward cocurrent fluid flow. They have the advantage of promoting nearly perfect plug flow of each of the phases and provide excellent transfer with the walls. There are few published correlations, however. Unfortunately, for large-diameter reactors, these catalysts present a serious drawback because of the difficulty of obtaining a balanced distribution of the fluids in all the channels.

8.2.3.3 Countercurrent flow reactors

In countercurrent reactors, the liquid, which is the dispersed phase, descends countercurrent to the gas, the continuous phase, through the fixed bed of catalyst. Little data exist for this type of reactor [Trambouze, 1990, Dudukovic *et al.*, 1999, Piché *et al.*, 2001] and for the most part they have been derived from packed columns. Readers are referred to Chapter 4, although the information presented there must be used with caution when catalytic reactors are involved, since they differ slightly from packed columns.

A. Hydrodynamics

The hydrodynamics for these reactors is very similar to that of countercurrent packed columns. The difference lies in the void fraction, which is generally low and considerably limits the operating range because of premature flooding. Pressure drop is calculated using the formulas presented in Chapter 4 for packed columns.

B. Mass transfer

As a result of systematic countercurrent flow, phase contact and transfer are quite efficient. There is little published data and it is limited to small reactors. The correlations for countercurrent packed columns can be used as a starting point for further calculations.

C. Technology

The technology used in these reactors is nearly identical to that used for countercurrent packed columns. The distribution of each of the phases, liquid as well as gas, must be designed carefully so that the fluids are forced to interact.

D. Concluding remarks

Although we know only few fixed-bed catalytic reactors with countercurrent fluid phases operating on an industrial scale, it is not inconceivable that such a technology could be used, possibly with certain advantages. We should point out that one of the limitations of this type of reactor is its reduced flexibility because of flooding, which limits the flow rates of each of the phases that must pass through the catalytic bed. To increase the range of acceptable flow rates, catalyst particles must be used whose dimensions or external void fractions are larger than those generally used for fixed beds, while remaining mechanically resistant to crushing. The larger catalyst particles would have the disadvantage of reduced effectiveness, however. Another solution consists in using catalyst particles shaped like conventional packing materials, such as Berl saddles or Raschig rings, which promote gas-liquid-solid contact without leading to excessive pressure drop. Catalysts deposited on structured packing represent another alternative [Ellenberger and Krishna, 1999], but this has to be developed on an industrial scale. These packings ensure good radial distribution, and pressure drop is much lower (100 to 1000 times less) than in conventional fixed beds. The coefficient of radial diffusion of the liquid is high (approximately 10 times greater than in a trickle bed and 100 times greater than the liquid alone traversing the fixed bed). This is because the liquid passes through filled catalyst channels as well as through open channels, where the gas passes preferentially.

Countercurrent operation is beneficial for some reactions because it promotes the systematic use of reactants and high conversion rates. For example, a more or less parasitic intermediate product can be eliminated in the gas phase and secondary reactions avoided. Thus, in the case of the hydrogenation of aromatics in a hydrocarbon cut containing traces of sulfur, the hydrogen sulfide can be stripped as soon it appears and the lower section of the catalytic bed will work in the absence of sulfur and, therefore, with maximum hydrogenating activity. Tests conducted for the hydroconversion and hydrodesulfurization of petroleum cuts [Ellenberger and Krishna, 1999] have resulted in conclusions that are distinctly favorable to this method of phase circulation.

8.2.4 Moving-bed reactors

Whenever it is necessary to frequently replace catalyst in a three-phase reactor, one possible option involves the use of a moving bed reactor. In moving-bed reactors the fluids pass through the catalytic bed as in a conventional fixed bed except that here the catalytic bed is systematically refreshed. New or regenerated catalyst is always introduced from the top of the reactor and, when inactive, withdrawn at its base. The catalyst moves slowly by gravity, continuously or in batches, in the plug-flow mode.

Two technologies have been developed to ensure such contact in the moving bed (Fig. 8.10). They differ in the direction of fluid flow:

- downward cocurrent fluid flow
- upward cocurrent fluid flow.

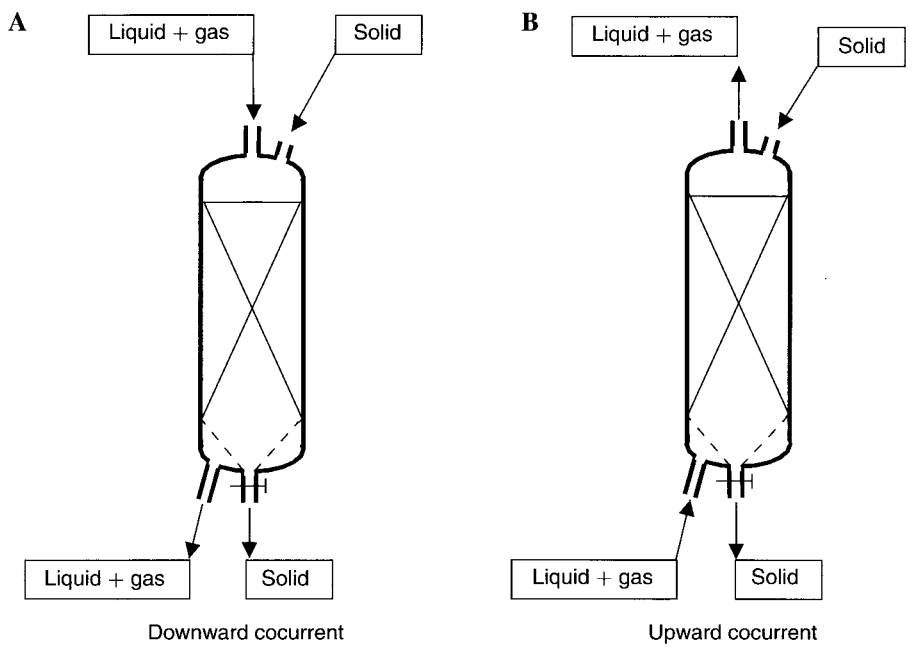


Figure 8.10 Three-phase moving-bed reactors. **A.** Downward cocurrent. **B.** Upward cocurrent.

In the first case, the fluids descend through the moving catalytic bed, which descends at the same time. Instantaneously, the reactor behaves like a cocurrent downflow fixed-bed reactor, for example, in the trickle bed regime. The catalyst moves slowly from top to bottom in the reactor, with plug flow. In the lower part of the reactor, a special conical zone helps separate the fluids and withdraw catalyst grains.

In the second case the fluids rise through the moving catalytic bed which, continues to descend [Burzynski *et al.*, 1988, Catros *et al.*, 1990]. The gas and liquid flow countercurrent to the solid catalyst. Instantaneously, the reactor operates as a fixed-bed reactor with upward

cocurrent liquid flow. Here too the catalyst moves with plug flow from top to bottom. In the bottom part of the reactor are located the fluids distributor and a cone used to remove the catalyst.

In this case the superficial velocities of the gas and liquid are chosen to avoid expansion of the bed, and the mixing and possible attrition of grains of solid [Euzen, 1991]. Examination of the hydrodynamic behavior leads to a determination of the most favorable domain on the basis of the characteristics of the catalyst (diameter, density) and the fluids (density, viscosity). There are several advantages to this solution:

- pressure drop through the bed is quite low
- liquid holdup is high, which provides good control of temperature homogeneity and limits the risk of local runaway reactions
- use of the catalyst is systematic and optimal: At the bottom of the reactor, fresh feed encounters the spent catalyst, which is about to be withdrawn. The feed can then react efficiently and, furthermore, deposit any accompanying sediment without the risk of plugging. At the top of the reactor, the feed, already mostly converted, encounters the most active catalyst, which has just entered the reactor and can push the conversion further.

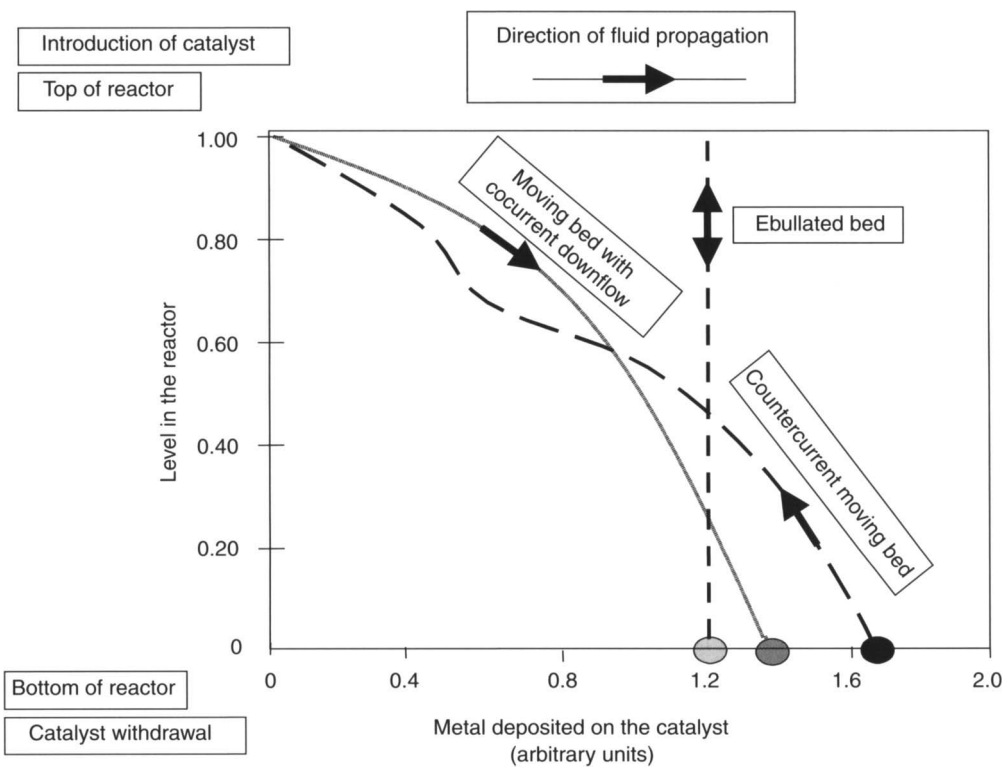


Figure 8.11 Comparison of metal deposit profiles in an ebullated bed, upward moving bed, and downward moving bed [from Euzen, 1991].

In the case of the hydrodemetallation of a heavy crude such as Boscan, a simplified reactor model illustrates this advantage. The countercurrent moving bed consumes approximately 25% less catalyst than the cocurrent fluid/solid moving bed and approximately half as much as an ebullated bed reactor (Fig. 8.11).

These moving-bed technologies provide an opportunity for systematic use of the catalyst. The reactors themselves must, of course, be equipped with devices for the sequential introduction and withdrawal of catalyst, without interrupting the continuous operation of the reactor. Reliable, automated technical solutions have been developed.

8.2.5 Three-phase fluidized beds or ebullated beds

Three-phase fluidized-bed reactors or ebullated bed reactors can be represented schematically as shown in Fig. 8.12. The liquid and gas phases traverse the reactor from bottom to top and maintain the catalytic solid, consisting of particles whose size is generally between 1 and 5 mm (values of u_t range as high as 0.5 m/s), in a fluidized state. The two fluid phases leave the upper part of the reactor without entraining the solid, which remains in a fluidized layer inside the reactor. If necessary, introduction or withdrawal of the solid catalyst is extremely easy, as in beds of particles fluidized by a single fluid.

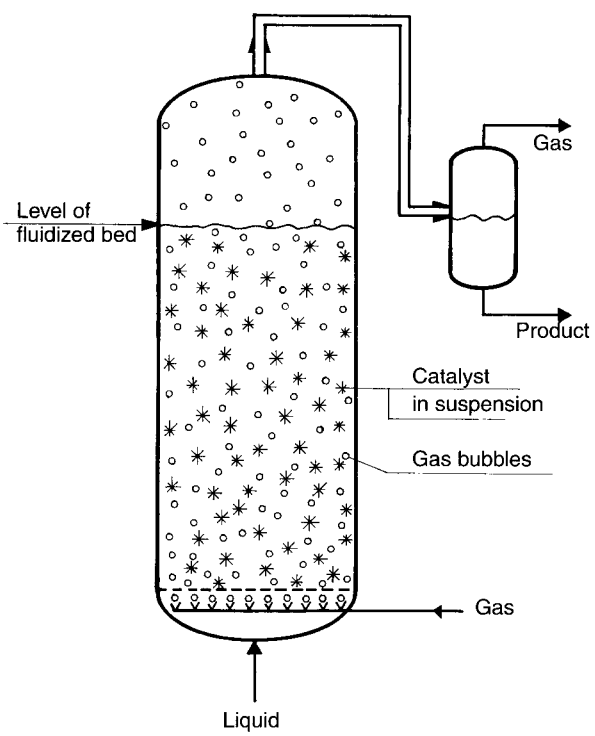


Figure 8.12 Three-phase fluidized-bed or ebullated-bed reactor.

At this point in time our understanding of three-phase fluidized beds is still fragmentary, especially for solids about a millimeter in size. In the following sections we provide some of the data found in the literature, which can be useful for a preliminary description of these systems. The indicated correlations have often been obtained from water-air systems in small devices. Their application to industrial situations, where large reactors often require high temperature and pressure, must be approached cautiously and, if possible, after verification. Good references in this field can be found in the work of Wild *et al.* [1982], Muroyama and Fan [1985], Fan [1989], Wild and Poncin [1996], Dudukovic *et al.* [1999], and in the databases and general correlations provided by Larachi *et al.* [2001].

8.2.5.1 Hydrodynamics

A. Flow regimes

Starting from a fixed bed at rest, the catalyst is fluidized as soon as the gas or liquid flow rate is capable of lifting the weight of the bed. If at least one of the flow rates continues to increase, the bed will gradually expand. For even greater flow rates, the fluids can even entrain the particles. The respective roles of each of the fluids varies on the basis of their flow rates.

If the liquid velocity is relatively high and the gas velocity low, the three-phase system will behave as a bed fluidized by the liquid alone, within which the gas phase will flow as in a bubble column. In contrast, when the gas velocity is high and the liquid velocity low, the situation is completely different, and accompanied by the appearance of a pulsed regime. For intermediate gas and liquid velocities, there is a gradual transition of the fixed bed to a completely fluidized bed that is more or less turbulent. These situations are illustrated in the diagram in Fig. 8.13. The illustration shows a homogeneous bubble regime and a turbulent bubble regime, separated by a transition regime; each has a specific signature of local pressure fluctuations. Although the regimes can be clearly identified in the laboratory, when dealing with large or industrial reactors, several regimes can coexist in the same bed, at different heights, as the characteristics of the medium evolve. In each of these regimes, however, the concentration of solid is homogeneous throughout the entire reactor cross-section.

Under the effect of pressure and temperature, the transition between the dispersed bubble regime and the coalesced bubble regime evolves toward higher superficial gas velocities. The transition velocity, U_{tr}, can be evaluated from the terminal velocity of an isolated particle falling in the liquid, u_t, according to the following correlation, derived from values obtained in the presence of water and air:

$$U_{tr} = 1.08u_t - 0.054 \quad \text{if } u_t < 0.27 \text{ m/s} \tag{8.99}$$

$$\text{and } U_{tr} = -0.81u_t + 0.46 \quad \text{if } u_t > 0.27 \text{ m/s} \tag{8.100}$$

B. Pressure drop

Once the bed is fluidized, the pressure drop from the bed alone can be calculated on the basis of the hydrostatic pressure, that is:

$$\Delta P \cong (\rho_s \varepsilon_s + \rho_L \varepsilon_L + \rho_G \varepsilon_G) Hg \tag{8.101}$$

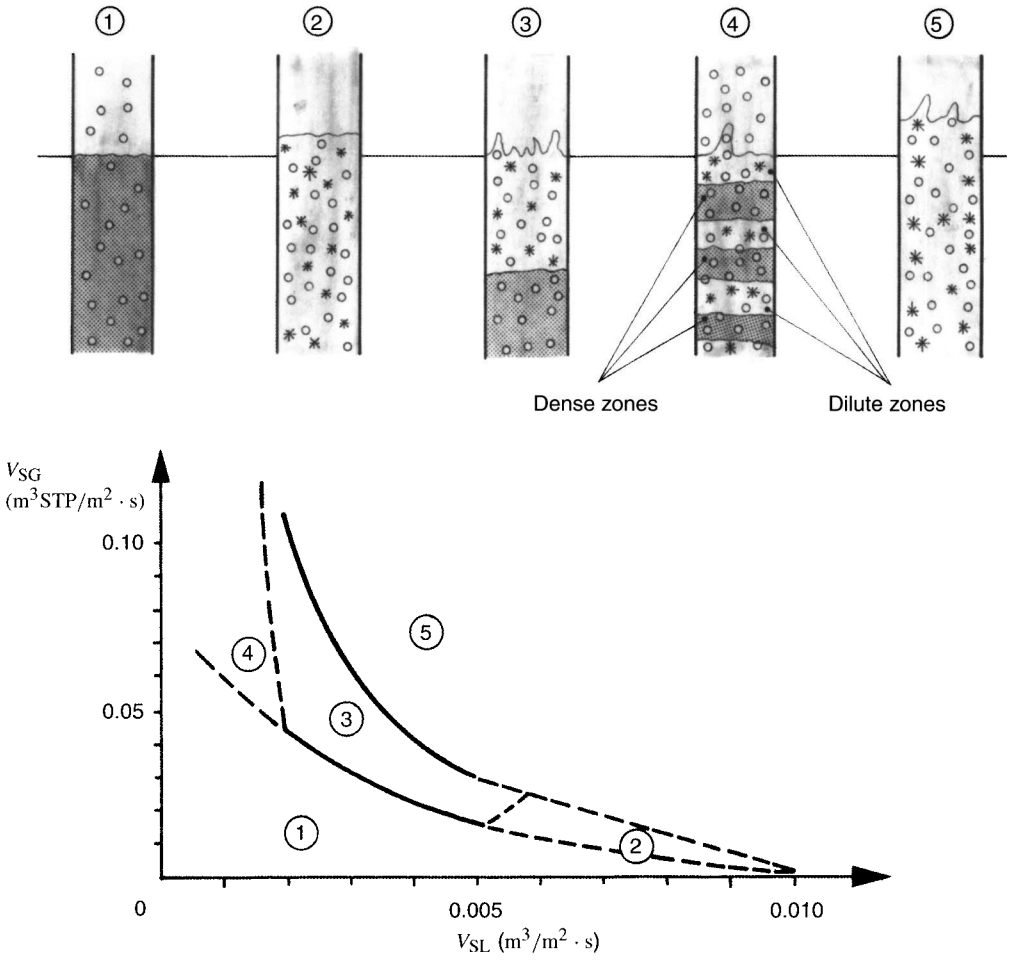


Figure 8.13 Flow regimes in a three-phase fluidized bed: 1) fixed bed, 2) pseudo-liquid-solid fluidized bed, 3) partially fluidized bed, 4) pulsed bed, 5) fluidized bed.

where H is the height of the fluidized layer. The calculation of holdup (ε_L and ε_G) is discussed below.

C. Minimum fluidization velocity

In Chapter 7 we showed how to calculate the minimum fluidization velocity for a single fluid phase (gas or liquid). Here we are interested in the interaction of the flow rates of the two fluids and the appearance of fluidization. This is generally expressed in the form of a minimum liquid velocity $(V_{SL})_m$, which depends on the gas flow rate, as in the Begovich and Watson equation (established with air and aqueous media in small size columns and

applicable only to high gas flow rates):

$$(Re)_{Lm} = \frac{\overline{d_p}(V_{SL})_m \rho_L}{\mu_L} = 5.12 \cdot 10^{-3} (Ar)_L^{0.662} (Fr)_G^{-0.118} \tag{8.102}$$

$$(Ar)_L = \frac{\rho_L \bar{d}_p^3 (\rho_s - \rho_L) g}{\mu_L^2} \quad \text{(Archimedes number)} \tag{8.103}$$

$$(Fr)_G = \frac{V_{SG}^2}{g\overline{d_p}} \quad \text{(Froude number)} \tag{8.104}$$

The following equation, derived from Song *et al.* [1989], is based on experiments conducted with hydroprocessing catalysts of various shapes. It can be used over large ranges of flow rates ($0.003 < V_{SL} < 0.15$ m/s and $V_{SG} < 0.08$ m/s):

$$(V_{SL})_m = (V_{SL})_{m_0} \left[1 - 376 V_{SG}^{0.33} \mu_L^{0.23} d_p^{0.21} (\rho_s - \rho_L)^{-0.42}\right] \tag{8.105}$$

where $(V_{SL})_{m_0}$ is the minimum fluidization velocity for the liquid alone, which was introduced previously (Eq. 7.38, Section 7.4.3):

$$(V_{SL})_{m_0} = \frac{33.7 \mu_L}{\overline{d_p} \rho_L} \left[\left(1 + \frac{3.6.10^{-5} g \rho_L (\rho_s - \rho_L) \bar{d}_p^3}{\mu_L^2}\right)^{1/2} - 1\right] \tag{8.106}$$

Some models are based on the pressure drop due to the liquid alone [Lee *et al.*, 2001], but use 180 instead of 150 as a constant in Ergun's equation. Larachi *et al.* [2000, 2001] have summarized current findings and proposed correlations based on a neural network approach. Their work is based on more than 500 different experimental data points; the precision is good within the limits of the domain covered.

D. Bed expansion and holdup

a. Bed expansion

Because the two fluid phases flow upward, the granular solid becomes fluidized after expansion of the initial fixed bed. This situation is somewhat more complicated than the case of a single fluid phase. It has been observed that the increase in the gas flow rate can, in some cases, be accompanied by a contraction of the fluidized bed—this occurs whenever particles smaller than 2.5 mm are fluidized by first introducing the liquid alone then gradually introducing the gas phase. For low but increasing gas flow rates, a weak contraction of the fluidized bed is observed, followed by expansion as the gas flow rate increases. Moreover, the axial profile of the solid concentration, ε_S, is generally exponential.

To calculate the expansion of the bed, we can use the equation of Saberian-Broudjenni *et al.* [1984], established on the basis of tests conducted in a variety of media, with a number of different industrial catalysts, spherical and extruded:

$$\varepsilon = (14\Phi_S)^{-1/3} \left(\frac{V_{SL}}{(V_{SL})_{m_0}}\right)^{0.27} \left(1 + 0.07 Re_{LG}^{0.34}\right) \tag{8.107}$$

where ε is the porosity of the bed ($\varepsilon = \varepsilon_G + \varepsilon_L$) and Φ_S is the sphericity factor:

$$\Phi_S = \frac{2d_{sph}^2}{\overline{d_p}^2 + 2\overline{d_p}L} \tag{8.108}$$

In the above equations d_{sph} is the diameter of the sphere of the same volume (see 6.2.2.1) and Re_{LG} is the Reynolds number relative to the liquid entrained by the gas bubbles:

$$Re_{LG} = \frac{\rho_L V_{SG} \overline{d_p}}{\mu_L} \tag{8.109}$$

Note that in industrial applications the level of the expanded three-phase bed is easily adjusted by modifying the liquid flow rate (which can also be recycled).

b. Liquid and gas holdup

Qualitatively, liquid holdup decreases as the gas flow rate increases. The holdup can be calculated using an equation developed by Saberian-Broudjenni *et al.* [1984], which takes into account the slip velocity of the gas in the liquid, defined as follows:

$$U_{GL} = \frac{1}{\varepsilon}\left(V_{SG}\varepsilon_L - V_{SL}\varepsilon_G\right) \tag{8.110}$$

and therefore:

$$\varepsilon_G = \varepsilon\frac{V_{SG} - U_{GL}}{V_{SG} + V_{SL}} \quad \text{and} \quad \varepsilon_L = \varepsilon\frac{V_{SL} + U_{GL}}{V_{SG} + V_{SL}} \tag{8.111}$$

A number of the experimental results obtained with water as well as with hydrocarbons and spherical or cylindrical particles at low superficial velocities ($V_{SL} < 0.03$ m/s and $V_{SG} < 0.15$ m/s) can be represented with acceptable precision by the following correlation:

$$U_{GL} = 0.017\left(\rho_L V_{SG}^2\right)^{0.45} \tag{8.112}$$

To calculate the gas holdup, using results obtained in a pilot unit for coal liquefaction, with gas holdup values of up to 50%, Fan, then Song [1989] introduced the effect of interfacial liquid tension by means of the Morton dimensionless number ($Mo = g\mu_L^4/\left(\rho_L\sigma^3\right)$). Its effect, however, is minimal ($(Mo^{0.02})$) compared to other uncertainties, so that a set of simplified equations, adapted to the various hydrodynamic regimes, can be proposed:

Large dispersed bubble regime: $$\varepsilon_G \cong 1.1 Fr_G^{0.22} Re_L^{-0.43} \tag{8.113}$$

Transition regime: $$\varepsilon_G \cong 0.4 Fr_G^{0.38} Re_L^{0.05} \tag{8.114}$$

Fine dispersed bubble regime: $$\varepsilon_G \cong 1.6 Fr_G^{0.21} Re_L^{-0.37} \tag{8.115}$$

Note that the liquid holdup increases slightly between the bottom and the top of the expanded bed, while the solid holdup decreases slightly. For the holdup of each of the phases, Larachi *et al.* [2001] have proposed some very complete polynomial correlations based on a large number of data points.

E. Backmixing

The majority of estimates are based on experiments made with columns of relatively narrow diameter (most often $D_C < 0.15$ m). It is clear, however, that backmixing in each of the three phases can increase considerably as the column diameter increases. So considerable caution is needed when making estimates. Below, we examine the behavior of each of the three phases in succession.

a. Gas phase

Mixing of the gas phase is essentially due to the fact that the gas bubbles have different sizes and, consequently, different velocities. Backmixing increases with the gas flow rate. Since the effect of the solid is not the determining factor, lacking specific correlations, a good approximation can be obtained by using the estimates given for bubble columns containing only a gas and a liquid.

The rise velocity of the bubbles relative to the liquid phase can be calculated from an equation by Kim *et al.* [1977]:

$$u_{Br} = 5.6 V_{SL}^{0.065} V_{SG}^{0.34} \mu_L^{0.025} \sigma^{0.18} \tag{8.116}$$

b. Liquid phase

The behavior of the liquid phase has been studied somewhat more extensively than the gas phase. This behavior depends considerably on the hydrodynamic regime.

- In the dispersed bubble regime, there is very little mixing of the liquid, so that the coefficient of axial dispersion is small and the corresponding Peclet number high.
- In the turbulent or pulsed bubble regime, there is significant axial mixing of the liquid, similar to that of a bubble column without solid particles. The correlation of Kim and Kim [1983] is one of the most precise but has been verified only up to a reactor diameter, D_C, of 0.15 m, although it is known that liquid mixing increases with the reactor diameter.

$$\frac{\overline{d_p} V_{SG}}{\mathcal{D}_{A,L}} \cong 20 \left(\frac{\overline{d_p}}{D_C} \right)^{1.66} \left(\frac{V_{SL}}{V_{SL} + V_{SG}} \right)^{1.03} \tag{8.117}$$

c. Solid phase

For fine particles it seems that backmixing of the solid is identical to that of the liquid phase. For larger particles the correlation of Kato *et al.* [in Shah, 1979] can be used to estimate the coefficient of axial dispersion of the solid, $\mathcal{D}_{A,S}$:

$$(Pe)_S = \frac{D_C V_{SG}}{\mathcal{D}_{A,S}} = 13 \left[\frac{Fr_G^{0.5} + 0.009 Fr_G^{0.1} (Re_L)_t}{1 + 8 Fr_G^{0.425}} \right] \tag{8.118}$$

where:

$$(Re_L)_t = \frac{\overline{d_p} u_t \rho_L}{\mu_L} \tag{8.119}$$

For particles of about one millimeter, backmixing is significant. Using mockups of various sizes ($D_C \leqslant 0.6$ m), Euzen and Fortin [1987] have shown that there is fairly systematic circulation of the particles, which rise in the center of the vessel in the wake of large bubbles and fall along the periphery.

8.2.5.2 Mass transfer

A. Gas-liquid mass transfer

The interfacial area, $\mathcal{A}_{GL}$, available for transfer between the gas and liquid phases varies considerably between 10 and 500 m^2/m^3. It depends on the gas holdup, ε_G, the size of the bubbles, d_B (and therefore directly on the gas and liquid flow rates), and the size of the particles, as indicated in the correlation proposed by Chang *et al.* [1986], which consolidates a number of different experimental results ($1.7 < \overline{d_p} < 6$ mm, $V_{SG} < 0.07$ m/s, $V_{SL} < 0.13$ m/s).

$$\mathcal{A}_{GL} \cong 2.08 \cdot 10^6 V_{SG}^{0.35} V_{SL}^{0.63} \overline{d}_p^{0.88} \tag{8.120}$$

Another method of determining interfacial area involves knowledge of the gas holdup and bubble diameter. In the homogeneous bubble regime, the bubble diameter, d_B, can be obtained from the correlation of Kim and Kang [1997], given that neither the viscosity nor the interfacial tension of the liquid have any appreciable effect:

$$\overline{d_B} \cong 0.14 V_{SL}^{0.05} V_{SG}^{0.25} \tag{8.121}$$

These bubbles rise with velocities of about 0.1 to 0.4 m/s within the three-phase medium.

For the transfer coefficients, the orders of magnitude are as follows:

$k_{l,L}\mathcal{A}_{GL}$ from 0.01 to 0.2 s^{-1}, k_L from $1 \cdot 10^{-4}$ to $2 \cdot 10^{-4}$ m/s. The group $k_{l,L}\mathcal{A}_{GL}$ depends strongly on the flow rates of the phases and the size of the particles but also, through more complex effects, on the nature of the liquid (viscosity, interfacial tension) and the particle concentration; k_L will be relatively unaffected by the size of the particles. Fan [1989], Zheng *et al.* [1995], and Koïde [1996] have proposed a number of correlations but, given the uncertainty associated with the specific behavior of the media and the influence of the size of the reactor, we suggest a fairly simple correlation, initially proposed by Chang *et al.* [1986]:

$$k_L \mathcal{A}_{GL} \cong 1\,600 V_{SG}^{0.68} V_{SL}^{0.63} \bar{d}_p^{1.21} \tag{8.122}$$

After examining a number of previous publications, Kim and Kang [1997] proposed a dimensionless correlation that gives good precision over a fairly broad range of gas and liquid flow rates ($0.005 < V_{SG} < 0.19$ m/s, $0.008 < V_{SL} < 0.18$ m/s), particle size ($0.8 < \overline{d_p} < 8$ mm) and liquid viscosity ($0.001 < \mu_L < 0.1$ Pa · s):

$$Sh_L = \frac{k_L \mathcal{A}_{GL} \overline{d}_B^2}{6\varepsilon_G \mathcal{D}_L} = 2.7\,(Sc_L)^{0.33}\,(Re_B)^{0.2} \tag{8.123}$$

where

$Sc_L = \frac{\nu_L}{\mathcal{D}_L}$ liquid Schmidt number

$(Re)_B = \frac{\Sigma_{VL}\bar{d}_B^4}{\nu^3}$ Reynolds number based on the bubble diameter, $\overline{d_B}$

Σ_{VL} rate of energy dissipation of liquid (m^2/s^3).

B. Liquid-solid mass transfer

Liquid-solid mass transfer depends primarily on the turbulence caused by the gas phase. The correlations change slightly, depending on the author, especially with respect to the exponents, but are based on similar factors. The correlation of Kikuchi, adopted by Fan [1989], is very similar in form to the correlation given for bubble columns and appears to do a good job at consolidating various results:

$$Sh_{LS} = 2 + 0.51\left(\Sigma_L^{0.33}\bar{d}_p^{1.33}\frac{\rho_L}{\mu_L}\right)^{0.59}(Sc_L)^{0.33} \tag{8.124}$$

Here, the estimate for the dissipated power per unit mass of liquid, designated by Σ_L, simply needs to be modified; in the case of three-phase fluidized beds, the following value is used:

$$\Sigma_L = \frac{\Delta P\,(V_{SL} + V_{SG})}{H\varepsilon_L\rho_L} \tag{8.125}$$

Comments: Gas-solid mass transfer can, in general, be neglected to the extent that the gas is practically never in direct contact with the solid particles.

8.2.5.3 Heat transfer

In three-phase fluidized-bed reactors, temperature uniformity is generally excellent as a result of fluid turbulence. Still, it is essential to be able to model heat transfer, at least for exchange with the walls of the reactor, to control the elimination of the heat produced by strongly exothermic reactions; consequently a good understanding of h_W is extremely important. Most often situated between 1 and 6 $kW/m^2 \cdot K$, the global transfer coefficient, h_W, for three-phase media, is greater than in two-phase liquid-solid fluidized reactors. In fact, h_W will increase sharply in the presence of a gas, and the flow rates and the diameter of the solid particles also have a positive influence. Below we provide two correlations that can be used together.

The first, by Baker *et al.* [1978], is based on tests conducted in the presence of water, air, and glass beads:

$$h_W = 10^4 V_{SL}^{0.070} V_{SG}^{0.059}\bar{d}_p^{0.106} \tag{8.126}$$

The second, established by Kato *et al.*, and included in Fan [1989], is dimensionless and introduces several variables, especially for the viscosity of the liquid, whose increase will slow the transfer:

$$Nu' = 0.044\left[(Re')_L\,(Pr)_L\right]^{0.78} + 2\,(Fr)_G^{0.17} \tag{8.127}$$

where:

$$Nu' = \frac{h_w \overline{d_p} \varepsilon_L}{\lambda_L (1 - \varepsilon_L)} \quad \text{Nusselt number} \tag{8.128}$$

$$\left(Re'\right)_L = \frac{\overline{d_p} V_{SL} \rho_L}{\mu_L (1 - \varepsilon_L)} \quad \text{Reynolds number} \tag{8.129}$$

$$(Pr)_L = \frac{\mu_L C_{PL}}{\lambda_L} \quad \text{Prandtl number} \tag{8.130}$$

$$(Fr)_G = \frac{V_{SG}^2}{g \overline{d_p}} \quad \text{Froude number} \tag{8.131}$$

In 1997 Kim and Kang, after summarizing a large number of existing correlations, proposed a correlation based on the concept of surface renewal and Kolmogoroff local isotropic turbulence. The correlation coefficient, calculated from a database of a thousand different experimental values, is 0.90, which is remarkable:

$$Nu = \left(\frac{h_W d_B}{\lambda_L}\right) = 0.436 \, (Pr)_L^{0.33} \, (Re)_B^{0.2} \tag{8.132}$$

8.2.5.4 Modeling a three-phase fluidized reactor

Given the uncertainty associated with estimating the parameters that characterize three-phase systems, there is little point in trying to develop sophisticated models of such reactors. However, the essential characteristics of these systems must be taken into account; these include:

- possibility of diffusion limitation within the catalyst grains
- possibility of limitation due to liquid-solid transfer
- possibility of limitation due to gas-liquid transfer
- weak backmixing in the gas phase
- strong backmixing in the liquid and solid phases.

We have a choice between two types of model:

- The reactor can be treated as a tubular reactor by assuming a plug flow model in the gas-phase, while in the liquid phase, axial turbulent diffusion is superimposed on plug flow.
- The fluidized bed can be treated as a series of M perfectly mixed stages with respect to the liquid and solid, while the gas is assumed to be characterized by plug flow.

In the first case we end up with a series of equations similar to those for downward cocurrent fixed-bed reactors (Eq. 8.72 to 8.77). The only difference will be the addition of a term for axial diffusion in the liquid phase balance Eqs. (8.73) and (8.74). The presence of these additional terms considerably complicates the solution of the system of equations, especially if thermal effects are taken into account.

The second type of model, which assumes a series of perfectly mixed stages, is easier to use in practice. We can write fundamental equations for the same reaction system covered in 8.2.3.1.D, which was:

$$\nu_1 A_1(\text{gas}) + \nu_2 A_2(\text{liquid}) \rightarrow \nu_3 A_3(\text{liquid})$$

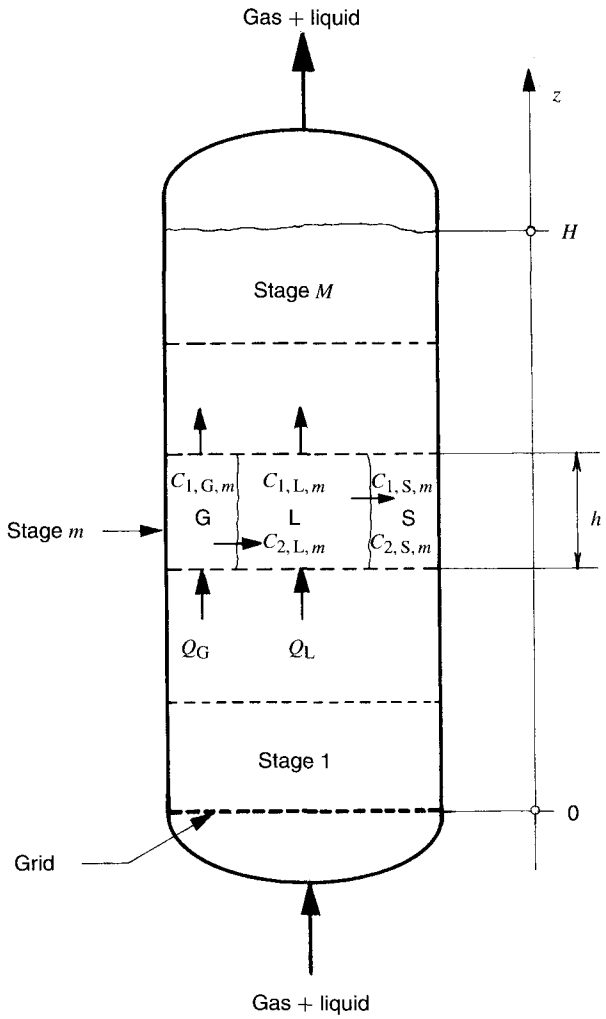


Figure 8.14 Basis for modeling a three-phase fluidized bed.

Referring to Fig. 8.14, we can write the molar balances for A_1 and A_2 for a stage m:

- In the gas phase:

$$(Q_G C_{1,G})_{m-1} - (Q_G C_{1,G})_m - \mathcal{A}_{GL} K_{1,L} \left(\frac{\overline{C_{1,G,m}}}{m_1} - C_{1,L,m} \right) Sh = 0 \qquad (8.133)$$

where

$\overline{C_{1,G,m}}$ logarithmic mean of $C_{1,G(m-1)}$ and $C_{1,G,m}$

m_1 partition coefficient of compound A_1 between the gas and liquid phases.

- In the liquid phase:

$$\left(Q_L C_{1,L}\right)_{m-1} - \left(Q_L C_{1,L}\right)_m + \left[\mathcal{A}_{GL} K_{1,L}\left(\frac{\overline{C_{1,G,m}}}{m_1} - C_{1,L,m}\right) - \mathcal{A}_S k_{1,S}\left(C_{1,L,m} - C_{1,S,m}\right)\right] Sh = 0 \quad (8.134)$$

$$\left(Q_L C_{2,L}\right)_{m-1} - \left(Q_L C_{2,L}\right)_m - \mathcal{A}_S k_{2,S}\left(C_{2,L,m} - C_{2,S,m}\right) Sh = 0 \quad (8.135)$$

- At the surface of the catalyst:

$$N_{1,m} = \mathcal{A}_S k_{1,S}\left(C_{1,L,m} - C_{1,S,m}\right) Sh = -\nu_1 r'_S S_p \rho_c \eta Sh \quad (8.136)$$

$$N_{2,m} = \mathcal{A}_S k_{2,S}\left(C_{2,L,m} - C_{2,S,m}\right) Sh = -\nu_2 r'_S S_p \rho_c \eta Sh \quad (8.137)$$

h is the height of a stage $= H/M$.

The number of stages M to use is determined from the liquid phase Peclet number (Eq. 8.117), so that the two flow models are equivalent (see Eq. 2.136).

The solution of Eqs. (8.133) to (8.135) is performed stage by stage, assuming, if need be, a different temperature for each stage, which implies that k_S and η vary with each stage. The inlet conditions in the reactor correspond to $m = 0$.

8.2.5.5 Technology

In principle the design of a three-phase fluidized reactor presents no specific problems. The method of distributing fluids at the base of the bed is identical to that in single-phase fluidized beds (perforated plates, for example). The two fluid phases can be introduced either by mixing them beneath the grid at the base of the bed or separately. If introduced separately, the liquid phase arrives beneath the grid while the gas phase is introduced just above the grid by means of a conventional distributor.

Difficulties can arise if the gas flow to liquid flow ratio is too high, since this results in what is effectively a pulsed regime (see Fig. 8.13), which is not recommended. To overcome this problem, some of the effluent liquid can be recycled, which generally leads to a drop in the efficiency of the reactor. It may also be necessary to recycle the liquid phase to ensure good temperature control in the case of exothermic reactions, or to keep the level of the fluidized bed constant. This is the method used when hydroprocessing oil residues using the H-Oil process, either by means of a pump submerged inside the reactor or an external pump [Kressmann *et al.*, 2000] (Fig. 8.15).

Sufficient height must be left at the top of the bed to avoid any entrainment of catalyst particles. However, it will be difficult to avoid entraining catalyst fines resulting from particle attrition outside the reactor. These fines are found in the gas-liquid separator tank, which must

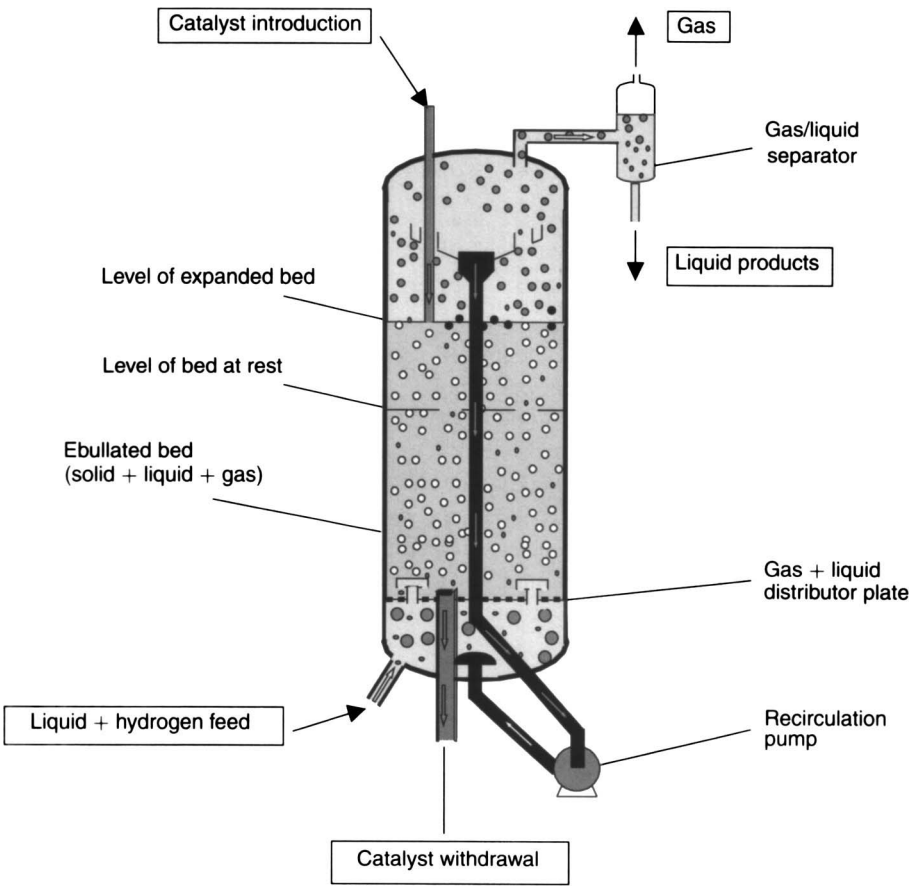


Figure 8.15 H-Oil ebullated bed reactor [Colyar and Wisdom, 1997].

be designed to easily separate and eliminate fines suspended in the liquid. The problem of solid/liquid separation is often difficult to resolve with long-term and cost-efficient methods.

8.2.5.6 Concluding remarks

The principal potential advantages of the fluidized bed compared to the fixed bed are:

- Spent catalyst can be removed and fresh catalyst introduced without shutting down the unit.
- Better temperature control is possible because of the significant backmixing of the liquid and solid phases and because of effective heat exchange inside the bed.
- Pressure drop through the reactor can remain low and constant for years because fouling and plugging of the bed are eliminated.

Fluidized bed reactors are well suited to highly exothermic reactions and reaction media that require frequent renewal of catalysts (deactivation or fouling). The problems associated

with pressure drop and plugging that are found in fixed beds are completely eliminated, making these a useful alternative to fixed-bed reactors. These reactors are also very flexible, since it is easy to change the catalyst or the feed, while maintaining an optimal environment for severe operating conditions and keeping catalyst activity stable. Additionally, the movement of liquid and solid produce fairly isothermal behavior. In some cases of high conversion, these reactors can be placed in series or used with a finishing reactor.

In industry fluidized-bed reactors are used quite often in large processing facilities (hydroprocessing of residues and heavy petroleum fractions, H-Oil processes, LC fining, methanation of synthesis gas, coal liquefaction, Fischer-Tropsch synthesis, water treatment, fermentation, etc.).

For example, the H-OIL process mentioned above makes use of these advantages. It employs an extruded catalyst of approximately 1 mm in diameter that is maintained in a fluidized state by a rising current of liquid (flow rate of feed + flow rate of recycled liquid) and a gas stream (fresh + recycled hydrogen). The height of the fluidized bed is controlled by adjusting the flow rate of the recycled liquid. New catalyst can be added and spent catalyst withdrawn to adjust the level of activity of the catalytic bed. Considerable backmixing in the reactor provides very homogeneous temperature distribution throughout the reactor. Cooling is provided by the introduction of low-temperature feedstock. These two significant advantages are used to maintain an optimum temperature that is high and stable throughout the reactor for months, and sometimes years.

Given the lack of precise knowledge of three-phase fluidized beds and the sensitivity of the gas-liquid medium to a variety of physicochemical parameters, the design of an industrial reactor must still be based on experiments conducted with mockups and relatively large pilot units.

8.3 CURRENT USES AND COMPARISON OF THREE-PHASE REACTORS

In comparing the various possibilities available to users for a given application, the principal characteristics of each reactor type (Table 8.4) as well as several criteria of varying importance must be taken into consideration to efficiently carry out a given reaction (Table 8.5). Among the many factors that need to be taken into account, the following are generally the most important:

- Chemical reaction: What is the reaction rate? Where does the reaction take place? What type of reaction kinetics is involved?
- Mass transfer: What are the principal limitations?
- Heat transfer: Is the reaction system highly exothermic or endothermic?
- What are the respective flow rates of the liquid and gas?
- What is the rate of catalyst deactivation?

This general information can help in the choice of reactor, the size of the particles, and the method of operation.

If the principal source of resistance occurs at the gas-liquid interface, reactors with considerable interfacial area may be of interest (the trickle-bed reactor or mechanically agitated reactor are well suited, although for different ranges of fluid flow rates).

Table 8.4 Principal characteristics of three-phase reactors.

Characteristic	Catalyst in suspension		Fixed bed			Three-phase fluidized bed
	Bubble column	Mechanically stirred tank	Downward cocurrent	Upward cocurrent	Counter-current	
ε_S (1)	0.01	0.01	0.6–0.7	0.6–0.7	0.5 (2)	0.1–0.6
ε_L (1)	0.8–0.9	0.8–0.9	0.05–0.25	0.2–0.3	0.05–0.1	0.2–0.8
ε_G (1)	0.1–0.2	0.1–0.2	0.2–0.35	0.05–0.1	0.2–0.4	0.05–0.2
$\overline{d_p}$ (mm)	$\leqslant 0.1$	$\leqslant 0.1$	1–5	1–5	> 5	0.1–5
$\mathcal{A}_S$ (m^{-1})	500	500	1 000–2 000	1 000–2 000	500	500–1 000
$\mathcal{A}_{GL}$ (m^{-1})	100–400	100–1 500	100–1 000	100–1 000	100–500	100–1 000
η	1	1	< 1	< 1	< 1	$\cong 1$

(1) The above values correspond only to that part of the reactor occupied by the catalyst and not to the entire reactor.

(2) This value is for special particle shapes.

If the maximum transfer resistance is situated at the liquid-solid interface or inside the grain, it is recommended that catalyst particles be as small as possible, which eliminates fixed-bed reactors because of pressure drop but favors the use of slurry or ebullated bed reactors. If the catalyst is rapidly deactivated, moving-bed or fluidized-bed reactors are preferred since they provide for continuous renewal of the catalyst.

We would again like to insist on the practical importance of three-phase catalytic reactors, which can be used for very high tonnage industrial units, including hydrodesulfurization, hydroconversion, various forms of hydrogenation in the petroleum refining industry, as well as a variety of chemical reactions such as oxidation, hydration, and amination.

Table 8.5 Comparison of three-phase reactors.

Criterion		Suspended catalyst	Three-phase fluidized bed	Fixed bed
Characteristics associated with the catalyst	Activity	Highly variable, but it is often possible to avoid the diffusion limitations found in fixed beds.	Highly variable. Internal and external mass transfer phenomena can appreciably decrease activity, especially in fixed beds.	
	Selectivity	Selectivity is generally little influenced by transfer phenomena.	As with activity, transfer phenomena can decrease selectivity.	
	Stability	Changing the catalyst between each batch operation can, under certain conditions, be used to overcome problems associated with rapid poisoning.	Ability to renew the catalyst continuously. The catalyst must have good resistance to wear.	Catalyst stability is essential for fixed-bed operation; plug flow may be of value following the establishment of an adsorption front for the poison.
	Cost	Most often, consumption depends on the impurities in the feed that act as poisons.		Catalyst consumption must be low.
Technological characteristics	Backmixing	Backmixing is unfavorable.	Backmixing is unfavorable.	Plug flow is favorable.
	Heat exchange	Fairly easy to carry out heat exchange operations.	Heat exchange can take place in the reactor itself.	Generally operates adiabatically.
	Difficulty of design	Separation of the catalyst is sometimes difficult. Potential problems with pumps and exchangers due to the risk of deposits or erosion.		Very simple technology in the case of the adiabatic bed with cocurrent downflow.
	Scale-up	No problems	Scale-up must take place in stages.	By paying careful attention to fluid distribution, large-size reactors can be constructed.

REFERENCES

Abraham M, Khare S, Sawant S, Joshi J. (1992) Critical Gas Velocity for Suspensions of Solid Particles in Three-Phase Bubble Columns. Ind Eng Chem Res 31, pp 1136–1147.

Al-Dahhan M, Dudukovic MP (1995) Catalyst Wetting Efficiency in Trickle Bed Reactors at High Pressure: Pressure Drop and Liquid Holdup in High Pressure Trickle Bed Reactors. Chem Eng Sci 50, 15, pp 2377–2389.

Al-Dahhan M, Larachi F, Dudukovic M, Laurent A (1997) High-Pressure Trickle-Bed Reactors: a Review. Ind Chem Eng Res, 36, pp 3292–3314.

Al-Dahhan M, Wu Y, Dudukovic MP (1995) Reproducible Technique for Packing Laboratory Scale Trickle Bed Reactors with a Mixture of Catalyst and Fines. Ind Eng Chem Res, 34, pp 741–747.

Al-Dahhan M, Wu Y, Dudukovic MP (1996) Catalyst Bed Dilution for Improving Catalyst Wetting in Laboratory Trickle-Bed Reactors. AIChE J. 42, 9, pp 2594–2606.

Al-Dahhan MH, Khadilkar M, Wu Y, Dudukovic MP (1998) Predictions of Pressure Drop and Liquid Holdup in High Pressure Trickle Bed Reactors. Ind Eng Chem Res37, pp 3292–3314.

Attou A, Boyer C (1999) Revue des aspects hydrodynamiques des réacteurs catalytiques gaz-liquide-solide à lit fixe arrosé. Oil and Gas Science and Technology – Revue de l'Institut Français du Pétrole, 54, 1, pp 29–66.

Attou A, Boyer C, Ferschneider G (1999) Modelling of the Hydrodynamics of the Cocurrent Gas-Liquid Trickle Flow through a Trickle Bed Reactor. Chem Eng Sci 54, pp 785–802.

Baker C, Armstrong E, Bergougnou M (1978) Heat Transfer in Three Phase Fluidized Beds. Powder Technology 21, pp 195–199.

Bartelmus G (1989) Local Solid-Liquid Mass Transfer Coefficients in a Three-Phase Fixed Bed Reactor. Chem Eng Proc 26, pp 111–120.

Bartelmus G (1993) Solid-Liquid Mass Transfer in a Fixed-Bed Reactor with Cocurrent Flow. Chem Eng Proc 32, pp 65–74.

Belfares L, Cassanello M, Grandjean B, Larachi F (2000) Liquid Backmixing in Packed Bubble Column Reactors: A State of the Art Correlation. Catalysis Today 2259, pp 1–12.

Bensetiti Z, Larachi F, Grandjean B, Wild G (1997) Liquid Saturation in Cocurrent Upflow Fixed-Bed Reactors: A State of the Art Correlation. Chem Eng Sci 52, 21/22, pp 4239–4247.

Burghardt A, Bartelmus G (1996) Hydrodynamics and Mass Transfer in Three-Phase Cocurrent Reactors. Chem Eng Sci 51, 2733–2738.

Burzynski JP, Euzen JP, Catros A, Trinquet G (1988) A New Three-Phase Counter-Current Moving Bed Reactor: Hydrodynamic Scale-Up. AIChE Spring Meeting New Orleans (1988).

CatrosA, Burzynski JP, Euzen JP, Morel F, Renard P, Trinquet G (1990) Étude et développement d'un réacteur à lit mobile triphasique. *In*: Récents Progrès en Génie des Procédés (Storck & Wild Eds.) 4 (10), p 165. Lavoisier, Paris.

Chang SK, Kang Y, Kim S (1986) Mass Transfer in Two- and Three-Phase Fluidized Beds. J Chem Eng Japan 19, pp 524–530.

Charpentier JC, Favier M (1975) Some Liquid Holdup Experimental Data in Trickle Bed Reactors for Foaming and Nonfoaming Hydrocarbons. AIChE J 21, pp 1213–1218.

Chaudhari RV, Ramachandran PA (1992) Modelling of Catalytic Trickle Bed Reactors. *In*: Heat and Mass Transfer in Porous Media (Quintard M et Todorovic M, Eds.). Elsevier, Amsterdam.

Chisti MY (1989) Airlift Bioreactors. Elsevier Applied Sciences, Londres et New York.

Colli-Serrano M, Midoux N (2000) Hydrodynamics and Heat Transfer in Packed Bed with Cocurrent Up Flow for Coalescing and Non-coalescing Liquids: A Simple Model. Chem Eng Sci 55, pp 4149–4157.

Colyar JJ, Wisdom LI (1997) The H-Oil Process: A Worldwide Leader in Vacuum Residue Processing. 1997 NPRA Annual Meeting, San Antonio, Texas.

De Swart JWA (1996) Scale-Up of a Fischer-Tropsch Slurry Reactor. Thesis. University of Amsterdam.

De Swart JWA, Krishna R, Sie ST (1997) Selection, Design and Scale-Up of the Fischer-Tropsch Slurry Reactor. Studies in Surface Science and Catalysis 107, pp 213–218.

Deckwer WD (1992) Bubble Column Reactors. John Wiley and Sons, New York.

Deckwer WD, *et al.* (1980) Hydrodynamic Properties of the Fischer-Tropsch Slurry Process. Ind Eng Chem Proc Des. Dev. 19, pp 699–708.

Dudukovic MP (2000) Opaque Multiphase Reactors: Experimentation, Modeling and Troubleshooting. Oil and Gas Science and Technology – Revue de l'Institut Français du Pétrole 55, 2, pp 135–158.

Dudukovic MP, Larachi F, Mills P (1999) Multiphase Reactors – Revisited. Chem Eng Sci 54, pp 1975–1995.

Ellenberger J, Krishna R (1999) Counter-Current Operation of Structured Catalytically Packed Distillation Columns: Pressure Drop, Holdup and Mixing. Chem Eng Sci 54, pp 1339–1345.

Ellman MJ, Midoux N, Laurent A, Charpentier JC (1988) A New Improved Pressure Drop Correlation for Trickle Bed Reactors. Chem Eng Sci 43, 8, pp 2201–2206.

Ellman MJ, Midoux N, Wild G, Laurent A, Charpentier JC (1990) A New improved Liquid Holdup Correlation for Trickle Bed Reactors. Chem Eng Sci 45, 7, pp 1677–1684.

Euzen JP (1991) Moving Bed Process for Residue Hydrotreating. Revue de l'Institut Français du Pétrole 46, 4, pp 517–527.

Euzen JP, Fortin Y (1987) Partikel Bewegung in einem Dreiphasen-fliessbett. Chem Ing Tech 59, 5, pp 416–419.

Fan LS (1989) Gas-Liquid-Solid Fluidization Engineering. Butterworths, Boston.

Fan LS, Yang GQ, Tsuchiya K, Luo X (1999) Some Aspects of High Pressure Phenomena of Bubbles in Liquid and Liquid-Solid Suspensions. Chem Eng Sci 54, pp 4681–4709.

Froment GF, Bishoff KB (1990) Chemical Reactor Analysis and Design, Second edition. John Wiley and Sons, New York.

Gianetto A, Silveston PI (1986) Multiphase Chemical Reactors Theory, Design, Scale Up. Hemisphere Publishing Corporation.

Gianetto A, Specchia V (1992) Trickle-Bed Reactors: State of Art and Perspectives. Chem Eng Sci 47, 13/14, pp 3197–3213.

Harnby N, Edwards M, Nienow A (1992) Mixing in the Process Industries. Butterworth-Heinemann, Boston.

Harter I, Boyer C, Raynal L, Ferschneider G, Gauthier T (2001) Flow Distribution Studies Applied to Deep Hydro-Desulfurization. Chemical Engineering Reactor CRE VIII, June 2001, Italy.

Illiuta I, Oritz A, Larachi F, Grandjean BP, Wild G (1999) Hydrodynamics and Mass Transfer in Trickle Bed Reactors: an Overview. Chem Eng Sci 54, 21, pp 5329–5337.

Jacobs GE, Milliken AS (2000) Evaluating Liquid Distributors in Hydroprocessing Reactors. Hydrocarbon Processing, Nov. 2000, pp 76–84.

Khadilkar MR, Al-Dahhan MH, Dudkovic MP (1999) Parametric Study of Unsteady-State Flow Modulation in Trickle Bed Reactors. Chem Eng Sci 54, pp 2585–2595.

Khadilkar MR, Wu YX, Al-Dahhan MH, Dudkovic MP, Colakyan M (1996) Comparison of Trickle Bed and Upflow Ractor Performance at High Presure: Model Predictions and Experimental Observations. Chem Eng Sci 51, 10, pp 2139–2148.

Kikuschi K, Sugawara Y, Ohashi H (1983) Correlation of Mass Transfer Coefficient between Particles and Liquid fluidized Beds. J Chem Eng Japan 16, pp 426–428.

Kim SD, Baker CGJ, Bergougnou MA (1977) Bubble Characteristics in Three Phase Fluidized Beds. Chem Eng Sci 32, 11, pp 1299–1306.

Kim SD, Kang Y (1997) Heat and Mass Transfer in three Phase Fluidized Bed Reactors – An Overview. Chem Eng Sci 52, pp 3639–3660.

Kim SD, Kim CH (1983) Axial Dispersion Characteristics of the three-Phase Fluidized Beds. J Chem Eng Japan 16, pp 172–178.

Kim SD, Laurent A (1988) L'état des connaissances sur le transfert de chaleur dans les lits fluidisés triphasiques. Entropie 143, pp 5–22.

Koïde K (1996) Design Parameters of Bubble Column Reactors with and without Solid Suspensions. J Chem Eng Japan 29, 5, pp 745–759.

Koïde K, Takazawa A, Komura M, Matsunaga H (1984) Gas Holdup and Volumetric Liquid-Phase Mass Transfer Coefficient in Solid Suspended Bubble Columns. J Chem Eng Japan 17, 5, pp 459–466.

Kressmann F, Boyer C, Colyar JJ, Schweitzer JM, Viguié JC (2000) Improvements of Ebullated Bed Technology for Upgrading Heavy Oils. Oil and Gas Science and Technology – Revue de l'Institut Français du Pétrole 55, 4, pp 397–406.

Krishna R (2000) A Scale-Up Strategy for a Commercial Scale Bubble Column Slurry Reactor for Fischer Tropsch Synthesis. Oil and Gas Science and Technology – Revue de l'Institut Français du Pétrole 35, 4, pp 359–393.

Lakota A, Levec J (1990) Solid-Liquid Mass Transfer in Packed Beds with Cocurrent Downward Two-Phase Flow. AIChE J. 36, 9, pp 1444–1448.

Lamine A, Colli Serano MT, Wild G (1992) Hydrodynamics and Heat Transfer in Packed Bed with Cocurrent Upflow. Chem Eng Sci 47, 13/14, pp 3493–3500.

Lamine A, Gerth L, Le Gall H, Wild G (1996) Heat Transfer in a Packed Bed Reactor with Cocurrent Downflow of a Gas and a Liquid. Chem Eng Sci 51, 15, pp 3813–3827.

Lara Marquez A, Larachi F, Wild G, Lurent A (1992) Mass Transfer Characteristics of Fixed Bed with Cocurrent Up Flow and Downflow: Effect of Pressure. Chem Eng Sci 47, 13/14, pp 3485–3492.

Larachi F (1991) Les réacteurs triphasiques à écoulement vers le bas et vers le haut de gaz et de liquide. Etude de l'influence de la pression sur l'hydrodynamique et le transfert de matière gaz-liquide. Thesis ENSIC–INPL.

Larachi F, Al-Dahhan MH, Dudukovic MH, Laurent A (1996) High Pressure Trickle Bed Reactors: a State of the Art Review. Proceedings of the 12th International Congress of Chemical and Process Enginnering, CHISA 12, Prague, Czech Rep. August 25–30.

Larachi F, Belfares L, Iliuta I, Grandjean P (2001) Three Phase Fluidization Macroscopic Hydrodynamics Revisited. Ind Eng Chem Res 40, pp 993–1008.

Larachi F, Cassanello M, Laurent A (1998) Gas-Liquid Interfacial Mass Transfer in Trickle Bed Reactors at Elevated Pressures. Ind Eng Chem Res 37, pp 718–734.

Larachi F, Iliuta I, Rival O, Grandjean B (2000) Prediction of Minimum Fluidization Velocity in Three Phase Fluidized Bed Reactors. Ind Eng Chem Res, 39, pp 563–572.

Larachi F, Laurent A, Wild G, Midoux N (1993) Effet de la pression sur la transition ruisselant-pulsé dans les réacteurs catalytiques à lit fixe arrosé. Can J Chem Eng 71, 319–321.

Larachi F, Laurent A, Midoux N, Wild G (1991) Experimental Study of a Trickle Bed Reactor Operating at High Pressure: Two Phase Pressure Drop and Liquid Saturation. Chem Eng Sci 46, 5/6, pp 1233–1246.

Larkins RP, White RR, Jeffrey DW (1961) Two-Phase Cocurrent Flow in Packed Beds. AIChE J 7, 2, p. 231–239.

Lee D, Epstein N, Grace J (2001) Models for Minimum Liquid Fluidization Velocity of Gas-Liquid Fluidized Beds. J Chem Eng Japan 34, 2, pp 95–101.

Levenspiel O (1999) Chemical Reaction Engineering (Third Edition). John Wiley and Sons, New York.

Li M, Iida N, Yasuda K, Bando Y, Nakamura M (2000) Effect of Orientation of Packing Structure On Liquid Flow Distribution in Trickle Bed. J Chem Eng Japan 33, 5, pp 811–814.

Luo X, Jiang P, Fan LS (1997) High Pressure Three Phase Fluidization: Hydrodynamics and Heat Transfer. AIChE J 43, 10, pp 2432–2445.

Marcandelli C, Lamine AS, Bernard JR, Wild G (2000) Liquid Distribution in Trickle Bed Reactor. Oil and Gas Science technology – Revue de l'IFP 55, 4, pp 407–415.

Matros Y (1996) Review: Forced Unsteady-State Processes in Heterogeneous Catalytic Reactors. Can J Chem Eng 74, october, pp 566–579.

Mears DE (1971) The Role of Axial Dispersion in Trickle-Flow Laboratory Reactors. Chem Eng Sci 26, pp 1361–1366.

Midoux N, Charpentier JC (1981) Les réacteurs gaz-liquide à cuve agitée mécaniquement. Partie 2 : aires interfaciales. Entropie, 101, pp 3–31.

Mochizuki S (1978) Mass Transport Phenomena and Hydrodynamics in Packed Bed With Gas-Liquid Concurrent Upflow. AIChE J 24, 6, pp 1138–1141.

Molga EJ, Westerterp K (1997) Experimental Study of a Cocurrent Upflow Packed Bed Bubble Column Reactor: Pressure Drop, Holdup and Interfacial Area. Chem Eng Proc 36, pp 489–495.

Moller LB, Halken C, *et al.* (1996) Liquid and Gas Distribution in Trickle Bed Reactors. Ind Eng Chem Res 35, pp 926–930.

Morsi BI, Midoux N, Charpentier JC (1978) Flow Patterns and some Holdup Experimental Data in Trickle Bed Reactors for Foaming, Nonfoaming and Viscous Organic Liquids. AIChE J 24, 2, Mars 1978, p. 357–360

Muroyama K, Fan L (1985) Fundamental of Gas-Liquid-Solid Fluidization. AIChE J 31, pp 1–34.

Ng KM (1986) Trickle Bed Reactors. Chem Eng Progr 83, pp 55–63.

Nieken U, Kolios G, Eigenberger G (1995) Limiting Cases and Approximate Solutions for Fixed Bed Reactors with Periodic Flow Reversal. AIChE J 41, 8, pp 1915–1925.

Oldshue J (1983) Fluid Mixing Technology. McGraw-Hill, New York.

Papayanakos N, Galtier P, Bigeard PH, Kasztelan S (1992) Hydrodynamic Effects in Bench Scale Hydrotreaters Operating in Cocurrent Gas-Liquid Upflow Mode. Chem Eng Sci 47, 9–11, pp 2275–2280.

Piché S, Larachi F, Grandjean P (2001) Flooding Capacity in Packed Towers: Data Base, Correlations and Analysis. Ind Chem Eng, 40, pp 476–487.

Reilly I, Scott D, De Bruijn T, Macintye D (1994) The Role of Gas Phase Momentum in Determining Gas Holdp and Hydrodynamic Flow Regime in Bubble Column Operations. Can J Chem Eng 72, pp 3–12.

Saberian-Broudjenni M, Wild G, Charpentier JC, Fortin Y, Euzen JP, Patoux R (1984) Contribution à l'étude hydrodynamique des réacteurs à lit fluidisé gaz-liquide-solide. Entropie 120, pp 30–44.

Sano Y, Yamaguchi N, Adachi Y (1974) Mass Transfer Coefficients for Suspended Particles in Agitated Vessels and Bubble Columns. J Chem Eng Japan 7, 4, p. 255–261.

Saroha A, Nigam K (1996) Trickle Beds Reactors. Rev Chem Eng 12, p 207.

Sato Y, Hirose T, Takahashi F, Toda M (1973) Pressure Loss and Liquid Holdup in Packed Bed Reactor With Cocurrent Gas-Liquid Downflow. J Chem Eng Japan 6, 2, p. 147–152.

Satterfield CN (1970) Mass Transfer in Heterogeneous Catalysis. Robert Krieger Publishing Co., New York.

Satterfield CN (1980) Heterogeneous Catalysis in Practice. McGraw-Hill, New York.

Saxena SC (1995) Bubble Column Reactors and Fischer-Tropsch Synthesis. Catal Rev Sci Eng 37 (2) pp 227–309.

Shaban HI, Khan A (1995) Pressure Related Operational Problems and their Remedies in Hydrotreating Reactors in Petroleum Refineries. J Petrol Sci Eng 14, pp 79–88.

Shah YT (1979) Gas Liquid-Solid Reactor Design. McGraw-Hill, New York.

Sie ST (1991) Scale Effects in Laboratory and Pilot-Plant Reactors for Trickle Flow Process. Revue de l'Institut Français du Pétrole 46, 4, pp 501–515.

Song GH, Bavarian LS, Fan RD, Buttke RD, Peck LB (1989) Hydrodynamics of Three-Phase Fluidized Bed Containing Cylindrical Hydrotreating Catalysts. Can J Chem Eng 67, pp 265–275.

Stegeman D, *et al.*, Westerterp kr (1996) Residence Time Distribution in the Liquid Phase in a Cocurrent Gas-Liquid Trickle Bed Reactor. Ind Eng Chem Res 35, pp 378–385.

Steiff A, Weinspach PM (1980) Heat Transfer in Agitated Vessels with Multiphase Systems. Chem Ing Techn 52, 6, pp 492–503.

Thanos A, Galtier P, Papayannakos (2001) Liquid Dispersion and Holdup in a Small Scale Upflow Hydrotreater at high Temperature and Pressure. Chem Eng Sci 56, pp 693–698.

Trambouze P (1990) Countercurrent Two-Phase Flow Fixed Bed Catalytic Reactors. Chem Eng Sci 45, 8, pp 2269–2275.

Trambouze P, Van Landeghem H, Wauquier JP (1988) Chemical Reactors: Design, Engineering, Operation. Editions Technip, Paris.

Vergel C, Euzen JP, Trambouze P, Wauquier JP (1995) Two-Phase Flow Catalytic Reactor, Influence of Hyrodynamics on Selectivity. Chem Eng Sci 50, 20, pp 3303–3312.

Wijngaarden RJ, Kronberg A, Westerterp KR (1998) Industrial Catalysis. Wiley-VCH

Wild G, Larachi F, Charpentier JC (1992) Heat and Mass Transfer in Gas-Liquid-Solid Fixed Bed Reactors. Heat and Mass Transfer in Porous Media (Quintard M., Todorovic M. Eds). Elsevier, Amsterdam pp 616–632.

Wild G, Larachi F, Laurent A (1991) The Hydrodynamic Characteristics of Cocurrent Downflow and Cocurrent Upflow Gas-Liquid-Solid Catalytic Fixed Bed Reactors: the Effect of Pressure. Revue de l'Institut Français du Pétrole 46, 4, pp 467–490.

Wild G, Poncin S (1996) Fluidized Beds and Slurry Bubble Reactors. Hydrodynamics. Topics in Chem Eng 8. Overseas Pub. Ass., Gordon & Breach Sc Pub, Amsterdam pp 11–112.

Wild G, Saberian M, Schwartz JL, Charpentier JC (1982) Les réacteurs à lits fluidisés gaz-liquide-solide. État de l'art et perspectives industrielles. Entropie, 106, 1982, pp 3–36.

Wilkinson PM (1991) Physical Aspects and Scale-up of High Pressure Bubble Columns. Thesis, Rijksuniversiteit Groningen.

Yang XL, Euzen JP, Wild G (1990) Residence Time Distribution of the Liquid in Gas-Liquid Cocurrent Upflow Fixed-Bed Reactors with Porous Particles. Chem Eng Sci. 45, 11, pp 3311–3317.

Yang XL, Wild G, Euzen JP (1992) A Comparison of the Hydrodynamics of Packed Bed Reactors with Cocurrent Upflow and Downflow of Gas and Liquid. Chem Eng Sci 47, 5, pp 1323–1325.

Yang XL, Wild G, Euzen JP (1993) Study of Liquid Retention in Fixed Bed Reactors With Upward Flow of Gas and Liquid. Int Chem Eng 33, pp 72–84.

Zheng C, Chen Z, Feng Y, Hofmann H (1995) Mass Transfer in Different Flow Regimes of Three-Phase Fluidized Beds. Chem Eng Sci 50, 10, pp 1571–1578.

NOMENCLATURE

(specific to Chapter 8)

Symbol	Definition	SI unit
$\mathcal{A}_{GL}$	Gas-liquid interfacial area	m^2/m^3
$\mathcal{A}_S$	External area of particles per unit volume of reactor	m^2/m^3
d_h	Hydraulic diameter of particles	m
d_p	Diameter of catalyst grain	m
E_L, E_G	Energy dissipated by the liquid, by the gas	W/m^3 of reactor
$FLGG$	Parameter defined in Eq. (8.52)	–
G, L	Mass flow of gas, of liquid per unit cross-section	$kg/m^2 \cdot s$
h	Height of a stage	m
H_S	Level of solid suspension	m
$\mathcal{K}_1'$	Apparent rate constant (Eq. 8.11)	$m^4/mol \cdot s$
$\mathcal{K}_1$	Apparent rate constant (Eq. 8.12)	m/s
k_S	Rate constant (Eq. 8.10)	variable
M	Number of stages	–
u_{Br}	Rise velocity of bubbles relative to the liquid phase (Eq. 8.116)	m/s
u_t	Terminal velocity of an isolated particle	m/s
β_L	Liquid saturation ratio: fraction of volume occupied by the liquid between the particles	–
ν	Kinematic viscosity $\nu = \dfrac{\mu}{\rho}$	m^2/s
μ	Dynamic or absolute viscosity	$Pa \cdot s$
λ	Parameter defined in Eq. (8.47)	–
λ_L, $\lambda_{L=0}$	Thermal conductivity of the liquid, of the bed in the absence of liquid flow	$W/m \cdot K$
ψ	Parameter defined in Eq. (8.48)	–
δ_L', δ_G', δ_{LG}'	Pressure drop from friction caused by the passage of one (or two) fluid(s) per unit length of catalytic bed	Pa/m
Σ_L	Power dissipated per unit mass of liquid	W/kg
$\left(\dfrac{\Delta P}{H}\right)_{GL,\,total}$	Absolute pressure difference between two points of the bed separated by height H	Pa/m
	Subscripts:	
GL	relative to the gas + liquid mixture	
m	relative to a stage m in a series of M stages	
w	relative to the wall	
S, s	relative to the solid	
SL	relative to the solid + liquid mixture	

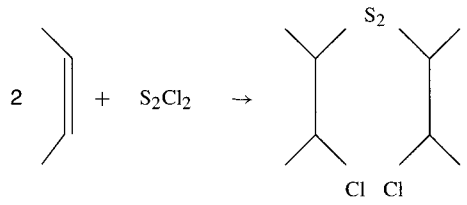
Copyrighted Materials
Copyright © 2004 Editions Technip Retrieved from www.knovel.com

9 Case Studies

9.1 BATCH AND SEMI-CONTINUOUS HOMOGENEOUS REACTORS

Production of an additive for a lubricant

Assume we want to produce 50 tons of an additive for a lubricant by reacting sulfur monochloride (S_2Cl_2) with methyl oleate ($C_{17}H_{33}COOCH_3$), according to the following reaction:



9.1.1 Fundamental data

Working with an inert solvent in the laboratory, Hugo [1980] determined the principal characteristics of this exothermic reaction.

$$\text{Reaction enthalpy:} \quad \Delta H_R = -2 \cdot 10^5 \text{ kJ/kmol}$$

$$\text{Activation energy:} \quad E = 5 \cdot 10^4 \text{ kJ/kmol}$$

The reaction temperature cannot exceed 80°C, otherwise byproducts appear that degrade the quality of the additive. The optimum temperature for the reaction was found to be 70°C. The kinetics can be expressed by a second-order global law, with partial orders equal to 1 for each of the reactants. The rate constant at 70°C was measured and found to be 11 $m^3/kmol \cdot h$. The physical data were also compiled (see Table 9.1).

Table 9.1

	Methyl oleate	Sulfur monochloride	Unit
Molecular weight	296.5	135	kg/kmol
Density	879	1 678	kg/m^3
Viscosity (70°C)	0.0047		Pa · s
Viscosity (50°C)	0.0073		Pa · s
Boiling point	216	135.6	°C
Specific heat	2.05	0.84	kJ/kg · K
Thermal conductivity	0.134		W/m · K

9.1.2 Batch reactor

Assume we wish to produce the additive in a batch reactor, using the reactants without a solvent but with an excess of oleate, that is, in terms of the stoichiometry, 2.75 moles of oleate for 1 mole of S_2Cl_2. The reaction takes place in the liquid phase, without any change in volume.

1. Referring to Chapter 2, we can first calculate the temperature increase when the reaction takes place under adiabatic conditions (ΔT_{ad}):

$$\Delta T_{ad} = \frac{-\Delta H_R}{\sum_1^2 n_i m_i C_{Pi}} = 112.1°C$$

   Given the high value of ΔT_{ad} and the narrow temperature range for optimum operation (70–80°C), temperature control must be carefully maintained.

2. We then calculate the maximum acceptable temperature difference (ΔT_C) between the reaction medium and the cooling fluid:

$$\Delta T_C = \frac{R \cdot T^2}{E} = 19.6°C$$

   The heat transfer should take place with a mean logarithmic temperature difference of less than 19°C.

3. Assume we have a stirred tank reactor equipped with a coil-shaped half-tube welded to the outside of the tank; the tank has the following characteristics (see Fig. 9.1 and Table 2.4) [De Dietrich, 1996]:
   - Total tank volume: 5.4 m^3
   - Working volume of tank: 4.0 m^3
   - Inside diameter: 1.74 m
   - Useful exchange surface (wall): 13.4 m^2
   - The half-tube welded to the outside of the tank has an inside diameter of 70 mm. Water from a production facility whose inlet temperature can be kept between 15 and 90°C is circulated in the coil with a linear velocity of 2.5 m/s.

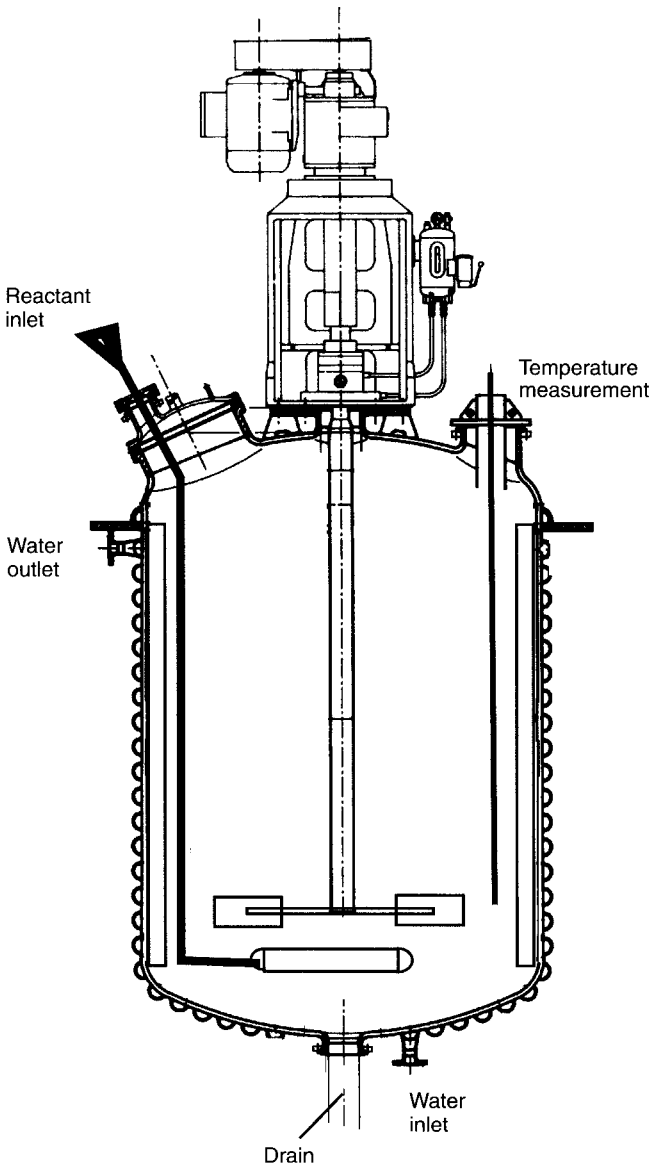


Figure 9.1 Cutaway drawing of the reactor used.

- The tank is equipped with a standard Rushton turbine impeller with 6 flat blades, driven by a 7.5 kW electric motor, together with a speed reducer operating at 125 rpm. The tank is equipped with 4 conventional 90° baffles.
- The reactants are introduced by means of a perforated pipe in the shape of a crown, located below the impeller.

- Given the working volume of the tank, we can load 11 kmol of oleate and 4 kmol of S_2Cl_2 at the start of the operation, the total corresponding to a volume $V_F = 4.032\ m^3$ and a weight of 3 801 kg.

4. Heat balance. The maximum heat is produced at the start of the reaction when the reaction rate is at a maximum. The concentrations of reactants are then, respectively:

$$C_{1,0} = \frac{11}{\frac{11 \cdot 296.5}{879} + \frac{4 \cdot 135}{1\,678}} = 2.728\ \text{kmol/m}^3 \quad \text{for the oleate}$$

$$C_{2,0} = \frac{4}{\frac{11 \cdot 296.5}{879} + \frac{4 \cdot 135}{1\,678}} = 0.992\ \text{kmol/m}^3 \quad \text{for the sulfur chloride}$$

Initial rate:

$$r_{ini} = kC_{1,0}C_{2,0} = 11 \cdot 2.728 \cdot 0.992 = 29.77\ \text{kmol/m}^3 \cdot \text{h}$$

The initial rate of heat production is then:

$$Q_P = r_{ini}(-\Delta H_R) = 29.77 \cdot 4.032 \cdot 2 \cdot 10^5 = 2.40 \cdot 10^7\ \text{kJ/h} = 6.67 \cdot 10^6\ \text{W}$$

► ***Calculating the heat exchange coefficient***

The equations given in Chapter 2 can be used.

- Inside the tank, Eq. (2.57) applies:

$$Nu_{int} = 0.74(Re)^{0.67}(Pr)^{0.33}(vis)^{-0.14}$$

The fluid is treated as pure oleate.

$$Re = \frac{\rho N_R D_A^2}{\mu} = \frac{879 \cdot 125 \cdot (1.74/3)^2}{0.00473 \cdot 60} = 1.30 \cdot 10^5$$

$$Pr = \frac{C_P \mu}{\lambda} = \frac{1\,000 \cdot 2.05 \cdot 0.00473}{0.134} = 72.4$$

$$vis = \frac{\mu_w}{\mu_L} = \frac{\mu(50°\text{C})}{\mu(70°\text{C})} = 1.55$$

$$Nu_{int} = 7.64 \cdot 10^3$$

$$h_{int} = Nu_{int} \cdot \frac{\lambda}{D_T} = 7\,640\frac{0.134}{1.74} = 589\ \text{W/m}^2 \cdot \text{K}$$

- Similarly, in the outside coil, the transfer coefficient is obtained by using Eq. (2.62). In this case the fluid is water:

$$Nu_{ext} = 0.027(Re)^{0.8}(Pr)^{0.33}\left(1 + \frac{3.5D_e}{D_T + 2e + 0.5D_e}\right)(vis)^{-0.14}$$

Effective diameter $D_e = \pi d_{Co}/2 = 3.14 \cdot 70/2 = 110$ mm.

$$Re = \frac{\rho v D_e}{\mu} = \frac{1\,000 \cdot 2.5 \cdot 110}{0.001 \cdot 1\,000} = 2.75 \cdot 10^5$$

$$Pr = \frac{C_P \mu}{\lambda} = \frac{1\,000 \cdot 4.18 \cdot 0.001}{0.627} = 6.67$$

We assume that $vis = 1$.

$$Nu_{ext} = 1.38 \cdot 10^3$$

$$h_{ext} = Nu_{ext} \cdot \frac{\lambda}{D_e} = 1.38 \cdot 10^3 \frac{0.627}{110 \cdot 10^{-3}} = 7.86 \cdot 10^3 \text{ W/m}^2 \cdot \text{K}$$

- The heat transfer resistance of the wall is normally calculated from the thickness e and the thermal conductivity λ: $h_p = e/\lambda$. In the present case, the wall is made of enameled steel and, consequently, has a specific resistance. The manufacturer provides measured values of λ/e of 750 kcal/m$^2 \cdot$ h $\cdot$ K $= 8.71 \cdot 10^2$ W/m$^2 \cdot$ K.
  Finally, according to Eq. (2.46):

$$\frac{1}{U} = \frac{1}{h_{int}} + \frac{1}{h_P} + \frac{1}{h_{ext}} = \frac{1}{5.89 \cdot 10^2} + \frac{1}{8.71 \cdot 10^2} + \frac{1}{7.86 \cdot 10^3}$$

$$U = 3.36 \cdot 10^2 \text{ W/m}^2 \cdot \text{K}$$ ◀

To ensure thermal stability, the maximum heat exchange capacity of the reactor is:

$$Q_E = US_{lat}\Delta T_C = 3.36 \cdot 10^2 \cdot 13.4 \cdot 19 = 8.56 \cdot 10^4 \text{ W}$$

and therefore much less than the heat produced (by a factor of approximately 80). Consequently, batch operation is not possible.

9.1.3 Semi-Continuous reactor

We can, however, operate the same reactor in semi-continuous mode with the gradual injection of sulfur chloride, adjusted so as to maintain a constant temperature of 70°C. In this way, it will be easy to control the production of heat and adjust it to match the exchange capacity of the reactor. For safety reasons, the thermal stability criterion (LMTD $< \Delta T_C$) should be maintained to avoid any temperature increase that might result from an accidental accumulation of the second reactant introduced.

1. The mean reaction rate can be calculated on the basis of the heat transfer. The energy dissipated by the impeller must be taken into account since it must be evacuated.
   Power dissipated by the impeller:

$$\mathcal{P} = N_P \rho D_A^5 N_R^3 \quad \text{where } N_P = 6$$

   Therefore, $\mathcal{P} = 3\,360$ W. In this way, we can also verify that the power of the motor installed (7.5 kW) is sufficient.

The heat capacity of the S_2Cl_2, which is introduced at 20°C but must be raised to the reaction temperature (70°C), must also be taken into account. The correction is easily made by subtracting from the heat of reaction the sensible heat needed for the transition from 20 to 70°C. We can then write:

$$r_{\text{adjusted}} = \frac{Q_E - \mathcal{P}}{1\,000\,[(-\Delta H_R) - (70 - 20) \cdot 0.84 \cdot 135]} = 4.3 \cdot 10^{-4} \text{ kmol/s}$$

The reaction time needed to produce 4 kmol of additive can be evaluated by using this mean rate:

$$t_R = \frac{1}{r_{\text{adjusted}}} = \frac{4 \cdot 10^4}{4.3} = 9.31 \cdot 10^3 \text{ s} = 2.59 \text{ h}$$

To produce 4 kmol of additive, 11 kmol of oleate are used at the outset. At the end of the operation, 3 kmol of excess oleate remain unreacted. The volume of liquid in the reactor is then:

$$V_F = 11 \cdot (296.5/879) + 4 \cdot (135/1\,678) = 4.032 \text{ m}^3$$

which is compatible with the volume of the tank. The concentration of oleate is then:

$$C_{1,F} = \frac{3}{V_F} = 0.744 \text{ kmol/m}^3$$

2. Writing the balances. To obtain a more realistic estimate of the time needed for the reaction, we can integrate the system of differential equations describing the reaction process as a function of time t:

- Oleate balance:

$$\frac{dn_1}{dt} = -2k_0 \exp\left(\frac{-E}{RT}\right) \frac{n_1 n_2}{V}$$

where

k_0 pre-exponential factor of the kinetic constant (m^3/kmol · s)
n_1 number of kmol of oleate in the reactor
n_2 number of kmol of S_2Cl_2 in the reactor
V total volume of liquid in the reactor (m^3).

- S_2Cl_2 balance:

$$\frac{dn_2}{dt} = -k_0 \exp\left(\frac{-E}{RT}\right) \frac{n_1 n_2}{V}$$

- Change in tota! volume:

$$\frac{dV}{dt} = Q_2$$

Q_2 is the volumetric flow rate of S_2Cl_2 (m^3/s) when it is introduced.

- Change in reaction temperature T:

$$\left(n_{1,0} P M_1 C_{P1} + (V - V_0)\rho_2 C_{P2} + w C_w\right) \frac{dT}{dt}$$
$$= \frac{\beta - 1}{\beta} [T_E - T] Q_E \rho_E C_{PE} + k_0 \exp\left(\frac{-E}{RT}\right) \frac{n_1 n_2}{V} (-\Delta H_R) - Q_2 \rho_2 C_{P2} (T - 20) + \mathcal{P}$$

where

PM_1	molecular weight of the oleate
C_{P1}	heat capacity of the oleate (kJ/kg)
C_{P2}	heat capacity of S_2Cl_2 (kJ/kg)
ρ_2	density of S_2Cl_2 (kg/m^3)
w	reactor weight subject to variations in temperature (kg)
C_w	heat capacity of the reactor weight w (kJ/kg)
T_E	inlet temperature of cooling water (K)
Q_E	flow rate of cooling water (m^3/s)
C_{PE}	heat capacity of water (kJ/kg)
ρ_E	density of water (kg/m^3)
$\beta = \exp\left(\frac{US}{Q_E \rho_E C_{PE}}\right)$	(see Chapter 2)
U	global heat transfer coefficient (W/m^2 · K)
S	exchange surface (m^2).

3. The initial conditions can be chosen as follows:

$$t = 0 \quad n_{1,0} = 11 \text{ kmol}$$

We can begin introducing S_2Cl_2 once the temperature reaches 65°C and take advantage of the reaction to raise the temperature to 70°C. For example, we can add 0.2 kmol of S_2Cl_2 at 65°C with the remainder, or 3.8 kmol, being added at a constant flow rate. In light of the initial feed, we can reduce the previously calculated feed time and round it off to 2.5 hours. Then:

$$n_{2,0} = 0.2$$
$$T_0 = 65 + 273 = 338 \text{ K}$$
$$V_0 = 3.71 + 0.2\frac{135}{1\,678} = 3.73 \text{ m}^3$$

The value of T_E can be chosen to be approximately 50°C to meet the requirements for stability. However, T_E can be adjusted as a function of the difference between T and the desired reaction temperature $T_R = 70$°C. For this calculation we can use a simple function for controlling the temperature of the cooling water, for example one that has only a proportional effect, such as:

$$T_E(°C) = 49 + 3(T_R - T)$$

4. Integrating the balances. With these boundary conditions, integration of the above differential equations can be used to obtain the change in temperature as a function of time ($0 < t < 2.5$ h) (Fig. 9.2) as well as the change in the number of kilomoles of oleate and S_2Cl_2 (Fig. 9.3). At the end of the feed period, the values of the two magnitudes are:

$$n_1 = 3.31 \quad n_2 = 0.156$$

The logarithmic mean temperature difference (LMTD) between the reaction fluid and the cooling water increases very rapidly up to around 19°C at the start of the reaction,

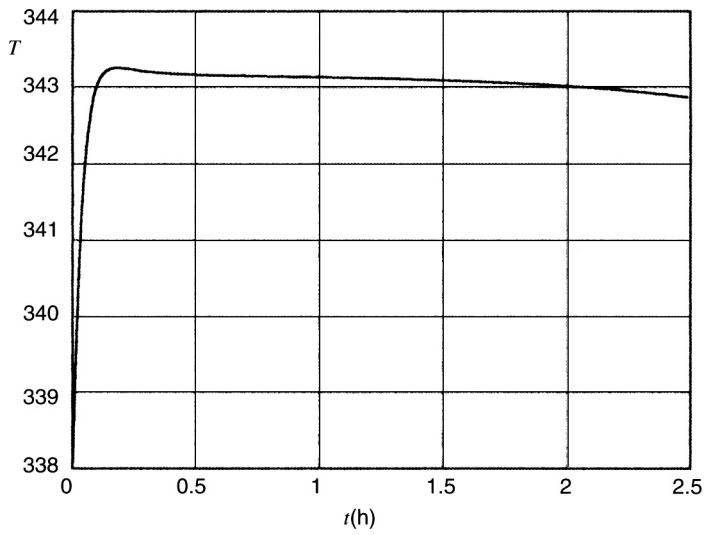


Figure 9.2 Curve giving the reaction temperature as a function of time during the S_2Cl_2 feed period.

then decreases steadily (Fig. 9.4). The time needed to complete the reaction and obtain a sufficiently low final concentration of S_2Cl_2 (10^{-5} kmol/m^3, for example) can be calculated by using the equations introduced in Chapter 2 (Table 2.1):

$$n_{1,0} = 3.312 \quad n_{2,0} = 0.156 \quad \xi = 0.156$$

We then find that $t = 1$ h and therefore, for the entire reaction, $t = 3.5$ h. This time can be compared to the time that would be needed if we were able to obtain the same overall extent of reaction under isothermal batch conditions, with a heat exchange surface sufficient to ensure stability. In this case (case E bis in Table 2.1):

$$t_{\text{isothermal}} = 0.25 \text{ h}$$

and the reaction time is much shorter. This should come as no surprise since the initial rate was, as we saw, 80 times greater than the acceptable mean rate.

5. Thermal stability of the reactor. The reactor's thermal stability is maintained by keeping the temperature difference between the reaction fluid and the cooling fluid below ΔT_C (LMTD < 19°C). We need to make sure, however, that an accidental accumulation of the coreactant (S_2Cl_2) and a runaway reaction do not occur in the reactor. Various factors can be examined to prevent this from happening.
   - Ensure there is no accumulation of S_2Cl_2 during the reaction (the maximum at the end of the feed period should be $n_2 = 0.156$ kmol). The potential adiabatic temperature increase, equal to $0.156/4 \cdot \Delta T_{ad} = 4.4$°C, which could result from a fault of some sort (stopping the impeller or reducing the flow rate of water) that reduces the heat exchange capacity, is then minimized and completely acceptable.

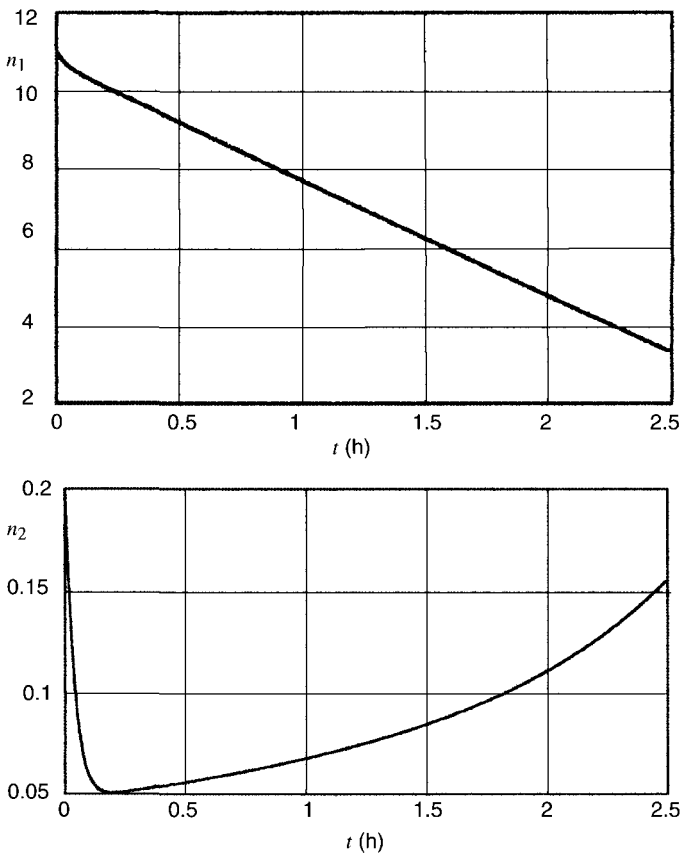


Figure 9.3 Variations in the number of kmol of oleate and S_2Cl_2 in the reactor throughout the S_2Cl_2 feed period.

• Local overconcentrations of S_2Cl_2 are not dangerous since feed is introduced just below the impeller and diluted as a result of the rate of circulation in the tank.

The rate of circulation is calculated by means of the equations given in Chapter 2. For a standard six-blade impeller with baffles:

$$Q_P = N_Q \cdot N_R \cdot D_A^3 \quad \text{where} \quad N_Q = 0.8$$

The pumping rate is then: $Q_P = 0.33\ m^3/s$.

In operation the rate of circulation resulting from this pumping rate doubles the value of Q_P. Since the feed is introduced below the impeller, the flow rate that entrains the S_2Cl_2 is only half the total flow rate of circulation. The concentration of reactant introduced is immediately brought to a value equal to:

$$\frac{4 - n_{2,0}}{Q_P t_R} = \frac{3.8}{0.33 \cdot 3\,600 \cdot 2.5} = 1 \cdot 10^{-3}\ \text{kmol/m}^3$$

a very low value incapable of causing thermal runaway.

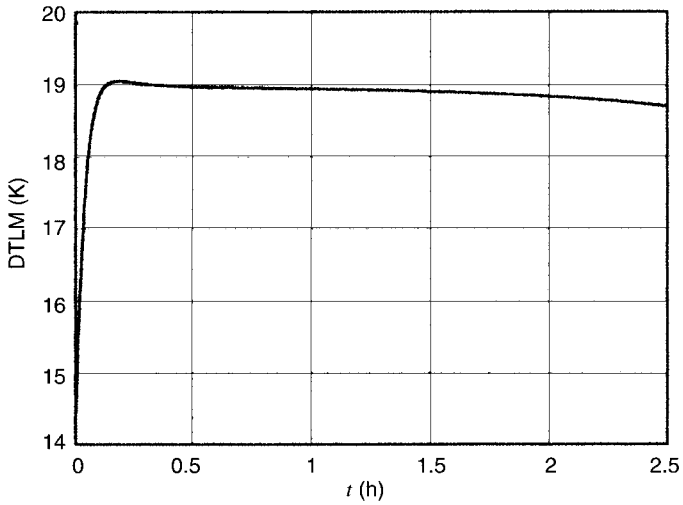


Figure 9.4 Variation of the logarithmic mean temperature difference (LMTD) between the reaction medium and the cooling water during the S_2Cl_2 feed period.

We can also estimate the mixing time resulting from agitation. The power number for the Rushton turbine is 6.

$$N_R = 125 \text{ tr/min}$$

The mixing time is calculated from the following simple equation:

$$t_M = \frac{300}{N_R N_P} = \frac{300 \cdot 60}{6 \cdot 125} = 24 \text{ s}$$

This time, during which there may be an excess concentration as calculated above, is itself very low.

6. Estimate of the time needed for production. To determine the total production time, it is necessary to estimate the time needed to reach the reaction temperature (heating) and cool the mixture before sending it to the storage tank (at 20°C), as well as the time needed for the initial introduction of oleate and for emptying the additive + oleate mixture.

• Heating and cooling time: The equations given in Chapter 2 (Eq. 2.47 and 2.48) are used. For heating, water at 90°C is circulated and oleate, assuming it is fed at a temperature of 20°C, is heated to 65°C. The introduction of 0.2 kmol of S_2Cl_2 is used to start the reaction and quickly raise the temperature to 70°C. During cooling, the mixture, which is at the reaction temperature (70°C), is brought to 20°C before pumping it to the storage tank. Water at 15°C is used for heat exchange. The calculations result as follows:

$$t_{heating} = 0.54 \text{ h} \quad \text{and} \quad t_{cooling} = 1.33 \text{ h}$$

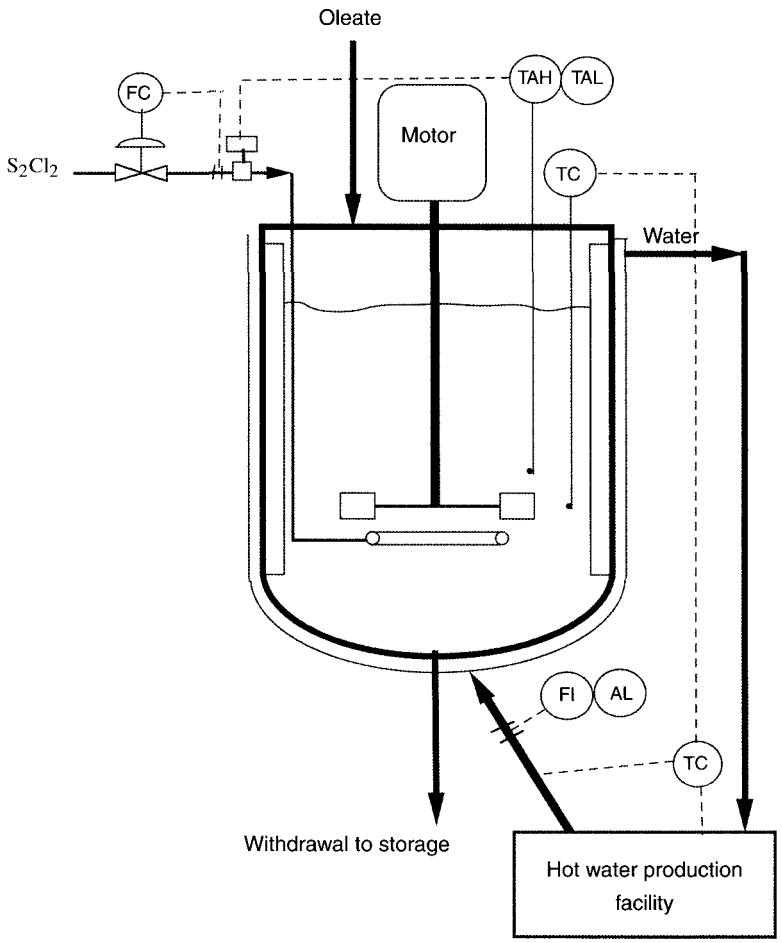


Figure 9.5 Reactor instrumentation diagram.

- The total time for all phases of the operation are broken down as follows:
  - filling (approximately 0.33 h)
  - heating the oleate from 20 to 65°C: 0.54 h
  - reaction with gradual introduction of S_2Cl_2: 2.5 h
  - completion of the reaction: 1 h
  - cooling the mixture from 70 to 20°C: 1.33 h
  - emptying the tank (approximately 0.33 h).

The total duration of the operation is 6 hours.

The reactor used can produce 14.5 tons of additive per week, performing one operation a day for 5 days, that is, 5 operations a week. It will, therefore, require 3.5 weeks to achieve the production goal (50 tons). Of course, it would be possible to increase the number of operations per week to reach the 50-ton production goal in a week.

- If larger quantities are needed, with a minimum investment, the same reactor could be equipped with an internal coil to increase its heat exchange capacity. In this way the time required to introduce the S_2Cl_2, as well as the heating and cooling times could be reduced. Other solutions are also possible such as an external heat exchanger with pump circulation.

7. Preliminary process design. We can now begin to design the reactor unit and the system needed to control the reaction (Fig. 9.5). The temperature regulator, set to 70°C, should control the cooling water temperature. The flow rate of S_2Cl_2 should, after the initial introduction of 0.2 kmol, be adjusted to a value of 1.52 kmol/h, or 122 l/h. For safety reasons a second temperature sensor, independent of the regulator, should function as a high- and low-temperature alarm:
   - high-temperature alarm at 75°C accompanied by cutoff of the S_2Cl_2 feed
   - low-temperature alarm at 65°C to inform the operator.

   The different stages of the operation could be managed by a programmable logic controller to ensure the transition from one phase to the next:
   - feed oleate
   - heat to 65°C
   - initial introduction of S_2Cl_2
   - introduction of S_2Cl_2 under control of the flow controller
   - continue the reaction once all the S_2Cl_2 has been introduced, with the temperature kept at 70°C for 1 h
   - cool by introducing 15°C water into the coil
   - drain the reactor.

9.1.4 Concluding remarks

The above example shows how a highly exothermic reaction that cannot be conducted in batch mode because of thermal instability, can be safely controlled by operating in semi-continuous mode.

9.2 PACKED COLUMN GAS-LIQUID REACTOR

***Washing natural gas through the simultaneous absorption of* CO_2 *and* H_2S**

In this case we have a natural gas effluent containing carbon dioxide and hydrogen sulfide that we want to eliminate before injecting the gas, similar to pure methane, into a distribution network. The gas is available at a pressure of 16 bar, with a flow rate of 26 m^3STP/s. To do this we will absorb the acidic gases (3.5% by volume of CO_2 and 0.75 by volume of H_2S) with an amine, diethanolamine (DEA) in this case. Elimination of acid compounds such as CO_2 and H_2S is commonly practiced in industry by using various basic solutions.

The process is simple and involves the use of two columns, one for absorption and the other for desorption, as shown in Fig. 9.6. The DEA solution circulates in a loop in the two columns, which can contain plates or packing.

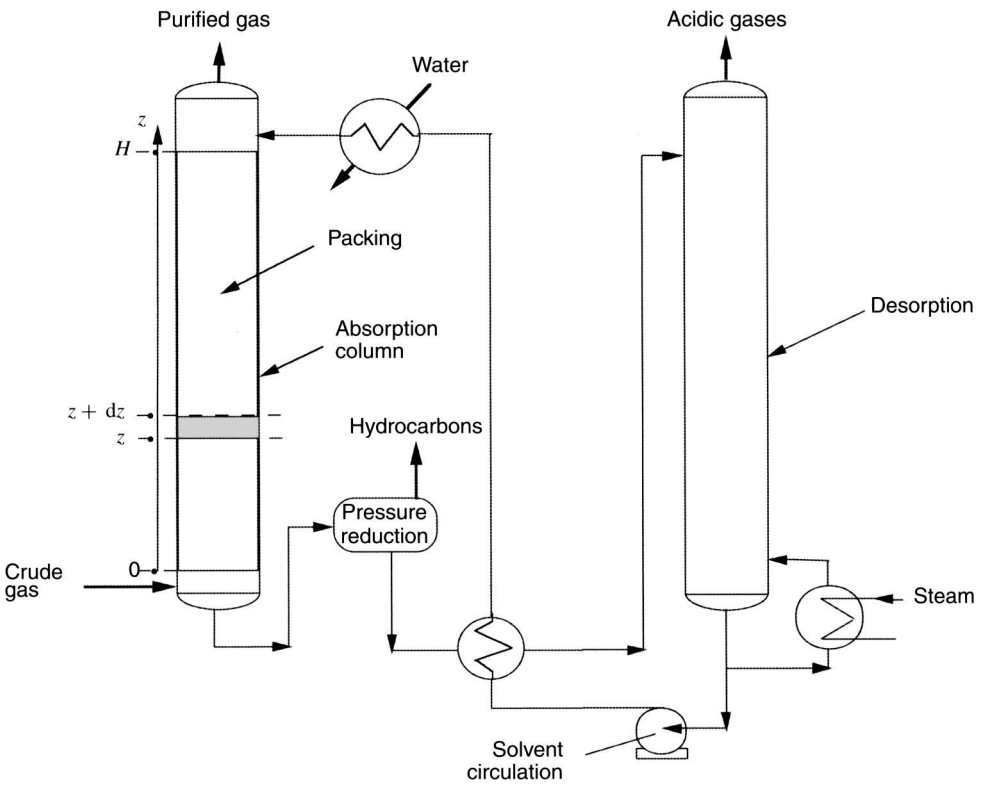


Figure 9.6 Treatment of natural gas with amines.

For this purpose various amines are used in solution in water or in an organic solvent. Here, we will use DEA in an aqueous solution, which is often done in practice because it presents a number of advantages including ease of regeneration, good stability, and low cost. There is considerable information in the literature on this subject [Danckwerts and Sharma, 1966; Kohl and Nielsen, 1997; Leprince *et al.*, 2000]; here we summarize the information needed to calculate the dimensions of the absorption column, to which we will limit our case study.

9.2.1 Fundamental data

9.2.1.1 Chemical reactions

The reactions between the acid compounds and DEA are written as follows:

$$CO_2 + 2R_2NH \rightarrow (R_2NCOO^- + R_2NH_2^+) \qquad \text{(Reaction 1)}$$

$$A_1 + 2A_3 \rightarrow A_4$$

$$H_2S + R_2NH \rightarrow (R_2NH_2^+ + SH^-) \qquad \text{(Reaction 2)}$$

$$A_2 + A_3 \rightarrow A_5$$

Therefore, we have two competing reactions and a single coreactant, DEA. The first reaction is fast; the second is considered to be very fast, according to the definitions given in Chapter 3.

The kinetics of the first reaction was studied by Danckwerts and Sharma [1966], who concluded that it was globally second-order and partially first-order for each of the reactants. The reaction rate can, therefore, be written:

$$r(CO_2) = k \cdot [CO_2] \cdot [DEA] \text{ kmol of } CO_2/m^3 \cdot s$$

The measured value of the constant k is 1 500 m^3/kmol · s at 25°C, the activation energy being approximately 9 575 kcal/kmol. This can be expressed by means of the following equation:

$$k = k_0 \exp\left(-\frac{E}{RT}\right) = 1.65 \cdot 10^{10} \exp\left(-\frac{9\,575}{RT}\right) \tag{9.1}$$

The only precise information available for the second reaction is that it is very rapid. We will use a rate constant that is five times greater than the one given above for CO_2.

Enthalpies of reaction have been provided by Leprince *et al.* [2000]. The overall influence on these values of the ratio (acidic gases/amine) in the liquid phase is reflected in a coefficient, here given a value of 0.85; this effect was reported by Kohl and Nielsen [1997].

This case is similar to the one discussed in Chapter 3 (Section 3.2.4.4, Simultaneous transfer of two compounds reacting with a third compound present in phase II). The two reactions are very fast and take place entirely in the liquid film near the interface.We indicated that the limit value of the enhancement factor E for fast reactions is obtained by means of the following equation:

$$E_{i,\,\mathrm{lim}} = \sqrt{\frac{\mathcal{D}_{i,\mathrm{II}}}{\mathcal{D}_{3,\mathrm{II}}}}\left[1 + \frac{\mathcal{D}_{3,\mathrm{II}} C_{3,\mathrm{IIb}}}{\frac{\nu_{3,1}}{\nu_{1,1}} C^*_{1,\mathrm{II}} \mathcal{D}_{1,\mathrm{II}} + \frac{\nu_{3,2}}{\nu_{1,2}} C^*_{2,\mathrm{II}} \mathcal{D}_{2,\mathrm{II}}}\right] \quad (i = 1, 2) \tag{9.2}$$

From this we can calculate the enhancement factor relative to each of the compounds by using Kishinevskii's equation (Eqs. 3.37 and 3.38) after introducing suitable values for the Hatta numbers and $\mathcal{N}_2$, that is:

$$Ha_i = \frac{\sqrt{k_i \mathcal{D}_{i,\mathrm{II}} C_{3,\mathrm{IIb}}}}{k_{\mathrm{L},i}} \quad (i = 1, 2) \tag{9.3}$$

$$\mathcal{N}_2 = \frac{\mathcal{D}_{3,\mathrm{II}} C_{3,\mathrm{IIb}}}{\frac{\nu_{3,1}}{\nu_{1,1}} C^*_{1,\mathrm{II}} \mathcal{D}_{1,\mathrm{II}} + \frac{\nu_{3,2}}{\nu_{1,2}} C^*_{2,\mathrm{II}} \mathcal{D}_{2,\mathrm{II}}} \tag{9.4}$$

9.2.1.2 Physicochemical data

• Solubility

The literature contains values for the solubilities of CO_2 and H_2S at various temperatures in the solvent, which is water. The solubility is most often expressed by means of Henry's

coefficient, H:

$$H_i = \frac{p_i}{C_i^*} \tag{9.5}$$

where:

$$\log(H_i) = \frac{\alpha_i}{T} - \beta_i \tag{9.6}$$

C_i^* being the concentration (kmol/m^3) in the liquid phase at equilibrium, with a partial pressure p_i (in atmospheres) of the compound A_i in the gas phase. We have used the values of α_i and β_i provided by Danckwerts and Sharma [1966] for CO_2 and calculated the corresponding values for H_2S using data provided in the literature.

• **Diffusivity**

In the gas phase, the diffusivities of CO_2 and H_2S can be calculated by means of the conventional correlations, those of Wilke and Lee, for example, [Poling *et al.*, 2001]. In the liquid phase, we refer to the experimental findings reported by Danckwerts and Sharma [1966], for both DEA and CO_2. We assume that the diffusivity of H_2S is identical to that of CO_2.

9.2.1.3 Physical data

The physical data used for our calculations are shown in Table 9.2, along with the physicochemical data mentioned above. For the gas phase, we will use the density, viscosity, specific heat, and thermal conductivity values of methane. For the liquid phase, values for density, viscosity, and heat capacity have been taken from Kohl and Nielsen [1997] and Leprince *et al.* [2000].

Table 9.2 The physical and physicochemical data used for the case study.

Compound	CO_2 $i=1$	H_2S $i=2$	CH_4 $i=6$	DEA $i=3$	Unit
Molecular weight	44	34	16.04	105.1	kg/kmol
Density				1 030 (solution)	kg/m^3
Solubility α	1 140	847			K
β	5.3	3.8			–
Diffusivity G	$1.16 \cdot 10^{-6}$	$1.19 \cdot 10^{-6}$			m^2/s
L	$1.40 \cdot 10^{-9}$	$1.40 \cdot 10^{-9}$		$4.0 \cdot 10^{-10}$	m^2/s
Viscosity			$1.2 \cdot 10^{-5}$	$2 \cdot 10^{-3}$ (solution)	Pa · s
Thermal conductivity			$3.5 \cdot 10^{-2}$		W/m · K
Interfacial tension				60	dyne/cm
Specific heat				3.8	kJ/kg · K
			39.5	(solution)	kJ/kmol · K
Enthalpy of reaction	−66.88	−40.46			kJ/kmol

9.2.1.4 Packing characteristics

We have decided to use a packed column filled with ceramic Intalox saddles with a nominal dimension of 25 mm (1"). The characteristics of the packing can be found in Table 4.5; here we summarize the values that will be used for our calculations:

- specific area: 250 m^{-1}
- void fraction: 0.74
- F factor: 320 m^{-1}.

9.2.2 Writing the molar and heat balances

9.2.2.1 Global balances

We begin by considering the column as a whole when writing the input-output molar balances. The composition of the raw gas entering the column is known. We can calculate the molar feed rates of the three constituents, as shown in Table 9.3. The amount of scrubbing required must be established in relation to the future use of the gas. We have chosen residual concentrations of the two acidic gases by making use of values common in industry—200 ppm by volume for CO_2 and 800 ppb by volume for H_2S.

Table 9.3 Input and output conditions for the column.

Incoming gas	CO_2	H_2S	CH_4
% vol	3.5	0.75	95.75
Partial P (kPa)	56	12	
Flow rate (kmol/s)	$4.06 \cdot 10^{-2}$	$8.71 \cdot 10^{-3}$	1.1
Outgoing gas	CO_2	H_2S	CH_4
% vol	$2 \cdot 10^{-2}$	$8 \cdot 10^{-5}$	
Partial P (kPa)	$3.2 \cdot 10^{-1}$	$1.3 \cdot 10^{-3}$	
Flow rate (kmol/s)	$2.2 \cdot 10^{-4}$	$8.8 \cdot 10^{-7}$	1.1
Incoming liquid	R_2NCOO^-	$SH^- + R_2NH_2^+$	free DEA
Conc. (kmol/m^3)	$2.4 \cdot 10^{-2}$	$7.0 \cdot 10^{-3}$	2.37
Flow rate (kmol/s)	$1.48 \cdot 10^{-3}$	$4.30 \cdot 10^{-4}$	$1.46 \cdot 10^{-1}$
Equilibrium P (kPa)	10^{-3}	10^{-3}	
Outgoing liquid	R_2NCOO^-	$SH^- + R_2NH_2^+$	free DEA
Conc. (kmol/m^3)	$6.81 \cdot 10^{-1}$	$1.49 \cdot 10^{-1}$	$9.16 \cdot 10^{-1}$
Flow rate (kmol/s)	$4.19 \cdot 10^{-2}$	$9.13 \cdot 10^{-3}$	$5.63 \cdot 10^{-2}$
Equilibrium P (kPa)	2	1.5	

The 25% by weight (2.43 M) DEA solution comes from the regeneration process, where the acidic compounds are removed by steam stripping; its temperature after heat exchange is

35°C. There remain traces of acidic compounds combined with a fraction of the amine. The following concentrations are used, which are easily obtained in practice:

- 0.024 kmol/m^3 of CO_2 in solution
- 0.007 kmol/m^3 of H_2S in solution.

The concentration of the free amine can be determined from the stoichiometric balance:

$$2.43 - 2 \times 0.024 - 0.007 = 2.37 \text{ kmol/m}^3$$

We must make sure that the concentrations of acidic gases in solution are in equilibrium, with partial pressures that are lower than those in the outgoing gas. The literature cited earlier contains equilibrium curves for CO_2 and H_2S with solutions of DEA:

- equilibrium pressure of CO_2 in a 25% by weight solution of DEA at 37°C = 0.001 kPa for a concentration of 0.024 kmol/m^3 in solution
- equilibrium pressure of H_2S in a 25% by weight solution of DEA at 37°C = 0.001 kPa for a concentration of 0.007 kmol/m^3 in solution.

These equilibrium pressures at 37°C are less than the partial pressures in the outgoing gas, which are respectively 0.32 kPa for the CO_2 and 0.0013 kPa for the H_2S.

We can now determine a liquid flow rate that ensures that the outgoing amine solution at the bottom of the column contains enough free amine (about 40%).

$$Q_L = \frac{2(F_{1,G,0} - F_{1,G,H}) + (F_{2,G,0} - F_{2,G,H})}{C_{3,T} \cdot 0.6} \tag{9.7}$$

where

Q_L flow rate of the liquid phase in m^3/s
$F_{1,G,0}$ molar flow rate of CO_2 in the gas phase at the column inlet ($z = 0$)
$F_{1,G,H}$ molar flow rate of CO_2 in the gas phase at the column outlet ($z = H$)
$F_{2,G,0}$ molar flow rate of H_2S in the gas phase at the column inlet ($z = 0$)
$F_{2,G,H}$ molar flow rate of H_2S in the gas phase at the column outlet ($z = H$)
$C_{3,T}$ total concentration of DEA in the liquid phase = 2.43 kmol/m^3.

We then obtain: $Q_L = 6.15 \cdot 10^{-2}$ m^3/s.

We can then verify that this choice leads to values of partial pressure at equilibrium, for each acidic compound, that are less than those in the gas entering the column. All the figures are shown in Table 9.3.

9.2.2.2 Differential balances

Here we examine an element of an absorption column of height dz, situated between height z and z + dz, the base of the packing being the origin of the z axis.

• Molar balances in the gas phase

For each gas phase constituent (CO_2 and H_2S), a molar balance can be written by considering the gas-liquid mass transfer, expressed as described in Chapter 3 for fast or instantaneous

reactions ($C_{1,L}$ and $C_{2,L}$ being zero).

$$-\frac{dF_{1,G}}{dz} = \mathcal{A}k_{G,1}\left(C_{1,G} - C^*_{1,G}\right)S = \mathcal{A}k_{L,1}E_1C^*_{1,L}S \tag{9.8}$$

$$-\frac{dF_{2,G}}{dz} = \mathcal{A}k_{G,2}\left(C_{2,G} - C^*_{2,G}\right)S = \mathcal{A}k_{L,2}E_2C^*_{2,L}S \tag{9.9}$$

where

$C_{1,G}$ and $C_{2,G}$	concentrations of CO_2 and H_2S in the gas phase (kmol/m^3)
$C^*_{1,G}$ and $C^*_{2,G}$	concentrations of CO_2 and H_2S at the gas-side interface in equilibrium with the concentrations $C^*_{1,L}$ and $C^*_{2,L}$ at the liquid-side interface (kmol/m^3)
E_1 and E_2	enhancement factors due to reactions 1 and 2
$k_{G,1}$ and $k_{G,2}$	mass-transfer coefficients in the gas phase for each constituent (m/s)
$k_{L,1}$ and $k_{L,2}$	mass-transfer coefficients in the liquid phase for each constituent (m/s)
$\mathcal{A}$	gas-liquid interfacial area (m^{-1})
S	column cross-section (m^2).

• Molar balance in the liquid phase

For the DEA a molar balance can be written by considering its disappearance resulting from the reactions with the two compounds transferred from the gas phase.

$$-\frac{dF_{3,L}}{dz} = 2\frac{dF_{1,G}}{dz} + \frac{dF_{2,G}}{dz} \tag{9.10}$$

Because of the countercurrent, the DEA concentration will vary along the length of the z axis in a manner opposite that of the acidic compounds in the gas phase.

• Heat balances

Heat balances can also be written for each of the phases:

$$\left(\Sigma F_{i,G}\right)C_{PG}\frac{dT_G}{dz} = h_{LG}\left(T_L - T_G\right)S \tag{9.11}$$

$$Q_LC_{PL}\frac{dT_L}{dz} = (\Delta H_1)\frac{dF_{1,G}}{dz} + (\Delta H_2)\frac{dF_{2,G}}{dz} + h_{LG}\left(T_L - T_G\right)S \tag{9.12}$$

where

$\left(\Sigma F_{i,G}\right)$	total molar flow rate ($i = 1, 2, 6$) of the gas phase (kmol/s)
T_G and T_L	respective temperatures of the gas and liquid phase (K)
ΔH_1 and ΔH_2	enthalpies of reactions 1 and 2 (kJ/kmol)
C_{PG}	specific heat of the gas phase (kJ/kmol · K)
C_{PL}	specific heat of the liquid phase (kJ/m^3 · K)
h_{LG}	heat transfer coefficient between the phases (kW/m^2 · K).

9.2.3 Calculating the transfer parameters

Before proceeding with the simultaneous integration of the five differential equations simulating the behavior of the column, it is necessary to calculate the transfer parameters that appear in the equations, namely:

- $k_{G,1}$ and $k_{G,2}$ as well as $k_{L,1}$ and $k_{L,2}$ for mass transfer
- h_{LG} for heat transfer
- $\mathcal{A}$ for both types of transfer.

For these values, we will make use of Honda's correlations, which were presented in Chapter 4 (Table 4.7, Eqs. 4.74 to 4.76). However, it is first necessary to determine the superficial velocities of the gas and the liquid, and then calculate the column diameter. For this we make use of the flooding equations (Eqs. 4.65 to 4.67) to determine the superficial velocity at flooding $V_{SG,e}$.

We successively calculate:

$$\pi_1 = \frac{Q_L}{Q_G}\sqrt{\frac{\rho_L}{\rho_G}} = 0.0235$$

$$\pi_2 = \frac{F}{g}\frac{\rho_G}{\rho_L}\frac{\rho_{water}}{\rho_L}\left(\frac{\mu_L}{\mu_{water}}\right)^{0.2} V_{SG,e}^2 = 0.232$$

For a packed column, a gas phase flow rate of approximately 60% of the flow rate that would cause flooding is generally used. In the case of an absorption column with amines, experience has shown that the pressure drop should be limited to a maximum, beyond which foaming phenomena will begin to occur [Trambouze *et al.*, 2000]. The maximum recommended pressure drop is 205 Pa/m.

The pressure drop is calculated by means of Eq. (4.68) in Table 4.6 and the ratio $\pi_2/\pi_{2,e} = \left(V_{SG}/V_{SG,e}\right)^2$ is adjusted in such a way that $\Delta P/L$ is equal to 205 Pa/m, which requires that the superficial velocity be $0.42 \cdot V_{SG,e} = 0.332$ m/s. The column diameter can then be easily determined from:

$$D = \sqrt{\frac{4Q_G}{3.14 \cdot V_{SG}}} = 2.62 \text{ m}$$

The mass transfer parameters can then be calculated using Eqs. (4.74) to (4.76) in Table 4.7:

$$\mathcal{A} = 162 \text{ m}^{-1}$$

$$k_{G,1} = 4.16 \cdot 10^{-3} \text{ m/s}$$

$$k_{G,2} = 4.27 \cdot 10^{-3} \text{ m/s}$$

$$k_{L,1} = k_{L,2} = 8.76 \cdot 10^{-5} \text{ m/s}$$

For the heat transfer, there is no specific correlation for determining h_{LG}. We will make use of the analogy between the two types of transfer generally considered valid, as presented in Chapter 7 for transfer between a fluid phase and a granular solid. We will use the factors

j_D and j_H defined in Table 7.1.

$$j_H = 1.2 \cdot j_D = \frac{h_{LG}}{C_{PMG}\rho_G V_{SG}} Pr^{2/3}$$

C_{PMG} is the specific heat of the gas phase in kJ/kg · K, and:

$$j_D = \frac{k_{G,1}}{V_{SG}} Sc_1^{2/3}$$

using the coefficient of mass transfer of compound 1 as a reference.

Based on the above equations, we can write:

$$h_{LG} = 1.2 \cdot C_{PMG} \cdot \rho_G \cdot k_{G,1} \left(\frac{Sc_1}{Pr}\right)^{2/3}$$

And therefore: $h_{LG} = 0.14\ \text{kW/m}^2 \cdot \text{K}$.

9.2.4 Integration of the differential balances

9.2.4.1 Boundary conditions

The above balance equations can now be integrated by using the initial conditions for $z = 0$, all of which are known except for T_L. With respect to the molar flow rates in the gas phase and the concentrations in the liquid phase, the boundary conditions were given in Table 9.3. The temperatures are known for the introduction of each phase, for example, in our case:

$$z = 0, \quad T_{G,0} = 20°\text{C} = 293\ \text{K},$$
$$z = H, \quad T_{L,H} = 35°\text{C} = 308\ \text{K}.$$

All that is required at this point is to assign a value to $T_{L,0}$, which will later be modified until a value for T_L is obtained at $z = H$ that is equal to the one given above.

9.2.4.2 Integration of the differential equations

One problem with integrating the system of differential equations arises from the fact that Eqs. (9.8) and (9.9), relative to the gas phase, contain variables for the concentration at the interface in each phase. We must therefore use, as is generally done, Eqs. (9.5), reflecting the solubilities of the two reactants in the liquid phase solvent.

The values of E_1 and E_2 must also be determined from the Kishinevskii equation, using the values for the Hatta number (Eq. 9.3) and $\mathcal{N}_2$ (Eq. 9.4). These two values depend on the concentrations $C^*_{1,L}$ and $C^*_{2,L}$ of the reactants at the interface in the liquid phase, which have to be calculated simultaneously at each step of the integration. For this, a system of two equations with two unknowns ($C^*_{1,L}$ and $C^*_{2,L}$) must be solved; the unknowns are obtained by

partially rewriting Eqs. (9.8) and (9.9) in the following form:

$$k_{G,1}\left(C_{1,G} - C^*_{1,G}\right) = k_{L,1}E_1C^*_{1,L}$$
$$k_{G,2}\left(C_{2,G} - C^*_{2,G}\right) = k_{L,2}E_2C^*_{2,L}$$

This system is transformed by using the partial pressures, p_1 and p_2, in the gas phase, as well as the coefficients H_i, reflecting the respective solubilities of the two acidic compounds in water:

$$\frac{k_{G,1}}{RT}\left(p_1 - \frac{C^*_{1,L}}{H_1}\right) = k_{L,1}E_1C^*_{1,L}$$
$$\frac{k_{G,2}}{RT}\left(p_2 - \frac{C^*_{2,L}}{H_2}\right) = k_{L,2}E_2C^*_{2,L} \qquad (9.13)$$

The reaction rate constants (1) and (2), along with the coefficients H_i, will be expressed as a function of the temperature of the liquid phase, T_L.

The equations can then be integrated by using the conventional Runge-Kutta method. Integration is stopped when the two values for molar flux $F_{1,G}$ and $F_{2,G}$, respectively for CO_2 and H_2S, reach the values assigned to them, as indicated in Table 9.3. We find that the value of $F_{2,G}$ is less than the target value and the value of $F_{1,G}$ is the only criterion for stopping the integration. The temperature of the liquid is then adjusted until an input temperature is obtained that corresponds to the boundary condition. Finally, after a few adjustments, we obtain the result shown by the curves in Figs. 9.7, 9.8 and 9.9.

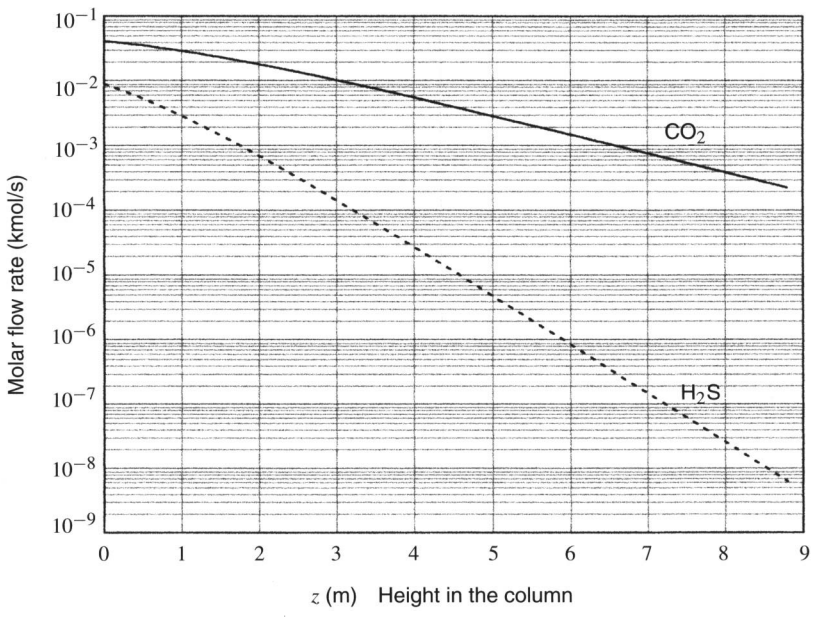


Figure 9.7 Curves for the variation in molar flow rate of CO_2 (solid line) and H_2S (dashed line) throughout the column.

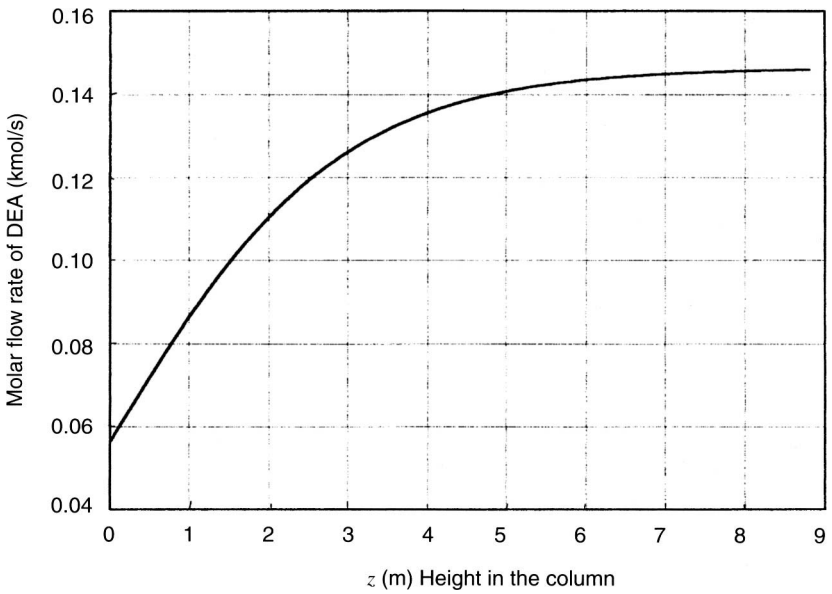


Figure 9.8 Variation in the molar flow rate of free DEA throughout the length of the column.

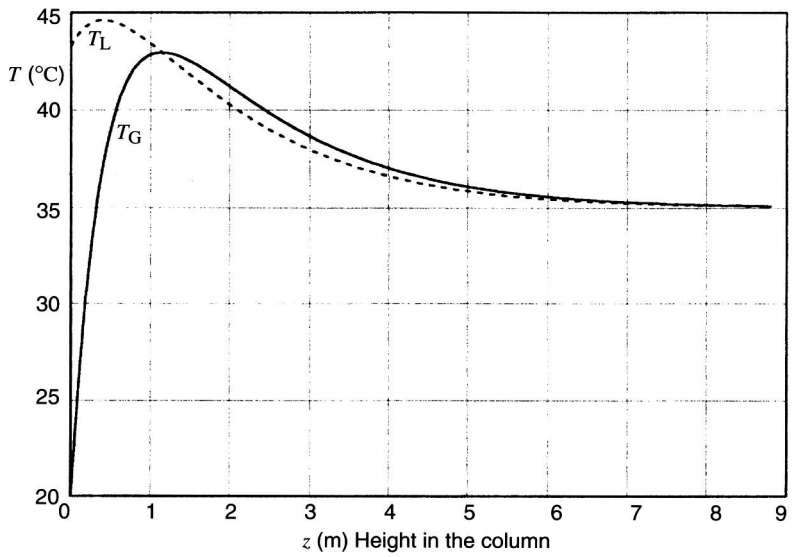


Figure 9.9 Temperature variation of the gas (solid line) and liquid (dashed line) phases throughout the length of the column.

The target outgoing concentrations in the column for CO_2 and H_2S are reached when the packing height is 8.8 m. For $z = 8.8$ the following values are obtained for the variables used in the differential Eqs. (9.8) to (9.12):

$$F_{1,G} = 2.2 \cdot 10^{-4} \text{ kmol/s}, \quad \text{corresponding to 200 ppm by volume;}$$
$$F_{2,G} = 6.2 \cdot 10^{-9} \text{ kmol/s}, \quad \text{that is, 5.6 ppb by volume;}$$
$$F_{3,L} = 0.146 \text{ kmol/s;}$$
$$T_{L,H} = 35°C \quad \text{for } T_{L,0} = 43.3°C \text{ at } z = 0\,;$$
$$T_{G,H} = 35°C.$$

We see that the reduction in the H_2S concentration is much greater than the target, primarily because of its high reactivity coupled with better solubility than CO_2. The packing height is fully comparable to the figures provided in the literature for existing units [Kohl and Nielsen, 1997]: between 20 and 30 plates, or 8 to 16 m of packing, depending on the operating conditions and required performance.

9.2.5 Column geometrical characteristics

Based on the results of the previous calculations, we can now determine the dimensions of absorption column needed to obtain the desired purification of natural gas. To be on the safe side, we will round up the numbers obtained from the calculations to take into account any lack of precision. The internal diameter of the column will be rounded up to 2.60 m and the height will be such that the total height of the packing is 10 m. To avoid any possible effects from poor phase distribution, it is recommended that the packing be split into two parts, each with a height of 5 m. The entire column is shown in Fig. 9.10. We will use a total height of 13 m to account for the heights needed respectively for:

- the introduction and distribution of the liquid as well as removal of the gas at the top of the column
- liquid redistribution in the middle of the column
- withdrawal of the liquid based on its level and introduction of the gas at the bottom of the column.

At the top of the column, a liquid phase distributor, with parallel channels and side openings (Fig. 9.11) ensures distribution of the liquid phase, while between the two sections of the bed, a distribution plate with openings and chimneys (Fig. 9.12) collects and redistributes the liquid.

9.2.6 Concluding remarks

The above case study illustrates how we can design a countercurrent gas-liquid reactor by taking into consideration the chemistry and transfer phenomena between phases. In the present case, two competing chemical reactions take place in the liquid phase at the same time as mass transfer. The reactions are sufficiently fast for them to occur entirely in the liquid film near the interface, the competition producing a slowdown in the transfer of the compound

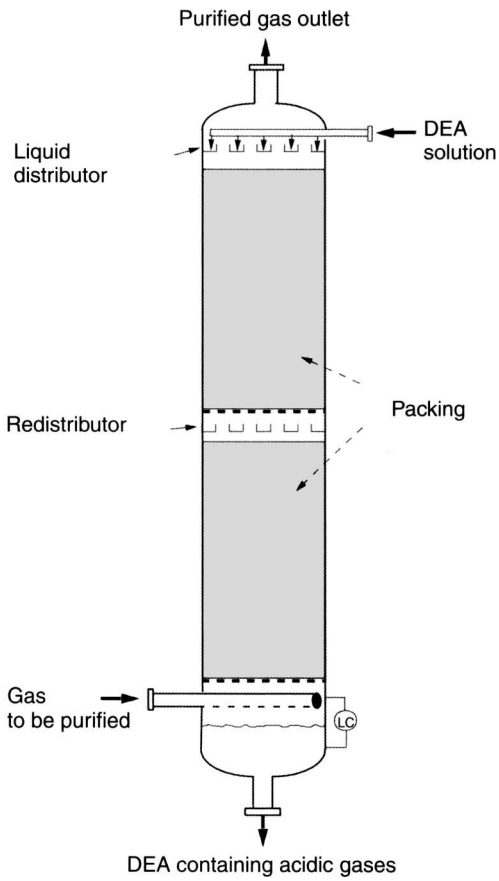


Figure 9.10 Diagram of the absorption column.

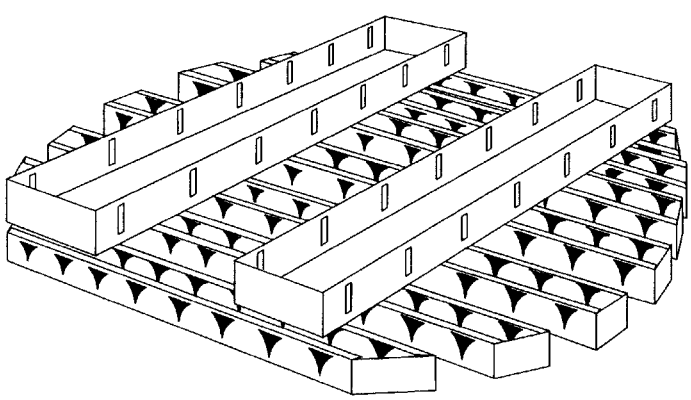


Figure 9.11 Liquid-phase distributor at the top of the column.

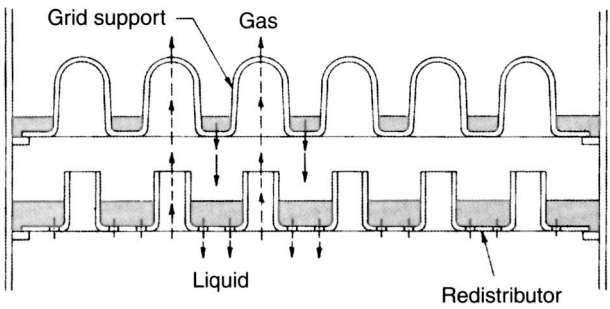


Figure 9.12 Liquid-phase distributor in the middle of the column.

that reacts most rapidly (H_2S). We could perform the same calculation with another type of packing or we could use a different dimension for the same packing and thus try to minimize the relative investment needed for the column-plus-packing assembly.

9.3 FIXED-BED CATALYTIC REACTOR WITH A SINGLE FLUID PHASE

Methanation as the finishing step in the production of hydrogen

The present case study illustrates the procedure for designing a fixed-bed catalytic reactor, taking into account both technical and economic factors. We consider a methanation reactor that is part of a chain in the synthesis of ammonia, shown schematically in Fig. 9.13. We are concerned with the final purification step for the mixture ($H_2 + N_2$) used for synthesis. We need to remove the last traces of CO and CO_2, which would poison the catalyst used to synthesize the ammonia.

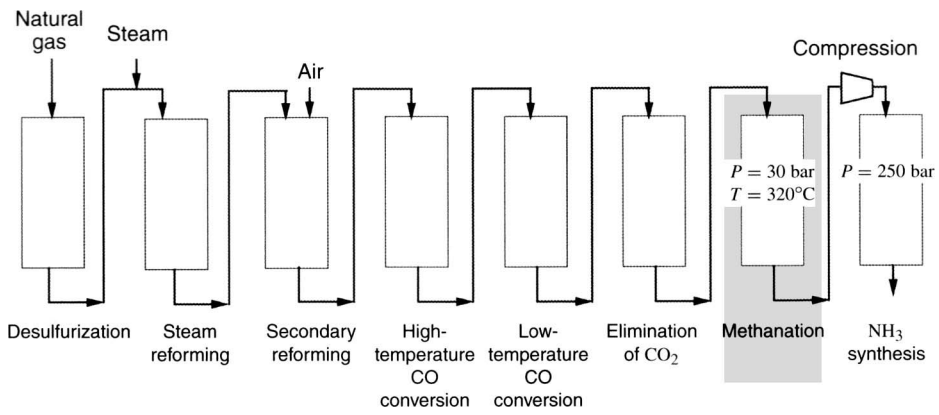


Figure 9.13 Ammonia production chain, indicating the various steps involved.

9.3.1 Fundamental data

The reactions that occur are primarily hydrogenation reactions:

$$\begin{aligned} CO + 3H_2 &\rightleftarrows CH_4 + H_2O \\ \text{that is } (A_1 + 3A_3 &\rightleftarrows A_4 + A_5) \\ CO_2 + 4H_2 &\rightleftarrows CH_4 + 2H_2O \\ \text{that is } (A_2 + 4A_3 &\rightleftarrows A_4 + 2A_5) \end{aligned}$$

These reversible reactions occur by means of a nickel-based catalyst deposited on a mixed oxide support. The operating conditions generally fall within the following ranges:

- temperature: 250–350°C
- pressure: 25 to 35 bar.

The equilibrium constants for the two reactions at 300°C are very large:

$$\begin{aligned} K_1 &= 0.152 \cdot 10^8 \ (\text{bar}^{-2}), \\ K_2 &= 0.387 \cdot 10^6 \ (\text{bar}^{-2}), \end{aligned}$$

so that it is possible to achieve very high conversions without the reverse reaction inhibiting the transformation.

The reactions can be treated as first-order reactions; the rates can be written as:

$$r_1 = -\frac{dn_1}{dt} = k_1 \cdot \exp\left(-\frac{E_1}{RT}\right) C_1$$

$$r_2 = -\frac{dn_2}{dt} = k_2 \cdot \exp\left(-\frac{E_2}{RT}\right) C_2$$

The activation energies are approximately 80 kJ/mol.

It is generally acknowledged that the kinetic constant for CO is twice that for CO_2, both depending on the total pressure.

The reaction enthalpies are high:

$$\begin{aligned} \Delta H_1 &= -206 \text{ kJ/mol} \\ \Delta H_2 &= -165 \text{ kJ/mol} \end{aligned}$$

Consequently, the adiabatic temperature increases are relatively large and can be estimated as follows:

$$\begin{aligned} (\Delta T_1)_{\text{adiabatic}} &= 74°C \quad \text{for 1\% of CO transformed;} \\ (\Delta T_2)_{\text{adiabatic}} &= 60°C \quad \text{for 1\% of } CO_2 \text{ transformed.} \end{aligned}$$

We will examine the case of a high-capacity synthesis chain (1 500 t/day of ammonia) [Appl, 1999], accompanied by the preliminary conversion of CO and elimination of CO_2, so that the

incoming gas for methanation has the following composition:

	mole %	
H_2	74.50	
N_2	24.45	
CO	0.40	(4 000 ppm by volume)
CO_2	0.01	(100 ppm by volume)
CH_4	0.64	

$\Delta T_{\text{adiabatic}}$ will then be: $0.4 \cdot 74 + 0.01 \cdot 60 = 30$ K.

Initially, we treat the reactions as being isothermal at $T_m = 593$ K.

Taking the practical data provided by Twigg *et al.* [1996], we will make use of the following equations at 593 K and 30 bar:

$$r_1 = -\frac{dn_1}{dt} = 3.6 \cdot C_1 \quad (\text{kmol/m}^3\text{of catalyst particle} \cdot \text{s})$$

$$r_2 = -\frac{dn_2}{dt} = 1.8 \cdot C_2 \quad (\text{kmol/m}^3\text{of catalyst particle} \cdot \text{s})$$

If we employ the notations defined in Chapter 6, the kinetic constants given above will correspond to $\rho_p k_M$.

The gas flow rate being processed is considerable, $Q = 50$ m^{3}STP/s.

The goal is to decrease the concentrations of CO and CO_2 to very low values (less than 1 ppm). Given the slow deactivation of the catalyst, we will use as our target at the start of the cycle the outlet concentrations, which are close to 0.5 ppm for each of the reactants. The required conversions can then be calculated:

$$X_1 = \frac{4\,000 - 0.5}{4\,000} = 0.999875$$

$$X_2 = \frac{100 - 0.5}{100} = 0.995$$

The catalyst selected for our calculations is a conventional catalyst with the following characteristics [Twigg *et al.*, 1996]:

- shape: cylindrical pellet with a diameter of 5.4 mm and height 3.6 mm
- porosity: $\theta = 0.42$
- tortuosity factor: $\tau = 3$
- void fraction of bed: $(1 - \varepsilon_p) = 0.4$
- specific weight of catalyst: $\rho_c = 1\,200$ kg/m^3 of catalytic bed.

9.3.2 Calculating the volume of catalyst

To calculate the volume of catalyst needed, we must successively determine the coefficient of external mass transfer and the global rate constant. Readers are referred to Chapters 6 and 7, where the relevant equations are given.

• **Coefficient of external mass transfer $k_{i,S}$**

To determine the coefficient of external mass transfer, we use the correlations given in Table 7.1:

$$k_{i,S} = j_D V_{SF} Sc_i^{-2/3}$$

where:

$$j_D = \frac{0.36}{(1-\varepsilon_p) Re^{0.36}}$$

$$\text{the Reynolds number:} \quad Re = \frac{\bar{d}_p V_{SF}}{\mu_F}$$

$$\text{the Schmidt number:} \quad Sc_i = \frac{\mu_F}{\rho_F \mathcal{D}_{i,F}} \quad (i = 1,2)$$

We need the respective diffusivities of CO and CO_2 in the hydrogen and nitrogen mixture. For this we use the correlation of Wilke and Lee [Poling *et al.*, 2001], already mentioned for the previous case. We then obtain:

$$\mathcal{D}_{1,F} = 4.30 \cdot 10^{-6} \text{ m}^2/\text{s}$$
$$\mathcal{D}_{2,F} = 3.54 \cdot 10^{-6} \text{ m}^2/\text{s}$$

• **Global transfer coefficient K_i**

We make use of Eq. (6.62):

$$\frac{1}{K_i} = \frac{1}{k_{i,S}} + \frac{\mathcal{A}_S}{-\nu_i k_{Mi} \eta_i \rho_C} \quad (i = 1,2)$$

where:

$$\mathcal{A}_S = \frac{6\varepsilon_p}{\bar{d}_p} = 778 \text{ m}^{-1} \quad \text{and} \quad k_{Mi}\rho_C = k_{Mi}\rho_p\varepsilon_p$$

The effectiveness factor η_i is calculated conventionally, using Eq. (6.23):

$$\eta_i = \frac{3}{\Phi_i}\left[\frac{1}{\text{th}(\Phi_i)} - \frac{1}{\Phi_i}\right] \quad (i = 1,2)$$

where:

$$\Phi_i = \frac{\bar{d}_p}{2}\sqrt{\frac{-\nu_i \rho_p k_{Mi}}{\mathcal{D}_{i,e}}} \quad (i = 1,2)$$

Given the dimensions of the catalyst particles (see Table 6.1), we have:

$$\bar{d}_p = \frac{3DH}{2H + D} = \frac{3 \cdot 0.0054 \cdot 0.0036}{2 \cdot 0.0054 + 0.0036} = 0.0046 \text{ m}$$

Based on the values given above, we obtain:

	$i = 1$	$i = 2$	
ν_i	-1	-1	
$k_{Mi}\rho_p$	3.6	1.8	$l/m^3 \cdot s$
$\mathcal{D}_{i,e}$	$6.02 \cdot 10^{-7}$	$4.96 \cdot 10^{-7}$	m^2/s
Φ_i	5.66	4.41	
η_i	0.436	0.526	

For a set of values for the superficial velocity V_{SF} (for example, between 0.1 and 1 m/s), we can then calculate the global transfer coefficient K_i.

• Volume of catalyst needed

For each of the reactions, we evaluate the length, L_i, of the catalyst bed that will be needed to obtain the desired conversion:

$$L_i = \frac{V_{SF}}{K_i \cdot \mathcal{A}_S} \ln\left[\frac{1}{1 - X_i}\right] \quad (i = 1, 2)$$

The two lengths obtained are in fact very close to one another because of the respective conversions used for CO and CO_2. We will retain the greater length (L_{iM}, relative to CO, $i = 1$) to determine the volume of catalyst needed:

$$V = L_{iM} \frac{Q}{V_{SF}}$$

where Q is the flow rate at the reaction conditions ($T = 593$ K and $P = 30$ bar) $= 3.62\ m^3/s$.

The reactor dimensions needed can then be easily determined. We add 1 m to the length of the bed so there is room at the top of the bed for a layer of alumina spheres and a fluid distributor:

$$H = L_{iM} + 1 \qquad S = \frac{V}{L_{iM}}$$

and, therefore, the diameter D is:

$$D = \sqrt{\frac{4S}{3.14}}$$

9.3.3 Cost optimization

To determine the superficial velocity to use in practice, overall operating costs must be minimized; the variable components are:

- investment associated with the reactor
- energy expenditure due to pressure drop in the catalytic bed
- additional investment to overcome pressure drop
- cost of the catalyst used.

• Reactor cost

Once we know the dimensions of the reactor, we can calculate the needed expenditure. To do this, we make use of the method proposed by Chauvel [1981]. We must first select the materiel that will be used for construction. Given the temperature and composition of the gas (rich in hydrogen) inside the reactor, Nelson's chart [Perry *et al.*, 1984] can be used to determine the proper grade of steel. A low-alloy steel such as AS357, which costs twice as much as ordinary steel, would be suitable.

The thickness e (mm) of the reactor wall is obtained from the following formula:

$$e = \frac{500PD}{\alpha t - 0.6P}$$

where

P pressure (bar)
D diameter (m)
α welding coefficient (here $\alpha = 1$)
t maximum acceptable stress for the metal ($t = 940$ bar for AS357 steel).

Once the thickness is determined, the total weight of the reactor can be calculated:

$$\text{Total weight} = \text{weight of the shell} + \text{weight of the elliptical heads}$$

An elliptical head corresponds to a metal disk of the same thickness as the shell and whose surface is equal to 1.4 times the cross-section of the shell. We can then write:

$$W = \pi e \rho_A \left[0.5 \cdot 1.4\,(D + 2e)^2 + H(D + e)\right] \quad \text{(kg)}$$

where ρ_A is the density of the steel $= 7.87 \cdot 10^3$ kg/m^3.

The price of the reactor is evaluated on the basis of the weight, by making use of corrections based on the diameter and thickness. We have converted the curves provided by Chauvel into the following equation:

$$P_R = 2W\left[2.01\left(D^{-0.21}\right)\right]\left[1.41\left(e^{-0.17}\right)\right][I_{\text{Price}}] \quad \text{(US\$)}$$

The cost index ratio I_{Price} can be used to readjust the 1975 costs given by Chauvel. We have adopted the Marshall & Swift Equipment Cost Index, which has a current (2001) value of 1095, compared to a value of 444 in 1975.

• Energy cost associated with pressure drop in the catalyst bed

The pressure drop through the catalyst bed is evaluated as indicated in Chapter 7. Equation (7.9) can be used to calculate the linear pressure drop for each value of the superficial velocity:

$$\frac{\Delta P}{\Delta L} = 150\frac{\varepsilon_p^2}{\left(1 - \varepsilon_p\right)^3}\frac{\mu_F V_{SF}}{\bar{d}_p^2} + 1.75\frac{\varepsilon_p}{\left(1 - \varepsilon_p\right)^3}\frac{\rho_F V_{SF}^2}{\bar{d}_p}$$

The pressure drop through the bed can then be easily calculated:

$$\Delta P = \frac{\Delta P}{\Delta L} L \quad \text{(Pa)}$$

The energy needed to overcome this pressure drop is determined as follows:

$$E_d = \frac{Q\Delta P}{10^3 R_{CT}} \quad \text{(kW)}$$

R_{CT} is the overall yield of the unit used for compression.

In the present case, the methanation reactor is located immediately downstream of the gas compressor, which is located ahead of the ammonia synthesis reactor. It consists of a set of centrifugal compressors with a number of stages, generally driven by a steam turbine. The overall yield of the entire unit (R_{CT}), measured on the basis of the primary fuel (natural gas), can be estimated to be 0.5. The operating cost resulting from the expenditure of energy will then be:

$$C_{En} = E_d P_{kWh} N_H$$

where

P_{kWh} price of a kWh of fuel

N_H number of hours of operation.

We have adopted a natural gas price of 0.0143 US$/kWh, which was the 2001 price for high gas consumption.

• Additional investment needed to overcome pressure drop

As indicated previously, the methanation reactor is located downstream of the high-pressure compressor in the synthesis chain. If additional investment for compression capacity must be taken into account, this is the compression unit that will be affected, since any change in pressure drop will directly influence the compressor's suction pressure. The corresponding investment for a compressor-plus-turbine assembly can be evaluated from the curves given by Chauvel [1981] and can be converted into the following correlation:

$$I_{C+T} = 110 \left(\frac{P_{kW}}{150} \right)^{0.68} \cdot I_{Price} \quad (10^3 \text{ US\$})$$

The additional power needed is approximately 10 kW, while the total power of the compression unit is approximately 8 MW. The additional investment required can be evaluated by calculating the logarithmic derivative of the above equation:

$$\frac{dI_{C+T}}{I_{C+T}} = d \ln \left[I_{C+T} \right] = 0.68 \cdot \frac{dP_{kW}}{P_{kW}}$$

and, therefore, the increased investment is obtained from:

$$\Delta I_{C+T} = 0.68 \cdot \frac{\Delta P_{kW}}{P_{kW}} \cdot I_{C+T} = 0.68 \cdot \frac{\Delta P_{kW}}{P_{kW}} \cdot 110 \left(\frac{P_{kW}}{150} \right)^{0.68} \cdot I_{Price}$$

where $P_{kW} = 8$ MW.

• Cost of the catalyst

The cost of the catalyst is easy to evaluate.

$$C_{cat} = V \rho_c P_{cat}$$

where

P_{cat} price of a kg of catalyst (6 US$/kg)

ρ_c mass of catalyst per unit volume of bed 1 200 kg/m^3).

An important element in the calculation of the operating cost is the catalyst life, t_{VC}.

• **Total operating cost**

Here we consider only the part of the total operating cost that depends on the superficial velocity. Therefore, we write the cost function we want to minimize as follows:

$$F_{\text{cost}} = C_{\text{cat}} + C_{\text{En}} t_{\text{VC}} + (P_{\text{R}} + I_{\text{C+T}}) \frac{t_{\text{VC}}}{t_{\text{Am}}}$$

The total variable expenses are spread out over a period equal to the catalyst life. The investment for the reactor and the compressor are evaluated as a function of the depreciation period, t_{Am}. For our calculations, we have used the following values:

- catalyst life, $t_{\text{VC}} = 4$ yr
- depreciation period, $t_{\text{Am}} = 10$ yr.

9.3.4 Presentation of the results

The above calculations can easily be performed with a spreadsheet, using the superficial velocity, V_{SF}, as the variable. In our case, V_{SF} varies from 0.1 to 1 m/s, in increments of 0.05 m/s. The variations in F_{cost} *versus* V_{SF} around an optimum value are shown in Fig. 9.14.

In this way we obtain a minimum value for the cost function for a superficial velocity of 0.31 m/s.

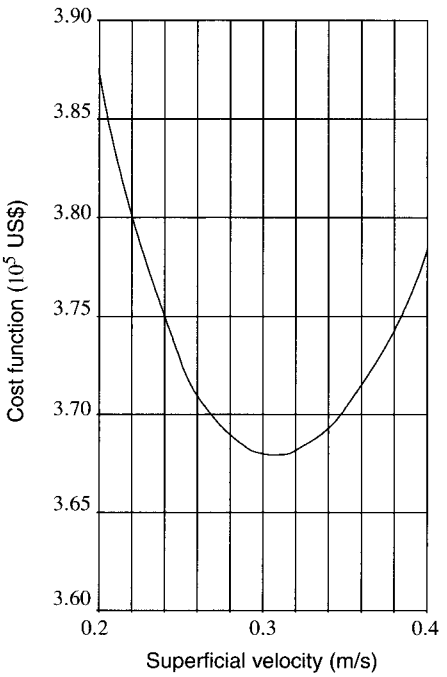


Figure 9.14 Variation of the cost function with superficial velocity near the optimum.

Next Page

In Fig. 9.15 we present the variations in the components of the cost function and, in Fig. 9.16, the percentage distributions of the various components at the optimum are shown.

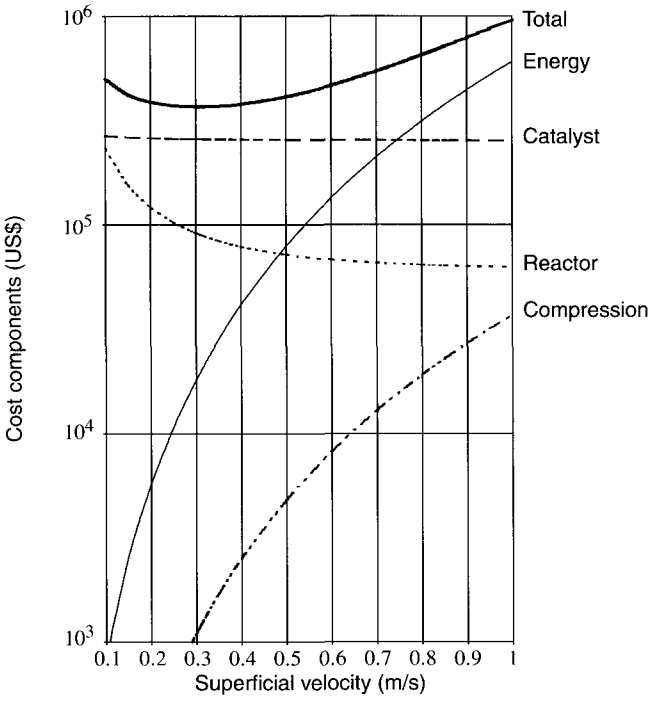


Figure 9.15 Variation of the various components of the cost function with superficial velocity.

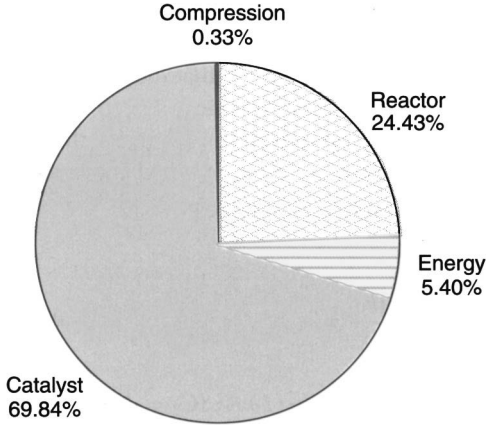


Figure 9.16 Percentage distribution of the various components of the cost function at the optimum.

Previous Page
Copyrighted Materials
Copyright © 2004 Editions Technip Retrieved from www.knovel.com

It can be seen from the graph that the cost of the catalyst is appreciably constant; this indicates that external mass transfer has practically no effect on cost, except at low superficial velocity, for which a slight influence can be observed. Moreover, for $V_{SF} = 0.31$ m/s, the portion of the cost due to energy expended is very low (only 2.36%), while the catalyst accounts for the majority of the cost.

The reactor characteristics can now be given:

- interior diameter: 3.92 m
- thickness: 67 mm
- height: 4.10 m
- weight: 44 969 kg.

The volume of catalyst needed is 36.9 m^3, that is, a space velocity (VVH) equal to 5 040 h^{-1}.

The total pressure drop through the bed is 6 000 Pa.

The height of the catalytic bed ($L = 3.06$ m) is low, less than the limit given in Chapter 7 (Eq. 7.22):

$$\frac{L}{\bar{d}_p} \geqslant 15.74 \left(\ln \frac{C_{1,0}}{C_{1,L}} \right) Re^{0.36} \cdot Sc^{0.67}$$

Here $Re = 376$ and $Sc = 0.88$, and therefore $L = 5.10$ m. The magnitude of the height is a result of the very high conversion sought. The height of 3.06 m has been obtained by taking into account the external mass transfer, which, under the conditions retained, plays a relatively minor role. Its importance can be estimated by comparing the value of the global constant ($K_1 = 1.172 \cdot 10^{-3}$) to its boundary value for a very high superficial velocity ($K_1 = 1.207 \cdot 10^{-3}$); the difference is only 3% and, therefore, acceptable. The reactor that has been described is shown schematically in Fig. 9.17.

9.3.5 Calculating concentration and temperature profiles

We have simplified our calculation by assuming that the reactor operates isothermally, while in practice it operates adiabatically. It is possible to complete our calculation by using the dimensions obtained from the cost optimization and verify that the approximation made is acceptable once the inlet temperature in the catalyst bed is adjusted.

We start with a series of differential equations that reflect the molar balances for CO and CO_2 as well as the heat balance.

$$-\frac{dF_1}{dz} = K_1(T) \mathcal{A}_S S C_1 = K_1(T) \mathcal{A}_S S \frac{F_1}{Q(T)}$$

$$-\frac{dF_2}{dz} = K_2(T) \mathcal{A}_S S C_2 = K_2(T) \mathcal{A}_S S \frac{F_2}{Q(T)}$$

$$\left(\sum F_i C_{Pi} \right) \frac{dT}{dz} = \Delta H_1 \frac{dF_1}{dz} + \Delta H_2 \frac{dF_2}{dz}$$

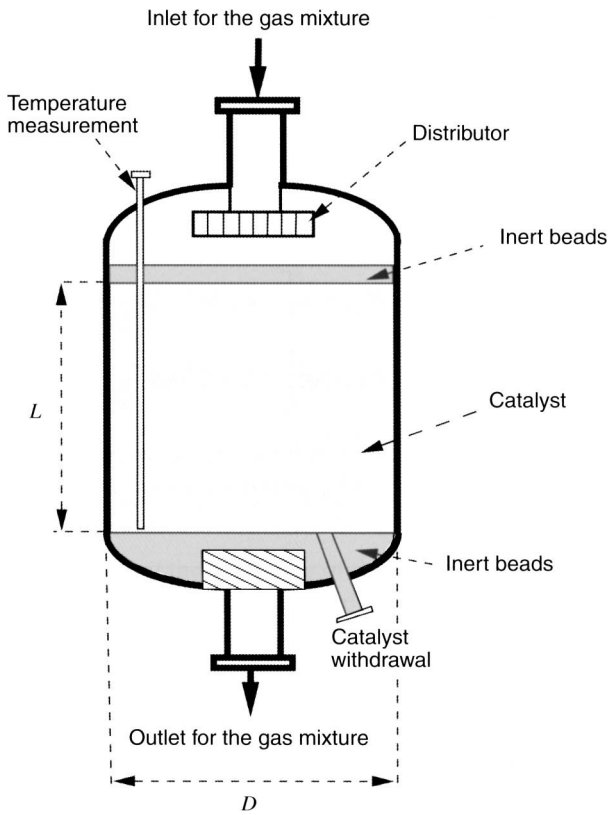


Figure 9.17 The catalytic reactor as determined by the optimization procedure.

where

F_1 and F_2	molar flow rates of CO and CO_2 (kmol/s)
C_1 and C_2	concentrations of CO and CO_2 (kmol/m^3)
$Q(T)$	total gas flow rate at the reaction conditions (m^3/s)
T	temperature of the reaction medium, assumed to be equal to that of the catalyst (K)
$\left(\sum F_i C_{Pi}\right)$	global heat capacity for the flow rate Q (J/K). This term is calculated for the H_2 and N_2 mixture (0.75/0.25) by using the values for C_{Pi} given by Twigg *et al.* [1996]:

$$C_{P3} = 27.67 + 3.39 \cdot T \cdot 10^{-3} \qquad \text{(kJ/kmol} \cdot \text{K)}$$

$$C_{P4} = 28.26 + 2.53 \cdot T \cdot 10^{-3} - 0.54\frac{10^5}{T^2} \qquad \text{(kJ/kmol} \cdot \text{K)}$$

$K_1(T)$ and $K_2(T)$	the global constants defined above, are functions of temperature, T; they undergo changes in their kinetic constant according to the Arrhenius law
S	cross-section of the catalytic bed $= \pi D^2/4 = 12.06$ m^2
z	position in the catalytic bed measured from the inlet (m).

The method of Runge-Kutta is used to integrate the equations, using the following initial conditions:

$$F_{1,0} = \frac{0.4}{100}\frac{Q_{TPN}}{22.4} \qquad F_{2,0} = \frac{0.01}{100}\frac{Q_{TPN}}{22.4}$$

The inlet temperature in the catalytic bed (T_0) must be specified so as to obtain molar flow rate profiles that are as close as possible to those obtained for isothermal operation. These last profiles can be easily calculated by means of the following equations:

$$F_1(\text{isothermal}) = F_{1,0}\exp\left[-K_1(593)\mathcal{A}_S\frac{S}{Q(593)}z\right]$$

$$F_2(\text{isothermal}) = F_{2,0}\exp\left[-K_2(593)\mathcal{A}_S\frac{S}{Q(593)}z\right]$$

By varying T_0, the value of the boundary condition can be determined in order to adjust the concentration profiles, as shown in Fig. 9.18. In this case $T_0 = 566.6$ K $= 293.6$°C.

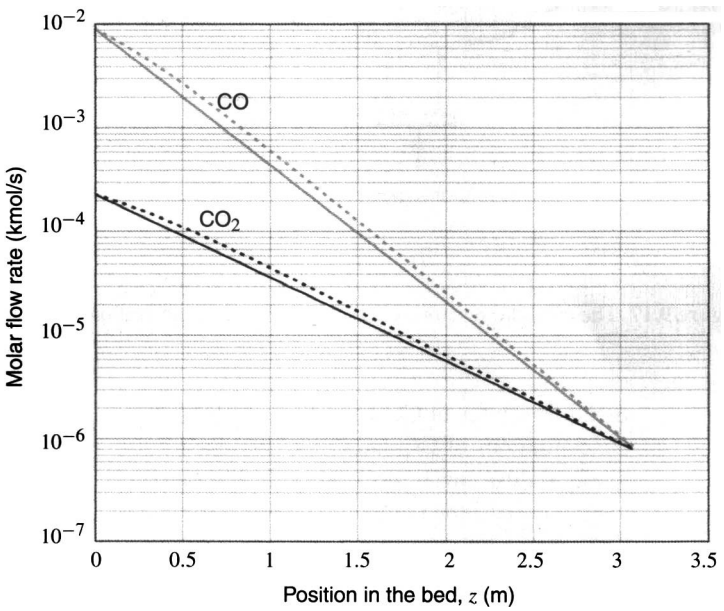


Figure 9.18 Variation in the molar flow rates of CO and CO_2 with the distance z in the catalytic bed; these values were obtained by integrating the balances for adiabatic (dashed lines) and isothermal operation (solid lines).

We can then plot the temperature profile in the catalytic bed, as shown in Fig. 9.19. The 30 K difference for the adiabatic temperature increase is clearly indicated.

The assumption concerning the equality of the temperatures of the gas and the solid can be justified by calculating the maximum value for the temperature difference at the point where

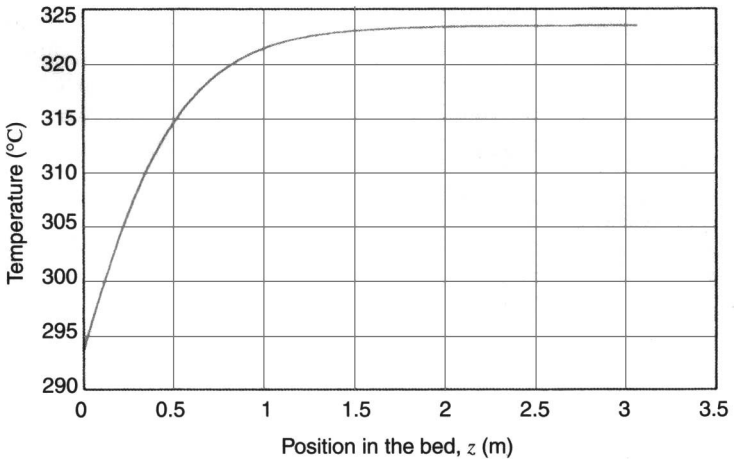


Figure 9.19 Temperature profile inside the catalytic bed.

the rate is a maximum, that is, at the beginning of the catalytic bed. The heat balance can be written for a unit volume of catalytic bed using the equations given in Chapter 7:

$$h\mathcal{A}_S(T_S - T_F) = r_{1m}(\Delta H_1) + r_{2m}(\Delta H_2) = (1 - \varepsilon_p)\left[3.6\eta_1 C_{1,0}\Delta H_1 + 1.8\eta_2 C_{2,0}\Delta H_2\right]$$

The heat transfer coefficient h can be evaluated from the correlations in Table 7.1, namely:

$$h = \frac{1.2 \cdot 0.36}{(1 - \varepsilon_p)Re^{0.36}} C_{PM}\rho_F V_{SF} Pr^{-2/3}$$

We know that $Re = 376$ for $V_{SF} = 0.31\,\text{m/s}$. Pr for the H_2+N_2 mixture is approximately 0.77. $C_{PM}\rho_F$ is evaluated using the equations given previously, and is 16.8 kJ/m^3. In this way we find that $h = 56\ \text{kW/m}^2 \cdot \text{K}$ and the maximum temperature difference at the inlet of the bed is 0.008 K, which is negligible.

We indicated that the catalyst undergoes a process of slow deactivation over time, associated with certain impurities arising from earlier steps in the synthesis. It is because of this that our initial conversion value was very high, since it can decrease with deactivation without leading to serious problems in the synthesis of ammonia.

The conversion of CO and CO_2 can be monitored using on-line analyzers, but a simpler method from the point of view of the operator consists in following the modification of the temperature profile in the reactor. The profile will shift, while retaining the shape shown in Fig. 9.19, and migrate slowly in the direction of fluid flow. By this simple means we can follow the deactivation of the catalyst and anticipate its life cycle.

9.3.6 Variants

The cost optimization process clearly shows the important role played by the catalyst in the cost factor (70%). It is normal, therefore, to try to decrease the amount of catalyst used. We can repeat the calculations to determine the influence of the size of the catalyst particles or their

geometry. The grain effectiveness factor (0.436 for reaction 1) indicates that it would be possible to decrease the catalyst volume by reducing the size of the particles. This will, however, result in an increase in the pressure drop. Calculation of the optimization will lead to a superficial velocity that is lower and, consequently, a larger reactor diameter, with a lower bed height.

We noted above that the bed height obtained from our calculations was already low and certainly at the limit of what is acceptable in practice. For, in addition to the mass transfer effect, which would become increasingly significant, there is another factor associated with the very high conversion target that could also play a decisive role in determining bed height. For conversions as high as those used here, every preferential path through the bed can have an appreciable effect by mixing the normal effluent from the catalytic bed with one or more fluid streams that have undergone much lower conversion. Because of this, it is undesirable to reduce the bed height below 3 m.

There is another way, however, to reduce the weight of catalyst used while maintaining the chemical performance and improving the cost balance. In Chapter 6 (Section 6.3.4.3) we demonstrated that the use of ring-shaped particles could result in a gain in effectiveness for a catalytic bed. Referring to Fig. 6.10, it can be seen that for values of Φ of about 6, we can easily obtain a 10% increase in effectiveness by using rings with a value of κ of approximately 2.5. Therefore, we can perform the previous calculation using the same external dimensions for the catalyst particles, but these will be ring shaped and characterized by a value of κ equal to 2.2. The equivalent diameter then becomes, based on Table 6.1: $\bar{d}_p = 0.0031$ m, and the catalytic bed has the following characteristics:

$$\varepsilon_p = 0.476$$

$$\mathcal{A}_S = 911 \text{ m}^{-1}$$

We will assume that the price per kg of ring-shaped catalyst is 10% more expensive per kg than solid pellets. By repeating the previous calculation, we obtain a minimum value for the cost function when $V_{SF} = 0.36$ m/s.

The reactor characteristics are as follows:

- diameter: 3.57 m
- height of the catalytic bed: 3.38 m
- reactor height: 4.38 m
- catalyst volume: 33.8 m^3
- VVH: 5 316 h^{-1}.

The cost function assumes a value that is 14% less than that obtained during the previous calculation. The percen age distribution of costs, however, has not been modified to any great extent (Fig. 9.20).

9.3.7 Concluding remarks

The calculations presented here show how the design of a catalytic reactor can be finalized and optimized by taking into account technical data as well as various economic factors associated with capital investments and operating costs. Examination of the various components of the cost function can often be useful in guiding the selection of certain parameters and can further improve the overall economics of the process.

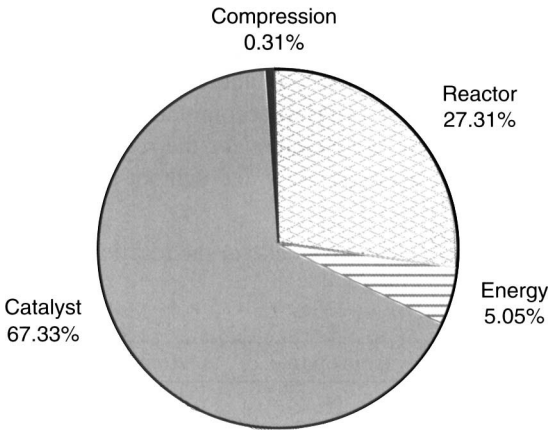


Figure 9.20 Percentage distribution of the various components of the cost function at the optimum for a ring-shaped catalyst.

9.4 LIQUID-PHASE REACTOR WITH A CATALYST IN SUSPENSION

Production of acetone

We want to produce 10 000 t/yr of acetone. With this as our target, we will outline the process and design the corresponding reactor.

9.4.1 Fundamental data

Laboratory studies have been made of the dehydrogenation of isopropyl alcohol to acetone:

$$CH_3-\underset{\displaystyle OH}{\underset{|}{CH}}-CH_3 \rightarrow \begin{matrix} CH_3 \\ \diagdown \\ \quad C = O \\ \diagup \\ CH_3 \end{matrix} + H_2$$

$$A_1 \rightarrow A_2 + A_3$$

The reaction is catalyzed with Raney nickel. The measured kinetics has been explained by means of the following simple equation:

$$\frac{1}{V}\frac{dn_1}{dt} = -\frac{km}{1+\dfrac{hx_2}{x_1}}$$

where

n_i	number of moles of compound A_i (mol)
k	kinetic constant $= 7 \cdot 10^{-5}$ mol/g · s at 150°C
m	catalyst mass per unit volume $= 100$ kg/m^3
h	ratio of the adsorption constants of A_1 and $A_2 = 120$ at 150°C
x_1 and x_2	molar fractions of A_1 and A_2 in the liquid phase.

The above kinetic expression represents the competition in the adsorption of compounds A_1 and A_2 on the active sites of the catalyst. It assumes that the overall kinetics is uninfluenced by the external mass transfer at the surface of the catalyst particles. Laboratory studies, made using a heavy inert solvent (paraffin) to accommodate temperatures up to 160°C, led to the conclusion that the optimum temperature for the reaction is 150°C. Here, we will use a temperature of 150°C, but under pressure and without a solvent, so as to simplify the separation step.

We must first gather the physicochemical data for the reaction system, which are available in the literature (see the following table).

Property	Isopropanol	Acetone	Hydrogen	Unit
Molecular weight	60	58	2	kg/kmol
Density				
– at 20°C	785	792		kg/m^3
– at 150°C	630	586		
Heat of vaporization at 150°C	29 700	22 200		kJ/kmol
Viscosity (150°C)	0.00014	0.00013		Pa · s
Mean specific heat (20–150°C)	196	147	15.8	kJ/kmol · K
Enthalpy of reaction at 150°C	12 210			kcal/kmol
Boiling point at normal pressure	82.5	56.2		°C

9.4.2 Process flowsheet

Because of the catalyst used (fine powder), the reactor will be a CSTR with a suspended catalyst (see Chapter 8). The impeller can be a three-blade helical device such as a multiple flat inclined paddle stirrer [Euzen, 2000], leading to a good circulation flow rate and ensuring adequate catalyst suspension.

The kinetic equation is of the Langmuir-Hinshelwood type, whose denominator reflects the competitive adsorption of the reactant and product. This results in a reduction of the rate, accentuated by the inhibition, whenever the extent of reaction increases. It will therefore be impossible to obtain complete conversion in the reactor.

Offtake is performed in the vapor phase, with the catalyst remaining in the reactor. After separation in a column of unreacted isopropanol, the latter is recycled to the reactor to obtain an overall conversion of 100%. The process can be diagramed as shown in Fig. 9.21. Heat must be supplied to the reactor to carry out the endothermic reaction and vaporize the acetone-isopropanol mixture that forms the reactor effluent. Steam at medium pressure circulating in the coil welded to the outside of the tank is used for this purpose.

If the surface of the tank is inadequate for carrying out the necessary heat transfer, an additional surface can be arranged inside the tank in the form of a guide cylinder around the stirrer, which will also be fed with steam at medium pressure.

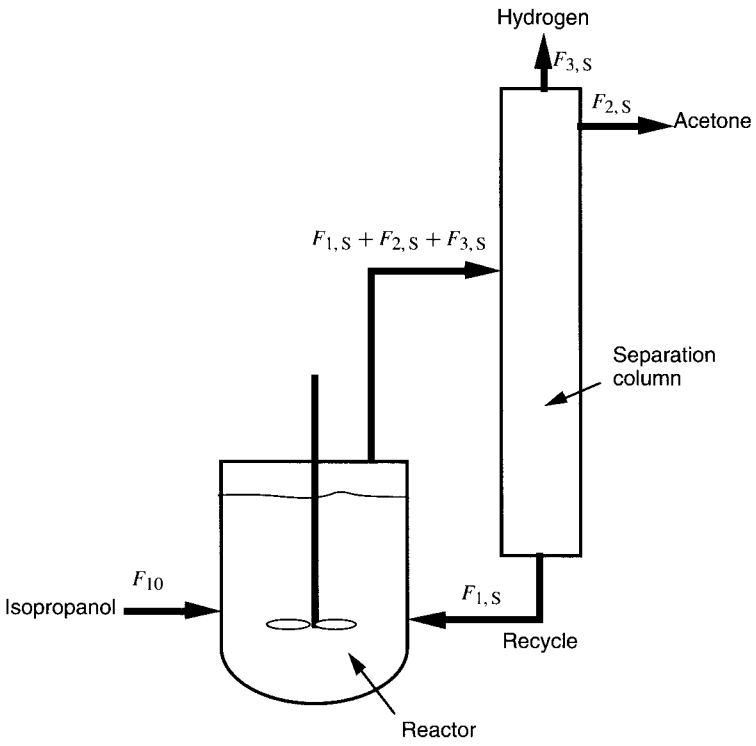


Figure 9.21 Acetone production process.

9.4.3 Molar balances

The reaction volume, V_R, is calculated from the equation for the chemical kinetics:

$$V_R = \frac{F_{1,0}}{km}\left[1 + \frac{hx_2}{x_1}\right]$$

$F_{1,0}$ is the rate of feed of the isopropanol, expressed in mol/s, that is totally transformed in the reactor. It is determined by the production capacity and is = 5.99 mol/s.

The reactor effluent in the form of a vapor consists of a mixture of hydrogen, acetone, and isopropanol. We can then write:

$$\text{Total outgoing molar flow rate} = F_{1,S} + F_{2,S} + F_{3,S}$$

where $F_{i,S}$ is the molar flow rate of A_i leaving the reactor.

Given the stoichiometry of the reaction, we also know that:

$$F_{3,S} = F_{2,S} = F_{1,0}$$

We assume that Raoult's law is applicable to the reaction mixture, in which case we can write:

$$\frac{F_{1,S}}{F_{2,S}} = \frac{\pi_1}{\pi_2}\frac{x_1}{x_2}$$

π_1 and π_2 are the respective vapor pressures of isopropanol and acetone.

Therefore, we need to know the vapor pressures π_1 and π_2 at the reaction temperature. In Table 9.4, we present the boiling temperatures as a function of pressure for isopropanol and acetone [Perry *et al.* 1984]. Knowing this data, it is easy to obtain an equation $\pi = f(T)$ by applying, for example, Antoine's law: $\log(\pi) = A + B/T$.

Table 9.4 Boiling temperature *versus* pressure.

	Boiling temperature (°C)	
Pressure (bar)	**Isopropanol**	**Acetone**
1	82.5	56.2
2	101.3	78.6
5	130.2	113
10	155.7	144.5
20	186	181
30	205	205
40	220.2	214.5
50	232	

We then obtain:

$$\log(\pi_1) = 5.824 - \frac{2\,070.48}{T} \quad \text{for isopropanol}$$

and:

$$\log(\pi_2) = 4.792 - \frac{1\,578.9}{T} \quad \text{for acetone}$$

These equations are shown graphically in Fig. 9.22, together with the experimental data from Table 9.2. The graph shows that the difference between the boiling temperatures of acetone and isopropanol decrease as the pressure increases. Distillation separation of the two compounds will, therefore, be easier at low pressure, which is why the column must operate at a pressure near atmospheric pressure. We will use a top pressure of 1.2 bar so the hydrogen can be easily removed for further processing. We assume a pressure of 1.5 bar at the bottom of the column, with a temperature corresponding to the bubble point of isopropanol at this pressure, that is, 94°C. The feed temperature will have to be adjusted to a value between the boiling points of acetone and isopropanol at a pressure of 1.4 bar. We will use the mean value of 79°C. The process defined is represented in Fig. 9.23.

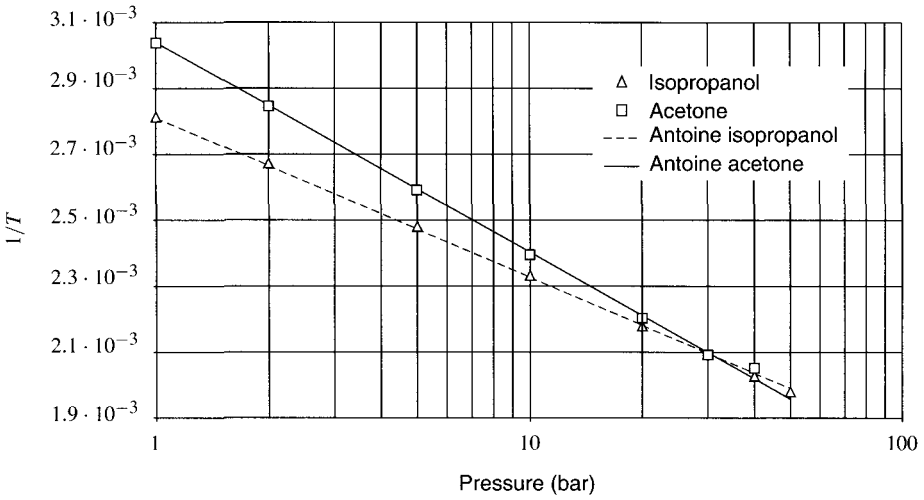


Figure 9.22 Variation of the vapor pressure of isopropyl alcohol and acetone as a function of temperature.

The rate of isopropanol recycling is equal to $F_{1,S}$, or:

$$F_{1,S} = F_{2,S}\frac{\pi_1}{\pi_2}\frac{x_1}{x_2} = F_{1,0}\frac{\pi_1}{\pi_2}\frac{x_1}{x_2} \quad \text{(mol/s)}$$

The ratio x_1/x_2 must be determined to calculate the reactor volume and the amounts of heat necessary to carry out the reaction and the vaporization of the effluent. This can be done so as to minimize the operating costs of the entire system. As a first approximation, we will assume that the characteristics of the column are not changed when the ratio x_1/x_2 varies. The separation column is in fact only slightly influenced by the recycling rate since its dimensions are associated with the top vapor flow rate, which remains constant and equal to $F_{2,S} + F_{3,S}$. The consumption of utilities (steam for reboiling and cooling water for condensation) can also be considered as relatively uninfluenced by x_1/x_2.

9.4.4 Energy balances

The amount of heat (Q_F) supplied to the reactor corresponds to the enthalpy of reaction, together with the heat of vaporization of the reactor effluent, less the energy expended for agitation (W_A). The total amount of heat that will be supplied to the system is equal to Q_F, plus the heat needed to raise the temperature of fresh and recycled feed to 150°C. The fresh feed will recover some of the enthalpy of the reactor effluent when it passes through exchanger E1 before being mixed with the recycled feed and passing through exchanger E3. The outgoing temperature of fresh feed from E1 can be chosen so it equals the temperature of the recycled feed from the bottom of the column, that is, 94°C.

We can then calculate the total heat (Q_T) that must be supplied:

$$Q_T = F_{1,0}(-\Delta H_R) + F_{1,S}\lambda_1 + F_{2,S}\lambda_2 - W_A + Q_C + Q_R \quad \text{(kJ/s)}$$

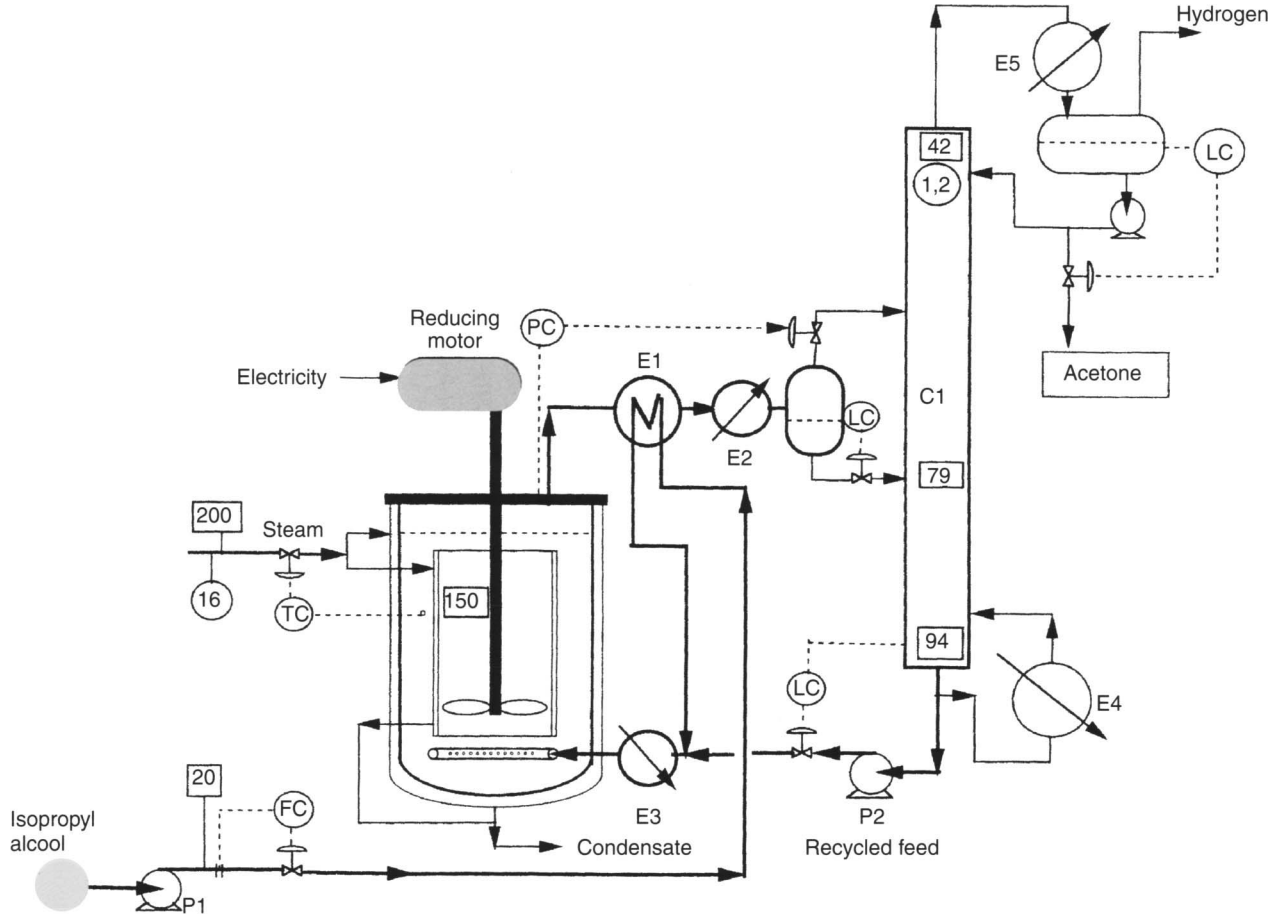


Figure 9.23 Detailed schema of an acetone production unit.

where

ΔH_R enthalpy of reaction (kJ/mol)

Q_R heat necessary to raise the recycled feed to the temperature of the reaction

Q_C heat necessary to raise the fresh feed to the temperature of the reaction

λ_i heat of vaporization of compound A_i ($i = 1, 2$) in kJ/mol.

$$Q_T = F_{1,0}\left[(-\Delta H_R) + \frac{\pi_1}{\pi_2}\frac{x_1}{x_2}\lambda_1 + \lambda_2\right] - W_A + Q_C + Q_R$$

Q_C is easy to calculate:

$$Q_C = F_{1,0}\overline{C_{P1}}\,(150 - 20) \quad \text{(kW)}$$

where $\overline{C_{P1}}$ is the mean specific heat of isopropanol, between 20 and 150°C, expressed in kJ/K · mol.

The recycle rate, F_2, is easily obtained:

$$F_2 = \frac{F_{1,0}}{1\,000}\frac{\pi_1}{\pi_2}\frac{x_1}{x_2}\frac{M_1}{\rho_1} \quad (\text{m}^3/\text{s})$$

where

M_1 molecular weight of isopropanol (kg/kmol)

ρ_1 density of isopropanol (kg/m^3).

Q_R can then be calculated:

$$Q_R = F_{1,0}\left(\frac{\pi_1}{\pi_2}\frac{x_1}{x_2}\right)\overline{C_{P1}}(150 - 94) \quad \text{(kW)}$$

9.4.5 Equipment design

The items directly influenced by the value of x_1/x_2 includes:

- the reactor (volume V and steam consumption)
- the mass of catalyst used ($= m \cdot V$)
- exchanger E1, which preheats the feed between 20 and 94°C, while partially condensing the reactor effluent at 150°C
- exchanger E2, which completes cooling of the reactor effluent from 150 to 79°C
- exchanger E3, which heats the mixture of recycled isopropanol and fresh feed from 94 to 150°C
- feed pump P1 is somewhat influenced by the pressure in the reactor
- recycling pump P2 (flow rate = F_2).

9.4.5.1 Reactor

We indicated that the reactor would have a helical stirrer with a welded half-tube forming a coil on the outside surface of the tank (see Chapter 2). These materials are currently designed to operate at pressures ranging from atmospheric to 15 bar. In addition to the volume required for the reaction, it is necessary to include a freeboard above the reaction medium so the vapor

effluent can be evacuated without entrainment (we will add 30% to the calculated volume V_R). The volume V needed to calculate the corresponding investment will then be: $V = 1.3 \cdot V_R$.

9.4.5.2 Heat exchangers

The heat exchange surfaces are calculated conventionally from the LMTD and the values of the heat transfer coefficient for each case, as recommended by Chauvel [1981]. We will use the following values:

- reactor (wall and guide cylinder): $U_R = 350$ kcal/K · m^2 · h
- exchanger E1: $U_1 = 500$ kcal/K · m^2 · h
- exchanger E2: $U_2 = 500$ kcal/K · m^2 · h
- exchanger E3: $U_3 = 350$ kcal/K · m^2 · h.

We can then write a heat balance for each exchanger.

For the reactor:

$$Q_F = U_R \Omega_R \mathrm{DTLM}_R = 350 \cdot 50 \cdot \Omega_R$$

For E1:

$$Q_1 = F_{1,0} \overline{C_{P1}} (94 - 20) = U_1 \Omega_1 \mathrm{LMTD}_1$$

$$\mathrm{LMTD}_1 = \frac{(150 - 20) - (150 - 94)}{\ln\left(\dfrac{150 - 20}{150 - 94}\right)} = 87.9$$

For E2:

$$Q_2 = F_{1,0}\left(\lambda_2 + \frac{\pi_1}{\pi_2}\frac{x_1}{x_2}\lambda_1\right) + F_{1,0}\left(1 + \frac{\pi_1}{\pi_2}\frac{x_1}{x_2}\right)\overline{C_{P1}}(150 - 79) - F_{1,0}\overline{C_{P1}}(94 - 20)$$

$$= U_2 \Omega_2 \mathrm{LMTD}_2$$

$$\mathrm{LMTD}_2 = \frac{(150 - 90) - (79 - 20)}{\ln\left(\dfrac{150 - 90}{79 - 20}\right)} = 59$$

For E3:

$$Q_3 = F_{1,0}\left(1 + \frac{\pi_1}{\pi_2}\frac{x_1}{x_2}\right)\overline{C_{P1}}(150 - 94) = U_3 \cdot \Omega_3 \cdot \mathrm{LMTD}_3$$

$$\mathrm{LMTD}_3 = \frac{(200 - 94) - (200 - 150)}{\ln\left(\dfrac{200 - 94}{200 - 150}\right)} = 75$$

The heat exchange area (Ω_i) needed can then be calculated along with the corresponding capital investment.

9.4.5.3 Pumps

The pump power is calculated with a formula taken from Chauvel [1981]:

$$P_W = KQ\Delta P$$

where

P_W in Watts

ΔP in bars, measured between the pump inlet and outlet

$K = 28 \cdot \frac{f_S}{\eta}$

f_S safety factor (1.2, for example)

η energy yield for the pump-plus-motor assembly, here taken to be 0.7.

The pressure P in the reactor varies as a function of the ratio x_2/x_1.

Here, we will use the simplified formula:

$$P_W = 48 \cdot Q \cdot \Delta P$$

Q being expressed in m^3/h.

9.4.6 Cost optimization

For various values of x_2/x_1 (between 0.08 and 0.44), it is easy to calculate V, Q_F, F_2, Q_T, the reactor's operating pressure, the mass of catalyst required, and the surface of the exchangers E1, E2, and E3. In Table 9.5 we list examples of some of the principal values to provide an idea of the orders of magnitude involved.

Table 9.5 Values of the principal variables calculated.

x_2/x_1	0.08	0.16	0.28	0.4
V (m^3)	9.05	17.25	29.55	41.85
F_2 (m^3/h)	15	7.5	4.28	3
Q_T (GJ/h)	9.52	5.51	3.77	3.05
P (bar)	9.45	10.39	11.57	12.55
M (kg)	905	1 725	2 955	4 185
E1 (m^2)	1.28	1.28	1.28	1.28
E2 (m^2)	72.57	38.26	23.56	17.68
E3 (m^2)	19.71	9.86	5.63	3.94

With this information the capital investment for all the equipment as well as the energy consumption required (steam for the reactor and E3, electricity for the impeller and pumps P1 and P2, water for exchanger E2) can be calculated using conventional means.

Equipment costs are evaluated by using formulas of the following type:

$$C = C_0 \left(\frac{K}{K_0} \right)^n$$

where

C cost of installed equipment (10^3 US$)
C_0 cost of equipment for some base capacity or size (10^3 US$)
K capacity or size of equipment installed
K_0 base capacity or size.

Depending on the nature of the equipment, the base capacity or size is defined specifically:

- for the reactor, the total volume is used (m^3)
- for the pumps and motors, power (kW)
- for the exchangers, the capacity is defined by the surface area (m^2). For determining the cost of the guide cylinder inside the reactor, the data for an exchanger (S and T) are used, with a factor of 0.5 applied to the base price.

Table 9.6, taken from Perry [1984], provides the information for the equipment in our study. These costs correspond to a reference index of 1 000 (Marshall & Swift Equipment Cost Index). The index was 1095 in 2001.

Table 9.6 Data for calculating FOB capital investments.

Type	Base	Unit	Cost (10^3 US$)	Range	Exponent
Centrifugal pump	7.5	kW	1.6	0.4–30	0.3
	75	kW	4.4	30–300	0.67
Electric motor	7.5	kW	0.7	7.5–19	0.56
	52	kW	3	19–150	0.77
Pump + motor	7.5	kW	2.3	0.4–30	0.38
Exchanger (S & T)	9.3	m^2	21.7	1.9–1800	0.59
Stirred reactor	0.4	m^3	9.3	0.04–15	0.53

The US$ is employed as the unit of measure because of its near parity with the euro.

The investments are reevaluated by multiplying them by 1.095. A multiplier of 4 is also applied for installation of the equipment.

With respect to the cost of utilities, average current values are used. For heat, we assume that the steam is supplied from an integrated network and the amounts of heat supplied are calculated on the basis of the price of a thermal GJ:

- electricity: 0.043 $/kWh
- steam: 3 $/GJ
- cooling water: 0.14 $/$m^3$
- catalyst: 43 $/kg.

The operating cost is then obtained by adding the various components:

$$\text{Operating cost} = \text{steam} + \text{electricity} + \text{water} + \text{investment} + \text{catalyst}$$

The calculation is adjusted for a year of operation (8 000 h); the depreciation period for the investment is taken as 10 years, while the life of the catalyst is estimated to be 18 months. The calculations can be performed easily with a spreadsheet, and the minimum total operating

cost can then be determined. The results of the calculations can be presented as shown in Fig. 9.24. Using the values retained for the various parameters involved, there is a minimum for $x_2/x_1 = 0.26$. Table 9.7 below lists the major characteristics of the essential equipment for optimal value.

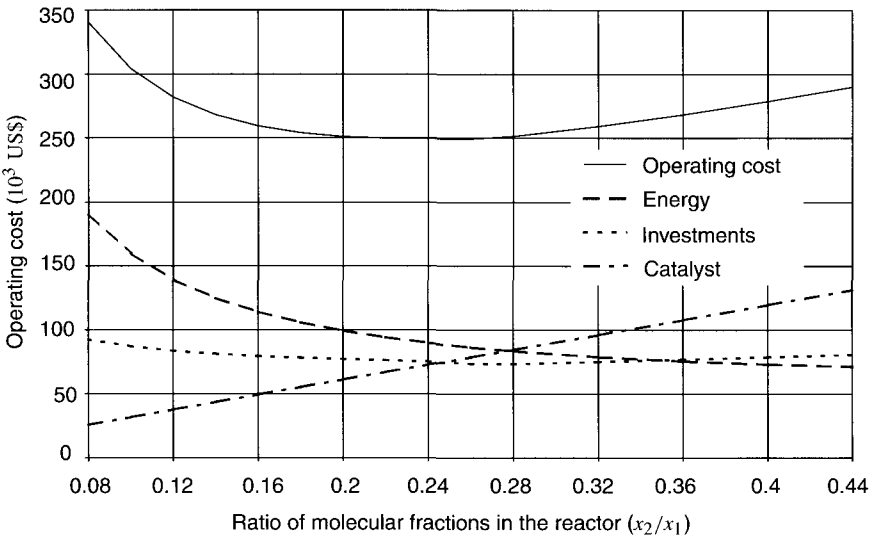


Figure 9.24 Curves for the operating cost and the key components as a function of the parameter x_2/x_1

Table 9.7 Characteristics of the principal equipment at the optimum.

Equipment	Characteristic dimension	Power	Cost (10^3 US$)
Reactor	27.5 m^3	$7.87 \cdot 10^5$ kcal/h	440.7
Pump P1	1.65 m^3/h	0.9 kW	4.5
Pump P2	4.61 m^3/h	2.52 kW	6.66
Exchanger E1	1.28 m^2	$5.6 \cdot 10^4$ kcal/h	29
Exchanger E2	25.07 m^2	$7.46 \cdot 10^5$ kcal/h	171
Exchanger E3	6.06 m^2	$1.58 \cdot 10^5$ kcal/h	74

Figure 9.25 provides the percentage distribution of the various components of the operating cost. The most important are the investment for the reactor and the exchangers; the pumps represent a much smaller investment. The steam and the catalyst are the most significant utility costs, while electricity and water are negligible. The total annual operating cost for our optimization is \$250 000 per year, or \$25 per ton of acetone produced. Some of the parameters involved could be easily modified to determine the sensitivity of operating cost to a given parameter.

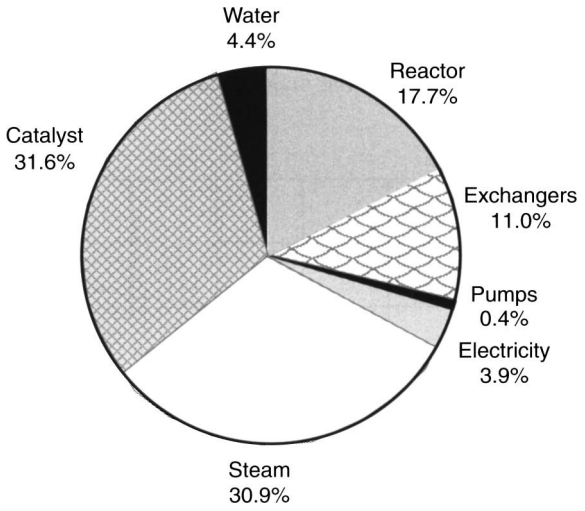


Figure 9.25 Percentage distribution of the various components of operating cost.

The cost of the catalyst is high. Note that the catalyst lifetime has a significant influence on the position of the optimum. However, very often the consumption of catalyst is associated with production capacity; this is the case whenever catalyst deactivation is the result of an impurity in the feedstock. The optimum value of $[x_2/x_1]$ is then independent of the catalyst lifetime, which plays a role in the operating cost as the price of a chemical product, expressed in \$/kg of acetone produced.

9.4.7 Final reactor design

Once the optimum has been determined, the reactor volume is established and its dimensions can be calculated:

- diameter $(D) = 3.23$ m
- height $= 4.20$ m.

The lateral surface of the tank available for heat exchange is easily calculated and is found to be 44 m^2. The heat exchange capacity of the wall, equipped with a welded coil on the outside, can then be evaluated by assuming that the hot fluid is steam at 16 bar and 200°C. The global heat exchange coefficient has been estimated to be 350 $kcal/m^2 \cdot K \cdot h$.

We see that the exchange surface is inadequate for exchanging the required amount of heat. Therefore, an additional surface will be added by arranging a double-wall guide cylinder around the impeller and by introducing steam into this cylinder. A cylinder whose diameter is equal to $D/1.414$ and whose height is equal to $D \cdot 0.75$ could easily be used and would supply a much larger heat exchange surface than is needed. In this case we would have excess exchange surface, which can be used to compensate for any fouling of the exchange surfaces. Also, the guide cylinder will serve as a baffle and channel the circulation of liquid in the vessel, thereby promoting transfer at the walls.

The impeller power (which, based on the previous calculations, is equal to 0.8 kW/m^3 with a power number $N_P = 0.65$) can be used to calculate the speed of rotation of the helical stirrer used as an impeller [Euzen, 2000]:

$$N_R = 1.54 \text{ rev/s}$$

and the mixing time based on the action of the impeller:

$$\text{Mixing time} = 40/(N_R \cdot N_P) = 40 \text{ s}$$

which can be compared to the mean residence time in the reactor:

$$\text{Mean residence time} = \text{volume}/(\text{feed flow rate} + \text{recycle flow rate}) = 3 \text{ h}$$

The assumption of perfect mixing is, therefore, justified.

We can also calculate the impeller's pumping rate:

$$Q(\text{helical stirrer}) = N_Q N_R D_A^3$$

When $N_Q = 0.73$, we obtain Q(helical stirrer) = 4.75 m^3/s.

We can also verify that the free surface at the top of the reactor is sufficient for the removal of the vapor effluent. The following equation can be used to calculate the critical entrainment velocity [Trambouze *et al.*, 2000]:

$$U_G^* = 0.381 \cdot 0.2 \cdot \sqrt{\frac{\rho_L - \rho_G}{\rho_G}} \quad \text{(m/s)}$$

Thus, given the conditions used for the reactor:

$$U_G^* = 0.075 \quad \text{(m/s)}$$

while the velocity of the vapor phase leaving the liquid surface at the top of the reactor is equal to 0.003 m/s, much lower than the critical entrainment velocity.

9.4.8 Concluding remarks

The above case is an example of how to design a catalytic reactor with a suspended catalyst, a reactor often found in practice, especially for the production of fine chemicals. We have tried to show that the technical information provided by the reaction chemistry is not always sufficient to determine the operating conditions and that cost factors must be taken into account to finalize our technical choices.

9.5 FIXED-BED CATALYTIC REACTORS WITH TWO FLUID PHASES

9.5.1 Fundamental data

Here we want to desulfurize a straight run gas-oil to reduce its sulfur content from 2.52% to 0.010% in a fixed-bed catalytic reactor. The flow rate to be processed is 43 400 kg/h. The gas-oil has the following characteristics:

- density at 15°C: 842 kg/m^3
- density at 350°C: 570 kg/m^3

- kinematic viscosity at 50°C: 2.8 mm^2/s
- kinematic viscosity at 360°C: 0.2 mm^2/s
- sulfur content: 2.52% by weight
- average molecular weight: 220 kg/kmol
- specific heat at 350°C: 0.77 kcal/kg ·°C (3.22 kJ/kg ·°C).

We want to establish the dimensions of the reactor, taking into account the following elements:

- the feedstock is heated to 363°C at the reactor inlet
- the total pressure at the reactor outlet is kept at 50 bar ($5 \cdot 10^6$ Pa), while the partial pressure of hydrogen must remain greater than or equal to 40 bar ($4 \cdot 10^6$ Pa) throughout the reactor.

The gas-oil contains a large number of constituents, not all of which contain sulfur. These are represented by two fictive compounds, one of which refers to the sulfur-containing molecules (A_4) and the other the unsulfured molecules (A_5). This leads to the following stoichiometric equation:

$$2.9A_1 + A_4 = A_2 + A_5$$

where

A_1 H_2
A_2 H_2S
A_3 inert CH_4 (5%) present in the feed hydrogen
A_4 sulfured gas-oil
A_5 desulfurized gas-oil.

Estimates of the molecular weights of the different gas-oil molecules:

$$M_5 = 220 \text{ kg/kmol}$$
$$M_4 = M_5 + M_2 - 2.9M_1 = 220 + 34 - 5.8 = 248.2 \text{ kg/kmol}$$

The results of desulfurization tests conducted in a fixed-bed pilot unit operating isothermally and using the same catalyst (Fig. 9.26) lead to the identification of only two families of sulfur-containing compounds, depending on whether the sulfur is easy (S_1) or difficult (S_2) to eliminate (see the sections on lumping in Chapter 1). The results can be correctly represented by means of an apparent kinetics comprising two first-order reactions of the following form:

$$S = S_1 + S_2 = 0.95S_0 \exp\left(\frac{-K_1}{LHSV}\right) + 0.05S_0 \exp\left(\frac{-K_2}{LHSV}\right)$$

where

S sulfur content (weight %)
S_0 sulfur content of gas-oil in the feedstock (weight %)
$LHSV$ liquid hourly space velocity, $LHSV = Q_L/V_{cata}$ (h^{-1})
Q_L volumetric flow rate, here measured at 15°C (m^3/h)
V_{cata} catalyst volume (m^3)
K_1 rate constant of the fastest reaction $K_1 = 19.2\ h^{-1}$ at 363°C
K_2 rate constant of the slowest reaction $K_2 = 2.9\ h^{-1}$ at 363°C.

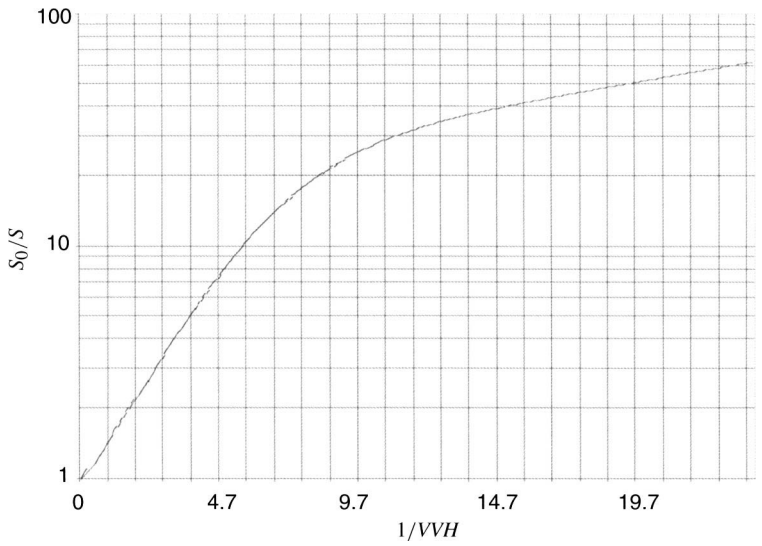


Figure 9.26 Kinetics of the hydrodesulfurization of gas-oil.

For each of the reactions the activation energy, E, is 30 kcal/mol (125 kJ/mol) and the enthalpy of reaction, ΔH_R, is −0.67 kcal/l STP (2.18 kJ/l STP of hydrogen consumed).

The global conversion is defined by:

$$X = \frac{S_0 - S}{S_0}$$

Here, we want to obtain $X = (2.52 - 0.01)/2.52 = 0.996$.

The catalyst consists of a cobalt molybdate type deposited on alumina extrudates and has the following characteristics:

- mean diameter of the extrudates: 1.2 mm
- mean length of extrudates: 3.6 mm
- equivalent diameter: $\overline{d_l} = 1.5$ mm
- density of the particles: $\rho_p = 1\,110$ kg/m^3
- porosity of the particles: $\theta = 0.5$
- tortuosity factor: $\tau = 3$
- density of the bed: $\rho_c = 670$ kg/m^3
- void fraction of the bed: $1 - \varepsilon_p = 0.4$.

9.5.2 Process flow diagram

Fresh hydrogen, possibly together with recycled hydrogen, is added to the raw feedstock before it enters a furnace that brings the mixture to the inlet temperature of the first bed (363°C) (Fig. 9.27).

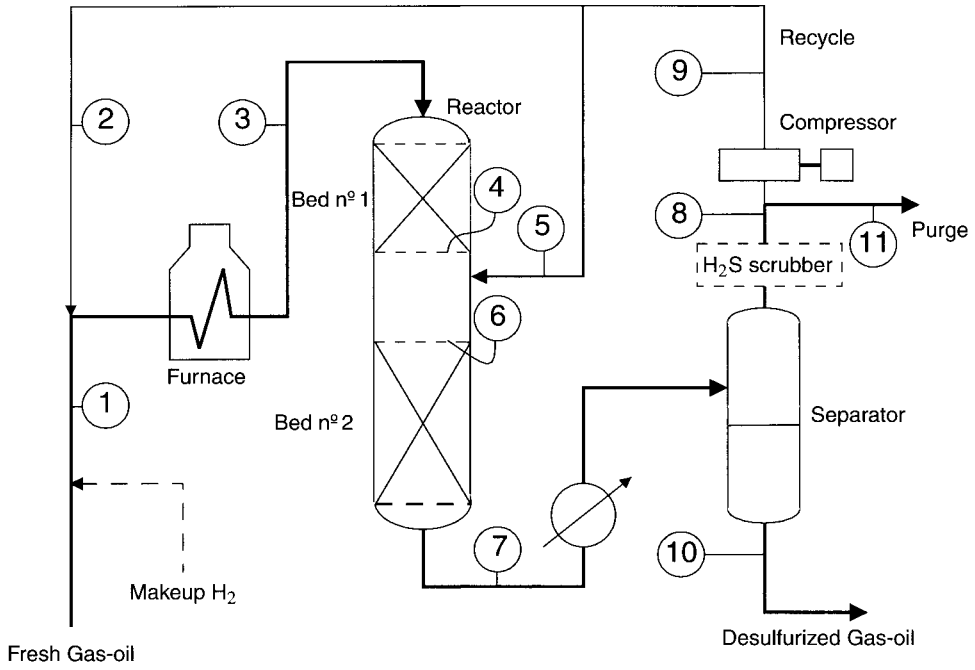


Figure 9.27 Process flow diagram for the hydrodesulfurization of gas-oil.

Due to the temperature increase in the first bed, effluents from the bed must be cooled with a stream of cold recycled hydrogen. The mixture, raised to the same temperature as the inlet temperature in the first bed, is fed into the second bed, where it undergoes the desired conversion. The reactor effluent is then cooled and separated into a liquid and a gas phase. The liquid phase is the desulfurized gas-oil according to the specifications. The gas mixture, which contains hydrogen, methane, and hydrogen sulphide, is stripped of its H_2S in a scrubber before being split into a purge line and a recycle line. After the pressure is restored, the recycled gas is returned to the inlet of the second catalytic bed and to the inlet of the furnace located upstream of the reactor. This arrangement can be used to reduce the consumption of make-up hydrogen.

9.5.3 Material and heat balances

The material balance is established, as weight and molar balances ($F_{i,j}$), for each compound i ($i = 1$ to 5, T for the total) and each line ($j = 1$ to 11), numbered as shown in the process flow diagram, taking into account the following elements:

- global balances
- local balances (at the network nodes)
- specific balances (kinetic, heat, physical equilibrium).

Below we examine some specific equations relating to these balances.

9.5.3.1 Global balances

• **Gas-oil**

The flow rate of sulfur in the feedstock is 43 400(0.0252/32) = 34.18 katoms/h of sulfur. If, for the purpose of simplification, it is assumed that each molecule of sulfur-containing gas-oil contains one atom of sulfur, we have:

$$F_{4,1} = 34.18 \text{ kmol/h of sulfur-containing gas-oil}$$

and, taking the difference:

$$F_{5,1} = \frac{43\,400 - 34.18 \cdot 248.2}{220} = 158.71 \text{ kmol/h of desulfurized gas-oil.}$$

At the separator outlet, the flow rate of unprocessed sulfur-containing gas-oil is:

$$F_{4,10} = (1 - X)F_{4,1} = 4 \cdot 10^{-3} F_{4,1} = 0.14 \text{ kmol/h}$$

• **Hydrogen**

The total consumption of hydrogen is:

$$CONSH = 2.9\left(F_{4,1} - F_{4,10}\right) = 2.9 \cdot 0.996 \cdot 34.18 = 98.72 \text{ kmol/h}$$

or

$$CONSH = 98.72 \cdot 22.4 = 2\,211 \text{ Nm}^3/\text{h}$$

The composition of make-up hydrogen leads to the following equation:

$$F_{1,1} = 19 \cdot F_{3,1}$$

• **H_2S**

Since 1 mole of H_2S is produced when 2.9 moles of hydrogen are consumed, the production of H_2S is as follows:

$$F_{2,7} = \frac{98.72}{2.9} = 34.04 \text{ kmol/h}$$

9.5.3.2 Local balances

For each constituent A_i, the following specific equations can be written:

$$F_{i,2} = R_2 \cdot F_{i,9} \quad \text{(this equation defines the recycle ratio } R_2\text{)}$$
$$F_{i,3} = F_{i,1} + F_{i,2}$$
$$F_{i,4} = F_{i,3} + \nu_i CONSH/(2 \cdot 2.9)$$
$$F_{i,5} = R_5 \cdot F_{i,9} \quad \text{(this equation defines the recycle ratio } R_5\text{)}$$
$$R_5 + R_2 = 1$$
$$F_{i,6} = F_{i,4} + F_{i,5}$$
$$F_{i,7} = F_{i,6} + \nu_i CONSH/(2 \cdot 2.9) \quad \text{(second catalytic bed)}$$
$$F_{i,8} = F_{i,7} - F_{i,10}, \quad \text{except when } i = 2 \text{ because of the scrubber}$$
$$F_{i,9} = R \cdot F_{i,8} \quad \text{(this equation defines the recycle ratio } R\text{)}$$
$$F_{i,11} = (1 - R)F_{i,8}$$

It is assumed that the scrubber is perfectly efficient and removes all, and only, the hydrogen sulphide ($F_{2,8} = 0$). Eighty percent of the gas flow that leaves the scrubber ($R = 0.80$) will be recycled.

9.5.3.3 Heat balance

The consumption of hydrogen results in the production of heat; this heat is equal to:

$$Q_R = 0.67 \cdot 2\,211 \cdot 10^3 = 1.48 \cdot 10^6 \text{ kcal/h}$$

To simplify the calculations we will assume that this heat warms the liquid feed only; the temperature increase in the reactor can then be estimated by:

$$\Delta T = \frac{Q_R}{43\,400 \cdot C_P} = \frac{1.48 \cdot 10^6}{43\,400 \cdot 0.77} = 44°C$$

There is a risk that this temperature increase will lead to catalyst degradation, and therefore the catalyst must be arranged in two beds, separated by an intermediate cooling unit. Here, we will distribute the heat of reaction equally between each of the beds.

The temperature of the effluents from the first bed must be brought to 363°C using a recycled gas whose temperature will rise from 60°C (the assumed temperature at the compressor outlet) to 363°C after mixing:

$$RR_5 \left(F_{1,8} + F_{2,8} + F_{3,8}\right) \overline{C_P}(363 - 60) = Q_R/2$$

$\overline{C_P}$ is the mean value, between 60 and 363°C, of the specific heat of the recycled gas mixture: $\overline{C_P} = 8$ cal/(mol · °C).

9.5.3.4 Liquid-vapor equilibrium equations

$$K_{ei} = \frac{y_i}{x_i}$$

x_i and y_i are the molar fractions of component A_i in the liquid and in the gas phase; the values of the coefficients K_{ei} are provided in the *API Technical Data Book*:

- at 50°C and 50 bar: $K_{e1} = 32$; $K_{e2} = 1.6$; $K_{e3} = 5$; $K_{e4} = K_{e5} \cong 0$
- at 370°C and 50 bar: $K_{e1} = 9.5$; $K_{e2} = 3.3$; $K_{e3} = 5$; $K_{e4} = K_{e5} = 0.08$.

9.5.3.5 Results

If we take into account all the equations and pressure constraints at the reactor outlet, we obtain the molar and mass flow rates shown in Tables 9.8 and 9.9.

9.5.4 Examination of diffusion limitations

For a first-order reaction, it is possible to evaluate the influence of the diffusion limitation inside the catalyst pores using the Thiele modulus, which can be written as shown below for each of the reactions (see Chapter 6):

$$\Phi_1 = \frac{\overline{d_p}}{2}\sqrt{\frac{k_{M1}\rho_p}{\mathcal{D}_{e4}}} \quad \text{and} \quad \Phi_2 = \frac{\overline{d_p}}{2}\sqrt{\frac{k_{M2}\rho_p}{\mathcal{D}_{e4}}}$$

Table 9.8 Molar balances (kmol/h).

Compound	Line	1	2	3	4	5	6	7	8	9	10	11
H_2	A1	190.98	22.16	213.14	163.78	324.08	487.86	438.50	432.80	346.24	5.70	86.56
H_2S	A2	0.00	0.00	0.00	17.02	0.00	17.02	34.04	0.00	0.00	7.10	0.00
CH_4	A3	10.05	1.81	11.86	11.86	26.47	38.34	38.34	35.36	28.28	2.98	7.07
Sulfur-containing gas-oil	A4	34.18	0.00	34.18	17.16	0.00	17.16	0.14	0.00	0.00	0.14	0.00
Desulfurized gas-oil	A5	158.71	0.00	158.71	175.73	0.00	175.73	192.76	0.00	0.00	192.76	0.00
Total		393.92	23.97	417.89	385.55	350.55	736.10	703.76	468.15	374.52	208.67	93.63

Table 9.9 Mass balances (kg/h).

Compound	Line	1	2	3	4	5	6	7	8	9	10	11
H_2	A1	382	44	426	328	648	976	877	866	692	11	173
H_2S	A2	0	0	0	579	0	579	1 157	0	0	241	0
CH_4	A3	161	29	190	190	424	613	613	566	453	48	113
Sulfur-containing gas-oil	A4	8 483	0	8 483	4 258	0	4 258	34	0	0	34	0
Desulfurized gas-oil	A5	34 917	0	34 917	38 662	0	38 662	42 406	0	0	42 406	0
Total		43 943	73	44 016	44 016	1 072	45 088	45 088	1 431	1 145	42 740	286

with the general relation,

$$\eta = \frac{3}{\Phi}\left[\frac{1}{\text{th}\,\Phi} - \frac{1}{\Phi}\right]$$

We will now estimate the various parameters for the equations:

- $\overline{d_p} = 6\Sigma V/\Sigma S = 1.5 \cdot 10^{-3}$ m.
- $\mathcal{D}_{e4} = \mathcal{D}_{4,L}\theta/\tau$, where $\mathcal{D}_{4,L}$ for the gas-oil, estimated by means of the equation of Wilke and Chang [Poling *et al.*, 2001], is:

$$\mathcal{D}_{4,L} = 0.18 \cdot 10^{-3}\ \text{cm}^2/\text{s}, \quad \text{then} \quad \mathcal{D}_{e4} = 2.8 \cdot 10^{-9}\ \text{m}^2/\text{s} \quad \text{or} \quad 1.0 \cdot 10^{-5}\ \text{m}^2/\text{h}$$

- Based on the apparent constants obtained at 363°C ($K_1 = 19.2\ \text{h}^{-1}$ and $K_2 = 2.9\ \text{h}^{-1}$), we will try to determine the "true" kinetic constants:

The global transfer coefficient K_4 can be calculated by means of the following formula:

$$\frac{1}{K_4} = \frac{1}{k_{4,S}} + \frac{\mathcal{A}_S}{-\nu_4 k_M \eta \rho_c}$$

which can be simplified since, as we show below, external transfer does not play a role: $K_4\mathcal{A}_S = -\nu_4 k_M \eta \rho_c$.

We then have, for each of the reactions:

$$k_{M1}\rho_p = k_{M1}\rho_c\frac{\rho_p}{\rho_c} = \frac{K_1}{\eta_1}\frac{1}{\varepsilon_p} = \frac{K_1}{0.6\eta_1}$$

$$k_{M2}\rho_p = k_{M2}\rho_c\frac{\rho_p}{\rho_c} = \frac{K_2}{\eta_1}\frac{1}{\varepsilon_p} = \frac{K_2}{0.6\eta_1}$$

At 363°C the effectiveness factor for each of the reactions is:

$$\eta_1 = 0.89 \quad \text{for the fastest reaction and}$$
$$\eta_2 = 0.98 \quad \text{for the slowest reaction}$$

The "true" kinetic constants can then be obtained:

$$k_{M1}\rho_p = \frac{K_1}{0.6\eta_1} = 35.8 \quad \text{and} \quad k_{M2}\rho_p = \frac{K_2}{0.6\eta_1} = 4.92$$

These "true" kinetic constants can be used to calculate, at each point in the catalytic beds, the corresponding Thiele modulus as a function of K_1 and K_2, which vary with the temperature according to the Arrhenius law, so that:

$$\Phi_1 = \frac{\overline{d_p}}{2}\sqrt{\frac{35.8 \cdot \exp\left[\dfrac{-E}{R}\left(\dfrac{1}{T} - \dfrac{1}{636}\right)\right]}{\mathcal{D}_{e4}}}$$

and:

$$\Phi_2 = \frac{\overline{d_p}}{2}\sqrt{\frac{4.92 \cdot \exp\left[\frac{-E}{R}\left(\frac{1}{T} - \frac{1}{636}\right)\right]}{\mathcal{D}_{e4}}}$$

The values for effectiveness factors, η_1 and η_2, can be determined directly from the general formula indicated above. Note that, as shown in Fig. 9.28, the values obtained change significantly depending on the reaction and the position in the catalytic bed. For the slowest reaction, the values remain greater than 0.95, which enables us to treat diffusion limitations as negligible for that reaction. In contrast, for the fastest reaction, the effectiveness factor decreases from 0.89 to about 0.80, and this cannot be ignored. The lowest values are found at the outlets of the beds, where the temperature is highest.

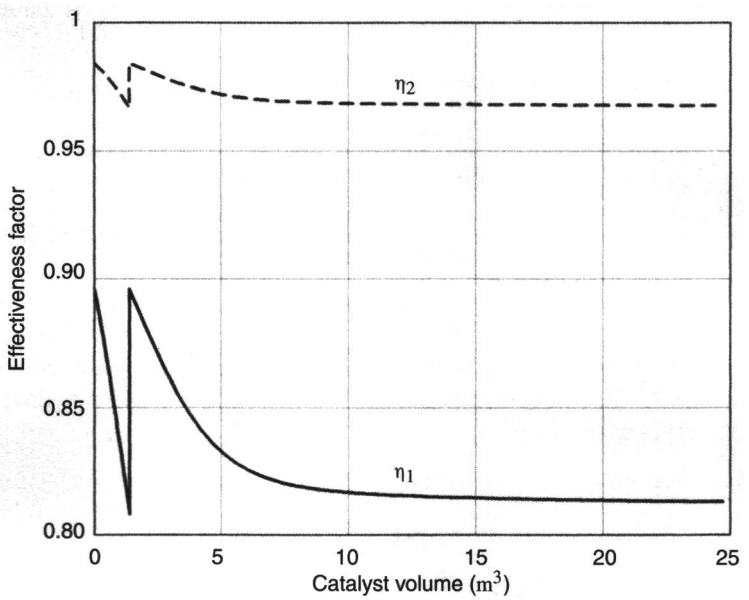


Figure 9.28 Profiles of effectiveness factors throughout each of the reactor's catalytic beds.

Calculations for the effectiveness factors must, therefore, be included in the system of equations shown below (see Section 9.5.6), which are then integrated step-by-step to obtain the reactor volume.

9.5.5 Calculating the transfer parameters

To evaluate the influence of transfer on the hydrogen and the gas-oil, the correlations shown in Section 8.2.3.1.B are used and applied to the inlet conditions for the first bed ($P \cong 50$ bar, $T = 640$ K), where the concentrations and gradients are the strongest.

9.5.5.1 Hydrogen

Since we are considering a steady state, there is no product accumulation at the interfaces or within the phases. The continuous consumption of hydrogen by the chemical reaction is then equal to the flux of hydrogen through each interface, which is expressed as follows:

$$N_{\mathrm{I}} = k_{\mathrm{I,G}}\mathcal{A}_{\mathrm{LG}}\left(C_{\mathrm{I,G}} - C^{*}_{\mathrm{I,G}}\right) = k_{\mathrm{I,L}}\mathcal{A}_{\mathrm{LG}}\left(C^{*}_{\mathrm{I,L}} - C_{\mathrm{I,L}}\right) = k_{\mathrm{I,S}}\mathcal{A}_{\mathrm{S}}\left(C_{\mathrm{I,L}} - C_{\mathrm{I,S}}\right)$$

The consumption of hydrogen must be evaluated at the reactor inlet, where it is at a maximum. Given the stoichiometry, we can write:

$$\frac{\mathrm{d}F_{\mathrm{I}}}{\mathrm{d}V} = -2.9\frac{\mathrm{d}S}{\mathrm{d}V}\frac{Q_{\mathrm{L}}\rho_{\mathrm{L}}}{100 \cdot 32}$$

where Q_{L}, ρ_{L} are evaluated at the same temperature, 15°C, and $\mathrm{d}S/\mathrm{d}V$ is the result of the kinetic expressions.

At the inlet of the first bed, we have:

$$\frac{\mathrm{d}F_{\mathrm{I}}}{\mathrm{d}V} = 2.9\frac{[0.95 \cdot 19.2 + 0.05 \cdot 2.9]}{3\,600}\frac{2.52}{100}\frac{842}{32} = 9.8\ \mathrm{kmol/s \cdot m^3}$$

For the diffusion of hydrogen in the gas film, the estimate of Wilke and Lee [Poling, 2001] yields:

$$\mathcal{D}_{\mathrm{I,G}} = 50 \cdot 10^{-6}\ \mathrm{m^2/s}$$

For the diffusion of hydrogen in the liquid film, the equation of Wilke and Lee [Poling, 2001] is used with $M_{\mathrm{L}} = 220$ g/mol of gas-oil, $V_{\mathrm{ML}} = 14.3\ \mathrm{cm^3/mol}$ of hydrogen, T in K, μ_{L} of gas-oil in cP, and $\mathcal{D}_{\mathrm{L}}$ in $\mathrm{cm^2/s}$:

$$\mathcal{D}_{\mathrm{I,L}} = 7.4 \cdot 10^{-8}\frac{M_{\mathrm{L}}^{0.5}}{V_{ML}^{0.6}}\frac{T}{\mu_{\mathrm{L}}} = 7.4 \cdot 10^{-8}\frac{220^{0.5}}{14.3^{0.6}}\frac{640}{0.11} = 1.25 \cdot 10^{-3}\ \mathrm{cm^2/s} = 1.3 \cdot 10^{-7}\ \mathrm{m^2/s}$$

The specific area of the catalyst is:

$$\mathcal{A}_{\mathrm{S}} = \frac{6\varepsilon_{\mathrm{p}}}{\overline{d_{\mathrm{p}}}} = \frac{6 \cdot 0.6}{1.5 \cdot 10^{-3}} = 2\,400\ \mathrm{m^2/m^3}$$

The hydraulic diameter of the grains can be calculated by means of the following formula:

$$d_{\mathrm{h}} = \overline{d_{\mathrm{P}}}\left(\frac{16 \cdot (1-\varepsilon_{\mathrm{P}})^3}{9\pi\varepsilon_{\mathrm{P}}^2}\right)^{0.33} = 1.5 \cdot 10^{-3}\left(\frac{16 \cdot (1-0.6)^3}{9 \cdot 3.14 \cdot 0.6^2}\right)^{0.33} = 7 \cdot 10^{-4}\ \mathrm{m}$$

based on which:

$$\varphi = \frac{\mathcal{A}_{\mathrm{S}}d_{\mathrm{h}}}{\varepsilon_{\mathrm{p}}} = \frac{2\,400 \cdot 7 \cdot 10^{-4}}{0.6} = 2.8$$

The relevant dimensionless numbers have the following values:

$$\chi_G = \frac{G}{L}\sqrt{\frac{\rho_L}{\rho_G}} = \frac{0.56}{5.7}\sqrt{\frac{570}{18}} = 0.55$$

$$Re_L = \frac{Ld_p}{\mu_L} = \frac{5.7 \cdot 1.5 \cdot 10^{-3}}{1.14 \cdot 10^{-4}} = 75$$

$$Sc_{l,L} = \frac{\mu_L}{\rho_L \mathcal{D}_L} = \frac{1.14 \cdot 10^{-4}}{570 \cdot 1.25 \cdot 10^{-7}} = 1.6$$

$$Sc_{l,G} = \frac{\mu_G}{\rho_G \mathcal{D}_G} = \frac{15 \cdot 10^{-6}}{19 \cdot 50 \cdot 10^{-6}} = 0.016$$

$$We_L = \frac{L^2 d_P}{\rho_L \sigma_L} = \frac{5.7^2 \cdot 1.5 \cdot 10^{-3}}{570 \cdot 20 \cdot 10^{-3}} = 4.3 \cdot 10^{-3}$$

$$We_G = \frac{G^2 d_P}{\rho_G \sigma_L} = \frac{0.56^2 \cdot 1.5 \cdot 10^{-3}}{18.4 \cdot 20 \cdot 10^{-3}} = 1.3 \cdot 10^{-3}$$

$$Sh_{l,G} = \frac{k_{lG} \mathcal{A}_{GL} d_h^2}{\mathcal{D}_{l,G}}$$

$$Sh_{l,L} = \frac{k_{lL} \mathcal{A}_{GL} d_h^2}{\mathcal{D}_{l,L}}$$

- To estimate $\mathcal{A}_{GL}$, Eq. (8.62) is used:

$$\frac{\mathcal{A}_{GL}}{\mathcal{A}_S} = 1\,550 \chi_G^{0.7} Re_L^{-0.35} We_L^{0.7} \varphi^{-3.5} \tag{8.62}$$

and:

$$\frac{\mathcal{A}_{GL}}{\mathcal{A}_S} = 0.13$$

therefore:

$$\mathcal{A}_{GL} = 321 \text{ m}^2/\text{m}^3 \tag{9.14}$$

- To estimate $k_{l,L}$, Eq. (8.60) is used:

$$Sh_L = 0.45 \chi_G^{0.65} Re_L We_L^{0.26} Sc_L^{0.65} \varphi^{0.32} \tag{8.60}$$
$$Sh_L = 10$$

that is:

$$k_{l,L} \mathcal{A}_{GL} = Sh_L \frac{\mathcal{D}_{l,L}}{d_h^2} = 2.6 \text{ s}^{-1}$$

and therefore:

$$k_{l,L} = 8.2 \cdot 10^{-3} \text{ m/s}$$

- To estimate $k_{l,G}$ Eq. (8.61) is used:

$$Sh_G = 0.123\chi_G^{0.45} Re_L^{0.72} We_G^{0.27} Sc_G^{0.45} \varphi^{0.22} \tag{8.61}$$
$$Sh_G = 0.07$$

and therefore:

$$k_{l,G}\mathcal{A}_{GL} = Sh_G \frac{\mathcal{D}_{l,G}}{d_h^2} = 7\ s^{-1}$$

and:

$$k_{l,G} = 21 \cdot 10^{-3}\ m/s$$

- To estimate $k_{l,S}$, Eqs. (8.63) and (8.64) are used:

$$Sh_S = 0.49 Sc_L^{-0.33} \left(Re_L^*\right)^{0.5} \tag{8.63}$$

$$\text{valid for } 0.2 < \left(Re_L^* = Re_L' \frac{1-\varepsilon_p}{\varepsilon_{L\,dynamic}}\right) < 600 \tag{8.64}$$

where:

$$Re_L' = \frac{L\overline{d_p}}{\varepsilon_P \mu_L} = \frac{75}{0.6} = 125 \quad \text{and} \quad Re_L^* = 125\frac{0.4}{0.18} = 278$$

and therefore:

$$Sh_{l,S} = 7$$

and:

$$k_{l,S} = \frac{Sh_{l,S}\mathcal{D}_{l,L}}{\overline{d_P}} \frac{\varepsilon_P}{1-\varepsilon_P} = 9 \cdot 10^{-4}\ m/s$$

so that:

$$k_{l,S}\mathcal{A}_S = 2.1\ s^{-1}$$

- To estimate $C_{l,G}^*$:

$$k_{l,G}\mathcal{A}_{GL}\left(C_{l,G} - C_{l,G}^*\right) = 9.8\ mol/(s \cdot m^3)$$
$$k_{l,G}\mathcal{A}_{GL} = 7\ s^{-1}$$
$$C_{l,G} - C_{l,G}^* = \frac{P_l - P_l^*}{RT} = \frac{9.8}{7} = 1.4\ mol/m^3$$
$$P_l - P_l^* = 1.4 \cdot 83 \cdot 10^{-6} \cdot 640 = 0.07\ bar$$

Since P_l is greater than 40 bar, the difference $P_l - P_l^*$ is negligible. Therefore, on the gas side there is no limitation for the transfer of hydrogen from the gas to the liquid phase.

- To estimate $C_{l,L}$:

  At the interface, the gas and liquid are in equilibrium, so that:

$$K_{el} = \frac{y_l^*}{x_l^*} = 9.5$$

since $P_1 \cong P_1^*$:

$$y_1^* \cong \frac{P_1}{P}$$

At the reactor inlet, P_1/P is approximately 0.95, therefore:

$$x_1^* \cong 0.95/9.5 = 0.1$$

and:

$$C_{1,L}^* = \frac{x_1^* \rho_L}{M_L} = \frac{0.1 \cdot 570}{0.220} = 259 \text{ mol/m}^3$$

$$N_1 = k_{1,L} \mathcal{A}_{GL} \left(C_{1,L}^* - C_{1,L}\right) = 9.8 \text{ mol/(s} \cdot \text{m}^3)$$

and therefore:

$$C_{1,L} = 259 - 9.8/2.6 = 255 \text{ mol/m}^3$$

Since $C_{1,L}$ is very close to $C_{1,L}^*$, on the liquid side we can neglect the limitation of hydrogen transfer toward the liquid.

- To estimate $C_{1,S}$:

$$k_{1,S} \mathcal{A}_S \left(C_{1,L} - C_{1,S}\right) = 9.8 \text{ mol/(s} \cdot \text{m}^3)$$

$$k_{1,S} \mathcal{A}_S = 2.1 \text{ s}^{-1}$$

$$C_{1,S} = 255 - 9.8/2.1 = 251 \text{ mol/m}^3$$

The difference is negligible compared to the value of $C_{1,L}$. Therefore, there is no limitation, on the liquid film side, to impede the transfer of hydrogen from the liquid phase to the porous grain of the catalyst.

Finally, the hydrogen concentration profile from the gas phase to within the catalyst grain is practically flat (see Fig. 9.29).

9.5.5.2 Sulfur-containing molecules

Similarly, we can write:

$$\mathcal{D}_{4,L} = 0.18 \cdot 10^{-7} \text{ m}^2/\text{s}$$

$$Sc_{4,L} = 11$$

$$Sh_{4,S} = 3.7$$

$$k_{4,S} = 7 \cdot 10^{-5} \text{ m/s}$$

$$k_{4,S} \mathcal{A}_S = 0.16 \text{ s}^{-1}$$

$$k_{4,S} \mathcal{A}_S \left(C_{4,L} - C_{4,S}\right) = 3.4 \text{ mol/(s} \cdot \text{m}^3)$$

$$C_{4,L} - C_{4,S} = 21 \text{ mol/m}^3$$

This difference is small compared to the concentration of gas-oil in the liquid $C_{4,L}$, which, at the reactor inlet, is $C_{4,L} = 34.18/70 = 486 \text{ mol/m}^3$. For the gas-oil as well, the concentration profile near the surface of the particles is practically flat.

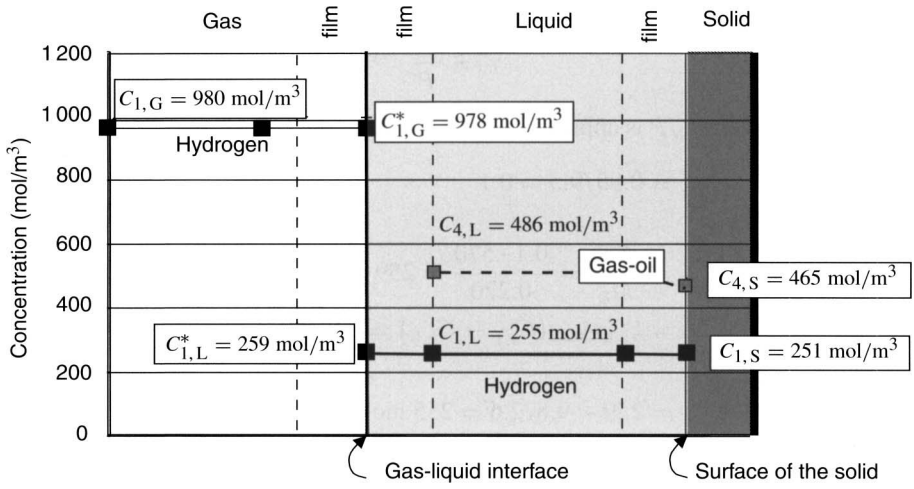


Figure 9.29 Concentration profiles of hydrogen and gas-oil at the reactor inlet.

9.5.6 Volume of catalyst needed

The volume of catalyst needed to reach the sulfur concentration required at the outlet can be calculated by assuming pure plug flow and by using the kinetic model, without neglecting the variation in the effectiveness factor. We must then simultaneously integrate the mass and heat balance equations and take into account the liquid-vapor equilibrium equations.

With respect to the mass balances, the kinetics gives us:

$$\frac{dS}{dV} = \frac{dS_1}{dV} + \frac{dS_2}{dV} = (k_{M1}\eta_1 S_1 + k_{M2}\eta_2 S_2)\,\rho_c \exp\left[\frac{E}{T}\left(\frac{1}{T_0} - \frac{1}{T}\right)\right]$$

With respect to the heat balances, we have:

$$\frac{dT}{dV} = \left(\frac{dS_1}{dV} + \frac{dS_2}{dV}\right)\frac{Q_R}{\Sigma F_i C_{Pi}}$$

where

T_0 temperature at the entrance to the bed = 636 K

Q_R heat of reaction for 1 atom of sulfur.

The curves in Fig. 9.30 illustrate the results of this calculation.

When the ratio of desulfurization reaches 0.498, half of the required value, the temperature is reduced to 363°C through the introduction of cold gas. At the entrance to the second bed, $\Sigma F_i C_{Pi}$ is reevaluated.

The catalyst volumes obtained are then:

$$V_1 = 1.40 \text{ m}^3$$

$$V_1 + V_2 = 24.70 \text{ m}^3$$

$$V_2 = 24.70 - 1.40 = 23.10 \text{ m}^3$$

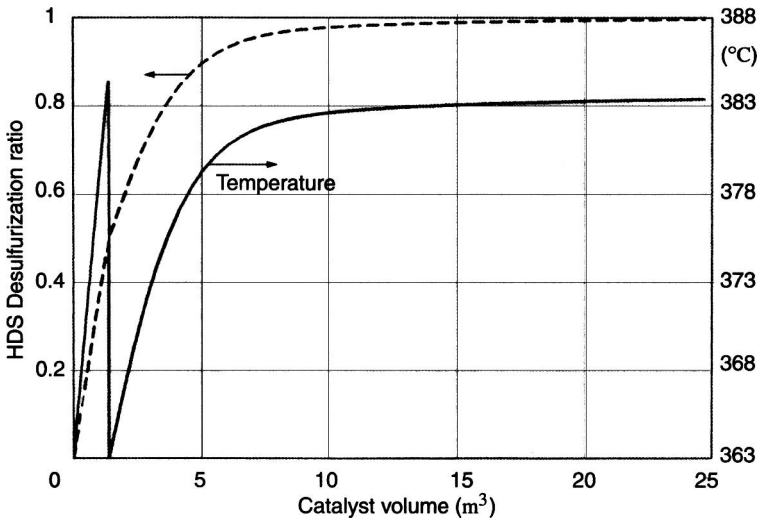


Figure 9.30 Change in temperature and desulfurization ratio in the reactor.

9.5.7 Calculating the reactor dimensions

The reactor dimensions are determined by the hydrodynamic criteria: we will use a liquid superficial velocity of 1 cm/s to maintain good distribution of the fluids in the bed. A calculation of the liquid-vapor equilibrium at the entrance of the first bed leads to a liquid phase mass flow rate of 40 085 kg/h, or a volumetric flow rate $Q_L = 40\,085/570 = 70.3\ m^3/h$, or $0.0195\ m^3/s$.

The reactor cross-section is $S = 0.0195/0.01 = 1.95\ m^2$ and consequently the internal diameter $D = 1.58$ m. The heights of the catalyst beds are then:

$$H_1 = 0.71 \text{ m}$$
$$H_2 = 11.93 \text{ m}$$

The total height of the reactor must take into account any internal components, that is, approximately 2 m for the fluid distribution zone and the fluid cooling zone between the beds, which gives:

$$H = 0.71 + 11.93 + 2 = 14.7 \text{ m}$$

9.5.8 Calculations for other equipment

9.5.8.1 Pressure drop through the bed

We will follow the procedure described in 8.2.3.1.A. If each of the fluid phases were to flow alone through the bed, the pressure drop could be calculated by means of Ergun's equation:

$$\delta = A\frac{\varepsilon_P^2}{(1-\varepsilon_p)^3}\frac{\mu_F V_{SF}}{\overline{d_P^2}} + B\frac{\varepsilon_p}{(1-\varepsilon_p)^3}\frac{\rho_F V_{SF}^2}{\overline{d_p}} \tag{8.49a}$$

where:

$$A = 150 \quad \varepsilon_p = 0.6$$
$$B = 1.75 \quad \overline{d_p} = 1.5 \cdot 10^{-3} \text{ m}$$

For the liquid phase, we have:

$$V_{SL} \cong 0.01 \text{ m/s}$$
$$\mu_L = 0.2 \cdot 10^{-6} \cdot 570 = 1.14 \cdot 10^{-4} \text{ Pa/s}$$
$$\rho_L = 570 \text{ kg/m}^3$$

and, therefore:

$$\delta'_L = 150 \cdot \frac{(0.6)^2}{(0.4)^3} \cdot \frac{1.14 \cdot 10^{-4} \cdot (0.01)}{(1.5)^2 \cdot 10^{-6}} + 1.75 \cdot \frac{0.6}{(0.4)^3} \cdot \frac{570 \cdot 10^{-4}}{1.5 \cdot 10^{-3}} \cdot \frac{570 \cdot (0.01)^2}{1.5 \cdot 10^{-3}}$$
$$\delta'_L = 1\,051 \text{ Pa/m}$$

For the gas phase, the flow rates and composition change between the inlet and outlet of the beds, but also from one bed to the other. Flash calculations lead to the following mean values:

	ρ_G (kg/m^3)	V_{SG} (m/s)
Bed 1: mean	18.4	0.03
Bed 2: mean	18.7	0.08

In the first bed, the pressure drop for the gas alone passing through the bed is then:

$$\delta'_G = 150 \cdot \frac{(0.6)^2}{(0.4)^3} \cdot \frac{\left(15 \cdot 10^{-6}\right) \cdot 0.03}{(1.5)^2 \cdot 10^{-6}} + 1.75 \cdot \frac{0.6}{(0.4)^3} \cdot \frac{19.1 \cdot (0.03)^2}{1.5 \cdot 10^{-3}}$$
$$\delta'_G = 360 \text{ Pa/m}$$

To calculate the pressure drop caused by the simultaneous passage of the two fluids, Eqs. (8.50) to (8.58) are used, which gives:

$$\chi_G = \sqrt{\frac{\delta'_G}{\delta'_L}} = 0.58$$

$$Re_L = \frac{\rho_L V_{SL} d_p}{\mu_L} = 75$$

$$We_L = \frac{(\rho_L V_{SL})^2 d_p}{\rho_L \sigma_L} = 0.0043$$

$$\kappa = \chi_G (Re_L We_L)^{0.25} = 0.44$$

$$FLGG = \kappa^{-1.5} \left(31.3 + 17.5 \cdot \kappa^{-0.5}\right) = 199$$

$$\delta_{GL} = FLGG \frac{2 \cdot \rho_G \cdot V_{SG}^2}{d_h} = 9\,620 \text{ Pa/m}$$

The liquid saturation ratio is:

$$\beta_L = 1 - 10^{-\Gamma}$$
$$\Gamma = 1.22 \cdot \chi_G^{-0.15} Re_L^{-0.20} We_L^{0.15} = 0.25$$

and, therefore:

$$\beta_L = 0.43$$

Finally, the pressure drop in the first bed is equal to:

$$\left(\frac{\Delta P}{H}\right)_{GL\,total} = \delta_{GL} - g\left[\beta_L \rho_L + (1 - \beta_L)\,\rho_G\right] = 7\,100 \text{ Pa/m}$$

Note that this pressure drop is much greater than the sum of the two pressure drops for the fluids by themselves.

In the second catalytic bed, the pressure drop, calculated in the same way, leads to:

$$\left(\frac{\Delta P}{H}\right)_{GL\,total} = 15\,200 \text{ Pa/m}$$

The global pressure drop through the reactor is then:

$$\Delta P = 0.71 \times 7\,100 + 11.93 \times 15\,200 \cong 190\,000 \text{ Pa} = 1.9 \text{ bar}$$

This pressure variation is sufficiently low compared to the total pressure to justify the approximations made above.

9.5.8.2 Recycling compressor

The flux considered is for line 9, whose flow rate is 374 kmol/h, mostly hydrogen. The coefficient of compressibility γ is 1.4. The input conditions are as follows:

$$F_T = 374 \text{ kmol/h}$$
$$T_A = 50°C$$
$$P_A = 50 \text{ bar}$$
$$V_A = 200 \text{ m}^3/\text{h}$$

If we use 54 bar as the output compressor pressure, the compression ratio ρ is:

$$\rho = \frac{P_{out}}{P_{in}} \cong \frac{54}{50} = 1.08$$

An evaluation of the theoretical adiabatic power P_{TA} leads, following Chauvel [1981], to:

$$P_{TA} = \frac{P_A V_A}{26.5} \frac{\gamma}{\gamma - 1}\left(\rho^{\frac{\gamma-1}{\gamma}} - 1\right)$$
$$P_{TA} \cong 29 \text{ CV}$$

which, for a reciprocating compressor operating at 50% efficiency, leads to a real power of 60 HP.

The outlet temperature T_R of the compressor is then:

$$T_R = T_A \rho^{\frac{\gamma-1}{\gamma}} = 330 \text{ K} = 57°\text{C}$$

This temperature is quite suitable for the gas that is injected between the two beds to cool the effluents from the first catalytic bed.

9.5.9 Concluding remarks

The desulfurization of gas-oil is feasible under classical conditions. One important aspect that needs to be accounted for is the deactivation of the catalyst, but it exceeds the scope of our example. The relation between the desulfurization conditions and the cycle periods could be used to completely optimize the design of the unit.

REFERENCES

Appl M (1999) Ammonia, Wiley-VCH.

Chauvel A *et al.* (1981) Manual of Economic Analysis of Chemical Processes, McGraw-Hill, New York.

Danckwerts PV, Sharma MM (1966) The absorption of carbon dioxide into solutions of alkalis and amines. Chem Eng, October 1966, CE 244–280.

De Dietrich (1996) Documentation Cat F 04/96 Programme de fabrication.

Euzen J-P (2000) Agitation and Mixing Techniques. *In*: Petroleum Refining. Vol. 4: Materials and Equipment. Editions Technip, Paris.

Hugo P (1980) Anfahr- und Betriebsverhalten von exothermen Batch-Prozessen. Chem Ing Tech 52, 9, pp 712–723.

Kohl A, Nielsen R (1997) Gas Purification, 5th edition, Gulf Publishing Co.

Leprince P *et al.* (2000) Petroleum Refining. Vol. 3: Conversion Processes. Editions Technip, Paris.

Perry *et al.* (1984) Perry's Chemical Engineers Handbook, 6th Edition. McGraw-Hill, New York.

Poling B, Prausnitz J, O'Connell (2001) The properties of Gases and liquids, 5th edition. McGraw-Hill, New York.

Trambouze P *et al.* (2000) Petroleum Refining. Vol. 4: Materials and Equipment. Editions Technip, Paris.

Twigg MV *et al.* (1996) Catalyst Handbook, 2nd edition, Manson Publishing.

Copyrighted Materials
Copyright © 2004 Editions Technip Retrieved from www.knovel.com

10 Multifunctional Reactors and Future Developments

For the past ten years or so, references to "multifunctional reactors" have appeared in the literature [Agar and Ruppel, 1988; Westerterp, 1992; Hoffmann and Sundmacher, 1997; Agar, 1999]. The term refers to a large number of devices within which a transfer phenomenon (mass, energy, or momentum) and a chemical reaction take place, the goal being to improve the performance of the chemical reaction from the point of view of conversion and selectivity. A good idea of the meaning of the term can be gleaned by consulting the proceedings of an international symposium held in Amsterdam in April 1999; all of the 36 presentations were included in a special issue of *Chemical Engineering Science* (vol. 54, 1999).

The underlying concept, which, as we will show below, can involve various combinations of unit operations with one or more reactions, has the advantage of systematizing a number of disparate approaches and stimulating the creativity of research personnel. Note that in some cases, it is the chemical reaction that is coupled to a unit operation to improve its effectiveness, as is the case with reactive separation processes [Kreul *et al.*, 1999].

10.1 CLASSIFICATION OF MULTIFUNCTIONAL REACTORS

We can begin with the reactor classification provided in Chapter 1, and use as our initial criterion the location of the chemical reaction, namely: homogeneous gas or liquid phase, catalytic solid, or reactive solid. The second criterion refers to the unit operation coupled to the reaction:

- mass transfer and separation between phases, and their various combinations:
  - gas-liquid: absorption, evaporation, distillation, condensation
  - liquid-liquid: extraction
  - fluid-solid: adsorption, filtration, permeation
  - gas/liquid-reactive solid: dissolution, crystallization, sublimation
- energy transfer, including the following variants:
  - conduction through a wall
  - contact between phases
  - radiation
  - electrical current

- transfer of momentum, including the following variants:
  - friction, shear
  - gravitational or centrifugal acceleration
  - impulse or pressure.

As can be seen, there are a large number of possible combinations and, far from being exhaustive, we will describe only those operations that have actually been studied or implemented and which have the greatest potential interest. Table 10.1 lists a number of these variants. In the remainder of the chapter, we will describe those we feel have the greatest current or future importance.

10.2 REACTION WITH MASS TRANSFER

10.2.1 Reaction with adsorption

The above combination has been the subject of numerous studies, especially in the form of moving-bed reactive chromatography. Adsorption separation using a simulated moving bed (for example, the separation of p-xylene) has been extended to situations involving a simultaneous catalytic reaction by means of a solid catalyst mixed with the adsorbent [Bjorlund and Carr, 1995]. For reactions limited by thermodynamic equilibrium (hydrogenation of aromatics, methanol synthesis, esterification) [Kruglov, 1994; Mazzotti *et al.*, 1996], it is possible to shift this equilibrium by means of *in situ* separation. When complex reactions such as the oxidative coupling of methane are involved, the ethylene selectivity can be increased [Kruglov, 1996].

Periodic operation, by modulating the pressure of a fixed bed containing catalyst mixed with an adsorbent, has also been tried with success [Vaporciyan and Kadlec, 1989].

Another possibility for reversible reactions such as the synthesis of methanol, is to add to the reaction mixture an adsorbing solid that will capture the reaction product as it appears during the catalytic reaction [Westerterp, 1992] (Fig. 10.1).

10.2.2 Reaction with distillation

It is this combination that has, until today, seen the most widespread use and led to the interest in multifunctional reactors. The reaction can take place in the homogeneous liquid phase, the distillation being used to eliminate one or more reaction products and shift the equilibrium. The process has been used for a long time to carry out esterification reactions (acetates, for example) in batch or continuous mode (Fig. 10.2) [Corrigan and Stichweh, 1968; Hartig and Regner, 1971; Sawistowski and Pilvakis, 1988; Bessling *et al.*, 1998; Kreul *et al.*, 1999; Stichlmair and Frey, 1999].

Another implementation, which has had numerous industrial applications over the past ten years, involves the use of a solid catalyst within a distillation column [Podrebarac *et al.*, 1997; Fair, 1998]. For example, there have been several configurations for the synthesis of MTBE from isobutene and methanol, using ion-exchange resins as a catalyst. The principle remains the same, however; MTBE being less volatile than the reactants, is separated at the bottom of the column while the excess methanol is removed at the top (Fig. 10.3).

Table 10.1 Various ways of coupling a chemical reaction with a mass, heat, or momentum transfer phenomenon, along with typical examples.

Unit operation		Reaction location			
		Gas	**Liquid**	**Catalytic solid**	**Solid**
Mass transfer	Adsorption	Adsorbing solid	Adsorbing solid	Adsorbing solid	
	Vaporization Distillation Condensation	Condensation	Reactive distillation	Catalytic distillation	
	Absorption		Gas absorption		
	Extraction		Liquid extraction		
	Filtration	Membrane	Membrane	Reactive membrane	Filter
	Fluid-solid transfer	Polymerization	Crystallization Dissolution		Sublimation Drying
Energy transfer	Wall conduction	Solid wall	Solid wall	Solid wall	Solid wall
	Contact between phases	Liquid or solid	Gas or solid	Gas and/or liquid	Gas, liquid and/or solid
	Radiation	Emitter/Receptor	Emitter/Receptor	Emitter/Receptor	Emitter/Receptor
	Electricity	Electrode	Electrode	Electrode	Electrolyte
Momentum transfer	Friction Shear	Ejector	Impeller	Fluidization Pneumatic transport	Fluidization Pneumatic transport Extrusion
	Acceleration	Venturi	Centrifuge Hydrocyclone	Cyclone	Cyclone
	Impulse	Ultrasound	Ultrasound		Grinder

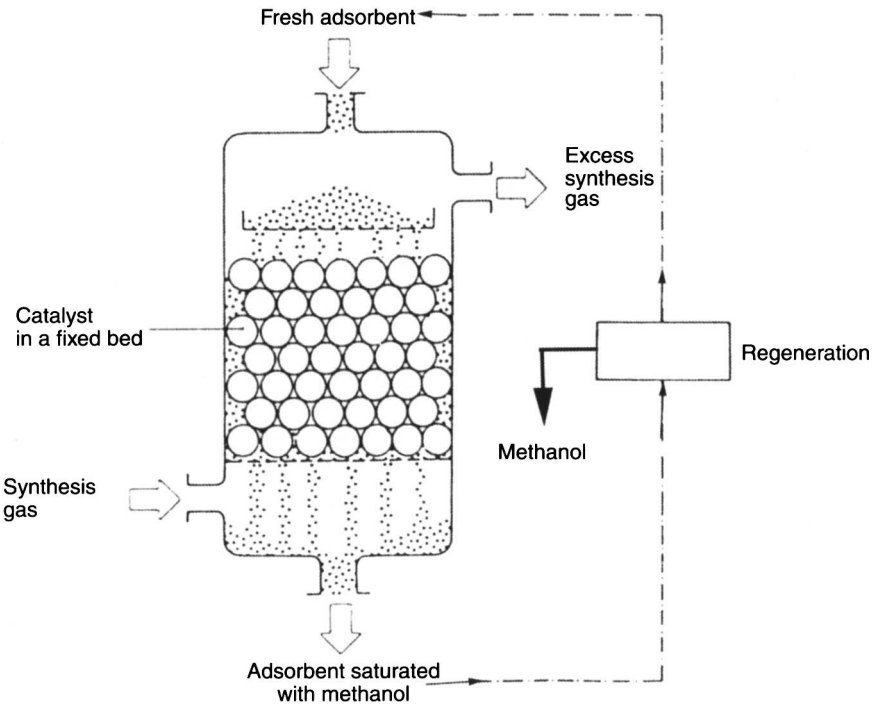


Figure 10.1 Catalytic reactor for the synthesis of methanol with adsorbent solid flow [based on Agar and Ruppel, 1988].

A number of other applications have been developed or are now in development: production of ETBE or TAME, hydration of olefins for the production of alcohol (TBA), dehydration of isopropyl alcohol, alkylation of benzene, esterification or hydrolysis [Podrebarac *et al.*, 1997]. The problem in these applications arises from the fact that the operating conditions for temperature and pressure required by the reaction are not always suitable for effective distillation. Moreover, conventional catalysts are not suitable for use as packing inside the column. Research has been conducted to develop suitable catalytic solids (rings and monoliths, for example) [Hoffmann and Sundmacher, 1997; Kapteijn *et al.*, 1999]. The use of structured packing has also been proposed; in this case catalyst is inserted into open areas within the packing structure. For such use the structured packing offered by Sulzer, where the packing consists of catalytic materials (Katapak), is an excellent solution [Stingaro and Luder, 1992].

The simple evaporation of a reaction product is also used for performing separations inside the reactor. In the hydrogenation of benzene, for example, the cyclohexane is entrained by the excess hydrogen (see Chapter 6), while the acetone obtained by the dehydrogenation of isopropyl alcohol is entrained by the hydrogen produced (see Chapter 9, Section 9.4).

The condensation of one of the reaction products has also been proposed, for example, for the synthesis of methanol [Hoffmann and Sundmacher, 1997; Amor and Halloin, 1999].

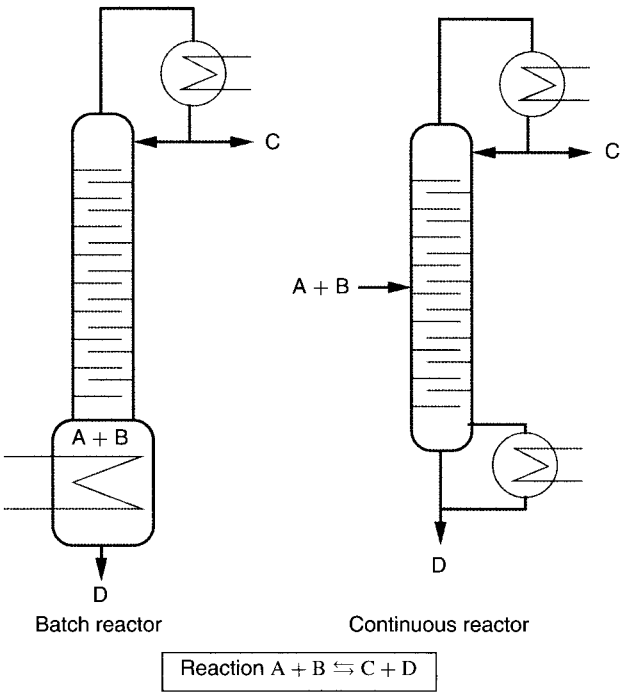


Figure 10.2 Reactive distillation: batch or continuous reaction.

10.2.3 Reaction with absorption

Gas-liquid reactors in which the reaction takes place in the liquid phase with one or more reactants supplied from the gas phase can also be considered multifunctional reactors. Liquid-phase oxidation, chlorination, and sulfonation are examples of such reactions. During the manufacture of nitric acid, the absorption of nitrous vapors is another noteworthy example since reactions occur in both phases (gas and liquid) with simultaneous absorption.

This coupling has also been practiced for years in the treatment of various gaseous elements for the elimination of impurities; the scrubbing of natural gas by amines is an example. In this case the process is primarily one of reactive separation, especially if we are also looking for a certain level of selectivity in the separation, as is the case for CO_2 and H_2S.

10.2.4 Reaction with extraction

As with gas-liquid systems, reactions with two liquid phases always involve extraction of at least one of the reactants. Frequently, one of the reaction products is itself re-extracted from the reaction phase and returned to the phase that provided the reactant [Samant and Ng, 1999].

An example of this process is the alkylation of olefins by isoparaffins in the presence of strong acids (sulfuric or hydrofluoric). The reaction takes place in the acid phase after

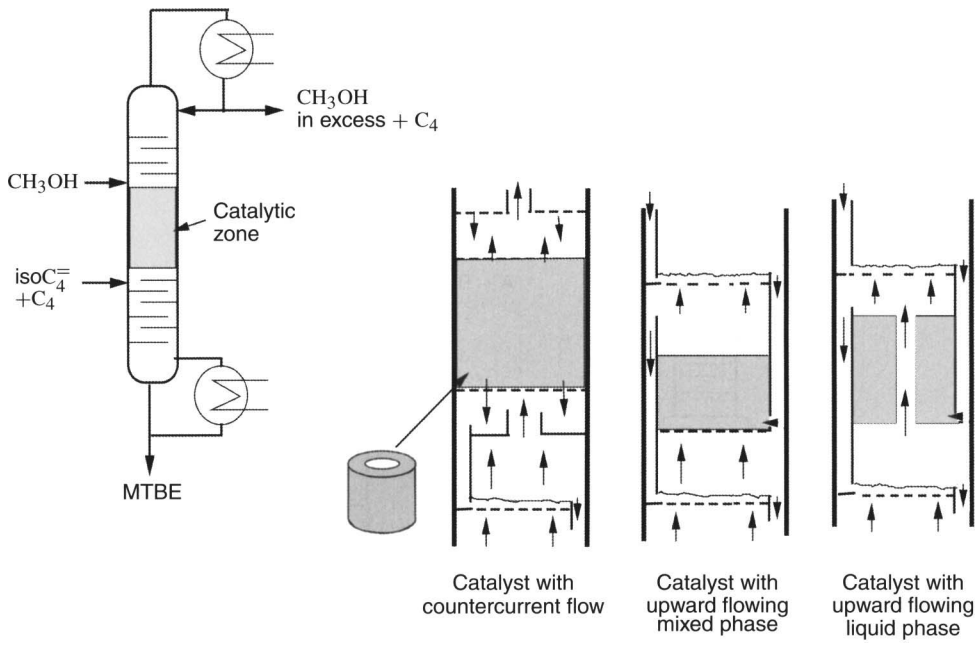


Figure 10.3 Catalytic distillation: basic procedure and possible variants.

extraction of the olefins and isoparaffins from the hydrocarbon phase. The reaction products (isooctanes) are again transferred to the organic phase. The selectivity of the transformation is heavily dependent on the rate of transfer between the phases [Trambouze *et al.*, 2000].

Many other reactions have been conducted in this way in industrial settings for years: nitration or sulfonation of aromatics, saponification of fatty acid esters, etc. Similarly, there are a number of industrial processes that involve extraction of a reactant by the reaction phase, followed by a re-extraction of the reaction products by the non-reaction phase. An example is the Merox process for sweetening gasoline or LPG [Leprince, 2000]. In this case the hydrocarbon cut contains mercaptans, which are extracted by an aqueous phase containing a catalyst, where they are transformed into disulfides. These are then re-extracted by the hydrocarbon phase.

Examples of coupling the reaction with gas absorption and extraction from the liquid reaction phase can also be found. For example, the Clauspol process is based on the simultaneous absorption of SO_2 and SH_2 in an organic phase in which the sulfur-producing reaction occurs. The sulfur leaves the reaction phase to form another liquid phase, which can be easily separated by decantation [Trambouze *et al.*, 1988].

Interesting applications will certainly be found for phase-transfer catalysis [Hoffmann and Sundmacher, 1997] and for the use of non-aqueous ionic media [Crabb, 2001], since such technologies can be used to resolve the difficult problem of separating homogeneous catalysts.

10.2.5 Reaction with filtration

Although filtration is essential during a catalytic reaction with a suspended catalyst, this is not, strictly speaking, a coupled operation. In contrast, if ultrafiltration or permeation are involved, the selectivity of this separation can benefit the reaction. A number of studies have been made in this field, using mineral or organic membranes [Tsotsis *et al.*, 1993; Saracco and Specchia, 1994; Dixon, 1999, Sanchez, 2002]. The membrane can be used only for the physical separation of a molecular species or can be catalytically active [Veldsink *et al.*, 1995; Neomagus *et al.*, 1998]. The introduction of one or more reactants through a membrane has also been proposed, so as to maintain the concentration of the key reactant at a low level, thereby increasing the selectivity (oxidative coupling of methane, for example).

Various types of membranes have been used: metallic, mineral, and organic polymers. The qualities required are selectivity of separation, rate of filtration, and resistance to temperature and pressure. Membrane separation can be coupled to a homogeneous or catalytic reaction. A number of basic configurations are possible (Fig. 10.4).

In general membranes can be used to improve the yield of reversible reactions or the selectivity to intermediate products for consecutive reactions [Agarwalla and Lund, 1992]. Palladium's permeability to hydrogen can be used for reactions that produce hydrogen, such as steam reforming, dehydrogenation, and the thermal decomposition of H_2S [Shu *et al.*, 1991; Edlund *et al.*, 1994; Amor, 1998]. In the case of catalytic reactions, membranes have also been studied for use with fixed beds [Tsotsis *et al.*, 1992] as well as with fluidized beds [Adris *et al.*, 1991].

Mineral and ceramic membranes have the great advantage of being capable of use at high temperature, although their selectivity is often poor.

Mention should also be made of the "particle filter," a technology that is likely to be rapidly put into widespread use and which is designed to catch fine particles contained in the exhaust gases of diesel engines. Particles are caught and burned *in situ* by various catalytic mechanisms.

The separation of a reaction product by pervaporation has also been proposed [Hoffmann and Sundmacher, 1997].

Polymer-based organic membranes provide considerable choice, often with very good selectivity. They are, however, limited to low-temperature use. A wide array of uses for these membranes exists in the field of biotechnology. Interesting applications have been found by coupling an ultrafiltration or pervaporation module to a fermenter or enzymatic reactor so as to selectively extract one of the reaction products [Cauwenberg *et al.*, 1999; Lipnizki *et al.*, 2000].

The concept of a catalytic liquid membrane has also been proposed; it involves inserting a porous solid impregnated with a liquid having catalytic properties between two conventional membranes (Fig. 10.4C). The reactants are introduced on either side of this membrane sandwich and react within the catalytic liquid phase, while the product of the reaction escapes through the membranes [Kim *et al.*, 1991].

Biofiltration couples several operations, with filtration being only a minor component of the process. The biofiltration process is designed to purify gas or liquid effluents containing

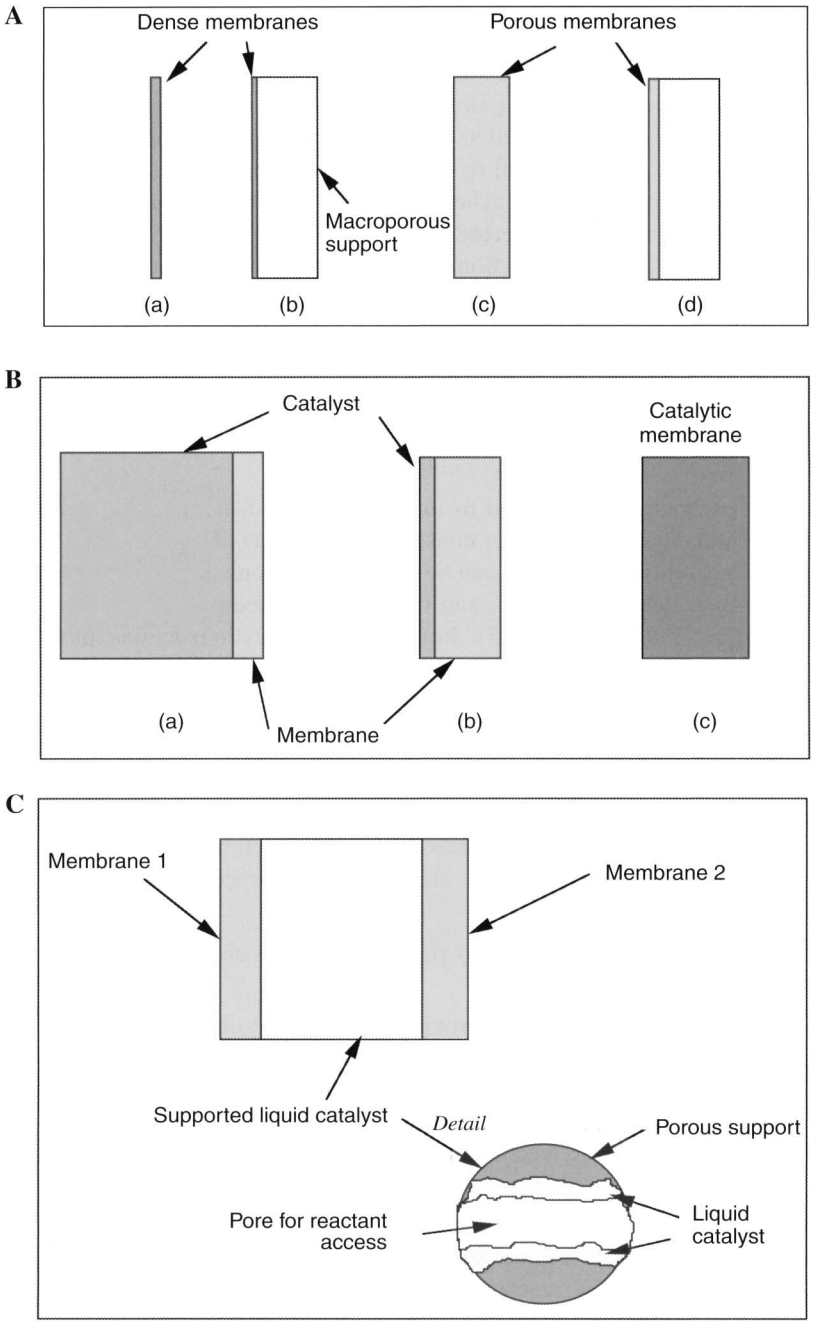


Figure 10.4 Various arrangements for the use of membranes: **A.** Dense and porous membranes used with a fluid phase. **B.** Membrane with an associated catalyst. **C.** Membranes with a supported liquid catalyst.

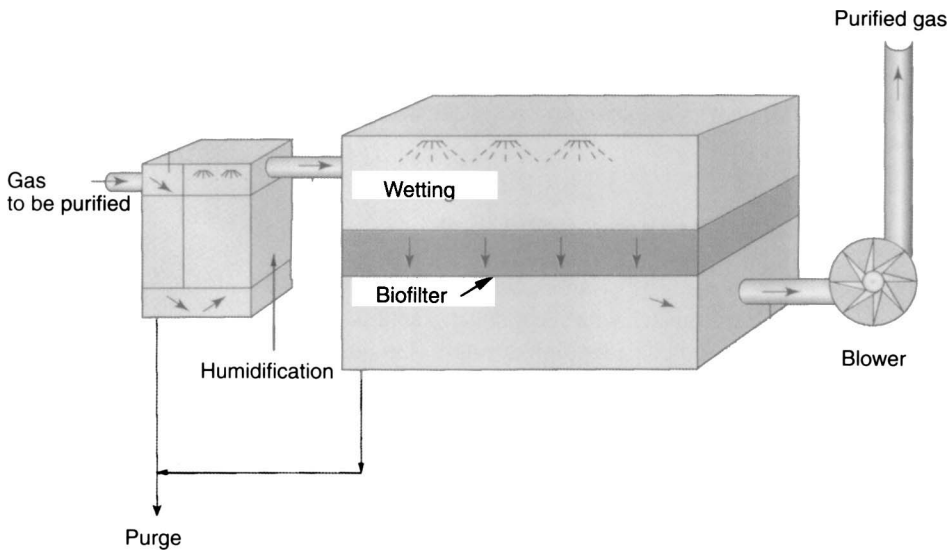


Figure 10.5 Configuration of a biofiltration system for treating gas effluents.

toxic products from various sources in generally low concentrations (Fig. 10.5). In the case of a gaseous effluent, the gas crosses a bed of porous materials containing microorganisms, forming what is sometimes referred to as a bacterial bed and which is wet by an aqueous phase needed to maintain the activity of the microorganisms [Adler, 2001].

10.2.6 Reaction with fluid-reactive solid transfer

Here the solid can be formed by precipitation or crystallization. The two operations are often inseparable and the texture of the solid obtained depends considerably on the reaction conditions [Mersmann *et al.*, 1994]. If the reaction is very fast, acid-base neutralization, for example, the solid obtained is highly divided and its properties (particle size, texture, crystallinity) may depend on the intensity of micromixing [Kim and Tarbell, 1996].

As in conventional crystallization, the supersaturation needed to obtain the solid can be produced by evaporation of a solvent, the heat of vaporization being supplied by the reaction [Harmsen and Chewter, 1999]. A number of examples of solid formation can be found in polymerization processes (Ziegler-Natta, metalocene, emulsion or melt), from either the gas or liquid phase.

The solid formation reaction can take place in a dryer by atomization, as is the case with several processes for SO_2 collection in flue gas, whether a liquid phase (sodium carbonate solution) or lime slurry is used. In both cases the evaporation of water enables the solid sulfite formation reaction to take place, the sulfite then being separated for further processing [Kohl and Nielsen, 1997].

The sublimation of a solid can also be coupled with a reaction to separate one of the reaction products, as in zinc metallurgy.

10.3 REACTION WITH ENERGY TRANSFER

The first method of energy transfer that comes to mind when we consider a reaction system is obviously heat transfer. This transfer can occur in various ways, but other energy vectors can also be used.

10.3.1 Heat transfer through the wall

It may appear to be something of an exaggeration to speak of a multifunctional reactor in the simple case of heat transfer with a chemical reaction. In fact, except in rare cases, heat transfer must be taken into consideration during a chemical reaction, whether exothermic or endothermic. However, the transfer is often designed to produce a temperature profile that is near an optimum, to obtain maximum conversion and selectivity. This is just as true for homogeneous phase (gas or liquid) reactions as it is for catalytic reactions.

Even if we consider the simple case of a batch reactor with a homogeneous reaction phase (see Chapter 2), the heat exchange capacity can be of considerable importance for ensuring the stability and, therefore, the safety of the operation.

In the case of exothermic catalytic reactions like the synthesis of ammonia or methanol, a large number of arrangements for reactor internals have been proposed for improving these high-tonnage yield processes (Fig. 10.6). In such cases it is legitimate to speak of multifunctional reactors, since synergy between various phenomena is sought for and achieved through the arrangement of heat exchange surfaces. The same could be said of multitubular, fluidized or entrained bed reactors. In this context another example is supplied by Fisher-Tropsch synthesis, which has made use of all the variants cited above for various industrial processes.

An interesting example of a case where heat transfer is tightly coupled to a highly exothermic reaction resulting from the absorption of a gaseous reactant is the sulfonation of olefins by SO_3 in a thin-film heat exchanger [Trambouze *et al.*, 1988].

10.3.2 Heat transfer by direct contact between the phases

Here too, it is a commonly held belief that in multiphase reaction systems, heat transfer between the phases is inevitable and, therefore, irrelevant to our subject. However, there are many occasions when the degree of this transfer must be modified to meet the requirements of the reaction. For example, the transition from a fixed bed to a fluidized bed may result from the need to increase heat exchange considerably with the solid, where the heat is generated or consumed, in order to keep the reaction temperature within the desired range.

A chemically inert phase can also be added to the reaction system; this phase, through heat exchange, will influence the change in temperature.

Similarly, it has been suggested that a liquid phase be added to a methanol synthesis reactor to provide better temperature control and avoid the quenching needed whenever the gas phase alone is in circulation [Galtier *et al.*, 1986]. The same idea has been proposed for the countercurrent circulation of a divided solid to eliminate heat.

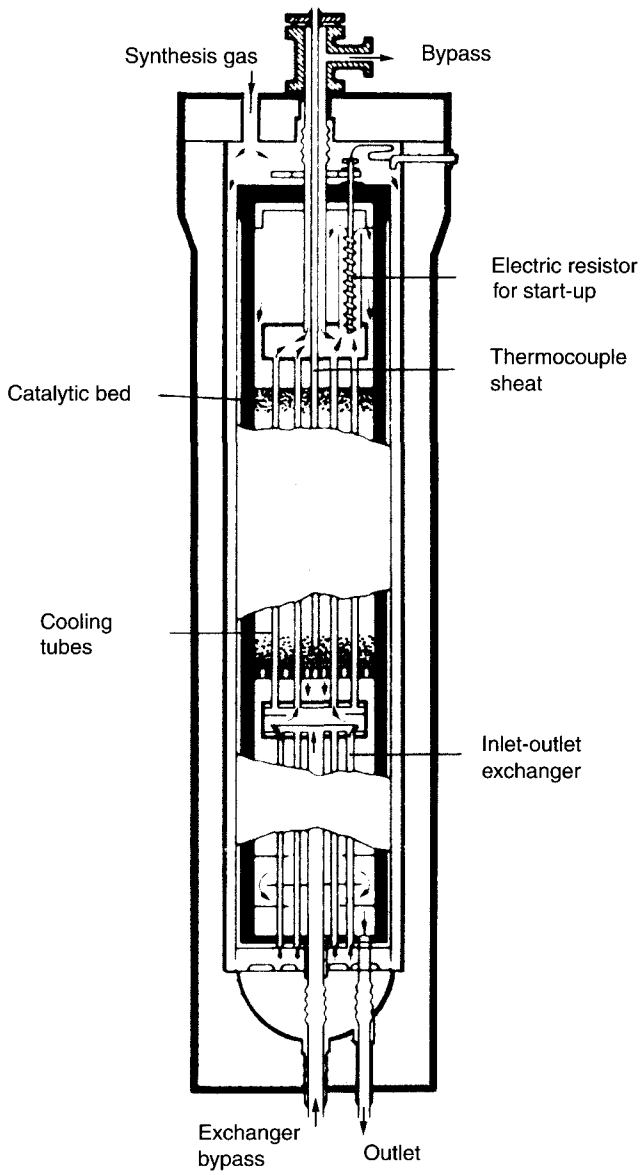


Figure 10.6 Configuration of a reactor for the synthesis of ammonia with internal heat exchange.

The recovery of heat through contact with solid elements has been practiced for years in a number of processes. Common in metallurgy, it has also been used for the cyclic cracking of hydrocarbons and for treating waste gases containing small amounts of organic compounds (VOC).

More recently, it has been suggested that periodic flow reversal be used, which has the advantage of keeping the heat within the catalytic or inert solid bed (Fig. 10.7) [Agar and Ruppel, 1988; Westerterp, 1992]. The method has also been proposed for the synthesis of styrene by the dehydrogenation of ethylbenzene, using the heat of combustion of the hydrogen produced as the heat source [Grigorios and Eigenberger, 1991]. Transfer within the reaction phase itself is also used, by coupling highly thermal reactions, exothermic and endothermic. These processes are referred to as "authothermal." They are used to obtain acetylene from methane, as part of the production chain when producing hydrogen by partial oxidation, or during secondary reforming (Fig. 10.8).

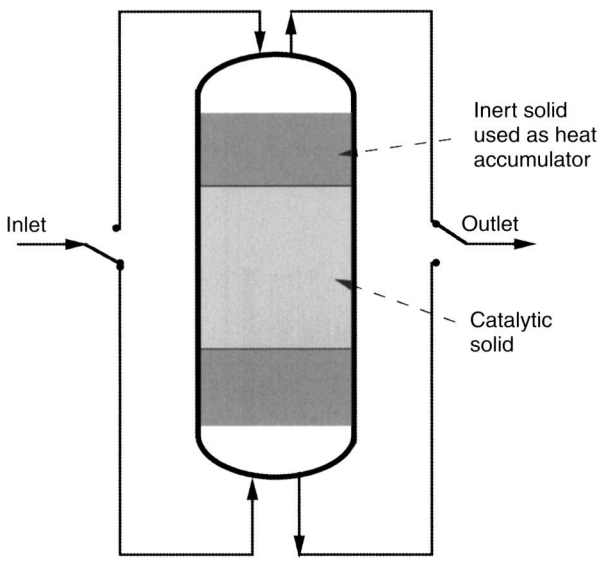


Figure 10.7 Flow diagram for the recovery of heat by periodic flow reversal.

10.3.3 Radiative transfer

For high temperature reactions, tubes must often be heated inside a furnace, where they are directly subjected to the radiation produced by flames in the burner. In this case, as with exchange through the wall, since radiative heating is a necessity, there is no reason to include it here. However, it is often necessary to accurately assess the needs of a frequently complex chemical reaction, modulating the heat flux in order to optimize yields and selectivities. Consequently, there is considerable synergy between the reactor (the interior of the tube) and the furnace, consisting of the burners, the various zones through which the combustion gases flow, and the radiative surfaces. Important examples of industrial use include steam cracking and steam reforming furnaces [Trambouze *et al.*, 2000].

Other cases where radiation is more specific are found in photochemical reactors, where radiation (most often visible or UV) is the activation source for the reactions that occur. Here,

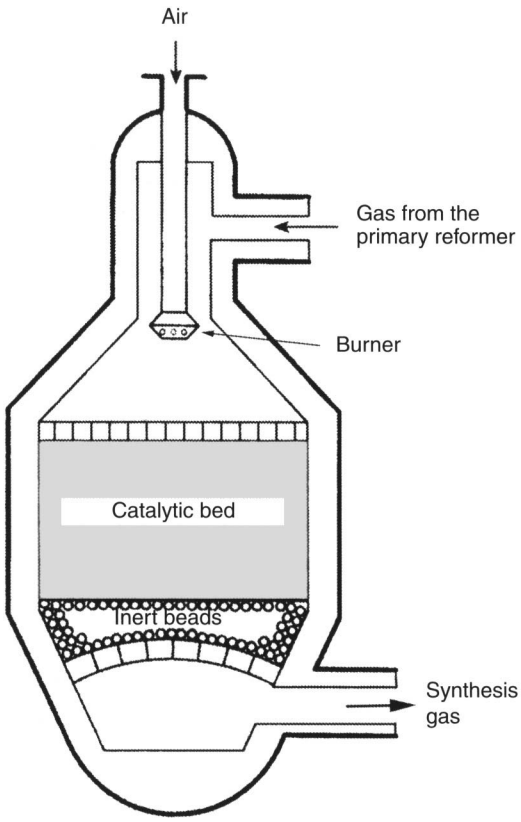


Figure 10.8 Design of an authothermal reactor for the production of hydrogen by secondary reforming.

the chemical transformations can only take place with the energy supplied by radiation and, frequently, good selectivity can be obtained by selecting the appropriate wavelengths.

Some applications have been practiced industrially for a number of years [Staff Report, 1962]. Aside from obtaining vitamin D3 from ergosterol, there are a number of other potential reactions, including chlorination, nitrosation, sulfoxidation, and, in some cases, oxidation. One problem associated with this type of reactor is the high cost of obtaining radiation from special lamps and using that radiation in an optimal way inside the reactor [Harano and Matsura, 1972; Cassano *et al.*, 1995].

Biotechnology is another promising field, especially for growing microorganisms (algae or bacteria) [Ogbonna and Tanaka, 1997]. Given the high costs associated with obtaining radiation, which are acceptable only for high added-value products, the use of solar radiation has been investigated, especially for the growth of algae. An example of a multifunctional photochemical reactor is shown in Fig. 10.9. This system was developed for the production of Spirulina algae. Here, combustion gas supplies CO_2 and is used to circulate the culture medium throughout the pond, which is exposed to the sun [Clément *et al.*, 1968].

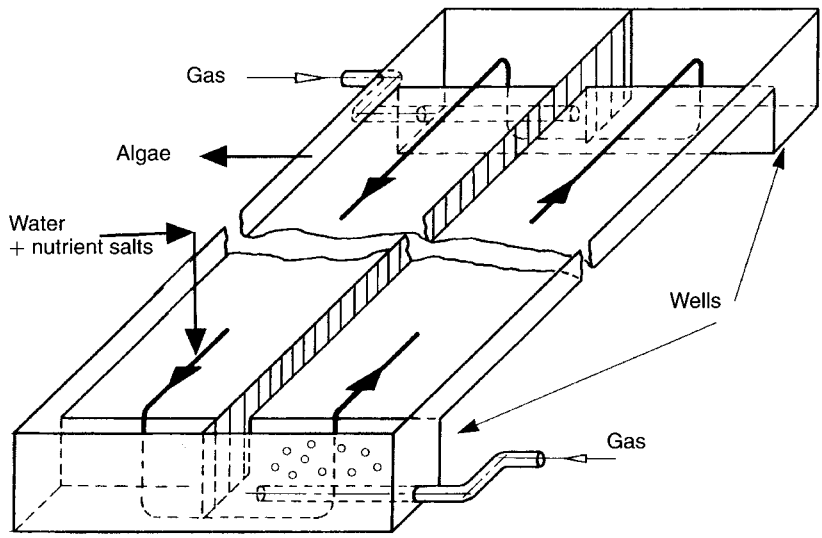


Figure 10.9 Schematic design of an algae pond.

It is even conceivable that some form of "solar" chemistry would involve the use of solar furnaces, which could be used to reach temperatures that are hard to obtain by other means [Lede, 1997].

As for the radiation source, radioisotopes have been used, either directly as a source of β radiation (radiochemistry) or to irradiate phosphorescent substances that then convert the β radiation into ultraviolet light [Staff Report, 1962].

Radiation can also be combined with a catalyst (homogeneous or heterogeneous). Such photocatalysis can be used for oxidation [Frei *et al.*, 1996] or the treatment of effluents [Pelizzetti *et al.*, 1992; Obuchi *et al.*, 1999; Dillert *et al.*, 1999].

More recently, another type of electromagnetic radiation (microwave) has been used to promote chemical reactions [Whittaker and Mingos, 1994; Majetich and Hicks, 1995; Bose *et al.*, 1997; Galema, 1997]. Derived from microwave heating, the technology can be used to accelerate certain reactions, typical of which are: Diels-Alder reactions, ene-reactions, the transformation of alcohols into alkyl bromide or iodide, isomerization, oxidation of alcohols into acids, esterification, ether synthesis, hydrolysis, polymerization, etc. These reactions generally take place in the liquid phase, but the use of reactive solids or catalysts is also possible.

10.3.4 Transfer of electricity

Electricity is often the best vector for energy transfer. The simplest means is Joule heating, even though induction heating is sometimes proposed (see Chapter 2). Here too, the use of electricity to carry out a chemical reaction may not be very specific compared

to the other methods of heating mentioned above. Nonetheless, there are situations in which electricity can be highly specific. Thus, for high-temperature gas-phase reactions with short residence times such as acetylene synthesis, an electric arc is use in industrial applications. Other reactions of this type or those that make use of electrical discharges for the formation of a plasma also fall into this category—the manufacture of ozone is one such example.

If we now consider liquid-phase reactions, electrolysis provides a vast field of application for the use of electricity to produce chemical compounds. High-tonnage processes for the production of chlorine, soda, aluminum, and copper have been carried out for years and have little commercial competition.

In addition to these common applications, there are a number of applications of electrochemistry that have come into prominence over the years, often in the field of organic chemistry [Chaussard, 1982; Toomey and Yu, 1989]. It is worth noting that more than 200 000 t/yr of adiponitrile is synthesized industrially by the dimerization of acrylonitrile. Some examples of industrial reactions carried out by electrosynthesis are:

- dimerization or hydrodimerization
- hydrogenation
- reduction of carboxylic acids
- reduction of nitro compounds
- oxidations
- halogenations.

Many other reactions are carried out on a small scale (pilot units) or as research for future developments (production of hydrogen peroxide, propylene oxide, ethylene glycol, etc.), especially for applications involving the treatment and depollution of effluents [Trassatti, 1995; Hairston, 1997].

Modern electrochemical reactors often take the form of filter presses in which elementary cells are stacked (Fig. 10.10) [Walsh and Robinson, 1995; Jackson and Moran, 2001]. Efforts are often made to accelerate the reaction involved and increase its selectivity by enabling the electrodes to function as sources of catalytic activity. Porous electrodes, often arranged in fixed- or fluidized-beds are also used [Fahidy, 1973].

In the future, applications for the production of energy using fuel cells will certainly represent an important field of research.

10.4 REACTION WITH TRANSFER OF MOMENTUM

10.4.1 Transfer by friction or shear

As soon as a fluid or granular solid begins to flow, it is subject to friction, if only with the walls of the conduit. If the system contains several phases, friction between the phases must also be considered. Here, we are only interested in friction that can promote the chemical reaction. Some of the types of friction we are interested in include:

- gas-liquid friction created in an ejector to suck the gas and induce a liquid-phase reaction after absorption of a reactive compound (see Figs. 4.23 and 4.24)

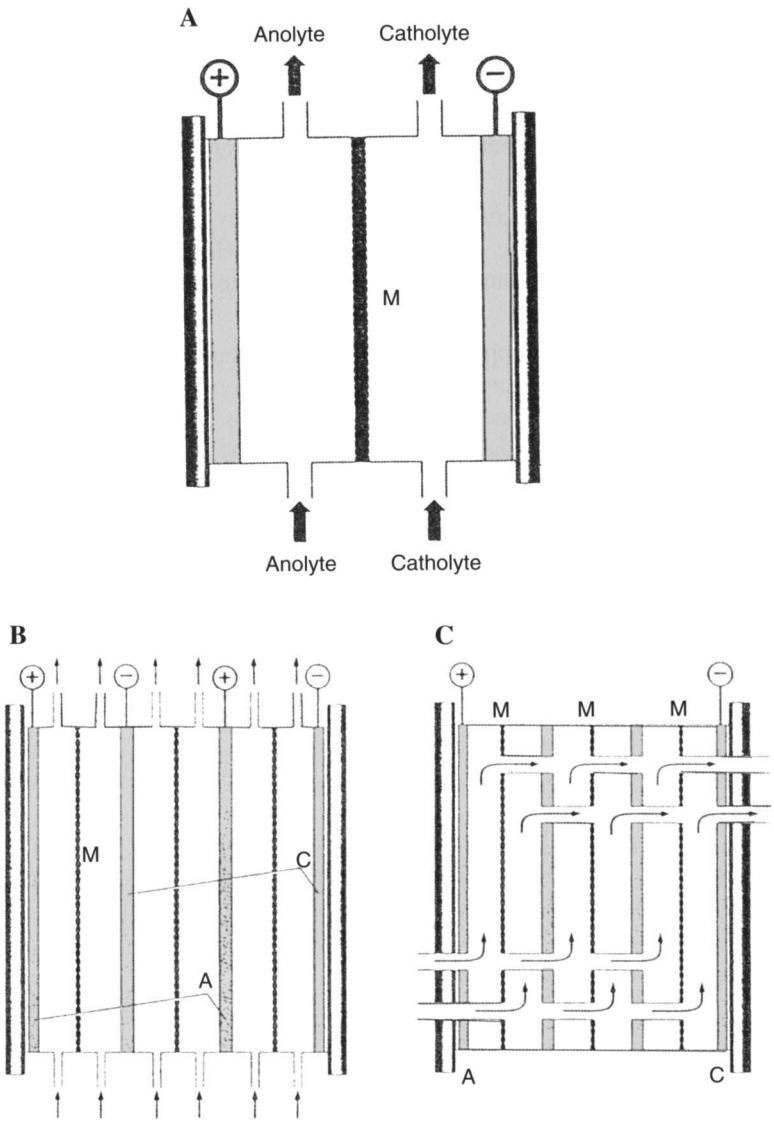


Figure 10.10 Illustration showing:
A. The basic structure of an electrochemical cell, together with two variant assemblies inside a filter press reactor. **B.** Single-pole connection. **C.** Bipolar connection. A = anode, C = cathode, M = membrane permeable to ions.

- the action of impellers in stirred reactors, whether homogeneous or heterogeneous; the impeller is often essential for accelerating macro- and micromixing, dispersal of a phase to increase the interfacial area, etc.

- use of inline mixers to conduct fast gas-liquid or liquid-liquid reactions
- pneumatic transport or fluidization of a solid (catalytic or reactive) for the purpose of carrying out a highly thermic reaction.

In a catalytic cracking unit, for example, we find all the elements of a highly multifunctional reactor: pneumatic transport with a reaction in the riser, gas-solid reaction in a fluidized bed in the regenerator, and transport of heat by the solid catalyst from the regenerator to the riser.

When pasty materials are involved, it is often suggested that extruders be used as reactors. Friction of the screw on the material causes shear effects that promote mixing and, therefore, reaction. This technique has been used in polymerization [Cassagnau *et al.*, 1998] and in the food processing industry.

10.4.2 Transfer by acceleration

In this case the acceleration can be gravitational or associated with centrifugal force. Gravity is involved, for example, in moving beds of solid (catalytic or reactive), which are needed because of the nature of the reaction being conducted (deactivation of a catalyst or the exhaustion of the reactive part of a solid).

Centrifugal force is employed for separation processes in cyclones or centrifuges. A reaction can be carried out at the same time as the separation, as has been proposed for the pyrolysis of sawdust inside a cyclone [Lede, 2000].

The use of an atomization dryer to carry out a reaction also makes use of centrifugal force to disperse the reaction mixture [Reinhold *et al.*, 2001].

10.4.3 Transfer by impulse or pressure

Rather than the influence of pressure on a chemical reaction, we will consider the effect of sudden changes in pressure. When two flow streams from opposite directions come into contact, this can lead to locally favorable conditions for a reaction between several phases. Gas-liquid and gas-solid flows have been studied to evaluate the performance increase that can be achieved [Gaddis *et al.*, 1992; Tamir, 1989].

Another combination of a physical process with a reaction system that has been developed recently involves the use of ultrasound to accelerate chemical transformation, sometimes referred to as "sonochemistry" [Gandhi and Kumar, 1994]. The technology can be used for reactions involving one or two fluid phases, as well as those involving a catalytic or reactive solid [Mason and Gordemans, 1996; Suslick *et al.*, 1995; Lickiss and McGrath, 1996; Pandit and Moholkar, 1996]. Some have even proposed that ultrasound be coupled with microwaves to accelerate a chemical process such as esterification or pyrolysis [Chemat *et al.*, 1996].

For reactions that involve a solid, a reaction can be carried out during the grinding operation, by using a specially designed ball grinder [Bade and Hoffmann, 1996, 1997]. The technique is applicable to gas-solid, liquid-solid, and even gas-liquid-solid reactions, but at present, only for batch operation.

10.5 FUTURE DEVELOPMENTS

Our cursory examination of the possibilities offered by multifunctional reactors illustrates the very broad range of potential applications as well as the large number of variant implementations that are "multifunctional" in essence if not in name. We have limited our examination, however, primarily to the field of conventional chemistry, including petroleum and gas refining, heavy petrochemistry, the production of major feedstocks, commodities, and specialty products.

The number of variants covered actually would be much greater and the inventory would doubtless be richer if we had considered fields that are traditionally not included in the chemical industry, such as the extractive industry and the treatment of mineral raw materials, metallurgy, and the food processing industry.

One example, among many, is the blast furnace, which can be described as an excellent embodiment of a multifunctional reactor. In it we find multiple simultaneous reduction and oxidation reactions, a moving bed of reactive solids (coke and iron oxides), a fluid current transporting another reactant (oxygen), and the final separation of the liquid pig iron. It also needs to be stressed that this technology has existed, along with all the constituent details we have described, for more than ten centuries (Fig. 10.11).

If we examine natural processes in both the plant and animal kingdoms, we can find many examples of multifunctional reactors. Thus, the human or animal intestine can be described as a rather remarkable multifunctional reactor. After food is premixed in the stomach with the gastric juices, the slurry that is formed enters the small intestine, where chemical digestion takes place, catalyzed by various enzymes. During its progression through the small intestine, the nutrient substances formed are extracted through the membrane walls and evacuated by blood flow. The parts that remain untransformed continue their path through the large intestine, which behaves as an extruder, rejecting them to the exterior.

If we now consider the leaves of plants, we find that they function as photochemical reactors with an external membrane (Fig. 10.12); the membrane allows sunlight and carbon dioxide to pass through. The CO_2 is reduced and transformed into various sugars, amino acids, and fatty acids, which are removed through the other internal membranes towards the plant's circulatory system. Moreover, the operation is cyclic, with oxygen being produced during the nocturnal phase.

These examples show that the field of application for multifunctional reactors is practically unlimited—the only practical limitation being the imagination of researchers and engineers.

More recently, we have seen the development of process intensification using multifunctional reactors [Stankiewicz and Moulijn, 2000; Dautzenberg and Mukherjee, 2001]. Here the objective is to reduce the size of the equipment and increase its efficiency, while at the same time trying to reduce the cost of the operation and protect the environment. There is little doubt that multifunctional reactors will play an important role in achieving these objectives.

In the future we can anticipate that new designs involving such equipment will be developed through the use of the sophisticated tools available to researchers and engineers, which provide new methods of measurement, visualization, and mathematical modeling, especially computational fluid dynamics [Euzen and Gauthier, 2000, Ranade, 2001].

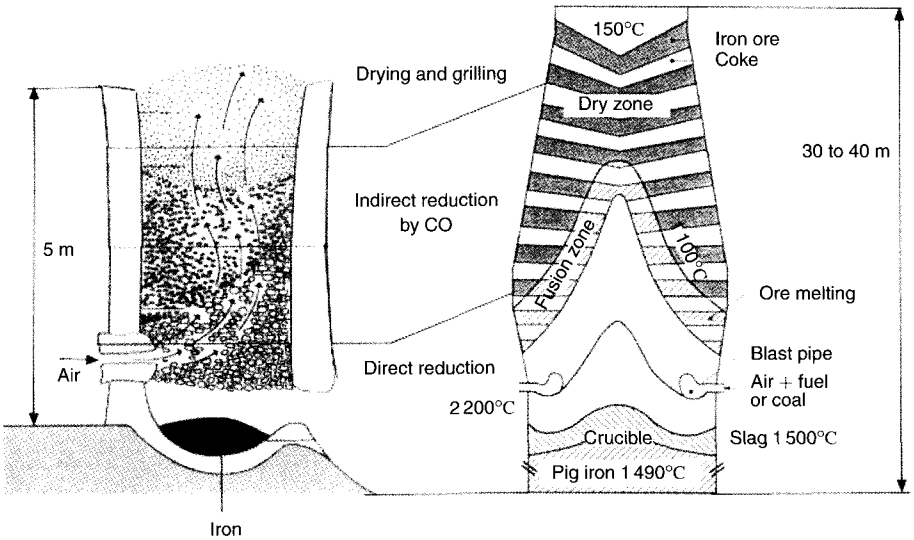


Figure 10.11 Comparison of a furnace for the production of iron dating from the thirteenth century and a modern blast furnace (right).

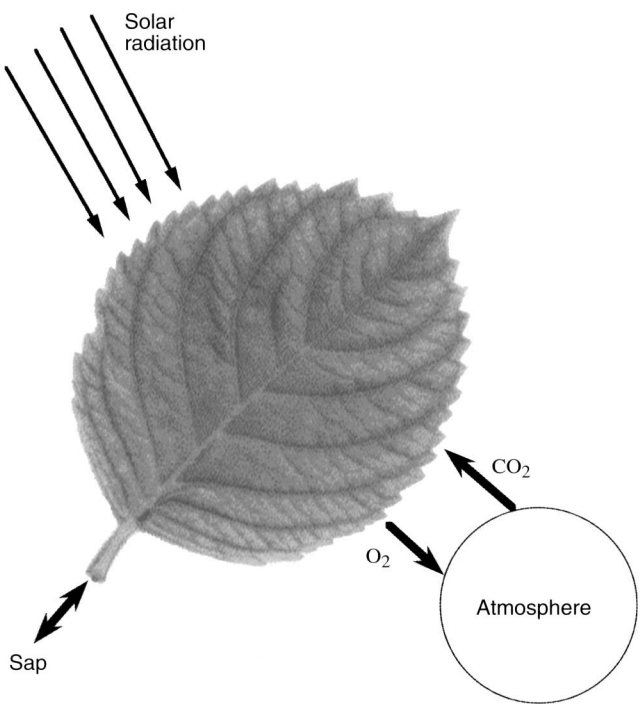


Figure 10.12 A plant leaf as a photochemical reactor.

REFERENCES

Adler SF (2001) Biofiltration - a Primer. Chem Eng Prog 97, 4, pp 33–41.

Adris AM *et al.* (1991) A fluidized bed membrane reactor for the steam reforming of methane. Can J Chem Eng 69, pp 1061–1070.

Agar DW (1999) Multifunctional Reactors: Old preconceptions and new dimensions. Chem Eng Sci 54, pp 1299–1305.

Agar DW, Ruppel W (1988) Multifunktionale Reaktoren für die heterogene Katalyse. Chemie-Ingenieur Technik 60, 10, pp 731–741.

Agarwalla S, Lund CRF (1992) Use of a membrane reactor to improve selectivity to intermediate products in consecutive catalytic reactions. J Memb Sci 70, pp 129–141.

Amor JN (1998) Applications of catalytic inorganic membrane reactors to refinery products. J Memb Sci, 147, pp 217–233.

Amor HB, Halloin VL (1999) Methanol synthesis in a multifunctional reactor. Chem Eng Sci 54, 10, pp 1419–1423.

Bade S, Hoffmann U (1996) Development of a new reactor for combined communition and chemical reaction. Chem Eng Comm 143, pp 169–193; (1997) Modelling of the simultaneous communition and chemical reaction in a non-catalytic gas-solid batch reactor. Chem Eng Sci 52, 16, pp 2715–2728.

Bessling B *et al.* (1998) Investigations on the synthesis of methyl acetate in a heterogeneous reactive distillation process. Chem Eng Tech 21, pp 393–400.

Bjorklund MC, Carr RW (1995) The simulated countercurrent moving bed chromatographic reactor: a catalytic and separative reactor. Catalysis Today, 25, pp 159–168.

Bose AK *et al.* (1997) More chemistry in a microwave. Chemtech (Sept. 1997), pp 18–23.

Cassagnau P *et al.* (1998) Polymérisation de polyuréthane en phase dispersée en réacteur extrudeuse. Entropie, 212/213, pp 19–24.

Cassano AE *et al.* (1995) Photoreactor analysis and design; Fundamentals and applications. Ind Eng Chem Res 34, pp 2155–2201.

Cauwenberg V *et al.* (1999) Integration of reaction and separation in manufacturing of pharmaceuticals: membrane-mediated production of S-Ibuprofen. Chem Eng Sci, 54, 10, pp 1473–1477.

Chaussard J (1982) L'électrolyse dans l'industrie de la chimie organique. L'actualité chimique, (Nov. 1982), pp 29–33.

Chemat F *et al.* (1996) An original microwave-ultrasound combined reactor suitable for organic synthesis. J Microwave Power and Electromagnetic Energy 31, 1, pp 19–22.

Clément G, Rebeller M, Trambouze P (1968) Utilisation massive du gaz carbonique dans la culture d'algues alimentaires. Revue de l'Institut Français du Pétrole 23, 5, pp 702–711.

Crabb C (2001) Exploring ionic liquids. Chem Eng 108, 3, pp 33–37.

Corrigan TE, Stichweh LA (1968) Esterification process development. Chem Eng Sci 23, pp 991–1002.

Dautzenberg FM, Mukherjee M (2001) Process intensification using multifunctional reactors. Chem Eng Sci 56, 2, 251–267.

Dillert R *et al.* (1999) Photocatalytic treatment of an industrial wastewater in the double-skin sheet reactor. Chem Eng Tech 22, pp 931–934.

Dixon AG (1999) Innovations in catalytic inorganic membrane reactors. Catalysis, 14, pp 40–92.

Edlund DJ *et al.* (1994) Catalytic platinum-based membrane reactor for removal of H_2S from natural gas streams. J Memb Sci, 94, pp 111–119.

Euzen JP, Gauthier Th (2000) Chemical reactors, from mock-up to industrial reactor: diagnostic methods. Oil and Gas science and Technology, Special Issue 55, 2, pp 131–229.

Fahidy TZ (1973) The chemical engineering approach to some electrochemical processes. Can J Chem Eng 51, pp 521–535.

Fair JR (1998) Design aspects for reactive distillation. Chem Eng 105, 11, pp 158–162.

Frei H *et al.* (1996) Photocatalyzed oxidation of hydrocarbons in zeolithe cages. Chemtech 26, 6, pp 24–30.

Gaddis ES *et al.* (1992) The impinging-stream loop reactor: a newly developed reactor with a high mass transfer performance. *In*: Transport Phenomena in Heat and Mass Transfer, Reizes JA, Ed., Elsevier.

Galema SA (1997) Microwave chemistry. Chem Soc Rev 26, pp 233–238.

Galtier P *et al.* (1986) Modeling of methanol synthesis in a 3-phase fixed bed reactor. Chem Eng Sci 41, 4, pp 973–979.

Gandhi KS, Kumar R (1994) Sonochemical reaction engineering. Sadhana 19, Part 6, pp 1055–1076.

Grigorios K, Eigenberger G (1999) Styrene synthesis in a revers-flow reactor. Chem Eng Sci 54, 13–14, pp 2637–2646.

Hairston D (1997) Electrosynthesis: the clean alternative. Chem Eng 104, 5, pp 40–45.

Hao XR *et al.* (1995) Novel catafractionation technology for the production of MTBE. Chem Eng J 56, pp 11–18.

Harano Y, Matsura T (1972) Problems in designing photochemical reactors. Int Chem Eng 12, 1, pp 131–143.

Harmsen GJ, Chewter LA (1999) Industrial applications of multi-functional multi-phase reactors. Chem Eng Sci 54, pp 1541–1545.

Hartig H, Regner H (1971) Verfahrenstechnische Auslesung einer Veresterungskolonne. Chemie Ingenieur Technik, 43, 18, pp 1001–1048.

Hoffmann U, Sundmacher K (1997) Multifunktionale Reaktoren. Chemie-Ingenieur Technik 69, 5197, pp 613–622.

Horst RM, Hoffmann U (2001) Experimental and theoretical investigations of a spray dryer with simultaneous chemical reaction. Chem Eng Sci 56(4), 13–14, pp 1657–1665.

Jackson B, Moran S (2001) Harnessing electrochemistry. Chem Eng 108, 4, pp 88–95.

Kapteijn F *et al.* (1999) Monoliths in multiphase catalytic processes: aspects and prospects. Cattech, 3(1), pp 24–41.

Kim JS *et al.* (1991) Supported liquid-phase catalytic membrane reactor-separator for homogeneous catalysis. AIChE J 37, 11, pp 1657–1667.

Kim W-S, Tarbell JM (1996) Micromixing effects on barium sulfate precipitation in NSMPR reactor. Chem Eng Comm 146, pp 33–56.

Kohl A, Nielsen R (1997) Gas Purification, 5th edition, Gulf Publishing Co.

Kreul LU *et al.* (1999) Modeling of homogeneous reactive separation processes in packed columns. Chem Eng Sci 54, pp 19–34.

Kruglov AY (1994) Methanol synthesis in a simulated countercurrent moving-bed adsorptive catalytic reactor. Chem Eng Sci 49, 24A, pp 4699–4716.

Kruglov AY (1996) Optimization of the simulated countercurrent moving-bed chromatographic reactor for the oxidative coupling of methane. Chem Eng Sci 51, 11, pp 2945–2950.

Lede J (1997) Chimie solaire dans le monde et en France. Entropie, 204, pp 47–55.

Lede J (2000) The cyclone: a multifunctional reactor for the fast pyrolysis of biomass. Ind Eng Chem Res 39(4), pp 893–903.

Leprince P (2000) Petroleum Refining. Vol. 3: Conversion Processes. Editions Technip, Paris.

Lickiss PD, McGrath VE (1996) Breaking the sound barrier. Chemistry in Britain, (March 1996), pp 47–50.

Lipnizki F *et al.* (2000) Use of pervaporation-bioreactor hybrid processes in biotecnology. Chem Eng Techn 23, 7, pp 569–577.

Majetich G, Hicks R (1995) Applications of microwave-accelerated organic synthesis. Radiat Phys Chem 45, 4, pp 567–579.

Mason TJ, Cordemans ED (1996) Ultrasonic intensification of chemical processing and related operations. Trans Inst Chem Eng 74, Part A, (July 1996), pp 511–516.

Mazzotti M *et al.* (1996) A continuous chromatographic reactor: SMBR. Chem Eng Sci 51, 10, pp 1827–1836.

Mersmann A *et al.* (1994) Controlled precipitation. Chem Eng Tech 17, pp 1–9.

Neomagus HW *et al.* (1998) The catalytic oxidation of H_2S in a stainless steel membrane reactor with separate feed of reactants. J Memb Sci, 148, pp 147–160.

Obuchi E *et al.* (1999) Photocatalytic decomposition of acetaldehyde over TiO_2/SiO_2, catalyst. Chem Eng Sci 54, 10, pp 1525–1530.

Ogbonna JC, Tanaka H (1997) Industrial-size photobioreactors. Chemtech, July 1997, pp 43–49.

Pandit AB, Moholkar VS (1996) Harness cavitation to improve processing. Chem Eng Prog 92, 7, pp 57–69.

Pelizzetti E *et al.* (1992) Photocatalytic processes for destruction of organic water contaminants. NATO ASI Series E 225, Kluwer Academic Publishers, pp 577–608.

Podrebarac GG *et al.* (1997) More uses for catalytic distillation. Chemtech, (May 1997), pp 37–45.

Ranade V (2001) Computational flow modeling for chemical reactor engineering. Ed. Academic Press.

Reinhold M *et al.* (2001) Experimental and theoretical investigations of a spray dryer with simultaneous chemical reaction. Chem Eng Sci 56, 4, pp 1657–1665.

Samant KD, Ng KM (1999) Systematic development of extractive reaction processes. Chem Eng Tech 22, 10, pp 877–880.

Sanchez J, Tsotsis T (2002) Catalytic membranes and catalytic membranes reactors. John Wiley and Sons.

Saracco G, Specchia V (1994) Catalytic Inorganic-Membrane Reactors: Present experience and future opportunities. Catal Rev Sci Eng 36(2), pp 305–384.

Sawistowski H, Pilvakis PA (1988) Performance of esterification in a reaction-distillation column. Chem Eng Sci 41, 2, pp 335–360.

Shu J *et al.* (1991) Catalytic Palladium-based membrane reactors: a review. Can J Chem Eng 69, pp 1036–1060.

Staff report (1962) Industrial photochemistry. Ind Eng Chem 54, pp 20–28.

Stankiewicz A, Moulijn J (2000) Process intensification: Transforming chemical engineering. Chem Eng Prog 96, 1, pp 22–34.

Stichlmair J, Frey T (1999) Reactive distillation processes. Chem Eng Technol 22, pp 95–103.

Stingaro J-P, Luder J (1992) Katalysatoren für heterogene Reaktionssystem. Chemi-Ankagen+Verfarhen, Nr 4.

Suslick KS *et al.* (1995) Sonochemical synthesis of nanostructured catalysts. Materials Sci Eng, A204, pp 186–192.

Tamir A (1989) Processes and phenomena in impinging-stream reactors. Chem Eng Prog 85 (9), pp 53–61.

Toomey JE, Yu JC (1989) Making organic chemicals via electrochemical processing. Chem Eng 96, p 6.

Trambouze P, Van Landeghem H, Wauquier JP (1988) Chemical Reactors: Design, Engineering, Operation. Editions Technip, Paris.

Trambouze P *et al.* (2000) Petroleum Refining. Vol. 4: Materials and Equipment. Editions Technip, Paris.

Trasatti S (1995) Electrochemistry and environment: the role of electrocatalysis. Int J Hydrogen Energy 20, 10, pp 835–844.

Tsotsis TT *et al.* (1992) Packed bed catalytic membrane reactors. Chem Eng Sci 47, 9–11, pp 2903–2908.

Tsotsis TT *et al.* (1993) Catalytic membrane reactors. *In*: Computer Aided Design of Catalysts, chap. 12. Dekker, New-York.

Vaporciyan GG, Kadlec RH (1989) Periodic separating reactors: Experiments and Theory. AIChE J 35, 5, pp 831–844.

Veldsink JW *et al.* (1995) A catalytically active membrane reactor for fast, highly exothermic, heterogeneous reactions. A pilot plant study. Ind Eng Chem Res 34, pp 763–772.

Walsh F, Robinson D (1995) Electrochemical synthesis and processing in modern filterpress reactors. Chem Tech Europe (May/June 1995) pp 16–23.

Westerterp KR (1992) Multifunctional Reactors. Chem Eng Sci 47, 9–11, pp 2195–2206.

Whittaker AG, Mingos DMP (1994) The application of microwave heating to chemical synthesis. Journal of Microwave Power and electromagnetic energy 29, 4, pp 195–219.

Copyrighted Materials
Copyright © 2004 Editions Technip Retrieved from www.knovel.com

General nomenclature

The general nomenclature below lists all the main symbols used throughout the ten chapters. Specific notations are also introduced chapter by chapter, as required.

Symbol	Definition	Dimension	SI unit
A_i	Chemical compound, always accompanied by a subscript	–	–
$\mathcal{A}$	Exchange surface area per unit volume	L^{-1}	m^2/m^3
$\mathcal{A}_p$	Geometric area of packing	L^{-1}	m^2/m^3
$\mathcal{A}_S$	External surface area of particles per unit volume	L^{-1}	m^2/m^3
C_i	Concentration, accompanied by a subscript	$mol \cdot L^{-3}$	mol/m^3
C_{Pi}	Molar specific heat, accompanied by a subscript	$mol^{-1} \cdot ML\theta^{-2}T^{-1}$	$J/mol \cdot K$
C_{PM}	Global specific heat	$L^2\theta^{-2}T^{-1}$	$J/kg \cdot K$
$\mathcal{D}_i$	Coefficient of molecular diffusion, accompanied by a subscript	$L^2\theta^{-1}$	m^2/s
$\mathcal{D}_A$	Coefficient of axial diffusion	$L^2\theta^{-1}$	m^2/s
d_p	Nominal diameter of a packing element	L	m
$\overline{d_l}$	Mean particle diameter	L	m
$\overline{d_B}$	Mean or bubble or drop diameter	L	m
D_C	Column diameter	L	m
D_T	Diameter of a stirred tank	L	m
D_A	Impeller diameter in a stirred tank	L	m
$\mathcal{D}_{ie}$	Coefficient of effective diffusion in a porous particle	$L^2\theta^{-1}$	m^2/s
d_O	Diameter of opening	L	m
E	Enhancement factor (Chapters 3, 4, 5)	–	–
E	Activation energy	$ML^2\theta^{-2} \cdot mol^{-1}$	J/mol
$\mathbf{E}$	Global effectiveness of a catalyst particle	–	–
F	Molar flow rate	$mol \cdot \theta^{-1}$	mol/s
Fr	Froude number	$\frac{[u]^2}{[L][g]}$	–
G	Free enthalpy	$ML^2\theta^{-2}$	J
g	Acceleration due to gravity	$L\theta^{-2}$	$9.81\ m/s^2$

Symbol	Definition	Dimension	SI unit
H	Enthalpy	$ML^2\theta^{-2}$	J
H	Total height	L	m
Ha	Hatta number	–	–
h	Height measured from the point of origin	L	m
h	Coefficient of heat transfer	$M\theta^{-3}T^{-1}$	$W/m^2 \cdot K$
j_D	$j_D = k_i Sc^{\frac{2}{3}}/V_{SF}$	–	–
j_H	$j_H = h/C_{P,M}\rho_F V_{SF}$	–	–
k	Reaction rate constant	variable	variable
k_i	Mass transfer coefficient relative to compound A_i	$L\theta^{-1}$	m/s
K_i	Global coefficient of mass transfer	$L\theta^{-1}$	m/s
K	Equilibrium constant	variable	variable
l	Length measured from the point of origin	L	m
L	Total length	L	m
M	Molecular weight	$M \cdot mol^{-1}$	kg/mol
n	Number of moles	–	–
N_i	Transfer flux of compound A_i per unit of surface	$mol \cdot L^{-2}\theta^{-1}$	$mol/m^2 \cdot s$
$\mathbf{N}_i$	Transfer flux per particle	$mol \cdot \theta^{-1}$	mol/s
$\mathcal{N}_i$	Transfer flux per unit volume	$mol \cdot L^{-3}\theta^{-1}$	$mol/m^3 \cdot s$
N_R	Rotational speed of rotor	θ^{-1}	s^{-1}
Nu	Nusselt number	$\frac{[U][L]}{[\lambda]}$	–
P	Pressure	$ML^{-1}\theta^{-2}$	Pa
$\mathcal{P}$	Power dissipated in a reactor	$ML^2\theta^{-3}$	W
Pe	Peclet number	$\frac{[L][u]}{[\mathcal{D}]}$	–
Pr	Prandtl number	$\frac{[C_{P,M}][\mu]}{[\lambda]}$	–
p_i	Partial pressure of compound A_i	$ML^{-1}\theta^{-2}$	Pa
q	Heat exchanged per unit of volume and unit of time	$ML^{-1}\theta^{-3}$	W/m^3
Q	Volumetric flow rate	$L^3\theta^{-1}$	m^3/s
Q_M	Mass flow rate	$M\theta^{-1}$	kg/s
R	Molar yield, accompanied by two subscripts	–	–
R	Ideal gas constant	$ML^2\theta^{-2} \cdot mol^{-1} \cdot T^{-1}$	8.31 J/mol·K
r_j	Intensive rate of the reaction of rank j	$mol \cdot L^{-3}\theta^{-1}$	$mol/m^3 \cdot s$
$\mathcal{R}_i$	Rate of generation or disappearance of compound $A_i = \Sigma \nu_{i,j} r_j$	$mol \cdot L^{-3}\theta^{-1}$	$mol/m^3 \cdot s$
Re	Reynolds number	$\frac{[L][u][\rho]}{[\mu]}$	–
$r_{obs}(A_i)$	Observable rate of generation or disappearance of A_i	$mol \cdot L^{-3}\theta^{-1}$	$mol/m^3 \cdot s$
r'_M	Rate of reaction (per unit mass of solid catalyst)	$mol \cdot M^{-1}\theta^{-1}$	$mol/kg \cdot s$

Symbol	Definition	Dimension	SI unit
r'_S	Rate of reaction (per unit surface of solid catalyst)	$\mathrm{mol \cdot L^{-2}\theta^{-1}}$	$\mathrm{mol/m^2 \cdot s}$
s	Instantaneous molar selectivity, accompanied by two subscripts	–	–
S	Integrated molar selectivity, accompanied by two subscripts	–	–
Sc	Schmidt number	$\frac{[\mu]}{[\rho][\mathcal{D}]}$	–
S	Cross-section of a reactor or column	$\mathrm{L^2}$	$\mathrm{m^2}$
Sh	Sherwood number	$\frac{[\mathrm{L}][k_i]}{[\mathcal{D}]}$	–
S_p	Specific surface of a catalyst	$\mathrm{L^2M^{-1}}$	$\mathrm{m^2/kg}$
T	Temperature	T	K
t	Time	θ	s
u	Velocity	$\mathrm{L\theta^{-1}}$	m/s
U	Global heat transfer coefficient	$\mathrm{M\theta^{-3}T^{-1}}$	$\mathrm{W/m^2 \cdot K}$
$\overline{v_\mathrm{m}}$	Molar volume	$\mathrm{L^3 \cdot mol^{-1}}$	$\mathrm{m^3/mol}$
V	Volume	$\mathrm{L^3}$	$\mathrm{m^3}$
V_R	Reactor volume	$\mathrm{L^3}$	$\mathrm{m^3}$
V_P	Porous volume of a catalyst	$\mathrm{L^3}M^{-1}$	$\mathrm{m^3/kg}$
V_SG	Superficial gas velocity	$\frac{[\mathrm{L^3\theta^{-1}}]}{[\mathrm{L^2}]}$	m/s
V_SL	Superficial liquid velocity	$\frac{[\mathrm{L^3\theta^{-1}}]}{[\mathrm{L^2}]}$	m/s
We	Weber number	$\frac{[\mathrm{L}][\mathrm{u}]^2[\rho]}{[\sigma]}$	–
x_i	Molar fraction of compound A_i in the liquid phase	–	–
X	Conversion	–	–
y_i	Molar fraction of compound A_i in the vapor phase	–	–
z	Length measured from the point of origin	L	m
Z	Total length	L	m
ε	Volume fraction of the reactor occupied by a phase, with a subscript	–	–
η	Effectiveness	–	–
θ	Residence time	θ	s
λ	Thermal conductivity	$\mathrm{ML\theta^{-3}T^{-1}}$	$\mathrm{W/m \cdot K}$
μ	Dynamic or absolute viscosity	$\mathrm{ML^{-1}\theta^{-1}}$	$\mathrm{Pa \cdot s}$
ν_i	Stoichiometric coefficient, accompanied by at least one subscript	–	–
ξ	Stoichiometric extent of reaction for closed systems	mol	mol
ξ'	Stoichiometric extent of reaction for open systems	$\mathrm{mol \cdot \theta^{-1}}$	mol/s

Symbol	Definition	Dimension	SI unit
π_i	Vapor pressure, accompanied by a subscript	$ML^{-1}\theta^{-2}$	Pa
ρ	Density	ML^{-3}	kg/m^3
σ	Superficial or interfacial tension	$M\theta^{-2}$	N/m
Σ	Injected power per unit of mass	$L^2\theta^{-3}$	W/kg
Ω	Heat exchange surface	L^2	m^2
	Subscripts:		
a	relative to the incoming phase		
ad	adiabatic		
b	within the fluid phase, far from the interface		
C	relative to the continuous phase		
c	relative to catalyst particle bed		
c	critical		
d	relative to the outgoing phase		
D	relative to the dispersed phase		
E	at flooding		
e	at the inlet		
eq	at equilibrium		
f	relative to the exchange fluid		
F	relative to the reaction fluid		
G	gas		
i	characterizes a definite compound A_i		
int	at the internal wall		
j	characterizes a definite reaction		
L	liquid		
m, min	minimum, or mean		
mf	relative to the exchange fluid and averaged		
M, max	maximum		
M	mass		
O	at the injector opening		
p	relative to a particle or a group of particles		
R	characterizes a single reaction (ΔH_R)		
s	at the outlet		
S	relative to the solid		
S	superficial		
T	total		
T	at temperature *T*		
w or p	at the wall		
0	at the inlet, at the initial instant		
I	relative to Phase I		

Symbol	Definition	Dimension	SI unit
II	relative to Phase II		
	Superscript:		
m, n, p, q	reaction order		
0	in the standard state		
	Other symbols:		
$\rightarrow$	Forward direction		
$\leftarrow$	Backward direction		
$\bar{}$	Mean value		
$>$	Greater than		
$<$	Less than		
$\neq$	Not equal to		
$\cong$	Approximately equal to		
$\approx$	Proportional to		
tanh	Hyperbolic tangent		
cosh	Hyperbolic cosine		
sinh	Hyperbolic sine		
d	Differential operator		
Δ	Difference operator		
Σ	Sum operator		
Π	Product operator		
ln	Naperian logarithm		
log	Logarithm base-ten		
exp	Exponential		

Copyrighted Materials
Copyright © 2004 Editions Technip Retrieved from www.knovel.com

INDEX

Index Terms	Links		
A			
absorption	564	625	
acetone	591		
activation	10		
adiabatic	396	404	430
	554		
adsorption	15	622	
age	35		
agitation, mechanical	269	399	404
	407		
anchor	76		
angle			
of internal friction	446		
of repose	445		
Archimedes (number)	459	533	
area			
external surface	353		
gas-liquid interfacial	203	222	261
	273	277	
liquid-liquid interfacial	302	309	313
	320	331	338
specific	241	352	
three-phase interfacial	508	536	
Arrhenius (number)	12	372	387
atomizer	286		

This page has been reformatted by Knovel to provide easier navigation.

Index Terms	Links		
attrition	454		
autothermal	110	632	
B			
backmixing	94	249	305
	309	310	316
	321	333	464
	496	522	535
balance			
energy	5	53	90
	105	595	
enthalpy	30	187	
heat	479	556	568
	570	606	608
mass	30	53	90
	105	185	411
	606		
molar	568	569	593
	606		
batch operation	25	53	184
	399	554	
bed			
ebullated	530		
entrained	348	404	
fixed	347	394	404
	407	411	502
	519	543	577
fixed adiabatic	403		
fixed with two fluid phases	603		
fluid or fluidized	348	400	404
	407	454	543
moving	348	396	404

This page has been reformatted by Knovel to provide easier navigation.

Index Terms	Links		
bed			
moving (*Cont.*)			
	407	445	528
trickle	504		
Biot (number)	524		
blast furnace	638		
Bodenstein (number)	130		
bypass	417		

C

cascade *see* multistage			
catalysis			
heterogeneous	347		
homogeneous	122		
catalyst	13	347	
entrained	401	407	
loading	417	433	516
suspended or in suspension	591		
catalytic converter	441		
centrifugal extractor	341		
channeling	462		
circulation			
catalyst	445	449	
external of a fluid	120		
cloud of particles	469		
coalescence	306	313	
bubble	221		
coalescer	286		
cocurrent	195		
downward	251	503	
upward	519		

This page has been reformatted by Knovel to provide easier navigation.

Index Terms	Links		
coefficient			
drag	460		
external mass transfer	384	419	580
heat transfer	81	274	472
	556	589	
Henry's	566		
mass transfer	224	261	273
	306	508	
of diffusion	147	382	
overall exchange	73		
overall transfer	145	384	580
	610		
stoichiometric	1		
coil	71	82	
column			
bubble	205	228	492
mechanically agitated	326		
packed	241	251	255
	319	564	571
perforated plate	313		
plate	233	255	
pulsed	313		
spray	287	308	
comparison (of reactors)	123	403	542
compound lumping	16		
condensation	624		
constant			
equilibrium	8		
reaction rate	12	347	
continuous	25	89	
stirred tank reactor (CSTR)	104	196	
tubular	89		

This page has been reformatted by Knovel to provide easier navigation.

Index Terms	Links		
conversion	2	127	441
	578	605	
cost	256	291	341
	343	582	599
countercurrent	28	193	503
	526		
cracking	17		
catalytic	401	402	405
	451	474	

D

Damköhler (number)	128		
deactivation	391		
dense loading	417	433	516
design (dimensions)	226	232	414
	454	575	602
	617		
desorption	16		
diameter			
bubble	217	278	465
hydraulic	324	612	
mean	348		
mean bubble	309	314	
of openings	227		
diffusion			
axial	95	310	
external (of the particle)	394		
internal (of the particle)	358	375	394
	455		
Knudsen	383		
limitation	384	392	608
molecular	382		

This page has been reformatted by Knovel to provide easier navigation.

Index Terms	Links		
diffusivity	496	567	
effective	491		
direct contact (heat transfer)	630		
disengagement	473	603	
dispersion	337		
axial	97	207	
radial	209		
distillation	622		
reactive	253	625	
distribution			
bubble size	290		
liquid	254		
of diameters	325		
of reactivity	18		
of the dispersed phase	322		
of the fluid phases	472	513	524
radial	417		
residence time	35	124	323
	515		
distributor	308	439	473
	479	513	
gas	227	500	
liquid-phase	575		
drop size	304	331	

E

earliness of mixing	43		
economy *see* cost			
effectiveness	161	360	363
	365	367	580
global	384	386	
ejector	279	282	

This page has been reformatted by Knovel to provide easier navigation.

Index Terms	Links		
electricity, electrochemistry	634	635	
elementary steps	23		
energy			
activation	12	22	372
	381		
apparent, of activation	172	388	
dissipated	557		
of expansion	222		
enthalpy	6		
free	7		
of reaction	372		
entrainment of droplets	239		
equilibrium	146	430	
chemical	7		
liquid-vapor	608		
Ergun	418		
esterification	268		
evaporation	624		
exchanger			
external	71		
heat	598		
tubular	102		
exothermic	541		
expansion	461		
bed	533		
extent of reaction	2	8	430
extraction	625		
extrapolation, scaling-up	307	336	
extrudate	352		

This page has been reformatted by Knovel to provide easier navigation.

Index Terms	Links		

F

factor			
acceleration	151	566	
effectiveness	490		
packing	241		
power	79		
Fick's law	147		
film			
agitated	260		
falling	257		
film theory, two-film theory	147	167	
filtration	627		
fines removal	285	291	
Fischer-Tropsch synthesis	542		
flooding			
gas-liquid	236	245-247	
liquid-liquid	311	317	321
	334		
three-phase reactor	527		
flow			
axial	429		
cross	28	445	448
	451		
parallel	28		
periodic	632		
plug	33	40	
radial	417	435	451
fluidization	400	455	
foaming	291		
Froude (number)	79	533	538

This page has been reformatted by Knovel to provide easier navigation.

Index Terms	Links		
furnace	394	442	
steam cracking	100		
G			
gas scrubber	285	564	625
gaslift	229		
gradient (concentration or temperature)	373	387	455
grain *see* particle			
H			
Hatta (number)	151	566	
heat exchange, thermal	29	69	99
	394	442	
heat transfer			
at the wall	232	262	425
	471	498	510
catalytic reactor	386	422	423
	471		
gas-liquid reactor	226	263	278
	571		
single-phase reactor	81		
three-phase reactor	502	509	523
	537		
helical stirrer	75	592	597
holdup	29	203	219
	230	302	303
	309	310	313
	320	330	338
	494		
gas	272	276	534
liquid	248	521	534

This page has been reformatted by Knovel to provide easier navigation.

Index Terms	Links		
hydrocracking	405	431	
hydrodesulfurization	18	405	431
	605		
hydrodynamics			
catalytic reactor	455	501	504
	527	531	
gas-liquid reactor	229	234	245
	259		
liquid-liquid reactor	302	309	313
	320	323	329
	337		
hydrogenation	405	406	527
hydroprocessing	542		
I			
impeller (mechanical)	279		
impulse (Dirac)	39		
instability, thermal	61	455	515
interface			
gas-liquid	263	487	
liquid-solid	487		
J			
jacket (water)	70	82	
K			
kinetics			
apparent	168		
chemical	9		
formal	13		

This page has been reformatted by Knovel to provide easier navigation.

Index Terms	Links		
L			
LHSV *see* space velocity			
LMTD *see* logarithmic mean temperature difference			
loading catalyst	417	433	516
logarithmic mean temperature difference (LMTD)	67	559	
lumping (procedure)	20		
M			
macromixing	42		
mass transfer			
catalytic reactor	384	422	471
external	419	424	586
gas-liquid reactor	203	209	232
	236	249	261
	277	280	497
	508	522	536
	571		
liquid-liquid reactor	305	311	317
	322	325	334
	338		
liquid-solid	498	509	523
	537		
three-phase reactor	501	527	
two fluid phases	148	173	
materials			
packing	250		
plastic	254		
mechanical strength (catalyst)	353	355	
membrane	627		

This page has been reformatted by Knovel to provide easier navigation.

Index Terms	Links		
methanation	577		
micromixing	42	46	
microreactor	342		
miniring	245		
mixer			
inline	288		
static	289	323	
mixer-settler	336		
model, modeling	463	499	502
	510	524	538
monolith	355	365	396
	417	419	422
	440	526	
Morton (number)	217	534	
multistage	27	115	131
	464		
multitubular	394	404	428
	442	518	

N

number			
aeration	278		
Archimedes	459	533	
Arrhenius	372	387	
Biot	524		
Bodenstein	130		
Damköhler	128		
Froude	79	533	538
Hattal	151	566	
Morton	217	534	
Nusselt	82	263	423
	472	538	

This page has been reformatted by Knovel to provide easier navigation.

Index Terms	Links		
number (*Cont.*)			
Peclet	97	249	260
	323	415	494
	510	517	522
power	79	270	329
Prandtl	82	422	538
Prater	372	387	
pumping	88		
Reynolds	78	82	98
	259	261	270
	325	422	459
	498	537	538
Schmidt	261	422	424
	537		
Sherwood	261	423	
Thiele	387		
Weber	325		
Nusselt (number)	82	263	423
	472	538	

O

offtake *see* withdrawal			
operation			
batch	25		
continuous	26	27	
semi-continuous	26		
optimization	433	581	599
order (apparent), reaction	13	168-170	
oxidation	405	481	632

This page has been reformatted by Knovel to provide easier navigation.

Index Terms	Links		
P			
packing	243	244	253
	322	568	624
flooded	251		
structured	241	254	323
	527		
particle	348		
Peclet (number)	97	249	260
	323	415	494
	510	517	522
perfect mixing	40		
perfectly stirred	26		
phase			
bubble	464	467	469
dense	467	471	
dispersed	302	306	
emulsion	464	469	
reaction	9	149	
separation	478	621	
pilot unit	526		
plate			
bubble-cap	233	237	238
distributor *see* distributor			
inclined baffle tray	239		
perforated	233	237	239
	318		
redistributor	575		
submerged	240		
plug flow	26		
polymerization	102	121	268
	481		

This page has been reformatted by Knovel to provide easier navigation.

Index Terms	Links		
porosity	352	394	
porous volume	352		
power			
absorbed	271	329	
dissipated	78		
input	270	337	339
PPH	413	513	
Prandtl (number)	82	422	538
Prater (number)	372	387	
pressure drop			
catalytic reactor	418	437	447
	457	582	
gas-liquid reactor	245	247	284
	291	571	
liquid-liquid reactor	322	324	
single-fluid phase reactor	94		
three-phase reactor	516	521	531
	617		
production capacity	123	320	
profile, concentration or temperature	586		
propeller	75	592	597
pump	599		
pumping flow rate	88	561	

Q

quenching	431		

R

radiation	632		
Raschig (ring)	244		

This page has been reformatted by Knovel to provide easier navigation.

Index Terms	Links		
rate			
minimum fluidization	454	457	532
minimum wetting	248		
of reaction	10	11	
RDC (Rotating Disc Contactor)	326		
reaction			
autocatalytic	134		
catalytic	15	347	486
fast	152	175	181
	187	192	291
	326		
instantaneous	157	175	
irreversible	149	151	164
pseudo-first-order	157		
reversible	112	165	370
	578	622	
simple (first order)	107	111	127
slow	152	185	189
	291		
surface	17	159	
very fast	440		
reactions			
competing	566		
consecutive	57	109	113
	178	377	
parallel	182	375	
twin	57	108	376
reactor			
adiabatic	29	92	429
batch	28	53	184
	553		
catalytic	577	603	

This page has been reformatted by Knovel to provide easier navigation.

Index Terms	Links		
reactor (*Cont.*)			
concentration gradient	26		
continuous	28		
continuous stirred tank	34	592	
gas-liquid	201	265	564
isothermal	29	92	
liquid-liquid	299		
multifunctional	621		
multistage	27	115	131
pilot	517	522	
semi-continuous	28	85	188
	553	557	
single-phase	53	264	
single-phase batch	32		
single-phase semi-continuous	33		
single-phase stirred tank	104		
stirred tank	196		
three-phase	491		
tubular	26	33	89
	192		
recycling	132	595	619
reforming			
catalytic	20	405	431
	451		
steam	405		
regenerability	394		
regeneration	423	478	
regime			
flow	504	519	531
heterogeneous	220		
homogeneous	219		
hydrodynamic	207	269	493

This page has been reformatted by Knovel to provide easier navigation.

Index Terms	Links		
regime (*Cont.*)			
laminar	80	94	
steady state	25	384	
trickle flow	504		
turbulent	80	87	94
Reynolds (number)	78	82	98
	259	261	270
	325	422	459
	498	537	538
ring	352		
Lessing	321		
Pall	241	244	
Raschig	241	321	
riser	402	476	
runaway reaction	68	375	
S			
saddle (Berl, Intalox)	244	245	321
	568		
scale-up	307	336	
Schmidt (number)	261	422	424
	537		
segregation	44		
selectivity	2	109	136
	173	375	394
global	136		
instantaneous	3	57	136
	141	377	381
integrated	3	57	381
mass	5		
molar	3		
semi-continuous	25		

This page has been reformatted by Knovel to provide easier navigation.

Index Terms	Links		
separation (of effluent)	603		
settling	313	336	339
	341		
Sherwood (number)	261	423	
slugging	462		
slurry	492		
solubility	566		
stability	394		
thermal	428	557	560
stage	115		
steam cracking	632		
step			
kinetics	23		
tracer	39		
stirred (continuous reactor)	196		
stirred tank	117	501	554
stoichiometry	1		
sulfonation	268		
surface exchange (heat)	226	228	281
suspension	348	398	404
	407	494	543
synthesis			
Fischer-Tropsch	405		
methanol	405		
system			
adiabatic	58	107	
agitation	75		
closed	2	25	
gas-liquid	173		
isothermal	55	107	
multiphase	24		
open	4	25	
single-phase	24		

This page has been reformatted by Knovel to provide easier navigation.

Index Terms	Links		
T			
technology			
catalytic reactor	404	500	502
	513	524	527
	540		
liquid-liquid reactor	312	317	322
	326	335	339
Tellerette	245		
thermal conductivity	425		
thermodynamics	5		
Thiele (modulus and number)	359	361	367
	369	377	387
	610		
Thiele's modulus *see* Thiele			
time			
mean residence	603		
mixing	87	562	603
residence	37	92	124
tracer	38		
transfer			
energy	621	630	
fluid-solid	629		
momentum	622	635	
trickle bed	504		
turbine	76	279	555
U			
ultrasound	637		

This page has been reformatted by Knovel to provide easier navigation.

Index Terms	Links		
V			
velocity			
characteristic	303		
minimum fluidization	454	457	532
minimum, of rotation	270		
of circulation	230		
of entrainment	460		
of rotation	270		
rise	469		
slip	303		
space	413	513	
superficial	246	437	584
terminal fall	460		
venturi scrubber	283		
void fraction	241	353	
VVH *see* space velocity			
W			
Weber (number)	325		
weight flow rate of feed related to the weight of the bed	413		
withdrawal	447	450	455
	473		
Y			
yield	2	57	
mass	5		
molar	3		

This page has been reformatted by Knovel to provide easier navigation.